

Talanta

The International Journal of Pure and Applied Analytical Chemistry

Aims & Scope

Talanta provides a forum for the publication of original research papers, preliminary communications, and reviews in all branches of pure and applied analytical chemistry. Analytical data should be submitted only if they are clearly related to new analytical measurements. Original research papers on fundamental studies and novel sensor and instrumentation development are especially encouraged. Novel or improved applications in areas such as clinical chemistry, environmental analysis, geochemistry, and materials science and engineering are welcome. Methods should be validated by comparison with a standard method or analysis of a certified reference material, and relevant literature should be cited. Since classical spectrophotometric measurements and applications, solvent extraction, titrimetry, chemometrics, etc. are well established, studies in such areas should demonstrate a unique and substantial advantage over presently known systems. New reagents or systems should demonstrate clear advantage, and their presentation should be comprehensive rather than generating a series of similar papers for several analytes. Modifications of reagents should demonstrate significant improvements. Solvent extraction methods in particular, but others as well, should focus on the use of non-hazardous material substitutes and the minimization of waste generation. But obvious application of known chemistries or methods to established techniques are discouraged. Application of classical analytical approaches to relatively sample matrices having no major interferences, such as pharmaceutical preparations or reconstituted samples, are discouraged unless considerable improvements over other methods in the literature are demonstrated. Papers dealing with analytical data such as stability constants, pK_a values, etc. should be published in more specific journals, unless novel analytical methodology is demonstrated, or important analytical data are provided which could be useful in the development of analytical procedures.

Editors-in-Chief

Professor G.D. Christian, University of Washington, Department of Chemistry, 36 Bagely Hall, P.O. Box 351700, Seattle, WA 98195-1700, U.S.A.

Professor J.-M. Kauffmann, Université Libre de Bruxelles, Institut de Pharmacie, Campus de la Plaine, C.P. 205/6, Boulevard du Triomphe, B-1050 Bruxelles, Belgium

Associate Editors

Professor J.-H. Wang, Research Center for Analytical Sciences, Northeastern University, Box 332, Shenyang 110004, China

Professor J.L. Burguera, Los Andes University, IVAQUIM, Faculty of Sciences, P.O. Box 542, 5101-A Mérida, Venezuela.

Assistant Editors

Dr R.E. Synovec, Department of Chemistry, University of Washington, Box 351700, Seattle, WA 98195-1700, U.S.A.

Professor J.-C. Vire, Université Libre de Bruxelles, Institut de Pharmacie, Campus de la Plaine, C.P. 205/6, Boulevard du Triomphe, B-1050 Bruxelles, Belgium

Talanta

R. Apak (Istanbul, Turkey)
E. Bakker (Auburn, AL, U.S.A.)
D. Barceló (Barcelona, Spain)
B. Birch (Luton, UK)
K. S. Booksh (Tempe, AZ, U.S.A.)
J.-L. Capelo-Martinez (Caparica, Portugal)
Z. Cai (Kowloon, Hong Kong)
O. Chailapakul (Thailand)
S. Cosnier (Grenoble, France)
D. Diamond (Dublin, Ireland)
W. Frenzel (Berlin, Germany)
A.G. Gonzales (Seville, Spain)
P. de B. Harrington (OH, U.S.A.)

A. Ho (Hsin-chu, Taiwan)
P. Hubert (Liège, Belgium)
J. Kalivas (Pocatella, ID, U.S.A.)
B. Karlberg (Stockholm, Sweden)
J.-M. Lin (Beijing, China)
Y. Lin (Richland, WA, U.S.A.)
M.D. Luque de Caastro (Cordoba, Spain)
I.D. McKelvie (Victoria, Australia)
S. Motomizu (Okayama, Japan)
J.-M. Pingarron (Madrid, Spain)
E. Pretsch (Zürich, Switzerland)
W. Schuhmann (Bochum, Germany)
M. Shamsipur (Kermanshah, Iran)

M. Silva (Porto Alegre, Brazil)
P. Solich (Hradec Králové, Czech Republic)
K. Suzuki (Yokohama, Japan)
D.G. Themelis (Thessaloniki, Greece)
D.L. Tsalev (Sofia, Bulgaria)
B. Walzac (Katowice, Poland)
J. Wang (Tempe, AZ, U.S.A.)
J.D. Winefordner (Gainesville, U.S.A.)
Xiu-Ping Yan (Tianjin, China)
E.A.G. Zagatto (Piracicaba, SP, Brazil)
X. Zhang (China)



Selective determination of doxorubicin and doxorubicinol in rat plasma by HPLC with photosensitization reaction followed by chemiluminescence detection

Sameh Ahmed, Naoya Kishikawa, Kaname Ohyama, Mitsuhiro Wada, Kenichiro Nakashima, Naotaka Kuroda*

Graduate School of Biomedical Sciences, Course of Pharmaceutical Sciences, Nagasaki University, 1-14 Bunkyo-machi, Nagasaki 852-8521, Japan

ARTICLE INFO

Article history:

Received 23 August 2008

Received in revised form 27 October 2008

Accepted 27 October 2008

Available online 5 November 2008

Keywords:

Doxorubicin

Doxorubicinol

Pharmacokinetics

Peroxyoxalate chemiluminescence detection

Photosensitization

ABSTRACT

A highly sensitive and selective high-performance liquid chromatography (HPLC) method was developed for the determination of doxorubicin (DXR) and its metabolite doxorubicinol (DXR-ol) in rat plasma. The method was based on photosensitization reaction followed by peroxyoxalate chemiluminescence detection (PO-CL). DXR and DXR-ol that were fluorescent quinones, served as a photosensitizer in the presence of a hydrogen atom donor such as ethanol under aerobic conditions to produce hydrogen peroxide. Then the generated hydrogen peroxide and DXR or DXR-ol were monitored through PO-CL reaction by mixing with aryloxalate as a single post-column reagent that enabled highly selective and sensitive determination of DXR and DXR-ol. The separation of DXR and DXR-ol by HPLC was accomplished isocratically on an ODS column within 15 min. The method involves a simple one step protein precipitation by methanol and a sample size of 50- μ L was sufficient. Besides, it can detect accurately the low plasma concentrations. The detection limits (signal-to-noise ratio = 3) were 4.5 and 3.8 fmol for DXR and DXR-ol, respectively. The percentage recovery was found to be 90.7–102.4% and the inter- and intra-assay RSD values in rat plasma were 2.5–8.9%. The method has been successfully used to study pharmacokinetic profiles of DXR and DXR-ol in rats after a single-dose of DXR.

© 2008 Elsevier B.V. All rights reserved.

1. Introduction

Doxorubicin (DXR) is a cytotoxic anthracycline antibiotic that is originally produced by *Streptomyces peucetius* var. *caesius* and has been used in the treatment of a wide range of malignant tumours, including leukemia and breast cancer. However, the clinical use of doxorubicin is limited by a cumulative dose-dependent irreversible chronic cardiomyopathy, which can subsequently lead to congestive heart failure, with an ultimate mortality rate of 20–40%. Moreover, DXR-induced cardiotoxicity may be reduced or prevented by an administration schedule that produces low peak plasma drug concentrations [1,2].

DXR is rapidly metabolized in liver by the cytoplasmic NADPH-dependent aldo–keto reductase to the secondary alcohol metabolite, doxorubicinol (DXR-ol), and by the NADPH-dependent cytochrome P450 reductase to a broad panel of hydroxy- or deoxyglycones. Of these metabolites, DXR-ol has been demonstrated to

be cardiotoxic. However, the role of doxorubicin aglycones in the cardiotoxicity remains unclear (Fig. 1) [3].

To date, a number of publications have been reported for the determination of DXR and its metabolite DXR-ol including capillary electrophoresis (CE) with UV detection [4] or laser-induced fluorescence (LIF) detection [5–7], radioimmunoassay [8], high-performance liquid chromatography (HPLC) with ultraviolet (UV) detection [9–10], fluorescence detection [11–21], chemiluminescence detection [22], electrochemical detection [23] and mass spectrometric detection [25–29]. However, many of these methods lack the enough sensitivity and selectivity which enable the determination of DXR and DXR-ol at small plasma concentration while the high cost and the need for technical experience limits the use of the others. In addition, some of these techniques are laborious and necessitate long analytical run times to achieve sufficient peak resolution, owing to structural similarities of DXR and DXR-ol. Besides, sample pre-treatment procedures in these methods vary greatly. Some of them include time-consuming solid-phase extraction processes [23–26], or liquid–liquid extraction procedures [4,12,17,20,28]. The instability of DXR and DXR-ol in plasma also limits the utility of otherwise promising extraction strategies.

* Corresponding author. Tel.: +81 95 8192894 fax: +81 95 8192444.
E-mail address: n-kuro@nagasaki-u.ac.jp (N. Kuroda).

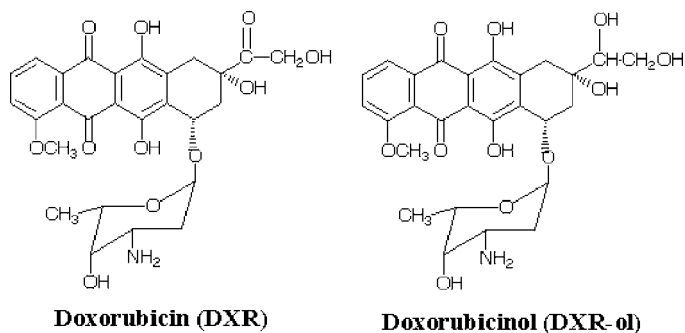


Fig. 1. Chemical structures of doxorubicin and its metabolite doxorubicinol.

From a practical point of view, a simple and rapid sample pre-treatment procedure is desirable in a single protein precipitation step.

Peroxyoxalate chemiluminescence (PO-CL) is based on the reaction between hydrogen peroxide and aryloxalate, which produces strong luminescence in the presence of fluorophore through the CIEEL (chemically initiated electron exchange luminescence) mechanism [30]. The PO-CL is easily combined with HPLC and applied to highly sensitive determination of fluorescent compounds and hydrogen peroxide. Previously, we had reported the determination of quinones by HPLC-PO-CL detection, without addition of hydrogen peroxide and fluorophore, combined with on-line photodegradation reaction [31] and this method was further adopted for the determination of vitamin K homologues [32]. This method was based on the production of hydrogen peroxide and conversion of non-fluorescent quinones to a fluorescent 3,6-dihydroxyphthalic acid through photodegradation reaction by UV irradiation, and then detected via PO-CL reaction by mixing with aryloxalate. Furthermore, it was reported that quinones served as sensitizer for photooxidation of hydrogen atom donor (HAD) under aerobic conditions to generate hydrogen peroxide and quinones were regenerated [33–34]. Moreover, DXR and DXR-ol are highly fluorescent quinones and can be used as fluorophore for PO-CL reaction after photosensitization reaction because they were regenerated along with the production of hydrogen peroxide.

Therefore, we aimed in this research to develop an HPLC method for their determination based on their unique photochemistry with UV irradiation (254 nm, 15 W) of DXR or DXR-ol in the presence of ethanol as an HAD under aerobic conditions to generate hydrogen peroxide followed by chemiluminescence reaction by mixing with

aryloxalate. The use of aryloxalate as a single post-column reagent provides advantages on the stability of CL reagent and subsequently reproducibility of the method in addition to the expected decrease of background noise. As a general case in PO-CL reaction, a mixture of aryloxalate together with hydrogen peroxide or a fluorophore is used as post-column CL reagent, which suffers from stability problems accompanied with high background noise. Interestingly, only fluorescent compounds with quinone moiety can give a response in our method that imparts the high selectivity that enabled us to determine small sample concentrations without any interference from plasma components.

2. Experimental

2.1. Chemicals and reagents

Doxorubicin hydrochloride was obtained from Wako Pure Chemical Industries (Osaka, Japan). Doxorubicinol hydrochloride was from Toronto Research Chemicals, Inc. (Toronto, Ontario, Canada). Stock solutions of DXR and DXR-ol (100 μ M) were prepared in methanol and stored in the dark at -30°C . These solutions were diluted appropriately with methanol to prepare the working solutions. Bis[2-(3,6,9-trioxadecyloxycarbonyl)-4-nitrophenyl]oxalate (TDPO), bis[2-(3,6-dioxaoctyloxycarbonyl)-4-nitrophenyl]oxalate (DOPO) and sodium dodecyl sulphate (SDS) were from Wako Pure Chemical Industries. Bis(2,4,6-trichlorophenyl)oxalate (TCPO), bis[(2,4,5-trichloro-6-pentoxycarbonyl) phenyl]oxalate (CPPO), bis(2,4-dinitrophenyl)oxalate (DNPO), bis(2,6-difluorophenyl)oxalate (DFPO) and bis(pentafluorophenyl)oxalate (PFPO) were from Tokyo Chemical Industry (Tokyo). Acetonitrile (LC/MS grade) were from Kanto Chemical (Tokyo). Imidazole was from Tokyo Chemical Industry; imidazole was recrystallized from acetonitrile before use. Distilled water was obtained using Simpli Lab-UV (Millipore, Bedford, MA, USA) water device. Other chemicals were of extra pure grade. All centrifuge tubes and HPLC vials were made of polypropylene to minimize adsorption effects of DXR and DXR-ol.

2.2. HPLC-PO-CL system

The HPLC system (Fig. 2) consisted of two LC-10AS liquid chromatographic pumps (Shimadzu, Kyoto, Japan), a Rheodyne 7125 injector (Cotati, CA, USA) with a 5- μ L sample loop, a Cosmosil 5C18-AR-II (150 mm \times 2 mm, i.d., Nacalai Tesque Inc., Kyoto) column, a low-pressure mercury lamp (15 W, 254 nm, Sigemi Standard,

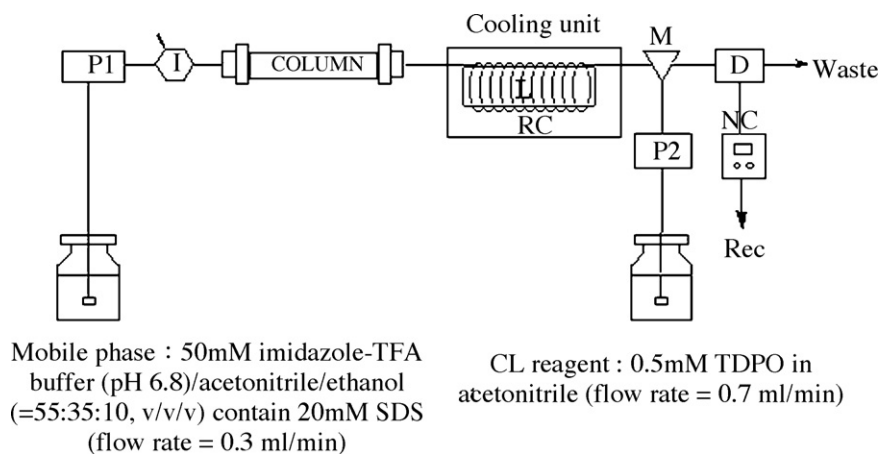


Fig. 2. HPLC-PO-CL system for the determination of DXR and DXR-ol. P1, pump 1; P2, pump 2; I, injector; Column, Cosmosil 5C18-AR-II (150 mm \times 2 mm, i.d.); cooling unit, oven equipped with cold insulator; L, low-pressure mercury lamp; RC, reaction coil (2.0 m \times 0.25 mm, i.d.); M, mixing tee; NC, noise cleaner; D, CL detector; Rec, recorder.

Tokyo), a CLD-10A chemiluminescence detector (Shimadzu) and SIC chromatorecorder (Tokyo, Japan). PTFE tubing (2.0 m × 0.25 mm i.d., GL Sciences, Tokyo) coiled around a low-pressure mercury lamp was used as on-line photoreactor. Temperature of the photoreactor was maintained at 50 °C by an oven (Jasco, Tokyo). A mixture of imidazole–trifluoroacetic acid (TFA) buffer (50 mM, pH 6.8), acetonitrile and ethanol (55:35:10, v/v/v) containing 20 mM SDS was used as a mobile phase and 0.5 mM TDPO in acetonitrile was used as the post-column CL reagent. The mobile phase and CL reagent were filtered through a 0.45- μ m filter prior to use. The flow-rates of the mobile phase and the CL reagent were set at 0.3 and 0.7 mL min⁻¹, respectively.

2.3. Experimental animals

Wistar male rats (285–317 g, Tagawa experimental animals, Nagasaki, Japan) were used for experiments. Animals were housed separately in a metabolic cage and kept on a 12-h light/dark cycle for 2 days before being used in experiment. Food and water were available *ad libitum*. Rats were anesthetized with ethyl carbamate i.p. (1.5 g/kg). DXR was administered (i.a.) via arteria femoralis to a group of three male Wistar rats at a dose of 5 mg/kg. Blood samples (150- μ L) were collected through indwelling arterial catheters, transferred to EDTA tubes and centrifuged for 10 min at 4 °C, 5000 × g then the plasma was separated and stored at –30 °C in dark until analysis. Sampling of blood was performed prior administration of DXR and then at 10, 20, 30, 45, 60, 120, 180, 240, 300, 360 and 420 min after administration of DXR. All animal procedures and care in this experiment were approved by the Nagasaki University Animal Care and Use Committee (approval no. 0807010676). Pharmacokinetic parameters were determined by moment analysis using a single-dose i.a. bolus drug administration model. The studied parameters are area under the curve (AUC), terminal phase half-life ($T_{1/2}$), clearance (CL), maximum concentration (C_{max}) and volume of distribution at steady state (V_{dss}).

2.4. Sample processing

Sample preparation involved a single protein precipitation step. A 50- μ L aliquot of plasma were pipetted into polypropylene Eppendorf micro test tube (Hamburg, Germany), followed by 150- μ L methanol for protein precipitation. The tube was vigorously mixed for 30 s and centrifuged for 10 min at 10,000 × g. A 5- μ L supernatant was injected directly into the HPLC system.

2.5. Method validation

The validation was done according to US FDA guidance for industry on bioanalytical method validation [35].

Three days of calibration curves with five replicates of quality controls (QC) over concentration range of 2–1000 nM were performed to assess linearity of the proposed method.

To evaluate intra-day and inter-day precision and accuracy, three sets of QC samples at three different concentration levels low-QC (50 nM), middle-QC (250 nM) and high-QC (1000 nM) with five replicates at 3 successive days. The samples were extracted by single protein precipitation step with methanol then 5 μ L of supernatant was injected directly to the HPLC system.

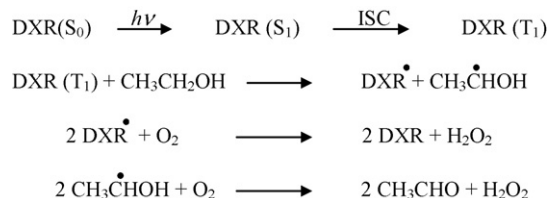
Pre-spiked plasma samples were used for the recovery study. The recovery was determined in triplicate at three concentration levels 50, 250 and 1000 nM by extraction of drug-free rat plasma fortified with standard DXR and DXR-ol. The fortified extracts were injected into HPLC system. The obtained results were compared with true concentration of the pure standard.

Finally, the stability of DXR and DXR-ol in rat plasma under various laboratory conditions was investigated in triplicate in both low-QC (50 nM) and high-QC (1000 nM). The quality control samples were freshly prepared and subjected to three-times freeze cycles, storing at room temperature for 1, 5 and 24 h, refrigeration overnight at 4 °C and storing in freezer at –30 °C for 3 weeks. The samples were extracted and analyzed by the proposed method.

3. Results and discussion

3.1. Photosensitization reaction of doxorubicin and its metabolite doxorubicinol

Photochemical reaction between anthraquinone or hydroxyanthraquinones and hydrogen atom-donating substrates has been widely studied [33,36]. Quinone sensitizers serve as catalysts for the reduction of oxygen and the oxidation of HAD substrates. Similarly, DXR and DXR-ol act as sensitizers for photooxidation of HAD such as ethanol. DXR is excited to its singlet-excited state (S_1) by UV irradiation and most of the excited DXR is converted by intersystem crossing (ISC) to the triplet state and subsequent by internal conversion to its lowest triplet state (T_1). Next, the excited DXR in the triplet state (T_1) abstract hydrogen from ethanol to produce two radical products, the semiquinone form of DXR and α -hydroxyethyl radical. Under aerobic conditions these two radical intermediates react with molecular oxygen to produce hydrogen peroxide and DXR is regenerated (Scheme 1 below).



3.2. Optimization of HPLC-PO-CL method

Since it was necessary to develop a highly sensitive and selective method for determination of DXR and DXR-ol at therapeutic level of the drugs in plasma, the conditions for separation and determination of DXR and DXR-ol with the proposed method were optimized in order to obtain the best resolution and sensitivity.

3.2.1. Optimization of separation and photochemical reaction conditions

Isocratic elution mode was employed for resolution and quantitation of DXR and DXR-ol. A mixture of imidazole buffer, acetonitrile and ethanol (55:35:10, v/v/v) containing SDS was used as a mobile phase. SDS was selected as ion-pair reagent not only for its effect on separation and peak shape of DXR and DXR-ol [10] but also for its enhancement and stabilization effect on PO-CL reaction [37]. Furthermore, SDS has a hydrogen atom-donating ability [38]. The influence of SDS concentration on separation and peak shape of DXR and DXR-ol peaks was tested. It was found that above its critical micellar concentration, reproducible and stable signals were obtained probably due to the protection of aryloxalate (TDPO) molecules in the micelles, thereby avoiding decomposition processes. In addition, the separation and peak symmetry were largely improved. Given this effect, a concentration of 20 mM was selected as optimum.

The presence of HAD in mobile phase such as methanol, ethanol and isopropanol was also studied (Fig. 3). Nevertheless, the presence of SDS in mobile phase, the presence of hydrogen atom

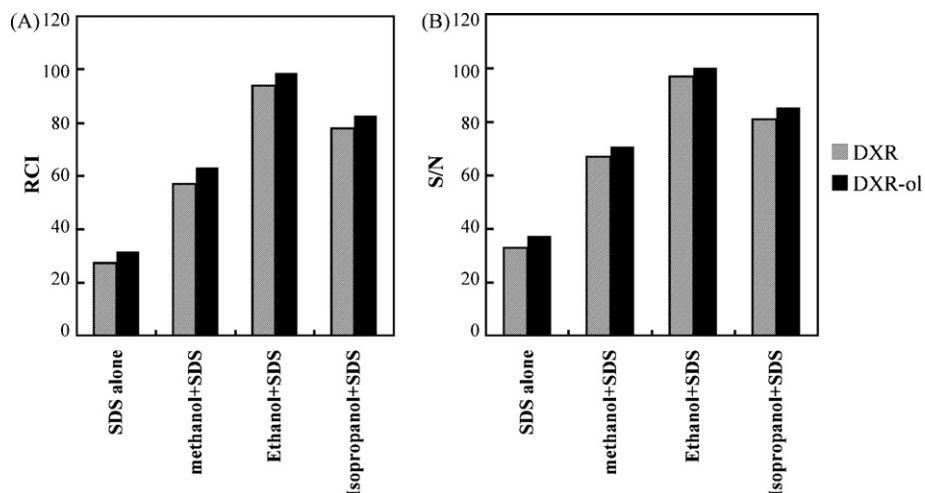


Fig. 3. Effects of hydrogen atom-donating substrates on (A) CL intensity and (B) S/N ratio. Samples were 500 nM DXR and DXR-ol.

donor enhance greatly CL intensity probably due to its effect on the amount of generated hydrogen peroxide. Ethanol was selected because it is effective as an enhancer of CL intensity and as eluent for DXR and DXR-ol. Moreover, the concentration of ethanol was studied and the best separation and CL intensity was obtained at ethanol concentration of 10% (v/v).

Furthermore, effect of photoreactor conditions such as UV irradiation lamps, the length of the reaction coil wrapped around UV lamp and photoreactor temperature were investigated. Three types of UV lamps were evaluated as UV sources; Toshiba GL-10 (10 W, 254 nm), Shigemi standard AL-15 H (15 W, 254 nm) and National FL-10 BL-B (10 W, 350 nm). We found that 15 W powered lamp, which emits at 254 nm wavelengths, gave higher CL intensity and signal-to-noise (S/N) ratio than the other two lamps. Therefore, it was chosen for subsequent work.

The effect of coil length ranging from 0.5 to 4.0 m with 0.25 mm internal diameter corresponding to 5–40 s of UV irradiation on CL intensity of DXR and DXR-ol was examined. It was found that CL intensity and S/N increased as the length of the reaction coil increased due to the increase in exposure time then decreased probably due to the decomposition of hydrogen peroxide by long UV irradiation time. From this experiment, 2.0 m of coil length, corresponding to 20 s of UV irradiation, was selected as optimal.

In addition, the influence of photoreactor temperature between 20 and 60 °C on CL of DXR and DXR-ol was investigated. It was found that both CL intensity and S/N ratio increased by the increase in temperature till 50 °C then decreased. This is probably due to the

increase in the amount of generated hydrogen peroxide by the rise in temperature then the more rise in temperature lead to increase decomposition of hydrogen peroxide. Therefore, 50 °C was selected.

3.2.2. Optimization of CL conditions

Imidazole has been reported as the most efficient catalyst for the PO-CL reaction, acting not only through a simple base catalysis but also nucleophilic catalysis pathway [30]. In this study, we have investigated the effect of different acids used in combination with imidazole. Several acids were tried such as HNO₃, HClO₄, H₃PO₄, HCl, H₂SO₄ and TFA. However, the highest CL intensity and S/N ratio was obtained when using a combination of imidazole-TFA. This may be attributed to the effect of TFA on PO-CL reaction kinetics and stability of CL reagent [39]. Next, the influence of imidazole-TFA buffer solution on CL intensity of DXR and DXR-ol was examined. It was found that the best CL intensity and S/N ratio were obtained at 50 mM imidazole-TFA buffer solution. Subsequently, the influence of pH of the imidazole-TFA buffer solution on CL was studied. CL intensity increased with the increase in pH value till 7.5 then decreased, which could be attributed to instability of DXR and DXR-ol at higher pH. Although, S/N ratio was decreased after pH 6.8 and therefore pH value of 6.8 was selected for subsequent work (Fig. 4).

In order to increase the quantum yield and light intensity produced for CL reaction of DXR and DXR-ol, we aimed to study the effect of different aryloxalates on CL intensity and S/N ratio of DXR and DXR-ol. Because it was reported that aryloxalates with strongly electron-withdrawing substituents provided the highest quantum yields [38], therefore we have tested; TCPO, TDPO, DNPO,

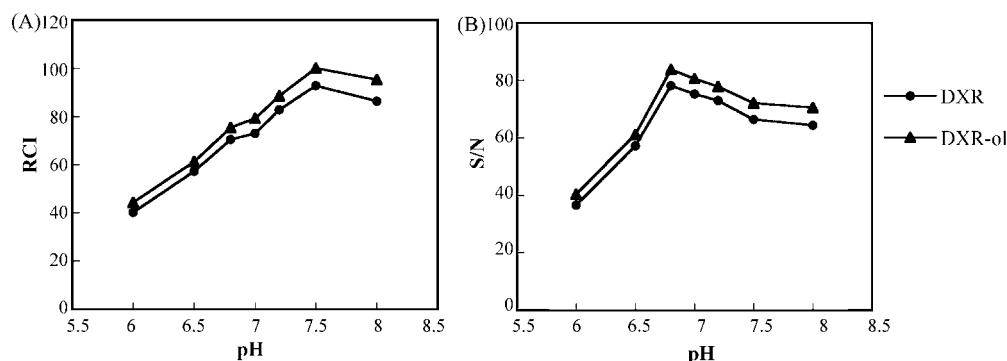


Fig. 4. Effects of pH of imidazole-TFA buffer on (A) CL intensity and (B) S/N ratio. Samples were 500 nM DXR and DXR-ol.

Table 1
Retention times, calibration curves and detection limits of DXR and DXR-ol.

Sample	t_R (min)	Calibration curve ^a				Detection limit ^b (fmol)/injection (nM)
		Range (nM)	Slope ^c (\pm SE)	Intercept ^c (\pm SE)	r	
DXR	14.1	2–1000	0.09 (\pm 0.01)	6.5 (\pm 0.52)	0.998	4.5 (0.90)
DXR-ol	9.2	2–1000	0.09 (\pm 0.02)	7.7 (\pm 0.65)	0.999	3.8 (0.76)

^a CL intensity (arbitrary unit) versus concentration (nM).

^b Detection limit at a S/N ratio of 3.

^c Data presented as mean \pm SE of three experiments.

DOPO, DFPO, PFPO and CPPO as the most efficient PO-CL reagents. We found that TDPO gave the best CL intensity and S/N ratio for both DXR and DXR-ol. Moreover, TDPO provides improved solubility (1010 mM) and chemical stability in acetonitrile relative to other aryloxalates that further provides superior reproducibility [40].

Furthermore, the effect of TDPO concentration on CL on DXR and DXR-ol was studied. It was found that CL intensity increases by increasing the concentration of TDPO whereas S/N ratio increases till 0.5 mM then decreased. The reason for this is the increase in background noise. Therefore, the concentration of 0.5 mM TDPO was selected for subsequent work. Subsequently, effect of TDPO flow-rate on CL of DXR and DXR-ol was investigated. It was found that CL intensity increased by the increase in flow-rate and reached maximum at 0.70 mL min⁻¹ then CL intensity decreased due to the decrease in reaction time between CL reagent, hydrogen peroxide and the analyte. From this experiment, flow-rate of 0.70 mL min⁻¹ was selected as optimal.

3.3. Validation of the proposed method

Under the optimum experimental conditions, linear relationship was observed by plotting drug concentration (nM) against relative chemiluminescence intensity (RCI). Calibration curve, retention time, calibration range, correlation coefficient and detection limit were recorded for DXR and DXR-ol (Table 1). The

correlation coefficients of 0.998 or more were obtained in the concentration ranges of 2–1000 nM for DXR and DXR-ol which indicate the good linearity of calibration graphs. Also, the detection limits obtained with the proposed method (S/N = 3) were 4.5 and 3.8 fmol for DXR and DXR-ol, respectively. A typical chromatogram of a standard mixture of DXR and DXR-ol using the proposed method is shown in Fig. 5(A). DXR and DXR-ol were fully separated and eluted within 15 min. Accuracy and precision of the proposed method were assessed at three different concentration levels; low (50 nM), middle (250 nM) and high (1000 nM) concentrations at 3 different days (Table 2). It was found that the accuracy of the determination was 92.3–101.5% and 90.4–102.5% for DXR and DXR-ol, respectively. The relative standard deviations (RSD) intra-day ($n = 5$) and inter-day ($n = 3$) were 3.5–8.9% and 2.5–7.6% for DXR and DXR-ol, respectively so good reproducibility was obtained. Moreover, extraction recovery was established with three different concentration levels; low (50 nM), middle (250 nM) and high (1000 nM). The percentage recovery was found to be 91.2–96.7% and 90.7–102.4% for DXR and DXR-ol, respectively. These results indicate the high efficiency of the extraction procedure in addition to its rapidity and simplicity. Besides, there is no matrix effect as the extracted samples can be determined without any interference from plasma matrix components that emphasize the bio-specificity of the proposed method.

The stability experiments of DXR and DXR-ol were carried out under various laboratory conditions such as three-times

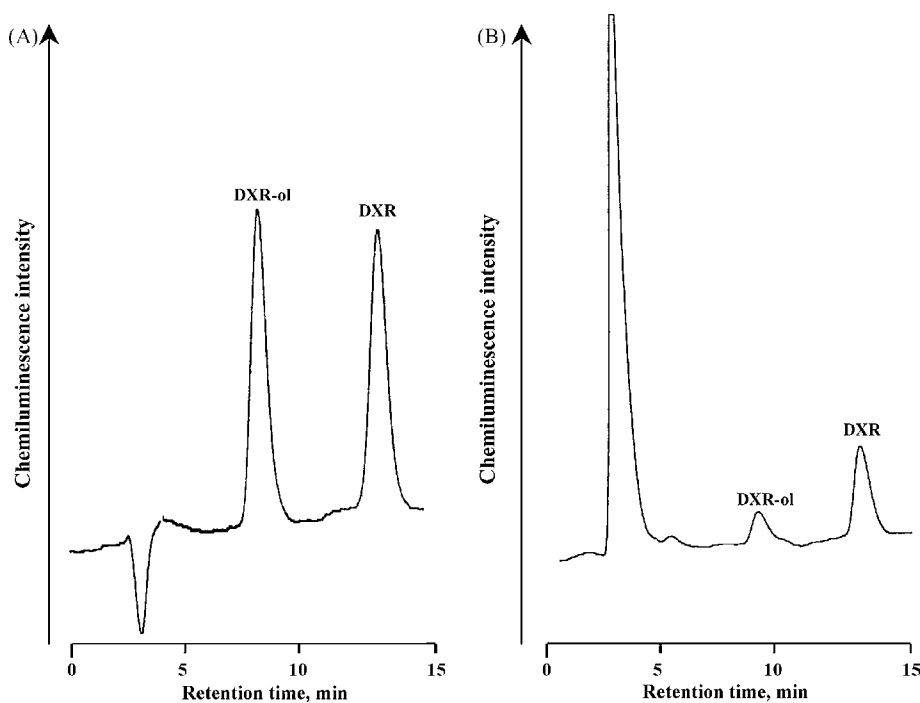


Fig. 5. Chromatogram of (A) a mixture of 500 nM standard DXR and DXR-ol (B) rat plasma collected after 60 min of single-dose administration of 5 mg/kg DXR and analyzed by the proposed HPLC-PO-CL method.

Table 2

Accuracy and precision of the proposed method in rat plasma.

Sample	Concentration (nM)	Intra-day assay (n = 5)		Inter-day assay (n = 3)	
		Accuracy (%)	Precision (RSD%)	Accuracy (%)	Precision (RSD%)
DOX	50	95.2	7.6	92.3	8.9
	250	93.3	5.7	101.5	7.5
	1000	100.7	4.6	97.4	3.5
DOX-ol	50	90.4	5.9	100.1	6.4
	250	102.5	2.5	94.1	5.7
	1000	96.1	3.9	91.2	4.8

Table 3

Stability of DXR and DXR-ol in rat plasma.

Condition	Percentage of initial concentration (%) (n = 3)			
	DXR		DXR-ol	
	High (1000 nM)	Low (50 nM)	High (1000 nM)	Low (50 nM)
Three-times freeze–thaw (−30 °C)	91.9	89.6	90.0	87.4
Room temperature (1 h)	102.3	96.8	98.9	97.2
Room temperature (5 h)	96.4	98.8	93.1	90.5
Room temperature (24 h)	85.0	82.7	81.9	80.3
Refrigeration over night (4 °C)	93.0	91.5	90.6	87.4
Freezer at −30 °C for 3 weeks	90.2	87.6	88.4	86.1

freeze–thaw stability, after storing at room temperature for 1, 5 and 24 h, refrigeration overnight at 4 °C and freezer stability at −30 °C for 3 weeks (Table 3). The variations of DXR and DXR-ol concentration in rat plasma for the freeze–thaw operations, room temperature stability for 1 and 5 h, refrigerator stability and freezer stability were within 13%. These results met with the acceptance criteria (+15%) according to US FDA guidance [35]. However, 24 h room temperature storage led to about 20% loss. Therefore, DXR and DXR-ol samples should be stored in cold as soon as possible, which is consistent with previous reports [11,24].

3.4. Application to pharmacokinetic studies of doxorubicin and its metabolite in rat

In order to test the applicability of the method to measure DXR and DXR-ol in the course of pharmacokinetic studies, the proposed HPLC-PO-CL method was used for simultaneous determination of DXR and DXR-ol in rat plasma after a single-dose administration of DXR. The smaller amount of plasma required for the determination enable many sampling points. DXR and

DXR-ol were detected in rat plasma up to 420 min after administration of DXR. A typical chromatogram of rat plasma collected after 60 min of single-dose administration of DXR is shown in Fig. 5(B) that fully confirms the high selectivity of the proposed method. Concentration–time profiles of DXR and DXR-ol in rat plasma after a single-dose administration of 5 mg/kg DXR are presented in Fig. 6. The pharmacokinetic parameters (mean ± SD, n = 3) are summarized as follows; for DXR, AUC_{0-420} 725.6 ± 26.1 µg h/L; $T_{1/2}$ 8.3 ± 0.8 h; CL 6.9 ± 2.1 L/h/kg; V_{dss} 15.3 ± 3.1 L/kg. For DXR-ol, C_{max} 53.9 ± 8.1 µg/L; T_{max} 23.3 ± 5.8 min; AUC_{0-420} 201.2 ± 26.1 µg h/L; $T_{1/2}$ 9.2 ± 1.3 h. These results indicate the higher conversion of DXR to DXR-ol when DXR was administered as free form compared to the pegylated liposomal form [28]. The results are consistent with previous studies for the free doxorubicin formulations [11,24]. Consequently, the obtained results demonstrate that the proposed HPLC-PO-CL method is suitable for pharmacokinetic studies of DXR and its metabolite DXR-ol in rats.

4. Conclusion

A highly sensitive and selective HPLC-PO-CL method has been developed and validated for the simultaneous determination of DXR and DXR-ol in rat plasma. The method was based on the unique photosensitization and fluorescence characteristics of DOX and DOX-ol, which enabled the use of aryloxalate as a single post-column CL reagent that provides advantages on the stability of CL reagent and subsequently reproducibility of the method in addition to the expected decrease of background noise. Because only fluorescent compounds with quinone moiety can give a response in our method, the high selectivity is expected for the proposed method. Furthermore, sample processing procedure involves a single protein precipitation step with a sample size of 50-µL which enabled many sampling points. Besides, it can detect accurately the low plasma concentrations due to its high selectivity and sensitivity which was comparable or even better than most of the published methods [6,8–25]. These advantages make our method strongly needed in cases where it is difficult to take larger sample volume with small sample concentration. Finally, the proposed method has been successfully applied to study pharmacokinetic profiles of DXR and DXR-ol in rats after a single-dose of DXR.

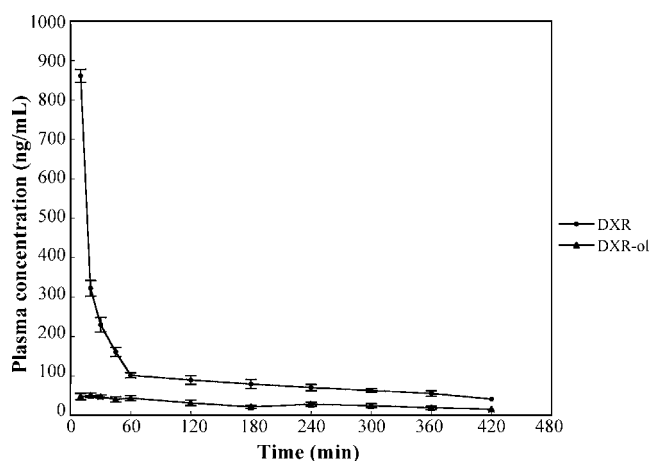


Fig. 6. Concentration–time profiles of DXR and its metabolite DXR-ol in rat plasma after a single-dose administration of 5 mg/kg DXR; data expressed as mean ± SD (n = 3).

References

- [1] G.N. Hortobagyi, *Drugs* 54 (Suppl. 4) (1997) 1.
- [2] D.L. Keefe, *Semin. Oncol.* 28 (Suppl. 12) (2001) 2.
- [3] G. Minotti, R. Ronchi, E. Salvatorelli, P. Menna, G. Cairo, *Cancer Res.* 61 (2001) 8422.
- [4] A. Gavenda, J. Sevcik, J. Psova, P. Bednar, P. Bartak, P. Adamovsky, V. Simanek, *Electrophoresis* 22 (2001) 2782.
- [5] A. Eder, J. Chen, E. Arriaga, *Electrophoresis* 27 (2006) 3263.
- [6] T. Pérez-Ruiz, C. Martínez-Lozano, A. Sanz, E. Bravo, *Electrophoresis* 22 (2001) 134.
- [7] N.J. Reinhoud, U.R. Tjaden, H. Irth, J. Vander Greef, *J. Chromatogr.* 574 (1992) 327.
- [8] R. Rahmani, P. Gil, M. Martin, A. Burand, J. Barbet, J. Cano, *J. Pharm. Biomed. Anal.* 1 (1983) 301.
- [9] I. Badea, L. Lazar, D. Moja, D. Nicolescu, A. Tudose, *J. Pharm. Biomed. Anal.* 39 (2005) 305.
- [10] O.T. Fahmy, M.A. Korany, H.M. Maher, *J. Pharm. Biomed. Anal.* 34 (2004) 1099.
- [11] Q. Zhou, B. Chowbay, *J. Pharm. Biomed. Anal.* 30 (2002) 1063.
- [12] C.M. Gilbert, R.P. McGeary, L.J. Filippich, R. Norris, B. Charles, *J. Chromatogr. B* 826 (2005) 273.
- [13] S. Emara, I. Morita, K. Tamura, S. Razee, T. Masujima, H. Mohamed, S. El-Gizawy, N. El-Rabbat, *Talanta* 41 (1994) 1973.
- [14] S. Emara, I. Morita, K. Tamura, S. Razee, T. Masujima, H. Mohamed, S. El-Gizawy, N. El-Rabbat, *J. Liq. Chrom. Rel. Technol.* 21 (1998) 681.
- [15] S.N. Mahnik, B. Rizovski, M. Fuerhacker, R.M. Mader, *Chemosphere* 65 (2006) 1419.
- [16] L. Alvarez-Cedron, M.L. Sayalero, J.M. Lanao, *J. Chromatogr. B* 721 (1999) 271.
- [17] S. Fogli, R. Danesi, F. Innocenti, A. Di Paolo, G. Bocci, C. Barbara, M. Del Tacca, *Ther. Drug Monit.* 21 (1999) 367.
- [18] N. Laubrock, G. Hempel, P. Schulze-Westhoff, G. Wurthwein, S. Flege, J. Boos, *Chromatographia* 52 (2000) 9.
- [19] P. de Bruijn, J. Verweij, W.J. Loos, H.J. Kolker, A.S.T. Planting, K. Nooter, G. Stoter, A. Sparreboom, *Anal. Biochem.* 266 (1999) 216.
- [20] J. van Asperen, O. van Tellingen, J.H. Beijnen, *J. Chromatogr. B* 712 (1998) 129.
- [21] L.H. Reddy, N. Meda, R.R. Murthy, *Acta Pharm.* 55 (2005) 81.
- [22] K. Imai, A. Nishitani, Y. Tsukamoto, *Chromatographia* 24 (1987) 77.
- [23] R. Ricciarello, S. Pichini, R. Pacifici, I. Altieri, M. Pellegrin, A. Fattorossi, P. Zucaro, *J. Chromatogr. B* 707 (1998) 219.
- [24] R. DiFrancesco, J.J. Griggs, J. Donnelly, R. DiCenzo, *J. Chromatogr. B* 852 (2007) 545.
- [25] F. Lachat, P. Marquet, S. Ragot, J.M. Gaulier, P. Cardot, J.L. Dupuy, *J. Chromatogr. B* 738 (2000) 281.
- [26] C. Sottani, G. Tranfo, M. Brettinelli, P. Faranda, M. Spagnoli, C. Minoia, *Rapid Commun. Mass Spectrom.* 18 (2004) 2426.
- [27] Y. Yang, *Talanta* 71 (2007) 596–604.
- [28] Y. Liu, Y. Yang, X. Liu, T. Jiang, *Talanta* 74 (2008) 887–895.
- [29] R.D. Arnold, J.E. Slack, R.M. Straubinger, *J. Chromatogr. B* 808 (2004) 141.
- [30] A.M. Garcia-Campana, W.R. Baeyens, *Chemiluminescence in Analytical Chemistry*, M. Dekker, New York, 2001, Chapter 7, p. 141.
- [31] S. Ahmed, S. Fujii, N. Kishikawa, Y. Ohba, K. Nakashima, N. Kuroda, *J. Chromatogr. A* 1133 (2006) 76.
- [32] S. Ahmed, N. Kishikawa, K. Nakashima, N. Kuroda, *Anal. Chim. Acta* 591 (2007) 148.
- [33] J.R. Poulsen, J.W. Birks, *Anal. Chem.* 62 (1990) 1242–1251.
- [34] T. Pérez-Ruiz, C. Martínez-Lozano, V. Tomás, J. Martín, *Analyst* 124 (1999) 197.
- [35] Department of Health and Human Services, Food and Drug Administration, Guidance for Industry on Bioanalytical Method Validation, Fed. Regist. 66 (2001) 28526.
- [36] K. Gollnick, S. Held, *J. Photochem. Photobiol. A: Chem.* 70 (1993) 135.
- [37] L. Gamiz-García, A.M. García-Campana, F. Ales Barrero, L. Cuadros Rodríguez, *Anal. Bioanal. Chem.* 377 (2003) 281.
- [38] T. Pérez-Ruiz, C. Martínez-Lozano, M.D. García, J. Martín, *J. Chromatogr. A* 1141 (2007) 67.
- [39] P. Prados, T. Santa, H. Homma, K. Imai, *Anal. Sci.* 11 (1995) 575.
- [40] K. Imai, H. Nawa, M. Tanaka, H. Ogata, *Analyst* 111 (1986) 209.



Comparison of ultrasonic and pressurized liquid extraction for the analysis of polycyclic aromatic compounds in soil samples by gas chromatography coupled to tandem mass spectrometry

N. Barco-Bonilla, J.L. Martínez Vidal, A. Garrido Frenich*, R. Romero-González

Research Group "Analytical Chemistry of Contaminants", Department of Analytical Chemistry, Almería University, 04071 Almería, Spain

ARTICLE INFO

Article history:

Received 27 June 2008

Received in revised form 20 October 2008

Accepted 31 October 2008

Available online 7 November 2008

Keywords:

Soils

PAHs

Pressurized liquid extraction

Ultrasonic extraction

GC–MS/MS

ABSTRACT

A pressurized liquid extraction (PLE) method has been optimized for the determination of polycyclic aromatic hydrocarbons (PAHs) in soil samples and it was compared with ultrasonic extraction. The extraction step was followed by gas chromatography–triple quadrupole mass spectrometry (GC–QqQ–MS/MS) analysis. Parameters such as type of solvent, extraction time, extraction temperature and number of extractions were optimized. There were no significant differences among the two extraction methods although better extraction efficiencies were obtained when PLE was used, minimizing extraction time and solvent consumption. PLE procedure was validated, obtaining limits of detection (LODs) ranging from 0.02 to 0.75 $\mu\text{g kg}^{-1}$ and limits of quantification (LOQs) ranging from 0.07 to 2.50 $\mu\text{g kg}^{-1}$ for the selected PAHs. Recoveries were in the range of 59–110%, except for naphthalene, which was the most volatile PAH. Finally, the method was applied to real soil samples from Southeast of Spain. PAHs concentrations were low, and phenanthrene, pyrene, fluorene, benzo[a]pyrene and chrysene were the most frequently detected analytes in the samples.

© 2008 Elsevier B.V. All rights reserved.

1. Introduction

Polycyclic aromatic hydrocarbons (PAHs) are hydrophobic compounds originating from natural or anthropogenic sources, such as incomplete combustion at high temperature or inappropriate agricultural practices [1]. It is well known that some PAHs, such as benzo[a]anthracene, benzo[a]pyrene, are recognized as potent carcinogens [2] and they are widely distributed in the environment. For instance, in soil, most of the PAHs come from wet and dry deposition due to the low water solubility, and the flux to the soil is determined by PAH concentration in the air. The amount of PAHs in soils is of importance because of their toxicity to humans and their effects on soil organisms and plants [3]. As a result of their widespread presence, PAHs are generally introduced in monitoring programs [4] and are listed by the US Environmental Protection Agency (EPA) and the European Community as priority pollutants [5].

Many analytical techniques have been developed and applied for the monitoring of these compounds in soil samples [6], including immunoassay tests [4,7], although PAHs are mainly determined

by chromatographic methods. Liquid chromatography (LC) with fluorescence [8,9] or diode array [10] detection has been used to separate and detect these compounds, due to the selectivity and sensitivity of fluorescence detection, although gas chromatography (GC) with flame ionization detector (FID) [11] has been also applied. Due to the lack of selectivity of this type of detector, it is being replaced by mass spectrometry (MS) detection using several analyzers such as single, triple quadrupoles or ion trap [12–14], providing good selectivity, low limits of detection (LODs) and reliable confirmation of PAHs.

However, sample preparation and especially extraction is a critical step in PAHs analysis, because these hydrophobic compounds are strongly sorbed to the soil material. In consequence, their extraction is time-consuming and in many cases becomes the origin of quantification errors. Traditionally, Soxhlet extraction was used for the extraction of PAHs in soils [15,16], but this procedure does not provide enough energy to release the analytes rapidly. It requires very long extraction time and large amounts of organic solvent. New approaches have been used in order to improve automation, reduce extraction times and the amount of solvent required, as well as to increase sample throughput. Thus, supercritical fluid extraction [17], ultrasonic extraction [18], microwave extraction [19], subcritical water extraction [11,20], matrix solid phase dispersion (MSPD) [9,21] and pressurized liquid extraction

* Corresponding author. Tel.: +34 950015985; fax: +34 950015483.
E-mail address: agarrido@ual.es (A. Garrido Frenich).

(PLE) [22,23] have been proposed as alternative techniques. PLE is mainly being used for the extraction of organic compounds from solid samples such as sediments, soils and particulate matter samples, obtaining high performance due to the disruption of surface equilibria, solubility and mass transfer effect [24]. Some studies compared the extraction efficiencies of PAHs from contaminated samples when different extraction techniques such as Soxhlet, ultrasound, microwave and PLE were used [11,12,25,26], indicating that differences between conventional and new techniques are negligible. However these studies are usually carried out at concentrations higher than 1 mg kg⁻¹ or with few compounds, so in order to get reliable conclusions related to these techniques more data are necessary.

In this study, PLE and ultrasonic extraction were compared for the extraction of more than 20 PAHs in soil, followed by gas chromatography coupled to triple quadrupole (GC-QqQ-MS/MS) determination. The PLE combined with the chromatographic method was used to determine PAHs at trace levels in soil samples taken from different agricultural areas of the southeast of Spain.

2. Experimental

2.1. Chemicals and materials

Acenaphthene, acenaphthylene, anthracene, benzo[*a*]anthracene, benzo[*a*]pyrene, benzo[*b*]fluoranthene, benzo[*g,h,i*]perylene, chrysene, dibenzo[*a,h*]anthracene, fluoranthene, fluorene, indeno[1,2,3-*cd*]pyrene, naphthalene, phenanthrene, pyrene and 2-bromonaphthalene were purchased from Supelco (Bellefonte, PA, USA) as mix solution of 2000 mg L⁻¹ in methylene chloride. 5-Methylchrysene (99.6% purity), benzo[*j*]fluoranthene (98.6% purity), benzo[*k*]fluoranthene (99.5% purity) and fluoranthene-*d*₁₀ (99.2% purity), which was used as internal standard, were also obtained from Supelco. Dibenzo[*a,e*]pyrene (99% purity), dibenzo[*a,i*]pyrene (99.9% purity), dibenzo[*a,h*]pyrene (99% purity), dibenzo[*a,l*]pyrene (99.5% purity) and cyclopenta[*cd*]pyrene (99%

purity) were purchased from Dr. Ehrenstorfer GmbH (Augsburg, Germany). Stock solutions were prepared in acetone (concentrations in the range from 10 to 900 mg L⁻¹) and stored at 4 °C. A multicomponent working standard solution (2 mg L⁻¹) was prepared by appropriate dilution with acetone and stored under refrigeration (4 °C). A working standard solution of fluoranthene-*d*₁₀ (20 mg L⁻¹) was prepared by appropriate dilution of the stock solution with acetone and stored under the aforementioned conditions.

Analytical grade organic solvents (acetone, dichloromethane, *n*-hexane and ethyl acetate) were obtained from Riedel-de Haën (Seelze-Hannover, Germany).

Cellulose filters of 30 mm from Whatman (Maidstone, England) and Hydromatrix (Varian, Harbour City, CA, USA) were used for PLE.

2.2. Apparatus

Chromatographic analyses were carried out using a GC system Varian 3800 (Varian Instruments, Sunnyvale, CA, USA) equipped with electronic flow control (EFC) interfaced to a 1200 L triple quadrupole mass spectrometer. Samples were injected into an SPI/1079 split/splitless programmed-temperature injector with a Combi Pal (CTC Analytics AG, Zwingen, Switzerland) using a 100 µL syringe. The glass liner was equipped with a plug of carbofrit (Resteck, Bellefonte, PA, USA). A fused-silica untreated capillary column 2 m × 0.25 mm i.d. from Supelco was used as guard column connected to a Factor Four Capillary Column VF-5 ms (30 m × 0.25 mm i.d. × 0.25 µm film thickness) purchased from Varian (Sunnyvale, CA, USA). The carrier gas was helium (99.999%) at a constant flow rate of 1 mL min⁻¹, and argon (99.999%) was used as collision gas. The mass spectrometer was operated in electron impact (EI) at 70 eV. From the ionization source the ions passed through a hexapole ion guide to the mass analyzers (mass range from 10 to 1500 u). The curved collision cell presented a 180° path. The mass spectrometer was calibrated weekly with perfluorotributylamine. Varian Workstation was used for instrument control and data analysis.

Table 1
Retention time windows (RTWs) and GC-MS/MS conditions for the selected PAHs.

Code	Compound	RTW (min)	Precursor ion (<i>m/z</i>)	Product ion (<i>m/z</i>) ^a
1	Naphthalene	8.08–8.26	128	78 (20); 102 (15); 127 (15)
2	Acenaphthylene	10.21–10.25	152	126 (20); 150 (25); 151 (15)
3	2-Bromonaphthylene	10.38–10.43	208	126 (25); 127 (20); 208 (5)
4	Acenaphthene	10.41 –10.46	153 154	126 (35); 152 (15) 153 (10)
5	Fluorene	11.07 –11.11	165 166	139 (25); 165 (15) 165 (10)
6	Phenanthrene	12.27–12.31	178	152 (15); 176 (25); 177 (10)
7	Fluoranthene	13.75–13.79	202	174 (50); 200 (35); 201 (10)
8	Fluoranthene- <i>d</i> ₁₀ (IS)	13.73–13.77	212	156 (50); 208 (35)
9	Pyrene	13.75–13.79	202	174 (40); 200 (25); 201 (20)
10	Benzo[<i>a</i>]anthracene	15.53–15.58	228	200 (50); 224 (50); 226 (25)
11	Cyclopenta[<i>cd</i>]pyrene	15.53–15.57	226	223 (30); 224 (45); 225 (20)
12	Chrysene	15.62–15.64	228	200 (50); 224 (50); 226 (25)
13	5-Methylchrysene	16.06–16.19	242	226 (35); 239 (35); 241 (10)
14	Benzo[<i>b</i>] + [<i>j</i>] + [<i>k</i>] fluoranthenes	17.12–17.16	252	224 (50); 249 (45); 250 (35)
15	Benzo[<i>a</i>]pyrene	17.72–17.76	252	224 (50); 249 (50); 251 (25)
16	Indeno[1,2,3- <i>cd</i>]pyrene + dibenzo[<i>a,h</i>]anthracene	20.40–20.44	276	273 (50); 274 (40); 275 (15)
17	Benzo[<i>g,h,i</i>]perylene	21.22–21.25	276	273 (45); 274 (50); 275 (20)
18	Dibenzo[<i>a,l</i>]pyrene	25.79–25.84	302	300 (35); 301 (15); 302 (5)
19	Dibenzo[<i>a,e</i>]pyrene	27.73–27.85	302	300 (25); 301 (5); 302 (5)
20	Dibenzo[<i>a,i</i>]pyrene	28.44–28.61	302	300 (45); 301 (40); 302 (5)
21	Dibenzo[<i>a,h</i>]pyrene	28.85–28.92	302	299 (45); 300 (35); 302 (5)

^a Collision energies are given in brackets (eV).

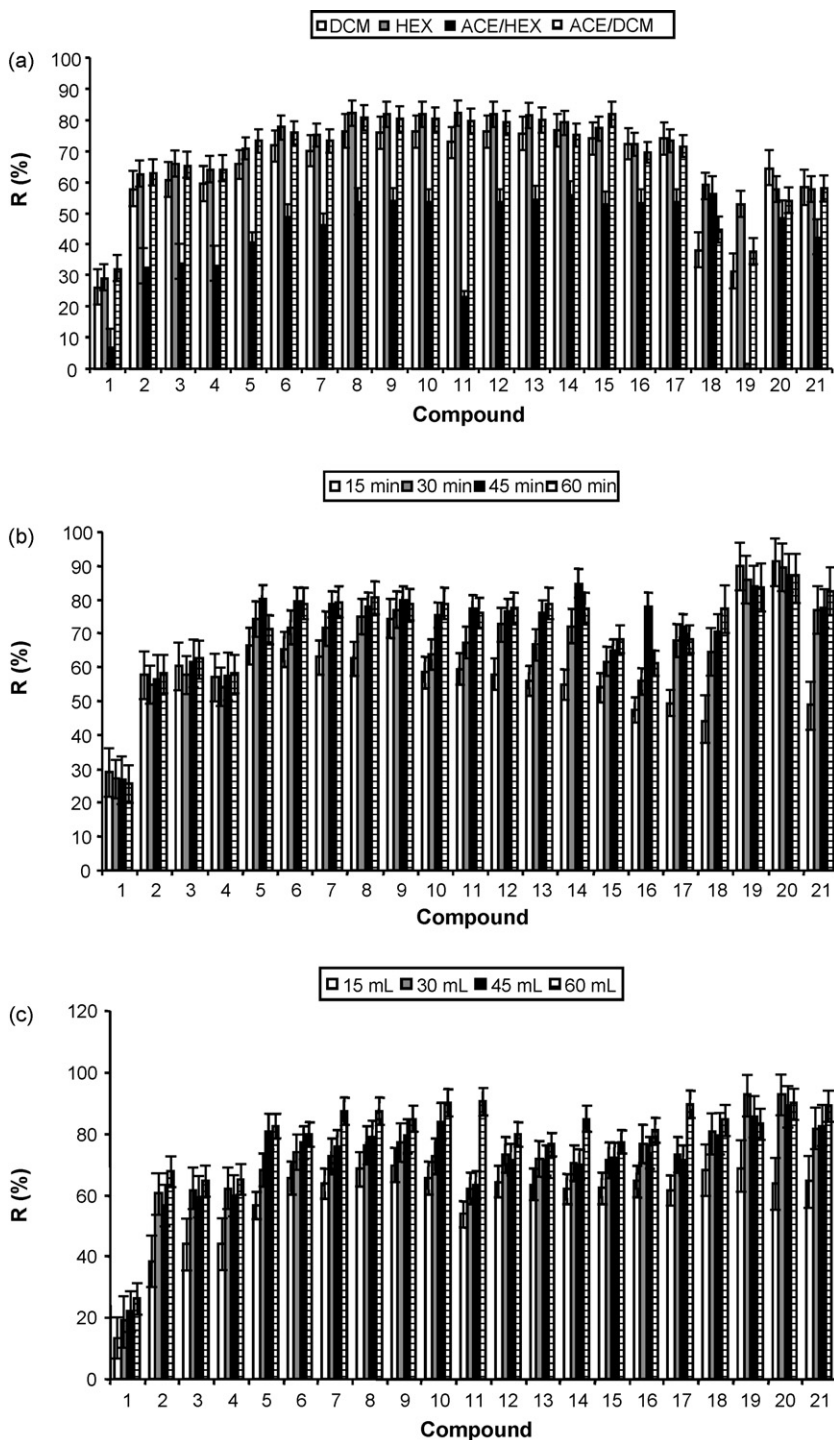


Fig. 1. Effect of (a) type of solvent; (b) extraction time and (c) solvent volume on the recoveries of the selected PAHs when a blank sample soil was spiked at $20 \mu\text{g kg}^{-1}$. DCM: dichloromethane; HEX: *n*-hexane; ACE: acetone. Error bars indicated the standard deviation ($n=3$). PAHs codes are shown in Table 1.

Ultrasonic extractions were carried out in a P-Selecta sonication bath (Selecta, Barcelona, Spain).

Pressurized liquid extraction was performed using an ASE 100 Accelerated Solvent Extraction system (Dionex, Sunnyvale, CA, USA) equipped with 34 mL stainless steel extraction cells.

An analytical balance AB204-S from Mettler Toledo (Greifensee, Switzerland), a P-Selecta Centromix mod S-549 centrifuge (Selecta, Barcelona, Spain) and a rotary evaporator R-114 (Büchi, Flawil, Switzerland) were used during extraction process.

2.3. GC-MS/MS analysis

Aliquots of $10 \mu\text{L}$ of sample extract were injected into the GC system operating at a syringe injection flow rate of $10 \mu\text{L s}^{-1}$. The initial injector temperature of 70°C was held for 0.4 min and then increased at $200^\circ\text{C min}^{-1}$ to 325°C , which was supported for 28 min. The injector split ratio was initially set at 30:1. The splitless mode was switched on from 0.4 to 4 min. At 4 min, the split ratio was set at 100:1 and reduced to 30:1 at 30 min. The column

oven temperature was initially at 70 °C, and was held for 4.0 min; then temperature was increased at 20 °C min⁻¹ to 300 °C, which was held for 15 min. Cryogenic cooling with CO₂ was applied when the injector temperature was 270 °C in order to reach the initial injector temperature as fast as possible before continuing with the next injection. The total running time was 30.50 min.

Triple quadrupole mass spectrometer was operated in MS/MS mode (selected reaction monitoring, SRM). The electron multiplier was set +200 V above the optimal value indicated by the software instrument. The temperatures of transfer line, manifold and source of ionization were set at 300, 40 and 280 °C, respectively. The optimal values for the scan time ranged from 0.105 to 0.330 s. Peak widths of *m/z* 2.0 and 1.5 were set in the first (Q1) and third quadrupole (Q3) respectively and the analysis was performed with a filament-multiplier delay of 7.5 min. MS/MS parameters for the selected PAHs are indicated in Table 1.

2.4. Sonication extraction

Dried soil sample (5 g) were extracted in a sonication bath for 45 min using 60 mL of *n*-hexane. After that, the extracts were centrifuged for 5 min at 3500 rpm, the supernatants were reduced to approximately 5 mL with a vacuum rotary evaporator at 45 °C and evaporated to almost dryness under a gentle stream of nitrogen. The concentrated extracts were then adjusted to 1 mL with ethyl acetate. Finally, 950 µL were taken and 50 µL of working internal standard solution was added before GC–MS/MS analysis.

2.5. Pressurized liquid extraction

A cellulose filter was placed at the bottom of the extraction cell. 6 g of soil sample was accurately weighed into a glass container and mixed with Hydromatrix, which removes moisture and also facilitates solvent penetration through the matrix, until the mixture became homogeneous. The mixture was then introduced into the cell, taking care to avoid loose mixture packing. The cell was refilled with Hydromatrix and it was tightly closed. The soil samples were extracted under the following conditions: solvent, hexane; pressure, 1500 psi; temperature, 150 °C; oven heat-up time, 7 min; static

time, 5 min; flush volume, 60% of extraction cell volume; purge N₂, 60 s; number of extraction cycles, 1.

The extracts were reduced to a volume of approximately 5 mL with a vacuum rotary evaporator at 45 °C and evaporated to almost dryness under a gentle stream of nitrogen. The concentrated extracts were then adjusted to 2 mL with ethyl acetate. Finally, 950 µL were taken and 50 µL of internal standard solution was added before chromatographic analysis.

2.6. Validation study

Linearity was evaluated using matrix-matched calibration, spiking blank extracts at four concentration levels (from 5 to 150 µg L⁻¹). Precision and accuracy of the method were evaluated by spiking blank samples. Thus, repeatability (intraday precision) was studied at 2 and 20 µg kg⁻¹, using five replicates per concentration level. Reproducibility (interday precision) was evaluated at the same concentration levels and spiked samples were analyzed at three different days. Accuracy was evaluated in terms of recovery which was determined for five replicates at two concentration levels (2 and 20 µg kg⁻¹). LODs and limits of quantification (LOQs) for each analyte were calculated as the concentrations for which signal-to-noise ratios were 3 and 10 respectively.

2.7. Sample collection

Soil samples were taken from agricultural and industrial areas located in Almeria, Spain. Samples were homogenized and sieved. After that, all samples were dried at ambient temperature and kept in brown glass bottles before analysis.

3. Results and discussion

The aim of this work was the development and comparison of ultrasonic and pressurized liquid extraction of PAHs in soil samples at low levels and the chromatographic analysis was based on a previously reported GC–MS/MS methodology [27], developed for the determination of PAHs in air, showing in Table 1 the characteristic ions used for GC–MS/MS analysis. It can be noticed that three isomers (benzo[*b*], [*j*] and [*k*] fluoranthenes) coeluted and had the

Table 2
Effect of the number of extractions on the recovery of the selected PAHs by ultrasonic extraction.

Compound	Recovery (%)		Total (%)
	1st extraction	2nd extraction	
Naphthalene	20.0	3.0	23.0
Acenaphthylene	43.5	5.3	48.9
2-Bromonaphthylene	45.7	5.9	51.6
Acenaphthene	46.9	5.0	52.0
Fluorene	62.7	5.4	68.1
Phenanthrene	72.7	6.9	79.7
Anthracene	69.6	6.4	76.0
Fluoranthene	73.3	7.5	80.7
Pyrene	73.5	7.5	81.0
Benzo[<i>a</i>]anthracene	67.7	7.9	75.6
Cyclopenta[<i>cd</i>]pyrene	54.7	6.9	61.6
Chrysene	58.6	8.6	67.2
5-Methylchrysene	63.5	7.2	70.7
Benzo[<i>b</i>] + [<i>j</i>] + [<i>k</i>] fluoranthenes	64.4	9.1	73.6
Benzo[<i>a</i>]pyrene	61.5	7.8	69.3
Benzo[<i>g,h,i</i>]perylene	63.3	9.3	72.5
Dibenzo[<i>a,h</i>]anthracene/indeno[1,2,3- <i>cd</i>]pyrene	58.1	9.5	67.6
Dibenzo[<i>a,l</i>]pyrene	63.5	10.0	73.5
Dibenzo[<i>a,e</i>]pyrene	72.5	Nd ^a	72.5
Dibenzo[<i>a,i</i>]pyrene	75.4	Nd	75.4
Dibenzo[<i>a,h</i>]pyrene	81.0	Nd	81.0

^a Nd: not detected.

same monitoring ions, so they were considered together, as well as indeno[1,2,3-*cd*]pyrene and dibenzo[*a,h*]anthracene.

3.1. Optimization of the ultrasonic extraction process

The different parameters that influence the extraction of PAHs between the soil and the extracting solution using sonication approach were optimized, spiking blank soils samples with $20 \mu\text{g kg}^{-1}$.

First, several solvents such as dichloromethane, *n*-hexane, a mixture of acetone/*n*-hexane (50:50, v/v) and acetone/dichloromethane (50:50, v/v) were tested, sonicating 5 g of spiked soil during 30 min with 30 mL of solvent. The obtained results for

the selected PAHs are shown in Fig 1a. It can be observed that the best results were obtained when pure *n*-hexane or acetone/dichloromethane (50:50, v/v) were used as solvents. Both solvents provide very similar results (recoveries higher than 60% in most of the cases), so pure *n*-hexane was chosen as solvent due to its lower toxicity.

In order to determine the optimum sonication time, 5 g of spiked soil was sonicated for 10, 30, 45 and 60 min, showing in Fig. 1b the influence of the extraction time on the recovery of the studied PAHs. In general, recovery increased with extraction time and kept constant between 45 and 60 min, although for naphthalene, dibenzo[*a,e*]pyrene and dibenzo[*a,i*]pyrene this trend is not fulfilled. It is necessary to highlight that the low values obtained

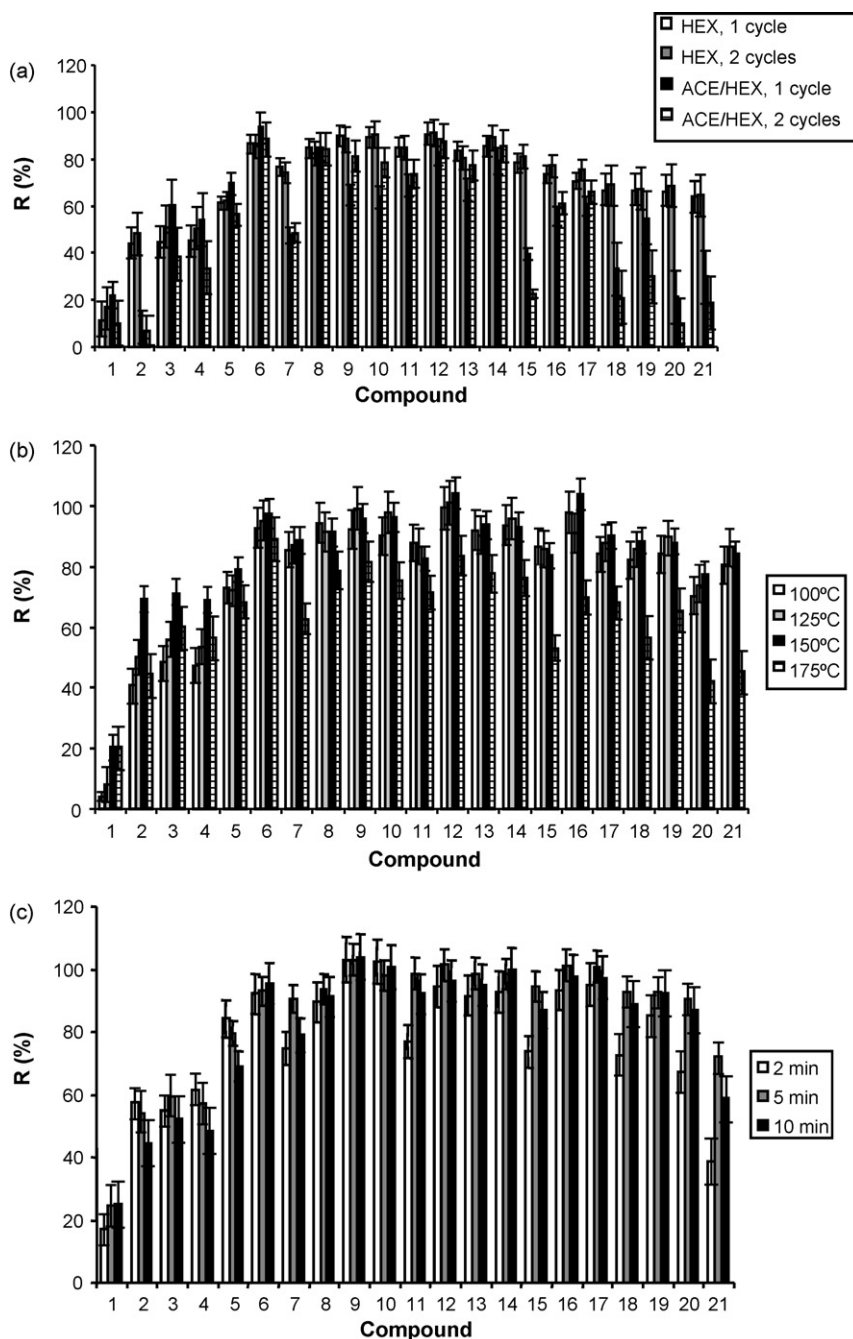


Fig. 2. Recoveries of the selected PAHs during the optimization of the pressurized liquid extraction, spiking a blank sample soil at $20 \mu\text{g kg}^{-1}$: (a) type of solvent and extraction cycles; (b) extraction temperature; (c) extraction time. HEX: *n*-hexane; ACE: acetone. Error bars indicated the standard deviation ($n=3$). PAHs codes are shown in Table 1.

Table 3Recoveries (*R*) and relative standard deviations (RSDs) obtained from spiked soil samples ($20 \mu\text{g kg}^{-1}$) using ultrasonic and pressurized liquid extraction (PLE)^a.

Compound	Ultrasonic extraction		PLE	
	<i>R</i> (%)	RSD (%)	<i>R</i> (%)	RSD (%)
Naphthalene	29.2	26.4	32.0	20.6
Acenaphthylene	56.5	47.1	62.1	17.2
2-Bromonaphthylene	59.5	39.3	65.3	7.4
Acenaphthene	59.7	38.6	64.0	12.3
Fluorene	70.8	24.0	72.5	5.9
Phenanthrene	77.2	9.6	95.7	3.6
Anthracene	75.9	9.4	87.6	7.7
Fluoranthene	78.8	6.6	97.5	3.1
Pyrene	79.2	6.8	97.7	0.6
Benzo[<i>a</i>]anthracene	74.1	6.9	99.6	3.5
Cyclopenta[<i>cd</i>]pyrene	63.5	6.0	91.7	5.3
Chrysene	71.6	8.4	93.1	1.7
5-Methylchrysene	71.3	6.5	98.3	1.2
Benzo[<i>b</i>] + [<i>j</i>] + [<i>k</i>] fluoranthenes	69.9	7.0	99.2	2.6
Benzo[<i>a</i>]pyrene	72.1	7.0	98.2	7.1
Benzo[<i>g,h,i</i>]perylene	73.7	8.4	97.4	4.0
Dibenzo[<i>a,h</i>]anthracene/indeno[1,2,3- <i>cd</i>]pyrene	71.3	7.4	97.7	4.3
Dibenzo[<i>a,l</i>]pyrene	79.5	7.5	98.1	13.9
Dibenzo[<i>a,e</i>]pyrene	80.6	19.7	104.4	10.6
Dibenzo[<i>a,i</i>]pyrene	79.1	13.6	100.1	12.5
Dibenzo[<i>a,h</i>]pyrene	82.5	15.2	95.8	16.1

^a Five replicates.

for naphthalene, observed in other papers [28,29], are due to the evaporation during the extraction process because its volatility. It can be noted that no significant differences were observed when extraction time was changed from 45 to 60 min except for compound 16, which corresponds with the simultaneous determination of indeno[1,2,3-*cd*]pyrene and dibenzo[*a,h*]anthracene. In order to increase sample throughput, 45 min was selected as optimum extraction time for further experiments. Then, the optimum solvent volume was evaluated, testing 15, 30, 45 and 60 mL of pure *n*-hexane. The obtained results for the selected PAHs are shown in Fig. 1c. The best results were obtained when 60 mL of solvent were used, observing a considerable increase of recovery in relation to lower solvent volumes.

To evaluate if a second extraction could improve the recovery, extraction procedure of the residue was repeated and the extract was also injected into the GC–MS/MS system. Recovery values obtained for the second extraction were always lower than 10% (see Table 2), whereas for the first extraction, recoveries were always higher than 50%, except for naphthalene, acenaphthylene, 2-bromonaphthylene and acenaphthene. In fact, reasonable results can be obtained when only one extraction is carried out for most of the selected compounds, although for some of them, such as cyclopenta[*c,d*]pyrene, and chrysene, better results were obtained when two extractions are used. Thus, although more extractions can improve recovery, it can be observed a decrease in extraction efficiency when the number of extraction increases [18] so some studies on ultrasonic extractions only used a single extraction [30].

Bearing in mind that further extractions did not improve considerably the results, and one extraction can provide suitable recoveries, reducing analysis time and use of solvents, only one extraction was used for further experiments.

3.2. Optimization of the pressurized liquid extraction process

Extraction of PAHs using PLE depends on the type of solvent, number of extraction cycles, extraction time and temperature, which were studied spiking 6 g of blank soil with $20 \mu\text{g kg}^{-1}$.

Bearing in mind that solvent was studied previously, a comparison between *n*-hexane and a mixture of acetone/*n*-hexane (50:50, v/v), which was commonly used in PLE for the extraction of these

type of compounds [31], were tested, extracting the spiked soil using the PLE process with one and two extraction cycles and using 5 min of extraction time and 100°C as extraction temperature. The obtained results are shown in Fig. 2a. It can be observed that the best

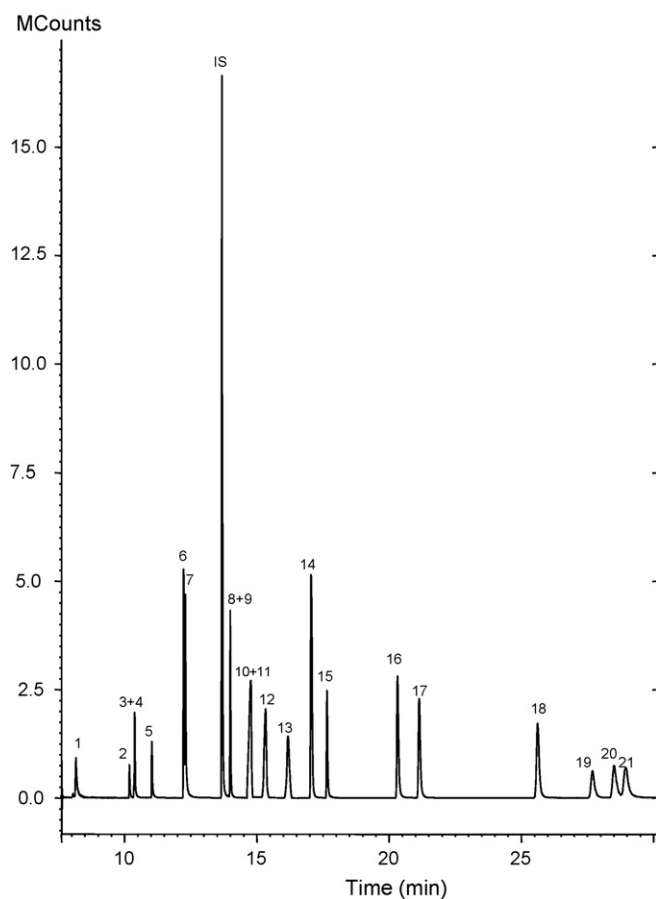


Fig. 3. Total ion chromatogram (TIC) of a soil sample spiked with the selected PAHs at $20 \mu\text{g kg}^{-1}$. PAHs codes are shown in Table 1.

Table 4
Validation parameters of the PLE method.

Compound	LOD ($\mu\text{g kg}^{-1}$)	LOQ ($\mu\text{g kg}^{-1}$)	Recovery ^a (%)		Interday precision (%RSD)	
			2 $\mu\text{g kg}^{-1}$	20 $\mu\text{g kg}^{-1}$	2 $\mu\text{g kg}^{-1}$	20 $\mu\text{g kg}^{-1}$
Naphthalene	0.30	1.00	35.2 (24.7)	39.3 (17.8)	26.7	22.8
Acenaphthylene	0.14	0.45	68.9 (19.3)	62.2 (15.0)	22.0	17.2
2-Bromonaphthylene	0.09	0.31	63.8 (14.4)	60.5 (7.4)	20.2	10.9
Acenaphthene	0.06	0.21	59.1 (18.4)	64.7 (12.3)	22.2	20.4
Fluorene	0.03	0.09	82.9 (12.5)	79.3 (5.9)	15.6	6.9
Phenanthrene	0.04	0.12	104.3 (8.0)	93.7 (3.6)	7.1	7.1
Anthracene	0.08	0.27	90.6 (8.5)	81.3 (7.7)	8.5	18.5
Fluoranthene	0.04	0.14	103.2 (2.1)	94.2 (3.1)	2.1	7.4
Pyrene	0.02	0.07	108.8 (5.5)	97.0 (0.6)	2.1	7.9
Benzo[a]anthracene	0.06	0.21	106.2 (2.9)	95.8 (3.5)	3.3	12.1
Cyclopenta[cd]pyrene	0.07	0.22	103.4 (5.6)	79.0 (15.3)	7.6	16.7
Chrysene	0.04	0.14	102.6 (1.5)	93.5 (1.7)	5.6	9.9
5-Methylchrysene	0.04	0.12	106.1 (1.7)	97.0 (1.2)	4.8	10.5
Benzo[b] + [j] + [k] fluoranthene	0.04	0.13	109.8 (5.8)	97.1 (2.6)	8.5	8.7
Benzo[a]pyrene	0.04	0.14	108.8 (15.3)	83.7 (7.1)	17.6	8.0
Benzo[g,h,i]perylene	0.08	0.27	106.6 (5.5)	93.3 (4.0)	16.3	18.5
Dibenzo[a,h]anthracene/indeno[1,2,3-cd]pyrene	0.07	0.23	102.6 (4.8)	93.3 (4.3)	5.7	4.9
Dibenzo[a,l]pyrene	0.38	1.25	95.6 (8.7)	85.0 (13.9)	8.9	14.8
Dibenzo[a,e]pyrene	0.50	1.67	106.7 (10.6)	94.3 (3.5)	12.4	6.5
Dibenzo[a,i]pyrene	0.75	2.50	104.5 (12.3)	79.4 (7.5)	14.3	13.2
Dibenzo[a,h]pyrene	0.60	2.00	102.2 (12.8)	80.8 (6.1)	16.4	8.7

^a Repeatability values, expressed as % RSD, are given in brackets.

results were obtained in general when pure *n*-hexane was used, although for some PAHs such as naphthalene, acetone/*n*-hexane provided better results. In relation to number of cycles, one cycle and two cycles provide very similar results, so one extraction cycle was used for further experiments in order to reduce analysis time and solvent. In order to determine the optimum extraction temperature, 6 g of spiked soil were extracted at temperatures of 100, 125, 150 and 175 °C showing in Fig. 2b the obtained results. 100, 125 and 150 °C provide good and similar recoveries noting that when temperature increased to 175 °C, recoveries decreased, so 150 °C was chosen as optimum extraction temperature.

Finally the extraction cycle time was evaluated, testing 2, 5 and 10 min of static time. The obtained results are shown in Fig. 2c. It can be observed that the best results were obtained when 5 min were used, except for the most volatile PAHs, which present better recoveries with 2 min. For the rest of compounds, no significant differences were observed when extraction time changed from 5 to 10 min, except for fluoranthene and dibenzo[a,h]pyrene, so the selected extraction time for further experiments was 5 min, in order to reduce extraction time and increase sample throughput.

3.3. Comparison of ultrasonic and pressurized liquid extraction

Both extraction methodologies were compared, showing in Table 3 recoveries and relative standard deviations (RSDs) obtained when five blank samples were spiked at 20 $\mu\text{g kg}^{-1}$ and the optimized procedures were carried out. PLE presents higher values of recoveries than ultrasonic extraction as well as the repeatability was better, obtaining lower RSD values, except for dibenzo[a,l]pyrene and dibenzo[a,h]pyrene. Furthermore, ultrasonic extraction is more tedious than PLE procedure since it involves centrifugation of the soil material after ultrasonication, whereas the extraction by PLE is fully automated and only an evaporation step is required after extraction. In addition, PLE is a technique that consumes less organic solvent and it is faster, offering better results, so it was selected as extraction technique for the determination of PAHs in soils. Due to the high selectivity of the GC-QqQ-MS/MS no further clean up steps were necessary prior to chromatographic determination. Finally, Fig. 3 shows a representative chromatogram obtained when the optimized extraction method was applied to a spiked blank soil sample with 20 $\mu\text{g kg}^{-1}$.

Table 5
PAHs found in real soil samples.

Compound	Concentration range ($\mu\text{g kg}^{-1}$)	Number of samples	Average value ($\mu\text{g kg}^{-1}$) ^a
Acenaphthylene	0.46	1	
2-Bromonaphthylene	0.37–0.54	6	0.44 (0.07)
Acenaphthene	0.21–0.35	10	0.27 (0.05)
Fluorene	0.15–0.65	12	0.30 (0.14)
Phenanthrene	0.33–31.61	12	3.31 (8.92)
Fluoranthene	0.19–15.88	10	2.24 (4.84)
Pyrene	0.11–15.75	11	1.94 (4.62)
Benzo[a]anthracene	0.21–4.67	4	1.30 (1.93)
Chrysene	0.23–8.22	8	1.81 (2.64)
5-Methylchrysene	0.13–0.28	3	0.19 (0.08)
Benzo[b] + [j] + [k] fluoranthenes	0.03–2.04	8	0.66 (0.67)
Benzo[a]pyrene	0.20–4.27	9	0.92 (1.32)
Benzo[g,h,i]perylene	0.82–1.48	2	1.15 (0.47)

^a Standard deviation is given in brackets.

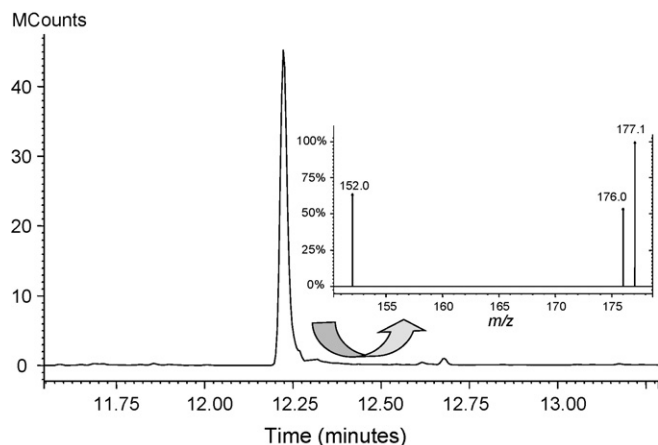


Fig. 4. GC-MS/MS chromatogram in SRM mode of a positive sample of phenanthrene ($31.61 \mu\text{g kg}^{-1}$) with the corresponding spectrum.

3.4. Validation of the pressurized liquid extraction process

A validation procedure was carried out to evaluate linearity, repeatability, interday precision, accuracy (expressed as recovery), LODs and LOQs.

First, matrix effect was studied to ensure bias-free analytical results, analyzing standard solutions of the selected PAHs in solvent (from 5 to $150 \mu\text{g L}^{-1}$) and extracts of blank soils spiked with the same concentrations. The calibration curves obtained using spiked extracted soils were not significantly different from that obtained by use of standard solutions (data not shown). In consequence, external calibration was used for quantification purposes, using fluoranthene- d_{10} as internal standard.

Accuracy was estimated in terms of recovery, by evaluating two different fortification levels (2 and $20 \mu\text{g kg}^{-1}$). Five blank samples were spiked with PAHs at each fortification level, showing the obtained results in Table 4. Good results were found, with recoveries between 59% and 110%, except for naphthalene, for which recovery was lower than 30%. For other volatiles PAHs such as acenaphthylene, 2-bromonaphthylene and acenaphthene, recoveries ranged from 60% and 70%.

Precision was studied by performing repeatability and reproducibility experiments. Repeatability was evaluated at the two concentration levels of the accuracy studies, extracting five replicates for each level (Table 4). Reproducibility (interday precision) was studied by extracting blank samples spiked at two concentration levels (2 and $20 \mu\text{g kg}^{-1}$) which were analyzed at three different days (Table 4). It can be observed that intraday and interday precision values, expressed as RSD, were lower than 25%, except for naphthalene.

Finally, LODs and LOQs were estimated analyzing blank spiked samples, and they were determined as the lowest concentration giving a response of three and ten times the average of the baseline noise, respectively. Results are shown in Table 4, with LODs ranging from 0.02 to $0.75 \mu\text{g kg}^{-1}$ and LOQs ranging from 0.07 to $2.50 \mu\text{g kg}^{-1}$, observing that the higher LODs and LOQs were obtained for the high molecular PAHs (dibenzo pyrenes). The low LOQs obtained allow the determination of PAHs at ultra trace levels in soils.

3.5. Application of the method to real samples

The optimized PLE procedure has been applied to the determination of PAHs in agricultural soil samples from Southeast of Spain. The results are shown in Table 5. It can be observed that the

most detected PAHs were acenaphthene, fluorene, phenanthrene, fluoranthene, pyrene, chrysene and benzo[a]pyrene, which can be found in soils basically by atmospheric deposition and by the action of agricultural practices, as it was indicated by other authors [13]. It can be noted that the high values of phenanthrene, fluoranthene and pyrene correspond to the same sample with a total concentration of PAHs of $85 \mu\text{g kg}^{-1}$, which was collected in an industrial area, whereas for the rest of the samples, the total PAHs concentration ranged from 1 to $7 \mu\text{g kg}^{-1}$, indicating very low concentrations of these contaminants in the studied soils.

Finally, Fig. 4 shows a positive sample of phenanthrene in soil. It can be observed that no interfering peaks appear on the chromatogram, indicating the high selectivity of the PLE process coupled to GC-QqQ-MS/MS.

4. Conclusions

A PLE process has been developed and validated for the determination of PAHs in soil. The analyses were carried out by GC-QqQ-MS/MS and due to the high selectivity of the triple quadrupole, no further clean up steps were necessary. PLE was compared with sonication extraction and better recovery and precision were obtained when PLE was used. Furthermore, PLE minimizes the volume of organic solvent used for the extraction as well as the extraction time. Although losses of the more volatile analytes appeared during the extraction process, accuracy, precision and selectivity of the proposed method are satisfactory for analysis of PAHs, and the proposed method can be used as a screening method for monitoring PAHs in soils.

Acknowledgements

The authors gratefully acknowledge Andalusian Regional Government (Regional Ministry of Innovation, Science, and Enterprise) for financial support (Project Ref. P07-AGR-02922). RRG is also grateful for personal funding through the Juan de la Cierva Program (Spain Ministry of Science and Innovation-EFS).

References

- [1] E. Martínez, M. Gros, S. Lacorte, D. Barceló, J. Chromatogr. A 1047 (2004) 181.
- [2] J. Cachot, M. Law, D. Pottier, L. Peluhet, M. Norris, H. Budzinski, R. Winn, Environ. Sci. Technol. 41 (2007) 7830.
- [3] S. Kahn, L. Aijun, S. Zhang, Q. Hu, Y.G. Zhu, J. Hazard. Mater. 152 (2008) 506.
- [4] M. Nording, K. Frech, Y. Persson, M. Forsman, P. Haglund, Anal. Chim. Acta 555 (2006) 107.
- [5] T. Wenzl, R. Simon, J. Kleiner, E. Anklam, Trends Anal. Chem. 25 (2006) 716.
- [6] C. Sluszný, V.V. Gridin, V. Bulatov, I. Schecter, Rev. Anal. Chem. 21 (2002) 77.
- [7] J.C. Chuang, J.M. Van Emon, Y.L. Chou, N. Junod, J.K. Finegold, N.K. Wilson, Anal. Chim. Acta 486 (2003) 31.
- [8] G.S. Peterson, R.P. Axler, K.B. Lodge, J.A. Schuldt, J.L. Crane, Environ. Monit. Assess. 78 (2002) 111.
- [9] M.T. Pena, M.C. Casais, M.C. Mejuto, R. Cela, J. Chromatogr. A 1165 (2007) 32.
- [10] C. Miège, J. Dugay, M.C. Hennion, J. Chromatogr. A 995 (2003) 87.
- [11] S.B. Hawthorne, C.B. Grabanski, E. Martin, D.J. Miller, J. Chromatogr. A 892 (2000) 421.
- [12] M.I.H. Helaleh, A. Al-Omar, A. Nisar, B. Gevao, J. Chromatogr. A 1083 (2005) 153.
- [13] C. Sánchez-Brunete, E. Miguel, J.L. Tadeo, J. Sep. Sci. 29 (2006) 2166.
- [14] B. Veyrand, A. Brosseau, L. Sarcher, V. Varlet, F. Monteau, P. Marchand, F. Andre, B. Le Bizec, J. Chromatogr. A 1149 (2007) 333.
- [15] O.H.J. Szolar, H. Rost, R. Braun, A.P. Loibner, Anal. Chem. 74 (2002) 2379.
- [16] H. Hamdi, L. Manusadzian, I. Aoyama, N. Jedidi, Chemosphere 65 (2006) 1153.
- [17] V. Librando, O. Hutzinger, G. Tringali, M. Aresta, Chemosphere 54 (2004) 1189.
- [18] D.R. Banjoo, P.K. Nelson, J. Chromatogr. A 1066 (2005) 9.
- [19] K. Li, M. Landriault, M. Fingas, M. Llopart, J. Hazard. Mater. 102 (2003) 93.
- [20] A.E. Mc Gowin, K.K. Adom, A.K. Obubuafo, Chemosphere 45 (2001) 857.
- [21] C. Sánchez-Brunete, E. Miguel, J.L. Tadeo, J. Chromatogr. A 1148 (2007) 219.
- [22] L. Ramos, J.J. Vreuls, U.A.Th. Brinkman, J. Chromatogr. A 891 (2000) 275.
- [23] M.A. Olivella, Anal. Bioanal. Chem. 383 (2005) 107.

- [24] J. Lintelmann, K. Fischer, E. Karg, A. Schröppel, *Anal. Bioanal. Chem.* 381 (2005) 508.
- [25] W. Wang, B. Meng, X. Lu, Y. Liu, S. Tao, *Anal. Chim. Acta* 602 (2007) 211.
- [26] N. Itoh, M. Numata, Y. Aoyagi, T. Yarita, *Anal. Chim. Acta* 612 (2008) 44.
- [27] A. Garrido Frenich, R. Martínez Ocaña, J.L. Martínez Vidal, *J. AOAC*, submitted for publication.
- [28] J.D. Berset, M. Ejem, R. Holzer, P. Lischer, *Anal. Chim. Acta* 383 (1999) 263.
- [29] S. Buco, M. Moragues, P. Doumenq, A. Noor, G. Mille, *J. Chromatogr. A* 1026 (2004) 223.
- [30] F. Sun, D. Litteljohn, M.D. Gibson, *Anal. Chim. Acta* 364 (1999) 1.
- [31] S. Lundstedt, P. Haglund, L. Oberg, *Anal. Chem.* 78 (2006) 2993.



Simultaneous determination of multibenzodiazepines by HPLC/UV: Investigation of liquid–liquid and solid-phase extractions in human plasma

Keyller Bastos Borges^{a,*}, Ellen Figueiredo Freire^b, Isarita Martins^c,
Maria Elisa Pereira Bastos de Siqueira^c

^a Department of Physics and Chemistry, Faculty of Pharmaceutical Sciences of Ribeirão Preto, University of São Paulo, 14040-903 Ribeirão Preto, Brazil

^b Department of Pharmaceutical Sciences, Faculty of Pharmaceutical Sciences of Ribeirão Preto, University of São Paulo, Ribeirão Preto, Brazil

^c Laboratory of Toxicological Analysis, Federal University of Alfenas, Alfenas, Brazil

ARTICLE INFO

Article history:

Received 28 July 2008

Received in revised form 3 November 2008

Accepted 4 November 2008

Available online 12 November 2008

Keywords:

Benzodiazepines
Flunitrazepam
Clonazepam
Oxazepam
Lorazepam
Chlordiazepoxide
Nordiazepam
Diazepam
N-Desalkylflurazepam
Human plasma
HPLC
LLE
SPE

ABSTRACT

A method for simultaneous determination of seven benzodiazepines (BZPs) (flunitrazepam, clonazepam, oxazepam, lorazepam, chlordiazepoxide, nordiazepam and diazepam using *N*-desalkylflurazepam as internal standard) in human plasma using liquid–liquid and solid-phase extractions followed by high-performance liquid chromatography (HPLC) is described. The analytes were separated employing a LC-18 DB column (250 mm × 4.6 mm, 5 μm) at 35 °C under isocratic conditions using 5 mM KH₂PO₄ buffer solution pH 6.0:methanol:diethyl ether (55:40:5, v/v/v) as mobile phase at a flow rate of 0.8 mL min⁻¹. UV detection was carried out at 245 nm. Employing LLE, the best conditions were achieved with double extraction of 0.5 mL plasma using ethyl acetate and Na₂HPO₄ pH 9.5 for pH adjusting. Employing SPE, the best conditions were achieved with 0.5 mL plasma plus 3 mL 0.1 M borate buffer pH 9.5, which were then passed through a C18 cartridge previously conditioned, washed for 3 times with these solvents: 3 mL 0.1 M borate buffer pH 9.5, 4 mL Milli-Q water and 1 mL acetonitrile 5%, finally the BZPs elution was carried with diethyl ether:n-hexane:methanol (50:30:20). In both methods the solvent was evaporated at 40 °C under nitrogen flow. The validation parameters obtained in LLE were linearity range of 50–1200 ng mL⁻¹ plasma ($r \geq 0.9927$), limits of quantification of 50 ng mL⁻¹ plasma, within-day and between-day CV% and E% for precision and accuracy lower than 15%, and recovery above 65% for all BZPs. In SPE, the parameter obtained were linearity range of 30–1200 ng mL⁻¹ plasma ($r \geq 0.9900$), limits of quantification of 30 ng mL⁻¹ plasma, within-day and between-day CV% and E% for precision and accuracy lower than 15% and recovery above 55% for all BZPs. These extracting procedures followed by HPLC analysis showed their suitable applicability in order to examine one or more BZPs in human plasma. Moreover, it could be suggested that these procedures might be employed in various analytical applications, in special for toxicological/forensic analysis.

© 2008 Elsevier B.V. All rights reserved.

1. Introduction

Benzodiazepines (BZPs) are an important class of drugs commonly used as minor tranquilizers, hypnotics, muscle relaxant and anticonvulsive. The usefulness of BZPs varies considerably because there are large differences in selectivity among these drugs. They are among the most frequently prescribed drugs for the treatment of anxiety, sleep disturbance and status epilepticus. In addition, BZPs are used in treatment of alcohol withdrawal, to relieve tension in the preoperative period and to induce amnesia in surgical procedures. The abuse of these drugs is very common among its users and illegal drug users. Moreover, the continued abuse of these drugs

leads to dependence. Therefore, these compounds may be involved in cases of sudden death and be linked to different crimes [1].

Laboratories, thus, frequently receive request for the determination of BZPs in plasma, serum, urine, or gastric lavage fluid. The analysis of BZPs in biological fluids is complicated by the diversity of these drugs commercially available and the fact that each product has a particular therapeutic and toxic range. The classical BZPs are chemically characterized by the presence of a benzene ring fused on the -10 and -11 positions of the 1,4-diazepine ring. All the important BZPs contain a 5-phenyl ring (in many cases, this ring suffers an additional substitution of halogen, F, Cl or Br, at R_H-position), a halogen or nitro group in the 7-position (Fig. 1).

Several methods have been described in the literature for the clinical, toxicological and biopharmaceutical study of the BZPs. Besides spectrophotometric, spectrofluorimetric [2–4], potentiometric [5,6] and immunoassay [7] methods, the majority of the

* Corresponding author. Tel.: +55 16 36024270; fax: +55 16 36024880.

E-mail addresses: keyller@fcrfp.usp.br, keyller@pop.com.br (K.B. Borges).

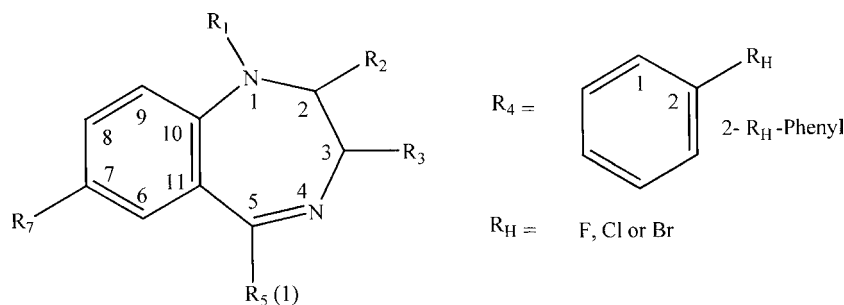


Fig. 1. Representative chemical structure for the classical BZPs.

papers describe methods employing HPLC (using UV or MS detector) [8–27], GC [28–38], and CE [14,31].

The sample preparation techniques commonly used involve liquid–liquid extraction (LLE) [39–41], solid-phase extraction (SPE) [28,33,37], solid-phase microextraction (SPME) [17,23,34], liquid phase microextraction (LPME) [34], column switching techniques [42,43] and direct LC analysis using restricted access materials (RAM) [44,45].

Since HPLC/UV assays are inexpensive and widely utilized, it has been a good choice in the analysis of BZPs for simultaneous separation and quantification. Moreover, SPE and LLE are still the most employed techniques for sample preparation more used in routine analysis. The presence of different methods in the literature using these techniques is a great advantage for analysts from different areas. In this context, there are numerous detection methods, but no one is ideal due to the large number of chemically similar compounds, the wide variation in therapeutic and toxic range, and the intensive metabolism suffered by BZPs. In addition, exhaustive extraction techniques, such as LLE and SPE, are necessary because many analyses require a significant pre-concentration step. The purpose of this investigation was to develop a simple analytical HPLC method alongside a liquid–liquid extraction and an off-line solid-phase extraction procedures for the simultaneous analysis

of seven benzodiazepines (flunitrazepam, clonazepam, oxazepam, lorazepam, chlordiazepoxide, nordiazepam and diazepam using *N*-desalkylflurazepam as internal standard) (Fig. 2) in plasma samples.

2. Experimental

2.1. Standard solutions and chemicals

BZPs, flunitrazepam, clonazepam, oxazepam, lorazepam, *N*-desalkylflurazepam (internal standard, I.S.), chlordiazepoxide, nordiazepam and diazepam were all obtained from Sigma–Aldrich® (St Louis, USA).

Stock standard solutions of flunitrazepam, clonazepam, oxazepam, lorazepam, chlordiazepoxide, nordiazepam and diazepam were prepared by dissolution of each drug in methanol to obtain a concentration of 1 mg mL^{-1} . These standard solutions were used in dilution series to result in the following concentrations: 30, 50, 75, 100, 300, 600, 900 and 1200 ng mL^{-1} of plasma. In the same way, a stock standard solution *N*-desalkylflurazepam at concentration of $3 \mu\text{g mL}^{-1}$ of plasma was also prepared to be used as internal standard. All these solutions were stored at -20°C in the absence of light.

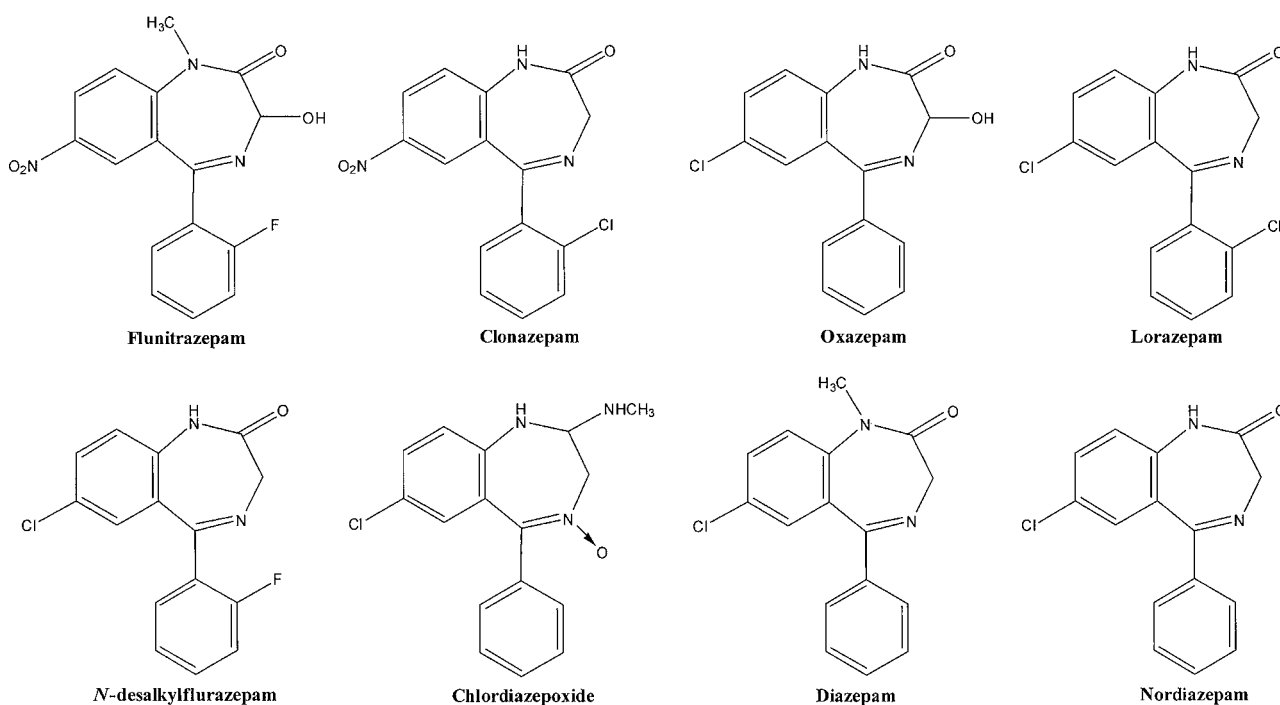


Fig. 2. Molecular structure of studied BZPs: flunitrazepam, clonazepam, oxazepam, lorazepam, *N*-desalkylflurazepam (internal standard, I.S.), chlordiazepoxide, nordiazepam and diazepam.

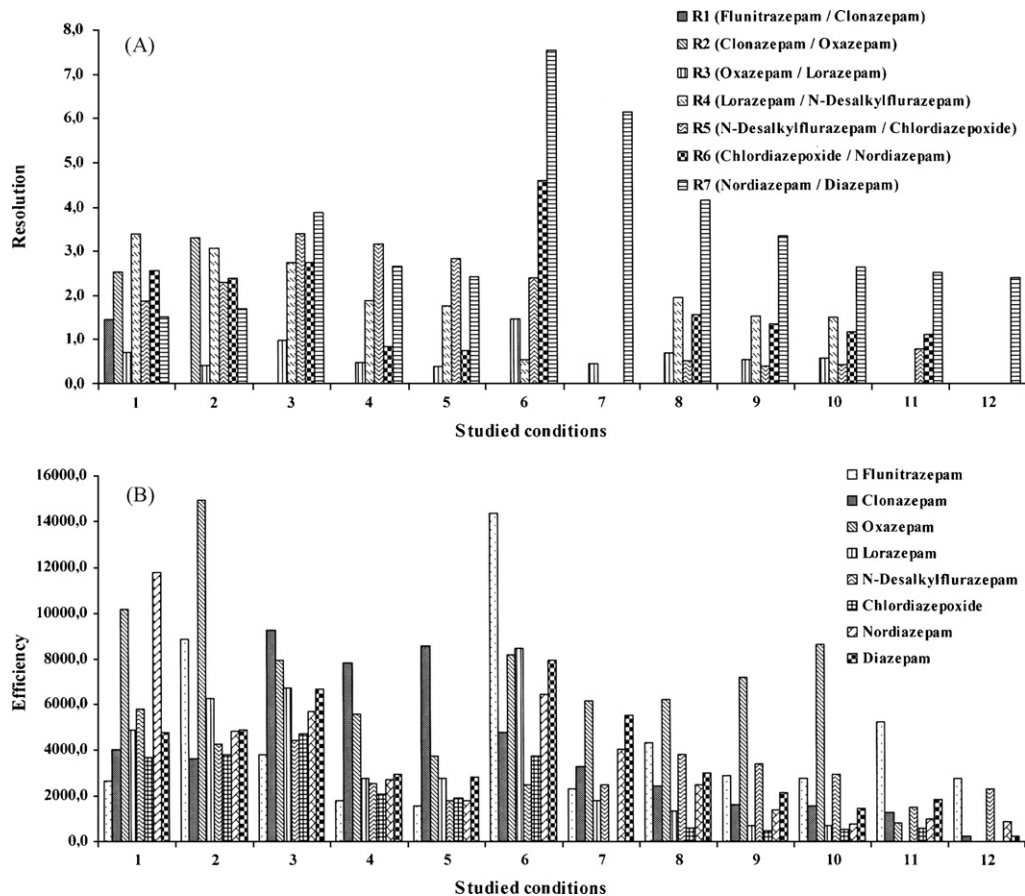


Fig. 3. (A) BZPs resolution obtained from some modifications in the analysis conditions; (B) BZPs efficiency (theoretical plates) obtained from some modifications in the analysis conditions. Chromatographic conditions studied: (1) 5 mM KH_2PO_4 buffer pH 6:methanol:diethyl ether (55:40:5), column 250 mm \times 4.6 mm \times 5 μm , flow rate 0.8 mL min^{-1} ; (2) 5 mM KH_2PO_4 buffer pH 6:methanol:diethyl ether (55:40:5), column 250 mm \times 4.6 mm \times 5 μm , flow rate 0.6 mL min^{-1} ; (3) 5 mM KH_2PO_4 buffer pH 6:methanol (45:55), column 250 mm \times 4.6 mm \times 5 μm , flow rate 0.8 mL min^{-1} ; (4) 5 mM KH_2PO_4 buffer pH 6:methanol (45:55), column 150 mm \times 4.6 mm \times 5 μm , flow rate 0.8 mL min^{-1} ; (5) 5 mM KH_2PO_4 buffer pH 6:methanol (45:55), column 150 mm \times 4.6 mm \times 5 μm , flow rate 1.2 mL min^{-1} ; (6) 5 mM KH_2PO_4 buffer pH 6:methanol:acetonitrile (55:25:20), column 250 mm \times 4.6 mm \times 5 μm , flow rate 0.6 mL min^{-1} ; (7) 5 mM KH_2PO_4 buffer pH 6:methanol:acetonitrile (55:25:20), column 250 mm \times 4.6 mm \times 5 μm , flow rate 1.0 mL min^{-1} ; (8) 5 mM KH_2PO_4 buffer pH 6:methanol:acetonitrile (55:25:20), column 150 mm \times 4.6 mm \times 5 μm , flow rate 0.4 mL min^{-1} ; (9) 5 mM KH_2PO_4 buffer pH 6:methanol:acetonitrile (55:25:20), column 150 mm \times 4.6 mm \times 5 μm , flow rate 0.8 mL min^{-1} ; (10) 5 mM KH_2PO_4 buffer pH 6:methanol:acetonitrile (55:25:20), column 150 mm \times 4.6 mm \times 5 μm , flow rate 1.5 mL min^{-1} ; (11) 5 mM KH_2PO_4 buffer pH 6:methanol:acetonitrile (55:35:15), column 150 mm \times 4.6 mm \times 5 μm , flow rate 1.5 mL min^{-1} ; (12) 5 mM KH_2PO_4 buffer pH 3.5:acetonitrile (69:31), column 150 mm \times 4.6 mm \times 5 μm ; flow rate 1.5 mL min^{-1} . The others conditions were the same used in the optimized method.

HPLC-grade methanol and diethyl ether were purchased from Vetec[®] (Duque de Caxias, Brazil). Hexane (HPLC-grade) was obtained from Merck[®] (Darmstadt, Germany). HPLC-grade acetonitrile was purchased from Mallinckrodt Baker Inc. (Paris, France). All other chemicals were of analytical-grade in the highest purity available. Water was distilled and purified using a Millipore[®] Milli-Q Plus system (Bedford, USA).

2.2. Plasma samples

Blood samples were collected from healthy subjects, not taking any kind of drug, in Vacutainer[®] heparinized tubes (Becton Dickinson, Meylan, France) and were used for optimization and validation

of the method. Real blood samples were collected from one volunteer after 4.5 h of a single oral administration of 10.0 mg of diazepam and from a patient 20 h after ingestion of 0.5 mg of flunitrazepam. The volunteers gave written informed consent to participate in the investigation.

The plasma samples were centrifuged at 1800 \times g for 5 min and the plasma was frozen and stored at -20°C , no longer than 72 h.

2.3. Instrumentation and analytical conditions

The analyses were carried out using a chromatographic system from Shimadzu[®] Corporation (Kyoto, Japan). This equipment consisted of a LC-10 AT_{VP} pump, a SPD-10 A_{VP} UV-vis detector

Table 1

Chromatographic parameters for the benzodiazepines on LC-18 DB column (250 mm \times 4.6 mm, 5 μm) using as mobile phase 5 mM KH_2PO_4 buffer solution pH 6.0:methanol:diethyl ether (55:40:5, v/v/v) at 35 $^\circ\text{C}$, under isocratic conditions, flow rate of 0.8 mL min^{-1} and detection at 245 nm.

BZPs	Flunitrazepam	Clonazepam	Oxazepam	Lorazepam	N-Desalkylflurazepam	Chlordiazepoxide	Nordiazepam	Diazepam
R_s		1.47	2.54	0.72	3.39	1.88	2.55	1.53
k	10.10	11.31	13.01	13.50	16.34	18.40	21.77	23.91
α		1.12	1.15	1.04	1.21	1.13	1.18	1.10
N	2630.47	4002.62	10128.56	4947.36	5780.81	3686.45	11748.43	4732.85

R_s , resolution; k , retention factor for the first eluted BZP ($t_M = 1.94$ min, defined as the first significant baseline disturbance, corresponding to the retention time of a non-retained solute); α , separation factor; N , theoretical plates. N-Desalkylflurazepam was used as internal standard.

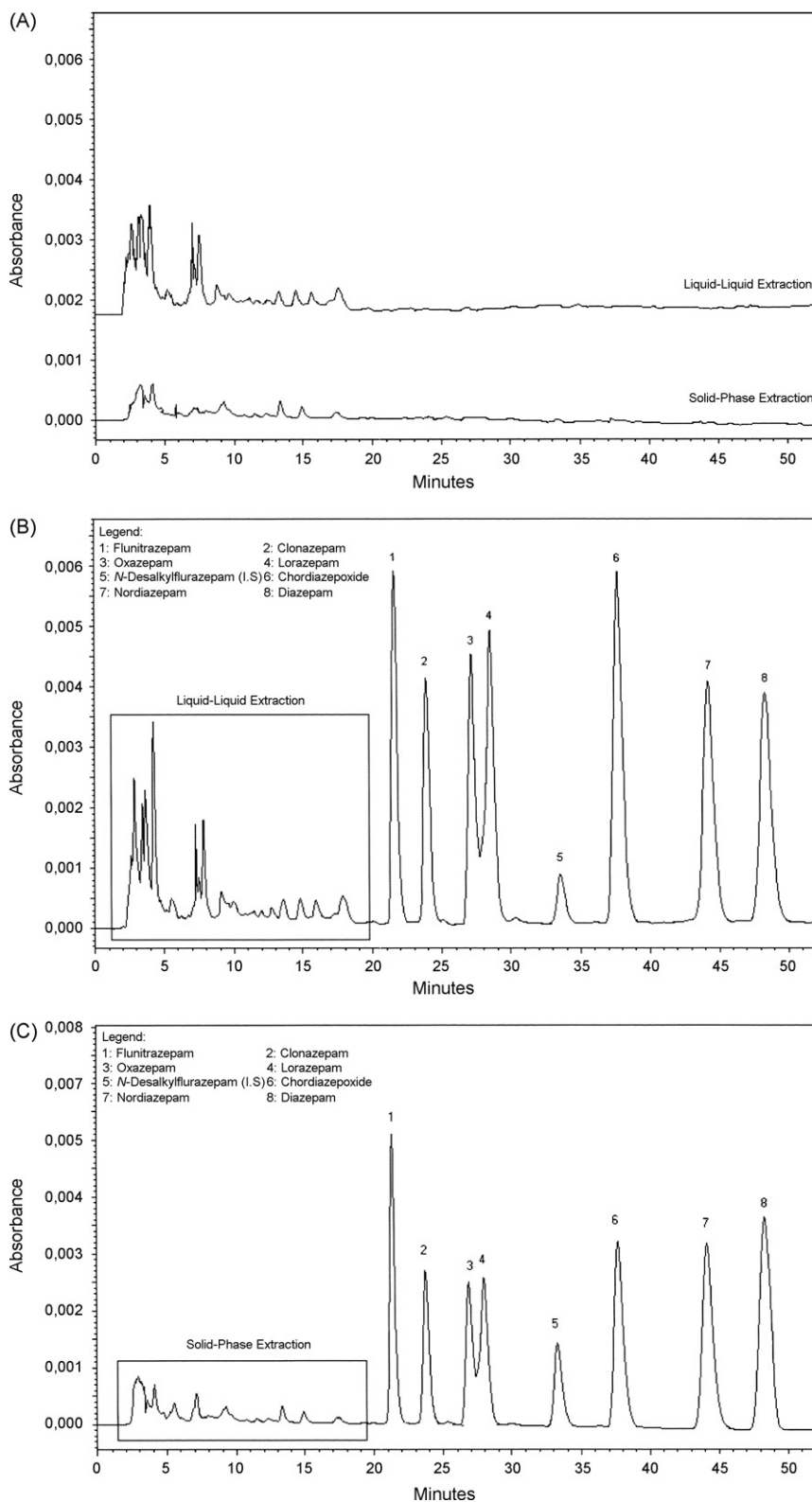


Fig. 4. (A) Representative chromatogram of blank human plasma employing LLE and SPE; (B) chromatogram referring to the separation of BZPs employing LLE, peak 1: flunitrazepam 600 ng mL⁻¹; peak 2: clonazepam 600 ng mL⁻¹; peak 3: oxazepam 600 ng mL⁻¹; peak 4: lorazepam 600 ng mL⁻¹; peak 5: *N*-desalkylflurazepam (internal standard, I. S.) 75 ng mL⁻¹; peak 6: chlordiazepoxide 600 ng mL⁻¹; peak 7: nordiazepam 600 ng mL⁻¹; peak 8: diazepam 600 ng mL⁻¹; (C) chromatogram referring to the separation of BZPs employing SPE, peak 1: flunitrazepam 300 ng mL⁻¹; peak 2: clonazepam 300 ng mL⁻¹; peak 3: oxazepam 300 ng mL⁻¹; peak 4: lorazepam 300 ng mL⁻¹; peak 5: *N*-desalkylflurazepam (internal standard, I. S.) 75 ng mL⁻¹; peak 6: chlordiazepoxide 300 ng mL⁻¹; peak 7: nordiazepam 300 ng mL⁻¹; peak 8: diazepam 300 ng mL⁻¹. Chromatographic conditions: Supelcosil LC-18 DB column (250 mm × 4.6 mm, I.D., 5 μm particle size) protected with a 4 cm × 4 mm, I.D., 5 μm particle size Supelguard LC-18-DB pre-column at 35 °C under isocratic conditions using 5 mM buffer KH₂PO₄ solution pH 6.0: methanol: diethyl ether (55:40:5) as mobile phase at a flow rate of 0.8 mL min⁻¹. UV detection was carried out at 245 nm.

Table 2
Linearity of the methods employing liquid–liquid and solid-phase extraction.

BZPs	Procedure extraction							
	Liquid–liquid extraction				Solid-phase extraction			
	Linear equation ^a	Correlation coefficient (<i>r</i>)	Range (ng mL ⁻¹)	CV (%) ^b	Linear equation ^b	Correlation coefficient (<i>r</i>)	Range (ng mL ⁻¹)	CV (%) ^b
Flunitrazepam	$y = 0.0042x - 0.1857$	0.9927	50–1200	8.9	$y = 0.0038x - 0.1572$	0.9905	30–1200	9.9
Clonazepam	$y = 0.0032x - 0.1407$	0.9968	75–1200	9.7	$y = 0.0018x - 0.1280$	0.9900	50–1200	14.1
Oxazepam	$y = 0.0036x - 0.1809$	0.9964	75–1200	12.3	$y = 0.0017x - 0.1197$	0.9960	50–1200	7.1
Lorazepam	$y = 0.0046x - 0.2320$	0.9967	75–1200	10.8	$y = 0.0018x - 0.1122$	0.9973	50–1200	13.4
Chlordiazepoxide	$y = 0.0062x - 0.3096$	0.9975	50–1200	11.5	$y = 0.0031x - 0.0647$	0.9942	30–1200	10.6
Nordiazepam	$y = 0.0057x - 0.4259$	0.9948	50–1200	10.2	$y = 0.0034x - 0.1721$	0.9974	30–1200	14.8
Diazepam	$y = 0.0056x - 0.3232$	0.9952	50–1200	12.3	$y = 0.0046x - 0.1234$	0.9930	30–1200	13.5

^a Calibration curves for liquid–liquid and solid-extraction were performed in triplicate ($n = 3$) for each concentration.

^b CV (%), coefficient of variation on the slope of the calibration curve.

(operating at 245 nm), a SCL-10 A_{VP} system controller, a SIL-10 AF automatic injector, and a CTO-10 AS_{VP} column oven. Class VP[®] software was used to control the LC system and data acquisition.

The simultaneous resolution of BZPs was performed on a Supelcosil[®] LC-18 DB column (250 mm × 4.6 mm, I.D., 5 μm particle size; Supelco Inc., Bellefonte, USA) protected with a 4 cm × 4 mm, I.D., 5 μm particle size Supelguard LC-18-DB pre-column at 35 °C under isocratic conditions using 5 mmol L⁻¹ KH₂PO₄ buffer solution pH 6.0: methanol: diethyl ether (55:40:5, v/v/v) as mobile phase at a flow rate of 0.8 mL min⁻¹. A Supelcosil[®] LC-18 DB column (150 mm × 4.6 mm, I.D., 5 μm particle size; Supelco[®], Bellefonte, USA) was also used. UV detection was carried out at 245 nm. The mobile phase was filtered through a Millipore membrane filter (0.45 μm) Millipore[®] (São Paulo, Brazil) and degassed ultrasonically prior to use, then by a stream of helium during use.

The SPE study was performed on a Vac-Elut vacuum manifold column processor obtained from Supelco[®] (Bellefonte, USA). LC-18 cartridges 500 mg/3 mL were supplied from Supelco[®] (Bellefonte, USA).

2.4. Extraction procedure

2.4.1. Liquid–liquid extraction

Aliquots of 0.5 mL of human plasma spiked with 25 μL of standard solutions of BZPs and 10 μL of standard solution of I.S. (3 μg mL⁻¹) were buffered with 2 mL of 0.1 mol L⁻¹ disodium monohydrogen phosphate buffer (Na₂HPO₄) pH 9.5 and extracted with 3 mL ethyl acetate. The tubes were capped and submitted to vortex mixing for 3 min and then centrifuged at 1800 × *g* for 8 min. The upper organic phases were transferred to conical tubes and separated. The aqueous phase was re-extracted with 3 mL ethyl acetate. The organic phases were evaporated at 40 °C under flow of nitrogen to obtain good results. The residues were dissolved in 400 μL of the mobile phase and 50 μL were chromatographed.

2.4.2. Solid-phase extraction

A C18 cartridge (500 mg, 3 mL) was activated with 2 mL of methanol and washed with 1 mL of Milli-Q water. After that, buffered aqueous sample (0.5 mL of human plasma spiked with 25 μL of standard solutions of BZPs and 10 μL of standard solution of I.S., 3 μg mL⁻¹, and 3 mL 0.1 mol L⁻¹ borate buffer pH 9.5) was added, and the sorbent was washed with 3 mL of 0.1 mol L⁻¹ borate buffer pH 9.5, 4 mL of Milli-Q water and 1 mL of acetonitrile 5% (dissolved in water, v/v). The cartridge was dried for 1 min. The elution was performed with 3 mL of diethyl ether: hexane: methanol (50:30:20, v/v/v) at constant flow rate of 2 mL min⁻¹. The collected solvent was evaporated at 40 °C under flow of nitrogen and the residue was dissolved in 400 μL of the mobile phase and 50 μL were chromatographed.

2.5. Method validation

Calibration curves were obtained by spiking aliquots of 0.5 mL human plasma with standard solutions of BZPs, prepared in methanol, resulting in concentrations ranging from 30 to 1200 ng mL⁻¹ for each drug depending on the technique used; *N*-desalkylflurazepam (I.S., 3 μg mL⁻¹ of human plasma) was added to all samples. Calibration standards of each concentration were analyzed in triplicate and curves of BZPs were constructed using peak area ratio of drug to the internal standard versus nominal concentrations of the analytes.

To determine the extraction recovery, human plasma samples (0.5 mL) were spiked with each BZP in the concentrations of 100, 600 and 1200 ng mL⁻¹ ($n = 3$) and submitted to the extracting procedures. Another set of samples were prepared extracting 0.5 mL aliquots of human plasma and then spiking the extract with the same amount of BZPs. The recovery was calculated by comparing the areas obtained before and after extraction and it was expressed as percentage of the amount extracted.

The detection limit (LOD) was determined by adding flunitrazepam, clonazepam, oxazepam, lorazepam, chlordiazepoxide, nordiazepam and diazepam in a pool of blank plasma ($n = 5$). LOD was considered the lowest concentration of these analytes corresponding to three times the background noise or relationship signal to noise ratio 3:1.

In addition, the quantification limit (LOQ) of the method was also evaluated. The LOQ was defined as the lowest concentration that could be determined with accuracy and precision below 20% [46] over five analytical run and it was obtained using human plasma samples (0.5 mL, $n = 5$) spiked with concentration from 30 to 75 ng mL⁻¹ of each BZP.

The precision and accuracy of the method were evaluated by within-day ($n = 5$) and between-day ($n = 3$) assays using human plasma samples spiked with BZPs at the concentrations of 100, 600 and 1200 ng mL⁻¹ of each BZP. The results obtained for precision and accuracy were expressed as coefficient of variation (CV, %) and relative error (*E*, %), respectively.

3. Results and discussion

The methods of BZPs analysis in plasma must present high detectability to allow detection of low quantities of analytes (ng mL⁻¹). The HPLC with UV detection employing LLE and SPE are still the most employed techniques used in routine analysis of BZPs. These drugs are amphoteric and relatively polar, moreover the biological sample preparation step using LLE is usually laborious and time consuming. SPE would, therefore, be a simple and reliable alternative, despite been expensive, since the cartridges are not reutilized.

Table 3
Detection and quantification limits of the methods employing liquid–liquid and solid–phase extraction^a.

BZPs	Procedure extraction		Liquid–liquid extraction				Solid–phase extraction			
	Liquid–liquid extraction		Liquid–liquid extraction		Solid–phase extraction		Solid–phase extraction		CV ^c (%)	F ^d (%)
	LOD ^a (ng mL ⁻¹)	LOQ ^b (ng mL ⁻¹)	Analyzed concentration (ng mL ⁻¹)	Analyzed concentration (ng mL ⁻¹)	LOD ^a (ng mL ⁻¹)	LOQ ^b (ng mL ⁻¹)	Analyzed concentration (ng mL ⁻¹)	Analyzed concentration (ng mL ⁻¹)		
Flunitrazepam	30	50	49.4	–1.2	20	30	28.7	6.6	–4.5	
Clonazepam	50	75	73.1	–2.5	20	50	53.7	8.5	7.3	
Oxazepam	50	75	78.0	4.3	20	50	50.1	5.3	0.2	
Lorazepam	50	75	79.3	6.4	20	50	51.1	1.8	2.1	
Chlordiazepoxide	30	50	48.6	4.2	20	30	26.6	13.1	–11.4	
Nordiazepam	30	50	53.5	4.8	20	30	30.7	10.4	2.3	
Diazepam	30	50	51.1	10.7	20	30	25.7	1.6	14.3	

^a LOD, detection limit was defined as a signal-to-noise ratio of 3:1, $n = 5$.

^b LOQ, quantification limit as defined as the lowest BZPz concentration that could be determined with accuracy and precision below 20%, $n = 5$.

^c CV (%), coefficient of variation of the quantification limit expressed in percentage.

^d E (%), relative error of the quantification limit expressed in percentage.

3.1. Chromatographic conditions

Several chromatographic conditions, such as mobile phase, type of column and its length, mobile phase flow rate, mobile phase pH, temperature, and volume injection were studied to obtain a satisfactory chromatographic separation (good resolution and efficiency) for all compounds. In addition, the total time required for the analysis was also an important factor because the analysis could be unfeasible since interfering compounds could eluate close to the BZPs if modifications were performed in order to reduce the analysis time. The resolution and efficiency of some modifications in the analysis conditions are presented in Fig. 3A and B, respectively. In general, the condition 1 showed the best results because it promoted the resolution for the seven BZPs studied.

Various solvents or mixture of solvents at different compositions were used to extract the BZPs from human plasma using LLE. A procedure of re-extraction of analytes was also studied because some BZPs need a double extraction due to their low lipid solubility. SPE procedure was optimized in terms of BZPs recovery prior to its application in the human plasma studies. Various procedures to activate and to wash the sorbent and to extract the analytes from the samples were studied. In addition, different solvents or mixture of solvents at different compositions for elution of the adsorbed analytes were tested.

3.2. Method validation

The optimized chromatographic conditions are described on Table 1, as well as the obtained chromatographic parameters. Under these chromatographic conditions, BZPs are well separated: flunitrazepam elutes at 21.5 min, clonazepam at 23.9 min, oxazepam at 27.2 min, lorazepam at 28.1 min, *N*-desalkylflurazepam at 33.6 min, chlordiazepoxide at 37.6 min, nordiazepam at 44.2 min, and diazepam at 48.3 min. Fig. 4A shows the chromatogram referring to the blank of human plasma using LLE and SPE. Fig. 4B and C shows the chromatograms referring to the separation of BZPs using LLE and SPE, respectively.

3.2.1. Linearity

Response ratio of peak areas between the corresponding compound and the internal standard versus theoretical concentration was fitted by a least-square linear regression. The calibration curves were linear over the concentration range of 50–1200 ng mL⁻¹ for flunitrazepam, chlordiazepoxide, nordiazepam and diazepam and 75–1200 ng mL⁻¹ for clonazepam, oxazepam and lorazepam employing LLE. For SPE, the calibration curves were linear over the concentration range of 30–1200 ng mL⁻¹ for flunitrazepam, chlordiazepoxide, nordiazepam and diazepam and 50–1200 ng mL⁻¹ for clonazepam, oxazepam and lorazepam. The correlation coefficients for BZPs employing LLE and SPE were ($r \geq 0.9927$ and ($r \geq 0.9900$, respectively (Table 2).

3.2.2. Detection and quantification limits

The lowest concentrations detected and quantified by the validated methods are presented in Table 3. The coefficients of variation and relative errors employing LLE and SPE were lower than 15%.

3.2.3. Recoveries for LLE and SPE

Recoveries of BZPs ranged from 61% to 91.1% employing LLE. For SPE, the recoveries ranged from 52.2% to 96.8%. The coefficients of variation for both techniques were lower than 15%. Results are summarized in Table 4.

3.2.4. Precision and accuracy for LLE and SPE

Precision of a quantitative method is the degree of agreement among individual test results when the procedure is applied

Table 4
Recoveries obtained from liquid–liquid and solid-phase extraction of BZPs.

BZPs	Procedure extraction															
	Liquid–liquid extraction ($n^a = 3$)								Solid-phase extraction ($n^a = 3$)							
	100 ng mL ⁻¹		600 ng mL ⁻¹		1200 ng mL ⁻¹		Mean		100 ng mL ⁻¹		600 ng mL ⁻¹		1200 ng mL ⁻¹		Mean	
	R ^b (%)	CV ^c (%)	R ^b (%)	CV ^c (%)	R ^b (%)	CV ^c (%)	R ^b (%)	CV ^c (%)	R ^b (%)	CV ^c (%)	R ^b (%)	CV ^c (%)	R ^b (%)	CV ^c (%)	R ^b (%)	CV ^c (%)
Flunitrazepam	72.7	1.6	65.7	3.2	81.3	2.6	73.3	8.7	85.1	5.8	96.7	4.3	89.6	0.1	90.5	5.3
Clonazepam	78.5	1.4	80.7	0.4	87.4	1.0	82.2	4.6	72.1	0.1	61.3	5.8	69.0	2.7	67.5	6.8
Oxazepam	78.2	4.1	62.7	1.0	73.5	0.6	71.5	9.1	82.9	0.6	89.2	8.6	86.6	3.6	86.2	3.0
Lorazepam	88.8	1.1	79.1	1.4	86.3	1.6	84.7	4.9	90.2	7.2	96.8	13.9	90.8	3.0	92.6	3.2
Chlordiazepoxide	76.4	7.6	66.9	6.1	91.1	0.8	78.1	12.7	64.6	1.6	53.3	3.0	52.2	2.0	56.7	9.9
Nordiazepam	64.7	1.1	76.2	2.7	86.3	1.0	75.9	11.9	87.3	7.2	98.2	0.8	94.2	2.5	93.2	4.8
Diazepam	61.0	5.6	66.0	1.3	79.2	1.3	68.8	11.2	79.3	2.8	93.1	4.6	96.4	1.3	89.6	8.2

^a n , number of replicates.

^b R , recoveries expressed as percentage (%).

^c CV, coefficient of variation expressed as percentage (%).

Table 5
Precision and accuracy of the method for analysis of BZPs in human plasma by liquid–liquid extraction.

	BZPs																				
	Flunitrazepam			Clonazepam			Oxazepam			Lorazepam			Chlordiazepoxide			Nordiazepam			Diazepam		
Within-day ($n = 5$) ^a																					
Nominal concentration (ng mL ⁻¹)	100	600	1200	100	600	1200	100	600	1200	100	600	1200	100	600	1200	100	600	1200	100	600	1200
Analyzed concentration (ng mL ⁻¹)	91	536	1325	91	596	1206	89.4	605.4	1186	94.5	609.6	1188	87.9	677.3	1158	102.2	664.4	1363	90.1	637.5	1237
Precision ^b (CV, %)	8.8	6.9	3.1	7.8	1.6	1.8	3.6	2.5	0.6	8.5	3.1	1.4	10.3	4.5	9.1	8.5	3.7	1.2	9.9	2.9	2.1
Accuracy ^c (E, %)	-8.3	-10.6	10.4	-8.6	-0.6	0.5	-10.6	0.9	-1.2	-5.5	1.6	-1.0	-12.1	12.9	-3.5	2.2	10.7	13.6	-9.9	6.3	3.1
Between-day ($n = 3$) ^d																					
Nominal concentration (ng mL ⁻¹)	100	600	1200	100	600	1200	100	600	1200	100	600	1200	100	600	1200	100	600	1200	100	600	1200
Analyzed concentration (ng mL ⁻¹)	114	656	1215	103	628	1193	102	630	1212	99	614	1153	97	572	1294	104	632	1248	103	640	1218
Precision ^b (CV, %)	11.9	13.1	12.7	5.1	6.7	5.1	6.3	7.1	6.1	1.9	3.3	3.7	12.8	6.6	11.0	5.5	7.5	5.7	8.6	9.5	2.1
Accuracy ^c (E, %)	13.6	9.3	1.3	3.5	4.7	-0.6	2.5	5.0	1.0	-1.3	2.3	-3.9	-2.6	-4.7	7.8	4.4	5.3	4.0	3.3	6.7	1.5

^a Number of replicates, $n = 5$.

^b Expressed as coefficient of variation in percentage, CV (%).

^c Expressed as relative error in percentage, E (%).

^d Number of days, $n = 3$.

Table 6
Precision and accuracy of the method for analysis of BZPs in human plasma by solid-phase extraction.

BZPs	Flunitrazepam		Clonazepam		Oxazepam		Lorazepam		Chlordiazepoxide		Nordiazepam		Diazepam	
	100	600	100	600	100	600	100	600	100	600	100	600	100	600
Within-day (n = 5) ^a														
Nominal concentration (ng mL ⁻¹)	100	600	100	600	100	600	100	600	100	600	100	600	100	600
Analyzed concentration (ng mL ⁻¹)	100	532	88	543	102	672	94	684	99	551	102	542	102	678
Precision ^b (CV, %)	9.0	5.0	8.3	9.2	3.1	7.5	2.9	0.6	5.3	6.1	4.0	2.8	8.1	0.7
Accuracy ^c (E, %)	-0.2	-11.3	11.4	-12.0	-9.6	12.0	1.4	-5.8	1.8	-0.9	-8.2	12.1	2.4	-9.8
Between-day (n = 3) ^d														
Nominal concentration (ng mL ⁻¹)	100	600	100	600	100	600	100	600	100	600	100	600	100	600
Analyzed concentration (ng mL ⁻¹)	111	633	107	634	96	598	94	623	111	563	111	628	94	590
Precision ^b (CV, %)	11.3	7.8	8.3	5.9	2.0	5.6	6.5	8.0	9.6	10.2	8.7	5.4	11.0	6.7
Accuracy ^c (E, %)	11.4	5.5	5.9	6.6	1.4	-0.4	4.6	-5.6	-8.8	11.0	-6.1	3.8	10.6	4.7

^a Number of replicates, n = 5.

^b Expressed as coefficient of variation in percentage, CV (%).

^c Expressed as relative error in percentage, E (%).

^d Number of days, n = 3.

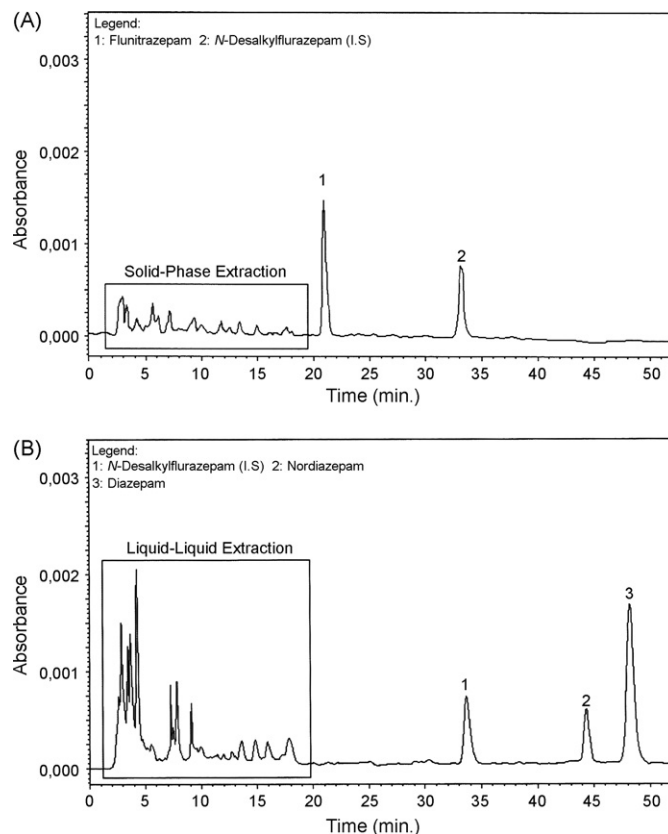


Fig. 5. Chromatograms of (A) human plasma of a patient in continuous use of 0.5 mg of flunitrazepam collected at 20 h after drug administration using SPE; (B) human plasma of healthy volunteer collected at 4.5 h after single oral administration of 10.0 mg of diazepam using LLE.

repeatedly to multiple samplings. It is measured by injecting repeatedly a ready-made sample pool and expressed as coefficient of variation of the results. In addition, the accuracy of the method is defined as the degree of agreement of test results generated by the method to the true value. Within-day ($n = 5$) and between-day ($n = 3$) precision and accuracy for LLE and SPE presented coefficients of variation and relative errors lower than 15%. These results are presented in Tables 5 and 6.

3.3. Other considerations

Several papers have been described in the literature for studies of stability of various BZPs in human plasma [47–53]. In this work, a study of stability was not achieved since the samples were not stored for long time.

The selectivity of the method employing LLE or SPE as extraction procedures was demonstrated by the analysis of some blank plasma matrices showing the absence of peaks with retention times close to the seven BZPs studied (Fig. 4A).

The diazepam, nordiazepam and flunitrazepam plasma concentrations in volunteers were successfully determined by LLE and SPE extraction (Fig. 5). Analysis of diazepam and its active metabolite nordiazepam in plasma of patients treated with diazepam has been studied by our group [54]. The results of the analysis of samples collected from volunteers after oral administration of diazepam and flunitrazepam are present in Table 7.

SPE procedure demonstrated superiority over LLE due to its higher selectivity in eluting compounds and its lower LOQ that permitted the quantification of diazepam and its active metabolite, nordiazepam, as well as flunitrazepam in the samples from the volunteers. In addition, this technique allows the treatment of smaller

Table 7

Diazepam, nordiazepam and flunitrazepam plasma concentrations of volunteers included in the study.

Drug	Oral dose (mg)	Plasma concentrations (ng mL ⁻¹) extraction procedure	
		ELL	SPE
Diazepam	10.0	303.0	280.1
Nordiazepam	–	<50 ^a	35.2
Flunitrazepam	0.5	<50 ^a	38.8

^a Below the limit of quantification.

volumes without the problem of possible emulsion formation, it offers the possibility of automation, and provides reproducibility and recoveries at least as good as LLE.

4. Conclusions

A suitable high-performance liquid chromatography method was developed and validated using LLE and SPE as extraction procedures for the determination of flunitrazepam, clonazepam, oxazepam, lorazepam, *N*-desalkylflurazepam (internal standard, I.S.), chlordiazepoxide, nordiazepam and diazepam simultaneously in human plasma. This HPLC method provides a good alternative to existing methods for analyzing BZPs employing LLE and SPE. The major advantage of this method over similar methods is that it is performed in isocratic mode and it is free from endogenous interferents. In addition, it is necessary relatively inexpensive equipment and sample preparation techniques, which are usually employed in routine analyses of drugs in biological specimens. The development of appropriate procedures for sample preparation and concentration might extend the applicability of this method to other matrices. In SPE, the selection of the best extraction conditions, such as sample pH, composition of the washing and eluting solvents, provided the cleanest samples for further chromatographic analysis.

Acknowledgements

The authors are grateful to Fundação de Amparo à Pesquisa do Estado de São Paulo (FAPESP), sub-program BIOTA/FAPESP (Rede BIOprospecTA), Financiadora de Estudos e Projetos - CT-INFRA (FINEP), Conselho Nacional de Desenvolvimento Científico e Tecnológico (CNPq), and to Coordenação de Aperfeiçoamento de Pessoal de Nível Superior (CAPES) for financial support and for granting research fellowships.

References

- [1] O.H. Drummer, *J. Chromatogr. B* 733 (1999) 27.
- [2] R.S. Guerrero, C.G. Benito, J.M. Calatayud, *J. Pharm. Biomed. Anal.* 11 (1993) 1357.
- [3] M.J. Walash, F. Belal, M.E. Metwally, M.M. Hefnawy, *J. Pharm. Biomed. Anal.* 12 (1994) 1417.
- [4] A.A. Salem, B.N. Barsoum, E.L. Izake, *Spectrochim. Acta A Mol. Biomol. Spectr.* 60 (2004) 771.
- [5] A.A. Salem, B.N. Barsoum, G.R. Saad, E.L. Izake, *J. Electroanal. Chem.* 536 (2002) 1.
- [6] A.A. Salem, B.N. Barsoum, E.L. Izake, *Anal. Chim. Acta* 498 (2003) 79.
- [7] M. Bogusz, R. Aderjan, G. Schmitt, E. Nadler, B. Neureither, *Forensic Sci. Int.* 48 (1990) 27.
- [8] A.M.A. Verweij, P.J.L. Lipman, P.G.M. Zweipfenning, *Forensic Sci. Int.* 54 (1992) 67.
- [9] H. Le Solleu, F. Demotes-Mainard, G. Vincon, B. Bannwarth, *J. Pharm. Biomed. Anal.* 11 (1993) 771.
- [10] E. Tanaka, M. Terada, S. Misawa, C. Wakasugi, *J. Chromatogr. B* 682 (1996) 173.
- [11] S.M. Sultan, A.H. El-Mubarak, *Talanta* 43 (1996) 569.
- [12] M. Kleinschnitz, M. Herderich, P. Schreier, *J. Chromatogr. B* 676 (1996) 61.
- [13] K.M. Höld, D.J. Crouch, D.G. Wilkins, D.E. Rollins, R.A. Maes, *Forensic Sci. Int.* 84 (1997) 201.
- [14] S. McClean, E. O'Kane, J. Hillis, W.F. Smyth, *J. Chromatogr. A* 838 (1999) 273.
- [15] A. El Mahjoub, C. Staub, *J. Pharm. Biomed. Anal.* 23 (2000) 447.
- [16] M. Wilhelm, H.-J. Battista, D. Obendorf, *J. Chromatogr. A* 897 (2000) 215.
- [17] W.M. Mullett, K. Levsen, D. Lubda, J. Pawliszyn, *J. Chromatogr. A* 963 (2002) 325.
- [18] C. Pistos, J.T. Stewart, *J. Pharm. Biomed. Anal.* 33 (2003) 1135.
- [19] X.-P. Lee, T. Kumazawa, J. Sato, Y. Shoji, C. Hasegawa, C. Karibe, T. Arinobu, H. Seno, K. Sato, *Anal. Chim. Acta* 492 (2003) 223.
- [20] T. Toyo'oka, Y. Kumaki, M. Kanbori, M. Kato, Y. Nakahara, *J. Pharm. Biomed. Anal.* 30 (2003) 1773.
- [21] A. Bugey, C. Staub, *J. Pharm. Biomed. Anal.* 35 (2004) 555.
- [22] B.E. Smink, J.E. Brandsma, A. Dijkhuizen, K.J. Lusthof, J.J. De Gier, A.C.G. Egberts, D.R.A. Uges, *J. Chromatogr. B* 811 (2004) 13.
- [23] M. Walles, W.M. Mullett, J. Pawliszyn, *J. Chromatogr. A* 1025 (2004) 85.
- [24] M. Chêze, M. Villain, G. Pépin, *Forensic Sci. Int.* 145 (2004) 123.
- [25] O. Quintela, A. Cruz, A. de Castro, M. Concheiro, M. López-Rivadulla, *J. Chromatogr. B* 825 (2005) 63.
- [26] A. Bugey, S. Rudaz, C. Staub, *J. Chromatogr. B* 832 (2006) 249.
- [27] V.F. Samanidou, A.P. Pechlivanidou, I.N. Papadopyannis, *J. Sep. Sci.* 30 (2007) 679.
- [28] P. Lillsunde, T. Seppälä, *J. Chromatogr. B* 533 (1990) 97.
- [29] H. Gjerde, E. Dahlin, A.S. Christophersen, *J. Pharm. Biomed. Anal.* 10 (1992) 317.
- [30] N.C. Van de Merbel, J.M. Teule, H. Lingeman, U.A.T. Brinkman, *J. Pharm. Biomed. Anal.* 10 (1992) 225.
- [31] M. Tomita, T. Okuyama, *J. Chromatogr. B* 678 (1996) 331.
- [32] R. Herráez-Hernández, A.J.H. Louter, N.C. Van de Merbel, U.A.T. Brinkman, *J. Pharm. Biomed. Anal.* 14 (1996) 1077.
- [33] A.J.H. Louter, E. Bosma, J.C.A. Schipperen, J.J. Vreuls, U.A.T. Brinkman, *J. Chromatogr. B* 689 (1997) 35.
- [34] J.K. Reubsæet, R.H. Norli, P. Hemmersbach, K.E. Rasmussen, *J. Pharm. Biomed. Anal.* 18 (1998) 667.
- [35] G.H. Ugland, M. Krogh, K.E. Rasmussen, *J. Chromatogr. B* 749 (2000) 85.
- [36] H. Inoue, Y. Maeno, M. Iwasa, R. Matoba, M. Nagao, *Forensic Sci. Int.* 113 (2000) 367.
- [37] D. Borrey, E. Meyer, W. Lambert, C. Van Peteghem, A.P. De Leenheer, *J. Chromatogr. B* 765 (2001) 187.
- [38] T. Gunnar, K. Ariniemi, P. Lillsunde, *J. Chromatogr. B* 818 (2005) 175.
- [39] H.M. Stevens, *J. Forensic Sci.* 25 (1985) 67.
- [40] M.A. Zilli, G. Nisi, *J. Chromatogr.* 378 (1986) 492.
- [41] G.L. Lensmeyer, C. Rajan, M.A. Evenson, *Clin. Chem.* 28 (1982) 2274.
- [42] I. Deinl, L. Angermaier, C. Franzelius, G. Machbert, *J. Chromatogr. B* 704 (1997) 251.
- [43] A. El Mahjoub, C. Staub, *J. Chromatogr. B* 754 (2001) 271.
- [44] W.M. Mullett, J. Pawliszyn, *J. Pharm. Biomed. Anal.* 26 (2001) 899.
- [45] A. El Mahjoub, C. Staub, *Forensic Sci. Int.* 123 (2001) 17.
- [46] Guidance for Industry, Bioanalytical Method Validation, US Department of Health and Human Services Food and Drug Administration, Center for Drug Evaluation and Research (CDER), Rockville, USA, 2001.
- [47] I.A. Zingales, *J. Chromatogr.* 75 (1973) 55.
- [48] J.M. Clifford, W.F. Smyth, *Analyst* 99 (1974) 241.
- [49] S.R. McCormick, J. Nielsen, P. Jatlow, *Clin. Chem.* 30 (1984) 1652.
- [50] N. Ratnaraj, V. Goldberg, P.T. Lascelles, *Analyst* 109 (1984) 813.
- [51] J.M.F. Douse, *J. Chromatogr.* 301 (1984) 137.
- [52] G. Skopp, L. Pötsch, I. König, R. Mattern, *Int. J. Legal Med.* 111 (1998) 1.
- [53] A. El Mahjoub, C. Staub, *J. Pharm. Biomed. Anal.* 23 (2000) 1057.
- [54] E.F. Freire, J.L. Miranda, P.P. Maia, E.P. Vieira, K.B. Borges, M.E.P.B. Siqueira, *Quim. Nova* 28 (2005) 773.



Surface IR applied to rapid and direct immunosensing of environmental pollutants

Souhir Boujday^{a,b,*}, Chunyan Gu^{a,b}, Marie Girardot^{a,b}, Michèle Salmain^c, Claire-Marie Pradier^{a,b}

^a UPMC Univ Paris 6, UMR CNRS 7609, Laboratoire de Réactivité de Surface, F75005 Paris, France

^b CNRS, UMR 7609, Laboratoire de Réactivité de Surface, F75005 Paris, France

^c Laboratoire de Chimie et Biochimie des Complexes Moléculaires, UMR CNRS 7576, Ecole Nationale Supérieure de Chimie de Paris, F75005 Paris, France

ARTICLE INFO

Article history:

Received 23 July 2008

Received in revised form 24 October 2008

Accepted 31 October 2008

Available online 14 November 2008

Keywords:

Immunosensor
PAHs
Benzo[a]pyrene
Protein G
QCM-D
PM-RAIRS

ABSTRACT

This paper describes the elaboration of a model immunosensor monitored by polarization modulation reflection absorption infrared spectroscopy (PM-RAIRS) and quartz crystal microbalance (QCM-D), as well as its reactivity using PM-RAIRS as transduction technique. To prove its relevance, this immunosensor was applied to the detection of benzo[a]pyrene (BaP), a carcinogenic polycyclic aromatic hydrocarbon. Very few immunoassays, and even fewer immunosensors, have been described for the assay of BaP, making it an interesting target for analytical device development. The PM-RAIRS immunosensor was constructed on planar gold-coated sensors functionalized with cystamine then glutaraldehyde. Antibodies were immobilized through their affinity to protein G, covalently coupled to the aldehyde layer. In a first stage, a model mouse IgG was utilized to optimize the elaboration parameters; then, a monoclonal anti-PAH antibody was used and detection tests were performed, monitored by PM-RAIRS. The successive functionalization steps were monitored by PM-RAIRS and QCM-D. The binding of the proteins to gold surface, their saturation coverages and association constants, as well as their capture efficiencies were discussed. BaP capture by the antibody layer was evidenced by the appearance of a new $\nu(\text{C-H})$ band at 3039 cm^{-1} typical of aromatic C-H bonds. The integrated area of this band varied linearly with the BaP concentration within the range of tested concentrations, with a limit of detection close to $3\text{ }\mu\text{M}$. This represents the first example of direct, label-free immunodetection of a low molecular weight molecule by PM-RAIRS transduction. The simplicity and the rapid response of this IR sensor make it already very worthwhile to preliminary on-site measurements.

© 2008 Elsevier B.V. All rights reserved.

1. Introduction

Immunosensors are a class of biosensors where the molecular receptor is an antibody [1]. They may be used to detect several types of targets such as toxins, bacteria or pollutants provided that the specific antibodies are available [2,3]. The crucial step in their elaboration is the immobilization of the antibodies on the transducer surface, that must guarantee an efficient and specific recognition of a target in a complex environment. Several studies pointed out the direct correlation between controlling the elaboration of immunosensors and their efficiency [1,4,5]. On gold transducers, the technique of self-assembled monolayers (SAMs) allows controlling the amount and orientation of the antibodies [6,7].

We have recently proposed a novel type of optical transduction device based on Modulated Polarization-Infrared Absorption Spectroscopy (PM-RAIRS) [4,8–11]. Biorecognition layers including a specific antibody were first built up onto planar gold-coated glass chips using the technique of self-assembled monolayers. PM-RAIRS technique takes advantage of the peptidic signals of the proteins, i.e. amide I and II absorption bands at 1550 and 1650 cm^{-1} , respectively. Binding of antigens or antibodies to the recognition layers led to an increase of the intensity of these bands, proportional to the amount of surface-bound proteic material. As a result, goat anti-rabbit IgG antibodies [9,11], the pesticide atrazine [10] and more recently the bacterial pathogen *Staphylococcus aureus* [8] could be assayed with good to excellent sensitivity. Other research groups made use of different spectral signatures to transduce interfacial antigen–antibody interactions by mid-IR spectroscopy [12,13].

We now apply this strategy to the detection of polycyclic aromatic hydrocarbons (PAHs). PAHs are a class of chemicals resulting from the incomplete combustion of organic substances

* Corresponding author at: Laboratoire de Réactivité de Surface, UMR CNRS 7609, Université Pierre et Marie Curie-Paris VI, 4 Place Jussieu, 75252 Paris Cedex 05, France. Tel.: +33 144276001; fax: +33 144276033.

E-mail address: souhir.boujday@upmc.fr (S. Boujday).

such as fossil fuels [14]. Some members of the PAHs family, such as the five-ring derivative benzo[a]pyrene (BaP) are identified carcinogens and displays also endocrine-disruptive activity. As a consequence, rules regarding PAHs assessment have been enacted, in particular regarding BaP whose concentration correlates well with the total PAHs contents in environmental samples.

Monitoring of BaP and of some other PAH derivatives in the air is currently performed off-site by HPLC analysis coupled with fluorescence detection of PAHs. Although this method is rather specific, it is not very sensitive (requires collection times of 24 h) and most importantly, the response may come a long time after exposition to BaP. There is therefore clearly a need for sensitive analytical devices that would allow on-site monitoring, at close proximity of emission sources. Immunosensors appear to be particularly attractive since antibodies, the biological recognition elements, can be developed for a large variety of species; because of their specificity they are able to recognize and capture a given analyte such as BaP (or several structurally related analytes such as PAHs) in a complex matrix [15].

A limited number of label-free and label-based immunosensors have been set up to detect and quantify PAHs in water samples. These immunosensors operate with electrochemical, [16,17] optical, [18–23] or piezoelectric [24] transduction modes. Because PAHs are low molecular weight compounds, all these devices operate in the indirect competitive or displacement formats. Interestingly, no immunosensor operating in the direct, label-free format (i.e. employing an immobilized antibody) has ever been set up although this format is very attractive because of its simplicity.

We describe herein the first example of PM-RAIRS immunosensor designed for the assay of the low molecular weight compound BaP operating in a direct, label-free format. PM-RAIRS and QCM analyses were first applied to optimize the elaboration parameters of a model immunosensor. Then, anti-BaP IgG were immobilized and BaP capture was assayed in the 1–10 μM concentration range. PM-RAIRS signal transduction was made possible by the appearance of a $\nu(\text{C-H})$ band characteristic to BaP at ca 3000 cm^{-1} upon its binding to the immobilized anti-PAH antibody.

2. Experimental

2.1. SAMs formation

Gold-coated sensor chips were immersed in 10 mL of a 10 mM solution of cystamine (CA; Aldrich) in water. After 12 h, the substrates were washed with the same volume of water or EtOH and dried under nitrogen flow.

2.2. Covalent immobilization of protein G

Amine-coated sensors were treated by a 0.1 M solution of glutaraldehyde in EtOH prepared from the 25% stock solution in water for 12 h, followed by extensive rinsing in EtOH. The activated sensors were submitted to a 20 mg L^{-1} solution of recombinant protein G (Pierce chemicals). After 2 h, substrates were washed three times with PBS and submitted to a 100 mg L^{-1} solution of BSA (Sigma) in PBS for 30 min to block non-specific binding sites then washed again in PBS.

2.3. Immobilization of mouse IgG₁ by affinity

Protein G-coated sensors were submitted to 5–100 mg L^{-1} solutions of mIgG₁ (Zymed) in 25 mM Bis-Tris buffer pH 6.5. After 2 h, they were washed three times with PBS.

2.4. Tests of anti-mouse IgG detection and of specificity

Protein G-coated sensors previously submitted to a 50 mg L^{-1} solution of mIgG₁ in 25 mM Bis-Tris buffer pH 6.5 and subsequently blocked by treatment with a 100 mg L^{-1} solution of BSA in PBS were exposed to a 40 mg L^{-1} solution of goat serum proteins ($150\ \mu\text{L}$, Sigma) in PBS or to a 20 mg L^{-1} solution of affinity purified goat anti-mouse IgG antibody ($150\ \mu\text{L}$, Sigma) in PBS. After 1 h, they were washed successively with PBS and water.

2.5. PAH immunosensor elaboration

IR sensor chips successively coated with CA, protein G and BSA were exposed to a 20 mg L^{-1} solution of monoclonal anti-PAH antibody ($150\ \mu\text{L}$, [BAP-13], Abcam) in PBS. After 1 h, they were washed with PBS.

2.6. Direct assay of BaP with IR immunosensor

A 1 mM stock solution of Benzo[a]pyrene (Supelco) in EtOH was first prepared. Then, standard solutions of BaP ranging from 1 to $10\ \mu\text{M}$ were prepared in PBS/EtOH 9:1 by successive dilutions from the stock solution. An IR immunosensor was exposed to 10 mL of BaP solution at the lowest concentration ($1\ \mu\text{M}$). After 1 h, the surface was rinsed with PBS/EtOH 9:1, then with ultra-pure water, and the PM-RAIRS spectrum was recorded. This sequence of events was repeated with the other standard BaP solutions of increasing concentration.

2.7. PM-RAIRS

PM-RAIRS spectra were recorded on a commercial NICOLET Nexus spectrometer. The external beam was focused on the sample with a mirror, at an optimal incident angle of 75° . A ZnSe grid polarizer and a ZnSe photoelastic modulator, modulating the incident beam between *p*- and *s*-polarizations (HINDS Instruments, PEM 90, modulation frequency = 37 kHz), were placed prior to the sample. The light reflected at the sample was then focused onto a nitrogen-cooled MCT detector. The presented spectra result from the sum of 124 scans recorded with 8 cm^{-1} resolution. The PM-RAIRS signal is given by the differential reflectivity $\Delta R/R = (R_p - R_s)/(R_p + R_s)$. IR sensors were glass substrates ($11\text{ mm} \times 11\text{ mm}$) successively coated with a 50 nm thick layer of chromium and a 200 nm thick layer of gold. These substrates were purchased from Arrandee (Werther, Germany). Before chemical functionalization, they were annealed in a flame, then rinsed in ultrapure water and dried under nitrogen flow.

2.8. QCM measurements

In situ studies of molecules adsorption to piezoelectric sensor chips were performed using a dissipative QCM (QCM-Z500, KSV Instruments, Finland). Experiments were carried out in static conditions, with AT-cut planar gold-coated quartz crystals (QCM sensors, 14 mm diameter) with a 5 MHz nominal resonance frequency (QuartzPro, Sweden). The measurement temperature was set to $25 \pm 0.1^\circ\text{C}$ using a thermal electric controller (Oven Industries, Inc.). Before use, quartz crystal electrodes were cleaned by ethanol and dried under nitrogen flow. They were then functionalized following the same procedure as for the IR sensors. Data was simultaneously acquired at the fundamental frequency *F* of 5 MHz (*N* = 1) and several overtone frequencies (15, 25, 35, 45, and 55 MHz). Two physical parameters are discussed: the frequency of oscillation and the dissipation. The frequency change can be correlated to the mass of the

adsorbed layer using the Sauerbrey equation [25]:

$$\Delta F = - \frac{N \Delta m}{C_f}$$

where C_f ($=17.7 \text{ ng cm}^{-2} \text{ Hz}$ at $F=5 \text{ MHz}$) is the mass-sensitivity constant, and N ($=1, 3, 5$, etc.) is the overtone number. In this paper, the presented frequency change (ΔF) and dissipation change (ΔD) are those measured at the third overtone ($N=3$; $F=15 \text{ MHz}$).

3. Results and discussion

3.1. Optimization of immunosensor elaboration using the model mouse IgG₁

The construction of a direct immunosensor for the assay of PAHs requires to immobilize anti-PAH antibodies onto the transducer (Fig. 1). The first investigations aiming at optimizing the conditions of antibody binding were carried out with a model of this antibody, a non-directed mouse IgG₁ (mIgG₁). As both anti-PAH IgG₁ and the model mIgG₁ antibodies belong to the same isotype, one can expect a similar behavior. Immobilization of mIgG₁ to gold-coated transducers was achieved by affinity capture to streptococcal protein G. This protein is known to bind a large range of IgG isotypes from a wide variety of mammalian species by association with their Fc fragment. Therefore, this approach allows the antibody molecules to be oriented with respect to the transducer surface with the antigen binding sites pointing away from the surface. Moreover, protein G can capture antibodies from complex media (serum, ascites) which obviates the need to work with purified antibodies [26]. Protein G was covalently attached to a SAM of cystamine using glutaraldehyde as cross-linking agent. Then, the protein G-coated chips were exposed to a solution of mIgG₁ so that it can be immobilized by bioaffinity. To avoid non-specific binding, blocking steps with BSA were carried out after protein G and mIgG₁ binding steps. The ability of the resulting model sensing layer to recognize and bind an associated antibody was then assessed as follows. The specificity of the resulting sensing layer was checked using goat serum proteins, while the antibodies accessibility was estimated by means of goat anti-mIgG antibody. This sequence of protein adsorption to the gold-coated sensors was monitored *ex-situ* by PM-RAIRS and *in situ* by QCM.

3.1.1. Grafting of the capture protein G and the model mouse IgG₁

Fig. 2A (trace a) depicts the PM-RAIRS spectrum, in the 1300–1900 cm^{-1} region, of the gold-coated sensor surface recorded after exposure to protein G solution. Two bands, characteristic of proteins (amide I and II bands), were observed at 1660 and 1550 cm^{-1} . Moreover, the $\nu(\text{C}=\text{O})$ band of the aldehyde functions, observed at 1734 cm^{-1} after addition of glutaraldehyde, disappeared. These results evidenced the covalent grafting of protein G via glutaraldehyde to the SAM of CA.

Covalent attachment of protein G to the CA surface was also monitored *in situ* by QCM with dissipation (data not shown). Binding of this protein resulted in a frequency shift at equilibrium of -14.5 Hz , corresponding to a mass uptake of 86 ng cm^{-2} (3.9 pmol cm^{-2} taking a molecular weight of 22,000 Da), assuming the Sauerbrey equation is applicable. Protein G was reported to have a Stokes radius of 3.53 nm ($\sim 39 \text{ nm}^2 \text{ molecule}^{-1}$) [27]. Thus a close-packed layer of protein G molecules should have a surface density of 93 ng cm^{-2} . Therefore, the amount of protein G chemisorbed to gold-coated sensor deduced from the QCM measurement indicated that the coverage in protein G was close to 90% of a full monolayer; this of course should be taken cautiously due

to the possible decrease of frequency owing to the water coupled to the protein layer [28]. The recorded dissipation upon protein G adsorption was very small ($\sim 1.5 \times 10^{-6} \text{ D}$), suggesting a weak, if any, over-estimation of the mass uptake [4]. One may thus consider that the coverage in protein G is likely slightly below one monolayer.

After protein G adsorption, sensors were exposed to a solution of BSA to block non-specific binding sites. From the PM-RAIRS spectrum displayed in Fig. 2A (trace b), the amide bands area increased from 2.1 to 3.7 ($\Delta A = 1.6$), upon BSA adsorption. This suggested that the sensor surface had not been entirely covered by protein G molecules. The amide bands area can be correlated to the amounts of bound proteins after correction by their respective molecular weights [4,6]. This leads to a molecular ratio, PrG over BSA, close to 5. On the basis of its size, the surface occupied by a molecule of BSA is about 56 nm^2 [29], for a molecular weight of 60 kDa; one sees that for equivalent masses, BSA occupies much lower area than PrG, likely due to the respective shapes of these two proteins. Thus, from the PrG over BSA molecular ratio, the fraction of the surface occupied by protein G molecules was found to be close to 78% of a monolayer; this is in agreement with a small over-estimation of the amount of protein G calculated from the QCM measurement.

3.1.2. Determination of the association constant between protein G and mouse IgG₁

Once the capture protein layer was constructed and characterized, the adsorption of mIgG₁ at different concentrations was monitored by both PM-RAIRS and QCM. The aim of this study was twofold, first: estimating the association constant between mIgG₁ and surface-bound protein G; second: evaluating the mIgG₁ saturation coverage to determine the optimal adsorption concentration in the upcoming steps.

PM-RAIRS spectra corresponding to the protein G-coated sensor after contact with solutions of mouse IgG₁ at increasing concentration are shown in Fig. 2A (traces c–h). The integrated area of the amide I and II bands recorded after each addition was plotted as a function of mIgG₁ concentration (Fig. 2B). The curve shape indicated a Langmuir type adsorption. The data points were fitted with a linear curve-fitting procedure applying the linear transform of the Langmuir isotherm equation (1).

$$\frac{1}{\Delta A} = \frac{1}{K \times \Delta A_{\max}} \times \frac{1}{[\text{mIgG}_1]} + \frac{1}{\Delta A_{\max}} \quad (1)$$

where ΔA is the variation of the area of the amide I and II bands and K the association constant.

A maximum variation of area ΔA_{\max} equal to 10.4 and an association constant K of 0.056 L mg^{-1} ($8.4 \times 10^6 \text{ M}^{-1}$) were measured from the experimental data points. This binding constant was smaller than that measured for the association between mouse IgG and protein G in solution ($K_a = 41 \times 10^9 \text{ M}^{-1}$) [30], and that measured between protein G physisorbed to an acoustic waveguide sensor and mIgG in solution ($K = 1.13 \times 10^8 \text{ M}^{-1}$) [31]. The difference with the first reference data is probably the result of protein G immobilization onto the gold transducer. Likewise, it is also difficult to compare our result with the second example as the buffers used for studying the association were different and the isotype of the mouse IgG used was not mentioned. The maximum mIgG₁ to protein G ratio obtained from the amide bands area, taking into account the respective proteins molecular weight, was equal to 0.5, which means that on an average half of the immobilized protein G molecules were able to bind one mIgG₁.

Association between chemisorbed protein G and mIgG₁ was also monitored *in situ* by QCM with dissipation measurement. Injection of mIgG₁ solutions of increasing concentration resulted in successive shifts of the vibration frequency of the crystal owing to the interfacial molecular association between the two macro-

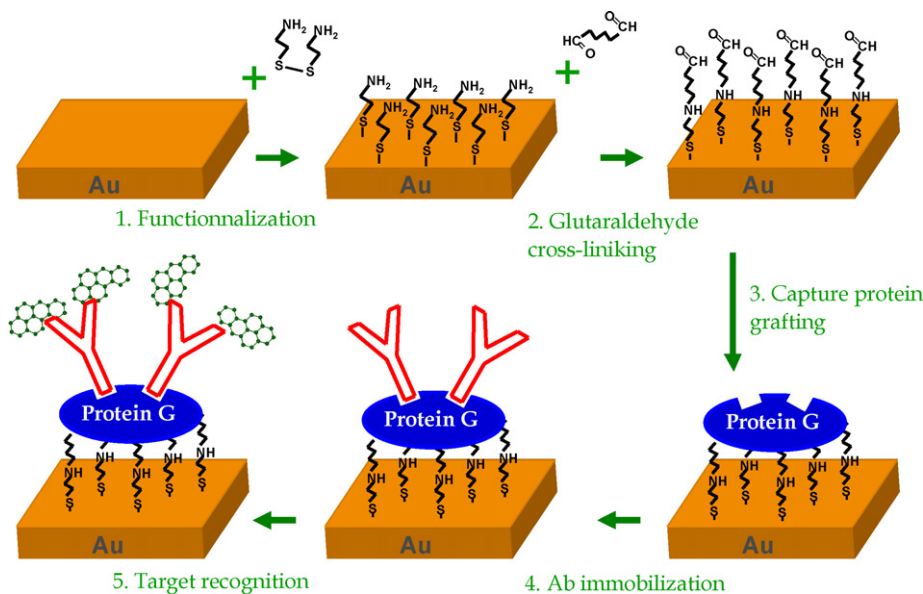


Fig. 1. Schematic drawing of PAH immunosensor elaboration and functioning.

molecules (Fig. 3A). The frequency shifts were plotted as a function of mIgG₁ concentration (Fig. 3B). Here again, the curve shape indicated a Langmuir type adsorption. The data points were also fitted following the linear transform of Langmuir isotherm equation (2).

$$\frac{1}{\Delta m} = \frac{1}{K \times \Delta m_{\max}} \times \frac{1}{[\text{mIgG}_1]} + \frac{1}{\Delta m_{\max}} \quad (2)$$

A maximum mass uptake of 303 ng cm⁻² (2 pmol cm⁻²) and an association constant K of 0.07 mg⁻¹ L were calculated from the data points. If one assumes an end-on orientation of IgG molecules with respect to the surface, the theoretical density of a close-packed monolayer is 370 ng cm⁻² [32]. This would mean that the amount of bound mIgG₁ at saturation was about 80% of a full monolayer, or even less, if one takes the potentially trapped water into account. However, this over-estimation cannot be considerable as the dissipation changes were low. Eventually in line with the PM-RAIRS data, the mIgG₁ to PrG ratio was close to 0.5 at saturation.

3.1.3. Specificity and antibody accessibility on the model sensing layer

A model sensing layer was constructed by exposing protein G-coated chips to a 50 mg L⁻¹ solution of mIgG₁ followed by a blocking step with BSA. The model immunosensor was then submitted to a solution of goat serum proteins. No noticeable change was recorded on the PM-RAIRS spectrum, indicating that no protein was adsorbed. Conversely, when the model immunosensor chip was submitted to a solution of anti-mouse IgG antibodies, the PM-RAIRS spectrum displayed a large increase of the amide bands area ($\Delta A = 7.3$). This corresponds to a molecular anti-mIgG to mIgG₁ ratio close to unity, indicating a very good accessibility of the grafted mIgG₁ molecules.

Thus, the strategy consisting in immobilizing the model antibody mIgG₁ to the transducer surface by affinity to a layer of protein G afforded a specific model recognition layer with a good accessibility of the capture antibodies, even at high surface density.

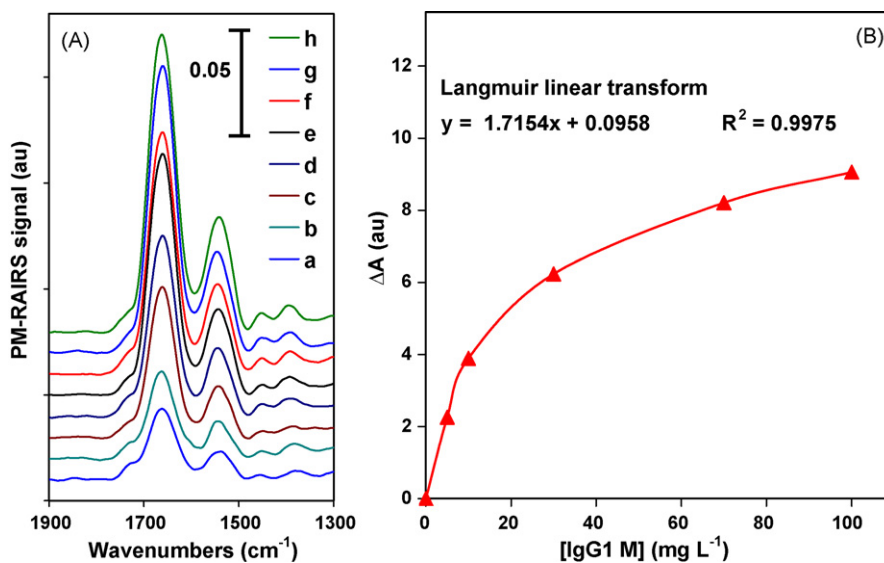


Fig. 2. (A) PM-RAIRS spectra recorded in the course of the model immunosensor elaboration; (a) protein G grafting; (b) BSA blocking; (c, d, e, f, g, and h) mIgG₁ at 5, 10, 30, 70, and 100 mg L⁻¹, respectively. (B) Amide band area increase as a function of mIgG₁ concentration.

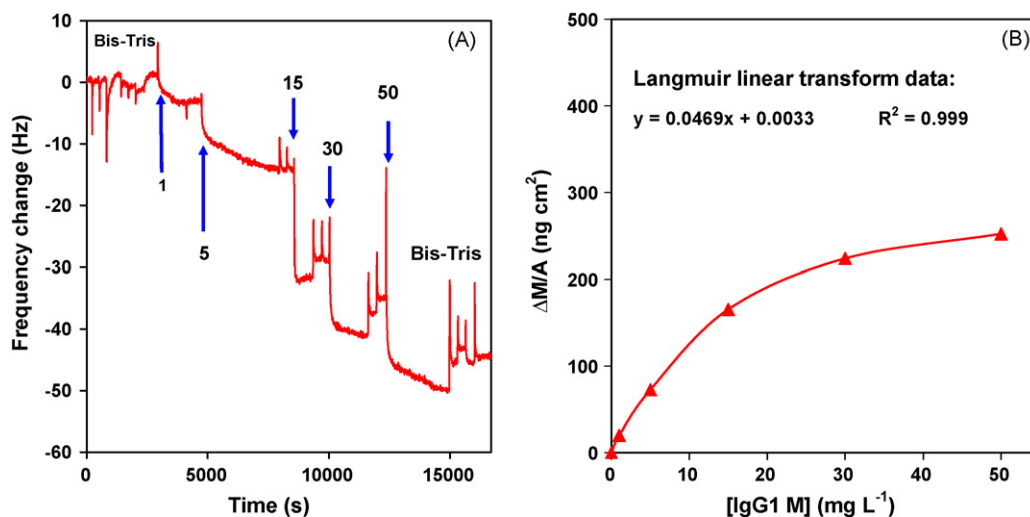


Fig. 3. (A) QCM curve recorded during mlgG₁ capture by protein G-coated piezoelectric sensor chip. mlgG₁ concentrations, in mg L⁻¹ are indicated by arrows. (B) QCM mass uptake as a function of mlgG₁ concentration.

3.2. Elaboration and reactivity of the PAH immunosensor

3.2.1. Elaboration of PAH immunosensor

The previously optimized conditions were applied to design a direct immunosensing platform for the assay of PAH. Protein G and BSA deposition steps were carried out under the same conditions as before. For the IR sensor chips, the anti-PAH IgG immobilization step was carried out with a 20 mg L⁻¹ solution of antibody. Indeed, this concentration led to an antibody coverage close to that obtained from a 50 mg L⁻¹ solution with a considerable saving of the rather expensive anti-PAH monoclonal antibody. Moreover, a slightly lower antibody coverage may enhance their accessibility, which is preferable for an optimized target recognition. For QCM monitoring of antibody capture, the anti-PAH concentration was lowered to 5 mg L⁻¹ because the volume required to make *in situ* measurements was larger (2 mL versus 0.15 mL for the IR measurements). The amount of anti-PAH antibody in contact with the transducer surface was

10 μg, i.e. three times higher than for the PM-RAIRS measurement (3 μg).

A significant increase (+126%, ΔA = 1.3) of the amide I and II bands integrated area was observed on the PM-RAIRS spectrum of the IR sensor upon anti-PAH IgG capture (data not shown). Similarly, exposition of protein G-coated QCM sensor to the solution of anti-PAH resulted in a frequency shift at equilibrium of -23.4 Hz, i.e. a mass uptake of 138 ng cm⁻², which corresponds to ca. 40% of a full monolayer of IgG molecules. Both methods indicated that a fraction of a monolayer of anti-PAH antibody was bound to the surface.

3.2.2. Direct detection of BaP

Due to the very low solubility of BaP in water, standard solutions of BaP were prepared in PBS/EtOH 9:1. This mixture of solvents was found necessary to maintain BaP in solution, a higher percentage of ethanol might affect the molecular recognition properties of the immobilized antibodies. Unfortunately, the use of such solvent

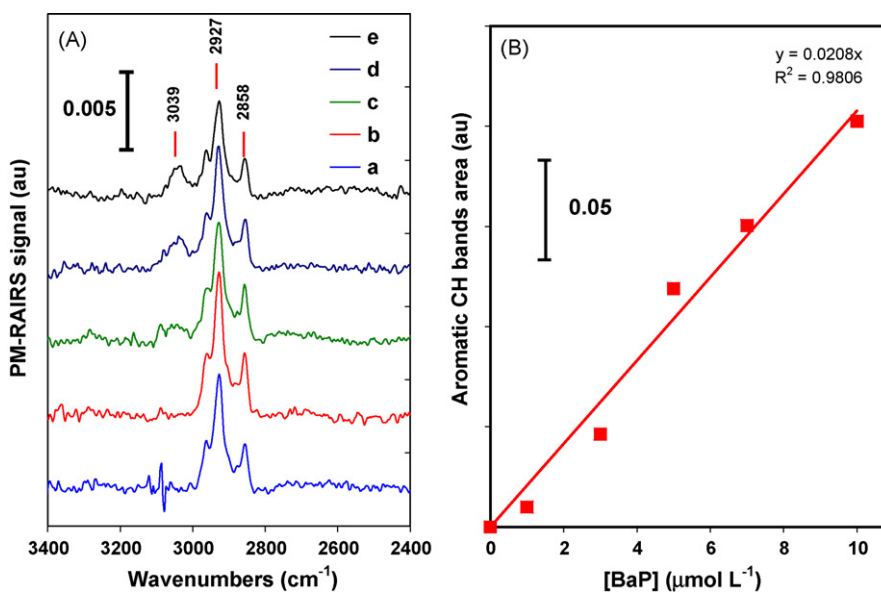


Fig. 4. A: PM-RAIRS spectra recorded after immunodetection of benzo[a]pyrene at 1, 3, 5, 7, and 10 × 10⁻⁶ M for a, b, c, d, and e, respectively. (B) Aromatic C-H band (3039 cm⁻¹) integrated area as a function of benzo[a]pyrene concentration.

strongly affected QCM measurements and induced considerable perturbation on the recorded frequencies. Moreover, because of the low molecular weight of BaP, we expected very low frequency shifts resulting from its binding, although previous examples of direct detection of small analytes by QCM immunosensor were published [33,34]. Thus QCM was not used as transducing technique.

However, very interestingly, the PM-RAIRS spectrum of the anti-PAH coated surface, recorded after the sensors were exposed to 1–10 μM (0.25–2.5 ppm) solutions of BaP, showed a new feature at ca. 3039 cm^{-1} (Fig. 4A). This band was readily assigned to the aromatic $\nu(\text{C-H})$ band of BaP that occurs at 3044 cm^{-1} in solution. The presence of captured BaP on the surface was evidenced from the 5 μM solution of analyte (Fig. 4A, trace c). The integrated area of the aromatic $\nu(\text{C-H})$ band was measured on each spectrum and plotted versus the initial concentration of BaP (Fig. 4B). A linear response was observed in the range of concentrations tested. Thus, the mid-IR immunosensor was able to directly recognize the target providing a linear response at the transducer with a limit of detection close to 5 μM .

4. Conclusions

In order to build up an immunosensor for direct detection of benzo[a]pyrene, preliminary studies were carried out to optimize the immobilization of mouse IgG on gold-coated sensors. A mouse IgG, mimicking anti-PAH antibody, was immobilized on a gold transducer surface using an affinity capture protein, streptococcal protein G. This capture protein was covalently bound to the gold surface by cross-linking to a thiolamine SAM. The binding to these proteins was monitored by both PM-RAIRS and QCM-D and we showed that protein G covered ca. 80% of the available surface whereas mIgG formed an almost complete monolayer at the surface, corresponding to a capture efficiency of 0.5 mIgG's per protein G. The resulting model immunosensor was found specific and the accessibility of antibodies, estimated using an anti-mouse IgG was promising (anti-mIgG/mIgG ratio close to unity). The optimized parameters were then used to immobilize the anti-PAH antibody and build up the PAH immunosensor. This immunosensor was able to directly detect and capture benzo[a]pyrene. Indeed, after exposure to BaP solutions, a new band at 3039 cm^{-1} , assigned to the BaP aromatic C-H stretching vibration, appeared on the surface PM-RAIRS spectra. The intensity of this band was linearly correlated to the initial concentration of BaP in the 1–10 μM concentration range. Hence, this work is the first example of direct detection of the association between an immobilized antibody and a small molecule by mid-IR transduction. The reached detection level, 5 μM , is very promising for future improvement, maybe including an enrichment

stage. However, the process simplicity and the rapid answer of the measurement make the so-built immunosensor a potential competitive tool for on-site preliminary measurements.

Acknowledgements

The City of Paris together with the CNRS and the French Ministry of Research are gratefully acknowledged for financial support.

References

- [1] P.B. Lippa, L.J. Sokoll, D.W. Chan, *Clin. Chim. Acta* 314 (2001) 1.
- [2] E. Delibato, M. Bancone, G. Volpe, D. De Medici, D. Moscone, G. Palleschi, *Anal. Lett.* 38 (2005) 1569.
- [3] M. Campas, B. Prieto-Simon, J.-L. Marty, *Talanta* 72 (2007) 884.
- [4] S. Boujday, A. Bantegnie, E. Briand, P.-G. Marnet, M. Salmain, C.-M. Pradier, *J. Phys. Chem. B* 112 (2008) 6708.
- [5] J.W. Chung, J.M. Park, R. Bernhardt, J.C. Pyun, *J. Biotechnol.* 126 (2006) 325.
- [6] E. Briand, M. Salmain, J.-M. Herry, H. Perrot, C. Compère, C.-M. Pradier, *Biosens. Bioelectron.* 22 (2006) 440.
- [7] N.K. Chaki, K. Vijayamohan, *Biosens. Bioelectron.* 17 (2002) 1.
- [8] S. Boujday, R. Briand, J.-M. Herry, M. Salmain, M. Gautier, P.-G. Marnet, C.-M. Pradier, *Microchim. Acta* 163 (2008) 203.
- [9] E. Briand, M. Salmain, C. Compère, C.-M. Pradier, *Biosens. Bioelectron.* 22 (2007) 2884.
- [10] M. Salmain, N. Fischer-Durand, C.-M. Pradier, *Anal. Biochem.* 373 (2008) 61.
- [11] E. Briand, C. Gu, S. Boujday, M. Salmain, J.-M. Herry, C.M. Pradier, *Surf. Sci.* 601 (2007) 3850.
- [12] C.W. Brown, Y. Li, J.A. Seelenbinder, P. Pivarnik, A.G. Rand, S.V. Letcher, O.J. Gregory, M.J. Platek, *Anal. Chem.* 70 (1998) 2991.
- [13] C. Yu, A. Ganjoo, H. Jain, C.G. Pantano, J. Irudayaraj, *Anal. Chem.* 78 (2006) 2500.
- [14] A.H. Miguel, T.W. Kirchstetter, R.A. Harley, S.V. Hering, *Environ. Sci. Technol.* 32 (1998) 450.
- [15] K.A. Fahrnich, M. Pravda, G.G. Guilbault, *Anal. Lett.* 35 (2002) 1269.
- [16] K.A. Fahrnich, M. Pravda, G.G. Guilbault, *Biosens. Bioelectron.* 18 (2003) 73.
- [17] M. Liu, Q.X. Li, G.A. Rechnitz, *Electroanalysis* 12 (2000) 21.
- [18] J. Dostalek, J. Pribyl, J. Homola, P. Skadal, *Anal. Bioanal. Chem.* 389 (2007) 1841.
- [19] K.V. Gobi, C. Kataoka, N. Miura, *Sens. Actuators, B* 108 (2005) 784.
- [20] K.V. Gobi, M. Sasaki, Y. Shoyama, N. Miura, *Sens. Actuators, B* 89 (2003) 137.
- [21] K.V. Gobi, H. Tanaka, Y. Shoyama, N. Miura, *Biosens. Bioelectron.* 20 (2004) 350.
- [22] K. Länge, G. Griffin, T. Vo-Dinh, G. Gauglitz, *Talanta* 56 (2002) 1153.
- [23] N. Miura, M. Sasaki, K.V. Gobi, C. Kataoka, Y. Shoyama, *Biosens. Bioelectron.* 18 (2003) 953.
- [24] M. Liu, Q.X. Li, G.A. Rechnitz, *Anal. Chim. Acta* 387 (1999) 29.
- [25] G. Sauerbrey, *Z. Phys.* 155 (1959) 206.
- [26] J. Quinn, P. Patel, B. Fitzpatrick, B. Manning, P. Dillon, S. Daly, R. O'Kennedy, M. Alcocer, H. Lee, M. Morgan, K. Lang, *Biosens. Bioelectron.* 14 (1999) 587.
- [27] C. Raman Suri, G.C. Mishra, *Biosens. Bioelectron.* 11 (1996) 1199.
- [28] F. Höök, B. Kasemo, T. Nylander, C. Fant, K. Sott, H. Elwing, *Anal. Chem.* 73 (2001) 5796.
- [29] D.C. Carter, X.M. He, S.H. Munson, P.D. Twigg, K.M. Gernert, M.B. Broom, T.Y. Miller, *Science* 244 (1989) 1195.
- [30] B. Akerstrom, L. Björck, *J. Biol. Chem.* 261 (1986) 10240.
- [31] K. Saha, F. Bender, E. Gizeli, *Anal. Chem.* 75 (2003) 835.
- [32] J. Buijs, J.W.T. Lichtenbelt, W. Norde, J. Lyklema, *Colloids Surf., B* 5 (1995) 11.
- [33] J. Pribyl, M. Hapel, J. Hal-mek, P. Skl-dal, *Sens. Actuators, B* 91 (2003) 333.
- [34] J. Pribyl, M. Hapel, P. Skl-dal, *Sens. Actuators, B* 113 (2006) 900.



An assay for identification and determination of toxic rodenticide valone in serum by ion chromatography–electrospray ionization tandem mass spectrometry with ion trap detector

Mei-Qiang Cai^a, Xin-Yan Dong^b, Xiao-Hong Chen^c, Mi-Cong Jin^{c,*}

^a College of Environmental Science and Engineering, Zhejiang Gongshang University, Hangzhou 310035, PR China

^b National Laboratory of Secondary Resources Chemical Engineering, Zhejiang University, Hangzhou 310027, PR China

^c Ningbo Key Laboratory of Poison Research and Control, Ningbo Municipal Center for Disease Control and Prevention, 237 YongFeng Road, Ningbo 315010, PR China

ARTICLE INFO

Article history:

Received 6 July 2008

Received in revised form 3 November 2008

Accepted 5 November 2008

Available online 25 November 2008

Keywords:

IC–MS/MS

Anticoagulant rodenticide

Valone

Serum

ABSTRACT

Valone has a chronic and toxic anticoagulant rodenticide that has widely used in China and has resulted in some accidental and intentional intoxication in recent years. The literature reported so far lacks sensitive and selective method for the confirmation of valone. The purpose of this study was to establish a novel assay for the identification and quantification of valone in serum by ion chromatography–electrospray ionization tandem mass spectrometry (IC–MS/MS). After serum sample was extracted with methanol/acetonitrile (10:90, v/v) and cleaned by Oasis[®] HLB solid-phase extraction cartridge, chromatographic separation was performed on an Ionpac[®] AS11 column with an eluent of methanol/30 mmol/L KOH (10:90, v/v). The overall extraction efficiency was >81.0%, and the limit of quantification was 0.5 ng/mL for valone. Regression analysis of the calibration data revealed good correlation ($r^2 > 0.99$) for valone. Intra- and inter-day precisions for quality-control samples were less than 8.0 and 13.7%, respectively. The proposed method enables the identification and quantification of valone in both clinical and forensic specimens.

© 2008 Elsevier B.V. All rights reserved.

1. Introduction

Valone (2-isovaleryl-1,3-indandione) is a registered anticoagulant rodenticide commonly used to control population of rats and mice in urban area. It belongs to the indandiones and often used as sodium valone (valone-Na). This anticoagulant is also effective in the control of other rodents such as pocket gophers in rangeland rodents. The extensive use had led to many suspected valone intoxications of both domestic animals and human beings in accidental and intentional species in China. Thus, development of effective analytical methods for confirmation of valone is an urgent requirement. Some months ago, our laboratory received some poisoned species with suspicion to identification the valone. To the best of our knowledge, there are no other assays for the determination of valone, except a spectrophotometric method reported by Menzie et al. [1] and a liquid chromatographic measurement with UV detector reported by Chen et al. [2], although many methods had been reported to determine the other anticoagulant rodenticides including the indandione-type and the coumarin-type rodenticides [3–10]. In 1962, Menzie et al. [1] developed a sensitive spectrophotometric method using KCN and 2,4-dinitrophenylhydrazone as the

chromogenic reagents at 540 nm for the determination of valone, the limit of detection was 1.0 mg/kg. In 2007, Chen et al. [2] reported a liquid chromatographic assay with UV detector at 280 nm using a Zorbax SB C18 column (250 mm × 4.6 mm i.d., 5 μm) and ternary gradient mobile phase (methanol, 0.8% acetic acid and 0.01 mol/L ammonium acid) for the analysis of valone in cereal, the limit of quantification was 0.1 mg/kg. Both methods could not be suitable for the analysis of trace valone in the serum. Recently, the combination of liquid chromatography with mass spectrometry (LC–MS) or tandem mass spectrometry (LC–MS/MS) had many applications in the analysis of toxic and polar species [11–19], and the ion chromatography with mass spectrometry (IC–MS) or tandem mass spectrometry (IC–MS/MS) had also some applications [20–22]. The purpose of this paper is to develop a novel, sensitive and selective method for the confirmation and analysis of valone residue in serum by ion chromatography in combination with electrospray ionization ion trap mass spectrometric detection in the multiple reaction monitoring (MRM) mode.

2. Experimental

2.1. IC–MS system

The separation was performed on a Dionex Model ICS2000 ion chromatograph system equipped with an isocratic pump, a

* Corresponding author. Tel.: +86 574 87274559; fax: +86 574 87361764.

E-mail address: jmcjc@163.com (M.-C. Jin).

column thermostat, an AS40 automated sampler, a 25 μ L sample loop, an ASRS-ULTRA-4 mm self-regenerating suppressor (recycle mode) (Dionex, Sunnyvale, CA, USA), a DS60 conductivity detector and an EG50 eluent generator. The eluent generator with CR-ATC continuously regenerated anion trap column was used to generate KOH gradient concentrations. The chromatographic separation was carried out on a Dionex Ionpac AS11 separation column (250 mm \times 4 mm, i.d.) using a Dionex Ionpac AG11 guard column (50 mm \times 4 mm, i.d.). The organic modifier was delivered by a Waters 510 pump. Detection was performed by an Agilent 1100 series LC/MSD Trap SL mass spectrometer with an electrospray interface (ESI) (Agilent Technologies, Waldbronn, Waldbronn, Germany). The schematic diagram of the IC-MS apparatus was shown in our previous paper [21]. The ICS2000 system was controlled on a personal computer equipped with Dionex Chromeleon 6.5 Software and the ESI-MS system was controlled, and data were analyzed, on a personal computer equipped with LC/MSD Trap Software 4.2 (Bruker Daltonik GmbH).

2.2. Solvents and materials

HPLC grade methanol and acetonitrile were purchased from Merck (Merck, Darmstadt, Germany). Deionized water was obtained by a Milli-Q water purification system from Millipore (Molsheim, France). The standards of warfarin (>99%, IS) and valone (>99.5%) were purchased from Sigma (St. Louis, MO, USA). Anhydrous sodium sulfate, ethanol and hydrochloric acid were of analytical grade and obtained from Shanghai Reagent Company (Shanghai, China). Blank human serum was collected from healthy blank volunteers (three women and three men), aged 21–25 years, come from Ningbo University (Ningbo, China), all were in good general health. Samples A, B and C were collected from three different patients who were suspected for incidental ingestion of valone rodenticide. All the blood samples were centrifugated in 5 mL polypropylene centrifuge tubes at once and the serum specimens were kept refrigerated until processing.

2.3. Preparation of standard stock solutions

Stock solutions of valone (1.0 mg/mL) and warfarin (IS, 1.0 mg/mL) were prepared in methanol. The stock solutions stored at 4 °C in tightly closed bottles until use. Working solutions of valone at the concentration of 0.5, 1.0, 2.0, 5.0, 8.0, 15.0, 40.0 and 100.0 ng/mL were diluted from the stock solution with MeOH, wherein the IS concentrations were the same amounts as valone in serum. Serum quality control samples were prepared in drug-free serum (2.0, 15.0 and 100.0 ng/mL for both valone and IS).

2.4. Preparation of sample

Sample preparation was as follows: 500 μ L serum samples were thawed to room temperature in a 2 mL polypropylene centrifuge tube before analysis, and 1.0 mg/L IS (10.0 μ L) were vortex-mixed and extracted using 1.0 mL methanol/acetonitrile (10:90, v/v) for 5 min. After centrifugation for 5 min at 7800 rpm, the upper organic layer was transferred to a disposable glass tube. The samples were re-extracted with 1.0 mL methanol/acetonitrile (10:90, v/v) as mentioned above. The organic layer was combined and evaporated to dryness under a stream of nitrogen on a heating block at 50 °C in a disposable glass tube. Then, the residues were dissolved in 2.0 mL methanol/water (80:20, v/v) by ultrasonication for 5 min. The solution was uploaded on an Oasis[®] HLB (200 mg/3 mL, Waters, USA) cartridge that first was conditioned with 2.0 mL dichloromethane, 2.0 mL methanol and 2.0 mL water. The flow rate of the sample was 5.0 mL/min. The elution was done with 2.0 mL MeOH and 2.0 mL dichloromethane, then evaporated to dryness by a gentle stream of

nitrogen, and the residues were reconstituted with 500 μ L of eluent by ultrasonication for 5 min to facilitate dissolution. Prior to analysis, the extract was filtered through a 0.45 μ m nylon syringe filter (Agilent Technologies, Waldbronn, Germany), and a 20 μ L aliquot was injected into the IC system.

2.5. IC-MS analysis

The separation was performed on a Dionex Ionpac AG11 guard column (50 mm \times 4 mm, i.d.) and a Dionex Ionpac AS11 analytical column (250 mm \times 4 mm, i.d.) using methanol/30.0 mmol/L KOH (10:90, v/v) as eluent at a constant flow rate of 1.0 mL/min. Column temperature was held constant at 35 °C. An ASRS-ULTRA-4 mm suppressor was operated at 60.0 mA in the external water mode. A Dionex ASRS Ultra II Self-regenerating suppressor (4 mm) was used in pressurized bottle mode to remove the sodium ions from the mobile phase. After suppression the flow from the chromatographic system was split in the ratio of 1:3, by means of a zero dead volume T-piece to allow 0.25 mL/min to enter an Agilent 1100 series LC/MSD Trap SL mass spectrometer equipped with an ESI interface operating in the negative ion mode. A portion (0.75 mL/min) of the flow was returned to the self-regenerating suppressor and, to ensure the proper operation of the suppressor, external water circulation (external pressurized bottle mode, flow 1.0 mL/min) was added to the suppressor to compensate for the removal of the 0.25 mL/min of the flow.

An Agilent ion trap mass spectrometer with an electrospray ionization (ESI) mass spectrometry was used for detection. Conditions were as follows: negative ion mode; capillary voltage 3.0 kV, capillary exit voltage –135 V, dry temperature 325 °C, high purity (99.99%) dry nitrogen gas 8.0 L/min, nitrogen nebulizer pressure of 35.0 psi and dwell time 200 ms. MS/MS experiments were performed using argon as collision gas at a pressure of 1.22×10^{-5} mbar and a collision energy setting adapted for each compound. To determine the product ions of valone and IS, the deprotonated ion $[M-H]^-$ at m/z 229 and 307 was isolated, and helium gas was introduced into the trap to induce collision. Throughout all the measurements the analytes were detected in multiple reaction monitoring (MRM) mode with a transition of m/z 229 \rightarrow 145 for valone, and m/z 307 \rightarrow 161 for IS, respectively. Table 1 outlines the MRM parameters for valone and IS.

2.6. Method validation

A calibration curve was constructed from a blank sample (a serum sample processed without the IS), a zero sample (a serum processed with the IS) and seven non-zero samples covering the total range 0.5–100.0 ng/mL. The calibration curves were generated using the valone-to-IS peak area ratios by weighted ($1/x^2$) least-squares linear regression on consecutive days.

The intra-day precision and accuracy were determined by analyzing three sets of QC samples (low, medium and high concentrations), each day for five replicates within 3 days. The inter-day precision and accuracy were determined by analyzing such QC samples in duplicate on each of eight different days within a 14-day period.

Table 1
The MRM parameters for valone and warfarin (IS).

Item	Valone	IS
Precursor ion (m/z)	239	307
Product ion for detection and quantification (m/z)	145	161
Additional ions for confirmation (m/z)	172, 187, 214	250, 117
Width (m/z)	2.0	2.0
Cutoff mass	73	84
CID (V)	1.50	1.15
Retention time (min)	3.42	4.15

Recovery of valone from the extraction procedure was determined by a comparison of the peak area of valone in spiked serum samples (low, medium and high QCs) with the peak area of valone in samples prepared by spiking extracted blank serum samples with the same amounts of valone at the step immediately prior to chromatography.

The stability of valone and IS in human serum under different temperature and timing conditions, as well as their stability in the stock solutions, was evaluated. QC samples were subjected to short-term room temperature conditions, to long-term storage conditions ($-20\text{ }^{\circ}\text{C}$) and to freeze–thaw stability studies. All the stability studies were conducted by QC samples with three replicates for each.

3. Results and discussion

3.1. Optimization of IC–MS/MS conditions

The ion trap mass spectrometer was used in MRM mode for highest selectivity and lowest limit of quantification (LOQ). The MS/MS spectra for valone and IS are shown in Fig. 1. Transition ion pair of m/z 229 \rightarrow 145, which was the deprotonated ion $[\text{M}-\text{H}]^-$ loss of was selected as MRM quantitative ion pair for valone. Both transition ion pairs of m/z 229 \rightarrow 172 and m/z 229 \rightarrow 187 were selected as the qualitative ions for valone. Signal intensities were about 100 times higher in MRM mode when the eluent consisted of 30 mmol/L KOH and 10% methanol than the eluent of 30 mmol/L KOH. Initially, we tested methanol and acetonitrile, respectively, as the organic modifier to improve the resolution and the sensitivity. The result indicate that methanol as the organic modifier gives better intensities than acetonitrile, and intensities are highest at 10–20% ratio in the eluent. Negative-ion mode was 100 times more sensitive than positive-ion mode in MRM mode for valone, whereas negative-ion mode was almost five times as sensitive for IS. We decided to use negative-ion mode for IC/MS/MS determination of valone in serum by use of isocratic eluent conditions on an Ionpac[®] AS11 analytical

column. Variability of the peak-area ratio of valone to IS under these conditions was <15% between injections. The apparent response at the retention time of valone ($t_R = 3.42$ min) and IS ($t_R = 4.15$ min) is shown in Fig. 2.

3.2. Sample preparation

Serum matrices are rich in protein and lipids components, the analysis of valone in serum required an adequate purification. Initially, liquid–liquid partition with acetonitrile was used to remove the protein in serum at neutral pH (7.0). We found that the absolute recovery of valone was lower owing to the behavior of the rapid precipitation by acetonitrile, which resulted to the analyte enwrapped into the precipitation particle. When adding 10% methanol in acetonitrile, the coprecipitation phenomenon was decreased, the absolute recovery of valone was improved to an acceptable range (63.3–76.5%). In order to increase further the absolute recovery of valone, repeated extraction was necessary. However, owing to the complexity of the serum matrix, a further clean-up was necessary to remove medium to interfering compounds. Crude sample extract cleanup was performed by SPE on the hydrophilic–lipophilic balance Oasis HLB cartridges because of their high capacity, good and reproducible recovery for both polar and non-polar compounds, and no loss of analytes due to dryness of the cartridge. And HLB cartridges have been used in the previous methods for the cleanup of coumarin rodenticides [21,24]. In the preliminary experiments, we paid careful attention to investigate the optimal conditions of critical SPE parameters for simultaneous extraction of valone and IS, and effective elimination of interferences.

First, the influence of pH of sample extract loading on the SPE was studied. The pH of the extract solution critically affected the retaining efficiency of valone in the HLB cartridge. In this work, fortified sample extracts were adjusted to pH values from 1 to 14 by 1% acetic acid and loaded on the SPE cartridges. After the sample loading, the cartridges were washed and eluted using the method reported by the literatures [21,24], which is absolute methanol

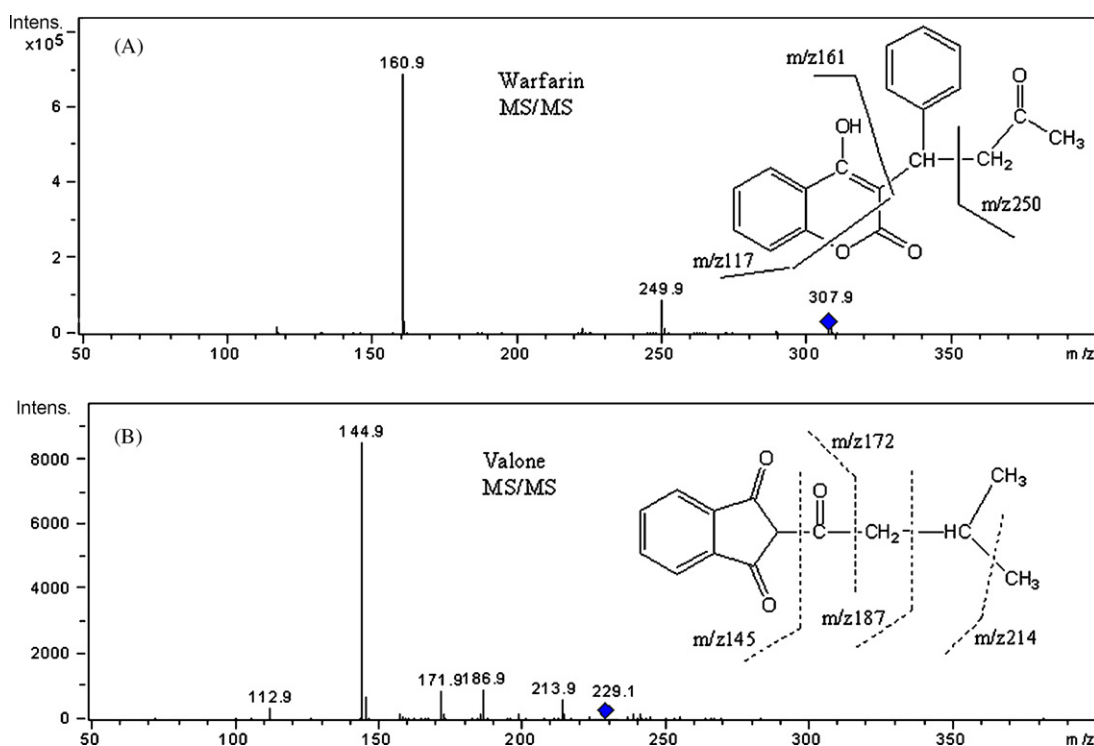


Fig. 1. The MS/MS spectra for IS (A) and valone (B). The diamond marked the precursor ion.

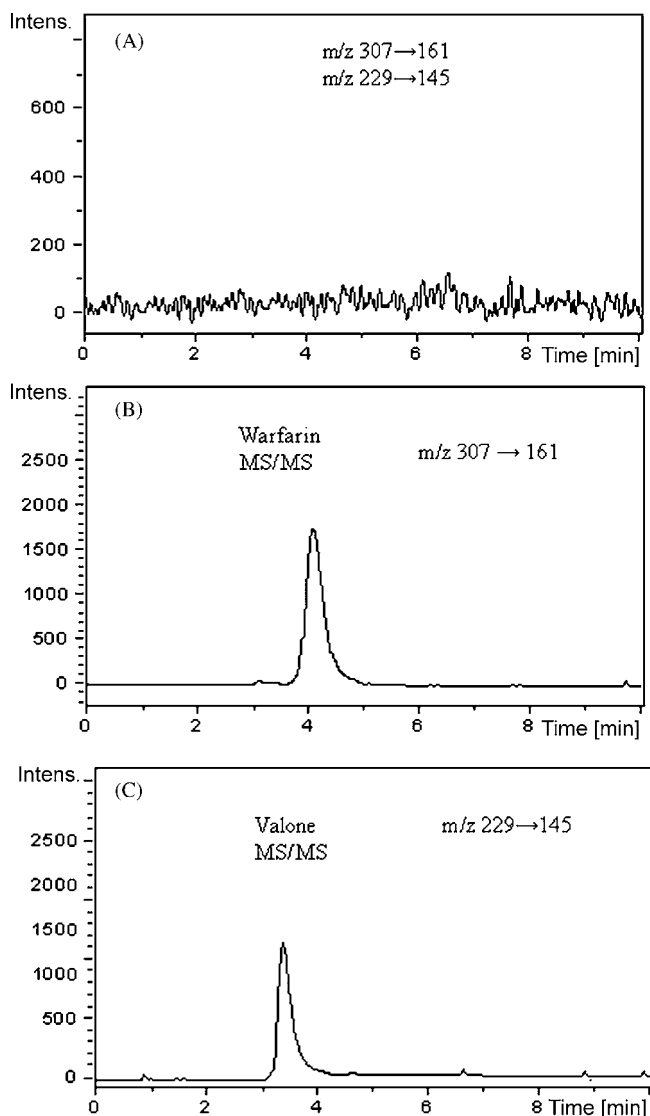


Fig. 2. MRM chromatograms of a blank serum with transitions of m/z 229 \rightarrow 145 for valone, and m/z 307 \rightarrow 161 for IS (A); spiked at 10.0 ng/mL IS with a transition of m/z 307 \rightarrow 161 (B); spiked at 10.0 ng/mL valone with a transition of m/z 229 \rightarrow 145 (C).

(2 mL) as washing solvent and absolute dichloromethane (2 mL) as eluent. It was observed that the recoveries of valone and IS decreased notably when the extract pH was above 8.5. At a high pH value (e.g., pH > 8.5), valone and IS are transformed to anions (through deprotonating the hydroxyl moiety) which tend to penetrate the HLB cartridge. Neutral (pH 7) was found to be optimal to remain the two groups of compounds on the cartridge simultaneously. Methanol was assessed for the washing step attempting to partially remove the interfering organics retained by the HLB cartridge prior to elution of the valone and IS. It was found that lit-

tle valone and IS was removed from the HLB cartridge if methanol was used as the washing solution. In this work, several eluting solvents including cyclohexane, dichloromethane, ethyl acetate and acetone were tested individually or in combination to achieve a high extraction efficiency of the valone and IS while retaining the matrix organics in the HLB cartridge. The results show that dichloromethane could achieve the highest recovery of valone and IS and the least elution of matrix organics. After the elution procedure, the extract was dried under a gentle stream of nitrogen gas. Thereafter, 500 μ L of methanol/30.0 mmol/L KOH (10:90, v/v) was added to reconstitute the dried residue for IC-MS/MS analysis.

3.3. Specificity and selectivity

To examine the effect of the human serum on ionization efficiency, we compared the peak areas of valone and IS in QC samples of three concentration levels with those in standard solutions that had been prepared in the same way as the QC samples except that water replaced the blank human serum. It shows that the mean peak areas from the three QC samples (2.0, 15.0 and 100.0 ng/mL) had relative errors of -5.8 , -5.2 and -4.3% for valone, compared with these standard solutions. For the IS, the relative errors were -6.7 , -4.9 and -6.2% . These indicated that there were no endogenous substances to influence significantly the ionization of valone and IS.

Six different sources of blank human serum samples were investigated for interferences from endogenous compounds. Fig. 2A shows a typical MRM chromatogram of a blank human serum sample for valone and IS. It indicates that no significant direct interference in the blank serum was observed from endogenous substances in blank human serum at the retention time of the analyte. Similarly, six different sources of blank human serum samples spiked with the analyte and IS were also examined for interferences from endogenous compounds. Fig. 2B and C shows typical MRM chromatograms of a blank human serum sample spiked 10 ng/mL for valone and IS, respectively. It also shows the absence of direct interference from the IS to the MRM channel of the analyte. The MRM transitions show valone and IS, and demonstrate that there are good specificity and selectivity.

3.4. Method development

The assay was validated in accordance with Food and Drug Administration guidelines [23]. Calibration curve for valone was obtained by a series of spiked human serum at the concentrations of 0.5, 1.0, 2.0, 5.0, 15.0, 50.0 and 100.0 ng/mL, respectively, wherein the IS concentrations were the same amounts as valone. Three replicates of standards at each concentration were performed. Calibration curve was constructed by using the ratio of area (Y, valone peak area to IS peak area) to the concentration (C, ng/mL) in human serum. The typical equation of the calibration curve was $C = 126.23Y - 0.52123$. It was linear in the tested concentration range of 0.5–100.0 ng/mL with a coefficient of determination $r^2 = 0.9973$, and consistent slope (3.7%) and intercept value (4.8%).

Table 2

The recoveries and the precisions of the method for spiked samples.

Analyte	Added (ng/mL)	Found (ng/mL) ^a	Recovery (%)	RSD (%)	
				Intra-day ^b	Inter-day ^c
Valone	2.0	1.62 \pm 0.13	81.0	8.0	13.7
	15.0	13.52 \pm 0.88	90.1	6.5	10.8
	100.0	85.16 \pm 3.67	85.2	4.3	7.9

^a Determined within 3 days.

^b $n = 5 \times 3$.

^c $n = 2$ replicates \times 8 days within a 14-day period.

The limit of quantification was determined as the lowest concentration in the standard curve that can be measured with acceptable accuracy and precision and was found to be 0.5 ng/mL in human serum. The mean response for the valone peak at the assay sensitivity limit (0.5 ng/mL) was 10-fold greater than the mean response for the peak in six blank human serum samples at the retention time of the analyte.

The intra-day precision was evaluated by performing five replicates on each day within 3 days for the spiked QC samples (2.0, 15.0 and 100.0 ng/mL) including extraction procedures. The inter-day precision was evaluated by performing duplicates on each of eight different days within a 14-day period. The intra-day precision (RSD) on the basis of peak area was less than 8.0% and the inter-day precision (RSD) on the basis of peak area was less than 13.7%, as shown in Table 2.

The extraction recoveries of valone were determined by comparing the peak area of valone at the three QC levels in the human serum samples that had been spiked with valone at three different concentrations (2.0, 15.0 and 100.0 ng/mL) before and after extraction. The recoveries were 81.0–90.1%, as shown in Table 2.

3.5. Stability

We assessed the stability of valone in serum matrix, the QC samples were analyzed under different condition. After three freeze and thaw cycles (room temperature to -20°C) was performed at three concentrations (2.0, 15.0 and 100.0 ng/mL) and the percent bias were evaluated to be -6.5 , -5.2 and -3.1% , respectively, in comparison with freshly prepared samples. Short-term room temperature stability was done for 24 h and the percent bias calculated by comparing with freshly prepared sample was found to be -8.5 , -7.3 and -4.4% for the three concentrations (2.0, 15.0 and 100.0 ng/mL), respectively. The long-term stability data of valone in human serum stored for a period of 10 days at below -20°C showed reliable stability behavior, the percent bias was found to be -10.4 , -9.3 and -5.6% for the three concentrations (2.0, 15.0 and 100.0 ng/mL), respectively. These findings indicate that storage of the analyte in serum samples at below -20°C is adequate, and no stability-related problems would be expected during routine analyses for clinical and forensic investigations.

3.6. Application to the real world samples

Samples A, B and C were analyzed by the established IC-ESI/MS/MS method. The results indicate that the valone concentrations are 14.7 and 401.3 ng/mL and less than LOQ for samples A, B and C, respectively, as shown in Table 3. In order to validate further the developed method, Fig. 3 depicts the MRM chromatograms for the three samples. It also indicates that small matrix effects or interferences from endogenous substances were detected in the real world samples.

In addition, we also determined the coagulation time of these samples by glasses test tube method (at room temperature). The coagulation time for samples A, B and C are 8.3, 13.8 and 6.4 min, respectively, as shown in Table 3. Based on the result obtained,

Table 3
Samples A, B and C information and the result of valone concentration in serum.

Sample	Gender	Age (year)	Coagulation time (min) ^a	Concentration (ng/mL)
A	Man	13	8.3	14.7
B	Woman	27	13.8	401.3
C	Woman	49	6.4	n.d. ^b

^a Determined by glasses test tube method (at room temperature), the normal value is between 4 and 12 min.

^b n.d.: less than 0.5 ng/mL.

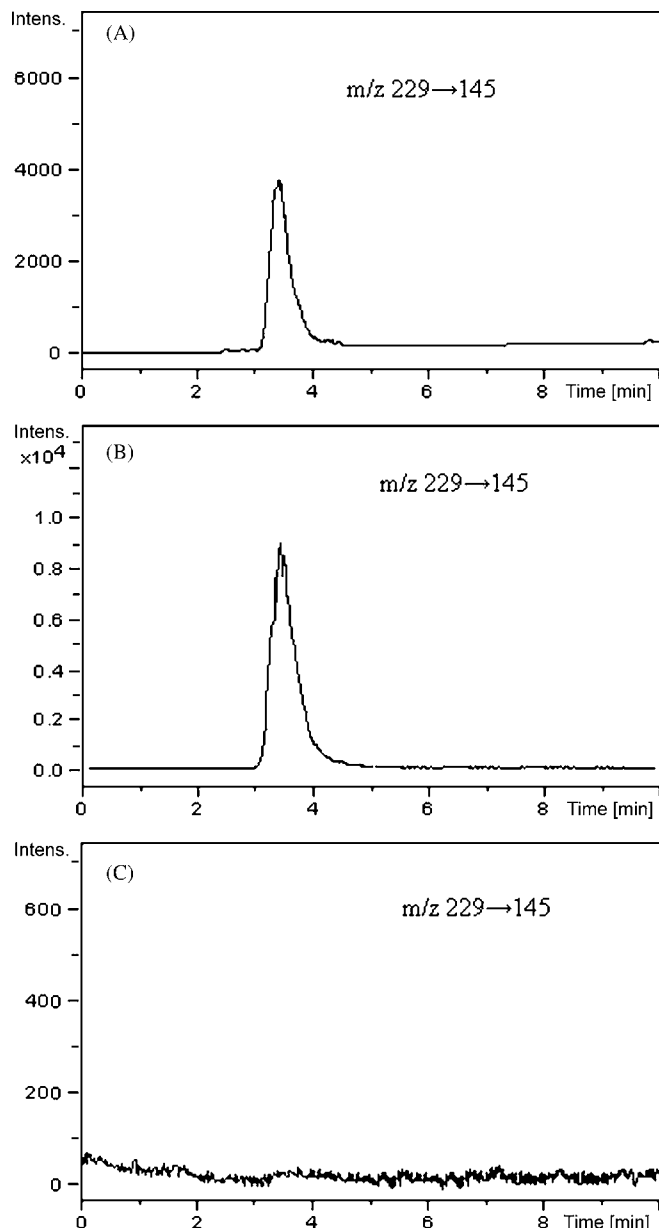


Fig. 3. MRM chromatograms of the real world samples with a transition of m/z 229 \rightarrow 145 for valone, sample A (A); sample B (beyond the linear range, dilution in 1:10) (B); sample C (C).

it indicates that the valone contents in serum are positive correlation with the blood coagulation time. It also shows that a low concentration of valone in serum cannot significantly delay the coagulation time. In fact, even if the coagulation time is between the normal values (4–12 min), the poison is still possibly existed in the human body. Therefore, the poison residue monitoring is necessary to achieve the best therapeutic effects and the least toxicity for person.

4. Conclusions

In this paper, a highly sensitive and selective method for the quantification of valone in serum was developed and validated by ion chromatographic separation with tandem mass spectrometric detection. This method combines a rapid solid-phase extraction procedure with an extremely fast chromatographic analysis. This proposed IC-MS/MS assay for identification and quantification

of valone has a lower limit of quantification of 0.5 ng/mL, wide linearity, and specificity without interferences from endogenous substances, and allows for applying in clinical and toxicological investigations.

Acknowledgements

This work was supported by the Natural Science Foundation of Ningbo, China (No. 2007A610072), the Agriculture and Social Development Funds of Ningbo, China (No. 2007C10084) and the Medical Health Youth Funds in Zhejiang Province, China (No. 2007QN014).

References

- [1] C.M. Menzie, V.A. Adomaitis, W.L. Reichel, *Anal. Chem.* 34 (1962) 516.
- [2] H.Y. Chen, X.H. Chen, M.C. Jin, J. Tang, *Chin. J. Health Lab.* 17 (2007) 1629.
- [3] M.C. Jin, X.H. Chen, *Rapid Commun. Mass Spectrom.* 20 (2006) 2741.
- [4] L.J. Marek, W.C. Koskinen, *J. Agric. Food Chem.* 55 (2007) 571.
- [5] F.Y. Guan, A. Ishii, H. Seno, K. Watanabe-Suzuki, T. Kumazawa, O. Suzuki, *J. Pharm. Biomed. Anal.* 21 (1999) 179.
- [6] M.Z. Mesmer, R.A. Flurer, *J. Chromatogr. A* 891 (2000) 249.
- [7] J.B. Addison, *J. Assoc. Off. Anal. Chem.* 65 (1982) 12.
- [8] T. Grobosch, B. Angelow, L. Schönberg, D. Lampe, *J. Anal. Toxicol.* 30 (2006) 281.
- [9] M.C. Jin, X.K. Ouyang, X.H. Chen, *J. Appl. Toxicol.* 27 (2007) 18.
- [10] M.C. Jin, Y.P. Ren, X.M. Xu, X.H. Chen, *Forensic Sci. Int.* 171 (2007) 52.
- [11] K.H. Yoon, S.Y. Lee, M. Jang, S.H. Ko, W. Kim, J.S. Park, I. Park, H.J. Kim, *Talanta* 66 (2005) 831.
- [12] B. Delmulle, S. De Saeger, A. Adams, N. De Kimpe, C. Van Peteghem, *Rapid Commun. Mass Spectrom.* 20 (2006) 771.
- [13] S.A. Chan, S.W. Lin, K.J. Yu, T.Y. Liu, M.R. Fuh, *Talanta* 69 (2006) 952.
- [14] B.K. Matuszewski, M.L. Constanzer, C.M. Chavez-Eng, *Anal. Chem.* 70 (1998) 882.
- [15] M. Gros, M. Petrović, D. Barceló, *Talanta* 70 (2006) 678.
- [16] E. Bermudo, E. Moyano, L. Puignou, M.T. Galceran, *Talanta* 76 (2008) 389.
- [17] R. Guo, Q.F. Zhou, Y.Q. Cai, G.B. Jiang, *Talanta* 75 (2008) 1394.
- [18] C. Lacey, G. McMahon, J. Bones, L. Barron, A. Morrissey, J.M. Tobin, *Talanta* 75 (2008) 1089.
- [19] O. Delhomme, M. Millet, P. Herckes, *Talanta* 74 (2008) 703.
- [20] M.C. Jin, Y.W. Yang, *Anal. Chim. Acta* 566 (2006) 193.
- [21] M.C. Jin, Y. Zhu, *J. Chromatogr. A* 1118 (2006) 111.
- [22] A. Meyer, S. Höffler, K. Fischer, *J. Chromatogr. A* 1170 (2007) 62.
- [23] *Guidance for Industry: Bioanalytical Method Validation*. US Department of Health and Human Services, Food and Drug Administration, Center for Drug Evaluation and Research, Rockville, MD (2001).
- [24] M.C. Jin, J.M. Ma, L. Wang, X.H. Chen, *Chin. J. Ind. Hyg. Occup. Dis.* 24 (2006) 682.



Ammonia gas sensor based on electrosynthesized polypyrrole films

Stéphanie Carquigny^{a,b}, Jean-Baptiste Sanchez^a, Franck Berger^a,
Boris Lakard^{b,*}, Fabrice Lallemand^b

^a LCPR-AC, UMR CEA E4, Université de Franche-Comté, Bâtiment Propédeutique, 16 route de Gray, 25030 Besançon Cedex, France

^b Institut UTINAM, UMR CNRS 6213, Université de Franche-Comté, Bâtiment Propédeutique, 16 route de Gray, 25030 Besançon Cedex, France

ARTICLE INFO

Article history:

Received 28 July 2008

Received in revised form 24 October 2008

Accepted 31 October 2008

Available online 11 November 2008

Keywords:

Gas sensor

Ammonia

Polypyrrole

Electrochemistry

ABSTRACT

In this work, design and fabrication of micro-gas-sensors, polymerization and deposition of poly(pyrrole) thin films as sensitive layer for the micro-gas-sensors by electrochemical processing, and characterization of the polymer films by FTIR, X-ray photoelectron spectroscopy (XPS) and scanning electron microscopy (SEM), are reported. The change in conductance of thin polymer layers is used as a sensor signal. The behaviours, including sensitivity, reproducibility and reversibility, to various ammonia gas concentrations ranging from 8 ppm to 1000 ppm are investigated. The influence of the temperature on the electrical response of the sensors is also studied. The experimental results show that these ammonia gas sensors are efficient since they are sensitive to ammonia, reversible and reproducible at room temperature.

© 2008 Elsevier B.V. All rights reserved.

1. Introduction

Polypyrrole (PPy) has attracted considerable attention because of the possibility to use redox reactions for transforming it into states of strongly differing electrical conductivity [1] and because PPy has a good stability in air and aqueous media. PPy and other conductive polymers have, therefore, also been classified as organic metals. There exists a wide range of applications to use organic metals, such as: cell culture substrates [2,3], field effect transistors [4–6], light-emitting diodes [7], solar cells [8–10], electrochromic devices [11,12], electronic circuits [13,14], elastic textile composites [15], supercapacitors for energy storage and secondary batteries [16], protection of metals [17,18], ion exchange membranes that respond to external stimulations [19,20], sensors and biosensors [21–27]. More, in recent years, attention has also been given to the use of conducting polymers as active layers in chemical gas sensors, and it has been proved that adsorbed gas molecules (ammonia, NO₂, CO₂) and organic vapors (alcohols, ethers, halocarbons) cause a change of electrical conductivity in the polymer matrix of organic metals [28–33]. In comparison with most of the commercially available sensors, based usually on metal oxides and operating at high temperatures, the sensors made of conducting polymers have many improved characteristics. They have high sensitivities and short response time; especially, these features are ensured at room temperature.

Thus, in this paper, an original ammonia gas sensor based on micropatterned microelectrodes functionalized by electropolymerization of polypyrrole films is studied. Electrochemical deposition has been chosen since it is the most convenient method to deposit conducting polymer films [34–36]. Indeed, the thickness of the film can be controlled by the total charge passed through the electrochemical cell during the film growing process. More, such a deposition also allows the preparation of films at a well-defined redox potential in the presence of a given counter-ion, which then also defines the level and characteristics of the doping reaction [37]. Thus, electropolymerization is used in this study to fabricate a gas sensor consisting in PPy films deposited on microstructured electrode arrays and also across the insulating gap separating the microstructured electrodes of the sensor. Indeed, if the insulating gap between the neighboring electrodes is close enough (a few micrometers), the growing film can cover the insulated gap and connect electrodes [38,39]. This is important in fabricating chemiresistors for gas sensing. A microstructured interdigitated electrode array was chosen since it represents the most suitable geometry to serve as a transducer in chemical gas sensors, based on conductivity changes. Following their deposition, the electropolymerized polypyrrole layers are characterized by infrared spectroscopy (IR), X-ray photoelectron spectroscopy (XPS) and scanning electron microscopy (SEM). Then, polymer films are tested as ammonia gas sensors. In particular, their response, in terms of conductance changes when exposed to different ammonia concentration, was studied. The reproducibility and the reversibility of the signal exhibited by the PPy films to ammonia exposure but also the influence of temperature on this response are also studied.

* Corresponding author. Tel.: +33 3 63 08 25 78.

E-mail address: boris.lakard@univ-fcomte.fr (B. Lakard).

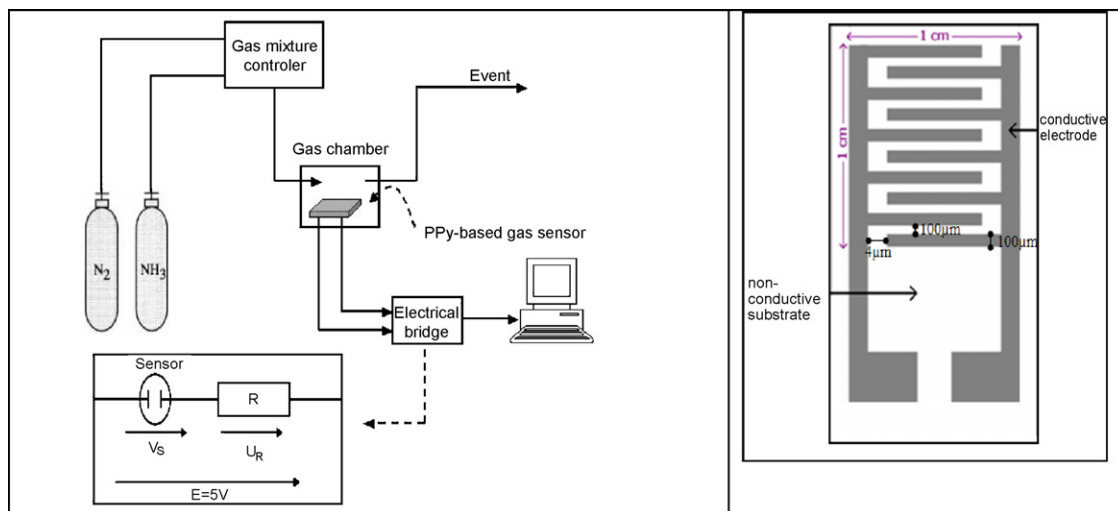


Fig. 1. (a) Experimental set-up used for the analysis of NH₃ vapors and (b) schematic drawing of the ammonia gas sensor.

2. Experimental

2.1. Fabrication of gas sensors

The gas sensors were fabricated using microsystem technologies, and in particular using lift-off process that consists in a photolithography followed by a sputtering of platinum on a SiO₂ wafer. The first step of the photolithography process consisted in drawing the required pattern (see Fig. 1) with commercial mask design software Cadence. Then a Cr/Glass mask, on which the shape of the pattern has been drawn, was made with an electromask optical pattern generator. The process started with a 100-oriented standard 3" silicon wafer, which was thermally wet-oxidized, at 1200 °C in water vapor, in order to produce a 1.3 μm thickness SiO₂ layer. Next, a 1.4-μm thickness layer of negative photoresist (AZ 5214, from Clariant), suitable for lift-off, was deposited by spin coating. Then, the wafer was first exposed with the mask to a 36-mJ/cm² UV radiation flux delivered by an EVG 620 apparatus, and then without any mask to a 210-mJ/cm² UV radiation flux. Thus, the pattern was transferred to the resist, which was then developed, using AZ 726 developer, to dissolve the resist where the metal was deposited. Then, a magnetron sputtering (Alcatel SCM 441 apparatus) was used to coat microsystems with titanium (30 nm, used to improve platinum layer), then platinum (150 nm). The fabrication parameters for Pt and Ti films were the following ones: base pressure: 4.6×10^{-7} mbar, pressure (Ar) during sputtering: 5×10^{-3} mbar, power: 150 W, target material purity: 99.99%, film thickness: 150 nm for Pt films and 30 nm for Ti films. The remaining resist layer was then dissolved using acetone. After the gas sensors have been fabricated, the pattern and the dimensions are controlled using an optical microscope. More details about the microsystem fabrication can be found in a previous paper [27]. A microstructured interdigitated electrode array was chosen since it represents the most suitable geometry to serve as a transducer in chemical gas sensors, based on conductivity changes. The width and length of the 100 bands (50 bands on each microelectrode array) were 100 μm and 9996 μm, respectively (Fig. 1). The width of the gap between the two microelectrode array was 4 μm to allow the coating of the gap by the polypyrrole film.

2.2. Electrochemistry

Pyrrole (Py) and LiClO₄ were obtained from Sigma–Aldrich (analytical grade). Pyrrole was used at the concentration of 0.05 M in

an aqueous solution of 0.1 M LiClO₄. The electrochemical apparatus was a classical three-electrode set-up using a Tacussel PGZ301, from Radiometer, potentiostat–galvanostat. The microsystem was used as working electrode. The reference electrode was a saturated calomel electrode (SCE) and the counter-electrode was a platinum wire. All electrochemical experiments were carried out at room temperature (293 K). Cyclic voltammetry experiments were carried out with a sweep rate of 100 mV s⁻¹ between -0.3 V/SCE and +1.5 V/SCE. Each solution was purged by ultrahigh purity argon. Chronoamperometry experiments were carried out at a potential of +1.3 V/SCE.

2.3. Characterization of the polymer films

2.3.1. XPS

The polymer surface was characterized by X-ray photoelectron spectroscopy (XPS, SSX-100 spectrometer). XPS was used to control the elemental composition and to determine the oxidation state of elements. All recorded spectra were recorded at a 35° take-off angle relative to the substrate with a spectrometer using the monochromatized Al Kα radiation (1486.6 eV). The binding energies of the core-levels were calibrated against the C_{1s} binding energy set at 285.0 eV, an energy characteristic of alkyl moieties. The peaks were analyzed using mixed Gaussian–Lorentzian curves (80% of Gaussian character).

2.3.2. SEM

Examinations of polymer morphologies were performed using a high-resolution scanning electron microscope. Once synthesized and dried, polymer samples were examined in a LEO microscope (SEM LEO stereoscan 440, manufactured by Zeiss–Leica, Köln, Germany) with an electron beam energy of 15 keV.

2.3.3. IRTF-ATR

All spectra were recorded using a Shimadzu spectrometer (IR-Prestige 21) in ATR reflexion mode. The specific accessory used for these analyses is the ATR Miracle Diamond/KRS5 which allowed us to record spectra between 4000 cm⁻¹ and 700 cm⁻¹. Resolution was fixed at 4 cm⁻¹ and 60 scans were realized to acquire each spectrum. All samples were constituted with PPy powder.

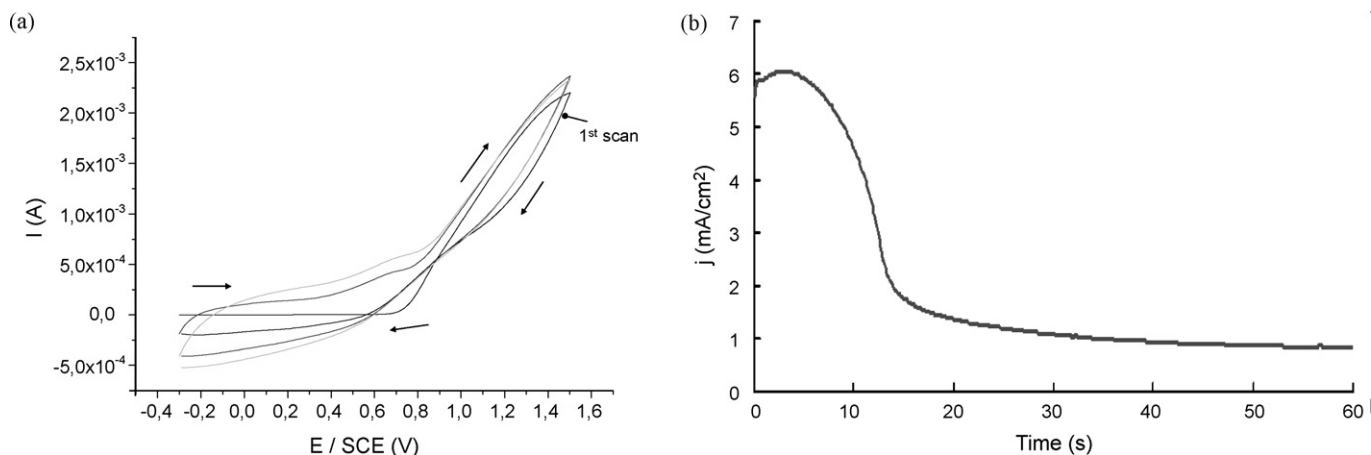


Fig. 2. Electrochemical synthesis of polypyrrole films by oxidation of an aqueous solution of pyrrole and LiClO_4 by cyclic voltammetry (a) or chronoamperometry (b).

2.4. Gas measurements

An initial ammonia concentration equal to 1000 ppm in nitrogen was used for the experiment. All the studies were carried out in nitrogen atmosphere. The sensor's electrical responses were obtained by monitoring the variations in the sensor's instantaneous conductance versus acquisition time, for a constant temperature of the sensitive layer. The conductance measurements lasted about 3 h for each acquisition. The protocol used for the conductance experiments was the same for each sensor. Each sensor's electrical response was obtained under a constant gas flow (N_2 or NH_3 diluted in N_2) rate of 50 mL min^{-1} . Specially designed equipment was developed for this study. Mass flowmeters were used to obtain different NH_3 concentrations. This experimental set-up allowed PPy-based gas sensors to be exposed to the different ammonia concentrations.

The effect of gases on the sensor's electrical properties was recorded using a basic divisor voltage bridge (Fig. 1). With these experimental conditions, the relationship between the variation of the sensor's conductance and the variation of the voltage U_R is defined as:

$$G_C = \frac{1}{R((E/U_R) - 1)}$$

Any decrease (or increase) of the sensor's conductance was recorded as a decrease (or increase) of the electrical signal.

Each new sensor was exposed to a constant nitrogen flow for 12 h before conducting each experiment. This process allowed for the desorption of pollutant chemical compounds adsorbed onto the sensitive layer during the storage.

3. Results and discussion

3.1. Electrochemical synthesis of polymer films

Electrochemical synthesis of polypyrrole was performed by cyclic voltammetry, from an aqueous solution containing 0.1 M pyrrole and 0.1 M LiClO_4 , on the platinum microelectrodes of the sensor using a potential sweep rate of 0.1 V s^{-1} between -0.3 V/SCE and $+1.5 \text{ V/SCE}$ (Fig. 2a). For this aqueous solution of pyrrole, the first scan showed the oxidation of pyrrole at $+1.25 \text{ V/SCE}$. Following scans showed the oxidation peak of polypyrrole at $+0.5 \text{ V/SCE}$ and the reduction peak of polypyrrole at about $+0.2 \text{ V/SCE}$. Moreover, the polymer film is a conductive one since the current remains constant during all the potential scans.

PPy films can also be formed at a constant potential. As in the case of polymer formation by potential scans, the films are homogeneous and very adherent to the substrate. From Fig. 2a, we chose to carry out the potentiostatic depositions at $+1.3 \text{ V/SCE}$. Fig. 2b shows the $I-t$ curves obtained for a fixed potential of $+1.3 \text{ V/SCE}$ and for a deposition time of 60 s. This chronoamperometric curve shows that, after an increase corresponding to the formation of pyrrole cation radicals, the current decreases following a linear relationship with $t^{-1/2}$. This behaviour indicates a diffusion-controlled process. This current response is due to the nucleation and growth of the polymer. At longer times, after the nucleation transient, the chronoamperometry shows a constant $I-t$ response for PPy.

3.2. XPS characterization of the polypyrrole films

Fig. 3a shows the XPS of the films obtained from the oxidation of an aqueous solution containing pyrrole and LiClO_4 since this technique is widely used to control the elemental composition of a solid film. The XPS analyses confirm the presence of PPy, incorporating ClO_4^- doping agents, on the platinum surfaces. Indeed, XPS spectra of polymer samples reveal the presence of C, N, O, Cl, Pt for all polymers. Thus, C_{1s} signal (Fig. 3b) can be fitted by five different carbon species at 284.0, 284.8, 286.1, 287.8 and 289.8 eV. The two components at the lowest binding energy relevant to β and α carbon atoms, respectively, revealed the first interesting finding. In fact, the comparison of these two carbon atoms areas showed that, following overoxidation, the β carbons in the film were less abundant than the α ones. This indicates, that the β positions were the ones involved in the polymer functionalization. The third peak at 286.1 eV is attributed to carbons of the polymer $\text{C}=\text{N}$ or $\text{C}-\text{N}^+$; the fourth one at 287.8 eV to $\text{C}=\text{N}^+$ carbons and the peak much weaker at 289.8 eV to carbonyl $\text{C}=\text{O}$ groups. The appearance of a $\text{C}=\text{O}$ component may be associated with the overoxidation of PPy at the β carbon site in the pyrrole rings. The N_{1s} spectra (Fig. 3c) indicate the presence of four peaks in the case of PPy. It contains a main signal at 399.6 eV which is characteristic of pyrrolylium nitrogens ($-\text{NH}-$ structure) and a high BE tail (BE = 400.4 and 402.0 eV) attributable to the positively charged nitrogen ($-\text{NH}^+$ (polaron) and $=\text{NH}^+$ (bipolaron)). The spectra also show a small contribution at 397.0 eV that we associate with $=\text{N}-$ structure. Fig. 3d represents the Cl_{2p} core-level XPS spectrum at 207.5 eV binding energy due to the perchlorate anions present in the film as a doping agent. Consequently, these XPS spectra confirm that polypyrrole films incorporating ClO_4^- doping agents are obtained from the oxidation of pyrrole in various solvents.

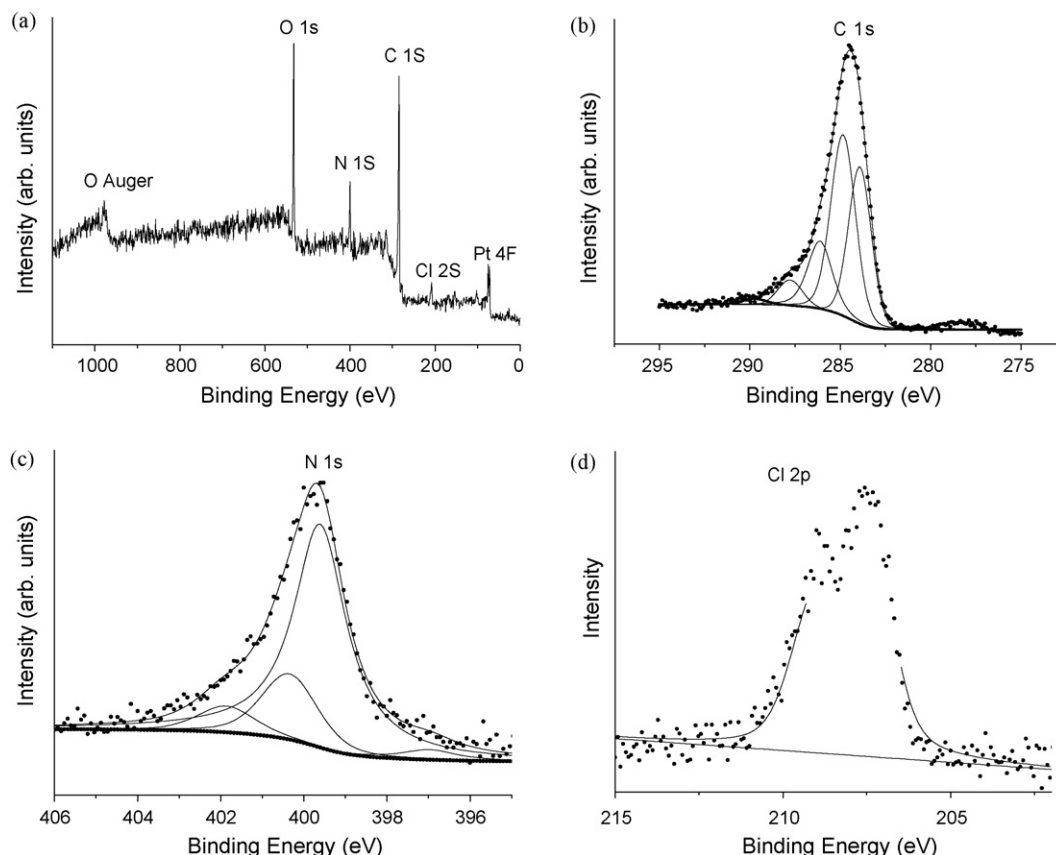


Fig. 3. Survey-scan XPS of polypyrrole films electro synthesized by oxidation of an aqueous solution of pyrrole and LiClO_4 (a). (b) C 1s (c) N 1s (d) Cl 2p XPS spectra of the same polypyrrole film.

3.3. Morphological characterization

Scanning electron microscopy was used to determine the surface morphology of the polypyrrole films on the microstructured electrode arrays but also to check that PPy films were deposited across the insulating gap on the microstructured electrode arrays. Thus, Fig. 4 shows that the whole surface of the platinum micro-electrodes is coated by a homogeneous and very compact film of polypyrrole composed of many nodules (1–2 μm long). The mean

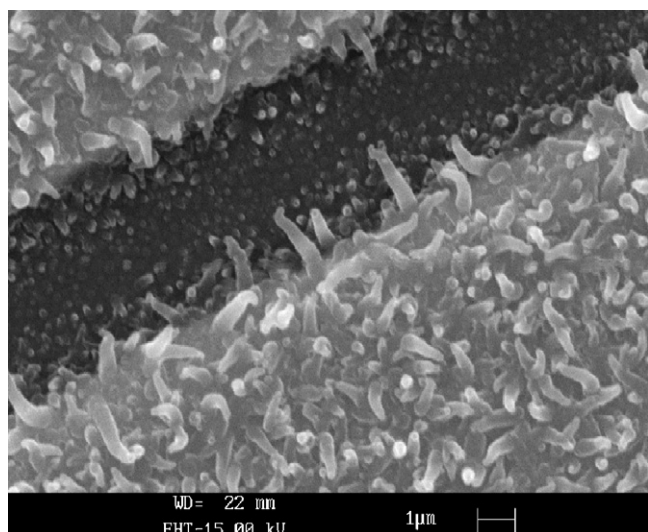


Fig. 4. SEM image of PPy film grown on the sensor surface.

film thickness of this polypyrrole film (x) was estimated to 2.25 μm from the electrical charge (q), associated with pyrrole oxidation by application of Faraday's law and assuming 100% current efficiency for polypyrrole formation: $x = qM/\rho AzF$, where M is the molar mass of the polymer, F is the Faraday constant, ρ is the density of the polymer and z is the number of electrons involved. The nominal density of the polypyrrole films (ρ) was taken as 1.5 g cm^{-3} and an electron loss z of 2.25 was considered.

More, Fig. 4 shows that nodules of PPy are also present in the insulating gap between the microelectrodes indicating that the growing film covers the insulated gap and connect microelectrodes. This point is important since the PPy layer must connect each pair of interdigitated electrodes in order to obtain the sensitive layer of the gas sensor.

3.4. Evaluation of the sensor's electrical signal under NH_3 flow

Firstly, the sensor was exposed to a NH_3 flow at a concentration equal to 500 ppm with a temperature of the sensitive layer near to room temperature. The signal's electrical variation was recorded versus time. Fig. 5a represents the evolution of the PPy's conductance in presence of ammonia and nitrogen. The curve shows the evolution of the electrical signal when the sensor is first stabilised under N_2 flow (until 300 s.), second exposed to NH_3 flow (from 300 s to 6000 s) and then to nitrogen flow (from 600 s to 14,000 s). This acquisition protocol was used for all the experiments described in this paper.

In presence of pollutant in the gas chamber (NH_3), we clearly notice a decrease in sensor's sensitive layer conductance. Ammonia reacts with the PPy and induces a modification of the sensor's sensitive layer electrical properties. After ammonia exposition, the

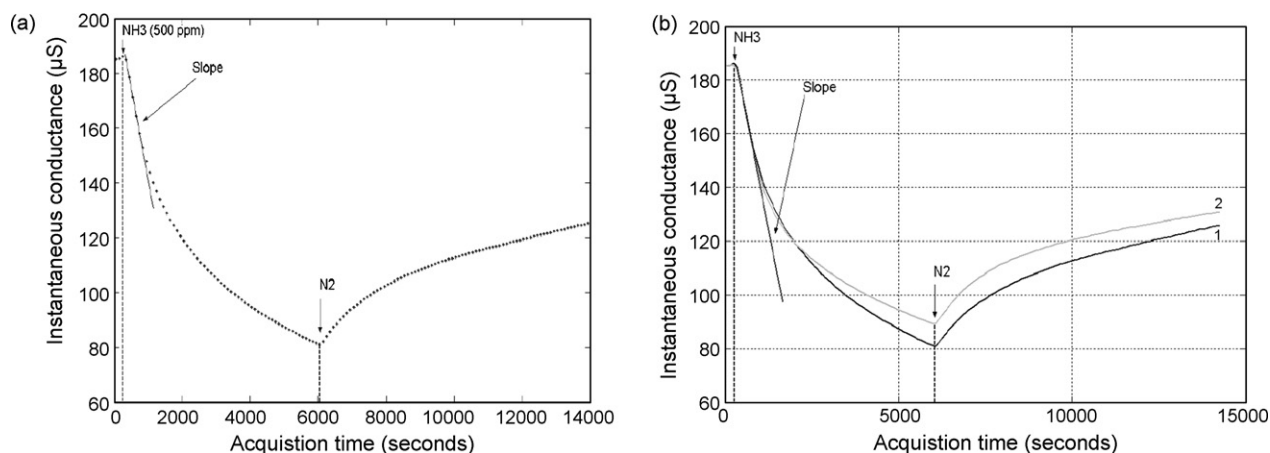


Fig. 5. Sensor's electrical response under NH_3 (500 ppm) and N_2 flow.

sensor is submitted to a nitrogen flow (after 6000 s). Fig. 5a indicates an increase of the sensor's conductance. This modification of conductance can be attributed to the desorption of ammonia from sensitive layer. Among to this electrical variation under NH_3 flow, it is possible to obtain one supplementary information. Looking at the beginning of the exposition to pollutant flow, the conductance variation is linear with time. In this way, the calculation of the slope value gives us information about the sensitivity of the gas sensor. For a concentration of ammonia equal to 500 ppm the value of the slope equals to 63.20 nS s^{-1} .

In order to evaluate a possible reproducibility of the gas sensor under ammonia flow at room temperature, we studied two successive electrical responses of the same gas sensor under pollutant. The purpose was to compare the sensor's conductance between two successive acquisitions. In Fig. 5b is represented the first electrical response obtained under a constant NH_3 flow and nitrogen flow. The second curve shows the successive response under NH_3 flow and N_2 flow after a nitrogen flow exposition of the sensitive layer during 12 h at room temperature. As shown in Fig. 5b, we notice a superposition of the signal under ammonia flow during the first minutes of acquisition. If we consider that the sensor's electrical response is measured by referring to experimental point obtained at the beginning of the exposition of the sensor, one can say that the electrical signal is reproducible with the same sensor at room temperature. The values of the slope are nearly the same (63.20 nS s^{-1} and 65.42 nS s^{-1}).

By comparing the two acquisitions (Fig. 5b curves 1 and 2), when the sensor is rinsed with nitrogen flow, the second electrical response is slightly shifted. This phenomenon is probably due to a

chemical modification of the sensitive surface after a first detection. This point will be confirmed with infrared analysis.

Various ammonia concentrations from 8 ppm to 1000 ppm were tested using the same sensor. Fig. 6a shows some of the electrical responses obtained for various ammonia concentrations. Before each pollutant expositions, the gas sensor is stabilised by nitrogen flow during 12 h at room temperature.

Fig. 6a shows a decrease of the instantaneous conductance for each NH_3 concentrations. This decrease depends on the concentrations of the pollutant in the gas chamber. In particular, if we determine the value of the slope of the electrical responses obtained for each ammonia concentrations, we can plot the variation of the slope versus ammonia concentrations. Fig. 6b represents the evolution of the slope versus the ammonia concentration. Above concentrations of 500 ppm, we noticed a smooth plate which was due to the saturation of the sensitive layer. For lower concentrations, there is a linear relationship between the value of the slope and the ammonia's concentration.

3.5. Influence of the sensitive layer's temperature on the sensor's electrical signal under NH_3 flow

Chemiresistors, based on metallic oxides, generally works at high temperatures (about 450°C) in order to optimize the electrical response. In order to evaluate the impact of temperatures on the electrical signal of the PPy-based gas sensor, the sensing layer was heated at temperatures ranging from 25°C to 100°C (Table 1). A concentration of ammonia equals to 500 ppm was used for this experiment. Curves show the evolution of the electrical signal when

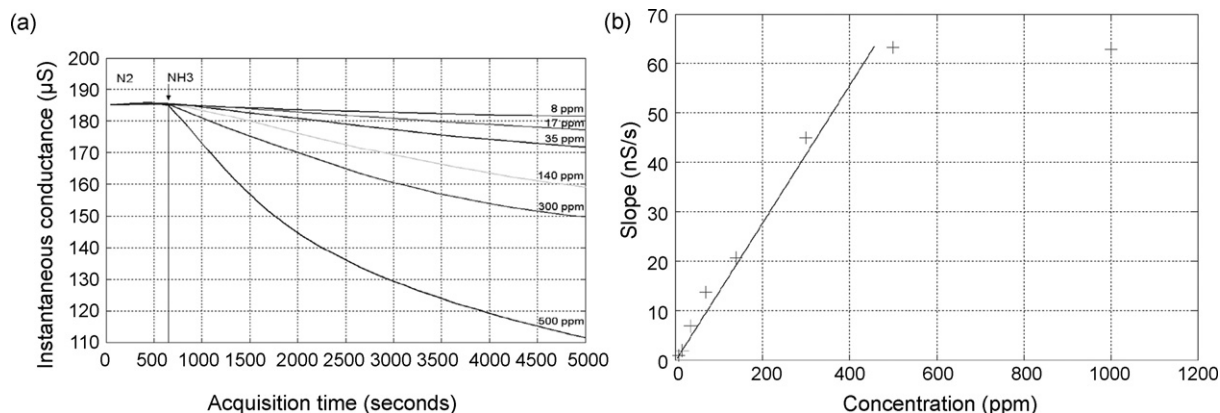


Fig. 6. Sensor's electrical responses to various ammonia concentrations (a). Slope of the gas sensor's electrical response vs. NH_3 concentrations (b).

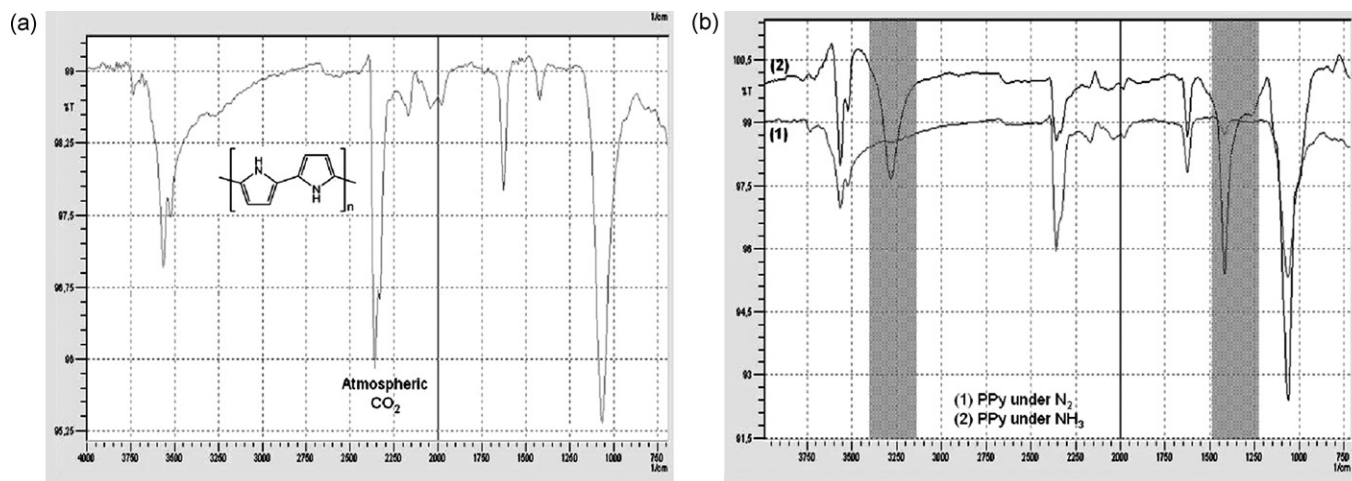


Fig. 7. Infrared spectra of polypyrrole powder before and after an exposition to ammonia flow for 1 h.

Table 1

Values of the slope under ammonia flow at different temperatures.

PPy's temperature (°C)	Slope (nS s ⁻¹)
25	116.72
50	72.29
75	74.04
100	78.57

the sensor is first stabilised under N₂ flow (until 400 s), second exposed to NH₃ flow (from 400 s to 1200 s) and then to nitrogen flow (from 1200 s to 3500 s).

Looking at Table 1 which represents the values of the slope for each temperature, we understand that an increase of the PPy's sensitive layer temperature decreases the sensitivity of the gas sensor.

The best sensitivity was obtained at room temperature. Consequently, in term of power consumption, the PPy-based gas sensor show very interesting detection properties compared to resistive sensors which have higher working temperatures (300–500 °C).

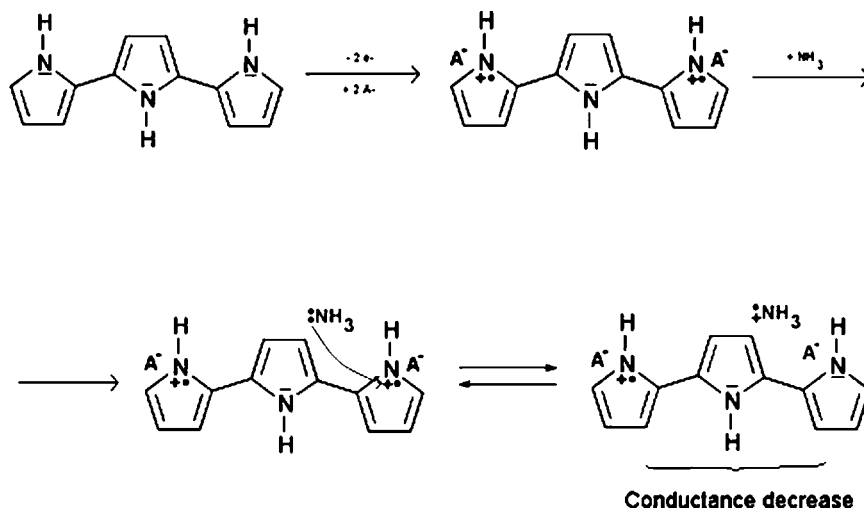
3.6. Interaction mechanism

In order to understand the interaction mechanism between ammonia and the gas sensor's sensitive surface we proceed to an infrared characterization of PPy powder before and after being exposed to NH₃ flow.

First we characterized the PPy powder unexposed to NH₃ vapors. The spectrum represented in Fig. 7a shows the presence of broad absorption bands characteristics of polypyrrole material. These absorption bands corresponds to: N–H stretching in secondary amine (3600 cm⁻¹), N–H deformation in secondary amine (1600 cm⁻¹), C=C aromatic stretching (1400 cm⁻¹) et C–N stretching (1050 cm⁻¹).

Then, in order to understand the mechanism of ammonia adsorption onto PPy surfaces, polypyrrole samples were exposed during 1 h to NH₃ 1000 ppm flow. The spectra obtained for this sample, compared to PPy under N₂, is represented in Fig. 7b. Compared to the PPy powder spectrum (Fig. 7a), two broad absorption bands appeared when PPy was exposed to NH₃ flow. The first one at 3260 cm⁻¹ may be attributed to the stretching vibration of N–H binding in NH₃⁺ radical group. The second one seems to be superposed to the C=C aromatic stretching band centered at 1400 cm⁻¹. This latter band may be attributed to N–H bending vibration. These results confirmed that the interaction between NH₃ and PPy-induced chemical modifications of the sensitive layer. These infrared analyses explained the shift observed between two successive NH₃ detections using PPy-based gas sensors.

According to the infrared results, we propose an interaction mechanism for the adsorption of ammonia onto polypyrrole thin films. The different stages of ammonia adsorption onto the PPy layer which is considered as a p-type semi-conducting material (positive hole conduction) are the following ones:



The first step of this mechanism is the loss of an electron by the doublet of nitrogen of some nitrogens of the polymer backbone. This electron transfer between ammonia molecule and the polymer's positive hole induces a diminution of the sensitive positive charge density which leads to a decrease in the conductance layer. After adsorption of NH_3 , the polymer becomes less conducting. In this mechanism, it is proposed that ammonia is adsorbed onto PPy surface forming $\text{NH}_3^{\cdot+}$ radical groups according to infra-red spectra. This mechanism is completing the various works realised on the ammonia detection studies using PPy-based gas sensors [40,41].

3.7. Comparison with other works

Before this study, other authors used conducting polymer films to develop gas sensors. These polymer films were obtained using different techniques. The most often used technique was the chemical deposition by dip-coating [42–45], and the others were: spin-coating from soluble conducting polymers [46,47], thermal evaporation by heating and deposition of the conducting polymer on a substrate [48], vapor deposition polymerization [49], drop-coating of a dried polymer solution [50,51], UV-photopolymerization [52], deposition of Langmuir–Blodgett film [53] and electrochemical deposition [54,55]. We decide to use this latter technique since the thickness of the film can be controlled by the total charge passed through the electrochemical cell during film growing process. Moreover, the film can be deposited on patterned microelectrode arrays [38]. However, if the insulating gap between the neighboring electrodes is close enough, the growing film can cover the insulated gap and connect electrodes [39].

Amongst the various polymer films, polypyrrole is one of the most studied and interesting in particular thanks to its high conductivity. Consequently, many papers have already used this polymer as active layer of gas sensors. Thus, PPy obtained by chemical oxidation was used for the detection of CO [56], CO_2 [57], xylene [58], alcohols [43,59,60] or acetone [61]. PPy obtained by vapor deposition polymerization was also used for the detection of methanol, ethanol, CCl_4 and benzene [62]. PPy obtained by UV-photopolymerization was used for the detection of sevoflurane [52]. It can also be noticed that the surfaces coated by PPy in all these studies were either gold microelectrode arrays deposited on alumina substrates [43,52,56,58,60] or ITO substrates [57,59,62]. Polypyrrole deposited by electrochemical way was also incorporated in gas sensors for the detection of ethanol gas [54], benzene, xylene and toluene [55].

Other studies focused on ammonia gas sensors using polypyrrole as sensitive layer. Thus, an ammonia gas sensor based on Langmuir–Blodgett PPy film was developed but its lower detectable limit was of 100 ppm of NH_3 in N_2 [53]. Bai et al. have electrochemically co-polymerized polypyrrole and sulfonated polyaniline on an ITO substrate to obtain an ammonia sensor but it was efficient only for ammonia concentration higher than 20 ppm [63]. Another study from Brie et al. presents an ammonia sensor using electro-synthesized PPy film, with various doping agents, but this study is limited to concentrations higher than 10 ppm [32]. Thus, only a study by Guernion et al. presented an ammonia sensor giving a response below 10 ppm but in this study PPy is chemically oxidized on a poly(etheretherketone) surface [64]. Concerning ammonia sensors using polymer films deposited on microelectrode arrays, an interesting work was carried out by Lin et al. [65]. In this work an electro-synthesized copolymer PPy–poly(vinyl alcohol) was used and was efficient for ammonia gas concentrations ranging from 50 ppm to 150 ppm. Consequently, the results obtained in our study are competitive with all these results since the ammonia gas sensors developed in this paper showed a detectable limit of 8 ppm

of NH_3 in N_2 . More, the best responses were obtained at room temperature and were reproducible.

4. Conclusion

The aim of this work was to validate the use of polypyrrole-based gas sensor for the detection of ammonia at concentrations lower than 10 ppm. From this study we first electro-synthesized PPy films doped with small anions ClO_4^- on metallic electrodes to develop a chemical resistor gas sensor. A homogeneous polymer deposited film with a thickness close to the micrometer was obtained. The various tests conducted under ammonia flow showed an interesting sensitivity (lower than 10 ppm) and a good reproductibility. By comparison with most of chemiresistors gas sensors, our PPy-based sensor presents best sensitivity at room temperature.

References

- [1] J. Albuquerque, L. Mattoso, D. Balogh, R. Faria, J. Masters, A.G. MacDiarmid, *Synth. Met.* 113 (2000) 19.
- [2] H.K. Song, B. Toste, K. Ahmann, D. Hoffman-Kim, G.T.R. Palmore, *Biomaterials* 27 (2006) 473.
- [3] W.R. Stauffer, X.T. Cui, *Biomaterials* 27 (2006) 2405.
- [4] C.D. Dimitrakopoulos, P.R.L. Malenfant, *Adv. Mater.* 14 (2002) 99.
- [5] R. Poddar, C. Luo, *Solid-State Electron.* 50 (2006) 1681.
- [6] H.E.A. Huitema, G.H. Gelinck, J.B.P.H. van der Putten, K.E. Kuijk, C.M. Hart, E. Cantatore, P.T. Herwig, A.J.J.M. van Breemen, D.M. de Leeuw, *Nature* 414 (2001) 599.
- [7] A. Kraft, A.C. Grimsdale, A.B. Holmes (Eds.), *Angew. Chem. Int.* 37 (1998) 402.
- [8] W.U. Huynh, J.J. Dittmer, A.P. Alivisatos, *Science* 295 (2002) 2425.
- [9] B. Sun, E. Marx, N.C. Greenham, *Nano Lett.* 3 (2003) 961.
- [10] G. Yu, J. Gao, J.C. Hummelen, F. Wudl, A.J. Heeger, *Science* 270 (1995) 1789.
- [11] A.A. Argun, A. Cirpan, J.R. Reynolds, *Adv. Mater.* 15 (2003) 1338.
- [12] R. DeLongchamp, P.T. Hammond, *Adv. Mater.* 13 (2001) 1455.
- [13] B. Crone, A. Dodabalapur, Y.Y. Lin, R.W. Filas, Z. Bao, A. LaDuca, R. Sarpeshkar, H.E. Katz, W. Li, *Nature* 403 (2000) 521.
- [14] C.J. Drury, C.M.J. Mutsaers, C.M. Hart, M. Matters, D.M. de Leeuw, *Appl. Phys. Lett.* 73 (1998) 108.
- [15] H.K. Kim, M.S. Kim, S.Y. Chun, Y.H. Park, B.S. Jeon, J.Y. Lee, Y.K. Hong, J. Joo, S.H. Kim, *Mol. Cryst. Liq. Cryst.* 405 (2003) 161.
- [16] M. Hughes, M.S.P. Shaffer, A.C. Renouf, C. Singh, G.Z. Chen, D.J. Fray, A.H. Windle, *Adv. Mater.* 14 (2002) 382.
- [17] S.U. Rahman, M.A. Abul-Hamayel, B.J. Abdul Aleem, *Surf. Coat. Technol.* 200 (2006) 2948.
- [18] C.M. Li, C.Q. Sun, W. Chen, L. Pan, *Surf. Coat. Technol.* 198 (2005) 474.
- [19] J.W. Gardner, P.N. Bartlett, *Sens. Actuators A* 51 (1995) 57.
- [20] T. Zama, S. Hara, W. Takashima, K. Kaneto, *Bull. Chem. Soc., Jpn.* 78 (2005) 506.
- [21] A. Mazzoldi, A. Della Santa, D.E. De Rossi, *Polymer Sensors and Actuators*, Springer-Verlag (Ed.), Heidelberg, 1999, pp. 207–244.
- [22] C. Hagleitner, A. Hierlemann, D. Lange, A. Kummer, N. Kerness, O. Brand, H. Baltes, *Nature* 414 (2001) 293.
- [23] G. Chen, Z. Guan, C.T. Chen, L. Fu, V. Sundaresan, F.H. Arnold, *Nat. Biotechnol.* 15 (1997) 354.
- [24] U. Lange, N.V. Roznyatovskaya, V.M. Mirsky, *Anal. Chim. Acta* 614 (2008) 1.
- [25] B. Lakard, O. Segut, S. Lakard, G. Herlem, T. Gharbi, *Sens. Actuators B* 122 (2007) 101.
- [26] S. Lakard, G. Herlem, N. Valles-Villareal, G. Michel, A. Propper, T. Gharbi, B. Fahys, *Biosens. Bioelectron.* 20 (2005) 1946.
- [27] O. Segut, B. Lakard, G. Herlem, J.Y. Rauch, J.C. Jeannot, L. Robert, B. Fahys, *Anal. Chim. Acta* 597 (2007) 313.
- [28] L. Torsi, M. Pezzuto, P. Siciliano, R. Rella, L. Sabbatini, L. Valli, P.G. Zambonin, *Sens. Actuators B* 48 (1998) 362.
- [29] R. Gangopadhyay, A. De, *Sens. Actuators B* 77 (2001) 326.
- [30] J. Janata, M. Josowicz, *Nat. Mater.* 2 (2003) 19.
- [31] A.C. Partridge, P. Harris, M.K. Andrews, *Analyst* 121 (1996) 1349.
- [32] M. Brie, R. Turcu, C. Neamtu, S. Pruneanu, *Sens. Actuators B* 37 (1996) 119.
- [33] M. Matsuguchi, J. Ito, G. Sugiyama, Y. Sakai, *Synth. Met.* 128 (2002) 15.
- [34] J.M. Slater, E.J. Watt, N.J. Freeman, I.P. May, D.J. Weir, *Analyst* 117 (1992) 1265.
- [35] J.W. Gardner, M. Vidic, P. Ingleby, A.C. Pike, J.E. Brignell, P. Scivier, P.N. Bartlett, A.J. Duke, J.M. Elliott, *Sens. Actuators B* 48 (1998) 289.
- [36] P. Ingleby, J.W. Gardner, P.N. Bartlett, *Sens. Actuators B* 57 (1999) 17.
- [37] M. Gross, D. Müller, H.G. Nothofer, U. Scherf, D. Neher, C. Bräuchle, K. Meerholz, *Nature* 405 (2000) 661.
- [38] G.W. Lu, L.T. Qu, G.Q. Shi, *Electrochim. Acta* 51 (2005) 340.
- [39] J. Reemts, J. Parisi, D. Schlettwein, *Thin Solid Films* 466 (2004) 320.
- [40] H. Bai, G. Shi, *Sensors* 7 (2007) 267.
- [41] I. Lähdesmäki, W.K. Kubiak, A. Lewenstam, A. Ivaska, *Talanta* 52 (2000) 269.
- [42] S.T. McGovern, G.M. Spinks, G.G. Wallace, *Sens. Actuators B* 107 (2005) 657.

- [43] J.H. Cho, J.B. Yu, J.S. Kim, S.O. Sohn, D.D. Lee, J.S. Huh, *Sens. Actuators B* 108 (2005) 389.
- [44] S. Brady, K.T. Lau, W. Megill, G.G. Wallace, D. Diamond, *Synth. Met.* 154 (2005) 25.
- [45] M.S. Silverstein, H.W. Tai, A. Sergienko, Y.L. Lumelsky, S. Pavlovsky, *Polymer* 46 (2005) 6682.
- [46] G.K. Prasad, T.P. Radhakrishnan, D.S. Kumar, M.G. Krishna, *Sens. Actuators B* 106 (2005) 626.
- [47] R. Tongpool, S. Yoriya, *Thin Solid Films* 477 (2005) 148.
- [48] N.E. Agbor, M.C. Petty, A.P. Monkman, *Sens. Actuators B* 28 (1995) 173.
- [49] E. Stussi, S. Cella, G. Serra, G.S. Venier, *Mater. Sci. Eng. C* 4 (1996) 27.
- [50] L. Ruangchuay, A. Sirivat, J. Schwank, *React. Funct. Polym.* 61 (2004) 11.
- [51] H.G.O. Sandberg, T.G. Backlund, R. Osterbacka, S. Jussila, T. Makela, H. Stubb, *Synth. Met.* 155 (2005) 662.
- [52] R.J. Wu, Y.C. Huang, M. Chavali, T.H. Lin, S.L. Hung, H.N. Luk, *Sens. Actuators B* 126 (2007) 387.
- [53] M. Penza, E. Milella, M.B. Alba, A. Quirini, L. Vasanelli, *Sens. Actuators B* 40 (1997) 205.
- [54] Q. Fang, D.G. Chetwynd, J.A. Covington, C.S. Toh, J.W. Gardner, *Sens. Actuators B* 84 (2002) 66.
- [55] J.N. Barisci, G.G. Wallace, M.K. Andrews, A.C. Partridge, P.D. Harris, *Sens. Actuators B* 84 (2002) 252.
- [56] S. Radhakrishnan, S. Paul, *Sens. Actuators B* 125 (2007) 60.
- [57] S.A. Waghuley, S.M. Yenorkar, S.S. Yawale, S.P. Yawale, *Sens. Actuators B* 128 (2008) 366.
- [58] C.W. Lin, Y.L. Liu, R. Thangamuthu, *Sens. Actuators B* 94 (2003) 36.
- [59] J.E.G. de Souza, F.L. dos Santos, B.B. Neto, C.G. dos Santos, M.V.B. dos Santos, C.P. de Melo, *Sens. Actuators B* 88 (2003) 246.
- [60] H.K. Jun, Y.S. Hoh, B.S. Lee, S.T. Lee, J.O. Lim, D.D. Lee, J.S. Huh, *Sens. Actuators B* 96 (2003) 576.
- [61] J.B. Yu, H.G. Byun, M.S. So, J.S. Huh, *Sens. Actuators B* 108 (2005) 305.
- [62] C.P. de Melo, B.B. Neto, E.G. de Lima, L.F.B. de Lira, J.E.G. de Souza, *Sens. Actuators B* 109 (2005) 348.
- [63] H. Bai, Q. Chen, C. Li, C. Lu, G. Shi, *Polymer* 48 (2007) 4015.
- [64] N. Guernion, R.J. Ewen, K. Pihlainen, N.M. Ratcliffe, G.C. Teare, *Synth. Met.* 126 (2002) 301.
- [65] C.W. Lin, B.J. Hwang, C.R. Lee, *Mater. Chem. Phys.* 58 (1999) 114.



Direct electrochemistry of cytochrome *c* on a phosphonic acid terminated self-assembled monolayers

Yu Chen^a, Xiao-Jing Yang^a, Li-Rong Guo^a, Bo Jin^b, Xing-Hua Xia^{b,*}, Li-Min Zheng^{a,*}

^a State Key Laboratory of Coordination Chemistry, Coordination Chemistry Institute, School of Chemistry and Chemical Engineering, Nanjing University, 22 Hankou Road, Nanjing 210093, PR China

^b Key Laboratory of Analytical Chemistry for Life Science, School of Chemistry and Chemical Engineering, Nanjing University, 22 Hankou Road, Nanjing 210093, PR China

ARTICLE INFO

Article history:

Received 6 August 2008

Received in revised form 5 November 2008

Accepted 5 November 2008

Available online 13 November 2008

Keywords:

Immobilization

Electrochemistry

Self-assembled monolayers

Cytochrome *c*

Direct electron transfer

ABSTRACT

The direct electrochemistry of cytochrome *c* (cyt *c*) on a gold electrode modified with 3-mercaptopropylphosphonic acid [HS-(CH₂)₃-PO₃H₂, MPPA] self-assembled monolayers (SAMs) was for the first time investigated. Electrochemical measurements and surface-enhanced infrared absorption spectroscopic reveal that the adsorption kinetics of cyt *c* on the MPPA-SAMs is very fast (saturation adsorption is completed within 5 s) and the immobilized cyt *c* molecules retain their native secondary protein structure. The nature of interaction between cyt *c* and -PO₃H₂ groups is mainly the electrostatic interaction. The direct electrochemistry of the immobilized cyt *c* on the -PO₃H₂ terminated SAMs with short chain is nearly reversible. Its formal potential ($E^{0'}$ = 18 ± 3 mV vs. SCE) is very close to that of cyt *c* in an aqueous solution ($E^{0'}$ = 18–22 mV vs. SCE). In addition, the electron transfer rate of cyt *c* immobilized on -PO₃H₂ terminated SAMs is relatively slow as compared to -SO₃H and -COOH terminated SAMs, indicating excess negative charge density on the SAMs surface will decrease the electron transfer rate of cyt *c*.

© 2008 Elsevier B.V. All rights reserved.

1. Introduction

Among the electroactive proteins, cytochrome *c* (cyt *c*) is usually used as a model system to study the direct electron transfer. Particularly, the direct electrochemistry of cyt *c* immobilized on metals coated with monolayers of organic molecules has attracted extensive attentions of several groups over the past few years, because these simple systems allow for a systematic study of the parameters that control the electron transfer kinetics. Self-assembled monolayers (SAMs) with -COOH [1] and -SO₃H [2] terminated thiolates, which provide a negatively charged surface for cyt *c* adsorption, have been extensively study to understand the electron transfer properties of electrostatically complexed cyt *c* and draw analogies to its physiological redox partners. As another very important anion (i.e. -PO₃H₂) terminated SAMs, there is no formal report on the electron transfer of cyt *c* although Murgida and his co-workers repetitiously proposed that electron transfer of cyt *c* on a Ag electrode modified with -PO₃H₂ terminated thiolates with long carbon chains can hardly occur [3,4].

Phosphate is an essential component in biologic system due to its pervasive existence in organs and tissues, such as cell membranes, bones and body fluids. For example, a lipid bilayer

membrane is composed of phospholipids containing various phosphate head groups. Based on the biomimetic concepts, the phosphate and phosphonate terminated SAMs have been studied. Tanahashi and Matsuda [5] reported that the negative charged functionalities strongly induced apatite formation on a -PO₃H₂ interface. Lin and co-workers [6] found that the ionic -PO₃H₂ surface exhibited a lower platelet reactivity than the -COOH. These studies show that the -PO₃H₂ groups play very important roles in biological systems.

In the present work, we for the first time study the immobilization of cyt *c* on a -PO₃H₂ terminated SAMs on an Au substrate. Electrochemical impedance spectroscopy and X-ray photoelectron spectroscopy (XPS) were used to characterize the immobilization of -PO₃H₂ functional interface on the gold electrode. Surface-enhanced infrared absorption spectroscopy (SEIRAS) affirms that the cyt *c* immobilized on MPPA-SAMs retain their native secondary protein structure. Voltammetry was used to understand the interaction between cyt *c* and surface-immobilized -PO₃H₂ groups, and the direct electron transfer behavior of the cyt *c* molecules immobilized on the -PO₃H₂ terminated SAMs.

2. Experimental

2.1. Materials

All the chemicals were of analytical grade (AR) and used without further purification. Cytochrome *c* from a horse heart

* Corresponding authors. Fax: +86 25 83314502.

E-mail addresses: xhxia@nju.edu.cn (X.-H. Xia), lmzheng@nju.edu.cn (L.-M. Zheng).

(type VI) was purchased from Sigma–Aldrich (St. Louis, USA). 11-Mercaptoundecanylphosphonic acid [$\text{HS}-(\text{CH}_2)_{11}-\text{PO}_3\text{H}_2$, MUPA] was synthesized according to the process reported in the literature [7]. 3-Mercaptopropylphosphonic acid [$\text{HS}-(\text{CH}_2)_3-\text{PO}_3\text{H}_2$, MPPA] was prepared according to the modified procedure by using 3-bromopropylene as the starting material [7].

2.2. Preparation of MPPA/Au electrode

After the Au electrode (CHI, 2 mm in diameter) was pretreated by the oxidation/reduction cycling in the potential region of hydrogen and oxygen evolution in a 0.5 M H_2SO_4 solution at a scan rate of 100 mV/s, it was immersed in a 4 mM MPPA solution in the dark for 24 h, followed by thoroughly rinsing with Millipore water, 0.1 M KOH, 0.1 M HClO_4 and Millipore water, consecutively. The process ensures the formation of a monolayer of MPPA on the gold electrode.

2.3. Immobilization of Cyt c

Immobilization of cyt c on the MPPA/Au electrodes was accomplished by immersing the MPPA/Au electrodes in a low-ionic-strength phosphate buffer containing cyt c (PBS, 10 mM, pH 7.0, $\sim 15 \mu\text{M}$ cyt c) at 4 °C for 30 min. After the cyt/MPPA/Au electrodes were rinsed with 10 mM PBS (pH 7.0), electrochemical measurements were carried out in 10 mM PBS (pH 7.0) without cyt c.

2.4. Apparatus

The cyclic voltammetry (CV) and electrochemical impedances spectroscopy (EIS) measurements were performed on a CHI 660 C electrochemical workstation (CH Instruments, Shanghai Chenghua Co.). A Pt plate auxiliary electrode and a saturated calomel reference electrode (SCE) were used. All potentials refer to the SCE. The modified Au electrodes were used as the working electrode. The electrolyte was purged with high purity nitrogen for at least 10 min prior to each measurement to remove the dissolved oxygen. Then, the electrochemical cell was kept under nitrogen atmosphere throughout the experiments. The EIS data were approximated using electronic equivalent circuits. For this purpose, ZView impedance software was employed. The impedance spectra were plotted in the form of complex plane diagrams (Nyquist plots). All measurements were performed at room temperature.

X-ray photoelectron spectroscopy (XPS) measurements were carried out on a Thermo VG Scientific ESCALAB 250 spectrometer using a monochromatic Al $\text{K}\alpha$ X-ray source (1486.6 eV photons). A Bruker Tensor 27 FT-IR spectrometer (Bruker, Germany) equipped with a liquid nitrogen cooled mercury–cadmium–telluride (MCT)

detector was used for surface-enhanced infrared absorption spectroscopy (SEIRAS) measurements. A gold film with nanostructures was deposited on the flat surface of a non-doped single reflection silicon (Si) hemispherical prism (180 mm radius) by a chemical deposition technique [8]. The MPPA-modified gold/Si was prepared using the same procedure as MPPA/Au. A reference spectrum of the MPPA-modified gold/Si in a 10 mM PBS (pH 7.0) was recorded in the absence of cyt c. After cyt c was added to the cell about 30 min, a sample spectrum of the cyt c was recorded. Spectra were averaged over 128 scans with a resolution of 4 cm^{-1} .

3. Results and discussion

3.1. XPS characterization of MPPA/Au electrode

XPS was used to monitor the characteristic elements of the assembled electrode surface and to confirm the successful formation of the S–Au bond. Fig. 1a presents the XPS spectra of the MPPA/Au in the $\text{S}_{(2p)}$ region. An asymmetric peak that can be fitted as a spin doublet at 162.0 and 163.2 eV is observed, which corresponds to the $\text{S}_{2p_{3/2}}$ and $\text{S}_{2p_{1/2}}$ peaks, in agreement with the reported values for the thiolates SAMs systems on a gold surface [6]. XPS scan of the $\text{P}_{(2p)}$ region shows a peak that is fitted as a spin doublet at 133.4 and 134.3 eV (Fig. 1b), corresponding to $\text{P}_{2p_{3/2}}$ and $\text{P}_{2p_{1/2}}$, respectively. The XPS spectra of the $\text{S}_{(2p)}$ and $\text{P}_{(2p)}$ indicate the formation of MPPA-SAMs on the gold surface. In the proposed SAMs structure, the $-\text{PO}_3\text{H}_2$ groups reside on the top-most layer of the SAMs whereas the sulfur atom is bound to the Au substrate.

3.2. Modification process of the gold electrode

Fig. 2 shows the Nyquist plots of a bare Au and MPPA/Au electrode using $\text{Fe}(\text{CN})_6^{3-/4-}$ as electrochemical probe. The electrochemical impedance spectra were collected at the formal potential (0.215 V) of the electrochemical probe in a frequency range of 1 Hz to 100 kHz with an ac amplitude of 5 mV. The charge transfer resistance (R_{ct}) of the bare Au electrode (Fig. 2a) is estimated as 9.5 k Ω . The R_{ct} increases to 52 k Ω when the gold electrode is covered by a monolayer of MPPA (MPPA/Au) (Fig. 2b). It further decreases to 25 k Ω when cyt c was immobilized on the MPPA/Au electrode (Fig. 2c). This result indicates that the cyt c was successfully immobilized on the surface of MPPA/Au electrode, resulting in the decrease of surface negative charges of MPPA-SAMs [9].

Surface-enhanced infrared absorption spectroscopy provides a sensitive means to observe the minute change of a protein at a gold surface at the molecular level [10]. It is generally accepted that the shape and position of the amide I and II infrared absorbance bands of proteins could provide detailed information on the secondary

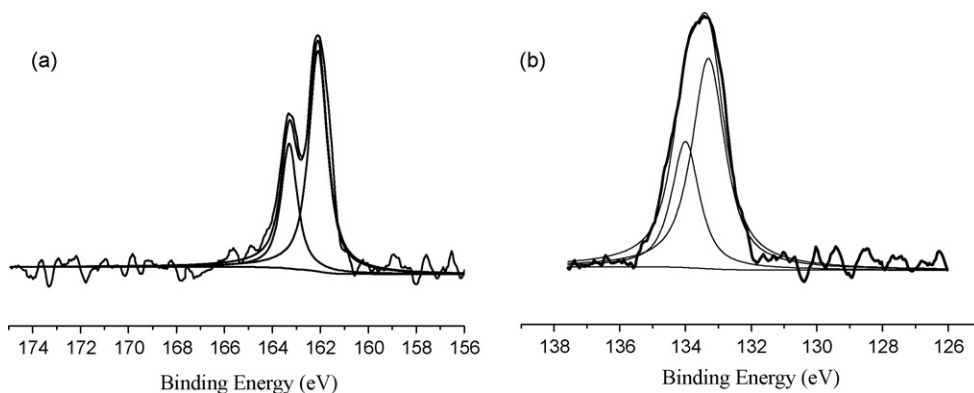


Fig. 1. XPS spectra of the MPPA/Au in the (a) $\text{S}_{(2p)}$ and (b) $\text{P}_{(2p)}$ region.

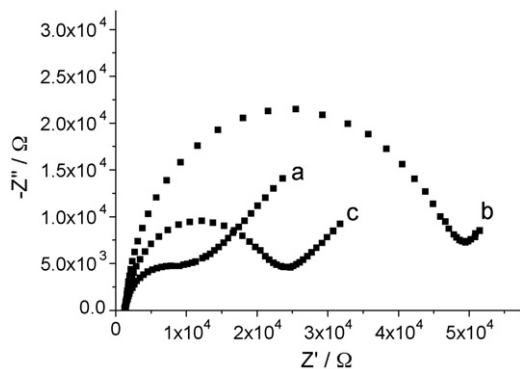


Fig. 2. Nyquist plots of (a) bare Au, (b) MPPA/Au and (c) cyt/MPPA/Au electrodes collected at 0.215 V in a frequency range of 1 Hz to 100 kHz with an ac amplitude of 5 mV from a solution of 1 mM $\text{Fe}(\text{CN})_6^{3-/4-}$ in 10 mM PBS (pH 7.0). Electrode area: 0.0736 cm^2 .

structure of the polypeptide chain [11]. As shown in Fig. 3, the shape and position of amide I and amide II bands of the cyt c immobilized on the MPPA-SAMs (1656.6 and 1548.6 cm^{-1}) are nearly the same as those of native cyt c (1656.6 and 1548.6 cm^{-1}). If cyt c is denatured, the shape of amide I and II bands will significantly change or even disappear. Similarities of the spectra of free cyt c and adsorbed cyt c in Fig. 3 indicate that the immobilized cyt c molecules retain their native secondary protein structure.

3.3. Electrochemistry of the cyt/MPPA/Au electrode

It is well known that the redox potential for unfolded cyt c species locates below -0.4 V (vs. SCE) [12]. To observe the state of cyt c immobilized on MPPA-SAMs, a larger potential range from 0.25 to -0.5 V was chosen. As shown in Fig. 4, curve a (dotted curve), the cyclic voltammogram (CVs) of a MPPA/Au electrode in 10 mM PBS (pH 7.0) at a scan rate of 100 mV/s shows a pair of peaks with the midpoint potential [$E^0 = (E_{\text{pa}} + E_{\text{pc}})/2$] of -335 mV , which could be attributed to the electric-field-induced protonation/deprotonation peak of $-\text{PO}_3\text{H}_2$ groups in the MPPA-SAM as in the case of $-\text{COOH}$ terminated SAMs [13,14]. When cyt c was assembled on this MPPA/Au electrode, the CV (Fig. 4, solid curve b) shows an additional pair of well-defined and nearly reversible redox peaks ($E^0 = 18 \pm 3\text{ mV}$, $\Delta E_p = 35 \pm 5\text{ mV}$, $i_{\text{pa}} \approx i_{\text{pc}}$) besides the protonation/deprotonation peak of $-\text{PO}_3\text{H}_2$ groups in MPPA-SAMs, which is the characteristics of the $\text{Fe}(\text{III})/\text{Fe}(\text{II})$ redox couple. Compared with the CV of MPPA/Au electrode, no redox peak of unfolded cyt c species was observed on the cyt/MPPA/Au electrode [12]. Com-

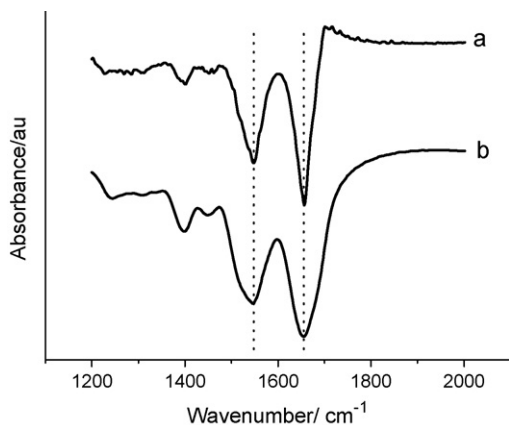


Fig. 3. (a) Surface-enhanced infrared absorption spectrum of cyt c immobilized on the MPPA-SAMs and (b) absorption infrared (IR) spectrum of free cyt c.

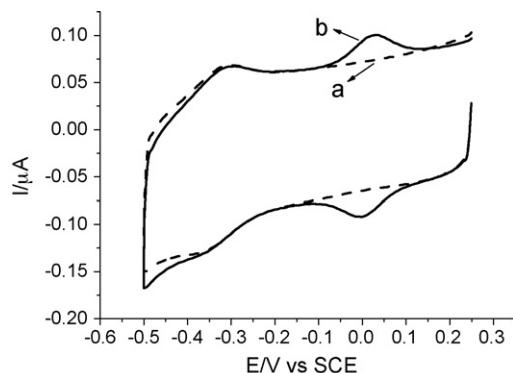


Fig. 4. Cyclic voltammograms for (a) MPPA/Au and (b) cyt/MPPA/Au electrodes in a 10 mM PBS (pH 7.0) at a scan rate of 100 mV/s.

pared with results of infrared spectroscopy in Fig. 3, it leads us to conclude that the adsorbed cyt c molecule remains its native structure. In addition, the peak current and position do not change within 500 times continuous potential scans in the potential range of 0.25 to -0.25 V , demonstrating that the electrochemistry of the cyt c is very stable.

To understand the nature of the interaction between cyt c and $-\text{PO}_3\text{H}_2$ groups, the cyt/MPPA/Au electrode was immersed in a 1.0 M KCl solution for 3 min. This immersion process resulted in disappearance of the electrochemical signal of cyt/MPPA/Au electrode in 10 mM PBS (pH 7.0), which suggests that the electrostatic interaction between the monolayer of MPPA and the cyt c occurs [12,15]. It should be noted that the decrease in current upon 1.0 M KCl exposure should be attributed to the desorption but not denaturation of the adsorbed cyt c. Herein, after the cyt/MPPA/Au electrode treated with 1 M KCl solution is re-immersed in cyt c solution, and the resulted cyt/MPPA/Au electrode gives the same electrochemical characteristics as in Fig. 4, curve b in 10 mM PBS (pH 7.0).

It is generally observed that immobilization of cyt c on electrodes with anionic surfaces causes a shift in the formal potential (E^0) [2,16,17], as compared to the native cyt c in solution ($E^0 = 18\text{--}22\text{ mV}$ vs. SCE) [1,2,16], because the ferric form of the cyt c binds more strongly than its ferrous form [18,19]. However, the formal potential of the cyt c immobilized on MPPA/Au electrode is very close to the one of cyt c in an aqueous solution, indicating that the Gibbs energies for the adsorption of the ferric and ferrous forms of cyt c at the $-\text{PO}_3\text{H}_2$ terminated SAMs are very similar.

The surface pK_a value of mercaptopropionic acid-SAMs is 8.0 [20], therefore, each carboxyl group on the mercaptopropionic acid-SAMs is partly dissociated in the neutral aqueous solution. For comparison, the sulfonic acid groups on the 2-mercaptoethanesulfonate-SAMs are fully dissociated in the neutral aqueous solution [2]. Recently, the apparent pK_{a1} and pK_{a2} values of 11-mercaptopundecanylphosphonic acid-SAMs on a gold surface were estimated to be 4.5 and 8.4 using chemical force microscopy [21]. It is well known that the acidity of the acid-terminated SAMs on gold electrodes increases with the decrease of carbon chain. Therefore, the pK_{a1} and pK_{a2} values of MPPA-SAMs are certainly smaller than 4.5 and 8.4, respectively, which demonstrates that the MPPA-SAMs should be negatively charged in the neutral aqueous solution, i.e., the first $-\text{OH}$ of the phosphonic acid group in the MPPA-SAMs may be expected to deprotonate completely, while the second $-\text{OH}$ of the phosphonic acid group dissociates partially. Every phosphonic acid group in MPPA-SAMs should possess more than one unit negative charges in the neutral solution. Thus, the order of the surface negative charge density for three SAMs is MPPA-SAMs > 2-mercaptoethanesulfonate-SAMs > 3-mercaptoethanesulfonate-SAMs. However, the formal potential of cyt c immobilized on the MPPA, 2-mercaptoethanesulfonate [2] and 3-

mercaptopropionic acid [17] SAMs consecutively decreases (18, 9 and -16 mV vs. SCE, respectively). Thus, the present results provide evidence that the value of formal potential shift is not simply proportional to the surface negative charge density of SAMs, implying that influence of the type of anion in SAMs should be considered as well.

On the other hand, an interesting phenomenon is observed. After the MPPA/Au electrode is immersed in a cyt *c* solution for 5 s, the cyclic voltammogram of the cyt/MPPA/Au electrode obtained is identical to that of the present cyt/MPPA/Au electrode (i.e., adsorption time of 30 min), indicating the adsorption kinetics of cyt *c* on the MPPA-SAMs is very fast (data not shown). Obviously, the adsorption kinetics of cyt *c* on MPPA-SAMs is much faster than that of cyt *c* on 3-mercaptopropionic acid-SAMs (the cyt *c* monolayer adsorption is accomplished within the 30 min) [10], in term of Coulomb's law, which is probably due to fact that the high negative charge density of MPPA-SAMs accelerates the adsorption of cyt *c* with positive charge due to strong electrostatic interaction.

3.4. Charge transfer rate constant of cyt *c* on MPPA/Au electrode

A typical data set is shown in Fig. 5 for the cyt *c* on a MPPA/Au electrode at 25 °C at different scan rate (from 20 to 1000 mV/s). With the increase of scan rate, the formal potential (E^0) of the immobilized cyt *c* is almost unchanged, while the anodic and cathodic currents increase linearly (Fig. 5a and b), showing a surface-controlled electrode process. According to the slope of the I_p - v curve of $I_p = n^2 F^2 v \Gamma A / 4RT$ [22], the average surface coverage (Γ) of the electroactive cyt *c* immobilized on MPPA/Au electrode was estimated to be 1.9×10^{-12} mol/cm², which is much lower than the theoretical monolayer coverage of electroactive cyt *c* (13×10^{-12} mol/cm²) [23]. Kakiuchi and co-workers [2] have reported that the surface coverage of electroactive cyt *c* immobilized on 2-mercaptoethanesulfonate SAMs was lower than that of mercaptopropionic acid SAMs due to the effect of surface charges. Similarly, the MPPA-SAMs possessing higher surface charges than the 2-mercaptoethanesulfonate SAMs may result in lower surface coverage of electroactive cyt *c*.

From the peak-to-peak separation in Fig. 5c, the direct electron transfer rate constant (k_s) was determined based on the Laviron's equation [22]. Assuming the charge-transfer coefficient $\alpha = 0.5$ and the number of electrons ($n = 1$) for a one electron transfer process, the electron-transfer rate constant was calculated to be $k_s = 8.0 \pm 2 \text{ s}^{-1}$. It is clear that the value ($8.0 \pm 2 \text{ s}^{-1}$) is much lower than that of the cyt *c* immobilized on a $-\text{SO}_3\text{H}$ terminated [2] and a $-\text{COOH}$ terminated SAMs [2,24,25] with short carbon chains. For example, k_s values of cyt *c* immobilized on SAMs of 2-mercaptoethanesulfonate (MES) and mercaptopropionic acid (MPA) are $100 \pm 15 \text{ s}^{-1}$ and $1450 \pm 210 \text{ s}^{-1}$. Obviously, the order of k_s values of cyt *c* on three SAMs is $k_{s\text{MPPA}} (8.0 \pm 2 \text{ s}^{-1}) \ll k_{s\text{MES}} (100 \pm 15 \text{ s}^{-1}) \ll k_{s\text{MPA}} (1450 \pm 210 \text{ s}^{-1})$. It has been reported that the k_s value of cyt *c* adsorbed on the $-\text{COOH}$ terminated SAMs decreases with the increase of pH because the surface negative charge density of SAMs increases as solution pH increases [23,26]. In addition, it is worth noting that the order of the surface negative charge density for the three SAMs is MPPA-SAMs > MES-SAMs > MPA-SAMs. Thus, those facts suggest that the high negative charge density on the SAMs surface appears to deteriorate the electron transfer rate between cyt *c* and electrode. A gated mechanism indicates that the electron transfer rate of cyt *c* is nearly distance and overpotential independent at SAMs with short carbon chains ($C_n < 9$), in which the rearrangement of cyt *c* from the stable binding orientation to the orientation optimal for efficient electron transfer is essential prior to the electron transfer event [2,23]. A big electric field generated by the high surface charge density of the MPPA-SAMs should make an effect on the orientation of cyt *c*

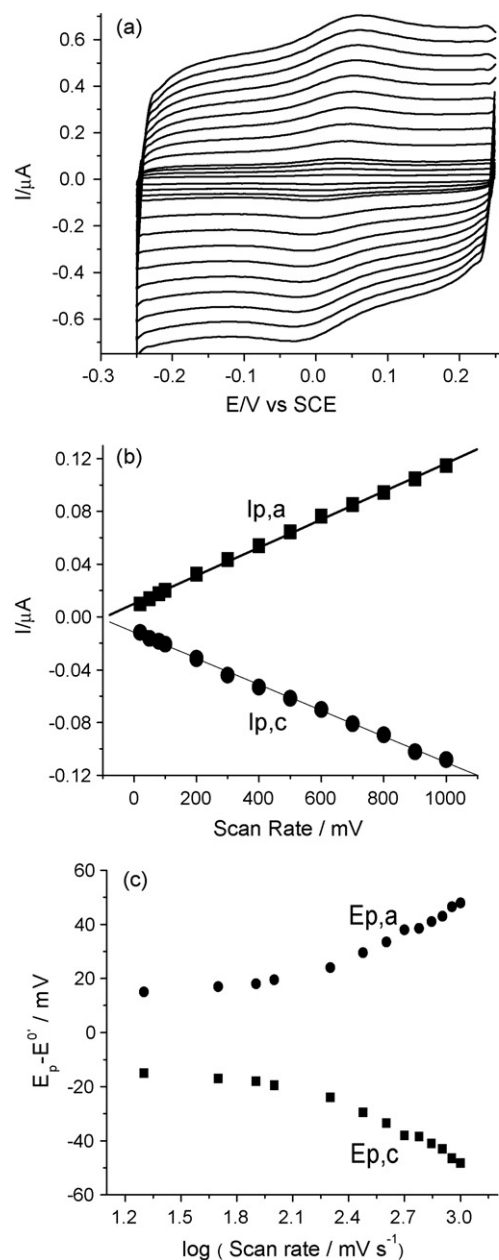


Fig. 5. (a) Cyclic voltammograms of the cyt/MPPA/Au electrode in a 10 mM PBS (pH 7.0) at different scan rate of 20, 50, 80, 100, 200, 300, 400, 500, 600, 700, 800, 900 and 1000 mV/s from inner to outer, respectively; (b) plots of the corresponding cathodic and anodic peak currents vs. scan rate, and (c) plots of the corresponding cathodic and anodic peak potentials vs. logarithm of scan rate.

molecules due to the large dipole moment of cyt *c*. Therefore, this reduction of the k_s of cyt *c* immobilized on MPPA-SAMs probably results from an orientation of adsorbed cyt *c* that is inappropriate for the electron transfer between the heme groups and the electrode due to the strong electrostatic interaction between cyt *c* and MPPA-SAMs.

The direct electron transfer of cyt *c* immobilized on long-chain alkanethiolates SAMs obeys the electron transfer kinetic theory [27]. Herein, the non-adiabatic electron transfer rate constant of cyt *c* has an exponential dependence on distance for methylene chain lengths. Consequently, the small k_s value ($8.0 \pm 2 \text{ s}^{-1}$) implies that the direct electron transfer of cyt *c* cannot occur upon remarkable increase of carbon chains length. As expected, the cyt *c* electrostatic immobilized on MUPA [$\text{HS}-(\text{CH}_2)_{11}-\text{PO}_3\text{H}_2$] modified Au electrode

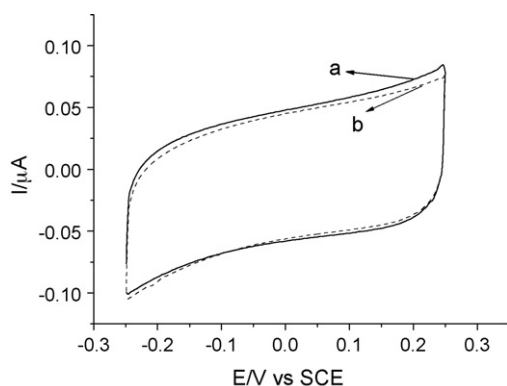


Fig. 6. Cyclic voltammograms of (a) MUPA/Au and (b) cyt/MUPA/Au electrode in 10 mM PBS (pH 7.0) at a scan rate of 100 mV/s. Preparation of the MUPA/Au and cyt/MUPA/Au electrode are similar to that of the MPPA/Au and cyt/MPPA/Au except that ethanol is used as the solvent in the course of formation of MUPA/Au electrode.

does not result in CV response in the applied potential range due to the longer electron transfer path (Fig. 6).

4. Conclusion

The cyt *c* immobilized on the $-\text{PO}_3\text{H}_2$ terminated SAMs via the electrostatic interactions retains its native secondary protein structure and the direct electron transfer can occur. The direct electrochemistry of the immobilized cyt *c* on MPPA/Au is nearly reversible, and its formal potential ($E^{0'} = 18 \pm 3$ mV vs. SCE) is very close to that of cyt *c* in an aqueous solution ($E^{0'} = 18\text{--}22$ mV vs. SCE). Compared with previous reported works, the present experimental results demonstrate that the value of formal potential shift is not simply proportional to the surface negative charge density of SAMs, implying that influence of the type of anion in SAMs should be considered as well. In addition, the electron transfer rate of cyt *c* immobilized on MPPA-SAMs is relatively slow ($k_s = 8.0 \pm 2$ s $^{-1}$) as compared to other acidic groups terminated SAMs, which is proba-

bly due to the fact that excess negative charges on the SAMs surface will decrease the electron transfer rate of cyt *c*.

Acknowledgments

This work is supported by NSFC (Nos. 20325103, 20775034, 20535010), the National Science Fund for Creative Research Groups (20521503, 20721002) and the National Basic Research Program of China (2007CB925102).

References

- [1] J. Petrovic, R.A. Clark, H. Yue, D.H. Waldeck, E.F. Bowden, *Langmuir* 21 (2005) 6308.
- [2] S.I. Imabayashi, T. Mita, T. Kakiuchi, *Langmuir* 21 (2005) 1470.
- [3] D.H. Murgida, P. Hildebrandt, *Acc. Chem. Res.* 37 (2004) 854.
- [4] D.H. Murgida, P. Hildebrandt, *Phys. Chem. Chem. Phys.* 7 (2005) 3773.
- [5] M. Tanahashi, T. Matsuda, *J. Biomed. Mater. Res.* 34 (1997) 305.
- [6] M.Y. Tsai, Y.T. Sun, J.C. Lin, *J. Colloid Interface Sci.* 308 (2007) 474.
- [7] T.M. Putvinski, M.L. Schilling, H.E. Katz, C.E.D. Chidsey, A.M. Majsce, A.B. Emerson, *Langmuir* 6 (1990) 1567.
- [8] H. Miyake, S. Ye, M. Osawa, *Electrochem. Commun.* 4 (2002) 973.
- [9] J.J. Xu, G. Wang, Q. Zhang, D.M. Zhou, H.Y. Chen, *Electrochem. Commun.* 6 (2004) 278.
- [10] K. Ataka, J. Heberle, *J. Am. Chem. Soc.* 126 (2004) 9445.
- [11] Y.Y. Song, W.Z. Jia, C. Yang, X.H. Xia, *Adv. Funct. Mater.* 17 (2007) 2377.
- [12] X. Chen, R. Ferrigno, J. Yang, G.M. Whitesides, *Langmuir* 18 (2002) 7009.
- [13] I. Burgess, B. Seivewright, R.B. Lennox, *Langmuir* 22 (2006) 4420.
- [14] H.S. White, J.D. Peterson, Q. Cui, K.J. Stevenson, *J. Phys. Chem. B* 102 (1998) 2930.
- [15] D. Millo, A. Bonifacio, A. Ranieri, M. Borsari, C. Gooijer, G. van der Zwan, *Langmuir* 23 (2007) 4340.
- [16] H.H. Liu, J.L. Lu, M. Zhang, D.W. Pang, H.D. Abruna, *J. Electroanal. Chem.* 544 (2003) 93.
- [17] K. Ataka, J. Heberle, *J. Am. Chem. Soc.* 125 (2003) 4986.
- [18] R.A. Clark, E.F. Bowden, *Langmuir* 13 (1997) 559.
- [19] X.P. Ji, B.K. Jin, J.Y. Jin, T.J. Nakamura, *Electroanal. Chem.* 590 (2006) 173.
- [20] T. Kakiuchi, M. Iida, S. Imabayashi, K. Niki, *Langmuir* 16 (2000) 5397.
- [21] J. Zhang, J. Kirkham, C. Robinson, *Anal. Chem.* 72 (2000) 1973.
- [22] E.J. Laviron, *Electroanal. Chem.* 100 (1979) 263.
- [23] A. Avila, B.W. Gregory, K. Niki, T.M. Cotton, *J. Phys. Chem. B* 104 (2000) 2759.
- [24] X. Jiang, K. Ataka, J. Heberle, *J. Phys. Chem. C* 112 (2008) 813.
- [25] J. Xu, E.F. Bowden, *J. Am. Chem. Soc.* 128 (2006) 6813.
- [26] D.E. Khoshdariya, J. Wei, H. Liu, H. Yue, D.H. Waldeck, *J. Am. Chem. Soc.* 125 (2003) 7704.
- [27] H. Yue, D. Khoshdariya, D.H. Waldeck, J. Grochol, P. Hildebrandt, D.H. Murgida, *J. Phys. Chem. B* 110 (2006) 19906.



Immunoaffinity extraction of testosterone by antibody immobilized monolithic capillary with on-line laser-induced fluorescence detection

Hong-Xu Chen, Ting Huang, Xin-Xiang Zhang*

Beijing National Laboratory for Molecular Sciences, BNLM; Key Laboratory of Bioorganic Chemistry and Molecular Engineering of MOE, Institute of Analytical Chemistry, College of Chemistry, Peking University, Beijing 100871, China

ARTICLE INFO

Article history:

Received 31 August 2008
Received in revised form 3 November 2008
Accepted 5 November 2008
Available online 13 November 2008

Keywords:

Affinity extraction
Azlactone
Immobilized antibody
Monolith
Testosterone

ABSTRACT

An immunoaffinity capillary column has been made with poly (2-vinyl-4, 4-dimethylazlactone-co-2-hydroxyethyl methacrylate-co-ethylene dimethacrylate) (VDA-co-HEMA-co-EDMA) monolith as a support for the immobilized antibody. The monolith is prepared by UV-initiated in situ polymerization, followed by immobilizing anti-testosterone polyclonal antibody through the rapid reaction with VDA. Fluorescence labeled testosterone at C₃ is designed as a tracer to estimate the extraction ability of this immunoaffinity column, and to optimize the immunoextraction process, such as washing, eluting, incubation and injection. The performance in a more realistic application is then demonstrated successfully for the rapid extraction of testosterone (T) by competitive immunoassay and on-line laser-induced fluorescence (LIF) detection. This immunoaffinity monolith is easily prepared, with high mechanical strength and low flow resistance. It is a satisfactory material as an immunoextractor to detect small molecular compounds specifically and rapidly with high sensitivity (sub ng/mL level).

© 2008 Elsevier B.V. All rights reserved.

1. Introduction

Immobilized antibodies as ligands for affinity supports have been widely used for the pretreatment of complex biological and clinical samples [1]. Compared with general extraction methods such as liquid–liquid extraction, solid phase extraction and supercritical fluid extraction, the immunoaffinity extraction method has exquisite specificity caused by specific antibody–antigen interaction, and thus will lead to the highly selective adsorption of a target analyte.

Off-line or on-line combination of immunoaffinity extraction and separation is a useful hybrid technique when cross-reactivity of antibody exists. A group of analytes with similar structure can be extracted by immunoaffinity and then separated by HPLC, GC or CE [1–5]. CE has the advantage of high separation efficiency and low sample consumption, thus on-line immunoaffinity capillary electrophoresis (IA-CE) has been applied widely [3,6–9]. Other than specific extraction, enrichment can also be achieved which can be applied to improve the sensitivity of CE. Packed [10–16] and open tubular [17–22] capillaries have been reported to be the mostly used modes to immobilize antibody. However the frits are required to maintain the porous beads in packed capillary. The preparation procedure is also difficult and the frits will also generate irregular

electroosmotic flow and irreproducible migration time. In the case of open tubular capillary, the amount of antibodies immobilized onto the surface of the capillary is usually restricted. These limitations provide motivation for further investigating new materials and strategies of antibody immobilization in IA-CE.

Monolith was first introduced as a chromatographic support by Hjerten et al. [23] in 1989 and further used in the field of capillary electrochromatography [24]. The porous structure has attractive features of high mechanical strength, low back pressure and fast mass transfer. Furthermore, no frits are required and the preparation is easy, with one-step in situ polymerization of initiator, monomer, crosslinker, and porogen initiated by heat or UV light. Recently, methacrylate-based monolith has been successfully used as enzyme [25], affinity ligands [26–28] or antibody [29] immobilized material within capillary.

In our study, an affinity monolithic capillary was prepared and evaluated for immunoextraction with testosterone (T) as a model analyte. The preparation of the monolith was based on a copolymer of 2-vinyl-4,4-dimethylazlactone (VDA), 2-hydroxyethyl methacrylate (HEMA) and ethylene dimethacrylate (EDMA). Anti-testosterone polyclonal antibody was immobilized onto the monolith via the reaction with VDA. Assay was carried out by competitive immunoassay mode and on-line laser-induced fluorescence (LIF) detection. Results demonstrated that the extraction and quantification was satisfactory. Once combining with CE, a rapid and simple on-line IA-CE system will be established for abusing control.

* Corresponding author. Tel.: +86 10 6275 4680 fax: +86 10 6275 1708.
E-mail address: zxx@pku.edu.cn (X.-X. Zhang).

2. Experimental

2.1. Apparatus

In the preparation of the monolith, capillary was rinsed using a CE-212 system (Peking University Instrument Factory, China; Micro Analytical, MO, USA) with a pressure of 0.25 MPa. A ZF-7A UV lamp (16 W) (Guchun, Shanghai, China) with a wavelength of 365 nm was used for UV initiation of the polymerization reaction. The on-line immunoaffinity extraction was performed by pressure driving (0.14 MPa) on a P/ACE 5000 CE system with LIF detector (Beckman Instruments, Fullerton, CA, USA). Fluorescence was excited by argon ion laser at 488 nm and detected after passing through a 488 nm cut-off and a 520 nm interference filter.

2.2. Material and reagents

EDMA, HEMA, γ -methacryloxypropyltrimethoxysilane (γ -MAPS), 1-decanol, azobisisobutyronitrile (AIBN), and testosterone were purchased from Acros (New Jersey, USA). VDA was bought from TCI (Tokyo, Japan). Bovine serum albumin (BSA), ovalbumin (OVA) were obtained from Sigma (St. Louis, MO, USA). Methanol (Siyou, Tianjin, China) was of HPLC grade. All other chemicals were of analytical grade. Deionized water was used throughout. EDMA, HEMA were purified by a basic alumina column. AIBN was purified by re-crystallization from methanol. Before filled into the capillary, solutions were filtered through 0.22 μ m PTFE membrane filters (Dikma, Beijing, China). PBST, consisting of phosphate buffer saline (PBS) and Tween-20, was prepared by dissolving 8.0 g of NaCl, 2.9 g of $\text{Na}_2\text{HPO}_4 \cdot 12\text{H}_2\text{O}$, 0.2 g of KH_2PO_4 , 0.2 g of KCl and 0.5 mL of Tween-20 in 1 L of water. Anti-testosterone polyclonal antibody was elaborated by collecting serum from the immunized rabbits (Monoclonal Laboratories, Department of Biology, Peking University, China). Fluorescence labeled tracers were synthesized in our lab. Fused silica capillary (100 μ m i.d.) was from Ruifeng Inc. (Hebei, China).

2.3. Preparation of antibody immobilized monolith

A transparent area with a length of 1.0 cm for UV-initiated polymerization, as well as the detection window was made on a capillary (100 μ m i.d.). The distances from the transparent area and the window to the outlet of the capillary were 2.0 and 7.0 cm, respectively. Reversed pressure (from outlet to inlet) was used through the preparation and assay procedure. Capillary pretreatment and silanization procedure was carried out in order to enhance the covalent attachment of the poly (VDA-co-HEMA-co-EDMA) monolith to the capillary walls. (a) Pretreatment and silanization: the capillary was rinsed with 1 M sodium hydroxide

for 60 min, water for 20 min and methanol for 5 min. It was then dried with air for 5 min. The pretreated capillary was filled with a 50% (v/v) solution of γ -MAPS in methanol, sealed at both ends, and then placed in an oven at 37 °C overnight. After taken out and unsealed, the capillary was rinsed with methanol for 5 min and dried with air for 5 min. (b) Polymerization: a polymerization solution consisting of 50 mg of EDMA, 30 mg of HEMA, 20 mg of VDA, 150 mg of 1-decanol and 1.0 mg of AIBN was prepared (mass ratio 20/12/8/60/0.4) [25]. This solution was ultrasonicated for 1 min and degassed with nitrogen for 15 min before being introduced into the pretreated capillary at a pressure of 0.25 MPa. The capillary was sealed at both ends and placed under the UV lamp. Only the 1 cm transparent area was exposed to UV light. Distance between the lamp and the capillary was 11.3 cm. Irradiated by UV with a wavelength of 365 nm for 3 h, polymerization would occur and form monolith inside the transparent area. The obtained monolith was purged with air at a pressure of 0.25 MPa for 15 min, methanol for 30 min and air for 15 min again to remove any unreacted monomers. (c) Immobilization of antibody: the antibody solution (5.3 mg/mL in 0.1 M NaHCO_3 and 0.5 M Na_2SO_4 , pH 9.0) reacted dynamically for 1 h at room temperature driven by a pressure of 0.25 MPa. (d) Quenching and equilibration: the monolith was rinsed with 1 M aqueous ethanolamine for 30 min to quench any unreacted azlactone groups, followed by equilibration with PBS for 2 h with a pressure of 0.25 MPa. A control monolithic capillary was prepared by the same steps without the immobilization of antibody.

2.4. On-line immunoextraction

Fluorescence labeled testosterone at C_3 (T3F) was synthesized and used as a monitoring compound for immunoextraction conditions. Steps were as follows: (1) loading: a known amount of T3F (3.6 μ M) in binding buffer (PBS) was loaded into the capillary by pressure for 2 min, and incubated for 2 min. (2) Washing: the capillary was rinsed with washing buffer (PBST) to remove all unbound and non-specifically adsorbed samples, until a smooth baseline was detected. (3) Eluting: specifically extracted sample was eluted by eluting buffer (80% methanol in water (v/v)) for 1 min, and followed by PBST until they were detected by LIF detector. (4) Regeneration and equilibration: the capillary was rinsed with PBST for 2 min to equilibrate the immunoaffinity monolith, and then ready for another run.

The quantification of testosterone was carried out by competitive immunoextraction format. A mixture of T3F with a fixed concentration (3.6 μ M) and testosterone standard sample (0.07–700 μ M) was injected into the immunoaffinity capillary. The procedure of loading, washing, eluting, detection and regeneration was the same as that described above. A general scheme for this competitive immunoextraction was shown in Fig. 1.

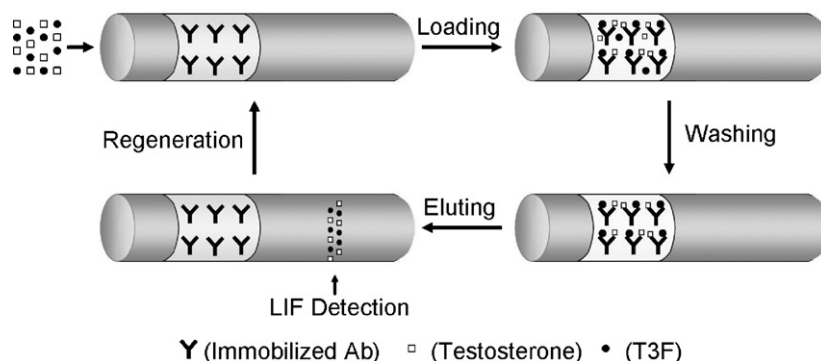


Fig. 1. Scheme of competitive immunoextraction.

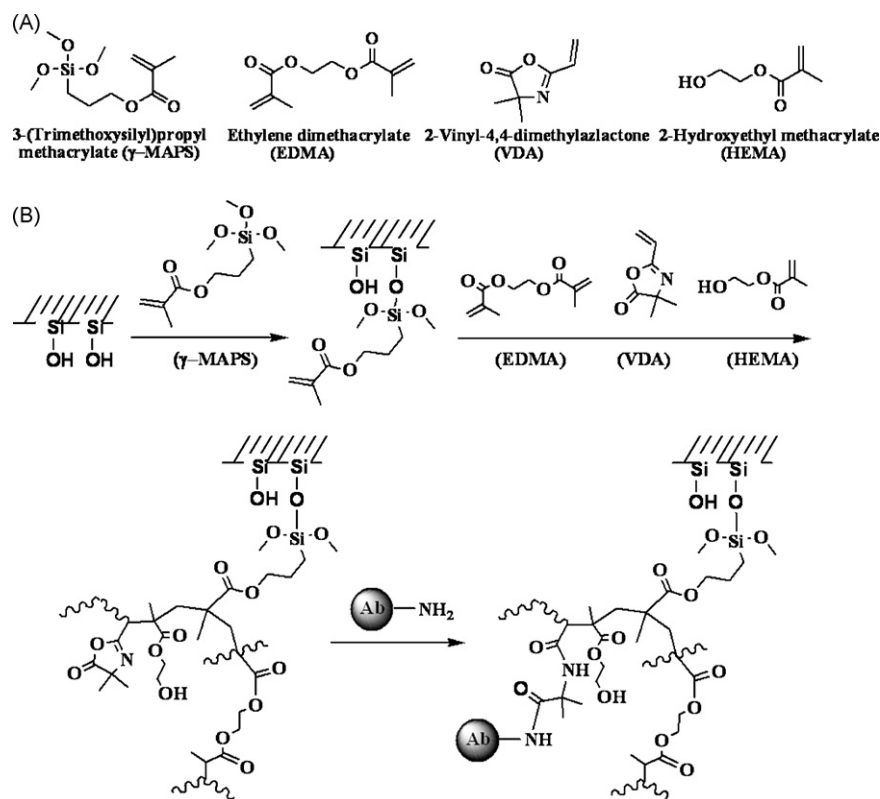


Fig. 2. (A) The structures of related monomers. (B) Schematic description of polymerization reaction and the coupling of antibody on poly (VDA-co-HEMA-co-EDMA) monolithic support.

3. Results and discussion

3.1. Preparation of polyclonal antibody and fluorescence labeled tracers

BSA conjugated T at C₃ (T-3-BSA) synthesized as our previous report [30] was used as immunogen to immunize two healthy New Zealand rabbits. The obtained antiserum was purified based on an octanoic acid-saturated ammonium sulfate method. The concentration of immunoglobulin (IgG) was measured with UV spectrophotometer and calculated according to the following equation: $C_{\text{protein}} \text{ (mg/mL)} = 1.45A_{280\text{nm}} - 0.74A_{260\text{nm}}$. The purified antibody was stored at -20°C . Titer-level and affinity constant measured by ELISA were $1:10^{4.4}$ and $2.75 \times 10^7 \text{ M}^{-1}$.

Since polyclonal antibody was prepared by immunizing with T-3-BSA, the exposed B, C, D rings of testosterone were the target binding sites with antibody. As the same theory, a competitive tracer T3F was designed and synthesized [30]. Fluorescein isothiocyanate (FITC) was conjugated with T at C₃ and the binding sites for immunoreaction were exposed. Thus, T3F could also be regarded as target molecule of the antibody, which could be used for the conditions optimization and competitive immunoassay. Fluorescence labeled testosterone at C₁₇ (T17F) was used as a control tracer. It was synthesized in a similar way as T3F.

3.2. Preparation of antibody immobilized monolith

UV-initiated polymerization was used because it was faster than thermally initiated process and well suited to achieve monolith formation within a specified area [31]. Obviously, UV transparent area was required for polymerization. Burning off the coating with an electric slender iron wire was an easy method to accurately control the length of the transparent area, and consequently the length of

the monolith. Longer monolith could immobilize more antibodies but would increase the back pressure of the capillary. Furthermore, when combined with CE, separation stability and efficiency will decrease. 1.0 cm of the monolith was chosen after making a compromise between these conditions.

Among different polymer materials such as polyacrylamide, polystyrene and so on, monolith made by methacrylate with a wide variety of functionalities was the most popular one [32]. Glycidyl methacrylate-based monoliths have been used as supports for immobilization of proteins [33]. However, epoxide functionalities reacted slowly with proteins. In contrast, the incorporation of VDA into the monolith appeared to be extremely attractive [34], which can react easily with amino or thiol groups of biomacromolecules to form stable covalent bonds at room temperature. After pretreatment, part of the silanol groups in the innerwall of the capillary reacted with γ -MAPS to form the anchor for the poly (VDA-co-HEMA-co-EDMA) monolith. The polymerization was initiated by AIBN, while the use of functional monomers VDA, HEMA, and EDMA enabled the preparation of monolith with reactive, hydrophilic and cross-linking functionalities, respectively. The structures of related monomers and polymeric reaction were shown in Fig. 2. Porogenic solvents were another essential part of the polymerization mixture. All monomers and initiator were dissolved in the porogenic solvents and the phase separation process was thus controlled during polymerization in order to achieve the desired porous structure. Although porogenic solvent with lower boiling points could safely be used in UV-initiated polymerization, the pore sizes were not easy to control to a narrow range [35]. 1-Decanol, which has been studied to be a good porogenic solvent for the preparation of monolith with controlled porous properties, was used in our study. The composition of the polymerization mixture used here was inspired from those optimized results reported by Svec's group [25]. In order to obtain low back pressure, the support must have large pores

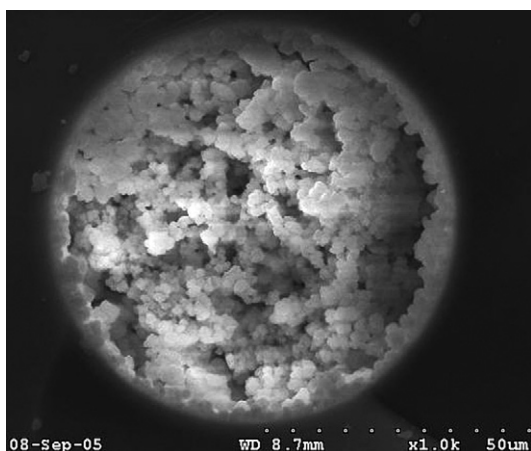


Fig. 3. Scanning electron microscope image of internal structure of the monolith.

through the entire monolith. Based on the work reported by the same group [25], the median pore diameter of the through pores in poly (VDA-co-HEMA-co-EDMA) supports measured by mercury intrusion porosimetry in the dry state was 1.02 μm . The pore sizes estimated from the scanning electron micrography in our experiment closely matched this value (Fig. 3).

3.3. Selective immunoextraction

The immunological studied showed that T3F had almost the same interaction as that of testosterone. T3F was used for the estimation and conditions optimization of the affinity column. On the contrary, the main binding sites of T17F were covered by FITC. Thus T17F was taken as the control labeled tracer to test the specificity of the affinity column. Peaks 2 and 1 in Fig. 4 represented the specially bound and unbound part, respectively. The ratio of them could reflect the retention of different samples on the immunoaffinity monolith. Results showed that the target tracer (T3F) had the ratio of 0.26, higher than that of 0.02 in the case of control tracer (T17F). These data indicated that this immunoaffinity monolith had the ability of extracting its target specifically.

3.4. Optimization for immunoextraction conditions

3.4.1. Eluting buffer

Since the labeled tracer released from the monolith was used for quantification, proper elution buffer becomes important in

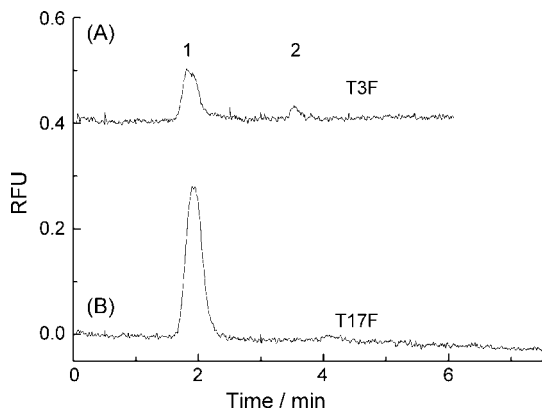


Fig. 4. Retention of different tracers on antibody immobilized monolith. The assay process was as follow: fluorescent tracers (A) T3F (0.60 μM), (B) T17F (2.5 μM), from 0 to 1.0 min, PBST from 1.0 to 3.0 min, 80% methanol from 3.0 to 4.0 min, and PBST again after 4.0 min. Peak 1: unbound or non-specifically adsorbed tracers; peak 2: specifically bound tracers.

this immunoassay procedure. A compromise needs to be made between complete elution of the bound targets and keeping the activity of the antibody. The targets (T or T3F) were captured by the immunosorbent due to electrostatic forces, hydrogen bonding and hydrophobic interaction. After removal of the unbound or non-specifically adsorbed part, the specifically bound targets can be dissociated by changing the chemical environment such as pH, salt content and organic solvent. Several elution conditions were investigated including organic solvent and acid pH buffer. Since no fluorescent signal was observed after eluting with acid Gly-HCl buffer (pH 2.0), organic solvent was tested. The appropriate composition of methanol and water was optimized. Taking 100% methanol as eluting buffer, signal was too weak though the elution was rapid and complete. This was most likely due to the low fluorescence response in absolute methanol. Severe tailing was observed in the case of 50% methanol, which caused by the weak elution ability. Finally 80% methanol was used, with which condition, the eluted peak of T3F was sharp and no tailing was observed. Complete dissociation was reassured by eluting again with 100% methanol and no T3F was detected any more. Since the pulse contact between organic solvent and antibody brought very little damage to the activity of antibody, even under this relatively high percent of methanol, immobilized antibody showed no obvious denaturation during the whole assay procedure and can be regenerated.

3.4.2. Optimization of washing buffer to decrease non-specific adsorption

Non-specific adsorption caused by the interaction with the monolithic material might interfere with the immunoextraction. Ideally, after loading and binding procedure, all the non-specifically adsorbed analytes should be washed away by appropriate solution, and only those bound with antibody retained. In order to investigate the effect of different washing buffer to decrease the non-specific adsorption, a control monolithic capillary without antibody was made, with three kinds of washing modes tested. The elution profiles were shown in Fig. 5. Using PBS as washing buffer, target could be captured even in the control capillary, which meant the adsorption from monolithic material existed. Alternatively, PBST solved this problem with nothing captured and eluted. In the case of the other mode, OVA solution was firstly rinsed to pre-saturate the sites for non-specific adsorption, followed by washing with PBS. Results demonstrated that effective elimination of non-specific adsorption could also be achieved. PBST was finally used as washing buffer due to its convenience in operation than pre-saturation with OVA.

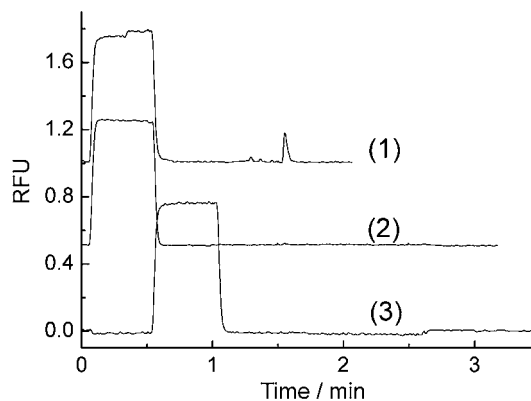


Fig. 5. Effect of washing buffer to decrease non-specific adsorption on a control capillary. The assay process was as follow (at a pressure of 0.14 MPa): loading samples: T3F (0.60 μM) for 0.5 min; washing: (1) PBS, (2) PBST for 1 min; elution: 80% methanol for 1 min; washing: washing buffer for 5 min. As for (3), OVA was firstly be rinsed for 0.5 min, the following steps were the same as process (1).

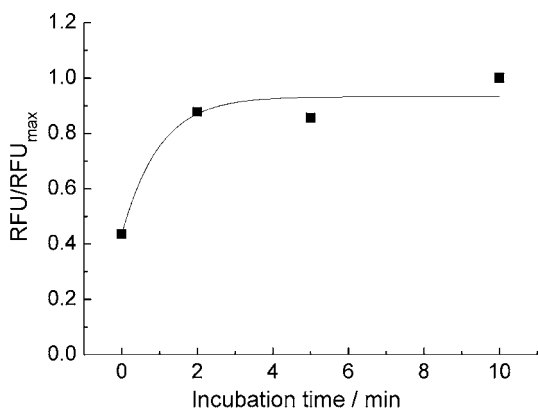


Fig. 6. Plot of relative peak height of bound T3F vs. different on-line incubation periods. The assay process was the same as that in Fig. 4 except stopping for different periods (from 0, 2, 5, 10 min) after the injection of T3F.

3.4.3. Incubation and injection periods

The interaction between targets and antibody in heterogeneous phase was slower than that in homogenous reaction because of the diffusion of targets from mobile phase to immobilized antibody. On-line incubation at different periods (0, 2, 5, 10 min) was investigated. As shown in Fig. 6, there was nearly no difference in the eluted peak height when incubation time was above 2 min. That meant the reaction had reached equilibrium within 2 min. Because of the high mass-transfer rates, benefited from the porous structure of the monolith, the interaction of the targets and antibody would be rapid. Consequently, it was possible to load and concentrate larger volumes of sample solution.

Relatively low sensitivity was a severe disadvantage of capillary electrophoresis method especially when trace analytes were determined. In general, an increase in the peak height or area will not be achieved by simply increasing the injection time or the sample plug length. However, by on-line combination of immunoextraction and CE, enrichment can be achieved. The ability of enrichment depends on the capacity of immobilized antibody. Experiments were performed to test the retention of T3F with fixed concentration but different injection periods. Fig. 7 showed that the peak height of specifically adsorbed T3F increased with longer loading period. However, due to the relatively low amount of antibody immobilized on the monolith, the affinity concentration was saturated soon and no increase was observed when the injection period was longer than 2 min. Oriented immobilization of antibody may be required in order to achieve higher enrichment efficiency.

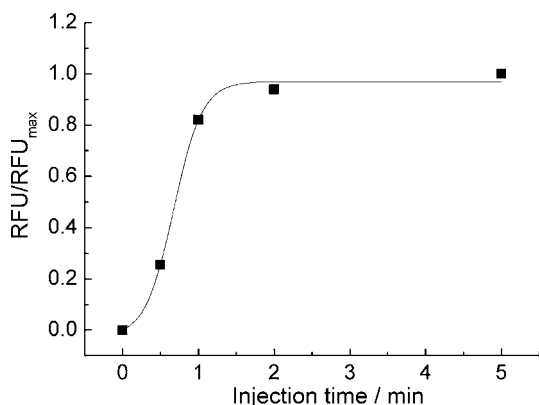


Fig. 7. Plot of relative peak height of bound T3F vs. different injection periods. The assay process was the same as that in Fig. 4 except the different injection periods.

3.5. Quantification of testosterone by competitive immunoextraction

The sensitivity of detection can be adjusted by altering the concentration of the antibody and competitive tracer, thereby producing assay with different working range. The concentration of T3F was chosen according to the best response and proper range for clinical detection. A fixed concentrated T3F (3.6 μM) competed with standard testosterone sample (0.07–700 μM) to react with limited antibody immobilized on the monolith. With increasing concentration of testosterone, the amount of bound tracer (T3F) decreased. A calibration curve was constructed by plotting RFU/RFU_{max} of eluted peak height as a function of the logarithm of different testosterone concentration. The corresponding equation was $Y = 0.25 - 0.13 \lg C_T$ (mg/mL), where C_T was the concentration of testosterone. The correlation coefficient (R) was 0.99. The linear range of 0.07–700 μM (or 0.02–200 $\mu\text{g/mL}$) was obtained, which was suitable for clinical application.

3.6. Repeatability

The run to run repeatability of the affinity monolithic capillary column was investigated by extracting T3F continuously. In each run, the whole procedure of loading, washing and eluting was carried out, and the peak height of eluted T3F was used to estimate the relative standard deviation (R.S.D.). The value of 7.3% ($n = 4$) was got, which indicated that the affinity monolithic capillary was stable for immunoextraction and quantitative analysis. However, the day to day or column to column reproducibility still need to be improved.

4. Conclusions

A monolithic capillary containing covalently immobilized antibody was prepared by in situ UV-initiated polymerization. The immobilized anti-testosterone polyclonal antibody was able to selectively capture its target molecules (T and T3F), and used for immunoextraction of testosterone by competitive mode. High sensitivity (LOD lower than 70 nM) was achieved through somewhat enrichment and LIF detection. The column was found to be reusable even after exposure to 80% methanol, with an R.S.D. of 7.3% ($n = 4$). Further study will be focused on the optimization of antibody immobilization, in order to achieve higher enrichment efficiency. The use of monoclonal antibody and oriented immobilization may be explored. This rapid immunoextraction system within capillary can be applied in developing on-line IA-CE which can be used to analysis a group of related compound simultaneously.

Acknowledgements

This work was supported by National Natural Science Foundation of China (Nos. 20475006 and 90713013) and the National Scientific Support Project 2006BAF07B03 (MOST, China).

References

- [1] D.S. Hage, J. Chromatogr. B 715 (1998) 3.
- [2] P. Su, X.-X. Zhang, W.-B. Zhang, J. Chromatogr. B 816 (2005) 7.
- [3] A.J. Tomlinson, L.M. Benson, N.A. Guzman, S. Naylor, J. Chromatogr. A 744 (1996) 3.
- [4] M.-C. Hennion, V. Pichon, J. Chromatogr. A 1000 (2003) 29.
- [5] N. Delaunay-Bertoncini, M.-C. Hennion, J. Pharm. Biomed. Anal. 34 (2004) 717.
- [6] N.A. Guzman, M.A. Trebilcock, J.P. Advis, J. Liq. Chromatogr. 14 (1991) 997.
- [7] N.A. Guzman, S.S. Park, D. Schaufelberger, L. Hernandez, X. Paez, P. Rada, A.J. Tomlinson, S. Naylor, J. Chromatogr. B 697 (1997) 37.
- [8] N.A. Guzman, R.J. Stubbs, Electrophoresis 22 (2001) 3602.
- [9] T. Stroink, E. Paarlberg, J.C.M. Waterval, A. Bult, W.J.M. Underberg, Electrophoresis 22 (2001) 2375.
- [10] N.A. Guzman, Electrophoresis 24 (2003) 3718.
- [11] N.A. Guzman, J. Chromatogr. B 749 (2000) 197.

- [12] L.J. Cole, R.T. Kennedy, *Electrophoresis* 16 (1995) 549.
- [13] L.G. Rashkovetsky, Y.V. Lyubarskaya, F. Foret, D.E. Hughes, B.L. Karger, *J. Chromatogr. A* 781 (1997) 197.
- [14] J.J. Dalluge, L.C. Sander, *Anal. Chem.* 70 (1998) 5339.
- [15] D.H. Thomas, D.J. Rakestraw, J.S. Schoeniger, V. Lopez-Avila, J. Van Emon, *Electrophoresis* 20 (1999) 57.
- [16] M. Mayer, A. Muscate-Magnussen, H. Vogel, M. Ehrat, G.J.M. Bruin, *Electrophoresis* 23 (2002) 1255.
- [17] T.M. Phillips, J.J. Chmielinska, *Biomed. Chromatogr.* 8 (1994) 242.
- [18] K. Ensing, A. Paulus, *J. Pharm. Biomed. Anal.* 14 (1996) 305.
- [19] T.M. Phillips, L.M. Kennedy, E.C. De Fabo, *J. Chromatogr. B* 697 (1997) 101.
- [20] T.M. Phillips, *Anal. Chim. Acta* 372 (1998) 209.
- [21] M.K. Little, C.D. Crawley, *Anal. Chim. Acta* 464 (2002) 25.
- [22] T.M. Phillips, P. Smith, *Biomed. Chromatogr.* 17 (2003) 182.
- [23] S. Hjertén, J.-L. Liao, R. Zhang, *J. Chromatogr.* 473 (1989) 273.
- [24] F. Svec, *J. Sep. Sci.* 28 (2005) 729.
- [25] D.S. Peterson, T. Rohr, F. Svec, J.M.J. Fréchet, *Anal. Chem.* 74 (2002) 4081.
- [26] M. Bedair, Z. El Rassi, *J. Chromatogr. A* 1044 (2004) 177.
- [27] J.M. Armenta, B. Gu, P.H. Humble, C.D. Thulin, M.L. Lee, *J. Chromatogr. A* 1097 (2005) 171.
- [28] Z. Pan, H. Zou, W. Mo, X. Huang, R. Wu, *Anal. Chim. Acta* 466 (2002) 141.
- [29] K. Faure, N. Delaunay, G. Alloncle, S. Cotte, J.-L. Rocca, *J. Chromatogr. A* 1149 (2007) 145.
- [30] H.X. Chen, X.X. Zhang, *Electrophoresis* 29 (2008) 3406.
- [31] D.S. Peterson, T. Rohr, F. Svec, J.M.J. Fréchet, *Anal. Chem.* 75 (2003) 5328.
- [32] E.C. Peter, M. Petro, F. Svec, J.M.J. Fréchet, *Anal. Chem.* 69 (1997) 3646.
- [33] M. Petro, F. Svec, J.M.J. Fréchet, *Biotechnol. Bioeng.* 49 (1996) 355.
- [34] S. Xie, F. Svec, J.M.J. Fréchet, *Biotechnol. Bioeng.* 62 (1999) 30.
- [35] C. Yu, M. Xu, F. Svec, J.M.J. Fréchet, *J. Polym. Sci. Pt. A, Polym. Chem.* 40 (2002) 755.



Silk fibroin as a sorbent for on-line extraction and preconcentration of copper with detection by electrothermal atomic absorption spectrometry

Xu-Wei Chen^a, Lin-Lin Huang^a, Rong-Huan He^{b,*}

^a Research Center for Analytical Sciences, Northeastern University, Shenyang 110004, China

^b Department of Chemistry, Northeastern University, Shenyang 110004, China

ARTICLE INFO

Article history:

Received 25 September 2008

Received in revised form 22 October 2008

Accepted 23 October 2008

Available online 6 November 2008

Keywords:

Silk fibroin

Copper

Solid-phase extraction

Sequential injection

Electrothermal atomic absorption spectrometry

ABSTRACT

Silk fibroin is a kind of polypeptide with functional amino acids in its structure. The electric charges in its molecular chains originating from the dissociation of acidic groups, i.e., hydroxyl, phenol and carboxyl, provide vast potentials for the retention of metal species of interest. In this study, the selective retention of Cu^{2+} with silk fibroin at pH 6.0 was investigated and a novel on-line procedure for separation/preconcentration of Cu^{2+} from complex sample matrices was thus developed by using a sequential injection system with an electrothermal atomic absorption spectrometry. A novel concept of enrichment index (EI), i.e., defined as enrichment factor (EF) obtained by consuming unity of sample volume (ml), was proposed for evaluating the enrichment efficiency of a flow-based preconcentration procedure. With a sampling volume of 900 μl , an EI of 30.3 (EF = 27.3) was achieved, which was much improved as compared to that of reported procedures. A detection limit of 8.0 ng l^{-1} was achieved within a linear range of 0.025–1.5 $\mu\text{g l}^{-1}$ along with a precision of 2.2% R.S.D. at 0.5 $\mu\text{g l}^{-1}$. The practical applicability of this procedure was validated by analyzing a certified reference material of riverine water (GBW08608) and a certified reference material of seawater (NASS-5) achieving satisfactory agreements between the certified and the obtained values. A spiking recovery was also performed by using a cave water sample.

© 2008 Elsevier B.V. All rights reserved.

1. Introduction

Copper is an essential trace element playing a complex role in the living organisms. At very low concentration levels, i.e., $\leq 40 \text{ ng ml}^{-1}$, Cu^{2+} is a necessary micro-nutrient to maintain the normal metabolism of carbohydrates and lipids, and to keep the activities of heart and blood vessel. While on the other hand, when exceeding a certain concentration threshold, Cu^{2+} may be toxic and is prone to bind to the cell membrane, hindering the transport process through the cell wall heavily [1]. Thus it is highly desirable for timely evaluation of the existing level of copper in biological and environmental samples. Up to now, various detection methodologies including UV–vis spectrophotometry [2,3], atomic adsorption spectrometry [4–6], fluorometry [7,8], electrochemical techniques [9,10], inductively-coupled plasma emission spectrometry [11,12] have been developed for the quantitative determination of Cu^{2+} . However, for accurate quantification of ultra-trace copper in practical applications, appropriate sample pretreatment procedures are usually necessary and helpful in order to eliminate the strong

interferences from the matrix components and at the same time facilitate the preconcentration of Cu^{2+} . As an efficient sample pretreatment methodology, solid-phase extraction is applied widely in the preconcentration/separation of ultra-trace metal species. The flow injection analysis techniques have also been demonstrated as a powerful manipulation platform for on-line extraction with distinct merits of automatic fluidic management, improved efficiency and precision, minimized sample/reagent consumption, and minimal risk of cross-contamination of samples [13,14]. As for the on-line separation/preconcentration of Cu^{2+} in environmental or biological samples with detection by atomic adsorption spectrometry, various solid substrates such as silica gel [15,16], PTFE [17–19], and resin [20,21] have been adopted successfully in real-world sample pretreatments.

There are usually two strategies exploited for the separation/preconcentration of metal ions in on-line solid-phase extraction system, i.e., forming a complex with chelating reagents or binding to the solid substrates directly. In the practical applications, the first protocol is usually puzzled by the selection of suitable chelating reagents and subsequent reagent purification for reducing the blank values. For the direct sorption protocol, the surface modifications of solid materials are frequently necessary in order to introduce appropriate functional groups and while practically,

* Corresponding author. Tel.: +86 24 83683429; fax: +86 24 83676698.
E-mail address: herh@mail.neu.edu.cn (R.-H. He).

the modification procedures are usually quite time-consuming and costly. From this point of view, it is highly necessary to exploit suitable and easy-to-obtained alternative sorbent materials for selective separation/preconcentration of analytes of interest in the presence of sample matrices. Recently, the exploitations of biomaterials including algae [22–25], bacteria [26], cellulose [27,28], collagen [29], egg-cell membrane [30] as solid substrates for solid-phase extraction of analytes have attracted extensive attentions since their structures are abundant of functional groups such as carboxyl, hydroxyl, sulfhydryl and amino groups. Silk fibroin is a linear polypeptide composed of various amino acid groups [31]. The excellent biological compatibility and unique chemical properties of the silk fibroin have made it a favorable sorbent material widely adopted in adsorption investigations [32–35].

In the present work, the preconcentration of ultra-trace Cu^{2+} by exploiting the silk fibroin as the sorbent was investigated in a sequential injection system with detection by electrothermal atomic absorption spectrometry (ETAAS). The practical applicability of the system was validated by preconcentration and determination of ultra-trace Cu^{2+} in two kinds of certified reference materials and spiking recovery in a cave water sample.

2. Experimental

2.1. Instrumentation

A SP-3530GA atomic absorption spectrometer (Shanghai Spectrum Instruments Co., Ltd., Shanghai, China) with deuterium background correction was exploited. A copper hollow cathode lamp (Rayleigh Analytical Instrument, Beijing, China) was used as light source at a wavelength of 324.8 nm and operated at 4.0 mA with a 0.7 nm spectral bandpass. Pyrolytically coated graphite tubes with L'vov platforms were used. Peak height values were adopted for quantification considering that a very good precision for the peak height was achieved within the concentration range studied. The temperature program of the ETAAS determination was summarized in Table 1, details for the optimization of the temperature program were not included.

A FIALab-3000 sequential injection system (FIALab Instruments Inc., Medina, WA, USA) equipped with a 1.0 ml syringe pump (SP) and a six-port selection valve was employed for fluidic delivery and sample processing. The silk fibroin packed micro-column was incorporated into port 4 of the selection valve.

All the external channels were made using narrow-bore PTFE tubing connected to the six-port selection valve with PEEK nuts/ferrules (Upchurch Scientific, Oak Harbor, WA, USA). The inner diameter of the PTFE tube was 0.75 mm, except for the holding coil, where 1.5 mm i.d. tubing with a length of 150 mm was used in order to achieve a large holding capacity.

Both the atomic absorption spectrometer and the sequential injection system were controlled by a computer in order to synchronize the sample processing and the ETAAS determination.

The pH measurements were performed by using an Orion Model 818 digital pH meter (Thermo Electron Co., USA).

Table 1
The temperature program for the determination of Cu^{2+} with ETAAS.

Step	Temperature (°C)	Ramp (s)	Hold (s)	Argon flow rate (ml min ⁻¹)
Preheating	80	5	15	250
Drying	120	10	15	250
Pyrolysis	600	10	15	250
Atomization	2600	0	3	0
Cleaning	2700	1	2	250

2.2. Chemicals

The reagents were all purchased from Sinopharm Chemical Reagent Co., Ltd (Shanghai, China) and were at least of analytical reagent grade. Double deionized water (18 M Ω cm) was used throughout.

A 1000 mg l⁻¹ Cu^{2+} stock solution was prepared by using 0.1 mol l⁻¹ HNO_3 as the solvent to dissolve 0.2683 g $\text{CuCl}_2 \cdot 2\text{H}_2\text{O}$ and diluted to 100 ml. Working standard solutions of various concentrations were obtained by step-wise dilution of the stock solution with double deionized water. The acidity of the sample solutions was adjusted with either 0.1 mol l⁻¹ NaOH or 0.1 mol l⁻¹ HNO_3 .

2.3. Preparation of the silk fibroin micro-column

The silk fibroin purchased commercially was first cut into granules within a size range of 0.1–0.3 cm. The granulated silk fibroin of 1.0 g was then immersed into a certain amount of 0.1 mol l⁻¹ HNO_3 for 3 h in order to remove the residual impurities, and afterwards rinsed with deionized water and heated at 80 °C for 4 h for desiccation.

About 8.0 mg of silk fibroin granules was put into a tube in PTFE to pack a micro-column (2.0 mm i.d./3.2 mm o.d.) and followed by plugging the column at both ends with small amount of glass wool and PTFE nuts/ferrules. The micro-column was rinsed thoroughly with 3.0 ml of HNO_3 (0.5 mol l⁻¹) and 5.0 ml of deionized water successively at a flow rate of 30.0 $\mu\text{l s}^{-1}$ before analytical manipulations.

2.4. Analytical procedure

The sequential injection system was illustrated in Fig. 1. The entire analytical processes run through the following steps:

System conditioning: 100 μl of carrier (deionized water) was first aspirated into the syringe pump. 200 μl of air and 200 μl of conditioning solution (blank solution with identical pH value as that of the sample solution employed in the ensuing sections) were subsequently aspirated from ports 1 and 5 into the holding coil, which were afterward dispensed through port 2 to flush the micro-column at a flow rate of 30.0 $\mu\text{l s}^{-1}$.

Sorption and de-sorption of Cu^{2+} : 900 μl of sample solution was aspirated into the holding coil from port 4 and directed to flow through the micro-column at a flow rate of 10.0 $\mu\text{l s}^{-1}$ to facilitate the sorption and preconcentration of Cu^{2+} , then 50 μl of air was introduced to evacuate the micro-column. Thereafter, 200 μl of air and 30 μl of 0.5 mol l⁻¹ nitric acid were sequentially aspirated into the holding coil, which were afterwards dispensed to flow through micro-column at 5.0 $\mu\text{l s}^{-1}$. The nitric acid zone was used to elute

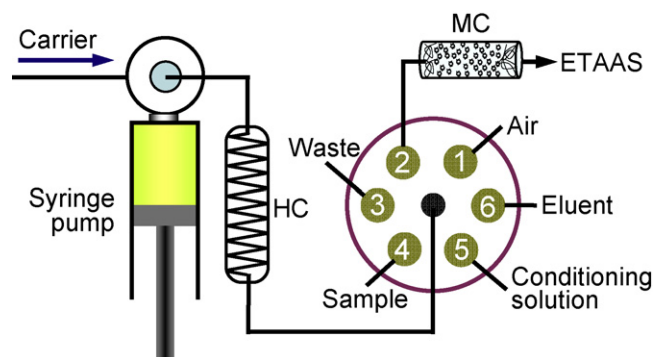


Fig. 1. Schematic diagram of sequential injection system for Cu^{2+} preconcentration coupled to ETAAS. HC: holding coil; MC: micro-column packed with silk fibroin.

the retained copper while the air zone was used to transport all of the eluate into the graphite tube of the ETAAS for quantification. *Micro-column refreshing*: Before the next operation cycle, 200 μl of air, 200 μl of conditioning solution and 200 μl of nitric acid (0.5 mol l^{-1}) were aspirated sequentially into the holding coil followed by directing them to flow through the micro-column to eliminate any potential residues on the surface of the silk fibroin.

3. Results and discussion

3.1. The adsorption of Cu^{2+} by silk fibroin

Silk fibroin is a natural biomaterial mainly composed of 18 amino acids including serine, tyrosine, aspartic acid, lysine, arginine, etc. There are abundant nucleophilic groups in the molecular chains of silk fibroin such as hydroxyl group provided by serine, carboxyl by aspartic acid, phenol group by tyrosine, side/terminal amino group by lysine and arginine [36]. The dissociation of these acidic groups as a function of pH value makes it chargeable and provides potential binding capacity to metal ions, e.g., Cu^{2+} , through electrostatic interactions, as illustrated in Fig. 2. The ETAAS signals showed that only very limited amount of Cu^{2+} was observed in the effluent after sorption of 900 μl sample with a concentration of $0.5 \mu\text{g l}^{-1}$ (Fig. 3A), indicating a high retention efficiency. At the same time, a large quantity of Cu^{2+} was detected in the eluate with 0.5 mol l^{-1} nitric acid as eluent (Fig. 3B), suggesting that the retained Cu^{2+} could be readily stripped off from the surface of the silk fibroin. The experimental results showed that an adsorption capacity of 3.66 mg g^{-1} for Cu^{2+} was achieved at the optimal conditions.

3.2. Effect of sample pH

It has been demonstrated that the pH value of solutions is a key parameter for bio-sorption of metal species due to its important influence not only on the site dissociation of the biomass surface, but also on the solution chemistry of the metals including hydrolysis, complexation by organic and/or inorganic ligands, redox reactions, precipitation, the speciation and the bio-sorption availability of the metals [37,38]. The effects of sample pH were

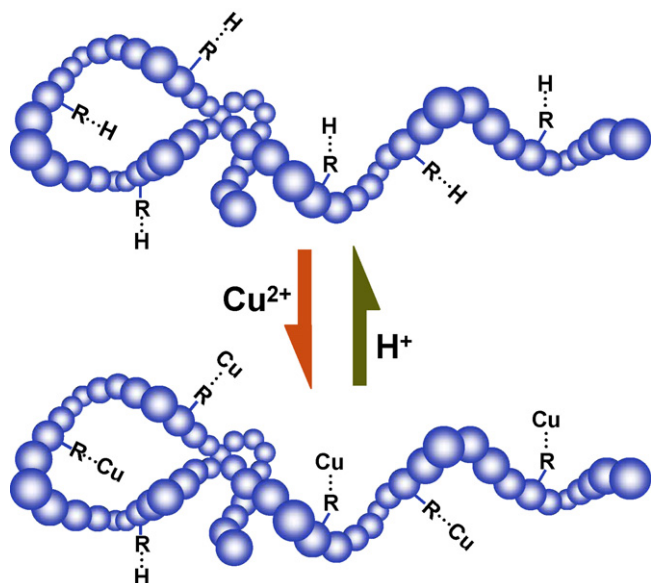


Fig. 2. Binding formation between Cu^{2+} ions and functional groups of silk fibroin molecular chains. R: active sites, e.g., CH_2O , CH_2COO , $\text{CH}_2\text{C}_6\text{H}_4\text{O}$.

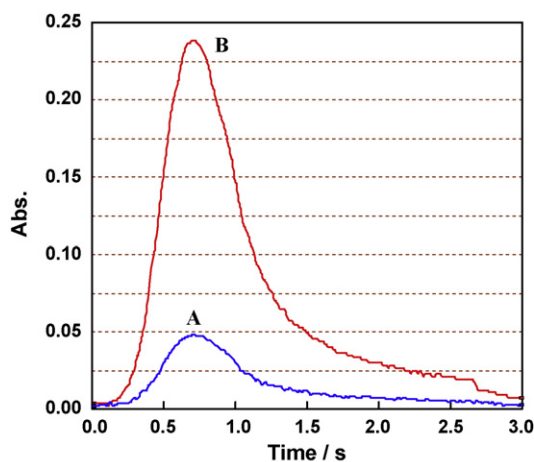


Fig. 3. Determination of Cu^{2+} in the effluent and the eluate with detection by ETAAS. (A) Signal derived from the effluent, (B) signal derived from the eluate. Sample volume: 900 μl , $0.5 \mu\text{g l}^{-1}$ Cu^{2+} ; sample loading flow rate: $10.0 \mu\text{l s}^{-1}$; eluent (0.50 mol l^{-1} nitric acid): 30 μl ; elution flow rate: $5.0 \mu\text{l s}^{-1}$.

investigated in the range of 2.0–8.0 by fixing a loading flow rate at $10.0 \mu\text{l s}^{-1}$ and the results were summarized in Fig. 4. An obvious increase in the retention efficiency was observed as the pH value increased from 2.0 to 6.0, and it kept virtually unchanged in the range of 6.0–7.0, thereafter a slight decline of the efficiency appeared when further increasing the pH value. This could be attributed to the fact that copper was presented in a free cation form (Cu^{2+}) in an acidic medium, i.e., $\text{pH} \leq 6.0$, and then the charge intensity of the functional groups of solid materials played a crucial role in the metal sorption. It has been known that the isoelectric point of serine, tyrosine and aspartic acid is 5.68, 5.66, and 2.97, respectively. As a function of pH value, the dissociations of the acidic functional groups on the silk fibroin, which providing binding sites for the metal ions, were governed by the acidity of the solution. At a low pH value, e.g., 2.0, the dissociations were suppressed greatly due to the excess H^+ in the sample solution and therefore nearly no sorption took place. The increase of pH value facilitated the dissociation of functional groups and thus more binding sites were released for the sorption of metals. As a result, increased retention efficiency was achieved. However, an even higher pH value, i.e., 7.0, tended to cause the precipitation of $\text{Cu}(\text{OH})_2$, which resulted in the

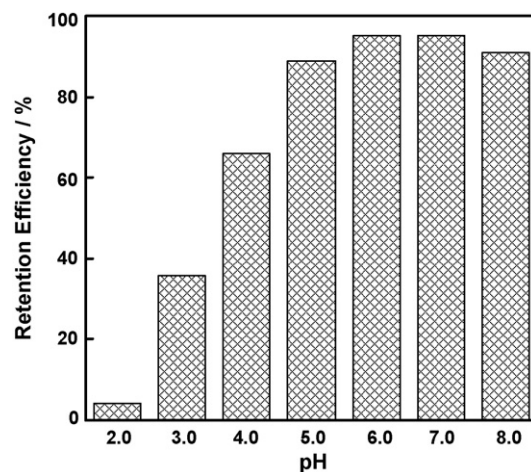


Fig. 4. Effects of pH of sample solutions on the retention efficiency. Sample volume: 900 μl , $0.5 \mu\text{g l}^{-1}$ Cu^{2+} ; sample loading flow rate: $10.0 \mu\text{l s}^{-1}$; eluent (0.5 mol l^{-1} nitric acid): 30 μl ; elution flow rate: $5.0 \mu\text{l s}^{-1}$.

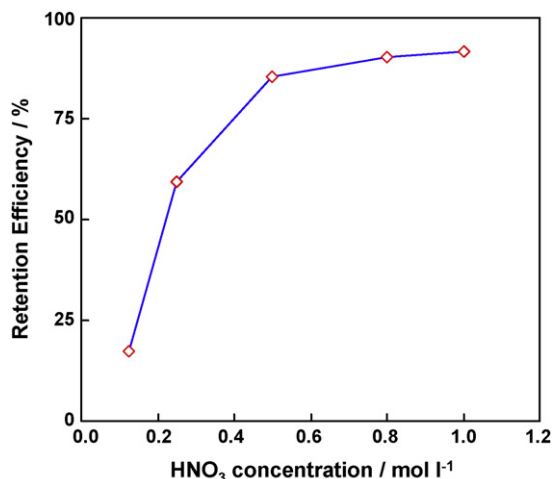


Fig. 5. Effects of HNO₃ concentrations on the elution efficiency. Sample volume: 900 μl, 0.5 μg l⁻¹ Cu²⁺; eluent: 30 μl; elution flow rate: 5.0 μl s⁻¹.

heterogeneity of the fluidic flow and the contamination of sorbent surface and hence a slight decline of the retention efficiency. Consequently a sample pH value of 6.0 was employed for the ensuing investigations.

3.3. Effect of sample loading flow rate

The effect of sample loading flow rate on the retention efficiency was investigated in the range of 2.0–30.0 μl s⁻¹. The experimental results indicated a decline of the retention efficiency of Cu²⁺ with the increase of flow rates. The retention efficiency was decreased from 100% to 94.9% with a variation of flow rate from 2.0 μl s⁻¹ to 10.0 μl s⁻¹, while a sharp drop to 45.8% was observed when further increase the flow rate to 30.0 μl s⁻¹. This might be attributed to the fact that the bio-sorption of Cu²⁺ with the silk fibroin was a relative slow process, which took certain time to accomplish the electrostatic interactions between Cu²⁺ and the acidic groups [35]. Therefore a suitable long of contacting time between the sample and the solid-phase material obviously facilitated the sorption process. For the comprehensive consideration of retention efficiency and analysis frequency, a sample loading flow rate of 10.0 μl s⁻¹ was adopted.

3.4. The acidity of eluent and the elution flow rate

Diluted nitric acid was employed as eluent for the strip of the retained Cu²⁺ from the surface of the silk fibroin granule packed micro-column. The effect of nitric acid concentration on the analytical performance of the entire system in terms of elution efficiency and detection limit was investigated in a concentration range of 0.125–1.0 mol l⁻¹. The results were illustrated in Fig. 5. It could be seen that the elution efficiency increased with the increase of HNO₃ concentration. This might be attributed to that more protons

Table 2
Analytical performance of this proposed system.

Sample volume	900 μl
Linear calibration range	0.025–1.5 μg l ⁻¹
Regression equation	Abs = 0.3389C _{Cu} + 0.0363
Analytical frequency	18 h ⁻¹
Detection limit (3σ, n = 11)	8.0 ng l ⁻¹
R.S.D. (0.5 μg l ⁻¹ , n = 9)	2.2%
Enrichment factor	27.3

provided by the acid displaced the adsorbed Cu²⁺ at a higher eluent concentration. While the experimental results indicated that a relative high HNO₃ concentration, i.e., ≥0.8 mol l⁻¹, would result in an increased blank and an irregular signal peak shape. Thus, a 0.5 mol l⁻¹ HNO₃ was employed as eluent for the ensuing investigations where an elution efficiency of ≥85% could be obtained.

By fixing an eluent volume of 30.0 μl, the effect of elution flow rate was examined in the range of 2.0–12.0 μl s⁻¹ and a decline of the elution efficiency was observed with the increase of the elution flow rate. It suggested that a long reaction time facilitated the displacement of the retained Cu²⁺ with H⁺. In the present case, an elution flow rate of 5.0 μl s⁻¹ was recommended for further studies.

3.5. The effects of foreign species

In order to evaluate the practical applicability of the present procedure for the determination of copper in real samples, the potential interfering effects of some species frequently encountered in biological and environmental samples were investigated by analyzing a standard solution containing 0.5 μg l⁻¹ Cu²⁺ and various amounts of coexisting species. The experiments indicated that within a ±5% error range, interfering effects from alkali and alkaline earth metal ions were not observed. In addition, 100 μg l⁻¹ of Fe³⁺, Al³⁺, Cr³⁺ and Cd²⁺; 50 μg l⁻¹ of Co²⁺, Pb²⁺, Ni²⁺, Mn²⁺, Hg²⁺ and Bi³⁺ do not interfere with the determination (no tests for higher concentration levels). For real-world samples, the contents of the above mentioned coexisting species are usually lower than the tolerant concentration levels, therefore the present protocol can be readily exploited directly, and no further sample treatment or masking reagents are needed.

3.6. Analytical performance and validation of the procedure

The characteristic analytical performance data of the proposed procedure for the preconcentration of Cu²⁺ by employing a silk fibroin granule packed micro-column with detection by ETAAS were summarized in Table 2, in terms of enrichment factor (EF), detection limit and sampling frequency. The enrichment factor was calculated as the ratio of the slope of the calibration graphs with and without preconcentration. For a copper sample with a sampling volume of 900 μl, an enrichment factor of 27.3, a detection limit of 8.0 ng l⁻¹ along with a sampling frequency of 18 h⁻¹ were obtained within a linear range of 0.025–1.5 μg l⁻¹, achieving a precision of 2.2% R.S.D. at the level of 0.5 μg l⁻¹.

Table 3
Analytical features of procedures for Cu²⁺ determination by ETAAS involving on-line solid-phase extraction separation/preconcentration.

Sorbent	Eluent	Vs (ml)	EF	El ^a	Detection limit (ng l ⁻¹)	Sampling rate (h ⁻¹)	Ref.
Silica-macrocyclic ligand	40 μl 2.5 mol l ⁻¹ HNO ₃	7.1	82	11.6	46	10	[15]
PTFE micro-beads	40 μl methanol	1.0	20	20	15	26	[17]
PTFE-based KR	45 μl methanol	5.9	33.6	5.7	5.7	21.6	[18]
PTFE-based KR	55 μl methanol	3.3	44	13.3	6.0	26	[19]
Poly-styrene-divinylbenzene resin	150 μl 3.0 mmol l ⁻¹ PDCA	200	1300	6.5	1.0	–	[21]
Silk fibroin	30 μl 0.5 mol l ⁻¹ HNO ₃	0.9	27.3	30.3	8.0	18	This method

^a The El values for the literatures are calculated from the reported data of sample volumes and enrichment factors.

Table 4

Determination results for real sample assays.

Sample	Certified ($\mu\text{g l}^{-1}$)	Found ($\mu\text{g l}^{-1}$)	Spiked ($\mu\text{g l}^{-1}$)	Recovery (% , $n = 3$)
NASS-5	0.297 \pm 0.046	0.299 \pm 0.011	–	–
GBW08608	0.508 \pm 0.020	0.506 \pm 0.014	–	–
Cave water	–	0.435 \pm 0.005	0.5	96.8%

For comparisons, the main analytical features of the proposed system and those attained by procedures for Cu^{2+} determination by ETAAS involving on-line solid-phase extraction separation/preconcentration were presented in Table 3. Although the detection limits obtained by using various sorbents were comparable, it should be emphasized that in the present system the silk fibroin was employed as the sorbent for direct adsorption of Cu^{2+} avoiding any pre-modifications of the sorbent surface and chelating reactions, which obviously simplified the manipulation of the entire operation.

Enrichment factor is an indispensable parameter for evaluation of the flow-based preconcentration systems. When the enrichment factor is used exclusively, however, it does not provide adequate information on the efficiency of a procedure. It should be kept in mind that a higher enrichment factor is not necessarily associated with high efficiency, as it might be achieved at the expense of a large sample volume. Therefore for comprehensive evaluation of the preconcentration efficiency of a flow-based system, a novel concept of enrichment index (EI), defined as enrichment factor obtained by consuming unity of sample volume (ml), is proposed, as expressed in the following equation:

$$\text{EI} = \frac{\text{EF}}{\sqrt{V_s}}$$

where V_s denotes the total sample volume consumed in the preconcentration process. Table 3 illustrates a comparison of the enrichment index of this procedure with some reported solid-phase extraction procedures for Cu^{2+} . It is obvious that the present system provides a much improved EI value.

The reusability and stability of this silk fibroin micro-column was tested by 50 repeated loading and elution cycles. No obvious change was observed in the obtained results, suggesting that this proposed micro-column was suitable for long-term repetitive sorption/desorption of metal species.

The practical applicability of the present system was demonstrated by analyzing Cu^{2+} contents in certified reference materials of riverine water (GBW08608) and seawater (NASS-5). The analytical results were summarized in Table 4. It is obvious that reasonable agreements were achieved between the certified and the found values.

In order to further validate this procedure, spiking recovery test of Cu^{2+} was also performed for a cave water sample using this method. The results listed in Table 4 showed that favorable recovery for the real environmental sample had been achieved.

4. Conclusions

An on-line solid-phase extraction procedure for preconcentration of Cu^{2+} by exploiting silk fibroin as the sorbent was developed. The silk fibroin provides abundant functional groups for retaining metal species of interest and the retained metal ions could readily be desorbed by employing a suitable stripping reagent. In addition, the silk fibroin entails a distinct advantage over the conventional

adsorbents as an environmental-friendly material which could be easily obtained and recycled after use facilitating rapid biodegradation. This material thus shows vast potentials as a bio-compatible material for sample pretreatment. Furthermore, a novel concept of enrichment index is proposed for evaluating the enrichment efficiency of a flow-based preconcentration procedure.

Acknowledgments

Financial supports from the Natural Science Foundation of China (Nos. 20575010, 20805004, National Science Fund for Distinguished Young Scholars No. 20725517 and Major International Joint Research Project 20821120292) are highly appreciated.

References

- [1] N.N. Greenwood, A. Earnshaw, Chemistry of the Elements, Pergamon, New York, 1984.
- [2] I.S. Balogh, M. Ruschak, V. Andruch, Y. Baze, Talanta 76 (2008) 111.
- [3] L. Morales, M.I. Toral, M.J. Álvarez, Talanta 74 (2007) 110.
- [4] D. Schiavo, J.Y. Neira, J.A. Nóbrega, Talanta 76 (2008) 1113.
- [5] Z. Ajtony, N. Szoboszlai, E.K. Suskó, P. Mezei, K. György, L. Bencs, Talanta 76 (2008) 627.
- [6] S. Walas, A. Tobiasz, M. Gawin, B. Trzewik, M. Strojny, H. Mrowiec, Talanta 76 (2008) 96.
- [7] J.M. Liu, L.Y. Xu, L. Chen, H. Wu, F.M. Li, S.X. Lin, Z.B. Shi, Z.M. Li, G.H. Zhu, X.M. Huang, Anal. Lett. 40 (2007) 295.
- [8] H.S. Kim, H.S. Choi, Talanta 55 (2001) 163.
- [9] M.B. Gholivand, A. Sohrabi, S. Abbasi, Electroanalysis 19 (2007) 1609.
- [10] H.M. Abu-Shawish, S.M. Saadeh, A.R. Hussini, Talanta 76 (2008) 941.
- [11] N. Oleszczuk, J.T. Castro, M.M. da Silva, M.G.A. Korn, B. Welz, M.G.R. Vale, Talanta 73 (2007) 862.
- [12] J.-H. Wang, E.H. Hansen, J. Anal. Atom. Spectrom. 17 (2002) 1284.
- [13] J.-H. Wang, E.H. Hansen, Trends Anal. Chem. 22 (2003) 836.
- [14] Z. Wan, Z.R. Xu, J.-H. Wang, Analyst 131 (2006) 141.
- [15] E. Hosten, B. Welz, Anal. Chim. Acta 392 (1999) 55.
- [16] Z.F. Queiroz, F.R.P. Rocha, G. Knapp, F.J. Krug, Anal. Chim. Acta 463 (2002) 275.
- [17] Y.-L. Yu, Z. Du, J.-H. Wang, Chinese J. Anal. Chem. 35 (2007) 431.
- [18] K. Benkhedda, E. Ivanova, F. Adams, J. Anal. Atom. Spectrom. 14 (1999) 957.
- [19] E. Ivanova, K. Benkhedda, F. Adams, J. Anal. Atom. Spectrom. 13 (1998) 527.
- [20] V.A. Lemos, M.A. Bezerra, F.A.C. Amorim, J. Hazard. Mater. 157 (2008) 613.
- [21] S. Scaccia, G. Zappa, N. Basili, J. Chromatogr. A 915 (2001) 167.
- [22] T.A. Davis, B. Volesky, A. Mucci, Water Res. 37 (2003) 4311.
- [23] A.-M. Zou, M.-L. Chen, Y. Shu, M. Yang, J.-H. Wang, J. Anal. Atom. Spectrom. 22 (2007) 392.
- [24] A.-M. Zou, M.-L. Chen, X.-W. Chen, J.-H. Wang, Anal. Chim. Acta 598 (2007) 741.
- [25] A.-M. Zou, X.-Y. Tang, M.-L. Chen, J.H. Wang, Spectrochim. Acta B 63 (2008) 607.
- [26] K. Vijayaraghavan, Y.S. Yun, Biotechnol. Adv. 26 (2008) 266.
- [27] F. Aloulou, S. Boufi, J. Labidi, Sep. Purif. Technol. 52 (2006) 332.
- [28] M.-L. Chen, Y. Tian, J.-H. Wang, J. Anal. Atom. Spectrom. 23 (2008) 876.
- [29] A. Pourjavadi, H. Salimi, M.S. Amini-Fazl, M. Kurdtabar, A.R. Amini-Fazl, J. Appl. Polym. Sci. 102 (2006) 4878.
- [30] A.-M. Zou, X.-W. Chen, M.-L. Chen, J.-H. Wang, J. Anal. Atom. Spectrom. 23 (2008) 412.
- [31] J. Magoshi, Y. Magoshi, S. Nakamura, Silk Polymers: Materials Science and Biotechnology, American Chemical Society, Washington, DC, 1993, p. 211.
- [32] P. Kongkachuichay, A. Shitangkoon, N. Chinwongamorn, Dyes Pigments 53 (2002) 179.
- [33] E. Altioik, D. Baycin, O. Bayraktar, S. Ulku, Sep. Purif. Technol. 62 (2008) 342.
- [34] D. Baycin, E. Altioik, S. Ulku, O. Bayraktar, J. Agric. Food Chem. 55 (2007) 1227.
- [35] C.S. Ki, E.H. Gang, I.C. Um, Y.H. Park, J. Membr. Sci. 302 (2007) 20.
- [36] G. Nalankilli, S. Padampat, Am. Dyest. Rep. 9 (1994) 28.
- [37] A. Esposito, F. Pagnanelli, F. Veglio, Chem. Eng. Sci. 57 (2002) 307.
- [38] J.L. Wang, C. Chen, Biotechnol. Adv. 24 (2006) 427.



Speciation of inorganic arsenic in a sequential injection dual mini-column system coupled with hydride generation atomic fluorescence spectrometry

Mingli Chen, Yumei Huo, Jianhua Wang*

Research Center for Analytical Sciences, Northeastern University, Box 332, Shenyang 110004, China

ARTICLE INFO

Article history:

Received 5 August 2008

Received in revised form 26 October 2008

Accepted 27 October 2008

Available online 12 November 2008

Keywords:

Arsenic speciation

Sequential injection

Dual mini-column

C18

717 anion exchange resin

Hydride generation atomic fluorescence spectrometry

ABSTRACT

The separation and speciation of inorganic arsenic(III) and arsenic(V) are facilitated by employing a novel sequential injection system incorporating two mini-columns followed by detection with hydride generation atomic fluorescence spectrometry. An octadecyl immobilized silica mini-column is used for selective retention of the complex between As(III) and APDC, while the sorption of As(V) is readily accomplished by a 717 anion exchange resin mini-column. The retained As(III)–PDC complex and As(V) are effectively eluted with a 3.0 mol L⁻¹ hydrochloric acid solution as stripping reagent, which well facilitates the ensuing hydride generation process via reaction with tetrahydroborate. With a sampling volume of 1.0 mL and an eluent volume of 100 μL for both species, linear ranges of 0.05–1.5 μg L⁻¹ for As(III) and 0.1–1.5 μg L⁻¹ for As(V) are obtained, along with enrichment factors of 7.0 and 8.2, respectively. Precisions of 2.8% for As(III) and 2.9% for As(V) are derived at the concentration level of 1.0 μg L⁻¹. The practical applicability of the procedure has been demonstrated by analyzing a certified reference material of riverine water (SLRS-4), in addition to spiking recovery in a lake water sample matrix.

© 2008 Elsevier B.V. All rights reserved.

1. Introduction

The toxic effects of arsenic have been widely demonstrated in some areas like environment, dairy food, etc. [1,2]. Recently, extensive attentions have been focused on the arsenic pollution of surface water [3]. In some cases, excessive high concentrations of arsenic caused serious health problems [4–6]. Thus, the World Health Organization is currently conducting the guidelines for drinking and environmental waters [3]. The wide distribution of arsenic in biosphere and its pronounced detrimental effects on the ecological system, biological organisms as well as human health not only depend on the total amount, but most significantly, depend strongly on its chemical forms and distribution [1,7]. It is well recognized that inorganic arsenic compounds are far more toxic than their organic counterparts [8], while as refer to the two inorganic arsenic forms, arsenite is more toxic than arsenate [9]. In this respect, it is highly desirable to develop suitable speciation approaches for arsenic in order to provide reliable information concerning the toxicity of arsenic in the sample matrices [10].

Atomic absorption spectrometry (AAS) and inductively coupled plasma mass spectrometry (ICPMS) have been widely employed

for the evaluation of total amount of arsenic as well as arsenic speciation hyphenated with various separation and preconcentration protocols [11,12]. ICPMS provides very high sensitivity for arsenic determination, but the operation and maintenance of the instrumentation is quite costly, thus limited its wide applications in routine laboratories. On the other hand, the detection sensitivity for arsenic species by using atomic absorption spectrometry is so far not favorable. In the last decade, a lot of efforts have been dedicated to the development of analytical procedures for hydride forming elements including arsenic with detection by atomic fluorescence spectrometry (AFS), which offers competitive sensitivity with ICPMS for their determination, while requires much lower running cost [13–15].

For many of real world samples, arsenic concentrations might be very low in the presence of complex sample matrices. In such circumstances, the insufficient detection sensitivity in addition to the matrix effects tends to block the accurate determination of arsenic and its speciation. Therefore, pertinent sample pretreatment schemes are required [16]. In this respect, flow/sequential injection on-line separation and preconcentration protocols are most suitable for this purpose, which provide extensive flexibilities in flow manifold design [17]. Among those the hyphenation of sample clean-up with hydride generation atomic fluorescence spectrometry has vast potentials because of its low running cost, ease of operation, improved selectivity and sensitivity [10,14]. In addition, the flow through characteristic of AFS well facilitates

* Corresponding author. Tel.: +86 24 83688944; fax: +86 24 83676698.
E-mail address: jianhuajrz@mail.neu.edu.cn (J. Wang).

its incorporation into various on-line separation/preconcentration and speciation systems [15,18,19].

Conventionally, the speciation of inorganic arsenic without employing chromatographic separation is performed by direct analysis of As(III) followed by quantification of total inorganic arsenic after reduction of As(V), and the amount of As(V) is thus obtained by subtraction [20,21]. In the present work, we developed a novel separation and preconcentration procedure for inorganic arsenic by designing a sequential injection system which incorporates two mini-columns packed with C18 and 717 anion exchange resin for selective retention of As(III)–APDC complex and As(V), respectively. Both species were collected with an appropriate eluent followed by quantification with hydride generation atomic fluorescence spectrometry.

2. Experimental

2.1. Instrumentation

A FIALab-3000 sequential injection system (FIALab Instruments, Bellevue, WA, USA) equipped with two syringe pumps (5.0 and 1.0 mL) and an 8-port selection valve was employed for fluids delivery and sample processing. An AFS-920 atomic fluorescence spectrometer equipped with two syringe pumps (5.0 mL) and a selection valve (Beijing Titan Instruments, China) was employed for hydride generation and quantification. A high-intensity arsenic hollow cathode lamp at 193.7 nm (Beijing General Research Institute for Nonferrous Metals, China) was used as radiation source. An argon flow was used to sweep the separated arsine from the gas–liquid separator to the quartz tube atomizer. A single computer was used to control both the atomic fluorescence spectrometer and the sequential injection system in order to synchronize the sample processing and the AFS determination.

All the external channels were made of PTFE tubing (0.8 mm i.d./1.0 mm o.d.). The mini-columns were made by filling 5 mg of C18 immobilized silica beads (100 μm) or 11 mg of 717 anion exchange resin (150 μm) into a piece of PTFE tubing (1.8 mm i.d./2.3 mm o.d.) and blocked at both ends with glass wool.

2.2. Reagents

All the reagents used were at least of analytical reagent grade, and deionized water of 18 M Ω cm as carrier solution was used throughout. Working standard solutions of As(III) and As(V) were prepared by stepwise dilution of 1000 mg L⁻¹ stock solutions. A 0.06% (m/v) ammonium pyrrolidine dithiocarbamate (APDC) (Sinopharm Chemical Reagent Co., China) solution as complexing reagent was prepared daily by dissolving appropriate amount of APDC in deionized water. A NaBH₄ solution of 1.0% (m/v) in 0.5% NaOH (m/v) solution was prepared daily with sodium tetrahydroborate (Sinopharm Chemical Reagent Co., China). Other chemicals used include suprapur hydrochloric acid (Sinopharm Chemical Reagent Co., China), octadecyl immobilized silica beads (nominal bead size: 100 μm , Tianjin Di-er Chemicals Co., Tianjin, China), 717 anion exchange resin (300–1200 μm in diameter, Sinopharm Chemical Reagent Co., China) was grounded and sieved to control the diameter at ca. 150 μm for mini-column packing.

2.3. Samples and sample pretreatment

A certified reference material of SLRS-4 (Riverine Water, National Research Council, Canada) is used for demonstrating the practical applicability of the proposed procedure. The pH value of the water sample is adjusted to pH 3 before undergoing the preconcentration process.

A lake water sample from Nan-Hu Lake outside the campus of Northeastern University is used for spiking recovery test. Appropriate amount of the lake water is filtered through a qualitative filter paper with aperture of 30–50 μm , the acidity of which is afterwards adjusted to pH 3 before preconcentration on the mini-columns.

2.4. Operating procedures

The flow manifold of the sequential injection system was illustrated in Fig. 1. The procedure includes the sorption of As(III)–PDC complex onto the C18 micro-column and the retention of As(V) by the 717 anion exchange resin column, followed by mini-columns rinsing, elution and hydride generation.

2.4.1. Preconcentration and determination of As(III)

Syringe pump SP1 was set to successively aspirate 800 μL air from port 2 and 1000 μL of sample solution from port 3 into holding coil HC1 at a flow rate of 100 $\mu\text{L s}^{-1}$. In the meantime, 1000 μL of APDC solution was aspirated into SP2 at a same flow rate. The sample solution was thereafter dispensed via port 4 at 15 $\mu\text{L s}^{-1}$ to meet the APDC solution zone delivered by P2 at a same flow rate, and the formed As(III)–PDC complex was adsorbed onto the C18 mini-column. The mini-column was then evacuated by the stored air zone, followed by a prewashing procedure with 600 μL of deionized water, and the mini-column was finally evacuated.

100 μL of hydrochloric acid (3 mol L⁻¹) solution was aspirated into holding coil HC1 via port 6 which was thereafter directed via port 4 at 10 $\mu\text{L s}^{-1}$ to collect the retained As(III)–PDC complex and the eluate was stored in holding coil HC2. Afterwards, the eluate and a sodium tetrahydroborate solution zone were directed by syringe pumps of the AFS system to confluence downstream and trigger the hydride generation process. The hydride was isolated in the gas–liquid separator and swept by an argon stream to flow through the atomic fluorescence spectrometer for quantification.

2.4.2. Preconcentration and determination of As(V)

1000 μL of sample solution was aspirated via port 3 into holding coil HC1, which was thereafter dispensed via port 5 at a flow rate of 15 $\mu\text{L s}^{-1}$ to flow through the 717 anion exchange resin mini-column for facilitating the sorption of As(V). Afterwards, the mini-column was thoroughly rinsed with 400 μL of deionized

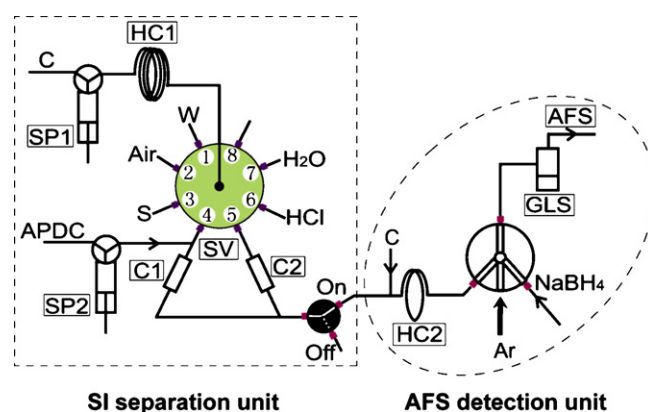


Fig. 1. The flow manifold for separation and preconcentration of As(III)–PDC complex and As(V) respectively onto C18 and 717 anion exchange resin mini-columns in a sequential injection system, followed by their speciation with detection by hydride generation atomic fluorescence spectrometry. SP1, SP2: syringe pumps; HC1, HC2: holding coils; SV: 8-port selection valve; C1: C18 packed mini-column; C2: a mini-column packed with 717 anion exchange resin; GLS: gas–liquid separator; AFS-920: atomic fluorescence spectrometer; S: sample; W: waste; C: carrier solution (deionized water).

Table 1
AFS operating parameters.

Parameters	Settings
Arsenic hollow cathode lamp	193.7 nm
Lamp current	60 mA
Atomizer height	8 mm
Integration time	3 s
Time delay	3 s
Negative high voltage of PMT	400 V
Carrier argon flow	1000 mL min ⁻¹
Shield argon flow	800 mL min ⁻¹
Reading mode	Peak area

water followed by evacuation with an air zone of 800 μL . The elution and hydride generation processes are exactly the same as those adopted for As(III).

2.5. The AFS parameters

The experimental parameters for AFS operations have been carefully scrutinized in terms of signal-to-noise ratio (sensitivity) as well as peak shapes by using As(III)/As(V) standard solutions of 1.0 $\mu\text{g L}^{-1}$, and peak area was employed for quantification. Details of the operating parameters employed in the present investigation for the AFS instrument were summarized in Table 1.

3. Results and discussion

3.1. On-line sorption of As(III) and As(V) by the dual mini-column system

3.1.1. The effect of acidity on the sorption of As(III)–PDC complex and As(V)

In the present work, pH of the sample solution has been demonstrated to be a critical factor for governing not only the stability of the As(III)–PDC complex in aqueous medium, but also the sorption efficiencies of the As(III)–PDC complex onto the C18 mini-column and that of the As(V) onto the 717 anion exchange resin mini-column. When employing a fixed concentration of APDC solution of 0.06% (m/v), the effect of pH of sample solution on the sorption of As(III)–PDC complex and As(V) onto the C18 mini-column was illustrated in Fig. 2A indicating the variation of fluorescence intensity within a range of pH 1–6. When considering the As(III)–PDC complex, it is obvious that a slight increment of the fluorescence intensity was observed by increasing the pH from 1 to 3, while thereafter an obvious decline was encountered when further increasing pH value of the sample solution. On the other hand, very limited fluorescence intensity was recorded attributed to As(V) within the pH range investigated, which indicated that the con-

tribution of the signal arising from As(V) at pH < 3 was controlled within ca. 8%.

When the 717 anion exchange resin mini-column was employed as sorption medium, a significant enhancement of fluorescence intensity was obtained attributed to As(V) by increasing pH from 1 to 4, as illustrated in Fig. 2B. It is obvious that a limited contribution of fluorescence signal derived from the As(III)–PDC complex was recorded, i.e., not exceed 9% at pH < 3, while thereafter a substantial increment of the fluorescence intensity was encountered up to pH 6.

This observation might be attributed to the fact that As(V) in an aqueous solution at pH < 1 is predominated by molecular H_3AsO_4 [22,23], its sorption onto the 717 anion exchange resin mini-column is unfavourable and thus virtually no signal was recorded. A gradual increase of the pH of sample solution gives rise to more anionic species, i.e., H_2AsO_4^- , HAsO_4^{2-} and AsO_4^{3-} , which facilitate their retention onto the mini-column via anion exchange effect. This has been illustrated by the increment of fluorescence intensity with an increase of pH value from 1 to 4 followed by a minor drop up to pH 6. As for the As(III)–PDC complex, it is neutral within the range of pH < 3 and thus no obvious sorption onto the 717 anion exchange resin mini-column was encountered. With the increase of pH value of the sample solution, on one hand, the complex tends to be negatively charged and thus facilitates sorption by the 717 mini-column. On the other hand, the As(III)–PDC complex is unstable at a higher pH, which gives rise to some free As(III) species in the forms of H_2AsO_3^- , HAsO_3^{2-} and AsO_3^{3-} [20,23]. These species could readily be retained by the 717 anion exchange resin mini-column. Thus, an obvious increment of fluorescence intensity was observed with the increase of pH value.

It is obvious from the above discussions that at pH 3, the C18 mini-column provides favourable retention of As(III)–PDC complex, while the sorption of As(V) is negligible. At same experimental conditions, the 717 anion exchange resin mini-column facilitates selective retention of As(V) in the presence of As(III) or As(III)–PDC complex. These observations offer a promising potential for selective separation/preconcentration and speciation of As(III) and As(V) by employing C18 and 717 anion exchange resin as sorbents, respectively.

3.1.2. The effect of APDC concentration on the sorption of As(III)–PDC complex

An appropriate amount of APDC should be used to provide sufficient chelating reagent for converting As(III) to As(III)–PDC complex in order to ensure its selective sorption onto the C18 mini-column. The experiments have shown that when a fixed volume of APDC solution of 1000 μL was employed, an obvious improvement of the fluorescence intensity was observed as APDC concentration

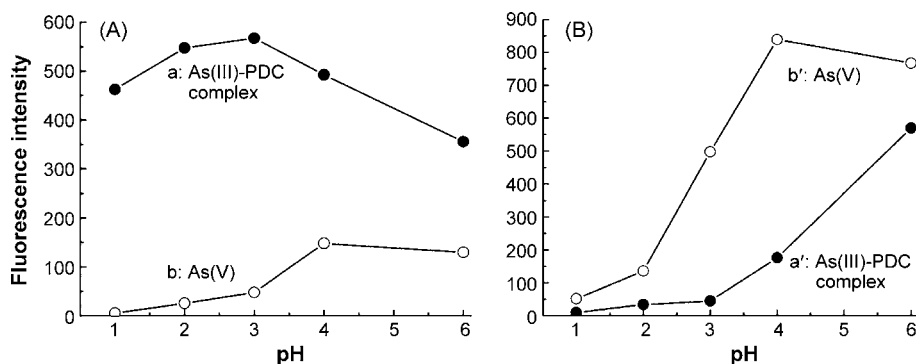


Fig. 2. The dependences of sorption of As(III)–PDC complex and As(V) on the pH of sample solution. A: sorption on the C18 mini-column; B: sorption on the 717 anion exchange resin mini-column. (a, a') sorption of As(III)–PDC complex; (b, b') sorption of As(V).

was increased from 0.02% (m/v) to 0.06% (m/v), and thereafter a decline of the signal was encountered when further increasing the APDC concentration up to 0.10% (m/v) (fluorescence data were not shown). This indicated that a concentration of 0.06% (m/v) APDC provides sufficient amount of chelating reagent for the conversion of As(III) to As(III)–PDC complex. While excessive amount of chelating reagent would compete for the active sites of the C18 surface [10], resulting in a decrease of the sorption efficiency and thus a drop of the fluorescence intensity in the following process. For further experiments, an APDC concentration of 0.06% (m/v) was employed.

3.1.3. The sample loading flow rates

In a flow configuration for sample pretreatment, it is highly desired to achieve favorable retention efficiency for the analyte of interest and at the same time give rise to satisfactory sampling frequency for the preconcentration process [14]. The selection of a suitable sample loading time or sampling flow rate is thus among the most important parameters. In the present system the complexation reaction between As(III) and APDC as well as the kinetics of the sorption of As(III)–PDC complex onto the C18 surface are not very fast processes, thus sample loading flow rates within a range of 5–30 $\mu\text{L s}^{-1}$ were investigated by fixing an APDC concentration at 0.06% and the acidity of sample solution at pH 3. The results showed that a decline of the fluorescence intensity was observed when the sampling flow rate was increased from 5 to 30 $\mu\text{L s}^{-1}$ (Fluorescence data were not shown). As a compromise between the preconcentration efficiency and the sampling frequency, a sampling flow rate of 15 $\mu\text{L s}^{-1}$ was chosen in the subsequent experiments for As(III)–PDC complex sorption. On the other hand, no obvious variation was observed for the sorption of As(V) onto the 717 anion exchange resin mini-column and corresponding fluorescent intensity within the same range of sampling flow rate, thus an identical sampling flow rate, i.e., 15 $\mu\text{L s}^{-1}$, was employed for loading the As(V) solution.

3.1.4. Prewashing of the mini-columns before elution

Our experiments have shown that a limited fluorescence signal was achieved when a small amount of eluent, i.e., 100 μL of hydrochloric acid (3 mol L^{-1}), was employed for eluting the adsorbed arsenic species. Thereafter, a second elution gave rise to a much higher signal by using a same amount of eluent, indicating that the first part of the hydrochloric acid zone was consumed to strip some of the concomitantly adhered matrix components or interfering species on the surface of the mini-columns. Thus, prewashing procedures were adopted before elution of the retained arsenic species on both mini-columns. The results indicated that losses of both As(III) and As(V) were encountered if diluted hydrochloric acid (0.1 mol L^{-1}) was used as prewashing solution. Further experiments showed that deionized water could effectively remove the adsorbed concomitants on the surface of both C18 and 717 anion exchange resin mini-columns, giving rise to improved recoveries of adsorbed arsenic species when a fixed amount of hydrochloric acid was afterwards used as eluent (Fig. 3). A prewash of the C18 mini-column with 600 μL of deionized water at a flow rate of 10 $\mu\text{L s}^{-1}$ facilitates a complete elution of the retained As(III)–PDC complex by employing 100 μL of hydrochloric acid (3 mol L^{-1}). On the other hand, the prewash of the 717 anion exchange resin mini-column by 400 μL of deionized water at a same flow rate ensures a complete recovery of As(V) by hydrochloric acid.

3.1.5. The elution process

Although both organic and inorganic reagents could be used for the elution of adsorbed metal complex from the surface of solid substrate [20], inorganic acids are preferential in the present case

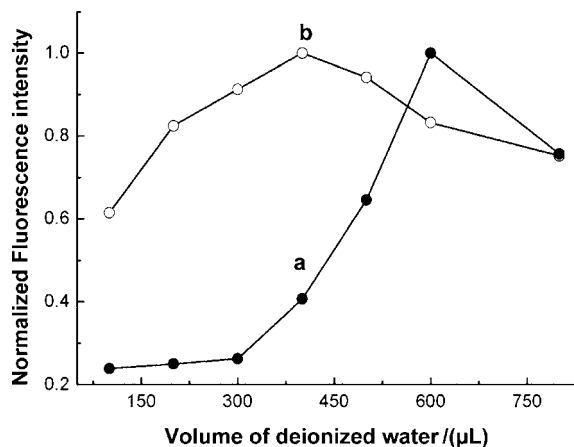


Fig. 3. The dependences of arsenic recoveries on the prewash of the mini-columns by using deionized water. (a) As(III)–PDC complex on C18 mini-column; (b) As(V) on 717 anion exchange resin mini-column.

considering the subsequent hydride generation and detection processes. When oxidizing acids were used, conversions of chemical forms of arsenic species might be encountered during the elution process [24], thus hydrochloric acid is the most suitable eluent for this system. Fig. 4 indicated that obvious increments on the fluorescence intensities for both As(III) and As(V) were observed with the increase of hydrochloric acid concentration in a range of 1.0–3.0 mol L^{-1} , and no further gains were obtained by using an even higher acid concentration. Considering that the ensuing hydride generation process requires a sufficient acid concentration in the eluate, a 3 mol/L hydrochloric acid was thus adopted as eluent for the recovery of both As(III)–PDC complex and As(V).

The volume of 3 mol/L hydrochloric acid as eluent was investigated within 50–150 μL . It indicated that complete recoveries of the retained As(III)–PDC complex and As(V) could only be achieved when a sufficient amount of eluent was employed. In the present system, 100 μL of hydrochloric acid ensures complete elution of both species. The experiments also indicated dependences of the recoveries of retained arsenic species from the mini-columns upon the elution flow rate, as illustrated in Fig. 5. It can be seen that maximum recoveries for As(III)–PDC complex and As(V) could be obtained at elution flow rates within 5–10 and 5–15 $\mu\text{L s}^{-1}$, respectively, while higher flow rates caused deteriorations on the

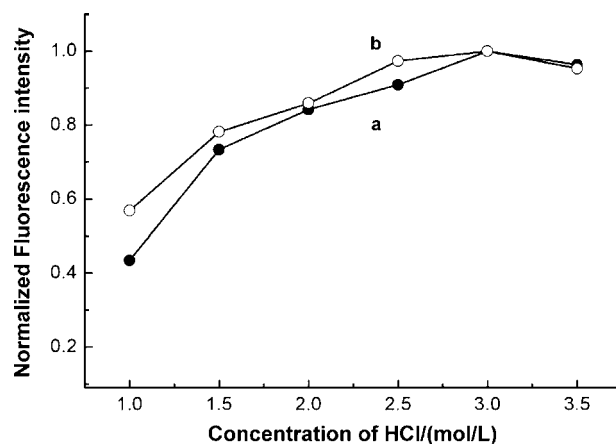


Fig. 4. The effect of hydrochloric acid concentration on the recovery of arsenic species from the mini-columns. (a) collection of As(III)–PDC complex from the C18 mini-column; (b) collection of As(V) from the 717 anion exchange resin mini-column.

Table 2The determination of inorganic arsenic species in a certified reference material of riverine water (SLRS-4) and a lake water sample ($n=3$).

Sample	Certified ($\mu\text{g L}^{-1}$)	Found ($\mu\text{g L}^{-1}$)		Spiked ($\mu\text{g L}^{-1}$)	Recovery	
		As(III)	As(V)		As(III)	As(V)
SLRS-4	0.68 ± 0.06	0.06 ± 0.01	0.64 ± 0.06			
Lake water	<d.l.	<d.l.	<d.l.	0.5	98%	103%

recovery rates of the adsorbed arsenic species. In this respect, elution flow rates of 10 and 15 $\mu\text{L s}^{-1}$ were employed for the recovery of As(III)–PDC complex and As(V), respectively.

3.1.6. The hydride generation process

The experiments have indicated that 1.0% (m/v) of NaBH_4 in a 0.5% (m/v) NaOH solution and 3 mol L^{-1} hydrochloric acid used for the elution of arsenic species from the mini-columns are sufficient for the ensuing hydride generation of the recovered As(III)–PDC complex and As(V). In order to ensure a complete reduction of the arsenic species, an excessive amount of NaBH_4 solution is required, i.e., a 500 μL of NaBH_4 solution was employed in the present system for the hydride generation of As(III)–PDC complex and As(V) in the eluates. We have previously demonstrated that the flow rates of both sample and NaBH_4 solution zones are most critical for the hydride generation and the ensuing atomic fluorescence detection [13]. Investigations in the present system have illustrated that a same flow rate of 100 $\mu\text{L s}^{-1}$ for the NaBH_4 solution and the eluates containing the recovered arsenic species, i.e., As(III)–PDC complex and As(V), produced maximum fluorescence intensities with better peak shapes (fluorescence data were not shown). Therefore, this flow rate was adopted for hydride generation in further investigations.

3.2. Interferences

The potential interfering effects of some foreign species which are frequently encountered in environmental samples were tested with the present procedure by gradually increasing the amount of foreign ions. All the tests were carried out under optimum operating conditions and evaluated with an arsenic concentration level of 1.0 $\mu\text{g L}^{-1}$ and within a 5% error range. Alkali and alkaline earth metal species can be tolerated up to 1.0 g L^{-1} without posing interfering effects for the determination of As(III) and As(V). As

for transition metal species, no interferences were identified for the determination of As(III) in the presence of 500 $\mu\text{g L}^{-1}$ Cu^{2+} , 400 $\mu\text{g L}^{-1}$ Fe^{3+} , 100 $\mu\text{g L}^{-1}$ Mn^{2+} , Pb^{2+} , Hg^{2+} and Zn^{2+} , 50 $\mu\text{g L}^{-1}$ Cd^{2+} , Ni^{2+} and Se(IV) . On the other hand, 500 $\mu\text{g L}^{-1}$ Cu^{2+} and Zn^{2+} , 400 $\mu\text{g L}^{-1}$ Fe^{3+} , 200 $\mu\text{g L}^{-1}$ Hg^{2+} and Pb^{2+} , 100 $\mu\text{g L}^{-1}$ Mn^{2+} , 50 $\mu\text{g L}^{-1}$ Cd^{2+} , Ni^{2+} and Se(IV) caused no obvious interferences when As(V) was analyzed.

3.3. Analytical performance and applications

At the above experimental conditions, when 1000 μL of sample solution was processed for the separation/preconcentration of As(III)–PDC complex or As(V) followed by elution with 100 μL of 3.0 mol L^{-1} HCl solution, enrichment factors of 7.2 and 8 were achieved for As(III) and As(V), respectively. The detection limits of 0.02 $\mu\text{g L}^{-1}$ for As(III) and 0.03 $\mu\text{g L}^{-1}$ for As(V) were obtained within linear ranges of 0.05–1.5 $\mu\text{g L}^{-1}$ As(III) and 0.1–1.5 $\mu\text{g L}^{-1}$ As(V). The precisions for As(III) and As(V) analyses are 2.8% RSD and 2.9% RSD at the concentration level of 1.0 $\mu\text{g L}^{-1}$. The present procedures result in sampling frequencies of 10 and 12 samples per hour for As(III) and As(V), respectively.

A certified reference material of SLRS-4 (Riverine Water) was employed to demonstrate the practical applicability of the present procedure by speciation of As(III) and As(V), the results are listed in Table 2. Although only total amount of arsenic is certified in this material and it provides no information about the distribution of inorganic arsenic species, a well agreement was achieved between the certified value of total arsenic and the sum of As(III) and As(V) concentrations determined. When analyzing a lake water sample by using this procedure, no As(III) and As(V) were detected. In the present work, 0.5 $\mu\text{g L}^{-1}$ of As(III) and As(V) were spiked and satisfactory recoveries were obtained.

4. Conclusions

The selective sorption of As(III)–PDC complex and As(V) onto the surface of C18 and 717 anion exchange resin provides a promising potential for the speciation of inorganic arsenic species in the presence of complex sample matrices. The separation and preconcentration of As(III)–PDC complex and As(V) on different mini-columns avoid the conversion of chemical states of the arsenic species, which facilitate direct quantification of both species and thus eliminate the error source arisen from the incomplete conversion of the arsenic species. The employment of a same chemical reagent at a fixed concentration for the recovery of the retained As(III)–PDC complex and As(V) from the solid substrates and their ensuing hydride generation significantly simplified the entire operation procedure. The use of a sequential injection system for sample processing improves the precision of the protocol, in addition to the downscaled sample/reagent consumption and automatic operation of the entire system.

Acknowledgements

Financial support from the Natural Science Foundation of China (no. 20575010, key project no. 20635010, National Science Fund

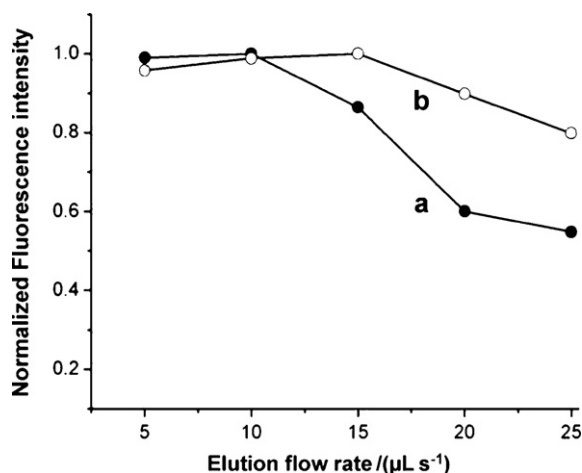


Fig. 5. The dependences of arsenic recoveries on the eluent flow rates. (a) collection of As(III)–PDC complex from the C18 mini-column; (b) collection of As(V) from the 717 anion exchange resin mini-column.

for Distinguished Young Scholars no. 20725517 and Major International Joint Research Project 20821120292) is highly appreciated.

References

- [1] M.N.M. Reyes, M.L. Cervera, R.C. Campos, M. de la Guardia, *Talanta* 75 (2008) 811.
- [2] K. Baba, T. Arao, Y. Maejima, E. Watanabe, H. Eun, M. Ishizaka, *Anal. Chem.* 80 (2008) 5768.
- [3] I.A. Katsoyiannis, S.J. Hug, A. Ammann, A. Zikoudi, C. Hatziliontos, *Sci. Total Environ.* 383 (2007) 128.
- [4] F.S. Islam, A.G. Gault, C. Boothman, D.A. Polya, J.M. Charnock, D. Chatterjee, J.R. Lloyd, *Nature* 430 (2004) 68.
- [5] T. Clarke, *Nature* 413 (2001) 556.
- [6] C.F. Harvey, C.H. Swartz, A.B.M. Badruzzaman, N. Keon-Blute, W. Yu, M.A. Ali, J. Jay, R. Beckie, V. Niedan, D. Brabander, P.M. Oates, K.N. Ashfaq, S. Islam, H.F. Hemond, M.F. Ahmed, *Science* 298 (2002) 1602.
- [7] M. Resano, E.G. Ruiz, V.G. Mihucz, A.M. Moricz, G. Zaray, F. Vanhaecke, *J. Anal. At. Spectrom.* 22 (2007) 1158.
- [8] M.N.M. Reyes, M.L. Cervera, R.C. Campos, M. de la Guardia, *Spectrochim. Acta B* 62 (2007) 1078.
- [9] Z.-L. Zhu, J.-L. Liu, S.-C. Zhang, X. Na, X.-R. Zhang, *Anal. Chim. Acta* 607 (2008) 136.
- [10] X.-P. Yan, X.-B. Yin, X.-W. He, Y. Jiang, *Anal. Chem.* 74 (2002) 2162.
- [11] T. Narukawa, T. Kuroiwa, K. Chiba, *Talanta* 73 (2007) 157.
- [12] L.S. Milstein, A. Essader, E.D. Pellizzari, R.A. Fernando, J.H. Raymer, K.E. Levine, O. Akinbo, *Environ. Health Persp.* 111 (2003) 293.
- [13] J.-H. Wang, Y.-L. Yu, Z. Du, Z.-L. Fang, *J. Anal. At. Spectrom.* 19 (2004) 1559.
- [14] X.-D. Tang, Z.-R. Xu, J.-H. Wang, *Spectrochim. Acta B* 60 (2005) 1580.
- [15] M.-L. Chen, A.-M. Zou, Y.-L. Yu, R.-H. He, *Talanta* 73 (2007) 599.
- [16] C.-J. Wei, J.-X. Liu, *Talanta* 73 (2007) 540.
- [17] X.-B. Long, M. Miro, E.H. Hansen, J.M. Estela, V. Cerda, *Anal. Chem.* 78 (2006) 8290.
- [18] M.-L. Chen, Y. Tian, J.-H. Wang, *J. Anal. At. Spectrom.* 23 (2008) 876.
- [19] Y. Wang, M.-L. Chen, J.-H. Wang, *J. Anal. At. Spectrom.* 21 (2006) 535.
- [20] A.N. Anthemidis, E.K. Martavaltzoglou, *Anal. Chim. Acta* 573–574 (2006) 413.
- [21] N.M.M. Coelho, A. Cósme da Silva, C. Moraes da Silva, *Anal. Chim. Acta* 460 (2002) 227.
- [22] K. Toda, T. Ohba, M. Takaki, *Anal. Chem.* 77 (2005) 4765.
- [23] A.D. Idowu, P.K. Dasgupta, *Anal. Chem.* 79 (2007) 9197.
- [24] D. Pozebon, V.L. Dressler, J.A.G. Neto, A.J. Curtius, *Talanta* 45 (1998) 1167.



Flow injection on-line displacement/solid phase extraction system coupled with flame atomic absorption spectrometry for selective trace silver determination in water samples

Chrysoula K. Christou, Aristidis N. Anthemidis*

Laboratory of Analytical Chemistry, Department of Chemistry, Aristotle University, Thessaloniki 54124, Greece

ARTICLE INFO

Article history:

Received 18 June 2008

Received in revised form 20 October 2008

Accepted 31 October 2008

Available online 7 November 2008

Keywords:

Flow injection

Silver

Displacement extraction

Solid phase

Atomic spectrometry

ABSTRACT

A novel flow injection (FI) on-line displacement solid phase extraction preconcentration and/or separation method coupled with FAAS in order to minimize interference from other metals was developed for trace silver determination. The proposed method involved the on-line formation and subsequently pre-sorption of lead diethyldithiocarbamate (Pb-DDTC) into a column packed with PTFE-turnings. The preconcentration and/or separation of the Ag(I) took place through a displacement reaction between Ag(I) and Pb(II) of the pre-sorbed Pb-DDTC. Finally, the retained analyte was eluted with isobutyl methyl ketone (IBMK) and delivered directly to nebulizer for measuring. Interference from co-existing ions with lower DDTC complex stability in comparison with Pb-DDTC, was eliminated without need for any masking reagent. With 120 s of preconcentration time at a sample flow rate of 7.6 mL min⁻¹, an enhancement factor of 110 and a detection limit (3 s) of 0.2 µg L⁻¹ were obtained. The precision (RSD, *n* = 10) was 3.1% at the 10 µg L⁻¹ level. The developed method was successfully applied to trace silver determination in a variety of environmental water samples and certified reference material.

© 2008 Elsevier B.V. All rights reserved.

1. Introduction

The widespread use of silver compounds and silver-containing procedures in industry, medicine, jewellery, cloud seeding and in the disinfection of drinking water has resulted in an increasing silver content of environmental samples. Silver impregnated filters are used in water disinfection, while silver concentrations up to 200 µg L⁻¹ are permitted for antimicrobial activities for human health [1]. Silver often presented as an impurity in Cu, Zn, As and Sb ores and thus it is possible to be entered into the environment from industrial wastes [2,3]. Bowen [4] suggested that silver may pose a potential risk as a water pollutant, because of the lack of recycling of mined silver. Also, recent information about the interaction of silver with essential nutrients, especially selenium, copper and vitamins E and B₁₂, has focused attention on its potential toxicity [1]. Consequently, determination of trace amounts of silver is important for many areas of chemical analysis.

Although, flame atomic absorption spectrometry (FAAS) is one of the most popular used techniques for metals determination with significant precision and accuracy, there are many limitations

to determine traces of analyte in environmental samples due to insufficient sensitivity or in some sample types matrix interference. Conventional off-line procedures for preconcentration and/or separation are usually effective, but they are time-consuming and tedious, requiring large quantities of sample and reagents, and thus potential prone to sample contamination and analyte losses. On-line flow injection (FI) preconcentration and/or separation coupled with atomic spectrometry has been shown to be very powerful in eliminating many of the above drawbacks for trace elements determination and offers advantages inherent in automatic methods of analysis [5,6].

Among on-line preconcentration techniques frequently used, FI micro-column based solid phase extraction presents many advantages, such as relatively high concentration factor and sampling frequency, simplicity of phase separation and suitability for automation [7,8]. Several methods have been reported to adapt FI on-line solid phase extraction coupled with FAAS, for the determination of silver in various types of samples. These methods usually make use of a packed column filled with a suitable stationary phase like: immobilized or modified silica gel [9–12], activated or immobilized alumina [13,14], sulfhydryl cotton fibers [3] and rhodamine fibers [15]. Alternatively, a knotted reactor (KR), which consists from a long polytetrafluoroethylene (PTFE) tube properly knotted, can be applied as a sorbent surface [16].

* Corresponding author. Tel.: +30 2310997826; fax: +30 2310997719.
E-mail address: anthemid@chem.auth.gr (A.N. Anthemidis).

However, preconcentration systems usually suffer undesirable interference from co-existing transition metals especially in complicated matrices, owing to metal competition for the complexing reagent and/or active sites of sorbent material in packed columns or in the inner walls of the KR [17]. Recently, Yan et al. [17] presented a FI on-line displacement solid phase extraction preconcentration method for interference-free determination of copper by FAAS. The methodology involved on-line formation, pre-sorption of the Pb-DDTC chelate onto the inner wall of the KR and subsequently retention of the analyte Cu(II) through a displacement reaction between the Cu(II) and the Pb(II) in the pre-sorbed Pb-DDTC complex because the stability of Cu-DDTC is greater than Pb-DDTC. Finally the retained analyte was eluted with ethanol and detected by FAAS. Interferences from co-existing ions with lower stability DDTC complexes relative to Pb-DDTC were eliminated without need for any masking agents, due to their competition with Cu(II) for DDTC and the active sorption sites on the inner walls of the KR. The same group also employed the above concept for mercury speciation and palladium determination, using cigarette filter as sorbent material [7,18–20]. To the best of our knowledge the above technique has not been applied for silver determination.

On the other hand PTFE-turnings have been proved as superior hydrophobic sorbent material for FI on-line column preconcentration systems for Cu, Pb, Cr, Co, As and Hg determination [8,21–25] but have not been used yet in on-line displacement solid phase extraction systems.

The aim of this work was to investigate the applicability of the micro-column packed with PTFE-turnings in FI on-line displacement solid phase extraction system in order to minimize interference from other metals, using sodium diethyl dithiocarbamate (NaDDTC) as complexing agent for selective and sensitive FAAS determination of trace silver in water environmental samples.

2. Experimental

2.1. Instrumentation

A PerkinElmer, Norwalk, Connecticut, USA (<http://las.perkinelmer.com>) model 5100 PC flame atomic absorption spectrometer with deuterium arc background corrector was exploited as detection system. A silver hollow cathode lamp (HCL) operated at 10 W was used as light source. The wavelength was set at 328.1 nm resonance line and the slit at 0.7 nm. A time-constant of 0.2 s was used for peak height evaluation. The flame conditions were slightly leaner than those recommended by the manufacturer, in order to compensate the effect of organic solvent isobutyl methyl ketone (IBMK), which serves as additional fuel during elution step. The air and acetylene flow rate was set at 10.0 L min⁻¹ and 0.9 L min⁻¹, respectively. In that case the nebulizer's free uptake rate was 5.9 mL min⁻¹. A flow spoiler was employed into the spray chamber for better nebulization conditions. The spectrometer was set to work in the FI-FAAS mode.

A PerkinElmer Norwalk, Connecticut, USA model FIAS-400 flow injection analysis system was coupled to the flame atomic absorption spectrometer for automatic processing of the method and operated in preconcentration mode. The whole system was controlled by a personal computer and the AA Lab. Benchtop version 7.2 application program. The FIAS-400 system consisted of two peristaltic pumps P1, P2 and a 5-port 2-position injection valve, while it was connected to the spectrometer's nebulizer, using a short PTFE capillary 20.0 cm length/0.35 mm i.d., in order to minimize the eluent dispersion. A third peristaltic pump P3 (Watson Marlow model 205U/BA) was also elaborated for the FI on-line displacement solid phase extraction method. A flow compensation (FC) unit was used

just before the nebulizer inlet, in order to compensate the lack of nebulizer free uptake flow rate. Peristaltic pump tubing of "Tygon" type was adopted to deliver the aqueous solutions and a displacement bottle (Tecator, Hoganas, Sweden, <http://www.foss.dk>) was used to deliver the organic solvent, isobutyl methyl ketone. All other conduits used for various connections were of 0.5 mm i.d. PTFE tubing.

The micro-column for retention of Ag-DDTC derivative complex was fabricated by firmly packing 100 mg of PTFE-turnings in a piece of narrow PTFE tube (20 mm length, 2.1 mm i.d./3.2 mm o.d.). PTFE-turnings were mechanically produced in our laboratory by lathe as described elsewhere [8]. The image from PTFE-turnings using an optical microscope has been given previously [25]. The turnings were washed thoroughly by ethanol followed by 1 mol L⁻¹ HNO₃ and finally with de-ionized water. No frits or glass wool were necessary at either end to block the PTFE-turnings. The column was initially flushed with de-ionized water and subsequently with IBMK. The performance of the column was stable at least for 1000 preconcentration cycles.

An Orion EA940 pH-meter was employed for the pH measurements with absolute accuracy limits at the pH measurements being defined by NIST buffers.

2.2. Reagents and samples

All chemicals were of analytical reagent grade and were provided by Merck (Darmstadt, Germany, <http://www.merck.de>). Ultra-pure quality water was used throughout which was produced by a Milli-Q system (Millipore, Bedford, USA, <http://www.millipore.com>). Working standard solutions of Ag(I) and Pb(II) were prepared by appropriate stepwise dilution of a 1000 mg L⁻¹ stock standard solution (Titrisol, Merck) to the required µg L⁻¹ levels. The acidity of the standards was adjusted with dilute HNO₃. The chelating reagent 0.1% (m/v) DDTC was prepared fresh daily by dissolving the appropriate amount of sodium diethyl dithiocarbamate (Aldrich) in water. Isobutyl methyl ketone was used after saturation with water, without any other purification.

Natural water samples (tap, lake, and coastal sea-water, from Northern Greece) and the industrial waste water treatment plant, filtered through 0.45 µm membrane filters, acidified to 0.1 mol L⁻¹ HNO₃ and stored at 4 °C in acid-cleaned polyethylene bottles, in order to determine the "dissolved metal" fraction. The standard reference material NIST CRM 1643d (National Institute of Standard and Technology, Gaithersburg, MD, USA, <http://www.nist.gov/>) containing trace elements in water, was also analyzed.

2.3. Procedure

The operation sequence (three steps) and the schematic diagram of the manifold for the FI on-line displacement solid phase extraction (FI-D/SPE-FAAS) method for silver determination are presented in Table 1 and Fig. 1, respectively. In step 1 (Fig. 1, Pre-sorption), the injection valve (IV) was set in the load position. Pump P2 fed a mixed solution 1.0 mg L⁻¹ Pb(II) and 0.05% (m/v) DDTC as complexing agent, through the column C for 30 s. The formed Pb(II)-DDTC complex was adsorbed on the surface of the PTFE-turnings of the packed column. In the mean time, pump P1 remained inactive and the nebulizer of the FAAS aspirated air through the flow compensation adapter (FC). During step 2, pump P2 was off, while pump P3 was activated and propelled the sample solution through the column for 120 s. In this step, the silver ions were retained onto the surface of the PTFE-turnings, by replacing the Pb(II) ions of the pre-sorbed Pb(II)-DDTC complex. Such displacement reaction could not be established between other co-existing metal ions and

Table 1
Operation sequences of the FI on-line displacement solid phase extraction (FI-D/SPE-FAAS) method and the conventional (FI/SPE-FAAS) one for silver determination.

Method	Step	Injection valve	Pumps			Delivered medium	Flow rate (mL min ⁻¹)	Time (s)	Operation
			P1	P2	P3				
FI-D/SPE	1	Load	Off	On	Off	1.0 mg L ⁻¹ Pb(II) 0.05% (m/v) DDTC	7.2 0.8	30	Pre-sorption
FI-D/SPE	2	Load	Off	Off	On	Sample	7.5	120	Preconcentration
FI-D/SPE	3	Inject	On	Off	Off	IBMK	2.6	40	Elution/measurement
FI/SPE	1	Load	Off	On	Off	Sample	9.5	90	Preconcentration
FI/SPE	2	Inject	On	Off	Off	0.1% (m/v) DDTC IBMK	0.6 2.6	40	Elution/measurement

Pb(II)–DDTC due to less stability of their DDTC chelates in comparison to Pb(II)–DDTC complex stability. Thus, possible interferences from co-existing metal were minimized or eliminated. In step 3 (Fig. 1, Elution), IV was turned in the elute position and the eluent, IBMK is propelled by pump P1 through the column in reverse direction than that of the sample loading to minimize eluent dispersion.

The procedure for the conventional FI on-line solid phase extraction (FI/SPE-FAAS) method was similar with the above FI-D/SPE-FAAS method, but without the use of the first step (pre-sorption). The Ag(I)–DDTC complex was formed through direct merging of sample solution with DDTC solution and subsequently it was sorbed on the PTFE-turnings. The operation sequences are given in Table 1.

In both methods, the eluted complex Ag(I)–DDTC was directly delivered to the nebulizer for atomization and measuring. The peak height of the signal was proportional to the Ag(I) concentration and was used for all measurements. In order to ensure complete elution of the silver complex, the elution time was fixed at 40 s. The recorded peaks were sharp and the baseline was stable. Five replicate measurements per sample were made in all instances.

3. Results and discussion

3.1. Development of the FI on-line displacement solid phase extraction system

Two points should be consulted developing an efficient displacement solid phase extraction system. The extent of the sorbent active surface, which should be covered thoroughly by the pre-sorption complex (M–DDTC) and the stability of the dithiocarbamate complex of the displaced ion, which should be less than that of Ag(I)–DDTC, and higher than that of interfering metal complexes. The stability of the DDTC–metal complex decreases in order [26]: Hg(II) > Pd(II) > Ag(I) > Cu(II) > Tl(III) > Ni(II) > Bi(III) > Pb(II) > Co(III) > Co(III) > Cd(II) > Tl(I) > Zn(II) > In(III) > Sb(III) > Fe(III) > Te(IV) > Mn(III) > Mn(II). Based on the above comments, a micro-column packed with 100 mg PTFE-turnings was adopted throughout the experiments. On the other hand, taking into account the kinetic of the complexation and displacement reaction, Cu(II) and Pb(II) are the most appropriate ions for on-line Ag(I) displacement preconcentration. Preliminary experiments have shown that in case of the pre-sorbed Cu(II)–DDTC, the concentration of Cu(II) solution should be higher than 1.0 mg L⁻¹, but at this Cu(II) concentration, precipitation of the Cu(II)–DDTC complex was observed resulting low precision. In contrast, the complex Pb(II)–DDTC was not precipitated at Pb(II) concentration at least up to 2.0 mg L⁻¹. Thus, Pb(II)–DDTC was employed for the displacement solid phase extraction technique.

In order to define the optimum performance characteristics of the on-line displacement solid phase extraction preconcentration procedure for Ag(I) determination, both chemical and FI variables were thoroughly studied using 10.0 µg L⁻¹ Ag(I) using the manifold shown schematically in Fig. 1.

3.2. Factors affecting the pre-sorption of Pb(II)–DDTC

The pH value of Pb(II) solution affects significantly the formation of the Pb(II)–DDTC complex and its pre-sorption on the sorbent surface. The effect of pH was studied within the range of 0.5–3.5 with a DDTC concentration of 0.1% (m/m) in water. The acidity of the Pb(II) solution was fixed with nitric acid and monitored in the effluents. As shown in Fig. 2, the absorbance increased with increasing the acidity up to 1.6, then leveled off. Hence, a pH of ca. 2 (0.01 mol L⁻¹ HNO₃ in the Pb(II) solution) was selected for further experiments.

The concentration of Pb(II) solution plays significant role on the displacement solid phase extraction, because it affects the

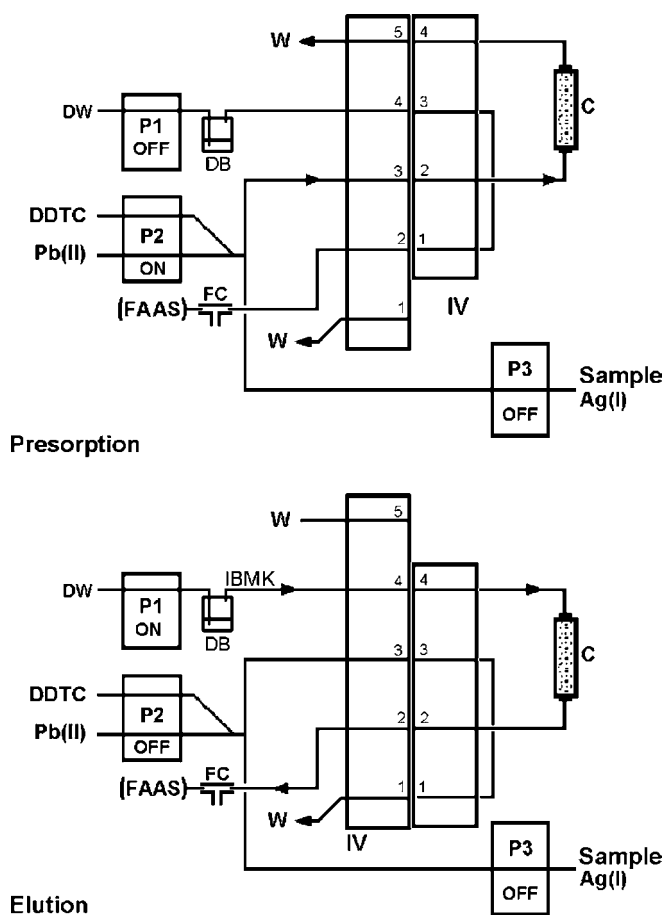


Fig. 1. Schematic diagram of the FI on-line displacement solid phase extraction manifold and the two of three operation sequences, for silver determination. DDTC, 0.05% (m/v) DDTC; P1, P2, P3, peristaltic pumps; IV, injection valve; DB, displacement bottle; C, packed column; FC, flow compensation adapter; DW, distilled water; W, waste.

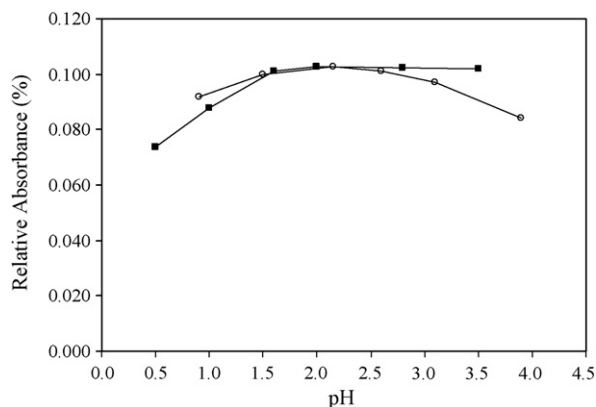


Fig. 2. Effect of pH of the Pb(II) solution (■) and the sample solution (○) on the peak height absorbance of $10.0 \mu\text{g L}^{-1}$ Ag(I) solution. All other conditions as in Table 1.

Pb(II)–DDTC pre-sorbed on the PTFE-turnings in the micro-column. The effect of Pb(II) concentration was investigated up to 5.0 mg L^{-1} . As it is presented in Fig. 3 in the absence of Pb(II), the absorbance of $10.0 \mu\text{g L}^{-1}$ Ag(I) is still about 70% of the optimum absorbance, probably because the silver is complexed with the pre-coated DDTC with lower kinetic reaction. The absorbance increased with the Pb(II) concentration up to 0.5 mg L^{-1} and then gradually leveled off up to 2.0 mg L^{-1} . A decreased absorbance with low precision which was observed for Pb(II) concentration higher than 2.0 mg L^{-1} is the result of the Pb(II)–DDTC complex precipitation. For further experiments, a concentration of 1.0 mg L^{-1} Pb(II) was employed for pre-sorption.

The formation of the complex Pb(II)–DDTC and its subsequent pre-sorption depends also on the DDTC concentration. The influence of DDTC concentration on the preconcentration of $10.0 \mu\text{g L}^{-1}$ Ag(I) was examined in the range 0.001% to 0.5% (m/v), at fixed 0.8 mL min^{-1} DDTC flow rate. The absorbance raised by increasing the DDTC concentration up to 0.05% (m/v), and then leveled off. For low reagent consumption, a concentration of 0.05% (m/v) DDTC was selected for further study.

The time for the pre-sorption of the lead solution and the Pb(II) solution flow rate affects significantly the effective formation of Pb(II)–DDTC complex and its retention on the PTFE-turnings surface. The effect of the pre-sorption time was investigated from 10 s to 60 s, with a concentration of 1.0 mg L^{-1} Pb(II) at a flow rate of 7.2 mL min^{-1} . The obtained absorbance of silver increased practically linearly with increasing pre-sorption time up to 30 s and then leveled off. Hence, a pre-sorption time of 30 s was selected

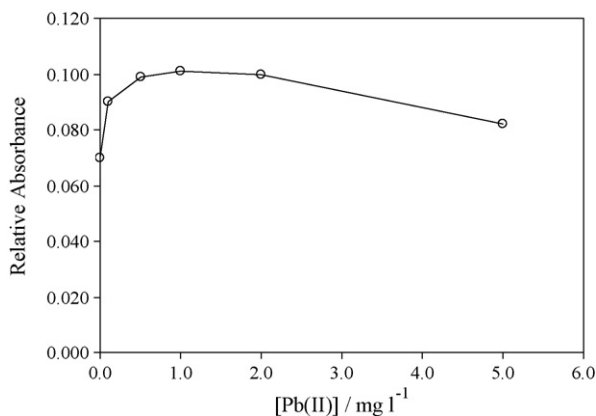


Fig. 3. Effect of the Pb(II) concentration on the absorbance of $10.0 \mu\text{g L}^{-1}$ Ag(I) for the pre-sorption. All other conditions as in Table 1.

for further experiments. The influence of the lead solution flow rate on the absorbance for pre-sorption was studied in the range $3.9\text{--}9.6 \text{ mL min}^{-1}$, for a pre-sorption time of 30 s and lead concentration of 1.0 mg L^{-1} . It was found that the absorbance of $10.0 \mu\text{g L}^{-1}$ Ag(I) increased almost linearly up to a flow rate of 7.2 mL min^{-1} , implying that the complexation was completed and the contact time was sufficient. For higher flow rates the signal is leveled off indicating the beginning of the partial leaching of the Pb(II)–DDTC complex. A flow rate of 7.2 mL min^{-1} was selected for further work.

3.3. Factors affecting the on-line displacement solid phase extraction preconcentration

Sample acidity is a critical variable of the on-line displacement affecting the displacement reaction between Ag(I) and Pb(II) in the pre-sorbed Pb(II)–DDTC complex, the retention of Ag(I)–DDTC complex on the sorbent surface. The effect of pH was studied from 0.9 to 3.9 by adjusting it in the silver solution with dilute nitric acid. As it is presented in Fig. 2, the recorded absorbance was optimum and practically stable in a wide pH window varied between 1.5 and 3.0. This fact enables the use of the method directly in many aqueous samples after common acid preservation, without any laborious precise pH adjustment.

The effect of sample flow rate on the silver absorbance was investigated in the range $4.1\text{--}9.5 \text{ mL min}^{-1}$ and it was found that the absorbance increased almost linearly, by increasing the sample loading flow rate. The kinetic of the complex formation was very fast and the contact time for complete displacement and sorption was sufficient. This is a significant advantage, because different loading flow rates can be used with proportional sensitivity. For all subsequent experiments a sample flow rate of 7.5 mL min^{-1} was adopted, as a compromise between high sensitivity and medium sample consumption.

The influence of preconcentration time (sample loading time) was studied in the range from 30 s to 180 s, at a sample flow rate of 7.5 mL min^{-1} . It was observed that the absorbance increased practically linearly as the sample loading time was increasing up to 120 s. When longer loading times were used, the analytical signal was increased with lower rate, probably, due to partial leaching of the complexes. Finally, a 120 s preconcentration time was chosen for the proposed method.

Organic solvents like, ethanol, methanol and IBMK have been extensively used as effective eluents in FI on-line solid phase extraction preconcentration systems. However, IBMK is considered to be more convenient for FAAS, because it produce higher and sharpest signals. These advantages are arising from the fact that IBMK serves as additional fuel improving the atomization conditions and also from its immiscibility with aqueous phase, decreasing the analyte dispersion. Thus, IBMK was adopted as eluent solvent and the elution time was fixed at 40 s for complete elution. The effect of IBMK flow rate was studied within the range $1.5\text{--}4.8 \text{ mL min}^{-1}$. Maximum absorbance was achieved within the range $2.2\text{--}3.0 \text{ mL min}^{-1}$. Above 3.0 mL min^{-1} the recorded absorbance decreases, mainly due to the dispersion, while at low flow rates ($<2.2 \text{ mL min}^{-1}$) due to the high flow rate difference between elution and nebulizer uptake flow rate. For further experiments a 2.6 mL min^{-1} flow rate was used for the eluent.

3.4. Investigation of the potential interferences

Sodium diethyl dithiocarbamate (DDTC) is a general chelating agent for preconcentration of many transition metals with LLE or SPE and has been used successfully either in batch or in on-line mode. Although, FAAS has significant inherent selectivity, interfer-

Table 2
Comparison of interference from co-existing ions on the determination of $5.0 \mu\text{g L}^{-1}$ Ag(I) between the conventional FI/SPE-FAAS method and the FI-D/SPE-FAAS one.

Ion	Concentration (mg L^{-1})	Recovery (%)	
		FI/SPE-FAAS	FI-D/SPE-FAAS
Cu(II)	0.3	94	99
	0.5	85	100
	2.0	73	95
Cd(II)	0.1	101	–
	0.5	75	100
	1.0	54	99
	2.0	15	95
Co(II)	0.2	95	–
	0.5	60	100
	1.0	–	101
	5.0	–	96
Fe(III)	0.5	94	101
	1.0	55	99
	5.0	–	100
	10.0	–	98
Zn(II)	2.0	99	100
	5.0	94	99
	10.0	–	100
Mn(II)	2.0	96	101
	10.0	67	100
Ni(II)	0.5	100	99
	1.0	95	101
	2.0	78	96
Hg(II)	0.1	101	100
	0.2	96	99
	0.4	80	95

ences from co-existing metals should be investigated in order to define the selectivity of the developed FI on-line displacement/solid phase extraction method (FI-D/SPE-FAAS) for the determination of trace silver. The effect of some potential interfering species on the preconcentration and determination of $5.0 \mu\text{g L}^{-1}$ Ag(I) were tested using the optimized manifold. Taking as criterion for interference the deviation of the recovery more than $\pm 5\%$, the obtained results showed that, Cu(II), Cd(II), Co(II), Fe(III), Zn(II), Mn(II), Ni(II) and Hg(II) were tolerated at least up to 0.5, 2.0, 5.0, 10.0, 10.0, 10.0, 2.0 and 0.4 mg L^{-1} , respectively. On the other hand DDTC does not form complexes with alkali and alkaline earth metals, which are usually found in high concentrations in natural waters. Some common matrix cations such as K(I), Ca(II), Mg(II) and Ba(II) at high concentrations were tested and it was found that they did not interfere at concentrations up to 1000 mg L^{-1} . Also NaCl did not interfere at concentrations up to 30.0 g L^{-1} .

For comparative purposes, the interference effect of the above metal ions was also examined using the conventional FI on-line

solid phase extraction method for determination of $5.0 \mu\text{g L}^{-1}$ Ag(I). The results are presented in Table 2. As it can be seen, the proposed FI on-line displacement/solid phase extraction method gave much higher selectivity for the separation and preconcentration of silver in the presence of high concentrations of Cu(II), Cd(II), Co(II), Fe(III), Zn(II), Mn(II), Ni(II) and Hg(II). These results clearly illustrate the high selectivity of the present FI on-line displacement preconcentration method for FAAS determination of silver.

3.5. Analytical characteristics

Under the optimum conditions described above, the analytical characteristics of the proposed FI-D/SPE-FAAS method for Ag(I) determination are summarized in Table 3. For a 30 s pre-sorption time and a 120 s preconcentration time, the sampling frequency was 19 h^{-1} and the enhancement factor calculated as the ratio of the slopes of calibration curves with and without preconcentration was 110. The detection limit calculated by 3 s criterion and found to be $c_L = 0.2 \mu\text{g L}^{-1}$. The precision of the method was also studied. The precision, as relative standard deviation (RSD), was $s_r = 3.1\%$, calculated from 10 replicate measurements at $10.0 \mu\text{g L}^{-1}$ level of Ag(I). For comparative purposes, the performance characteristics of the proposed FI-D/SPE-FAAS method and the conventional FI on-line solid phase extraction FI/SPE-FAAS method, using the same packed column, for silver determination are given in Table 3. As it is expected the conventional FI/SPE-FAAS method appears higher sensitivity and better enhancement factor with lower detection limit, because the kinetic of complex retention is more effective than the kinetic of the displacement. Consequently, for simple matrices and for higher sensitivity the conventional FI/SPE-FAAS method can be used, while for complicated matrices the FI-D/SPE-FAAS method can be successfully elaborated.

In Table 4, the figures of merit of the proposed method FI-D/SPE-FAAS and other selected on-line solid phase extraction preconcentration FAAS methods are summarized for comparative purposes. The proposed method shows very good sensitivity and precision and has some good advantages over other on-line preconcentration methods reported in the literature.

In order to evaluate the accuracy of the proposed method FI-D/SPE-FAAS and the conventional one FI/SPE-FAAS for silver determination, certified reference material CRM 1643d (Trace elements in water) were analyzed. As it is shown in Table 5, the found values were in good agreement with the certified one and the calculated recoveries (R) were satisfactory. The two methods were also applied to the analysis of natural water (tap, lake and coastal seawater) and waste water samples and were validated by spiking the samples with known amounts of silver. The obtained results are presented in Table 5. The recoveries (R) from spiked samples were varied in the range 94–99% and student t -test was applied in order to test the significance of differences between certified or added

Table 3
Analytical performance of the FI-D/SPE-FAAS and the conventional FI/SPE-FAAS method for determination of Ag(I) by FAAS.

Parameter	Method	
	FI-D/SPE-FAAS	FI/SPE-FAAS
Pre-sorption time (s)	30	–
Preconcentration time (s)	120	90
Sample consumption (mL)	15.0	14.2
Sampling frequency (h^{-1})	19	27
Enhancement factor	110	218
Linear range ($\mu\text{g L}^{-1}$)	0.5–30.0	0.3–15.0
Regression equation ($n = 5$)	$A = 0.0111 [\text{Ag(I)}] + 0.0028$	$A = 0.0218 [\text{Ag(I)}] + 0.0010$
Correlation coefficient, r	0.9979	0.9992
Detection limit, c_L ($\mu\text{g L}^{-1}$)	0.2	0.1
Precision (RSD, $n = 10$) (%)	3.1 ($10.0 \mu\text{g L}^{-1}$)	2.5 ($5.0 \mu\text{g L}^{-1}$)

Table 4

Comparison of the characteristic data between recent published on-line SPE methods and the developed FI-D/SPE-FAAS one for silver determination with FAAS.

Ref.	Sorbent material/reagent	Eluent	EF	PT (s)	SF (h ⁻¹)	cL (μg L ⁻¹)	sr (%)
*	PTFE-turnings/Pb-DDTC	IBMK	110	120	19	0.2	3.1
[9]	DPT-silica gel	Thiourea	–	60	24	0.3	0.9
[10]	ATu-silica gel	Thiourea	–	60	–	1.1	1.2
[11]	Tu-silica gel	Thiourea	–	60	–	1.3	3.0
[12]	MBT-silica gel	Thiourea	–	60	60	0.6	1.0
[14]	DDTC-alumina	EtOH	125	30	16	0.6	4.0
[3]	S-cotton fiber	KCN	300	300	9	1.0	3.5
[13]	Activated alumina	HNO ₃	150	180	–	2.9	< 5
[16]	KR-PTFE/Fe-DDTC	IBMK	26	45	62	0.5	2.1
[27]	Atu-glass beads	Thiourea	–	60	–	0.5	0.9
[28]	KR-PTFE/Cu-DDTC	IBMK	26	30	72	0.6	2.0

* This work; EF, enhancement factor; PT, preconcentration time; SF, sampling frequency; c_L, detection limit; s_r, relative standard deviation.**Table 5**Analytical results of silver determination in the certified reference material and water samples (determination in “dissolved metal” fraction) by FI-D/SPE-FAAS and FI/SPE-FAAS method (concentrations values in μg L⁻¹).

Sample	Certified value	Added	FI-D/SPE-FAAS			FI-SPE-FAAS		
			Found ^a	R (%)	t _{exp} ^b	Found ^a	R (%)	t _{exp} ^b
CRM 1643d	1.27 ± 0.057	–	1.2 ± 0.1	95	1.21	1.2 ± 0.1	96	1.21
Tap water	–	5.0	<cL	–	–	<cL	–	–
Lake water	–	–	4.8 ± 0.3	96	1.15	4.9 ± 0.3	99	0.58
	–	10.0	<cL	–	–	<cL	–	–
Sea-water	–	–	9.6 ± 0.5	96	1.39	9.8 ± 0.3	98	0.69
	–	10.0	<cL	–	–	<cL	–	–
Waste water	–	–	9.4 ± 0.7	94	1.48	9.5 ± 0.5	95	1.24
	–	5.0	0.68 ± 0.07	–	–	0.65 ± 0.05	–	–
			5.4 ± 0.5	95	1.39	5.5 ± 0.3	97	1.73

^a Mean value ± standard deviation based on three (N = 3) replicate determinations.^b t_{exp} = |(μ - x̄)| √N/s, t_{crit} = 4.30 for 95% probability level.

and found concentrations. In all cases the differences were proved to be not significant at 95% probability level. The relative standard deviation (RSD) for silver determination in the examined samples varied in the range 3.1–10.6%.

4. Conclusions

The FI on-line displacement solid phase extraction system has been evaluated and demonstrated for eliminating the major interferences in FAAS determination of silver. Compared with conventional FI on-line sorption preconcentration methodology, the proposed method proved to be effectively minimized the interference from co-existing metal ions, giving much higher selectivity, without the need of any masking agents. The developed on-line system offers rapid and reliable preconcentration of Ag(I) on the PTFE-turnings in relative high sample flow rates improving thus the sensitivity. The obtained detection limit was thus comparable to those obtained by ETAAS. To our knowledge this is the first work dealing with PTFE-turnings as sorbent material in on-line displacement solid phase extraction column preconcentration for metal determination. The unlimited life time sorbent material, the easy operation and the high sensitivity of the proposed system make it attractive for routine determination of the silver in natural waters.

References

- [1] Environment Protection Agency (EPA), Ambient Water Quality Criteria for Silver, EPA 4405-80-071, Office of Water Regulations, Washington, DC, 1980.
- [2] R. Soager, Metallic Raw Materials Dictionary, Bank Tobel, Zurich, 1984, p. 63.
- [3] M.M. Gomez Gomez, M.M. Hidalgo Garsia, M.A. Palacios Corvillo, Analyst 120 (1995) 1911.
- [4] H.J.M. Bowen, Trace Element Biochemistry, Academic Press, London, 1996.
- [5] Z.-L. Fang, Flow Injection Atomic Absorption Spectrometry, Wiley & Sons Ltd., West Sussex, England, 1995.
- [6] M. Trojanowicz, Flow Injection Analysis Instrumentation and Applications, World Scientific Publishing Co. Ltd., Singapore, 2000.
- [7] J. Fang, Y. Jiang, X.-P. Yan, Z.-M. Ni, Environ. Sci. Technol. 39 (2005) 288.
- [8] A.N. Anthemidis, G.A. Zachariadis, J.A. Stratis, J. Anal. At. Spectrom. 17 (2002) 1330.
- [9] P. Liu, Z. Su, X. Wu, Q. Pu, J. Anal. At. Spectrom. 17 (2002) 125.
- [10] S. Zhang, Q. Pu, P. Liu, Q. Sun, Z. Su, Anal. Chim. Acta 452 (2002) 223.
- [11] P. Liu, Q. Pu, Z. Su, Analyst 125 (2000) 147.
- [12] Q. Pu, Q. Sun, Analyst 123 (1998) 239.
- [13] P.P. Coetzee, I. Taljaard, H. de Beer, Fresenius J. Anal. Chem. 336 (1990) 201.
- [14] S. Dadfarnia, A.M. Haji Shabani, M. Gohari, Talanta 64 (2004) 682.
- [15] C.S. Gong, X.W. Guo, Z.X. Su, Yejin Fenxi 16 (1996) 9.
- [16] S. Pei, Z. Fang, Anal. Chim. Acta 294 (1994) 185.
- [17] X.-P. Yan, Y. Li, Y. Jiang, J. Anal. At. Spectrom. 17 (2002) 610.
- [18] X.-P. Yan, Y. Li, Y. Jiang, Anal. Chem. 75 (2003) 2251.
- [19] L.-M. Dong, X.-P. Yan, Y. Li, Y. Jiang, S.-W. Wang, D.-Q. Jiang, J. Chromatogr. A 1036 (2004) 119.
- [20] J. Fang, L.-W. Liu, X.-P. Yan, Spectrochim. Acta. B 61 (2006) 864.
- [21] A.N. Anthemidis, G.A. Zachariadis, J.-S. Kougoulis, J.A. Stratis, Talanta 57 (2002) 15.
- [22] G.A. Zachariadis, A.N. Anthemidis, P.G. Bettas, J.A. Stratis, Talanta 57 (2002) 919.
- [23] A.N. Anthemidis, G.A. Zachariadis, Ch.E. Michos, J.A. Stratis, Anal. Bioanal. Chem. 379 (2004) 764.
- [24] A.N. Anthemidis, E.K. Martavaltzoglou, Anal. Chim. Acta 573–574 (2006) 413.
- [25] G.A. Zachariadis, A.N. Anthemidis, J.A. Stratis, Talanta 57 (2002) 919.
- [26] Z.B. Alfassi, C.M. Wai, Preconcentration Techniques for Trace Elements, CRC Press Inc., London, 1992, p. 113.
- [27] P. Liu, Q. Pu, Q. Sun, Anal. Sci. 19 (2003) 409.
- [28] X. Mao, H. Chen, J. Liu, Microchem. J. 59 (1998) 383.



Comparison of ICP-MS and SIMS techniques for determining uranium isotope ratios in individual particles

F. Esaka*, M. Magara, C.G. Lee, S. Sakurai, S. Usuda, N. Shinohara

Research Group for Analytical Science, Japan Atomic Energy Agency, 2-4 Shirakata-Shirane, Tokai, Naka, Ibaraki 319-1195, Japan

ARTICLE INFO

Article history:

Received 15 October 2008

Received in revised form

10 November 2008

Accepted 10 November 2008

Available online 21 November 2008

Keywords:

Uranium
Isotope ratio
Particles
ICP-MS
SIMS

ABSTRACT

The determination of uranium isotope ratios in individual particles is of great importance for nuclear safeguards. In the present study, an analytical technique by inductively coupled plasma mass spectrometry (ICP-MS) with a desolvation sample introduction system was applied to isotope ratio analysis of individual uranium particles. In ICP-MS analysis of individual uranium particles with diameters ranging from 0.6 to 4.2 μm in a standard reference material (NBL CRM U050), the use of the desolvation system for sample introduction improved the precision of $^{234}\text{U}/^{238}\text{U}$ and $^{236}\text{U}/^{238}\text{U}$ isotope ratios. The performance of ICP-MS with desolvation was compared with that of a conventionally used method, i.e., secondary ion mass spectrometry (SIMS). The analysis of test swipe samples taken at nuclear facilities implied that the performance of ICP-MS with desolvation was superior to that of SIMS in a viewpoint of accuracy, because the problems of agglomeration of uranium particles and molecular ion interferences by other elements could be avoided. These results indicated that ICP-MS with desolvation has an enough ability to become an effective tool for nuclear safeguards.

© 2008 Elsevier B.V. All rights reserved.

1. Introduction

Isotope ratio analysis of individual particles is increasingly important in the field of nuclear safeguards. Here, individual uranium particles in environmental samples taken at nuclear facilities are measured to reveal the presence of undeclared nuclear activities [1]. For this purpose, two kinds of analytical techniques are utilized, i.e., a fission track method combined with thermal ionization mass spectrometry (FT-TIMS) [2–4] and secondary ion mass spectrometry (SIMS) [5–7]. The FT-TIMS technique allows us to identify uranium particles easily and to measure isotope ratios precisely. However, it needs a nuclear reactor to irradiate samples with thermal neutrons for obtaining fission tracks and it is complicated and time-consuming to prepare samples. The SIMS technique is efficient in analyzing samples when uranium particles are large enough both in numbers and size. There is a difficulty in analyzing $^{234}\text{U}/^{238}\text{U}$ and $^{236}\text{U}/^{238}\text{U}$ isotope ratios accurately because of isobaric interferences caused by molecular ions of other elements. In a previous paper, we developed a combination method of particle manipulation and SIMS (manipulation-SIMS), removing the interferences from other elements in other particles [7]. A remaining problem is the interferences from other elements in the same particle.

Recently, inductively coupled plasma mass spectrometry (ICP-MS) has been increasingly applied for isotope ratio analysis of long-lived radionuclides [8]. The high sensitivity suggests that it will become an effective analytical tool for individual particles. Boulyga and Prohaska [9] applied laser ablation – ICP-MS for determination of uranium isotope ratio in individual particles with sub-millimeter in diameter. Further studies would be, however, needed to measure smaller particles precisely. Degueldre et al. [10] performed ICP-MS analysis for single uranium particles introduced as diluted suspensions. However, it is difficult to apply these approaches to isotope ratio analysis because only transient signals are obtained.

In a previous work [11], we developed an experimental technique for isotope ratio analysis of individual particles, including particle manipulation and chemical dissolution of individual particle for subsequent isotope ratio analysis with ICP-MS. This technique also has a possibility to remove isobaric interferences from other elements existing in the same particle by a combination with chemical separation. Although the developed technique enabled us to acquire stable signals needed for isotope ratio measurement, it was difficult to obtain precise results for $^{234}\text{U}/^{238}\text{U}$ and $^{236}\text{U}/^{238}\text{U}$ isotope ratios due to the lack of sensitivity.

In the present study, a desolvation sample introduction system was used to improve sensitivity in ICP-MS analysis for individual particles. Moreover, the performance for isotope ratio analysis of individual particles was evaluated by using test swipe samples

* Corresponding author. Tel.: +81 29 282 6165; fax: +81 29 282 6950.
E-mail address: esaka.fumitaka@jaea.go.jp (F. Esaka).

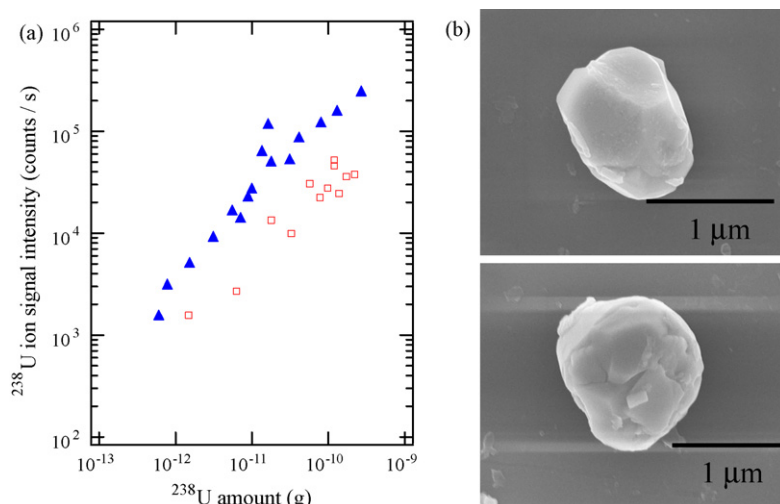


Fig. 1. (a) The ^{238}U ion signal intensities measured for individual NBL CRM U050 particles by ICP-MS with (\blacktriangle) and without (\square) desolvation. (b) Example of the SEM images of measured uranium particles.

containing uranium particles and compared with that of SIMS and manipulation-SIMS methods.

2. Experimental procedure

2.1. Samples

Uranium particles in a certified reference material (grains of U_3O_8 powder, CRM U050, New Brunswick Laboratory (NBL), USA) were used in this study. The uranium particles were smeared onto a cotton cloth (TexWipe[®] TX304, used for safeguards environmental sampling by IAEA inspectors). In addition, two kinds of test swipe samples taken at nuclear facilities were used to compare the performance of ICP-MS with SIMS.

2.2. Sample preparation for ICP-MS

Particles on the cotton cloth were recovered onto a Si disk (Nihon Exceed Co. Ltd., Japan) with a diameter of 25 mm and a thickness of 3 mm by an impaction method [12]. Si chips (5 mm \times 5 mm, Semitec Co. Ltd., Japan) were cleaned, in sequence, with 40%, 2% HNO_3 (high purity, Tama Chemicals Co. Ltd.) and deionized Milli-Q water (18 $\text{M}\Omega$). The Si disk and the Si chips were introduced into a chamber of a scanning electron microscope (SEM, JSM-6700F, Jeol Co. Ltd., Japan) simultaneously. Individual uranium particles on the Si disk were observed with SEM and identified with energy dispersive X-ray (EDX) analysis. Single uranium particle was manipulated with a glass needle attached to a manipulator and transferred onto the center of each Si chip. Teflon bottles with a volume of 8 mL were cleaned with 4% HNO_3 and deionized Milli-Q water. The 8 mL of 4% HNO_3 was, then, added to the bottle and the count rate at a mass 238 was measured with ICP-MS to check the cleanliness of the bottle. Each Si chip containing a single uranium particle was dropped into the bottle and 250 μL of 40% HNO_3 was added. The particle was soaked overnight and dissolved at 55 $^\circ\text{C}$ for 4 h under ultrasoneration. The solution was finally adjusted to 4% HNO_3 by adding 2.75 mL of deionized Milli-Q water.

2.3. Sample preparation for SIMS

Particles on the cotton cloth were collected onto a glassy carbon disk ($\text{O}25$ mm, Hitachi Chemical Co. Ltd., Japan) by the impaction method. Both the planchet containing particles and a blank disk were introduced into the main chamber of the SEM. Each ura-

anium particle to be analyzed was manipulated with the glass needle attached to the manipulator and transferred onto the blank planchet. For test swipe samples, uranium particles without manipulation were also prepared for SIMS analysis.

2.4. Instrumentation

An Apex-Q desolvation system (Elemental Scientific Inc., USA) was used for sample introduction to ICP-MS. This system consists of a heated cyclonic spray chamber, a Peltier cooled condenser and an ACM Naflon fluoropolymer membrane desolvation module, allowing high efficient sample introduction. Uranium isotope ratios were measured using a high resolution ICP-MS model ELEMENT 1 (Thermo Fisher Scientific, USA), which has an ICP ion source with Guard electrode and a double-focusing mass spectrometer. The instrument was operated in electric scanning (E-scan) modes with a mass resolution ($M/\Delta M$) of 300. A PFA micro-flow nebulizer (self-aspirating mode) was used in combination with a Scott-type double pass spray chamber cooled at 4 $^\circ\text{C}$. The instrument without desolvation was tuned daily for optimal ^{238}U sensitivity (2300 cps/ppt). Four mono-atomic ions ($^{234}\text{U}^+$, $^{235}\text{U}^+$, $^{236}\text{U}^+$ and $^{238}\text{U}^+$) were measured in a peak-jumping mode. The signal intensity of $^{238}\text{U}^{16}\text{O}^+$ was also measured for monitoring the stability of the instrument. The formation rate of $^{238}\text{U}^{16}\text{O}^+$ to $^{238}\text{U}^+$ was between 2 and 3%. The operating condition for the ICP-MS is listed in Table 1. The interference of $^{235}\text{U}^{1}\text{H}^+$ on $^{236}\text{U}^+$ was corrected with prelimi-

Table 1
Analytical condition in ICP-MS.

Parameter	Setting
<i>ICP-MS</i>	
RF power	1148 W
Cooling gas flow rate	16.0 L/min
Auxiliary gas flow rate	0.85 L/min
Sample gas flow rate	0.79–0.86 L/min
Solution uptake rate	0.18 mL/min
Sampling time per isotope	50 ms
Scan per replicate	400
Number of replicates	5
Resolution ($\Delta M/M$)	300
<i>Apex-Q desolvation system</i>	
Spray chamber temperature	100 $^\circ\text{C}$
Condenser temperature	2 $^\circ\text{C}$
Nitrogen flow	1.5 mL/min
Additional gas (Ar)	0.08–0.15 L/min

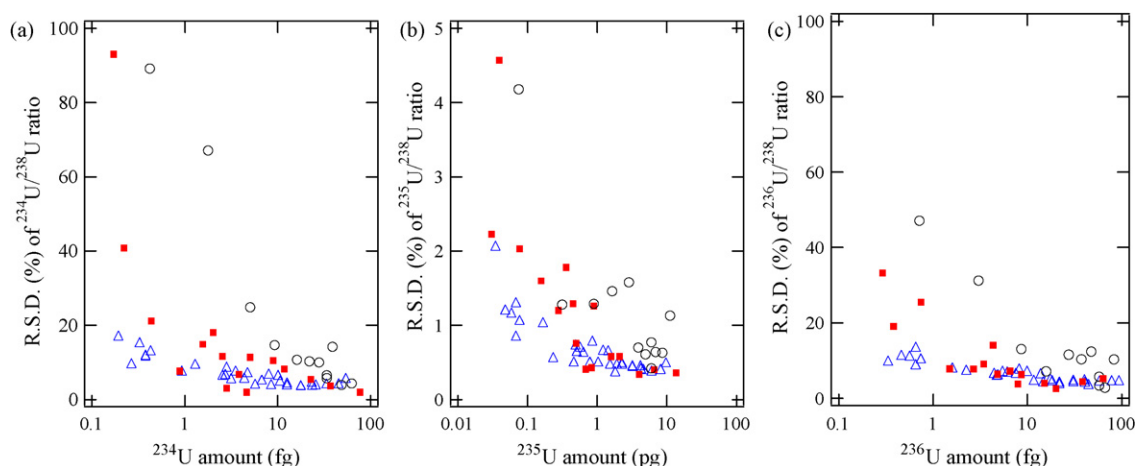


Fig. 2. The precision of (a) $^{234}\text{U}/^{238}\text{U}$, (b) $^{235}\text{U}/^{238}\text{U}$ and (c) $^{236}\text{U}/^{238}\text{U}$ isotope ratios obtained for individual NBL CRM U050 particles by (Δ) manipulation-SIMS, (\circ) ICP-MS and (\blacksquare) ICP-MS with desolvation.

narily measured $^{238}\text{U}^1\text{H}/^{238}\text{U}$ ratio, 5.0×10^{-5} . The mass bias factor assuming the following equation was determined using a 4 pg/mL NBL CRM U015 standard solution:

$$R_t = R_m(1 + C)^{\Delta M} \quad (1)$$

where R_t is the certified isotope ratio, R_m is the measured isotope ratio, ΔM is a difference in mass and C is a mass discrimination factor.

A secondary ion mass spectrometer (IMS-6f, Cameca, France) was used for measuring uranium isotope ratios in individual particles. In SIMS analysis, an O_2^+ focused beam of 15 keV with a current of 1.0–20 nA was rastered over a $50 \mu\text{m} \times 50 \mu\text{m}$ area. Positive secondary ions emitted from a particle were accelerated through 5 keV. Transfer optics of $150 \mu\text{m}$ and a field aperture of $1800 \mu\text{m}$ were used. An energy slit was adjusted for a band pass of 50 eV. The mass resolution was set at 300. Secondary ions at masses 234, 235, 236, 238 and 239 were counted in an automatic peak-jumping mode. An electron multiplier was operated in an ion counting mode with a dead time of 39 ns. Mass calibration was performed each time before starting measurements of particles. Mass bias corrections were conducted by comparing the measured isotope ratios for a certified uranium reference material (NBL CRM U350) with the reference values. The ratio of certified $^{235}\text{U}/^{238}\text{U}$ to measured $^{235}\text{U}/^{238}\text{U}$ was around 0.991. The hydride formation rate of uranium ($^{238}\text{UH}/^{238}\text{U}$) was determined (approximately 4×10^{-4}) for each particle and used to subtract the contribution of ^{235}UH from the signal of a mass 236.

3. Results and discussion

3.1. Effect of Apex-Q desolvation system in ICP-MS

The Apex-Q desolvation system was used to improve sensitivity for analysis of individual uranium particles. Prior to the analysis of uranium particles, procedural blank solution was prepared by performing the same sample preparation procedure without particles. Count rates on masses 234, 235, 236 and 238 were measured for procedural blank solution by ICP-MS with and without desolvation and are given in Table 2. No obvious differences in the count rates on masses 234 and 236 were found between the results obtained with and without desolvation. In contrast, the use of the desolvation system caused the increases of the count rates on masses 235 and 238, which would be due to the memory effect of the system.

The ^{238}U ion signal intensities were measured for individual U050 particles with the diameters ranging from 0.6 to $4.2 \mu\text{m}$ by

ICP-MS with and without desolvation. These results were plotted against the ^{238}U amount calculated using the diameter as an average value between the lengths of major and minor axes of each particle observed with SEM in Fig. 1(a). Fig. 1(b) shows examples of the SEM images of the particles. As shown in Fig. 1(a), the ^{238}U count rate obtained with desolvation was several times higher than that without desolvation. The increases of count rates were also observed on masses 234, 235 and 236. In the result measured with desolvation, approximate chemical recovery rate was about 90%, which was calculated using the uranium amount estimated from particle size and the signal intensity obtained with ICP-MS. This recovery rate would depend on the chemical composition of particles to be measured. Therefore, chemical dissolution procedure should be optimized to perform sensitive measurement.

In isotope ratio analysis, precision is an important factor to evaluate performance of measurements. In order to compare the performance between ICP-MS and SIMS, relative standard deviation (R.S.D.) values of uranium isotope ratios obtained by analyzing individual U050 particles were plotted against the amounts of uranium isotopes and are shown in Fig. 2. The R.S.D. values of $^{234}\text{U}/^{238}\text{U}$ and $^{236}\text{U}/^{238}\text{U}$ isotope ratios obtained by ICP-MS with desolvation were smaller than those without desolvation. These implied that the use of the desolvation system improved the precision of these isotope ratios. In contrast, no obvious improvement was found in the analysis of $^{235}\text{U}/^{238}\text{U}$ isotope ratio. This is related to the increase of ^{235}U intensity of procedural blank by using the desolvation system. Thorough cleaning of the system to reduce the blank value is necessary to perform more precise analysis.

For all isotope ratios, manipulation-SIMS gave better R.S.D. values than ICP-MS analysis. However, in the analysis of relatively large uranium particles, the R.S.D. values obtained by ICP-MS with desolvation were nearly equal to those by manipulation-SIMS. This means that ICP-MS analysis with desolvation has enough performance for individual particle analysis. It should be noted that all

Table 2

The procedural blank values on masses 234, 235, 236 and 238 in ICP-MS with and without desolvation.

Mass	Counts/s	
	Procedural blank	Procedural blank with desolvation
234	0.5 ± 0.3^a	0.7 ± 0.3
235	0.9 ± 0.5	2.3 ± 1.7
236	0.2 ± 0.2	0.0 ± 0.1
238	12.6 ± 6.6	115.8 ± 18.6

^a One standard deviation.

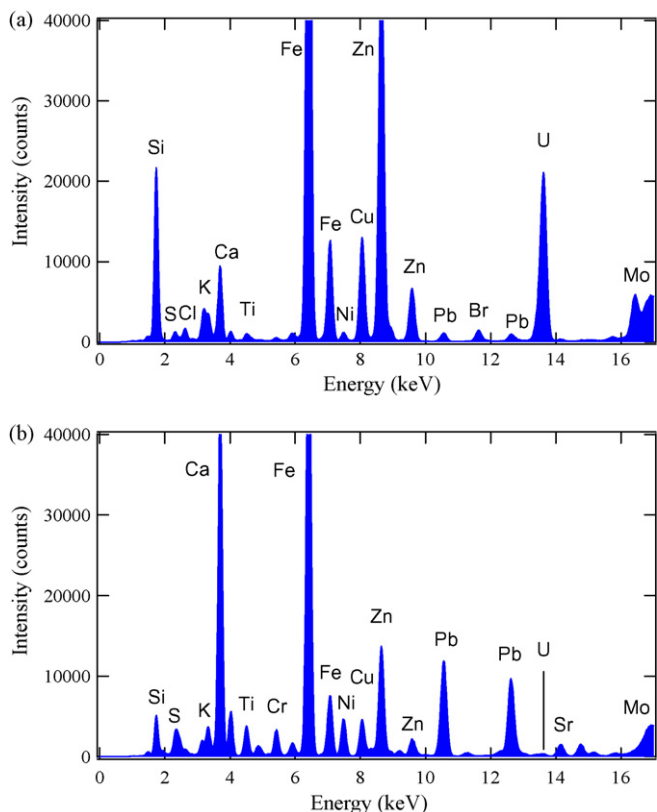


Fig. 3. Total-reflection X-ray fluorescence spectra of test swipe samples: (a) 1 and (b) 2 measured at an incident angle of 0.05° for 1000 s.

R.S.D. values of $^{235}\text{U}/^{238}\text{U}$ isotope ratios in Fig. 2 were within 5%, which is an acceptable precision in the analysis of individual uranium particles for nuclear safeguards [13].

3.2. Analysis of test swipe samples

Swipe samples taken at nuclear facilities contain various kinds of particles having different size, morphology and elemental composition. Typically, swipe samples contain a large number of non-uranium particles and a small number of uranium particles. In this study, two kinds of test swipe samples were analyzed to compare performance of SIMS and ICP-MS with desolvation. Fig. 3

represents the total-reflection X-ray fluorescence (TXRF) spectra of these samples. Here, the particles on Si disks were irradiated with molybdenum X-rays at an incident angle of 0.05° . The TXRF analysis implied that sample 1 contained iron, zinc and a relatively larger amount of uranium. Sample 2 contained iron, calcium, lead and a small amount of uranium. The iron and zinc are used for equipment and the lead is utilized as a shielded material for neutron in nuclear facilities. Thus, swipe samples taken at nuclear facilities normally contain these elements.

Fig. 4 shows the $^{234}\text{U}/^{238}\text{U}$ and $^{236}\text{U}/^{238}\text{U}$ isotope ratios measured for sample 1, plotted against $^{235}\text{U}/^{238}\text{U}$ isotope ratios. For comparison, the result obtained by SIMS without manipulation, used as a standard method for nuclear safeguards, is also shown in Fig. 4(a). The result in Fig. 4(a) indicated that all particles had almost the same isotope ratios. The average values were 4.22×10^{-4} , 4.00×10^{-2} and 6.50×10^{-5} for $^{234}\text{U}/^{238}\text{U}$, $^{235}\text{U}/^{238}\text{U}$ and $^{236}\text{U}/^{238}\text{U}$ isotope ratios, respectively. In contrast, the result obtained by manipulation-SIMS (Fig. 4(b)) and ICP-MS with desolvation (Fig. 4(c)) indicated the presence of uranium particles with different isotopic ratios. For example, the range of $^{235}\text{U}/^{238}\text{U}$ isotope ratio measured by ICP-MS was from 2.52×10^{-2} to 5.14×10^{-2} . In addition, the $^{234}\text{U}/^{238}\text{U}$ isotope ratio had a good correlation with the $^{235}\text{U}/^{238}\text{U}$ isotope ratio. The correlation between $^{234}\text{U}/^{238}\text{U}$ and $^{235}\text{U}/^{238}\text{U}$ isotope ratios is a signature in enrichment plants [1]. The discrepancy of the results between Fig. 4(a) and (c) is presumably due to agglomeration of uranium particles having different isotope ratios. In fact, the averaged $^{235}\text{U}/^{238}\text{U}$ isotope ratio (4.06×10^{-2}) in ICP-MS analysis was well consistent with that (4.00×10^{-2}) in SIMS without manipulation.

When the sample has a large number of uranium particles, agglomeration is a severe problem in SIMS analysis. This can be avoided by using single particle manipulation before SIMS analysis. Since ICP-MS analytical procedure also has a process of single particle manipulation, the problem of agglomeration of uranium particles could be avoided.

The results for sample 2 are shown in Fig. 5. In the result of SIMS without manipulation (Fig. 5(a)), the variations of $^{234}\text{U}/^{238}\text{U}$ and $^{236}\text{U}/^{238}\text{U}$ isotope ratios were larger, compared to those in manipulation-SIMS (Fig. 5(b)) and ICP-MS with desolvation (Fig. 5(c)). This discrepancy can be explained by an effect of molecular ion interferences in SIMS analysis. This sample has a small amount of uranium and larger amounts of other elements, as shown in Fig. 3. In particular, lead is known as a typical element giving molecular ion interferences on uranium mass region [7]. Molecular ions such as $^{206}\text{Pb}^{12}\text{C}^{16}\text{O}$, $^{207}\text{Pb}^{12}\text{C}^{16}\text{O}$ and $^{208}\text{Pb}^{12}\text{C}^{16}\text{O}$ can give

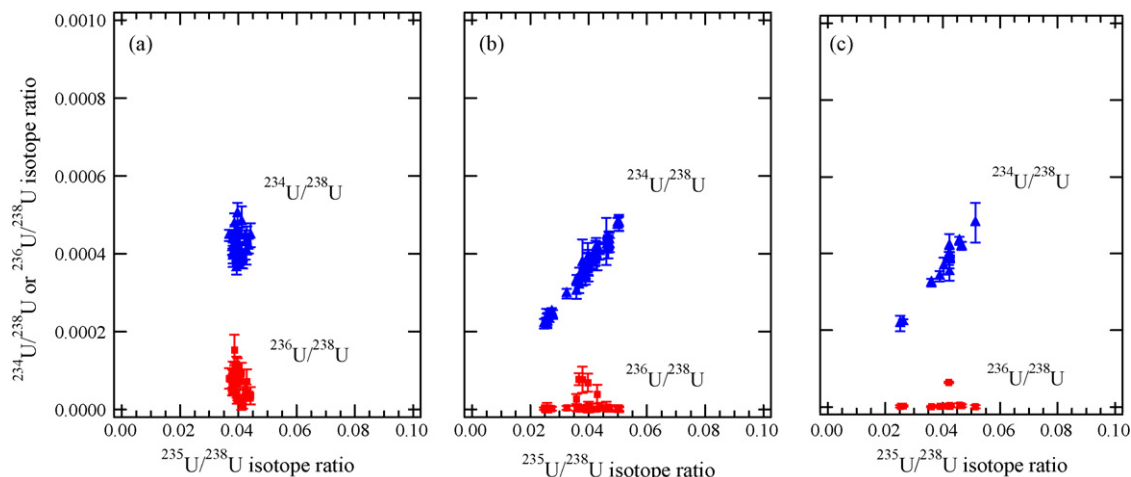


Fig. 4. The $^{234}\text{U}/^{238}\text{U}$ or $^{236}\text{U}/^{238}\text{U}$ isotope ratio against the $^{235}\text{U}/^{238}\text{U}$ isotope ratio measured for test swipe sample 1 by: (a) SIMS, (b) manipulation-SIMS and (c) ICP-MS with desolvation. The error bars represent one standard deviation.

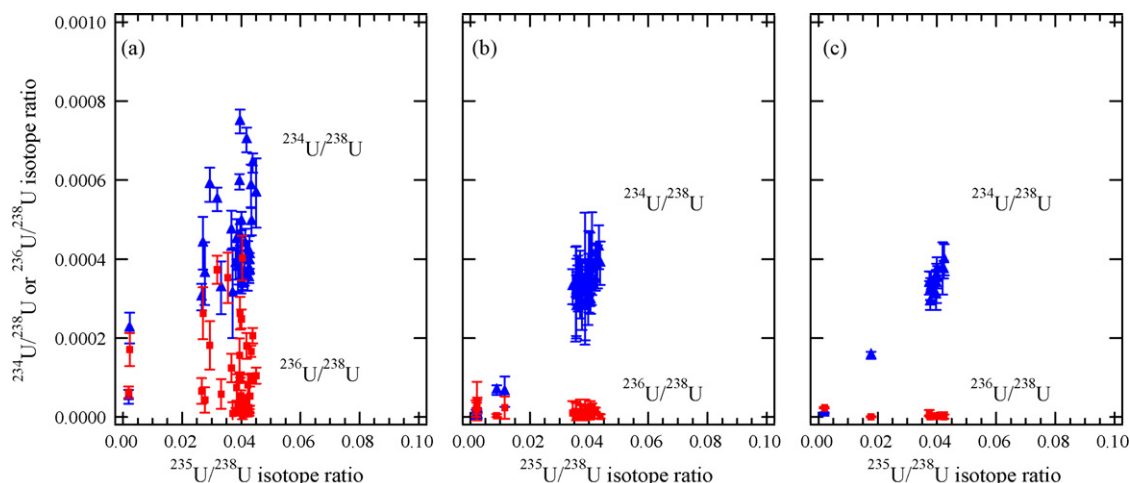


Fig. 5. The $^{234}\text{U}/^{238}\text{U}$ or $^{236}\text{U}/^{238}\text{U}$ isotope ratio against the $^{235}\text{U}/^{238}\text{U}$ isotope ratio measured for test swipe sample 2 by: (a) SIMS, (b) manipulation-SIMS and (c) ICP-MS with desolvation. The error bars represent one standard deviation.

interferences on masses 234, 235 and 236, respectively. Uranium minor isotopes (^{234}U and ^{236}U) are easily affected by these interferences because the count rates of these isotopes obtained in SIMS analysis are considerably low. The problem of interferences could also be removed by using single particle manipulation in SIMS and ICP-MS analyses as shown in Fig. 5(b) and (c). It should be noted that the correlation between the $^{234}\text{U}/^{238}\text{U}$ and $^{235}\text{U}/^{238}\text{U}$ isotope ratios was clearly observed in Fig. 5(b) and (c).

4. Conclusions

A desolvation system was used for determination of individual uranium particles in ICP-MS analysis. The improvement of precision in the analysis of $^{234}\text{U}/^{238}\text{U}$ and $^{236}\text{U}/^{238}\text{U}$ isotope ratios was achieved, though the increase of procedural blank values on masses 235 and 238 prevented the improvement of precision of $^{235}\text{U}/^{238}\text{U}$ isotope ratio. The ability of ICP-MS with desolvation for determination of uranium isotope ratios in individual particles was compared with that of SIMS by using test swipe samples. As well as manipulation-SIMS, the use of ICP-MS allowed us to perform precise isotope ratio analysis without problems of agglomeration of uranium particles and molecular ion interferences. In conclusion, ICP-MS with desolvation has almost the same ability as manipulation-SIMS, becoming an effective tool for individual particle analysis for nuclear safeguards.

Acknowledgements

This work was supported by the Ministry of Education, Culture, Sports, Science and Technology of Japan.

References

- [1] D.L. Donohue, *J. Alloys Compd.* 271–273 (1998) 11.
- [2] S. Baude, R. Chiappini, Proceedings of Symposium on International Safeguards, Vienna, Austria, 2001, IAEA-SM-367/10/05.
- [3] K.T. Esaka, F. Esaka, J. Inagawa, K. Iguchi, C.G. Lee, S. Sakurai, K. Watanabe, S. Usuda, *Jpn. J. Appl. Phys.* 43 (2004) L915.
- [4] C.G. Lee, K. Iguchi, F. Esaka, M. Magara, S. Sakurai, S. Usuda, *Jpn. J. Appl. Phys.* 45 (2006) L1121.
- [5] D.S. Simons, G. Gillen, C.J. Zeissler, R.H. Fleming, P.J. McNitt, *Secondary Ion Mass Spectrometry XI*, John Wiley & Sons, New York, 1998, pp. 59–62.
- [6] G. Tamborini, M. Betti, V. Forcina, T. Hiernaut, B. Giovannone, L. Koch, *Spectrochim. Acta B* 53 (1998) 1289.
- [7] F. Esaka, K.T. Esaka, C.G. Lee, M. Magara, S. Sakurai, S. Usuda, K. Watanabe, *Talanta* 71 (2007) 1011.
- [8] D. Lariviere, V.F. Taylor, R.D. Evans, R.J. Cornett, *Spectrochim. Acta B* 61 (2006) 877.
- [9] S.F. Boulyga, T. Prohaska, *Anal. Bioanal. Chem.* 390 (2008) 531.
- [10] C. Degueldre, P.-Y. Favarger, R. Rossé, S. Wold, *Talanta* 68 (2006) 623.
- [11] X.Z. Zhang, F. Esaka, K.T. Esaka, M. Magara, S. Sakurai, S. Usuda, K. Watanabe, *Spectrochim. Acta B* 62 (2007) 1130.
- [12] F. Esaka, K. Watanabe, H. Fukuyama, T. Onodera, K.T. Esaka, M. Magara, S. Sakurai, S. Usuda, *J. Nucl. Sci. Technol.* 41 (2004) 1027.
- [13] V.M. Pikaikin, G.M. Pshakin, V.A. Roshchenko, *Sci. Global Secur.* 14 (2006) 49.



Biomimetic sensor based on Mn^{III}Mn^{II} complex as manganese peroxidase mimetic for determination of rutin

Ana Cristina Franzoi^a, Rosely A. Peralta^b, Ademir Neves^b, Iolanda Cruz Vieira^{a,*}

^a Departamento de Química, LaBios-Laboratório de Biossensores, Universidade Federal de Santa Catarina, CEP 88040-900 Florianópolis, SC, Brazil

^b Departamento de Química, LABINC-Laboratório de Bioinorgânica e Cristalografia, Universidade Federal de Santa Catarina, CEP 88040-900 Florianópolis, SC, Brazil

ARTICLE INFO

Article history:

Received 24 September 2008

Received in revised form 3 November 2008

Accepted 4 November 2008

Available online 14 November 2008

Keywords:

Biomimetic sensor

Manganese peroxidase

Mn^{III}Mn^{II} complex

Rutin

ABSTRACT

A novel biomimetic sensor for rutin determination based on a dinuclear complex [Mn^{III}Mn^{II}(Ldtb)(μ -OAc)₂]BPh₄ containing an unsymmetrical dinucleating ligand, 2-[N,N-bis(2-pyridylmethyl)aminomethyl]-6-[N-(3,5-di-*tert*-butyl-2-oxidoben-zyl)-N-(2-pyridylamino)aminomethyl]-4-methylphenol (H₂Ldtb), as a manganese peroxidase mimetic was developed. Several parameters were investigated to evaluate the performance of the biomimetic sensor obtained after the incorporation of the dinuclear complex in a carbon paste. The best performance was obtained in 75:15:10% (w/w/w) of the graphite powder:Nujol:Mn^{III}Mn^{II} complex, 0.1 mol L⁻¹ phosphate buffer solution (pH 6.0) and 4.0 × 10⁻⁵ mol L⁻¹ hydrogen peroxide. The response of the sensor towards rutin concentration was linear using square wave voltammetry in the range of 9.99 × 10⁻⁷ to 6.54 × 10⁻⁵ mol L⁻¹ ($r=0.9998$) with a detection limit of 1.75 × 10⁻⁷ mol L⁻¹. The recovery study performed with pharmaceuticals ranged from 96.6% to 103.2% and the relative standard deviation was 1.85% for a solution containing 1.0 × 10⁻³ mol L⁻¹ rutin ($n=6$). The lifetime of this biomimetic sensor was 200 days (at least 750 determinations). The results obtained for rutin in pharmaceuticals using the biomimetic sensor and those obtained with the official method are in agreement at the 95% confidence level.

© 2008 Elsevier B.V. All rights reserved.

1. Introduction

Enzymes are remarkable biomolecules which, besides having as their main characteristic an extraordinary catalytic efficiency, have a high degree of specificity for their substrates and are the biological component most commonly used in biosensors [1]. A field of enormous interest is the development of mimetic complexes, which function as analogous synthetic metalloenzymes for catalytic oxidation reactions, and can mimic the active site of different enzymes [2–8].

The majority of peroxidases are heme proteins and contain Fe^{III} in the active site. A large number of peroxidases have been identified in fungal species and are being characterized at the molecular level [9]. Manganese peroxidase (MnP) is the most common lignin-modifying peroxidase and is produced by almost all wood-colonizing basidiomycetes which cause white-rot *Phanerochaete chrysosporium* and various soil-colonizing litter-decomposing fungi. This enzyme requires hydrogen peroxide as a cosubstrate and oxidizes Mn²⁺, always present in wood and soils, to Mn³⁺ which then acts as an obligatory redox coupler, oxidizing

various organic substrates. Mn³⁺ is stabilized by fungal chelators such as oxalic acid. Chelated Mn³⁺ in turn acts as a low-molecular weight, diffusible redox mediator that attacks phenolic lignin structures resulting in the formation of unstable free radicals that tend to disintegrate spontaneously [10]. It is unique among plant and fungal peroxidases since it catalyzes the hydrogen peroxide-dependent oxidation of Mn²⁺ to Mn³⁺, which in turn oxidizes a wide variety of organic phenolic substrates including lignin itself [11]. MnP is a glycoprotein with one iron protoporphyrin IX prosthetic group. The primary product of the peroxidase reaction with H₂O₂ is the oxidized intermediate compound I – MnP I – Fe⁴⁺-oxo-porphyrin-radical complex. The spectral characteristics of MnP I are most similar to those of HRP compound I and LiP compound I. One-electron reduction of MnP I by a peroxidase substrate results in the formation of compound II – MnP II – Fe⁴⁺-oxo-porphyrin complex [12].

Another metalloenzyme class is purple acid phosphatases (PAPs), that contain a homodinuclear Fe^{III}Fe^{II} (isolated from animals) or heterodinuclear Fe^{III}M^{II} (M=Mn or Zn; isolated from plants) in their active sites. The characteristic pink to purple color is due to a charge transfer transition involving a tyrosine residue coordinating a ferric ion [7,8,13]. Our research group employed homodinuclear Fe^{III}Fe^{II} [14] and heterodinuclear Fe^{III}Zn^{II} [15] complexes, in the construction of biomimetic sensors. These were then

* Corresponding author. Tel.: +55 48 37216844; fax: +55 48 372119711.
E-mail address: iolanda@qmc.ufsc.br (I.C. Vieira).

used in the determination of dopamine in pharmaceutical formulations and rosmarinic acid in plant extract samples, respectively.

Polyphenols include a large group of structurally related compounds widely distributed in nature and there is an increasing interest in polyphenols due to their potentially positive effect against certain diseases. They can act as free radical scavengers neutralizing dangerous reactive oxygen species and metal ion chelators, and these activities are responsible for their antioxidant properties [16].

Rutin is a natural flavonoid with a wide spectrum of biochemical and pharmacological activities, including antioxidant, antiviral, antitumor, anti-inflammatory, and antiallergic, and is a stimulant of the immune system [17]. Methods for the determination of rutin include spectrophotometry [18], capillary electrophoresis [19] and electrochemistry [20–22]. Franzoi et al. [20] have developed a poly(vinylpyrrolidone) (PVP)-modified carbon paste electrode for the determination of rutin in pharmaceutical formulations. The excellent properties of PVP effectively facilitate the adsorption of rutin on the surface of the modified electrode and improve sensitivity in the determination of this flavonoid. Linear sweep voltammetry measurements have shown that the modified electrode exhibited a linear response for rutin concentrations from 3.9×10^{-7} to 1.3×10^{-5} mol L⁻¹ and the detection limit was 1.5×10^{-7} mol L⁻¹. Cathodic stripping square-wave voltammetry has been reported [21] for the determination of rutin based on the accumulation of rutin on the surface of a hanging mercury drop electrode. The peak current is proportional to the concentration of rutin over the range of 2.0–85.0 nmol L⁻¹ and the limit of detection is 0.5 nmol L⁻¹. Mousty et al. [22] have investigated the amperometric detection of rutin with a biosensor using polyphenol oxidase (PPO) as the bioelement. The biosensor was fabricated by entrapment of PPO within a laponite clay film coated on an electrode surface. The amperometric detection of rutin was carried out at -0.1 V via the direct electrochemical reduction of the product of the enzymatic reaction or its reduction mediated by a phenothiazine redox mediator (Azure B) intercalated within the clay matrix.

In this study, the fully characterized dinuclear mimetic complex [Mn^{III}Mn^{II}(Ldtb)(μ -OAc)₂]BPh₄ [2] was utilized as a manganese peroxidase mimetic in the construction of a novel biomimetic sensor. The influence of different experimental conditions including the percentage of the Mn^{III}Mn^{II} complex, pH, hydrogen peroxide concentration and square wave voltammetry parameters, such as frequency, pulse amplitude, and scan increment, was investigated to optimize the proposed sensor. Of the several phenolic compounds available (adrenaline, caffeic acid, catechin, catechol, chlorogenic acid, dopamine, hydroquinone and rutin) rutin was selected. The results obtained for rutin determination in pharmaceutical formulations using the biomimetic sensor and the official method [20] are in good agreement.

2. Experimental

2.1. Reagents and solutions

All reagents used in this study were of analytical grade. All solutions used in the experiments were prepared with ultrapure water (18.2 M Ω) obtained from a Milli-Q purification system. Adrenaline, caffeic acid, catechin, catechol, chlorogenic acid, dopamine and hydroquinone were acquired from Aldrich and a 1.0×10^{-3} mol L⁻¹ stock solution was prepared in 0.1 mol L⁻¹ phosphate buffer solution at pH 6.0. Rutin was purchased from Sigma and a 1.0×10^{-3} mol L⁻¹ stock solution was prepared daily in 30% (v/v) ethanol and 0.1 mol L⁻¹ phosphate buffer solution at pH 6.0. Graphite powder (grade #38) and Nujol were supplied by Fisher Scientific and Aldrich, respectively. Hydrogen peroxide, sodium

chloride, sucrose, lactose, magnesium stearate, poly(ethylene glycol) and starch were purchased from Sigma.

2.2. Synthesis and characterization of the ligand and the complex

Neves and co-workers [2] reported the synthesis of the ligand 2-[N,N-bis(2-pyridylmethyl)-aminomethyl]-6-[N-(3,5-dimethylphenol (H₂Ldtb)) and its characterization by ¹H NMR [δ H (200 MHz, CDCl₃), in ppm: 8.54, 7.61, 7.53, 7.15, 6.97, 6.84 (16H, aromatic H); 3.92, 3.85, 3.84, 3.80 (s, 12H, CH₂); 2.23 (s, CH₃); 1.42, 1.25 (s, *tert*-butyl)], as well as the X-ray crystal structure of its corresponding manganese complex di- μ -acetato- μ -{2-[N,N-bis(2-pyridylmethyl)-aminomethyl]-6-[N-(3,5-dimethylphenol (H₂Ldtb))-N-(2-pyridylamino)aminomethyl]-4-methylphenolate}dimanganese(II,III)tetraphenylborate [Mn^{III}Mn^{II}(Ldtb)(μ -OAc)₂]BPh₄. Yield 82%.

2.3. Biomimetic sensor preparation

Recent studies by our group have described the construction and application of several sensors based on carbon paste [14,15]. The carbon paste was obtained by homogenizing graphite powder (135.0 mg; 75%, w/w) and Mn^{III}Mn^{II} complex powder (18.0 mg; 10%, w/w) in a mortar for 20 min to ensure uniform dispersion. Subsequently, the biomimetic sensor was obtained by adding Nujol (27.0 mg; 15%, w/w) to this paste and mixing for 20 additional min to produce the final paste. The resulting paste was packed firmly into the cavity (3.0 mm diameter) of a syringe and a copper wire was inserted to obtain the external electrical contact. For comparison, a carbon paste electrode without Mn^{III}Mn^{II} complex (bare CPE) was prepared following the same steps.

2.4. Instrumentation and electrochemical measurements

Square wave voltammetry measurements using the biomimetic sensor were performed on an Autolab PGSTAT12 potentiostat/galvanostat (Eco Chemie, Utrecht, The Netherlands) connected to data processing software (GPES, version 4.9.006, Eco Chemie). Voltammetric measurements were carried out in an unstirred, non-de-aerated phosphate buffer solution (pH 6.0) at 25.0 ± 0.5 °C and all potentials were measured and reported vs. Ag/AgCl (3.0 mol L⁻¹ KCl). A three-electrode assembly was used in which a biomimetic sensor, an Ag/AgCl (3.0 mol L⁻¹ KCl) and a platinum-wire served as the working, reference and auxiliary electrodes, respectively. First, 10 mL of the supporting electrolyte and 4.0×10^{-5} mol L⁻¹ of the hydrogen peroxide solution were transferred to a clean, dry cell and the required volume of the rutin or pharmaceutical samples was added by micropipette. After a stirring period of 60 s in order to homogenize the solution, a square wave voltammogram was recorded, applying a sweep potential between +0.6 and -0.4 V, at a frequency of 20 Hz, pulse amplitude of 10 mV and increment of 5.0 mV, after successive additions of rutin.

2.5. Analytical application

Three Brazilian pharmaceutical formulations containing rutin (A=manipulated rutin, B=Novarrutina tablet form and C=Novarrutina liquid form) were obtained from a local drugstore in Florianopolis (Santa Catarina, Brazil). The solid samples (A or B) were dissolved in 30% (v/v) ethanol and added to 0.1 mol L⁻¹ phosphate buffer solution (pH 6.0). For the liquid rutin sample (C), 1.0 mL of the pharmaceutical sample was added to ethanol:phosphate buffer solution, pH 6.0 (30/70%, v/v), to give 50 mL of the solution. Aliquots of pharmaceutical samples were transferred to the cell

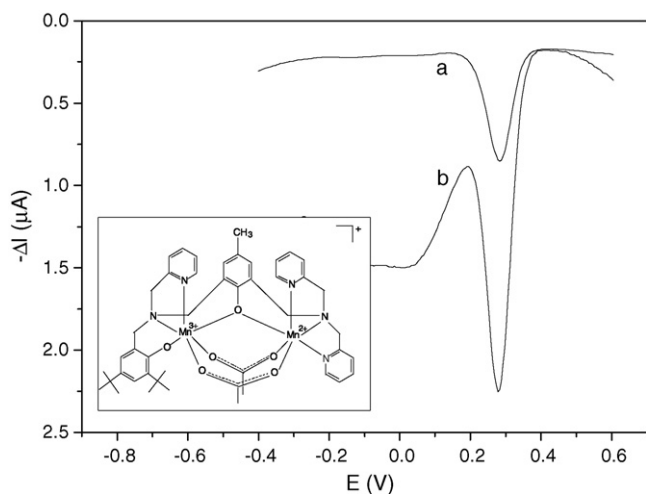


Fig. 1. Square wave voltammograms obtained using (a) bare carbon paste electrode and (b) biomimetic sensor, in $2.91 \times 10^{-5} \text{ mol L}^{-1}$ rutin and $4.0 \times 10^{-5} \text{ mol L}^{-1}$ hydrogen peroxide in 0.1 mol L^{-1} phosphate buffer solution (pH 6.0) at frequency 20 Hz, pulse amplitude 10 mV and scan increment 5.0 mV. Inset: schematic representation of the dinuclear complex $[\text{Mn}^{\text{III}}\text{Mn}^{\text{II}}(\text{Ldtb})(\mu\text{-OAc})_2]\text{BPh}_4$ containing the dinucleating ligand H_2Ldtb .

and quantified using square wave voltammetry, after successive additions of rutin standard solutions.

3. Results and discussion

3.1. Voltammetric behavior of rutin in the biomimetic sensor and bare CPE

The electrochemical behavior of rutin in relation to the biomimetic sensor based on the $\text{Mn}^{\text{III}}\text{Mn}^{\text{II}}$ complex and the bare carbon paste electrode (CPE) was investigated by square wave voltammetry in the potential range of +0.6 and -0.4 V vs. Ag/AgCl . Fig. 1 shows the voltammograms obtained using the (a) carbon

paste electrode and (b) biomimetic sensor in $2.91 \times 10^{-5} \text{ mol L}^{-1}$ rutin and $4.0 \times 10^{-5} \text{ mol L}^{-1}$ hydrogen peroxide in 0.1 mol L^{-1} phosphate buffer solution (pH 6.0). A peak reduction of *o*-quinone to rutin can be seen at +0.28 V for both the electrodes. The response of the biomimetic sensor with addition of the $\text{Mn}^{\text{III}}\text{Mn}^{\text{II}}$ complex (inset Fig. 1) was higher and three times more sensitive than the carbon paste electrode.

3.2. $\text{Mn}^{\text{III}}\text{Mn}^{\text{II}}$ complex and catalytic cycle of mimetic manganese peroxidase

The mixed-valence diacetate-bridged manganese complex $[\text{Mn}^{\text{III}}\text{Mn}^{\text{II}}(\text{Ldtb})(\mu\text{-OAc})_2]\text{BPh}_4$ was prepared in good yield according to the synthetic procedures described in the literature and was characterized through X-ray crystallography [2]. Manganese ions are known to play a role in the catalytic cycle of fungal peroxidases [23] which resembles those of other peroxidases, such as horseradish peroxidase (HRP) [24] and lignin peroxidase (LiP) [25,26] both associated with lignin degradation. It has also been demonstrated that MnP oxidizes Mn^{2+} to Mn^{3+} and that the Mn^{3+} produced, in turn, oxidizes the organic substrates. Thus, the manganese ion participates in the reaction as a redox couple rather than as an enzyme-binding activator [10–12].

The $\text{Mn}^{\text{III}}\text{Mn}^{\text{II}}$ complex at the biomimetic sensor surface catalyzes the reaction between the rutin and hydrogen peroxide, as shown in Fig. 2. The catalytic cycle was proposed by Wariishi [12] and is initiated by the binding of H_2O_2 to the $\text{Mn}^{\text{III}}\text{Mn}^{\text{II}}$ complex forming MnP compound I (MnP I) and one water molecule. The cleavage of the peroxide oxygen–oxygen bond requires a two-electron transfer in the formation of MnP I. The Mn^{2+} ion acts as a one-electron donor and is oxidized to Mn^{3+} which, in turn, oxidizes the molecule of rutin by hydrogen abstraction, forming a free radical of the rutin. The single electron on the oxygen atom may be dispersed by the double bond and the carbonyl forming a very stable radical. In this step it is assumed that the Mn^{2+} is capable of reducing MnP I to the corresponding MnP II compound. The reduction of MnP II proceeds in a similar way and another Mn^{3+} is formed from Mn^{2+} thereby leading to generation of the native enzyme, $\text{Mn}^{\text{III}}\text{Mn}^{\text{II}}$

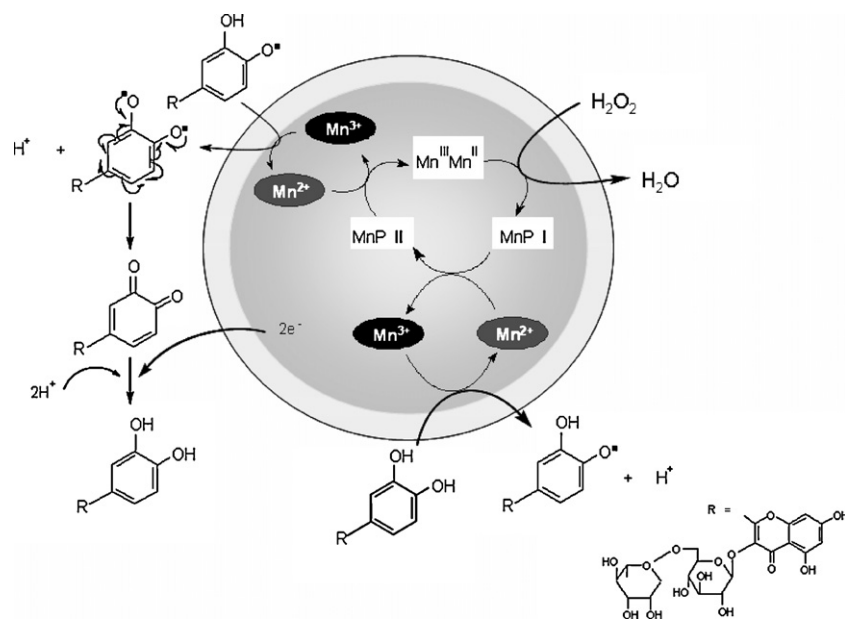
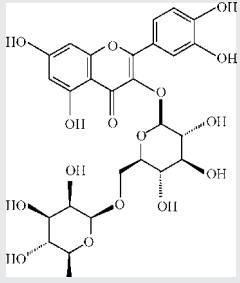
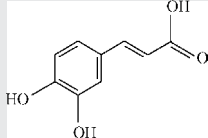
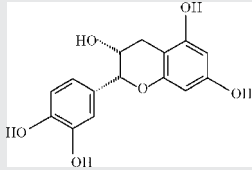
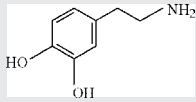
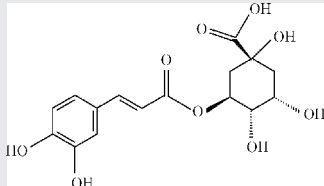
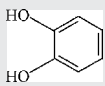
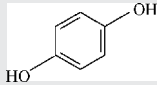
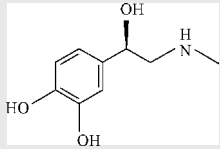


Fig. 2. Reaction between the rutin and hydrogen peroxide in the biomimetic sensor surface catalyzed by $\text{Mn}^{\text{III}}\text{Mn}^{\text{II}}$ complex: catalytic cycle of manganese peroxidase (MnP) mimetic.

Table 1
Relative response of the biomimetic sensor to different phenolic compounds.

Phenolic compound	Structure	E_{pc} (V)	Relative response (%)
Rutin		+0.28	100
Caffeic acid		+0.16	33
Catechin		+0.18	17
Dopamine		+0.11	14
Chlorogenic acid		+0.18	13
Catechol		+0.03	6
Hydroquinone		-0.11	4
Adrenaline		-0.22	3

complex. It has been demonstrated that the Mn^{3+} ion can be subsequently stabilized by chelation with organic acids such as oxalate and malonate (secreted by the fungus) and diffuses from the surface of the enzyme to oxidize the phenolic and amino-aromatic compounds [10,27–29]. When both H_2O_2 and an aromatic electron donor, e.g. hydroquinone or catechol, are present at the surface of a peroxidase electrode, direct electron transfer coexists with the common enzymatic reaction [30,31]. In addition, Mn^{3+} oxidizes the radical forming a diradical of rutin and one proton. This diradical of rutin is converted into the most stable form (*o*-quinone) with the arrows in Fig. 2 showing a sequence of one-electron transfers. Finally, the last step shows the electrochemical reduction of *o*-quinone to rutin involving two electrons and two protons.

3.3. Study of phenolic compounds

A comparative study was carried out in order to investigate the response of the biomimetic sensor to different phenolic compounds (adrenaline, caffeic acid, catechin, catechol, chlorogenic acid, dopamine, hydroquinone and rutin). Table 1 shows the potential E_{pc} (cathodic peak current) and relative response (%). The biomimetic sensor sensitivity decreased in the following order: rutin, caffeic acid, catechin, dopamine, chlorogenic acid, catechol, hydroquinone and adrenaline. Thus, in this study, rutin was selected for the optimization of the proposed biomimetic sensor and application to pharmaceutical samples.

3.4. Analytical performance of the biomimetic sensor

Initially, the effect of the $\text{Mn}^{\text{III}}\text{Mn}^{\text{II}}$ complex composition varying from 5% to 20% (w/w) in a fixed ratio of graphite powder:Nujol of 75:15% (w/w) was investigated. The analytical response to $2.91 \times 10^{-5} \text{ mol L}^{-1}$ rutin increased with the $\text{Mn}^{\text{III}}\text{Mn}^{\text{II}}$ complex percentage used up to 10%. Thus, the biomimetic sensor containing 10% (w/w) of complex powder showed the best response, and this composition was used in the construction of further biomimetic sensors.

In the biomimetic sensor optimization studies several experimental parameters were investigated in order to obtain the maximum peak current and optimum performance of the biomimetic sensor. The effect of the pH of the 0.1 mol L^{-1} phosphate buffer solution, in the range of 5.0–8.0, on the biomimetic sensor response to a $2.91 \times 10^{-5} \text{ mol L}^{-1}$ rutin solution was studied. The highest response was obtained at pH 6.0. Therefore, this pH was selected and used for subsequent experiments.

Another important parameter evaluated was the hydrogen peroxide concentration. The effect on the sensor response of varying the rutin concentration from 0.0 to $2.0 \times 10^{-4} \text{ mol L}^{-1}$ to $1.0 \times 10^{-3} \text{ mol L}^{-1}$, in phosphate buffer solution (0.1 mol L^{-1} , pH 6.0), was examined. In the range studied, the analytical response increased with an increase in the concentration of the hydrogen peroxide solution up to $4.0 \times 10^{-5} \text{ mol L}^{-1}$ and then leveled off between 4.0×10^{-5} and $2.0 \times 10^{-4} \text{ mol L}^{-1}$. Therefore, a hydrogen peroxide concentration of $4.0 \times 10^{-5} \text{ mol L}^{-1}$ was used in this study.

In the square wave voltammetry method, the choice of the best parameters such as frequency, pulse amplitude and scan increment, offers a higher sensitivity and lower detection limit of the electrochemical signal. Thus, these parameters were investigated and the responses were analyzed through the cathodic peak current for a $2.91 \times 10^{-5} \text{ mol L}^{-1}$ rutin solution. The optimum values found were a frequency of 20 Hz, pulse amplitude of 10 mV and scan increment of 5.0 mV. Table 2 summarizes the range over which each variable was investigated and the optimum value found. The best experimental conditions were selected for subsequent experiments.

3.5. Repeatability, reproducibility and stability of the biomimetic sensor

To investigate the precision of the determination, the same biomimetic sensor was used for six parallel determinations of $2.91 \times 10^{-5} \text{ mol L}^{-1}$ rutin solution and $4.0 \times 10^{-5} \text{ mol L}^{-1}$ hydrogen peroxide in phosphate buffer solution (0.1 mol L^{-1} ; pH 6.0). The relative standard deviation was calculated as 1.85%. Three biomimetic sensors were constructed using the same procedure and were independently used for the determination of rutin under the conditions described above. All the biosensors showed an acceptable reproducibility with a relative standard deviation of 2.08%, indicating that the results obtained with the proposed biosensor have a good reproducibility.

The stability and lifetime of the sensor are very important and were investigated through consecutive measurements, with-

out surface renewal over a 200-day period (over 750 samples were determined for each quantity of carbon paste used in the syringe), of its response (cathodic peak currents) to $2.91 \times 10^{-5} \text{ mol L}^{-1}$ rutin solution (pH 6.0) and $4.0 \times 10^{-5} \text{ mol L}^{-1}$ hydrogen peroxide. When the biomimetic sensor was stored at room temperature and measurements taken every 1–2 days using this substance, no change was observed in its response.

3.6. Square wave voltammograms and analytical curve

Under the optimum conditions established (75:15:10% (w/w/w) graphite powder:Nujol: $\text{Mn}^{\text{III}}\text{Mn}^{\text{II}}$ complex, phosphate buffer solution pH 6.0, $4.0 \times 10^{-5} \text{ mol L}^{-1}$ of hydrogen peroxide, frequency 20 Hz, amplitude 10 mV and scan increment 5.0 mV), the electrocatalytic behavior of the biomimetic sensor in the electrochemical reduction of *o*-quinone was investigated using square wave voltammetry (Fig. 3). As can be seen the cathodic peak current at +0.28 V vs. Ag/AgCl increased with increasing rutin concentration. The analytical curve (Fig. 3 inset) obtained with the biomimetic sensor was linear from 9.99×10^{-7} to $6.54 \times 10^{-5} \text{ mol L}^{-1}$ ($\Delta I = -0.398 + 0.0776 \times 10^6 [\text{rutin}]$; $r = 0.9998$) where ΔI is the cathodic current peak, and [rutin] is the rutin concentration in mol L^{-1} . Additionally, the detection limit (three times the signal blank/slope) was calculated using the linear range, and was found to be $1.75 \times 10^{-7} \text{ mol L}^{-1}$.

3.7. Recovery and determination

The accuracy of the biomimetic sensor was evaluated through a recovery study on pharmaceuticals after standard addition of 6.1, 9.0 and 12.0 mg L^{-1} of rutin. The rutin recoveries of 96.6–103.2% (Table 3) show that the sensor gave satisfactory results, indicating the absence of matrix effects in these determinations.

Also, to evaluate the applicability of the biomimetic sensor, the proposed method was validated by applying it to the determination of rutin in pharmaceutical formulations. The results for pharmaceutical samples (A, B and C) using the proposed biomimetic sensor, compared with the values obtained using the official method [20] and the declared values, are given in Table 4. According to the Student's *t*-test, at a 95% confidence level, a good agreement was

Table 2
Optimization of biomimetic sensor experimental conditions.

Parameter investigated	Range studied	Optimum value
$\text{Mn}^{\text{III}}\text{Mn}^{\text{II}}$ (% w/w)	5–20	10
pH	5.0–8.0	6.0
Hydrogen peroxide concentration (mol L^{-1})	1.0×10^{-5} – 2.0×10^{-4}	4.0×10^{-5}
Frequency (Hz)	10–100	20
Pulse amplitude (mV)	10–100	10
Scan increment (mV)	0.5–5.0	5.0

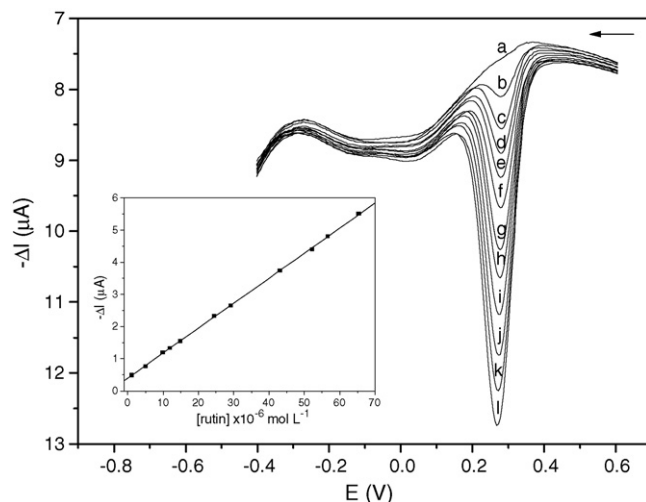


Fig. 3. Square wave voltammograms obtained using the proposed biomimetic sensor for (a) blank in phosphate buffer solution (0.1 mol L^{-1} ; pH 6.0) and rutin solutions at the following concentrations: (b) 9.99×10^{-7} ; (c) 4.98×10^{-6} ; (d) 9.90×10^{-6} ; (e) 1.19×10^{-5} ; (f) 1.48×10^{-5} ; (g) 2.44×10^{-5} ; (h) 2.91×10^{-5} ; (i) 4.31×10^{-5} ; (j) 5.21×10^{-5} ; (k) 5.66×10^{-5} and (l) $6.54 \times 10^{-5} \text{ mol L}^{-1}$ at frequency 20 Hz, pulse amplitude 10 mV and scan increment 5.0 mV. Inset: the analytical curve of rutin.

Table 3
Rutin recovery in pharmaceutical formulations using the biomimetic sensor.

Rutin (mg L ⁻¹)			
Sample	Added	Found	Recovery (%)
A	6.1	6.0	98.3
	9.0	9.1	101.1
	12.0	12.1	100.8
B	6.1	6.3	103.2
	9.0	8.8	97.7
	12.0	12.2	101.6
C	6.1	5.9	96.6
	9.0	8.8	97.7
	12.0	12.0	100

n = 3.

Table 4
Determination of rutin in pharmaceutical formulations using the biomimetic sensor and the official method.

Sample	Label value	Official method [24]	Biomimetic sensor	<i>R</i> _{e1}	<i>R</i> _{e2}
A ^a	20.0	19.8 ± 0.1	19.3 ± 0.1	-3.6	-2.6
B ^a	20.0	20.8 ± 0.1	19.4 ± 0.1	-3.1	-7.2
C ^b	20.0	20.4 ± 0.1	19.1 ± 0.1	-4.7	-6.8

*R*_{e1} = biomimetic sensor vs. label value; *R*_{e2} = biomimetic sensor vs. official method. *n* = 3; confidence level of 95%.

^a mg tablet⁻¹.

^b mg mL⁻¹.

obtained within an acceptable range of error. Thus, it can be concluded that the method is suitable for the determination of rutin in commercial pharmaceutical formulations.

4. Conclusions

In this paper, a dinuclear Mn^{III}Mn^{II} complex was successfully used in the construction of a new biomimetic sensor for the determination of phenolic compounds. The ability of the complex to mimic the active site of the manganese peroxidase, catalyzing the reaction between rutin and hydrogen peroxide at the biomimetic sensor surface, is observed through an increase in the response in terms of rutin reduction. Additionally, the biosensor with the complex was shown to offer an excellent performance especially in terms of rutin determination. This promising sensor offers attractive analytical features including high sensitivity, low detection limit, and rapid response, as well as showing excellent long-term stability. Furthermore, the biomimetic sensor is accurate, reliable, simple, quick to prepare and offers a low cost procedure. Satisfactory results were obtained using this sensor when compared with

the official method and, thus, it represents an alternative method to determine rutin in pharmaceutical formulations.

Acknowledgments

Financial support from CNPq (Process 472169/2004-1 and 472541/2006-4), MCT/CNPq/PADCT, FAPESC and also a scholarship granted by CNPq to ACF are gratefully acknowledged.

References

- [1] M.D.P.T. Sotomayor, A.A. Tanaka, R.S. Freire, L.T. Kubota, *Encyclopedia Sens.* 10 (2005) 1.
- [2] A.J. Bortoluzzi, A. Neves, R.A.A. Couto, R.A. Peralta, *Acta Cryst. C* 62 (2006) m27.
- [3] A. Neves, M. Lanznaster, A.J. Bortoluzzi, R.A. Peralta, A. Casellato, E.E. Castellano, P. Herral, M.J. Riley, G. Schenk, *J. Am. Chem. Soc.* 129 (2007) 7486.
- [4] N.A. Rey, A. Neves, A.J. Bortoluzzi, C.T. Pich, H. Terenzi, *Inorg. Chem.* 46 (2007) 348.
- [5] M.U. Triller, D. Pursche, W. Hsieh, V.L. Pecoraro, A. Rompel, B. Krebs, *Inorg. Chem.* 42 (2003) 6274.
- [6] P. Karsten, A. Neves, A.J. Bortoluzzi, J. Strähle, C. Maichle-Mössmer, *Inorg. Chem. Commun.* 5 (2002) 434.
- [7] N. Mitić, S.J. Smith, A. Neves, L.W. Guddat, L.R. Gahan, G. Schenk, *Chem. Rev.* 106 (2006) 3338.
- [8] M. Lanznaster, A. Neves, A.J. Bortoluzzi, B. Szpoganicz, E. Schwingel, *Inorg. Chem.* 41 (2002) 5641.
- [9] A. Conesa, P.J. Punt, C.A.M.J.J. van den Hondel, *J. Biotechnol.* 93 (2002) 143.
- [10] M. Hofrichter, *Enzyme Microb. Technol.* 30 (2002) 454.
- [11] H. Wariishi, K. Valli, M.H. Gold, *Biochem. Biophys. Res. Commun.* 176 (1991) 269.
- [12] H. Wariishi, L. Akileswaran, M.H. Gold, *Biochemistry* 27 (1988) 5365.
- [13] W.W. Clelland, A.C. Hengge, *Chem. Rev.* 106 (2006) 3252.
- [14] I.R.W.Z. Oliveira, A. Neves, I.C. Vieira, *Sens. Actuators B* 129 (2008) 424.
- [15] M. Santhiago, R.A. Peralta, A. Neves, G.A. Micke, I.C. Vieira, *Anal. Chim. Acta* 613 (2008) 91.
- [16] T.M. Penning, M.E. Burczynski, C.F. Hung, K.D. McCoul, N.T. Palackal, L.S. Tsuruda, *Chem. Res. Toxicol.* 12 (1999) 1.
- [17] D. Odaci, S. Timur, N. Pazarlioglu, M.R. Montereali, W. Vastarella, R. Pilloton, A. Telefoncu, *Talanta* 71 (2007) 312.
- [18] M.L. Calabrò, S. Tommasini, P. Donato, R. Stancanelli, D. Raneri, S. Catania, C. Costa, V. Vilari, P. Ficarra, R. Ficarra, *J. Pharm. Biom. Anal.* 36 (2005) 1019.
- [19] G. Chen, H.W. Zhang, J.N. Ye, *Anal. Chim. Acta* 423 (2000) 69.
- [20] A.C. Franzoi, A. Spinelli, I.C. Vieira, *J. Pharm. Biom. Anal.* 47 (2008) 973.
- [21] A.A. Ensafi, R. Hajian, *Electroanalysis* 18 (2006) 579.
- [22] C. Mousty, S. Cosnier, M.S.-P. Lopez, E. Lopez-Cabarcos, B. Lopez-Ruiz, *Electroanalysis* 19 (2007) 253.
- [23] M.J.R. Marañón, R.B. van Huystee, *Phytochemistry* 37 (1994) 1217.
- [24] H.B. Dunford, *Peroxidases in Chemistry and Biology*, CRC Press, Boca Raton, 1991, p. 1.
- [25] H. Wariishi, J. Huang, H.B. Dunford, M.H. Gold, *J. Biol. Chem.* 266 (1991) 20694.
- [26] K. Valli, H. Wariishi, M.H. Gold, *Biochemistry* 29 (1990) 8535.
- [27] K. Kishi, H. Wariishi, L. Marquez, H.B. Dunford, M.H. Gold, *Biochemistry* 33 (1994) 8694.
- [28] H. Wariishi, H.B. Dunford, I.D. MacDonald, M.H. Gold, *J. Biol. Chem.* 264 (1989) 3335.
- [29] H. Wariishi, K. Valli, M.H. Gold, *Biochemistry* 28 (1989) 6017.
- [30] T. Ruzgas, E. Csöregi, J. Emnéus, L. Gorton, G. Marko-Varga, *Anal. Chim. Acta* 330 (1996) 123.
- [31] A. Lindgren, T. Ruzgas, L. Gorton, E. Csöregi, G.B. Ardila, I.Y. Sakharov, I.G. Gazaryan, *Biosens. Bioelectron* 15 (2000) 491.



A new electrochemical method for trace water determination in methanol

Monika Gašiorowska*, Jacek A. Soroka, Marta J. Sawicka, Elwira K. Wróblewska

Section of Instrumental Analysis, Institute of Chemistry and Environmental Protection, Szczecin University of Technology, Piastów Avenue 42, 71-065 Szczecin, Poland

ARTICLE INFO

Article history:

Received 7 July 2008

Received in revised form 17 October 2008

Accepted 24 October 2008

Available online 31 October 2008

Keywords:

Conductivity

Trace water determination

Electrolyte

Alkali metal chlorides

ABSTRACT

A new electrochemical method for the determination of trace water in methanol has been developed. This method is based on the effect, that a minor change in the water content affects the value of conductivity measured for dissolved in the solutions electrolyte. The conductivity measurements were performed for four inorganic salts, i.e. NaCl, KCl, RbCl, and CsCl in solutions with different amounts of water traces in methanol and the calibration curves for three of them were determined. With the exception of cesium chloride the high values of correlation coefficients for the regression lines as well as low limits of detection were achieved in all cases which indicates that this method is a useful tool for the determination of the trace amounts of water in methanol.

© 2008 Elsevier B.V. All rights reserved.

1. Introduction

There are a number of organic solvents, which are strongly hygroscopic in nature. This feature can be a problem when a solvent of high purity is required, since even a small amount of a contamination changes the properties of the medium. The methods for the determination of trace amounts of water have been of interest to the chemists for many years. A lot of these methods are based on the spectroscopic measurements [1–8] such as: solvatochromic effects [5], spectrofluorimetric method [5] or NIR spectrophotometry in which the determination of a low water level in organic solvents is possible due to aggregation of a near-infrared dye monomer [7] or the appearance of O–H stretch absorbance band [8]. All these methods require expensive equipment and sometimes special dyes which are usually not commercially available [5,7]. Moreover, a lot of these methods can be used only for aprotic solvents.

Other methods of a trace water determination are based on: gas chromatography with thermal conductivity detector [9], or the most widely used—the Karl Fisher titration [10]. The last one requires special, expensive equipment and the use of toxic reagent, although there have been carried out some researches on less harmful solvent systems recently [10,11].

Accuracy of measurements, simplicity, and convenience are considered to be the most desirable features in the laboratory. In this paper a new simple and convenient method for the determina-

tion of a trace amount of water in methanol using electrochemical technique was described. The aim was to find such electrolyte (an inorganic salt), which exhibits significant changes in its conductivity due to the interaction with the analyte (water).

2. Experimental

2.1. Chemicals

Methanol Rothidry® was purchased from Carl Roth with water concentration of ≤ 50 ppm. Inorganic salts were of analytical – reagent grade and were obtained from: rubidium chloride – Fluka, cesium chloride – Sigma–Aldrich, potassium and sodium chlorides – POCh, Gliwice.

2.2. Apparatus

Corning electronic conductometer with Checkmate II Conductivity/TDS Sensor Module was used for conductivity measurements. The measurement range is from 20.0 to 199.9 $\mu\text{S}/\text{cm}$, resolution automatically variable by range, and accuracy 0.3 $\mu\text{S}/\text{cm}$ (0.2% of maximal range value). Moulinex microwave oven, 700 W was used to dry the salts. All glassware was cleaned with methanol, dried in oven at 100 °C for few hours, and was then cooled and kept in a desiccator before use. Z.M.P Gdansk analytical balance with accuracy 1×10^{-5} g was used to weigh the salts. VEB PRÜFGERÄTE-WERG MLW thermostat with accuracy 0.1 °C was used to keep all samples at constant temperature. The salts were dissolved in methanol using Polned ultrasonic bath.

* Corresponding author.

E-mail address: monka@ps.pl (M. Gašiorowska).

Table 1
Solubility of the examined inorganic salts (25 °C).

Solubility	NaCl	KCl	RbCl	CsCl
Water (g salt/100 g water)	36.0 [12]	34.0 [12]	83.6 [12]	162 [12]
Methanol (g salt/100 g anhydrous methanol)	1.41 [13]	0.5 [14]	1.41 [15]	Insoluble [12]

Table 2
Differences in conductivity ($\Delta\kappa$) of the electrolytes.

Salt	$\Delta\kappa^*$ ($\mu\text{S}/\text{cm}$)												
	0.015 mg/ml	0.030 mg/ml	0.045 mg/ml	0.060 mg/ml	0.075 mg/ml	0.090 mg/ml	0.105 mg/ml	0.120 mg/ml	0.135 mg/ml	0.150 mg/ml	0.165 mg/ml	0.175 mg/ml	
NaCl	0.2	2.0	1.4	3.5	3.5	4.6	7.0	10.9	9.5	8.0	7.2	7.0	
KCl	0.2	0.3	0.4	2.2	3.1	4.5	6.0	7.0	6.2	4.9	3.5	3.3	
RbCl	6.5	6.5	7.0	6.6	6.4	6.5	6.4	6.6	6.7	7.6	8.6	3.1	
CsCl	5.0	4.5	3.9	4.2	3.5	3.7	0.8	1.3	7.5	4.0	4.0	4.1	

* $\Delta\kappa$: the difference in conductivity between 0.060 and 0.015% water content solutions in methanol at 20 °C.

2.3. Procedure

The dry chloride (30 mg) was dissolved in 10 ml of anhydrous methanol with the use of ultrasonic bath (the stock solutions). To avoid moistness the solutions were kept in desiccator. The standard solutions were prepared in a tightly closed volumetric flasks, capacity 100 ml by adding: 0.000; 0.015; 0.030; 0.035; 0.045; 0.055; 0.065; 0.075 ml water and filling up to the mark with methanol. To 10 ml of each standard solution constant, in the series, amount of the stock solution of the salt was added and then conductivity was measured at constant temperature (20 ± 0.1 °C). All procedures were performed under a nitrogen atmosphere.

3. Results and discussion

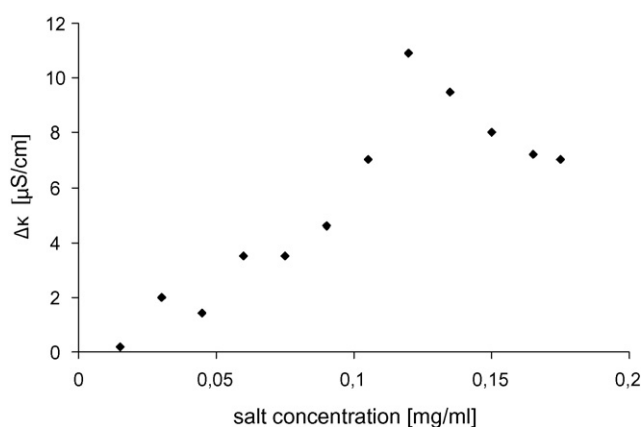
Electrolytes can conduct electricity due to their ionic structures. The value of conductivity depends on the concentration of an electrolyte in solution, temperature, or the nature of the solvent, and it is higher for aqueous solutions in comparison to other solvents. A kind of solvent determines degree of dissociation of an electrolyte. A high value of the dielectric constant of water (78.4 in 25 °C) facilitates the dissociation of electrolyte in solution. For smaller value of the dielectric constant of a solvent (32.6 for methanol) the dissociation degree of electrolyte is smaller.

It was assumed, that even a small amount of water in methanol can influence the dissociation degree of an electrolyte and consequently the conductivity of electrolyte solution. In this work the chlorides of sodium, potassium, rubidium, and cesium, respectively were used as electrolytes. These salts characterize the difference in their solubility in water and methanol (see Table 1), thus, they are strong electrolytes in water but weak electrolytes in methanol.

In order to verify the above mentioned assumption and to chose the optimal concentration of the electrolytes the measurements were carried out using two solutions of water in methanol (0.015% and 0.060% of water, respectively). The conductivity was measured for the concentrations of the electrolytes, i.e. NaCl, KCl, RbCl, and CsCl ranging from 0.015 to 0.255 mg/ml. All electrolytes exhibited significant differences in conductivity with changes of water concentration.

Moreover, these differences are not constant. They reach the maximum value and then decrease (see Table 2) in most cases. Only for CsCl there is no dependency between the differences in conductivity and the salt contents. An exemplary course of the changes in conductivity for NaCl is shown in Fig. 1.

It is well known, that a steep slope of a calibration curve determines a high sensitivity of a method therefore the concentrations

**Fig. 1.** Differences in conductivity ($\Delta\kappa$) for NaCl.

of electrolytes for which are observed the biggest differences in conductivity with the change in water content were selected, i.e. 0.120 mg/ml for NaCl, 0.120 mg/ml for KCl, 0.165 mg/ml for RbCl, and 0.135 mg/ml for CsCl.

The conductivity measurements for eight standard solutions of varied water content were performed and the results are collected in Table 3.

A linear dependency of the measured value in relation to the water content was found for NaCl, KCl, and RbCl (see Fig. 2 and Table 4), thus, they can be used as the calibration curves. A low value of the correlation coefficient for cesium chloride which amounts to 0.693 indicates, that this salt is less sensitive to the changes in water content in the measured range of its concentrations and for that reason is not interesting for the application.

Table 3
Changes in conductivities of the electrolytes with the variable water concentration in methanol.

Water content (%)	Conductivity ($\mu\text{S}/\text{cm}$)			
	NaCl	KCl	RbCl	CsCl
0.000	163.7 \pm 0.5	134.6 \pm 0.1	139.3 \pm 0.4	96.0 \pm 1.1
0.015	154.3 \pm 0.1	137.3 \pm 0.0	143.1 \pm 0.4	97.6 \pm 0.0
0.030	155.9 \pm 0.2	137.5 \pm 0.1	144.5 \pm 0.3	100.2 \pm 1.0
0.035	157.8 \pm 0.2	138.3 \pm 0.2	145.3 \pm 0.1	96.8 \pm 1.0
0.045	160.4 \pm 0.0	138.5 \pm 0.1	146.5 \pm 0.1	95.3 \pm 0.0
0.055	162.8 \pm 0.3	138.5 \pm 0.0	147.5 \pm 0.3	91.2 \pm 1.1
0.060	165.4 \pm 0.3	141.6 \pm 0.5	147.9 \pm 0.1	95.1 \pm 0.2
0.075	–	–	–	89.70 \pm 1.50

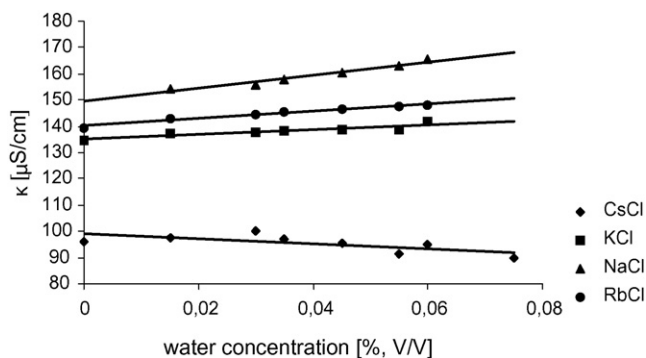


Fig. 2. Calibration curves.

Table 4

Data describing calibration curves of the method.

Salt	Equation $y = ax + b$	r	S.D. ($\mu\text{S}/\text{cm}$)	Limits of detection (v/v, %)
NaCl	$A = 247.50 \pm 1.28$ $b = 149.53 \pm 0.77$	0.997	0.0845	0.0209
KCl	$a = 86.85 \pm 0.38$ $b = 135.06 \pm 0.59$	0.972	0.1183	0.0025
RbCl	$a = 135.98 \pm 0.36$ $b = 140.21 \pm 0.38$	0.995	0.0817	0.0080

The value of conductivity of sodium chloride in pure methanol is not consistent with those for the rest of the results (Table 3). This can be associated with the size of the Na^+ ion, and its atomic weight, and consequently with a different kind of interactions of the salt with methanol in comparison to the methanol–water system. In highly associated solvents mixtures, where concentration of each component is relatively high the selective solvation results from the solvent structure rather than from ion–solvent interactions. Above 30 mol% of water concentration, the binary solvent can be treated as a mixture of water globules and methanol monomers [16–18]. Water prefers to create self-associates rather than the solute–solvent solvates because it is energetically favorable. As it is known [19–22] Na^+ in the methanol–water system is selectively solvated by methanol over the whole range of its concentration and only in methanol-rich solutions shows preferential hydration. This kind of researches for trace concentration of water have not been carried out yet, however we suppose that in this range of water concentration the preferential hydration also occurs, which can affect the conductivity value of the examined salts. Na^+ ion is of a small size. Its positively charged atomic nucleus strongly interact with a surroundings, especially with a polar one (here water), which facilitates the formation of associates. The bigger ion is, the weaker are the interactions with the surroundings since a distance between the nucleus and medium is long. That is probably a reason why in case of the other cations examined here this phenomenon is not observed. The largest mobility is observed for the free ion, which exists in pure methanol. An associate of Na^+ with even one molecule of water changes noticeably the weight of the cation and

consequently its size and mobility. The conductivity is proportional to the mobility, thus, the value of conductivity of NaCl in methanol is higher than that in the methanol–water mixture. The atomic weights of K^+ , Rb^+ , and Cs^+ are larger than that of Na^+ and even if they create the associates with water, the weight of one molecule of water would not influence such noticeably the weight of solvate.

The results describing the calibration curves and thereby the method are summarized in Table 4.

From the above data results (Table 4) that the highest sensitivity of the method is for sodium chloride (247.50 slope) whereas the lowest sensitivity was observed for potassium chloride (86.85 slope). The correlation coefficient for the regression lines ranges from 0.972 to 0.997 and the standard deviation from 0.0817 $\mu\text{S}/\text{cm}$ for RbCl to 0.1183 $\mu\text{S}/\text{cm}$ for KCl. The limits of detection for sodium chloride amounts to 0.0209, for potassium chloride – 0.0025, and rubidium chloride – 0.0080.

4. Conclusions

Our studies demonstrate that there are significant and reproducible changes in conductivity of the electrolyte solutions with the change of water content in methanol. Among four inorganic salts studied here, three of them NaCl, KCl, and RbCl exhibited a linear and strictly monotonic dependency of conductivity on the examined range of low water concentrations in methanol. This enables to detect a trace amount of water in polar solvent (methanol). Unfortunately, cesium chloride is insensitive and does not exhibit this dependency.

The sensitivity of the method is high and the limit of water detection in methanol is low, thus, this method seems to be useful in the studied range of water concentrations. Moreover, the method is simple, convenient, fast, and the cost of the analysis is very low.

References

- [1] J.S. Kim, M.G. Choi, Y. Huh, M.H. Kim, S.Y. Wang, Suk-Kyu Chang, Bull. Korean Chem. Soc. 27 (12) (2006) 2058–2060.
- [2] C. Pinheiro, J.C. Lima, A.J. Parola, Sens. Actuators, B 114 (2006) 978–983.
- [3] H. Hisamoto, H. Tomha, T. Yamada, Ki-ichiro Yamuachi, D. Siswanta, N. Yoshioka, K. Suzuki, Anal. Chim. Acta 373 (1998) 271–289.
- [4] H. Langhals, Anal. Lett 23 (12) (1990) 2243–2258.
- [5] A. Cedergrén, C. Orrad, Anal. Chem. 66 (1994) 2010–2016.
- [6] Y. Ci, X. Jia, Talanta 31 (7) (1984) 556–558.
- [7] M. Li, G.E. Pacey, Talanta 44 (1997) 1949–1958.
- [8] S. Garrigues, M. Gallignani, M. Guardia, Anal. Chim. Acta 281 (1993) 259–264.
- [9] T. Mitchell Jr., D.M. Smith, Aquametry, Part I. A Treatise on Methods for the Determination of Water, Wiley-Interscience, Publication, Wiley, 1997.
- [10] I. Nordin-Andersson, A. Cedergrén, Anal. Chem. 57 (1985) 2571–2575.
- [11] C. Oradd, A. Cedergrén, Anal. Chem. 66 (1994) 2603–2607.
- [12] Collective Work, Physical–Chemical Handbook, 2nd ed., WNT, Warszawa, 1974.
- [13] C.A. Lobry de Bruyn, Rec. Trav. Chim. 11 (1892) 788.
- [14] C.A. Lobry de Bruyn, Rec. Trav. Chim. 11 (1892) 145–1145.
- [15] C.A. Lobry de Bruyn, Z. Phys. Chem. 10 (1892) 783.
- [16] E. Hawlicka, D. Swiatla-Wojcik, Chem. Phys. 195 (1995) 221–230.
- [17] E. Hawlicka, D. Swiatla-Wojcik, Phys. Chem. Chem. Phys. 2 (2000) 3175–3182.
- [18] A. Laaksonen, P.G. Kusalik, I. Svischev, J. Phys. Chem. 101 (1997) 5910–5918.
- [19] E. Hawlicka, D. Swiatla-Wojcik, J. Phys. Chem. A 106 (2002) 1336–1345.
- [20] E. Hawlicka, D. Swiatla-Wojcik, J. Mol. Liq. 78 (1998) 7–18.
- [21] G. Palinkas, E. Hawlicka, K. Heinzinger, Chem. Phys. 158 (1991) 65–71.
- [22] A.K. Convington, M. Dunn, J. Chem. Soc., Faraday Trans. 85 (1989) 2827–2835.



Improvement in protein separation in Barretts esophagus samples using two-dimensional capillary electrophoresis analysis in presence of cyclodextrins as buffer additives

David Gonzalez-Gomez^{a,*}, Daniella Cohen^a, Jane A. Dickerson^a, Xingguo Chen^a, Florentina Cañada-Cañada^b, Norm J. Dovichi^a

^a Department of Chemistry, University of Washington, Seattle, WA 98195-1700, USA

^b Department of Analytical Chemistry, University of Extremadura, Badajoz 06071, Spain

ARTICLE INFO

Article history:

Received 28 July 2008

Received in revised form 20 October 2008

Accepted 31 October 2008

Available online 14 November 2008

Keywords:

Two-dimensional capillary electrophoresis

Protein

Cyclodextrins

ABSTRACT

In two-dimensional capillary electrophoresis (2DCE) components are separated based on their size and hydrophobicity. A preliminary run separates analytes in the first capillary based on size (CSE). Following that, fractions are electrokinetically transferred across an interface into a second capillary, where components are further resolved according to hydrophobicity. In order to succeed in this analysis, two orthogonal methods should be selected for the different modes. The transfers from the first to the second capillary must be efficient in order to reduce tailing effects and lost of resolution. We report a new method to improve the resolution with our 2DCE instrumentation using CD doped buffers. When methyl beta cyclodextrin (m β CD) is added to the 2DCE interface buffer a stacking effect is described in the transfers from the first to the second dimension. In addition to that, changes in retention times are observed when proteins form complex with CD's helping in the separation. Protein fingerprints were obtained from BE homogenates using this method in presence of methyl beta cyclodextrin (m β CD). Within-day and between-day precision has been studied in order to establish the reproducibility of the methodology proposed.

© 2008 Elsevier B.V. All rights reserved.

1. Introduction

Capillary electrophoresis (CE) became popular in the early 1980s, when Jorgenson and Lukacs demonstrated that the efficiency of electrophoresis can be substantially increased if the process is conducted in quartz capillaries with an internal diameter of 75 μ m [1]. CE is widely considered one of the most important tools in separation science. The popularity of this analytical method is because CE uses a distinct separation mechanism that can serve as alternative for samples that are not easily resolved by traditional methods. Many different separation modes are compatible with CE; this flexibility makes it an attractive tool for a variety of analytical fields such as pharmaceutical analysis, small ion analysis, inorganic and organic compounds [2,3]. But it is in the bioanalytical field where CE application has increased drastically [4,5]. CE has proved to be a fast and convenient technique for protein analysis due to its efficiency [6].

The separation and identification of proteins in a biological complex sample is one of the major challenges in bioanalytical chemistry because complex samples contain a large number of different proteins, which have different molecular weights, *pI*, and they vary considerably in concentration. To achieve good resolution, instrumental improvements have been reported by our research group [7,8]. High-speed fully automated two-dimensional capillary electrophoresis (2DCE) allows us to resolve complex biological samples experiments in less than 1 h. However, the resolutions of proteins still remain unsatisfactory [6]. The incorporation of pseudophases such as micelles and cyclodextrins (CDs) would provide additional selectivity through the introduction of hydrophobic interaction or molecular inclusion complexations [9].

CDs are a series of oligosaccharides produced by the enzyme amylase in *Bacillus macerans* on starch and related compounds. The CDs were discovered in 1891 by Villiers [10]. These compounds are composed of alpha-(1,4)-linkages of a number of D(+)-glucopyranose units. CDs are doughnut-shaped with all the glucose units in substantially undistorted C1 (D) (chair) conformations. These structures require special arrangements of functional groups in cyclodextrin molecules; thus the secondary hydroxyl groups are located on one side of the torus, whereas the primary

* Corresponding author at: Technological Institute of Food and Agriculture (INTAEX), Junta de Extremadura, Badajoz 06071, Spain.

E-mail address: david.gonzalezgo@juntaextremadura.net (D. Gonzalez-Gomez).

hydroxyl groups are located on the opposite side of the torus. The torus interior is relatively apolar compared to water. One of the most important characteristics of cyclodextrins is its formation of inclusion complexes with various compounds (guest). These guest compounds are included in the cavity of the cyclodextrins (host). Guest compounds range from polar reagents such as acids, amines, small ions, and highly apolar aliphatic and aromatics hydrocarbons. The nature of the binding force is mainly attributed to Van der Waals interactions between guest and host and/or hydrogen bonding between the guest and the hydroxyl groups of cyclodextrin among others factors.

In this paper, we improve a previously published method [6] by increasing the resolution between proteins. Different changes have been introduced in the 2DCE interface in order to accomplish these improvements. The presence of m β CD in the 2DCE interface and in the second dimension reservoir helps the cyclic transfers from the first to the second dimension, thereby increasing the resolution between proteins.

2. Experimental

2.1. Materials and chemicals

2-(Cyclohexylamino)ethanesulfonic acid (CHES), 2-Amino-2-(hydroxymethyl)-1,3-propanediol (Tris), dextran (513 kDa), sodium hydroxide, sodium dodecyl sulfate (SDS), m β CD and standard proteins were purchased from Sigma–Aldrich (St. Louis, MO). Water was from a Barnstead Nanopure water supply (Boston, MA). FQ and potassium cyanide were purchased from Molecular Probes (Eugene, OR). Fused-silica capillaries were purchased from Polymicro Technologies (Phoenix, AZ). The dynamic coating reagent UltraTrol LN was purchased from Target Discovery (Palo Alto, CA).

2.2. Cell culture and preparation of cellular homogenate

Barrett's esophagus cell line (CP18821) was obtained from the Fred Hutchinson Cancer Research Center, Seattle, WA. Roughly 4 million cells were lysed and homogenized in 500 μ L of fresh 1% SDS solution using a pulsed high-power probe sonicator equipped with a cooled water bath (Branson Ultrasonics, Danbury, CT). Typically, cells were homogenized after 5 min of pulsed sonication. Cellular homogenates were stored at -80°C in 20 μ L aliquots.

To prepare a tryptic digest, homogenates were exposed to trypsin at 33 $\mu\text{g}/\text{mL}$ and incubated at 37°C overnight to digest the protein content. The digest was reconstituted in 1% SDS and stored at -80°C in 20 μ L aliquots.

2.3. Sample preparation

Samples were labeled with 3-(2-furoyl)-quinoline-2-carboxaldehyde (FQ) and KCN using the procedure described in a previous paper [6,11].

2.4. Capillary electrophoresis/laser-induced fluorescence detection

Capillary electrophoresis was performed with a locally constructed instrument. Separation was performed in a 30 cm long, 31 μm i.d., and 148 μm o.d. fused silica capillary (Polymicro Technologies, Phoenix, AZ, USA). Detection was performed with a locally constructed ultra-sensitive laser-induced fluorescence detector based on a sheath-flow cuvette. Fluorescence was excited with a 12 mW solid state diode laser (Lasermate Group, Pomona, CA, USA) operating at 473 nm and detected through a 580 nm long-pass filter from Omega Optical (Brattleboro, VA, USA). High voltage

was applied by CZE1000R high-voltage power supplies (Spellman, Hauppauge, NY, USA).

2.5. Data collection and processing

Data was collected with a computer using software written in LabView. Data processing was performed using software written in Matlab [7].

3. Results and discussion

3.1.1. CE separation

The separation is performed in two 25 cm long, 31 μm inner diameter, 146 μm outer diameter fused-silica capillaries. The polyamide coating was burned from the capillary ends with a gentle flame, and the tip was cleaned with an ethanol-soaked tissue. UltraTrol LN was used as a dynamic coating to reduce electroosmotic flow for the 2D separation.

The first dimension separation was performed by capillary sieving electrophoresis (CSE) in a 100 mM CHES, 100 mM Tris, 3.5 mM SDS and 5% dextran (513 kDa) buffer. The second dimension separation was performed by micellar electrokinetic capillary chromatography (MECC) in a 50 mM CHES, 50 mM Tris, 15 mM SDS and 10 mM m β CD buffer. The buffer in the interface and in the second dimension reservoir was the same as the second dimension running buffer.

The voltage program for 2D separations has been reported previously [6]. After an electro kinetic injection (4 kV for 4 s) a preliminary separation was then performed by applying -21 kV to the injection block buffer and -1 kV to the interface for 115 s, at this point the fastest moving analyte approaches the end of the first dimension capillary. Fractions of analyte were electrokinetically transferred from the first to the second capillary by applying -26 kV the injection block buffer and -16 kV the interface for 1 s. Then, -18 kV was applied to both dimension for 12 s. This set of voltages produced zero potential across the first capillary so that components were stationary in that capillary; the voltage drop applied across the second capillary drove the second dimension separation.

3.2. Methy- β cyclodextrin buffer modified

We previously reported the best conditions found for the electrophoretic studies of Barrett's esophagus tissues using 2DCE [6]. The resolution between proteins reported in this paper was unsatisfactory. In order to solve this issue, modifications were made to this procedure. The literature has reported the use of cyclodextrins to increase the resolution in complex mixtures. CDs would provide additional selectivity to the established conditions by providing hydrophobic interactions or molecular inclusion complexation. When m β CD is added to the running buffer we observe changes in the electropherograms. These changes can be noticed in Fig. 1 between the CSE cycles 200–350. In this area the numbers of resolved components increase when the interface and the second dimension buffer is doped with CD. Also, the unresolved ridge in the no-CD experiment is further resolved when CD is added to the interface and second dimension running buffer. The best resolution is obtained when the concentration of CD is 10 mM. Above this concentration no improvements are observed. We previously reported that proteins appear in the first part of the electropherogram in the no-CD proposed conditions. When the BE homogenate samples are treated with trypsin to digest proteins and then separated in the proposed conditions (Fig. 2) we observe that the unresolved peak in the 1DCE experiment is gone (Fig. 2C and D). In the digested sample,

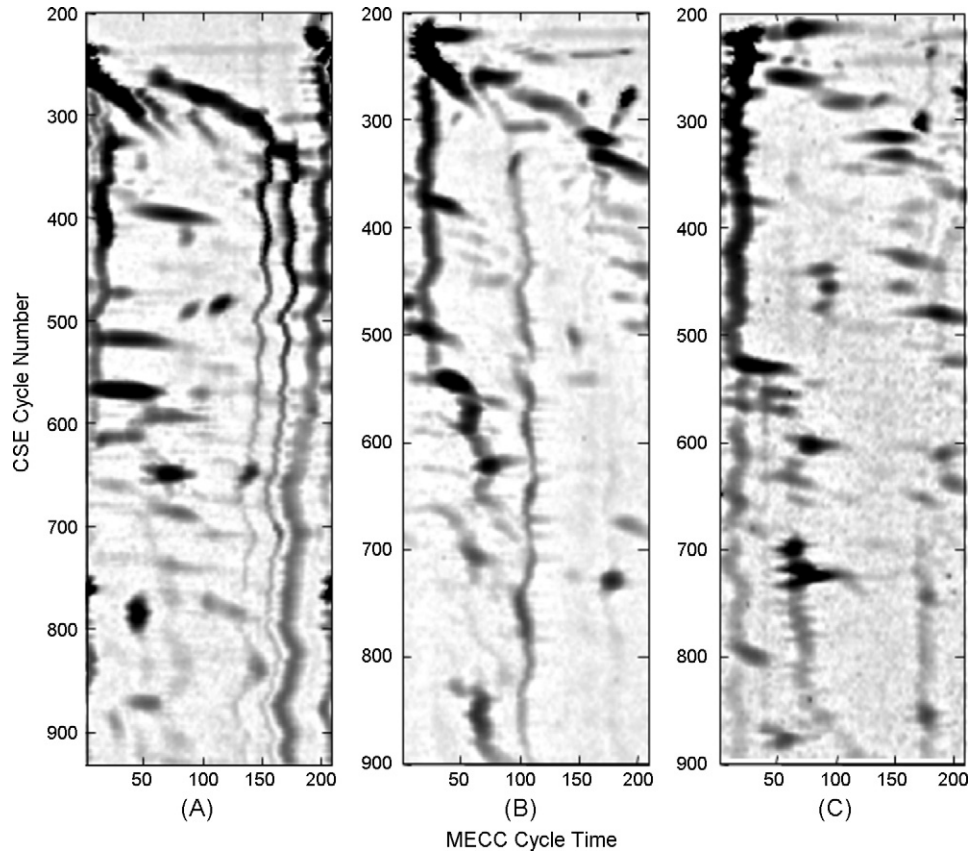


Fig. 1. 2D-CE gel plot for BE culture homogenate sample in the following conditions: 100–100–3.5 mM CHES, Tris, SDS, 5% Dextran (513 kDa) for the first dimension buffer in all the experiments; 50–50–15 mM CHES, Tris, SDS for the second dimension buffer in A doped with 0.5 mM of m β CD in B and 10 mM of m β CD in C respectively.

new peaks appear in the first area of the electropherogram (Fig. 2D). These same samples were injected in the 2DCE system. Again the group of non-resolved components is gone after the digestion (see Fig. 2A). Several new appear in the bottom part of the electrophero-

gram. Also, the effect that the CD's have on resolution between proteins is also noticed with a set of eight standard proteins (Fig. 3). Improvements in the separation are observed when the m β CD is present in the interface buffer (Fig. 3B). The CD helps to reduce

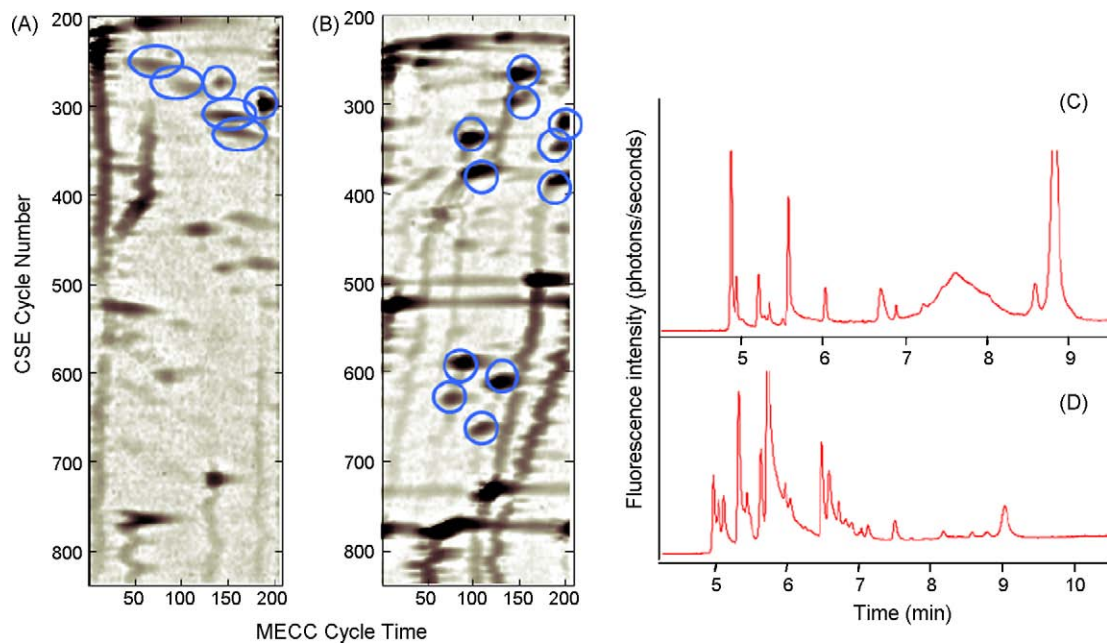


Fig. 2. Separation of BE cellular homogenate untreated (A and C) and treated with trypsin enzyme (B and D). 2DCE conditions 100–100–3.5 mM CHES, Tris, SDS, 5% Dextran (513 kDa) for the first dimension buffer; 50–50–15 mM CHES, Tris, SDS for the second dimension buffer doped with 10 mM of m β CD. 1DCE second dimension buffer conditions.

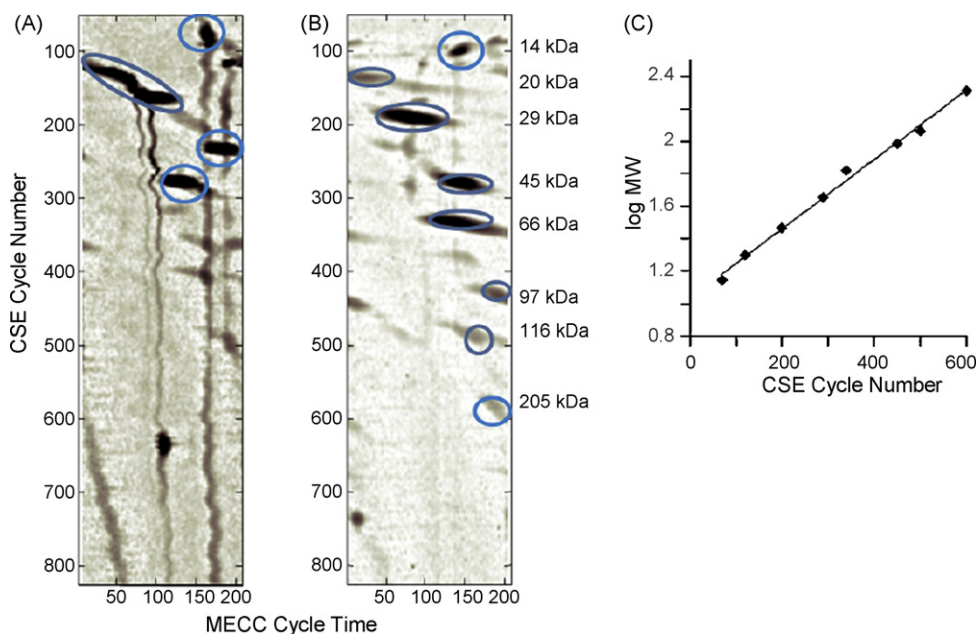


Fig. 3. Separation of eight protein mixture 2DCE conditions 100–100–3.5 mM CHES, Tris, SDS, 5% Dextran (513 kDa) for the first dimension buffer; 50–50–15 mM CHES, Tris, SDS for the second dimension buffer (A) and doped with 10 mM of m β CD (B). The relationship of log MW (kDa) and migration time of standard proteins in presence of m β CD (C).

the tailing in the first dimension, in that way an increment of the resolution is observed. As it can be observed in Fig. 3B the separation between the studied standard of proteins is achieved, while in Fig. 3A poor resolution is observed in the first part of the electropherogram. A calibration curve was constructed when m β CD is

present, between migration time (CSE cycle number) and molecular weight by analysis of a set of standard proteins (Fig. 3C). Migration time increased with the logarithm of molecular weight. The least-squares regression equation for this line was $y = 0.002133x + 1.033$ with a correlation coefficient $r = 0.994$.

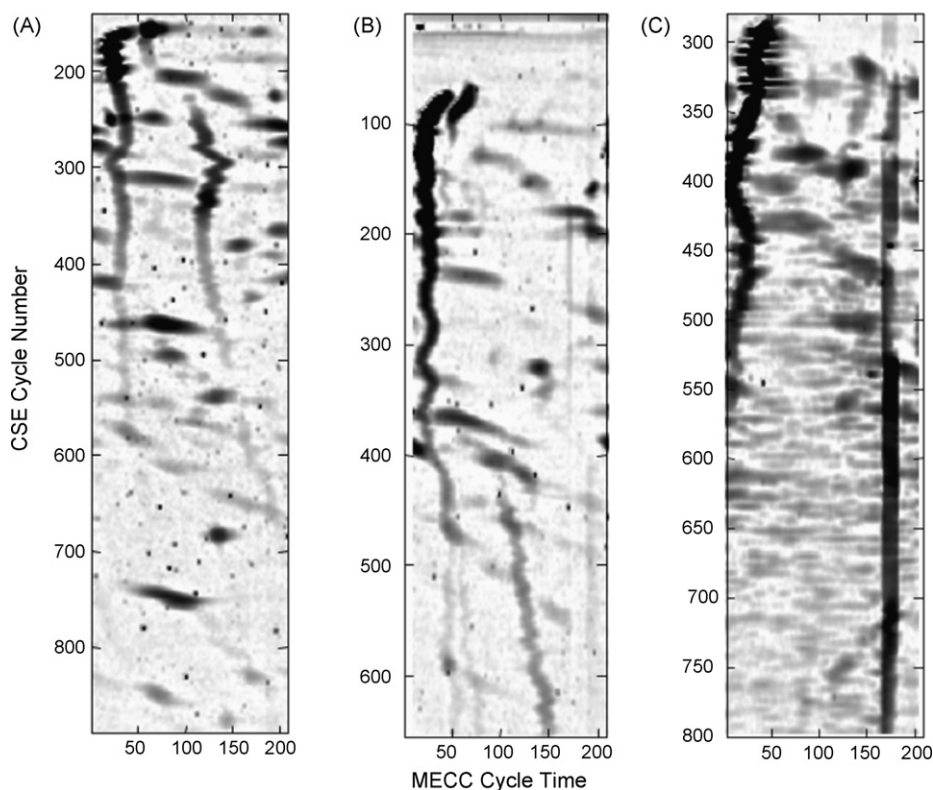


Fig. 4. 2DCE gel plot for BE culture homogenate sample in the following conditions: 100–100–3.5 mM CHES, Tris, SDS, 5% Dextran (513 kDa) first dimension buffer in all the experiments; 50–50–15 mM CHES, Tris, SDS for the second dimension buffer. In (A) and (B) the interface buffer was doped with 10 mM of m β CD, in (B) the conductivity for the first dimension was adjusted to 1500 μ S/cm adding NaCl and in (C) the conductivity of the interface buffer was adjusted to 1500 μ S/cm adding sodium acetate.

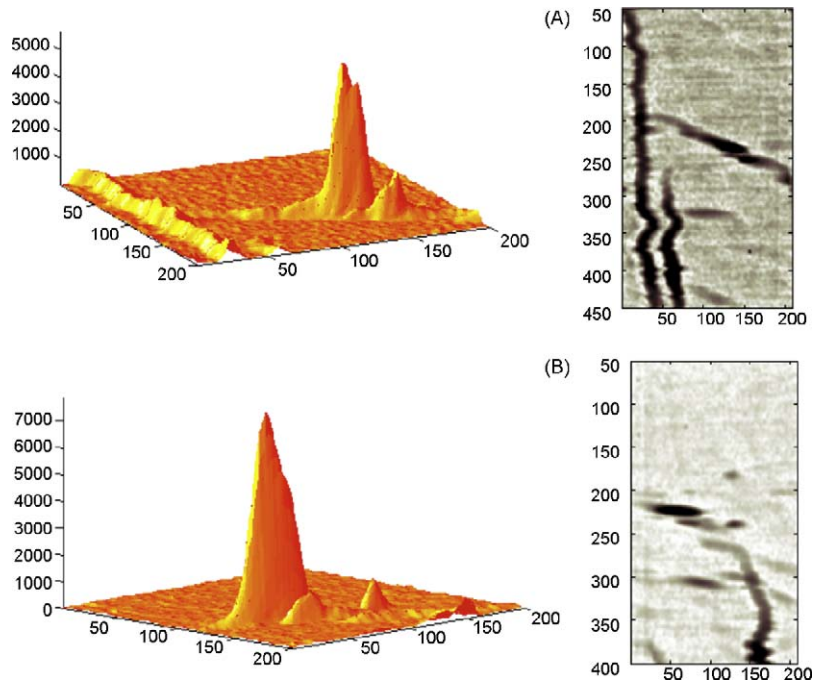


Fig. 5. (A) Separation of ovalbumin standard sample (45 kDa) using 100–100–3.5 mM CHES, Tris, SDS and 5% dextran for the first dimension, and 100–100–15 mM CHES, Tris, SDS for the 2nd dimension. In experiment (B), the interface was filled with 50–50–15–10 mM CHES, Tris, SDS, m β CD buffer.

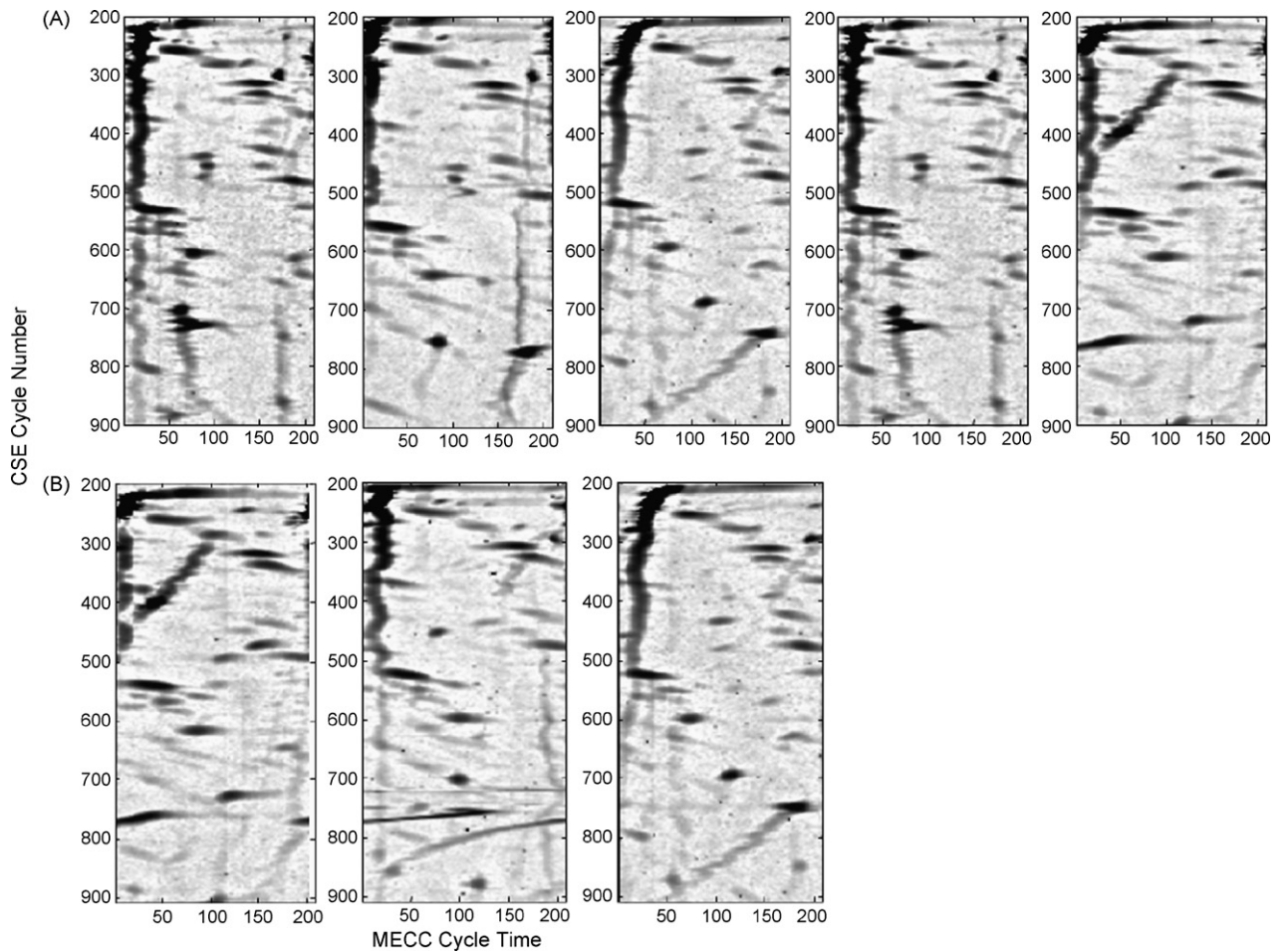


Fig. 6. Between-day (A) and within-day (B) precision experiments for BE cell homogenate for the proposed conditions. 2DCE conditions 100–100–3.5 mM CHES, Tris, SDS, 5% Dextran (513 kDa) for the first dimension buffer; 50–50–15 mM CHES, Tris, SDS for the second dimension buffer (A) and doped with 10 mM of m β CD.

We know that the stacking effect can be observed in our 2DCE system when a lower conductive buffer is placed in the 1st D capillary relative to the 2nd D capillary. This condition is achieved when the ionic strength of the first buffer is lower compared to the ionic strength of the second buffer. In our previous conditions, the difference in conductivities between the first dimension and the interface was around $200 \mu\text{S}/\text{cm}$ (Fig. 1A). When the CD doped buffer is in the interface (50–50–15 mM CHES, Tris, SDS doped 10 mM of $m\beta\text{CD}$), the conductivity in the interface increases from $1100 \mu\text{S}/\text{cm}$ to $1500 \mu\text{S}/\text{cm}$; the stacking effect is observed more noticeably (Fig. 4A). But, this stacking effect is not the only factor. Additional experiments have been performed in order to check these results. The conductivity in the first dimension has been adjusted to $1500 \text{S}/\text{cm}$ using a concentrated solution of sodium chloride. CD doped buffer was used in the interface and in the second dimension reservoir ($1500 \mu\text{S}/\text{cm}$). For these conditions, there is no difference in conductivity between first and second buffer, the resolution is not as good as the resolution in previously mentioned experiment, but it is still better than the resolution obtained without CD (Fig. 4B). These results suggest, that the stacking effect is not the only factor. Thus, the CD must be playing an additional role in the separation or transfer. To prove that conclusion, and additional experiment was done. No-CD CSE buffer was used for the first dimension (100–100–3.5 mM CHES–Tris–SDS and 5% dextran and $900 \mu\text{S}/\text{cm}$) and for the interface and second dimension reservoir, and no-CD CHES–Tris–SDS buffer was titrated with sodium acetate to adjust its conductivity as $1500 \mu\text{S}/\text{cm}$, in that way, the increment of conductivity in the interface has the same value as the no-CD/CD conditions (100–100–3.5 mM CHES–Tris–SDS 5% dextran for the first dimension and 50–50–15–10 mM CHES–Tris–SDS– $m\beta\text{CD}$). With these conditions, it can be observed that the stacking effect helps the resolution of the components but without the presence of CD, this resolution is not complete. Those experiments are showed in Fig. 4C and Fig. 5.

The literature suggests [12,13] that βCD interacts with peptides and proteins and thus changes their mobilities. It has been proved that cyclodextrins form sufficiently strong complexes with some amino acids and, their relative mobilities are affected. To test the grade in which proteins react with CD, a protein solution was prepared in the running buffer. Different amounts of $m\beta\text{CD}$ were added to this solution and the fluorescence signal was monitored at tryptophan's excitation wavelength (253 nm). An increase of fluorescence signal was observed when $m\beta\text{CD}$ was added to a protein solution in basic conditions up to 10 mM. This fact is in accordance with Hjerten's paper [12] where cyclodextrins interact with peptides and proteins to form sufficiently strong complexes. Due to that, changes in mobility terms can be noticed.

3.3. Reproducibility of 2DCE analysis

To determine the between-day precision, five aliquots of the same cell homogenate batch were labeled and analyzed on successive days. The average R.S.D. in CSE mobility was 1.23%. Similar experiments were done to study the precision within-day. The same aliquot was analyzed in a single day and the CSE mobility was compared. The average R.S.D. was 1.14% (Fig. 6).

4. Conclusions

In summary, we proved that the presence of $m\beta\text{CD}$ in the interface buffer improve the resolutions for our 2DCE system. When the interface and second dimension buffer is doped with 10 mM of this CD the number of resolved components increase. We propounded that this improvement is due to two principal factors; the new complexes formed when the CD increase the electrophoretic differences between similar compounds, in that way unresolved peak now appear in separated spots. In addition, the presence of $m\beta\text{CD}$ in the interface and the second dimension buffer make more conductive this buffer. The stacking effect during the transfers is now more highlighted and less tailing peaks are observed resulting in a better resolution.

The precision of the method has been studied within the day and between days. R.S.D. below 1.3% were achieved in both studies.

Acknowledgment

D.G.G and F.C.C. thanks the Ministerio de Ciencia e Innovacion of Spain (Project CTQ2008-00468/BQU) for financial support.

References

- [1] J.W. Jorgenson, K.D. Lukacs, *Anal. Chem.* 53 (1981) 1298.
- [2] H.J. Issaq, *Electrophoresis* 21 (2000) 1921.
- [3] R.A. Frazier, J.M. Ames, H.E. Nursten, *Capillary Electrophoresis for Food Analysis. Method Development*, Royal Society of Chemistry, London, 2000, Chapter 9.
- [4] J. Kraly, M.A. Fazal, R.M. Schoenherr, R. Bonn, M.M. Harwood, E. Turner, M. Jones, N.J. Dovichi, *Anal. Chem.* 78 (2006) 4097.
- [5] E. Turner, D. Cohen, H.R. Pugsley, D. Gonzalez Gomez, C.D. Whitmore, C. Zhu, N.J. Dovichi, *Anal. Bioanal. Chem.* 390 (2008) 223.
- [6] J.R. Kraly, M.J. Jones, D.G. Gomez, J.A. Dickerson, M.M. Harwood, M. Eggertson, T.G. Paulson, C.A. Sanchez, R. Odze, F. Ziding, B.J. Reid, N.J. Dovichi, *Anal. Chem.* 78 (2006) 5977.
- [7] D.A. Michels, S. Hu, R.M. Schoenherr, M.J. Eggertson, N.J. Dovichi, *Mol. Cell. Proteomics* 1 (2002) 69.
- [8] C. Zhu, X. He, J.R. Kraly, M.R. Jones, C.D. Whitmore, D.G. Gomez, M. Eggertson, W. Quigley, A. Boardman, N.J. Dovichi, *Anal. Chem.* 79 (2007) 765.
- [9] C. Quand, A. Malek, M.G. Khaledi, *Electrophoresis* 24 (2003) 824.
- [10] M.L. Bender, M. Komiyama, *Cyclodextrin Chemistry*, Springer-Verlag, 1978.
- [11] D. Pinto, E. Arriaga, R.M. Schoenherr, S.S.H. Chou, N.J. Dovichi, *J. Chromatogr. B* 793 (2003) 107.
- [12] R. Zhang, H.-X. Zhang, D. Eaker, S. Hjerten, *J. Capillary Electrop.* 4 (1997) 105.
- [13] C.E. Sanger-van de Griend, K. Groningsson, T. Arvidsson, *J. Chromatogr. A* 782 (1997) 271.



A novel stir bar sorptive extraction coating based on monolithic material for apolar, polar organic compounds and heavy metal ions

Xiaojia Huang^{a,*}, Ningning Qiu^a, Dongxing Yuan^a, Benli Huang^b

^a State Key Laboratory of Marine Environmental Science, Environmental Science Research Center, Xiamen University, Xiamen 361005, China

^b Department of Chemistry & The MOE Key Laboratory of Analytical Sciences, Xiamen University, Xiamen 361005, China

ARTICLE INFO

Article history:

Received 24 August 2008

Received in revised form 23 October 2008

Accepted 26 October 2008

Available online 11 November 2008

Keywords:

Stir bar sorptive extraction

Coating

Monolithic material

Enrichment

Poly(vinylpyrrolidone-divinylbenzene)

ABSTRACT

In this study, a novel stir bar sorptive extraction (SBSE) based on monolithic material (SBSEM) was prepared. The monolithic material was obtained by in situ copolymerization of vinylpyrrolidone and divinylbenzene in the presence of a porogen solvent containing cyclohexanol and 1-dodecanol with azobisisobutyronitrile as initiator. The influences of polymerization conditions on the extraction efficiencies were investigated, using phenol and *p*-nitrophenol as detected solutes. The monolithic material was characterized by various techniques, such as elemental analysis, scanning electron microscopy, mercury intrusion porosimetry, infrared spectroscopy. Polycyclic aromatic hydrocarbons were used to investigate the extraction efficiencies of SBSEM for apolar analytes. Hormones, aromatic amines and phenols were selected as test analytes to investigate the extraction efficiencies of SBSEM for weakly and strongly polar compounds. The results showed that the new SBSEM could enrich the above-mentioned organic compounds effectively. It is worthy to mention that the SBSEM can enrich some heavy metal ions, such as Cu²⁺, Pb²⁺, Cr³⁺ and Cd²⁺, through coordination adsorption. To our best knowledge, that is the first to use SBSE to enrich heavy metal ions.

© 2008 Elsevier B.V. All rights reserved.

1. Introduction

Stir bar sorptive extraction (SBSE) is an “environmental friendly” sample preparation technique that was developed by P. Sandra et al. [1] in 1999 based on the same principles as those of SPME. The SBSE has been widely used for enrichment and sensitive determination of priority organic micro-pollutants in water samples, as well as in other matrices [2–6]. Polydimethylsiloxane (PDMS) is typical coating material in the commercial stir bars and the amount of PDMS is 25–125 μL, which is substantially higher than that on a SPME fiber with a maximum volume of 0.5 μL. The phase ratio of SBSE is about 50–250 times lower than SPME, resulting in much higher recoveries, especially for organic compounds with higher octanol–water partition coefficients (K_{ow}) [7,8].

Because of the apolar character of PDMS, which is the only commercialized coating for SBSE, therefore, SBSE has been mainly applied to extract non-polar and weakly polar compounds, and failed in the extraction of strongly polar compounds unless they have been previously derivatised [9,10]. However, sample derivati-

sation of polar analytes to produce more hydrophobic species is not always possible. In order to solve the bottleneck of the development of SBSE, it is important to develop novel extraction phases that have better affinities to polar compounds. A new dual-phase stir bar commercialized by Gerstel was consisted of a short PDMS tube packed with different carbons [11]. The new stir bar showed enhanced extraction yield for polar compounds compared with those by using conventional PDMS stir bar. Sol-gel technique has also been used to prepare stir bar that provides direct chemical binding of the coating to the substrate [12], and applied to the extraction of polycyclic aromatic hydrocarbons and organophosphorus pesticides [13]. In order to improve the polarity of the coating on stir bars, a PDMS/β-cyclodextrin extraction phase has been prepared by sol-gel technique and showed better selectivity to medium polar compounds estrogen and bisphenol A compared to the PDMS stir bar [14]. However, the coatings prepared by sol-gel technology reported previously suffered from cracking of polymer layer. Polyurethane foam [15] and poly(phthalazine ether sulfone ketone) [16] also were selected as SBSE coating. Although there were a few of SBSE coatings and SBSE has been widely used for enriching organic compounds, there was no any research about using SBSE to enrich heavy metal ions. Therefore, developing new SBSE coating which not only directly extract apolar, polar organic compounds but also can extract heavy metal ions may be an interesting topic of SBSE.

* Corresponding author at: State Key Laboratory of Marine Environmental Science, Environmental Science Research Center, P.O. Box 1009, Xiamen University, Xiamen 361005, China. Tel.: +86 0592 2183661.

E-mail address: hxj@xmu.edu.cn (X. Huang).

In our previous research [17], poly(octyl methacrylate-ethylene dimethacrylate) was prepared and acted as the extractive media of SBSE, which showed ideal extraction performance to apolar compounds but low affinity to polar compounds. Poly(methacrylic acid stearyl ester-ethylene dimethacrylate) also was used as SBSE coating and was used to effectively extract medium polar steroid sex hormones [18]. In order to directly extract strongly polar compounds without derivatisation, a more polar monolithic material which based on the copolymerization of vinylpyridine and ethylene dimethacrylate was synthesized and acted as the SBSE coating, the new coating can directly extract strong polar phenols without derivatisation and excellent detected limits were obtained. However, the recoveries were not as good as expected [19]. To our best knowledge, there is no any research which use SBSE to extraction metal ions. Therefore, developing new SBSE coatings which not only extract apolar, polar organic compounds effectively but also can extract heavy metal ions may be very interesting and can expand the application field of SBSE. In this study, a novel stir bar coating based on poly(vinylpyrrolidone and divinylbenzene) monolithic material (SBSEVD) was designed and prepared. The influences of preparation conditions on the extraction efficiencies were studied in detail. Apolar and polar organic compounds were used to preliminarily evaluate extraction performance of SBSEVD. Furthermore, SBSEVD can enrich some heavy metal ions, such as Cu^{2+} , Pb^{2+} , Cr^{3+} and Cd^{2+} , through coordination adsorption. The research results give us a novel idea that SBSE can be used to enrich metal ions if some suitable coating is prepared.

2. Experimental

2.1. Chemicals

Vinylpyrrolidone (VPL) (99%), divinylbenzene (DVB) (80%) and 3-(trimethoxysilyl)propyl methacrylate (γ -MAPS) (95%) were supplied by Alfa Aesar LTD. (Tianjin, China); Azobisisobutyronitrile (AIBN) (97%, recrystallized before use), cyclohexanol (96%) and 1-dodecanol (97%) were purchased from Shanghai Chemical Co. (China); HPLC-grade acetonitrile (ACN), methanol and *n*-hexane were purchased from Tedia Company (Fairfield, USA); Water used throughout the study was purified using a Milli-Q water purification system (Millipore, USA). Polycyclic aromatic hydrocarbons (PAHs), phenols, anilines and hormones compounds were supplied from Sigma–Aldrich (USA), Alfa Aesar LTD. (Tianjin, China), Shanghai Chemical Co. (China) and Jjubang Chemical Co. Ltd. (Shanghai, China), respectively. The heavy metal ions were prepared by using nitric acid to dissolve corresponding pure metals and diluting to the required concentration (100 ng/mL) with ultra pure water.

Water was used to dilute the stock standard solutions of 16 PAHs (1.0 $\mu\text{g/mL}$) to prepare the spiked PAHs sample (1.0 ng/mL); the spiked phenols, anilines and hormones water samples (50 ng/mL each) were prepared by diluting corresponding stock standard solutions (1.0 $\mu\text{g/mL}$) with water.

2.2. Equipments and materials

HPLC analyses were carried out on a LC chromatographic system (Shimadzu, Japan) equipped with a binary pump (LC-20AB) and a diode array detector (SPD-M20A) and LC solution workstation and CBM-20A controller. Sample injection was carried out using a RE3725i manual sample injector with a 20 μL loop (Rheodyne, Cotati, CA, USA); all experiments were performed at room temperature.

The morphologies of monolithic materials were examined by a Model XL30 scanning electron microscopy (SEM) instrument (Philips, Eindhoven, The Netherlands). The pore size distribution of the monolith was measured on mercury intrusion porosimeter (MIP) (Porous Materials Inc., Ithaca, NY). Elemental analysis (EA) was carried out on PerkinElmer (Shelton, CT, USA) Model PE 2400. FT-IR was performed on an Avatar-360 FT-IR instrument (Thermo Nicolet, Madison, WI, USA). Heavy metal ions were analysed on Thermo Solar 6 atomic adsorption spectrometer (Massachusetts, USA).

2.3. Preparation of SBSEVD

The procedure of preparation of glass bar, pretreatment and chemical modifications of the glass bar was described previously [17–19]. AIBN was used as polymerization initiator (1% (w/w) of the total monomer amount) in the all polymerization reaction. Different monomers and porogen concentrations were used for different SBSEVD (Table 1). The monomer mixtures and porogen (90% (w/w) cyclohexanol, 10% (w/w) 1-dodecanol) were mixed ultrasonically into a homogenous solution then the reactant solution was purged with nitrogen for 3 min. Subsequently, the reactant mixture was poured into a glass tube with definite diameter. The stir bar that has been pretreated was vertically immersed into the reactant mixture. The tube was sealed with septa and kept at 70 °C for 12 h. After the polymerization, the glass tube was cut off carefully with grindstone. Firm, integrated and polished monoliths could be obtained. The monolithic material on the bar was then Soxhlet-extracted with methanol for 24 h to remove the residue monomers, porogen, uncross-linked polymers and initiator. Finally, the stir bar was dried in air for 1 h to obtain the final SBSEVD (30 mm in length and 1.0 mm monoliths thickness).

Table 1
Extraction efficiency of different SBSEVD for phenol and *p*-nitrophenol.

SBSEVD	Monomer mixture ^a		Polymerization mixture		Extraction efficiency ^b	
	VPL (% w/w)	DVB (% w/w)	Monomer mixture (% w/w)	Porogen solvent (% w/w)	Phenol (%)	<i>p</i> -Nitrophenol (%)
1	10	90	30	70	32.3	48.1
2	15	85	30	70	36.3	55.7
3	20	80	30	70	30.6	51.3
4	25	75	30	70	34.3	52.9
5	30	70	30	70	31.4	53.6
6	35	65	30	70	30.0	47.8
7	15	85	25	75	35.0	52.5
8	15	85	35	65	32.4	60.0
9	15	85	40	60	39.4	52.5
10	15	85	45	55	36.9	59.0
11	15	85	50	50	36.7	59.2

^a Weight fraction in monomer mixture.

^b The extraction efficiency is calculated from the equation: $E = ((C_b - C_a)/C_b) \times 100\%$, the E is the extraction efficiency, C_b and C_a are the concentrations before and after extraction, respectively.

2.4. Extraction and desorption mode

Stirring extraction and stirring liquid desorption modes were used. The samples were stirred with 400 rpm at room temperature. The influences of polymerization conditions on the extraction efficiencies were performed using 50 mL (5.0 µg/mL) solution of the mixture of phenol and *p*-nitrophenol. In the study of the enrichment of the PAHs, phenols, anilines, hormones and heavy metal ions on SBSEVD, 50 mL stock mix solution of corresponding compounds was used. In the extraction of PAHs, phenols, anilines and hormones samples, the stir bars stirred 2 h for extraction, then the stir bars were removed and immersed in 3.0 mL mixture of methanol/*n*-hexane (V/V = 10/90) for PAHs and 3.0 mL ACN for phenols, anilines and hormones, respectively, and stirred for another 2 h to release the extracted analytes. After that, the stir bars were removed by means of a magnetic rod, while the stripping solvent was evaporated to dryness under a gently stream of nitrogen. For phenols, anilines and hormones, the dried residues were redissolved in 0.5 mL ACN for HPLC/DAD analysis, for PAHs, dried residues were redissolved in 0.5 mL *n*-hexane for GC–MS analysis.

In the study of the enrichment of heavy metal ions, the concentrations of metal ions before and after extracting 2 h were measured by atomic adsorption spectrometer. The extraction efficiency was calculated from the equation:

$$E = \frac{C_b - C_a}{C_b} \times 100\%$$

where the *E* is the extraction efficiency, *C_b* and *C_a* are the concentrations of metal ions before and after extraction, respectively.

2.5. Chromatographic conditions

The separation of phenol and *p*-nitrophenol for the investigation of the influences of the polymerization parameters on extraction efficiencies were performed on the Supelco C18 (5.0 µm particle size, 250 mm × 4.6 mm i.d.). The mobile phase consisted of a mixture of 40% (v/v) ACN aqueous solution. The detector was set at 271 nm; the flow rate was 1.0 mL/min and injection volume was 20 µL. The separations of phenols, anilines, hormones were performed on a Phenomenex Luna ODS column (5 µm particle size, 250 × 2.0 mm i.d.). ACN and water were used as the mobile phase, the flow rate was 0.3 mL/min and the injection volume was 10 µL.

The PAHs were analyzed using a Hewlett–Packard 6890 gas chromatography equipped with a mass spectroscopy detector (HP5975B). The HP-5MS column (Agilent Co., USA) was 30 m in length, with an internal diameter of 0.25 mm and a film thickness of 0.25 µm. The temperature was raised from 60 to 150 °C at a rate of 15 °C/min, increased to 220 °C at 5 °C/min, and increased to 300 °C at 10 °C/min, then held at 300 °C for 5 min. Helium was used as the carrier gas. The injector and detector temperatures were 280 and 300 °C, respectively. The electron-impact energy was 70 eV and the mass to charge ratio scan (*m/z*) was from 50 to 400 amu. The selected ion mode (SIM) was chosen. The injection volume was 2.0 µL.

3. Results and discussion

3.1. Effect of the polymerization parameters on extraction efficiency

Phenol (P) and *p*-nitrophenol (p-NP) had been selected as detected solutes to investigate the effect of the polymerization parameters including different monomers and porogen concentrations on extraction efficiency. Table 1 shows the effect of the content of monomer and porogen concentrations on the extrac-

tion efficiency. It could be seen from the table that when the ration of monomer mixture to porogen was kept 30%/70%, the extraction efficiency reached highest at the content of monomer 15%, then decreased when the usage of monomer increased continuously. This may be due to the content of VPL, which provides the main adsorptive site in the monoliths for P and p-NP compounds, with the content of VPL increased, higher extraction capacity should be obtained. However, the increase of VPL would decrease the content of DVB, which resulted in less surface area in the monoliths [20]. The decrease of surface area led to the lower extraction efficiency. As the result, the highest extraction efficiency could be obtained when the content of monomer was 15% (Bar 2) under the opposite effects mentioned above.

In order to enhance the extraction efficiency, more VPL groups should be expected in the SBSEVD. Another approach to enhance the content of VPL groups was to increase the proportion of monomer mixture in the reactant mixture. The monomer mixture was increased from 25% to 50% when the proportion of VPL to DVB was kept 15% to 85%. The results showed that the optimal extraction efficiency for P and p-NP appeared in 45% (Bar 10) (Table 1). When the monomer mixture increased to 50% (Bar 11), although high extraction efficiency for P and p-NP also could be obtained, the monolithic material was too soft and the coating would crack during stirring.

Based on the experimental results shown above, the optimal conditions for preparation of poly(VPL-DVB) monolithic material was the proportion of VPL kept 15% in the monomer mixture, while the ratio of monomer mixture to porogen was 45%/55% (Bar 10). The optimal conditions were used to prepare SBSEVD for the further experiments.

3.2. Characterization of the monolithic material

The monolithic material under the optimal conditions (Bar 10) was characterized by EA, IR, SEM and MIP. Elemental analysis on the monolith demonstrated that its carbon content was 84.0% (w/w) and nitrogen content was 2.16% (w/w), indicating that VPL and DVB were successfully incorporated into the monolith during the polymerization process. By theoretical calculation from the reactant ratio, the carbon content should be around 89.7% (w/w) and nitrogen content should be around 1.69% (w/w) in the final product. Obviously, some of the DVB had not taken part in the polymerization process.

Diffuse reflectance Fourier-transform IR measurement (Fig. 1) of the final monolithic structure further confirmed the polymer-

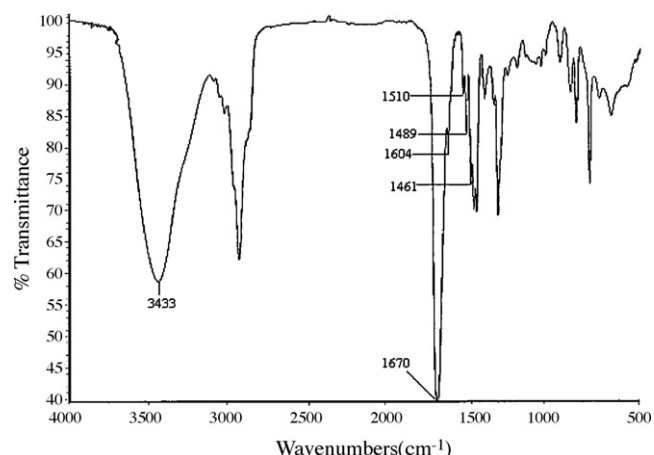


Fig. 1. IR spectroscopy of the poly(VPL-DVB) monolith.

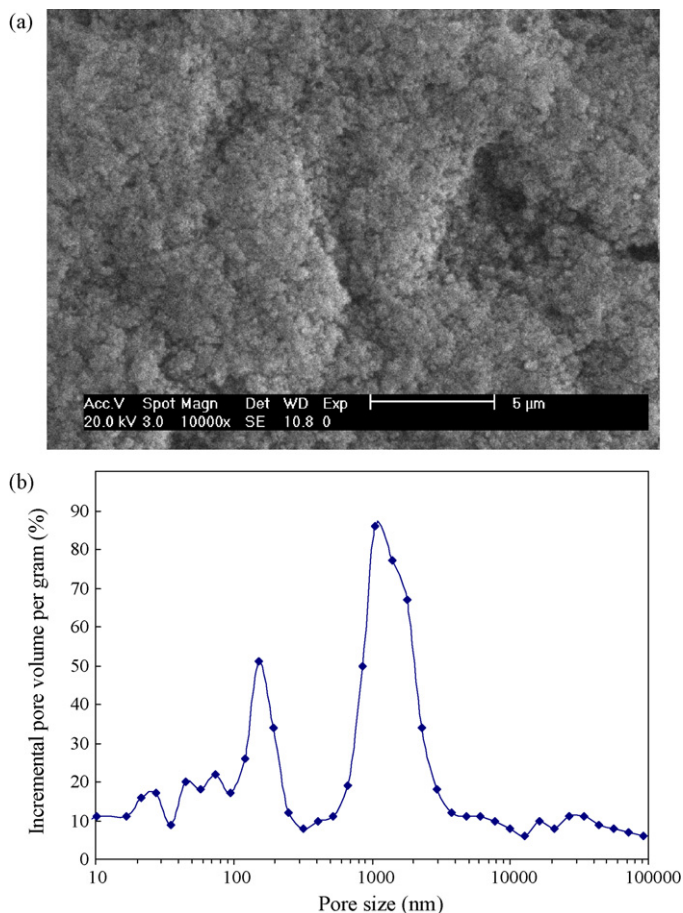


Fig. 2. (a) SEM image of the poly(VPL-DVB) monolith at 10,000 \times magnification. (b) Pore size distribution profiles of the poly(VPL-DVB) monolithic material.

ization of VPL and DVB. The spectrum shows a broad peak around 3433 cm^{-1} which may be attributed to the adsorbed water. Strong adsorption in the 1670 cm^{-1} can be due to C=O stretching bands. The adsorption observed at 1604, 1489 and 1461 cm^{-1} indicates the existence of phenyl groups. The weak adsorption in the 1510 cm^{-1} can be due to C–N stretching bands.

Fig. 2a shows the SEM image of the poly(VPL-DVB) monolith at 10,000 \times magnification. The interconnected skeletons and textural pore of the monolithic material can be clearly observed. The skeletons and the structure pores were evenly distributed in the monolith. At the same time, they were interwoven together, leading to the formation of an interpenetrating network. Fig. 2b shows the pore size distribution plot. It was found that there were two types pore size existing in the monoliths. One was large pore, the pore size about 1000 nm; the other was mesopore, the pore size about 150 nm. The existence of large pore ensures monolithic material possess very good permeability and favorable mass transfer in extraction applications. While the existence of mesopore ensures monolithic material possess surface area and high extraction capacity.

3.3. The enrichment performance of SBSEVD

Fig. 3 represents the GC–MS chromatograms of a water sample spiked with 16 PAHs before (a) and after (b) the extraction with SBSEVD for 120 min. It could be seen that PAHs could be enriched effectively by SBSEVD. For example, the enrichment factors and the LODs, calculated at $S/N=3$ for naphthalene, fluorene and flouran-

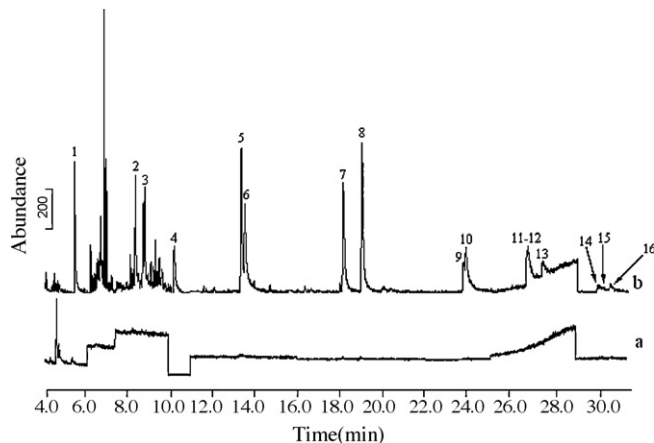


Fig. 3. GC–MS chromatograms of a water sample spiked with 16 PAHs before (a) and after (b) the extraction with SBSEVD. Peaks number: 1, naphthalene; 2, acenaphthylene; 3, acenaphthene; 4, fluorine; 5, phenanthrene; 6, anthracene; 7, flouranthene; 8, pyrene; 9, chrysene; 10, benzo(a)anthracene; 11, benzo(b)fluoranthene; 12, benzo(k)fluoranthene; 13, benzo(a)pyrene; 14, indeno(1,2,3-cd)pyrene; 15, dibenz(a,h)anthracene; 16, benzo(g,h,i)perylene.

there were 80 and 0.045, 98 and 0.093, 90 and 0.074 ng/mL, respectively. The high enrichment results may be own to the π – π interaction between the phenyl in SBSEVD and the phenyl in PAHs.

Hormones, phenols and aromatic amines were used to evaluate the extraction performance of SBSEVD for weakly and strongly polar compounds. Fig. 4 shows the HPLC chromatograms of a water sample spiked with seven hormones before (a) and after (b) the extraction with SBSEVD. The result showed that all the hormones were enriched effectively by SBSEVD. The enrichment factors varied from 38 to 55. Ideal LODs could be obtained after enrichment. For example, the detection limits for nandrolone, testosterone and progesterone were 0.036, 0.041 and 0.068 ng/mL, respectively.

Fig. 5 depicts the enriched results of five aromatic amines by SBSEVD. The results showed that aromatic amines also could be enriched by SBSEVD effectively. The enrichment factors varied from 9 to 73 and good detection limits could be obtained. For example, the LODs for *p*-nitroaniline and *p*-toluidine were 0.095 and 0.038 ng/mL, respectively.

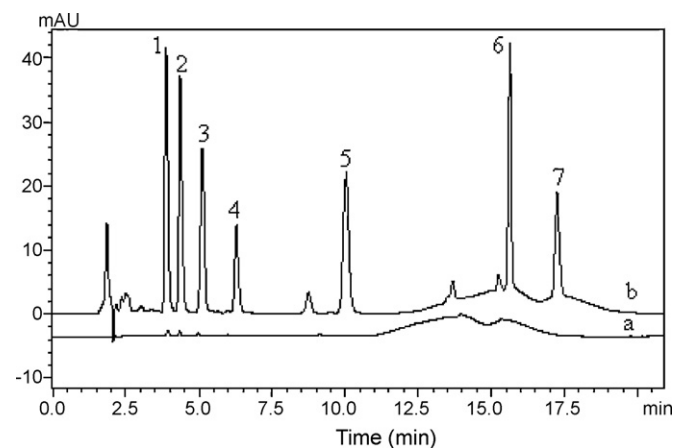


Fig. 4. HPLC chromatograms of a water sample spiked with seven hormones before (a) and after (b) the extraction with SBSEVD. Peaks number: 1, nandrolone; 2, testosterone; 3, diethylstilbestrol; 4, methyltestosterone; 5, progesterone; 6, testosterone propionate; 7, nandrolone phenylpropionate. Mobile phase: the composition gradient started with 40% water and 60% ACN and held until 8.0 min, then increased to 100% ACN in 4.0 min, then decreased to 60% ACN in 3.0 min and held until the end of analysis. The detector wavelength was set at 240 nm.

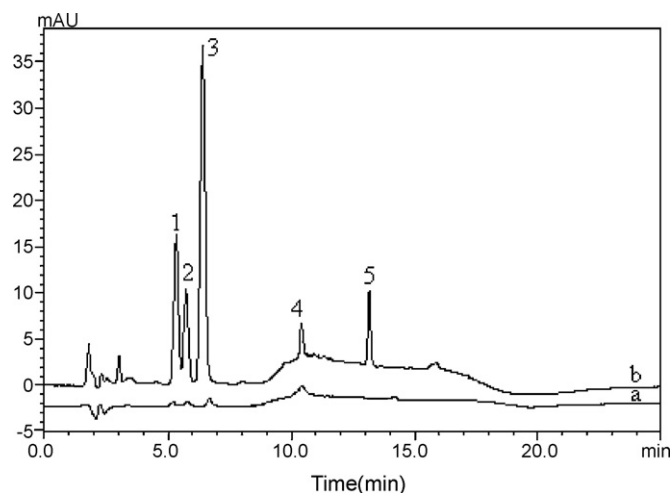


Fig. 5. HPLC chromatograms of a water sample spiked with five anilines before (a) and after (b) the extraction with SBSEVD. Peaks number: 1, *p*-nitroaniline; 2, *m*-nitroaniline; 3, *p*-toluidine; 4, diphenylamine; 5, *N*-ethyl aniline. Mobile phase: the composition gradient started with 60% water and 40% ACN and held until 4.0 min, then increased to 70% ACN in 2.0 min and held until 12.0 min, then decreased to 40% ACN in 3.0 min and held until the end of analysis. The detector wavelength was set at 230 nm.

Phenols are strongly polar compounds, for example, the $\log K_{o/w}$ of phenol is 1.49. Because of the strong polarity, derivatisation process should be taken before extracting by SBSE [9,10]. However, the derivatisation of polar analytes to produce more hydrophobic species is inconvenient and not always possible especially for those with $\log K_{o/w} < 3$ [21]. Therefore, if there is a SBSE coating which can directly enrich phenols may simple the extraction process of SBSE. Fig. 6 represents the HPLC chromatograms of a water sample spiked with nine phenols before (a) and after (b) the direct extraction with SBSEVD. It could be seen from the figure that all the phenols were directly enriched. Enrichment factors varied from 23 (for phenol) to 50 (for 2,4-dimethylphenol) and acceptable LODs could be obtained. For example, the LODs for phenol and 2,4-dimethylphenol were 0.50 and 0.24 ng/mL, respectively.

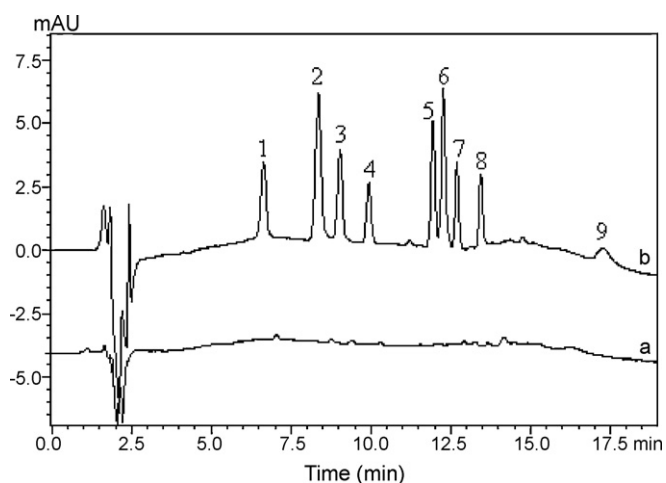


Fig. 6. HPLC chromatograms of a water sample spiked with nine phenols before (a) and after (b) the extraction with SBSEVD. Peaks number: 1, phenol; 2, 4-nitrophenol; 3, *m*-methylphenol; 4, bisphenol A; 5, 2-chlorophenol; 6, 2,4-dichlorophenol; 7, 2,4-dimethylphenol; 8, 4-chloro-3-methylphenol; 9, 2,4,6-trichlorophenol. Mobile phase: the composition gradient started with 70% water and 30% ACN, then increased to 50% ACN in 8.0 min and increased continuously to 60% in 2.0 min, then decreased to 30% ACN in 5.0 min and held until the end of analysis. The detector wavelength was set at 271 nm.

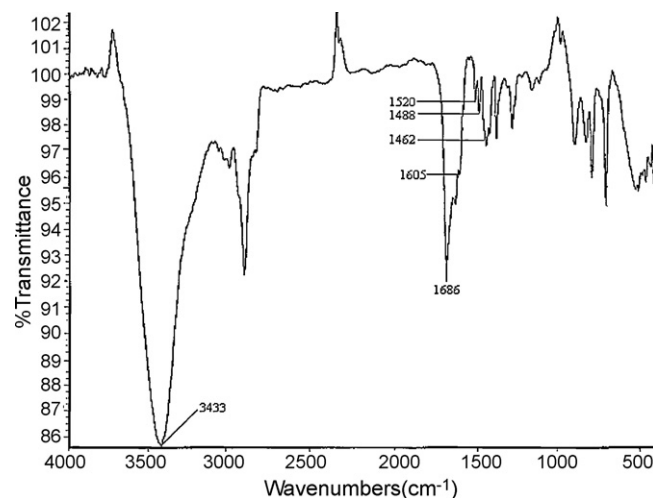


Fig. 7. IR spectroscopy of poly(VPL-DVB) after absorption Cu^{2+} .

There are nitrogen and oxygen atoms in the poly(vinylpyrrolidone-divinylbenzene) monolithic materials. Therefore, SBSEVD may be used to extract heavy metal ions except for adsorption of organic compounds. Four heavy metal ions included Cu^{2+} , Pb^{2+} , Cr^{3+} and Cd^{2+} were used to investigate the adsorption performance of SBSEVD for metal ions. After extraction 2 h, the extraction efficiencies (E) were 19.6%, 15.3%, 10.1% and 16.6% for Cu^{2+} , Pb^{2+} , Cr^{3+} and Cd^{2+} , respectively. The adsorption of SBSEVD to heavy metal ions may be the existence of nitrogen and oxygen atoms in the VPL groups and could coordinate with metal ions. The FT-IR of poly(VPL-DVB) after adsorption Cu^{2+} showed that the adsorption peaks of C–N (1510 cm^{-1}) and C=O (1670 cm^{-1}) shifted to 1520 and 1686 cm^{-1} , respectively (Fig. 7). The FT-IR demonstrated that nitrogen and oxygen atoms played a key role in the extraction of metal ions. Although the E is not as high as expected, it gives us a new idea that SBSE can be used to enrich metal ions if some suitable coating is prepared and the applied field of SBSE can be extended.

3.4. Bar-to-bar reproducibility and stability investigation of SBSEVD

The bar-to-bar reproducibility of SBSEVD was studied used phenol and *p*-nitrophenol as target analytes. The RSD ($n=5$) of enrichment factors for phenol and *p*-nitrophenol were 1.74% and 1.52%, respectively. Good rigidity of SBSEVD could be obtained under optimal polymerization conditions. No decomposition had been found during stirring and the bar could be used at least 10 times. The good reproducibility and stability indicate that poly(VPL-DVB) monolithic material is suitable to prepare coating layer of SBSE. In our future research, the optimally extractive conditions for hormones, phenols and aromatic amines on SBSEVD would be investigated in detail and would couple with HPLC-MS or GC-MS to highly sensitive detect above compounds in real water samples. Some new SBSE coating for concentration metal ions would be further developed in order to extend the applied field of SBSE.

4. Conclusion

A new coating based on poly(VPL-DVB) monolithic material for SBSE was prepared. The polymerization conditions were optimized and EA, FT-IR, SEM and MIP were used to characterize the monolithic material. In comparison with previous research, the SBSEVD not only could directly concentrate apolar and polar organic compounds effectively, but also can extracted some heavy metal ions

through coordination reaction between nitrogen and oxygen atoms in the coating and metal ions.

Acknowledgements

The project was supported by National Nature Science Foundation of China (grant: 20805039), Youth Talent Foundation of Fujian Province (No. 2006F3117) and Innovation Foundation of Xiamen University (No. XDKJCX20063007).

References

- [1] E. Baltussen, P. Sandra, F. David, C. Cramers, J. Microcol. Sep. 11 (1999) 737.
- [2] S. Nakamura, S. Daishima, Anal. Bioanal. Chem. 382 (2005) 99.
- [3] A. Juan-Garcia, Y. Pico, G. Font, J. Chromatogr. A 1073 (2005) 229.
- [4] A. Stopforth, A. Tredoux, A. Crouch, P. Van Helden, P. Sandra, J. Chromatogr. A 1071 (2005) 135.
- [5] E.D. Guerrero, R.N. Marin, R.C. Mejias, C.G. Barroso, J. Chromatogr. A 1104 (2006) 47.
- [6] S. Nakamura, S. Daishima, J. Chromatogr. A 1038 (2004) 291.
- [7] M. Kawaguchi, R. Ito, K. Saito, H. Nakazawa, J. Pharm. Biomed. Anal. 40 (2006) 500.
- [8] F. David, B. Tienpont, P. Sandra, LC-GC N. Am. 21 (2003) 108.
- [9] D. Juan, D. Cristina, A.G. Dominico, V. Rafael, G.B. Carmelo, J. Chromatogr. A 1025 (2005) 263.
- [10] M. Kawaguchi, K. Inoue, M. Yoshimura, R. Ito, N. Sakui, N. Okanouchi, H. Nakazawa, J. Chromatogr. B 805 (2004) 41.
- [11] C. Bicchi, C. Cordero, E. Liberto, P. Rubiolo, B. Sgorbini, F. David, P. Sandra, J. Chromatogr. A 1094 (2005) 9.
- [12] W. Liu, H. Wang, Y. Guan, J. Chromatogr. A 1045 (2004) 15.
- [13] W. Liu, Y. Hu, J. Zhao, Y. Xu, Y. Guan, J. Chromatogr. A 1095 (2005) 1.
- [14] Y. Hu, Y. Zheng, F. Zhu, G. Li, J. Chromatogr. A 1148 (2007) 16.
- [15] N.R. Neng, M.L. Pinto, J. Pires, P.M. Marcos, J.M.F. Nogueira, J. Chromatogr. A 1171 (2007) 8.
- [16] W.N. Guan, F. Xu, W.M. Liu, J.H. Zhao, Y.F. Guan, J. Chromatogr. A 1147 (2007) 59.
- [17] X.J. Huang, D.X. Yuan, J. Chromatogr. A 1154 (2007) 152.
- [18] X.J. Huang, D.X. Yuan, B.L. Huang, Talanta 75 (2008) 172.
- [19] X.J. Huang, N.N. Qiu, D.X. Yuan, J. Chromatogr. A 1194 (2008) 134.
- [20] N. Fontanals, R.M. Marce, F. Borrull, Trends Anal. Chem. 24 (2005) 394.
- [21] F. David, P. Sandra, J. Chromatogr. A 1152 (2007) 54.



Determination of strontium and simultaneous determination of strontium oxide, magnesium oxide and calcium oxide content of Portland cement by derivative ratio spectrophotometry

K.A. Idriss*, H. Sedaira, S.S. Ahmed

Chemistry Department, Faculty of Science, Assiut University, 3716 Assiut, Egypt

ARTICLE INFO

Article history:

Received 30 July 2008

Received in revised form 26 October 2008

Accepted 27 October 2008

Available online 5 November 2008

Keywords:

Strontium determination

Portland cement analysis

Derivative spectrophotometry

ABSTRACT

A derivative spectrophotometric method has been developed for the determination of strontium in Portland cement. The method is applied successfully for the simultaneous determination of SrO, MgO and CaO. It is based on the use of Alizarin Complexone (AC) as a complexing agent and measurement of the derivative ratio spectra of the analytes. Interferences of manganese(II) and zinc(II) were eliminated by precipitation. The validity of the method was examined by analyzing several Standard Reference Material (SRM) Portland cement samples. The strontium complex formed at pH 9.5 allows precise and accurate determination of strontium over the concentration range of 1.5–18 mgL⁻¹ of strontium. The MDL (at 95% confidence level) was found to be 25 ng mL⁻¹ for strontium in National Institute of Standards and Technology (NIST) cement samples using the proposed method.

© 2008 Elsevier B.V. All rights reserved.

1. Introduction

As given by the current ASTM Standard Test Methods for chemical analysis of hydraulic cement (C 114) [1], strontium, usually present in Portland cement as a minor constituent, was precipitated with calcium as the oxalate and was subsequently titrated and calculated as CaO, or alternatively correction of CaO for SrO was made, if the SrO content is known. Many analysts and ASTM members have expressed the opinion that (C 114) does not make the distinction between CaO and SrO and the statement referred therein may direct the analyst to not correct the CaO for SrO. Accordingly, the development of a new, direct, sensitive and accurate method for the determination of Sr as a minor constituent in cement is of utmost importance. The objective of this work is to accomplish this.

However, little information is available concerning the determination of Sr in cement matrix, although several works have been published about the determination of strontium. Strontium in presence of higher levels of calcium concentrations has been determined using separation techniques [2–5], many of these methods are not simple and usually they have low selectivity. An atomic absorption spectrometric method for the determination of calcium, magnesium and strontium in soils has been reported [6], for the determination of calcium and strontium, it was necessary to remove silicon.

Derivative spectrophotometry opens up possibilities, not only for increasing selectivity [7–11], but also for increasing sensitivity [12–14]. The scale of this increase depends on the shape of the normal absorption spectra of the analyte and the interfering substances, as well as on the instrumental parameters and the measurement technique (e.g. peak-to-trough or zero-crossing), chosen by the analyst in a given analytical procedure [15–17].

Salinas et al. [18] developed a derivative spectrophotometric method for resolving binary mixtures when the spectra of the components are overlapped. The method is based on the use of the first-derivative of the ratios of the spectra. The absorption spectrum of the mixture is obtained and divided (amplitude by amplitude at appropriate wavelengths) by the absorption spectrum of a standard solution of one of the components (previously stored in a computer), and the first-derivative of the ratio spectrum is obtained. The concentration of the other component is then determined from a calibration graph. Later, the method was extended to the resolution of ternary mixtures in combination with zero-crossing method [19].

Alizarin Complexone (alizarin-3-methylamine-N, N-diacetic acid, AC) is one of the most commonly reagents used for spectrophotometric determination of metal ions [20–23]. No studies have yet been reported demonstrating the solution equilibria of strontium with AC or the use of this reagent for the analytical determination of strontium. As an extension to our previous studies for spectrophotometric determinations of some constituents [24–26] in Portland cement, a rapid and sensitive first-derivative ratio spectrum zero-crossing method is undertaken to determine Sr and its

* Corresponding author. Fax: +20 88 2342708.

E-mail address: kamalidriss@hotmail.com (K.A. Idriss).

closely related cations Mg and Ca in mixtures using Alizarin Complexone as a complexing agent. Specific conditions are applied for simultaneous determination of Sr, Mg and Ca in Portland cement.

2. Experimental

2.1. Chemicals and solutions

A 1×10^{-3} mol L⁻¹ stock standard solution of Alizarin Complexone was prepared by dissolving an accurately weighed amount of Sigma (St. Louis, MO, USA) pure grade reagent in absolute ethanol. A 10^{-3} mol L⁻¹ stock standard solution of strontium chloride, calcium chloride and magnesium chloride were prepared using the AnalaR grade product. The metal content of the solution was determined by conventional methods [27]. Solutions of perchloric acid, sodium perchlorate and standard sodium hydroxide solution were all prepared from analytical-reagent grade reagents. Solutions of diverse ions used for interference studies were prepared from AnalaR chloride salts of the metal ions and potassium or sodium salts of the anions to be tested.

2.2. Cement samples

National Institute of Standards and Technology (NIST) Standard Reference Materials (SRMs) 1881, 1885 and 1886 were used as the Portland cement matrix in this study. Precautions for handling and use were taken in accordance with the instructions on the NIST data sheet. A complete composition of SRMs samples according to NIST certificates of analysis [28] is given in Table 1. Other samples of ordinary Portland cement (OPC) were supplied by Assiut Cement (Cemex, Egypt).

2.2.1. Dissolution of cement samples

Weigh accurately 0.3–0.4 g of the sample (dried at 110 °C) into a beaker and dissolve it in the minimum volume of hydrochloric acid. Heat to dryness, add 10 mL of HCl (6 mol L⁻¹) to the residue, digest and filter the insoluble residue into a 100 mL calibrated flask and then dilute to volume with doubly distilled water.

2.3. Apparatus

A PerkinElmer (Norwalk, CT, USA) Lambda 35 double beam spectrophotometer was used for ordinary and first-derivative spectral measurements using 1 cm matched quartz cells. The first-derivative

spectra were recorded at a scan speed of 240 nm min⁻¹, $\Delta\lambda = 5$ nm and a slit width of 2 nm. The smoothing and differentiation calculation are based on a least-squares polynomial convolution function using 17 data points.

pH values were measured using a Radiometer (Copenhagen, Denmark) M 201 pH meter equipped with a Radiometer combined glass electrode. The pH meter was calibrated regularly before use with standard buffer solutions and the pH values in water–ethanol medium were corrected as described elsewhere [29].

2.4. Procedures

2.4.1. Ordinary spectrophotometry

Transfer an aliquot of a sample solution containing strontium(II) (25–500 µg) and/or magnesium(II) (10–150 µg) and/or calcium(II) (15–250 µg) into 25 mL calibrated flasks. Add 5 mL of 1×10^{-3} mol L⁻¹ Alizarin Complexone solution and 5 mL of absolute ethanol to ensure a final ethanol content of 40% (v/v). Adjust the pH to 9.5 using 0.008 M sodium hydroxide, while keeping the ionic strength constant at 0.1 (NaClO₄). Dilute to volume with doubly distilled water and record the normal spectrum from 700 to 500 nm against a reagent blank as the reference.

2.4.2. Derivative ratio spectrum zero-crossing method

The stored spectra of Sr–AC complex, Ca–AC complex and their ternary mixture with Mg–AC complex were divided by a standard spectrum of Mg–AC complex. The first-derivative of the ratio spectra were recorded from 650 to 550 nm. In the ternary mixture, the concentrations of strontium and calcium were proportional to the first-derivative divided signals (¹DD) at 587 and 612.5 nm (zero-crossing points for Ca/Mg) and 594 nm (zero-crossing point of Sr/Mg), respectively. By the same procedure, the stored spectra of Mg–AC complex, Ca–AC complex and their ternary mixture with Sr-complex were divided by a standard spectrum of Sr–AC complex and the first-derivative of the obtained ratio spectra was recorded. The concentrations of calcium and magnesium in the ternary mixture were proportional to the first-derivative divided signals (¹DD) at 594 nm (zero-crossing point of Mg/Sr) and 602.5 nm (zero-crossing point of Ca/Sr), respectively. In this case the concentration of calcium in ternary mixture has been determined twice.

2.4.3. Simultaneous determination of SrO, MgO and CaO in Portland cement

Weigh accurately 0.3–0.4 g of the sample (dried at 110 °C) into a beaker and prepare the sample solution as indicated earlier. Transfer a 25-mL aliquot of the sample solution into a 150-mL beaker. To overcome the presence of calcium in a high level relative to strontium in Portland cement (600:1) add 0.5 mL of 1×10^{-3} mol L⁻¹ Sr(II) solution. Add 5 mL of (1:1) ammonium hydroxide solution to precipitate [1] and eliminate the interferences due to manganese and zinc. Filter into a 100 mL calibrated flask and dilute to the volume with doubly distilled water.

Transfer a 0.5–1.0 mL aliquot of the prepared cement solution into a 25 mL calibrated flask and add 5 mL of AC (1×10^{-3} M). Adjust the pH to 9.5 by the addition of 0.008 M sodium hydroxide. Dilute to volume while keeping final ethanol content of 40% (v/v). Record the absorbance of the solution from 700 to 500 nm against a reagent blank as the reference. Divide the obtained normal spectrum by a standard one for Mg-complex or Sr-complex. Record the first-derivative of the ratio spectrum and measure the amplitudes (¹DD) at proper zero-crossing wavelengths as mentioned above. Mg and Ca content in Portland cement were calculated directly using regression equations, only the Sr content was corrected due to the added amount.

Table 1
Complete composition of SRM(s) samples according to NIST certificates of analysis [28].

Constituent	1886 (wt%)	1885 (wt%)	1881 (wt%)
CaO	67.43 ± 0.15	62.14 ± 0.14	58.67
SiO ₂	22.53 ± 0.06	21.24 ± 0.06	22.25
Al ₂ O ₃	3.99 ± 0.04	3.68 ± 0.07	4.16
Fe ₂ O ₃	0.31 ± 0.01	4.40 ± 0.02	4.68
SO ₃	2.04 ± 0.02	2.22 ± 0.02	3.65
MgO	1.60 ± 0.04	4.02 ± 0.10	2.63
K ₂ O	0.16 ± 0.01	0.83 ± 0.01	1.17
TiO ₂	0.19 ± 0.01	0.20 ± 0.01	0.25
Na ₂ O	0.02 ± 0.01	0.38 ± 0.04	0.04
SrO	0.11 ± 0.01	0.037 ± 0.014	0.11
P ₂ O ₅	0.025 ± 0.010	0.10 ± 0.01	0.09
Mn ₂ O ₃	0.013 ± 0.004	0.12 ± 0.01	0.26
F	(0.01)	(0.05)	0.09
Cl	(0)	(0.02)	0.01
ZnO	(<0.01)	(0.03)	0.01
Cr ₂ O ₃	(<0.01)	(<0.01)	–

Values in parentheses are not certified, but are presented for use as Information Only.

3. Results and discussion

3.1. Acid–base properties of the reagent

The AC reagent yields five coloured acid–base forms in solutions of pH ~3.2–10.5: H_4L , H_3L^- , H_2L^{2-} , HL^{3-} and L^{4-} , exhibiting the absorption maxima at 270, 335, 423, 525, and 580 nm, respectively. Distinct isosbestic points are observed for the particular acid–base equilibrium.

The absorbance versus pH graphs were interpreted assuming that a particular equilibrium is established under selected conditions. Under our experimental conditions, pK_{a1} (H_4L/H_3L^-) = 4.5, pK_{a2} (H_3L^-/H_2L^{2-}) = 5.0, pK_{a3} (H_2L^{2-}/HL^{3-}) = 5.4 and pK_{a4} (HL^{3-}/L^{4-}) = 8.5 ($I=0.1$, $25^\circ C$).

3.2. Complexation equilibria of Sr^{2+} with AC

The complexation equilibria of Sr^{2+} with AC were studied in solutions containing 40% (v/v) ethanol over the pH range of 7.0–10.5. The solution spectra were recorded in equimolar solutions and in solutions containing an excess of the reagent. The absorption spectra reflect the formation of a complex with a double-headed band (λ_{max} at 575 and 622 nm), where the reagent Alizarin Complexone does not absorb. The complex formation starts at pH 7.5 and increases up to pH 9.5 as evidenced by increase in absorbance. Maximum colour development is attained at pH 9.5–10.0. At higher pH values, a decrease of absorbance is observed which is presumably due to the hydrolysis effect.

The absorbance versus pH graphs for the Sr–AC system (Fig. 1a) were interpreted using the relationships reported by Voznica et al. [30] and Idriss et al. [31,32]. The number of protons released during complexation (q) and the equilibrium constant (K_{eq}) were proved graphically from the plots obtained (Fig. 1b) with the solutions investigated. The following Eqs. (1) and (2) are valid for equimolar solutions and solutions with an excess of ligand,

respectively.

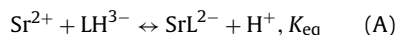
$$K_{eq} = \frac{AA_0^2[H^+]^q}{4C_M^2(A_0 - A)^3} \quad (1)$$

$$K_{eq} = \frac{\Delta A[H^+]^q}{(\Delta A_0 - \Delta A)C_L^2} \quad (2)$$

All symbols have their usual meanings.

The logarithmic transformation of these equations are straight lines with a slope (q) and an intercept including (K_{eq}). By considering the acid–base equilibria of Alizarin Complexone in 40% (v/v) ethanol and the distribution ratio of the reagent species at different pH values, one can assume that the trianionic form of the reagent (HL^{3-}) is the prevalent ligand species in the pH range of complexation (7.0–10.0).

At this pH range, the graphical analysis of the absorbance versus pH graphs, for solutions with different component ratios, indicated the best fit for the formation of SrL^{2-} complex with the liberation of one proton according to equilibrium (A).



3.3. Equilibrium and stability constants

The equilibrium constant K_{eq} was determined by considering equilibrium (A). The stability constant (β) of strontium–AC complex is related to the equilibrium constant (K_{eq}) by the expression $\beta = K_{eq} K_{a4}^{-1}$. The calculated values of the apparent equilibrium constant and stability constant at pH 9.5 are 1.6×10^5 and 4.9×10^{13} , respectively.

3.4. Stoichiometry of the complex

The composition of the complex was further verified by the method of continuous variations. In solutions having

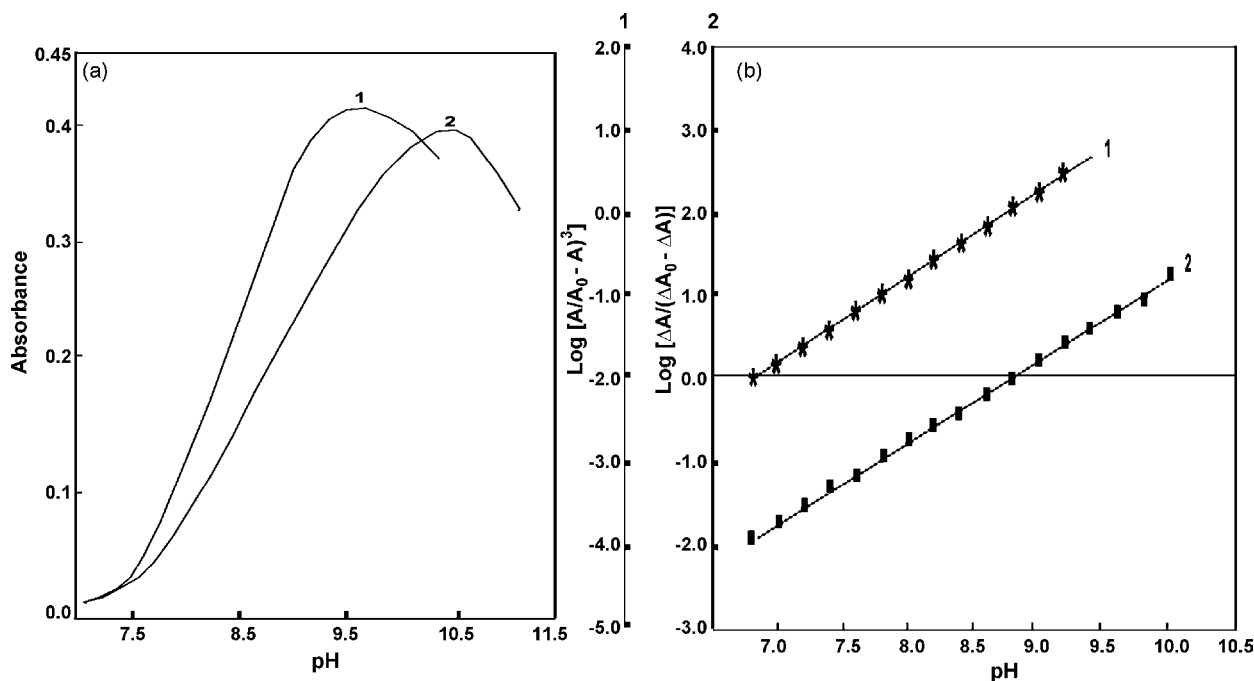


Fig. 1. (a) Absorbance vs. pH graphs and (b) graphical analysis of the absorbance vs. pH graphs for Sr(II)–AC complexes. $\lambda = 622$ nm, 40% (v/v) ethanol, 0.1 mol L^{-1} (NaClO_4). (1) $C_M = C_L = 2 \times 10^{-4} \text{ mol L}^{-1}$. (2) $C_M = 1 \times 10^{-4} \text{ mol L}^{-1}$; $C_L = 2 \times 10^{-4} \text{ mol L}^{-1}$.

$C_o = C_M + C_L = 4.0 \times 10^{-4} \text{ mol L}^{-1}$ at pH 9.5, the plot of absorbance at 622 nm versus mole fraction of strontium shows a maximum at 0.5, suggesting the formation of 1:1 (M:L) complex.

3.5. Analytical characteristics of the method

Under the optimum conditions, a linear calibration graph for the Sr–AC system was obtained up to a concentration of $12.26 \mu\text{g mL}^{-1}$ of Sr with a molar absorptivity of $3.4 \times 10^3 \text{ L mol}^{-1} \text{ cm}^{-1}$ at 622 nm. A Ringbom plot showed that the optimum concentration range for the determination of strontium was $3.5\text{--}12.2 \mu\text{g mL}^{-1}$. The sandell's sensitivity of the reaction was found to be 3.35 ng cm^{-2} .

The reproducibility of the method was checked by analyzing a series of five solutions with a Sr concentration of $8.7 \mu\text{g mL}^{-1}$. The relative standard deviation (R.S.D.) was found to be 0.96%.

3.6. Effect of diverse ions

To assess the usefulness of the proposed method, the effects of diverse ions that are often associated with Sr^{2+} were studied. The tolerance of the method to foreign ions was investigated with solutions containing 0.2 mg of Sr per 25 mL and various amounts of foreign ions. The tolerance criterion for a given ion was taken to be the deviation of the absorbance values by more than $\pm 2\%$ from the expected value. The determination of strontium as SrL^{2-} complex was possible in the presence of Li^+ , Na^+ , K^+ , Cs^+ , Cd^{2+} , Al^{3+} , Fe^{3+} , Mo^{6+} , SO_4^{2-} , SO_3^{2-} , NO_3^- , Cl^- , Br^- , I^- and PO_4^{3-} (20.0 mg); Co^{2+} , Ni^{2+} , Pb^{2+} , Cr^{3+} , Ti^{4+} , $\text{C}_2\text{O}_4^{2-}$ and CO_3^{2-} (1.0 mg). The investigated ions Ca^{2+} , Mg^{2+} , Mn^{2+} and Zn^{2+} interfered seriously, even when present in amounts of 0.1 mg. The interference due to Mn and Zn was eliminated by the addition of ammonium hydroxide, and that due to Ca and Mg was overcome by using derivative ratio zero-crossing method.

3.7. Reaction of magnesium(II) and calcium(II) with AC

The complexation equilibria of Mg^{2+} and Ca^{2+} with AC were studied over the pH range of 7–10. The absorption spectra reflect the formation of Mg–AC complex with λ_{max} at 560, 600 nm, and the formation of Ca–AC with λ_{max} at 570, 608 nm. The analysis of

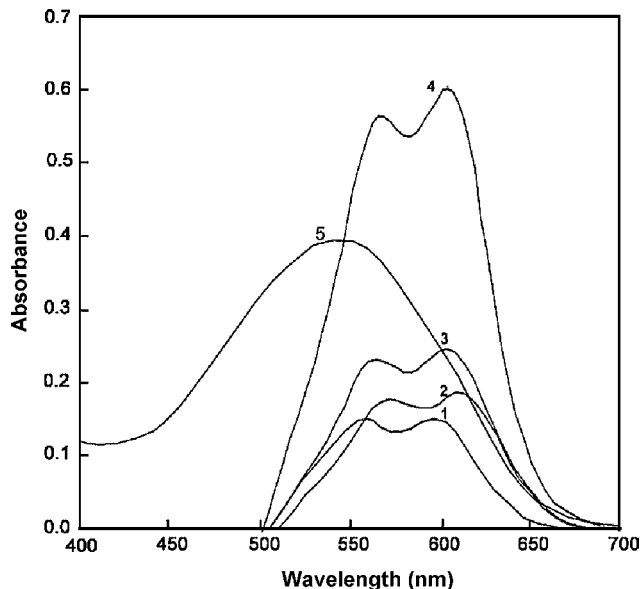
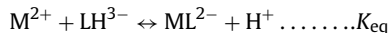


Fig. 2. Absorption spectra of (1) Mg(II)–AC complex, (2) Sr(II)–AC complex, (3) Ca(II)–AC complex, (4) their mixture–AC complexes. $[\text{Mg(II)}] = 0.5 \text{ mg L}^{-1}$, $[\text{Sr(II)}] = 3.5 \text{ mg L}^{-1}$ and $[\text{Ca(II)}] = 2.4 \text{ mg L}^{-1}$, $[\text{AC}] = 4 \times 10^{-4} \text{ mol L}^{-1}$ and (5) AC ($1 \times 10^{-4} \text{ mol L}^{-1}$), 40% (v/v) ethanol, 0.1 mol L^{-1} (NaClO_4), pH 9.5. (1)–(4) Against reagent blank and (5) against water–ethanol medium.

the absorbance versus pH graphs in the pH range studied indicated the best fit for equilibrium.



At pH 9.5 the complex conformed Beer's law up to $4.0 \mu\text{g mL}^{-1}$ of Mg^{2+} and $7.5 \mu\text{g mL}^{-1}$ of Ca^{2+} .

3.8. Simultaneous determination of strontium, magnesium and calcium in mixtures

3.8.1. Absorption spectra

The absorption spectra of Sr–AC, Mg–AC and Ca–AC complexes are shown in Fig. 2. The total absorption spectrum of a mixture of

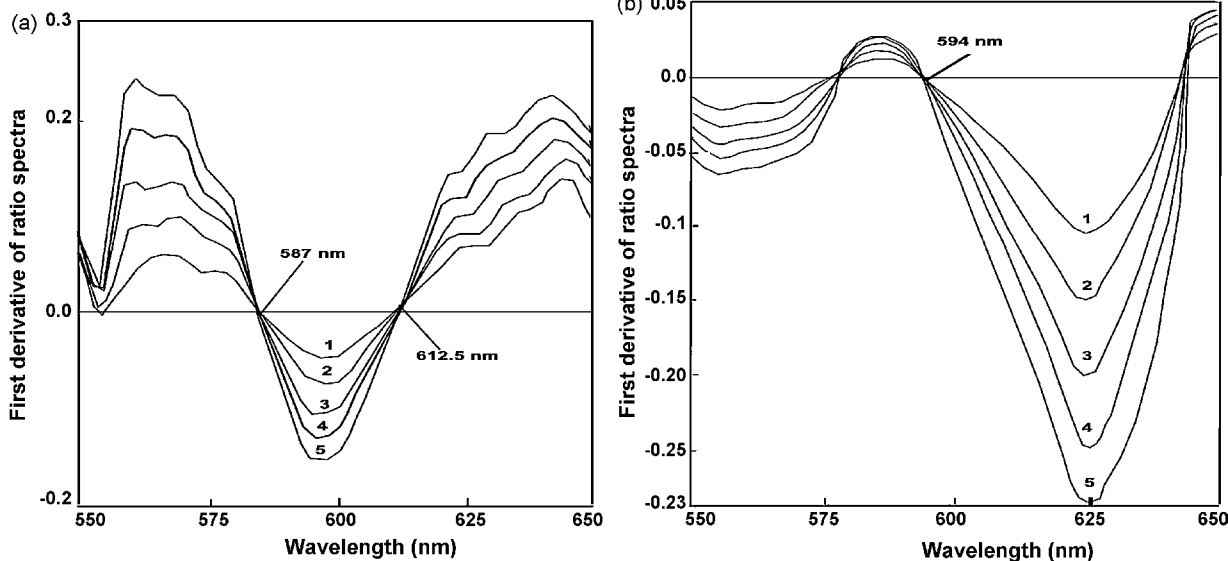


Fig. 3. First-derivative ratio spectra of Ca–AC (a) and Sr–AC (b) complexes. $[\text{Ca(II)}] = (1) 0.8 \text{ mg L}^{-1}$, (2) 1.2 mg L^{-1} , (3) 1.6 mg L^{-1} , (4) 2.0 mg L^{-1} , (5) 2.4 mg L^{-1} ; $[\text{Sr(II)}] = (1) 3.5 \text{ mg L}^{-1}$, (2) 5.2 mg L^{-1} , (3) 7.0 mg L^{-1} , (4) 8.7 mg L^{-1} , (5) 10.5 mg L^{-1} ; $[\text{Mg(II)}] = 0.5 \text{ mg L}^{-1}$ as divisor, $[\text{AC}] = 4 \times 10^{-4} \text{ mol L}^{-1}$, 40% (v/v) ethanol, 0.1 mol L^{-1} (NaClO_4), pH 9.5.

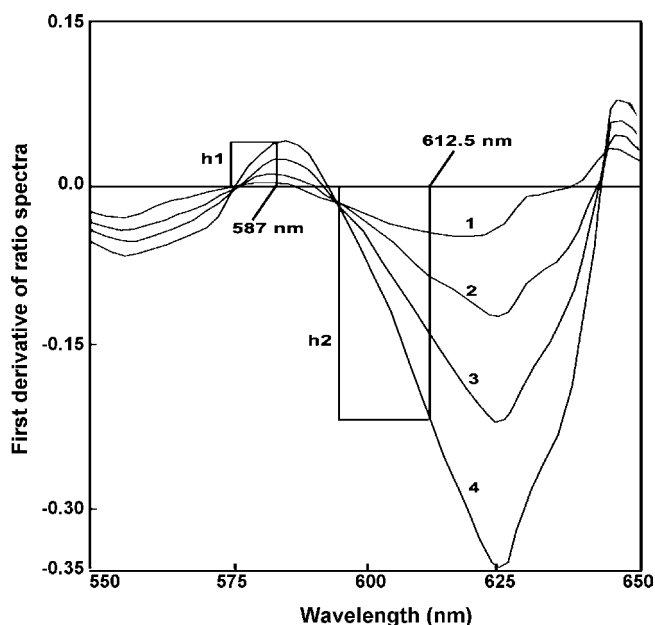


Fig. 4. First-derivative ratio spectra of ternary mixtures of (Sr^{2+} , Mg^{2+} and Ca^{2+})-AC complexes containing increment amounts of strontium. [$\text{Sr}(\text{II})$]= (1) 3.5 mg L^{-1} , (2) 7.0 mg L^{-1} , (3) 10.5 mg L^{-1} , (4) 14.0 mg L^{-1} ; [$\text{Mg}(\text{II})$]= 0.5 mg L^{-1} and [$\text{Ca}(\text{II})$]= 0.8 mg L^{-1} , [$\text{Mg}(\text{II})$]= 0.5 mg L^{-1} as divisor, [AC]= $4 \times 10^{-4} \text{ mol L}^{-1}$, 40% (v/v) ethanol, 0.1 mol L^{-1} (NaClO_4), pH 9.5.

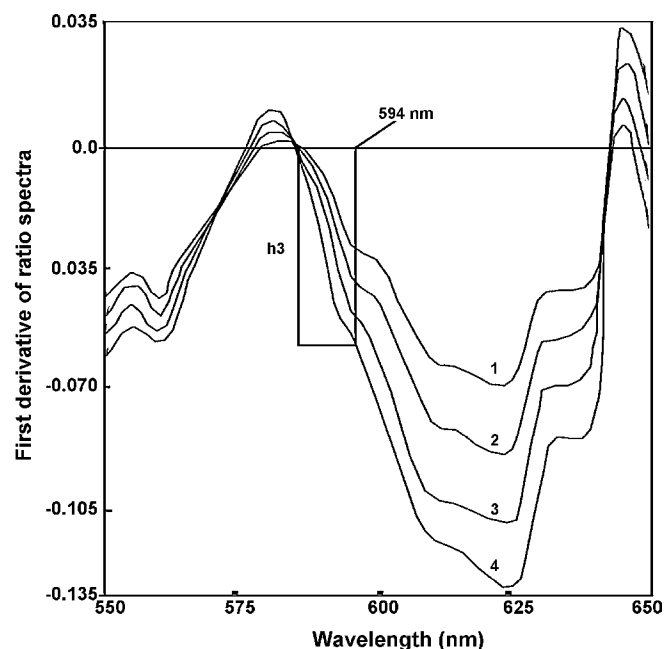


Fig. 5. First-derivative ratio spectra of ternary mixtures of (Sr^{2+} , Mg^{2+} and Ca^{2+})-AC complexes containing increment amounts of calcium. [$\text{Ca}(\text{II})$]= (1) 0.8 mg L^{-1} , (2) 2.4 mg L^{-1} , (3) 4.0 mg L^{-1} , (4) 5.6 mg L^{-1} ; [$\text{Sr}(\text{II})$]= 3.5 mg L^{-1} and [$\text{Mg}(\text{II})$]= 0.5 mg L^{-1} ; [$\text{Mg}(\text{II})$]= 0.5 mg L^{-1} as divisor, [AC]= $4 \times 10^{-4} \text{ mol L}^{-1}$, 40% (v/v) ethanol, 0.1 mol L^{-1} (NaClO_4), pH 9.5.

strontium, magnesium and calcium complexes is given. The absorption spectra of all complexes are characterized by a double-headed band in the range of 560–622 nm whereas the reagent (AC) has a maximum absorption at 520 nm. Due to the fact that absorption spectra of these complexes overlap, the determination of strontium, magnesium and calcium in their mixtures by zero-order spectrophotometry is frequently difficult. This disadvantage has been overcome by use of derivative ratio zero-crossing method.

3.8.2. Derivative ratio spectrum zero-crossing method

In order to resolve the ternary mixture, we needed to select the appropriate zero-crossing wavelengths that permitted the determination of each component in the presence of the other two. The reproducibility of zero-crossing wavelengths of derivative ratio spectra was checked by recording the first-derivative ratio spectra of Ca-AC and Sr-AC systems, at different concentrations of the analytes and using a standard spectrum of Mg-AC complex as a divisor (Fig. 3). The zero-crossing wavelengths were obtained at 587 and

612.5 nm for Ca/Mg (Fig. 3a) and at 594 nm for Sr/Mg (Fig. 3b). The zero-crossing wavelengths of Mg/Sr and Ca/Sr were obtained at 594 and 602.5 nm, respectively.

Figs. 4 and 5 show the derivative ratio spectra of two series of ternary mixtures containing increasing amounts of strontium or calcium, using Mg-complex as a divisor. Strontium and calcium can be determined using the absolute value of the total first-derivative divided spectrum (^1DD) at a wavelength corresponding to the zero-crossing point of the other component. The heights h_1 and h_2 , Fig. 4, corresponding to values taken at 587 and 612.5 nm (zero-crossing points of calcium complex) are proportional to strontium concentration, and the height h_3 , Fig. 5, corresponding to value taken at 594 nm (zero-crossing point of strontium complex) is proportional to calcium concentration. By the same way, with the use of Sr-AC complex as a divisor, ^1DD values obtained at 602.5 (zero-crossing point for calcium complex) are proportional to magnesium concentration.

Table 2

Results of analyzing synthetic mixtures prepared in our laboratory containing varying amounts of Sr, Mg and Ca using the proposed method.

Composition of mixture (mg L^{-1})			0.5 mg L^{-1} Mg (divisor)				3.5 mg L^{-1} Sr (divisor)			
Sr	Mg	Ca	$^1\text{DD}_{587 \text{ nm}}$		$^1\text{DD}_{594 \text{ nm}}$		$^1\text{DD}_{602.5 \text{ nm}}$		$^1\text{DD}_{594 \text{ nm}}$	
			Sr, found (mg L^{-1})	Recovery (%)	Ca, found (mg L^{-1})	Recovery (%)	Mg, found (mg L^{-1})	Recovery (%)	Ca, found (mg L^{-1})	Recovery (%)
1.5	1.0	2.0	1.52	101.3	1.91	95.50	0.97	97.00	1.92	96.00
7.0	1.0	2.0	6.97	99.57	1.96	98.00	0.98	98.00	1.97	98.50
10	1.0	2.0	9.98	99.80	1.95	97.50	0.99	99.00	1.95	97.50
18	1.0	2.0	18.1	100.5	1.92	96.00	0.96	96.00	1.93	96.50
4.0	0.5	2.0	4.05	101.2	2.05	102.5	0.49	98.00	2.03	101.5
4.0	2.0	2.0	3.98	99.50	1.97	98.50	1.95	97.50	2.00	100.0
4.0	3.5	2.0	3.99	99.75	1.98	99.00	3.44	98.28	1.99	99.50
4.0	5.0	2.0	3.95	98.75	1.92	96.00	4.46	89.20	1.94	97.00
4.0	1.0	2.0	4.03	100.7	1.99	99.50	0.94	94.00	1.98	99.00
4.0	1.0	4.0	3.97	99.25	3.97	99.25	0.99	99.00	3.98	99.50
4.0	1.0	6.0	3.96	99.00	5.94	99.00	0.97	97.00	5.95	99.16
4.0	1.0	8.0	3.91	97.75	7.90	98.75	0.95	95.00	7.92	99.00

Table 3
Statistical data for calibration graphs.

Regression equations	<i>r</i>	<i>S_m</i>	<i>S_b</i>
Standard divisor 0.5 mg L ⁻¹ Mg			
¹ DD ₅₈₇ = 3.89 × 10 ⁻³ C _{Sr} - 0.01775	0.9998	2 × 10 ⁻⁴	2 × 10 ⁻⁵
¹ DD _{612.5} = 1.19 × 10 ⁻² C _{Sr}	0.9999	1 × 10 ⁻³	5 × 10 ⁻⁷
¹ DD ₅₉₄ = 2.79 × 10 ⁻³ C _{Ca} + 7.5 × 10 ⁻³	0.9997	3 × 10 ⁻⁴	1 × 10 ⁻⁴
Standard divisor 3.5 mg L ⁻¹ Sr			
¹ DD _{602.5} = 0.0206C _{Mg} + 0.011	0.9999	2 × 10 ⁻³	1 × 10 ⁻³
¹ DD ₅₉₄ = 4.58 × 10 ⁻³ C _{Ca} + 7 × 10 ⁻³	0.9998	5 × 10 ⁻³	2 × 10 ⁻⁴

¹DD: the first-derivative divided signal; C_{Sr}: Sr concentration (mg L⁻¹); C_{Mg}: Mg concentration (mg L⁻¹); C_{Ca}: Ca concentration (mg L⁻¹); *r*: regression coefficient; *S_m*: standard deviation of slope; *S_b*: standard deviation of intercept.

In order to test the validity of the method, several synthetic mixtures of strontium, magnesium and calcium were prepared and tested between 1.5 and 18 mg L⁻¹ for strontium, 0.5–5 mg L⁻¹ for magnesium and 1.0–8.0 mg L⁻¹ for calcium in the ternary mixture (Table 2). Mean recoveries and the relative standard deviations were found to be 101 and 0.72 for strontium, 98 and 0.64 for calcium using Mg-AC as a divisor, also 99 and 0.98 for magnesium, 99.6 and 0.87 for calcium using Sr-AC as a divisor.

3.8.3. Effect of divisor

The standard spectrum of any of the three components can be used as a divisor. Favorable results were obtained using the standard spectrum of strontium (2.0–5.0 mg L⁻¹) or magnesium (0.2–1.0 mg L⁻¹). In consequence we used 3.5 mg L⁻¹ strontium and 0.5 mg L⁻¹ magnesium as suitable values of the divisor concentrations for obtaining the ratio spectra. In such cases a good recovery was obtained.

3.8.4. Calibration graphs and statistical analysis of the results

The calibration graphs, prepared by plotting the first-derivative divided value, ¹DD, (*h*) versus strontium, magnesium or calcium concentration gave a straight line passing through the origin confirming the mutual independence of the derivative signals of the three complexes. The calibration graphs obtained were linear over a range of 1.5–18 mg L⁻¹ of strontium, 0.5–5 mg L⁻¹ of magnesium and 1–8 mg L⁻¹ of calcium. A critical evaluation of the proposed method as obtained by statistical analysis of the experimental results is given in Table 3. The detection limits (at the 95% confidence level) of the proposed method for the mean of five analyses were determined [33,34]. The calculated detection limits are 25 ng mL⁻¹ for strontium and 42 ng mL⁻¹ for calcium using Mg-complex as a divisor, and 36 ng mL⁻¹ for magnesium using Sr-complex as a divisor.

4. Applications

The potential of AC as a reagent for the direct spectrophotometric determination of strontium prompted us to explore the

Table 4
Spectrophotometric determination of SrO, MgO and CaO in some Portland cement materials.

Material	Strontium determination (%SrO), statistical term			Magnesium determination (%MgO), statistical term			Calcium determination (%CaO), statistical term		
	<i>x</i> ⁻	<i>s</i>	95% CI	<i>x</i> ⁻	<i>s</i>	95% CI	<i>x</i> ⁻	<i>s</i>	95% CI
Cement (OPC)	0.1200	1.0 × 10 ⁻³	<i>x</i> ⁻ ± 0.0010	3.52	5.8 × 10 ⁻²	<i>x</i> ⁻ ± 0.06	60.8	0.42	<i>x</i> ⁻ ± 0.4
NIST SRM cement									
1886	0.1040	1.4 × 10 ⁻³	<i>x</i> ⁻ ± 0.0014	1.64	4.7 × 10 ⁻²	<i>x</i> ⁻ ± 0.05	65.1	0.33	<i>x</i> ⁻ ± 0.3
1885	0.0378	5.0 × 10 ⁻⁴	<i>x</i> ⁻ ± 0.0005	4.11	7.0 × 10 ⁻²	<i>x</i> ⁻ ± 0.07	62.2	0.45	<i>x</i> ⁻ ± 0.5
1881	0.1043	1.5 × 10 ⁻³	<i>x</i> ⁻ ± 0.0015	2.64	5.0 × 10 ⁻²	<i>x</i> ⁻ ± 0.05	57.4	0.35	<i>x</i> ⁻ ± 0.4

Number of determinations for each sample: *n* = 5. *x*⁻: mean recovery; *s*: standard deviation. Test solutions of the samples investigated contained 0.2–1.0 mg of cement material per 25 mL. Certified amounts (%SrO): SRM 1886, 0.11; 1885, 0.037; 1881, 0.11; (%MgO): SRM 1886, 1.60; 1885, 4.02; 1881, 2.63; (%CaO): SRM 1886, 67.43; 1885, 62.14; 1881, 58.67.

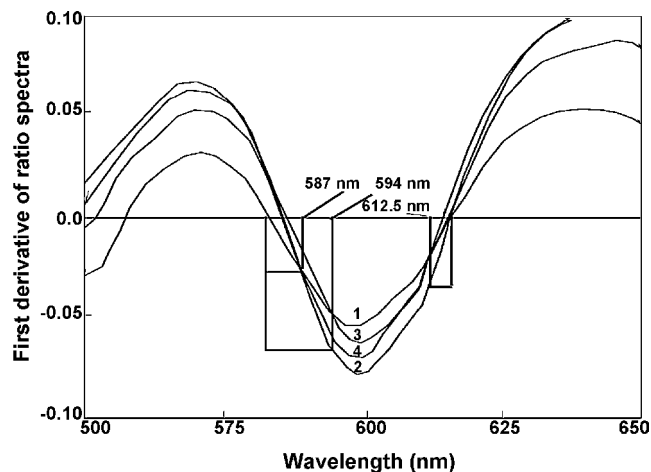


Fig. 6. First-derivative ratio spectra of (1) ordinary Portland cement sample, (2) 1881 SRM, (3) 1885 SRM, and (4) 1886 SRM-AC complexes using 0.5 mg L⁻¹ Mg(II) as divisor, [AC] = 4 × 10⁻⁴ mol L⁻¹, 40% (v/v) ethanol, 0.1 mol L⁻¹ (NaClO₄), pH 9.5.

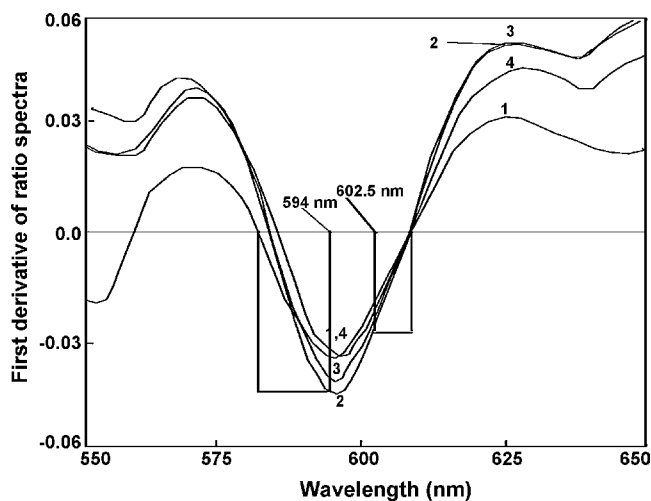


Fig. 7. First-derivative ratio spectra of (1) ordinary Portland cement sample, (2) 1881 SRM, (3) 1885 SRM, and (4) 1886 SRM-AC complexes using 3.5 mg L⁻¹ Sr(II) as divisor, [AC] = 4 × 10⁻⁴ mol L⁻¹, 40% (v/v) ethanol, 0.1 mol L⁻¹ (NaClO₄), pH 9.5.

applicability of the method for determination of strontium and simultaneous determination of SrO, MgO and CaO content in Portland cement. The validity of first-derivative ratio spectra zero-crossing method was thoroughly examined. Replicate analysis of ordinary Portland and NIST cement samples SRM 1881, 1885 and 1886 were performed (representative spectra are shown in Figs. 6 and 7). SrO, MgO and CaO concentrations were determined by measuring ¹DD signals at appropriate wavelengths and using the

regression equations indicated in Table 3. Using Mg–Ac complex as a divisor, Fig. 6, SrO concentration determined by measuring ¹DD signals at 587 and 612.5 nm (zero-crossing points for calcium complex), and the concentration of CaO was determined by measuring ¹DD signal at 594 nm (zero-crossing point of strontium complex). The concentration of MgO was determined by using Sr–AC complex as a divisor, Fig. 7, and measuring ¹DD signal at 602.5 nm (zero-crossing point of for calcium complex). In the precision study, five determinations were carried out for each sample (Table 4). A good precision of the proposed method was obtained, which allow the application of the method to the routine analysis of cement.

5. Conclusion

Using the proposed method, it is possible to determine Sr, Mg, and Ca simultaneously in mixtures containing 1.5–18 μg mL⁻¹ strontium, 0.5–5.0 μg mL⁻¹ magnesium and 1.0–8.0 μg mL⁻¹ calcium. Simplicity, sensitivity, large range of linearity besides accuracy and precision are the main advantages of the proposed method.

This paper demonstrate the potential of the first-derivative ratio spectrophotometry as an analytical technique and its usefulness to accurate, rapid, simple and simultaneous quantification of SrO, MgO and CaO in Portland cement.

References

- [1] American Society for Testing and Materials (ASTM), Annual Book of ASTM Standards, vol. 04.01, C-114, Philadelphia, PA, USA, 2004.
- [2] Z. Grahek, M.R. Macefat, Anal. Chim. Acta 534 (2005) 271.
- [3] M. Macka, B. Paull, P. Andersson, P.R. Haddad, J. Chromatogr. A 767 (1997) 303.
- [4] P. Jones, M. Foulkes, B. Poull, J. Chromatogr. 637 (1994) 173.
- [5] P. Robinson, Chem. Geol. 28 (1980) 135.
- [6] Z. Arslan, J.F. Tyson, Talanta 50 (1999) 929.
- [7] H. Sedaira, Talanta 51 (2000) 39.
- [8] N.K. Agnihotri, S. Ratnani, V.K. Singh, H.B. Singh, Anal. Sci. 9 (2003) 1297.
- [9] H. Eskandari, A.G. Saghseloo, Anal. Sci. 19 (2003) 1513.
- [10] A. Bhalotra, B.K. Puri, Microchim. Acta 134 (2000) 139.
- [11] M. Benamor, N. Aguerssif, Spectrochim. Acta A 69 (2008) 676.
- [12] T.C. O'Haver, Anal. Proc. 19 (1982) 22.
- [13] H. Ishii, K. Satoh, Z. Anal. Chem. 312 (1982) 114.
- [14] P. Levilain, D. Fompeydie, Analusis 14 (1986) 1.
- [15] T.C. O'Haver, G.L. Green, Anal. Chem. 48 (1976) 312.
- [16] J. Medinilla, F. Ales, F. Garcia Sanchez, Talanta 33 (1986) 329.
- [17] F.G. Sanchez, M.H. Lopez, J.C.M. Gomez, Talanta 34 (1987) 639.
- [18] F. Salinas, J.J. Berezas, A. Espinosa-Mansilla, Talanta 37 (1990) 347.
- [19] J.J. Berezas Nevada, C.G. Cabanillas, F. Salinas, Talanta 39 (1992) 547.
- [20] H. Wada, H. Mori, G. Nakagawa, Anal. Chim. Acta 172 (1985) 297.
- [21] H.-W. Gao, J. Braz. Chem. Soc. 13 (2002) 78.
- [22] V.Y. Fain, V.G. Avakyan, B.E. Zaitsev, M.A. Ryabov, Russ. J. Coord. Chem. 30 (2004) 671.
- [23] K. Shimada, T. Shimoda, H. Kokusen, S. Nakano, Talanta 66 (2005) 80.
- [24] H. Sedaira, K.A. Idriss, M.S. Abdel-Aziz, Analyst 121 (1996) 1079.
- [25] K.A. Idriss, E.Y. Hashem, M.S. Abdel-Aziz, H.M. Ahmed, Analyst 125 (2000) 221.
- [26] K.A. Idriss, H. Sedaira, H.M. Ahmed, Talanta 54 (2001) 369.
- [27] A.I. Vogel, Text Book of Quantitative Chemical Analysis, 5th ed., ELBS, London, 1988.
- [28] NIST, Certificate of Analysis, SRMs, 1881, 1885, 1886, National Institute of Standards and Technology, Gaithersburg, MD, USA, 1989.
- [29] K.A. Idriss, M.K. Hassan, M.S. Abu-Bakr, H. Sedaira, Analyst 109 (1984) 1389.
- [30] P. Voznica, J. Havel, L. Sommer, Collect. Czech. Chem. Commun. 45 (1980) 54.
- [31] K.A. Idriss, M.M. Sleim, M.S. Saleh, M.S. Abu-Bakr, H. Sedaira, Analyst 113 (1988) 1643.
- [32] K.A. Idriss, E. Hashem, M.Sh. Abdel Aziz, H.M. Ahmed, Analyst 125 (2000) 221.
- [33] D.A. Skoog, D.M. West, F.J. Moller, Fundamentals of Analytical Chemistry, 6th ed., Saunders, Florida, 1992.
- [34] American Society for Testing and Materials (ASTM), Annual Book of ASTM Standards, vol. 03.06, E-876, PA, USA, 1997.



Artificial neural networks in analysis of indinavir and its degradation products retention

B. Jančić-Stojanović^{a,*}, D. Ivanović^a, A. Malenović^a, M. Medenica^b

^a Faculty of Pharmacy, Department of Drug Analysis, Vojvode Stepe 450, 11000 Belgrade, Serbia

^b Faculty of Pharmacy, Department of Physical Chemistry, Vojvode Stepe 450, 11000 Belgrade, Serbia

ARTICLE INFO

Article history:

Received 10 March 2008

Received in revised form 4 June 2008

Accepted 30 October 2008

Available online 17 November 2008

Keywords:

Experimental design

Artificial neural networks

Liquid chromatography

Indinavir

Degradation products

ABSTRACT

Artificial neural networks (ANN) are biologically inspired computer programs designed to simulate the way in which the human brain processes the information. In the past few years, coupling of experimental design (ED) and ANN became useful tool in the method optimization. This paper presents the application of ED-ANN in analysis of chromatographic behavior of indinavir and its degradation products. According to preliminary study, full factorial design 2^4 was chosen to set input variables for network training. Experimental data (inputs) and results for retention factors from experiments (outputs) were used to train the ANN with aim to define correlation among variables. For networks training multi-layer perceptron (MLP) with back propagation (BP) algorithm was used. Network with the lowest root mean square (RMS) had 4–8–3 topology. Predicted data were in good agreement with experimental data (correlation was higher than 0.9713 for training set). Regression statistics confirmed good ability of trained network to predict compounds retention.

© 2008 Elsevier B.V. All rights reserved.

1. Introduction

Analysis of chromatographic retention of active substance and its impurities demands serious access because of similar structure, similar physical and chemical properties as well as huge difference in concentration level. Application of experimental design (ED) in the first phase of investigation enables extraction of important data about the system. Usually, number of experiments required for ED is up to 20 (for full factorial design or central composite design if the number of factors is three or four). It is well known that many factors can influence to chromatographic separation. However, it is possible to reduce the number of factors, because in many cases only a few factors really significantly influence to chromatographic analysis. The second stage in method development is optimization. With a view to optimize method the appropriate ED can be used in combination with artificial neural networks [1–6]. Significance of proposed approach and all the mathematical methods for optimization are reviewed [7]. Generally, artificial neural networks are applicable in many area of pharmacy, such as the optimization of formulation parameters [8–11] or definition of the quantitative structure–retention relationship (QSRR) [12,13] and so on.

Analysis of indinavir in pharmaceutical dosage forms was presented only in three papers [14–16]. Our previous paper was the first dealing with the determination of degradation products in capsules [15]. On the other hand, a lot of published papers concern analysis of indinavir and its metabolites in biological fluids [17–23] or indinavir in combination with other anti-HIV drugs in biological fluids [24–51]. In those methods the various isocratic and gradient modes of elution column packing and detectors were employed.

The main goal of this study was to develop and describe effective approach to examine and predict chromatographic separation of indinavir and its degradation products, *cis*-aminoindanol and lactone (Fig. 1). For that purpose coupling of experimental design and artificial neural networks was used. The authors wanted to confirm all the presumed advantages of such approach, because multi-objective simultaneous optimization enables prediction of non-linear relationship between causal factors and response variables, i.e. chromatographic behavior of the investigated substances.

2. Theory

2.1. Experimental design and artificial neural networks

In definition of chromatographic separation, when the number of influencing factors can be limited up to four, application of full factorial design (FFD) is recommended. In FFD each factor is anal-

* Corresponding author. Tel.: +381 11 3951 333; fax: +381 11 3972 840.
E-mail address: jancic.stojanovic@pharmacy.bg.ac.yu (B. Jančić-Stojanović).

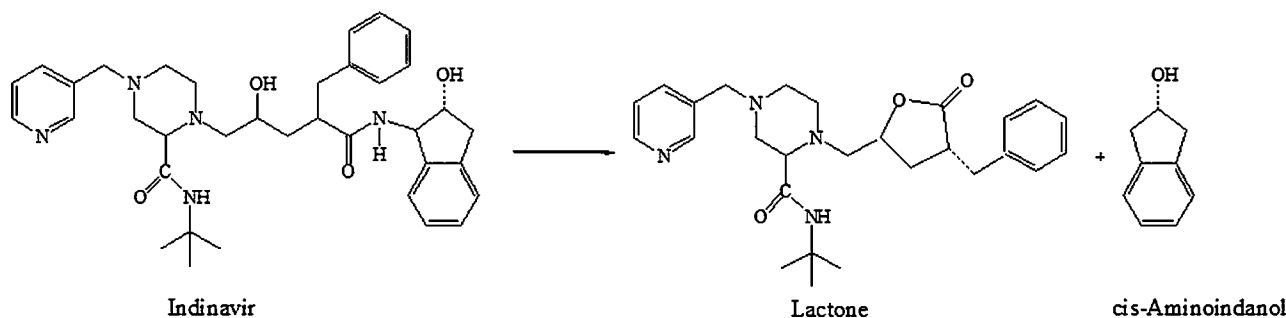


Fig. 1. Structures of indinavir, lactone and *cis*-aminoindanol.

Table 1
Factors and their lower (–) and upper (+) level.

Symbol	Factors	Factors levels	
		(–)	(+)
x_1	Temperature (°C)	20	50
x_2	pH of the water phase	6.0	8.4
x_3	Content of SDS (g L ⁻¹)	0.8	2.2
x_4	Acetonitrile (%)	32	45

used in two levels (in coded units +1 or –1). That means that the number of experiments will be 2^n , where n presents the number of factors being investigated. Using FFD, not only basic effects but also interactive effects of given factors, with maximum precision, can be estimated. In this case the experiments were conducted according to 2^4 FFD. Experimental data (inputs) and results from experiments (outputs) were used to train the ANN with aim to define correlation among variables. This paper present application of, perhaps the most popular architecture in use, multi-layer perceptrons (MLP). MLP as architecture with supervised learning, can be trained with different kind of algorithm, but the most often used in analytical application is backpropagation algorithm (BP). Such kind of network has one input layer, one or more hidden layers and one output layer. Each layer has a few units corresponding to neurons. The units in neighbouring layers are fully interconnected with links corresponding to synapses. The strengths of connections between two units are called “weights” [10]. Training of ANN is performed by adjusting weights in order to minimize the RMS of the training data and on that way prevent the same error happening again. When the

network fulfills the appropriate demands, it is presumed that it has good predictive capabilities and ability to accurately describe the system.

3. Experimental

3.1. Reagents and samples

All reagents used were of an analytical grade. Acetonitrile: gradient grade (Lab Scan, Ireland), water: HPLC grade, sodium-dodecylsulphate (SDS) (Merck, Darmstadt, Germany), triethylamine (TEA) (Merck, Darmstadt, Germany) and orthophosphoric acid (Carlo Erba, Milan, Italy) were used to prepare a mobile phase. Working standards of indinavir monohydrate, lactone and *cis*-aminoindanol were obtained from Merck Sharp & Dohme Ltd., Hertford Road Hoddesdon, United Kingdom.

3.2. Chromatographic conditions

The chromatographic system Hewlett Packard 1100 (Agilent, Technologies, Germany) consisted of HP 1100 pump, HP 1100 UV–vis detector and HP ChemStation integrator. Separations were performed on a X Terra™ 4.6 mm × 150 mm, 5 μm particle size column. The flow rate was 1.25 mL min⁻¹ with UV detection at 214 nm. The samples were introduced through a Rheodyne injector valve with a 20 μL sample loop.

Water phase was prepared as follows: appropriate mass of SDS was dissolved in water, than 0.3 mL L⁻¹ of TEA was added and pH was adjusted with orthophosphoric acid. After that, acetonitrile

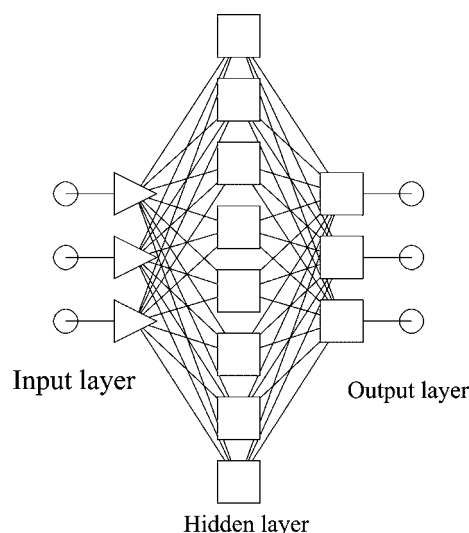
Table 2
Matrix for experiments for a full factorial design 2^4 and the obtained results.

No. exp.	x_1	x_2	x_3	x_4	Responses		
					k_1	k_2	k_3
1	–1	–1	–1	–1	12.53	11.06	4.19
2	+1	–1	–1	–1	10.30	10.30	3.02
3	–1	+1	–1	–1	8.46	9.97	2.09
4	+1	+1	–1	–1	8.75	9.34	1.03
5	–1	–1	+1	–1	10.77	10.77	4.93
6	+1	–1	+1	–1	8.59	8.59	4.93
7	–1	+1	+1	–1	7.85	9.16	3.11
8	+1	+1	+1	–1	7.86	8.48	1.50
9	–1	–1	–1	+1	2.83	3.62	1.53
10	+1	–1	–1	+1	2.74	3.33	0.78
11	–1	+1	–1	+1	1.82	2.49	0.52
12	+1	+1	–1	+1	2.07	2.64	0.49
13	–1	–1	+1	+1	2.26	2.93	1.13
14	+1	–1	+1	+1	2.76	2.76	1.17
15	–1	+1	+1	+1	2.83	2.83	1.0
16	+1	+1	+1	+1	1.89	1.89	0.33

k_1 , retention factor of indinavir; k_2 , retention factor of lactone; k_3 , retention factor of *cis*-aminoindanol.

Table 3
Calculated factor effects.

Factor effects	Indinavir	Lactone	cis-Aminoindanole
b_0	5.894	6.26	1.984
b_1	-0.274	-0.344	-0.328
b_2	-0.703	-0.41	-0.726
b_3	-0.293	-0.334	0.278
b_4	-3.494	-3.449	-1.116
b_{12}	0.226	0.081	-0.093
b_{13}	0.052	-0.152	0.048
b_{23}	0.209	0.074	-0.052
b_{14}	0.239	0.187	0.152
b_{24}	0.456	0.061	0.442
b_{34}	0.328	0.125	-0.239
b_{123}	-0.132	0.01	-0.197
b_{124}	-0.363	-0.122	0.094
b_{134}	-0.023	0.031	-0.029
b_{234}	-0.037	0.033	0.093
b_{1234}	-0.091	-0.161	0.018

**Fig. 2.** Graphical presentation of network.

trile was added and mobile phase was degassed on ultrasonic bath for 15 min. Mobile phase was filtered through a 0.2 μm Millipore membrane filter.

Laboratory mixture was prepared of 0.6 mg mL^{-1} of indinavir, 9 $\mu\text{g mL}^{-1}$ of lactone and 3 $\mu\text{g mL}^{-1}$ of cis-aminoindanol in mixture of acetonitrile–water (35:65, v/v).

4. Results and discussion

In evaluation of liquid chromatographic method analysis of chromatographic retention takes an important part. As many factors could influence on retention and separation, experimentators experience is indispensable for extraction of three or four important factors during appropriately conducted preliminary investigations. When the factors and their regions are settled, adequate method optimization has to be selected. There are many literature data dealing with different kinds of ED such as full factorial, fractional, central composite, Plackett–Burman and so on employed in method optimization. In last decade, the combination of ED and ANN as a powerful technique in method optimization can be found in literature. The most important is that coupling ED and ANN offers more informations then ED alone and that ED–ANN can handle linear and non-linear models also.

In this study of indinavir and its degradation products, lactone and cis-aminoindanol, the chromatographic retention was analysed by ED–ANN. During the preliminary investigations some chromatographic parameters, like column characteristics, flow rate and detection wavelength were defined. As important factors the mobile phase composition (acetonitrile content, SDS concentration and pH of the water phase) and column temperature were extracted [15]. The influence of four selected factors on retention factor (k) was examined. Factors and their levels are presented in Table 1.

Matrix of experiment and obtained results for k are given in Table 2.

Factor effects presenting coefficients of appropriate mathematical model (Eq. (1)) were calculated (Table 3). Mathematical model had the following form:

$$y = b_0 + b_1x_1 + b_2x_2 + b_3x_3 + \dots + b_{N-1}x_{N-1} + b_Nx_N + b_{12}x_1x_2 + b_{13}x_1x_3 + b_{23}x_2x_3 + \dots + b_{(N-1)N}x_{N-1}x_N \quad (1)$$

where y presents the estimate response, b_0 the average experimental response, the coefficients b_1 – b_N are the estimated effects of the factors considered and the extend to which these terms affect the

Table 4
Retention factor values predicted by ANN and corresponding errors.

Predicted k values			Errors		
Indinavir	Lactone	cis-Aminoindanol	Indinavir	Lactone	cis-Aminoindanol
11.52	11.37	4.11	-1.00	0.317	-0.08
10.77	10.13	3.09	0.47	-0.169	0.07
9.01	10.02	2.02	0.55	0.055	-0.06
8.31	8.87	1.20	-0.44	-0.467	0.169
10.57	10.67	4.87	-0.19	-0.10	-0.06
9.92	9.59	3.87	1.33	1.00	-1.06
8.06	9.33	2.72	0.21	0.17	-0.39
7.44	8.41	1.74	-0.42	-0.07	0.241
4.45	4.68	1.72	1.62	1.06	0.19
4.25	4.15	1.01	1.51	0.82	0.228
2.22	3.15	0.33	0.397	0.66	-0.188
2.02	2.64	-0.14	-0.04	0.00	-0.63
3.24	3.67	2.27	0.981	0.74	1.14
2.61	2.69	1.40	-0.14	-0.066	0.24
1.16	2.44	0.50	-1.67	-0.39	-0.50
0.56	1.52	-0.09	-1.33	-0.367	-0.42
11.52	11.38	4.11	-1.01	0.317	-0.08
10.77	10.13	3.09	0.47	-0.169	0.07

performance of the method is called main effect. The coefficients $b_{12}–b_{(N-1)N}$ are called the interaction terms [52].

The obtained effects indicate the strongest influence of acetonitrile content in mobile phase on chromatographic retention. The second important factor was pH of the water phase. Two other factors, content of SDS and column temperature had low influence on retention.

Hereafter, chromatographic conditions (input) defined by matrix of experiment and resulting k (outputs) were used to train ANN. Multiple layer perceptron architecture with three layers was chosen. First layer was input layer consisting of four nodes which present factors to be analysed (acetonitrile content, SDS concentration, pH of the water phase and column temperature), second is hidden layer of which the nodes will be determined during training and the third is output layer consisting of three nodes (retention factors for indinavir, lactone and *cis*-aminoindanol). In order to define the optimal network three groups of experiments were selected. One group had 10 experiments and it was used for network training, two other groups of three data were used for network testing and verification. The number of experiments in each group can be varied and in this case it was defined during the preliminary study. MLP feed forward network with the back-propagation (BP) learning algorithm was used for network training. The number of nodes in hidden layer was optimized and the network with the smallest RMS had eight nodes. Network with 4–8–3 topology was defined as optimal and its graphical presentation is given in Fig. 2.

During the network training, the difference between predicted and obtained results was observed to define the optimal number of epochs and learning rate. The momentum was settled at 0.3 in the beginning of the training and kept constant all the time. Training was stopped at 88 epochs and at 0.1 values for learning rate when the correlations for training cases were 0.9860 for indinavir, 0.9943 for lactone and 0.9713 for *cis*-aminoindanol. The results for predicted k values and corresponding errors are presented in Table 4.

Experimental data vs. predicted data had the good correlation (0.9673 for indinavir, 0.9903 for lactone and 0.9499 for *cis*-aminoindanol) and appropriate graphs are presented in Fig. 3A–C for indinavir, lactone and *cis*-aminoindanol, respectively.

Regression statistics for training, verification and testing sets are given in Table 5.

The weight distribution was between -1.25 and $+1.25$.

According to the coefficients of the mathematical model acetonitrile content in the mobile phase and pH of the water phase were distinguished as important factors, and on the basis of the predicted values obtained with ANN 3D graphs for the investigated substances were constructed (Fig. 4A–C for indinavir, lactone and *cis*-aminoindanol, respectively).

Temperature and content of SDS as the factors with significant influence were set at 20°C and 1.6 g L^{-1} , respectively. Two other factors must be considerably set in order to maintain system performances. Chromatogram of laboratory mixture where the content

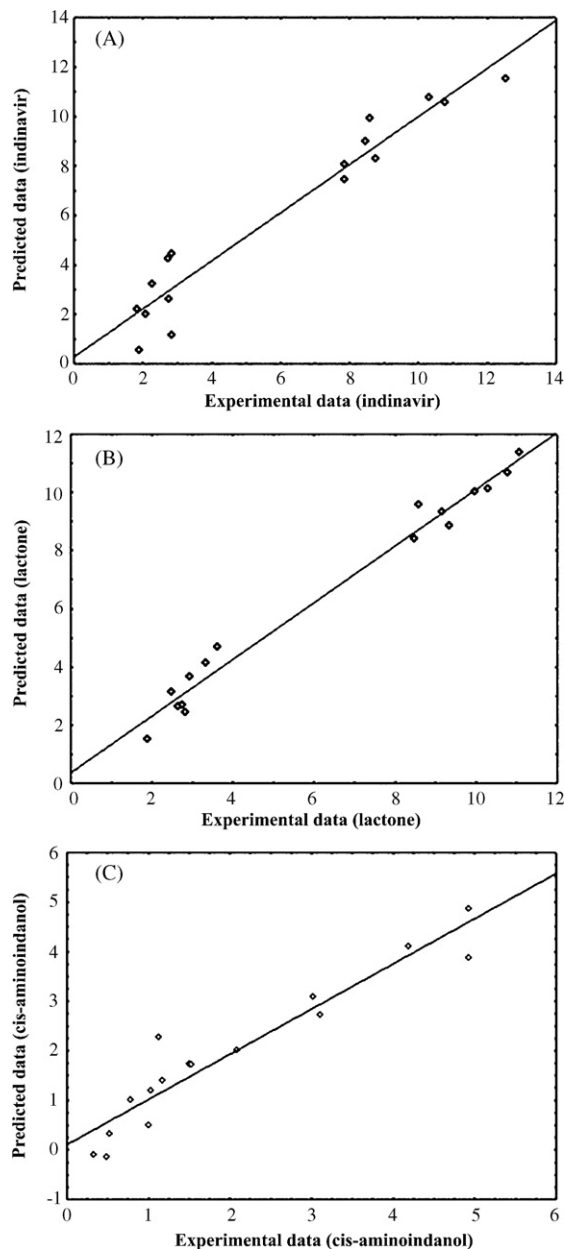


Fig. 3. Correlation of observed retention factor vs. ANN predicted retention factors for (A) indinavir, (B) lactone and (C) *cis*-aminoindanol.

Table 5
Regression statistics for training (Tr.), verification (Vr.) and testing (Te.) set.

	Indinavir			Lactone			<i>cis</i> -Aminoindanol		
	Tr.	Vr.	Te.	Tr.	Vr.	Te.	Tr.	Vr.	Te.
Data mean	7.301	4.803	2.300	7.622	5.263	2.717	2.595	1.187	0.747
Data S.D.	3.801	3.418	0.426	3.547	3.553	0.743	1.703	0.298	0.401
Error mean	0.116	-0.163	0.389	0.179	0.067	0.397	-0.193	-0.047	0.314
Error S.D.	0.634	1.664	1.511	0.379	0.859	0.663	0.405	0.393	0.786
Abs. E. mean	0.478	1.244	1.274	0.262	0.638	0.641	0.303	0.287	0.597
S.D. ratio	0.170	0.487	3.545	0.107	0.242	0.891	0.238	1.319	1.959
Correlation	0.9860	0.8880	0.9462	0.9943	0.9717	0.9952	0.9713	0.8486	0.9939

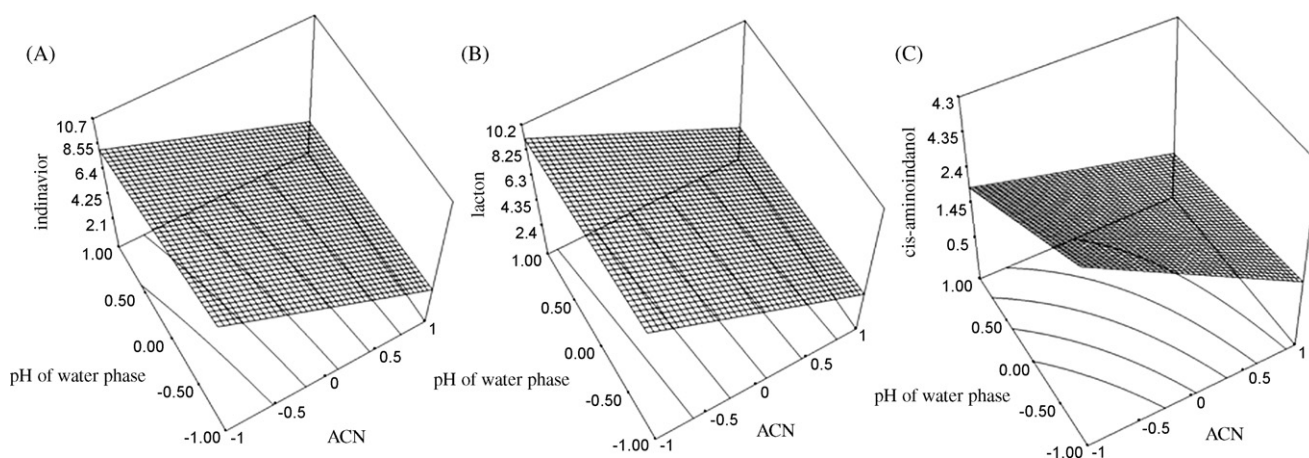


Fig. 4. 3D graph: (A) $k(\text{indinavir}) = f(\% \text{ ACN}, \text{pH of the water phase})$; (B) $k(\text{lactone}) = f(\% \text{ ACN}, \text{pH of the water phase})$; (C) $k(\text{cis-aminoindanol}) = f(\% \text{ ACN}, \text{pH of the water phase})$.

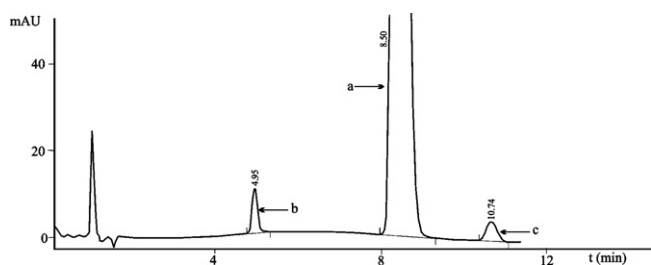


Fig. 5. The chromatogram of laboratory mixture of (A) indinavir (B) *cis*-aminoindanol and (C) lactone (mobile phase: acetonitrile–water phase (35:65, v/v); water phase consisted of 1.6 g L^{-1} SDS, 0.3 mL L^{-1} TEA and pH of the water phase was adjusted to 7.0 with orthophosphoric acid, flow rate 1.25 mL min^{-1} ; UV detection 214 nm).

of acetonitrile in mobile was 35% (v/v) and pH of the water phase 7.0 is given in Fig. 5.

5. Conclusion

ED–ANN presents useful tool in many areas of pharmacy. In this paper, authors presented the modality of ED–ANN application in analysis of indinavir and its degradation products (lactone and *cis*-aminoindanol) retention. The study indicated that ED alone offer important data about the investigated system. However, after coupling with ANN prediction of chromatographic retention, as the most significant information, can be easily done. This paper describes complete procedure for ED–ANN employment in method evaluation. In this situation, FFD 2^4 design with ANN trained by BP algorithm was applied. The optimal network with the lowest RMS had 4–8–3 topology. Regression statistics for training, verification and testing sets gave acceptable results. The obtained network has good ability to predict chromatographic retention of active substance, its structurally similar degradation product lactone and the most polar compound in mixture *cis*-aminoindanol.

Acknowledgement

The authors thank to Ministry of Science for supporting these investigations in Project 142077G.

References

- [1] A.B. Hamed, S. Elost, J. Havel, J. Chromatogr. A 1084 (2005) 7.
- [2] K. Novotna, J. Havliš, J. Havel, J. Chromatogr. A 1096 (2005) 50.

- [3] E. Marengo, V. Gianotti, S. Angioi, M.C. Gennaro, J. Chromatogr. A 1029 (2004) 57.
- [4] A.T.K. Tran, R.V. Hyne, F. Pablo, W.R. Day, P. Doble, Talanta 71 (2006) 1268.
- [5] J. Havel, J.E. Madden, P.R. Haddad, Chromatographia 49 (1999) 481.
- [6] H. Wang, W. Liu, J. Sep. Sci. 27 (2004) 1189.
- [7] A.M. Siouffi, R. Phan-Tan-Luu, J. Chromatogr. A 892 (2000) 75.
- [8] N. Arulsudar, N. Subramanian, R.S.R. Murthy, J. Pharm. Pharmaceut. Sci. 8 (2005) 243–258.
- [9] B.D. Glass, S. Agatonovic-Kustrin, M.H. Wisch, Curr. Drug Discov. Technol. 2 (3) (2005) 195.
- [10] K. Takayama, M. Fujikawa, T. Nagai, Pharmaceut. Res. 16 (1) (1999) 1.
- [11] M. Gašperlin, L. Tušar, M. Tušar, J. Kristl, J. Šmid-Korbar, Int. J. Pharm. 168 (1998) 243.
- [12] S.Z. Tham, S. Agatonovic-Kustrin, J. Pharm. Biomed. Anal. 28 (2002) 581.
- [13] F. Ruggieri, A.A. D'Archivio, G. Carlucci, P. Mazzeo, J. Chromatogr. A 1076 (2005) 163.
- [14] D.M. Kreuz, A.L. Howard, D. Ip, J. Pharm. Biomed. Anal. 19 (1999) 725.
- [15] B. Jančić, M. Medenica, D. Ivanović, A. Malenović, Chromatographia 62 (2005) 233.
- [16] R. Yekkala, H. Lei, J. Hoogmartens, E. Adams, J. Pharm. Biomed. Anal. 42 (2006) 71–80.
- [17] D.M. Burger, M. De Graaff, E.W. Wuis, P.P. Koopmans, Y.A. Hekster, J. Chromatogr. B: Biomed. Appl. 703 (1997) 235.
- [18] M.L. Foisy, J.P. Sommadossi, J. Chromatogr. B: Biomed. Sci. Appl. 721 (1999) 239.
- [19] M.R. Fizzano, L. Valvo, M.L. Dupuis, V. Mennella, M. Cianfriglia, J. Pharm. Biomed. Anal. 22 (2000) 307.
- [20] L. Zhong, K.C. Yeh, J. Chromatogr. B: Biomed. Sci. Appl. 734 (1999) 63.
- [21] I. Fu, E.J. Woolf, B.K. Matuszewski, J. Pharm. Biomed. Anal. 18 (1998) 347.
- [22] X. Yu, D. Cui, M.R. Davis, J. Am. Soc. Mass Spectrom. 10 (1999) 175.
- [23] A.L. Jayewardene, B. Kearney, J.A. Stone, J.G. Gambertoglio, F.T. Aweeka, J. Pharm. Biomed. Anal. 25 (2001) 309.
- [24] U.S. Justesen, C. Pedersen, N.A. Klitgaard, J. Pharm. Biomed. Anal. 783 (2003) 491.
- [25] R. Panchagnula, T. Bansal, M.V.S. Varma, C. Lal Kaul, J. Chromatogr. B 806 (2004) 277.
- [26] J. Faux, N. Venisse, G. Le Moal, A. Dupuis, S. Bouquet, Chromatographia 58 (2003) 421.
- [27] P.W.H. Hugen, C.P.W.G.M. Verweij-van Wissen, D.M. Burger, E.W. Wuis, P.P. Koopmans, Y.A. Hekster, J. Chromatogr. B: Biomed. Appl. 727 (1999) 139.
- [28] M. Sarasa-Nacenta, Y. Lopez-Pua, J. Mallolas, J.L. Blanco, J.M. Gatell, X. Carne, J. Chromatogr. B: Biomed. Appl. 757 (2001) 325.
- [29] E. Dailly, L. Thomas, M.F. Kergueris, P. Jolliet, M. Bourin, J. Chromatogr. B: Biomed. Appl. 758 (2001) 129.
- [30] P. Langmann, H. Klinker, D. Schirmer, M. Zilly, A. Bienert, E. Richter, J. Chromatogr. B: Biomed. Appl. 735 (1999) 41.
- [31] C. Marzolini, A. Beguin, A. Telenti, A. Schreyer, T. Buclin, J. Biollaz, L.A. Decosterd, J. Chromatogr. B: Biomed. Sci. Appl. 774 (2002) 127.
- [32] S. Notari, A. Bocedi, G. Ippolito, P. Narciso, L.P. Pucillo, G. Tossini, R.P. Donnorso, F. Gasparrini, P. Ascenzi, J. Chromatogr. B 831 (2006) 258.
- [33] N.L. Rezk, R.R. Tidwell, A.D.M. Kashuba, J. Chromatogr. B 805 (2004) 241.
- [34] C. Marzolini, A. Telenti, T. Buclin, J. Biollaz, L.A. Decosterd, J. Chromatogr. B: Biomed. Sci. Appl. 740 (2000) 43.
- [35] M.L. Turner, K. Reed-Walker, J.R. King, E.P. Acosta, J. Chromatogr. B: Biomed. Sci. Appl. 784 (2003) 331.
- [36] J. Ray, E. Panga, D. Carey, J. Chromatogr. B: Biomed. Sci. Appl. 775 (2002) 225.
- [37] A.L. Jayewardene, F. Zhu, F.T. Aweeka, J.G. Gambertoglio, J. Chromatogr. B: Biomed. Sci. Appl. 707 (1998) 203.

- [38] R.P.G. Van Heeswijk, R.M.W. Hoetelmans, R. Harms, P.L. Meenhorst, J.W. Mulder, J.M.A. Lange, J.H. Beijnen, *J. Chromatogr. B: Biomed. Sci. Appl.* 719 (1998) 159.
- [39] G. Aymard, M. Legrand, N. Trichereau, B. Diquet, *J. Chromatogr. B: Biomed. Sci. Appl.* 744 (2000) 227.
- [40] E. Gangl, I. Utkin, N. Gerber, P. Vouros, *J. Chromatogr. A* 974 (2002) 91.
- [41] V.A. Frerichs, R. DiFrancesco, G.D. Morse, *J. Chromatogr. B: Biomed. Sci. Appl.* 787 (2003) 393.
- [42] M.J. Rose, S.A. Merschman, R. Eisenhandler, E.J. Woolf, K.C. Yeh, L. Lin, W. Fang, J. Hsieh, M.P. Braun, G.J. Gatto, B.K. Matuszewski, *J. Pharm. Biomed. Anal.* 24 (2000) 291.
- [43] J. Chi, A.L. Jayewardene, J.A. Stone, T. Motoya, F.T. Aweeka, *J. Pharm. Biomed. Anal.* 30 (2002) 675.
- [44] L. Dickinson, L. Robinson, J. Tjia, S. Khoo, D. Back, *J. Chromatogr. B* 829 (2005) 82.
- [45] S. Colombo, A. Beguin, A. Telenti, J. Biollaz, T. Buclin, B. Rochat, L.A. Decosterd, *J. Chromatogr. B* 819 (2005) 259.
- [46] K.M.L. Crommentuyn, H. Rosing, L.G.A.H. Nan-Offerga, M.J.X. Hillebrand, D.R. Huitema, J.H. Beijnen, *J. Mass Spectrom.* 38 (2003) 157.
- [47] W. Gao, T. Kishida, K. Kimura, M. Kageyama, M. Sumi, Y. Yoshikawa, N. Shibata, K. Takada, *Biomed. Chromatogr.* 16 (2002) 267.
- [48] W. Gutleben, N.D. Tuan, H. Stoiber, M.P. Dierich, M. Sarcletti, A. Zemann, *J. Chromatogr. A* 922 (2001) 313.
- [49] H. Rebiere, B. Mazel, C. Civade, P.A. Bonnet, *J. Chromatogr. B* 850 (2007) 376.
- [50] D.R. Weller, R.C. Brundage Jr.H.H., H.E. Balfour, Vezina, *J. Chromatogr. B* 848 (2007) 369.
- [51] R. Verbesselt, E. Van Wijngaerden, J. de Hoon, *J. Chromatogr. B* 845 (2007) 51.
- [52] P.W. Araujo, R.G. Brereton, *Trends Anal. Chem.* 15 (1996) 26.



Computer-aided target optimization for traditional Chinese medicine by ultra-performance liquid chromatography

Gaowa Jin^a, Xingya Xue^a, Feifang Zhang^a, Yu Jin^b, Xinmiao Liang^{a,b,*}

^a Dalian Institute of Chemical Physics, Chinese Academy of Sciences, Dalian 116023, China

^b School of Pharmacy, East China University of Science and Technology, 130 Meilong Road, Shanghai 200237, China

ARTICLE INFO

Article history:

Received 1 August 2008

Received in revised form 7 November 2008

Accepted 10 November 2008

Available online 18 November 2008

Keywords:

Target optimization

Computer-aided software

Moved overlapping separation ranging map

Traditional Chinese medicine

Ultra-performance liquid chromatography

ABSTRACT

A new strategy of target optimization was developed for resolving the separation problems of complex samples. Computer-aided target optimization for separation of complex samples by ultra-performance liquid chromatography (UPLC) was studied. Taking traditional Chinese medicine (TCM) (*Rhizoma Coptidis*) as an example, separation conditions of target compounds – overlapping peaks and all components – were optimized based on moved overlapping separation ranging map (OSRM) and artificially intervention. After calculating retention parameters and peak shape parameters of the target peaks, the optimization was operated in an emulational picture through the computer without further experiments. The emulational chromatogram was proved to be authentic by the estimated values, which were almost identical to experimental results. The method was very helpful for obtaining the satisfied separation conditions of target compounds rapidly and efficiently.

© 2008 Elsevier B.V. All rights reserved.

1. Introduction

Ultra-performance liquid chromatography (UPLC) has been proved to give high peak capacity and separation efficiency [1] and has shown great potential for separating complex samples (e.g., metabolites [2–6], proteins [7–8] and pharmaceutical products [9,10]). Gradient conditions are necessary for these more complicated samples. Multi-step gradient elution is the most efficient method because the concentration of the mobile phase and gradient duration in each step can be changed to adjust separation selectivity and analysis time. UPLC can bring higher sensitivity, but it may be difficult (or not necessary) to optimize separation conditions for all compounds in complex samples. Many peaks overlapped and the traditional optimization method may not give satisfactory separation. For these “black box” systems, it is difficult and unfeasible to obtain the best resolution for all the components. Optimization of target compounds is a good option for rapid acquisition of information, enabling more convenient subsequent qualitative, quantitative and preparative analysis to be made. In practice, the requirements for separation of target components vary. For example, quality control of traditional Chinese medicines (TCMs) requires separation of the active (diagnostic) components, not all the components. For complex samples, the target com-

ponents and separation requirement change continuously. These target components can be the full components, the normal-quantity component, the micro-quantity component, the analogue series of component and the overlapping peaks. Developing a suitable target optimization method to resolve the separation problem of complex samples rapidly and efficiently is necessary. Different targets have different optimized separation conditions. To get the requisite separation, computer-aided target optimization is necessary to simulate the chromatogram without carrying out experiments. This helps to obtain adequate resolution in the shortest run time.

Trial-and-error optimizations are frequently used to find out the appropriate gradients, although they are particularly slow and inefficient. Computer-assisted strategies can avoid these limitations. To simplify and accelerate the optimization process, several computer simulation software packages, such as Dry-Lab, Preopt-W, Osiris and ChromSword, have been widely used in reversed-phase high performance liquid chromatography (RP-HPLC) with isocratic, linear gradient, non-linear gradient and step-gradient models [11–16]. DryLab computer simulation is probably the most widespread approach to optimize the operation parameters in RP-HPLC. It uses retention data from two initial gradient runs to subsequently adjust the steepness and range of the gradient and other working parameters (if necessary) [17–19]. Our laboratory developed a complex sample analysis software system (CSASS) to resolve separation of complex samples [20]. Retention parameters and peak shape parameters can be calculated based on five initial gradient mobile phase conditions. Then the simulated chromatogram under other mobile phase conditions can be exported, and the moved

* Corresponding author at: Dalian Institute of Chemical Physics, Chinese Academy of Sciences, Dalian 116023, China. Tel.: +86 411 8437 9539; fax: +86 411 8437 9519.
E-mail address: liangxm@dicp.ac.cn (X. Liang).

overlapping separation ranging mapping (OSRM) was drawn so that the satisfactory separation condition of target peaks can be selected. It can save optimization time and improve optimization quality.

The major objective of this contribution was to propose a novel method for the rapid optimization of binary gradient elution in UPLC for target compounds in a TCM. The retention equation of solutes can be obtained by running several linear gradient elutions, and then the satisfactory elution condition optimized according to the moved OSRM. This method was validated by the separation of the TCM *Rhizoma Coptidis* extract, in which good prediction precision and separation performance were obtained.

2. Theory: CSASS software

2.1. Prediction of retention times and peak shapes

Accuracy of predicted retention times and peak shapes are key factors that influence the reliability of the optimization study. The calculation method was identical to that previously described [20,21]. The basis of CSASS software was the statistical thermodynamic equation: the dependence of the logarithm of retention factor of solute $\ln k$ on the composition of strong modifier C_B in a binary solvent system in RP-LC for gradient elution can be written as the following equation:

$$\ln k = a + c C_B \quad (1)$$

where k is the retention factor ($k = (t - t_0)/t_0$ in which t and t_0 are the retention time and the dead time at the concentration of the organic phase C_B , respectively), and a and c are the intercept and the slope of the plot of $\ln k$ vs. C_B , respectively. a is a constant and relates to the molecular volume of the solutes, the interaction energy between the solutes with the stationary phase and the mobile phase. c is the coefficient of C_B in the retention equation and relates to the interaction energy between solutes and solvents.

Five initial linear gradient experiments were carried out to obtain the retention times of every target compound. Considering the dead time and the gradient delay in the system, the initial retention parameters (a and c) of target compounds were assigned. Euler's method was used to calculate the predicted retention times under five gradient mobile phase conditions. Final retention parameters of target compounds were calculated using the Levenberg–Marquardt method, and the retention parameters of target compounds were obtained. Retention times under other mobile phase conditions could then be predicted.

For chromatographic kinetics, the EMG model is used to describe the chromatographic elution curve [20,21]. Zone broadening that arises from symmetrical processes is quantified by σ , whereas broadening that arises from asymmetrical processes is quantified by τ . The computer-assisted automatic curve-fitting method is helpful for the resolution of overlapping peaks, and is used to obtain initial σ and τ values. The Levenberg–Marquardt method is used to calculate peak shape parameters. A lot of research has been carried out to prove that σ and τ have good linear relationships with t_R^* (Eqs. (2) and (3)).

$$\sigma = s_a + s_b \times t_R^* \quad (2)$$

$$\tau = t_a + t_b \times t_R^* \quad (3)$$

The half-peak width ($W_{h/2}$) also has a good linear relationship with t_R^* :

$$W_{h/2} = w_a + w_b \times t_R^* \quad (4)$$

The regulation of peak shapes can be obtained from Eqs. (2)–(4), where s_a , s_b , t_a , t_b , w_a and w_b are dynamically related coefficients that can be obtained by the regression of each peak under the

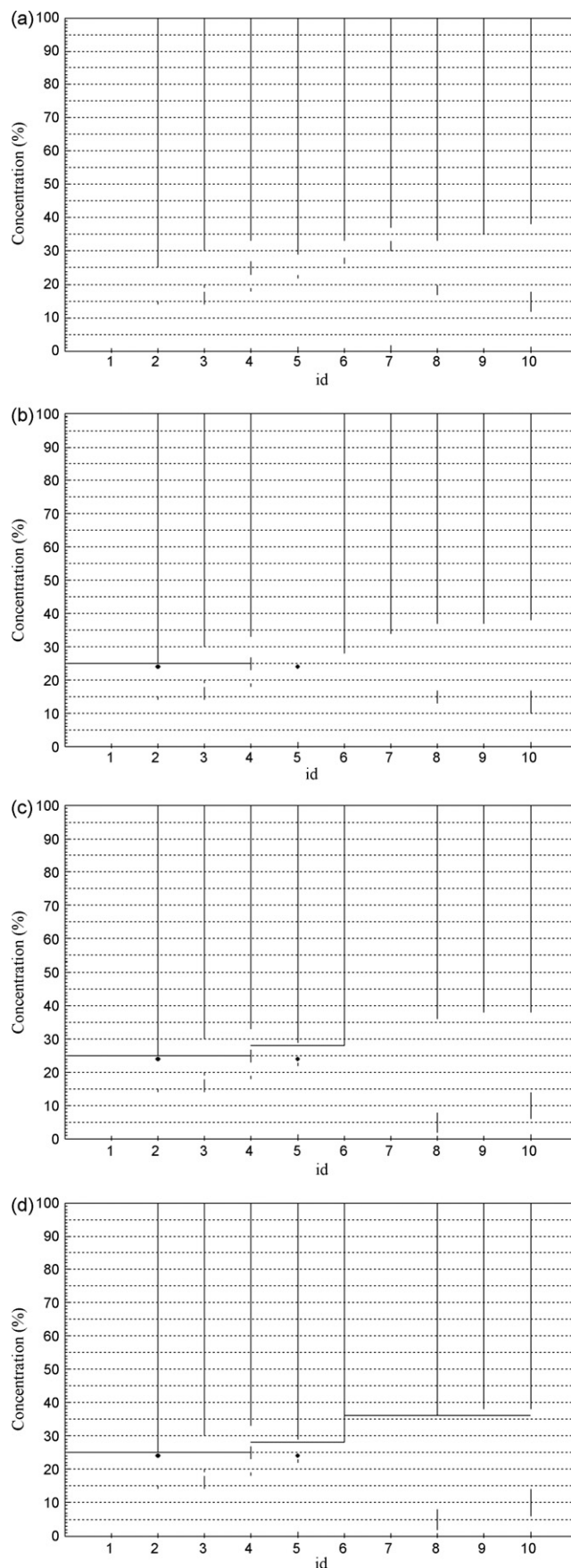


Fig. 1. The example of optimization progress with OSRM.

five mobile phase conditions. t_R^* is the equivalent retention time which is equal to t_R under corresponding isocratic concentration at t moment.

2.2. Simulation of the chromatogram

After the chromatographic retention parameters a and c , and the chromatographic peak shape parameters σ , τ and $W_{h/2}$ of target compounds were obtained, precise retention times and the separation of each target peak under other mobile phase gradient conditions in this chromatographic system could be predicted. We can therefore interpret these unknown chromatographic samples. Once prediction of the retention time and asymmetry for target solutes under any gradient program has been completed, the corresponding theoretical chromatogram can be simulated. The stimulated chromatogram based on predicted retention time and peak shape parameters at a given gradient condition can be directly obtained by CSASS.

2.3. Target optimization

2.3.1. Resolution

Resolution is the most important factor for evaluating the separation quality of the chromatogram. Half-peak width resolution (K_1) is selected to reflect the separation of two peaks in a target optimization:

$$K_1(i, j) = \frac{t_{R,i} - t_{R,j}}{(W_{h/2,i} + W_{h/2,j})/2} \quad (5)$$

2.3.2. Moved OSRM

Five linear gradient elutions were done to get each peak's a and c values and the linear regression chart of $\ln k$ vs. C_B for each peak. From the $\ln k$ vs. C_B curve of target components, the finding that some peaks cannot be separated at certain organic concentrations can be seen; if the curves of different compounds intersected, it implied that these compounds could not be separated at this organic concentration. After retention parameters and peak shape parameters were calculated, with the required resolution (in this paper, $K_1 = 2.5$), the OSRM in the range of full concentration (0–100% organic concentration) could be drawn. An example of optimization progress with OSRM is shown in Fig. 1. Fig. 1a was the initial OSRM for ten target peaks; the y-axis was the concentration of organic solvent and the x-axis was the peak number. On the OSRM, the vertical

line expressed that this peak could not attain the required resolution with the previous peak. The blank expressed that this peak could attain the required resolution with the previous peak. For separating complex samples, using the condition of higher organic concentration first meant that decreasing organic concentration was not practical because analysis time would be too long. Selecting the initial organic concentration should be done carefully; in general, the initial concentration was at the highest concentration of target components (Fig. 1b) and 25% organic concentration was selected for the anterior four peaks. But if the selected concentration considerably influenced the separation of latter peaks, the concentration step should be reselected. After the initial isocratic concentration was determined, the effect of this isocratic condition on un-eluted components in the column was considered. The resolution at full concentration of these un-eluted components was recalculated, and the OSRM updated to select the second isocratic concentration (Fig. 1c); 28% organic concentration was selected for peaks 5–6. Then the third isocratic condition, 36% organic concentration, was selected until all components were eluted (Fig. 1d). The OSRM was moved; when the condition for the front peaks was selected, the separation of the back peaks would change. Separation of the front peaks influenced the separation of the back peaks, reflecting the real separation of sample in the column. In practice, the sudden change of the isocratic concentration will bring unwanted fluctuation to the baseline and affect the eluting curve. We therefore added a linear gradient condition between the two-isocratic steps. The separation of target components can be rapidly seen by a simulated chromatogram from CSASS, so we can adjust separation conditions to get satisfactory separation. The OSRM, an artificially intervention method and simulated chromatogram can produce satisfactory separation for target compounds.

3. Experimental

3.1. Materials and instrument

HPLC-grade acetonitrile purchased from Fisher (Fairlawn, NJ, USA) and methanol obtained from Yuwang (Shandong, China) filtered with 0.22- μm membranes were used for UPLC analysis. The water was purified using a Milli-Q water purification system (Bedford, MA, USA). Trifluoroacetic acid (TFA) from Tedia (Fairfield, OH, USA) was the mobile phase additive.

Experiments were done on a Waters ACQUITY UPLC™ system (Milford, MA, USA), including binary solvent manager, column

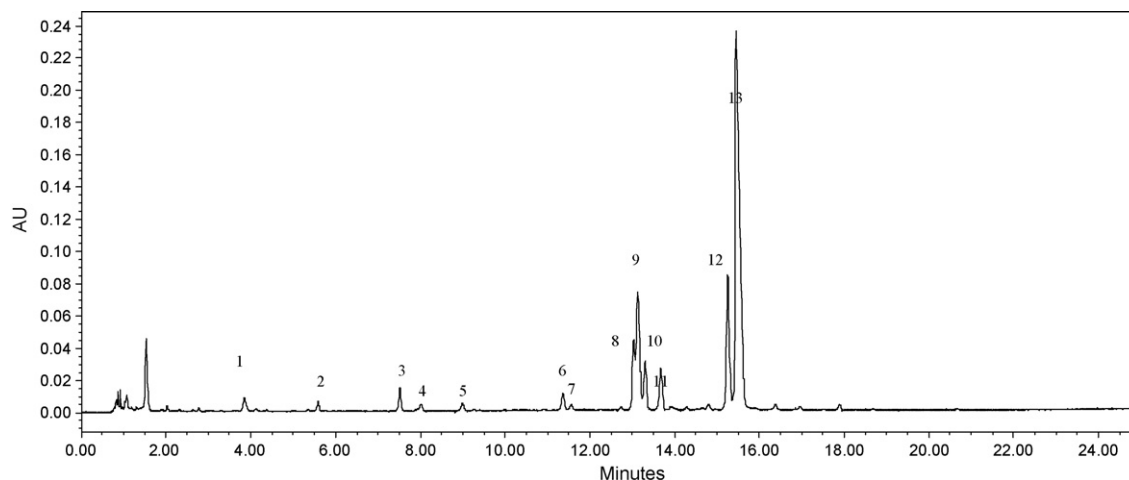


Fig. 2. Chromatogram of *Rhizoma Coptidis* extract. Column: ACQUITY UPLC™ BEH shield RP18 (100 mm × 2.1 mm i.d., 1.7 μm); flow rate: 0.35 mL min⁻¹; column temperature: 30 °C; eluent: (A) water–TFA (100:0.016, v/v) and (B) acetonitrile–TFA (100:0.016, v/v); 5% B to 30% B through 20 min, then through 5 min to 60% B. The wavelength was 254 nm: (12) palmatine and (13) berberine

Table 1
Retention parameters and optimization results of total 13 compounds in *Rhizoma Coptidis*.

No	a	c	t (exp, min)	t (pre, min)	t, error(%)	Error (s)		
						σ	τ	$W_{h/2}$
1	1.61	-8.21	1.90	1.89	0.57	0.22	0.07	0.49
2	2.21	-12.18	2.01	1.95	2.91	0.21	0.06	0.48
3	4.64	-24.96	2.77	2.66	4.15	0.21	0.16	0.42
4	4.64	-23.96	2.98	2.85	4.39	0.18	0.13	0.36
5	4.88	-23.26	3.46	3.35	2.97	0.17	0.08	0.36
6	5.78	-23.90	4.76	4.66	1.94	0.38	0.39	0.64
7	5.96	-24.78	4.79	4.71	1.69	0.37	0.40	0.60
8	6.17	-23.11	5.75	5.68	1.35	0.27	0.34	0.41
9	5.77	-20.43	5.99	5.90	1.42	0.35	0.59	0.42
10	6.35	-23.72	5.86	5.78	1.27	0.28	0.12	0.57
11	6.33	-22.94	6.11	6.04	1.16	0.24	0.10	0.60
12	6.59	-21.79	7.36	7.41	0.70	0.35	0.41	0.53
13	6.38	-20.34	7.79	7.76	0.32	0.18	1.61	0.70

heater, sample manager and PDA detector, connected to a Waters Empower 2 software. Chromatographic conditions were as follows: column: ACQUITY UPLC™ BEH shield RP₁₈ (100 mm × 2.1 mm i.d., 1.7 μm); eluent: (A) water–TFA (100:0.016, v/v) and (B) acetonitrile–TFA (100:0.016, v/v); the five initial experiments were 5% B to 30% B through 16.6, 20, 25, 33.3 and 50 min, respectively, then through 5 min to 60% B. Flow rate was 0.35 mL min⁻¹ and the column temperature was 30 °C. The wavelength was set at 254 nm. Retention parameters were calculated and analyzed by CSASS.

3.2. Plant material and sample preparation

Rhizoma Coptidis was collected from Shizhu county, Sichuan province, China. The herb was authenticated by the China Academy of Traditional Chinese Medicine Research–Institute of Traditional Chinese Medicine. The herb was dried and 10 g was weighed; and refluxed with 10-fold water for twice. The solution was filtered; the filtrate was concentrated to about 10 mL in which 100 μL was taken and diluted to 2 mL with water, and then 100 μL diluted solution was taken and re-diluted to 2 mL with water. After that 1 mL solution was filtered through 0.22-μm membrane before injection into the UPLC column for the analysis.

3.3. Determination of dead time and gradient delay in the system

Uracil was the measurement marker of dead time. The mobile phase was isocratic with a composition of 85/15 of methanol/water. The detection wavelength was 254 nm. Dead time was 0.7220 min ($n=3$).

A specific step gradient with methanol and water was designed to measure the gradient delay in the system when no sample was injected. The detection wavelength was at 203 nm. The concentration of methanol was changed from 100 to 90% at 2 min, but the absorbance changed at 2.9613 min (middle of the decreasing curve, $n=3$). By subtraction of the dead time, the gradient delay of the system was 0.2393 min.

4. Results and discussion

4.1. Accurate calculation of retention parameters and peak shape parameters

When optimizing target components, retention times and peak shape parameters of the peaks were required to simulate chromatograms. Accuracy of the predicted retention times is a key factor that influences the reliability of optimization. In addition to, peak shape is the most important factor that influences separation efficiency. The evaluation and prediction of peak shape parameters is important to foresee the resolution between closely eluting peaks

and to select the satisfactory analytical conditions for efficient and rapid separation. The chromatogram of *Rhizoma Coptidis* extract was shown in Fig. 2. Thirteen peaks were labeled. According to CSASS, the retention parameters a and c values of 13 peaks in *Rhizoma Coptidis* under five gradient mobile phase conditions were calculated (Table 1, column 2–3). The retention time under other mobile phase conditions can be predicted with these a and c values.

The peak shape parameters can be predicted with the linear relationship of σ , τ , $W_{h/2}$ vs. the equivalent retention time t_R^* . σ , τ and $W_{h/2}$ can be calculated according to the EMG model and the computer-assisted automatic peak curve-fitting method under each linear gradient mobile phase condition. The equivalent retention time t_R^* could be calculated by loading the retention concentration in Eq. (1) with the obtained a and c values. Then the linear relationships of the peak shape parameters σ , τ and $W_{h/2}$ vs. t_R^* for 13 peaks were obtained by regression under gradient conditions, respectively.

$$\sigma = 0.2839 + 0.3764t_R^* (R^2 = 0.9675)$$

$$\tau = -0.4164 + 0.2802t_R^* (R^2 = 0.9907)$$

$$W_{h/2} = 0.4036 + 0.9680t_R^* (R^2 = 0.9854)$$

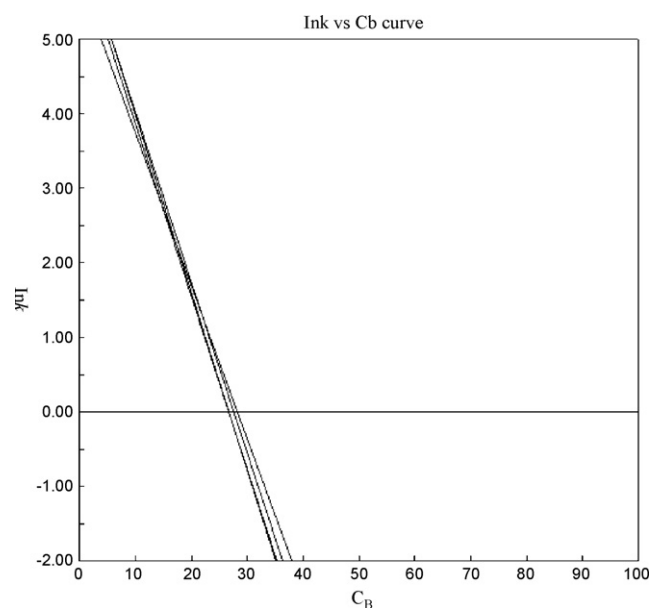


Fig. 3. The relationship between $\ln k$ vs. C_B of peaks 8–11 in *Rhizoma Coptidis* extract.

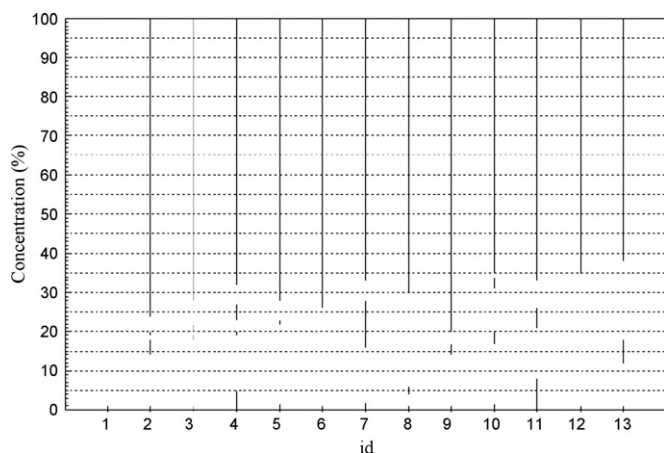


Fig. 4. Moved overlapping separation ranging map (OSRM) of 13 peaks in *Rhizoma Coptidis* extract.

The results showed that the linearity between σ , τ and $W_{h/2}$ vs. t_R^* was quite good. They were used for calculation of peak shape parameters under other separation conditions. The precise prediction of peak profiles met the requirement for realistic simulation of chromatograms.

4.2. Target optimization of overlapping peaks

Peaks 8–11 were overlapped (Fig. 2). Their linear relationship between $\ln k$ vs. C_B was shown in Fig. 3. Their separation was difficult due to their adjacent retention factors. Their plot intersected considerably, so they were selected as targets for better separation. According to the CSASS, the OSRM of peak 1–13 was drawn (Fig. 4). According to the OSRM of peaks 8–11 and the simulated chromatogram, isocratic condition of 19% B can make overlapping peaks 8–11 attain the required resolution without considering the separation of other peaks, the experimental result proved it. The simulated and experimental chromatograms were shown in Fig. 5, and the predicted error of retention times were 0.08%, 0.31%, 1.04%, and 2.41% for peaks 8–11, respectively. Good separation of peaks 8–11 can be achieved under this condition and the analysis time was less than 10 min. Further qualitative, quantitative and preparative analysis for peaks 8–11 would now be easier.

4.3. Target optimization of all components

All components (peaks 1–13) can also be considered as a target fraction to obtain good separation and short analysis time. From Fig. 4, the initial concentration of organic phase at 13% was selected. In practice, mutation of the gradient always leads to high fluctuation of the baseline and “ghost” peaks. Therefore a gradient condition was required between two-step conditions. The simulated chromatogram can adjust and then obtain the optimized separation condition. For peaks 1–13, after determination of the initial condition of 13% B, with computer-aided software and artificial intervention, the condition of 13% B through 5 min to 23% B and hold 4 min was selected for optimization of all components. As shown in Fig. 6, simulated and experimental chromatograms were very similar. The predicted errors of retention times were shown in Table 1 (columns 4–6). The largest relative error of retention time was 4.39%. The predicted peak shapes can truly reflect experimental peak shapes; the absolute error between experimental and predicted peak shape parameters was shown in Table 1 (columns 7–9). After optimization, the analysis time was only 8 min for full analysis and satisfactory separation was obtained. We can select any peaks as target peaks and obtain their separation situation in any mobile phase conditions without conducting further experiments.

4.4. Effect of flow rate

In general, increasing the flow rate can decrease analysis time. UPLC adopted 1.7 μm particles as the column solid phase, so according to the Van Deemter curve, a realm of chromatography is entered where not only are higher efficiencies gained, but also these efficiencies no longer diminish with flow rate. Experiment at 0.15, 0.25, 0.35, 0.45 and 0.55 mL min^{-1} under five gradient conditions was done. After conversion of the dead times and system delay, retention values under each flow rate were calculated, and the retention factors (k) of each peak were calculated from a , c values. The calculated relative retention factors (α) under each flow rate were shown in Fig. 7:

$$\alpha = \frac{k_n}{k_{n-1}} \quad (6)$$

From Fig. 7, most values of α at different flow rates were constant. Flow rate has little influence on relative retention values. Increasing flow rate did not affect retention behavior. When the flow rate increased from 0.35 to 0.55 mL min^{-1} , the analysis time was less than 5 min with the same gradient condition for all 13

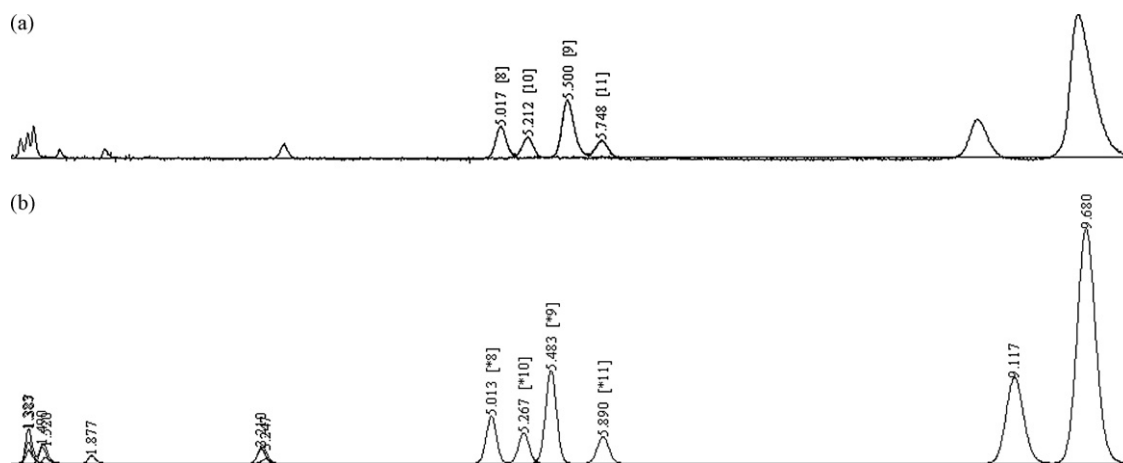


Fig. 5. The experimental chromatogram (a) and the simulated chromatogram (b) for optimizing peaks 8–11 in *Rhizoma Coptidis* extract. Gradient elution of (A) water–TFA (100:0.016, v/v) and (B) acetonitrile–TFA (100:0.016, v/v), isocratic 19% B. Other conditions were same to Fig. 2.

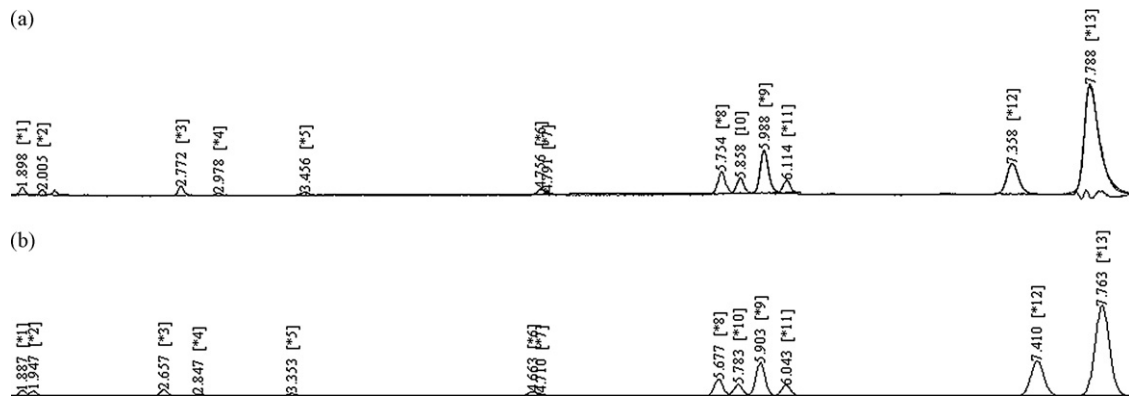


Fig. 6. The experimental chromatogram (a) and the simulated chromatogram (b) for optimizing total 13 peaks in *Rhizoma Coptidis* extract. Gradient elution of (A) water–TFA (100:0.016, v/v) and (B) acetonitrile–TFA (100:0.016, v/v), and the gradient program: 13% B to 23% B through 5 min and hold 4 min. Other conditions were same to Fig. 2.

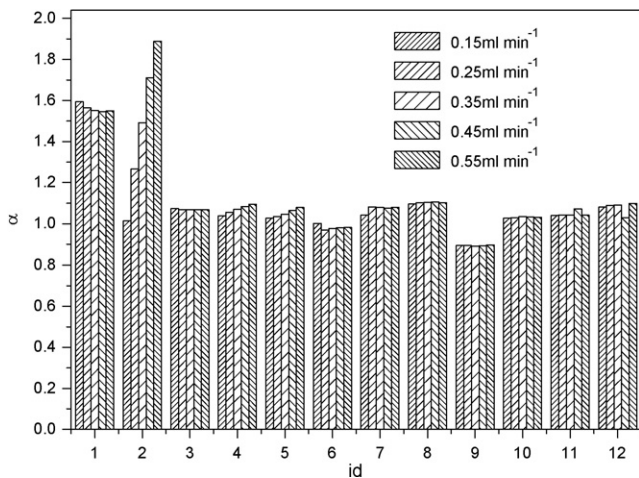


Fig. 7. Comparing the relative retention factors under different flow rates, column: ACQUITY UPLC™ BEH shield RP18 (100 mm × 2.1 mm i.d., 1.7 μm), column temperature: 30 °C.

peaks. It could save analysis time further and did not affect retention behavior.

5. Conclusions

Target optimization is an effective way to analyze TCMs. An effective method developed in this study was to optimize the separation conditions of target components in TCMs by UPLC. Retention parameters and peak shape parameters of each target component in TCM – *Rhizoma Coptidis* – were calculated accurately. The OSRM was drawn. Thus, the initial concentration of organic phase can be obtained for target components, and simulated chromatograms exported automatically. Then, with artificially intervention, the satisfactory separation condition can be selected based on the required resolution for target components. Four overlapped compounds and all compounds were selected as targets, and optimized separation conditions for each target fraction were obtained. The experimen-

tal and simulated chromatograms matched well. The proposed methodology is based on computer simulation using a few numbers of experimental runs to predict UPLC separation for a wide range of conditions. This reduces time and effort in looking for the satisfactory chromatographic conditions for target compounds.

Acknowledgements

This work was supported by the “Science and Technology plan of Liaoning Province (2006226002)”, “Science and Technology plan of Dalian (2007J23JH032)” and “the Knowledge Innovation Program of DICP, CAS (K2006A4)”.

References

- [1] S.A.C. Wren, J. Pharm. Biomed. Anal. 38 (2005) 337.
- [2] R. Plumb, J. Castro-Perez, J. Granger, I. Beattie, K. Joncour, A. Wright, Rapid Commun. Mass Spectrom. 18 (2004) 2331.
- [3] L. Nováková, D. Solichová, P. Solich, J. Sep. Sci. 29 (2006) 2433.
- [4] D.J. Crockford, E. Holmes, J.C. Lindon, R.S. Plumb, S. Zirah, S.J. Bruce, P. Rainville, C.L. Stumpf, J.K. Nicholson, Anal. Chem. 78 (2006) 363.
- [5] S. Inagaki, T. Noda, J.Z. Min, T. Toyooka, J. Chromatogr. A 1176 (2007) 94.
- [6] H.G. Gika, G.A. Theodoridis, I.D. Wilson, J. Sep. Sci. 31 (2008) 1598.
- [7] I.D. Wilson, J.K. Nicholson, J. Castro-Perez, J.H. Granger, K.A. Johnson, B.W. Smith, R.S. Plumb, J. Proteome Res. 4 (2005) 591.
- [8] R.A. Everley, T.R. Croley, J. Chromatogr. A 1192 (2008) 239.
- [9] M. Mezcuca, A. Agüera, J.L. Lliberia, M.A. Cortés, B. Bagó, A.R. Fernández-Alba, J. Chromatogr. A 1109 (2006) 222.
- [10] E.C.Y. Chan, S.L. Yap, A.J. Lau, P.C. Leow, D.F. Toh, H.L. Koh, Rapid Commun. Mass Spectrom. 21 (2007) 519.
- [11] N. Lundell, J. Chromatogr. A 639 (1993) 97.
- [12] P. Jandera, J. Chromatogr. A 845 (1999) 133.
- [13] R.G. Wolcott, J.W. Dolan, L.R. Snyder, J. Chromatogr. A 869 (2000) 3.
- [14] V. Morris, J. Hughes, P. Marriott, J. Chromatogr. A 1008 (2003) 43.
- [15] G. Vivó-Truyols, J.R. Torres-Lapasí, M.C. García-Alvarez-Coque, J. Chromatogr. A 1018 (2003) 183.
- [16] P. Nikitas, A. Pappa-Louisi, K. Papachristos, J. Chromatogr. A 1033 (2004) 283.
- [17] J.W. Dolan, D.C. Lommen, L.R. Snyder, J. Chromatogr. 535 (1990) 55.
- [18] L.R. Snyder, J.W. Dolan, D.C. Lommen, J. Chromatogr. 535 (1990) 75.
- [19] I. Molnar, J. Chromatogr. A 965 (2002) 175.
- [20] Y. Jin, X.Y. Xue, Y.F. Liu, Y.S. Xiao, J. Zhang, H. Shi, F.F. Zhang, X.M. Liang, J. Chromatogr. A 1183 (2008) 76.
- [21] G.W. Jin, X.Y. Xue, F.F. Zhang, X.L. Zhang, Q. Xu, Y. Jin, X.M. Liang, Anal. Chim. Acta 628 (2008) 95.



Direct electrochemistry and electrocatalysis of horseradish peroxidase immobilized in hybrid organic–inorganic film of chitosan/sol–gel/carbon nanotubes

Xinhuang Kang^{a,b}, Jun Wang^b, Zhiwen Tang^b, Hong Wu^b, Yuehe Lin^{b,*}

^a College of Science, Guangdong Ocean University, Zhanjiang, 524088, PR China

^b Pacific Northwest National Laboratory, 902 Battelle Boulevard, Richland, WA 99352, USA

ARTICLE INFO

Article history:

Received 18 September 2008

Received in revised form 29 October 2008

Accepted 30 October 2008

Available online 14 November 2008

Keywords:

Direct electrochemistry

Horseradish peroxidase

Multi-walled carbon nanotubes

Sol–gel

ABSTRACT

A hybrid organic–inorganic nanocomposite film of chitosan/sol–gel/multi-walled carbon nanotubes was constructed for the immobilization of horseradish peroxidase (HRP). This film was characterized by scanning electron microscopy. Direct electron transfer (DET) and bioelectrocatalysis of HRP incorporated into the composite film were investigated. The results indicate that the film can provide a favorable microenvironment for HRP to perform DET on the surface of glassy carbon electrodes with a pair of quasi-reversible redox waves and to retain its bioelectrocatalytic activity toward H₂O₂.

© 2008 Elsevier B.V. All rights reserved.

1. Introduction

The direct electron transfer between electrodes and redox proteins, particularly enzymes, has aroused increasing interest because of its significance in both theoretical and practical applications in electrochemistry [1–5]. Studies based on electrochemistry were used to investigate enzyme structure, and these have contributed to a better understanding of the kinetics and thermodynamics of the biological redox process [6,7]. Moreover, DET can establish a foundation for fabricating new kinds of mediator-free biosensors, enzymatic bioreactors, and biomedical devices [8–10]. However, DET between the enzyme and a conventional electrode is usually prohibited because enzymatic redox centers embed deeply into the structure of the enzyme. Also, low electronic conductivity of the surrounding amino acid chains makes electron transfer rates slow in most orientations around the redox center [11,12]. Therefore, it is necessary to find new materials to modify the electrode and a suitable means to immobilize enzymes on the electrode surface to obtain their direct electrochemical reactions and retain their bioactivities. These new materials include nanomaterials [2–6,], room-temperature ionic liquids [4], biomaterials [5,9,10], and sol–gel matrices [6]. Nanomaterials have become the

focus of scientific research because of their unique electronic, optical, and catalytic properties [2–11,13]. Carbon nanotubes (CNTs) are superior to other carbon materials, and they have been extensively used in physics and chemistry. CNTs have demonstrated good performance in their high surface/volume ratio and fast electron transfer kinetics for a wide range of electroactive species in constructing sensors and biosensors [2–4,13–17]. Recently, CNTs have been used for research into the DET of proteins or enzymes because their unique structure and electronic properties allow good communication between CNT and redox active centers of proteins. For example, a pair of well-defined voltammograms for horseradish peroxidase (HRP) has been obtained at the modified electrodes with a CNT/thionine/gold composite [3], a sol–gel-derived ceramic–CNT nanocomposite [6], CNT powder [8], and N-CNT [18]. The CNT-modified electrodes have also been used to study the DET of cytochrome *c* [2,4,19], hemoglobin (Hb) [20,21], myoglobin (Mb) [22,23], catalase (CAT) [24], and glucose oxidase (GOD) [10,25–28].

However, immobilizing enzymes is a crucial process for fabricating biosensors. The common methods for immobilizing enzymes on electrodes include encapsulation [6,29], electrochemical copolymerization entrapment techniques [30], covalent or cross-linking [31], and adsorption [23]. Lately, sol–gel-derived materials have been applied to immobilize biomolecules to improve the performance of biosensors [6,29,32]. These improvements include high thermal stability, a wide potential window, chemical inertness, the capability to form films, and fabrication under mild conditions.

* Corresponding author.

E-mail address: Yuehe.lin@pnl.gov (Y. Lin).

Moreover, porous and open frameworks of sol–gel verify that the analytes can quickly and effectively access the active functionalities immobilized at the interface between electrode and solution, which results in a high sensitivity to the electrochemical response. However, the silica sol–gel, which is commonly used, is brittle and has a low biocompatibility. Silica-based organic–inorganic hybrids are adopted as attractive composite materials for fabricating biosensors [33]. Some polymers are hybridized into a silica sol–gel matrix, such as chitosan [6,29,31], polyhydroxyle (PVA–g–PVP) [34], and poly(vinyl alcohol) (PVA) [35], which can effectively avoid the brittleness of pure inorganic sol–gel and the swelling of some pure polymers, and it can enhance the biocompatibility of the silica-based organic–inorganic hybrids. These films facilitate the DET process between the biomolecules and the electrodes [9,19].

These advantages of organic–inorganic hybrids of the sol–gel component coupled with the striking properties of the CNT essentially suggest that the sol–gel–CNT should be useful for electrochemical biosensors [6,30]. In the present work, the homogenous hybrid composite film of chitosan/sol–gel/CNT is attractive both for electrochemical investigations of heme proteins and for the development of an amperometric biosensor. Chitosan, a natural organic polymer with abundant amino and hydroxyl groups, possesses many special properties, such as low cost, high mechanical strength, high hydrophilicity, good film-forming capability, biocompatibility, and no toxicity [36]. It has been widely used as an immobilization matrix for biosensors and biocatalysis [5,9,30,32,36]. So chitosan was chosen to react with methyltrimethoxysilane (MTOS) and CNT functionalized with carboxylic acid, which were introduced to form an organic–inorganic sol–gel hybrid nanocomposite film to immobilize HRP. The hybrid nanocomposite film-modified glassy carbon electrodes (GCE) can provide a favorable microenvironment for HRP to perform DET and retain its bioactivity. The electrocatalytic reduction of hydrogen peroxide by HRP entrapped in the hybrid film has been studied in detail.

2. Experimental

2.1. Chemicals

Phosphate buffer saline (PBS 0.01 M, pH 7.4) with 0.1 M KCl was used as the supporting electrolyte. HRP (1080 U mg⁻¹, type VI-A), K₄[Fe(CN)₆], K₃[Fe(CN)₆], PBS, H₂O₂, chitosan, and MTOS were purchased from Sigma–Aldrich. A stock HRP solution was prepared in PBS buffer and stored at 4 °C. An H₂O₂ solution (10 mM) was prepared and stored at 4 °C. CNT were purchased from Nano-lab (Brighton, MA). All other chemicals and reagents are of analytical grade and were prepared using deionized or ultrapure water (18 MΩ cm).

2.2. Apparatus and procedure

The electrochemical experiments were performed with a CHI660a electrochemical workstation (CHI, Austin, TX). A three-electrode system consists of a GCE ($\Phi = 3$ mm) as the working electrode, a platinum wire as the auxiliary electrode, and an Ag/AgCl electrode as the reference electrode. All experiments were performed at room temperature in a conventional electrochemical cell. Electrochemical impedance measurements were performed in a 0.1 M KCl solution containing 5 mM K₃[Fe(CN)₆] + K₄[Fe(CN)₆] (1:1) and plotted in the form of complex plane diagrams (Nyquist plots) with a frequency range of 0.1 Hz to 10 kHz. The amplitude of the applied sine wave potential is 5 mV, whereas the formal potential of the system was set at 0.174 V. Cyclic voltammogram (CV)

experiments were carried out in quiescent solution at 100 mV s⁻¹ in an electrochemical cell filled with 5.0 mL of PBS. The current–time curves were recorded in a stirred cell with a successive addition of H₂O₂ standard solution to the cell at an operating potential of –0.3 V. LEO-982 scanning electron microscopy (SEM; German) was used for the SEM experiment.

2.3. Fabrication of the film-modified GCE

Before modification, GCE was polished with 1.0-, 0.3-, and 0.05- μ m alumina powders in sequence, rinsed thoroughly with deionized water between each polishing step, sonicated in 1:1 HNO₃, ethanol, and doubly distilled water, respectively, and dried at room temperature. The HRP stock solution was prepared by dissolving 10 mg of HRP in 1 mL of PBS. Chitosan solution (1.0%) was prepared by dissolving 0.5 g chitosan in 50 mL of 1.0% (v/v) acetic acid solution with ultrasonication for 30 min, and the pH of the solution was adjusted to 5.5 with 0.2 M NaOH solution. A homogenous stock sol–gel solution with 1 mL of 1.0% chitosan and 1 mL of MTOS was sonicated for 30 min and then stored at room temperature for 3 h. One milligram of CNT functionalized with carboxylic acid [29] was dispersed in 1 mL of the sol–gel that was mentioned above (chitosan/sol–gel/CNT). Then, 0.2 mL of HRP solution was mixed with 0.8 mL of the chitosan/sol–gel/CNT suspension. Six microliters of mixture was dropped on the surface of the GCE and dried in air. Finally, the modified electrode was immersed in PBS to wash off the loosely adsorbed HRP and nanocomposite and dried. Then, the electrode was stored at 4 °C in a refrigerator before use.

3. Results and discussion

3.1. Characterization of the composite by SEM

The SEM images showed that the chitosan/sol–gel hybrid film was porous with an open framework (Fig. 1A), CNTs functionalized with carboxylic acid were well dispersed into the chitosan/sol–gel (Fig. 1B), and the enzyme of HRP was entrapped into the chitosan/sol–gel/CNT film (Fig. 1C).

Silica sol–gel is brittle and has a low biocompatibility. Chitosan reacts with MTOS to form a more stable and biocompatible organic–inorganic sol–gel [29,37] according to Scheme 1. Incorporation of CNT into the chitosan/sol–gel matrix increase the electron transfer property and porosity of the nanocomposite film, which will lead to fast diffusion of the analytes. The organic–inorganic hybrid chitosan/sol–gel/CNT matrix offers a non-aggressive HRP enzyme immobilization approach at room temperature, which may improve some properties in relation to other immobilization methods, such as enzyme activity, biosensor sensitivity and larger linear response range to analyte [38,39].

3.2. Electrochemical impedance spectroscopy (EIS) study of the composite film

The preparation process of electrodes was also monitored by EIS, which is an effective means for probing the features on the surface of modified electrodes [29]. The Nyquist plot of impedance spectra includes a semicircle portion and a linear portion, with the former at higher frequencies corresponding to the electron-transfer limited process and the latter at lower frequencies corresponding to the diffusion process. The electron-transfer resistance (R_{ct}) at the electrode surface is equal to the semicircle diameter, which can be used to describe the interface properties of the electrode. Fig. 2 exhibits the EIS of the bare and modified GCEs. The R_{ct} (1450 Ω , Fig. 2b) of the chitosan/GCE was much larger than that of the bare

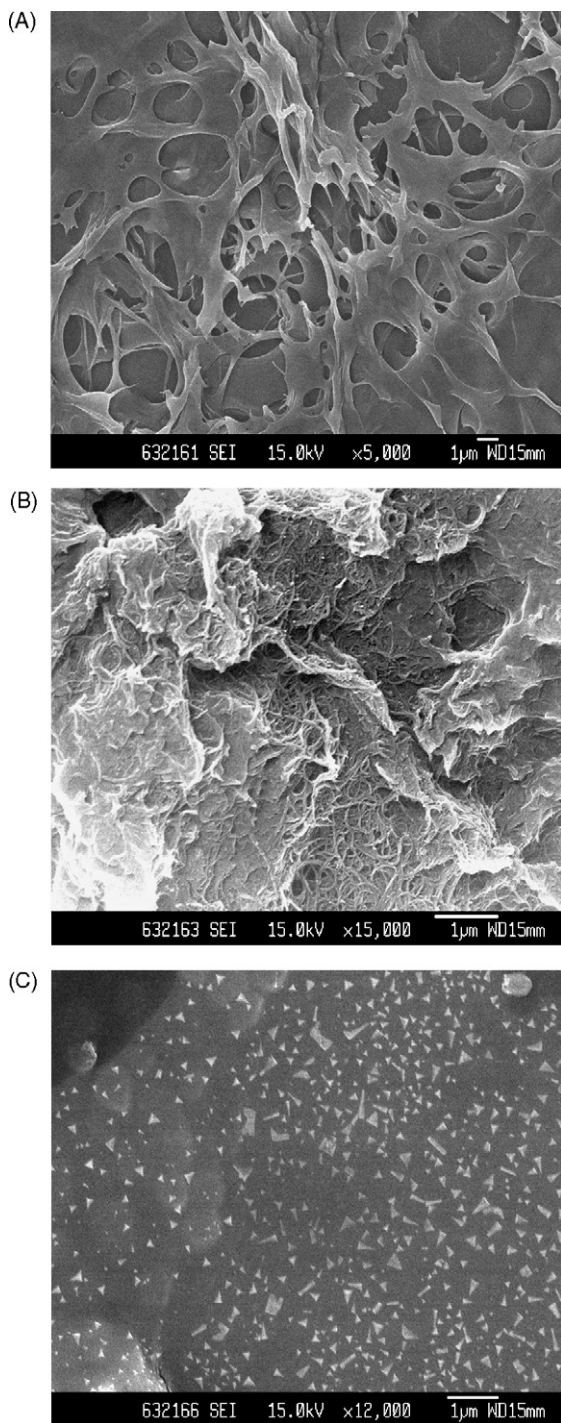


Fig. 1. SEM images of the chitosan/sol-gel (A), chitosan/sol-gel/CNT (B), and HRP/chitosan/sol-gel/CNT films (C).

GCE (350Ω , Fig. 2a), showing that a layer of chitosan hydrogel formed on the electrode surface, and that could inhibit the electron transfer of the redox probe of $[\text{Fe}(\text{CN})_6]^{3-/4-}$ to the electrode surface to some degree. For the porous film of chitosan/sol-gel (Fig. 2c), the R_{ct} decreased to 700Ω compared with that of the chitosan film because of the ease of the electron transfer of the redox probe of $[\text{Fe}(\text{CN})_6]^{3-/4-}$. After the film of chitosan/sol-gel/CNT was formed, the R_{ct} decreased unceasingly to about 280Ω (Fig. 2d), indicating that CNT have good conductivity and the chitosan/sol-gel/CNT composite can make the electron transfer easier. However, the R_{ct}

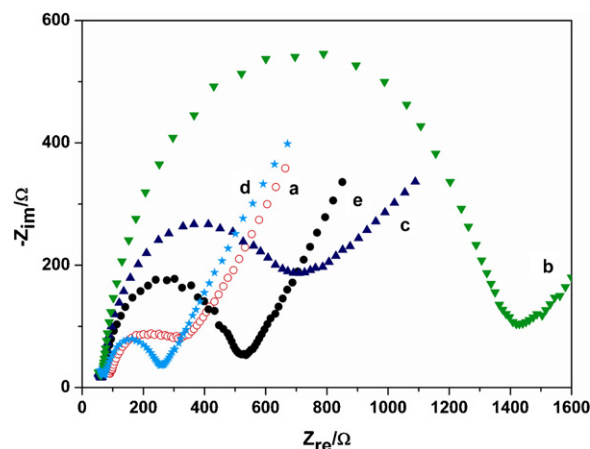


Fig. 2. Nyquist plot of EIS for (a–e) bare GCE, chitosan/GCE, chitosan/sol-gel/GCE, chitosan/sol-gel/CNT/GCE, and HRP/chitosan/sol-gel/CNT/GCE.

increased to 520Ω (Fig. 2e), which showed that the HRP was immobilized steadily into the chitosan/sol-gel/CNT film.

3.3. Direct electrochemistry of HRP immobilized in the chitosan/sol-gel/CNT film

HRP contains heme as the protein active site, which can catalyze the H_2O_2 dependent one-electron oxidation. Under appropriate conditions, the DET of HRP can be achieved, and the bioelectrocatalytic activity of HRP is often used to fabricate a third-generation biosensor [6,8,18,40]. The electrochemical behavior of HRP immobilized in the chitosan/sol-gel/CNT film was investigated. Fig. 3 shows the cyclic voltammograms of various films of modified GCE in N_2 -saturated PBS at a scan rate of 0.1 V s^{-1} . No peaks were observed at the chitosan/sol-gel/GCE and the HRP/chitosan/sol-gel/GCE (Fig. 3a and b). A pair of small redox peaks around 0 V in curve c is attributed to the redox process of the oxygen-containing groups on CNT, and this indicates that the surface of the CNT has been activated, which is similar to reported results [6,41]. Obviously, it can be seen that one pair of waves has an anodic peak potential (E_{pa}) at -0.24 V and a cathodic peak potential (E_{pc}) at -0.305 V with the peak separation about 65 mV in curve d. This corresponds to the conversion between HRP-Fe(III) and HRP-Fe(II), which exhibited a stable, well-defined and nearly reversible

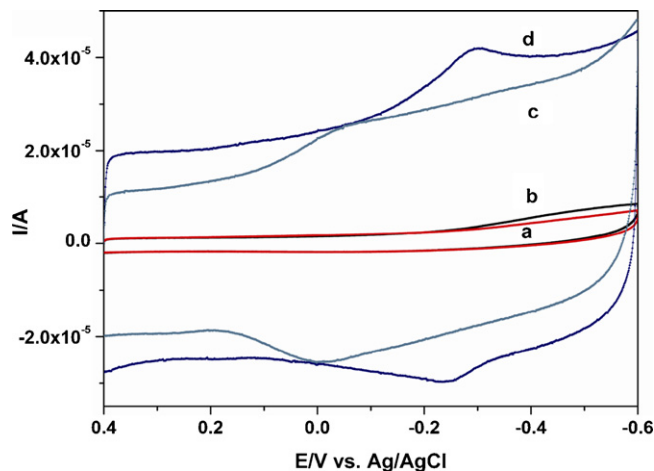
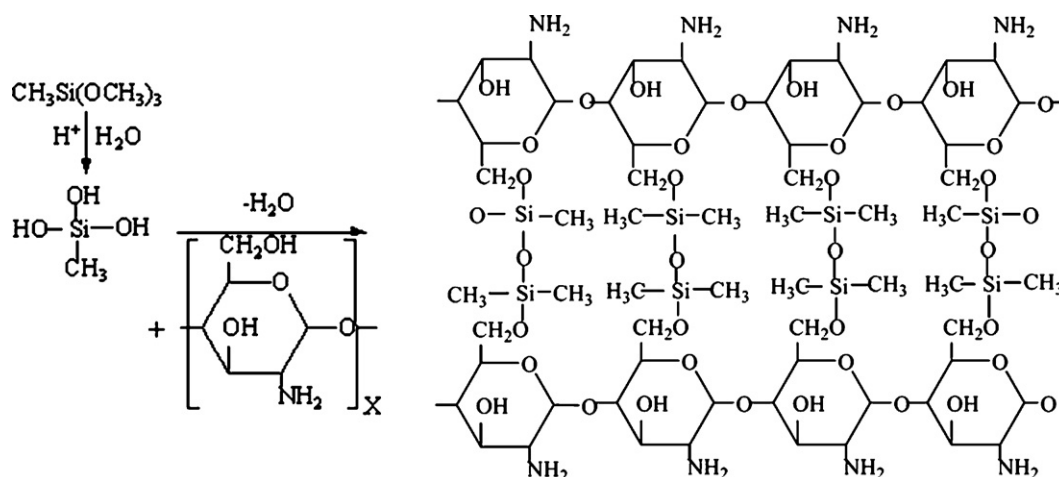


Fig. 3. Cyclic voltammograms of the modified GCE with (a–d) chitosan/sol-gel, HRP/chitosan/sol-gel, chitosan/sol-gel/CNT, and HRP/chitosan/sol-gel/CNT films in PBS with 0.1 M KCl at the scan rate of 100 mV s^{-1} .



Scheme 1. Formation of the sol-gel with MTOS and chitosan.

couple for HRP immobilized on the chitosan/sol-gel/CNT/GCE. The formal potentials (E°), taken by averaging potential values of the E_{pa} and E_{pc} , was -0.273 V, which is close to the -0.22 V of native HRP in solution, suggesting that most HRP molecules preserve their native structure after being entrapped in chitosan/sol-gel/CNT composite film. The E° shifts positively at 59 mV as compared with those reported previously in the literature (-0.332 V) [42], which means that the HRP immobilized in the chitosan/sol-gel/CNT film may need less activation energy to conduct the DET with the electrode. This may be ascribed to the favorable microenvironment for the proteins provided by the composite film.

Fig. 4 shows that both the cathodic and anodic peak currents of HRP increased linearly with scan rates from 0.02 to 0.3 V s $^{-1}$ with a small shifting of the peak potentials and a small increase in the peak-to-peak separation. The results indicated that the electron transfer of HRP with the modified GCE was a typical surface-controlled electrochemical process [43]. The electron transfer rate constant (k_s) can be estimated from the peak potential separation value (ΔE_p) according to the model of Laviron [44]. The plot of ΔE_p versus the logarithm of the scan rates yielded a straight line in which α was estimated as 0.52. Assuming that one electron was transferred, the k_s of the HRP in the chitosan/sol-gel/CNT film was calculated to be about 3.52 ± 0.34 s $^{-1}$. It is higher than

that of HRP adsorbed at carbon nanotube powder microelectrode (2.48 ± 0.03 s $^{-1}$) [8]. The higher k_s indicates that the resultant electrode can facilitate the electron transfer between HRP and the electrode surface. On the one hand, the two values were in the ranges of typical surface-controlled quasi-reversible electron transfer processes [5,43]. On the other hand, the surface average concentration of the electroactive HRP (Γ^* , mol cm $^{-2}$) in the chitosan/sol-gel/CNT film can be estimated from the charge integrating redox wave of the cyclic voltammogram, using Faraday's law $Q = nFA\Gamma^*$, where Q is the charge (C) integrated from the reduction peak area of the cyclic voltammogram, A is the electrode real area (cm 2), F is the Faraday constant, and n stands for the number of electrons transferred. In the experiment, the value of Γ^* was estimated to be $(2.21 \pm 0.21) \times 10^{-10}$ mol cm $^{-2}$ at scan rates of 20–300 mV s $^{-1}$, which was 10 times more than that of the theoretical monolayer coverage (about 2×10^{-11} mol cm $^{-2}$) [45]. This indicates that multi-layers of intercalated HRP in the porous chitosan/sol-gel/CNT matrix participated in the electron transportation process.

3.4. Influence of pH on voltammetry

The direct electrochemistry of HRP entrapped in the composite of chitosan/sol-gel/CNT revealed a dependence on the pH of the supporting electrolyte (Fig. 5). Both reduction and oxidation peak potentials of the HRP-Fe(III)/HRP-Fe(II) redox couple for the

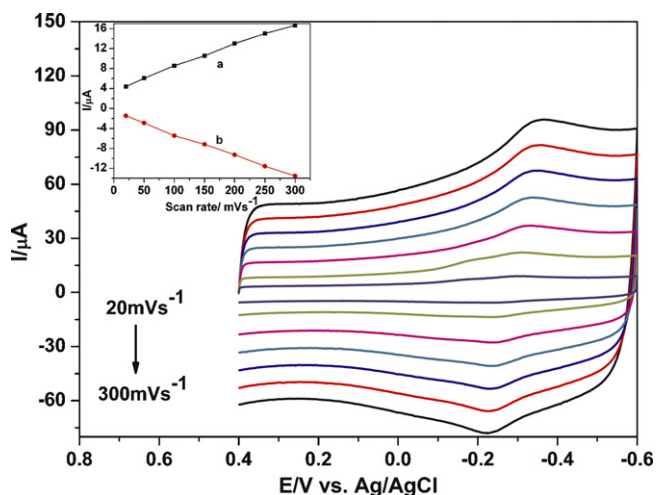


Fig. 4. Cyclic voltammograms of the modified GCE with HRP/chitosan/sol-gel/CNT film in PBS with 0.1 M KCl at different scan rates: 20, 50, 100, 150, 200, 250, 300 mV s $^{-1}$; and the plot of peak current vs. scan rates (insert).

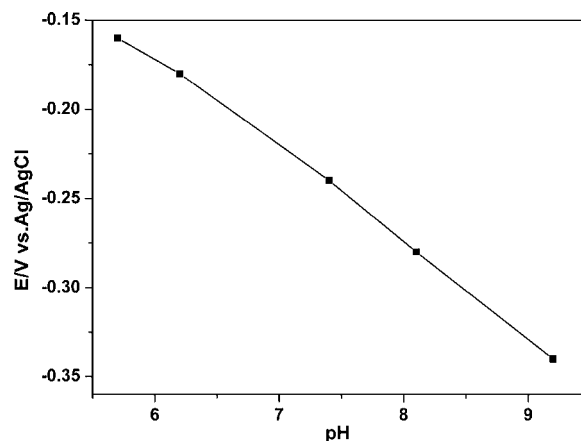


Fig. 5. Relationship of the formal potentials with pH for the modified GCE with HRP/chitosan/sol-gel/CNT film.

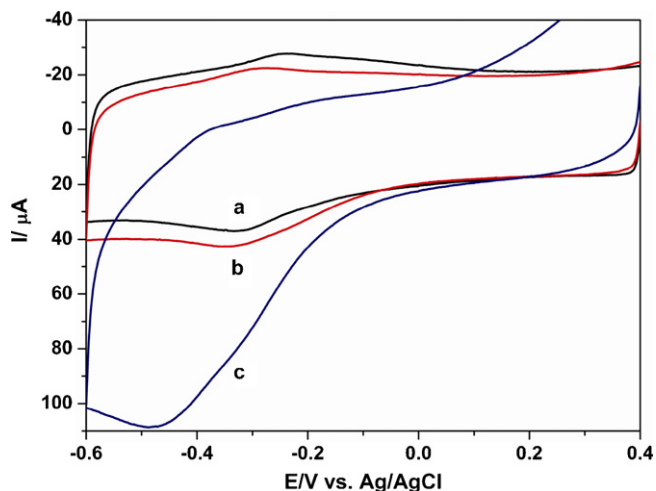


Fig. 6. Cyclic voltammograms of HRP/chitosan/sol-gel/CNT/GCE in PBS at 100 mV s^{-1} with different amount of H_2O_2 (a) without H_2O_2 , (b) 0.2 mM , and (c) 1.0 mM .

film shifted negatively with an increase in pH. The $E^{o'}$ of HRP varied linearly in the range of pH from 5.6 to 9.2 with a slope of -54.2 mV pH^{-1} that was very close to the theoretical value of -59 mV pH^{-1} at 25°C , showing the transfer of one proton and one electron in a reversible reduction [5]. The result displayed in the film could provide an appropriate microenvironment for HRP.

3.5. Bioelectrocatalytic reduction of H_2O_2

The bioelectrocatalytic activity of the HRP/chitosan/sol-gel/CNT composite film toward hydrogen peroxide was investigated by CV, which is one of the most commonly used techniques in electrochemical sensors. Fig. 6 indicates that as H_2O_2 was included in the PBS buffer, the cathodic response of the sensor was remarkably enhanced as the anodic peak decreased concomitantly, and the reductive peak potential shifted negatively (curves b and c in Fig. 6). The reduction peak current increases with increasing concentration of H_2O_2 , indicating that the catalytic reduction of H_2O_2 was performed on the sensor and that HRP entrapped in the chitosan/sol-gel/CNT nanocomposite kept its bioelectrocatalytic activity. The electrocatalytic mechanism of HRP immobilized in the chitosan/sol-gel/CNT nanocomposite film to H_2O_2 reduction can be presented as follows [9]:

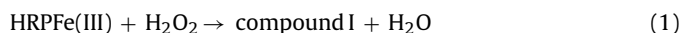


Fig. 7 is a typical current–time plot for chitosan/sol-gel/CNT/GCE (curve a), HRP/chitosan/sol-gel/GCE (curve b) and HRP/chitosan/sol-gel/CNT/GCE (curve c). As expected, the electrocatalytic current of the HRP/chitosan/sol-gel/CNT/GCE increases much more than those of the chitosan/sol-gel/CNT/GCE and HRP/chitosan/sol-gel/GCE with each addition of H_2O_2 to the supporting electrolyte. It can be seen from this figure that the most contribution of the reduction current is directly from the HRP catalysis. However, CNT also have the significant contribution because the high surface area of the CNT allows loading more HRP and the excellent electric conductivity of CNT makes the electron transfer easier between HRP and electrode. Besides, CNT increase the porosity of the film, which will lead to fast diffusion of the analytes. For the HRP/chitosan/sol-gel/CNT/GCE, the response time required to reach 95% of the maximum steady-state current is 5 s, which is faster than that of HRP/chitosan/sol-gel/GCE

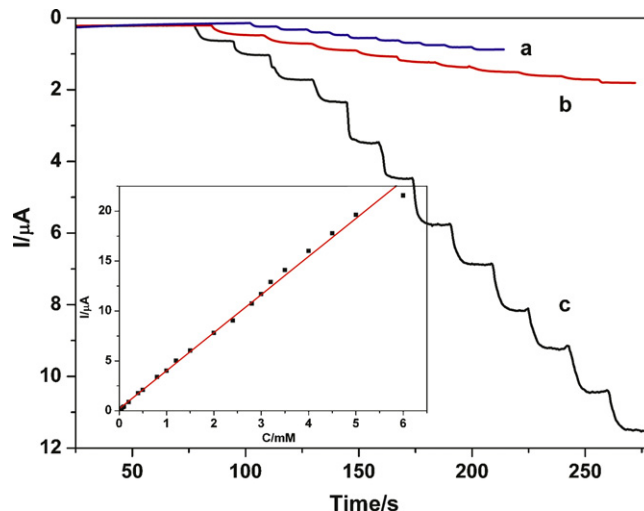


Fig. 7. Typical steady-state responses of the chitosan/sol-gel/CNT/GCE (a), HRP/chitosan/sol-gel/GCE (b) and HRP/chitosan/sol-gel/CNT/GCE (c) on successive injection of different concentration of H_2O_2 into PBS while stirring, with an applied potential of -0.3 V .

(10 s). The fast response can be ascribed to the CNT acceleration of electron transfer in a three-dimensional sol-gel matrix. The inset shown in Fig. 7 demonstrates the calibration curve with a linear range of the H_2O_2 concentration from $4.8 \mu\text{M}$ to 5.0 mM , which was wider than that reported in the literature [5,9]. The detection limit is estimated to be $1.4 \mu\text{M}$ at a signal-to-noise ratio of 3, which is lower than those reported in the literatures [6,15]. The Michaelis–Menten constant (K_m) can give information regarding the enzyme-substrate kinetics. The K_m was estimated about 6.51 mM for HRP/chitosan/sol-gel/CNT/GCE ($I^{-1} = 0.03454 + 0.22497C^{-1}$, $R = 0.9985$), which is lower than those reported in the literatures [5,6]. The smaller K_m value means that the immobilized HRP in chitosan/sol-gel with a CNT film possesses higher enzymatic activity and a higher affinity to H_2O_2 . The reproducibility of the sensor was examined, and its relative standard deviation (RSD) was 4.2% for six successive determinations in the solution with 0.2 mM H_2O_2 . The stability of the modified electrode was also estimated. When stored at 4°C for 2 weeks, the sol-gel modified GCE with a nanocomposite film showed nearly the same behavior for DET of HRP and the current response to H_2O_2 as its initial measurement. The sensor still kept more than 85% of its initial response to H_2O_2 after 1 month of storage. The good stability may attributed to the high biocompatible microenvironment around the enzyme provided by the inorganic–organic hybrid sol-gel with a CNT film and the three-dimensional network structure of the nanocomposite film preventing the leaching of the enzyme.

4. Conclusions

A biocompatible organic–inorganic nanocomposite of chitosan/sol-gel/CNT was prepared and applied in HRP immobilization and biosensor construction. The DET and electrocatalytic activity of HRP were investigated. The results indicated that the quasi-reversible and surface-controlled electron transfer kinetics for HRP was realized on chitosan/sol-gel/CNT/GCE. The uniform three-dimensional porous structure of composite film provided a favorable microenvironment around HRP to retain its native structure and bioelectrocatalytic activity with good stability and fast response to H_2O_2 . The unique chitosan/sol-gel/CNT nanocomposite film can be applied to further study the DET of other redox proteins and may find wide potential applications in biosensors.

Acknowledgments

The work was supported by a LDRD program at Pacific Northwest National Laboratory (PNNL). The research described in this paper was performed at the Environmental Molecular Sciences Laboratory, a national scientific user facility sponsored by the DOE's Office of Biological and Environmental Research and located at PNNL. PNNL is operated for the U.S. Department of Energy by Battelle under Contract DE-AC05-76RLO1830. X. Kang gratefully acknowledges the award of a PNNL fellowship to perform this work at PNNL.

References

- [1] M. El Kaoutit, I. Naranjo-Rodriguez, K.R. Tamsamani, M. Domínguez, J.L.H. Cisneros, *Talanta* 75 (2008) 1348–1355.
- [2] J.X. Wang, M.X. Li, Z.J. Shi, N.Q. Li, Z.N. Gu, *Anal. Chem.* 74 (2002) 1993–1997.
- [3] Z.J. Wang, M.Y. Li, P.P. Su, Y.J. Zhang, Y.F. Shen, D.X. Han, A. Ivaska, L. Niu, *Electrochem. Commun.* 10 (2008) 306–310.
- [4] C.L. Xiang, Y.J. Zou, L.X. Sun, F. Xu, *Electrochem. Commun.* 10 (2008) 38–41.
- [5] X.J. Zhao, Z.B. Mai, X.H. Kang, X.Y. Zou, *Biosens. Bioelectron.* 23 (2008) 1032–1038.
- [6] H.J. Chen, S.J. Dong, *Biosens. Bioelectron.* 22 (2007) 1811–1815.
- [7] J.J. Gooding, R. Wibowo, J.Q. Liu, W.R. Yang, D. Losic, S. Orbons, F.J. Mearns, J.G. Shapter, D.B. Hibbert, *J. Am. Chem. Soc.* 125 (2003) 9006–9007.
- [8] Y.D. Zhao, W.D. Zhang, H. Chen, Q.M. Luo, S. Fong, Y. Li, *Sens. Actuators B* 87 (2002) 168–172.
- [9] Q. Xu, C. Mao, N.N. Liu, J.J. Zhu, J. Sheng, *Biosens. Bioelectron.* 22 (2006) 768–773.
- [10] Y. Zhou, H. Yang, H.Y. Chen, *Talanta* 76 (2008) 419–423.
- [11] W.Y. Cai, Q. Xu, X.N. Zhao, J.J. Zhu, H.Y. Chen, *Chem. Mater.* 18 (2006) 279–284.
- [12] R. Andreu, E.E. Ferapontova, L. Gorton, J.J. Calvente, *J. Phys. Chem. B* 111 (2007) 469–477.
- [13] J. Wang, Y.H. Lin, *Trends Anal. Chem.* 27 (2008) 619–626.
- [14] J. Wang, M. Musameh, Y.H. Lin, *J. Am. Chem. Soc.* 125 (2003) 2408–2409.
- [15] Y.H. Lin, F. Lu, Y. Tu, Z.F. Ren, *Nano Lett.* 4 (2004) 191–195.
- [16] G. Liu, Y.H. Lin, *J. Nanosci. Nanotechnol.* 6 (2006) 948–953.
- [17] G. Liu, Y.H. Lin, *Electrochem. Commun.* 8 (2006) 251–256.
- [18] J.L. Lyon, K.J. Stevenson, *Electrochim. Acta* 53 (2008) 6714–6721.
- [19] G.C. Zhao, Z.Z. Yin, L. Zhang, X.W. Wei, *Electrochem. Commun.* 7 (2005) 256–260.
- [20] Y. Yan, W. Zheng, M. Zhang, L. Wang, L. Su, L.Q. Mao, *Langmuir* 21 (2005) 6560–6566.
- [21] Y.D. Zhao, Y.H. Bi, W.D. Zhang, Q.M. Luo, *Talanta* 65 (2005) 489–494.
- [22] X. Yu, D. Chattopadhyay, I. Galeska, F. Papadimitrakopoulos, J.F. Rusling, *Electrochem. Commun.* 5 (2003) 408–411.
- [23] G.C. Zhao, L. Zhang, X.W. Wei, Z.S. Yang, *Electrochem. Commun.* 5 (2003) 825–829.
- [24] X.L. Luo, A.J. Killard, M.R. Smyth, *Electroanalysis* 18 (2006) 1131–1134.
- [25] J.D. Zhang, M.L. Feng, H. Tachikawa, *Biosens. Bioelectron.* 22 (2007) 3036–3041.
- [26] C.Y. Deng, J.H. Chen, X.L. Chen, C.H. Xiao, L.H. Nie, S.Z. Yao, *Biosens. Bioelectron.* 23 (2008) 1272–1277.
- [27] A. Guiseppi-Elie, C.H. Lei, R.H. Baughman, *Nanotechnology* 13 (2002) 559–564.
- [28] Y. Liu, M.K. Wang, F. Zhao, Z. Xu, S. Dong, *Biosens. Bioelectron.* 21 (2005) 984–988.
- [29] X.H. Kang, Z.B. Mai, X.Y. Zou, P.X. Cai, J.Y. Mo, *Talanta* 74 (2008) 879–886.
- [30] X. Luo, J. Xu, Q. Zhang, G. Yang, H. Chen, *Biosens. Bioelectron.* 21 (2005) 190–196.
- [31] X.H. Kang, Z.B. Mai, X.Y. Zou, P.X. Cai, J.Y. Mo, *Anal. Biochem.* 369 (2007) 71–79.
- [32] M. Collinson, A.R. Howells, *Anal. Chem.* 72 (2000) 702A–709A.
- [33] A. Walcarius, D. Mandler, J.A. Cox, M. Collinson, O. Lev, *J. Mater. Chem.* 15 (2005) 3663–3689.
- [34] B. Wang, B. Li, Q. Deng, S. Dong, *Anal. Chem.* 70 (1998) 3170–3174.
- [35] B. Wang, J. Zhang, G. Cheng, S. Dong, *Anal. Chim. Acta* 407 (2000) 111–118.
- [36] H. Yi, L.Q. Wu, W.E. Bentley, R. Ghodssi, G.W. Rubloff, J.N. Culver, G.F. Payne, *Biomacromolecules* 6 (2005) 2881–2894.
- [37] X. Tan, Y. Tian, P. Cai, X. Zou, *Anal. Bioanal. Chem.* 381 (2005) 500–507.
- [38] A.M. Chiorcea-Paquim, R. Pauliuraitė, C.M.A. Brett, A.M. Olivera-Brett, *Biosens. Bioelectron.* 24 (2008) 297–305.
- [39] R.R. Naik, M.M. Tomczak, H.R. Luckarift, J.C. Spain, M.O. Stone, *Chem. Commun.* 15 (2004) 1684–1685.
- [40] J.B. Jia, B.Q. Wang, A.G. Wu, G.G. Cheng, Z. Li, S.J. Dong, *Anal. Chem.* 74 (2002) 2217–2223.
- [41] H. Luo, Z. Shi, N. Li, Z. Gu, Q. Zhuang, *Anal. Chem.* 73 (2001) 915–920.
- [42] H. Huang, N. Hu, Y. Zeng, G. Zhou, *Anal. Biochem.* 308 (2002) 141–151.
- [43] S.F. Wang, T. Chen, Z.L. Zhang, X.C. Shen, Z.X. Lu, D.W. Pang, K.Y. Wong, *Langmuir* 21 (2005) 9260–9266.
- [44] E. Laviron, *J. Electroanal. Chem.* 101 (1979) 19–28.
- [45] L. Zhang, Q. Zhang, X.B. Lu, J.H. Li, *Biosens. Bioelectron.* 23 (2007) 102–106.



Nanocrystalline $\text{Ni}_{0.6}\text{Zn}_{0.4}\text{Fe}_2\text{O}_4$: A novel semiconducting material for ethanol detection

V.D. Kapse^{a,*}, S.A. Ghosh^a, F.C. Raghuwanshi^b, S.D. Kapse^c, U.S. Khandekar^d

^a P.G. Department of Physics, Government Vidarbha Institute of Science & Humanities, Amravati 444604, Maharashtra, India

^b P.G. Department of Physics, Vidyabharati Mahavidyalaya, Amravati 444604, Maharashtra, India

^c Department of Physics, G.S. College, Khamgaon 444303, Maharashtra, India

^d Department of Chemistry, Arts, Science and Commerce College, Amravati 444606, Maharashtra, India

ARTICLE INFO

Article history:

Received 12 September 2008

Received in revised form 21 October 2008

Accepted 22 October 2008

Available online 31 October 2008

Keywords:

Gas sensor

Selectivity

Nickel ferrites

Sensor response

Recovery

ABSTRACT

The structure and crystal phase of the nanocrystalline powders of $\text{Ni}_{1-x}\text{Zn}_x\text{Fe}_2\text{O}_4$ ($0 \leq x \leq 0.5$) mixed ferrite, synthesized by ethylene glycol mediated citrate sol–gel method, were characterized by X-ray diffraction and microstructure by transmission electron microscopy. Further studies by Fourier transform infrared spectroscopy were also conducted. Moreover, DC electrical properties of the prepared nanoparticles were studied by DC conductivity measurements. The response of prepared $\text{Ni}_{1-x}\text{Zn}_x\text{Fe}_2\text{O}_4$ mixed ferrites to different reducing gases (ethanol, hydrogen sulfide, ammonia, hydrogen and liquefied petroleum gas) was investigated. In particular, $\text{Ni}_{0.6}\text{Zn}_{0.4}\text{Fe}_2\text{O}_4$ composition exhibited high response to 100 ppm ethanol gas at 300 °C. Incorporation of palladium further improved the response, selectivity and response time of $\text{Ni}_{0.6}\text{Zn}_{0.4}\text{Fe}_2\text{O}_4$ to ethanol gas with the blue shift in the operating temperature by 25 °C.

© 2008 Elsevier B.V. All rights reserved.

1. Introduction

Gas sensors based on metal oxides are commonly used in the monitoring of toxic pollutants and can provide the necessary sensitivity, selectivity and stability required by such systems. A variety of semiconductor metal oxides such as SnO_2 , ZnO , WO_3 and In_2O_3 are representative sensing layer materials for the detection of various gases [1–4]. At 200–450 °C, a resistive electron depletion layer is established near the surface of the n-type oxide semiconductor by the adsorption of negatively charged oxygen, which has an oxidative or reductive interaction with the target gases that induce a large change in electrical conductivity. But, these sensing layer materials react with a number of gases simultaneously.

Among the methods used, the fabrication of a new sensor composition by making a composite or solid solution between sensing materials has a great potential accomplishing better gas-sensing characteristics such as sensitivity and selectivity. In general, ferrites with high density are used for magnetic or electrical applications. But, for gas or humidity sensors, for which lower density and nano-sized structures are preferred. As suggested by several authors

nanosized grains of sensing layer materials are preferred to increase the specific surface area exposed to analyte gas [5,6]. Spinel of the type $\text{M}^{2+}\text{M}_2^{3+}\text{O}_4$ attract the research interest because of their versatile practical applications [7–9]. In the case of $\text{M}^{3+} = \text{Fe}$, the resulting spinel ferrites having a general chemical composition of MFe_2O_4 ($\text{M} = \text{Mn}, \text{Mg}, \text{Zn}, \text{Ni}, \text{Co}, \text{Cd}, \text{etc.}$) are widely used as magnetic materials. Currently it is a topic of increasing interest to study the gas-sensing properties of ferrites [10–12]. However, information on the gas-sensing properties of nanocrystalline ferrites (MFe_2O_4) is still limited.

Ethyl alcohol is the most important alcohol owing to its varied applications. It is a solvent for various alcohol soluble active ingredients and also an alternative to automotive fuels. Ethanol is widely used as well in food industry, brewing process control, medical and clinical applications and bio-technological processes. Detection of alcohol vapour is one of the most popular needs in our daily life. The more common application of an alcohol sensor is as a breath checker and to detect ethanol vapour in human breaths, which is said to be correlated with the alcohol concentration in the blood and to monitor the alcohol vapours in air.

The current efficient ethanol sensors are based on LaNiO_3 [13] as well as pure and doped SnO_2 [14–16], In_2O_3 [17], TiO_2 [18], WO_3 [19], and ZnO [20]. There are almost no literature reports concerning gas-sensing properties of $\text{Ni}_{1-x}\text{Zn}_x\text{Fe}_2\text{O}_4$. In this paper, nanocrystalline powders of $\text{Ni}_{1-x}\text{Zn}_x\text{Fe}_2\text{O}_4$ ($x = 0 \leq x \leq 0.5$) complex

* Corresponding author. Tel.: +91 9422157790.

E-mail addresses: vdk_research@yahoo.com, vdk.nano@gmail.com, ath135@rediffmail.com (V.D. Kapse).

oxides were prepared by ethylene glycol mediated citrated sol–gel method. In an attempt to enhance the response and impart selectivity, the nanoparticles of NiFe_2O_4 have been partly replaced with Zn in place of Ni. Further, Palladium (Pd) modified $\text{Ni}_{0.6}\text{Zn}_{0.4}\text{Fe}_2\text{O}_4$ demonstrated enhanced response to $\text{C}_2\text{H}_5\text{OH}$ with better selectivity.

2. Experimental

2.1. Material preparation

Ferrites of various compositions with general formulas $\text{Ni}_{1-x}\text{Zn}_x\text{Fe}_2\text{O}_4$ ($x = 0 \leq x \leq 0.5$) were prepared by the ethylene glycol mediated citrate sol–gel method [5].

2.2. Palladium incorporation

Palladium (Pd) was incorporated into the prepared sample by dissolving PdCl_2 in water along with the sample and then calcining at 250°C for 2 h to decompose the PdCl_2 . Pd was varied from 0.5 to 1.5 wt.%.

2.3. Structure and morphology studies

The crystal phases of calcined samples were analyzed using X-ray diffraction (XRD). The average grain size has been calculated from the XRD peaks using Debye–Scherrer formula. The lattice parameters of the prepared powder samples were calculated from the XRD peaks by indexing corresponding peaks in a cubic space group $Fd3m$, using least square refinement. The structure, morphology and grain size of the samples were observed using transmission electron microscopy along with electron diffraction patterns (TEM-ED).

2.4. DC electrical conductivity measurements

Fabricated sample holder was used to study DC characteristics of the $\text{Ni}_{1-x}\text{Zn}_x\text{Fe}_2\text{O}_4$ ($x = 0 \leq x \leq 0.5$) nanoparticles in the range $50\text{--}350^\circ\text{C}$ with a step of 10°C . The samples were used in the form of circular pellets of diameter 1.3 and 0.3 cm thickness. The sur-

faces of the pellets were polished well, coated with silver paste as contact materials for the electrical measurements. The pellets were sandwiched between two spring-loaded gold electrodes. To study the semiconducting nature of prepared materials, the DC electrical conductivity, σ_{dc} , was determined from the DC I–V characteristics for each sample at different temperatures, in the range $50\text{--}350^\circ\text{C}$ with a step of 10°C , using Ohm's law. The $\ln \sigma$ vs. $10^3/T$ plots for the samples have been plotted and the activation energy has been calculated.

The relationship between electrical conductivity and temperature may be expressed as

$$\sigma = \sigma_0 \exp \left\{ -\frac{\Delta E_a}{kT} \right\} \quad (1)$$

where ΔE_a denotes the thermal activation energy of electrical conduction, σ_0 represents a parameter depending on the semiconductor nature and k is the Boltzmann's constant.

2.5. Gas-sensing properties

The calcined $\text{Ni}_{1-x}\text{Zn}_x\text{Fe}_2\text{O}_4$ powders were mixed with α -terpineol as a binder to form pastes. The paste was coated onto an alumina tube on which two gold leads had been installed at each end. For this, the alumina tube was dipped several times in the prepared paste. The thickness of sensing layer was kept $\sim 40\text{--}41 \mu\text{m}$ for each composition. The alumina tube was about 8 mm in length, 2 mm in external diameter and 1.6 mm in internal diameter. A small Ni–Cr alloy coil was placed through the tube as a heater. The heater provide operating temperatures from 200 to 450°C . The temperature was controlled by adjusting the heating power. In order to improve their stability and repeatability, the gas-sensing elements were heated at 500°C for 5 days in air. The description of the schematic sensor assembly and the circuitry for the sensor characteristics measurement was reported in our earlier publication [21]. The sensor response to a test gas, S , is defined as the ratio $\Delta R/R_a$, i.e. change in resistance of the sensor (R_a) in air and in the gas (R_g), normalized to the sensor resistance in air [22]:

$$S = \frac{\Delta R}{R_a} = \frac{|R_a - R_g|}{R_a} \quad (2)$$

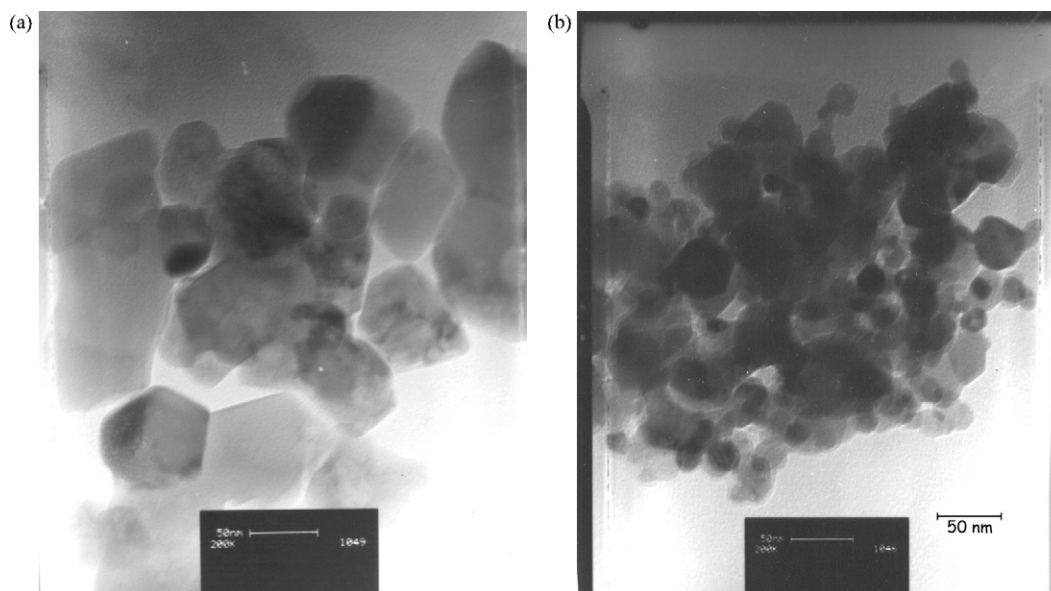


Fig. 1. TEM images of $\text{Ni}_{1-x}\text{Zn}_x\text{Fe}_2\text{O}_4$ powders with (a) $x = 0$ and (b) $x = 0.4$.

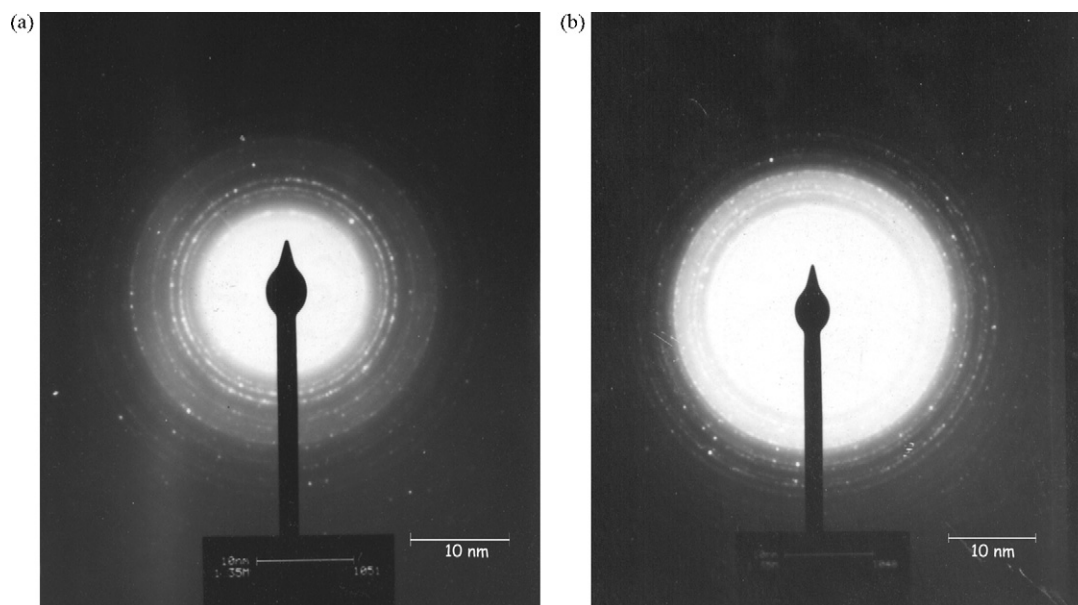


Fig. 2. Selected area diffraction pattern of $\text{Ni}_{1-x}\text{Zn}_x\text{Fe}_2\text{O}_4$ powders with (a) $x=0$ and (b) $x=0.4$.

3. Results and discussion

3.1. Structural characterization

From the previous results by X-ray diffraction analysis [5], it was found that all the ferrite samples calcinated at 700°C have a spinel cubic structure. The lattice parameters were found to increase from 8.332 ± 0.002 to $8.389 \pm 0.002 \text{ \AA}$ with the increase in Zn content. The TEM micrographs and selected area electron diffraction patterns of $\text{Ni}_{1-x}\text{Zn}_x\text{Fe}_2\text{O}_4$ ($x=0$ and 0.4) powders calcinated at 700°C are shown in Figs. 1(a and b) and 2(a and b), respectively. The resulting powder consists of nanoparticles (Table 1), which are well dispersed and are seen to be nearly spheroidal with irregular polyhedron (Fig. 2). The average crystallite size estimated from XRD data corroborates with the TEM investigations. The small amount of agglomerations is observed in the micrographs. Moreover, the amount of agglomeration is found to decrease with increase in the Zn content.

The selected area electron diffraction (SAED) patterns, presented in Fig. 2(a and b), correspond to that of a spinel phase, agreeing with the results obtained from powder XRD analysis. The rings on the diffraction pattern depicted a spinel crystal structure of nickel ferrite. Several lines [2 2 0], [3 1 1], [4 0 0], [5 1 1] and [4 4 0] could be identified in the diffraction pattern. Their positions and intensities confirm clearly the spinel crystallographic structure.

3.2. Fourier transform infrared spectroscopy (FT-IR)

The IR spectra of the $\text{Ni}_{1-x}\text{Zn}_x\text{Fe}_2\text{O}_4$ samples with $x=0, 0.2, 0.3, 0.4$ calcinated at 700°C , presented in Fig. 3, show small dif-

ferences in the range $4000\text{--}400 \text{ cm}^{-1}$. The intensive broadband, around 3450 cm^{-1} is due to O–H stretching vibration interacting through H bonds. The second one, observed at $\sim 1600 \text{ cm}^{-1}$, is less intensive.

In the range $1000\text{--}100 \text{ cm}^{-1}$, the IR bands of solids are usually assigned to vibration of ions in the crystal lattice [23]. Two main broad metal–oxygen bands are seen in the IR spectra of all spinels, and ferrites in particular. The highest one, ν_1 ; generally observed in the range $600\text{--}550 \text{ cm}^{-1}$, corresponds to intrinsic stretching vibrations of the metal at the tetrahedral site, $M_{\text{tetra}} \leftrightarrow \text{O}$, whereas the ν_2 -lowest band, usually observed in the range $450\text{--}385 \text{ cm}^{-1}$, is assigned to octahedral–metal stretching, $M_{\text{octa}} \leftrightarrow \text{O}$ [24]. The band values of the $\text{Ni}_{1-x}\text{Zn}_x\text{Fe}_2\text{O}_4$ are given in Table 2. In the present spectrum band, ν_1 and ν_2 appeared near 589 and 420 cm^{-1} . These two strong absorption bands are typical of inverse spinel ferrites and the positions of these infrared bands are in the range which corresponds to nickel ferrite [25].

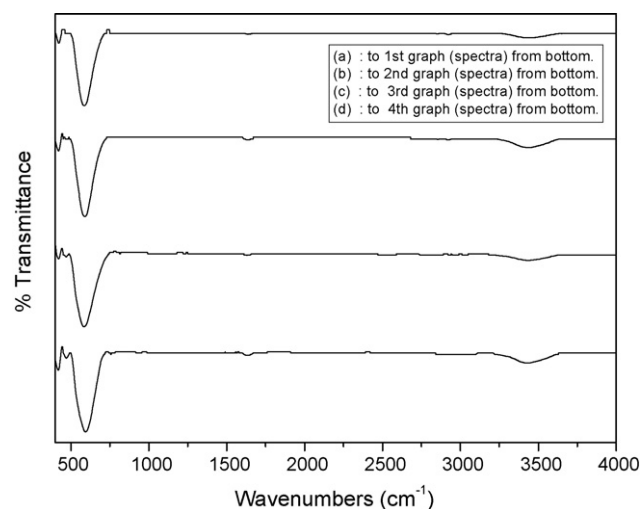


Fig. 3. The IR spectra of $\text{Ni}_{1-x}\text{Zn}_x\text{Fe}_2\text{O}_4$ powders with (a) $x=0$, (b) $x=0.2$, (c) $x=0.3$ and (d) $x=0.4$ calcinated at 700°C .

Table 1

Average crystallite size and activation energies E_{HT} and E_{LT} (eV) of $\text{Ni}_{1-x}\text{Zn}_x\text{Fe}_2\text{O}_4$ with $x=0, 0.2, 0.3, 0.4$ and 0.5 .

Compound	Average grain size (nm)	E_{HT} (eV)	E_{LT} (eV)
NiFe_2O_4	39	0.6156	0.38
$\text{Ni}_{0.8}\text{Zn}_{0.2}\text{Fe}_2\text{O}_4$	42	0.5232	0.3824
$\text{Ni}_{0.7}\text{Zn}_{0.3}\text{Fe}_2\text{O}_4$	30	0.4769	0.4018
$\text{Ni}_{0.6}\text{Zn}_{0.4}\text{Fe}_2\text{O}_4$	31	0.4735	0.3438
$\text{Ni}_{0.5}\text{Zn}_{0.5}\text{Fe}_2\text{O}_4$	28	0.4714	0.3158

Table 2

FT-IR vibrations for $\text{Ni}_{1-x}\text{Zn}_x\text{Fe}_2\text{O}_4$ compounds calcined 6 h at 700 °C; ν_1 and ν_2 correspond to the transition ions stretching vibrations in tetrahedral and octahedral sites, respectively.

Compound	ν_1 (cm^{-1})	ν_2 (cm^{-1})
NiFe_2O_4	594.454	419.515
$\text{Ni}_{0.8}\text{Zn}_{0.2}\text{Fe}_2\text{O}_4$	583.879	421.045
$\text{Ni}_{0.7}\text{Zn}_{0.3}\text{Fe}_2\text{O}_4$	589.533	420.786
$\text{Ni}_{0.6}\text{Zn}_{0.4}\text{Fe}_2\text{O}_4$	586.005	422.638

A new band ν_3 around 470 cm^{-1} appears and which gets diminished with the increase in the Zn content. This may be due to $n \rightarrow \sigma^*$ transition which indicates the formation of co-ordinate bond in the compound formation. On the basis of FT-IR spectrum, it is concluded that the ethylene glycol mediated citrate sol-gel method results into the deposition of single-phase cubic spinel nanocrystalline NiFe_2O_4 at 700 °C.

3.3. DC electrical conductivity measurements

Temperature dependence of DC electrical conductivity, σ_{DC} , is presented in Fig. 4. As expected for semiconductors, the conductivity of ferrites increases with rising temperature according to the well-known relation provided in Eq. (1). The increase in the electrical conductivity as temperature increases may be related to the increase in drift mobility of the thermally activated charge carriers (electron and hole) according to hopping conduction mechanism.

The semilogarithmic relations for σ_{DC} represent almost a straight line for each sample, the line changes its slope at the Curie temperature T_c , as was expected theoretically. It was reported that, on passing through the Curie point a change in the gradient of the straight line (Fig. 4) must take place. The magnitude of this effect (gradient or slope) depends on the exchange interaction, which determines the Curie point T_c . The activation energy for electric conduction E_{LT} in the low temperature and E_{HT} in the high temperature regions were calculated from the slopes of lines on both sides of Curie temperature T_c . From Fig. 4, it can be seen that the DC electrical conductivity shows almost a linear increase with temperature for all the samples. The variation of conductivity is explained on the basis of actual location of cation in the spinel structure. Occurrence of ions in more than one valence states is caused by the prepara-

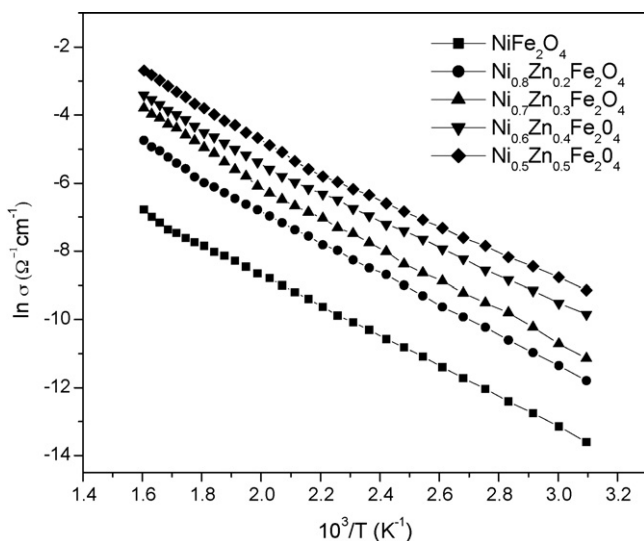


Fig. 4. Effect of temperature on DC electrical conductivity of $\text{Ni}_{1-x}\text{Zn}_x\text{Fe}_2\text{O}_4$ with (a) $x=0$, (b) $x=0.2$, (c) $x=0.3$, (d) $x=0.4$ and (e) $x=0.5$.

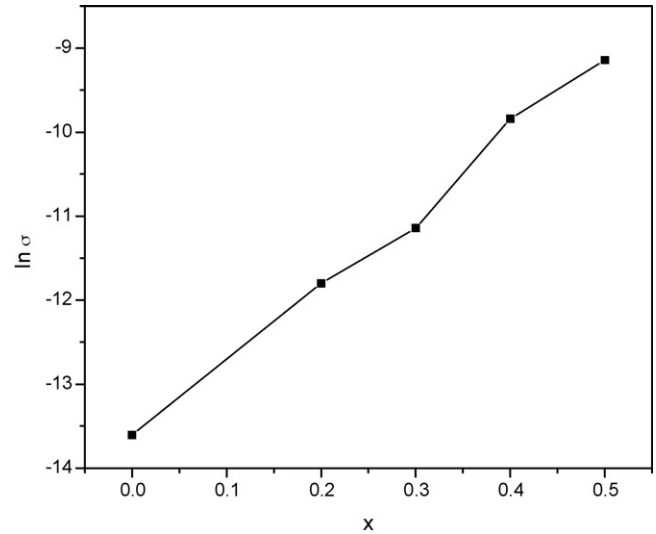


Fig. 5. Effect of Zn-ion substitution on DC electrical conductivity at 50 °C.

tion conditions, especially, the sintering temperature: Fe^{2+} ions in the lattice are created due to zinc loss during the sintering process. Loss of Zn results in cation vacancies and unsaturated oxygen ions. The excess electrons on oxygen then bond with the neighboring Fe^{3+} ions in the spinel lattice due to electrostatic interaction giving rise to Fe^{2+} ions. The overall charge balance is restored by oxygen loss from the sample. Formation of Fe^{2+} ions leads to deviations from ferrite stoichiometry. The number of Fe^{2+} ions depends on the amount of zinc lost from the sample on volatilization, which in turn is dependent on the sintering temperature of the ferrite. Higher the sintering temperature, greater is the possibility of Fe^{2+} formation. Creation of Fe^{2+} ions gives rise to electron hopping between the Fe ions in +2 and +3.

The effect of Zn-ion addition on DC electrical conductivities is represented in Fig. 5 at 50 °C. The σ_{DC} increases as Zn-ion substitution increases. On increasing Zn ion substitution (at A sites), the Ni ion concentration (at B sites) will decrease. This leads to the migration of some Fe ions from A sites to B sites to substitute the reduction in Ni ion concentration at B sites. As a result, the number of Fe^{2+} and Fe^{3+} ions (on the B-sites between which the electron exchange interaction takes place) increases while the number of Ni^{2+} and Ni^{3+} ions (between which the hole hopping takes place) decreases as Zn-ions substitution increases. Therefore, σ_{DC} increase as Zn-ion addition increases. Another reason for the increase in σ on increasing Zn ion substitution is that, zinc is less resistive ($\rho = 5.92 \mu\Omega \text{ cm}$) than nickel ($\rho = 6.99 \mu\Omega \text{ cm}$) [26].

The activation energy calculated from the slope of inverse temperature vs. $\ln \sigma$ plot lies within the range 0.6156–0.4714 eV in the high temperature region. It is seen from that value of activation energy decreases with zinc concentration (Table 1). The decrease in the activation energies E_{HT} , E_{LT} and Curie temperature T_c , as zinc ion substitution increases could be related to the same reasons for the decrease in the electrical resistivity. This result is in good accordance with the conclusion that the lower activation energy (as Zn ion substitution increases) is associated with higher electrical conductivity [27].

3.4. Gas-sensing characteristics

The gas-sensing responses of $\text{Ni}_{1-x}\text{Zn}_x\text{Fe}_2\text{O}_4$ ($x=0 \leq x \leq 0.5$) to different reducing gases like ethanol ($\text{C}_2\text{H}_5\text{OH}$), ammonia (NH_3), hydrogen sulfide (H_2S), hydrogen (H_2) and liquefied petroleum

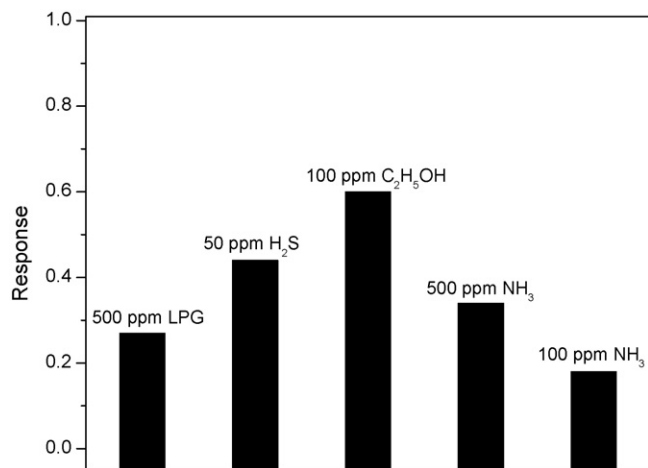
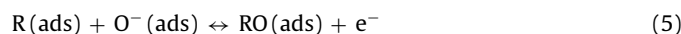


Fig. 6. Response of $\text{Ni}_{0.6}\text{Zn}_{0.4}\text{Fe}_2\text{O}_4$ towards $\text{C}_2\text{H}_5\text{OH}$ (100 ppm), NH_3 (500 ppm), H_2S (50 ppm), H_2 (500 ppm) and LPG (500 ppm) at 300°C .

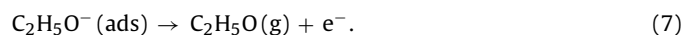
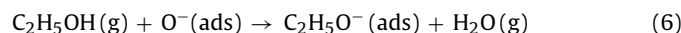
gas (LPG) as a function of operating temperature were studied. In our previous work [5], we have reported that the $\text{Ni}_{0.6}\text{Zn}_{0.4}\text{Fe}_2\text{O}_4$ nanocrystalline powder calcined at 700°C for 6 h exhibited good response to 100 ppm $\text{C}_2\text{H}_5\text{OH}$ at 300°C . The response of $\text{Ni}_{0.6}\text{Zn}_{0.4}\text{Fe}_2\text{O}_4$ towards $\text{C}_2\text{H}_5\text{OH}$ (100 ppm), NH_3 (500 ppm), H_2S (50 ppm), H_2 (500 ppm) and LPG (500 ppm) at 300°C is depicted in Fig. 6. It was found that the sensor element based on $\text{Ni}_{0.6}\text{Zn}_{0.4}\text{Fe}_2\text{O}_4$ could detect $\text{C}_2\text{H}_5\text{OH}$ at 300°C with poor selectivity.

The reducing gas R acting on the $\text{Ni}_{1-x}\text{Zn}_x\text{Fe}_2\text{O}_4$ surface can be described as



In the absence of R, electrons are removed from $\text{Ni}_{1-x}\text{Zn}_x\text{Fe}_2\text{O}_4$ conduction band by the reduction of O_2 , resulting in the formation of O^- species and consequently the resistance of $\text{Ni}_{1-x}\text{Zn}_x\text{Fe}_2\text{O}_4$ sensor increases. When R is introduced, it reacts with $\text{O}^-(\text{ads})$ to form RO, and electrons enter the conduction band of $\text{Ni}_{1-x}\text{Zn}_x\text{Fe}_2\text{O}_4$ leading to decrease of resistance.

The reactions involved during the ethanol sensing are summarised below (taking O^- and $\text{C}_2\text{H}_5\text{O}$ for example) [28]:



3.5. Effect of palladium (Pd)

Sensor should be such that it could sense a particular gas in the presence of other interfering gases. Selectivity is the capacity of sensor to distinguish between the gases in mixture. To achieve selective gas sensing, different approaches like controlling the sensing temperature [29,30], the addition of a noble metal [31] or oxide catalysts [32] and the design of multi-compositional sensing materials [33,34] have been instigated.

The effect of noble metal addition on the gas-sensing properties of metal oxide has formally been classified as chemical or electronic according to two basic sensitization mechanisms. The two mechanisms are so-called spill over mechanism and Fermi energy control. The observed increase in sensor response of Pd is mainly due to the change, which is termed as the electronic sensitization [35–37]. In this case, the close electronic contacts of the semicon-

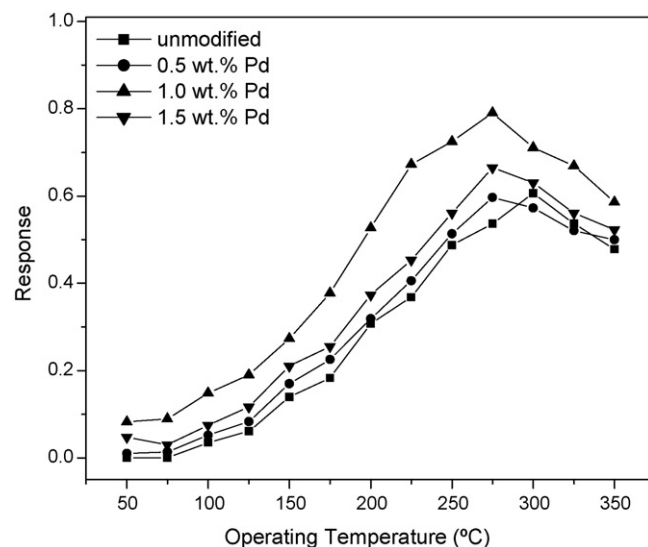


Fig. 7. Sensor response as a function of operating temperature for unmodified and Pd modified $\text{Ni}_{0.6}\text{Zn}_{0.4}\text{Fe}_2\text{O}_4$ to 100 ppm $\text{C}_2\text{H}_5\text{OH}$.

ductor with the catalyst dominate the sensor signal. Oxygen species at the surface of the catalyst trap electrons from the semiconductor. Since the density of electrons in the bulk changes by this process, a depletion layer is created and band bending occurs. Under the influence of the ambient gas atmosphere, the catalyst particles become oxidized. The stoichiometry of the catalyst (MO_{2-x}) depends on the composition of the ambient air and so does the position of its Fermi level. At equilibrium, the Fermi level of the catalyst and the semiconductor are at the same height. Since the gas reacts with the semiconductor via the catalyst, the chosen catalyst can strongly change the selectivity of semiconducting material.

Fig. 7 illustrates the response of unmodified and Pd (0.5–1.5 wt.%) modified $\text{Ni}_{0.6}\text{Zn}_{0.4}\text{Fe}_2\text{O}_4$ as a function of the operating temperature towards 100 ppm $\text{C}_2\text{H}_5\text{OH}$. From the plots it is clearly evident that on impregnation of the $\text{Ni}_{0.6}\text{Zn}_{0.4}\text{Fe}_2\text{O}_4$ with 1.0 wt.% Pd, there was notable enhancement in the response to 100 ppm $\text{C}_2\text{H}_5\text{OH}$ with reduction in the optimal operating temperature. The operating temperature for maximum response towards 100 ppm $\text{C}_2\text{H}_5\text{OH}$ was observed at about 275°C . This indicates a catalytic activity for Pd.

To know about the selective behavior of 1.0 wt.% Pd sensitized $\text{Ni}_{0.6}\text{Zn}_{0.4}\text{Fe}_2\text{O}_4$ towards $\text{C}_2\text{H}_5\text{OH}$ at optimal operating temperature, its response to H_2S (50 ppm), LPG (500 ppm), NH_3 (500 ppm) and H_2 (500 ppm) was also studied. The results are shown in Fig. 8. Furthermore, the response of $\text{Ni}_{0.6}\text{Zn}_{0.4}\text{Fe}_2\text{O}_4:\text{Pd}$ (1.0 wt.%) to $\text{C}_2\text{H}_5\text{OH}$ was also measured at 275°C in the presence of other tested interfering gases. For this, 100 ppm $\text{C}_2\text{H}_5\text{OH}$ was injected in the testing chamber, and then, in its presence, LPG (500 ppm), NH_3 (500 ppm), H_2 (500 ppm) and H_2S (50 ppm) were also injected. Thereafter, the change in the response of sensor element to 100 ppm of $\text{C}_2\text{H}_5\text{OH}$ was measured. The results are depicted in Table 3. It can

Table 3
Response of sensor element to $\text{C}_2\text{H}_5\text{OH}$ and other interfering gases.

Sensor element	Operating temperature ($^\circ\text{C}$)	Gas species (ppm)	Response
$\text{Ni}_{0.6}\text{Zn}_{0.4}\text{Fe}_2\text{O}_4:\text{Pd}$ (1.0 wt.%)	275	100 $\text{C}_2\text{H}_5\text{OH}$	0.79
		100 $\text{C}_2\text{H}_5\text{OH} + 50 \text{H}_2\text{S}$	0.90
		100 $\text{C}_2\text{H}_5\text{OH} + 500 \text{LPG}$	0.82
		100 $\text{C}_2\text{H}_5\text{OH} + 500 \text{NH}_3$	0.81
		100 $\text{C}_2\text{H}_5\text{OH} + 500 \text{H}_2$	0.79

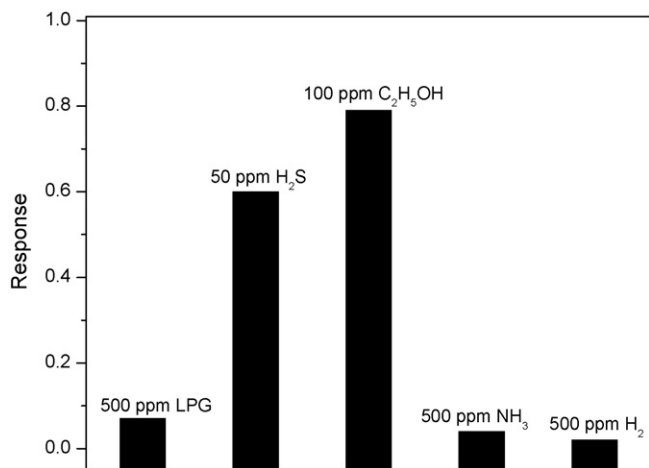


Fig. 8. Sensor response of Pd (1.0 wt.%) modified $\text{Ni}_{0.6}\text{Zn}_{0.4}\text{Fe}_2\text{O}_4$ to different gases at 275 °C.

be seen that the response of sensor elements to $\text{C}_2\text{H}_5\text{OH}$ remains high after the introduction of interfering gases like H_2 , LPG and NH_3 besides $\text{C}_2\text{H}_5\text{OH}$ in the testing chamber. The influence of other reducing gases that are additionally present on the $\text{C}_2\text{H}_5\text{OH}$ characteristics was found to be nearly 0–14% at 275 °C. So, it can be seen that Pd (1.0 wt.%) modified $\text{Ni}_{0.6}\text{Zn}_{0.4}\text{Fe}_2\text{O}_4$ increases the response along with enhancing the selectivity to $\text{C}_2\text{H}_5\text{OH}$.

The variations of response of unmodified and Pd (1.0 wt.%) modified $\text{Ni}_{0.6}\text{Zn}_{0.4}\text{Fe}_2\text{O}_4$ sensor elements at their respective optimal operating temperature for different concentrations of $\text{C}_2\text{H}_5\text{OH}$ is provided in Fig. 9. The sensor element $\text{Ni}_{0.6}\text{Zn}_{0.4}\text{Fe}_2\text{O}_4$:Pd (1.0 wt.%) is able to detect $\text{C}_2\text{H}_5\text{OH}$ upto 25 ppm at 275 °C with the response of 0.40. The sensors exhibited an increase in response as a function of $\text{C}_2\text{H}_5\text{OH}$ concentration up to 250 ppm and it is observed that the sensor has tendency to saturate at 250 ppm of $\text{C}_2\text{H}_5\text{OH}$. Moreover, it is important to note here that the sensor response is not linear from 40 to 250 ppm.

3.6. Response and recovery

The response-recovery characteristics of the $\text{Ni}_{0.6}\text{Zn}_{0.4}\text{Fe}_2\text{O}_4$ and $\text{Ni}_{0.6}\text{Zn}_{0.4}\text{Fe}_2\text{O}_4$:Pd (1.0 wt.%) sensor elements to 100 ppm

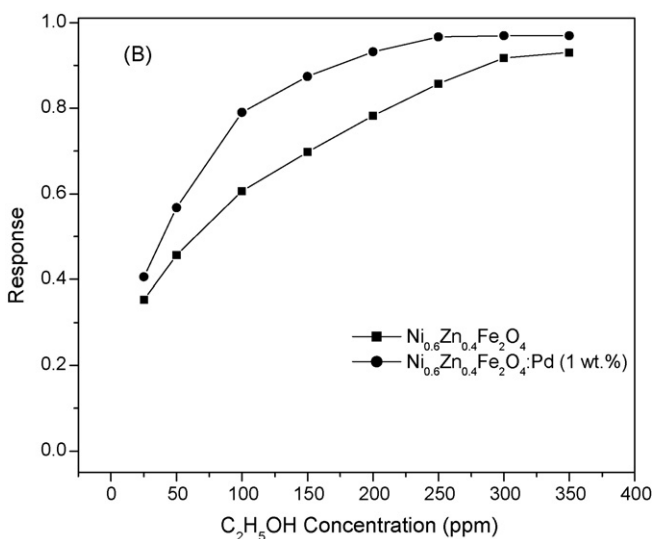


Fig. 9. The response vs. $\text{C}_2\text{H}_5\text{OH}$ concentration of unmodified and Pd (1.0 wt.%) modified $\text{Ni}_{0.6}\text{Zn}_{0.4}\text{Fe}_2\text{O}_4$ sensor element at 300 and 275 °C, respectively.

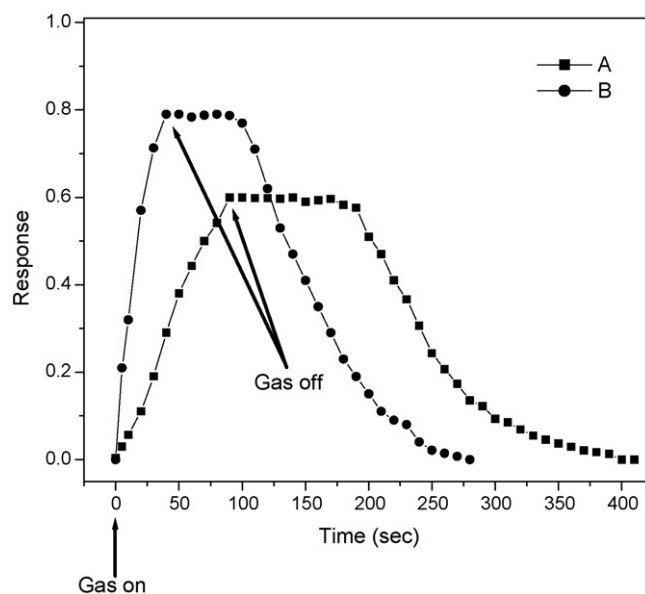


Fig. 10. Response characteristics of (A) $\text{Ni}_{0.6}\text{Zn}_{0.4}\text{Fe}_2\text{O}_4$ at 300 °C and (B) $\text{Ni}_{0.6}\text{Zn}_{0.4}\text{Fe}_2\text{O}_4$:Pd (1.0 wt.%) at 275 °C to 100 ppm $\text{C}_2\text{H}_5\text{OH}$.

$\text{C}_2\text{H}_5\text{OH}$ at 300 and 275 °C are shown in Fig. 10. The response and recovery time of the Pd modified $\text{Ni}_{0.6}\text{Zn}_{0.4}\text{Fe}_2\text{O}_4$ was found to reduce as compared with unmodified $\text{Ni}_{0.6}\text{Zn}_{0.4}\text{Fe}_2\text{O}_4$. The result indicates that the $\text{Ni}_{0.6}\text{Zn}_{0.4}\text{Fe}_2\text{O}_4$:Pd (1.0 wt.%) sensor can meet the practical application for $\text{C}_2\text{H}_5\text{OH}$ detection.

3.7. Stability

In order to check the stability of $\text{Ni}_{0.6}\text{Zn}_{0.4}\text{Fe}_2\text{O}_4$, $\text{Ni}_{0.6}\text{Zn}_{0.4}\text{Fe}_2\text{O}_4$:Pd (1.0 wt.%) sensor element, its response towards 100 ppm $\text{C}_2\text{H}_5\text{OH}$ at their respective optimal operating temperature was measured for 60 days, at an interval of 10 days, after the first measurement. The results are illustrated separately in Fig. 11. The sensors have nearly constant response to 100 ppm $\text{C}_2\text{H}_5\text{OH}$ indicating the good stability of the sensor elements.

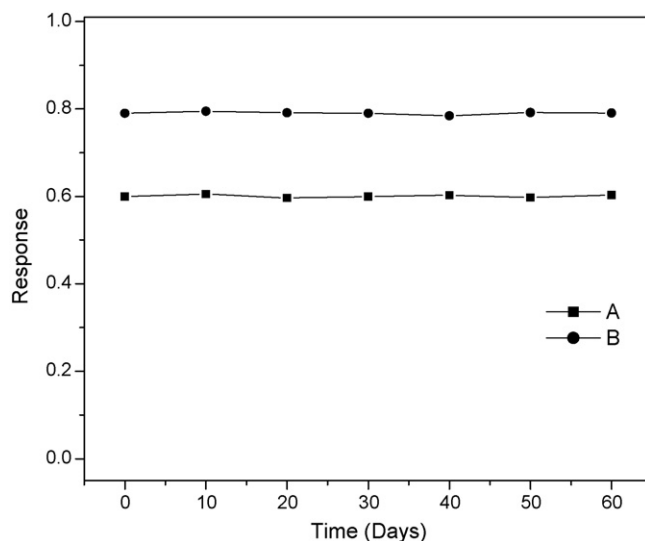


Fig. 11. Stability of (A) $\text{Ni}_{0.6}\text{Zn}_{0.4}\text{Fe}_2\text{O}_4$ at 300 °C and (B) $\text{Ni}_{0.6}\text{Zn}_{0.4}\text{Fe}_2\text{O}_4$:Pd (1.0 wt.%) at 275 °C to 100 ppm $\text{C}_2\text{H}_5\text{OH}$.

4. Conclusion

The presence of Zn^{2+} ions causes appreciable change in the structural, electrical and gas-sensing properties of $Ni_{1-x}Zn_xFe_2O_4$. The unit cell parameter 'a' increases linearly with the zinc concentration from 8.332 ± 0.002 to 8.389 ± 0.002 Å. The samples $Ni_{1-x}Zn_xFe_2O_4$ have semiconducting behaviour. Activation energy calculated from the DC electrical conductivity vs. temperature for all the samples ranges from 0.6156 to 0.4714 eV. DC electrical conductivity increases while activation energy (E_{HT}) was found to decrease with Zn content.

The gas-sensing properties of $Ni_{1-x}Zn_xFe_2O_4$ ($0 \leq x \leq 0.5$) sensors indicate that $Ni_{0.6}Zn_{0.4}Fe_2O_4$ sensor exhibits the highest sensitivity and quick response behavior to 100 ppm C_2H_5OH at 300 °C, which is mainly attributed to its small grain size. The sensor is found to exhibit good selectivity against NH_3 , H_2 and LPG but poor selectivity against H_2S . $Ni_{0.6}Zn_{0.4}Fe_2O_4$ incorporated with 1.0 wt.% Pd was found to be further increase the response to C_2H_5OH at an operating temperature of 275 °C with good selectivity. This may be attributed to Pd sensitization and selective oxidation and reduction of C_2H_5OH . This means that sensor elements based on $Ni_{0.6}Zn_{0.4}Fe_2O_4$ can be good candidates for practical use in detecting C_2H_5OH on account of the good characteristics mentioned.

The investigated unmodified and Pd (1.0 wt.%) modified $Ni_{0.6}Zn_{0.4}Fe_2O_4$ sensors exhibited rapid adsorption and desorption kinetics at 300 and 275 °C, respectively. Sensitivity, stability, reversibility, and response time are very important parameters for evaluating sensor properties. We found that the $Ni_{0.6}Zn_{0.4}Fe_2O_4$:Pd (1.0 wt.%) sensor element exhibits very attractive performances at 275 °C: high sensitivity to ethanol, good stability, total reversibility, good reproducibility, as compared to the current ethanol sensors.

Acknowledgements

The authors thank Sophisticated Analytical Instrument Facility, Indian Institute of Technology (I.I.T.), Bombay for carrying out FT-IR and TEM-ED characterizations. VDK thanks University Grant Commission (U.G.C.) for awarding Teacher Fellowship under Faculty Improvement Programme (F.I.P.). VDK thanks Principal, Arts, Science and Commerce College, Chikhaldara for his constant encouragement during the course of this work.

References

- [1] G. Neri, A. Bonavita, G. Rizzo, S. Galvagno, N. Pinna, M. Niederberger, S. Capone, P. Siciliano, *Sens. Actuators B* 122 (2007) 564.
- [2] S.T. Shishiyano, T.S. Shishiyano, O.I. Lupan, *Sens. Actuators B* 107 (2005) 379.
- [3] W. Belkacem, A. Labidi, J. Guérin, N. Mliki, K. Aguir, *Sens. Actuators B* 132 (1) (2008) 196.
- [4] V.D. Kapse, S.A. Ghosh, G.N. Chaudhari, F.C. Raghuvanshi, *Talanta* 76 (2008) 610.
- [5] V.D. Kapse, S.A. Ghosh, F.C. Raghuvanshi, S.D. Kapse, *Mater. Chem. Phys.* 113 (2009) 638.
- [6] C. Xu, T. Jun, N. Miura, N. Yamazoe, *Chem. Lett.* 3 (1990) 441.
- [7] R.D. McMichael, R.D. Shull, L.J. Swartzendruber, L.H. Bennett, R.E. Watson, *J. Magn. Magn. Mater.* 111 (1992) 29.
- [8] M. Sugimoto, *J. Am. Ceram. Soc.* 82 (1999) 269.
- [9] K. Raj, B. Moskowitz, R. Casciari, *J. Magn. Magn. Mater.* 149 (1995) 174.
- [10] C.V. Gopal Reddy, S.V. Manorama, V.J. Rao, *J. Mater. Sci. Lett.* 9 (2000) 775.
- [11] Y.-L. Liu, Z.-M. Liu, Y. Yang, H.F. Yang, G.-L. Shen, R.-Q. Yu, *Sens. Actuators B* 107 (2005) 600.
- [12] N.-S. Chen, X.-J. Yang, E.-S. Liu, J.-L. Huang, *Sens. Actuators B* 66 (2000) 178.
- [13] H. Obayashi, Y. Sakurai, T. Geo, *J. Solid State Chem.* 17 (1976) 299.
- [14] T. Sahm, L. Mäßler, A. Gurlo, N. Barsan, S.E. Pratsinis, U. Weimar, *Sens. Actuators B* 98 (2004) 148.
- [15] P. Ivanov, J. Hubalek, K. Prášek, X. Vilanova, E. Llobet, X. Correig, *Sens. Actuators B* 100 (2004) 221.
- [16] O.K. Tan, W. Cao, W. Zhu, J.W. Chai, J.S. Pan, *Sens. Actuators B* 93 (2003) 396.
- [17] K.K. Makhija, A. Ray, R.M. Patel, U.B. Trivedi, H.N. Kapse, *Bull. Mater. Sci.* 28 (2005) 9.
- [18] A. Teleki, S.E. Pratsinis, K. Kalyanasundaram, P.I. Gouma, *Sens. Actuators B* 119 (2006) 683.
- [19] K. Galatsis, Y.X. Li, W. Wlodarski, E. Comini, G. Sberveglieri, C. Cantalini, S. Santucci, M. Passacantando, *Sens. Actuators B* 83 (2002) 276.
- [20] P.P. Sahay, S. Tewari, S. Jha, M. Shamsuddin, *J. Mater. Sci.* 40 (2005) 4791.
- [21] V.D. Kapse, S.A. Ghosh, G.N. Chaudhari, F.C. Raghuvanshi, *Vacuum* 83 (2008) 346.
- [22] B. Baruwati, D. Kishore Kumar, S.V. Manorama, *Sens. Actuators B* 119 (2006) 676.
- [23] V.A.M. Brabers, *Phys. Stat. Sol.* 33 (1969) 563.
- [24] R.D. Waldron, *Phys. Rev.* 99 (1955) 1727.
- [25] M. Gotic, I. Czako-Nagy, S. Popovic, S. Music, *Philos. Magn. Lett.* 78 (1998) 193.
- [26] C. Kittel, *An Introduction to Solid State Physics*, 5th ed., Wiley, London/New York, 1976, pp. 170.
- [27] J. Smit, J. Wijn, *Ferrites*, Cleaver-Hume Press, London, 1959, Ch. XII.
- [28] M. Ivanovskaya, D. Kotsikau, G. Faglia, P. Nelli, *Sens. Actuators B* 96 (2003) 498.
- [29] A. Chiorino, G. Ghiotti, F. Prinetto, M.C. Carotta, D. Gnani, G. Marinelli, *Sens. Actuators B* 58 (1999) 338.
- [30] S. Chakraborty, A. Sen, H.S. Maiti, *Sens. Actuators B* 115 (2006) 610.
- [31] U.-S. Choi, G. Sakai, K. Shimanoe, N. Yamazoe, *Sens. Actuators B* 107 (2005) 397.
- [32] J. Tamaki, K. Shimanoe, Y. Yamada, Y. Yamamoto, N. Miura, N. Yamazoe, *Sens. Actuators B* 49 (1998) 121.
- [33] M. Ivanovskaya, D. Kotsikau, G. Faglia, P. Nelli, S. Irkaev, *Sens. Actuators B* 93 (2003) 422.
- [34] B.P.J. de, L. Costello, R.J. Ewen, N.M. Ratcliffe, P.S. Sivenand, *Sens. Actuators B* 92 (2003) 159.
- [35] P. Montmeat, J.-C. Marchand, R. Lalaue, J.-P. Viricelle, G. Tournier, C. Pijolat, *Sens. Actuators B* 95 (2003) 83.
- [36] M. Schweizer-Berberich, J.G. Zheng, U. Weimar, W. Gopel, N. Barsan, E. Pentia, A. Tamescu, *Sens. Actuators B* 31 (1996) 71.
- [37] N. Yamazoe, *Sens. Actuators B* 5 (1991) 7.



Indicator-based and indicator-free magnetic assays connected with disposable electrochemical nucleic acid sensor system

Hakan Karadeniz^a, Arzum Erdem^{a,*}, Filiz Kuralay^b, Frantisek Jelen^c

^a Ege University, Faculty of Pharmacy, Analytical Chemistry Department, 35100 Bornova, Izmir, Turkey

^b Department of Chemistry, Faculty of Science, Hacettepe University, 06532 Beytepe-Ankara, Turkey

^c Institute of Biophysics, Academy of Sciences of the Czech Republic, Kralovopolska 135, 612 65 Brno, Czech Republic

ARTICLE INFO

Article history:

Received 9 July 2008

Received in revised form 26 October 2008

Accepted 31 October 2008

Available online 11 November 2008

Keywords:

Magnetic particles

Echinomycin

Guanine

Adenine

Electrochemical nucleic acid sensors

Pencil graphite electrode

ABSTRACT

An indicator-based and indicator-free magnetic assays connected with a disposable pencil graphite electrode (PGE) were successfully developed, and also compared for the electrochemical detection of DNA hybridization. The oxidation signals of echinomycin (ECHI) and electroactive DNA bases, guanine and adenine, respectively were monitored in the presence of DNA hybridization by using differential pulse voltammetry (DPV) technique. The biotinylated probe was immobilized onto the magnetic beads (magnetic particles, microspheres) and hybridization with its complementary target at the surface of particles within the medium was exhibited successfully using electrochemical sensor system. For the selectivity studies, the results represent that both indicator-based and indicator-free magnetic assays provide a better discrimination for DNA hybridization compared to duplex with one-base or more mismatches. The detection limits ($S/N=3$) of the magnetic assays based on indicator or indicator-free were found in nM concentration level of target using disposable sensor technology with good reproducibility. The characterization and advantages of both proposed magnetic assays connected with a disposable electrochemical sensor are also discussed and compared with those methods previously reported in the literature.

© 2008 Elsevier B.V. All rights reserved.

1. Introduction

The development of advanced biological sensor systems could impact significantly the areas of genomics, proteomics, biomedical diagnostics and drug discovery [1–3]. Recent advances in biosensors based on nucleic acid have led to the development of genosensor technology for gene sequence analysis and for nucleic acid ligand binding studies [2–6].

Electrochemical biosensors coupling the inherent specificity of DNA recognition reactions with the high sensitivity of physical transducers, hold great promise for sequence-specific detection for clinical, environmental or forensic investigations. DNA hybridization biosensors can be used for early and precise determination of infectious agents in various environments [2–5]. These biosensing devices can monitor sequence-specific hybridization processes [7–11] based on the oxidation signal of the most electroactive bases of DNA; guanine and adenine or by DNA intercalators (some metal coordination complexes, antibiotics, etc.) which form complexes with the nitrogenous bases of DNA [10–11] or by detecting the oxidation signal at some metal tags such as gold

and silver nanoparticles in the presence of DNA hybridization [8–12].

The nanoscale sensors based on nanowires, nanotubes and other nanomaterials have recently received considerable attention [13–21]. There has been a great interest for the development of double surface techniques in combination with magnetic separation and the electrochemical nucleic acid sensor systems [8,12,22–29]. The use of monosized magnetic beads gives the convenience of magnetic separation. These particles are superparamagnetic, meaning that these microparticles can be easily separated from the liquid phase with a small magnet, but can be redispersed immediately after the magnet is removed [30]. Bioanalysis has benefited from the use of magnetic beads in electrochemical immunosensors [31] or for fluorescence DNA hybridization approaches [32]. The basic concept in magnetic bioseparations is to selectively bind the biomaterial of interest (e.g., specific cell, protein, or DNA sequence) to a magnetic particle and then separate it from its surrounding matrix using a magnetic field.

The electrochemical nucleic acid sensor system based on magnetic particles [12,21–27,29], labeling with an enzyme [23,24], using label-free system [21,22,26,27] or combining with metal nanoparticles [12,25,29], enables the sequence specific detection of DNA hybridization observed in low detection limits resulting from efficient magnetic separation.

* Corresponding author. Tel.: +90 232 388 0110x5131; fax: +90 232 388 5258.
E-mail address: arzum.erdem@ege.edu.tr (A. Erdem).

A biomagnetic assay of DNA sequences related to breast-cancer gene (BRCA1) was reported based on label-free detection [22]. Coupling the label-free guanine detection with the efficient magnetic isolation of the hybrid as using biotinylated inosine-substituted probes, streptavidin-coated magnetic beads with potentiometric stripping analysis (PSA) measurements at a renewable graphite pencil electrode. An enzyme-linked sandwich hybridization was also studied in another study of Wang's group [23] where, the electrochemical detection of DNA sequences related to BRCA1 gene used magnetic particles labeled probe which hybridized to a biotinylated DNA target capturing a streptavidin-alkaline phosphatase (AP) enzyme. After DNA hybridization, 1-naphthol was measured consequently as a product of enzymatic reaction.

An enzyme-linked immunoassay coupling with magnetic particles for the detection of the DNA hybridization was performed by using pyrolytic graphite electrode (PrGE), and the magnitude of signals of 1-naphthol as the product of this enzymatic reaction due to DNA hybridization by using linear square voltammetry (LSV) technique [24].

The novel label-free assays in connection with magnetic particles developed by using different electrochemical transducers were also shown in the literatures [21,22,26,27]. The magneto graphite-epoxy composite electrodes (m-GECEs) were developed and effectively used for the electrochemical detection of a sequence specific for *Salmonella* spp. [28]. The chronopotentiometric detection of label-free DNA hybridization for BRCA1 by using an electrically heated carbon-paste transducer [26] was also developed successfully based on magnetic assays.

The application of the magnetic assay connected with a disposable graphite electrochemical sensor system in real samples was reported as the first time in the literature for the specific label-free detection of wild type hepatitis B virus (HBV) DNA in polymerase chain reaction (PCR) amplicons in length 437-bp [27]. The magnetic assays connected with nanoparticles labeled with different metals were also reported in the literatures [12,25,29]. Two different particle-based assays for monitoring DNA hybridization based on PSA detection of an iron tracer were reported [25]. The selectivity of this assay was also checked by co-existing of the larger excess of different point mutations in oligonucleotides and noncomplementary sequences.

In this study, an indicator-based and indicator-free magnetic assays connected with a disposable graphite sensor (pencil graphite electrode, PGE) were successfully developed, and also compared for the electrochemical detection of DNA hybridization. The changes at the oxidation signals of echinomycin (ECHI) and electroactive DNA bases, guanine and adenine, respectively were monitored in the presence of DNA hybridization by using differential pulse voltammetry (DPV) technique. The selectivity of these magnetic assays for DNA hybridization was also checked in the presence of single base mismatch and noncomplementary DNA sequences. There have not been yet any reports about both indicator-based and indicator-free magnetic assays connected with disposable sensor system by measuring the oxidation signals of ECHI, guanine and adenine in the same measurement scale. The characterization and advantages of both proposed magnetic assays connected with a disposable electrochemical sensor are also discussed and compared with those methods previously reported in the literature.

2. Experimental

2.1. Apparatus

The oxidation signals of ECHI and DNA bases, guanine and adenine were investigated by using DPV with an AUTOLAB PGSTAT electrochemical analysis system and GPES 4.8 software package

(Eco Chemie, The Netherlands). The raw data were also treated using the Savitzky and Golay filter (level 2) of the GPES software, followed by the moving average baseline correction with a "peak width" of 0.01. The three-electrode system consisted of the PGE, an Ag/AgCl/KCl reference electrode and a platinum wire as the auxiliary electrode.

The preparation of magnetic beads and hybridization process were performed on the magnetic separators, Dynal MPC-C and MCB 1200 (respectively, Dynal Biotech ASA, Norway and Sigris, USA).

2.2. Chemicals

The 17-mer biotin capped probe, complementary, noncomplementary (NC) and one-base mismatch (MM) DNA oligonucleotides (ODN), were purchased (as lyophilized powder) from Thermo Electron Corp. (Germany). The base sequences of ODNs are:

Probe

5'-biotin-TTT TTT TTT CGA TCG AG-3'.

Complementary

5'-CTC GAT CGA AAA AAA AA-3'.

Noncomplementary (NC)

5'-TGA AAC GAT TAT GAT AC-3'.

One-base mismatch (MM)

5'-CTC GAT CGA AGA AAA AA-3'.

All ODN stock solutions were prepared with ultrapure tri-distilled water and kept frozen. More dilute solutions of ODNs were prepared with either 0.50 M acetate buffer (ABS) containing 20 mM NaCl (pH 4.80) or 20 mM Tris-HCl buffer (TBS) (pH 7.00) containing 20 mM NaCl, according to the hybridization protocol. Other chemicals were in analytical reagent grade and they were supplied from Sigma and Merck.

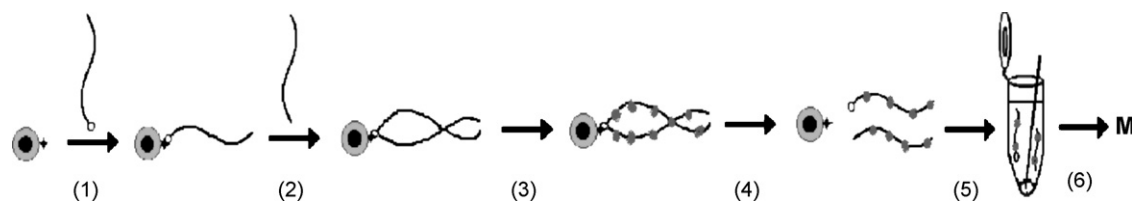
Proactive streptavidin-coated microspheres (Dynalbeads M-280 Streptavidin, Prod. No. 112.06) were purchased from Dynal Biotech ASA (Oslo, Norway). The size of magnetic particles (magnetic beads) is 2.8 μm , their binding capacity is DNA fragment length dependent (1.0 mg beads binds 5 pmol of a 2–4-kb dsDNA fragment). The further details about magnetic particles, including size and binding capacity, can be supplied from the following web sites: www.dynal.no or www.invitrogen.com.

2.3. Electrode preparation

The disposable PGE was used in voltammetric measurements for the electrochemical detection of DNA hybridization. A Tombo[®] pencil was used as a holder for the graphite lead. Electrical contact with the lead was obtained by soldering a metallic wire to the metallic part. The pencil was held vertically with 14 mm of the lead extruded outside (10 mm of which was immersed in the solution).

2.4. Preparation of probe-coated magnetic beads and DNA hybridization on surface of the magnetic beads

The preparation of ODN-coated microspheres (magnetic beads) performed by using the magnetic separators Dynal MPC-C and MCB 1200 was performed following the reported procedure [22,27]: 5 μl of streptavidin-coated magnetic beads was transferred into a 1.5-ml centrifuge tube. The microspheres were washed with 90 μl TTL



Scheme 1. Electrochemical detection of hybridization based on magnetic assays connected with indicator-based or indicator-free methods: (1) the immobilization of biotinylated probe onto streptavidin-coated magnetic beads; (2) hybridization in the presence of target (or noncomplementary (NC), or single base mismatch (MM)); (3) accumulation of ECHI; (4) after alkaline treatment to magnetic beads in order to dissociate of DNA hybrids from the surface of magnetic beads; (5) wet-adsorption procedure by using PGE; (6) electrochemical measurement based on the oxidation signals of indicator, ECHI and electroactive DNA bases; guanine and adenine, by using disposable sensor; PGE.

buffer (100 mM Tris–HCl, pH 8.0, and 0.1% Tween20 and 1 M LiCl) and resuspended in 25 μl TTL buffer. 25 μl of biotinylated probe was added and incubated for 15 min at room temperature with gentle mixing. The immobilized probe was then separated and washed twice with 90 μl TT buffer (250 mM Tris–HCl, pH 8.0, and 0.1% Tween20), resuspended in 40 μl hybridization solution (sodium citrate buffer (NaCB) (pH 7.00); 750 mM NaCl and 75 mM sodium citrate) containing 20 $\mu\text{g ml}^{-1}$ of complementary (target of probe) or MM or NC sequences. The hybridization reaction was carried out for 20 min at room temperature. The hybridized microsphere conjugates were then washed with 90 μl NaCB.

Indicator binding to DNA

The hybridized microsphere conjugates were resuspended in 50 μl 20 mM TBS containing 5 μM ECHI, indicator was accumulated onto the hybridized microsphere for 5 min at room temperature with gentle mixing. The microspheres were washed twice with 90 μl of 50 mM phosphate buffer solution (PBS) (pH 7.40) and resuspended in 25 μl of 0.05 M NaOH solution for alkaline treatment step during 5 min.

After the alkaline treatment step, 25 μl of resulted sample was transferred into the vial containing 85 μl PBS. Then the PGEs were dipped into these vials and kept for adsorption during 15 min. The electrodes were then rinsed with TBS for 5 s. The PGEs were replaced to the three-electrode system of electrochemical cell containing PBS for DPV measurement. Whole hybridization protocol is depicted in Scheme 1.

Voltammetric transduction

The oxidation signals of ECHI and DNA bases, guanine and adenine, were measured by using DPV in sample by scanning from -0.80 V to $+1.40\text{ V}$ at the pulse amplitude as 50 mV and the scan rate as 30 mV s^{-1} .

3. Results and discussion

Fig. 1A shows the cyclic voltammogram of $5\text{ }\mu\text{g ml}^{-1}$ ECHI by using PGE. Both reduction and oxidation signals of ECHI were earlier presented on cyclic voltammograms at hanging mercury drop electrode (HMDE) [33]. However, the changes at the reduction signal of ECHI were used for detection of interaction between ECHI and single and double stranded DNA immobilized onto the surface of gold and HMDE electrodes [29,33], the magnitude of oxidation signal of ECHI (about -0.6 V) at PGE was used in this study for the first time in order to detect DNA hybridization effectively in contradiction of other procedures earlier reported in literature. Besides, it was aimed to investigate DNA hybridization while measuring ECHI oxidation signal in the same measurement scale as the first time with the ones of DNA bases, guanine and adenine.

Fig. 1B shows the calibration plot based on ECHI signals in different concentrations from $0.1\text{ }\mu\text{g ml}^{-1}$ to $10\text{ }\mu\text{g ml}^{-1}$ measured by DPV and bare PGE. In our study, we used ECHI at a concentration of $5\text{ }\mu\text{g ml}^{-1}$.

In this study, both indicator-based and indicator-free magnetic assays connection with disposable graphite sensor; PGE were successfully developed for the electrochemical detection of DNA hybridization. In the presence of DNA hybridization, the changes at the oxidation signals of ECHI (E) and electroactive DNA bases; guanine (G) and adenine (A) were monitored using DPV technique in the same scale of measurement. The representative voltammogram showing the electrochemical detection of DNA hybridization were shown in Fig. 2.

The overall performance of the magnetic assay was strongly dependent upon experimental variables influencing the hybridization efficiency, such as probe and target concentration, the amount of streptavidin-coated magnetic beads and the hybridization time.

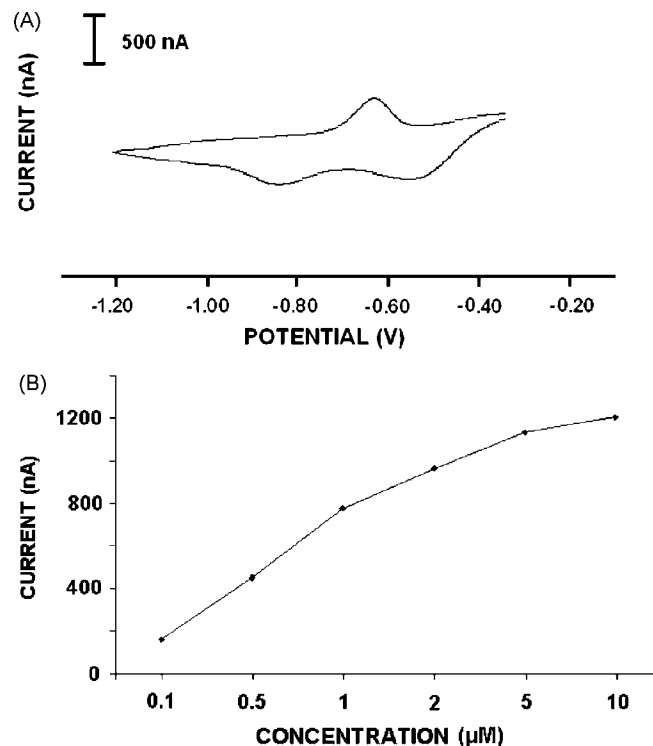


Fig. 1. (A) Cyclic voltammogram of $5\text{ }\mu\text{g ml}^{-1}$ ECHI in 50 mM PBS. ECHI accumulation: $5\text{ }\mu\text{g ml}^{-1}$ ECHI, at open circuit in 50 mM PBS for 5 min; CV measurement performed by 0.1 V s^{-1} scan rate between the potential range as -0.25 V and -1.20 V by using PGE. (B) Calibration plot obtained from the current dependence of the ECHI signal in PBS by using bare PGE in different concentrations of ECHI as 0.1, 0.5, 1.0, 2.0, 5.0 and $10.0\text{ }\mu\text{g ml}^{-1}$. ECHI accumulation at open circuit system for 5 min; DPV measurement scanning between -0.80 V and -0.20 V in 50 mM PBS.

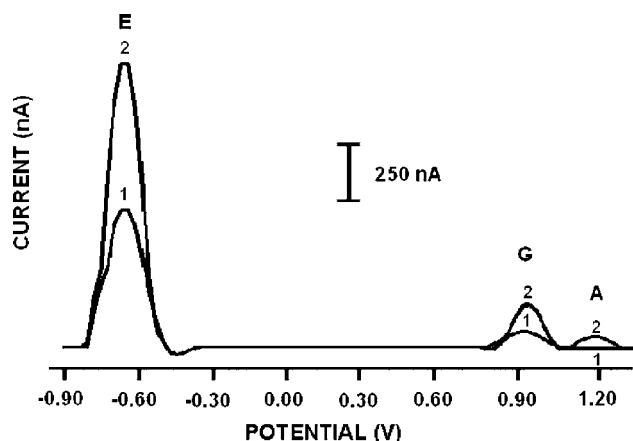


Fig. 2. Differential pulse voltammograms of the oxidation signals of ECHI, guanine and adenine, by pencil graphite electrode (PGE). (E: ECHI; G: guanine; A: adenine signal observed before (1) and after (2) hybridization between probe and its complementary, $20 \mu\text{g ml}^{-1}$. DPV measurement scanning between -0.90 V and $+1.30 \text{ V}$ in 50 mM PBS by using PGEs.

The effect of these experimental parameters was also explored earlier for optimum analytical performance [10,22,27,33].

Fig. 3A shows the ECHI signals obtained after hybridization between probe and either complementary or NC or MM sequences. The oxidation signal of ECHI obtained with the hybrid was higher than the one obtained with probe signal. The hybridization between

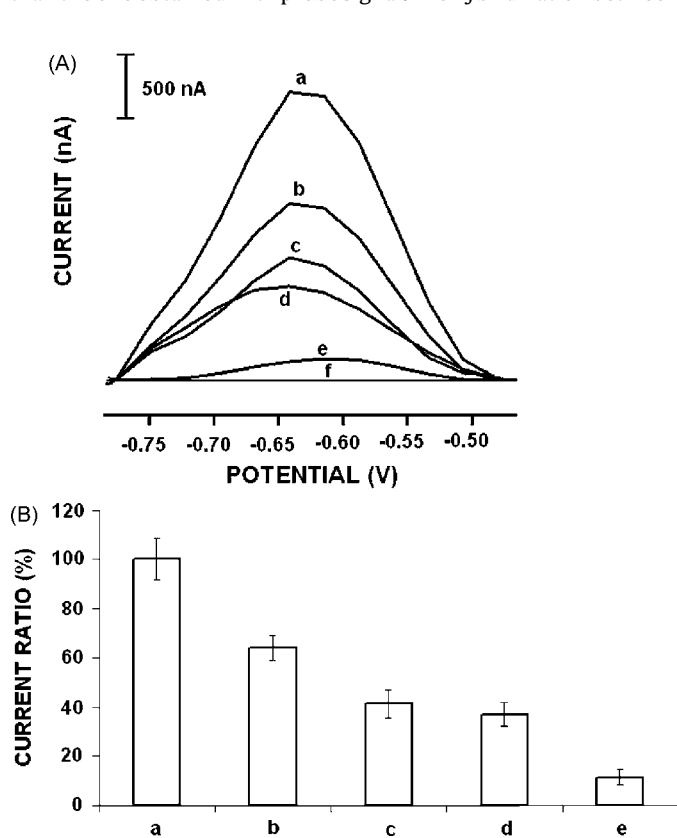


Fig. 3. (A) Differential pulse voltammograms of ECHI oxidation signal: (a) hybridization of the probe with its complementary, $20 \mu\text{g ml}^{-1}$; (b) hybridization of probe with mismatch, $20 \mu\text{g ml}^{-1}$; (c) hybridization of the probe and noncomplementary, $20 \mu\text{g ml}^{-1}$; (d) probe alone; (e) bare electrode and (f) blank PBS without ECHI. Other conditions are as in Fig. 2. (B) Histograms for the relative oxidation signals of ECHI obtained: (a) after hybridization of the probe with its complementary, (b) interaction of probe and mismatched, (c) hybridization between probe and noncomplementary, (d) probe alone and (e) blank PBS. Other conditions are as in Fig. 2.

probe and NC was investigated (Fig. 3A, -c) and the signal was measured as similar to the one with probe alone. The hybridization between probe and MM was also investigated (Fig. 3A, -b). It was found that the signal was higher than probe signal, but quite lower than the signal observed in the presence of hybridization. In view of the fact that the single base mismatch is guanine at the end of poly(A) tail from the 3' end of MM sequence, it was not easier to prevent incompletely hybridization of MM with probe immobilized onto the magnetic particles. This can be prevented by using different rinsing procedures (by employing surfactant, e.g., SDS, etc. or increasing the temperature of medium) after hybridization step, which could eliminate the non-specific absorption at the surface. The histogram based on the relative oxidation signal of ECHI that was taken as 100%, upon hybridization between probe with complementary or NC or MM ODN was also shown in Fig. 3B.

Three subsequent experiments for detection of hybridization by using an indicator-based magnetic assay upon $20 \mu\text{g ml}^{-1}$ concentration of target gave reproducible results as a mean ECHI signal of 2120 nA and a R.S.D. value of 8.6% ($n=3$) by using disposable sensor, PGE in 20 min hybridization time. The detection limit (DL) estimated from $S/N=3$, corresponds to 1.82 nM concentration level of target (i.e., 0.2 pmol in $110 \mu\text{l}$ sample).

Figs. 4 and 5 represent the voltammograms and histograms based on the magnitude of oxidation signals of electroactive DNA bases: guanine and adenine measured after hybridization between probe and complementary or NC or MM sequences. In parallel to the results obtained with an indicator-based magnetic assay by

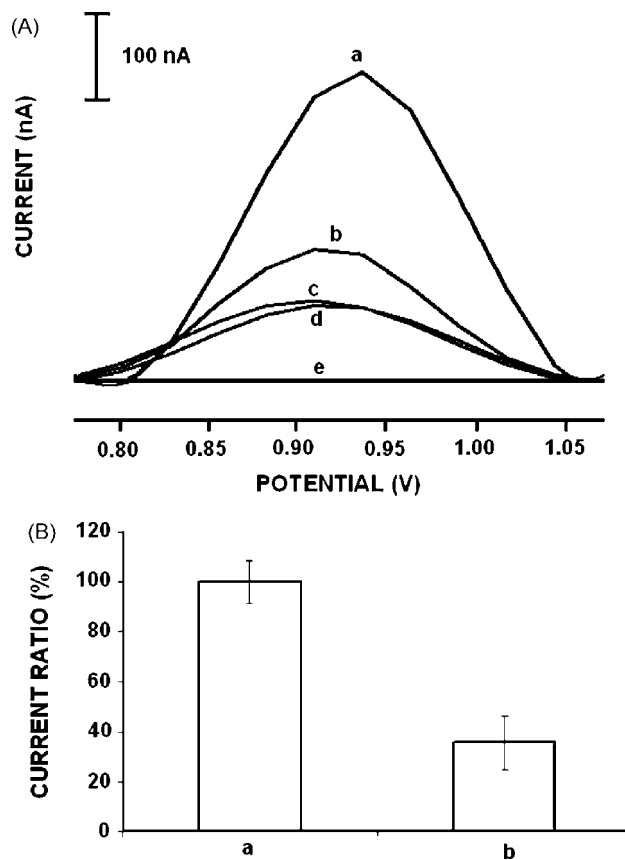


Fig. 4. (A) Differential pulse voltammograms of guanine oxidation signal: (a) hybridization of the probe with complementary, $20 \mu\text{g ml}^{-1}$; (b) hybridization of probe with mismatch, $20 \mu\text{g ml}^{-1}$; (c) hybridization of the probe and noncomplementary, $20 \mu\text{g ml}^{-1}$; (d) probe alone and (e) blank PBS. Other conditions are as in Fig. 2. (B) Histograms for the relative oxidation signals of guanine obtained: (a) after hybridization of the probe with its complementary and (b) probe alone. Other conditions are as in Fig. 2.

using the ECHI signal, the similar results were obtained by using an indicator-free magnetic assay based on the changes at the oxidation signals of guanine and adenine measured at almost +1.00 and +1.25 V, respectively.

The hybridization between probe and NC was investigated by measuring guanine signal and the result was shown in Fig. 4(A, -c). It was found that the oxidation signal of guanine was measured almost same to the one obtained with probe alone (shown in Fig. 4A, -d). The hybridization of probe with MM was also investigated (shown in Fig. 4A, -b) and the guanine signal was measured little higher than the probe signal, but substantially lower than the signal observed in the presence of hybridization. Note also that 50% decrease at the hybrid signal was measured in the case of hybridization between probe and MM, however, three guanine bases are available in MM sequences comparison to the complementarity of probe having two guanine bases.

Fig. 4B represents the histogram based on the relative oxidation signal of guanine that was taken as 100%, measured in the absence or presence of hybridization between probe and its complementary sequence.

The oxidation signal of adenine was also measured in the presence of hybridization of probe with complementary or NC or MM and the representative voltammograms were shown in Fig. 5A. DNA hybridization between probe and its target was detected by using

the oxidation signal of adenine (shown in Fig. 5A, -a) in similar to the result obtained by using guanine signal. Note that the number of adenine bases available in NC and MM sequences, respectively are seven and nine, there is no adenine signal was observed in the presence hybridization between probe and NC (in Fig. 5A, -c), or between probe and MM (in Fig. 5A, -d). Fig. 5B represents the histogram based on the relative oxidation signal of adenine that was taken as 100%, measured in the absence or presence of hybridization between probe and its complementary.

A possible non-specific adsorption that might have occurred on surface of magnetic particles, can be effectively removed by efficient washing during the magnetic separation. The successful application of magnetic particles for indicator-based and indicator-free-based DNA detection combined with electrochemical techniques provides the most important advantages for the prevention of non-specific adsorption in the presence of NC or unwanted constituents in the sample, and the detection especially the point mutations at DNA sequences.

Three subsequent experiments for detection of hybridization by using an indicator-free-based magnetic assay upon $20 \mu\text{g ml}^{-1}$ concentration of target gave reproducible results respectively, as a mean guanine and adenine signal of 340 and 180 nA with the calculated R.S.D. values % ($n=3$) as 9.1% and 12.0% using disposable sensor and 20 min hybridization time. The detection limits (DLs) estimated from $S/N=3$, correspond to 11 and 20 nM concentration level of target (i.e., 1.21 pmol and 2.20 pmol in 110 μl samples), respectively for both indicator-based and indicator-free magnetic assays.

4. Conclusion

The reported magnetic assays based on indicator-based and indicator-free methods connected with a disposable graphite sensor (PGE) were successfully developed for the electrochemical detection of DNA hybridization. There have not yet been any reports of both indicator-based and indicator-free magnetic assays connected with a disposable sensor system through measurement of the oxidation signal of indicator ECHI with the signals of DNA bases, guanine and adenine, in the same measurement scale. Easier, quicker and more sensitive detection scheme for DNA hybridization based on magnetic assay was explored herein in comparison to the traditional techniques reported earlier in the literature [11,34–37], in which several external indicators $[\text{Co}(\text{phen})_3]^{3+}$, methylene blue, meldola's blue or $[\text{Os}(\text{bpy})_2\text{Cl}_2]^+$ have been applied by using advanced surface modification or regeneration schemes. The use of PGE brings the other advantage to our assay with a better reproducibility; such as, being cheaper, easy to use (single-use) and portable, which are crucial properties of devices for DNA chip technology contrary to other transducers; such as, AuE and HMDE.

The magnetic separation brings another advantage to our assay in combination with the selection of specific synthetic probes starting with poly(T), that may be further progressed in our lab, especially for the detection of messenger RNA (mRNA), since the polyadenylation is part of the path by which eukaryotes produce mature mRNA for translation in the larger process of protein synthesis to produce proteins [38].

Such coupling of indicator-free magnetic hybridization surfaces with disposable electrochemical transducers and label-free electrical detection eliminates the needs for external indicators and advanced surface modification or regeneration schemes, resulting in a greatly simplified protocol.

The work represented here has also shown a realistic potential application as being carried out real PCR amplicons. Future work in our labs will be focused on the applications of indicator-based and indicator-free magnetic assays for the detection of mRNA,

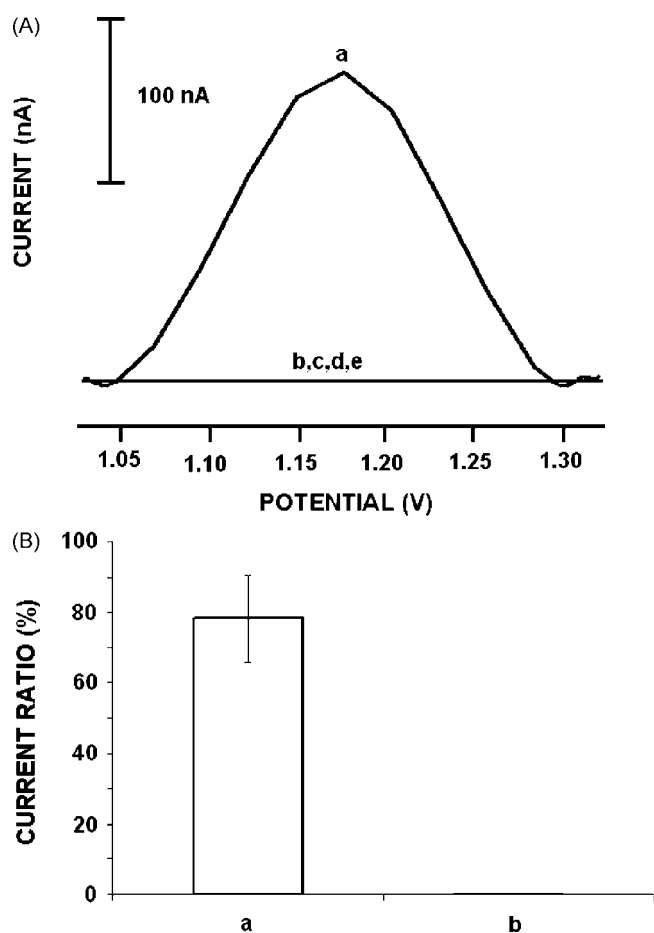


Fig. 5. (A) Differential pulse voltammograms of adenine oxidation signal: (a) hybridization of the probe with complementary, $20 \mu\text{g ml}^{-1}$; (b) hybridization of probe with mismatch, $20 \mu\text{g ml}^{-1}$; (c) hybridization of the probe and noncomplementary, $20 \mu\text{g ml}^{-1}$; (d) probe alone and (e) blank PBS. Other conditions are as in Fig. 2. (B) Histograms for the relative oxidation signals of adenine obtained: (a) after hybridization of the probe with its complementary and (b) probe alone. Other conditions are as in Fig. 2.

the quantification of target DNA, and also to detect specific DNA sequences related to inherited and genetic diseases in PCR products obtained from real samples.

Acknowledgements

Authors acknowledge the financial support from Turkish Scientific and Technological Council (TUBITAK; Project No. 106S181), Turkish Academy of Pharmacists and Turkish Pharmacists Association (TEB), support from Grant Agency of the Czech Academy of Sciences (Grant Nos. A100040602 and A400040804, and by institutional grant AV0Z50040702). The experimental work includes the doctoral thesis of H.K. supported by Ege University, Faculty of Pharmacy, project coordination (Project 06/ECZ/002). A.E. would like to express her gratitude to the Turkish Academy of Sciences (TUBA) as the associate member of TUBA for their support. H.K. and F.K. acknowledges a scholarship for Ph.D. students from Scientific and Technical Research Council of Turkey (TUBITAK).

References

- [1] P.M. Dean, E.D. Zanders, D.S. Bailey, Trends Biotechnol. 19 (2001) 288.
- [2] J. Wang, Analyst 130 (2005) 421.
- [3] E. Palecek, M. Fojta, Anal. Chem. 73 (2001) 74A.
- [4] E. Palecek, F. Jelen, F. Crit. Rev. Anal. Chem. 32 (2002) 261.
- [5] E. Palecek, F. Jelen, in: E. Palecek, F. Scheller, J. Wang (Eds.), Perspectives in Bioanalysis, vol. 1, Elsevier, New York, 2005, pp. 74–173.
- [6] A. Erdem, M. Ozsoz, Electroanalysis 14 (2002) 965.
- [7] D. Ozkan, A. Erdem, P. Kara, K. Kerman, B. Meric, B.J. Hassmann, M. Ozsoz, Anal. Chem. 74 (2002) 5931.
- [8] M. Ozsoz, A. Erdem, K. Kerman, D. Ozkan, B. Tugrul, N. Topcuoglu, N.H. Ekren, M. Taylan, Anal. Chem. 75 (2003) 2181.
- [9] A. Erdem, M.I. Pividori, M. del Valle, S. Alegret, J. Electroanal. Chem. 567 (2004) 29.
- [10] H. Karadeniz, B. Gulmez, A. Erdem, F. Jelen, M. Ozsoz, E. Palecek, Front. Biosci. 11 (2006) 1870.
- [11] A. Erdem, K. Kerman, B. Meric, U.S. Akarca, M. Ozsoz, Anal. Chim. Acta 422 (2000) 139.
- [12] J. Wang, D.K. Xu, R. Polsky, J. Am. Chem. Soc. 124 (2002) 4208.
- [13] A.D. McFarland, R.P. Van Duyne, Nano Lett. 3 (2003) 1057.
- [14] A.K. Salem, J. Chao, K.W. Leong, P.C. Searson, Adv. Mater. 16 (2004) 268.
- [15] J.E. Koehne, H. Chen, A.M. Cassell, Q. Yi, J. Han, M. Meyyappan, J. Li, J. Clin. Chem. 50 (2004) 1886.
- [16] K.B. Wu, J.J. Fei, W. Bai, S.S. Hu, Anal. Bioanal. Chem. 376 (2003) 205.
- [17] H. Cai, X.N. Cao, Y. Jiang, P.G. He, Y.Z. Fang, Anal. Bioanal. Chem. 375 (2003) 287.
- [18] M. Guo, L.D. Chen, D. Liu, L. Nie, S. Yao, Bioelectrochemistry 62 (2004) 29.
- [19] J. Hahm, C.M. Lieber, Nano Lett. 4 (2004) 51.
- [20] F. Patolsky, C.M. Lieber, Mater. Today 8 (2004) 20.
- [21] A. Erdem, P. Papakonstantinou, H. Murphy, Anal. Chem. 78 (2006) 6656.
- [22] J. Wang, A.N. Kawde, A. Erdem, M. Salazar, Analyst 126 (2001) 2020.
- [23] J. Wang, D.K. Xu, A. Erdem, R. Polsky, M.A. Salazar, Talanta 56 (2002) 931.
- [24] E. Palecek, R. Kizek, L. Havran, S. Billova, M. Fojta, Anal. Chim. Acta 469 (2002) 73.
- [25] J. Wang, G.D. Liu, A. Merkoci, Anal. Chim. Acta 482 (2003) 149.
- [26] J. Wang, G.U. Flechsig, A. Erdem, O. Korbut, P. Grundler, Electroanalysis 16 (2004) 928.
- [27] A. Erdem, D.O. Ariksoysal, H. Karadeniz, P. Kara, A. Sengonul, A. Sayiner, M. Ozsoz, Electrochem. Commun. 7 (2005) 815.
- [28] A. Erdem, M.I. Pividori, A. Lermo, A. Bonanni, M. del Valle, S. Alegret, Sens. Actuators B: Chem. 114 (2006) 591.
- [29] J. Wang, G.D. Liu, R. Polsky, A. Merkoci, Electrochem. Commun. 4 (2002) 722.
- [30] S. Sole, A. Merkoci, S. Alegret, TrAC-Trends Anal. Chem. 20 (2001) 102.
- [31] A.G. Gehring, J.D. Brewster, P.L. Irwin, S.I. Tu, L.J. Van Houten, J. Electroanal. Chem. 469 (1999) 27.
- [32] M. Dequaire, C. Degrand, B. Limoges, Anal. Chem. 71 (1999) 2571.
- [33] F. Jelen, A. Erdem, E. Palecek, Bioelectrochemistry 55 (2002) 165.
- [34] A. Erdem, K. Kerman, B. Meric, U.S. Akarca, M. Ozsoz, Electroanalysis 11 (1999) 586.
- [35] H.X. Ju, Y.K. Ye, J.H. Zhao, Y.L. Zhu, Anal. Biochem. 313 (2003) 255.
- [36] Y.K. Ye, J.H. Zhao, F. Yan, Y.L. Zhu, X.H. Ju, Biosens. Bioelectron. 18 (2003) 1501.
- [37] K. Kerman, Y. Matsubara, Y. Morita, Y. Takamura, E. Tamiya, Sci. Technol. Adv. Mater. 5 (2003) 351.
- [38] D. Munroe, A. Jacobson, Mol. Cell. Biol. 10 (1999) 3441.



Effect of a carboxyl group on the chemiluminescent reaction of tris(2,2'-bipyridine)ruthenium(III) with aliphatic amines

Hitoshi Kodamatani^a, Yu Komatsu^b, Shigeo Yamazaki^c, Keiitsu Saito^{d,*}

^a Department of Earth and Environmental Sciences, Faculty of Science, Kagoshima University, 1-21-35 Korimoto, Kagoshima 890-0065, Japan

^b Environmental Research Institute, Kanazawa Institute of Technology, 3-1 Yatsukaho, Hakusan 924-0838, Japan

^c Department of Applied Science, Okayama University of Science, 1-1 Ridaicho, Okayama 700-0005, Japan

^d Division of Human Environment, Graduate School of Human Development and Environment, Kobe University, 3-11 Tsurukabuto, Nada, Kobe 657-8501, Japan

ARTICLE INFO

Article history:

Received 14 October 2008

Accepted 3 November 2008

Available online 11 November 2008

Keywords:

Aliphatic amine

Amino acid

Carboxyl group

Tris(2,2'-bipyridine)ruthenium(III)

Chemiluminescence

ABSTRACT

The effect of a carboxyl group beside nitrogen of aliphatic amines on the tris(2,2'-bipyridine)ruthenium(III), Ru(bpy)₃³⁺, chemiluminescent reaction was examined. It has been shown that a carboxylate anion promotes the chemiluminescent reaction at a lower pH and then the aliphatic amines with this substituent can be sensitively detected compared with corresponding aliphatic amines without this substituent. Based on this finding, preliminary studies on simultaneous determination of 4-hydroxyproline, *N*-methylglycine, *N*-methylalanine, proline, and pipecolic acid in human serum have been performed using isocratic reversed-phase ion-pair high-performance liquid chromatography (HPLC) with electrogenerated Ru(bpy)₃³⁺ chemiluminescent detection. The detection limits (signal-to-noise ratio of 3) with the proposed method were 3.0, 12, 2.7, 4.6, and 10 nM for 4-hydroxyproline, *N*-methylglycine, *N*-methylalanine, proline, and pipecolic acid, respectively.

© 2008 Elsevier B.V. All rights reserved.

1. Introduction

A chemiluminescent detection system using tris(2,2'-bipyridine)ruthenium(III), Ru(bpy)₃³⁺, as a chemiluminescent reagent was shown to be a sensitive detection method for the reducing agents such as oxalate [1], aliphatic amines [2], active methylenes [3], aliphatic conjugated dienes [4], and five-membered heteroaromatic compounds [5]. Among these compounds, aliphatic tertiary amines are the most suitable reducing agents for Ru(bpy)₃³⁺ chemiluminescence. Hence, Ru(bpy)₃³⁺ is used as a detection reagent for a variety of compounds having an amine moiety; various analytical methods are employed, such as high-performance liquid chromatography (HPLC) [6,7], flow injection analysis (FIA) [8,9] capillary electrophoresis [10,11], and micro-total analysis system [12]. Since Ru(bpy)₃³⁺ can be electrochemically recycled, Ru(bpy)₃²⁺-derivatives are also used as chemiluminescent labels for immunoassay and DNA probe assay with Ru(bpy)₃²⁺/tri-*n*-propylamine electrogenerated chemiluminescence (ECL) system. The Ru(bpy)₃²⁺ ECL-label can be sensitively determined at subpicomolar concentrations, over a wide dynamic range. These analytical applications are shown in recent reviews [13,14] and in a book [15].

The reaction mechanism of Ru(bpy)₃³⁺ with aliphatic amines has been investigated by many workers [15]. It is generally accepted that the reaction of Ru(bpy)₃³⁺ with aliphatic amines proceeds as follows. The aliphatic amine is oxidized with Ru(bpy)₃³⁺, generating a radical cation. The α -carbon of the amine is then deprotonated, forming a strongly reducing electron-deficient radical. This radical intermediate produces the excited state, Ru(bpy)₃^{2+*}, in an electron transfer reaction with Ru(bpy)₃³⁺. When this excited state decays to the ground state, an orange emission is produced. The relationship between the molecular structure and chemiluminescent activity of the reaction has also been investigated [16]. In general, electron-donating substituents attached to the nitrogen or the α -carbon will stabilize the radical cation and the electron-deficient radical, and hence tend to increase the chemiluminescent activity of amines. Therefore, the chemiluminescent intensity for the aliphatic amines increases in the order primary < secondary < tertiary. Conversely, electron-withdrawing substituents attached to the nitrogen or the α -carbon will destabilize the radical cation and the electron-deficient radical, and hence tend to reduce the chemiluminescent activity. Although these general trends are found out, it is still difficult to predict what kind of compound will give emission of light upon the reaction with Ru(bpy)₃³⁺ and the intensity of light that will be obtained.

Proline, despite being a secondary amine, is one of the suitable reducing agents for the Ru(bpy)₃³⁺ chemiluminescent reaction. Previously, Lee and Nieman have reported that the relative

* Corresponding author. Fax: +81 78 803 7761.

E-mail address: keisaito@kobe-u.ac.jp (K. Saito).

chemiluminescent intensities observed for proline, Pro-Gly, and Gly-Pro were of 49,600, 2800, and 72, respectively [17]. As regards Gly-Pro in which a carbonyl group links to nitrogen of proline, the chemiluminescent intensity will decrease because of the electron-withdrawing character of carbonyl oxygen. However, it cannot be interpreted by the general trends mentioned above that the chemiluminescent intensity of Pro-Gly is about 20 times lower than that of proline. Other researchers have also reported similar results [18,19]. These previous reports suggest that the carboxyl group attached to the α -carbon of aliphatic amines may play an important role in the $\text{Ru}(\text{bpy})_3^{3+}$ chemiluminescent reaction. We have focused attention on the molecular structure of aliphatic secondary amines possessing a carboxyl group at the α -carbon and have found that $\text{Ru}(\text{bpy})_3^{3+}$ reacts with domoic acid and pipercolic acid to emit intense chemiluminescence. Based on this finding, we have proposed highly sensitive methods for determination of domoic acid [6] and pipercolic acid [7]. However, the reason why aliphatic secondary amines possessing a carboxyl group at the α -carbon have strong chemiluminescent activity was still unclear.

The objective of this study is to understand the role of a carboxylate anion beside nitrogen of aliphatic amines on the $\text{Ru}(\text{bpy})_3^{3+}$ chemiluminescent reaction; the carboxyl group is deprotonated to the carboxylate anion under the chemiluminescent reaction condition. As a result, we have confirmed that the carboxylate anion attached to the α -carbon of aliphatic amines promotes the chemiluminescent reaction. Based on this finding, preliminary studies on simultaneous determination of five amino acids containing a secondary amine in human serum have been performed using isocratic reversed-phase ion-pair HPLC with $\text{Ru}(\text{bpy})_3^{3+}$ chemiluminescent detection.

2. Experimental

2.1. Reagents

All chemicals were of analytical reagent grade and were used without further purification, except for tris(2,2'-bipyridine) ruthenium(II) chloride hexahydrate ($\text{Ru}(\text{bpy})_3\text{Cl}_2 \cdot 6\text{H}_2\text{O}$). $\text{Ru}(\text{bpy})_3\text{Cl}_2 \cdot 6\text{H}_2\text{O}$ was prepared in our laboratory. A 0.5 mM $\text{Ru}(\text{bpy})_3^{2+}$ solution was prepared by dissolving a weighed quantity of $\text{Ru}(\text{bpy})_3\text{Cl}_2 \cdot 6\text{H}_2\text{O}$ in 100 mM sodium sulfate containing 1 mM sulfuric acid. Stock standard solutions of the tested compounds were prepared in water and/or acetonitrile and were kept cool and in the dark; these solutions were diluted with the eluent or the carrier before use. A 0.4 M Britton–Robinson (BR) buffer solution was prepared as an acid solution with 27.2 mL of phosphoric acid, 22.8 mL of acetic acid, and 24.8 g of boric acid in 1 L of water, followed by pH adjustment with 2 M sodium hydroxide. Water for all solutions was purified using a GS-200 automatic water distillation apparatus (Advantec, Tokyo, Japan) and then a Milli-QII water purification system (Millipore, Bedford, MA, USA).

2.2. Apparatus

HPLC experiments were performed with the 3-pump chemiluminescent detection system shown in Fig. 1. A GL Science PU611 pump (GL Science, Tokyo, Japan) was used to deliver solutions. All the solutions were purged with a Shodex Degas (Showa Denko, Tokyo, Japan). Injection was made using a Rheodyne 7125 sample injector (Rheodyne, Cotati, CA, USA) equipped with a 20 μL injector loop. Electrochemical oxidation of $\text{Ru}(\text{bpy})_3^{2+}$ was performed by the controlled-current electrolysis method using an electrochemical reactor in a COMET 3000 ECL detector (Comet, Kawasaki, Japan). All connecting PTFE tubing was 0.5 mm i.d. A Hitachi D-2500

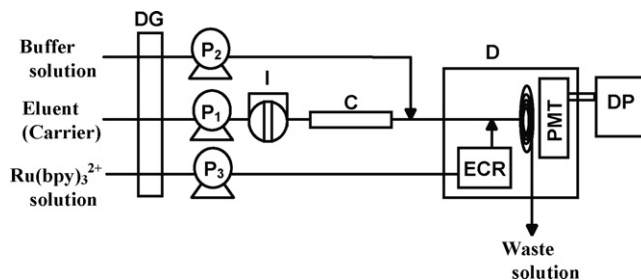


Fig. 1. Schematic diagram of the HPLC-chemiluminescent detection system. DG, degasser; P, pump; I, injector; C, column; D, CL detector; ECR, electrochemical reactor; PMT, photomultiplier tube; DP, data processor.

Chromato-Integrator (Hitachi, Tokyo, Japan) was used as the data processor. For FIA experiments, the column was removed from the system represented in Fig. 1.

2.3. Measurement of chemiluminescent intensities of amines

Chemiluminescent intensities of various amines were measured with the FIA system. The carrier solution of 50% (v/v) aqueous acetonitrile was delivered at a flow rate of 0.5 mL min^{-1} . The 0.4 M BR buffer solution was delivered at a flow rate of 0.1 mL min^{-1} and was mixed with the carrier after the injector in order to control the pH of the chemiluminescent reaction. Note, however, that the reaction pH value was decided from the effluent pH value. The 0.5 mM $\text{Ru}(\text{bpy})_3^{2+}$ solution was delivered at a flow rate of 0.3 mL min^{-1} . The electrolytic current of the electrochemical reactor was set at 50 μA .

2.4. Determination of unconsumed piperidine derivatives after reaction with $\text{Ru}(\text{bpy})_3^{3+}$

A $\text{Ru}(\text{bpy})_3^{3+}$ solution was prepared from the 0.5 mM $\text{Ru}(\text{bpy})_3^{2+}$ in 100 mM sodium sulfate containing 1 mM sulfuric acid. $\text{Ru}(\text{bpy})_3^{2+}$ was oxidized to $\text{Ru}(\text{bpy})_3^{3+}$ by the controlled-current electrolytic method at 5 mA for about 30 min with stirring by the use of a potentiostat/galvanostat HA-151 (Hokuto denko, Tokyo, Japan) with a standard three-electrode arrangement consisting of a platinum-gauze working electrode (5 cm \times 12.2 cm), an Ag/AgCl reference electrode, and a platinum-wire auxiliary electrode. The formation of $\text{Ru}(\text{bpy})_3^{3+}$ was noted through a color change from red-orange to green.

Three milliliters portions of a water–acetonitrile (1:1, v/v) mixture and 1 mL portions of a 0.1 mM piperidine derivative were successively placed in six of 10 mL volumetric flasks. Next graded amounts (0, 200, 400, 600, 800, 1000 μL) of the $\text{Ru}(\text{bpy})_3^{3+}$ solution were pipetted into each flask. The flasks were shaken well and set aside for a few hours in the dark. After the solutions changed from green to red-orange, the solutions were made up to 10 mL with the water–acetonitrile (1:1, v/v) mixture. In order to determine the residual piperidine derivative, the resulting solutions were injected into the FIA system, in which the pump 2 and the buffer solution reservoir represented in Fig. 1 were removed. The carrier was a 0.4 M BR buffer (pH 7.5)–50% (v/v) aqueous acetonitrile (1:5, v/v) and was delivered at a flow rate of 0.6 mL min^{-1} . Conditions for the $\text{Ru}(\text{bpy})_3^{2+}$ solution were the same as those described in Section 2.3.

2.5. Sample preparation and HPLC conditions for determination of amino acids containing a secondary amine in human serum

In order to precipitate proteins, 200 μL of acetonitrile was added to 200 μL of pooled human serum (NESCOL-N, Oriental Yeast,

Table 1
Relative luminescent intensities of the selected compounds.

Compound	R.L.I. ^a
Pipecolic acid	182
Nipecotic acid	108
Isonipecotic acid	50
Piperidine	16
Cyclohexanecarboxylic acid	0
2-Methylpiperidine	13
Proline	135
Diethylamine	23
N-Methylalanine	195
N-Methylglycine	76
Methylaminoacetonitrile	1
N-Methylbenzylamine	46

Sample: 10 μ M. pH value of BR buffer, 7.5.

^a Relative luminescent intensity.

Tokyo, Japan). The mixture was well shaken and then centrifuged at 3500 rpm for 10 min. To 200 μ L of the supernatant, 800 μ L of 30 mM phosphoric acid was added. The mixture was shaken and then loaded onto a solid-phase extraction cartridge (Strata C18-E, 50 mg/mL, phenomenex) and the first 0.5 mL of eluate was discarded. The following 0.5 mL was collected for chromatographic analysis. An aliquot of this solution (20 μ L) was injected into the HPLC system. Recovery experiments were made by adding the standard solutions of amino acids containing a secondary amine to the pooled human serum before the addition of acetonitrile.

Amino acids containing a secondary amine were separated on a CAPCELL PAK C18 120A (150 mm \times 4.6 mm i.d., Shiseido, Tokyo, Japan) analytical column. The eluent was 5 mM sodium octanesulfonate prepared with 10 mM phosphoric acid–acetonitrile (98:2, v/v) and was delivered at a flow rate of 0.5 mL min⁻¹. The 0.4 M BR buffer (pH 9.1) was delivered at a flow rate of 0.1 mL min⁻¹. The 0.5 mM Ru(bpy)₃²⁺ solution was delivered at a flow rate of 0.3 mL min⁻¹ and was oxidized at 150 μ A.

3. Results and discussion

3.1. Chemiluminescent intensities of secondary amines

The generation of chemiluminescence upon reaction of Ru(bpy)₃³⁺ with selected compounds was examined with the FIA system in order to evaluate the effect of a carboxylate anion on the chemiluminescent activity of secondary amines. Table 1 shows the obtained results. Strong chemiluminescence was observed for amino acids containing a secondary amine such as proline, pipecolic acid, and N-methylalanine. Although pipecolic acid, N-methylalanine, piperidine, and diethylamine are all aliphatic

secondary amines, the chemiluminescent intensities of pipecolic acid and N-methylalanine were nearly 10 times stronger than those of piperidine and diethylamine, respectively. In addition, the chemiluminescent intensities of pipecolic acid, nipecotic acid, and isonipecotic acid decreased in the order pipecolic acid > nipecotic acid > isonipecotic acid with increasing distance between the carboxylate anion and the nitrogen atom (Fig. 2). These results suggest that the carboxylate anion plays an important role in the chemiluminescent reaction of Ru(bpy)₃³⁺ with secondary aliphatic amines.

3.2. Role of a carboxyl group on the chemiluminescent reaction

It has been proposed in the previous report that an anionic species of a α -keto acid be generated in the chemiluminescent reaction between amino acids and Ru(bpy)₃³⁺ [20]. Furthermore, it is known that the anionic species of a α -keto acid such as pyruvate reacts with Ru(bpy)₃³⁺ to emit chemiluminescence [21]. Therefore, we initially thought that the strong chemiluminescence of amino acids containing a secondary amine resulted from sequential reactions, that is, the chemiluminescent reaction between the secondary amine moiety of the amino acids and Ru(bpy)₃³⁺ occurred first and then the reaction product successively reacted with Ru(bpy)₃³⁺. To confirm this assumption, residual concentrations of piperidine and its carboxyl derivatives after being allowed to react with a definite amount of Ru(bpy)₃³⁺ were measured. If pipecolic acid brings on the sequential reactions, the amount of pipecolic acid consumed in the reaction will be less than that of piperidine. However, contrary to our expectation, the opposite result was obtained. As shown in Fig. 3, more than 90% pipecolic acid was consumed by the addition of 1000 μ L of the Ru(bpy)₃³⁺ solution, while piperidine was consumed only 40%. The amount consumed in the reaction with Ru(bpy)₃³⁺ decreased in the order pipecolic acid > nipecotic acid > isonipecotic acid > piperidine, consistent with the sequence of chemiluminescent intensity. These results suggest that the carboxylate anion promotes the chemiluminescent reaction between Ru(bpy)₃³⁺ and aliphatic secondary amines. Since the chemiluminescent intensity is generally very low when the basicity of a solution is not high enough to deprotonate an amine or an amine radical cation [16,22] and the pK_a values of secondary amines possessing a carboxyl group at the α -carbon are lower than those of corresponding simple secondary amines (e.g. pipecolic acid, pK_a = 10.72; piperidine, pK_a = 11.12; N-methylglycine, pK_a = 10.12; dimethylamine, pK_a = 10.77), we have thought that the presence of a carboxylate anion at the α -carbon is advantageous to dissociation of the proton. Therefore, the effect of the pH on the chemiluminescent intensity for piperidine and its derivatives was examined. Fig. 4A shows the obtained results. The chemiluminescent reaction occurred at a lower pH with decreasing distance

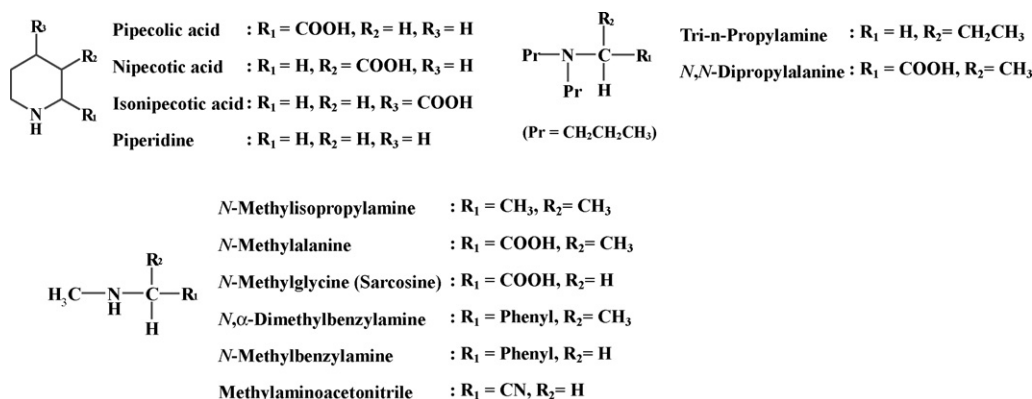


Fig. 2. Structure of selected aliphatic amines.

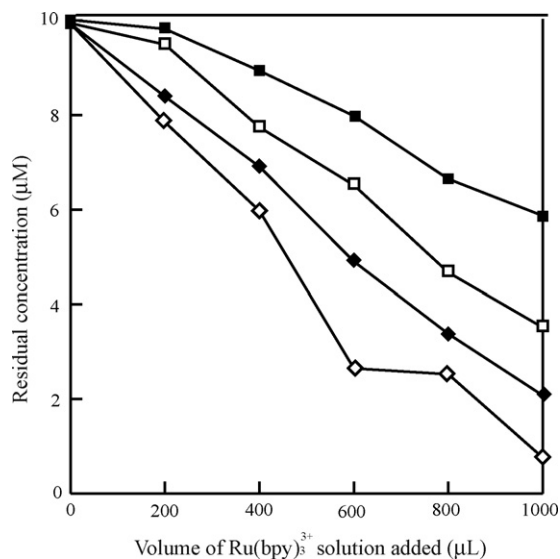


Fig. 3. The relationship between the residual concentration of piperidine derivatives and the volume of the Ru(bpy)₃³⁺ solution added. Sample: 1 μM each; pipecolic acid (◇), nipecotic acid (◆), isonipecotic acid (□), piperidine (■).

between the carboxyl group and the nitrogen atom in accord with expectation. The difference in chemiluminescent intensity between pipecolic acid and piperidine at each optimal pH is not so great. However, background chemiluminescence increased with increasing pH because hydroxide ions react with Ru(bpy)₃³⁺, as shown in the inset of Fig. 4A. Since high background chemiluminescence results in a high noise level, a lower reaction pH leads to more sensitive detection.

These results suggest that the chemiluminescent reaction occurs at a lower pH by the presence of specific substituents. Therefore, the effect of the pH on the chemiluminescent intensity was investigated in detail for aliphatic secondary amines having various substituents at the α-carbon (Fig. 2). As shown in Fig. 4B, diethylamine which is a simple aliphatic secondary amine showed the maximum chemiluminescent intensity at pH 9.4. Similarly, *N*-methylisopropylamine which has a methyl group at the α-carbon showed the maximum chemiluminescent intensity at the same pH value. On the other hand, the compounds having a carboxylate anion or a phenyl group, such as *N*-methylalanine, *N*-methylglycine (sarcosine), *N*,α-dimethylbenzylamine, and *N*-

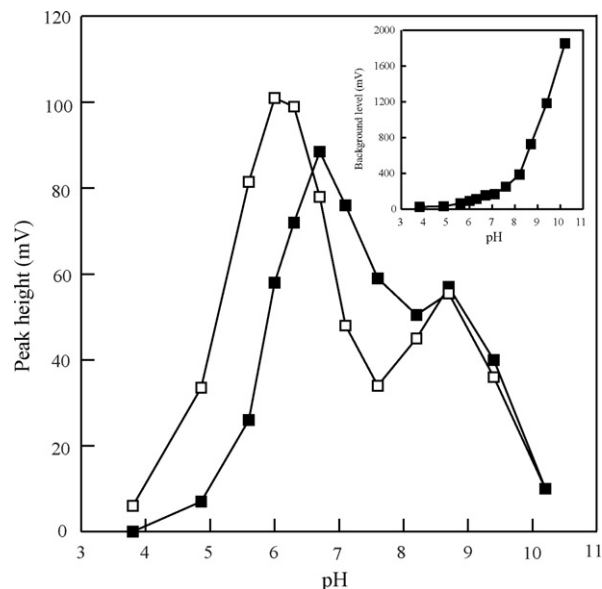


Fig. 5. Effect of the pH on the chemiluminescent intensity for aliphatic tertiary amines. Sample: 1 μM each; tri-*n*-propylamine (■), *N,N*-dipropylamine (□).

methylbenzylamine, showed the maximum chemiluminescent intensity at pH 8.2. However, these compounds showed significant difference in chemiluminescent intensity. The chemiluminescent intensities of *N*-methylalanine and *N*,α-dimethylbenzylamine were nearly two times stronger than those of *N*-methylglycine and *N*-methylbenzylamine, respectively. A possible explanation for the difference in chemiluminescent intensity is that the electron-donating methyl groups attached to the α-carbon of *N*-methylalanine and *N*,α-dimethylbenzylamine stabilize electron-deficient radicals and then increase the chemiluminescent activity. On the other hand, methylaminoacetonitrile which has a strong electron-withdrawing cyano group hardly produced chemiluminescence regardless of the reaction pH.

Since the aliphatic secondary amines having a carboxylate anion or a phenyl group at the α-carbon tended to have maximum chemiluminescent intensity at a lower pH compared with corresponding aliphatic secondary amines without these substituents, it was examined whether such tendency is observed for aliphatic tertiary and primary amines or not. Fig. 5 shows the results obtained for aliphatic tertiary amines. Although the chemilumi-

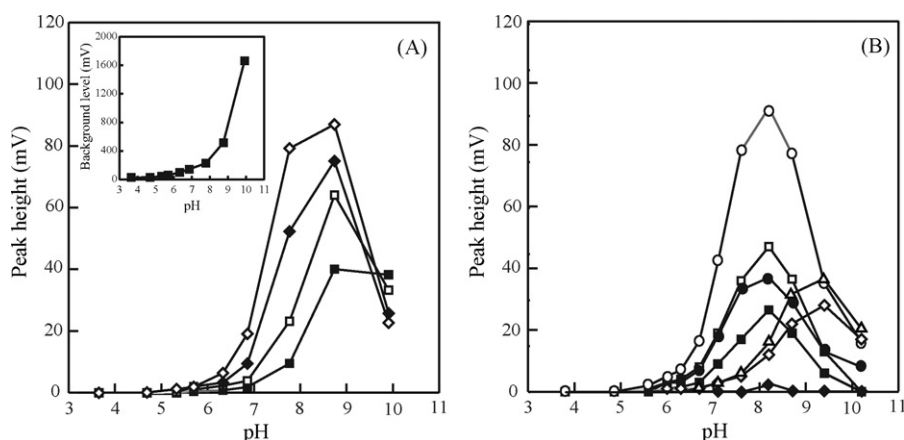


Fig. 4. Effect of the pH on the chemiluminescent intensity for aliphatic secondary amines. Sample: 1 μM each; (A) pipecolic acid (◇), nipecotic acid (◆), isonipecotic acid (□), piperidine (■); (B) diethylamine (Δ), *N*-methylisopropylamine (◇), *N*-methylalanine (○), *N*-methylglycine (●), *N*,α-dimethylbenzylamine (□), *N*-methylbenzylamine (■), methylaminoacetonitrile (◆).

nescent intensity of *N,N*-dipropylalanine was almost equal to that of tri-*n*-propylamine, the optimum pH with *N,N*-dipropylalanine shifted to a lower pH compared with tri-*n*-propylamine. It has been reported that the aliphatic tertiary amines having a phenyl group at the α -position such as emetine showed maximum chemiluminescence at a lower pH [23]. Recently, Morita and Konishi have reported that the aliphatic tertiary amines containing an alkoxyphenyl group tended to have maximum chemiluminescent intensity at a lower pH compared with the aliphatic amines not containing an alkoxyphenyl group. Based on the finding, they have developed a highly sensitive pre-column derivatization reagent for Ru(bpy)₃³⁺ chemiluminescent detection [24]. However, they did not describe why the aliphatic amines containing an alkoxyphenyl group tended to have maximum chemiluminescent intensity at acidic conditions. As regards aliphatic primary amines, we previously reported that the chemiluminescent intensity of histidine was stronger by twenty times than that of histamine at pH value around neutrality [5]. The structural difference between histidine and histamine is that only histidine has a carboxyl group at the α -carbon of the primary amine.

On the basis of the discussion in the preceding sections, the presence of the specific substituent, at least a carboxylate anion and a phenyl group, at the α -carbon of aliphatic amines, is advantageous for the chemiluminescent reaction at a lower pH. Therefore, the aliphatic amines having these substituents at the α -carbon can be sensitively detected compared with the corresponding aliphatic amines without such groups.

3.3. Simultaneous determination of amino acids containing a secondary amine in human serum

Although amino acids containing a secondary amine, such as proline, 4-hydroxyproline, and pipecolic acid, in human body fluid are important biomarkers for various illnesses [7,25–29], concentrations of amino acids containing a secondary amine except proline are very low compared with other amino acids. Therefore, amino acids containing a secondary amine have been currently determined by using HPLC coupled to sensitive fluorescence detection after pre-column derivatization [25,26]. However, the methods involve multisteps manipulation and gradient elution because the methods are subject to interference from other compounds mainly amino acids. Therefore, simultaneous determination of amino acids containing a secondary amine is very difficult. As will be appre-

Table 2

Parameters of calibration graphs and precision values obtained for standard solutions of amino acids.

Compound	Linear range (μ M)	Detection limit (nM)	R.S.D. (%) ^a	R ²
4-Hydroxyproline	0.01–20	3.0	0.3	1.000
<i>N</i> -Methylglycine	0.02–20	12	2.6	1.000
<i>N</i> -Methylalanine	0.01–20	2.7	0.8	1.000
Proline	0.01–20	4.6	1.1	0.9998
Pipecolic acid	0.02–20	10	1.9	1.000

R², determination coefficient.

^a Six determinations at 50 nM.

ciated from the forgoing, detection of amino acids containing a secondary amine with Ru(bpy)₃³⁺ chemiluminescent reaction can be expected to be sensitive and selective. Since it has been known that proline is one of the suitable reducing agents for the Ru(bpy)₃³⁺ chemiluminescent reaction, the determination method of proline and 4-hydroxyproline has been already reported [27,28]. However, it has not been so far reported that *N*-methylglycine and *N*-methylalanine can be also sensitively detected. Therefore, preliminary studies on simultaneous determination of five amino acids containing a secondary amine, 4-hydroxyproline, *N*-methylglycine, *N*-methylalanine, proline, and pipecolic acid, in human serum have been performed using isocratic reversed-phase ion-pair HPLC with post-column Ru(bpy)₃³⁺ chemiluminescent detection.

The optimal conditions for the chemiluminescent detection of pipecolic acid [7] were employed for the simultaneous determination of these amino acids in human serum because the lowest concentration compound among these amino acids was pipecolic acid. Fig. 6A shows a typical chromatogram obtained for the mixed solution of the five amino acids containing a secondary amine. Although *N*-methylalanine was not detected in human serum in previous reports, the determination of *N*-methylalanine was performed concurrently. The detection limits, the linear range, and the relative standard deviations obtained with HPLC-Ru(bpy)₃³⁺ chemiluminescent detection are shown in Table 2. This detection method exhibited high sensitivity, wide linear range (3 orders of magnitude), and good reproducibility. Fig. 6B shows a typical chromatogram obtained for the 10 times diluted human serum. 4-Hydroxyproline, *N*-methylglycine, proline, and pipecolic acid were detected. However, the peak of *N*-methylalanine overlapped with the peaks of the sample matrices. Since this problem is dependent

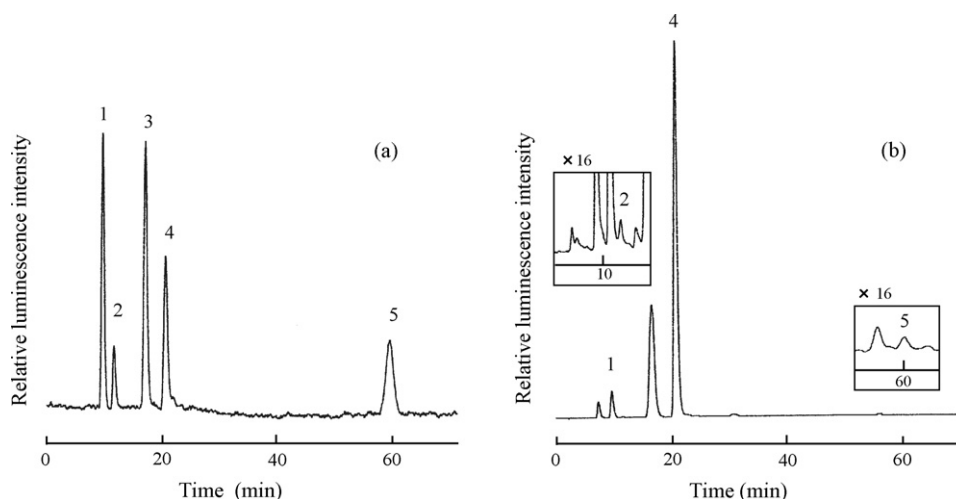


Fig. 6. Typical chromatograms obtained with the proposed HPLC method for (A) a mixed standard solution of amino acids (50 nM each) and (B) a 10 times diluted human serum sample. Peak identification: 1, 4-hydroxyproline; 2, *N*-methylglycine; 3, *N*-methylalanine; 4, proline; 5, pipecolic acid.

Table 3
Contents of amino acids in human serum.

Compound	Found (μM) ^a	Recovery (%) ^b
4-Hydroxyproline	3.65 \pm 0.14	94.2 \pm 3.7 ^c
N-Methylglycine	0.60 \pm 0.01	112.6 \pm 2.5 ^d
N-Methylalanine	–	–
Proline	95.1 \pm 3.3	110.7 \pm 4.0 ^e
Pipecolic acid	0.33 \pm 0.05	92.0 \pm 5.4 ^d

–, not determined.

^a Values are means for four determination \pm S.D.

^b Values are means for four operation \pm S.D.

^c Added 5 μM .

^d Added 2 μM .

^e Added 50 μM .

on the separation efficiency, it would be resolved by employing high-resolution separation methods such as capillary electrophoresis [11] or effective pretreatment techniques [26,29]. The contents of amino acids containing a secondary amine obtained for the human serum sample are shown in Table 3. Recovery values were of 92–113%, as shown in Table 3. These results suggest that the present methodology should be applied to the simultaneous determination of amino acids containing a secondary amine in human serum.

4. Conclusions

We have shown here that a carboxylate anion attached to the α -carbon of aliphatic amines play an important role in the chemiluminescent reaction of Ru(bpy)₃³⁺ with aliphatic amines. The carboxylate anion promotes the chemiluminescent reaction and then aliphatic amines having this substituent at the α -carbon can be sensitively detected compared with corresponding amines without this substituent. This information is very important in order to predict which compounds having amine moieties will give intense emission of light upon reaction with Ru(bpy)₃³⁺ and the intensity of light that will be obtained. To investigate the effect of substituents at the α -carbon of aliphatic amines in detail will lead to the development of more effective co-reagents for Ru(bpy)₃²⁺ ECL system. This study also indicates that the Ru(bpy)₃³⁺ chemiluminescence is effective for detecting various amino acids containing a secondary amine.

Acknowledgements

The present work was partially supported by a Grant-in-Aid for Scientific Research (No. 18550073) from the Ministry of Education, Culture, Sports, Science and Technology, Japan.

References

- [1] I. Rubinstein, C.R. Martin, A.J. Bard, *Anal. Chem.* 55 (1983) 1580–1582.
- [2] J.B. Noffsinger, N.D. Danielson, *Anal. Chem.* 59 (1987) 865–868.
- [3] K. Saito, S. Murakami, S. Yamazaki, A. Muromatsu, S. Hirano, T. Takahashi, K. Yokota, T. Nojiri, *Anal. Chim. Acta* 378 (1999) 43–46.
- [4] H. Kodamatani, K. Saito, A. Muromatsu, N. Niina, S. Yamazaki, *Anal. Lett.* 38 (2005) 291–301.
- [5] H. Kodamatani, Y. Komatsu, S. Yamazaki, K. Saito, *Anal. Sci.* 23 (2007) 407–411.
- [6] H. Kodamatani, K. Saito, N. Niina, S. Yamazaki, A. Muromatsu, I. Sakurada, *Anal. Sci.* 20 (2004) 1065–1068.
- [7] H. Kodamatani, Y. Komatsu, S. Yamazaki, K. Saito, *J. Chromatogr. A* 1140 (2007) 88–94.
- [8] T. Pérez-Ruiz, C. Martínez-Lozano, V. Tomás, J. Martín, *Talanta* 58 (2002) 987–994.
- [9] N.A. Al-Arfaj, *Talanta* 62 (2004) 255–263.
- [10] X. Wang, D.R. Bobbitt, *Talanta* 53 (2000) 337–345.
- [11] X.B. Yin, S. Dong, E. Wang, *Trend Anal. Chem.* 23 (2004) 432–441.
- [12] P.A. Greenwood, C. Merrin, T. McCreedy, G.M. Greenway, *Talanta* 56 (2002) 539–545.
- [13] K.A. Fährlich, M. Pravda, G.G. Guilbault, *Talanta* 54 (2001) 531.
- [14] B.A. Gorman, P.S. Francis, N.W. Barnett, *Analyst* 131 (2006) 616–639.
- [15] A.J. Bard (Ed.), *Electrogenerated Chemiluminescence*, Marcel Dekker, New York, 2004.
- [16] A.W. Knight, G.M. Greenway, *Analyst* 121 (1996) 101R–106R.
- [17] W.Y. Lee, T.A. Nieman, *Anal. Chem.* 67 (1995) 1789–1796.
- [18] L. He, K.A. Cox, N.D. Danielson, *Anal. Lett.* 23 (1990) 195–210.
- [19] N. Egashira, J. Piao, E. Hifumi, T. Uda, *Bunseki Kagaku* 49 (2000) 1029–1031.
- [20] S.N. Brune, D.R. Bobbitt, *Anal. Chem.* 64 (1992) 166–170.
- [21] I. Rubinstein, A.J. Bard, *J. Am. Chem. Soc.* 103 (1981) 512–516.
- [22] J.K. Leland, M.J. Powell, *J. Electrochem. Soc.* 137 (1990) 3127–3131.
- [23] K. Tsukagoshi, K. Miyamoto, R. Nakajima, N. Ouchiya, *J. Chromatogr. A* 919 (2001) 331–337.
- [24] H. Morita, M. Konishi, *Anal. Chem.* 75 (2003) 940–946.
- [25] H. Inoue, K. Moritani, Y. Date, K. Kohashi, Y. Tsuruta, *Analyst* 120 (1995) 1141–1145.
- [26] H. Inoue, Y. Sakata, K. Fukunaga, H. Nishio, Y. Tsuruta, *Anal. Chim. Acta* 511 (2004) 267–271.
- [27] K. Uchikura, K. Sakurada, K. Tezuka, K. Koike, *Bunseki Kagaku* 51 (2002) 953–957.
- [28] T. Ikehara, N. Habu, I. Nishino, H. Kamimori, *Anal. Chim. Acta* 536 (2005) 129–133.
- [29] M. Moulin, C. Deleu, F.R. Larher, A. Bouchereau, *Anal. Biochem.* 308 (2002) 320–327.



Iron (III) porphyrin bearing 2,6-di-*tert*-butylphenol pendants deposited onto gold electrodes for amperometric determination of L-histidine

Katarzyna Kurzatkowska^a, Dmitry Shpakovsky^b, Jerzy Radecki^a, Hanna Radecka^{a,*}, Zhang Jingwei^b, Elena Milaeva^b

^a Institute of Animal Reproduction and Food Research of Polish Academy of Sciences, Tuwima 10, 10-747 Olsztyn, Poland

^b Organic Chemistry Department, Faculty of Chemistry, Moscow State Lomonosov University, Lenin Hill 119992 Moscow, Russia

ARTICLE INFO

Article history:

Received 22 April 2008

Received in revised form 23 October 2008

Accepted 31 October 2008

Available online 7 November 2008

Keywords:

Iron(III) Porphyrin

Histidine

Gold electrodes

Osteryoung square-wave voltammetry

ABSTRACT

A sensitive amperometric sensor for determination of L-histidine was developed using gold electrode modified with Fe(III)-porphyrin bearing three 2,6-di-*tert*-butylphenol groups and one palmitoyl chain. Two methods of electrode modification were applied: direct chemisorption and embedment into dodecanethiol monolayer. Both types of electrodes were used for detection of L-histidine using Osteryoung square-wave voltammetry. The sensitivity of sensors presented towards L-histidine depends on the method of electrode modification. The detection limits observed for the electrodes incorporating with Fe(III)-porphyrin host by embedment and chemisorption were in 1 and 100 nM ranges, respectively. In addition, the determination of L-histidine with electrode modified by embedment technique was more precise, in comparison to that obtained by the direct chemisorption.

Applicability of gold electrodes modified with Fe(III)-porphyrin for the direct electrochemical determination of L-histidine was demonstrated using the artificial matrix mimicking human serum.

© 2008 Elsevier B.V. All rights reserved.

1. Introduction

L-Histidine, one of the 20 natural amino acids, plays an important role as a neurotransmitter, or neuromodulator in mammalian central-nervous system including the retina [1]. It controls the transport of metals in biologically important bases. Due to the high reactivity of imidazole group, L-histidine is often found at the active site of enzymes and is directly involved in catalysis. L-Histidine can be converted to histamine, which is a major neurotransmitter in the brain and throughout the nervous system [2]. It was found that ingestion of sufficiently high levels of histamine could result in symptoms of the intoxication. Thus, the specific analysis of L-histidine in biological samples is of great importance for biochemical studies [3,4].

The methods most frequently applied for the determination of trace amount of L-histidine are capillary electrophoresis [5–8], colorimetric [9], fluorimetric [4,10], chromatographic [11–13]. The electrochemical methods used in this particular field have been also reported [14–20].

In the present approach, an electroactive Fe(III)-porphyrin bearing 2,6-di-*tert*-butylphenol pendants was selected as a sensing element of amperometric sensor for L-histidine determination.

Metalloporphyrins have attracted a great deal of interest owing to the diversity of their structures and interaction between the central metal and the analyte. Metalloporphyrin macrocycle is almost planar molecule and it can easily form stable complexes with uncharged molecules possessing donor atoms such as oxygen or nitrogen. Among the metal complexes, iron and manganese porphyrins can be selected as biomimetics. Metal atoms in their molecules possess a high coordination number. The specific structures and properties of the metalloporphyrins confirm that they might be useful as probes in analytical chemistry for the molecular recognition [21,22]. On the other hand, the redox activity of both metal centre and porphyrin macrocycle improves the ability of these compounds to act as the recognition element of electrochemical sensors.

The goal of the study presented was the development of an amperometric sensor for detection of L-histidine based on Fe(III)-porphyrin bearing redox active 2,6-di-*tert*-butylphenol pendants in the periphery of porphyrin ring – 5-(4-palmitoyloxyphenyl)-10,15,20-tris[3,5-di-*tert*-butyl-4-hydroxyphenyl]porphyrinato iron (III) chloride (Fig. 1) [23,24].

* Corresponding author. Tel.: +48 895234636; fax: +48 895240124.
E-mail address: hanna.radecka@pan.olsztyn.pl (H. Radecka).

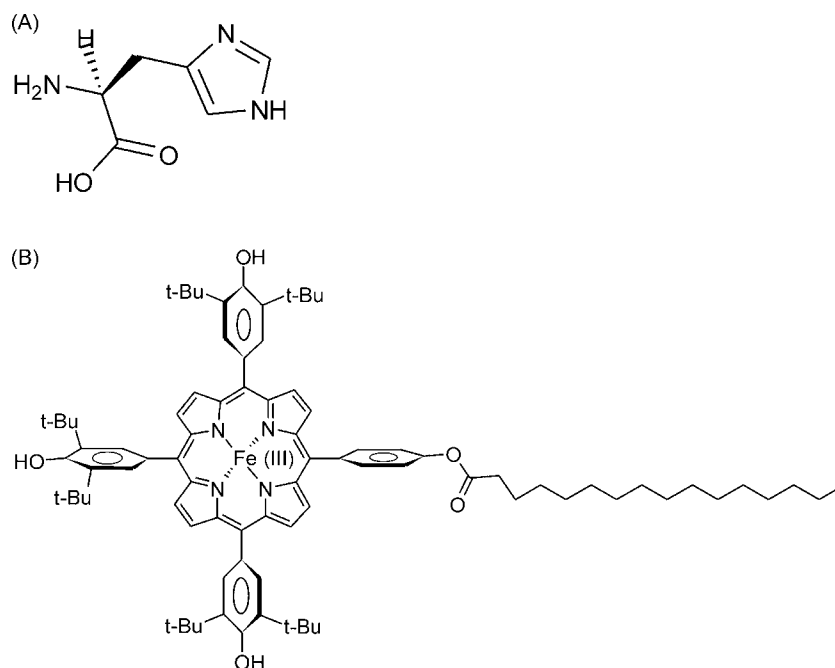


Fig. 1. The structures of L-histidine (A) and 5-(4-palmitoyloxyphenyl)-10,15,20-tris[3,5-di-tert-butyl-4-hydroxyphenyl]porphyrinato iron (III) chloride (Fe(III)-porphyrin) (B).

A well-known method of the direct immobilization of thiol-tailored metalloporphyrin on the surface of gold might bring some disadvantages. It has been reported that thiol can coordinate the metal ion of the porphyrin resulting in multilayer formation as well as a blocking of metal coordinative ability [19,20]. Therefore, in this study the gold electrodes were modified with Fe(III)-porphyrin by the embedment and chemisorption methods.

The influence of the immobilization method of porphyrin molecules on the gold surface on the sensitivity and precision of presented sensor was discussed.

2. Experimental

2.1. Reagents

5-(4-Palmitoyloxyphenyl)-10,15,20-tris[3,5-di-tert-butyl-4-hydroxyphenyl]porphyrinato iron (III) chloride (Fig. 1) was synthesized as described previously [23]. 1-Dodecanethiol, L-histidine, chloroform were purchased from Sigma–Aldrich (Poznań, Poland). KOH, KCl, KNO₃, ethanol were obtained from ABCChem, Gliwice, Poland. All aqueous solutions were prepared with deionised and charcoal-treated water (resistivity of 18.2 MΩcm) purified with a Milli-Q reagent grade water system (Millipore, Bedford, MA).

2.2. Electrodes preparation

Gold disk electrodes 2 mm² area (Bioanalytical Systems (BAS), West Lafayette, IN) were used for the experiments. The electrodes were polished with wet 0.3 and 0.05 μm alumina slurry (Alpha and Gamma Micropolish, Buehler, Lake Bluff, IL) on a flat pad for at least 10 min and rinsed repeatedly with water and finally in a sonicator (30 s). The polished electrodes were then dipped in 0.5 M KOH solution deoxygenated by purging with argon for 15 min, and the potential was cycled between –400 and –1200 mV (versus Ag/AgCl referents electrode) with scan rate of 100 mV s⁻¹ until cyclic voltammograms did not change any more.

2.2.1. Chemisorption's modification

5 μl portions of 1.0 × 10⁻³ M Fe(III)-porphyrin solution in chloroform were dropped on the surface of clean gold electrodes. Next, the electrodes were covered with a small glass beaker and left for 15 min. After deposition of Fe(III)-porphyrin the electrodes were washed with chloroform, next with ethanol and water. The modified electrodes were stored in 0.1 M potassium chloride solution at room temperature until use.

2.2.2. Embedment modification

Clean electrodes were soaked in 1.0 × 10⁻⁵ M 1-dodecanethiol solutions in chloroform at the room temperature for 30 min. Next, after washing with chloroform, the electrodes were dipped in 1.0 × 10⁻³ M Fe(III)-porphyrin solution in chloroform at room temperature for 24 h. The modification solutions were put into the tubes (8 mm diameter, with no flat bottom). After dipping the electrodes, the tubes were sealing with Teflon tape in order to avoid solvent evaporation. After modification, the electrodes were washed with chloroform, next with ethanol and water. The modified electrodes were stored in 0.1 M potassium chloride solution at room temperature until use.

2.3. Electrochemical measurements

All electrochemical measurements were performed with a potentiostat-galvanostat AutoLab (Eco Chemie, Utrecht, Netherlands) with a three-electrode configuration. Potentials were measured versus the Ag/AgCl electrode, and a platinum wire was used as the auxiliary electrode. Osteryoung square-wave voltammetry (OSWV) was performed in the potential range from –100 to –600 mV, with a step potential of 1 mV, a square-wave frequency of 100 Hz, and amplitude of 25 mV.

2.4. Determination of L-histidine in the presence of an artificial matrix mimicking physiological sample

The amperometric responses of gold electrode incorporating Fe(III)-porphyrin towards L-histidine were checked in the

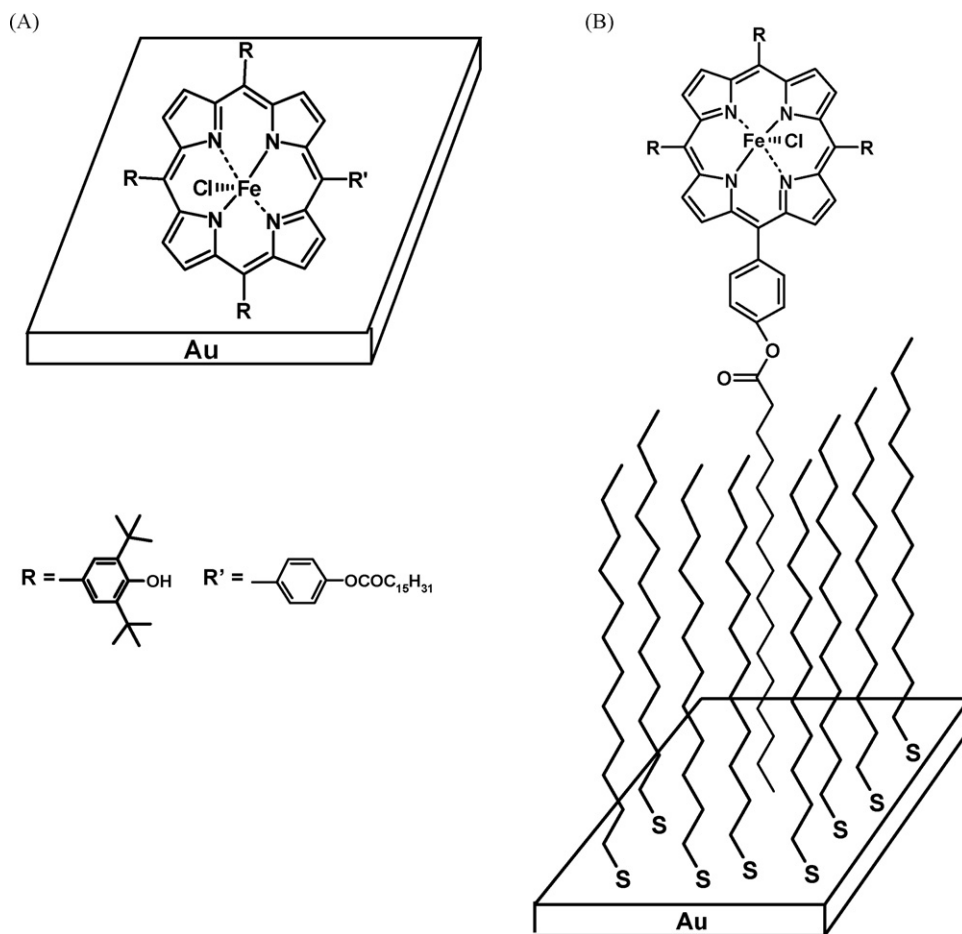


Fig. 2. The schematic illustration of immobilization of Fe(III)-porphyrin on the surface of gold electrodes by: A–chemisorption; B–embedment.

presence of an artificial matrix with following composition: 0.09% NaCl, 0.05% BSA; pH 5.5.

In order to perform the recovery test, 8 mL of the artificial matrix were spiked using a stock solution of L-histidine (1 mM in the presence of artificial matrix). The changes of current generated by a known amount of L-histidine were recorded and L-histidine concentrations were determined based on the calibration curve obtained in the presence of the artificial matrix.

2.5. UV–vis conformation of L-histidine–Fe(III)-porphyrin complex formation

A stock solution of 1.0×10^{-3} M was prepared by dissolving L-histidine in water. The working solution of Fe(III)-porphyrin for spectrophotometric measurements in DMSO was 1.0×10^{-5} M.

The UV–vis spectra of 1.0×10^{-5} M of Fe(III)-porphyrin in the presence of different concentrations of L-histidine: 1.0×10^{-5} M (2); 3.0×10^{-5} M (3); 4.0×10^{-5} M (4); 5.0×10^{-5} M (5) were recorded by Helios Gamma spectrophotometer.

3. Results and discussion

3.1. Immobilization of Fe(III)-porphyrin on gold electrodes

At the last few decades, the modifications of solid surfaces with porphyrins monolayers and multilayers are of great interest due to their potential applications in optical and chemical sensors [18,25].

In the study presented two methods of gold electrodes modification with Fe(III)-porphyrin were applied: the chemisorption (Fig. 2A) [25,26] and the embedment (Fig. 2B) [27,28].

The CPK model of Fe(III)-porphyrin (Fig. S1–supplementary materials) shows, that in spite of the presence of three 2,6-ditert-butylphenyl substitutions, the contact of porphyrin macrocycle with the gold surface is possible. This is mainly due to the presence in its structure one palmitoyl chain. Having such properties, the Fe(III)-porphyrin was suitable for both modification techniques applied.

Fig. 2B illustrates the scheme of gold electrode modification by the embedment method, which consists of two steps. In the first step, dodecanethiol self-assembled monolayer (DDT-SAM) was deposited on electrochemically clean gold surface through Au–S covalent bonds. In next step, the molecules of Fe(III)-porphyrin substituted with palmitoyl alkyl chain were incorporated into DDT SAM via hydrophobic and van der Waals forces. The concentration 1.0×10^{-5} M DDT for creation of DDT SAM was optimal. When higher concentration of DDT was used, gold surface was totally blocked and alkyl chains of Fe(III)-porphyrin could not penetrate into thiol monolayer.

In the case of embedment modification, the host molecule had no direct contact with gold surface. Therefore the porphyrin ring immobilized by this technique was relatively richer in π -electrons and more flexible than in the case of chemisorption.

The process of modification of gold surface electrode was controlled by means of OSWV technique. Fig. 3A illustrates the OSWV

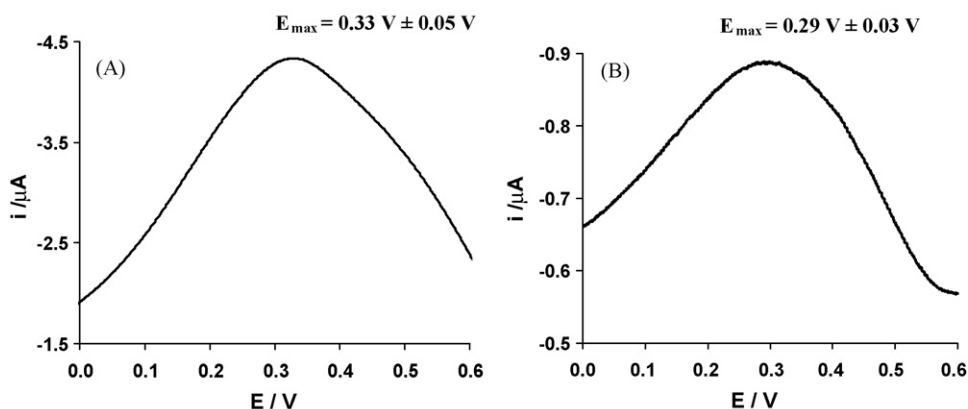


Fig. 3. OSWV curve of gold electrode modified with Fe(III)-porphyrin, by: A–chemisorption; B–embedment. The measurements were done vs. Ag/AgCl electrode in 0.1 M KCl.

curves of gold electrode modified with Fe(III)-porphyrin by direct chemisorption. The electrochemical measurements were done in 0.1 M KCl vs. Ag/AgCl electrode. The presence of a current maximum at 330 ± 50 mV indicated the presence of molecules of Fe(III)-porphyrin on the surface of electrode. The maximum peak current measured by OSWV for gold electrode modified by DDT and Fe(III)-porphyrin was observed at 290 ± 30 mV (Fig. 3B). The difference in position of maximums current was probably due to the different way of immobilization of host on the surface of gold electrode, which influences the electron density distribution in porphyrin molecules.

3.2. Electrochemical sensing of L-histidine with Fe(III)-porphyrin incorporated gold electrodes

The sensing of L-histidine by using gold electrodes modified with Fe(III)-porphyrin by direct chemisorption as well as by embedment method has been examined with OSWV technique. The concentration of L-histidine was determined in the range from 1.0×10^{-9} M to 1.0×10^{-4} M. The representative OSWV curves obtained for the gold electrode modified by the direct chemisorption in the presence of various concentration of L-histidine were illustrated in Fig. 4. The increase of L-histidine concentration decreased current values of OSWV peak (Fig. 4A). Also the potential of maximum peak currents were slightly shifted into more negative direction. The maximum current values correlated with L-histidine concentration logarithms as linear function, but repro-

ducibility was poor (Fig. 4B). Using this method (for details, see Section 2), the molecules of Fe(III)-porphyrin could be attached to the gold surface in rather random way. Some of them might be overlapped. Thus, receiving the reproducible modification using direct chemisorption's method was difficult. This was a main reason of large error bars on the calibration curves presented in Fig. 4 B. The detection limit observed for this type of electrodes estimated as $S/N=3$ was 2.08×10^{-7} M L-histidine.

The responses towards L-histidine were also examined using the electrodes modified by embedment method (Results not showed). This type of electrodes showed better detection limit ($S/N=3$, 8.9×10^{-10} M) and better accuracy in comparison to those modified by the chemisorption. Thus, the electrodes containing Fe(III)-porphyrin might be recommended for the direct electrochemical determination of L-histidine in aqueous solutions with sensitivity in nM range.

3.3. Determination of L-histidine in the presence of an artificial matrix mimicking physiological sample

In order to show the applicability of the sensors based on Fe(III)-porphyrin, the amperometric determinations of L-histidine were performed in the presence of an artificial matrix, which mimics the 10 times diluted human plasma (see Section 2).

The gold electrodes modified with Fe(III)-porphyrin by embedment technique, being more precise, were selected for this experiment.

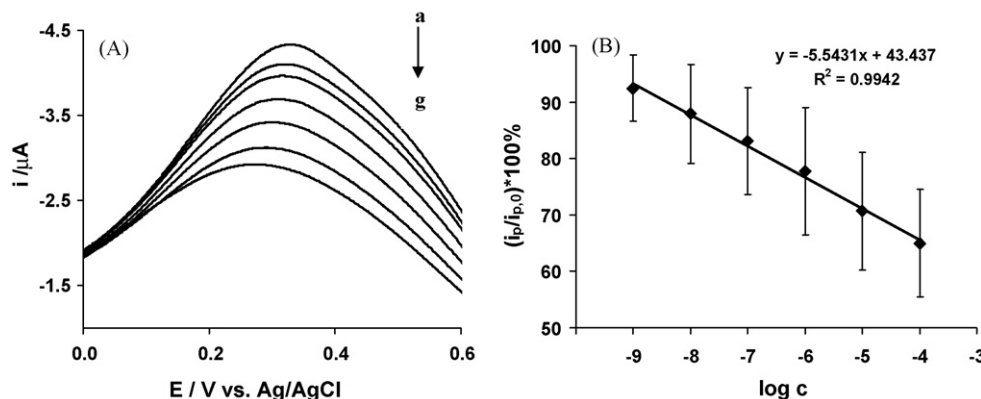


Fig. 4. The response towards L-histidine of gold electrode modified with Fe(III)-porphyrin by chemisorption's method. Concentrations of L-histidine: (a) 0 M, (b) 1.0×10^{-9} M, (c) 1.0×10^{-8} M, (d) 1.0×10^{-7} M, (e) 1.0×10^{-6} M, (f) 1.0×10^{-5} M, (g) 1.0×10^{-4} M. (A) OSWV; (B) linear relationship of relative current changes vs. concentration of L-histidine; (i_t)– current maximum in the presence of given concentrations of L-histidine; (i_0)– current maximum in 0.1 M KCl (average from 5 separate repetitions). The measuring conditions were as in Fig. 3.

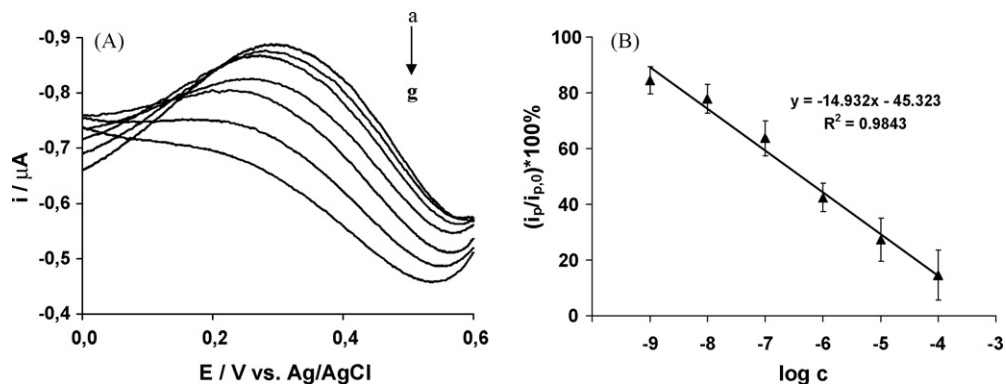


Fig. 5. The response towards L-histidine of gold electrode modified with Fe(III)-porphyrin by embedment method. Concentrations of L-histidine: (a) 0 M, (b) 1.0×10^{-9} M, (c) 1.0×10^{-8} M, (d) 1.0×10^{-7} M, (e) 1.0×10^{-6} M, (f) 1.0×10^{-5} M, (g) 1.0×10^{-4} M. (A) OSWV; (B) linear relationship of relative current changes vs. concentration of L-histidine in the presence of artificial matrix (0.09% NaCl + 0.05% BSA); (i_p)- current maximum in the presence of given concentrations of L-histidine; (i_0)- current maximum in the background solution free of analyte (average from 5 separate repetitions). The measuring conditions were as in Fig. 3.

Table 1
Recovery test in an artificial physiological matrix using L-histidine determination with Fe(III)-porphyrin gold electrode (measuring conditions Fig. 5 B; $n = 3$).

L-Histidine added (mol/L)	Embedment modification		Chemisorption modification	
	L-Histidine determined (mol/L)	Recovery (%)	L-Histidine determined (mol/L)	Recovery (%)
1.00×10^{-8}	$9.73 \times 10^{-9} (\pm 0.25)$	97.3 (± 7.6)	$9.85 \times 10^{-9} (\pm 0.51)$	98.5 (± 0.6)
1.00×10^{-6}	$9.91 \times 10^{-7} (\pm 0.20)$	99.1 (± 6.6)	$9.94 \times 10^{-7} (\pm 0.15)$	99.4 (± 1.6)
1.00×10^{-4}	$9.86 \times 10^{-5} (\pm 0.14)$	98.6 (± 5.1)	$1.01 \times 10^{-4} (\pm 0.46)$	101.2 (± 0.9)

Fig. 5A illustrates the responses of electrodes modified by embedment method towards L-histidine in the presence of artificial matrix. The addition of L-histidine in the range of concentrations from 1.0×10^{-9} to 1.0×10^{-4} M decreased the redox peak current at 290 ± 30 mV and shifted the potential at maximum of peak in the more negative region. The linear amperometric responses towards L-histidine were observed within the concentration range from 1.0×10^{-9} to 1.0×10^{-4} M. The detection limit estimated as the $S/N = 3$ was 4.9×10^{-10} M (Fig. 5B). This indicated that the presence of artificial matrix components influenced very little the response of sensor proposed towards L-histidine.

The L-histidine calibration curve obtained in the presence of an artificial physiological matrix was used for performing a recovery test. 8.0 mL samples of matrix were spiked with a known amount of L-histidine and the generated current changes were recorded. Next,

L-histidine concentrations were determined based on the calibration curve (Fig. 5B).

The recovery data collected in Table 1 suggested that the sensor presented might be applied for L-histidine determination in the wide concentration range from 1.0×10^{-9} to 1.0×10^{-4} M with good precision (98.5–101.2%).

Taking into account the simply way of preparation, low detection limit and wide dynamic range, the sensor based on Fe(III)-porphyrin is superior to those already reported. The detection limit ($S/N = 3$) of 4.9×10^{-10} M is ca 3 range of magnitude lower than those obtained with electrochemical sensors based on carbon paste electrode incorporating Cu(II)-porphyrin complex [17] or carbon nanotubes modified with copper microparticles [16].

The proposed sensor could compete even with that base on quite expensive fluorescent probe, which displayed detection limits in a range 1.0×10^{-9} – 9.2×10^{-8} M [10,29].

3.4. Mechanism of amperometric signal generation by Fe(III)-porphyrin containing gold electrodes after stimulation with L-histidine

The proposed mechanism of the recognition between the porphyrin host and L-histidine guest molecules might be associated to the Fe(III) centre coordination ability. It is well known that iron porphyrins display a selective affinity towards imidazole group in histidine due to strong coordination ability of Fe(III) centre to nitrogen atoms [30]. In water solution, on the surface of electrode modified with investigated host, $PFe^{3+}(Cl^-)(H_2O)$ (where $P = 5-(4\text{-Palmitoyloxyphenyl})-10,15,20\text{-tris}[3,5\text{-di-tert-butyl-4-hydroxyphenyl}]porphyrinato dianion$) could be expected as the dominant species [31]. In the presence of guest studied, which has high coordination ability, the reaction proceeds by displacement of H_2O by L-histidine. The interaction of Fe(III) centre in the porphyrin with π -donor imidazole group of the L-histidine results in the increase in electron density in the macrocycle. This

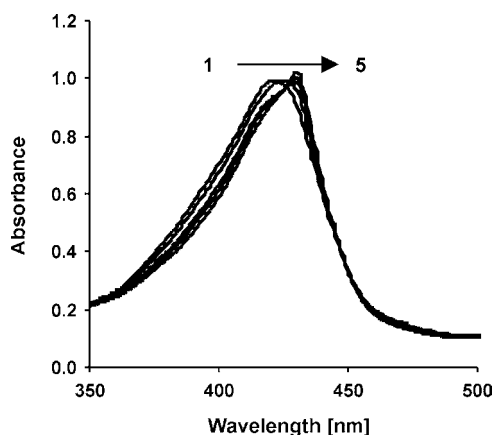


Fig. 6. The absorption spectra of 1.0×10^{-5} M Fe(III)-porphyrin in DMSO without additives (1) and in the presence of different concentrations of L-histidine: 1.0×10^{-5} M (2); 3.0×10^{-5} M (3); 4.0×10^{-5} M (4); 5.0×10^{-5} M (5).

stabilized the complex Fe(III)-porphyrin-L-histidine. Similar mechanism was observed for complex formation between L-histidine and Mn(III)-porphyrin [29,32].

The formation of intermolecular complex between Fe(III)-porphyrin and L-histidine was proved by UV-vis spectroscopy. Fig. 6 shows the absorption spectra of Fe(III)-porphyrin in the presence of various concentrations of L-histidine. It was observed that the Soret band at 421 nm of porphyrin was shifted to 431 nm with increased intensity by the addition of L-histidine. The Soret band was influenced by the oxidation state of metal centre. The red shifted Soret band of Fe(III)-porphyrin observed upon the addition of L-histidine to the solution confirmed that the imidazole group of L-histidine was bounded to the Fe(III) centre. The analogous interaction was observed by the UV-vis spectroscopy and resonance light scattering technique for Mn(III)-tetraphenylporphyrin interaction with histidine [29].

Presented results conformed that between both methods of immobilization of Fe(III)-porphyrin on the surface of gold, the embedment was more suitable. This technique provided a better flexibility of porphyrin host in comparison with rigid chemisorption. The better host flexibility guarantees better accessibility of a guest. Similar phenomenon was observed for the electrodes modified with macrocyclic polyamines [27,28].

The embedment method, being more reproducible, might be recommended for the porphyrin host immobilization on the surface of gold electrodes destined for the sensitive amperometric determination of L-histidine.

4. Conclusions

Gold electrodes could be modified with Fe(III)-porphyrin by direct chemisorption, as well as by embedment.

The method of host immobilization on the surface of gold electrodes influenced their accuracy. The electrodes modified with Fe(III)-porphyrin by embedment showed better reproducibility and sensitivity towards L-histidine than the electrodes modified by direct chemisorption.

The redox centre of host, Fe(III), played two roles, binding sites for L-histidine guest, as well as marker of electrochemical signal generation. The electrochemical properties of host immobilized on the surface of gold electrodes were changed upon formation of Fe(III)-porphyrin-L-histidine supramolecular complex. This was a base of electroanalytical signal generation of the sensor proposed.

Taking into account the good sensitivity and reproducibility, relatively easy way of preparation, the gold electrodes modified with Fe(III)-porphyrin host by embedment technique might be recommended for the direct determination of L-histidine using Osteryoung square wave voltammetry.

Acknowledgements

The work was supported by NATO project CBP.NR.CLG.982211, Russian Foundation for Basic Research (grants N 08-03-00844, 06-03-32773, 07-03-12110).

Appendix A. Supplementary data

Supplementary data associated with this article can be found, in the online version, at doi:10.1016/j.talanta.2008.10.051.

References

- [1] T.E. Creighton, *Encyclopedia of Molecular Biology*, vol.2, Wiley, New York, 1999, p. 1147.
- [2] H. Liao, Z. Zhang, L. Nie, S. Yao, *J. Biochem. Biophys. Methods* 59 (2004) 75.
- [3] L.Y. Zhang, M.X. Sun, *J. Chromatogr. A* 1040 (2004) 133.
- [4] X. Li, H. Ma, L. Nie, M. Sun, S. Xiong, *Anal. Chim. Acta* 515 (2004) 255.
- [5] P. Tuma, E. Samcova, P. Balynova, *J. Chromatogr. B* 821 (2005) 53.
- [6] S. Zhao, Y.M. Liu, *Anal. Chim. Acta* 426 (2001) 65.
- [7] M.J. Heravi, Y. Shen, M. Hassanisadi, M.G. Khaledi, *Electrophoresis* 26 (2005) 1874.
- [8] L.Y. Hang, M.X. Sun, *J. Chromatogr. A* 1040 (2004) 133.
- [9] S. Lata, A. Reichel, R. Brock, R. Tampe, J. Piehler, *J. Am. Chem. Soc.* 127 (2005) 10215.
- [10] X. Li, H. Ma, S. Dong, X. Duan, S. Liang, *Talanta* 62 (2004) 367.
- [11] S.W. Hovorka, T.D. Williams, C. Schoneich, *Anal. Biochem.* 300 (2002) 206.
- [12] A. Namera, M. Yashiki, M. Nishida, T. Kojima, *J. Chromatogr. B* 776 (2002) 49.
- [13] Z.P. Yang, W.S. Hancock, T.R. Chew, L. Bonilla, *Proteomics* 5 (2005) 3353.
- [14] X.L. Zhang, C.S. Ma, L.A. Deng, *Chin. J. Anal. Chem.* 6 (1995) 783.
- [15] R.I. Stefan-van Staden, B. Lal, L. Holo, *Talanta* 71 (2007) 1434.
- [16] G.L. Luque, N.F. Ferreyra, G.A. Rivas, *Talanta* 71 (2007) 1282.
- [17] A. Abbaspour, A. Ghaffarnejad, E. Safaei, *Talanta* 64 (2004) 1036.
- [18] R.H. Yang, K.M. Wang, L.P. Long, D. Xiao, X.H. Yang, W.H. Tan, *Anal. Chem.* 74 (2002) 65.
- [19] M. Nishimura, M. Doi, K. Shimazu, K. Fujii, K. Uosaki, *J. Electroanal. Chem.* 473 (1999) 75.
- [20] H. Imahori, H. Norieda, Y. Nishimura, K. Iwao Yamazaki, N. Higuchi, T. Kato, H. Motohiro, K. Yamada, M. Tomaki, Y. Arimura, M. Sakata, *J. Phys. Chem. B* 104 (2000) 1253.
- [21] P.D. Gale, *Coord. Chem. Rev.* 240 (2003) 17.
- [22] H. Radecka, I. Grzybowska, J. Radecki, P. Jakubowski, S. Lateran, C. Orlewska, W. Maes, W. Dehaen, *Analit. Lett.* 40 (2007) 387.
- [23] E.R. Milaeva, O.A. Gerasimova, Z. Jingwei, D.B. Shpakovsky, S.A. Syrbu, A.S. Semeykin, O.I. Koifman, E.G. Kireeva, E.F. Shevtsova, S.O. Bachurin, N.S. Zefirev, *J. Inorg. Biochem.* 120 (2008) 1348.
- [24] E.R. Milaeva, D.B. Shpakovsky, Yu. Gracheva, O. Gerasimova, V.Yu. Tyurin, V.S. Petrosyan, *J. Porphyrins Phthalocyanines* 8 (2003) 701.
- [25] R.I. Stefan-van Staden, L. Holo, *Sens. Actuators, B* 120 (2007) 399.
- [26] D.L. Pilloud, X. Chen, P.L. Dutton, C.C. Moser, *J. Phys. Chem. B* 104 (2000) 2868.
- [27] J. Radecki, I. Szymańska, L. Bulgariu, M. Pietraszkiewicz, *Electrochim. Acta* 51 (2006) 2282.
- [28] H. Radecka, I. Szymańska, M. Pietraszkiewicz, O. Pietraszkiewicz, H. Aoki, Y. Umezawa, *Chem. Anal. (Warsaw)* 50 (2005) 85.
- [29] Z. Chen, J. Liu, Y. Han, L. Zhu, *Anal. Chim. Acta* 570 (2006) 109.
- [30] F.A. Walker, *J. Am. Chem. Soc.* 95 (1975) 1150.
- [31] M. Mumenteu, M. Rougee, B. Look, *Eur. J. Biochem.* 71 (1976) 63.
- [32] E.V. Antina, N.S. Lebedeva, A.I. Vugin, *Russ. J. Coord. Chem.* 27 (2001) 784.



Amperometric tape ion sensors for cadmium(II) ion analysis

Hye Jin Lee^{a,*}, Grégoire Lager^b, Carlos M. Pereira^c, Antonio F. Silva^c, Hubert H. Girault^b

^a Department of Chemistry, Kyungpook National University, 1370 Sankyuk-dong, Buk-gu, Daegu 702-701, Republic of Korea

^b Laboratoire d'Electrochimie Physique et Analytique, Station 6, Ecole Polytechnique Fédérale de Lausanne, CH-1015 Lausanne, Switzerland

^c Centro de Investigação em Química-L4, Departamento de Química, Faculdade de Ciências da Universidade do Porto, P-4169-007 Porto, Portugal

ARTICLE INFO

Article history:

Received 27 August 2008

Received in revised form 23 October 2008

Accepted 24 October 2008

Available online 11 November 2008

Keywords:

Cadmium ion

ETH 1062 ligand

Complexation

ITIES

Liquid | gel interface

Ionode

Assisted ion transfer

ABSTRACT

This paper describes a novel tape platform ion sensing methodology specific to the detection of cadmium(II) ions in aqueous solution based on assisted ion transfer reactions across a polarized water | organic gel micro-interface. The tape ion sensors were constructed to incorporate the micro-water | polyvinylchloride-2-nitrophenylethyl ether (PVC–NPOE) gel interfaces referred to as *ionodes*. The sensors have overall thicknesses less than 300 μm , allowing their packaging in a disposable tape format. The detection methodology is based on the selective assisted transfer of the cadmium ion in aqueous phase by ETH 1062 present in the PVC–NPOE gel layer and was first investigated using cyclic voltammetry. Quantitative analysis of cadmium(II) ions in aqueous solution using the tape sensors was then conducted under stop-flow conditions. Detection limits as low as 20 ppb (178 nM) for Cd(II) ions in very small volumes as low as a single 20 μl droplet without any sample preconcentration was achieved in an analysis time of approximately 20 s, which could be easily employed for the direct measurement of Cd(II) ion levels in various field applications. The tape ion sensor can also be used in a flow-cell geometry to preconcentrate Cd(II) ions from aqueous samples and further improve the detection limit.

© 2008 Elsevier B.V. All rights reserved.

1. Introduction

Amperometric ion selective electrodes (ISE) have been powerfully employed in the sensing of a wide range of ionic species [1–6]. The most common approach is to utilize solidified polymeric membranes composed of a plasticizer and an ion carrier (ionophore or ligand), which selectively complexes to a target ion [7–9]. The same design principle can be applied to construct an amperometric ion sensor to monitor ion transfer reactions at the interface between two immiscible liquids where one of the phases, typically being the organic phase, is gelified [10–17]. This approach has been successfully demonstrated by several authors during the last decade, mainly using a nitrobenzene gel as the organic phase for the direct and assisted ion transfer, in a stagnant aqueous solution or combined with flow systems [18–22]. Due to the increasing concern with environmental issues, the organic phase must have a reduced toxicity and a long-term stability as well as maintaining good electrochemical characteristics. *O*-Nitrophenyloctylether (NPOE) together with polyvinylchloride (PVC) as a gelifying agent fulfils these criteria and can be printed at a temperature above its sol–gel transition (hot casting method)

[23,24]. This water | PVC–NPOE gel interface has been implemented into an array of microholes using a standard cell arrangement for studying the selective transfer of alkali metal ions and anions from the aqueous to the organic phase via direct and assisted transfer reactions [25–27].

The ion transfer reaction across the polarized water | organic gel interface can ideally be employed for the selective and sensitive detection of heavy metal ionic species. For example, Katano and Senda [28] have shown that the low ppb detection limit can be attained by stripping voltammetry of heavy-metal ions across a water | gel interface. Electrochemical extraction of large ionic concentrations with the use of micro-machined supported liquid membranes has also been reported, particularly for lead extraction from a lead/zinc solution [29]. In this paper, we demonstrate a novel disposable tape ion sensor utilizing the assisted transfer reaction of Cd^{2+} ions by ETH 1062 across the micro-interface of water | PVC–NPOE gel. The thin strip tape ion sensor was fabricated using a combination of laser micro-machining and screen-printing techniques. A cyclic voltammetry was used to characterize the electrochemical response of Cd^{2+} ion transfer by ETH 1062 at the interfaces. As a first demonstration, the quantitative analysis of cadmium(II) ions using the tape sensors was conducted under stop-flow condition with a small aqueous sample volume (about 20 μl) as well as under continuous flow conditions for achieving a higher preconcentration effect.

* Corresponding author. Tel.: +82 53 950 5336; fax: +82 53 950 6330.
E-mail address: hyejinlee@knu.ac.kr (H.J. Lee).

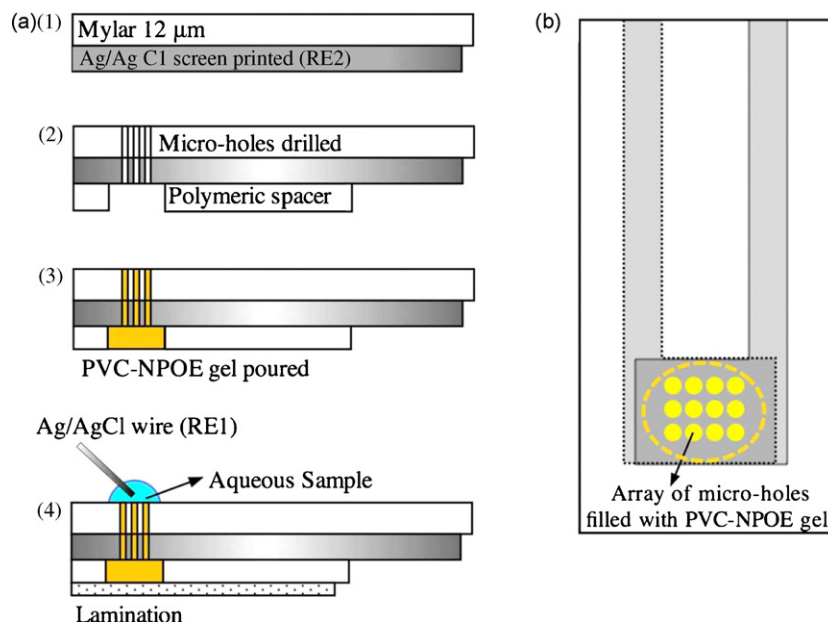


Fig. 1. (a) Schematic showing a four-step fabrication method for creating disposable tape sensors based on metal ion transfer reactions at the water | PVC–NPOE gel micro-interface. The overall thickness of the strip is about 300 μm . (b) A top view of the interface featuring the array of micro-holes containing the PVC–NPOE gel.

2. Experimental

2.1. Chemicals

ETH 1062 (Fluka), polyvinylchloride (PVC, high molecular weight, Sigma), *o*-nitrophenyloctylether (NPOE, Fluka), CdCl_2 (Fluka >96%) and LiCl (Fluka >99%) were all used as received. The supporting electrolytes for the organic phase was bis(triphenylphosphoranylidene) ammonium tetrakis(4-chlorophenyl)borate (BTTPATPBCl) or tetrabutylammonium tetrakis(4-chlorophenyl)borate (TBATPBCl) prepared as described in a previous paper [23,30]. Most of the cases, 10 mM BTTPATPBCl were used unless otherwise specified. Millipore-filtered water was used for preparing all aqueous solutions.

2.2. Fabrication of thin tape sensor

To fabricate the tape sensors, a supporting film of polyethylene terephthalate (12 μm thick, Melinex type “S”, ICI Films) supplied on a reel was first cut into strips (30 cm long). After cleaning with ethanol, a silver/silver chloride ink (RE 2) was screen-printed as illustrated in Fig. 1a and cured at 80 $^\circ\text{C}$ for 24 h. In a second step, an array of 66 microholes (11 \times 6) was drilled through the film using a UV Excimer laser (ArF, 193 nm, Spectra-Physics). The process of laser micro-machining of the polyester film was performed as described previously [24], but the differences here were the number of laser pulses used to drill through the metallised film and the silver layer being placed at the bottom. The entrance diameter of the microholes is 20 μm and the exit 13 μm due to the optics used to focus the laser beam so as to drill through the metallic ink layer. After drilling, an adhesive tape that had been punched with a circular aperture was placed on the silver/silver chloride layer. This microfabricated structure acts as a supporting film to deposit the gelified NPOE phase containing PVC. The gel layer was prepared by dissolving PVC (2.8% m/m) in a solution of 10 mM BTTPATPBCl or TBATPBCl and ETH 1062 in NPOE, at a temperature of approximately 120 $^\circ\text{C}$. Five microliters of the hot PVC–NPOE liquid at around 80 $^\circ\text{C}$ was manually casted on the arrays via the aperture in the adhesive film. Finally, the casted PVC–NPOE solution was allowed to

cool for a minimum of 6 h to form the gel followed by laminating the underside of the tape with a polyethylene (PE)–polyethylene terephthalate (PET) film (35 μm thick). In the present work, the screen-printing of Ag/AgCl ink was carried out after cutting the tape into sections adapted to the size of the screen used (30 cm \times 30 cm). The strip sensor was employed in two different ways for the amperometric measurements of small volumes of Cd^{2+} ions; (i) simply placing a drop of aqueous solution containing Cd^{2+} ions onto the sensing part, with the aqueous reference electrode dipped in the drop (see Fig. 1a), and (ii) placing the sensor in the flow cell prototype (see also Fig. 5). All the processes used here *i.e.* screen printing of Ag/AgCl ink, laser ablation, adhesion of a spacer film and lamination could be mounted in a continuous reel-to-reel assembly line for high-throughput industrial production of the tape.

2.3. Electrochemical measurements

The electrochemical experiments were performed using a computer controlled potentiostat (Sycopel Scientific Ltd.) with the data acquired without IR drop compensation. Half-wave potential measurements for ion transfer reactions are referred to Ag/AgCl ($c_{\text{Cl}^-} = 0.01 \text{ M}$) unless otherwise stated. The interfacial ion transfer and ion-ligand complexation processes across the water | PVC–NPOE fabricated in a tape platform sensor were studied by cyclic voltammetry using Cell I.

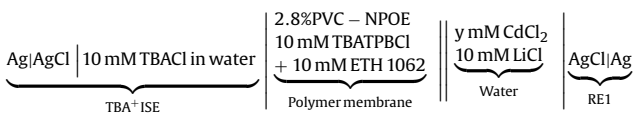
Cell I:



Ion transfer reactions across micro-interfaces which involve small currents (in all cases here, lower than 100 nA), only two reference electrodes are necessary, each one acting as both the reference and counter for the aqueous and organic phase. The aqueous phase reference electrode was made of silver/silver chloride in equilibrium with a chloride aqueous solution (RE 1). For the organic phase reference system, a pseudo-reference electrode (screen printed Ag/AgCl, RE 2) was utilized where the Ag/AgCl was

directly in contact with PVC–NPOE gel in the absence of organic supporting electrolyte. This was essential to conveniently assemble it to the tape sensing platform. On the other hand, for the case of Fig. 3 where we used a conventional micro-water/PVC–NPOE gel configuration, the cyclic voltammogram for the Cd(II) ion transfer was obtained using the TBA⁺ISE organic reference system and Cell II. TBA⁺Ion selective electrodes (TBA⁺ISE) were composed of a Ag/AgCl reference electrode in contact with the organic supporting electrolyte solution (e.g. 10 mM TBACl).

Cell II:



The electrochemical set-up used here was similar to that for the study of alkali metal ion transfer reactions across micro-water | PVC–NPOE gel interface as described previously [23]. Briefly, two reference electrodes for both the aqueous and organic phases were made of silver/silver chloride in equilibrium with a chloride aqueous solution; for the organic phase, a TBA⁺ISE reference system was used. The water | organic gel interface was formed by water phase containing CdCl₂ in contact with micro-fabricated membranes featuring 66 microholes in a 12 μm thick PET film filled up with PVC–NPOE gel as described above.

3. Results and discussion

Measurements of Cd²⁺ ion concentrations are very important since overexposure is extremely dangerous to public health and our ecology. Consequently, all countries in the world have established regulations on permissible concentrations of Cd²⁺ ions. For example, guidelines supplied world health organization [31], suggest an upper cadmium ion concentration of 3 ppb (26.7 nM) in drinking water. Also, the US Environmental Protection Agency set the permissible Cd ion concentrations in water as 10 ppb (89 nM) [32]. More details on allowed levels of cadmium in various environments can also be found from [33]. A disposable sensor that is easy to use, reliable, free of toxic elements as well as inexpensive to fabricate can be powerfully used for trace cadmium metal ion analysis. We have designed a disposable thin strip type ion sensor featuring micro-water | gel interfaces (see Fig. 1a) that utilizes very small sample volumes below 20 μl. Additional advantages of this sensor include: (i) the sensor packaging can be promptly achieved using a simple printing procedure, and (ii) the sensor strips can be placed on a dispenser such as a tape and consequently used under a flow system.

The electrochemical response of the thin strip sensor associated with the interfacial transfer of cadmium(II) ions facilitated by the ligand, ETH 1062, present in the PVC–NPOE gel layer was first characterized. A series of cyclic voltammograms obtained using Cell I for various cadmium ion concentrations are displayed in Fig. 2a. A small aqueous solution with a volume of about 20 μl containing various concentrations of cadmium(II) ions ranging from 1 to 100 μM and 10 mM of ETH 1062 were used. The transfer of Cd²⁺ ions can be clearly seen within the potential window limited by the transfer of Cl[−] ion at the negative end potential and the transfer of Li⁺ ion at the positive end potential. The steady-state current observed on the forward scan linearly increased as the cadmium concentration increased when the ligand concentration (10 mM) is in excess (see Fig. 2b). This indicates that the sensing method involving excess ligand concentrations compared to the metal analytes can be usefully employed for the quantitative analysis of Cd²⁺ ions in aqueous samples. However, above 40 μM concentrations of Cd²⁺ ions, the steady state current no longer increases and the top

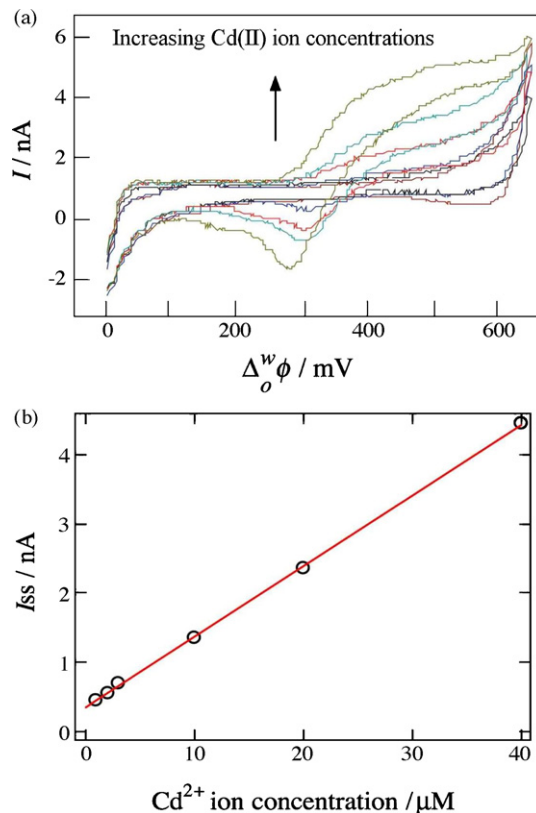


Fig. 2. (a) A series of cyclic voltammograms obtained for the assisted transfer of various concentrations of Cd²⁺ ions by 10 mM ETH 1062 in the PVC–NPOE gel across the water | gel interface using the strip sensor. The aqueous phase contains 10 mM LiCl and the PVC–NPOE gel phase contains 10 mM BTBAPBCl as a supporting electrolyte respectively. Cell I was used and Cd²⁺ ion concentrations were 1, 2, 5, 20, 40 and 100 μM. Scan rate was 10 mV s^{−1}. (b) Plot of steady-state currents for the assisted transfer of Cd²⁺ by ETH 1062 (10 mM) as a function of Cd²⁺ ion concentrations (calibration curve in the excess ligand case). Some of the data are taken from (a).

curve in Fig. 2a shows two transferring waves for a 100 μM concentration of Cd²⁺ ions on the forward scan. In this region where no clear excess is present from any of the species due to the slow diffusion of the ligand in the gel, a second peak at a more positive potential occurs which can be assigned as the formation of the 1:1 complex [Cd–ETH 1062]²⁺. On the reverse scan, a peak shape of signal was observed mainly due to the fact that the [Cd–ETH 1062] complex formed during the forward scan is diffusing along the hole, up to the interface where the ion is released. When using the hole length is 12 μm (thickness of the PET film), a major part of the complex previously formed is diffusing towards the bulk of the gel even when the potential across the interface allows the transfer back of the metal ion in the aqueous phase [34]. This has the main effect of limiting the possibility of ionic preconcentration in the gel. In an analytical point of view, a compromise must be found between small micro-holes with smaller IR drop and larger ones with higher preconcentration effect but also increased IR drop [24]. It should be noted that the data presented in Fig. 2 appears to be slightly noisy mainly due to the fact that the measured current associated with both the low concentration of Cd²⁺ ions and the small interface is as low as below ~1 nA. In addition, some instability issues may arise from the use of the pseudo-organic reference electrode where the Ag/AgCl layer is directly in contact with the PVC–NPOE gel. Nevertheless, the pseudo-electrode behaves similarly to the organic Ag/AgCl reference electrode which is referenced with the organic supporting electrolyte such as TBACl solution (TBA⁺ISE) (see also Fig. 3). The successful application with the pseudo-electrode also

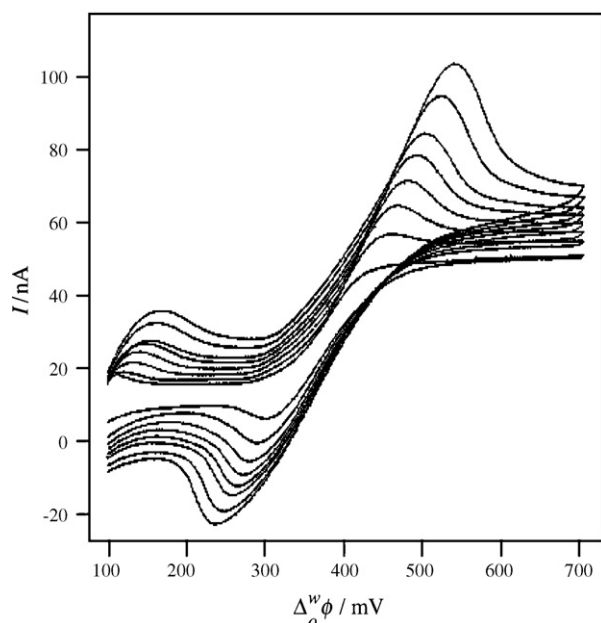


Fig. 3. Cyclic voltammograms obtained for the assisted transfer reaction of Cd^{2+} ions by the ligand ETH 1062 at various scan rates using Cell II. The concentrations used for Cd^{2+} ions and ETH 1062 were 120 mM and 10 mM, respectively. Scan rates were 5, 10, 15, 20, 25, 30, 40 and 50 mV s^{-1} . 10 mM TBATPBCl was used as an organic supporting electrolyte. The IR drop is estimated here to be 200 mV.

makes the tape sensor more convenient to fabricate and easy to utilize in field applications.

Further studies elucidating the peak shape of the ion transfer reaction were performed when the Cd^{2+} ion concentration is in excess compared to the ligand ETH 1062 concentration. Fig. 3 shows a series of cyclic voltammograms obtained at different scan rates using the organic reference electrode with Ag/AgCl in contact with the organic supporting electrolyte such as TBACl solution and 10 mM TBATPBCl in the PVC–NPOE gel. For short periods of time (higher scan rates above 50 mV s^{-1}), a strong peak shape voltammogram on the forward scan was observed because the ligand depletion region stays within the hole owing to much lower diffusion coefficients of the ligand in the gel compared to that of the metal ions in the aqueous phase. When the scan rate is of the order of 50 mV s^{-1} or lower, the two successive regimes of ligand diffusion are visible in the peak shapes (peak, then steady-state). At very low scan rates (below 10 mV s^{-1}), the linear diffusion behavior is becoming insignificant and the diffusion is mainly spherical over the forward scan period. At the potential of the transition point between linear and spherical diffusions, it is possible to estimate the diffusion coefficient of the ligand in the gel, knowing the micro-hole length ($12 \mu\text{m}$ long in this experiment), which is calculated to be $3 \times 10^{-11} \text{ m}^2 \text{ s}^{-1}$. This diffusion coefficient is in relatively good agreement with the values estimated for similar systems in a previous paper [23].

Following the well-defined electrochemical behaviour of Cd^{2+} ion transfer process at the interface of thin strip sensor platforms, we have further employed the strip sensor for the quantitative analysis of Cd^{2+} ion concentration in aqueous sample. Differential pulse stripping voltammetry was applied for Cd^{2+} concentrations ranging from 0 to 391 nM (44 ppb) when the ligand ETH 1062 (10 mM) is in excess. Fig. 4 demonstrates a series of differential pulse stripping voltammograms acquired for aqueous drops ($20 \mu\text{l}$) in the absence of Cd^{2+} ions, and also Cd^{2+} ions at concentrations of 196 nM and 391 nM. These were obtained without any preconcentration (plating) of Cd^{2+} ions. For comparison, the very top voltammogram in Fig. 4 was obtained at a Cd^{2+} ion concentration of 391 nM after a

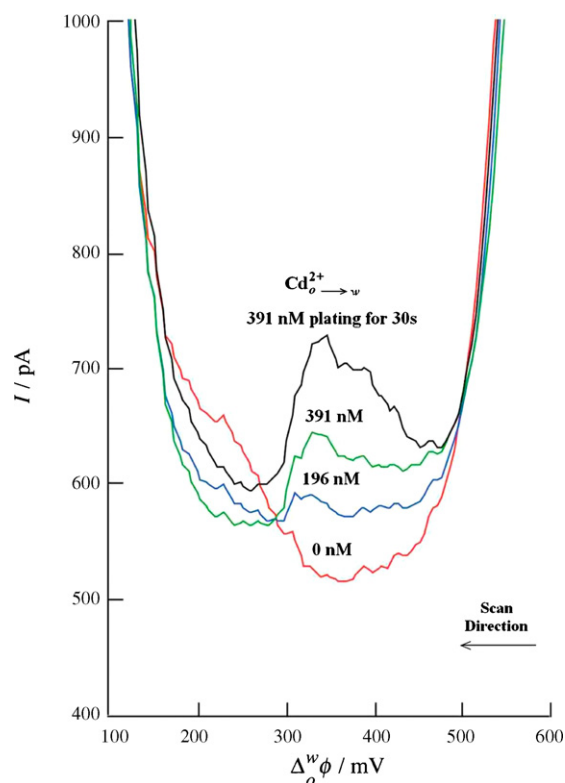


Fig. 4. Differential pulse stripping voltammograms of Cd^{2+} ion transfer from the gel, after the assisted transfer by ETH 1062 (10 mM). The pulse conditions were potential increment of 2 mV, pulse potential of 10 mV and pulse duration of 50 ms (scan rate is 20 mV s^{-1}). The scan was directed from high to low potentials to drive Cd^{2+} ion transfer from the organic to aqueous phase. From bottom to top: curve obtained without any cadmium ions, with 196 nM of Cd^{2+} ions in water, followed by 391 nM without any preconcentration (plating) of Cd^{2+} ions. The top voltammogram was obtained after a preconcentration step for 391 nM Cd^{2+} ions in water by applying the potential at 600 mV for 30 s prior to analysis.

preconcentration step by applying a potential of 600 mV for 30 s prior to analysis. It can be clearly seen that the preconcentration process enhances the detection signal by approximately a factor of two compared to that obtained without any preconcentration step. All these signals represent the extraction of the Cd^{2+} ions from the organic gel (where they are complexed by the ligand), back to the aqueous phase. The detection limit was found to be about 178 nM (20 ppb) of Cd^{2+} ions in a $20 \mu\text{l}$ volume assay (about 4 pmol), allowing the direct application of the sensor to determine Cd^{2+} ion levels in various environmental samples. The sensitivity of the ion tape sensor is better than commercially available ion-selective electrodes (e.g. 890 nM (100 ppb) of Cd^{2+} ions) [35] and comparable to conventional atomic absorption spectrometry (AAS) and inductively coupled plasma (ICP) atomic emission spectrometry [36]. Nevertheless, the ion sensor has a distinct advantage in requiring smaller sample volumes with additional possibilities for multiplexed and selective sensing as well as portability. Typically, AAS or ICP requires a minimum sample loading volume of over $50 \mu\text{l}$. In principle, even smaller volumes of sample drops (below $5 \mu\text{l}$) could be applied in the tape sensor, which would still cover the entire micro-hole interface; however, the rate of evaporation of the aqueous sample must be taken into account at such low volumes.

The tape ion sensor was finally integrated into a flow system (Metrohm flow cell prototype) to achieve a higher preconcentration of Cd^{2+} ions in the gel layer under a continuous solution flow (see Fig. 5). A representative differential pulse voltammogram of $1 \mu\text{M}$ Cd^{2+} ion detection is displayed in a right inset of the figure. The assisted transfer of Cd^{2+} ions by the ligand ETH 1062 across the

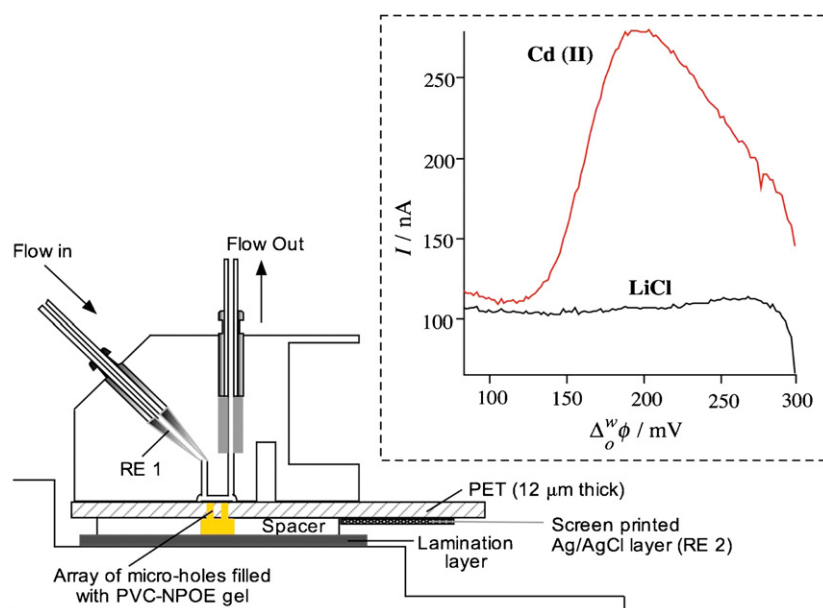


Fig. 5. Schematic of the disposable strip sensor featuring the microinterface of water|PVC-NPOE gel integrated into the Metrohm flow cell prototype. The aqueous phase reference electrode (RE 1) is a silver/silver chloride wire in a saturated KCl solution and is part of the cell construction. No auxiliary electrode is used as the current is always kept small (below 300 nA). The right inset of the figure shows a differential pulse voltammetry of 1 μM CdCl₂ using the flow cell. The pulse conditions were potential increment of 2 mV, pulse potential of 10 mV and pulse duration of 50 ms (scan rate is 20 mV s⁻¹). 10 mM ETH 1062 and flow rate of 1 ml/min were used.

aqueous/gel interface was clearly observed. Note that a large electrochemical signal for Cd²⁺ ion sensing was also observed due to the preconcentration of Cd²⁺ ions in the gel. A practical detection limit based on signal to noise ratio of 3:1 is set here at approximately 100 nM when using the flow cell geometry, which could be even further improved by a better handling of fluid flow. In the present configuration of the pumping system a large electrical noise is generated, which results in reducing the signal to noise ratio.

4. Conclusions

A novel disposable tape sensor for the sensitive detection of cadmium ions has been demonstrated. The detection method is based on the assisted transfer reaction of Cd²⁺ ion by the ligand, ETH 1062 across a water|PVC-NPOE gel microinterface. This sensor can be utilized not only in a stagnant mode but also under analyte flow systems with a simple pseudo-reference electrode system. The total thickness of the sensor typically 300 μm allows its packaging in a dispensing tape shape, which could be incorporated into a continuous reel-to-reel assembly line for industrial production of the tape. Detection limits as low as 20 ppb (178 nM) for Cd²⁺ ions in a stagnant aqueous solution volume of about 20 μl for the tape sensor have been achieved within 20 s of analysis time without preconcentration processes. Further improvements in the integration of the continuous flow aspect of the sensors to preconcentrate Cd²⁺ ions from aqueous samples as well as applications to the real sample analysis are currently underway.

Acknowledgement

This work was supported by the Korea Research Foundation Grant funded by the Korean Government (KRF-2008-331-C00190).

References

[1] B.K. Jena, C.R. Raj, *Talanta* 76 (2008) 161.

- [2] N.H. Chou, J.C. Chou, T.P. Sun, S.K. Hsiung, *Sens. Actuators B* 130 (2008) 359.
- [3] E. Pretsch, *Trends. Anal. Chem.* 26 (2007) 46.
- [4] L. Nagy, M. Kálmán, G. Nagy, *J. Biochem. Biophys. Methods* 69 (2006) 133.
- [5] F. Faridbod, M.R. Ganjali, R. Dinarvand, P. Norouzi, *Sensors* 8 (2008) 2331.
- [6] R. Long, E. Bakker, *Electroanalysis* 15 (2003) 1261.
- [7] E. Bakker, Y. Qin, *Anal. Chem.* 78 (2006) 3955.
- [8] E. Bakker, P. Bühlmann, E. Pretsch, *Talanta* 63 (2004) 3.
- [9] E. Bakker, E. Pretsch, *Anal. Chem.* 74 (2002) 420A.
- [10] J.A. Ortuno, A. Gil, C. Sanchez-Pedreno, *Sens. Actuators B* 122 (2007) 369.
- [11] J.A. Ortuno, I.C. Sanchez-Pedreno, A. Gil, *Anal. Chim. Acta* 554 (2005) 172.
- [12] Z. Samec, E. Samcová, H.H. Girault, *Talanta* 63 (2004) 21.
- [13] T. Osakai, H. Katano, *Bunseki Kagaku* 54 (2005) 251.
- [14] L. Lasse Murtomaki, M.H. Barker, J.A. Manzanares, K. Kontturi, *J. Electroanal. Chem.* 560 (2003) 95.
- [15] Y. Tong, P. Sun, Z. Zhang, Y. Shao, *J. Electroanal. Chem.* 504 (2001) 52.
- [16] H. Katano, M. Senda, *Anal. Sci.* 17 (2001) i337.
- [17] V. Marecek, H. Janchenova, M. Brezina, M. Betti, *Anal. Chim. Acta* 244 (1991) 15.
- [18] H. Katano, M. Senda, *J. Electroanal. Chem.* 496 (2001) 103.
- [19] S. Wilke, H. Franzke, H. Mueller, *Anal. Chim. Acta* 268 (1992) 285.
- [20] T. Osakai, T. Nuno, Y. Yamamoto, A. Saito, M. Senda, *Bunseki Kagaku* 38 (1989) 479.
- [21] E. Wang, H. Ji, *Electroanalysis* 1 (1989) 75.
- [22] V. Marecek, M.P. Colombini, *J. Electroanal. Chem.* 241 (1988) 133.
- [23] H.J. Lee, C. Beriet, H.H. Girault, *J. Electroanal. Chem.* 453 (1998) 211.
- [24] H.J. Lee, P.D. Beattie, B.J. Seddon, M.D. Osborne, H.H. Girault, *J. Electroanal. Chem.* 440 (1997) 73.
- [25] F. Bianchi, H.J. Lee, H.H. Girault, *J. Electroanal. Chem.* 523 (2002) 40.
- [26] H.J. Lee, C.M. Peirera, A.F. Silva, H.H. Girault, *Anal. Chem.* 72 (2000) 5562.
- [27] H.J. Lee, H.H. Girault, *Anal. Chem.* 70 (1998) 4280.
- [28] H. Katano, M. Senda, *Anal. Sci.* 14 (1998) 63.
- [29] S. Wilke, H.M. Wang, M. Muraczewska, H. Muler, *Fresenius J. Anal. Chem.* 356 (1996) 233.
- [30] Z. Ding, D.J. Fermin, P.F. Brevet, H.H. Girault, *J. Electroanal. Chem.* 458 (1998) 139.
- [31] World Health Organization (WHO/SDE/WSH/03.04/80) Guidelines, World Health Organization, Geneva, 2003.
- [32] <http://www.inchem.org/documents/pims/chemical/cadmium.html>.
- [33] http://www.cadmium.org/env_lev.html.
- [34] J. Jossierand, J. Morandini, H.J. Lee, R. Ferrigno, H.H. Girault, *J. Electroanal. Chem.* 468 (1999) 42.
- [35] http://www.astisensor.com/lab_organic.html.
- [36] <http://www.thermo.com/eThermo/CMA/PDFs/Articles/articlesFile.18407.pdf>.



Specific mercury(II) adsorption by thymine-based sorbent

Xiangjun Liu, Cui Qi, Tao Bing, Xiaohong Cheng, Dihua Shangguan*

Beijing National Laboratory for Molecular Sciences, Institute of Chemistry, Chinese Academy of Sciences, Beijing 100190, China

ARTICLE INFO

Article history:

Received 18 August 2008
Received in revised form 31 October 2008
Accepted 5 November 2008
Available online 13 November 2008

Keywords:

Selective adsorption
Thymine
Polymer sorbent
Mercury(II)

ABSTRACT

A new kind of polymer sorbent based on the specific interaction of Hg(II) with nucleic acid base, thymine, is described for the selective adsorption of Hg(II) from aqueous solution. Two types of sorbents immobilized with thymine were prepared by one-step swelling and polymerization and graft polymerization, respectively. The maximum static adsorption capacity of the new polymer sorbents for Hg(II) is proportional to the density of thymine on their surface, up to 200 mg/g. Moreover, the new kind polymer sorbent shows excellent selectivity for Hg(II) over other interfering ions, such as Cu(II), Cd(II), Zn(II), Co(II), Ca(II) and Mg(II), exhibits very fast kinetics for Hg(II) adsorption from aqueous solution, and can be easily regenerated by 1.0 M HCl. It also has been successfully used for the selective adsorption of spiked Hg(II) from real tap water samples. This new thymine polymer sorbent holds a great promise in laboratory and industrial applications such as separation, on-line enrichment, solid-phase extraction, and removal of Hg(II) from pharmaceutical, food and environmental samples.

© 2008 Elsevier B.V. All rights reserved.

1. Introduction

Heavy metal ion pollution has become widespread throughout the world as a result of industrialization, which significantly threatens the ecosystem, especially the people's health due to their severe toxicity. Mercury, as one of the most toxic heavy metal, can cause human disease, such as kidney toxicity, neurological damage and chromosome breakage, even at low concentration [1]. Mercury and mercury compounds are included in all lists of priority pollutants. Different regulations and guidelines have been developed for limiting their levels in water and sediments [2,3]. Burning coal, inorganic mercury used in chloro-alkali cells, electrical apparatus and chemical engineering process are the main sources of mercury pollutants introduced into the environment. Hg(II) is one of the main species of mercury pollutants in the environment, thus monitoring or removal of Hg(II) is quite necessary. However, in real samples, there are many coexisting interferences which seriously influence the detection or the removal efficiency of Hg(II), so the specific adsorption material for separation, preconcentration and removal of Hg(II) from the complex matrix is essential.

Many methods have been reported for the adsorption of Hg(II) from aqueous media, such as solvent extraction [4], solid-phase extraction by polymer sorbents [5,6], activated carbon [7], chitosan [8], clay [9] and other materials [10,11]. Particularly polymer sorbents have recently attracted more attention because of their larger adsorption capacity, higher efficiency and easier prepara-

tion. However, these sorbents commonly lack selectivity for Hg(II). Some attempts have been made to solve this problem, for example, thiol [12,13] or amide [14,15] modified sorbents have improved the selectivity, but it is still not enough since the interaction of these functional groups with Hg(II) is not specific. Recently, molecularly imprinted polymers (MIPs) for Hg(II) have been developed [16–18]. Although the MIPs sorbent showed better selectivity for Hg(II), the preparation process of the MIPs is complex and the adsorption capacity for Hg(II) is low. Moreover, using Hg(II) as template during the preparation of MIPs introduces a potential new source of mercury contamination.

In recent years, Hg(II) has been reported to selectively bind to thymine/thymine (T/T) mismatched base pairs in DNA sequences, by forming T–Hg(II)–T complexes (Fig. 1a) [19–21]. NMR studies have demonstrated that Hg(II) binds directly to N-3 of two thymidine residues in place of two imino protons and forms N–Hg(II)–N bond (Fig. 1a) [21,22]. Several Hg(II) probes or sensors based on the specific interaction of T and Hg(II) have also been developed and showed great selectivity and sensitivity [23–25]. To date, all these studies focused on the single nucleotide polymorphisms analysis and Hg(II) detection, no attempts have been carried out to adsorb Hg(II) using this specific interaction. In this study, we extend the application of this specific interaction to selective adsorption of Hg(II) from aqueous solution samples. Thymine-modified polymer sorbents were prepared by copolymerizing of allyl thymine (AT, Fig. 1b) with ethylene dimethacrylate (EDMA) or by grafting of AT onto the surface of a support. The characteristic of these sorbents was evaluated by SEM micrographs, infrared (IR) spectra and X-ray photoelectron spectrometer (XPS). The adsorption capability, adsorption kinetics, selectivity, and reusability of the new kind

* Corresponding author. Tel.: +86 10 62528509; fax: +86 10 62528509.
E-mail address: sgdh@iccas.ac.cn (D. Shangguan).

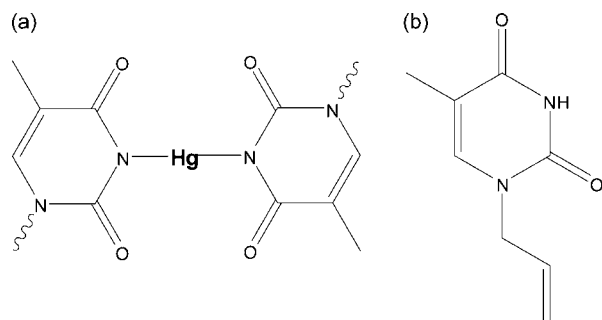


Fig. 1. Chemical structure of (a) proposed structure of T-Hg(II)-T and (b) allyl thymine (AT).

thymine polymer sorbent were investigated. Finally, the thymine polymer sorbent was successfully applied for the selective adsorption of Hg(II) which spiked in real water samples.

2. Experimental

2.1. Materials

Thymine (T) was purchased from Sigma (USA). Allyl bromide was purchased from Beijing Xingjin Chemical Plant (Beijing, China). Sodium hydride (NaH) was purchased from Tianjin Fuchen Chemical Reagent Plant (Tianjin, China). Chloromethylstyrene (CMSt) and EDMA were purchased from Acros Organics (USA). Glycidyl methacrylate (GMA) and *N,N,N',N',N''*-pentamethyldiethylenetriamine (PMDETA) were purchased from Aldrich (USA). 2,2-Azobis(2-isobutyronitrile) (AIBN), benzoyl peroxide (BPO), poly(vinyl pyrrolidone) (PVP), poly(vinyl alcohol) (PVA) and sodium dodecylsulphonate (SDS) were purchased from Beijing Chemical Plant (Beijing, China). Dithizone and cuprous bromide (CuBr) were purchased from Beijing Chemical Reagent Company (Beijing, China). All other reagents (AR) used were purchased from Beijing Chemical Plant (Beijing, China). Doubly deionised water was used throughout this work. AIBN, BPO, CuBr and dithizone were re-purification prior to use.

2.2. Instrumentation

^1H NMR spectra were recorded on Bruker AV400 instrument. UV-vis absorption spectra were recorded on Shimadzu UV-1601PC spectrophotometer. FT-IR spectra in KBr were recorded on Bruker Tensor 27 instrument. SEM micrographs of the sorbent were obtained on a JEOL JSM-6700F field emission scanning electron microscopy. The concentration of mercury and other ions in a mixed solution were measured using an Inductive Coupled Plasma Optical Emission Spectrometer (ICP-OES) (PE-Optima 2000DV). The nitrogen content on the surface of the sorbents was determined by ESCALab220i-XL X-ray photoelectron spectrometer (XPS).

2.3. Synthesis of allyl thymine (AT)

The synthesis of AT was performed as describing previously [26]. To a suspension of 2 g of thymine in 80 mL of dry DMF was slowly added 0.72 g of NaH. The suspension was stirred at room temperature for 1 h until no more gas evolved. Then 1.8 mL of allyl bromide was added dropwise. After 24 h, the excess NaH was quenched with saturated NH_4Cl aqueous solution. The mixture was concentrated under a vacuum and subjected to column chromatography (eluent: 40% ethyl acetate/petroleum ether) to yield some white solid. ^1H NMR (CDCl_3): δ 8.61 (s, 1H, pyrimidine NH), 6.96 (d, 1H, pyrimidine H-6), 5.81–5.92 (m, 1H, $-\text{CH}=\text{}$), 5.24–5.33 (m, 2H, $=\text{CH}_2$), 4.33 (d, 2H, $-\text{CH}_2-$), 1.92 (d, 3H, pyrimidine- CH_3).

2.4. Preparation of thymine polymer sorbent

2.4.1. Preparation of polyglycidyl methacrylate (PGMA) and polychloromethylstyrene (PCMSt)

PGMA and PCMSt were prepared using dispersion polymerization [27]. Five milliliters of GMA or CMSt, 0.15 g of AIBN and 0.5 g of PVP were dissolved in 50 mL of ethanol and purged with N_2 for 10 min. And then the reaction was carried out at 70°C for 24 h. The resultant beads were washed with ethanol and dried under vacuum at room temperature.

2.4.2. Preparation of copolymerized thymine polymer sorbent

The copolymerized thymine polymer sorbent (P1, P2 and P3) was prepared using a one-step swelling and polymerization method [27]. The typical process is as follows: A suspension of 0.1 g PGMA seeds in 10 mL of homogeneous solution containing PVA, SDS and distilled water was stirred at room temperature. Then an emulsion made of PVA, SDS, distilled water, 40 mg of BPO, 2 mL of chloroform and 1 mL of acetonitrile and monomer mixture (10 mmol) of AT and EDMA (molar amount of AT/EDMA: P1, 0/10; P2, 1/9 and P3, 5/5) was added dropwise to the suspension of PGMA seeds. After the monomer mixture was absorbed by the PGMA seeds completely, the polymerization was carried out at 60°C for 24 h. The polymer beads were washed with water and ethanol, and dried under vacuum at room temperature.

2.4.3. Preparation of grafted thymine polymer sorbent

The grafted thymine polymer sorbent (P4) was prepared using the atom transfer radical polymerization (ATRP) method [28]. 0.5 g PCMSt was suspended in a solution of 5 mL of distilled water and methanol (1:1, v/v) containing 0.5 g of AT, and then 32 mg of CuBr and 140 μL of PMDETA were added. The polymerization was carried out at room temperature for 24 h. The resultant beads (P4) were washed with water and ethanol, and dried under vacuum at room temperature.

2.5. Equilibration adsorption studies

Adsorption of Hg(II) from aqueous solutions was investigated in batch experiments. Fifty milligrams of sorbent was equilibrated with 30 mL of different solutions at room temperature. Then, an aliquot of the supernatant was separated, and the quantity of the ion was determined by the dithizone spectrophotometric method (GB 7469-87, China). The adsorption capacity of the sorbent and the removal efficiency of the ion could be calculated using the following equations:

$$Q = \frac{(C_0 - C_e)V}{W} \quad (1)$$

$$E (\%) = \frac{C_0 - C_e}{C_0} \times 100 \quad (2)$$

where Q represents the adsorption capacity (mg/g), C_0 and C_e are the initial and equilibrium concentration (mg/L), and E is the removal efficiency (%).

2.6. Recycling test

0.1 g of thymine polymer sorbent was equilibrated with 30 mL of 2.0 mg/L Hg(II) solution (pH 8.0, 20 mM $\text{Na}_2\text{HPO}_3/\text{H}_3\text{PO}_4$). After 2 h, the sorbent was regenerated for the next cycle by washing with 20 mL of 1.0 M HCl solution once, 10 mL of water twice and 20 mL of pH 8.0 $\text{Na}_2\text{HPO}_3/\text{H}_3\text{PO}_4$ buffer once. The equilibrium concentration was determined using the dithizone spectrophotometric method (GB 7469-87, China) and the removal efficiency was calculated according to Eq. (2).

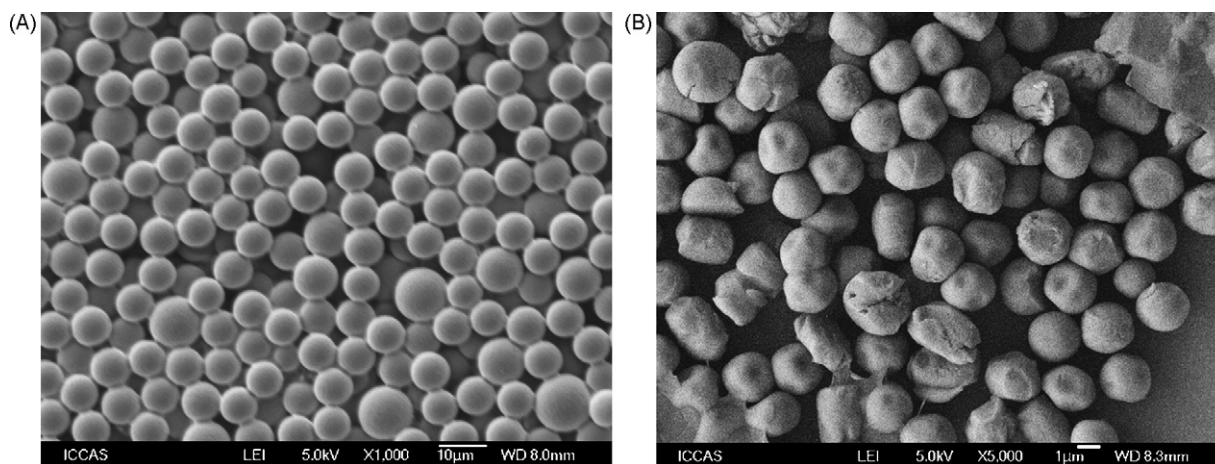


Fig. 2. SEM image of (A) copolymerized thymine polymer sorbent P3 and (B) grafted thymine polymer sorbent P4.

2.7. Selectivity studies

The selectivity of the thymine polymer sorbent was investigated by ICP-OES. Fifty milligrams of thymine polymer or blank sorbent was suspended in 30 mL of aqueous solution of containing Hg(II) and other ions. After adsorption equilibrium, the concentration of each ion in the remaining solution was measured by ICP-OES.

2.8. Adsorption test in real tap water sample

Tap water samples were taken from our research laboratory and filtered through a cellulose membrane filter (pore size 0.22 μm) prior to use. Different concentration of Hg(II) were spiked to tap water samples, and then disposed with the sorbents. After adsorption equilibrium, the concentration of Hg(II), Ca(II) and Mg(II) in the solution was measured by ICP-OES.

3. Results and discussion

3.1. Preparation and characterization of thymine polymer sorbent

Thymine has been previously reported to form T–Hg–T complexes (Fig. 1a) with Hg(II) between DNA sequences [19–22], polymer chains [24] and fluorophore-modified thymine [23,25]. Therefore by immobilizing thymine on solid support, we expected to obtain a Hg(II) specific sorbent. In order to prove the feasibility

of this approach, we prepared two kinds of sorbents with different densities of thymine by radical polymerization using two different methods. Since the N-3 of thymine has been reported to be the specific binding site to Hg(II), the thymine was allylated at N-1 position by allyl bromide and used as the polymerization monomer (Fig. 1b). Using the first method, sorbent P1 (blank sorbent), P2 and P3 were synthesized by copolymerization of three different ratios of AT and EDMA (0/10, 1/9 and 5/5, respectively) using a one-step swelling and polymerization method, a simple and convenient technique to prepare beads several microns in diameter. The other kind of sorbent (P4) was synthesized by grafting AT onto the surface of PCMSt beads using the ATRP method. SEM micrographs of the two kinds of thymine polymer sorbents showed that the diameter of the beads was about 7 μm and 3 μm for copolymerizing and grafting beads, respectively (Fig. 2). The sorbent with the small beads will have high adsorption capacity because of its high surface area. Moreover, it may have the potential to be used for on-line enrichment of Hg(II) or as a specific ion chromatography stationary phase directly.

The IR spectra (Fig. 3) demonstrated that thymine was copolymerized (P2 and P3) or grafted (P4) on the polymer beads successfully. IR spectra of different copolymerizing thymine polymer sorbent (P1, P2 and P3) are shown in Fig. 3A. In the three spectra, the adsorption peaks of C=O bond at 1732 cm^{-1} , C–O bond at 1155 cm^{-1} and aliphatic C–H at 2958 and 2991 cm^{-1} showed the presence of polymethacrylate. Furthermore, when compared the

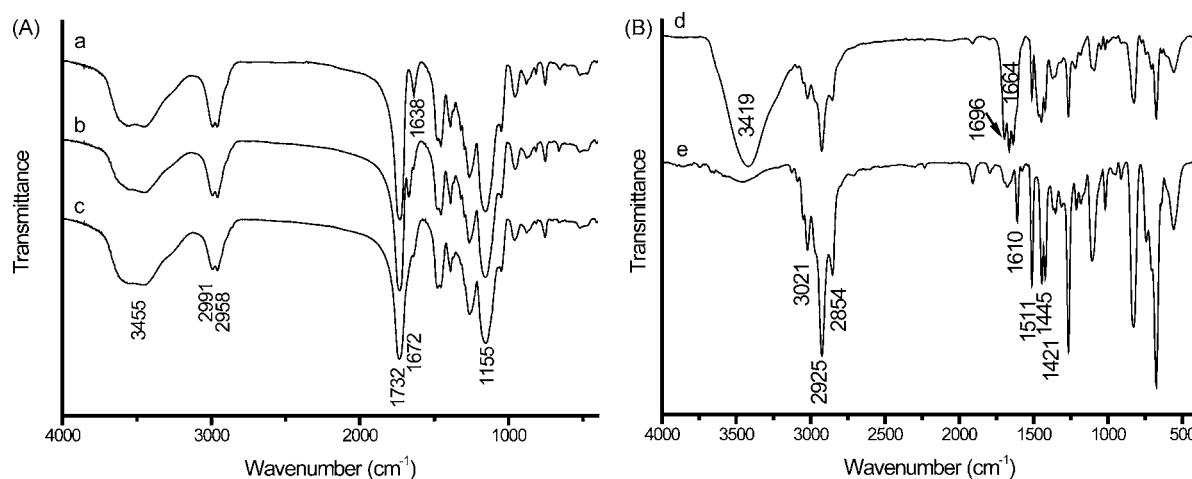


Fig. 3. FT-IR spectra of polymer sorbent (a) P1, (b) P2, (c) P3, (d) P4 and (e) PCMSt.

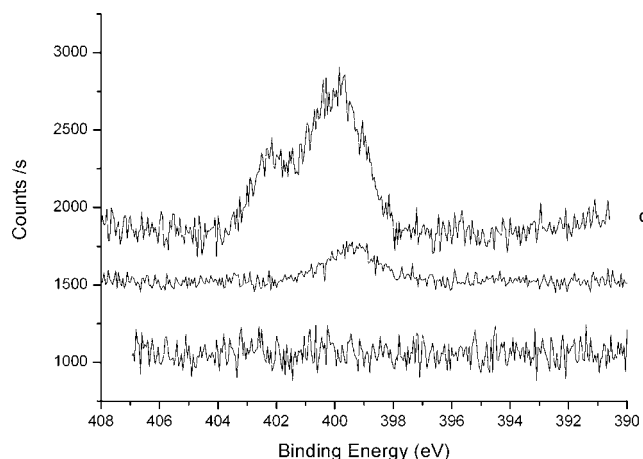


Fig. 4. XPS of N1s of (a) P2, (b) P3 and (c) P4 thymine polymer sorbent.

IR spectra of P2 (b) with P1 (a), it could be clearly found that a new peak of C=O band of acylamide group appeared at 1672 cm^{-1} which indicates that the AT was copolymerized with EDMA in the sorbent successfully. And this peak was weak adsorption because of the lower content of AT in the sorbent P2. But this peak disappeared when the AT content rising (P3, c), and compared the spectra c with b and a, it could be found that the peak at 1732 cm^{-1} was become broader obviously. The phenomenon might be caused from the overlap of peaks of C=O band of acylamide and ester.

IR spectra of grafting sorbent (P4) and PCMSt are shown in Fig. 3B. The peaks of C=C bond at 1610 , 1511 , 1445 , and 1421 cm^{-1} and aliphatic C-H at 3021 cm^{-1} indicated that the presence of benzene. Compared the IR spectra of d with e, it could be clearly found that some new peaks appeared. The new broad peak at 3419 cm^{-1} showed the presence of O-H or N-H in P4, and new peaks at 1696 and 1664 cm^{-1} indicated the presence C=O band of acylamide group. All these new peaks showed that AT had grafted on the surface of the PCMSt beads successfully.

Additionally, since no nitrogen is contained in blank sorbent beads (P1 and PCMSt), any nitrogen content represents the amount of thymine immobilized on polymer beads. As the adsorption capability of the sorbent was determined by the amount of thymine located on the surface of sorbent, the nitrogen content on the surface of P2, P3 and P4 were measured by XPS (Fig. 4). The nitrogen content on P2 surface was below the detection limit and the P3 was 1.75%. Whereas, the nitrogen content on the surface of P4, which was obtained by graft polymerization method, was 4.76% (about 2.7 times of P3). This might led to the larger adsorption capacity for Hg(II) of the grafting polymer sorbent P4. XPS results also clearly showed that the thymine polymer sorbent was prepared successfully.

3.2. Effect of pH on adsorption

Hg(II) probes based on thymine were reported to be pH sensitive [23]. This indicated that the adsorption capability of our thymine polymer sorbent may also depend on the pH of the solution. The effect of pH on the Hg(II) adsorption of sorbent beads P3 is shown in Fig. 5. The thymine sorbent shows weak sorption ability for Hg(II) at lower pHs. Only 22% of Hg(II) was adsorbed onto the P3 sorbent when the pH was 2.0. This might be due to that low pH is unfavorable for dissociation of the imino protons of thymine residues, which reduce the coordination ability of thymine with the Hg(II) in aqueous solution. As the pH of the solution is increased, the extent of dissociation of the imino protons becomes easier causing the Hg(II) adsorption to greatly increase. As shown in Fig. 5, when the

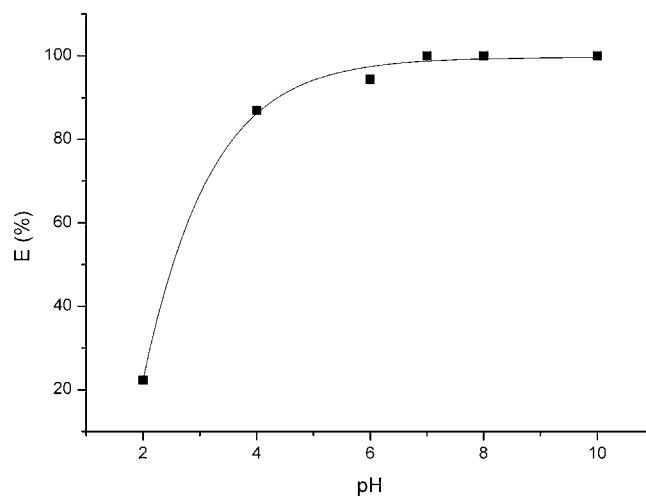


Fig. 5. Effect of pH on adsorption of Hg(II) on the thymine polymer sorbent. Hg(II) concentration: 2.0 mg/L; pH 2.0 (20 mM $\text{NaH}_2\text{PO}_4/\text{H}_3\text{PO}_4$); pH 4.0 (20 mM $\text{CH}_3\text{COONa}/\text{CH}_3\text{COOH}$); pH 6.0 (20 mM $\text{CH}_3\text{COONa}/\text{CH}_3\text{COOH}$); pH 7.0 (20 mM $\text{NaH}_2\text{PO}_4/\text{NaOH}$); pH 8.0 (20 mM $\text{Na}_2\text{HPO}_4/\text{H}_3\text{PO}_4$); pH 10.0 (20 mM $\text{Na}_2\text{HPO}_4/\text{NaOH}$); sorbent P3: 50 mg; sample volume: 30 mL.

pH was 4.0, more than 80% of Hg(II) was removed; the removal efficiency reached 100% in the pH range of 7.0–10.0. Moreover, the loss of the thymine polymer's adsorption ability at low pH indicates that this kind of Hg(II) sorbent may be regenerated conveniently by an acidic solution.

3.3. Adsorption capacity of thymine polymer sorbent for Hg(II)

Adsorption capacity of the new thymine polymer sorbents for Hg(II) from aqueous solution was investigated in batch experiments. Different initial concentrations of Hg(II) aqueous solutions were equilibrated with polymer sorbents P1, P2, P3, P4 and PCMSt, respectively. Fig. 6 shows the amount of the Hg(II) adsorbed on the different sorbent depends on the initial concentration of Hg(II) in solution. Hg(II) was hardly adsorbed on the blank sorbent P1 (0.78 mg/g dry weight) and PCMSt (0.98 mg/g dry weight). For P2, P3 and P4, however, the amount of Hg(II) adsorbed increased with increasing concentrations of Hg(II) in the initial solution. Finally at a high enough concentration the curve reached a plateau, which

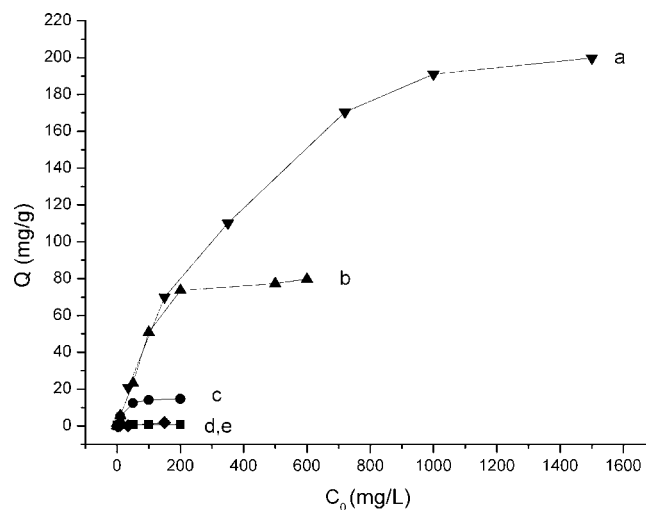


Fig. 6. The adsorption curve of Hg(II) on different sorbent: (a) P4, (b) P3, (c) P2, (d) and (e) P1 and PCMSt. Fifty milligrams of each sorbent in 30 mL of buffer (20 mM $\text{NaH}_2\text{PO}_4/\text{NaOH}$, pH 7.0) with different concentration of Hg(II). Q denote the adsorption capacity (mg/g), C_0 denote the initial concentration of Hg(II) (mg/L).

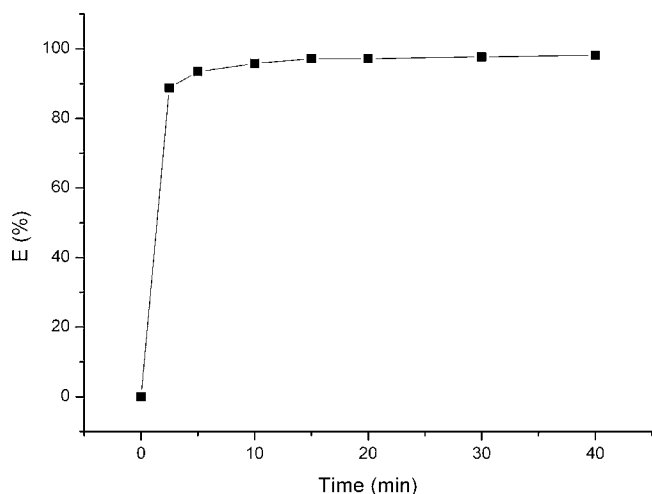


Fig. 7. Kinetics of Hg(II) adsorption on thymine polymer sorbent. Hg(II) concentration: 100.0 mg/L; pH 7.0 (20 mM NaH₂PO₄/NaOH buffer); sorbent P3: 100 mg; sample volume: 20 mL. *E* denote removal efficiency.

represents saturation of the active binding sites. The maximum adsorption capacity of P2, P3 and P4 is about 14.4, 78.5 and 200 mg/g dry sorbent, respectively, which agree well with the amount of thymine immobilized on the surface of different polymer beads (Fig. 4). Although the nitrogen content on P2 sorbent is undetectable, the molar amount of thymine used for preparation of sorbent P2 is one fifth of that for sorbent P3, this ratio is similar to the ratio of maximum adsorption capacity of P2 to P3. And the maximum adsorption capacity of P4 is about 2.55 times that of P3, which also agrees well with the ratio of the surface nitrogen content of P4 to P3. These results indicate that the adsorption capacity for Hg(II) depends on the density of thymine on the surface of the polymer sorbent, which illuminate that the specific coordination interaction of thymine and Hg(II) is the key factor for the adsorption performance of the new thymine polymer sorbent. The adsorption capacity of P4 is 200 mg/g, which is lower than the reported thiol (696 mg/g) [13] or amide (496 mg/g) [14] modified polymer sorbents, but higher than the MIP sorbent (41 mg/g [16] and 78.5 mg/g [17]). Because the adsorption capacity of the new sorbent is determined by the surface density of thymine, improvement of the surface density of thymine on the polymer sorbent would further increase the adsorption capacity.

3.4. Adsorption kinetics

The speed of adsorption of Hg(II) on P3 sorbent is shown in Fig. 7. Nearly 90% of Hg(II) was adsorbed within 2.5 min, and more than 95% of Hg(II) was removed from water after 5 min. This is much faster than some MIPs and other commonly used Hg(II) sorbents, which require 20 or more minutes for 95% adsorption of Hg(II) [13–16]. This unique pace could make the thymine polymer sorbent suitable for chemical sensing, chromatographic separation, solid-

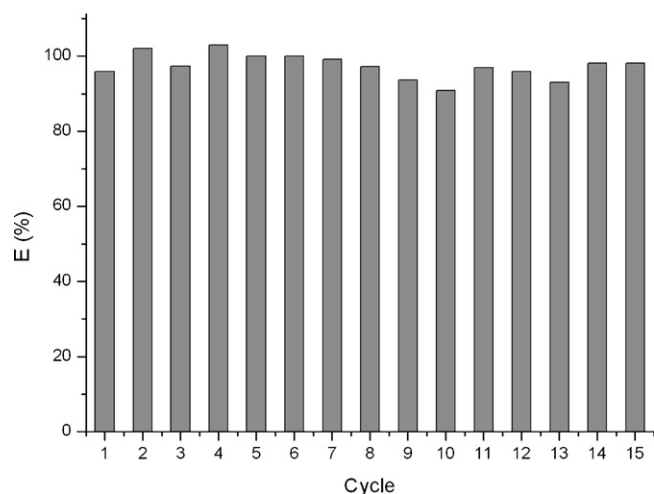


Fig. 8. Reusability of the thymine polymer sorbent. Hg(II) concentration: 2.0 mg/L; pH 8.0 (20 mM Na₂HPO₄/H₃PO₄ buffer); sorbent P3: 100 mg; sample volume: 30 mL.

phase extraction or other applications that require fast adsorption of Hg(II).

3.5. Recycling test

1.0 M HCl was found to elute the adsorbed Hg(II) from the P3 sorbent completely. Thus it was used to regenerate the thymine polymer. To test the reusability of the thymine polymer sorbent, we subjected it to a series of loading and elution batch experiments. As shown in Fig. 8, the Hg(II) adsorption ability of the thymine sorbent did not decrease even after 15 cycles of loading and elution, which shows good reusability and stability.

3.6. Selectivity studies

To investigate the selectivity of the thymine polymer sorbent, competitive adsorption of Hg(II) with other ions, such as Cu(II), Cd(II), Zn(II), Co(II), Ca(II) and Mg(II) was performed. From Fig. 9, it can be seen that only Hg(II) was completely removed by thymine polymer sorbent, while less than 10% of the Co(II), Ca(II) and Mg(II) ions were removed by both thymine and blank polymer sorbent. About 60% of Cu(II), 30% of Cd(II) and Zn(II) were adsorbed by the thymine polymer sorbent as well as by the blank polymer sorbent, indicating that the adsorption of Cu(II), Cd(II), and Zn(II) was caused by the non-specific adsorption of the matrix, and not by thymine. Since Cu(II), Cd(II) and Zn(II) were found to be adsorbed by the sorbent matrix, the adsorption capacities for these ions were further investigated. The maximum adsorption capacities of thymine polymer sorbent P3 for Cu(II), Cd(II) and Zn(II) were found to be 0.4, 0.2 and 0.1 mg/g, respectively, which are much lower than that for Hg(II) (78.5 mg/g), indicating the good selectivity of the thymine polymer sorbent for Hg(II).

Table 1

Adsorption of Hg(II) by thymine polymer sorbent from real tap water samples ($n = 3$)^a.

Hg(II) added (mg/L)	After adsorption by thymine polymer sorbent (P3) (mg/L)			After adsorption by blank polymer sorbent (P1) (mg/L)		
	Hg(II)	Ca(II)	Mg(II)	Hg(II)	Ca(II)	Mg(II)
1.0	– ^b	50.99 ± 0.39	24.45 ± 0.32	1.03 ± 0.16	50.25 ± 0.97	24.40 ± 0.45
5.00	0.37 ± 0.07	49.48 ± 0.21	24.19 ± 0.14	4.61 ± 0.04	49.65 ± 1.07	24.27 ± 0.11
20.0	0.59 ± 0.14	49.83 ± 0.74	24.87 ± 0.31	19.42 ± 0.87	51.08 ± 0.11	24.71 ± 0.76

^a The concentration of Ca(II) and Mg(II) in real tap water samples were measured to be 50.71 ± 1.54 and 25.02 ± 0.50 mg/L, respectively.

^b (–) means not detected.

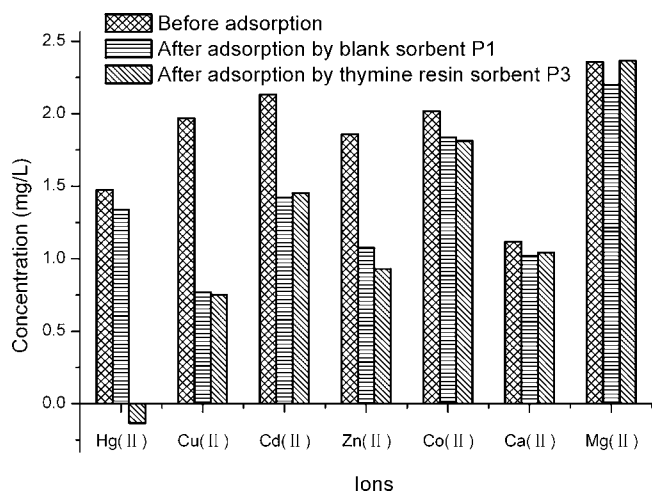


Fig. 9. Selectivity of thymine polymer sorbent. Mixture of different ions in 20 mM $\text{Na}_2\text{HPO}_4/\text{NaOH}$ (pH 7.0); sorbent P1 or P3: 50 mg; sample volume: 30 mL.

3.7. Application to real tap water sample

Water is probably the most studied environment sample and Hg(II) is the main species of mercury pollutant existed in natural water. The thymine polymer was also investigated for the selective adsorption and removal of spiked Hg(II) in tap water samples. Twenty milliliters of tap water sample spiked with Hg(II) at different concentrations were disposed with 50 mg of thymine sorbent P3 and blank sorbent P1, respectively. The concentrations of Hg(II), Ca(II) and Mg(II) before and after treatment are shown in Table 1. Ca(II) and Mg(II), the main interference ions existed in tap water, were hardly adsorbed by the thymine polymer sorbent and blank sorbent. The spiked Hg(II) was almost adsorbed by the thymine polymer sorbent completely, but was hardly adsorbed by the blank polymer sorbent. These results indicate that the thymine polymer sorbent can be used for the selective separation, preconcentration, or removal of Hg(II) from real water samples.

4. Conclusions

A new kind of sorbent for specific Hg(II) adsorption based on thymine was developed, which was stable, reusable, and easy to be prepared and environment friendly. The good specificity of this sorbent for Hg(II) relies on the specific interaction of Hg(II) with thymine. The Hg(II) adsorption capacity is highly depended on the

amount of thymine located on the sorbent surface. This kind of sorbent can be easily regenerated by acidic solution, showing great potential for selective separation and removal of Hg(II) from real water samples. Furthermore, the fast adsorption kinetics of Hg(II) onto the thymine polymer sorbent make it an attractive option for chemical sensing, solid-phase extraction, or selective on-line preconcentration and separation of Hg(II) from complex samples.

Acknowledgements

We gratefully acknowledge financial support from NSF of China (20775082 and 90717119), grant 973 Program (2007CB935601), 863 Program (2007AA02Z221 and the Center for Molecular Science, Institute of Chemistry, Chinese Academy of Sciences. We would also like to thank Meghan B. O'Donoghue for carefully reading and correcting this manuscript.

References

- [1] B. Hultberg, A. Andersson, A. Isaksson, *Toxicology* 126 (1998) 203.
- [2] G. Jiang, J. Shi, X. Feng, *Environ. Sci. Technol.* 40 (2006) 3673.
- [3] R.B. Hayes, *Cancer Causes Control* 8 (2002) 258.
- [4] M. Huebra, M.P. Elizalde, A. Almela, *Hydrometallurgy* 68 (2003) 33.
- [5] M.V.B. Krishna, D. Karunasagar, S.V. Rao, J. Arunachalam, *Talanta* 68 (2005) 329.
- [6] Y. Guo, B. Din, Y. Liu, X. Chang, S. Meng, M. Tian, *Anal. Chim. Acta* 504 (2004) 319.
- [7] C. Namasivayam, K. Kadirvelu, *Carbon* 37 (1999) 79.
- [8] C.P. Huang, Y.C. Chung, M.R. Liou, *J. Hazard. Mater.* 45 (1996) 265.
- [9] N.L. Dias Filho, D.R.D. Carmo, *Talanta* 68 (2006) 919.
- [10] S. Babel, T.A. Kurniawan, *J. Hazard. Mater.* 97 (2003) 219.
- [11] S.R. Segade, J.F. Tyson, *Talanta* 71 (2007) 1696.
- [12] X. Feng, G.E. Fryxell, L.Q. Wang, A.Y. Kim, J. Liu, K.M. Kemner, *Science* 276 (1997) 923.
- [13] M.C. Dujardin, C. Caze, I. Vroman, *React. Funct. Polym.* 43 (2000) 123.
- [14] C. Jeon, W.H. Holl, *Water Res.* 37 (2003) 4770.
- [15] A. Denizli, S. Senel, G. Alsancak, N. Tuzmen, R. Say, *React. Funct. Polym.* 55 (2003) 121.
- [16] Y. Liu, X. Chang, D. Yang, Y. Guo, S. Meng, *Anal. Chim. Acta* 538 (2005) 85.
- [17] Z. Fan, *Talanta* 70 (2006) 1164.
- [18] G. Wu, Z. Wang, J. Wang, C. He, *Anal. Chim. Acta* 582 (2007) 304.
- [19] A. Ono, T. Togashi, *Angew. Chem. Int. Ed.* 43 (2004) 4300.
- [20] A. Okamoto, Y. Ochi, I. Saito, *Bioorg. Med. Chem. Lett.* 15 (2005) 4279.
- [21] Y. Miyake, H. Togashi, M. Tashiro, H. Yamaguchi, S. Oda, M. Kudo, Y. Tanaka, Y. Kondo, R. Sawa, T. Fujimoto, T. Machinami, A. Ono, *J. Am. Chem. Soc.* 128 (2006) 2172.
- [22] Y. Tanaka, S. Oda, H. Yamaguchi, Y. Kondo, C. Kojima, A. Ono, *J. Am. Chem. Soc.* 129 (2007) 244.
- [23] Z. Wang, D. Zhang, D. Zhu, *Anal. Chim. Acta* 549 (2005) 10.
- [24] Y. Tang, F. He, M. Yu, F. Feng, L. An, H. Sun, S. Wang, Y. Li, D. Zhu, *Macromol. Rapid Commun.* 27 (2006) 389.
- [25] Y. Che, X. Yang, L. Zang, *Chem. Commun.* (2008) 1413.
- [26] J. Thibon, L. Latxague, G. Deleris, *J. Org. Chem.* 62 (1997) 4635.
- [27] X. Liu, Z. Chen, R. Zhao, D. Shangguan, G. Liu, Y. Chen, *Talanta* 71 (2007) 1205.
- [28] D.M. Jones, W.T.S. Huck, *Adv. Mater.* 13 (2001) 1256.



Reverse flow injection analysis of nanomolar soluble reactive phosphorus in seawater with a long path length liquid waveguide capillary cell and spectrophotometric detection

Jian Ma, Dongxing Yuan*, Min Zhang, Ying Liang

State Key Laboratory of Marine Environmental Science, Environmental Science Research Center, Xiamen University, 422 Siming South Road, Xiamen 361005, Fujian Province, PR China

ARTICLE INFO

Article history:

Received 24 July 2008

Received in revised form 11 November 2008

Accepted 13 November 2008

Available online 25 November 2008

Keywords:

Reverse flow injection analysis

Liquid waveguide capillary cell

Seawater

Nanomolar

Soluble reactive phosphorus

ABSTRACT

A novel reverse flow injection analysis method coupled with a liquid waveguide capillary cell (LWCC) and spectrophotometric detection for the determination of nanomolar soluble reactive phosphorus in seawater was established. Reagent was injected into the sample stream and detected in a 2-m path length LWCC with detection wavelength set at 710 nm. Experimental parameters, including the reagent concentration, the injection volume, the flow rate and the length of the mixing coil, were optimized based on univariate experimental design. The interference of silicate and arsenate were also investigated. Under optimized conditions, the linearity and the detection limit of the proposed method were found to be 0–165.0 nM and 0.5 nM, which was estimated to be three times the standard deviation of the measurement blanks ($n=9$). The relative standard deviations for the determination of 24.7 and 82.5 nM samples were 1.54% and 1.86% ($n=9$), respectively. Three seawater samples were analyzed with recoveries ranging from 87.8% to 101.8%. Using the Student's t -test at the 95% confidence level, the results of the proposed method and a segmented flow analyzer reference method for determination of the two samples showed no significant difference. The proposed method had the advantages of being less reagent consuming, more sensitive and with higher throughput (15 h^{-1}).

© 2008 Elsevier B.V. All rights reserved.

1. Introduction

Phosphorus is an essential element for all life in both terrestrial and aquatic environments, and its major inorganic form, orthophosphate, which is immediately biologically available, plays a key role in photosynthesis (i.e. primary productivity) [1]. Because of the biological uptake of phosphate, the concentrations of phosphate in the surface waters of some oligotrophic regions such as the North Pacific, the Western North Atlantic Ocean and the South China Sea, are usually down to nanomolar levels and could be a typical limiting nutrient in the marine environment [2–4]. Thus, in order to understand the biogeochemical behavior of phosphorus in oligotrophic systems, it is essential to determine accurately the phosphate concentration at such low levels.

The most widely recommended method for the determination of phosphate in aqueous samples is the phosphomolybdenum blue (PMB) method, because of its higher sensitivity and lower susceptibility to interference [5]. Soluble reactive phosphorus (SRP) is the phosphate measured using this PMB technique, and includes

orthophosphate and a small amount of acid hydrolysable organic or condensed phosphorus compounds [6,7]. However, the PMB method is unable to quantify SRP at nanomolar level without the assistance of other techniques. Consequently many methods have been developed for trace analysis of SRP [8], including optimization and modification of the PMB method to improve its sensitivity. Concentrating the analyte [4,7,9] and extending the detection cell path length [10–13] are the two most efficient techniques. The typical enrichment method which has been widely accepted by oceanographers is the magnesium hydroxide-induced coprecipitation (MAGIC) method [2,3,7]. This method is unavoidably labor-intensive and time consuming, and its applicability for shipboard usage is limited, although many modifications have been made to simplify the procedure and minimize the analytical time [14]. Increasing the detection cell path length is an alternative method developed in recent years. Long path length absorbance spectrophotometry can be achieved through the application of a liquid waveguide capillary cell (LWCC), which has a flexible fluoropolymer material (AF-2400, Dupont) with a refractive index (1.29) less than that of water and seawater (1.33 and 1.34, respectively). LWCC enables light introduced into the capillary core to be totally internally reflected down the capillary towards the detector, resulting in an enhancement of sensitivity and

* Corresponding author. Tel.: +86 592 2184820; fax: +86 592 2180655.
E-mail address: yuandx@xmu.edu.cn (D. Yuan).

improved limits of detection compared with conventional spectroscopic techniques [15]. In 2002, Zhang and Chi firstly published the paper about automatic analysis of nanomolar concentrations of phosphate in natural waters with LWCC [10]. Recently, the feasibility of combining MAGIC preconcentration and long path length absorbance spectrophotometry for the determination of nanomolar/sub-nanomolar concentration of phosphate was demonstrated. The limit of detection was taken down to 0.3 nM, but the above-mentioned disadvantages of the MAGIC method were unavoidably encountered [16].

Flow injection analysis (FIA), which involves injection of a small volume of sample into a stream of reagent flowing through the system, is considered as normal FIA (nFIA) and has the merits of simplicity, automation and less risk of contamination. It is a widespread and well established approach for the determination of phosphorus [17–19]. Different from this nFIA technique is reverse flow injection analysis (rFIA), where the reagent to be injected into the flowing system is mixed with the sample and other solutions. In 1982, Johnson and Petty published the first paper about rFIA and the analyte was phosphate with a detection limit of 50 nM [20]. In rFIA, with the injection of reagent into the sample flow, the determination concentration in the reagent zone increase with increasing dispersion, therefore the determination is carried out with only slight dilution and higher sensitivity could be obtained. rFIA could be suitable for in situ analysis or industrious process for the simple sample preparation. The rFIA also has advantageous features such as high selectivity and very low consumption of reagent, and has been applied for the determination of phosphate and other analytes [21–26].

In this work, a simple rFIA procedure and an LWCC were successfully used for the direct determination of nanomolar SRP in seawater based on the PMB reaction. Operative conditions for the rFIA procedures, including reagent concentration, injection loop, flow rate and length of the mixing coil, were investigated and optimized, and the interference of silicate and arsenate with SRP determination was also studied.

2. Experimental

2.1. Reagents and solutions

All the chemicals used in this study were of analytical grade, and supplied by Sinopharm Chemical Reagent Co., China, unless stated otherwise. Ammonium heptamolybdate tetrahydrate ($(\text{NH}_4)_6\text{Mo}_7\text{O}_{24}\cdot 4\text{H}_2\text{O}$) was re-crystallized from ethanol to remove any possible remaining phosphate and other impurities. The other chemicals were used as purchased without further purification. All solutions were prepared in Milli-Q water obtained from a Millipore water purification system (Millipore Co., MA, USA).

A mixed reagent (MR) for color development was prepared by mixing 100 mL of 14 g/L $(\text{NH}_4)_6\text{Mo}_7\text{O}_{24}\cdot 4\text{H}_2\text{O}$ solution, 100 mL of 0.35 g/L potassium antimony tartrate and 300 mL of 1.0 mol/L H_2SO_4 (G.R.). The solution was stored at 4 °C in a refrigerator while not in use. 10 g/L ascorbic acid solution (AA) was prepared daily.

Silicate stock solution of 10 mM was prepared from Na_2SiF_6 dried at 105 °C for 1 h. Phosphate stock solution (1000 mg/L, $\text{H}_2\text{PO}_4^{2-}$) and arsenate stock solution (1000 mg/L, As) were purchased from the National Research Center for Certified Reference Materials (Beijing, China). Working standards were prepared daily as required by stepwise dilution with Milli-Q water.

Low-nutrient seawater was collected from the surface of the South China Sea and phosphate was removed using the MAGIC method [7,10]. This phosphate-free seawater was used as the matrix for preparing standard curve solutions.

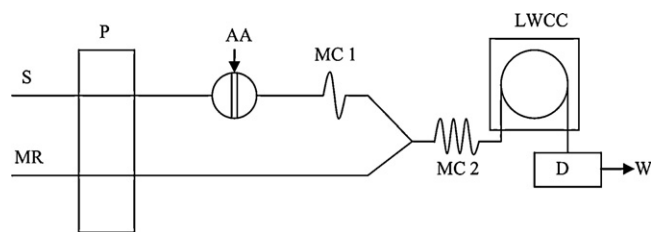


Fig. 1. Schematic diagram of reverse flow injection analysis. S: sample; P: peristaltic pump; MR: mixed reagent solution; AA: ascorbic acid solution; MC 1, MC 2: mixing coil 1, 2; LWCC: liquid waveguide capillary cell; D: detector; W: waste.

2.2. Apparatus and procedure for the reverse flow injection analysis system

As shown in Fig. 1, the rFIA system used in this study included the following parts: an FIA 3110 flow injection analysis processor (Beijing Titan Instruments Co., Beijing, China), including two 6-channel peristaltic pumps and an 8-way rotary valve; a BT100-1J 2-channel peristaltic pump (Baoding Longer Precision Pump Co., Hebei, China), equipped with Tygon tubing; an LWCC of 2 m length, 550 μm internal diameter and about 500 μL internal volume (World Precision Instruments, FL, USA); a miniature USB 2000+ fiber-optic spectrophotometer, with a miniature LS-1-LL tungsten halogen lamp and two QP400-2-VIS/NIR fiber-optic cables (Ocean Optics Inc., FL, USA); and 1.0 mm i.d. Teflon tubing for the reagent transport lines and mixing coils.

The rFIA procedure was based on AA injection into the flowing sample and MR mixing reagent, where any phosphate present formed PMB with the reagent in the mixing coil. The PMB solution was delivered to the spectrophotometer and LWCC for detection at 710 nm. The detector output was recorded using a computer and the “counts” value was converted to absorbance with Excel software (Microsoft Co. WA, USA).

Before and after use, the LWCC was sequentially flushed with ultrapure water followed by 1 M NaOH (10 mL) and 1 M HCl (10 mL) and again with ultrapure water (30 mL) as recommended by Gimbert et al. [12,15].

The blank and a 24.7 nM phosphate solution were used as data quality control samples throughout the experiments in order to check the measurement deviation and provide sound data.

3. Results and discussion

Although rFIA and LWCC have been, respectively employed to improve the sensitivity of spectrophotometric determination of phosphorus, the two techniques have not been reported to be simultaneously utilized in a FI-spectrophotometry system. However, combining the two has significant challenge such as baseline stability and bubble problem. For rFIA with conventional flow cell of 10 mm \times 1 mm (i.d.), it is easy to preclude the bubble by a higher flow rate, but for LWCC, higher flow rate may result in a much noisier baseline due to the pressure fluctuation. Thus, while changing samples, it is recommended to stop the sample pump or use a multi-position valve that is always employed in sequential injection analysis for sample change in order to avoid bubble introduction.

The effect of various parameters, including the reagent concentration, injection volume, flow rate and the length of the mixing coil were investigated and optimized based on univariate experimental design. During the optimization of these parameters, a blank and an 82.5 nM standard solution were used as testing samples and the results were evaluated. Each sample was determined three times and the result was shown as the average value \pm the standard deviation ($n = 3$). To evaluate the optimum parameters for the proposed

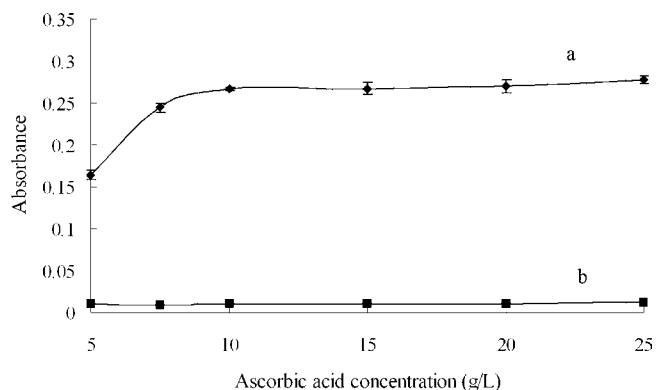


Fig. 2. Effect of ascorbic acid (AA) concentrations on signal at variation from 5 to 25 g/L at an injection volume of 300 μ L, MC 1 of 7 cm, MC 2 of 200 cm and sample flow rate of 1.0 mL/min on absorbance. Error bars are \pm S.D. for $n = 3$: (a) 82.5 nM P and (b) blank.

method, the sensitivity, analysis time and peak shape were the most important.

3.1. Effect of concentration of the color developing reagents (MR and AA)

In the MR solution, the $[H^+]/[MoO_4^{2-}]$ ratio was found to be a very important factor affecting the formation of PMB, and the optimum $[H^+]/[MoO_4^{2-}]$ ratio is between 50 and 80 [5]. Based on this, in this work the ratio was fixed at 74. The final pH of the reaction solution was another important factor in the PMB reaction. It was found that at pH 1.0, the PMB method was more sensitive and there was less interference from other elements [10,27]. Thus, the flow rate ratio of MR solution to the sample was fixed at 1:5 in order to obtain a pH of 1.0 in the final reaction solution.

The effect of AA concentration on the PMB reaction was studied in the range 5–25 g/L. As shown in Fig. 2, the absorbance increased as the AA concentration increased up to 10 g/L but, thereafter, the increase in AA concentration resulted in no significant variation in the observed signal. Thus, an AA concentration of 10 g/L was chosen for further experimental work.

3.2. Effect of injection volume

Once the AA concentration was fixed it was necessary to define the injection volume, which is the amount of AA to be added to the sample. An injection volume from 80 to 500 μ L was studied in order to determine the optimum value and, as shown in Fig. 3, the greatest signal was obtained at 300 μ L. It was observed that a double peak

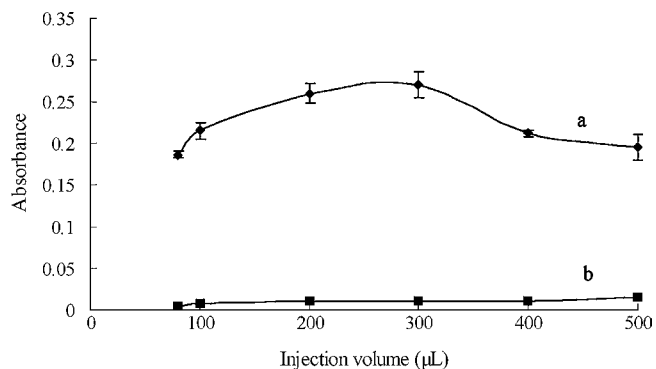


Fig. 3. Effect of injection volume on signal at variation from 80 to 500 μ L at an AA concentration of 10 g/L, MC 1 of 7 cm, MC 2 of 200 cm and sample flow rate of 1.0 mL/min on absorbance. Error bars are \pm S.D. for $n = 3$: (a) 82.5 nM P and (b) blank.

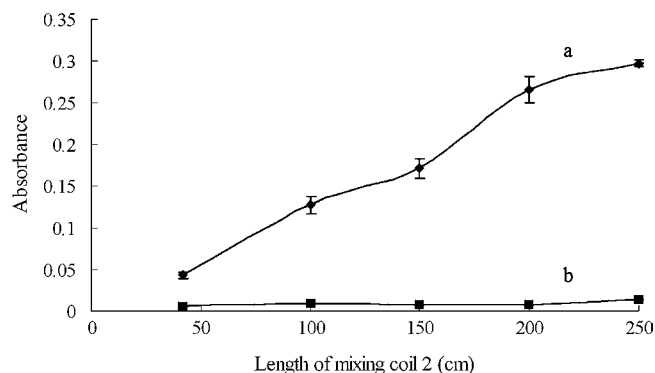


Fig. 4. Effect of mixing coil (MC) 2 length on signal at variation from 42 to 250 cm at an AA concentration of 10 g/L, injection volume of 300 μ L, MC 1 of 7 cm and sample flow rate of 1.0 mL/min on absorbance. Error bars are \pm S.D. for $n = 3$: (a) 82.5 nM P and (b) blank.

could occur if the injection volume was larger than 300 μ L, suggesting that for larger injections, the AA solution was excessive in the mid-portion of the AA zone, and complete reaction only occurred at the leading and trailing edges of the AA zone. Although this double peak could be eliminated by more efficient mixing (including enlarging the mixing coil and lowering flow rate) a broader peak or longer analysis time resulted. For these reasons, 300 μ L was chosen as the injection volume for subsequent measurements.

3.3. Effect of the mixing coil lengths

As illustrated in Fig. 1, in mixing coil 1 (MC 1) the sample and AA were mixed, and in MC 2, the sample-AA and MR were mixed together for PMB formation. The effects of MC 1 and MC 2 length on the signal were compared by varying their lengths. Because no reaction occurred in MC 1, increasing the length of MC 1 from 7 to 250 cm did not speed up the reaction but caused further dilution of the injected AA, resulting in a decreased absorbance. Therefore an MC 1 of 7 cm was chosen for further study.

As shown in Fig. 4, increasing the length of MC 2 from 42 to 250 cm resulted in an increased signal response, since a longer MC 2 meant a longer reaction time and better mixing of the sample and reagents, which were favorable for PMB formation. And the analytical time would be enlarged and prolonged. A length of 200 cm was chosen for MC 2 as a balance between the detection sensitivity and sample throughput.

3.4. Effect of sample flow rate

Higher sample flow rate could cause shorter retention time and incomplete reaction for the target analyte; on the other hand, lower flow rate could cause higher dispersion and a broader peak. The effect of sample flow rate on the signal was investigated in the range 0.6–1.6 mL/min. As shown in Fig. 5, the maximum signal was obtained in a flow rate range of 0.8–1.0 mL/min, and so a flow rate of 1.0 mL/min was selected as the optimum.

3.5. Effect of salinity

In continuous flow analysis, refractive index changes (Schlieren effect) caused by salinity difference between samples and the washing solution leads to interference in absorbance measurements [28]. In this study, the effect of salinity was studied followed the procedure introduced by Zhang and Chi [10]: waters of different salinity were analyzed as phosphate samples, but the MR solution was replaced by sulfuric acid solution at the same acidity. Therefore the

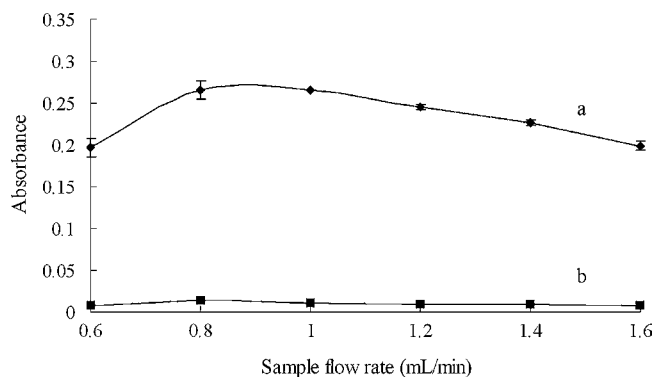


Fig. 5. Effect of sample flow rate on signal at variation from 0.6 to 1.6 mL/min at an AA concentration of 10 g/L, injection volume of 300 μ L, MC 1 of 7 cm and MC 2 of 200 cm on absorbance. Error bars are \pm S.D for $n=3$: (a) 82.5 nM P and (b) blank.

Table 1
Recommended analytical parameters.

Parameters	Selected value
Detection wavelength, λ (nm)	710
Tubing i.d. (mm)	1.0
Volume ratio of MR to sample	1:5
Final pH of mixture solution	1.0
AA concentration (g/L)	10
AA injection volume (μ L)	300
Length of mixing coil 1 (cm)	7
Length of mixing coil 2 (cm)	200
Sample flow rate (mL/min)	1.0

detected signals were caused only by the salinity difference and not the PMB because of the absence of MR solution.

There was no detectable refractive index interference in the proposed analytical system. Because in this rFIA method the sample also served as the carrier solution, the refractive index differences between the AA solution and different samples were almost the same after dispersion in MC 1 and MC 2. Therefore, the proposed method could be applied to various seawater samples without salinity correction.

3.6. Analytical figures of merit

Table 1 summarizes the optimization of the proposed method. Under the optimized parameters, a calibration curve was obtained over the concentration range 0–165.0 nM. The regression equation was $A = (0.000327 \pm 0.00002) + (0.002973 \pm 0.00001) C_P$ (nM), with $R^2 = 0.9990$ ($n=6$), where A was the absorbance and C_P was the concentration of phosphate. A typical detector signal output of the proposed method is shown in Fig. 6. In 1 h, 7 samples could be analyzed in triplicate with 2 min between each sample for sample

Table 2
Interference of silicate in the determination of SRP in seawater ($n=3$).

C_P (nM)	C_{Si} added (μ M)	Absorbance	Calculated t -value	Critical t -value ($P=0.95$)
0	0	0.0099 ± 0.0009	–	2.78
0	20	0.0099 ± 0.0010	0	2.78
0	40	0.0107 ± 0.0006	1.28	2.78
0	80	0.0111 ± 0.0010	1.54	2.78
0	160	0.0102 ± 0.0009	0.41	2.78
0	240	0.0112 ± 0.0008	1.87	2.78
82.5	0	0.2579 ± 0.0085	–	2.78
82.5	20	0.2565 ± 0.0041	0.26	2.78
82.5	40	0.2607 ± 0.0053	0.48	2.78
82.5	80	0.2593 ± 0.0047	0.25	2.78
82.5	160	0.2642 ± 0.0006	1.28	2.78
82.5	240	0.2571 ± 0.0058	0.24	2.78

changing and tubing flushing. If the analysis was only once for one sample, the analytical time was 4 min/sample (2 min for analysis and 2 min for flushing).

The relative standard deviations (R.S.D.)s for repetitive determination of phosphate samples at 24.7 nM and 82.5 nM were 1.54% and 1.86% ($n=9$), respectively, showing good and reproducible analytical results.

The method detection limit (MDL), estimated as three times the standard deviation of the measurement blanks ($n=9$), was 0.50 nM. The MDL was thus low enough to allow the determination of SRP in oligotrophic regions such as the South China Sea.

Compared with another method using a 2 m LWCC [10], the regression equation slope of the proposed method was about double, indicating higher sensitivity. In the proposed method, the sample consuming volume was at least 10 mL for triplicate analysis, which was larger than other methods, such as in the FIA-LWCC method introduced by Gimbert et al. [12] whose sample injection volume was only 0.5 mL. However, for seawater analysis, the sample volume was usually sufficient and 10 mL consumption could be accepted.

3.7. Interference of silicate and arsenate

Silicate and arsenate are two of the main species interfering with the determination of SRP using the PMB method, because of the formation of similar molybdate heteropolyacide compounds that contribute to the detection signal [29]. The effects of silicate and arsenate in seawater samples on SRP determination using the proposed method were studied, with samples containing 0 or 82.5 nM phosphate and various amounts of silicate and arsenate. The Student's t -test was used for evaluating whether there was significant signal difference with and without silicate and arsenate addition.

As shown in Table 2, the absorbance showed no significant difference within silicate concentrations between 0 and 240 μ M, which is the common concentration range for different seawaters. Because the kinetics of the silicate reaction is much slower than that for phosphate [30], using shorter reaction time could eliminate the formation of the silicomolybdate complex. The elimination of silicate interference has been studied by other researchers. Gimbert et al. found that the addition of tartaric acid could be effective to mask silicate interference [12]. Zhang et al. pointed out that silicate interference could be minimized under optimal reaction conditions, including a pH of 1.0 in the final solution, a room temperature of 30 $^{\circ}$ C, a $[H^+]/[Mo]$ ratio of 70 and the addition of potassium antimony tartrate [27]. The proposed method had the similar reaction parameter with Zhang et al. except that the little difference with $[H^+]/[Mo]$ ratio was 74 and the experimental result turned out to be in accordance with Zhang's conclusion.

As shown in Table 3, the calculated t -value of samples after the addition of different concentrations of arsenate were less than the

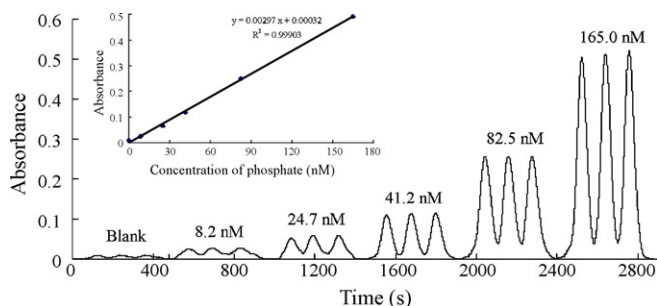


Fig. 6. Typical signal output and, inset, calibration curve with standards in the range 0–165.0 nM P obtained using an LWCC of 2 m path length. Error bars are \pm S.D. for $n=3$.

Table 3
Interference of arsenate in the determination of SRP in seawater ($n = 3$).

C_p (nM)	C_{As} added (nM)	Absorbance	Calculated t -value	Critical t -value ($P = 0.95$)
0	0	0.0103 ± 0.0008	–	2.78
0	6.7	0.0096 ± 0.0004	1.35	2.78
0	13.3	0.0107 ± 0.0006	0.69	2.78
0	26.7	0.0115 ± 0.0009	1.72	2.78
0	40.0	0.0106 ± 0.0006	0.52	2.78
0	53.3	0.0109 ± 0.0009	0.86	2.78
82.5	0	0.2639 ± 0.0067	–	2.78
82.5	6.7	0.2610 ± 0.0071	0.51	2.78
82.5	13.3	0.2603 ± 0.0070	0.64	2.78
82.5	26.7	0.2567 ± 0.0085	1.15	2.78
82.5	40.0	0.2598 ± 0.0057	0.81	2.78
82.5	53.3	0.2704 ± 0.0067	1.19	2.78

Table 4
Recovery of SRP in seawater samples using the proposed method ($n = 3$).

Sample No.	Added concentration (nM)	Found concentration (nM)	Recovery (%)
1	0	3.7 ± 0.1	–
	8.2	12.0 ± 0.1	101.2 ± 0.4
	24.7	27.4 ± 0.5	96.0 ± 1.8
	41.2	41.9 ± 0.7	92.7 ± 1.6
	82.5	84.4 ± 1.7	97.9 ± 2.0
165.0	171.6 ± 3.0	101.8 ± 1.8	
2	0	28.8 ± 0.5	–
	8.2	36.1 ± 0.9	88.7 ± 4.6
	24.7	50.6 ± 0.7	87.8 ± 0.7
	41.2	66.6 ± 1.8	91.6 ± 3.1
	82.5	109.4 ± 1.4	97.6 ± 1.0
165.0	189.4 ± 2.5	97.4 ± 1.2	
3	0	32.2 ± 0.5	–
	8.2	39.6 ± 0.8	90.1 ± 2.8
	24.7	54.8 ± 0.6	91.4 ± 0.2
	41.2	70.6 ± 1.8	93.2 ± 3.1
	82.5	113.1 ± 1.8	98.1 ± 1.6
165.0	192.0 ± 2.4	96.9 ± 1.2	

critical t -value ($P = 0.95$), showing that with the proposed method, arsenate interference could be neglected when its concentration was less than 53.3 nM. This result was probably due to the slower formation of arsenomolybdate at room temperature compared to that of PMB [30,31], and the faster reaction time (2 min) in the proposed method. Since arsenate concentration is at a much lower level in most natural waters, for example 20 nM in the open ocean [2], the influence of arsenate could be ignored in most cases. Since arsenite is non-reactive to molybdate reagents, in areas with arsenic pollution or hydrothermal activity, a third reagent line could be added in the system to introduce sulfite, L-cysteine or thiosulfate solution to reduce arsenate to arsenite for samples with arsenate more than 50 nM [32–34].

3.8. Recovery

To evaluate the degree of interference from the matrix, recovery tests were prepared using three seawater samples collected from the South China Sea. As shown in Table 4, the results obtained were within 87.8–101.8%, indicating high recovery by the proposed method and little matrix interference in the determination of SRP.

3.9. Comparison with the reference method

An intercomparison experiment was carried out for the proposed method and an automated segmented flow analyzer (Bran+Luebbe AA3), which is commonly used in ocean nutrient analysis research. The analytical method of AA3 is based on the

Table 5
Comparison of analytical results of the proposed method and reference method of automated segmented flow analyzer.

Sample No.	$C_p \pm S.D.$ ($n = 3$, nmol/L)		Calculated t -value	Critical t -value ($P = 0.95$)
	Proposed method	Reference method		
1	83.2 ± 1.9	85.4 ± 1.0	1.77	2.78
2	153.4 ± 2.4	150.5 ± 3.2	2.34	2.78

product manual and EPA method 365.5 [35]. The results are shown in Table 5. There was no statistically significant difference between the proposed and reference methods with the paired Student's t -test at the 95% confidence level. However, the proposed method was more sensitive, with a detection limit of 0.5 nM compared with about 25 nM for the reference method.

4. Conclusions

An rFIA method incorporating a 2 m liquid waveguide capillary cell and a miniature fiber-optic spectrophotometer for the determination of nanomolar SRP in seawater was established. The advantages of the proposed method included low method detection limit, high precision and high sample throughput. There was no statistically significant difference between the results obtained from the proposed and a reference method. 240 μ M silicate and 53.3 nM arsenate showed no statistically significant effect on the sample signal (blank and 82.5 nM). Of course, quantifying the dissolved organic phosphorus interference in SRP determination requires further study. The method could be applied for shipboard or *in situ* analysis.

Acknowledgments

The work was financially supported by the National High Technology Research and Development Program of China ("863" project) through grants # 2006AA09Z174 and 2007AA061501. We would like to thank Qing Li and Lifang Wang for their help during this work. Professor John Hodgkiss is thanked for polishing the English.

References

- [1] A. Paytan, K. McLaughlin, Chem. Rev. 107 (2007) 563.
- [2] D.M. Karl, G. Tien, Mar. Chem. 56 (1997) 77.
- [3] J. Wu, W. Sunda, E.A. Boyle, D.M. Karl, Science 289 (2000) 759.
- [4] J. Ma, D.X. Yuan, Y. Liang, Mar. Chem. 111 (2008) 151.
- [5] J. Murphy, J.P. Rilly, Anal. Chim. Acta 27 (1962) 31.
- [6] J.D.H. Strickland, T.R. Parsons, A Practical Handbook of Seawater Analysis, 2nd ed., Bull. Fish. Res. Bd. Can., 1972.
- [7] D.M. Karl, G. Tien, Limnol. Oceanogr. 37 (1992) 105.
- [8] M.D. Patey, M.J.A. Rijkenberg, P.J. Statham, M.C. Stinchcombe, E.P. Achterberg, M. Mowlem, Trends Anal. Chem. 27 (2) (2008) 169.
- [9] Y. Liang, D.X. Yuan, Q.L. Li, Q.M. Lin, Mar. Chem. 103 (2007) 122.
- [10] J.Z. Zhang, J. Chi, Environ. Sci. Technol. 36 (2002) 1048.
- [11] L.R. Adornato, E.A. Kaltenbacher, D.R. Greenhow, R.H. Byrne, Environ. Sci. Technol. 41 (2007) 4045.
- [12] L.J. Gimbert, P.M. Haygrath, P.J. Worsfold, Talanta 71 (2007) 1624.
- [13] M.S.A.C. Neves, M.R.S. Souto, I.V. Tóth, S.M.A. Victal, M.C. Drumond, A.O.S.S. Rangel, Talanta 77 (2008) 527.
- [14] P. Rimmelin, T. Mountin, Anal. Chim. Acta 548 (2005) 174.
- [15] L.J. Gimbert, P.J. Worsfold, Trends Anal. Chem. 26 (9) (2007) 914.
- [16] Q.P. Li, D.A. Hansell, Anal. Chim. Acta 611 (2008) 68.
- [17] J. Ruzicka, E.H. Hansen, Anal. Chim. Acta 78 (1975) 145.
- [18] J.M. Estela, V. Cerdà, Talanta 66 (2005) 307.
- [19] S. Motomizu, Z.H. Li, Talanta 66 (2005) 332.
- [20] K.S. Johnson, R.L. Petty, Anal. Chem. 54 (1982) 1185.
- [21] S. Auflitsch, D.M.W. Peat, I.D. McKelvie, P.J. Worsfold, Analyst 122 (1997) 1477.
- [22] M. Saowapha, I.D. McKelvie, M.R. Grace, M. Rayanakorn, K. Grudpan, J. Jakmunee, D. Nacapricha, Talanta 58 (2002) 1285.
- [23] G. Albenidín, M.P. Manuel-Vez, C. Moreno, M. García-Vargas, Talanta 60 (2003) 425.
- [24] Z.H. Xie, J.C. Zhao, Talanta 63 (2004) 339.
- [25] M. Grünhut, M.E. Palomeque, A.G. Lista, B.S.F. Band, Talanta 71 (2007) 1520.
- [26] W. Ruengsitagoon, Talanta 74 (2008) 1236.

- [27] J.Z. Zhang, C.J. Fischer, P.B. Ortner, *Talanta* 49 (1999) 293.
- [28] I.D. McKelvie, D.M.W. Peat, G.P. Matthews, P.J. Worsfold, *Anal. Chim. Acta* 351 (1997) 265.
- [29] H. Levine, J.J. Rowe, F.S. Grimaldi, *Anal. Chem.* 27 (2) (1955) 258.
- [30] K. Grasshoff, *Methods of Seawater Analysis*, Verlag Chemie, New York, 1976.
- [31] D.B. Johnson, P.J. Wangersky, *Limnol. Oceanogr.* 30 (1985) 966–971.
- [32] D.L. Johnson, *Environ. Sci. Technol.* 5 (1971) 411.
- [33] H.W. Chen, I.D. Brindel, X.C. Le, *Anal. Chem.* 64 (6) (1992) 667.
- [34] K.L. Linge, C.E. Oldham, *Anal. Chim. Acta* 450 (2001) 247.
- [35] C.F. Zimmermann, C.W. Keefe, *EPA Method 365* (1997) 5.



Review

Atmospheric pressure photoionization for coupling liquid-chromatography to mass spectrometry: A review

Ivano Marchi, Serge Rudaz, Jean-Luc Veuthey*

Laboratory of Pharmaceutical Analytical Chemistry, School of Pharmaceutical sciences, University of Geneva, University of Lausanne, Bd d'Yvoy 20, 1211 Geneva 4, Switzerland

ARTICLE INFO

Article history:

Received 23 June 2008

Received in revised form 17 November 2008

Accepted 20 November 2008

Available online 28 November 2008

Keywords:

Atmospheric pressure photoionization

APPI

Photoionization

PI

ABSTRACT

This review presents the state-of-the-art techniques that couple liquid chromatography (LC) and mass spectrometry (MS) via atmospheric pressure photoionization (APPI). The different ionization mechanisms are discussed as well as the influence of the mobile phase composition, the nature of the dopant, etc. A comparison with other ionization sources, such as electrospray ionization (ESI) and atmospheric pressure chemical ionization (APCI), is reported, and the combination of APPI with these sources is also discussed. Several applications, covering the time period of 2005–2008, for the analysis of drugs, lipids, natural compounds, pesticides, synthetic organics, petroleum derivatives, and other substances are presented.

© 2008 Elsevier B.V. All rights reserved.

Contents

1. Introduction	2
2. Theory	2
2.1. Reactional mechanisms	2
2.2. Light sources	3
2.3. Commercially available sources	3
3. LC solvents in APPI	3
3.1. Methanol	4
3.2. Acetonitrile	4
3.3. Water	4
4. Dopant-assisted APPI	5
4.1. Benzene	5
4.2. Acetone and toluene	5
4.2.1. Dopant-only situation	5
4.2.2. Analytes ionization	6
4.3. Anisole	7
4.4. Tetrahydrofuran and hexafluorobenzene	7
5. APPI in the negative mode	7
6. APPI versus ESI, APCI and dual sources	8
6.1. APPI compared to ESI	8
6.2. ESI/APPI dual mode	8

Abbreviations: AA, anion attachment; API, atmospheric pressure ionization; APCI, atmospheric pressure chemical ionization; APPI, atmospheric pressure photoionization; BGE, background electrolyte; CE, capillary electrophoresis; CI, chemical ionization; CX, charge exchange; CZE, capillary zone electrophoresis; EA, electron affinity; EC, electron capture; EI, electron ionization; ESI, electrospray ionization; FID, flame ionization detector; IE, ionization energy; LC, liquid chromatography; LOD, limit of detection; LOQ, limit of quantification; MEKC, micellar electrokinetic chromatography; MEEKC, microemulsion electrokinetic chromatography; MS, mass spectrometry; PA, proton affinity; PAH, polycyclic aromatic hydrocarbon; PI, photoionization; PID, photoionization detector; SE, solvation energy; SDS, sodium dodecyl sulfate; S/N, signal to noise; VUV, vacuum-ultraviolet.

* Corresponding author. Tel.: +41 22 379 63 36; fax: +41 22 379 68 08.

E-mail address: jean-luc.veuthey@unige.ch (J.-L. Veuthey).

6.3.	APPI compared to APCI	8
6.4.	APCI/APPI dual mode	9
7.	Matrix effects	9
8.	CE-APPI/MS	9
9.	Applications	11
9.1.	Drugs	11
9.2.	Lipids	12
9.3.	Natural compounds	15
9.4.	Pesticides	15
9.5.	Synthetic organics	15
9.6.	Petroleum derivatives	16
10.	Other applications	16
11.	Conclusion	16
	References	17

1. Introduction

Due to its universality, selectivity and sensitivity, mass spectrometry (MS) is considered the gold standard detector for liquid chromatography (LC). The first coupling of LC to MS was performed in the 1970s but became widely used only with the appearance of atmospheric pressure ionization (API) sources in the early 1990s. Among these interfaces, electrospray ionization (ESI) and atmospheric pressure chemical ionization (APCI) are currently the most widely employed API sources. ESI is particularly adapted to the analysis of polar molecules, and its ionization occurs in the liquid phase, while APCI allows the ionization of less polar molecules in the gas phase. Atmospheric pressure photoionization (APPI) is the last soft ionization technique able to ionize those molecules that are poorly amenable to ESI and APCI [1–3].

Photoionization (PI) was already used at low pressure as a detection method (PID) in gas chromatography (GC) in the mid-1970s. PID provided better sensitivity for apolar compounds (benzene), than a flame ionization detector (FID), and a dynamic range greater than 10^7 [4–7]. During the same decade, PI was also used as a detection method in LC, and the early studies in LC-PID [8] presented a similar set-up to the one employed in GC-PID. However, only a few applications of these techniques were published [9–11].

The use of PI at atmospheric pressure was first presented by Baim et al. in 1983 where it was coupled with ion mobility spectrometry (IMS) [12]. It was implemented with the same vacuum-ultraviolet (VUV) lamp used in GC [1]. Various examples of APPI coupled to IMS were proposed [12–15], and other applications have been recently published [16–18]. Moreover, in 1991, one patent reported the coupling of PI at atmospheric pressure with MS [19]. This study demonstrated the possibility of a direct infusion of analytes operating with helium as a carrier gas. Finally, the first studies using APPI as an ionization source for coupling LC to MS were published in 2000 by Robb et al. [1] and Syage et al. [20] (Table 1). Thanks to these results, two interfaces are currently commercially available, namely, the PhotoSpray and the PhotoMate sources (see Section 2.3).

The number of publications related to the use of PI has rapidly grown since its implementation at atmospheric pressure. Indeed,

Table 1
Historical overview of PI.

Subject	1st Publication	Authors
GC-PID	Middle 70s	Driscoll et al.
LC-PID	Middle 70s	Schermund et al.
APPI-IMS	1983	Baim et al.
APPI-MS	1991	Revel'skii et al.
LC-APPI-MS	2000	Robb et al. and Syage et al.

the use of PI at reduced pressure yields only poor ionization due to the low sample density in the ionizing region [21].

The objective of this review is to present the state-of-the-art of APPI and its recent developments. Indeed, only applications from papers published since 2005 are considered, as two reviews on APPI concerning the time periods 2000–2002 [22] and 2003–2004 [23] were previously published.

2. Theory

2.1. Reactional mechanisms

PI is based on the interaction of a photon beam produced by a discharge lamp with the vapors formed by the nebulization of a liquid solution. PI occurs in several steps. First, the absorption of a photon ($E = h\nu$) by a molecule (M) leads to an electronically excited molecule:



If the ionization energy (IE) of the analyte is lower than $h\nu$, the molecule releases an energetic electron ($E_{e^-}(\max) = h\nu - IE_M$) leading to the corresponding odd-electron cation (a phenomenon typically occurring with molecules with conjugated double bonds, such as aromatic compounds [24]):



At atmospheric pressure, the ion's free pathway is 65 nm [24]. Thus, molecular ions ($M^{\bullet+}$) with an unpaired electron show a tendency to react in collisional environments [2]. Moreover, molecules with low IE and/or high gas phase basicity, called proton affinity (PA), tend to dominate the positive ion spectra due to their high collision frequency [25].

However, when the $IE > h\nu$, M^* may undergo a de-excitation process, such as photodissociation (3), photon emission (4) or collisional quenching (5) with a non-excited molecule (C):

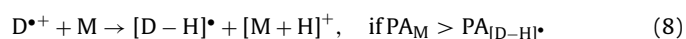
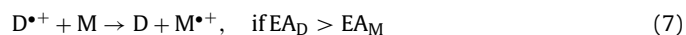


In such cases, the use of a preferentially ionized substance, called a dopant (D), has been proposed to promote the ionization of M:



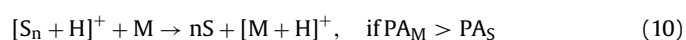
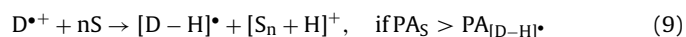
The dopant is added in large quantities compared to the analytes, and it acts as an intermediate between the photons and the analytes. The dopant must therefore produce photoions with a high recombination energy and/or a low PA. The ionization mechanism

depends on the PA values of the involved molecules (dopant, solvent, analyte) and on their capacity to capture an electron in the gas phase, called electron affinity (EA) [1]. Two mechanisms can occur, namely charge transfer (7) and proton transfer (8):



However, a dopant molecule can react only once. The dopant can also be used to improve the ionization yield of the analyte (even if $IE < h\nu$) because photons cannot penetrate deeply into the dense mixture of gases [26] (the photon beam produced by a krypton lamp loses 50% of its intensity each 1.5 mm [18]). Therefore, the probability for direct ionization of analytes, present in small proportion compared to solvent molecules, is very low.

Moreover, in the case of a chromatographic separation, solvent molecules are also present and can react according to the following equations:



It has to be noted that APPI is operated in the gas-phase because the IE values are generally lower in the liquid phase, making it impossible to discriminate between the analyte and solvent molecules (i.e., 6.1 eV in the liquid-phase versus 12.6 eV in the gas-phase for water [9]).

2.2. Light sources

The greater part of the studies conducted in APPI were performed with a krypton lamp, which can produce photons of 10.03 and 10.64 eV in a 4:1 ratio [27,28]. Krypton was selected mainly because most analytes have lower IE values than the photon's energy, while commonly used solvents and gases present in the source (O_2 , N_2 , etc.) have higher values. It should be noted that, in general, the IE tends to decrease with the size of the organic molecules (see anthracene, naphthalene and benzene series, Table 2) [3].

Besides krypton, xenon and argon were also used. Xenon was employed by Locke et al. in the early years of PI [11], and it presents the best penetration depth in the ionizing region but is less adapted to efficient PI due to the low energy of produced photons. Argon produces more energetic photons than krypton (11.7 eV), which are absorbed by the solvent only after a few millimeters. Thus, argon lamps give higher intensities (100 times) in the solvent ions and produce more abundant molecular ions than krypton lamps [28]. Regarding the ionization efficiency of the analytes as a function of the flow rate, krypton lamps produce a better S/N ratio at a low solvent flow rate, whereas argon lamps are better at higher solvent flow rates.

2.3. Commercially available sources

Only two APPI sources are commercially available. The first was based on the prototype developed by Robb et al. in 2000 (Fig. 1) and is available under the PhotoSpray trademark name. The second source is called PhotoMate and differs by its orthogonal geometry (Fig. 2). Both sources incorporate magnesium fluoride (MgF_2) lamp windows to ensure the photon's transmission [1].

The main difference between both sources stands in the compulsory presence of a dopant for the PhotoSpray source. With the latter, the offset potential (the electrical potential applied between the lamp and the mounting bracket) has a tremendous effect on the method's sensitivity because the ion production is low (10 nA of ion

Table 2

Gas-phase IE and PA values of commonly used solvents and compounds from [22].

Compound	IE (eV)	PA (kJ mol ⁻¹)
Nitrogen	15.58	493.8 ^a
Water	12.62	691.0 ^b
Acetonitrile	12.20	779.2 ^c
Oxygen	12.07	421.0 ^b
Ar: 11.7		
Chloroform	11.37 ^c	n.a.
Methanol	10.84	754.3 ^c
Acetic acid	10.65 ^b	783.7 ^b
Kr: 10.6		
Isopropanol	10.17	793.0 ^a
Hexane	10.13	n.a.
Ammonia	10.07 ^b	853.6 ^b
Kr: 10.0		
Heptane	9.93	n.a.
Isooctane	9.80	n.a.
Methanol dimer	9.74 ^d	899.1 ^d
Acetone	9.70	812.0 ^c
Tetrahydrofuran	9.4 ^a	822.1 ^a
Pyridine	9.26	930.0 ^a
Testosterone	9.2 ^c	880.0 ^c
Benzene	9.24	750.4 ^c
Furan	8.88	803.4 ^a
Toluene	8.83	784.0 ^c
Xe: 8.4		
Anisole	8.2 ^c	839.6 ^c
Naphthalene	8.14 ^c	802.9 ^c
Anthracene	8.10 ^c	877.3 ^c
Acridine	7.8 ^c	972.6 ^c
Triethylamine	7.53	981.8 ^a
Benzyl radical	7.2 ^b	831.4 ^b

n.a.: not available.

^a <http://webbook.nist.gov/chemistry/>.

^b [31].

^c [24].

^d [139].

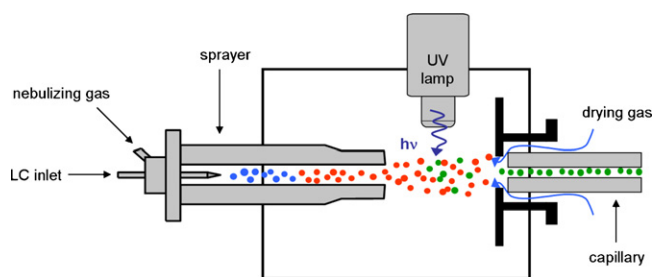


Fig. 1. Schematic representation of the APPI prototype source used by Robb et al. [1].

current measured at the MS curtain plate versus 2.5 μ A in APCI) [1]. This phenomenon is not observed on the PhotoMate source since the lamp ignition is different. Finally, the latter was also found to be able, under particular conditions, to ionize highly polar compounds (see Section 9).

3. LC solvents in APPI

Solvents commonly used in reversed-phase liquid chromatography (RPLC) have been studied regarding their influence on the ionization process. This section is dedicated to the most commonly used solvents in RPLC, namely, methanol, acetonitrile and water. The influence of buffers will be discussed in Section 8.

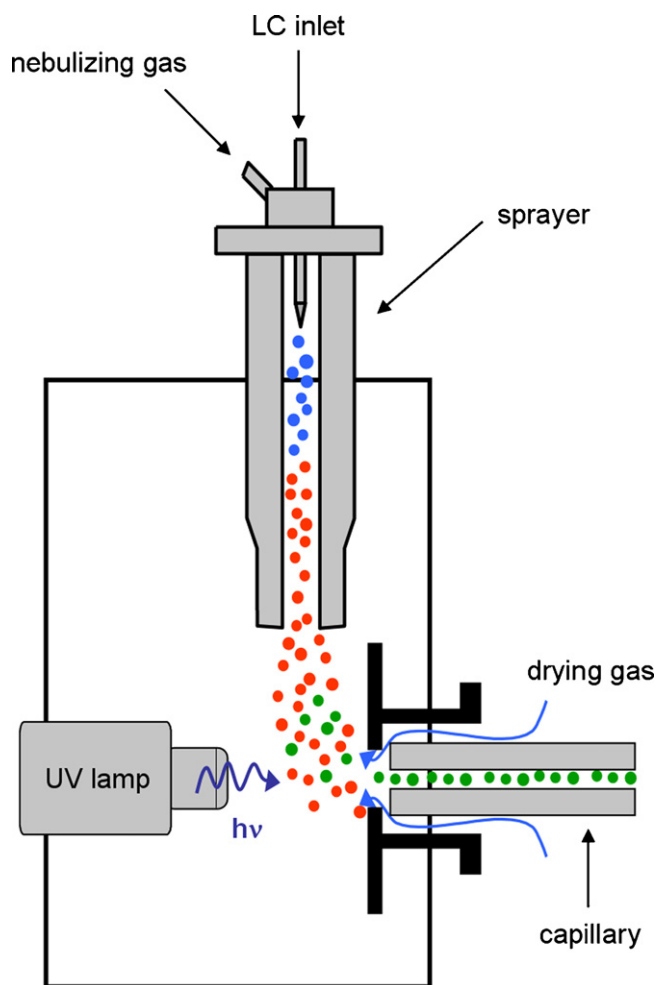


Fig. 2. Schematic representation of the PhotoMate source inspired from Agilent documents.

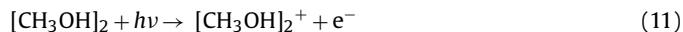
3.1. Methanol

In spite of its low IE (see Table 2), the use of methanol in aqueous mobile phases provided a 2- or 3-fold increase in the production of molecular ions $[M]^{*+}$ of naphthalene and diphenyl sulfide in comparison to water/acetonitrile mixtures, using the source developed by Robb et al. However, almost no influence of solvent's nature was observed on protonated molecules $[M+H]^+$ of carbamazepine and acridine [1]. This observation was recently confirmed with the PhotoMate ionization of PAH, providing much higher sensitivities for the molecular ions in pure methanol than in pure acetonitrile [28].

Furthermore, methanol was found to produce clusters in the gas phase [29,30], which concentration was correlated to the production of protonated analytes. Indeed, the influence of charged methanol clusters on the ionization of PAH was investigated [28]. Production of $[PAH+H]^+$ was maximum in the 300–400 $\mu\text{L min}^{-1}$ range, corresponding to the highest concentration of the protonated methanol dimer. A proton transfer from the protonated methanol dimer to a PAH molecule (due to the PA value of the protonated methanol dimer generally lower than that of PAH) was suggested. This mechanism is similar to the signal enhancement obtained with a dopant [28].

A mathematical model was also proposed for calculating the proportion of methanol clusters in the gas region. It was estimated that, at 50 $\mu\text{L min}^{-1}$, the vapor contained 99.98% of the methanol monomer (IE = 10.84 eV) and 0.02% of the dimer (IE = 9.74 eV) [28]. When using a krypton lamp, only the dimer could be ionized. This

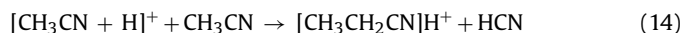
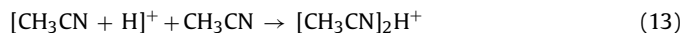
occurred through dissociative ionization:



The cluster size was found to depend on the applied cone voltage using the PhotoSpray. At low values (<10V), the dimer and the trimer were dominant, whereas, at higher voltages, both clusters were accelerated during their introduction in the low vacuum MS region, leading to their fragmentation into protonated monomer and dimethyl ether ($[\text{CH}_3]_2\text{OH}^+$) ions [31]. Besides, formation of large protonated clusters was favored by the large binding energy between methanol and a protonated cluster, $\text{CH}_3\text{OH} + [\text{CH}_3\text{OH}]_n\text{H}^+$ ($-33 \text{ kcal mol}^{-1}$ for $n=1$, $-22 \text{ kcal mol}^{-1}$ for $n=2$ and $-16 \text{ kcal mol}^{-1}$ for $n=3$) [32]. In the presence of water in the mobile phase, clusters such as $[\text{CH}_3\text{OH}]_n\text{-H}_2\text{O}$ were also formed, and their occurrence increased as the water/methanol ratio approached one. Enlargement of such clusters by the addition of a methanol molecule was thermodynamically favored ($-24.6 \text{ kcal mol}^{-1}$) [33].

3.2. Acetonitrile

In comparison with methanol, acetonitrile ionization with the PhotoMate was found to be lower, probably due to its higher IE value (12.2 eV) [28]. Robb et al. also observed that proton transfer was almost not affected by the solvent's nature, but charge transfer was lowered by a factor of 2–3 in acetonitrile [1]. In order to investigate ionization mechanisms in presence of acetonitrile, Marotta et al. observed that the latter participated to the formation of the $[M+H]^+$ ions of furcoumarins [21,34]. Indeed, in the presence of CD_3CN , protonated molecules were replaced by $[M+D]^+$ ions, proving unambiguously the role of acetonitrile in the proton transfer mechanism. An irradiated molecule of acetonitrile gave various structures reported in Fig. 3a [21,34]. For various reasons, structure 3 appeared to be the most stable isomer. With a calculated IE value of 9.5 eV, structure 3 could be ionized to the corresponding odd-electron ion (Fig. 3b), which might then sequentially react with neutral acetonitrile and water. Finally, the charged cluster could ionize the analytes by proton transfer (Fig. 3c) [21,34]. However, two consecutive bimolecular reactions with continuous and incoherent lights sources (such as krypton or argon lamps) were deemed unlikely by Short et al. [28]. According to their results, the $[M]^{*+}$ ions produced by direct ionization can abstract a hydrogen atom from acetonitrile. This hypothesis relied on the higher production of protonated acetonitrile clusters with a krypton lamp than with an argon lamp. Acetonitrile was also found in the source atmosphere in a variety of forms, mainly the protonated monomer, dimer and propionitrile ions ($[\text{CH}_3\text{CH}_2\text{CN}]\text{H}^+$). The cone voltage values seemed to have an influence on the cluster populations. Indeed, the dimer was essentially found at low cone voltages (13), while the propionitrile ion was present at higher values (14):



In presence of water, acetonitrile formed homologous clusters to those observed with water/methanol (see Section 3.1). However, ionization of the analytes was higher in pure acetonitrile than in water/acetonitrile mixtures, independently on the lamp (Xe, Kr, and Ar) [28].

3.3. Water

The influence of water on the PI was not widely investigated, and no mechanistic studies are available. Nevertheless,

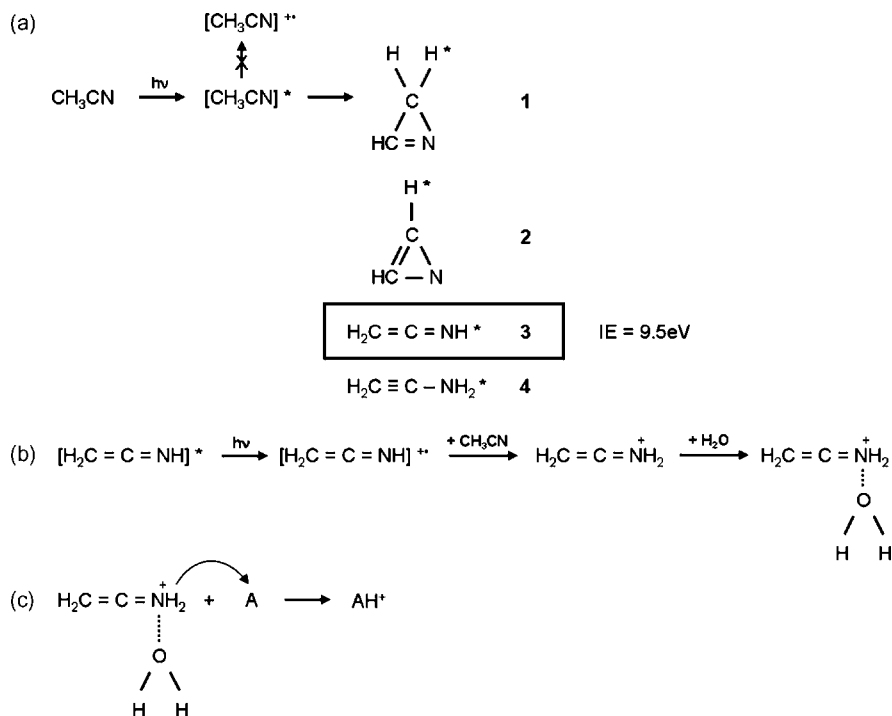


Fig. 3. Acetonitrile photoisomerization (a) followed by PI (b). Ionization by proton transfer from protonated acetonitrile to an analyte molecule (c).

Giuliani et al. studied the ionization of hexamethonium bromide salt (a bisquaternary salt) in aqueous solutions. It appeared that only minor in-source fragmentations occurred in the APPI conditions, namely, dequaternization (*i.e.*, loss of a single methyl group) and charge separation from the two major precursors (M^{2+} and $[\text{M}+\text{Br}]^+$). Moreover, fragmentation was greatly enhanced in presence of a dopant (see Section 4.2) [35]. Rauha et al. investigated the effect of various solvents on the ionization of flavonoids by proton transfer with the PhotoSpray and the highest responses were observed in pure water with toluene as a dopant [36].

As a conclusion, it is recommended to utilize as far as possible methanol rather than acetonitrile when compounds ionized *via* charge transfer are analyzed. However, in the case of analytes ionized by proton transfer, the solvent has only a small influence and both acetonitrile and methanol can be employed. Indeed, proton transfer is often attributable to the presence of protonated clusters of solvent molecules which reactivity (related to their PA) seems to be comparable for both solvents. Water favors proton transfer, probably due to its low PA (691 kJ mol^{-1} , see Table 2), inferior to anthracene ($877.3 \text{ kJ mol}^{-1}$) and naphthalene ($802.9 \text{ kJ mol}^{-1}$). However, no information was available for charge transfer.

4. Dopant-assisted APPI

The use of a dopant was already applied in 1994 with acetone and in 1997 with benzene, toluene and xylene for PI-IMS ionization enhancement. Benzene was also employed in 1991 as a charge transfer media for improving the chemical ionization in APCI [37]. Regarding LC-APPI-MS, acetone [38–61] and toluene [26,27,51,54,55,62–104] have been largely used, studied and compared, whereas anisole [24,35,49,51,55,59,60,77,78], benzene [66,105], hexafluorobenzene [35,59] and THF [53] have been employed to a lesser extent. The use of dopants in the negative mode is presented in Section 5.

4.1. Benzene

The use of benzene as dopant mainly leads to the formation of protonated analytes, while the production of molecular ions is less efficient. In order to understand reactional mechanisms involved, Tubaro et al. investigated the ionization of benzene and toluene with the PhotoMate source [105]. The formation of benzene $[\text{M}]^+$ ions was found to be related to its partial pressure in the source. At low values, only molecular ions of benzene were formed, while, with increasing partial pressures, the $[\text{M}]^+$ ions almost disappeared, and six new ions emerged ($m/z=94, 156, 170, 171, 186$ and 187), implicating oxygen present in the source (Fig. 4a and b). The produced phenol radical cation reacted with a neutral benzene molecule leading to the production of ions at $m/z=170$ and $m/z=171$ (Fig. 4c). Analytes ionization was therefore attributed to a proton transfer from ion $m/z=171$ and possibly to a charge transfer from its radical cation ($m/z=170$). As the phenol radical cation participates to the reactional mechanisms, the addition of large quantities of phenol to benzene was tested. It resulted that the phenol radical cation ($m/z=94$) reacted with a neutral phenol molecule to produce ions at $m/z=186$ and $m/z=187$ (Fig. 4d), also able to transfer a charge ($m/z=186$) or a proton ($m/z=187$). It seems therefore that phenol could also be used as a dopant.

4.2. Acetone and toluene

In order to explain ionization of analytes assisted with acetone and toluene as dopants, investigations of reactional pathways are divided into two sections. Ionization mechanisms of both dopants are first described in Section 4.2.1 whereas Section 4.2.2 is dedicated to the reactional pathways between these dopant ions and the analytes.

4.2.1. Dopant-only situation

Robb et al. already hypothesized in 2000 that dopant ionization may result in several reactions. The predominant mechanism

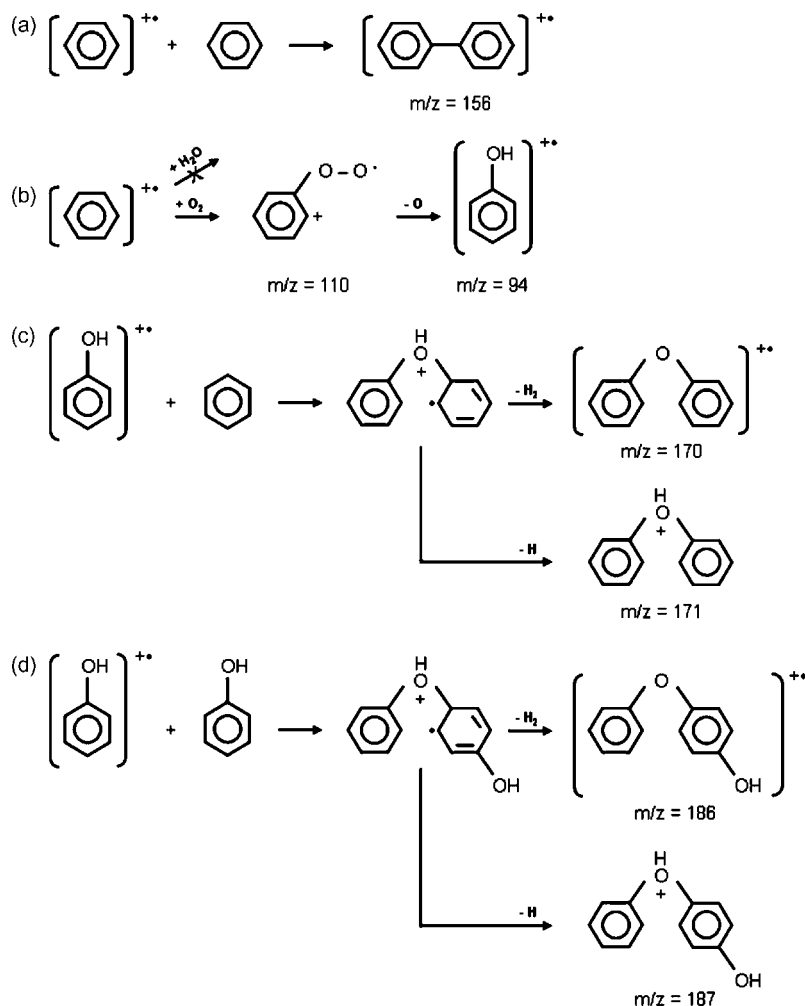


Fig. 4. Chemical reactions leading to the formation of the six ions detected at high partial pressure of benzene. Formation of $m/z = 156$ (a), $m/z = 94$ (b), $m/z = 186$ and 187 (c) when phenol is added in the source and $m/z = 170$ and 171 (d) with no phenol adjunction.

was identified as the reaction between dopant ions and solvent molecules. The solvent, once charged, ionized in turn the analytes either by proton or charge transfer (depending on the analytes' PA and IE values). This early suggestion was partially confirmed by Tubaro et al. [105] regarding the ionization mechanisms of toluene using the orthogonal commercially available source (PhotoMate). Reactions similar to those presented in Section 4.1 with benzene were observed with toluene. The intermediate reactive ion (homologous to phenol with benzene) was cresol, already observed in a previous study [31]. Nevertheless, more complex ions were produced at higher m/z values with toluene than with benzene, which involved a large number of reactional pathways, thereby complicating the elucidation of the reaction mechanisms. Furthermore, Robb and Blades showed that the production of the toluene photoions using the PhotoSpray source was directly proportional to the dopant flow and/or the lamp current [27,80]. From 0.2 to 2.0 mA, the signal intensity of the toluene ions was even found to increase by 300% [27]. However, the production of toluene ions was inversely proportional to the solvent flow rate, the key factor for dopant ion production being the dopant/solvent ratio.

4.2.2. Analytes ionization

In the first study dedicated to LC–APPI–MS with the prototype linear source, Robb et al. observed the influence of the dopant nature on the ionization of high PA (carbamazepine and acridine) and low PA (naphthalene and diphenyl sulfide) compounds [1].

With toluene, proton transfer leading to $[M+H]^+$ ions was the most efficient ionization mechanism [24,31]. Analytes with high PA presented signals about 100 times higher than those obtained from the low PA molecules. Acetone could ionize analytes only through proton transfer and was less efficient than toluene, regardless the source [1,2].

Ionization of naphthalenes with toluene was also studied by Kaupilla et al. with the PhotoSpray [31]. In presence of water, hexane or chloroform, toluene was ionized only in $[\text{C}_7\text{H}_8]^+{}^{++}$ because PA values of the solvents are sufficiently low (*i.e.*, no proton transfer possible from the dopant to the solvent). Abundant ionization of the analytes occurred by charge transfer only with these solvents. Nevertheless, with acetonitrile or methanol, clusters of both solvents possessing higher PA values than toluene were found to be protonated by $[\text{C}_7\text{H}_8]^+{}^{++}$, leading to their disappearance. As reported in Section 3.2, methanol formed monomers, dimers and trimers also in presence of toluene. The monomer formation was favored by increasing the vaporizer temperature from 200 to 500 °C, indicating that the latter had an effect on the APPI process. Besides, it was shown that both proton and charge transfer were not the unique ionization pathways with toluene. Indeed, in the presence of chloroform as solvent, $[\text{CHCl}_2]^+$ and $[\text{C}_7\text{H}_7\text{CHCl}]^+$ were formed, implicating chloroform in the ionization mechanisms with toluene [31].

Besides the influence of the vaporizer temperature, other factors such as the dopant proportion, the lamp current and the solvent

flow rate presented an incidence on the ionization efficiency of the analytes. For example, with the PhotoSpray, signals reached a maximum at 10% of added dopant. Regarding the lamp current, 0.8 mA was the value allowing the highest efficiency whatever the source [2,80]. Considering the solvent flow, as in the dopant-only situation, the ionization of acridine and 9-methylanthracene diminished with both sources as a function of the solvent flow rate. Ionization was higher between 50 and 100 $\mu\text{L min}^{-1}$ [3,26]. Kauppila et al. showed that sensitivity loss at high solvent flow rates was predominant for charge transfer, whatever the source, but had also an deleterious effect on proton transfer [26]. This decrease in $[\text{M}+\text{H}]^+$ ions at high solvent flow rate was attributed to in-source formation of solvent–solvent or dopant–solvent clusters when using polar solvents such as methanol, acetonitrile or water (see also Sections 3.1 and 3.2). Different sizes of clusters were observed, and the population of each cluster size was dependent on the temperature of the vaporizer, on the strength of the solvent–dopant bonds and especially on the solvent concentration, indicating that high solvent flow rates promoted the formation of large clusters. The loss and the gain of solvent molecules in the clusters were found to be in equilibrium. Ionization of low PA analytes by proton transfer was not efficient since large, protonated clusters were stabilized by a high solvation energy (SE). Proton transfer was therefore almost inefficient at high solvent flow rates. These large, protonated clusters can undergo two neutralization mechanisms. Moreover, the effect of the solvent flow rate on the ionization appeared to be compound dependent. For example, acridine (relatively high PA and SE) possessed a minor loss in sensitivity with an increase in the solvent flow rate compared with 9-methylanthracene (lower PA and SE) under the same conditions [31].

Furthermore, Robb and Blades showed that DA–APPI could be used for the simultaneous ionization of polar and non-polar compounds [104]. Indeed, by using toluene as a dopant and by applying a low solvent flow rate, toluene photoions remained in the source and ionized the non-polar compounds by charge transfer, while the polar molecules were preferentially ionized by the protonated solvent molecules *via* proton transfer. For example, by decreasing the mobile phase (water/methanol 1:1) flow rate from 200 to 50 $\mu\text{L min}^{-1}$, ionization by charge exchange increased by a factor of 10 [104].

However, the use of a dopant in APPI has also been shown to have, in some cases, a deleterious effect on the ionization performance. Hanold et al. observed that, in the case of the ionization of fat-soluble vitamins (A, D₂, E and K₁) with the PhotoMate source, toluene could enhanced the background noise, leading to a decrease of the S/N ratio. However, both the analyte signal and the background noise were enhanced with acetone [2].

Finally, two studies compared the benefit obtained by either single dopants or mixtures of dopants. Itoh et al. [60] evaluated the use of acetone, toluene, anisole and six mixtures of toluene and anisole on the ionization of PAH with an APPI-2010 source (Shimadzu), and found that a 99.5:0.5 toluene/anisole mixture gave the best sensitivity (around 4–40 times greater than that found using pure toluene). Himmelsbach et al. also investigated the efficiency of a 1:1 toluene/acetone mixture for the ionization of various drugs [52]. This mixture did not increase signals compared to either toluene or acetone alone. The advantage of dopant mixtures largely depends on the analytes, the dopant proportions and their natures.

4.3. Anisole

To overcome the problem of the sensitivity loss in presence of acetonitrile whatever the dopant, Kauppila et al. proposed anisole as an efficient dopant for charge transfer using the PhotoSpray source [24]. It was observed that anisole mostly promoted the formation of molecular ions, whereas toluene generated several

protonated molecules. The analytes' ionization mechanisms mainly depended on the nature of the molecules. Indeed, carbamazepine, previously used by Robb et al. [1], exhibited both $[\text{M}+\text{H}]^+$ and $[\text{2M}+\text{H}]^+$ ions when infused in water/acetonitrile with toluene (in agreement with the study presented in Section 4.2 [21,34]). Similar observations were made with luteolin and catechin using toluene, whereas $[\text{M}+\text{H}]^+$ and $[\text{2M}+\text{H}]^+$ ions were replaced by $[\text{M}]^{*+}$ ions with anisole.

Globally, intensities of the $[\text{M}+\text{H}]^+$ ions obtained with toluene were comparable to $[\text{M}]^{*+}$ intensities achieved with anisole. For compounds with low PA and IE that are still ionized with toluene [1], such as 2-naphthol, anthracene and diphenyl sulfide, anisole appeared to be more efficient and produced more intense signals (*ca.* 100 times) [24]. However, charge exchange became ineffective for compounds with higher IE values than anisole. Testosterone was for example poorly ionized due to its high IE value.

4.4. Tetrahydrofuran and hexafluorobenzene

Only two papers related to the use of other dopant molecules such as tetrahydrofuran [36] and hexafluorobenzene [35]. However, no significant performance enhancement was observed. The ionization of flavonoids with tetrahydrofuran decreased by a factor of two relative to the use of toluene [36], and hexafluorobenzene was shown to provide similar signal intensities than both toluene and anisole for the ionization of the hexamethonium bromide salt in aqueous solutions [35].

As a conclusion, toluene was found to be the most effective dopant for proton transfer while charge transfer was less favored. In the latter case, anisole was the most helpful dopant and therefore complementary to toluene. Other dopants were found to be less useful for various reasons. Indeed, acetone promoted only proton transfer, but less efficiently than toluene. Benzene presented performance similar to toluene, but due to health issues, its use is not recommended and, finally, tetrahydrofuran and hexafluorobenzene did not present interesting properties.

5. APPI in the negative mode

Only a small number of papers have investigated negative ionization in APPI [2,31,36,64,94,106], where three major mechanisms [31], namely charge exchange (CX (15)), electron capture (EC (16)) and proton transfer (analyte deprotonation (17)) were evidenced:



Recently, Song et al. discussed another ionization mechanism, anion attachment (AA), as a potential chemical reaction for molecules not ionized by EC, CX or proton transfer. AA results in hydrogen bonding, dipole attraction and polarization [94]. With the PhotoMate, Basso et al. showed in 2003 that negative ionization was mainly due to the generation of slow electrons produced by the irradiated, stainless steel surface in front of the krypton lamp [106]. This mechanism was investigated 1 year later by Hanold et al. [2]. The ionization almost disappeared when the metallic surface was covered with a dielectric plate in order to avoid the production of slow electrons with an energy around 3 eV ($E_{\text{lamp}} (10.6 \text{ eV}) - I\text{E}_{\text{Fe}} (7.7 \text{ eV}) = 2.9 \text{ eV}$). This was confirmed with the replacement of the dielectric surface by glass, thereby maintaining the electric fields in the source.

Negative APPI generated less background noise than the positive mode [36] and was found to ionize a wider range of molecules than other negative API sources [94]. On the other hand, Kauppila et al.

observed the ionization of only 3 of 7 naphthalenes [31]. The addition of toluene as a dopant produced a tremendous signal increase, indicating that the ionization was initiated by thermal electrons originating from toluene ions [2,31].

Oxidation products were also observed to be in abundance, leading to the conclusion that oxygen present in the source plays an important role. As an example, oxygen (O_2), with an EA of 0.45 eV, was ionized in $O_2^{\bullet-}$ by the capture of thermal electrons and subsequently ionized 1,4-naphthoquinone (EA, 1.8 eV) *via* various reactions due to the difference in their EA values. These oxidation products were more abundant than the expected $[M]^{\bullet-}$, particularly in presence of methanol. For 2-naphthol ionization, $[M-H]^-$ was probably formed *via* proton transfer from 2-naphthol (possessing an acidic group) to $O_2^{\bullet-}$ (which is a strong base in the gas-phase [107]). These oxidation products were not associated with the dopant proportion or the applied voltage between the source block and the curtain plate, and they obviously originated from trace oxygen in the ionization source. The latter was searched for, but neither oxygen dissolved in the solvents nor oxygen originating from the solvent molecules breaking down in the source was responsible for the formation of the oxidation products. The influence of the nebulizing gas was therefore evaluated, and the presence of a low quantity of oxygen (1 ppm) could induce oxidation [31,64]. Kauppila et al. evaluated its influence by the use of high purity nitrogen (99.999%) or by purified air as nebulizing gases with the PhotoSpray. It was found that, with high quality nitrogen, $[M]^{\bullet-}$ and $[M-H+O]^-$ ions were in a relative abundance of 100% and 81%, respectively, whereas with air, $[M]^{\bullet-}$ decreased to 48%, and $[M-H+O]^-$ increased to 100%.

The addition of an acid (acetic) or a base (ammonium hydroxide) to the mobile phase hampered the formation of both 1,4-naphthoquinone and 2-naphthol $[M]^{\bullet-}$ ions; furthermore, it decreased the abundance of the oxidation products, which was probably due to the consumption of thermal electrons by H^+ to form H_2 and/or by NH_4^+ to form NH_3 and H_2 [31,36,94]. Nevertheless, Rauha et al. observed higher signal intensities with ammonium hydroxide, in the analysis of glycosides (flavonoids) [36]. The addition of a salt (ammonium acetate) inhibited the formation of $[M]^{\bullet-}$ without influencing the oxidation products [31,36]. For compounds with gas-phase acidity higher than $O_2^{\bullet-}$ and lower than toluene, Song et al. showed that the presence of di-*tert*-butyl peroxide improved analyte deprotonation *via* the formation of a basic anion generated from toluene, $C_6H_5CH_2^-$ [94]. Due to the capture of thermal electrons, ionization was suppressed for naphthalenes with low, gas-phase acidity by halogenated solvents (chloroform and TFA). For naphthalenes with high gas-phase acidity, $[M-H]^-$ ions were observed [64].

6. APPI versus ESI, APCI and dual sources

APPI appears to be a good alternative to ESI and APCI for the coupling of low flow rate separation techniques ($<50 \mu\text{L min}^{-1}$, see Section 6.3) such as CE and capillary LC, due to the lower concentration of the solvent vapor in the ion source. Furthermore, APPI is generally considered to be a compatible ionization technique for apolar compounds. In fact, APPI was found by various authors to be more complementary to ESI than APCI, due to its ability to ionize molecules with lower polarity than can be ionized in APCI.

While several authors have directly compared the performance of the various available API sources on a variety of analytical compounds, others have tried to implement a dual source strategy. The latter principle was first reported in 1996 [108] with the electron ionization/chemical ionization (EI/CI) for GC-MS applications. Using a dual-source may expand the range of ionizable molecules during a single chromatographic run. The dual mode generally gave

lower sensitivities and better repeatability than running each ionization mode separately [3].

6.1. APPI compared to ESI

APPI and ESI are relatively orthogonal ionization sources with regards to the range of tested compounds [3]. Therefore, depending on the analytes and the separation conditions, APPI and ESI can either be complementary or one can be more appropriate than the other. For example, APPI was more efficient for olive oil identification in ionizing mono- and diacylglycerols while ESI was better for triacylglycerols [93]. For the analysis of unconjugated hormones in river water, APPI showed a better sensitivity than ESI, but the opposite situation was encountered for conjugated hormones [86]. In numerous cases, APPI was more sensitive than ESI, as in the analysis of aflatoxin M1 in milk [109], trifluorobenzoic acid [2], lipids (with cleaner MS spectra) [110], amininopyrene and dinitropyrene [74] and estrone (steroid) [3]. In this case, the ionization intensity was more than one order of magnitude higher in APPI. Ionization performance was also compared *via* an analysis of 201 drugs with a wide range of chemistry, and APPI ionized 98% of the compounds of the set whereas ESI only produced ions in 91% of the cases [81]. APPI also provided a wider, linear dynamic range (3–4 orders of magnitude versus 2–3 for ESI) [68]. Finally, ESI was more sensitive for the analysis of cyclosporin A in rat plasma [73], anabolic steroids (even using a buffered mobile phase) [42], and flavonoids [36], and it probably remains the most adaptable source for the ionization of charged compounds, such as apomorphine, dobutamine, and entacapone phase II thermolabile metabolites in biological samples. Indeed, ESI allowed for the detection of 22 molecules, whereas APPI only helped to detect 14, which was due to the lower probe temperatures applied in ESI [66].

6.2. ESI/APPI dual mode

Progesterone and testosterone were used to evaluate the ionization efficiency of the ESI/APPI dual source [3]. In a single ESI, only low intensity signals of multiple ions were observed, which disappeared in the dual mode, while abundant protonated molecules were formed in both the single and the dual-mode APPI. The ESI/APPI combination was shown to be very efficient in the simultaneous analysis of testosterone and horse myoglobin. ESI was more effective in protein (myoglobin) ionization, whereas APPI was found to be particularly adapted for testosterone. Similar results were described in the analysis of melittin and 2,7-dibromo-9,9-bis(2-ethylhexyl)fluorine [3]. Therefore, the dual ESI/APPI interface would be very useful, for example, in clinical diagnostics for the concomitant determination of pharmaceutical molecules with various polarity and protein and drug/macromolecule interactions. This concept was recently explored by Short and Syage [111], who have published a study using an electrospray photo-ionization (ESPI) source for the simultaneous analysis of low polarity (pharmaceutical, hormone or sterol) and polar compounds (cyclodextrin). The ESPI source provided several advantages over the separate use of both modes, including better performance at low flow-rates. Data acquisition was performed by alternating the ESI and APPI modes. In comparison to electrospray chemical ionization (ESCI), ESPI possessed better S/N ratios for all of the studied complexes of cyclodextrin (naproxen, flurbiprofen, nimesulide, progesterone and cholesterol).

6.3. APPI compared to APCI

One important difference between APPI and APCI concerns their ionization efficiency versus the mobile phase flow rate. APPI worked properly below $50 \mu\text{L min}^{-1}$, while better results are

obtained with APCI for larger values ($>1 \text{ mL min}^{-1}$, for mechanistic considerations, see Sections 2 and 4). Despite APPI is commonly considered as a mass flow sensitive detector, it behaves like a concentration flow sensitive detector at flow rates below $50 \mu\text{L min}^{-1}$. The lower sensitivity of APPI at high flow rates could not be compensated by an increase of either the dopant flow or the discharge lamp current [80].

For values comprised between 50 and 1 mL min^{-1} , the APPI signal was found to be directly proportional with the flow rate. The APPI ionization was, therefore, believed to be a first-order process in the analyte mass (a mass-dependent process) and a zero-order process in the solvent mass, suggesting that the methanol solvent was not involved in the PI process. On the other hand, APCI was dependent on both the solvent and analyte density since a CI process depends on the presence of solvent for charge transfer, thus explaining the loss in sensitivity at low solvent flow rates [2]. For high PA compounds, however, Kauppila et al. did not observe any significant decrease in the ion production with both APPI sources (Sciex prototype or Agilent/Syagen PhotoMate) [26], indicating that proton transfer is less dependent on the solvent flow rate compared to charge transfer.

Generally, APPI ionized more compounds (98%) than APCI (91%) among the set of 201 molecules previously cited [81]. In the positive mode, the dynamic range measured for reserpine with the PhotoMate source was about 1 pg to over 100 ng, comparable to APCI [2]. Signal stability was excellent, with an RSD less than 3% for 600 injections over a 15 h time span. With toluene as a dopant and methanol as a chromatographic solvent, the $[\text{M}+\text{H}]^+$ ions of carbamazepine and acridine were found to be about eight times higher in APPI than in APCI, whereas no molecular ions were observed in APCI. With toluene and acetonitrile, APPI was only slightly better than APCI for charge transfer but was significantly better for proton transfer [1]. Estrone ionization was also about five times higher in APPI than in APCI, and naphthalene PI was less sensitive to the solvent conditions than was APCI [3]. Besides, Cai et al. observed in normal-phase LC that APPI provided better repeatability and higher signal to noise ratios than APCI, which led to better sensitivities depending on the analyte (a factor 3–530). As expected, APPI was found to be particularly suitable when using a flammable solvent such as hexane and offered a decisive advantage compared to APCI with regards to potential explosions. Besides, APCI generates a deposit of carbon on the corona discharge needle and on the cone face, which can lead to instabilities and a decrease in signal over time [56].

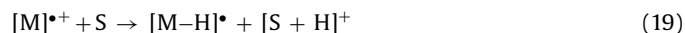
6.4. APCI/APPI dual mode

Syage et al. demonstrated that the dual mode can induce signals with intensities different from the sum of both single modes [3]. This suggested that either positive or negative interferences can occur when running both modes simultaneously. For example, the $[\text{M}]^{\bullet+}$ naphthalene ions were produced in a single APPI, whereas they disappeared when APCI was simultaneously operated. The mechanism was not elucidated but certainly involved a large number of free electrons generated by the corona discharge needle, thereby neutralizing the positive charges. For injections of hydrocortisone between 1 pg and 1 ng, the three modes (APCI, APPI and APCI/APPI) possessed a similar, linear domain. The hydrocortisone signal was found to be slightly higher with APPI than with APCI, whereas its ionization in the dual-mode produced more signal than the sum of independent analyses.

7. Matrix effects

Due to the principle of APPI, PI should not be subject to interfering mechanisms in the analytes' ionization [2]. However, ion

suppression could occur through proton transfer from the ionized analyte to other molecules present in the source (such as the solvent, matrix and endogenous compounds). Solvents with low IE values, such as DMSO, could transfer a charge from the ionized analyte to the solvent molecule. Solvents with high PA values could operate the same way by proton transfer through two possible mechanisms:



In 2004, Hanold et al. compared the effect of endogenous compounds from rat plasma on the ionization of fluphenazine with ESI, APCI and APPI. ESI possessed more significant ionization suppression in comparison to both APCI and APPI [2].

Another study compared ESI, APCI and APPI ionization sources with regards to matrix effects arising from endogenous compounds in human plasma by using a dedicated set-up inspired from Bonfiglio et al. [112]. The PhotoMate source was observed to be the least sensitive to matrix effects on the analysis of basic analytes as model compounds. APPI provided ion enhancement, indicating a possible dopant effect of the endogenous compounds [57]. The authors concluded that the choice of ionization source should be made by evaluating the best compromise between the achievable sensitivity and any encountered matrix effects.

8. CE-APPI/MS

The parameters influencing CE-APPI-MS were investigated by Schappler et al. with an experimental design methodology using a sheath-liquid interface [113]. It was observed that with sheath-liquid flow, the drying gas flow and the vaporizer temperature were the most important parameters for the detection of amphetamines. Other experimental parameters, such as the nebulizer pressure, capillary voltage and drying gas temperature, were not significant. When a dopant is necessary, it can be added to the sheath-liquid [43,45]. By adjusting the position of the nebulizer, a 10-fold increase in the signal intensity could be obtained [114]. As already mentioned in Section 6.1, the use of APPI in miniaturized techniques such as CE-MS is particularly interesting due its compatibility with low flow rates and commonly used background electrolytes (BGE). Non-volatile BGE did not induce any signal alterations in APPI, thereby resulting in a wider choice of CE buffers when transferring analytical conditions from CE-UV to CE-MS [43,45,54,114,115]. For the analysis of labetalol, salbutamol and terbutaline, both borate and phosphate BGE provided better signal/noise (S/N) ratios in APPI than in ESI, as demonstrated by Hanold et al. [2]. Higher abundances and an important reduction of the background noise were also observed, particularly with the phosphate buffer, while the formation of borate clusters contributed to higher noise. The ammonium buffer was shown by Nilsson et al. to have a deleterious effect on the toluene DA-APPI of naphthalenes, due to the high PA of ammonium ions [114].

Sodium dodecyl sulfate (SDS) did not lead to signal alteration in APPI [43,45], which is particularly important for coupling microemulsion electrokinetic chromatography (MEEKC) and micellar electrokinetic chromatography (MEKC) with APPI-MS. The latter allowed the simultaneous separation and detection of charged/polar and neutral/apolar compounds in a single run. This approach could be very useful in sample profiling, where unknown analytes with various physico-chemical properties are analyzed [45]. In the case of the analysis of drugs as standards, Himmelsbach et al. presented in 2007 the on-line coupling of MEEKC-APPI-MS for the determination of nine drugs in water [116]. The limits of detection (LOD) ranged between 0.5 and $5.0 \mu\text{g mL}^{-1}$. The same group also presented a MEEKC-APPI-MS/MS method for the analysis

Table 3
Summary of APPI applications for the analysis of drugs.

Analyte	Matrix	Source	Dual source	Dopant	Proportion	Polarity	Ref.
Stigmasterol β-Sitosterol Campesterol Brassicasterol Cholesterol Cholesteryl stearate	Human serum	PS	–	Toluene	15%	P	[78]
Omeprazole 5-Hydroxyomeprazole Omeprazole sulfone	Human serum	PM	–	None	–	P	[119]
Isosorbide-5-mononitrate	Human plasma	PS	–	Acetone	5%	N	[61]
Betamethasone	Human plasma	PS	–	Toluene	3%	N	[120]
Venlafaxine O-Desmethyivenlafaxine	Human plasma	PS	–	Toluene	36%	P	[98]
Cladribine Clofarabine Ketoconazole	Mouse plasma	PS	–	None Acetone Toluene THF	– 17% 17% 17%	P	[53]
Cyclosporin A	Rat plasma	PS	–	Toluene	2%	P	[73]
Ivermectin Doramectin Eprinomectin Milbemycin moxidectin	Cow milk	PM	APCI/APPI	Acetone	5%	P/N	[44]
Sulfanilamide Dapson Sulfapyridine Sulfadiazine Sulfamethoxazole Sulfathiazole Sulfamerazine Sulfamoxole Sulfabenzamide Sulfisomidine Slfamethiazine Sulfamethoxypyridiazine Sulfameter Sulfachlorpyridiazine Sulfaquinoxaline Sulfadoxine Sulfadimethoxine Sulfasalazine	Honey	PS	–	Toluene	10%	P	[51]
Pentoxifylline Trimethoprim Phenacetin Metoprolol Carbazepine Trazodone Diltiazem Clomipramine	Standard	PM	–	Toluene	n.a.	P	[52]
Pentoxifylline Phenacetin 4-Dimethylaminobenzaldehyde Quinoline Isoquinoline Metoprolol Carbamazepine 3-Methylquinoline 6-Methylquinoline	Standard	PM	–	Acetone	5%	P	[116]
Dopamine Salsolinol 3,4-Dihydroxybenzylamine Norsalsolinol Tetrahydropapaveroline Norepinephrine Epinephrine	Rat brain tissue	PM	–	Acetone	7.5%	P	[118]
Testosterone 4-Androstene-3,17-dione Androsterone Epiandrosterone Dehydroepiandrosterone (DHEA)	Environmental water	PS	–	Toluene	25%	P/N	[86]

Table 3 (Continued)

Analyte	Matrix	Source	Dual source	Dopant	Proportion	Polarity	Ref.
5 α -Dihydrotestosterone							
Estrone							
17 β -Estradiol							
Estriol							
Dehydroepiandrosterone-3-sulfate							
Estrone-3-sulfate							
17 β -Estradiol 3-sulfate							
Estriol 3-sulfate							
Estrone-3- β -D-glucuronide							
17 β -Estradiol 3- β -D-glucuronide							
Estriol 3- β -D-glucuronide							
Estrogen ethynylestradiol							

P: positive polarity; N: negative polarity; P/N: positive and negative polarities; PS: PhotoSpray source; PM: PhotoMate source.

of eight moderately polar drugs in water [52]. The LOD comprised between 3 and 41 $\mu\text{g mL}^{-1}$ in a single MS and between 0.6 and 6.0 $\mu\text{g mL}^{-1}$ in MS² were achieved. Moreover, other MEEKC formulations were tested (oil-phase buffer systems and other surfactants) without any interferences on the MS detection. On the other hand, Schappler et al. found that the compatibility of SDS with APPI depended on the analytes and the selected polarity. Indeed, MEEKC-APPI-MS used in the negative mode for the analysis of various diuretics showed a 15 to 20-fold loss in sensitivity compared to CZE-ESI-MS, which can be mainly attributed to the presence of [SDS-Na]⁻ adduct [117].

An interesting feature was observed with the PhotoMate source by Hommerson et al. [115]. Non-polar compounds with low PA were preferentially ionized by APPI or DA-APPI, whereas quaternary ammonium compounds were found to generate higher sensitivities when the lamp was switched off [115]. This phenomenon was attributed to an ESI-like liquid phase ionization, and it existed only for very specific conditions, such as when the capillary voltage was set to a low value (600 V). The same authors compared ESI and APPI for the analysis of basic amines, quaternary amines and steroids. A moderate ion suppression in the ESI with phosphate buffers was found, while no signal alteration in the APPI was observed. Nevertheless, sensitivities achieved in ESI-MS for basic amines were better than in APPI-MS by a factor of 2–5. Steroids presented similar signal intensities with both sources.

9. Applications

Articles appearing after the publications of the previous reviews [22,23] have been considered, covering the time period from January 2005 to April 2008. Among the studies published in this period, several classes of analytes emerged: drugs [44,51–53,61,73,78,86,98,116,118–120] (Table 3), lipids [46,47,87,91,110,121,122] (Table 4), natural compounds [48,49,82,85,93,95,109,123–125] (Table 5), pesticides [83,101] (Table 6), synthetic organics [58,92,97,100,103,126–131] (Table 7) and petroleum derivatives [96,132,133] (Table 8).

9.1. Drugs

The majority of APPI applications were dedicated to the determination of drugs in biofluids, such as serum [78,119] and plasma [53,61,73,98,120]. Serum was investigated by Lembcke et al. [78], who proposed an LC-APPI-MS/MS method for the analysis of phytosterols in 15 min instead of in GC-MS, which required about 3 h. The LOD ranged between 0.25 and 0.68 $\mu\text{g L}^{-1}$. Another LC-APPI-MS/MS application was proposed by Martens-Lobenhoffer et al. [119] for the stereoselective quantification of omeprazol and its two major metabolites (5-hydroxyomeprazole and omeprazole sulfone) in serum. The analytical range was

between 5 and 750 ng mL^{-1} for both omeprazole and omeprazole sulfone and was between 2.5 and 375.0 ng mL^{-1} for the 5-hydroxy-metabolite.

Regarding the analysis of drugs in plasma, Wang et al. compared five reversed-phase and normal-phase LC-MS methods using ESI, APCI and APPI sources for the analysis of cyclosporine A in rat plasma [73]. Normal-phase LC-APPI-MS was very efficient in terms of ionization since solvents used in the mobile phase (such as isooctane and ethanol) promoted the analytes' ionization. Hsieh et al. determined cladribine and clofarabine in plasma (mouse) [53]. Different fast separation techniques, including UHPLC, coupled to various MS systems (linear ion trap and triple quadrupole MS) equipped with APPI or APCI were evaluated. No significant matrix effects or ionization differences were observed. APPI was used by Theron et al. to overcome large matrix effects in ESI for the analysis of venlafaxin and its major metabolite (*O*-desmethylvenlafaxine) in human plasma [98]. Indeed, the use of APPI resulted in negligible ion suppression. Validation of the method was performed in the 2.4–605.0 ng mL^{-1} range. Silva et al. presented a LC-APPI-MS/MS method for the analysis of isosorbide-5-mononitrate in human plasma for a bioequivalence study of tablet formulations [61]. The calibration curve was linear in the 20–2000 ng mL^{-1} domain. Repeatability was 7.9% at 60 ng mL^{-1} , 5.2% at 300 ng mL^{-1} and 7.0% at 1800 ng mL^{-1} , with a trueness of 94.6, 94.1 and 88.8%, respectively. Pereira et al. proposed a LC-APPI-MS/MS method for the quantification of betamethasone in human plasma [120]. The calibration curve was linear in the 0.05–50 ng mL^{-1} domain, and the repeatability was lower than 12% for all tested concentration levels with a relative bias lower than 10%. Drugs have also been analyzed in food. Mohamed et al. validated a LC-APPI-MS/MS method for the analysis of 16 antibiotics in honey, with a LOD in the 0.4–4.5 $\mu\text{g kg}^{-1}$ range for a targeted concentration of 50 $\mu\text{g kg}^{-1}$ [51].

Turnipseed et al. compared ESI, APCI, APPI and APCI/APPI ionization methods for the analysis of anthelmintics in cow milk [44]. As expected, the MS responses varied as a function of the source and of the analytes. The best results were found when running the dual APCI/APPI source in the APPI-only configuration.

Only two applications of APPI in the field of compounds naturally present in the human body, such as hormones or neurotransmitters, have been published during the 2005–2008 period (see Table 4). The first application was dedicated to human hormones present in water. Yamamoto et al. compared ESI and APPI for the analysis of steroids in Osaka City rivers and estuaries [86]. ESI was found to provide better sensitivities for conjugated steroids, whereas APPI was better in ionizing unconjugated steroids. Estrone, estrone 3-sulfate and 4-androstene-3,17-dione were observed at maximal concentrations of 51, 5.1 and 6.4 ng L^{-1} , respectively. The LODs were in the 0.06–7.0 ng L^{-1} range, depending on the analyte. The second paper presented a LC-APPI-MS method for the

Table 4
Summary of APPI applications for the analysis of lipids.

Analyte	Matrix	Source	Dopant	Proportion	Polarity	Ref.
Eicosapentaenoic acid methyl ester Monoarachidin Diarachidin Docosahexaenoic acid Trielaidin	Standard	PM	None	–	P/N	[121]
Glucosylceramide Galactosylceramide Lactosylceramide Globoside Globopentaosylceramide Globotriaosylceramide	Standard	PS	Acetone	25%	P/N	[47]
Eicosapentaenoic acid methyl ester Monoarachidin Diarachidin Trielaidin	Fish oil	PM	None	–	P/N	[110]
Globotriaosylceramides	Urine	PS	Acetone None	12.5 and 25% –	P/N	[46]
Conjugated linoleic acids	Human coronary artery smooth muscle cells	PS	Toluene	5%	P	[87]
Cholesterol Free fatty acids Ceramide Cerebrosides	House sparrows stratum corneum	PS	Toluene	1%	P/N	[91]
Water Sphingolipids	House sparrows stratum corneum	PS	Toluene	1%	P/N	[122]

P: positive polarity; N: negative polarity; P/N: positive and negative polarities; PS: PhotoSpray source; PM: PhotoMate source.

Table 5
Summary of APPI applications for the analysis of natural compounds.

Analyte	Matrix	Source	Dual source	Dopant	Proportion	Polarity	Ref.
Anthocyanins	Red wine	PS	–	Toluene	12.50%	P	[85]
Various	Olive oil	PS	–	Toluene	10%	P	[93]
Various	Olive oil	PS	–	Toluene	10%	P	[82]
Aflatoxin M1 Aflatoxin B1	Cow milk	PS	–	None	–	P	[109]
Ergosterol	Wheat	PM	–	Toluene	1%	P	[49]
Wheat straw lignin polymer	Wheat	PS	–	Toluene	n.a.	P/N	[95]
Trans-resveratrol Trans- ϵ -viniferin α -Viniferin Trans- δ -viniferin Trans-pterostilbene	Grapevine leaves	PM	–	Acetone	n.a.	N	[48]
Serotonin Melatonin Indole-3-acetic acid	Higher plants	PM	–	None	–	P	[123]
Domoic acid Amber	Shellfish Amber	PM	APCI/APPI	None	–	P	[124] [125]

n.a.: not available; P: positive polarity; N: negative polarity; P/N: positive and negative polarities; PS: PhotoSpray source; PM: PhotoMate source.

quantitation of salsolinol and related catecholamines in rat brain tissue [118]. The calibration curve presented an R^2 value above 0.96 for over two orders of magnitude.

9.2. Lipids

This class of compounds was of particular interest for APPI due to their low polarity. Cai et al. compared ESI, APCI and APPI for the

normal-phase LC–MS analysis of free fatty acids in fish oil and their esters, monoglyceride, diglyceride and triglyceride, which are usually analysed by reversed-phase chromatography [110]. APPI provided the lowest LOD and the highest S/N ratios. It was two to four times more sensitive than APCI or ESI. APPI's linear dynamic range was found to be 4–5 orders of magnitude with an upper limit around 1250–2500 ng. This was confirmed in another study con-

Table 6
Summary of APPI applications for the analysis of pesticides.

Analyte	Matrix	Source	Dopant	Proportion	Polarity	Ref.
Diastereoisomers of metolachlor	Environmental water	PS	Toluene	1%	P	[83]
p,p'-Dichlorodiphenyltrichloroethane (DDT)	Environmental water	PS	Toluene	5%	P/N	[101]

P: positive polarity; P/N: positive and negative polarities; PS: PhotoSpray source.

Table 7
Summary of APPI applications for the analysis of synthetic organics.

Analyte	Matrix	Source	Dual source	Dopant	Proportion	Polarity	Ref.
2,4-Dibromodiphenylether 4,4'-Dibromodiphenylether 2,2',4'-Tribromodiphenylether 2,2',4,4'-Tetrabromodiphenylether 2,2',6,6'-Tetrabromodiphenylether 3,3',4,4'-Tetrabromodiphenylether 2,2',3,4,4'-Pentabromodiphenylether 2,2',4,4',5'-Pentabromodiphenylether 2,3',4,4',6'-Pentabromodiphenylether 3,3',4,4',5'-Pentabromodiphenylether 2,2',3,4,4',5'-Hexabromodiphenylether 2,2',4,4',6,6'-Hexabromodiphenylether 2,2',3,4,4',5,6'-Heptabromodiphenylether 2,2',3,4,4',5',6'-Heptabromodiphenylether 2,2',3',4,4',6,6'-Heptabromodiphenylether 2,3,3',4,4',5,6'-Heptabromodiphenylether 2,2',3,3',4,4',5,5',6,6'-Decabromodiphenylether	Standard	PM	–	Toluene	1%	P/N	[126]
1-Methylbenzo[α]pyrene 2-Methylbenzo[α]pyrene 3-Methylbenzo[α]pyrene 4-Methylbenzo[α]pyrene 5-Methylbenzo[α]pyrene 6-Methylbenzo[α]pyrene 7-Methylbenzo[α]pyrene 8-Methylbenzo[α]pyrene 9-Methylbenzo[α]pyrene 10-Methylbenzo[α]pyrene 11-Methylbenzo[α]pyrene 12-Methylbenzo[α]pyrene	Standard	PM	–	None	–	P	[127]
Bis(2,4-di-tert-butyl)pentaerythritol diphosphite (Alkanox P24)	Standard	PS	–	Toluene	10%	P/N	[92]
Fullerene Perfluoropentane Perfluoromethylcyclohexane Perfluoroadamantane Hexafluorobenzene Octafluorotoluene Octafluoronaphthalene Perfluorotributylamine Pentafluorobenzyl	Standard	PS	–	Toluene	400%	N	[100]
Tetrabromobisphenol A Octabromodiphenylether Decabromodiphenylether Monobromodiphenylether	Standard	PM	–	Toluene	2.5%	P/N	[130]
1-Naphthoic acid 2-Naphthoic acid Coumarine 4-Oxa-benzo[def]chrysene-5-one 1-Naphthol 2-Naphthol 2-Hydroxyphenanthrene 3-Hydroxyphenanthrene 4-Hydroxyphenanthrene 9-Hydroxyphenanthrene 1-Hydroxypyrene 1,5-Dihydroxynaphthalene 2,7-Dihydroxynaphthalene Cis-4,5-dihydro-dihydroxy-benzo[a]pyrene Tertralone Fluoren-9-one Benzanthrone 1,4-Naphthoquinone 9,10-Phenanthrenequinone 1,4-Anthraquinone 9,10-Anthraquinone 1,4-Chrysenequinone Benzo[a]pyrene-3,6-dione Benzo[a]pyrene-4,5-dione Benzo[a]pyrene-7,10-dione 5-Hydronaphthoquinone 2-Carboxy-9,10-anthraquinone 1-Hydroxy-9,10-anthraquinone 2-Hydroxy-9,10-anthraquinone 1,8-Dihydroxy-9,10-anthraquinone	Standard	PM	–	Acetone	10%	P/N	[58]

Table 7 (Continued)

Analyte	Matrix	Source	Dual source	Dopant	Proportion	Polarity	Ref.
Benz[a]anthracene 5-Methylchrysene Benzo[j]fluoranthene Benzo[b]fluoranthene Benzo[k]fluoranthene Benzo[a]pyrene Indeno[1,2,3-cd]pyrene Dibenz[a,h]anthracene Dibenzo[a,e]pyrene Dibenzo[a,i]pyrene	Cigarette smoke	PS	–	Toluene	60% and 75%	P	[97]
Hexabromocyclodecane	Environmental water	PM	–	None	–	N	[129]
1,3,5-Trinitrobenzene Tetryl-2,4,6,N-tetranitrotoluene 2,4,6-Trinitrotoluene 1,2-Dinitrobenzene 1,3-Dinitrobenzene 1,4-Dinitrobenzene 2-Amino-4,6-dinitrotoluene 4-Amino-2,6-dinitrotoluene 2,6-Diamino-4-nitrotoluene 2,3-Dinitrotoluene 2,4-Dinitrotoluene 2,5-Dinitrotoluene 2,6-Dinitrotoluene 3,5-Dinitrotoluene 1,3,5-Trinitro-1,3,5-triazacyclohexane 1,3,5,7-Tetranitro-1,3,5,7-tetrazacyclooctane Pentaerythritol tetranitrate 1,3-Bis-nitrooxy-2,2-bis-nitrooxymethyl-propane	Environmental water	PM	–	None	–	P/N	[128]
Benzidine 3,3'-Dichlorobenzidine 2-Chloroaniline 3-Chloroaniline 4-Chloroaniline 2,3-Dichloroaniline 2,4-Dichloroaniline 2,5-Dichloroaniline 2,6-Dichloroaniline 3,4-Dichloroaniline 3,5-Dichloroaniline 2,3,4-Trichloroaniline 2,4,5-Trichloroaniline 2,4,6-Trichloroaniline	Environmental water	PS	–	Toluene	15%	P/N	[103]
Decabromodiphenyl ether	Rat tissues	Riu	APCI/APPI	Toluene	1%	N	[131]

P: positive polarity; N: negative polarity; P/N: positive and negative polarities; PS: PhotoSpray source; PM: PhotoMate source.

cerning the analysis of fatty acids and acylglycol lipids [121]. APPI provided very clean MS spectra, which were stable and repeatable. It also appeared that non-aqueous mobile phases provided better sensitivities and peak shapes than aqueous mobile phases, which required higher vaporizer temperatures for the analyte desolvation. Low vaporizer temperatures were found to significantly reduce the analyte's thermal decomposition, and the signals were, therefore, improved. The cone voltage was determined as a key parameter determining the sensitivity of this method. The on-column LOD was estimated to 94 pg for an EPA methyl ester, 90 pg for monoarachidin and diarachidin and 24 pg for trielaidin. Roy et

al. proposed a porous, graphitic carbon LC-APPI-MS/MS method for the analysis of glycosphingolipids, thereby providing structural information on the fatty acid and sphingoid base [47]. This set-up allowed for the efficient discrimination of isobaric compounds. In the paper of Delobel et al., a LC-APPI-MS method was proposed for the analysis of globotriaosylceramides in human urine, which are connected with Fabry disease [46]. Collision-induced dissociation (CID) in the positive mode provided very useful information for the determination of alkyl chains structures. Another concern about the use of APPI for the analysis of lipids was proposed by Müller et al. [87]. They suggested a (Ag⁺)-HPLC-APPI-MS/MS method for the

Table 8
Summary of APPI applications for the analysis of petroleum derivatives.

Analyte	Matrix	Source	Dopant	Proportion	Polarity	Ref.
Naphtha[2,3- α]pyrene Various	Standard Crude oil	PM	Toluene	m.p.	P/N	[132]
Sulfur compounds	Petroleum	PM	None	–	P	[133]
Nitrogen aromatics	Petroleum	PM	Toluene	m.p.	P	[96]

P: positive polarity; P/N: positive and negative polarities; m.p.: dopant used as mobile phase.

analysis of conjugated linoleic acid's elongation and β -oxidation products usually operated in GC-MS. The use of APPI provided a 40-fold better sensitivity than APCI and allowed for the determination of the double bond positions, the configurations and the chains lengths of the conjugated linoleic acids. Finally, a LC-APPI-MS/MS method was proposed by Muñoz-García et al. for the identification of sphingolipids mixtures in the stratum corneum of house sparrows [91,122]. Seven families of cerebrosides (97 compounds) and four families of ceramides (79 compounds) were brought out, for which fatty acids carbon chains typically contained 40 carbons, longer than those generally reported for mammalian stratum corneum.

9.3. Natural compounds

The use of APPI was also investigated for the analysis of natural, low polarity compounds. For example, Gómez-Ariza et al. have published two studies on APPI performance, one for an olive oil analysis and one for the classification of unknown wine samples [85]. In the case of olive oil authentication, the authors first compared ESI and APPI for LC-MS analysis [93]. Both sources were found to be complementary to one another, as APPI was more sensitive for the monoacyl- and diacylglycerols and ESI for triacylglycerols. Flow injection analysis-APPI-MS, using a QqTOF apparatus, was used in a complementary fingerprinting study. This method was able to discriminate olive, extra-virgin olive, olive-pomace, hazelnut, sunflower, corn and several mixed oils in about 1 min per sample [82]. The same apparatus was also used for wine classification according to anthocyanins profiles [85]. Performance of ESI and APPI sources was also compared by Cavaliere et al. for the LC-MS/MS analysis of aflatoxins M1 and B1 in cow milk [109] and by Pardo et al. for the LC-MS/MS analysis of domoic acid in shellfish [124], who included evaluation of APCI and APCI/APPI sources. Both groups selected ESI either due to its lower LOD [124] or to its higher robustness [109]. Ergosterol quantitation was operated by Varga et al. with an LC-APPI-MS method to evaluate the fungal biomass in wheat [49]. The calibration curve was linear between 0.05 and 50 ng μL^{-1} with a repeatability value between 2.1 and 5.2%. Concerning the elucidation of the straw lignin molecular structure, Banoub et al. found the presence of 57 specific oligomers with an LC-APPI-QqTOFMS apparatus [95]. The latter was demonstrated to be a powerful analytical tool for the ionization of small and large lignin oligomers. The paper of Cao et al. compared ESI, APCI and APPI sources for the rapid LC-MS analysis of melatonin, serotonin and auxin in plants [123]. The performance was comparable, and a LOD was found to be 0.2 ng mL^{-1} for melatonin, 5 ng mL^{-1} for serotonin and 0.7 ng mL^{-1} for auxin. The linear dynamic ranges were 0.02 ng mL^{-1} to 0.1 mg mL^{-1} , 5 ng mL^{-1} to 0.1 mg mL^{-1} and 0.7 ng mL^{-1} to 0.1 mg mL^{-1} , respectively. Tonidandel et al. classified various samples of amber with the help of laser desorption ionization (LDI), APCI and APPI-ionization techniques with multivariate data analysis [125]. APPI was the most suitable ionization mode for the analysis of amber, as fossilization produced highly stable, insoluble polymers. Finally, Jean-Denis et al. proposed a rapid screening of stilbenes in grapevine leaves infected by *P. viticola* by LC-APPI-MSⁿ, which required only 1–2 mg of sample [48].

9.4. Pesticides

Within the selected time period, only two papers reported analyses of pesticides using APPI, and both were applied to surface and ground water determinations of DDT [101] and metolachlor [83]. For the former, a linear dynamic range of the method was found between 20 and 1000 ng mL^{-1} with a LOD of 7 ng mL^{-1} , higher than the LOD achieved by conventional GC-MS. For metolachlor

diastereoisomers and s-metolachlor analysis, Kabler and Chen proposed an enantioselective LC-APPI-MS/MS method with a LOD of 0.10 ppb, with a repeatability lower than 20% [83].

9.5. Synthetic organics

Among the papers published for the analysis of organic compounds, four concerned the determination of flame retardants [126,129–131]. In case of brominated substances, Riu et al. proposed an LC-APPI-MSⁿ as an alternative to the generally used GC-ESI/MS method [126]. Br₂ loss was the major ionization process for polybrominated flame retardants, and the ionization polarity modes were found complementary with regards to the degree and position of bromination. The positive mode favored the loss of Br₂ for the ortho-substituted compounds and COBr[•] for the non-ortho-substituted compounds, while the loss of both Br₂ and HBr was observed in the negative mode. The second study presented the determination of decabromodiphenyl ether in rat tissues [131], which allowed the identification of a very toxic derivative, namely, the hydroxylated octa-decabromodiphenyl ether, in liver. The third paper was dedicated to the analysis of tetrabromobisphenol A and polybromodiphenylethers [130]. The former was well ionized in the negative mode without dopant, while the positive mode was preferentially used for the mono- to penta-polybromodiphenylethers. For higher bromo-substitutions, the negative mode provided [M-Br+O]⁻ ions, required toluene as dopant, and was finally selected. To finish, Davis et al. proposed the identification of α -, β - and γ -hexabromocyclododecane metabolites in both wastewater sludge and freshwater [129]. Hexabromocyclododecane was found to be sequentially debrominated with the loss of two bromines at each step, giving rise to tetrabromocyclododecane, dibromocyclododecane and cyclododecatriene.

Concerning the analysis of PAH, Zheng et al. proposed a CEC-APPI-MS method for the analysis of the 12 monomethylated benzo[α]pyrene isomers [127]. APPI, which was compared to ESI and APCI, provided the highest signals. The method showed a linear domain of 2.5–50 $\mu\text{g mL}^{-1}$, and an LOD of 400 ng mL^{-1} for the 1-, 3-, and 11-methylbenzo[α]pyrene, which was 100 times lower than the CEC-UV results. Ten carcinogenic PAH were analyzed in mainstream cigarette smoke by Ding et al. who developed and validated the LC-APPI-MS/MS method with an LOD in the 11–166 pg range [97]. The last investigation of PAH was run by Grosse et al. who proposed a μ -LC-MS method for the determination of partially oxidized PAH [58]. ESI, APPI and/or APCI ionization techniques were tested. No ionization for any compound was achieved with ESI. APPI produced mainly negative ions, whereas APCI was found to be best adapted for the ionization of partially oxidized PAH since it produced both positive and negative ions. The dual mode was found to be the best regarding cost, time, the amount of sample required and structural information.

Other studies were dedicated to various compounds, such as alkanox P24 (a commercial phosphite antioxidant), nitroaromatics, perfluorinated compounds, pentafluorobenzyl derivatives and benzidine and related compounds. Alkanox P24 was analyzed by LC by Papanastasiou et al. to assess its hydrolysis in water [92]. APPI and APCI were compared, and APPI was selected for further investigations since it showed a lower LOD. In the positive mode, the [M+H]⁺ ions were produced, and in the negative mode, the [M-H]⁻ ions were predominant, and no protonated molecules were detected. Alkanox P24 was exclusively hydrolyzed by scission of both P-O_{phenol} bonds, thereby yielding 2,4-di-*tert*-butyl phenol. Crescenzi et al. also compared APCI and APPI for on-line-SPE-LC-MS methods dedicated to the determination of nitroaromatics and related compounds at trace levels in water [128]. APCI gave better ionization for the cyclic nitramines and

nitrate esters. Song et al. proposed a LC–APPI–MS method for the analysis of fullerenes, perfluorinated compounds and pentafluorobenzyl derivatives, where an electron capture mechanism provided very good sensitivities in the negative mode [100]. In the flow injection analysis, the LOD was 0.15 pg for fullerene and 1.5 pg for perfluoromethylcyclohexane. Finally, Bacaloni et al. proposed a normal-phase LC–APPI–MS/MS method for the determination of benzidine, 3,3'-dichlorobenzidine, mono-, di-, and tri-chloroanilines in water. LOQs were comprised in the 7–112 ng L⁻¹ range [103].

9.6. Petroleum derivatives

The analyses of petroleum derivatives were published by Purcell et al. with a FT–ICR–MS set-up. For sulfur speciation in petroleum, ESI and APPI sources were compared [133]. APPI produced more ions and was able to ionize samples without requiring chemical derivatization. The elemental composition of the aromatic nitrogen model compounds and the petroleum samples [96] revealed that nitrogen speciation could be obtained by APPI. In-source fragmentation phenomena were avoided by adjusting the instrumental parameters. Finally, Purcell et al. observed [M+H]⁺, [M–H][–] and protonated molecules in the analysis of naphtho[2,3- α]pyrene and crude oil [132], and the latter complex mixture generated more than 12,000 peaks. Contrary to ESI, APPI was able to ionize non-polar compounds and, therefore, led to non-polar sulfur speciation in the petrochemical mixtures.

10. Other applications

Low pressure photoionization (LPPI) is another type of source employing PI. Because it operates at low pressure (<1 Torr), this technique limits the collisions between ions and molecules that can lead to ionization competition phenomena. However, as mentioned in the introduction, only poor ionization can be achieved at reduced pressure due to the low sample density in the ionization region. The use of a dopant is therefore mandatory. LPPI is usually applied to gas or liquid samples with volatile or semi-volatile analytes [20]. Direct PI in LPPI was found to produce [M]^{•+} ions (Eqs. (1) and (2)), followed by proton transfer from the solvent (Eq. (8)) by replacing the dopant with the solvent) to the analyte, thereby leading to the [M+H]⁺ ions [134].

PI was also implemented in atmospheric pressure laser ionization (APLI). For some non-polar or low polar compounds [135], APLI gave a lower LOD compared to APPI due to the higher photon flux than could be obtained with conventional lamps. In fact, APLI photons are typically produced by a KrF excimer laser emitting 5 eV photons for efficiently ionizing nonpolar compounds [28]. The main drawbacks to APLI are the large dimension of the source, the tedious maintenance associated with the laser source, and the difficulty in changing the wavelength compared to APPI.

As previously mentioned, APPI has been coupled to IMS [12–15]. Borsdorf et al. compared APPI–IMS with APPI–DMS (differential mobility spectrometry) [16,17]. Both techniques provided the same number of ions, indicating that the ionization mechanisms were similar. Besides, the ions' behavior in a radiofrequency, asymmetric electric field was found to be dependent on the molecular structure (the functional groups and the saturations arrangement). As an example, significant differences in the spectra of aromatic and cyclic hydrocarbons were observed.

Recently, APPI was implemented in miniaturized systems. Haapala et al. proposed a microchip nebulizer made of two plates (silicon/glass or glass/glass) for combining APPI/MS with LC or GC capillary [136]. It contained all the classical parts present in a conventional APPI source, namely, a sample inlet channel, auxiliary gas and dopant inlets, vaporizer channels, nozzle and a platinum heater.

Luosjärvi et al. compared the performance achieved by APCI and APPI microchips for the analysis of polychlorinated biphenyls in a negative-mode GC–APPI–MS [137]. APPI exhibited a wider linear range and a better repeatability.

Furthermore, the use of an APPI source in GC–MS originally designed for LC–MS was presented in 2007 by McEwen for the analysis of standards [138]. GC–APPI–MS was found to produce similar odd-electron fragment ions as those observed in low energy GC–EI–MS, which are useful for the identification of unknown molecules by comparison with the mass spectra in computer libraries. Ionization with APPI was initiated by the production of the [M]^{•+} ions, which were stable enough to be detected. The [M]^{•+} ions could capture a hydrogen atom from either water vapor, an impurity or a neutral analyte, thereby leading to the [M+H]⁺ ions. With a homemade lamp model producing 9.8 eV photons, lower fragmentation and more selective ionization were achieved.

Finally, APPI was also used by Haapala et al. for the analysis of compounds of various polarities after desorption from different surfaces [102]. With a similar principle to desorption electrospray ionization (DESI), DAPPI required the use of a discharge lamp and a dopant. In this case, the ionization mechanism was found to be a combination of thermal and chemical processes.

11. Conclusion

APPI is the most recent ionization source for the LC–MS coupling. It is a photoinduced chemical ionization process with two major ionization mechanisms in the positive mode, namely, proton and charge transfer. Ionization can only occur for molecules that possess low IE values, while for the other compounds, the use of a dopant is mandatory. The latter can also be employed to enhance the ionization yield of compounds exhibiting low IE values. Acetone and toluene are the most largely reported dopants, but benzene, anisole, hexafluorobenzene and THF have also been used. Toluene was found to produce [M]^{•+} ions and favored the production of [M+H]⁺ ions by proton transfer. Besides, acetone formed exclusively [M+H]⁺ ions, but a study of this ionization mechanism is currently not available. In a few cases, the use of a dopant could present a deleterious effect on the ionization. For reversed-phase chromatography and without any dopant, the production of [M]^{•+} ions by charge transfer was dependent on the mobile phase composition. Methanol was particularly suited with an APPI source. In negative APPI, ionization occurs *via* six major ionization mechanisms: electron/analyte interaction, charge exchange (electron capture, EC), proton transfer (analyte deprotonation), association/displacement reactions and the newly discovered anion attachment. It generates less background noise than the positive mode and could ionize a broader range of molecules than both negative APCI and ESI. The APPI ionization yield in the positive mode is generally lower than both the ESI and the APCI ionization yields, but, since the solvents used in reversed-phase LC possess IE values that are higher than photon energy, the generated background noise is very low, and high S/N ratios can be obtained. APPI can also be used in combination with other API sources. Because ESI is an orthogonal ionization technique, the dual source ESI/APPI is particularly attractive for the detection of apolar and polar compounds within the same chromatographic run. APPI proved to be an ionization method adapted to a wide panel of compounds and was particularly tailored to separation techniques with low flow rates. Thus, APPI–MS was also found to be particularly adapted to CE due to its high sensitivity at low flow rates and to its compatibility with non-volatile buffers. Regarding APPI applications, this ionization technique was found to be particularly useful in the analysis of drugs, human endogenous compounds, lipids, natural compounds, pesticides, synthetic organics and petroleum derivatives. The PI mechanisms have been systematically studied and partially elucidated. Never-

- [107] I. Dzidic, D.I. Carroll, R.N. Stillwell, E.C. Horning, *J. Am. Chem. Soc.* 96 (1974) 5258.
- [108] F.G. Kitson, B.S. Larsen, C.N. McEwen (Eds.), *Gas Chromatography and Mass Spectrometry*, Academic Press, San Diego, 1996.
- [109] C. Cavaliere, P. Foglia, E. Pastorini, R. Samperi, A. Lagana, *J. Chromatogr. A* 1101 (2006) 69.
- [110] S.S. Cai, J.A. Syage, *Anal. Chem.* 78 (2006) 1191.
- [111] L.C. Short, J.A. Syage, *Rapid Commun. Mass Spectrom.* 22 (2008) 541.
- [112] R. Bonfiglio, R.C. King, T.V. Olah, K. Merkle, *Rapid Commun. Mass Spectrom.* 13 (1999) 1175.
- [113] J. Schappler, D. Guillarme, J. Prat, J.L. Veuthey, S. Rudaz, *Electrophoresis* 28 (2007) 3078.
- [114] S.L. Nilsson, C. Andersson, P.J.R. Sjöberg, D. Bylund, P. Petersson, M. Jornten-Karlsson, K.E. Markides, *Rapid Commun. Mass Spectrom.* 17 (2003) 2267.
- [115] P. Hommerson, A.M. Khan, T. Bristow, W. Niessen, G.J. de Jong, G.W. Somsen, *Anal. Chem.* 79 (2007) 5351.
- [116] M. Himmelsbach, M. Haunschmidt, W. Buchberger, C.W. Klampfl, *Anal. Chem.* 79 (2007) 1564.
- [117] J. Schappler, D. Guillarme, S. Rudaz, J.L. Veuthey, *Electrophoresis* 29 (2008) 11.
- [118] J.A. Starkey, Y. Mechref, J. Muzikar, W.J. McBride, M.V. Novotny, *Anal. Chem.* 78 (2006) 3342.
- [119] J. Martens-Lobenhoffer, I. Reiche, U. Troeger, K. Moenkemüller, P. Malfertheiner, S.M. Bode-Boeger, *J. Chromatogr. B* 857 (2007) 301.
- [120] A.d.S. Pereira, L.S.O.B. Oliveira, G.D. Mendes, J.J. Gabbai, G. De Nucci, *J. Chromatogr. B* 828 (2005) 27.
- [121] S.S. Cai, J.A. Syage, *J. Chromatogr. A* 1110 (2006) 15.
- [122] A. Munoz-Garcia, J. Ro, J.C. Brown, J.B. Williams, *J. Exp. Biol.* 211 (2008) 447.
- [123] J. Cao, S.J. Murch, R. O'Brien, P.K. Saxena, *J. Chromatogr. A* 1134 (2006) 333.
- [124] O. Pardo, V. Yusa, N. Leon, A. Pastor, *J. Chromatogr. A* 1154 (2007) 287.
- [125] L. Tonidandel, E. Ragazzi, G. Roghi, P. Traldi, *Rapid Commun. Mass Spectrom.* 22 (2008) 630.
- [126] A. Riu, D. Zalko, L. Debrauwer, *Rapid Commun. Mass Spectrom.* 20 (2006) 2133.
- [127] J. Zheng, S.A. Shamsi, *Anal. Chem.* 78 (2006) 6921.
- [128] C. Crescenzi, J. Albinana, H. Carlsson, E. Holmgren, R. Batlle, *J. Chromatogr. A* 1153 (2007) 186.
- [129] J.W. Davis, S.J. Gonsior, D.A. Markham, U. Friederich, R.W. Hunziker, J.M. Ariano, *Environ. Sci. Technol.* 40 (2006) 5395.
- [130] L. Debrauwer, A. Riu, M. Jouahri, E. Rathahao, I. Jouanin, J.P. Antignac, R. Cariou, B. Le Bizec, D. Zalko, *J. Chromatogr. A* 1082 (2005) 98.
- [131] A. Riu, J. Cravedi, L. Debrauwer, A. Garcia, C. Canlet, I. Jouanin, D. Zalko, *Environ. Int.* 34 (2008) 318.
- [132] J.M. Purcell, C.L. Hendrickson, R.P. Rodgers, A.G. Marshall, *Anal. Chem.* 78 (2006) 5906.
- [133] J.M. Purcell, P. Juyal, D.G. Kim, R.P. Rodgers, C.L. Hendrickson, A.G. Marshall, *Energy Fuels* 21 (2007) 2869.
- [134] J.A. Syage, *J. Am. Soc. Mass Spectrom.* 15 (2004) 1521.
- [135] M. Constapel, M. Schellentraeger, O.J. Schmitz, S. Gaeb, K.J. Brockmann, R. Giese, T. Benter, *Rapid Commun. Mass Spectrom.* 19 (2005) 326.
- [136] M. Haapala, L. Luosujaervi, V. Saarela, T. Kotiaho, R.A. Ketola, S. Franssila, R. Kostiaainen, *Anal. Chem.* 79 (2007) 4994.
- [137] L. Luosujarvi, M.M. Karikko, M. Haapala, V. Saarela, S. Huhtala, S. Franssila, R. Kostiaainen, T. Kotiaho, T.J. Kauppila, *Rapid Commun. Mass Spectrom.* 22 (2008) 425.
- [138] C.N. McEwen, *Int. J. Mass Spectrom.* 259 (2007) 57.
- [139] S.T. Tsai, J.C. Jiang, Y.T. Lee, A.H. Kung, S.H. Lin, C.K. Ni, *J. Chem. Phys.* 111 (1999) 3434.



Fast analysis of catecholamine metabolites MHPG and VMA in human plasma by HPLC with fluorescence detection and a novel SPE procedure

Laura Mercolini^a, Gilberto Gerra^b, Marco Consorti^a, Lorenzo Somaini^c, Maria Augusta Raggi^{a,*}

^a Faculty of Pharmacy, Department of Pharmaceutical Sciences, Alma Mater Studiorum – University of Bologna, Via Belmeloro 6, I-40126 Bologna, Italy

^b United Nations Office on Drugs and Crime, Global Challenges Section, Division for Operations, P.O. Box 500, A-1400 Vienna, Austria

^c Addiction Treatment Centre, Health Local Unit ASL BI, Via Pier Maffei 59, 13836 Cossato (BI), Italy

ARTICLE INFO

Article history:

Received 23 June 2008

Received in revised form 26 October 2008

Accepted 31 October 2008

Available online 7 November 2008

Keywords:

MHPG

VMA

HPLC-F

Human plasma

Solid-phase extraction

ABSTRACT

A fast and sensitive high-performance liquid chromatographic method has been developed for the determination in human plasma of MHPG (3-methoxy-4-hydroxyphenylethylglycol) and VMA (vanillyl mandelic acid), the main metabolites of epinephrine and norepinephrine. Analyses were carried out at 325 nm while exciting at 285 nm on a reversed-phase column (Atlantis C18, 150 mm × 4.6 mm I.D., 5 μm) using a mobile phase composed of 2% methanol and 98% aqueous citrate buffer at pH 3.0. A careful solid-phase extraction procedure, based on mixed-mode reversed-phase – strong anion exchange Oasis cartridges (MAX, 30 mg, 1 mL), was developed for the pre-treatment of plasma samples. Extraction yields were satisfactory, always higher than 90%. Calibration curves were linear over the 0.2–40.0 ng mL⁻¹ concentration range for MHPG and over the 0.5–40.0 ng mL⁻¹ concentration range for VMA. The method was successfully applied to plasma samples of former drug users undergoing detoxification therapy and subjects “at risk” of developing drug addiction.

© 2008 Elsevier B.V. All rights reserved.

1. Introduction

Epinephrine and norepinephrine are the two most important catecholamines, involved in several central and peripheral neuroendocrine responses to different kinds of stress [1,2]. Their two main metabolites found in blood are 3-methoxy-4-hydroxyphenylethylglycol (MHPG, Fig. 1a) and vanillyl mandelic acid (VMA, Fig. 1b). MHPG is produced from both epinephrine and norepinephrine by the sequential action of monoamine oxidase (MAO) and catechol-O-methyl transferase (COMT) and is then further metabolised to VMA by alcohol dehydrogenase (ADH). Both compounds can be used as markers of the neurometabolic state of the organism and of the relative state of activation (or lack thereof) of the noradrenergic system [3]. It has been known for a long time that this system is deeply involved in the onset and the maintaining of drug addiction [4], however the precise mechanisms of this involvement are not yet clear. On the other hand, it has been found that habitual drug users and subjects “at risk” of developing addiction show neuroendocrine responses to stress, and possibly to pain, which are different from those of subjects without any previous

addiction history [5,6]. Moreover, some researchers have correlated drug abuse with psychic trouble and depression [7], which are well-known to be closely linked with imbalances in adrenergic transmission. This has led to the hypothesis that a different state of arousal of the adrenergic system could be a marker of liability to drug abuse [8]. Within this frame, the determination of MHPG and VMA plasma levels could be an important tool in the study of the mechanisms underlying drug addictions [9] and in the development of new kinds of strategies for their treatment and prevention.

Consequently, there is an increasing need for the development of reliable, sensitive and fast analytical methods for the determination of these compounds in plasma samples.

Some analytical methods have been published for the determination of MHPG and VMA in different biological matrices [10–12] and mainly in urine [13–16]. Only a few methods for their analysis in plasma have been published, based on the use of HPLC with electrochemical detection [17–20] sometimes using a multi-electrode detector [17,20]. This technique surely has high selectivity and sensitivity, however it is also quite complex and difficult to optimise; moreover, the instrumentation is not easily found outside specialised laboratories. The methods based on multi-electrode detection [17,20] use even more complicated and less widespread instrumentation.

The aim of the study presented herein is the development of a sensitive, selective and fast method for the determination of MHPG

* Corresponding author at: Laboratory of Pharmaco-Toxicological Analysis, Department of Pharmaceutical Sciences, Via Belmeloro 6, I-40126 Bologna, Italy. Tel.: +39 051 2099700; fax: +39 051 2099740.

E-mail address: mariaaugusta.raggi@unibo.it (M.A. Raggi).

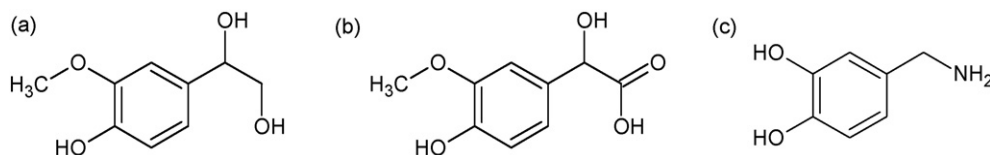


Fig. 1. Chemical structures of (a) MHPG, (b) VMA and (c) 3,4-dihydroxybenzylamine (IS).

and VMA levels in human plasma. The proposed method is based on the use of high-performance liquid chromatography with spectrofluorimetric detection, which exploits the native fluorescence of the analytes to obtain high sensitivity and selectivity without needing complicated derivatisation steps. This analytical paper is part of a broader interdisciplinary research, with the aim of studying neurobiological correlates of drug addictions and developing new strategies for their prevention and therapy [4].

2. Experimental

2.1. Chemicals

The analytes 3-methoxy-4-hydroxyphenylethylglycol (MHPG, Fig. 1a), vanillyl mandelic acid (α ,4-dihydroxy-3-methoxybenzeneacetic acid, VMA, Fig. 1b), the Internal Standard 3,4-dihydroxybenzylamine hydrobromide (IS, Fig. 1c) and bovine albumin were purchased from Sigma Chemicals (St. Louis, MO-USA).

Sodium metabisulfite, sodium carbonate, 37% (w/w) hydrochloric acid, 2 M sodium hydroxide, sodium chloride (NaCl), potassium chloride (KCl), potassium dihydrogen phosphate (KH_2PO_4), disodium hydrogen phosphate anhydrous (Na_2HPO_4), glacial acetic acid and methanol were analytical grade from Carlo Erba (Milan, Italy).

Ultrapure water (18.2 M Ω cm) from a MilliQ apparatus by Millipore (Milford, Mass., USA) was used.

2.2. Apparatus and chromatographic conditions

The chromatographic system was composed of a Jasco (Tokyo, Japan) PU-2089 PLUS chromatographic pump and a Jasco FP-2020 spectrofluorimetric detector set at $\lambda_{\text{exc}} = 285$ nm, $\lambda_{\text{em}} = 325$ nm.

Separations were obtained on an Waters (Milford, Mass., USA) Atlantis C18 reversed-phase column (150 mm \times 4.6 mm I.D., 5 μm) kept at room temperature. The mobile phase was composed of a mixture of methanol (2%, v/v) and a pH 3.0, 50 mM citrate buffer (98%, v/v).

The mobile phase was filtered through a Phenomenex (Torrance, CA, USA) membrane filter (47 mm nylon membrane, 0.2 μm) and degassed by an ultrasonic bath. The flow rate was 1.0 mL min^{-1} and the injections were carried out through a 50 μL loop. Data processing was handled by means of a Jasco Borwin 3.0 software.

Solid-phase extraction (SPE) was carried out on a Varian (Palo Alto, CA, USA) VacElut apparatus.

A Crison (Barcelona, Spain) Basic 20 pHmeter and a Hettich (Tutlingen, Germany) Universal 32 R centrifuge were used.

2.3. Solutions

The stock solutions of the analytes and the IS were 1 mg mL^{-1} and were prepared by dissolving 20 mg of the substance in 20 mL of ultrapure water to which 20 mg of sodium metabisulfite, 160 mg of sodium chloride and 10 μL of concentrated hydrochloric acid (37%) had been previously added. This saline solution prepared at acidic pH and containing an antioxidant is useful to avoid analyte degra-

dation. Standard solutions were prepared daily by diluting the stock solutions with the mobile phase.

Simulated "blank" plasma was prepared by dissolving 160 mg of NaCl, 23 mg of Na_2HPO_4 , 4 mg of KH_2PO_4 , 4 mg of KCl and 800 mg of bovine albumin in 20 ml of ultrapure water.

2.4. Plasma sample collection

The study was carried out in collaboration with the Ser.T. (Addiction Research Centers) of Cossato (BI) Italy, on plasma samples from former drug users undergoing detoxification therapy and subjects "at risk" of developing drug addiction. Blood was stored in glass tubes containing EDTA as the anticoagulant, then centrifuged (within 2 h from collection) at $1400 \times g$ for 15 min; the supernatant (plasma) was then transferred to polypropylene test tubes and stored at -20°C until HPLC analysis.

2.5. Sample pre-treatment: SPE procedure

The plasma pre-treatment procedure was carried out by means of solid-phase extraction (SPE) on Waters (Milford, Mass., USA) Oasis MAX cartridges (30 mg, 1 mL). Cartridges were activated and conditioned with 2×1 mL of methanol and 2×1 mL of pH 9.0, 200 mM carbonate buffer, respectively. After adding 50 μL of the IS standard solution (60 ng mL^{-1}) and 600 μL of water to 300 μL of plasma, the resulting mixture was loaded onto the previously conditioned cartridge. The cartridge was then washed with 2×1 mL of pH 9.0, 200 mM carbonate buffer and dried applying full vacuum (-30 kPa) for 1 min. Analyte elution was carried out with 1 mL of 5% acetic acid in methanol, applying full vacuum again for 1 min. The eluate was brought to dryness with a rotary evaporator and the residue was re-dissolved in 150 μL of mobile phase.

2.6. Method validation

2.6.1. Linearity

Analyte standard solutions at seven different concentrations were added to 300 μL of blank plasma, subjected to the SPE procedure and analysed. The volume of standard solution added was 50 μL and each spiked blank plasma sample was prepared in triplicate. The analyte/IS peak area ratios were plotted against the corresponding concentrations and the calibration curves were set up by means of the least squares method. The considered analyte linearity ranges were 0.2–40.0 ng mL^{-1} for MHPG and 0.5–40.0 ng mL^{-1} for VMA.

2.6.2. Extraction yield (absolute recovery)

Spiked blank plasma samples were prepared and analysed as described in Section 2.6.1, however three plasma analyte concentrations were prepared and analysed (0.2, 20.0 and 40.0 ng mL^{-1} for MHPG; 0.5, 10.0 and 40.0 ng mL^{-1} for VMA), corresponding to the lower limit, middle point and upper limit of the linearity curve. The analyte chromatographic peak areas thus obtained were compared to those obtained from standard solutions at the same concentration, and the percentage extraction yield was calculated.

2.6.3. Precision

Spiked blank plasma samples were prepared and analysed, as described in Section 2.6.2. The procedure was repeated six times within the same day to obtain repeatability (intraday precision) values and six times over six different days to obtain intermediate (interday) precision values, both expressed as percentage relative standard deviation (R.S.D.%).

2.6.4. Selectivity

Standard solutions of monoamines, their metabolites, some commonly used psychiatric drugs (antidepressants) and abuse drugs were injected into the HPLC system at levels higher than their physiological, therapeutic or usual concentrations. The acceptance criterion was: no peak should be detected at the retention times of the analytes or the IS.

2.6.5. Accuracy

Analyte standard solutions at three different concentrations were added to 300 μL of plasma (in order to obtain plasma analyte additions of 0.2, 10.0 and 20.0 ng mL^{-1} for MHPG; 0.5, 5.0 and 20 ng mL^{-1} for VMA) and the mixture subjected to the SPE procedure. Recovery values were calculated according to the following formula: $100 \times ([\text{after spiking}] - [\text{before spiking}]) / [\text{added}]$. The procedure was repeated three times at each concentration level to obtain standard deviation (S.D.) values.

3. Results and discussion

3.1. Choice of the chromatographic conditions

Fluorescence detection was used for the analysis, exploiting the native fluorescence of the analytes. In fact, standard solutions of the analytes were prepared in a mixture of acidic phosphate buffer and acetonitrile and subjected to spectrofluorimetric analysis. It was found that both MHPG (3-methoxy-4-hydroxyphenylethylglycol) and VMA (vanillyl mandelic acid) possess native fluorescence under acidic conditions and an emission intensity maximum was present at 325 nm for both analytes when exciting at 285 nm.

Chromatographic conditions similar to those already used in our previous papers on the determination of catecholamines and their metabolites [21–24] were chosen as the starting point for the analysis of MHPG and VMA. However, very long column conditioning times and some variability in analyte retention times were noted under these conditions. These problems were attributed to the high hydrophilicity of the analytes, which are scarcely retained on traditional reversed-phase columns and thus need high percentages of water (90–98%) in the mobile phase. This can cause the so-called “dewetting” of the stationary phase, decreasing its performance over time with low reproducibility of retention times. Thus, a specific kind of stationary phase was tried, namely the “Atlantis” C18 sorbent. As claimed by the manufacturer, this sorbent contains proprietary modifications in the silica matrix, which grant selectively higher retention toward hydrophilic compounds. Moreover, it is highly resistant to dewetting, allowing the use of very high percentages of aqueous solvent in the mobile phase (up to 100%), without any significant decrease in performance.

Using an Atlantis C18 column (150 mm \times 4.6 mm, 5 μm), different percentages of methanol (0%–10%) were tested. It was found that satisfactory analyte retention could be obtained with 2% methanol, without any decrease in column performance or in reproducibility of results.

Under these conditions, the analytes are eluted within 6 min. A run time of 10 min was necessary to elute 3,4-dihydroxybenzylamine hydrobromide, used as the IS. Fig. 2

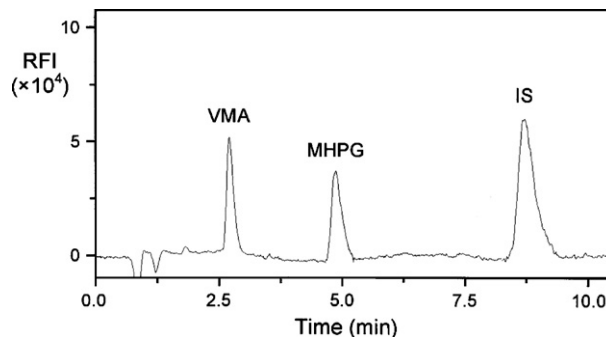


Fig. 2. Chromatogram of a standard solution containing 10 ng mL^{-1} of MHPG, 20 ng mL^{-1} of VMA and 20 ng mL^{-1} of the IS.

shows a chromatogram of a standard solution containing MHPG (10 ng mL^{-1}), VMA (20 ng mL^{-1}) and the IS (10 ng mL^{-1}): as can be seen, retention is satisfactory.

3.2. Analysis of standard solutions

Good linearity ($r^2 > 0.9997$) was obtained over the following concentration ranges: 0.4–80.0 ng mL^{-1} for MHPG, 1.0–80.0 ng mL^{-1} for VMA. Precision assays carried out at three different levels gave satisfactory results: repeatability (intraday precision), expressed as R.S.D., was always lower than 5.0% for MHPG and than 5.5% for VMA. Intermediate (interday) precision was also satisfactory, with R.S.D. values always lower than 6.1% for MHPG and than 6.2% for VMA.

3.3. Development of the solid-phase extraction procedure

Due to the very low concentrations of the analytes in human plasma and to the complexity of the plasma matrix, a very efficient sample pre-treatment procedure is needed to obtain satisfactory

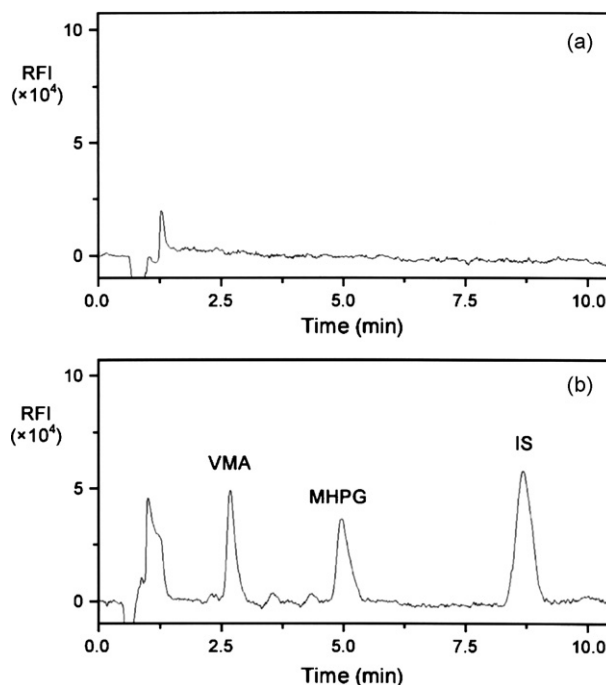


Fig. 3. Chromatograms of a blank plasma sample (a) and of the same sample spiked with 5 ng mL^{-1} of MHPG, 10 ng mL^{-1} of VMA (plasma concentrations, corresponding to 10 ng mL^{-1} of MHPG and 20 ng mL^{-1} of VMA) and 20 ng mL^{-1} of the IS (b).

Table 1
Linearity parameters.

Compound	Linearity (ng mL ⁻¹) ^a	Equation coefficients, $y = a + bx^b$		r^2	LOQ (ng mL ⁻¹) ^a	LOD (ng mL ⁻¹) ^a
		a	b			
MHPG	0.2–40.0	0.0011	0.0247	0.9992	0.2	0.1
VMA	0.5–20.0	0.0013	0.0110	0.9994	0.5	0.2

^a Plasma concentrations; the concentrations of the injected solutions can be found by multiplying the reported values by 2.

^b $y = \text{analyte/IS peak area ratio}$; $x = \text{analyte concentration, ng mL}^{-1}$.

Table 2
Extraction yield values and precision results.

Compound	Concentration (ng mL ⁻¹) ^a	Extraction yield (%) ^b	Repeatability (intra-day precision), RSD% ^b	Intermediate precision (inter-day precision), RSD% ^b
MHPG	0.2	92	5.5	6.3
	20.0	92	3.1	3.7
	40.0	94	2.8	3.3
VMA	0.5	91	5.8	6.6
	10.0	91	3.5	4.0
	20.0	92	3.0	3.2
IS	20.0	95	2.2	2.5

^a Plasma concentrations; the concentrations in the injected solutions can be found by multiplying the reported values by two.

^b $n = 6$.

results. SPE was chosen for this purpose, because it allows to obtain good sample purification and high extraction yields.

Since MHPG and VMA are endogenous compounds, it is not possible to find real “blank” plasma, i.e. plasma completely devoid of the analytes. For this reason, it was simulated with a solution of bovine albumin and salts (sodium and potassium phosphate and chloride) buffered at pH 7.4, which closely mimics the behaviour of real plasma for the purpose of SPE procedure development.

The two analytes have different chemical-physical properties: in fact, MHPG possesses two alcoholic functions and one phenolic group, while VMA has one alcoholic, one phenolic and one carboxylic group. As a consequence, finding a sorbent suitable for the extraction of both compounds by SPE is not easy. A procedure has been reported, which involves the use of two different cartridges (C18 and HLB, hydrophilic-lipophilic balance) and complexation with diphenylborate [11]. In order to develop a more feasible, less complicated and less time-consuming procedure,

different sorbents were thus tested, some possessing structural similarities with the analytes (such as phenol and diol), others for the possibility of interactions such as weak (diethylaminopropyl, DEA) and strong (trimethylaminopropyl, SAX) anionic exchange, others still for their versatility, such as HLB. None of these sorbents gave satisfactory extraction yield results for both compounds, however anionic exchange proved to be suitable for VMA while HLB was successful for MHPG and the IS. Thus, it was decided to work with a MAX mixed-mode sorbent, possessing both HLB and anionic exchange properties. This stationary phase is based on a divinylbenzene–polyvinylpyrrolidone copolymer having good affinity towards both lipophilic and hydrophilic compounds; it is modified to contain anionic exchange sites. This sorbent proved to be highly successful in the extraction of the analytes, providing suitable retention for all of them and granting good purification of the matrix.

The steps of washing and elution were carefully examined. If the washing step was carried out with neutral or acidic water/methanol mixtures it resulted in a sharp drop in analyte recovery, while basic buffers (phosphate, borate, carbonate) gave satisfactory sample purification and good analyte retention. The best results were obtained when washing the cartridge twice with 1 mL of pH 9.0 carbonate buffer.

For the elution step, a mixture of methanol and a weak organic acid (acetic acid) was suitable to displace the analytes from the sorbent. This is probably due to a combination of reversed-phase (methanol) and anion exchange (acetic acid) mechanisms. The eluate was then dried under vacuum and re-dissolved in 150 μ L of mobile phase to increase two times the concentrations of the analytes with respect to the original sample (whose volume was 300 μ L).

When the above described SPE procedure is carried out on spiked blank plasma samples, the chromatograms do not show any interference from the matrix and the analytes and the IS are detected as neat and symmetric peaks. As an example, the chromatogram of a blank plasma sample spiked with MHPG, VMA and the IS is reported in Fig. 3.

Table 3
Compounds tested for interference.

Class	Compound	t_R (min)
Monoamines and metabolites	3,4-Dihydroxybenzeneacetic acid (DOPAC)	n.d. ^a
	Dopamine	n.d.
	Epinephrine	n.d.
	5-Hydroxyindoleacetic acid (5-HIAA)	n.d.
	Norepinephrine	7.2
Antidepressants	Serotonin	n.d.
	Citalopram	n.d.
	Fluoxetine	n.d.
	Imipramine	n.d.
	Paroxetine	n.d.
	Trazodone	n.d.
Abuse drugs	Venlafaxine	n.d.
	Amphetamine	n.d.
	Buprenorphine	n.d.
	Cocaine	n.d.
	Codeine	n.d.
	Ecstasy (MDMA)	n.d.
	Ketamine	n.d.
	Lysergic acid diethylamide (LSD)	n.d.
	Methadone	n.d.
	Morphine	n.d.
	Δ^9 -Tetrahydrocannabinol (THC)	n.d.

^a n.d.: not detected within a 20 min chromatographic run.

3.4. Method validation

Having thus assured the suitability of the SPE procedure, calibration curves were set up on blank plasma by adding to the plasma

known amounts of analyte standard solutions at different concentrations and of IS standard solution at constant concentration and subjecting the resulting mixture to the SPE procedure.

Calibration curves were set up in the 0.2–40.0 ng mL⁻¹ range for MHPG and in the 0.5–40.0 ng mL⁻¹ range for VMA (corresponding, in the injected solutions, to 0.4–80.0 and 1.0–80.0 ng mL⁻¹ for MHPG and VMA, respectively). Good linearity ($r^2 > 0.9991$) was found over these concentration ranges; LOQ values were 0.2 ng mL⁻¹ for MHPG and 0.5 ng mL⁻¹ for VMA, while LOD values were 0.1 ng mL⁻¹ for MHPG and 0.2 ng mL⁻¹ for VMA. Both values were calculated according to the United States Pharmacopeia [25] and “Crystal City” guidelines [26]. Complete linearity details are reported in Table 1. Extraction yield (absolute recovery) and precision assays were carried out on simulated plasma spiked with analyte concentrations corresponding to the lower limits, middle levels and upper limits of the respective calibration curves. The results of these assays are reported in Table 2.

As one can note, mean extraction yields were always higher than 90%. Precision results were also satisfactory: R.S.D. values for repeatability were always lower than 5.9%; R.S.D. values for intermediate precision were lower than 6.7%.

3.5. Method selectivity

Selectivity was evaluated by injecting into the HPLC standard solutions of monoamines (epinephrine, norepinephrine, dopamine and serotonin), metabolites and some drugs (antidepressants, abuse drugs). The complete list of these compounds is reported in Table 3. It should be noted that some commonly used central nervous system drugs, such as antipsychotics and benzodiazepines, were not tested since it is known that they are not detected under

the chosen conditions; among antidepressants, only those possessing native fluorescence (such as fluoxetine, paroxetine and imipramine) were injected. Some monoamines and metabolites are fluorescent at the same wavelengths as MHPG and VMA, however none of them interferes with the analysis. Thus, selectivity is good.

3.6. Analysis of real plasma samples

Having thus successfully validated the method, it was then applied to the analysis of MHPG and VMA in plasma of several subjects who were either drug addicts undergoing detoxification therapy or subjects “at risk” of developing a drug addiction, as well as in the plasma of control subjects without any previous history of abuse drug consumption. A chromatogram of a plasma sample from a former drug user undergoing detoxification is reported in Fig. 4a, while a chromatogram of a plasma sample from a subject “at risk” is shown in Fig. 4b. As can be seen, the sample pre-treatment allows to obtain chromatograms devoid of interference from the biological matrix. The plasma sample shown in Fig. 4a contained an MHPG concentration of 21 ng mL⁻¹ and a VMA concentration of 15 ng mL⁻¹, and the plasma sample shown in Fig. 4b contained an MHPG concentration of 15 ng mL⁻¹ and a VMA concentration of 11 ng mL⁻¹.

These values are slightly higher than those found in healthy volunteers, in good agreement with the literature.

Method accuracy was evaluated by means of recovery studies at three different concentration levels ($n = 3$ for each level), as reported in Section 2.6.4 Accuracy.

Results were very satisfactory: mean recovery values were always higher than 90% for MHPG and higher than 91% for VMA. Standard deviation values were also good, always lower than 6.1 and 7.3 for MHPG and VMA, respectively.

4. Conclusion

The method developed for the determination of MHPG and VMA in human plasma, based on HPLC with fluorimetric detection, shows satisfactory precision and accuracy, good feasibility and rapidity, high sensitivity and selectivity due both to the fluorimetric detection and to the original and efficient SPE procedure. In fact the SPE step, carried out by means of MAX cartridges, has allowed obtaining high extraction yields (> 90%) and good selectivity.

When compared to the few other methods found in the literature, the present method does not require expensive or not readily available instrumentation [17–20]. The method by Unceta et al. [20] is more laborious and time-consuming: in fact, it requires several different reagents and a complex SPE procedure involving two different sorbents, a complexation reaction and plasma deproteinisation. Furthermore, the HPLC apparatus coupled to coulometric detection is more expensive and less widespread than HPLC with fluorescence detection.

Moreover, the sample pre-treatment procedure grants higher extraction yield results with respect to other methods which use protein precipitation [19] or dual-cartridge SPE [20].

In conclusion, the proposed HPLC method is suitable and advantageous for the reliable analysis of MHPG and VMA in human plasma.

Acknowledgements

This research was financially supported by Ministero dell'Istruzione, dell'Università e della Ricerca (MIUR) with RFO (ex-60%) funds.

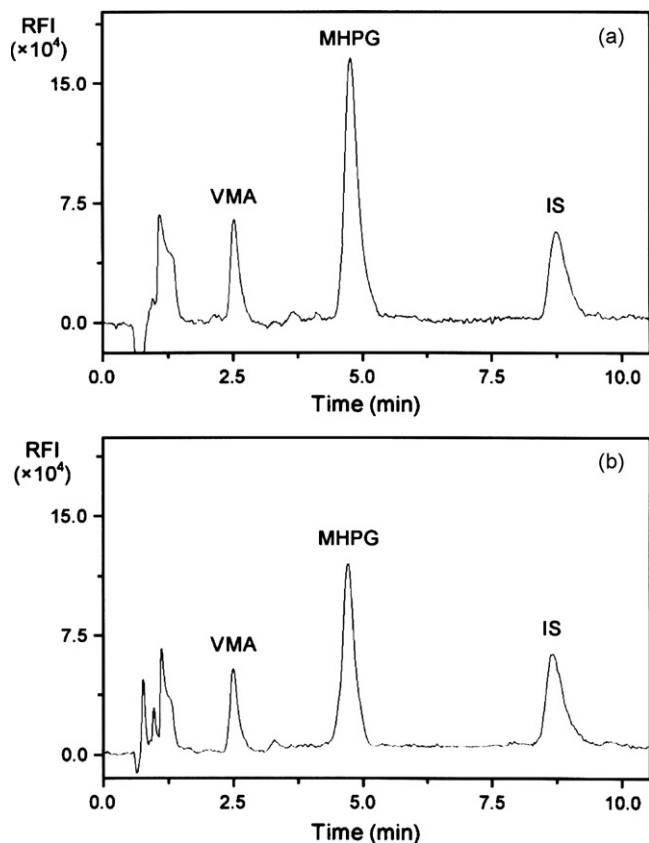


Fig. 4. Chromatograms of a plasma sample from a former drug user undergoing detoxification (a) and a subject “at risk” of developing drug addiction (b).

The Authors would like to thank Dr. Bruno Saladini for his technical assistance.

References

- [1] M. Codispoti, G. Gerra, O. Montebanocci, A. Zaimovic, M.A. Raggi, B. Baldaro, *Psychophysiology* 40 (2003) 863.
- [2] G. Gerra, A. Zaimovic, G. G. Mascetti, S. Gardini, U. Zambelli, M. Timpano, M.A. Raggi, F. Brambilla, *Psychoneuroendocrinology* 26 (2001) 91.
- [3] M. Fukuda, A. Hata, S.-I. Niwa, K.-I. Hiramatsu, H. Honda, K. Nakagome, A. Iwanami, *Psychiat. Res.* 63 (1996) 7.
- [4] L. Jasmin, M. Narasiah, D. Tien, *Vasc. Pharmacol.* 45 (2006) 243.
- [5] G. Gerra, A. Zaimovic, G.G. Mascetti, S. Gardini, U. Zambelli, M. Timpano, M.A. Raggi, F. Brambilla, *Psychoneuroendocrinology* 26 (2001) 91.
- [6] G. Gerra, B. Baldaro, A. Zaimovic, G. Moi, M. Bussandri, M.A. Raggi, F. Brambilla, *Drug Alcohol Depen.* 71 (2003) 25.
- [7] G. Gerra, A. Zaimovic, U. Zambelli, R. Delsignore, M.C. Baroni, G. Laviola, T. Macchia, F. Brambilla, *Psychiat. Res.* 96 (2000) 221.
- [8] G. Gerra, A. Zaimovic, G. Moi, M. Bussandri, C. Bubici, M. Mossini, M.A. Raggi, *Prog. Neuro-Psychoph.* 28 (2004) 129.
- [9] G. Laviola, W. Adriani, M.L. Terranova, G. Gerra, *Neurosci. Biobehav. R* 23 (1999) 993.
- [10] C.J. Drebing, R. Freedman, M. Waldo, G.A. Gerhardt, *Biomed. Chromatogr.* 3 (1989) 217.
- [11] M. Levitt, S. Kowalik, A.I. Barkai, *J. Neurosci. Meth.* 8 (1983) 155.
- [12] R.B. Taylor, R. Reid, K.E. Kendle, C. Geddes, P.F. Curle, *J. Chromatogr* 277 (1983) 101.
- [13] G.-M. Cao, T. Hoshino, *Chromatographia* 47 (1998) 396.
- [14] A.M. Kumar, J.B. Fernandez, K. Goodkin, N. Schneiderman, C. Eisdorfer, *J. Liq. Chromatogr. R. T.* 20 (1997) 1931.
- [15] A.M. Kumar, M. Kumar, J.B. Fernandez, N. Schneiderman, C. Eisdorfer, *J. Liq. Chromatogr.* 16 (1993) 1329.
- [16] M.H. Joseph, B.V. Kadam, D. Risby, *J. Chromatogr.* 226 (1981) 361.
- [17] H. Kuzuya, K. Fujita, H. Sakamoto, K. Kawai, K. Shimpō, H. Beppu, M. Ishida, T. Ito, *Biogenic Amines* 12 (1996) 9.
- [18] H. Ong, F. Capet-Antonini, N. Yamaguchi, D. Lamontagne, *J. Chromatogr.* 233 (1982) 97.
- [19] W.J. Burke, H.D. Chung, S.W. Li, *Anal. Biochem.* 273 (1999) 111.
- [20] N. Unceta, E. Rodriguez, Z.G. de Balugera, C. Sampedro, M.A. Goicolea, S. Barondo, J. Salles, R.J. Barrio, *Anal. Chim. Acta* 444 (2001) 211.
- [21] C. Sabbioni, M.A. Saracino, R. Mandrioli, S. Pinzauti, S. Furlanetto, G. Gerra, M.A. Raggi, *J. Chromatogr. A* 1032 (2004) 65.
- [22] M.A. Raggi, C. Sabbioni, G. Nicoletta, R. Mandrioli, G. Gerra, *J. Sep. Sci.* 26 (2003) 1141.
- [23] M.A. Raggi, C. Sabbioni, G. Casamenti, G. Gerra, N. Calonghi, L. Masotti, *J. Chromatogr. B* 730 (1999) 201.
- [24] M.A. Saracino, R. Mandrioli, L. Mercolini, A. Ferranti, A. Zaimovic, M.A. Raggi, *J. Pharmaceut. Biomed.* 42 (2006) 107.
- [25] The United States Pharmacopeia, 28th edn., United States Pharmacopeial Convention, Rockville (MD), 2005, pp. 2748–2751.
- [26] V.P. Shah, K.K. Midha, J.W.A. Findlay, H.M. Hill, J.D. Hulse, I.J. McGilveray, G. Mckay, K.J. Miller, R.N. Patnaik, M.L. Powell, A. Tonelli, C.T. Viswanathan, A. Yacobi, *Pharm. Res.* 17 (2000) 1551.



Development of a method for the analysis of seven banned azo-dyes in chilli and hot chilli food samples by pressurised liquid extraction and liquid chromatography with electrospray ionization-tandem mass spectrometry

Olga Pardo^{a,*}, Vicent Yusà^a, Nuria León^a, Agustín Pastor^b

^a Public Health Laboratory of Valencia, Conselleria de Sanitat, Camí de la Marjal, s/n 46470 Albal, Valencia, Spain

^b Analytical Chemistry Department, University of Valencia, Valencia, Spain

ARTICLE INFO

Article history:

Received 30 July 2008

Received in revised form 26 October 2008

Accepted 31 October 2008

Available online 7 November 2008

Keywords:

Sudan dyes

Azo-dyes

LC-MS-MS

Pressurised liquid extraction

Gel permeation chromatography

Experimental design

ABSTRACT

An automated, confirmatory and sensitive procedure has been developed and validated for the determination of Sudan (I–IV), Sudan Orange G, Sudan Red 7B and Para Red in hot chilli food samples. The proposed method includes pressurised liquid extraction (PLE) with acetone, gel permeation chromatography (GPC) clean-up and detection by liquid chromatography (LC) coupled to electrospray ionization in positive mode tandem mass spectrometry (ESI-MS-MS). The main parameters affecting the performance of the different ionization sources and PLE parameters were previously optimised using statistical design of experiments (DOE). The method was in-house validated on chilli powder and chilli meat. Linear calibrations were obtained with correlation coefficients $R^2 > 0.999$. The limits of detection (LOD) and quantification (LOQ) of the method were in the ranges of 0.002–0.012 ng g⁻¹ and 0.006–0.036 ng g⁻¹, respectively for chilli powder. The decision limit and detection capability were between 0.005–0.022 ng g⁻¹ and 0.007–0.026 ng g⁻¹, respectively for chilli meat. Recoveries ranged from 94% to 105%. The applicability of the method to the determination of azo-dyes in hot chilli products was demonstrated.

© 2008 Elsevier B.V. All rights reserved.

1. Introduction

Food quality is closely associated with colour and the use of food colourants has been an age-old practice, enhancing the aesthetic appeal of foods [1]. The use of synthetic organic dyes has been recognised as the most reliable and economical method of restoring or providing colour to a processed product. Azocompounds are by far the most widely used synthetic colourants [2]. Azo-dyes are synthetic organic colourants, characterised by chromophoric azo groups (–N=N–). Next to Sudan I–IV, Para Red, Butter Yellow, Sudan Red and Sudan Orange G belongs to the group of azo-dyes. Currently, there are over 3000 azo-dyes in use worldwide and they offer a wide spectrum of colours [3].

In order to prevent indiscriminate use, laws and regulations have been developed by many countries limiting types, purity, uses and amounts of authorised food dyes. The list of permitted synthetic dyes is progressively being reduced [1]. The list of authorised food colours and the maximum permitted levels in foodstuff are laid down in the annexes of Council Directive 94/36/EC [4]. Among organic colourants most of azo-dyes are recognised to be carcino-

gens [5]. Belonging to the azo-dye class, Sudan dyes may cause cancer to people and their presence at any level is not safe for the human [6].

Sudan I is not permitted colour under the Colours in Food Regulations [7] and is considered to be a genotoxic carcinogen [8]. Sudan II is the dimethyl derivate of Sudan I and has been tested in mice bladder implantation, resulting in a high incidence of bladder carcinomas [9]. Sudan III and Sudan IV are fat-soluble dye predominantly used for demonstrating presence of triglycerides in frozen sections. In addition, Sudan III and IV are commonly used for colouring waxes, oils and spirit varnishes. Sudan I, II, III and IV have been classified as a category 3 carcinogen by the International Agency for Research Cancer [10]. Consequently, the fraud identified by adulteration of chilli and chilli products by Sudan dyes constitutes a risk for public health. Para Red is chemically very similar to Sudan I and the Food Standards Agency (FSA) independent scientific experts have advised that it could be a genotoxic carcinogen [11].

In recent years, several processed food products, including chilli powder, curry sauce, and mustard sauce have been rejected or withdrawn by the European Union (EU) because of the presence of Sudan dyes. In particular, discovery of the azo-dye Sudan I in hot chilli and hot chilli products originating from India and marketed in the EU does not comply with the EU food safety requirements [12]. As a consequence, in June 2003, the European Union Commission

* Corresponding author.

E-mail address: pardo.olg@gva.es (O. Pardo).

adopted a decision on emergency measures concerning hot chilli and hot chilli products intended for human consumption [13]. On January 2004 the next emergency measures Decision 2004/92/EC were adopted by the Commission on Sudan I–IV [14].

According to the data collected through the Rapid Alert System for Food and Feed (RASFF), a sharp decrease in numbers of notifications about the fraudulent use of dyes in food has been observed since 2003. The 2006 RASFF annual report showed contamination with either Sudan I or Sudan IV or a combination of both in spices from the Region of India and Pakistan. Spice mixtures from the Russian Federation contained Sudan I, Para Red and a few times toluidine red and Sudan Red G. Few notifications on spices from Far East (Vietnam, China) showed the detection of Rhodamine B. In chilli from Nigeria, higher levels of Orange II were detected [15].

In this context, the use of banned dyes in food products exported in the European Union has led to an increasing demand for quantitative and confirmatory methods for compliance verification of these foodstuffs.

Several chromatographic methods have been proposed for the quantitative determination of azo-dyes in foodstuff, among them liquid chromatography with spectrophotometric [16] or fluorimetric detection [9]. Due to its high sensitivity, selectivity and minimal sample treatment required, liquid chromatography coupled to mass spectrometry (LC–MS) has become the preferred method for confirmatory analysis. LC methods with atmospheric pressure chemical ionization (APCI) [17] and electrospray ionization [6,12] for the identification of these substances have been developed and tandem mass spectrometry LC–APCI and [18] LC–ESI [19] combined with isotope dilution methods were described for the determination of Sudan dyes in foodstuff. A capillary liquid chromatography–electrospray tandem quadrupole orthogonal-acceleration time of flight mass spectrometry was used to accurate mass measurements for the confirmation of Sudan (I–IV) in hot chilli tomato sauce with detection limits from 0.4 to 11 $\mu\text{g g}^{-1}$ [20] and a LC–diode array detection–electrospray mass spectrometry was developed for simultaneous determination of water-soluble and fat-soluble synthetic colourants in foodstuff by high-performance liquid chromatography–diode array detection–electrospray mass spectrometry with detection limits from 1.25 to 5 $\mu\text{g g}^{-1}$ [21]. Some authors used internal standards [20,21] or standard addition techniques [22] in the analysis of Sudan dyes in order to improve their quantification.

The most frequently used extraction technique in these works is conventional solvent extraction. These procedures are laborious and time consuming. Pressurised liquid extraction has been frequently used for analysis of trace residues and contaminants in foods [23–27]. This paper describes the application of PLE for the determination of azo-dyes in foodstuffs in order to increase the speed of the extraction, the efficiency, the quantity of sample and the automatization and decrease the solvent consumption [28]. Various solvents (acetone, acetonitrile and methanol) were investigated and the dependence of the extraction yield from different parameters such as the static extraction time, pressure and oven temperature was studied.

Matrix interference from the large pigment and lipophilic compounds in foodstuffs is a serious hindrance to accurate quantification of lipophilic synthetic dyes in the foodstuffs [6], so gel permeation chromatography has been used by other authors [6,29] as clean-up technique to eliminate co-extractives molecular interferences such as fatty and wax from these kind of samples, based on the great difference in molecular size between them and the azo-dyes. In this work we developed a modified GPC method in order to purify the samples.

This study is focused on the development of an automated and sensitive method for the confirmatory detection of Sudan I, Sudan

II, Sudan III, Sudan IV, Sudan Orange G, Sudan Red 7B and Para Red in hot chilli products. It entails pressurised liquid extraction of azo-dyes from the hot chilli products followed by a GPC clean-up and analysis by LC–ESI–MS–MS, using Sudan I–D5, Sudan IV–D6 and Para Red–D6 as internal standards. The sensitivity of the method was improved by using GPC clean-up and by choosing the better ion source settings and LC conditions that maximised the analytical response provided by ESI. PLE parameters and ion source settings were optimised using statistically designed experiments [30]. The optimisation of both systems requires studying a multitude of parameters and can be very tedious by the approach of changing-one-factor-at-a-time (COST). In addition, this approach does not give information on interactions between experiments, so it can miss the optimal settings when interactions exist. Statistically designed experiments such as Plackett–Burman designs (P–B) and central composite designs (CCD) [31] can help optimise these kind of analytical parameters much more efficiently and in less runs than the COST approach [32,33].

The optimised method was applied to the determination of Sudan I, Sudan II, Sudan III, Sudan IV, Sudan Orange G, Sudan Red 7B and Para Red in hot chilli products selected from local supermarkets in Valencia (Spain) between January 2005 to December 2007 and can be used in the national monitoring programs to detect the presence of these illegal dyes in the framework of the European legislation.

2. Experimental

2.1. Standards and reagents

HPLC grade ethanol, acetone, dichloromethane, acetonitrile, formic acid and ammonium formate were supplied by Merck (Darmstadt, Germany) and ultrapure water was obtained from a Milli-Q filter system (Millipore, Bedford, MA, USA). Diatomaceous earth was from Sigma–Aldrich (Steinheim, Germany). The solvents for HPLC were filtered by 0.22 μm nylon membrane (Whatman, UK) and degassed in ultrasonic bath.

Standards of Sudan I, Sudan II, Sudan III, Sudan IV, Sudan Orange G, Sudan Red 7B and Para Red and internal standard Para Red–D6 were purchased from Dr. Ehrenstorfer GmbH (Augsburg, Germany). The purities of all standards were more than 90%. Internal standards Sudan I–D5 and Sudan IV–D6 were obtained from Witega Laboratorien Berlin–Adlershof GmbH (Berlin, Germany). The purities of the internal standards were more than 95%.

Individual stock solutions containing 200 $\mu\text{g mL}^{-1}$ approximately, were prepared in dimethylsulfoxide and stored at 4 °C in the dark. Intermediate mix solution at 1 $\mu\text{g mL}^{-1}$ and working solutions containing 1–1000 ng mL^{-1} approximately of each standard and 50 ng mL^{-1} of internal standards were prepared in methanol/water (9:1) and stored at 4 °C in the dark.

Sudan I and IV reference test material FAPAS T2031 (chilli powder), was provided by CSL (Central Science Laboratory, York, UK).

Statistical data manipulation and numerical analysis of data resulting from experimental design were carried out by means of the statistical package MINITAB for Windows, Release 14 (Minitab Inc., Birmingham, UK).

2.2. Equipment

Extractions were carried out using an accelerated solvent extraction system (ASE 200, Dionex, Sunnyvale, CA, USA) equipped with 22 mL stainless steel extraction cells. The waters gel permeation chromatography clean-up system employed for the purification was integrated by a Waters 515 high-pressure liquid chromatog-

Table 1
Estimated effects of the four factors on the analytes responses; statistical significance at 95% confidence level ($p < 0.05$).

Compound	Seath gas	Auxiliary gas	Capillary temperature	Spray voltage
Sudan I	3273405 (0.008)	796001 (0.435)	−699620 (0.491)	−9094 (0.993)
Sudan II	11631179 (0.006)	2461256 (0.462)	−1267341 (0.702)	1175041 (0.723)
Sudan III	3228829 (0.004)	1130031 (0.206)	−1505922 (0.103)	941183 (0.286)
Sudan IV	2011189 (0.001)	766381 (0.097)	−505099 (0.253)	791972 (0.088)
Sudan Red 7B	5569754 (0.001)	−180283 (0.885)	1794808 (0.173)	1642187 (0.208)
Sudan Orange G	1038895 (0.058)	−3265 (0.995)	−345585 (0.489)	33974 (0.945)
Para Red	3458528 (0.006)	2349856 (0.088)	−678429 (0.289)	875643 (0.112)

The minimum, central and maximum values used in the P–B design were: seath gas pressure 5–23–40 psi; auxiliary gas 5–13–20 arbitrary units; capillary temperature 200–275–350 °C; and spray voltage 2000–3500–5000 A.

raphy pump, a Waters 717 sample input module, tandem columns Envirogel GPC clean up 19 mm × 150 mm and 19 mm × 300 mm, and a Waters 2487UV detector (254 nm) together with a Gilson FC 204 Fraction Collector. To concentrate the extracts, a TurboVap II Concentration Workstation from Zymac (Hopkinton, MA, USA) was used.

The high performance liquid chromatography HPLC–MS system consists on a Finnigan Surveyor Autosampler, a Finnigan Surveyor LC Pump and a Finnigan TSQ Quantum Ultra triple quadrupole analyser detector (San José, CA, USA). Separations were obtained at 30 °C under isocratic conditions using a Luna C18 column, 150 mm × 2 mm i.d., 3 μm from Phenomenex (Macclesfield, UK).

2.3. Samples

Retail sampling was undertaken over the period January 2005 to December 2007. Different chilli tomato sauces, chilli powder, curry powder, curcumin powder and chilli meat were collected by public health inspectors from different supermarkets in the Valencia region (Spain) and stored at room temperature until analysis.

2.4. Sample preparation

After homogenising the whole samples (Ultra-Turrax TR-50, Germany), the sub-samples of the homogenate were stored at 4 °C in high-density polyethylene bottles with plastic screw-capped lids. As for sampling, an analytical aliquot of approximately 5 g was weighed and spiked with Sudan I–D5, Sudan IV–D6 and Para Red–D6 as internal standards to achieve a final concentration of 50 ng g^{−1}. After that the sub-samples were extracted by PLE.

The fortified samples were prepared by spiking 5 g of sample with the corresponding amount of intermediate mix solution. Homogenised spiked samples were stored at 4 °C during at least 6 h until analysis.

2.5. PLE conditions

The analytical aliquot was mixed and dried with diatomaceous earth with a spatula. Then the sample mixed with diatomaceous earth was placed into the 22 mL stainless-steel cell. After closing, to finger tightness, the sample cells were situated in the PLE 200 system carousel.

The samples were extracted using the following optimised conditions: Oven temperature of 95 °C, acetone as extraction solvent, 5 min heat-up time under a pressure of 1000 psi and two static cycles with a static time of 5 min. A volume equivalent to 60% of the extraction cell capacity was selected as flush volume. After the extraction a purge using pressurised nitrogen during 3 min was established.

The resultant extract (approximately 30 mL) was evaporated to dryness at 40 °C under nitrogen. Prior to the GPC clean-up, the

extracts were dissolved to 2.5 mL with dichloromethane and passed through 0.22 μm nylon membrane filter.

2.6. Solvent extraction conditions

The analytical aliquot was blended with 10 mL acetone [12]. After mixing for 2 min on a vortex the extract was centrifuged at 4500 rpm for 10 min. The resultant extract (approximately 30 mL) was evaporated to dryness at 40 °C under nitrogen. Prior to the GPC clean-up, the extracts were dissolved to 2.5 mL with dichloromethane and passed through 0.22 μm nylon membrane filter.

2.7. Gel permeation chromatography clean-up

The experimental conditions were as follows: a mobile phase of dichloromethane, a flow rate of 5 mL min^{−1}, and a volume injection of 2.5 mL. The collected fractions extended from 12.5 min to 17 min. Before each multiple-sample procedure, the GPC was calibrated by establishing an elution profile with a calibration solution which consisted of corn oil, bis(2-ethylhexyl)phthalate, methoxychlor and perylene [34]. The calibration chromatograms were examined to ensure that the relative retention times (RRTs) and peak shapes were as expected.

The collected fractions were evaporated under nitrogen flow at 40 °C, and re-dissolved in 250 μL of a solution containing acetonitrile/water (9:1, v/v) prior to their analysis by LC–MS–MS.

2.8. Liquid chromatography–electrospray ionization mass spectrometry (LC–ESI–MS–MS)

Separations were obtained at 30 °C under isocratic conditions using a 150 mm × 2 mm, 3 μm particle size Phenomenex Luna column from Phenomenex (Barcelona, Spain). The mobile phase system consisted of A (acetonitrile/water (9:1, v/v) containing of 2 mM ammonium formiat and 0.2% formic acid) and B (formiat buffer solution containing of 2 mM ammonium formiat and 0.2% formic acid) (97:3, v/v). The flow rate was set at 200 μL min^{−1} while the column temperature was maintained at 30 °C. The LC eluent was directed to the ESI interface within the retention time window 2–16 min using a diverter valve (Rheodyne, Cotati, USA) to prevent contamination of the ion optic region. The total run time of the chromatograms was 20 min and was divided into 10 segments in order to increase the sensitivity.

MS measurements were performed using a ESI source in positive selected reaction monitoring (SRM) mode. The ESI optimised experimental design parameters were as follows: Seath gas 10 psi, capillary temperature 200 °C, spray voltage 5000 V and auxiliary gas value 20 arbitrary units.

Table 2

Effect of different solvents on the extraction of the different Sudan dyes by PLE from a spiked chilli powder (2.5 ng g⁻¹).

Compound	Recovery (%) ±S.D.		
	Acetone	Acetonitrile	Ethanol
Sudan I	100 ± 5	81 ± 5	85 ± 7
Sudan II	98 ± 4	85 ± 4	82 ± 5
Sudan III	95 ± 8	86 ± 5	89 ± 4
Sudan IV	97 ± 6	82 ± 7	81 ± 6
Sudan Red 7B	105 ± 7	95 ± 6	84 ± 7
Sudan Orange G	99 ± 6	78 ± 3	79 ± 6
Para Red	94 ± 4	80 ± 8	81 ± 4

n = 5. S.D.: standard deviation.

2.9. Quantification and confirmation

Azo-dyes in incurred samples were quantified using a linear calibration function that was established with standard solutions in the range 1–1000 ng mL⁻¹. Each solution contained 50 ng mL⁻¹ of internal standards. Internal standard methodology was applied to quantify the different dyes. Sudan I-D5 was used as internal standard for the quantification of Sudan Orange G, Sudan I and Sudan II; Sudan IV-D6 was employed for Sudan III, Sudan Red 7B and Sudan IV and Para Red-D6 was used to quantify Para Red. Daily response curves for each analyte were plotted and six-point linear calibration plots with correlation coefficient (R^2) > 0.995 were used. The results were reported without correction for recovery because of the use of internal standards.

The confirmation criteria were according to the European Decision 2002/657/CE [35]: (1) the two product ions intensity must be, at least, three times greater than the base noise of the MS detector, (2) relative abundance between ions in the sample should be the same as in the standard, with the acceptable deviations described in this legislation (3) and the ratio between the chromatographic retention time of the analyte and its internal standard must be equal to those obtained for one of the calibration solutions, with a tolerance of ±0.5%.

Table 3

Pressurised liquid extraction conditions and analytical responses used for the central composite design optimisation of the three significant factors in the analysis of the seven azo-dyes^a.

Run	Analytical response						
	Area (au) ^b						
	Sudan I (m/z 156)	Sudan II (m/z 121)	Sudan III (m/z 77)	Sudan IV (m/z 91)	Sudan Red 7B (m/z 183)	Sudan Orange G (m/z 93)	Para Red (m/z 153)
1	198473	1199069	3641075	1585956	499593	931467	488364
2	206636	782327	5508337	2230954	546400	1086100	395745
3	149449	655020	4492418	1646519	603029	1221053	321783
4	87235	549478	4189808	1905404	447099	1006082	259916
5	51230	444908	3186072	1633086	313078	999537	235517
6	55263	430036	3233990	1613318	544646	1163442	229270
7	196027	342285	2608649	1218211	404591	986137	179318
8	222868	372589	3019306	1029076	551420	728519	186880
9	188975	317427	2803513	1085404	400176	952017	160827
10	192268	334821	2894748	1349566	636348	1060639	162034
11	155957	334286	2602197	1329046	621535	950908	169217
12	201882	403049	2443767	1478451	755726	1182468	179912
13	221239	444082	2878701	1784316	769325	1467518	224150
14	144956	287088	2524145	1240495	562718	1168293	139496
15	99263	148053	1159228	629699	284844	540887	80023
16	124510	235952	2187411	1232803	516916	1084472	124132
17	89132	407725	3280149	1907130	723119	1754230	214033
18	93700	276395	1993190	1275523	430106	953019	121174
19	94465	371314	2739258	1781080	931308	1884607	170076
20	88508	299007	2549908	1704043	858107	1679743	173314

The minimum, central and maximum values used in the CCD design were: pressure 1000–1250–1500 psi; temperature 40–95–150 °C and static time 2–5–8 min.

^a A spiked chilli powder at 2.5 ng g⁻¹ of azo-dyes was used.

^b au: analytical response in arbitrary units.

2.10. Analytical quality assurance

Each set of samples were analysed under quality-assurance protocols, including duplicate samples, reagent blanks and a quality control test materials (FAPAS T2031 chilli powder).

During this study, the laboratory participated in one interlaboratory proficiency testing provided by the Central Science Laboratory (CSL) with a satisfactory z-score. The laboratory works under the quality assurance system established by ISO/IEC/EN 17025.

3. Results and discussion

3.1. Detector settings optimisation

3.1.1. Preliminary experiments for optimisation of MS–MS parameters

In this work, ESI–MS–MS behavior of azo-dyes was investigated in positive mode, in order to maximize the responses. The first step of the MS–MS optimisation was to select the most abundant ions from the full scan spectra as the precursor ion, corresponding in all cases to the protonated molecule [M + H]⁺. The full scan spectra were monitored eluting at 50 μL min⁻¹, infusions of 10 μg mL⁻¹ individual standard solutions were realised.

The ESI(+)-MS–MS spectra of azo-dyes had been studied by other authors [6,12]. For Sudan I and Sudan II, the fragment corresponding to the loss of an OH[•] was observed at m/z 232 and m/z 260, respectively, with a relative intensity greater than 30%, whereas in the case of Sudan III and Sudan IV the relative intensity of such fragments was lower than 10%. The fragment ion at m/z 156 common to all dyes seems to originate from the cleavage of the C–N bond on the opposite side of the naphthalene group with hydrogen transfer to form a radical cation of the type [C₁₀H₈N₂]^{•+}. For all the azo-dyes studied, product ions originated by division of the molecules by the azo-group were formed, giving fragments ions like 121, 224 and 183 for Sudan II, Sudan IV and Sudan Red 7B, respectively.

After study the fragmentation of the precursor ions, parent ions and the two most abundant transitions for each analyte were

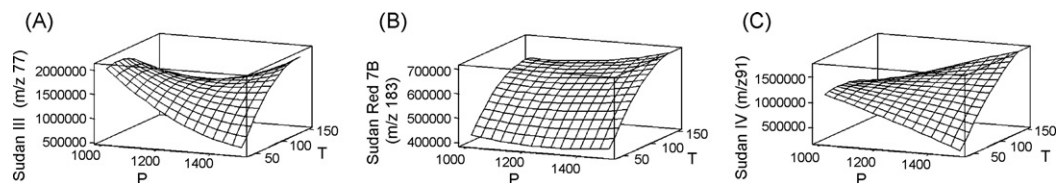


Fig. 1. Response surface for Sudan III (m/z 77), Sudan Red 7B (m/z 183) and Sudan IV (m/z 91) obtained in the central composite design optimisation of the PLE conditions. Pressure versus temperature. Fixed value: time (5 min).

selected. Collision energy and tubes lens were optimised automatically.

3.1.2. Ion source settings optimisation

The most important percentage of MS–MS response is source related. Although the TSQ Quantum detector has an automated source tuning, better improvement in the analyte responses could be achieved using a statistical design of experiments [30].

Considering the literature and previous studies carried out in our laboratory [24], four factors ($k=4$) were selected as potentially affecting the ESI efficiency: capillary temperature, auxiliary gas pressure, sheath gas pressure and spray voltage. A P–B design [30] was chosen as a screening method to estimate the relative influence of the four factors on the analytical response. With this screening design the main effects are calculated with a reduced number of experiments (12 runs, 1 block), and the experiment run order was randomized to provide protection against the effect of hidden variable. Although P–B designs for studying four factors require as few as eight runs, we used 12 runs plus a triplicate centre point in order to have generous degrees of freedom for testing the statistical significance.

The minimum, central and maximum values used in the P–B were: sheath gas pressure 5–23–40 psi; auxiliary gas 5–13–20 arbitrary units; capillary temperature 200–275–350 °C; and spray voltage 2000–3500–5000 A. The estimated effects of the five factors on all the analyte responses and their statistical significance at 95% confidence level are shown in Table 1. As can be seen only sheath gas had a significant effect on the analytical response for most of compounds studied. The selected values for the non-significant factors were as follows: auxiliary gas 20 au, capillary temperature 200 °C

and discharge current 5 A depending on their negative, positive or indistinct effect in the responses.

The sheath gas optimisation was realised by testing values from 5 to 40 psi and 10 psi were selected due to the maximum responses obtained for all the compounds.

3.2. ASE extraction optimisation

3.2.1. Effect of extraction solvent

The use of solvents at elevated temperatures increases the capacity of solvents to solubilise analytes and the diffusion rate. In addition, elevated temperatures also decrease the viscosity of liquid solvents (better penetration of matrix particles) and can disrupt the strong solute–matrix interactions caused by van der Waals forces, hydrogen bonding and dipole attractions of the solute molecules and active sites of the matrix [36].

The extraction efficiency of acetone, ethanol and acetonitrile, previously verified by others to be suitable extractants for Sudan dyes [21], was tested under the following PLE operating conditions: pressure, 1000 psi; temperature, 100 °C; static time, 5 min; and two cycles. The experiments were carried out on a spiked chilli powder sample (2.5 ng g^{-1}). Table 2 illustrates the effect of the solvent on the yield of the extractions.

Statistical analysis of the obtained data was carried out using a two-sample t -test approach at 95% confidence level [37]. Acetonitrile and ethanol gave similar responses and signal to noise ratios. The extracts obtained using acetone as extraction solvent were ‘clear’, and around 10 times higher signal responses were obtained due to less ion suppression effects. Finally, acetone was chosen as extraction solvent because statistically higher recover-

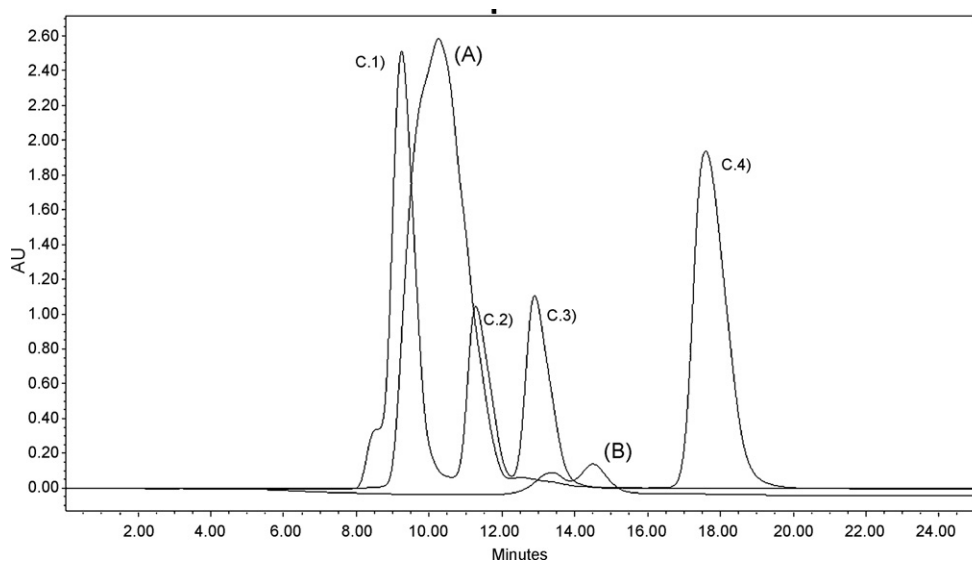


Fig. 2. GPC chromatograms of: (A) chilli powder extract; (B) mix solution containing about $10 \mu\text{g mL}^{-1}$ of each azo-dye; (C) GPC calibration solution, (C.1) corn oil, (C.2) bis(2-ethylhexyl)phthalate, (C.3) methoxychlor and (C.4) perylene.

Table 4

Analytical features of the proposed method; chilli powder validation.

	Fortified concentration (0.05 ng g ⁻¹)			Fortified concentration (2.5 ng g ⁻¹)			Fortified concentration (50 ng g ⁻¹)			LOD ^b (ng g ⁻¹)	LOQ ^b (ng g ⁻¹)
	Recovery ^a	Inter-assay R.S.D. ^a (%)	Intra-assay R.S.D. ^a (%)	Recovery ^a	Inter-assay R.S.D. ^a (%)	Intra-assay R.S.D. ^a (%)	Recovery ^a	Inter-assay R.S.D. ^a (%)	Intra-assay R.S.D. ^a (%)		
Sudan I	94	7	10	101	5	6	102	3	5	0.006	0.018
Sudan II	95	6	9	99	5	7/7	101	4	4	0.002	0.006
Sudan III	98	7	9	96	4	5/7	97	2	4	0.006	0.018
Sudan IV	96	5	8	94	4	6/6	99	3	5	0.010	0.030
Sudan Red/B	94	6	9	105	6	8/7	103	4	6	0.003	0.009
Sudan Orange G	99	5	7	100	5	6/5	100	5	5	0.012	0.036
Para Red	101	7	9	94	4	7	96	2	3	0.004	0.012

^a Validation schedule: 5 days, 3 replicates minimum each day; intra-assay: 5 replicates/1 day.^b Average of 10 replicates; LOD and LOQ calculated as three and ten times the noise level, respectively.

ies ($p < 0.05$) were obtained for the majority of the analytes studied than using acetonitrile or ethanol.

3.2.2. Optimisation of PLE conditions

The main parameters that have an influence on the performance of the PLE are temperature, pressure and extraction time [38]. A CCD design was chosen for screening the relative influence of these three parameters on the recovery of the different azo-dyes and was carried out with a spiked chilli powder (2.5 ng g⁻¹). The CCD model selected consisted of a full factorial design including eight cube points, six axial points and six central points in cube, with an alpha value of 1.682, involving 20 chromatographic injections. The 20 runs were randomized to provide protection against the effect of hidden variables. The minimum, central and maximum values used in the CCD were: pressure 1000–1250–1500 psi; temperature 40–95–150 °C and static time 2–5–8 min. The analytical responses are shown in Table 3. The analytical responses obtained were fitted into a linear equation that included second-order (curvature) and interaction terms. The equation model for the analytical responses (Y) was as follows:

$$Y = b_0 + b_1x_1 + b_2x_2 + b_3x_3 + b_{11}x_1^2 + b_{22}x_2^2 + b_{33}x_3^2 + b_{12}x_1x_2 + b_{13}x_1x_3 + b_{23}x_2x_3$$

where b_0 is the average response factor; x_1 , x_2 , x_3 are the temperature, pressure, and extraction time respectively; b_1 , b_2 , b_3 and b_4 are the coefficients for the main effect (1 for the temperature, 2 for the pressure and 3 for the extraction time; b_{11} , b_{22} and b_{33} are the coefficients for the quadratic effect; b_{12} , b_{13} and b_{23} are the coefficients for the two-factor interaction.

Three-dimensional response surfaces display the effect of the two independent variables on the analytical response (arbitrary units of peak areas). The following step was to select the factor settings that simultaneously optimise the responses of the seven compounds. This could be done using the “response optimiser” from response surface design in the MINITAB program. As we have

multiple responses for the seven compounds considered, and as the response surfaces are different for each one (see Fig. 1), there is no factor setting that simultaneously maximizes the desirability for each dependent variable. It must be noticed that the desirability is 0.00 for the lowest values obtained in the CCD; increases as response values increase; and is 1.0 for the highest response obtained in the experiments. For this reason, we maximize a composite desirability that combines the individual desirability of all the response variables into a single measure, taking into account that all the response variables have the same importance. The optimised factor settings were temperature 95 °C, pressure 1000 psi and 5 min extraction time. The composite desirability was 0.95.

3.3. Gel permeation chromatography study

Food samples are, in general, very complex matrixes. The GPC, based on the great difference in molecular size between some of the interferences and the target compounds, was chosen in order to remove coextractables, mainly lipids, from the extract. The GPC clean-up can decrease the presence of interferences in the final extract and also avoid the deterioration of the chromatographic column. At same time, interferences can also contaminate the ion source along with the analytic course of samples [6]. If the extracts were not treated through the clean-up steps, the interferences increased HPLC–MS–MS background noise, decreased the sensitivity of analytes and suppression or enhancement of the signal (matrix effects), affecting the reproducibility and accuracy of the method, were observed during the LC–MS–MS analysis. The use of this clean-up technique has been reported to avoid the use of matrix matched calibration [6] or standard addition methodology in order to quantify the dyes.

The GPC separation efficiency was investigated. The chromatogram corresponding to a 1 mL injection of a mix solution containing about 10 µg mL⁻¹ of each analyte was compared with the elution profile of a chilli powder extract and a calibration solution which consisted of corn oil, bis(2-ethylhexyl)phthalate,

Table 5

Analytical features of the proposed method; chilli meat validation.

	Fortified concentration (0.05 ng g ⁻¹)			Fortified concentration (2.5 ng g ⁻¹)			Fortified concentration (50 ng g ⁻¹)			CC α (ng g ⁻¹)	CC β (ng g ⁻¹)
	Recovery ^a	Inter-assay R.S.D. ^a (%)	Intra-assay R.S.D. ^a (%)	Recovery ^a	Inter-assay R.S.D. ^a (%)	Intra-assay R.S.D. ^a (%)	Recovery ^a	Inter-assay R.S.D. ^a (%)	Intra-assay R.S.D. ^a (%)		
Sudan I	97	6	9	102	4	7	98	4	5	0.010	0.013
Sudan II	99	6	10	94	5	7	94	4	6	0.005	0.007
Sudan III	95	5	9	101	5	7	102	4	4	0.014	0.017
Sudan IV	99	5	9	99	4	6	105	3	4	0.022	0.026
Sudan Red 7B	100	7	7	96	6	7	98	3	4	0.012	0.016
Sudan Orange G	96	6	9	94	6	5	97	4	4	0.018	0.022
Para Red	97	7	10	104	6	7	104	4	5	0.009	0.012

^a Validation schedule: 5 days, 3 replicates minimum each day; intra-assay: 5 replicates/1 day.

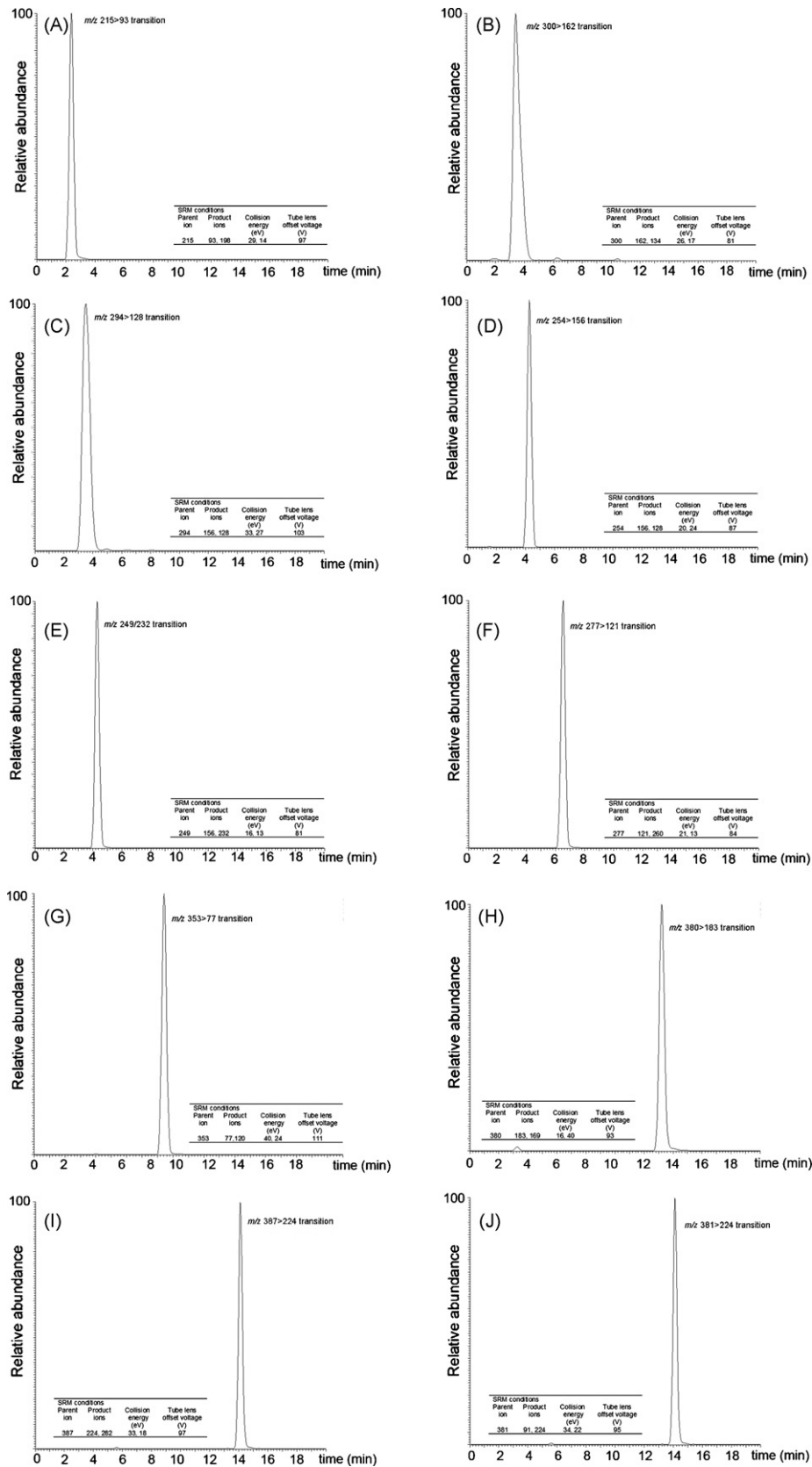


Fig. 3. Chromatogram of a spiked chilli meat at 2.5 ng g⁻¹; (A) Sudan Orange G; (B) Para Red-D6; (C) Para Red; (D) Sudan I-D5; (E) Sudan I; (F) Sudan II; (G) Sudan III; (H) Sudan Red 7B; (I) Sudan IV-D6; (J) Sudan IV.

Table 6

Comparison of PLE and conventional solvent extraction for a spiked chilli powder at 2.5 ng g⁻¹ of azo-dyes.

	PLE		Solvent extraction	
	Recovery (n = 10)	R.S.D. (%)	Recovery (n = 10)	R.S.D. (%)
Sudan I	100	5	82	9
Sudan II	98	4	68	9
Sudan III	95	8	75	8
Sudan IV	97	6	86	9
Sudan Red 7B	105	7	75	11
Sudan Orange G	99	6	72	10
Para Red	94	4	68	10

methoxychlor and perylene (Fig. 2). The experimental conditions were mobile phase of dichloromethane and a flow rate of 5 mL min⁻¹. Finally, the time of collection was fixed from 12.5 to 17 min in order to eliminate the main interference (the lipidic fraction) and collect the entire fraction corresponding to the elution of the azo-dyes.

3.4. Evaluation of matrix effects

Signal suppression or enhancement as a result of matrix effect (ME) can severely compromise quantitative analysis of the azo-dyes at trace levels. Matrix effects must be evaluated and discussed in the context of method development before method qualification and appropriate calibration techniques compensating for these effects should be used.

ME was studied and described by others [39]. In this way, two different sets of solutions were prepared (set A: standard solutions in mobile phase; set B: spiked blank sample extracts) and determined using the ESI interface and the optimised factor settings. The absence or presence of matrix effects on the quantification was evaluated by comparing the absolute peak areas of the two sets (ME% = B/A × 100). Both A and B sets had concentrations of 50 ng mL⁻¹.

No compound presented matrix effect, the ME ranged from 98% to 102%, indicating that it is not necessary to use the matrix-matched standard calibrations.

3.5. Performance characteristics of the method

Calibration solutions (1, 10, 50, 100 and 1000 ng mL⁻¹ of the 7 azo-dyes and 50 ng mL⁻¹ of internal standards) were used to construct calibration curves. The linear model was statistically validated taking into account that residual values were randomly distributed about the regression line, the *p*-value of the *F*-test statistic was <0.05, and the coefficient of determination (*R*²) was better than 0.999 [40].

The validation of the method was carried out over 3 days with a chilli powder and a chilli meat spiked at three different levels: 0.05, 2.5 and 50 ng g⁻¹. These samples were used to assess accuracy and intra-assay and inter-assay precision in each level. Detection and quantification limits were calculated for the chilli powder as the signal three or ten times higher of the noise level, respectively.

According to the criteria specified in the 2002/657/EC European decision [35], decision limit and detection capability were calculated for the chilli meat. The decision limits (CC_α) were estimated by analysing 20 blank materials and calculating the signal-to-noise ratio at the time window in which the analytes are expected. The detection capability (CC_β) was estimated by analysing 20 blank materials fortified with the analytes decision limits. The value of the decision limit plus 1.64 times the standard deviation of the within-laboratory reproducibility of the measured content equals the detection capability (*β* = 5%).

Analytical features of the method are shown in Table 4 (for chilli powder) and Table 5 (for chilli meat) and Fig. 3 illustrates a chromatogram of a spiked chilli meat at 2.5 ng g⁻¹. The LOD values are lower than those reported by others [6,12,17].

The recoveries obtained of all the compounds using PLE were compared with the recoveries obtained with solvent extraction, the most widely used technique for the extraction of these compounds in food samples. In all of the cases, the recoveries using PLE are statistically higher (*p* < 0.05) than those obtained by solvent extraction (Table 6). Moreover conventional solvent extraction suppose 30 min of manual handling for each sample, front only 5 min of manual handling and 12 min of automatic work for PLE.

3.6. Analysis of real samples

Once the operating conditions had been optimised, analysis of real samples was performed. In this study, 46 spice samples (curry, curcumin and chilli powder), 29 chilli tomato sauces and 6 chilli meats were analysed for their azo-dyes content. Samples were selected from local supermarkets in Valencia from January 2005 to December 2007. No peaks of interest were detected in any case, which demonstrates the safety of the foods tested and the fulfilment of the Spanish and European legislation that do not permit the use of these colourants as food additives [4,41].

4. Conclusions

This work describes an automated, rapid, confirmatory and sensitive procedure for the simultaneous determination of seven azo-dyes hot chilli food samples suitable to monitoring the presence of these banned substances in a large number samples each day. The method requires a minimum hand-working; PLE and GPC purification provide a readily automation.

The GPC clean-up procedure avoids some interference and the matrix effect during the MS–MS detection and the use of internal standard correct the losses of analytes during the process. The ESI(+)-MS–MS detection can provide the confirmation and accurate determination of the dyes.

Validation data demonstrate that this method is suitable to monitoring the presence of azo-dye residues in hot chilli food samples at trace levels in the framework of national control programmes. The estimated LOD and LOQ were in the range of 0.02–0.12 ng g⁻¹ and 0.05–0.36 ng g⁻¹, respectively and recoveries ranged from 94% to 105%. Using the optimised method azo-dye levels were investigated in 46 spice samples (curry, curcumin and chilli powder), 29 chilli tomato sauces and 6 chilli meats, demonstrating that the samples were in compliance with European and Spanish Legislation.

References

- [1] E.C. Vidotti, J.C. Cancino, C.C. Oliveira, M.E. Rollemberg, Anal. Sci. 21 (2005) 149.
- [2] M.S. Reisch, Chem. Eng. News 66 (1988) 7.
- [3] F. Rafii, J.D. Hall, C.E. Cerniglia, Food Chem. Toxicol. 25 (1997) 897.
- [4] European Parliament and Council Directive 94/36/EC of 30 June 1994 on colors for use in foodstuff, Off. J. Eur. Commun. L237 (1994) 13–29.
- [5] M.F. Boeninger, Department of Health and Human Service, Publication No. NIOSH 80, 1980.
- [6] H. Sun, F. Wang, L. Ai, J. Chromatogr. 164 (2007) 120.
- [7] The Colours in Food Regulations 1995, ISBN 0110537319.
- [8] M. Stiborová, V. Martinek, H. Rýdlová, P. Hodek, E. Frei, Cancer Res. 63 (2002) 5678.
- [9] A. Pielesz, I. Baranowska, A. Rybak, A. Wlochowicz, Ecotoxicol. Environ. Saf. 53 (2002) 42.
- [10] IARC Monographs on the Evaluation of the Carcinogenic Risk of Chemicals to Man, vol. 8, IARC, Lyon, 1975, p. 125.
- [11] Food Standards Agency: <http://www.food.gov.uk>
- [12] F. Calbani, M. Careri, L. Elviri, A. Mangia, L. Pistrà, I. Zagnoni, J. Chromatogr. A 1042 (2004) 123.

- [13] Commission Decision of 20 June 2003 on emergency measures regarding hot chilli and hot chilli products, notified under document number C (2003) 1970, (2003/460/EC), O J no L. 154/114, 21.6.2003.
- [14] Commission Decision 2004/92/EC on emergency measures regarding hot chilli and hot chilli product, notified under document number C (2004) 68, (2004/92/EC), O J no. L. 27/52, 30.1.2004.
- [15] Activities of the European Union and Summaries of legislation: <http://europa.eu>.
- [16] M. Nagase, Y. Osaki, T. Matesuda, J. Chromatogr. 465 (1989) 434.
- [17] F. Tateo, M. Bononi, J. Agric. Food Chem. 52 (2004) 655.
- [18] L. Di Donna, L. Maiuolo, F. Mozzotti, D. DeLuca, G. Sindona, Anal. Chem. 76 (2004) 5104.
- [19] F. Mazzotti, L. Di Donna, L. Maiuolo, A. Napoli, R. Salerno, A. Sajjad, G. Sindona, J. Agric. Food Chem. 56 (2008) 63.
- [20] F. Calbiani, M. Careri, L. Elviri, A. Mangia, I. Zagnoni, J. Chromatogr. A 1058 (2004) 127.
- [21] M. Ma, X.B. Luo, B. Chen, S.P. Su, S.Z. Yao, J. Chromatogr. A 1103 (2006) 170.
- [22] L.-H. Ahlström, S. Amon, L. Mathiasson, J. Sep. Sci. 28 (2005) 2407.
- [23] O. Pardo, V. Yusà, N. León, A. Pastor, J. Chromatogr. A 1107 (2006) 70.
- [24] D.E. Breithaupt, Food Chem. 86 (2004) 449.
- [25] K. Ridway, S.P.D. Lalljie, R.M. Smith, J. Chromatogr. A 1153 (2007) 36.
- [26] G.F. Barbero, M. Palma, C.G. Barroso, J. Agric. Food Chem. 54 (2006) 3231.
- [27] M. Villagrasa, M. Guillamón, A. Navarro, E. Eljarrat, D. Barceló, J. Chromatogr. A 1179 (2) (2008) 90.
- [28] V. Yusà, O. Pardo, P. Martí, A. Pastor, Food Addit. Contam. 22 (2005) 482.
- [29] M. Mazzetti, R. Fascioli, I. Mazzoncini, G. Spinelli, I. Morelli, A. Bertoli, Food Addit. Contam. 21 (2004) 935.
- [30] D.L. Massart, B.G.M. Vandeginste, C.M.C. Buydens, S. de Jong, P.J. Lewi, J. Smeyers-Vrbeke, Handbook of Chemometrics and Qualimetrics, Amsterdam, The Netherlands, 1997 (Part A).
- [31] DIONEX, Technical Note 208, Sunnyvale, CA, USA, 2000.
- [32] C. Peña-Farfal, A. Moreda-Piñeiro, A. Bermejo-Barrera, P. Bermejo-Barrera, H. Pinochet-Cancino, I. de Gregori-Henríquez, Talanta 64 (2004) 671.
- [33] V. Flotron, J. Houessou, A. Bosio, C. Delteil, A. Bermond, V. Camel, J. Chromatogr. A 999 (2003) 175.
- [34] EPA method 3640 A: Gel-permeation clean-up, 1994, Revision 1, <http://www.epa.gov/epaoswer/hazwaste/test/pdfs/3640a.pdf>.
- [35] EU, Commission of the European Communities 2002/657/EC, Off. J. Eur. Commun. L221 (2002) 8.
- [36] E. Ritcher, B.A. Jones, J.L. Ezell, N.L. Porter, N. Avdalovic, C. Pohl, Anal. Chem. 68 (1996) 1033.
- [37] W.P. Gardiner, Methods for chemists, Cambridge RSC, 1997, p. 51.
- [38] L.J. Fitzpatrick, O. Zuloaga, N. Etxebarria, J.R. Dean, Rev. Anal. Chem. 19 (2000) 75.
- [39] B.K. Matuszewsky, M.L. Constanzer, C.M. Chavez-Eng, Anal. Chem. 75 (2003) 3019.
- [40] Eurachem Guide, The fitness purpose of analytical methods, A laboratory guide to method validation and related topics, LGC, Teddington, Middlesex, UK, 1998.
- [41] Real Decreto 142/2002, BOE 44 (2002) 6756.



Detection of water in jet fuel using layer-by-layer thin film coated long period grating sensor

Sean D. Puckett, Gilbert E. Pacey*

Miami University Center for Nanotechnology, Department of Chemistry and Biochemistry, Miami University, Oxford, OH 45056, United States

ARTICLE INFO

Article history:

Received 6 October 2008

Received in revised form 11 November 2008

Accepted 12 November 2008

Available online 19 November 2008

Keywords:

Water in jet fuel

Long period gratings

Layer-by-layer multilayers

ABSTRACT

The quantitative measurement of jet fuel additives in the field is of interest to the Air Force. The “smart nozzle” project was designed as a state-of-the-art diagnostics package attached to a single-point refueling nozzle for assessing key fuel properties as the fuel is dispensed. The objective of the work was to show proof of concept that a layer-by-layer thin film and long period grating fibers could be used to detect the presence of water in jet fuel. The data for the nafion/PDMA film and a long period grating fiber is a combination capable of quantitative measurement of water in kerosene. The average response (spectral loss wavelength shift) to the kerosene sample ranged from -6.0 for 15 ppm to -126.5 for 60 ppm water. The average calculated value for the check standard was 21.71 and ranged from 21.25 to 22.00 with a true value of 22.5 ppm water. Potential interferences were observed and are judged to be insignificant in real samples.

© 2008 Elsevier B.V. All rights reserved.

1. Introduction

The quantitative measurement of jet fuel additives in the field is of interest to the Air Force. The “smart nozzle” project was designed as a state-of-the-art diagnostics package attached to a single-point refueling nozzle for assessing key fuel properties as the fuel is dispensed. Smart nozzle does not currently exist; however, several emerging sensor technologies offer key capabilities that are critical to the development of the smart nozzle concept.

Research efforts are in progress to develop next-generation gas-turbine-engine technologies with improved performance specifications. These advanced engines will operate at much higher temperatures than current engines, exposing engine components to greater levels of thermal stress and necessitating the development of improved thermal-dissipation technologies. One approach that has been quite successful involves increasing the thermal stability of the aircraft fuel (currently demonstrated by JP-8 + 100 with $T_{\max} \sim 425$ °F) to make it capable of absorbing greater quantities of excess heat without excessive thermal degradation. This advanced aircraft fuel, identified as JP-8 + 225, will possess an upper operating temperature T_{\max} of ~ 550 °F. This operating temperature is achieved through the addition of a package of additives that enable the fuel to meet this temperature specification. Failure to provide the proper fuel to aircraft using advanced gas-turbine-engine technologies will result in dramatically higher costs of operation due to

down time, excessive maintenance, and potential engine damage resulting from thermal stressing of the fuel and engine components.

In order to achieve the desired fuel performance, additives are mixed into the Jet A fuel. Additives are fuel-soluble chemicals added in small amounts to enhance or maintain properties important to fuel performance or fuel handling. Typically, additives are derived from petroleum-based raw materials and their function and chemistry are highly specialized. They produce the desired effect in the parts per million concentration range. These additives fall into the general categories such as thermal stabilizers, antioxidants, metal deactivators, defoamers, and electrical-conductivity. Water is not an additive but can occur in three different forms in jet fuel: dissolved in the fuel, as a separate liquid phase (free water), and as a fuel-water emulsion. Some amount of dissolved water is present in all fuels. This dissolved water is not a problem; free water or a water emulsion are potentially hazardous and must be avoided.

One of the sensor technologies being investigated is the long period grating, LPG, [1–10]. The important elements of an LPG are identified as the fiber core into which the grating is written, the fiber cladding that surrounds the core, and the coating that is bonded to the cladding surface. An LPG fiber-optic sensor operates as a spectral-loss element. When broadband light is coupled through the fiber core, selected wavelengths are diffracted by the LPG from the fiber-core modes to the fiber cladding modes. The selected wavelengths that are coupled to the latter are lost when the light exiting the fiber core is analyzed. The result is an attenuation band in the spectral profile of the light that passes through

* Corresponding author.

E-mail address: paceyge@muohio.edu (G.E. Pacey).

the fiber core. The position and shape of the attenuation band is dependent on the grating period of the LPG, the refractive indices of the fiber core, the fiber cladding, and the surrounding environment (some type of coating), the local temperature, and strain–bending [11] and geometry of the optical fiber.

Measurement of a chemical concentration by LPG is predicated on local changes in the density around the sensor. These changes result in a change in the refractive index, which induces a change in the spectral profile of the attenuation band. Analyses have been performed heretofore in an equilibrium mode in which the fiber is allowed to equilibrate with the surroundings prior to measurement of the spectral profile change. This approach for quantification of chemicals has been used for antifreeze [12], volatile organic compounds, [13] corrosion products, [14,15] aqueous sugar solutions, [16] aromatic compounds dissolved in alkanes, [17] and biological compounds [18,19]. In previous studies the analytical measurements have shown relatively high limits of detection. The lowest limits of detection reported to date with the use of an LPG are 3×10^{-4} M obtained in solutions of cane sugar and 90 parts per 106 (ppm) for trichloroethylene and toluene in air. The majority of the early LPG reports have used some type of affinity coating that swells when in contact with the analyte of interest. We have shown that kinetic methods can describe the slow responses from the affinity coating LPG sensors but the speed of this measurement is problematic. As a result an investigation into faster responding materials such as layer-by-layer multilayer nanostructures was initiated. From this work it is clear that the slow response is eliminated and increased sensitivity is observed [20].

The research present in this publication aims to show proof of concept that a long period grating fiber that has been coated has the ability to detect the amount of water saturation in jet fuel.

2. Materials and methods

2.1. Reagents

All chemicals were purchased from Sigma–Aldrich. They were Reagent Grade unless otherwise specified. Poly(diallyldimethylammonium chloride) (PDMA), solution was prepared by pipetting 0.5 mL of PDMA medium molecular weight, 20% weight in water in to 19.5 mL double distilled deionized water (DDDI). Poly acrylic acid (PAA) solution was prepared by weighing 1.0 g of PAA sodium salt and mixing into 20 mL DDDI. Nafion solution was prepared by pipetting 1 mL of Nafion 117 solution ~5% in a mixture of lower aliphatic alcohols and water into 19 mL methanol. Fresh piranha solution was prepared by mixing 30 mL of H_2SO_4 with 70 mL of 30% H_2O_2 . The pH 12.1 solution was prepared by adding drop-wise a concentrated potassium hydroxide solution to DDDI until the pH meter read 12.1 on the readout. Kerosene was obtained from local sources. The kerosene was dried by adding magnesium sulfate certified anhydrous to an Erlenmeyer flask filled with kerosene and placing on a magnetic stirrer for 30 min. The kerosene was allowed to sit for 10 min to allow the magnesium sulfate to settle before samples were prepared. Water saturated kerosene was prepared by adding DDDI to an Erlenmeyer flask filled with kerosene and shaking to mix and allowing to settle for 10 min until the drops of DDDI could be seen clumped into pools. Kerosene samples were prepared by pipetting in proper ratio dried and saturated kerosene into three dram vial until a total volume of 8 mL is reached. The fiber is exposed to the sample solutions in an increasing saturation percentage. After the daily experiment is completed the fiber is immersed into dry methanol to rinse the remaining kerosene off the fiber before being placed into the dry box overnight.

2.2. Layer-by-Layer assembly long period gratings

The LPG fibers, which were obtained from Luna Innovations, were initially cleansed by immersion in piranha solution for 2 min and then rinsed with DDDI and blown dried. The fibers were first modified by immersion in pH 12.1 KOH/DDDI solution for 30 min. The LPG fiber is then blown dried. The fibers are then soaked in the Nafion or poly acrylic acid (PAA) solution for 10 min. After soaking in the first layer the fiber is blown dried and soaked for 10 min in the PDMA solution. After film build up is complete the fiber is dried and placed into a desiccator overnight.

2.3. Instrumentation

The LPG data were collected with a Lunascan III (Luna Innovations Blackburn, VA). The fiber was held using a 3 prong clamp during individual experiments. The instrument operates by using a LED light source centered at 820 nm; the optical fiber with the LPG grating written on the core had approximate dimensions of: exposed length, 2 cm; optical elements diameter (inner plus outer core), 0.1 mm; and diameter including the cladding, 1 mm.

3. Results and discussion

3.1. Development of the process to analyze LPG kerosene samples

The LPG produces a spectrum where the wavelength location of the spectral loss is used as the analytical measurement. The location of the spectral loss is a function of the refractive index of the media in direct contact with the LPG fiber. The effective refractive index region is governed by the fiber material. In the case of the current fiber obtained with the Luna Scan III instrument, they are designed to be used in an aqueous environment that has a refractive index of 1.33. Jet fuel has higher baseline refractive index, 1.45, which is at the high wavelength range of these fibers. As a result a new method to determine the analytical signal had to be developed to process the LPG results. Fig. 1 shows the LPG fiber response in the presence of air and immersed into water.

As shown in Fig. 1 when the LPG fiber is immersed into water the single peak that is centered on 815 nm undergoes a spectra loss effect resulting in two smaller peaks with a wavelength shift centered in between 819 and 820 nm. When the wavelength shift is present between 805 and 830 nm an algorithm in the instrumental software lists the wavelength shift minimum to within 0.0001 nm. Fig. 2 shows the spectra for a LPG that has been exposed to kerosene samples that contained between 0 ppm to a maximum of 60 ppm water.

Starting with the data shown in Fig. 2, the value at 750 nm is subtracted from each point value for that given spectra produc-

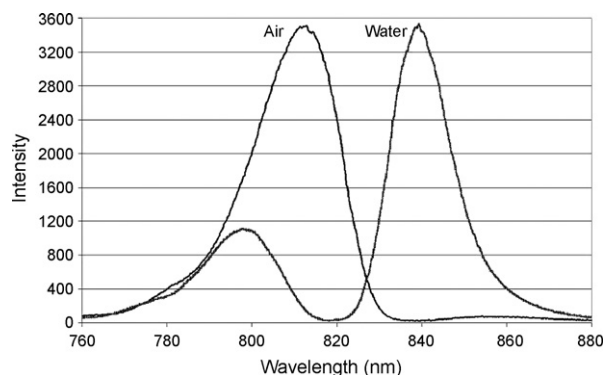


Fig. 1. Long period grating fiber response spectra to air and water.

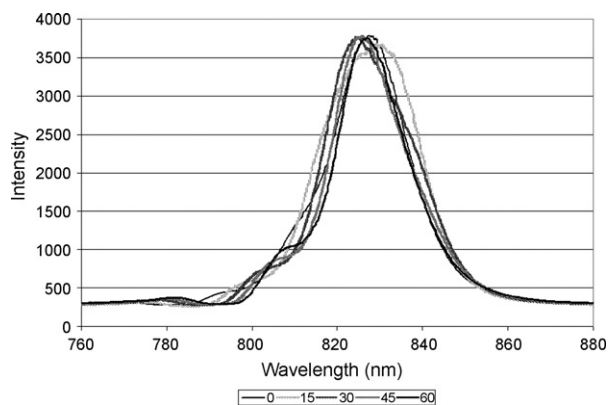


Fig. 2. Long period grating fiber response spectra to water present in kerosene as obtained from instrument.

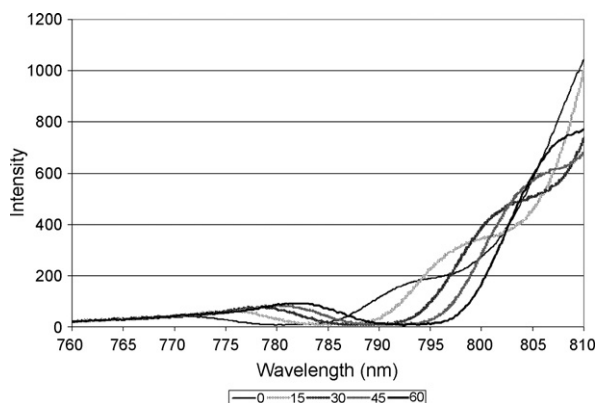


Fig. 3. Long period grating fiber response spectra to water present in kerosene normalized zoomed in.

ing the data shown in zoomed in region between 760 and 810 nm shown in Fig. 3. The next step is to take the values for the 0% water in kerosene spectrum and subtract it. The results for this step are shown in Fig. 4. These wavelength shift minimum are used as the Y-axis and are plotted to generate the calibration plots.

3.2. Bare LPG fiber exposed to kerosene

It would be expected that the bare LPG would respond at some level to the refractive index changes produced by the addition of water to kerosene. The water measured was dissolved water. In the initial experiments the bare fiber responded to different levels of

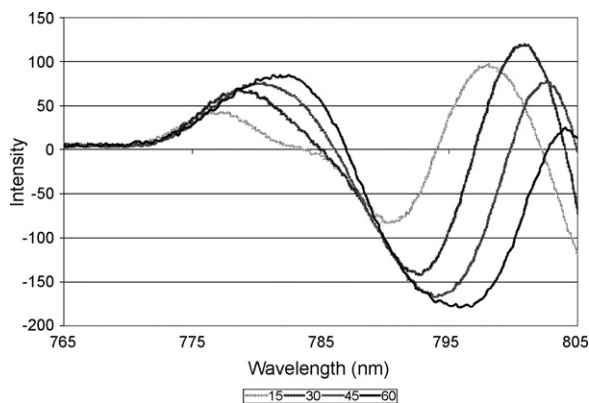


Fig. 4. Long period grating fiber response spectra to water present in kerosene 0% subtracted from other samples.

water in kerosene. The refractive index does change and the bare LPG exhibited a small response change to water. But given that this is a bare fiber, any change in refractive index produces a response; therefore, there is no specificity in this measurement. A coating will be needed to provide that specificity. From preliminary experiments two candidate emerged; PAA/PDMA and Nafion/PDMA.

3.3. PAA/PDMA pair films exposed to kerosene

Experiments were performed to determine the optimal thickness for PAA/PDMA film. Table 1 shows the results for these experiments. Films were prepared with alternating layers of PAA/PDMA. Films with one to three pairs of layers were tested.

The wavelength shift values for single, double and triple pairs are shown in Table 1. The average slope of the trend line was -0.0364 , -0.0173 , and -0.0073 for single, double, and triple pair films. Based on the slope values the single film has 2.1 times and 5 times the sensitivity of the double and triple pair films respectively. The coefficients of correlation for the film were 0.998, 0.997, and 0.989 for single to triple pair films respectively. These results show that additional film pairs did not provide any analytical benefit. Indeed the single pair films not only produced the most sensitivity, but also, as expected responded quicker than multiple pair films.

3.4. PAA/PDMA reproducibility–reversibility kerosene

Using single pair films, the reproducibility and reversibility of the PAA/PDMA film system to the exposure of 0 to 60 ppm maximum dissolved water present in kerosene was evaluated. The average response to the kerosene sample ranged from -32.5 for 15 ppm water to -368.6 for 60 ppm water present in kerosene. The average calculated value for the check standard was 22.43 and ranged from 22.09 to 22.99 with a true value of 22.5 ppm water producing a 0.3% RSD. Surprisingly, the wavelength shift movement values (0–60 ppm) between daily runs were not constant. For example a particular fiber exhibited wavelength shift movement values of -528.7 , -248.7 , and -328.3 on three different days. Yet on each of the individual days the films displayed a low percent error on the check standard indicating that the PAA/PDMA film system accurately detects dissolved water levels in kerosene.

Although the sensitivity of this coating is superior to the Nafion, the wide amount of error on the daily runs peak size show that the repeatability of the PAA/PDMA layer-by-layer was not acceptable.

3.5. Nafion/PDMA pair films exposed to kerosene

The effect of Nafion/PDMA pair films on the response to water levels in kerosene was investigated. Table 2 shows the results for these experiments. The average slopes of the trend lines were -0.0144 , -0.0071 , and 0.0002 for single, double, and triple pair films respectively. Based on the slope values the single film has 2 times the sensitivity and 72 times the sensitivity of the double and triple pair films respectively. The coefficients of correlation for the responses with each pair films were 0.995, 0.999, and 0.999 for single to triple pair films, respectively.

3.6. Nafion/PDMA reproducibility–reversibility kerosene

Using a single pair films the reproducibility and reversibility of the Nafion/PDMA film system to the exposure to varying levels of water in kerosene was tested. In addition to the five samples used for the pair films study an additional sample, 22.5 ppm water in kerosene (check standard), was added to test the accuracy of the results shown. The average response to the kerosene sample ranged from -6.0 for 15 ppm to -126.5 for 60 ppm water. The average calculated value for the check standard was 21.71 and ranged from

Table 1

Single, double, and triple poly acrylic acid/poly(diallyldimethyl ammonium chloride) film coated long period grating fiber response to water in kerosene.

	ppm water	Reading 1	Reading 2	Reading 3	Average reading	Standard deviation
Single film	0	0	0	0	0	0
	15	-4.3	-4.0	-5.3	-4.5	0.68
	30	-33.0	-36.3	-39.0	-36.1	3.00
	45	-74.7	-76.3	-82.0	-77.7	3.84
	60	-136.0	-127.7	-140.0	-134.6	6.27
	Double film	0	0	0	0	0
15		-10.7	-10.7	-11.3	-10.9	0.35
30		-21.3	-22.3	-23.7	-22.4	1.21
45		-44.3	-44.3	-45.3	-44.6	0.58
60		-75.0	-83.0	-74.3	-77.4	4.83
Triple film		0	0	0	0	0
	15	-10.7	-10.7	-11.3	-10.9	0.35
	30	-22.0	-21.3	-23.0	-22.1	0.85
	45	-31.0	-32.0	-33.3	-32.1	1.15
	60	-54.7	-55.0	-55.7	-55.1	0.51

21.25 to 22.00 with a true value of 22.5 ppm water. The average error associated with the check standard was 3.53 and ranged from 5.56 on the high side to 2.21 on the low side. The average peak wavelength shift for 0 ppm water to 60 ppm water was -126.5. The wavelength shift values for each run were -127.3, 124.3, and 128.0 for a percent difference from the average of -1.17% to 1.19%. The low percent difference on the total wavelength shift difference between daily runs and the similar error for the check standards show that the results for the detection of water in kerosene are both reproducible.

3.7. Nafion/PDMA 12.5% ethanol, 1,4-dioxane, THF spiked

Potential interferents, ethanol, 1,4-dioxane, or THF were addition and the response of the Nafion/PDMA film system to the exposure to varying saturation levels of water in kerosene was observed. Lower percentages of these compounds did not exhibit any significant interference. Table 2 shows the results. As in the experiment described above a check standard was employed. The amount of spiked additive, 12.5%, was well above the expected level of an additive, less than 5%, present in normal fuel samples.

For the addition of 12.5% ethanol the average response to the kerosene sample ranged from -82.9 for 15 ppm water to -180.2 for 60 ppm water in kerosene. The average calculated value for the check standard was 24.43 and ranged from 20.34 to 22.80 with a true value of 22.5 ppm water in kerosene. The average error associated with the check standard was 0.40 and ranged from 9.59 on the high side to -8.57 on the low side. The average peak wavelength shift for 0 ppm water to 60 ppm water was -180.2. The wavelength shift values for each run were -175.3, -192.7, and -172.7 for a percent difference from the average of -6.92% to 4.18%.

For the addition of 12.5% 1,4-dioxane the average response to the kerosene sample ranged from -47.8 for 15 ppm to -178.9 for 60 ppm water in kerosene. The average calculated value for the check standard was 21.64 ppm water and ranged from 21.20 to 21.89 with a true value of 22.5 ppm water. The average error associated with the check standard was 3.84 and ranged from 5.76 on the high side to 2.72 on the low side. The average peak wavelength shift for 0 ppm to 60 ppm water in kerosene was -178.9. The wavelength shift values for each run were -170.3, -182.0 and -184.3 for a percent difference from the average of -3.04% to 4.79%.

Table 2

Single, double, and triple nafion/poly(diallyldimethylammonium chloride) film coated long period grating fiber response to water in kerosene.

	ppm water	Reading 1	Reading 2	Reading 3	Average reading	Standard deviation
Single film	0	0	0	0	0	0
	15	-11.3	-11.6	-23.3	-15.4	6.84
	30	-50.0	-50.3	-55.7	-52.0	3.21
	45	-86.3	-84.3	-103.0	-91.2	10.27
	60	-107.3	-132.0	-144.7	-128.0	19.02
	Double film	0	0	0	0	0
15		-16.3	-9.2	-5.0	-10.2	5.71
30		-31.5	-26.3	-20.0	-25.9	5.76
45		-45.0	-45.6	-36.5	-42.4	5.09
60		-68.3	-69.6	-52.3	-63.4	9.63
Triple film		0	0	0	0	0
	15	-3.7	-5.0	-3.1	-3.9	0.97
	30	-5.7	-10.1	-9.1	-8.3	2.31
	45	-8.9	-12.1	-14.7	-11.9	2.91
	60	-13.4	-15.2	-19.2	-15.9	2.97

For the addition of 12.5% THF the average response to the kerosene sample ranged from -62.2 for 15 ppm water to -194.6 for 60 ppm water. The average calculated value for the check standard was 17.28 and ranged from 15.95 to 19.29 with a true value of 22.5 ppm water in kerosene. The average error associated with the check standard was 23.22 and ranged from 29.11 on the high side to 14.27 on the low side. The average peak wavelength shift for 0 ppm water to 60 ppm water in kerosene was -194.6 . The wavelength shift values for each run were -192.7 , -195.3 , and -195.7 for a percent difference from the average of -0.58% to 0.96% . The high levels of potential interferences needed to create an interfering signal are well above the expected levels and are judged to be insignificant in real samples.

4. Conclusions

The objective of the work presented here was to show proof of concept that a LBL thin film and LPG fiber could be used to detect the presence of water in fuel. To achieve this goal a different way of data analysis had to be devised. The data for the nafion/PDMA film and a long period grating fiber is a combination capable of quantitative measurement of water in kerosene. Potential interferences were observed at very high levels and are judged to be insignificant in real samples. In order for the LPG to be a viable sensor for the “Smart Nozzle” project, the fiber must be optimized for the wavelength range needed for kerosene and the spectral reproducibility of the bare fiber spectrum must be significantly improved.

Acknowledgements

The authors thank DAGSI, PR-MU-01-16, and the National Science Foundation, ECS 0304297 for their support of this project.

References

- [1] A.M. Vengsarkar, P.J. Lemaire, J.B. Judkins, V. Bhatia, T. Erdogan, J.E. Sipe, *J. Lightwave Technol.* 14 (1996) 58–65.
- [2] V. Bhatia, A.M. Vengsarkar, *Opt. Lett.* 21 (1996) 692–694.
- [3] B.A.L. Gwandu, X. Shu, T.P.D. Allsop, *Electron. Lett.* 38 (2002) 695–696.
- [4] C.C. Ye, S.W. James, R.P. Tatam, *Opt. Lett.* 25 (2000) 1007–1009.
- [5] H.J. Patrick, *Electron. Lett.* 36 (2000) 1763–1764.
- [6] Y. Liu, L. Zhang, J.A.R. Williams, I. Bennion, *IEEE Photon. Technol. Lett.* 12 (2000) 531–533.
- [7] H.J. Patrick, S.T. Vohra, C.C. Chang, *Electron. Lett.* 34 (1998) 1773–1775.
- [8] S.R.M. Kueh, R.S. Parnas, S.G. Advani, *Compos. Sci. Technol.* 62 (2002) 311–327.
- [9] Y. Liu, L. Zhang, J.A.R. Williams, I. Bennion, *Opt. Commun.* 193 (2001) 69–72.
- [10] Y.-G. Han, B.H. Lee, W.-T. Han, U.-C. Paek, Y. Chung, *Meas. Sci. Technol.* 12 (2001) 778–781.
- [11] L.A. Wang, C.Y. Lin, G.W. Chern, *Meas. Sci. Technol.* 12 (2001) 793–799.
- [12] R. Falciai, A.G. Mignani, A. Vannini, *Sens. Actuators B* 74 (2001) 74–77.
- [13] H.J. Patrick, A.D. Kersey, F.J. Bucholtz, *Lightwave Technol.* 16 (1998) 1606–1612.
- [14] K. Goswami, J. Prohaska, A. Menon, E. Mendoza, R. Lieberman, X. Proc. SPIE 3540 (1998) 115–122.
- [15] J.A. Greene, M.E. Jones, T.A. Tran, K.A. Murphy, P.M. Schindler, V. Bhatia, R.G. May, D. Sherrer, R.O. Claus, *Proc. SPIE* 2718 (1996) 170–174.
- [16] J. Elster, J. Greene, M. Jones, T. Bailey, S. Lenahan, W. Velandar, R. Van Tassel, W. Hodges, X. Proc. SPIE 3540 (1998) 251–257.
- [17] X. Shu, D. Huang, *Opt. Commun.* 171 (1999) 65–69.
- [18] T. Allsop, L. Zhang, I. Bennion, *Opt. Commun.* 191 (2001) 181–190.
- [19] T.A. Tran, V. Bhatia, T. D’Alberty, K.A. Murphy, R.O. Claus, *Proc. SPIE* 2676 (1996) 165–170.
- [20] J. Widera, G.E. Pacey, C. Bunker, J.R. Gord, V.R. Katta, J. Elster, M.E. Jones, S.W. Buckner, *Appl. Opt.* 44 (2005) 1011–1017.



An electrochemiluminescent biosensor for glucose based on the electrochemiluminescence of luminol on the nafion/glucose oxidase/poly(nickel(II)tetrasulfophthalocyanine)/multi-walled carbon nanotubes modified electrode

Bin Qiu^{a,b}, Zhenyu Lin^{a,b,*}, Jian Wang^{a,b}, Zhihuang Chen^{a,b}, Jinhua Chen^{a,b}, Guonan Chen^{a,b,*}

^a Ministry of Education Key Laboratory of Analysis and Detection Technology for Food Safety (Fuzhou University), Fuzhou, Fujian 350002, China

^b Department of Chemistry, Fuzhou University, Fuzhou, Fujian 350002, China

ARTICLE INFO

Article history:

Received 22 July 2008

Received in revised form 26 October 2008

Accepted 28 October 2008

Available online 17 November 2008

Keywords:

Electrochemiluminescent sensor

Glucose

Nickel phthalocyanine

Multi-walled carbon nanotubes

Luminol

ABSTRACT

A poly(nickel(II) tetrasulfophthalocyanine)/multi-walled carbon nanotubes composite modified electrode (polyNiTSPc/MWNTs) was fabricated by electropolymerization of NiTSPc on MWNTs-modified glassy carbon electrode (GCE). The modified electrode was found to be able to greatly improve the emission of luminol electrochemiluminescence (ECL) in a solution containing hydrogen peroxide. Glucose oxidase (GOD) was immobilized on the surface of polyNiTSPc/MWNTs modified GC electrode by Nafion to establish an ECL glucose sensor. Under the optimum conditions, the linear response range of glucose was 1.0×10^{-6} to 1.0×10^{-4} mol L⁻¹ with a detection limit of 8.0×10^{-8} mol L⁻¹ (defined as the concentration that could be detected at the signal-to-noise ratio of 3). The ECL sensor showed an outstanding well reproducibility and long-term stability. The established method has been applied to determine the glucose concentrations in real serum samples with satisfactory results.

© 2008 Elsevier B.V. All rights reserved.

1. Introduction

Recently, the development of electrochemiluminescent (ECL) sensors has been paid more and more attention by the analysts since they not only retain the advantages of chemiluminescence (CL) sensor, such as excellent sensitivity, wide dynamic concentration response range, but also have some additional advantages [1–5]. For example, the applied potential to produce the CL reaction can be easily controlled, which can improve its selectivity. Furthermore, the generation of light in the vicinity of the electrode would improve the spatial control for sensitive detection of analyte [6,7]. Besides the widely used Ru(bpy)₃²⁺-based ECL sensors [8,9], luminol-based ECL systems have also been developed to construct the ECL sensors because of its low oxidation potential, inexpensive reagent consumption and the high emission yields [10–16].

The luminol ECL intensity is directly proportional to the amount of luminol or hydrogen peroxide, and glucose can react with the dissolved oxygen to produce hydrogen peroxide in presence of glucose oxidase (GOD) [17], so a lot of ECL based glucose sensors have been

developed [18–23]. Many efforts had been paid to develop more sensitive and durable glucose ECL sensors, such as using iron species in the clay to enhance the ECL intensity [18], using photo-cross-link polymer [19,20], sol–gel composite [21] or proactive membrane [22,23] to immobilize the GOD, and a lot of work still needs to be done.

Since the rediscovery of carbon nanotubes (CNT) in 1991 [24], intensive attention has been paid on the analytical application of CNT for its high aspect ratio, excellent electrical conductivity, good chemical stability and extremely high mechanical strength [25,26]. These remarkable mechanical and electrical properties endow them with a wide range of applications [27–32]. On the other hand, conducting polymer/CNTs composites have received great interests in recent years because the incorporation of CNTs into conducting polymers can lead to produce the new composite materials with individual properties of each component, and their synergistic effect would be useful in some particular applications [33]. Among the various conducting polymers, metallophthalocyanine has become the most attractive one because of its electrocatalytic property [34]. Ni-phthalocyanine, using as the electrocatalyst to prepare the modified electrodes has shown interesting electrocatalytic properties [35–39]. Nickel(II) tetrasulfophthalocyanine (NiTSPc) polymerized on the GCE can retain phthalocyanine's macrocycle structure, Ni atom can play as a role

* Corresponding authors at: Department of Chemistry, Fuzhou University, Fuzhou, Fujian 350002, China. Tel.: +86 591 87893315; fax: +86 591 83713866.
E-mail addresses: zylin@fzu.edu.cn (Z. Lin), gnchen@fzu.edu.cn (G. Chen).

similar to that in Ni(OH)₂, which can catalyze ECL of luminol [39]. When it is immobilized on the electrode and used as the ECL sensor, the ECL sensitivity of the sensor can be greatly enhanced.

In our early study, we found that the presence of polyNiTSPc could catalyze the ECL of luminol, and the ECL intensity was increased with the thick of polyfilm, but if the film was too thick, it would block the charge transfer, and ECL intensity would not be enhanced anymore [39]. So if the charge transfer rate can be enhanced, the ECL behavior can be further improved. It is well known that MWNT can accelerate the electron transfer and can enhance ECL of luminol [46]. So the purpose of this study is to couple the catalyzing ability of NiTSPc with the charge transfer ability of MWNT to improve the performance of the luminol-based ECL sensor.

A polyNiTSPc/MWNT modified electrode has been fabricated by electropolymerization of NiTSPc on MWNT-modified glassy carbon electrode (GCE). GOD has been immobilized on the surface of the modified electrode to establish a glucose ECL sensor.

2. Experimental

2.1. Chemicals

Luminol, GOD (Aldrich Chem. Co., USA) and NiTSPc (Fluka, Switzerland,) were used as received without further purification. A stock solution of $1.0 \times 10^{-3} \text{ mol L}^{-1}$ luminol was prepared and stored at 4 °C. H₂O₂ working solution was prepared freshly daily from 30% (v/v) H₂O₂ (Bengbu, China Xinke Electrochemical Reagent Factory). Nafion (5 wt% aqueous alcoholic solution, Aldrich) was prepared as 0.1% by dilution with ethanol. The MWNT was obtained from Shenzhen Nanotech Port Co. Ltd. and purified according to the literature method [40]. Working solutions were made by dilution of these stock solutions. Serum samples were kindly provided by the Hospital of Fuzhou University (Fuzhou, China). Glucose concentration of the samples had been tested by sysmex CHEMIX-180 automated biochemistry analyzer (Tokyo, Japan, SYSMEX Corporation). All other reagents were of analytical grade or better, double-distilled water was used throughout the experiments.

2.2. Apparatus

ECL detection system consisted of a BPCL ultraweak luminescence analyzer (Institute of Biophysics, Chinese Academy of Science, Beijing, China) and a CHI660a electrochemical analyzer (Shanghai Chenhua Instrument Co., China). A three-electrode system was used, a modified GCE (diameter 3 mm) was used as working electrode, platinum wire and Ag/AgCl (sat. KCl) were used as counter electrode and reference electrode, respectively. A commercial 5 mL cylindroid glass cell was used as an ECL cell, which was washed with 0.2 mol L^{-1} nitric acid and water in sequence before using.

2.3. Procedure

2.3.1. Fabrication of the modified electrode

The GCE was pretreated by polishing its surface with aqueous slurries of alumina powders ($1.0 \mu\text{m}$ and $0.3 \mu\text{m}$ $\alpha\text{-Al}_2\text{O}_3$) on polishing cloth and carefully rinsed with water to give a smooth and clean electrode surface. Followed by cyclic voltammetry (CV) scanning in 0.1 mol L^{-1} H₂SO₄ aqueous solution from -0.2 to 0.8 V at 0.05 V s^{-1} until a stable CV current obtained. $10 \mu\text{L}$ of the black suspension (which was prepared by dispersing the desired amount of purified MWNTs in N,N-dimethyl formamide (DMF) solution) was dropped on GCE surface and evaporated under an infrared lamp. PolyNiTSPc film was formed by using CV scanning in the

range of $0.2\text{--}0.8 \text{ V}$ (versus Ag/AgCl) with a scanning rate of 0.1 V s^{-1} in 0.20 mol L^{-1} NaOH solution containing $5.0 \times 10^{-3} \text{ mol L}^{-1}$ NiTSPc under argon deoxygenated conditions. After the electropolymerization, the electrode was rinsed with water, and transferred to the buffer solution for preservation. The thickness of the film can be controlled by varying the CV scanning times. Appropriate concentration of GOD mixed with Nafion was directly dropped onto the polyNiTSPc/MWNT/GCE surface and dried in the air. The established modified electrode was stored in buffer solution at 4 °C when it was not used.

2.3.2. Static ECL measurement

Luminol and glucose were mixed just before the experiment in borate buffer solution (pH 7.4). A potential from 0.0 to 0.80 V was applied to the working electrode and the ECL signal was recorded simultaneously. The emission at 0.50 V was used for the quantitative analysis.

3. Results and discussion

3.1. Electrode characterization

3.1.1. Formation of polyNiTSPc

The electropolymerization of NiTSPc was obtained by repetitive CV scanning in range of $0.2\text{--}0.8 \text{ V}$ at a scan rate of 0.10 V s^{-1} , which resulted in the oxidation of Ni(II) ions to electrodeposit the corresponding electroactive polymers on the MWNT/GCE surface. Fig. 1 shows the typical CV curves recorded during the electropolymerization of NiTSPc on GCE and MWNT/GCE. It can be seen from Fig. 1A that a pair of reversible redox peaks appeared at $E_c = 0.43 \text{ V}$ and $E_a = 0.55 \text{ V}$ while in Fig. 1B appeared at $E_c = 0.40 \text{ V}$ and $E_a = 0.52 \text{ V}$ respectively. The area of polymer film on the MWNT/GCE is larger than that on the bare GCE, the reason for this maybe due to the presence of MWNT, which can increase the charge transfer rate, so more conductive polymer film has been deposited on the surface of the electrode.

3.1.2. Effect of amount of MWNTs attached on the electrode

ECL response of polyNiTSPc/MWNT/GCE to luminol is expected to be affected by the amount of MWNTs on the electrode surface. Fig. 2 shows the relationship between the ECL intensity and amount of MWNTs (represented as the MWNTs concentration of the suspension solution) on the modified electrode (the thickness of the polyNiTSPc is 80 cycles). With the increasing of MWNTs concentra-

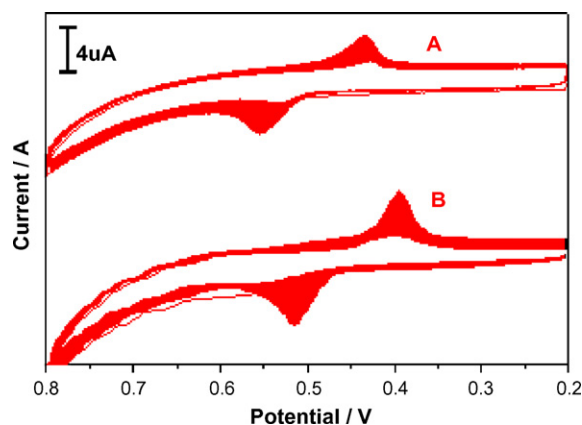


Fig. 1. CV curves of the electrodeposition of NiTSPc film on GCE (A) and MWNT/GCE (B) by consecutive potential cycling in a fresh solution containing $5.0 \times 10^{-3} \text{ mol L}^{-1}$ NiTSPc and 0.20 mol L^{-1} NaOH in the potential range of $0.20\text{--}0.80 \text{ V}$ (versus Ag/AgCl) at a scan rate of 0.10 V s^{-1} .

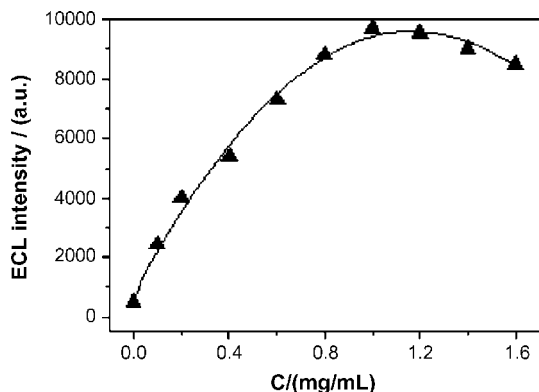


Fig. 2. Effect of MWNTs concentration on the ECL response of polyNiTSPc/MWNT modified electrode in borate buffer solution (pH 7.4) with $1.0 \times 10^{-5} \text{ mol L}^{-1}$ luminol and $8.0 \times 10^{-4} \text{ mol L}^{-1} \text{ H}_2\text{O}_2$.

tion, the ECL intensity of luminol enhances accordingly. When it is higher than 1 mg mL^{-1} , the ECL intensity decreases slightly. In this work, a moderate MWNTs concentration of 1 mg mL^{-1} was selected for the fabrication of polyNiTSPc/MWNT composite modified GCE.

3.1.3. Effect of NiTSPc film thickness

NiTSPc thickness can be easily controlled by the cycles of CV scanning during electropolymerization process. Fig. 3 shows the correlation between the thickness of the polymeric NiTSPc film and the ECL signal of luminol. The ECL intensity increases with the growing of the polymer film, but after 80 cycles of polymerizing scans the intensity tends towards constant. The ECL intensity obtained on the NiTSPc/MWNT modified GCE is about 10 times of that on MWNT modified electrode, indicating that the polymeric NiTSPc film can effectively enhance the ECL intensity of luminol.

3.1.4. Electro-oxidation and enhanced ECL of luminol on polyNiTSPc/MWNT/GCE

Fig. 4(I) (inset of Fig. 4) showed the CV curves of luminol on different electrodes in borate buffer solution (pH 7.4). On the bare GCE, only a small oxidation peak of luminol can be observed, while on MWNT modified electrode, the background current and the luminol oxidation peak current increase greatly. These results can be attributed to the large surface effect of the carbon nanotubes and the facilitation of electron-transfer by carbon nanotubes. Comparing curve C (for MWNT/GCE) with curve

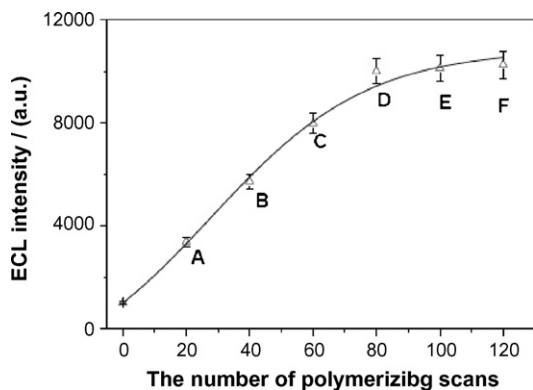


Fig. 3. ECL response of luminol on the different thickness polyNiTSPc/MWNT-modified GCE in borate buffer solution (pH 7.4) with $1.0 \times 10^{-5} \text{ mol L}^{-1}$ luminol and $8.0 \times 10^{-4} \text{ mol L}^{-1} \text{ H}_2\text{O}_2$. The polymers with different thickness were obtained by controlling the number of the electropolymerizing scans. A: 20 cycles, B: 40 cycles, C: 60 cycles, D: 80 cycles, E: 100 cycles, F: 120 cycles.

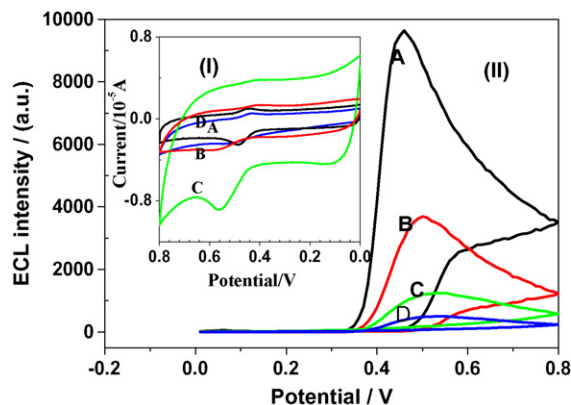


Fig. 4. ECL and CV (inset) response of luminol on the different electrodes in a borate buffer solution (pH 7.4) with $1.0 \times 10^{-5} \text{ mol L}^{-1}$ luminol and $8.0 \times 10^{-4} \text{ mol L}^{-1} \text{ H}_2\text{O}_2$. A: polyNiTSPc/MWNT/GCE; B: polyNiTSPc/GCE; C: MWNT/GCE; D: bare GCE.

A (for polyNiTSPc/MWNT/GCE) in Fig. 4(I), the background current reduces greatly if the polyNiTSPc has been deposited on the MWNT surface, the reason for this maybe due to the block of charge transfer by polyfilm.

Fig. 4(II) shows the ECL response of luminol on the different electrodes. The light emission on the bare GC electrode was quite small, on MWNT/GCE and polyNiTSPc/GCE, the ECL intensity increases about 2 and 8 times respectively. And on polyNiTSPc/MWNT/GC modified electrode, the maximum ECL intensity was about 21.3 times of that at the bare electrode, which means such kind of modification can combine the merits of both compounds.

3.2. Development of an ECL sensor for glucose

3.2.1. Principle of the ECL sensor

The principle of this ECL sensor can be shown in Fig. 5. On the surface of GCE, a MWNT layer had been modified. And the nickel complex was attached to the electrode surface through an O–Ni^{II} [41,42]. GOD was fixed on this modified electrode with the help of Nafion. Glucose reacts with the dissolved oxygen in the presence of GOD and produce gluconolactone and H_2O_2 [43]. The oxidation product of luminol at the surface of the electrode reacts with H_2O_2 to produce ECL. The adsorbed Ni(II)Pc took part in the catalytic oxidation of luminol and H_2O_2 generated in the reaction [39]. When the electrode potential was more positive than the redox potential of Ni(II)/Ni(III) (about 0.45 V), the oxidation production Ni(III) of Ni(II) would catalyze the oxidation of luminol (which also appeared

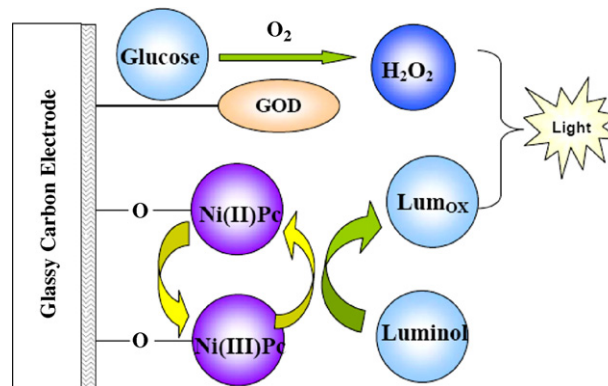


Fig. 5. The principle of the ECL biosensor. The marked layer on the surface of the GCE is MWNT. Lum_{ox} means the oxidation production of luminol.

at about 0.45 V) and H_2O_2 , and itself would be reduced to Ni(II), which shows the redox cycling of Ni ion.

3.2.2. Effect of nafion on the sensor performance

Nafion, as a cation-exchange polymer, has been widely used for modification of electrode and for construction of biosensors and chemical sensor [44]. GOD can be firmly immobilized in the Nafion film and its activity can be retained [45]. Moreover, the oxidation product of luminol is an anion, which can be adsorbed strongly onto the surface of the modified electrode without Nafion coating, which will affect the reaction between GOD and glucose. In addition, some interferences, such as ascorbic acid and uric acid were anions in the studied pH value, the presence of Nafion film will block off these anions.

3.2.3. Effect of pH on the ECL

It is well known that ECL reaction of luminol is more efficient in alkaline media, but the optimum pH condition for the activity of GOD was usually below neutral pH. Therefore, in this study, the effect of pH value on the enhanced ECL intensity (ΔI_{ECL}) was investigated in the range of 5.0–9.0. The results showed that ΔI_{ECL} would increase with the increase in pH in the range of 5.0–7.0, and remain constant in the range of 7.0–8.0, after that the ECL intensity would decrease with the increase in pH value. Considering that 7.4 is the physiological pH value, it has been chosen in this study.

3.2.4. Effect of luminol concentration on the ECL sensor

The concentration of the luminol also affects ΔI_{ECL} . Fig. 6 shows the relationship between ΔI_{ECL} and luminol concentration. The enhanced ECL intensity was increased with the increasing of luminol concentration, but if the concentration were higher than $1.0 \times 10^{-5} \text{ mol L}^{-1}$, the ΔI_{ECL} would not increase anymore. Higher luminol concentration would cause more fouling on the electrode surface, so in this study $1.0 \times 10^{-5} \text{ mol L}^{-1}$ was chosen as the optimized concentration of luminol.

3.2.5. Calibration curve for glucose

A calibration curve was obtained for determination of glucose in aqueous solution under the optimal conditions. As shown in Fig. 7, the ECL intensity was linear with the concentration of glucose in the range of 1.0×10^{-6} to $1.0 \times 10^{-4} \text{ mol L}^{-1}$. The linear regression equation was

$$\log \Delta I_{\text{ECL}} = 1.10 \log \left(\frac{C_{\text{glucose}}}{\text{mol L}^{-1}} \right) + 8.26 \quad (R = 0.9942)$$

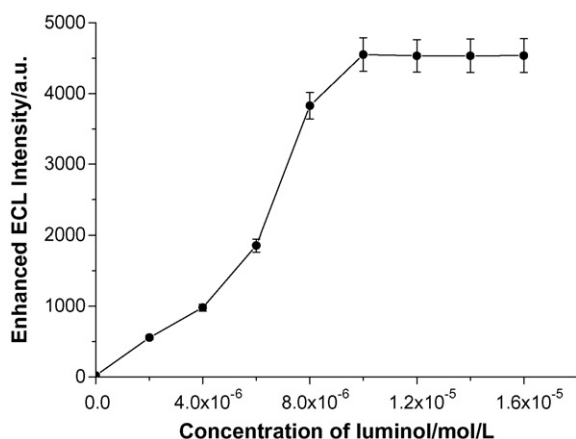


Fig. 6. Effect of the luminol concentration on the enhanced ECL intensity [glucose] = $6.0 \times 10^{-5} \text{ mol L}^{-1}$; borate buffer: pH 7.4.

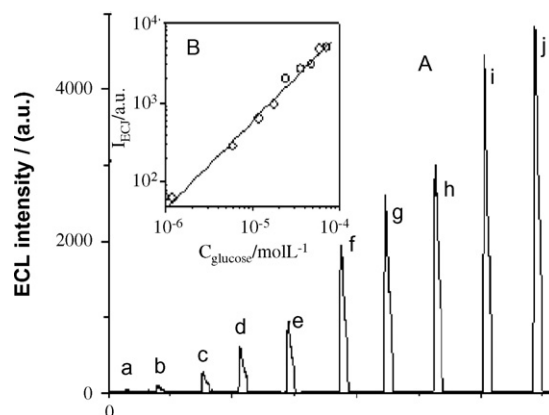


Fig. 7. The calibration curve for glucose [luminol] = $1.0 \times 10^{-5} \text{ mol L}^{-1}$, Borate buffer: pH 7.4. A: ECL curves with various glucose concentration: (a) 0.0; (b) 1.2×10^{-6} ; (c) 6.0×10^{-6} ; (d) 1.2×10^{-5} ; (e) 1.8×10^{-5} ; (f) 2.4×10^{-5} ; (g) 3.6×10^{-5} ; (h) 4.8×10^{-5} ; (i) 6×10^{-5} ; (j) $7.2 \times 10^{-5} \text{ mol L}^{-1}$. B: linear relationship between ECL intensity and glucose concentration.

where ΔI_{ECL} is the enhanced ECL intensity, C_{glucose} is the concentration of glucose, R is the regression coefficient. The detection limit (defined as the concentration that could be detected at the signal-to-noise ratio of 3) was $8.0 \times 10^{-8} \text{ mol L}^{-1}$. The relative standard deviation for $5.0 \times 10^{-6} \text{ mol L}^{-1}$ glucose was 1.2%. Compared with the glucose ECL sensor prepared early in our laboratory [46,47] or different enzyme immobilized methods [48–50], the ECL sensor established in this study has lower detection limits and large linear response range. But the method for sensor establishment was a little more complicated in this study.

3.2.6. Interference studies

Some species that commonly existed and possibly interfered with determination of glucose in biological samples were tested. Increasing amounts of foreign species were added into the solution containing $6.0 \times 10^{-5} \text{ mol L}^{-1}$ of glucose. A foreign species was considered not to interfere if it caused a relative error <5% during the measurement of the glucose sample. It was found that 5 times of sucrose, fructose, 7 times of lactose, maltose, 8 times of phenylformic acid and 15 times of uric acid and 17 times of ascorbic acid, 5 times of Cu^{2+} , Fe^{3+} , Mn^{2+} , Ni^{2+} and 0.05 times of Co^{2+} has no interference with the determination of glucose.

3.2.7. Reproducibility and stability of Nafion/GOD/polyNiTSPc/MWNT/GC electrode

It is important to study the stability and the reproducibility of the enzyme electrode response for practical applications. Fig. 8 shows the ECL response of the sensor in 10 different solutions containing $6.0 \times 10^{-5} \text{ mol L}^{-1}$ glucose and $1.0 \times 10^{-5} \text{ mol L}^{-1}$ luminol, the RSD was 5.0% ($n = 10$). The long-term stability of the established sensor had also been studied, the sensor was used to detect $6.0 \times 10^{-5} \text{ mol L}^{-1}$ glucose 10 times/day, the ECL response of $6.0 \times 10^{-5} \text{ mol L}^{-1}$ glucose only found to be decreased 7.8% and 10% after two weeks and two months, respectively. Such reproducibility and stability could be acceptable for most practical applications.

In spite of Nafion film, small amount of oxidized products of luminol can be adsorbed on the electrode surface after many times of application, which can be removed easily through successive scanning (10 circles) in the buffer solution in potential range of -1.0 to 1.0 V . The modified electrode can be applied for at least 10 times determination without any obvious decrease in reproducibility.

Table 1
Glucose content and recovery in serum samples (diluted 1:100).

Sample	Detected ^a (mmol/L)	Reference ^b (mmol/L)	RSD (%)	Added (mmol/L)	Found ^a (mmol/L)	Recovery (%)
1	4.82	4.93	1.05	2.00	6.91	105
2	4.02	3.95	1.36	2.00	5.98	98
3	5.13	5.28	1.31	2.00	7.18	103
4	6.98	6.95	1.71	2.00	8.89	96

^a Average of 5 times of determination.

^b Determined by sysmex CHEMIX-180.

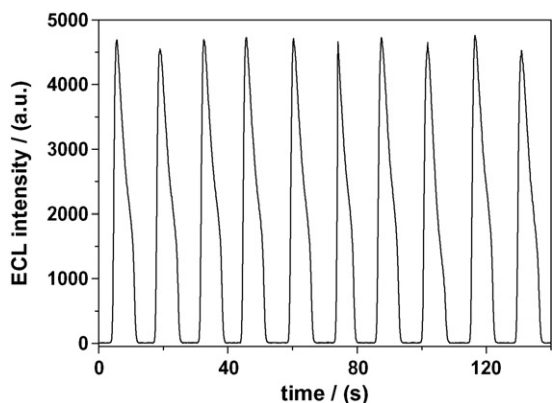


Fig. 8. The reproducibility of ECL on Nafion/GOD/polyNiTSPc/MWNT/GCE [luminol] = 1.0×10^{-5} mol L⁻¹, [glucose] = 6.0×10^{-5} mol L⁻¹; borate buffer: pH 7.4.

3.2.8. Application of the biosensors for determination of glucose in human serum samples

The proposed method has been applied to evaluate glucose content in serum samples. Before determination, the samples were diluted by buffer solution to the appropriate concentration. Under the optimum condition, the ECL of the samples had been tested, the results are shown in Table 1. These values obtained are consistent with the reference values. The recovery values ranged from 96% to 105%, which indicates that the sensor can be used clinically.

4. Conclusions

The oxidation of luminol could be catalyzed by the polyNiTSPc/MWNT-modified glassy carbon electrode, and the modified electrode could effectively enhance the luminol ECL. Based on which, an ECL biosensors have been successfully developed for detection of glucose by immobilizing GOD on the polyNiTSPc/MWNT/GC modified electrode. The proposed biosensor shows good response for glucose in the range of 1×10^{-6} to 1×10^{-4} mol L⁻¹ with a detection limit of 8.0×10^{-8} mol L⁻¹. The response of the biosensor was very fast and achieved the maximum intensity within 10 s.

Acknowledgements

This project was financially supported by the National Nature Sciences Funding of China (20735002, 20575011, 20877019), the Special Foundation for Young Scientists of Fujian Province, China (2008F3057) and the Science and Technology Developing Funding of Fuzhou University (2007-XQ-07).

References

- [1] A.W. Knight, Trends Anal. Chem 18 (1999) 47.
- [2] A.W. Knight, G.M. Greenway, Analyst 119 (1994) 879.
- [3] M.M. Richter, Chem. Rev. 104 (2004) 3003.
- [4] Y.B. Zu, Z.F. Ding, J.F. Zhou, Y.M. Lee, A.J. Bard, Anal. Chem. 73 (2001) 2153.
- [5] S.M. Buck, H. Xu, M. Brasuel, M.A. Philbert, R. Kopelman, Talanta 63 (2004) 41.
- [6] X.W. Zheng, Z.H. Guo, Z.J. Zhang, Anal. Chim. Acta 441 (2001) 81.
- [7] A. Chovin, P. Garrigue, N. Sojic, Electrochim. Acta 49 (2004) 3751.
- [8] Y. Zhao, A. Richman, C. Storey, N.B. Radford, P. Pantano, Anal. Chem. 71 (2001) 3887.
- [9] H.N. Choi, J.Y. Lee, Y.K. Lyu, W.Y. Lee, Anal. Chim. Acta 565 (2006) 48.
- [10] W. Qin, Z.J. Zhang, H.J. Liu, Anal. Chem. 70 (1998) 3579.
- [11] S.C. Shu, C.M. Wang, J. Electrochem. Soc. 145 (1998) 154.
- [12] S.M. Chen, K.C. Lin, J. Electroanal. Chem. 523 (2002) 93.
- [13] C.H. Wang, S.M. Chen, C.M. Wang, Analyst 127 (2002) 1507.
- [14] L.D. Zhu, Y.X. Li, G.Y. Zhu, Sens. Actuators, B 98 (2004) 115.
- [15] K.C. Lin, S.M. Chen, J. Electroanal. Chem. 589 (2006) 52.
- [16] L.L. Zhang, X.W. Zheng, Anal. Chim. Acta 570 (2006) 207.
- [17] I. Fridovich, J. Biol. Chem. 240 (1965) 2491.
- [18] C.S. Ouyang, C.M. Wang, J. Electroanal. Chem. 474 (1999) 82.
- [19] C.A. Marquette, L.J. Blum, Anal. Chim. Acta 381 (1999) 1.
- [20] V.C. Tsafack, C.A. Marquette, B. Leca, L.J. Blum, Analyst 125 (2000) 151.
- [21] C.A. Marquette, L.J. Blum, Anal. Lett. 33 (2000) 1779.
- [22] A. Salimi, R.G. Compton, R. Hallaj, Anal. Biochem. 333 (2004) 49.
- [23] B.C. Dave, B. Dunn, J.S. Valentini, J.J. Zink, Anal. Chem. 66 (1994) 1120A.
- [24] S. Lijima, Nature 354 (1991) 56.
- [25] P.M. Ajayan, Chem. Rev. 99 (1999) 1787.
- [26] S.B. Sinnott, J. Nanosci. Nanotech. 2 (2002) 113.
- [27] Y. Tzeng, Y. Chen, N. Sathitsuksanoh, C. Liu, Diamond Relat. Mater. 13 (2004) 1281.
- [28] G.C. Zhao, L. Zhang, X.W. Wei, Z.S. Yang, Electrochim. Commun. 5 (2003) 825.
- [29] K.B. Wu, J.J. Fei, S.S. Hu, Anal. Biochem. 318 (2003) 100.
- [30] N.S. Lawrence, R.P. Deo, J. Wang, Anal. Chim. Acta 517 (2004) 131.
- [31] Y. Xu, Y. Jiang, H. Cai, P.G. He, Y.Z. Fang, Anal. Chim. Acta 516 (2004) 19.
- [32] S.J. Wang, S.F. Yin, L. Li, B.Q. Xu, C.F. Ng, C.T. Au, Appl. Catal. B 52 (2004) 287.
- [33] G.Z. Chen, M.S.P. Shaffer, D. Coleby, G. Dixon, W. Zhou, D.J. Fray, A.H. Windle, Adv. Mater. 12 (2000) 522.
- [34] C.C. Leznoff, A.B.P. Lever (Eds.), Phthalocyanines: Properties and Applications, VCH Publications, New York, 1989 (vol. I); 1992 (vol. II); 1993 (vol. III); 1996 (vol. IV).
- [35] E.F. Perez, L.T. Kubota, A.A. Tanaka, G.D.O. Neto, Electrochim. Acta 43 (1998) 1665.
- [36] M.S. Ureta, C. Berryos, J. Pavez, J. Zagal, C. Gutierrez, J.F. Marco, J. Electroanal. Chem. 553 (2003) 147.
- [37] Z.H. Wen, T.F. Kang, Talanta 62 (2004) 351.
- [38] M.S. Ureta, A. Alarcon, C. Berrios, G.I. Cardenas-Jiron, J. Zagal, C. Gutierrez, J. Electroanal. Chem. 580 (2005) 94.
- [39] J. Wang, G.N. Chen, L. Huang, Analyst 130 (2005) 71.
- [40] Y.S.C. Tsang, K. Chen, P.J.F. Harris, M.L.H. Green, Nature 372 (1994) 159.
- [41] G. Roslonek, J. Taraszewska, J. Electroanal. Chem. 325 (1992) 285.
- [42] J. Bukowska, G. Roslonek, J. Taraszewska, J. Electroanal. Chem. 403 (1992) 47.
- [43] R. Wilson, J. Kremeskoetter, D.J. Schiffrin, Biosens. Bioelectron. 11 (1996) 805.
- [44] J. Wang, M. Musameh, Y.H. Lin, J. Am. Chem. Soc. 125 (2003) 2408.
- [45] B.Q. Wang, S.J. Dong, Talanta 51 (2000) 565.
- [46] Z.Y. Lin, J.H. Chen, G.N. Chen, Electrochim. Acta 53 (2008) 2396.
- [47] J.H. Chen, Z.Y. Lin, G.N. Chen, Anal. Bioanal. Chem. 388 (2007) 399.
- [48] L.D. Zhu, Y.X. Li, F.M. Tian, B. Xu, G.Y. Zhu, Sens. Actuators, B 84 (2002) 265.
- [49] L.D. Zhu, Y.X. Li, G.Y. Zhu, Sens. Actuators, B 86 (2002) 209.
- [50] C.A. Marquette, L.J. Blum, Sens. Actuators, B 90 (2003) 112.



Label-free electrochemical aptasensor for the detection of lysozyme

Marcela C. Rodríguez*, Gustavo A. Rivas

INFIQC, Departamento de Físico Química, Facultad de Ciencias Químicas, Universidad Nacional de Córdoba, Ciudad Universitaria, 5000 Córdoba, Argentina

ARTICLE INFO

Article history:

Received 3 September 2008

Received in revised form 3 November 2008

Accepted 4 November 2008

Available online 11 November 2008

Keywords:

Aptamer

Carbon paste electrode

Lysozyme

Electrochemical aptasensor

Protein detection

Biosensor

ABSTRACT

This work reports the advantages of a label free electrochemical aptasensor for the detection of lysozyme. The biorecognition platform was obtained by the adsorption of the aptamer on the surface of a carbon paste electrode (CPE) previously blocked with mouse immunoglobulin under controlled-potential conditions. The recognition event was detected from the decrease in the guanine and adenine electro-oxidation signals produced as a consequence of the molecular interaction between the aptamer and lysozyme. The biosensing platform demonstrated to be highly selective even in the presence of large excess (9-fold) of bovine serum albumin, cytochrome C and myoglobin. The reproducibility for 10 repetitive determinations of 10.0 mg L⁻¹ lysozyme solution was 5.1% and 6.8% for guanine and adenine electro-oxidation signals, respectively. The detection limits of the aptasensor were 36.0 nmol L⁻¹ (if considering guanine signal) and 18.0 nmol L⁻¹ (if taking adenine oxidation current). This new sensing approach represents an interesting and promising alternative for the electrochemical quantification of lysozyme.

© 2008 Elsevier B.V. All rights reserved.

1. Introduction

Since its discovery in 1990 [1–3], aptamers have demonstrated important advantages in the biosensing field, especially for the development of devices that allow the detection of proteins, toxins, peptides and neurotransmitters [4–9]. Aptamers are artificial single-stranded nucleic acids ligands, that present unique properties such as relatively easy production, multiple possibilities of modification, specific binding and high stability. These properties have made them very attractive recognition elements for a wide range of bioassays [4,5,10,11], and strong competitors of antibodies in the development of affinity biosensors.

The first aptamer-based biosensor has been proposed in 1998 by Ellington and co-workers [12] for the detection of thrombin and it has been based on the use of an aptamer labeled with a fluorescent marker. Aptamers modified with enzymes [13,14], fluorophores [15,16] and metallic nanoparticles [17,18] have been used as alternative to enhance the sensitivity of the determinations.

Different transduction modes have been reported for the development of aptasensors. Among them, Quartz Crystal Microbalance (QCM) has been proposed for the investigation of protein–nucleic acid and protein–aptamer interactions [19–21]. A comparative work using QCM and Surface Plasmon Resonance (SPR) for the transduction of the bioaffinity event has been also described [22]. Ostatná et al. [23] have proposed a sensitive and selective SPR-

aptasensor for the quantification of thrombin [23]. A fiber-optic evanescent aptasensor for the detection of trinitrotoluene at the ppb level has been developed by Ehrentreich-Förster et al. [24]. Fourier Transform Infrared Attenuated Total Reflection (FTIR-ATR) has been used for the quantification of thrombin using an anti-thrombin DNA aptamer [25]. The advantages of using field effect transistor based on single-wall carbon nanotubes (SWCNT-FET) for the quantification of thrombin has been reported [26]. More recently, there has been an increasing interest for the development of electrochemical aptasensors for the detection of proteins [19,27–37] and small molecules as adenosine monophosphate, cocaine and potassium [38–41]. The electrochemical detection of thrombin and lysozyme using quantum dots has also been proposed [36]. Electrochemical impedance spectroscopy (EIS) has been used in several devices for the development of label-free aptasensors [28–31]. A highly sensitive thrombin quantification by employing EIS in combination with gold nanoparticles has been reported [42,43]. Numnuam et al. [44] have proposed the thrombin detection through the potentiometric quantification of Cd²⁺ using an anti-thrombin aptamer labeled with CdS quantum dots. Just few electrochemical aptasensors for the detection of lysozyme have been described [27,28,32].

In this work we propose an electrochemical aptasensor based on the use of carbon paste electrodes (CPE) modified with an anti-lysozyme aptamer for the direct detection of lysozyme without using electroactive markers. Lysozyme, also called muramidase or peptidoglycan *N*-acetylmuramoyl-hydrolase (EC 3.2.1.17), is an ubiquitous enzyme widely distributed in diverse organisms such as bacteria, bacteriophages, fungi, plants and animals. It catalyzes

* Corresponding author. Tel.: +54 351 4334169/80; fax: +54 351 4334188.
E-mail address: marcela.rodriguez@fcq.unc.edu.ar (M.C. Rodríguez).

in vivo the hydrolysis of the $\beta(1-4)$ glycosidic linkage between *N*-acetylmuramic acid and *N*-acetylglucosamine alternating sugar residues in the bacterial peptidoglycan and causes bacterial cell lysis. Its primary sequence contains 129 amino acid residues. The molecular weight is 14,351 Da and its isoelectric point is 11.0 [45,46]. This enzyme works as a natural inner body antibiotic because it possesses lytic activity against the polysaccharide wall of bacteria. Lysozyme also exhibits antiviral activity and could be a potential marker for rheumatoid arthritis [47–49].

Due to its relatively small size lysozyme can be taken as a model analyte for the development of aptamer-based platforms for the detection of proteins [46]. In this work, we propose the use of a lysozyme aptasensor as an innovative strategy for the quantification of lysozyme based on the changes in guanine and adenine oxidation signals once the protein was bound to the aptamer immobilized at a graphite paste electrode (CPE) previously blocked with mouse immunoglobulin G. The influence of the aptasensor preparation conditions on the analytical performance of the resulting electrode is also discussed.

2. Experimental

2.1. Materials

2.1.1. Oligonucleotides sequences

The synthetic sequence of the DNA-anti-lysozyme aptamer designed by Ellington et al. [50] (5'-ATC TAC GAA TTC ATC AGG GCT AAA GAG TGC AGA GTT ACT TAG-3'), and the scrambled control sequence (5'-AAG ATG CTG AAA TAG TGC GCA CTT AAG TCT CAA TGA ATG CGT-3') were purchased from Invitrogen Argentina S.A. The anti-lysozyme aptamer was treated before using by heating at 70 °C for 3 min and allowed to slowly cool down at room temperature. Such heating and cooling steps are essential for maintaining the structural capabilities of the aptamer for the target capture [50]. The purified scrambled DNA sequence was treated following the same protocol. Lysozyme from chicken egg white, purified mouse immunoglobulin G (IgG), bovine serum albumin (BSA), cytochrome C (cyt C) and myoglobin (myo) from equine heart were obtained from Sigma-Aldrich. Other chemicals were reagent grade and used without further purification.

Ultrapure water ($\rho = 18.2 \text{ M}\Omega \text{ cm}$) from a Millipore-MilliQ system was used for preparing all the solutions.

2.2. Apparatus

The electrochemical measurements were performed with an EPSILON potentiostat (BAS). The three electrodes system consisted of a carbon paste electrode (CPE), a platinum wire and an Ag/AgCl, 3.0 mol L⁻¹ NaCl (BAS, Model RE-5B) as working, counter and reference electrodes, respectively. All potentials are referred to the latter. The electrodes were inserted into the cell (BAS, Model MF-1084) through holes in its Teflon cover.

2.3. Aptasensor preparation conditions and biosensing procedure

2.3.1. Preparation of the aptamer-based biorecognition platform

2.3.1.1. Pretreatment of the CPE surface. The CPE was first pretreated by applying +1.700 V for 1.0 min in a 0.020 mol L⁻¹ acetate buffer, pH 5.00.

2.3.1.2. Blockage of the CPE surface. This blocking step avoids unspecific interactions and ensures the efficient recognition of the target protein. In this case, a layer of mouse immunoglobulin G (IgG) was immobilized before adsorbing the DNA-aptamer. This molecule is widely used in immunoassay methodologies as blocking molecule

to prevent the non-specific adsorption of the target antigen (protein) [57,58].

After a careful rinsing with 0.100 mol L⁻¹ phosphate buffer solution pH 7.30, the pretreated CPE was immersed in a 0.100 M saline phosphate buffer solution pH 7.30 containing 100.0 mg L⁻¹ IgG for 10.0 min at open circuit potential.

2.3.1.3. Aptamer immobilization. After a rinsing step with acetate buffer, the aptamer was immobilized at the CPE blocked with IgG at +0.500 V for 2.0 min from a solution containing 100.0 mg L⁻¹ of anti-lysozyme aptamer (in 0.020 mol L⁻¹ acetate buffer, pH 5.00). Finally, the electrode was carefully rinsed with acetate buffer solution for 10.0 s.

2.3.2. Lysozyme-aptamer association step

The CPE blocked with IgG and modified with the aptamer was immersed in lysozyme solutions of different concentration (from 0.0 to 100.0 mg L⁻¹, prepared in a 0.100 mol L⁻¹ phosphate buffer solution pH 7.30) at open circuit potential for 10.0 min.

2.3.3. Electrochemical transduction

The aptasensor containing the protein was rinsed with acetate buffer solution for 10.0 s and then it was placed in a 0.020 mol L⁻¹ acetate buffer solution pH 5.00. The transduction was performed by Square Wave Voltammetry (SWV) between -0.200 V and 1.500 V with a frequency of 25 Hz, amplitude of 0.025 V and a step potential of 0.010 V. The same procedure was followed when the target protein was captured in the presence of interferents (bovine serum albumin, cytochrome C and myoglobin). All measurements were conducted at room temperature.

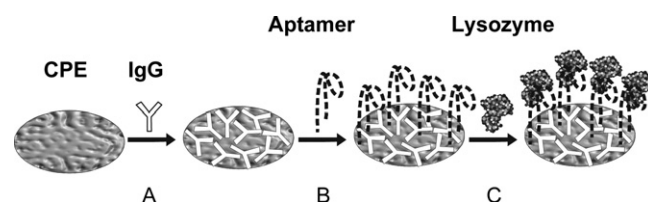
Scheme 1 shows the different steps during the preparation/operation of the aptasensor.

3. Results and discussion

3.1. Electrochemical behavior of carbon paste electrodes modified with the anti-lysozyme aptamer

Fig. 1 shows the electrochemical response of pretreated CPE modified with the anti-lysozyme-aptamer by immobilization for 2.0 min at 0.500 V from a 0.020 mol L⁻¹ acetate buffer solution pH 5.00 containing 100.0 mg L⁻¹ aptamer. Two well-defined oxidation processes are observed at +1.030 V and +1.330 V, attributed to the oxidation of guanine (a) and adenine (b), respectively [52–55].

The dependence of the peak currents for guanine and adenine oxidation on the accumulation time of the anti-lysozyme aptamer at 0.500 V was evaluated (not shown). For 10.0 mg L⁻¹ aptamer solution the current increased slightly from 30.0 s to 5.0 min adsorption suggesting a fast adsorption of the aptamer under these conditions [56]. When performing the same study using a 100.0 mg L⁻¹ DNA-aptamer solution, almost no changes were observed in the guanine and adenine oxidation currents for the different accumulation times. Consequently, in order to make sure



Scheme 1. Preparation steps of an anti-lysozyme aptasensor: (A) carbon paste electrode (CPE)-blocking step, (B) aptamer immobilization, and (C) lysozyme binding event.

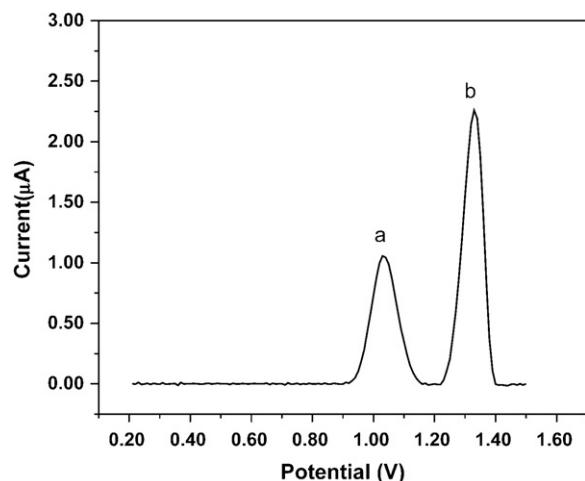


Fig. 1. Electrochemical response of the anti-lysozyme aptamer immobilized on CPE. CPE pretreatment: +1.700 V for 1.0 min in 0.020 mol L⁻¹ acetate buffer, pH 5.00; accumulation conditions: +0.500 V for 2.0 min in the 100.0 mg L⁻¹ aptamer solution prepared in 0.020 mol L⁻¹ acetate buffer, pH 5.00; transduction step: square wave voltammograms were recorded between -0.200 V and +1.500 V, frequency: 25 Hz, amplitude: 0.025 V and step potential: 0.010 V. Supporting electrolyte: 0.020 mol L⁻¹ acetate buffer solution, pH 5.00.

that the surface was completely covered and to avoid non-specific interactions, an immobilization time of 2.0 min from a 100.0 mg L⁻¹ aptamer solution was selected for further experiments.

3.2. Lysozyme aptasensor

3.2.1. Analytical performance of the lysozyme aptasensor

The guanine and adenine oxidation signals obtained at CPE blocked with IgG and modified with the aptamer were compared with those obtained at the unblocked CPE (Section 3.1). The presence of the blocking agent produced a decrease of 23.0% and 35.0% in the guanine and adenine oxidation signals, respectively. This decrease is attributable to a lower accessibility for electro-oxidation of the electroactive residues of the aptamer. In the case of the blocked surface, a new small peak appears at around 0.80 V as a result of the oxidation of electroactive amino acids of IgG.

Fig. 2A shows SWV recordings for increasing concentrations of lysozyme from 0.0 to 30.0 mg L⁻¹ at the aptamer-IgG-CPE. As the concentration of lysozyme increases, there is a decrease in the guanine and adenine oxidation signals as a consequence of the efficient capture of the protein by the aptasensor. The structural changes produced in the aptamer due to the interaction with lysozyme pockets would be responsible for the decrease in the oxidation signals of the electroactive residues. Aptamers preferentially interacts with pockets or clefts on proteins such as active and allosteric sites and the binding process involves the whole aptamer molecule and produces important structural changes in the aptamer and in the protein. For instance, the inhibition of the enzymatic action of the protein bound to the aptamer has been strongly demonstrated [51].

Fig. 2B displays calibration plots obtained from the electro-oxidation signal for guanine (I) and adenine (II). There is a linear relationship between lysozyme concentration and guanine (I) or adenine (II) oxidation signals up to 20.0 mg L⁻¹ of lysozyme. The sensitivities for lysozyme are $(-0.049 \pm 0.003) \mu\text{A mg}^{-1} \text{L}$ and $(-0.025 \pm 0.002) \mu\text{A mg}^{-1} \text{L}$ obtained from adenine and guanine oxidation signals, respectively. The saturation was reached for lysozyme levels higher than 20.0 mg L⁻¹ (Fig. 2B). The detection limits, taken as the ratio between 3.3 times the standard deviation of the blank solution and sensitivity of the calibration curve are $3.60 \times 10^{-8} \text{ mol L}^{-1}$ (0.52 mg L⁻¹) and $1.80 \times 10^{-8} \text{ mol L}^{-1}$

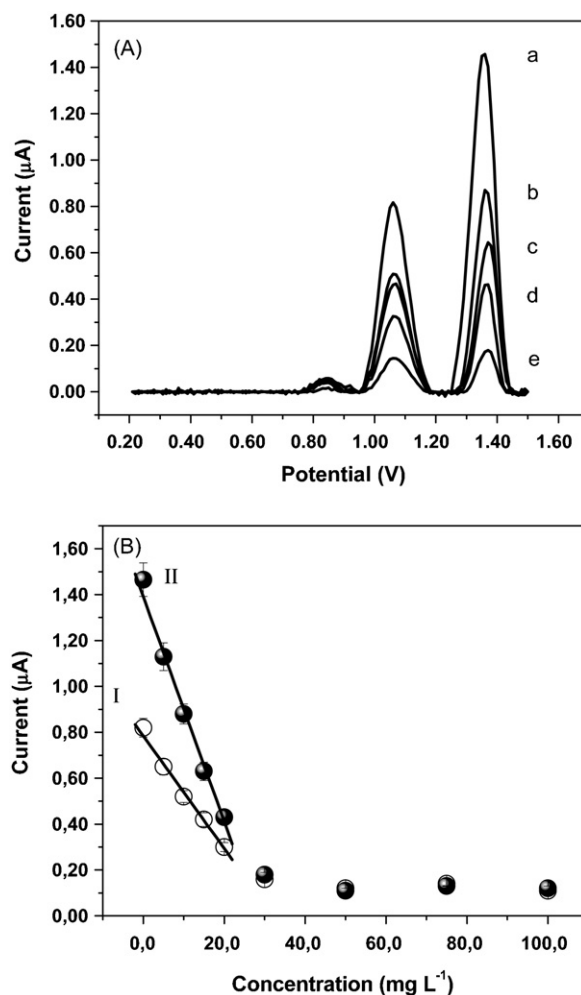


Fig. 2. (A) Square wave voltammograms for increasing concentration of lysozyme solutions: 0.0 mg L⁻¹ (a), 10.0 mg L⁻¹ (b), 15.0 mg L⁻¹ (c) 20.0 mg L⁻¹ (d) and 30.0 mg L⁻¹ (e) obtained at the anti-lysozyme aptamer modified-Ig G blocked-CPE. CPE pretreatment: +1.700 V for 1.0 min in 0.020 mol L⁻¹ acetate buffer, pH 5.00; blocking step: 10.0 min at open circuit potential in a 100.0 mg L⁻¹ IgG in phosphate buffer solution 0.100 M pH 7.30; aptamer accumulation conditions: 2.0 min at +0.500 V in 0.020 mol L⁻¹ acetate buffer, pH 5.00 containing 100.0 mg L⁻¹ aptamer; capture step: in buffer phosphate solution 0.100 mol L⁻¹ pH 7.30 containing lysozyme for 10.0 min at open circuit potential. Transduction step: square wave voltammograms: initial potential: -0.200 V, final potential: +1.500 V, frequency: 25 Hz, amplitude: 0.025 V and step potential: 0.010 V. Supporting electrolyte: 0.020 mol L⁻¹ acetate buffer solution, pH 5.00. (B) Calibration plots for lysozyme. I and II correspond to guanine and adenine oxidation signals, respectively.

(0.21 mg L⁻¹) depending if considering guanine or adenine oxidation signals, respectively. The quantification limits, taken as the ratio between 10 times the standard deviation of the blank solution and sensitivity of the calibration curve, are $1.10 \times 10^{-7} \text{ mol L}^{-1}$, taken from guanine oxidation signal, and $0.60 \times 10^{-7} \text{ mol L}^{-1}$, taken from the adenine oxidation response. The detection limits are one order of magnitude lower than that for the optical aptamer-based sensor array proposed by Ellington and co-workers [50] and comparable to those reported in the literature for electrochemical aptasensors (which goes from 0.2 $\mu\text{g mL}^{-1}$ to 0.5 $\mu\text{g mL}^{-1}$) [27,28,32]. Therefore, the decrease in the oxidation signals for adenine and guanine observed when increasing lysozyme concentrations provides an excellent, easy and fast way to quantify lysozyme.

The platform containing the aptamer shows good reproducibility. Ten repetitive measurements obtained in the presence of

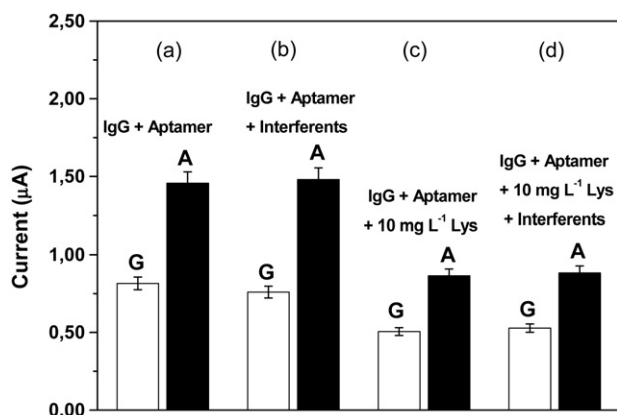


Fig. 3. Evaluation of the aptasensor selectivity. Electrochemical oxidation signals for anti-lysozyme aptamer modified-Ig G blocked-CPE prepared according to the conditions stated in Fig. 2 in different solutions: (a) in the absence of lysozyme and interferents, (b) in the presence of 30.0 mg L⁻¹ BSA + 30.0 mg L⁻¹ cytochrome C (cyt C) + 30.0 mg L⁻¹ myoglobin (myo), (c) in the presence of 10.0 mg L⁻¹ lysozyme, and (d) in the presence of 10.0 mg L⁻¹ lysozyme + 30.0 mg L⁻¹ BSA + 30.0 mg L⁻¹ cyt C + 30.0 mg L⁻¹ myo (d). Other conditions as in Fig. 2.

10.0 mg L⁻¹ lysozyme gave R.S.D of 5.0% and 6.8% for guanine and adenine redox signals, respectively.

To analyze the selectivity of the proposed protocol, the aptamer sensor was challenged with a large (9-fold) excess of common interferents such as bovine serum albumin (BSA), cytochrome C (cyt C) and myoglobin (myo). Fig. 3 shows the guanine and adenine electro-oxidation currents obtained at the aptasensor under different experimental conditions. The signal obtained in supporting electrolyte (a), was taken as 100.0%. The presence of 30.0 mg L⁻¹ BSA, cyt C and myo (in the absence of lysozyme), (b) has a negligible influence on the response of the electrode, with interferences of 3.2% and 1.6% for guanine and adenine oxidation signals, respectively. When the aptasensor is challenged with 10.0 mg L⁻¹ lysozyme (c) a clear decrease of the guanine and adenine oxidation signals is observed, as expected according to Fig. 2. If 10.0 mg L⁻¹ lysozyme is determined in the presence of 30.0 mg L⁻¹ BSA, cyt C and myo (d), the response remains almost constant. In fact, signals of (0.51 ± 0.02) µA and (0.53 ± 0.03) µA are attained for guanine oxidation signals; and (0.87 ± 0.04) µA and (0.88 ± 0.04) µA are obtained for the oxidation of adenine, in the presence and absence of interferents, respectively (c vs. d). These results are strong proof of the highly selective detection of lysozyme. No cross-reactions with interferent proteins were found even when they have very close structural similarities with lysozyme as in the case of cytochrome C (MW: 12 kDa and pI ~ 11) [59,60].

3.2.2. Specificity of the anti-lysozyme aptamer sequence

The specificity of the aptasensor was also evaluated from the aptamer sequence used for performing the biorecognition event by employing a DNA-scrambled sequence (disordered aptamer sequence) (Fig. 4). The oxidation signals for adenine and guanine are smaller than those obtained when using the right sequence (a). Even when the bases are the same, their particular array in the scrambled sequence leads to a structure with different exposure of the electroactive bases and makes more difficult the electron transfer with the electrode surface. A decrease of 3.2% and 2.7% for guanine and adenine oxidation signal, respectively, was obtained in the presence of 30.0 mg L⁻¹ lysozyme at the electrode containing the scrambled sequence (c). This change in the signal is largely different from that found when using the right aptamer sequence where a reduction of 82.1% and 87.6% for guanine and adenine oxidation signals, respectively, is obtained (d). These results suggest

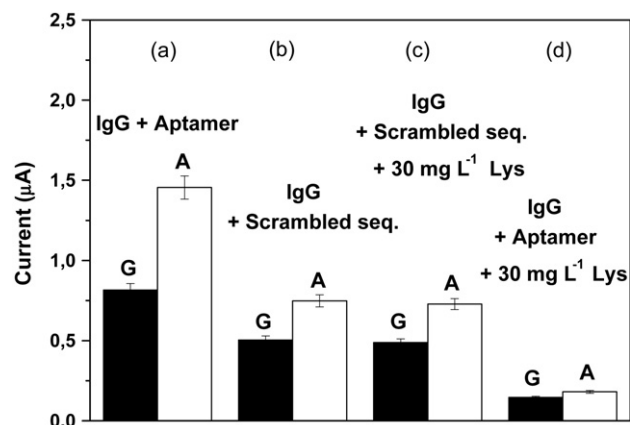


Fig. 4. Guanine and adenine oxidation signals obtained at an anti-lysozyme aptamer modified-Ig G blocked-CPE (a and d) and at a scrambled sequence modified-Ig G blocked-CPE (b and c) in the absence (a and b), and presence (c and d) of 30.0 mg L⁻¹ lysozyme. Other conditions as in Fig. 2.

that the unique structure of the anti-lysozyme aptamer sequence is absolutely required for the highly specific lysozyme binding.

4. Conclusions

This work proposes an elegant label-free electrochemical aptasensor for lysozyme detection based on the use of an anti-lysozyme aptamer modified CPE. The substantial drop in guanine and adenine electro-oxidation signals obtained after the recognition event takes place has allowed us to obtain a highly sensitive (detection at nM levels) and selective (no interference of BSA, cytochrome C and myoglobin) aptasensor for lysozyme quantification.

Compared to EIS, the most typical electrochemical transduction mode in aptasensors, the voltammetric transduction mode represents a faster detection and results-processing alternative. In addition, the use of CPE as electrode material offers multiple advantages such as easy surface renewal, fast conditioning and simple aptamer immobilization at variance with other electrode materials such as gold, glassy carbon or indium tin oxide, that present special requirements for surface preparation and the immobilization of the aptamer is time consuming. These features make the aptamer-IgG-CPE proposed here, an excellent biosensing platform for the development of a highly sensitive and selective lysozyme aptasensor with detection limits lower than those reached with optical aptasensors and comparable to those obtained by other reported electrochemical sensors.

This original and novel method of sensing aptamer-protein interactions at the transducer surface opens new promising routes for future applications in proteomics and diagnostics. The concept can be widely extended to the aptamer-based detection of a large range of proteins and small molecules taking advantages of several specific aptamer structures identified lately by SELEX.

Acknowledgements

The authors want to thank CONICET, SECyT-UNC, ANPCyT (PICT-2005 38111 and PICT-2006 02324) and Becas Banco Santander-Río for the financial support.

References

- [1] D.L. Robertson, G.F. Joyce, Nature 344 (1990) 467.
- [2] A.D. Ellington, J.W. Szostak, Nature 346 (1990) 818.

- [3] C. Tuerk, L. Gold, *Science* 249 (1990) 505.
- [4] S. Tombelli, M. Minunni, M. Mascini, *Biosens. Bioelectron.* 20 (2005) 2424.
- [5] C.L.A. Hamula, J.W. Guthrie, H. Zhang, X.-F. Li, X.C. Le, *TrAC* 7 (2006) 681.
- [6] E. Bakker, Y. Qin, *Anal. Chem.* 78 (2006) 3965.
- [7] T. Mairal, V.C. Özalp, P.L. Sánchez, M. Mir, I. Katakis, C.K. O'Sullivan, *Anal. Bioanal. Chem.* 390 (2008) 989.
- [8] J.-O. Lee, H.-M. So, E.-K. Jeon, H. Chang, K. Won, Y.H. Kim, *Anal. Bioanal. Chem.* 390 (2008) 1023.
- [9] S. Song, L. Wang, J. Li, J. Zhao, C. Fan, *TrAC* 27 (2008) 108.
- [10] R. Mukhopadhyay, *Anal. Chem.* 77 (2005) 115A.
- [11] S. Balamurugan, A. Obubuafo, S.A. Soper, D.A. Spivak, *Anal. Bioanal. Chem.* 390 (2008) 1009.
- [12] R.A. Potyrailo, R.C. Conrad, A.D. Ellington, G.M. Hieftje, *Anal. Chem.* 70 (1998) 3419.
- [13] S.E. Osborne, I. Matsumura, A.D. Ellington, *Curr. Opin. Chem. Biol.* 1 (1997) 5.
- [14] E. Baldrich, A. Restrepo, C.K. O'Sullivan, *Anal. Chem.* 76 (2004) 7053.
- [15] E.J. Merino, K.M. Weeks, *J. Am. Chem. Soc.* 125 (2003) 12370.
- [16] T.G. McCauley, N. Hamaguchi, M. Stanton, *Anal. Biochem.* 319 (2003) 244.
- [17] J. Liu, Y. Lu, *Anal. Chem.* 76 (2004) 1627.
- [18] V. Pavlov, Y. Xiao, B. Shlyabovskiy, I. Willner, *J. Am. Chem. Soc.* 126 (2004) 11768.
- [19] T. Hianik, V. Ostatná, M. Sonlajtnerova, I. Grman, *Bioelectrochemistry* 70 (2007) 127.
- [20] N. Tassew, M. Thompson, *Anal. Chem.* 74 (2002) 5313.
- [21] M. Liss, B. Petersen, H. Wolf, E. Prohaska, *Anal. Chem.* 74 (2002) 4488.
- [22] S. Tombelli, M. Minunni, E. Luzzi, M. Mascini, *Bioelectrochemistry* 67 (2005) 135.
- [23] V. Ostatná, H. Vaisocherová, J. Homola, T. Hianik, *Anal. Bioanal. Chem.* 391 (2008) 1861.
- [24] E. Ehrentreich-Föster, D. Orgel, A. Krause-Griep, B. Cech, V.A. Erdmann, F. Bier, F.W. Scheller, M. Rimmel, *Anal. Bioanal. Chem.* 391 (2008) 1793.
- [25] W. Liao, F. Wei, D. Liu, M.X. Qian, G. Yuan, X.S. Zhao, *Sens. Actuators B* 114 (2006) 445.
- [26] H.-M. So, K. Won, Y.H. Kim, B.-K. Kim, B.H. Ryu, P.S. Na, H. Kim, J.-O. Lee, *J. Am. Chem. Soc.* 127 (2005) 11906.
- [27] A.-N. Kawde, M.C. Rodríguez, T.M.-H. Lee, J. Wang, *Electrochem. Commun.* 7 (2005) 537.
- [28] M.C. Rodríguez, A.-N. Kawde, J. Wang, *Chem. Commun.* (2005) 4267.
- [29] A.-E. Radi, J.L. Acero Sánchez, E. Baldrich, C.K. O'Sullivan, *Anal. Chem.* 77 (2005) 6320.
- [30] J.A. Lee, S. Hwang, J. Kwak, S.I. Park, S.S. Lee, K.-C. Lee, *Sens. Actuators B* 129 (2008) 372.
- [31] H. Cai, T.M.-H. Lee, I.M. Hsing, *Sens. Actuators B* 114 (2006) 433.
- [32] A.K.H. Cheng, B. Ge, H.-Z. Yu, *Anal. Chem.* 79 (2007) 5158.
- [33] A.-E. Radi, J.L. Acero Sánchez, E. Baldrich, C.K. O'Sullivan, *J. Am. Chem. Soc.* 128 (2006) 117.
- [34] Y. Xiao, A.A. Lubin, A.J. Heeger, K.W. Plaxco, *Angew. Chem. Int. Ed.* 44 (2005) 5456.
- [35] M. Mir, M. Vreeke, I. Katakis, *Electrochem. Commun.* 8 (2006) 505.
- [36] J.A. Hansen, J. Wang, A.-N. Kawde, Y. Xiang, K.V. Gothelf, G. Collins, *J. Am. Chem. Soc.* 128 (2006) 2228.
- [37] K.I. Papamichael, M.P. Kreuzer, G.G. Guilbault, *Sens. Actuators B* 121 (2007) 178.
- [38] L. Shen, Z. Chen, Y. Li, P. Jing, S. Xie, S. He, P. He, Y. Shao, *Chem. Commun.* 21 (2007) 2169.
- [39] Y. Li, H. Qi, Y. Page, J. Yang, C. Zhang, *Electrochem. Commun.* 9 (2007) 2571.
- [40] B.R. Baker, R.Y. Lai, M.S. Wood, E.H. Doctor, A.J. Heeger, K.W. Plaxco, *J. Am. Chem. Soc.* 128 (2006) 3138.
- [41] A.-E. Radi, C.K. O'Sullivan, *Chem. Commun.* 32 (2006) 3432.
- [42] B. Li, Y. Wang, H. Wei, S. Dong, *Biosens. Bioelectron.* 23 (2008) 965.
- [43] X. Li, L. Shen, D. Zhang, H. Qi, Q. Gao, F. Ma, C. Zhang, *Biosens. Bioelectron.* 23 (2008) 1624.
- [44] A. Numnuan, K.Y. Chumbimuni-Torres, Y. Xiang, R. Bash, P. Thavarungkul, E. Prestch, J. Wang, *E. Anal. Chem.* 80 (2008) 707.
- [45] J. Huang, L. Wu, D. Yalda, Y. Adkins, S.L. Kelleher, M. Crane, B. Lonnerdal, R.L. Rodriguez, N. Huang, *Transgenic Res.* 11 (2002) 229.
- [46] Y. Wan, J. Lu, Z. Cui, *Sep. Purif. Technol.* 48 (2006) 133.
- [47] P. Jollès, *Lysozymes: Model Enzymes in Biochemistry and Biology*, Birkhauser Verlag, Basel, Switzerland, 1996.
- [48] S. Lee-Huang, P.L. Huang, Y. Sun, H.F. Kung, D.L. Blithe, H.C. Chen, *Proc. Natl. Acad. Sci. U.S.A.* 96 (1999) 2678.
- [49] J. Ireland, J. Herzog, E.R. Unanue, *J. Immunol.* 177 (2006) 1421.
- [50] R. Kirby, E.J. Cho, B. Gehrke, T. Bayer, Y.S. Park, D.P. Neikirk, J.T. McDevitt, A.D. Ellington, *Anal. Chem.* 76 (2004) 4066.
- [51] J.C. Cox, A.D. Ellington, *Bioorg. Med. Chem.* 9 (2001) 2525.
- [52] J. Wang, J.R. Fernandes, L.T. Kubota, *Anal. Chem.* 70 (1998) 3699.
- [53] J. Wang, *Anal. Chem.* 67 (1995) 487R.
- [54] E. Palacek, M. Fojta, *Anal. Chem.* 73 (2001) 74A.
- [55] M. Ligaj, J. Jasnowska, W.G. Musial, M. Filipiak, *Electrochim. Acta* 51 (2006) 5193.
- [56] G.A. Rivas, M.L. Pedano, in: C.A. Grimes, E.C. Dickey, M. Pishko (Eds.), *Electrochemical DNA-based Biosensors*, Encyclopedia of Sensors, American Scientific Publishers, The Pennsylvania State University, University Park, USA ISBN 1-5883-059-4. vol. 3, 2006, pp. 45–91.
- [57] S.S. Levinson, J.J. Millar, *Clin. Chim. Acta* 325 (2002) 1.
- [58] <http://www.sigmaldrich.com/sigma/datasheet/i5381dat.pdf>.
- [59] E. Margoliash, E.L. Smith, *J. Biol. Chem.* 237 (1962) 2151.
- [60] E. Margoliash, E.L. Smith, G. Kreil, H. Tuppy, *Nature* 192 (1961) 1121.



On-line solid phase extraction coupled to capillary LC-ESI-MS for determination of fluoxetine in human blood plasma

Amr L. Saber*

Department of Chemistry, Faculty of Science, Zagazig University, Zagazig, Egypt

ARTICLE INFO

Article history:

Received 15 August 2008
 Received in revised form
 10 November 2008
 Accepted 11 November 2008
 Available online 24 November 2008

Keywords:

Capillary liquid chromatography
 Column switching
 Fluoxetine hydrochloride
 Mass spectrometry

ABSTRACT

An instrumental setup including on-line solid phased extraction coupled to capillary liquid chromatography-electrospray ionization-mass spectrometry (SPE-capLC-ESI-MS) has been constructed to improve the sensitivity for quantification of fluoxetine hydrochloride in human plasma. Prior to injection, 0.5 mL of plasma spiked with metronidazole (internal standard) was mixed with ammonium formate buffer for effective chloroform liquid–liquid extraction. The method was validated in the range 5–60 ng mL⁻¹ fluoxetine, yielding a correlation coefficient of 0.999 (r^2). The within-assay and between-assay precisions were between (8.5 and 11%) and (6.6 and 7.5%), respectively. The method was used to determine the amount of fluoxetine in a healthy male 14 h after an intake of one capsule of the antidepressant and anorectic Flutin[®], which contains 20 mg fluoxetine per each capsule. Fluoxetine was detected, and the concentration was calculated to 9.0 ng mL⁻¹ plasma. In the preliminary experiments, conventional LC–UV instrumentation was employed. However, it was found that employing a capillary column with an inner diameter of (0.3 mm I.D. × 50 mm, Zorbax C₁₈) increased the sensitivity by a factor of ~100, when injecting the same mass of analyte. Incorporating an easily automated C₁₈ reversed phase column switching system with SPE (1.0 mm I.D. × 5.0 mm, 5 μm) made it possible to inject up to 100 μL of solution, and the total analysis time was 5.5 min.

Published by Elsevier B.V.

1. Introduction

Fluoxetine (N-methyl-*c*-[4-(trifluoromethyl)phenoxy]benzene-propanamine) (FLU) is a derivative of phenoxyphenyl propylamines. FLU (Fig. 1) is the parent drug of the selective serotonin reuptake inhibitor (SSRI) antidepressant class, which has emerged as a major therapeutic advance in psychopharmacology. It has been approved worldwide in the therapy of major depression [1] and has also demonstrated to be effective in the treatment of other syndromes, such as bulimia nervosa, panic fits and obsessive–compulsive disorder [2,3].

Several methods for sample preparation of fluoxetine in biological fluids have been described in the literature. Among them the most common are liquid–liquid extraction (LLE) [4–10] and solid phase extraction (SPE) [11–17]. These methods, however, present some disadvantages, being laborious and time-consuming. Moreover, they employ expensive and toxic solvents. Solid-phase microextraction (SPME), a solventless technique, has also been employed for the determination of FLU in urine and plasma [3,18]. Column switching, a rapid and modern approach, has been found in the literature for this analysis [19,20]. However, this tech-

nique requires more expensive and complex instrumentation to be utilized. Both gas chromatography (GC), often employing a derivatization step, and capillary electrophoresis have been used for the determination of FLU in biological samples [21,22]. However, high performance liquid chromatography (HPLC) has been the most common analytical technique used for fluoxetine analysis in plasma, because of the structural features of the analyte. Fluorescence and ultraviolet detectors have been widely used with HPLC in these analyses [10,15,26]. Mass spectrometry (MS) detectors have also been employed, presenting some advantages over spectroscopy systems [17,27–30]. In-tube SPME/LC [31] and comparison of LC with fluorescence detection to LC/MS [32] have been used for analysis of nontricyclic antidepressants in human plasma. MS provides high sensitivity and selectivity, being the favorite tool for complex matrices.

However, the concentration of FLU in plasma is expected to be low and hence a highly sensitive method is needed. Several instrumental steps can be made to improve sensitivity; reducing the inner diameter of the analytical column (e.g. replacing a 4.6 mm I.D. LC column with a 0.3 mm I.D. capillary LC column) will reduce chromatographic band dilution and will therefore increase sensitivity when employing concentration sensitive detectors [6]. However, if a narrower column is used (using a standard pump → injector → column setup), the injection volume must be significantly smaller than what can be injected into a regular

* Tel.: +20121530134; fax: +20552375354.
 E-mail address: amrlotfy2000@yahoo.com.

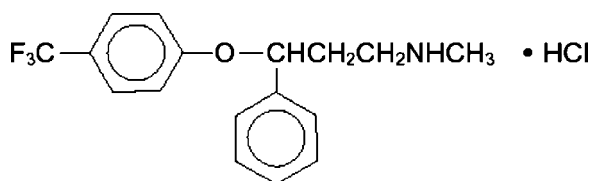


Fig. 1. Structure of fluoxetine hydrochloride.

column. To overcome the problem of potentially not being able to inject enough sample for analyte detection/quantification, a column switching system (on-line SPE-capLC [3–6]) can be employed. The principle of column switching is that a weak mobile phase is used for transfer of the sample to an enrichment column. The mobile phase must be weak enough so that the analyte(s) are retained on the enrichment column. When a reversed phase system is used, solvent, salts and less hydrophobic compounds which are not retained will pass through the enrichment column and to waste. When the entire sample has been loaded into the enrichment column, the easily automated plumbing of the system is set so that a second mobile phase (from a second pump) passes through the enrichment column in the backflush mode, and is strong enough to elute the analyte(s) of the enrichment column and into an analytical reversed phased column for chromatographic separation. In addition to being a tool for loading large injection volumes into a narrow column, column switching also replaces time-consuming off-line SPE steps.

The sensitivity will most often be further increased by replacing a UV detector with a mass spectrometer with an electrospray interface, which provides high sensitivity when operated with low flow rates as those used with capillary LC.

A method for determining fluoxetine in plasma using capLC-MS was described here. The decision to employ such instrumentation instead of conventional HPLC-UV instrumentation was based on expected improvements with regards to analysis time, selectivity and sensitivity, and these points are addressed in this paper. In order to avoid possible ion suppression during MS detection, the method includes a selective sample preparation based on liquid-liquid extraction (LLE). To lower the demands on the operator, the method also includes a column switching system, and the performance and limitations of this system are described. The performance of the method is demonstrated by quantifying fluoxetine in plasma from a volunteer who had taken one dose of fluoxetine-containing one capsule 14 h prior to sampling.

2. Experimental

2.1. Chemicals, buffers and materials

Fluoxetine hydrochloride was purchased from Egyptian International Pharmaceutical Industries Company (EIPICO). Metronidazole

was purchased from Sigma-Aldrich (Steinheim, Germany). HPLC grade acetonitrile (ACN) was obtained from Rathburn Chemicals Ltd. (Walkerburn, UK). Gradient quality water and reagent grade ammonium formate were obtained from Fluka (Buchs, Switzerland). Chloroform was purchased from Merck KGaA (Darmstadt, Germany). Nitrogen (99.99%) was obtained from AGA (Oslo, Norway). Ammonium formate buffer pH 4.0 (0.05 mol L^{-1}) was prepared as follows [23]: 3.15 g of ammonium formate was dissolved in 950 mL water, pH was adjusted to value 4.0 ± 0.1 with formic acid (diluted with water in the ratio 1:5), the buffer was diluted to 1000 mL with water and then was filtered through a $0.45\text{-}\mu\text{m}$ (HVLP, Germany) membrane filter.

Drug-free human plasma was purchased from Ullevaal University Hospital (Oslo, Norway). Plasma samples from volunteers who had taken fluoxetine-containing antidepressant capsule were frozen within 1 h of collection, and kept frozen until analyzed.

All fused silica capillaries were purchased from Polymicro Technologies Inc. (Phoenix, AZ, USA). $0.3 \text{ mm I.D.} \times 50 \text{ mm}$ Zorbax C_{18} columns were purchased from Agilent (Palo Alto, CA, USA). For pre-concentration of the analytes, HotSep[®] Tracy trace enrichment (SPE) columns (G & T SepTech, Kolbotn, Norway) were employed. The dimensions were $1 \text{ mm} \times 5 \text{ mm}$, and the columns were packed with $5 \mu\text{m}$ Kromasil C_{18} particles, with a pore size of 100 \AA . The enrichment column's inner dimensions were a compromise between column capacity and system dead volumes. The stationary phase particle size of the enrichment column was larger than that of the analytical column to assist refocusing on the column and for minimizing back pressure. A particle size larger than $5 \mu\text{m}$ was not used due to concern that larger particles would not retain the analytes well enough during the enrichment stage.

2.2. Chromatographic system

A Hitachi L-7110 isocratic LC pump from Merck (Darmstadt, Germany) was used for sample loading (pump 1 in Fig. 2). An Agilent Series 1100 capillary gradient pump with an incorporated on-line vacuum degasser was used to deliver the mobile phase (pump 2 in Fig. 2) providing *back-flushed* desorption from the pre-column and elution into the analytical column. The back-flush mode is used to avoid analyte band broadening which can occur if the analyte(s) pass through the entire enrichment column before entering the analytical column.

Elution of the analytes was conducted isocratically ($25\% \text{ ACN}/75\% \text{ } 0.05 \text{ mol L}^{-1}$ ammonium formate buffer, v/v). The mobile phase was delivered at a constant flow of $5 \mu\text{L min}^{-1}$ through the analytical column. The sample loading solution consisted of $\text{ACN}/0.05 \text{ mol L}^{-1}$ ammonium formate buffer (5/95, v/v). The loading flow rate was $200 \mu\text{L min}^{-1}$. Valco Cheminert C2 six-port valves were used for manually injecting the samples and manual column switching. A schematic drawing of the system is presented in Fig. 2.

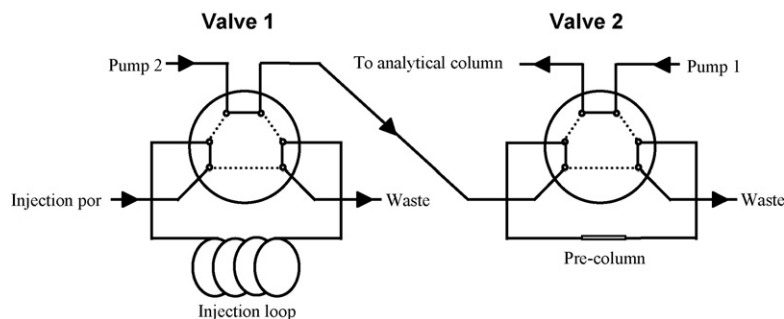


Fig. 2. Scheme of the switching system employed.

The on-line solid phased extraction-liquid chromatography-mass spectrometry (SPE-LC-MS) system times were as follows: 100 μL of sample was injected, and loaded at a flow rate of 200 $\mu\text{L min}^{-1}$. After 1.0 min, the SPE-retained compounds were back-flushed on to the analytical column. At the time of the void volume (2.0 min), valve 2 was switched to re-equilibrate the enrichment column with loading solvent, which took only approximately 20 s. At the time where the analyte began to elute from the analytical column (5.1 min), a new sample could be loaded on to the SPE column. Hence, immediately after completing data collection of one sample, data collection of the next sample could begin.

The analytical column was connected to a Micromass LCT TOF-MS (Micromass, Manchester, UK). The TOF-MS was equipped with a Z-spray atmospheric pressure ionization source for ESI, which was modified to handle flow rates in the low $\mu\text{L min}^{-1}$ range. Ionization was performed in positive ion mode and fluoxetine was observed at $m/z = 309.6$ and metronidazole was observed at 172.44 ($[M+H]^+$ for both compounds). The following voltages were used: 3.2 kV on the capillary, 20V on the sample cone and 5.0V on the extraction cone. In order to obtain a stable spray performance and aid solvent vaporization, nebulizer gas and desolvation gas were applied at 50 L h^{-1} and 300 L h^{-1} , respectively. The TOF-MS instrument was controlled by MassLynx v4.0 software, and mass spectra were acquired in the m/z range 100–1000. The instrument was calibrated with a sodium iodide and cesium iodide solution. For preliminary experiments a Spectra 100 UV detector (Spectra Physics, Mountain View, CA, USA) modified for miniaturized LC was employed.

Ion suppression studies were conducted by chromatographing a blank plasma sample with the conditions described above, and mixing the eluent by a t -coupling with a 1 $\mu\text{g mL}^{-1}$ standard solution of fluoxetine, pumped with a direct infusion pump at 5 $\mu\text{L min}^{-1}$. The mixed eluent/analyte solution was introduced to the TOF-MS, and the analyte signal was monitored at $m/z = 309.6$.

2.3. Preparation of stock and working solutions

Stock solutions of 100 $\mu\text{g mL}^{-1}$ were made by dissolving respectively 10 mg free base in 100 mL of methanol. Aqueous working solutions and calibration standards were prepared by appropriate dilution of the stock solutions with water. Spiked plasma samples (working, calibration and validation samples) were prepared by adding diluted solutions of the compounds to drug-free plasma in volumes not exceeding 10% of the plasma volume. Aqueous solutions of 5.0, 25 and 50 $\mu\text{g mL}^{-1}$ of both internal standard and analyte were used for recovery studies with LC-UV instrumentation. Aqueous calibration solutions used with the column switching method were prepared to the levels 5.0, 20, 40 and 60 ng mL^{-1} of analyte. Plasma calibration samples at 5.0, 20 and 40 ng mL^{-1} concentration levels and validation plasma samples at 5.0, 10, 20, 30 and 40 ng mL^{-1} were used. All samples and solutions used with the switching system were spiked to 20 ng mL^{-1} of internal standard. The stock solutions and plasma samples were stored at -10°C , and the aqueous solutions were stored at $+5^\circ\text{C}$.

2.4. Sample preparation

Plasma (0.5 mL) spiked with fluoxetine (analyte) and metronidazole (I.S.) was mixed with 1 mL 0.05 mol L^{-1} ammonium formate buffer. 5 mL of chloroform was added and the solution was shaken for 5 min. The solution was removed and centrifuged for 10 min (10 krpm). The organic layer was evaporated with nitrogen, and the residue was dissolved in 1 mL of ammonium formate buffer. 100 μL of this solution was injected into the column switching system.

Table 1

Retention times, precisions and accuracy of (FLU-HCl) and IS.

Analysis materials	Retention times (min)	RSD %	Recovery ^a %
Internal Standard (IS)	2.9	0.66	91 \pm 2
Analyte	5.1	0.71	95 \pm 4

^a Average of three determinations.

2.5. Recovery and accuracy

For the liquid-liquid extraction step, the recovery (%) of the target compounds was determined by comparing the chromatographic peak areas of the aqueous calibration solutions subject to the extraction procedure to the peak areas of the aqueous calibration solutions without extraction. But for the column switching step, the recovery was defined as: (The peak areas injecting 5 μL of 15 $\mu\text{g mL}^{-1}$ analyte + I.S. into the switching system/the chromatographic peak areas injecting 5 μL of 15 $\mu\text{g mL}^{-1}$ analyte + I.S. directly into the analytical column) \times 100%. The total recovery of the method was defined as [24]: (The chromatographic peak areas of plasma calibration samples/the peak areas of aqueous calibration solutions) \times 100%. The accuracy (%) of the (total) method was defined as the ratio of a known amount of analyte spiked to a plasma sample and the amount found, multiplied by 100%.

2.6. Calibration curves

The calibration curves were obtained by weighted linear regression, using the formula (Concentration_{analyte}/Concentration_{I,S}) = constant \times (Area_{analyte}/Area_{I,S}).

2.7. Limit of quantification (cLOQ) and limit of detection (cLOD) [25]

The cLOQ was defined as the analyte concentration that would produce a peak height of ~ 10 times the intensity of the baseline noise. The cLOD was defined as the concentration that would provide a signal-to-noise ratio of ~ 3 .

3. Results and discussion

3.1. Sample preparation

The use of dichloromethane as organic solvent for the extraction of target compound produced extraction efficiency between 52 and 57% for the analyte and internal standard, respectively, illustrating that chloroform was crucial to obtain high extraction efficiency.

The peak areas of the compounds in solutions subjected/not subjected to the liquid-liquid extraction procedure were compared using a t -test, and the difference in mean was insignificant at $p = 0.05$ for all three concentration levels using UV-detection (see Section 2), implying a recovery of 100%. The extraction recovery of the analyte and internal standard was shown in Table 1, when spiked plasma samples were extracted ($n = 3$, three levels).

3.2. Large volume injection SPE-capLC-MS

In preliminary experiments, conventional LC-UV instrumentation utilizing a 4.6 mm bore C_{18} column was employed and was intended to be used throughout the study. However, it was found that employing capillary columns (0.3 mm I.D.) enhanced the sensitivity of the method by a factor of ~ 100 , due to reduced radial dilution of the chromatographic band over the column. Although it was feared that this approach could be less robust than a conventional HPLC system, the capillary LC system performance was satisfactory. The back pressure over the 0.3 mm analytical column

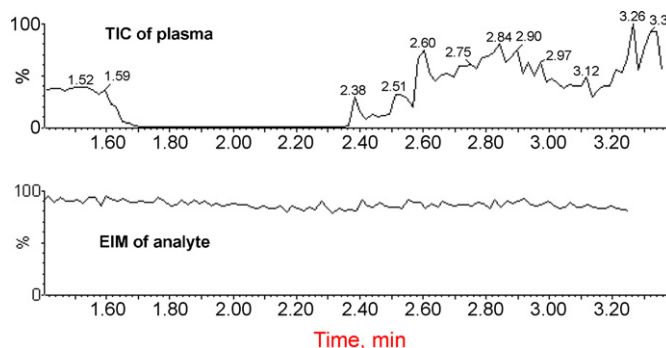


Fig. 3. TIC of blank plasma and EIM of analyte recorded for ion suppression monitoring.

was 65 bar (± 1 bar) during the entire study. The retention times and relative standard deviations of the internal standard and the analyte were stable throughout the study (Table 1). The peak areas of the target compounds were unaltered by including a switching system, tested by injecting equal amounts on to the column directly or by a switching system ($n = 3$ for each system), and comparing the mean and deviations of the two sets by Student's t -test ($p = 0.05$). No reduction of chromatographic performance was observed when utilizing the switching system. The chromatographic performance and recovery of the target compounds were also unaffected by the loading flow rate, tested up to $200 \mu\text{L min}^{-1}$. Injecting volumes up to $100 \mu\text{L}$ did not affect the performance of the system or recovery, but for injection volumes of $150 \mu\text{L}$, peak broadening was observed. Hence $100 \mu\text{L}$ was considered to be the maximum allowable injection volume. The back pressure of the enrichment column during sample loading was stable at $32 (\pm 1)$ bars throughout the study at a flow rate of $200 \mu\text{L min}^{-1}$.

When employing capillary LC with UV detection, a buffer/ACN gradient was employed to separate the internal standard from system void volume peaks and other early eluting compounds. This approach, although successful separation-wise, required a reconditioning of the system for 10 min before another sample could be injected. When employing a TOF-MS, co-elution issues were eliminated by monitoring single ion masses, allowing the use of isocratic elution, with no reconditioning step and no ion suppression was observed (see below).

With the on-line SPE-LC-MS system times described in Section 2, the target compounds can be subject to different eluting conditions depending on the sequence, since late eluting compounds from one injection may elute at the same time as the target compounds eluting from a second injection and possibly give ion suppression. However, analysis of a blank plasma sample when monitoring the signal of a constant supply of analyte (using a direct injection pump) showed no intensity drops in the analyte's extracted ion monitoring (EIM) signal during this experiment, showing that analyte suppression did not occur for plasma samples (Fig. 3).

The TOF-MS did not require recalibration during the study, since the measured masses of the target compounds did not drift more than 0.01 Da .

Table 2

Inter- and Intra-day assay variation of (FLU-HCl). The inter-day data were obtained by choosing randomly one replicate for each day.

Spiked levels of analyte (ng mL^{-1})	Inter-day variation		Intra-day variation	
	RSD%	Recovery ^a %	RSD%	Recovery ^a %
5	8	101	103	
20	10	99	99.8	
40	12	105	9	99.2

^a Average of six determinations.

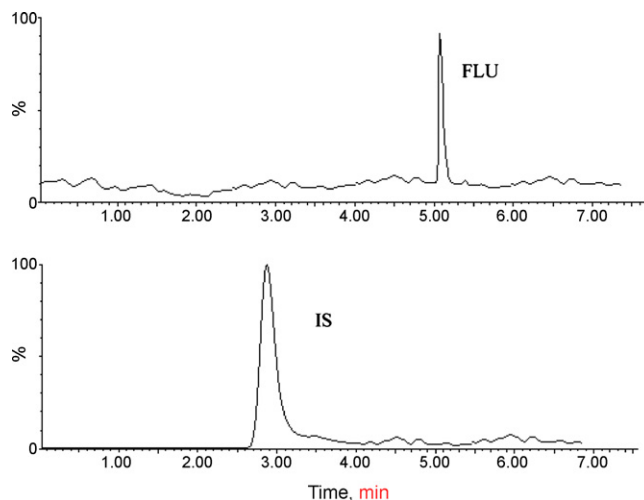


Fig. 4. Fluoxetine detected in plasma of volunteer who took Flutin[®]-containing fluoxetine 14 h prior to sampling. The concentration was determined to be 9 ng mL^{-1} .

3.3. Method validation

The correlation coefficient of the analyte (r^2) was 0.999 for aqueous calibration curves, plasma sample calibration curves and plasma validation samples. For spiked plasma samples, the lower limit of quantification (the lowest concentration of spiked plasma standard employed) was $\sim 5.0 \text{ ng mL}^{-1}$. The cLOD of the method was approximately 3.0 ng mL^{-1} .

The accuracy and precision for inter- and intra-day variation of spiked levels of 5.0 , 20 and 40 ng mL^{-1} of fluoxetine were shown in Table 2.

The method was used to determine the amount of fluoxetine in a healthy male 14 h after an intake of one capsule of Flutin[®], which contains 20 mg fluoxetine hydrochloride. Fluoxetine was detected (Fig. 4), and the concentration was calculated to 9.0 ng mL^{-1} plasma.

4. Conclusions

The on-line SPE-capillary LC-ESI-MS method described in this paper provided selective, fast and sensitive determination of fluoxetine in human plasma with acceptable precision and accuracy. This easily automated system was found to be robust; the retention times and back pressures were constant throughout the study. This approach is thus an attractive alternative to off-line SPE procedures prior to LC injection. Miniaturizing the system for increased sensitivity was a useful step, since the level of fluoxetine in a volunteer's plasma 14 h after exposure was as low as 9.0 ng mL^{-1} , and this concentration is almost impossible to determine employing a larger column diameter.

References

- [1] J.P. Feighner, W.F. Boyer, Selective Serotonin Re-Uptake Inhibitors, Wiley, New York, 1991.
- [2] P. Benfield, R.C. Heel, S.P. Lewis, *Drugs* 32 (1986) 481.
- [3] D. Wong, F. Bymaster, E. Engleman, *Life Sci.* 57 (1995) 411.
- [4] A.L. Peyton, R. Carpenter, K. Rutkowski, *Pharm. Res.* 8 (1991) 1528.
- [5] G. Misztal, H. Hopkala, *Pharmazie* 52 (1997) 854.
- [6] M.A. Raggi, F. Bugamelli, G. Casamenti, R. Mandrioli, D. De Ronchi, V. Volterra, *J. Pharm. Biomed. Anal.* 18 (1998) 699.
- [7] A. Zarghi, A. Kebriaeezadeh, R. Ahmadkaniha, M. Akhgari, N. Rastkari, *J. AOAC Int.* 84 (2001) 1735.
- [8] A. Llerena, P. Dorado, R. Berecz, A. Gonzalez, M.J. Norberto, A. de la Rubia, M. Caceres, *J. Chromatogr. B* 783 (2003) 25.
- [9] J. Atta-Politou, P. Fraskou, M. Koupparis, *J. Liq. Chromatogr. Relat. Technol.* (2004) 2957.
- [10] L. Vlase, S. Imre, S. Leucuta, *Talanta* 66 (2005) 659.
- [11] R.N. Gupta, M. Steiner, *J. Liq. Chromatogr.* 13 (1990) 3785.

- [12] S. Pichini, S. Pacifici, I. Altieri, M. Pellegrini, P. Zuccaro, J. Liq. Chromatogr. Relat. Technol. 19 (1996) 1927.
- [13] L. Kristoffersen, A. Bugge, E. Lundanes, L. Slordal, J. Chromatogr. B 734 (1999) 229.
- [14] P. Molander, A. Thomassen, L. Kristoffersen, T. Greibrokk, E. Lundanes, J. Chromatogr. B 766 (2002) 77.
- [15] C. Sabbioni, F. Bugamelli, G. Varani, L. Mercolini, A. Musenga, M.A. Saracino, S. Fanali, M.A. Raggi, J. Pharm. Biomed. Anal. 36 (2004) 351.
- [16] K.M. Li, M.R. Thompson, I.S. McGregor, J. Chromatogr. B 804 (2004) 319.
- [17] H. Juan, Z. Zhiling, L. Huande, J. Chromatogr. B 820 (2005) 33.
- [18] C. Fernandes, A.J. Santos-Neto, J.C. Rodrigues, C. Alves, F.M. Lanças, J. Chromatogr. B 874 (2007) 217.
- [19] S. Souverain, M. Mottaz, S. Cherkaoui, J.L. Veuthey, Anal. Bioanal. Chem. (2003) 880.
- [20] A.J. Santos-Neto, J.C. Rodrigues, C. Fernandes, G.M. Titato, C. Alves, F.M. Lanças, J. Chromatogr. A 1105 (2006) 71.
- [21] P. Fontanille, N. Jourdil, C. Villier, G. Bressard, J. Chromatogr. B 692 (1997) 337.
- [22] L. Labat, M. Deveaux, P. Dallet, J.P. Dubost, J. Chromatogr. B 773 (2002) 17.
- [23] D. Zivanov-Stakic, L. Djeric, Arh. Farm 27 (1977) 223.
- [24] ICH Validation of Analytical Procedures Methodology, ICH Harmonised Tripartite Guidelines, Adopted 6 NOV, 1996.
- [25] A. Jedlička, J. Klimeš, T. Grafnetterova, Pharmazie 59 (2004) 178.
- [26] B. Venkateswara Reddy, K.V.N. Suresh Reddy, J. Sreeramulu, G.V. Kanumula, Chromatographia 66 (2007) 111.
- [27] A. de Castro, M. Concheiro, O. Quintela, A. Cruz, M. López-Rivadulla, J. Pharm. Biomed. Anal. 48 (2008) 183.
- [28] C. Fernandes, E.V. Hoeck, P. Sandra, F.M. Lanças, Anal. Chim. Acta 614 (2008) 201.
- [29] J.M. Conley, S.J. Symes, S.A. Kindelberger, S.M. Richards, J. Chromatogr. A 1185 (2008) 206.
- [30] N. Unceta, A.G. Caballero, A. Sánchez, S. Millán, M.C. Sampedro, M.A. Goicolea, J. Sallés, R.J. Barrio, J. Pharm. Biomed. Anal. 46 (2008) 763.
- [31] B.J. Goncalves, F. Mauro, M.E. Costa, J. Chromatogr. B 862 (2008) 181.
- [32] I. Kovacevic, M. Pokrajac, B. Miljkovic, D. Jovanovic, M. Prostran, J. Chromatogr. B 830 (2006) 372.



Fast and selective determination of triterpenic compounds in olive leaves by liquid chromatography–tandem mass spectrometry with multiple reaction monitoring after microwave-assisted extraction

N. Sánchez-Ávila, F. Priego-Capote*, J. Ruiz-Jiménez, M.D. Luque de Castro

Department of Analytical Chemistry, Annex C-3 Building, Campus of Rabanales, University of Córdoba, Córdoba, Spain

ARTICLE INFO

Article history:

Received 30 June 2008

Received in revised form 20 October 2008

Accepted 24 October 2008

Available online 31 October 2008

Keywords:

Triterpenic compounds

LC–MS–MS

Multiple reaction monitoring (MRM)

Natural products

Microwave-assisted extraction

ABSTRACT

A method for fast and selective determination of the main triterpenic compounds present in olive leaves – oleanolic, ursolic and maslinic acids as triterpenic acids and, uvaol and erythrodiol as triterpenic dialcohols – is reported here. Quantitative isolation of the analytes has been accomplished in 5 min by microwave assistance using ethanol as extractant. Due to the medium polarity of triterpenic acids and dialcohols, different ethanol–water ratios were tested in order to select the optimum extractant composition for their solubilisation. Microwave assistance provided a significant shortening of the leaching time as compared to conventional procedures by maceration, which usually requires at least 5 h. After extraction, determination was carried out by liquid chromatography–tandem mass spectrometry (LC–MS–MS) with a triple quadrupole (qQq) mass detector without any clean-up step prior to chromatographic analysis. Highly selective identification of triterpenes was confirmed by multiple reaction monitoring (MRM) using the most representative transitions from the precursor ion to the different product ions, while the most sensitive transitions were used for MS–MS quantitation. Total analysis performed in 25 min enables the characterization of a fraction with particular interest in the pharmacological area.

© 2008 Elsevier B.V. All rights reserved.

1. Introduction

The main endeavour of the pharmaceutical industry is at present aimed at the prevention and/or treatment of pathological disorders and diseases affecting our society. This is accomplished by synthesis of new drugs and isolation of compounds with pharmacological properties from natural products. Despite pharmacological properties of natural products have for centuries been investigated, their tremendous diversity makes them an inexhaustible source of new drugs [1]. Thus, natural products continue at present being a great promise for discovery and development of new pharmaceuticals [2]. In addition, new properties of well-known natural drugs are proved, thus contributing to the relevance of research on products isolated from plants.

The inherent diversity and interest on natural products justify the present demand for development of fast and selective analysis methods. These methods involve first an extraction (leaching) step, which is the key for subsequent steps of the overall analytical process leading to identification and/or quantitation of target

plant constituents. An ideal leaching procedure should be exhaustive with respect to the constituents to be analysed, fast, simple, inexpensive, environmental friendly and amenable to automation for routine analysis. Looking for these characteristics, alternative leaching techniques such as ultrasound- and microwave-assisted extraction, pressurized liquid extraction and supercritical fluid extraction have been applied to this field [3–6]. Based on these techniques, extraction methods in which both the extract volume and the process time are drastically shortened have been developed.

Concerning individual separation of the target analytes, a powerful separation technique such as gas chromatography (GC) has for decades been applied to the analysis of volatile natural products or derivatives. Despite this technique interfaced to mass spectrometry (MS) is especially effective with identification and quantitation purposes, the role recently played by liquid chromatography (LC) for analysis of natural products is invaluable. This is supported on the fact that approximately 80% of all known natural compounds are non-volatile or thermally unstable, and thus incompatible with GC [7]. In this sense, although LC has lower resolution capability than GC (ultra-performance LC has considerably improved this aspect), the former shortens the analysis time because derivatization is not required. In addition, the LC–MS coupling and, particularly

* Corresponding author. Tel.: +34 957218615; fax: +34 957218615.
E-mail address: q72prcaf@uco.es (F. Priego-Capote).

Table 1

Optimization of the chromatographic conditions for separation of triterpenic compounds.

Variable	Tested range	Optimum value
Flow rate (mL min ⁻¹)	0.7–1.2	1.2
Temperature (°C)	5–35	15
Water content (%)	0–20	7.9
Acetonitrile content (%)	0–100	90
Polarity modifier	Methanol Ethanol 2-Propanol	Methanol
Polarity modifier (%)	1–10	2
Ammonia	0–1	0.05
Ammonium formate	0–1	0.05

LC–MS–MS, provide powerful tools for quantitative and qualitative analysis [8].

One important bioactive fraction isolated from plants is that composed by triterpenic compounds, either in the form of free acids or aglycones of triterpenoid saponins. The literature abounds on their pharmacological properties which include anti-inflammatory

[9], hepatoprotective [10], anti-tumour [11], anti-viral [12], anti-HIV [13], anti-microbial [14], anti-fungal [15], anti-diabetic [16], gastroprotective [17], and anti-hyperlipidemic effects [18]. Bioactive pentacyclic triterpenoids are widely distributed in medicinal herbs and plants, *Olea europaea* included [19]. In Spain, approximately 110 tonnes of olive leaves are annually generated both from pruning and after separation of olive fruit in mills prior to olive oil production. This residue is a potential source for isolation of oleanolic and maslinic acid together with other triterpenic compounds.

Due to the low volatility and high molecular weight of triterpenes, a derivatization step is mandatory prior to GC analysis. Derivatization of triterpenes has traditionally been carried out by silylation, a tedious procedure requiring reaction times from 30 min to 3 h [20–24]. Recent investigations carried out by our research group have shortened the silylation step by virtue of the assistance with an auxiliary energy such as ultrasound [25]. One alternative to avoid the derivatization step is the use of LC separation. Thus, an LC–LC coupling to MS with electrospray ionization (ESI) has been used to analyse boswellic acids [26]. Triterpene glycosides have been determined by a photoarray absorptiometric–mass-spectrometric–evaporative-light scattering

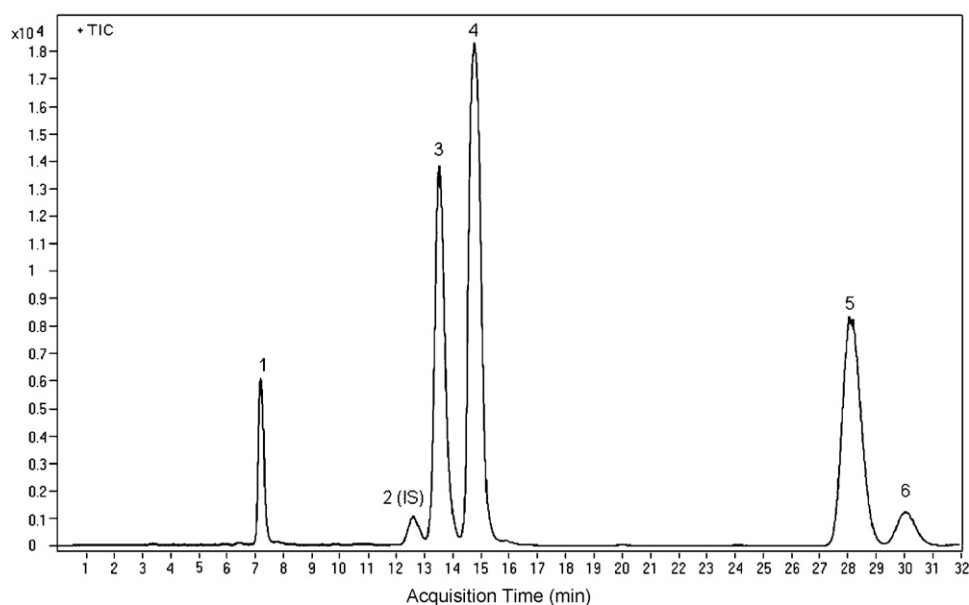


Fig. 1. Total ion chromatogram obtained with a standard solution of the target triterpenes under the optimum chromatographic conditions (Section 2.5). (1) maslinic acid, 15 $\mu\text{g mL}^{-1}$; (2) betulinic (IS) 5 $\mu\text{g mL}^{-1}$, (3) oleanolic and (4) ursolic acids, 30 $\mu\text{g mL}^{-1}$; (5) erythrodiol, 30 $\mu\text{g mL}^{-1}$ and (6) uvaol, 10 $\mu\text{g mL}^{-1}$.

Table 2

Optimization of the MS–MS step for qualitative and quantitative determination of terpenic compounds.

Analyte	Voltage MS1 ^a (V)	Precursor ion (<i>m/z</i>)	Collision energy (eV)	Product ions (<i>m/z</i>)	Quantitation transition (<i>m/z</i>)
Maslinic acid	160	409	10	203 189	409 → 203
Betulinic acid	160	439	10	203 191	439 → 191 439 → 203
Oleanolic acid	160	439	10	203 191	439 → 191 439 → 203
Ursolic acid	160	439	10	203 191	439 → 191 439 → 203
Erythrodiol	140	425	10	217 191	425 → 217 425 → 191
Uvaol	140	425	10	217 191	425 → 217 425 → 191

^a Voltage of the first quadrupole to focus the precursor ion for each analyte.

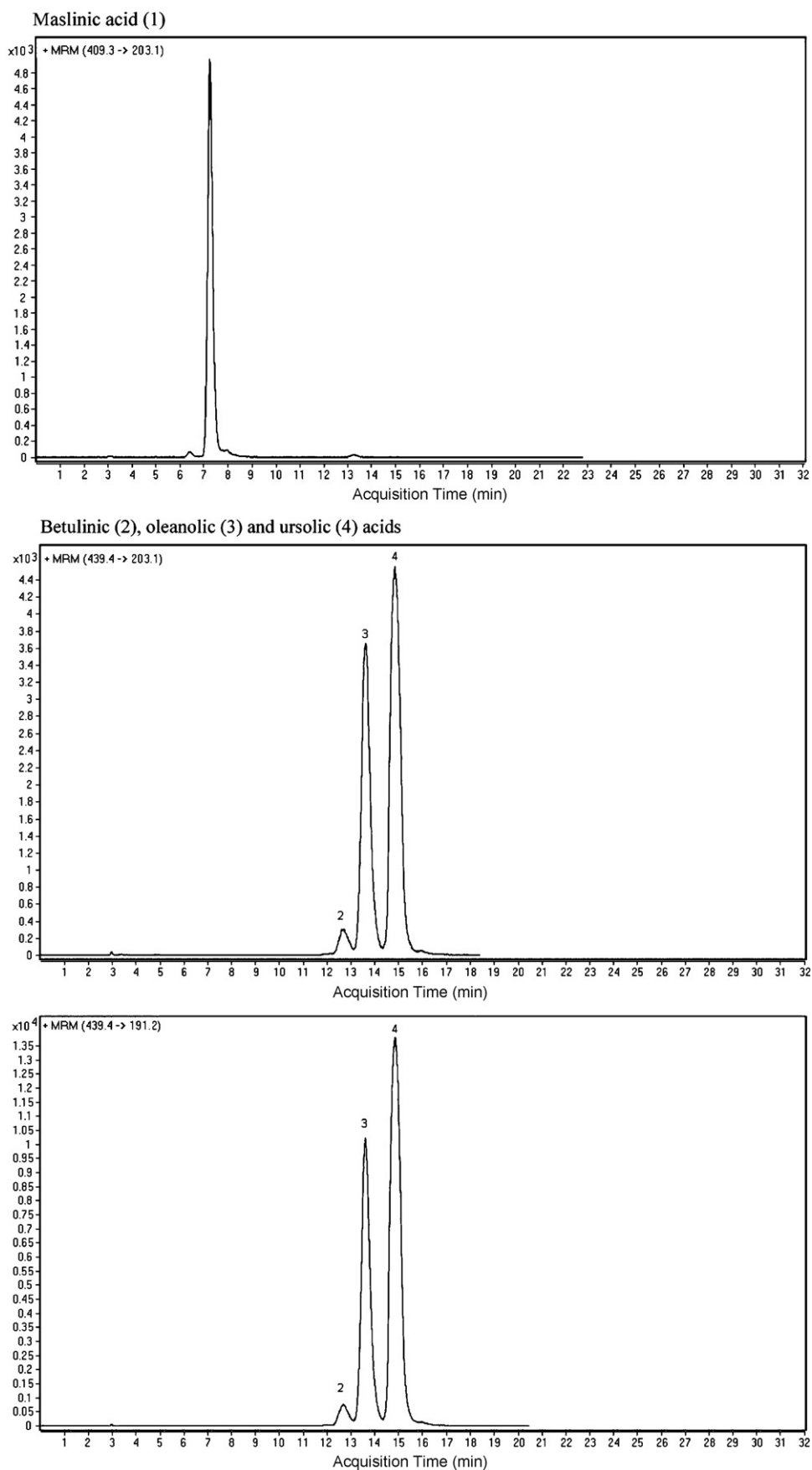


Fig. 2. Selected transitions from precursor ions to product ions used for quantitation of the terpenes after optimization by MRM. (1) maslinic acid, 15 $\mu\text{g mL}^{-1}$; (2) betulinic (IS) 5 $\mu\text{g mL}^{-1}$, (3) oleanolic and (4) ursolic acids, 30 $\mu\text{g mL}^{-1}$; (5) erythrodiol, 30 $\mu\text{g mL}^{-1}$ and (6) uvaol, 10 $\mu\text{g mL}^{-1}$.

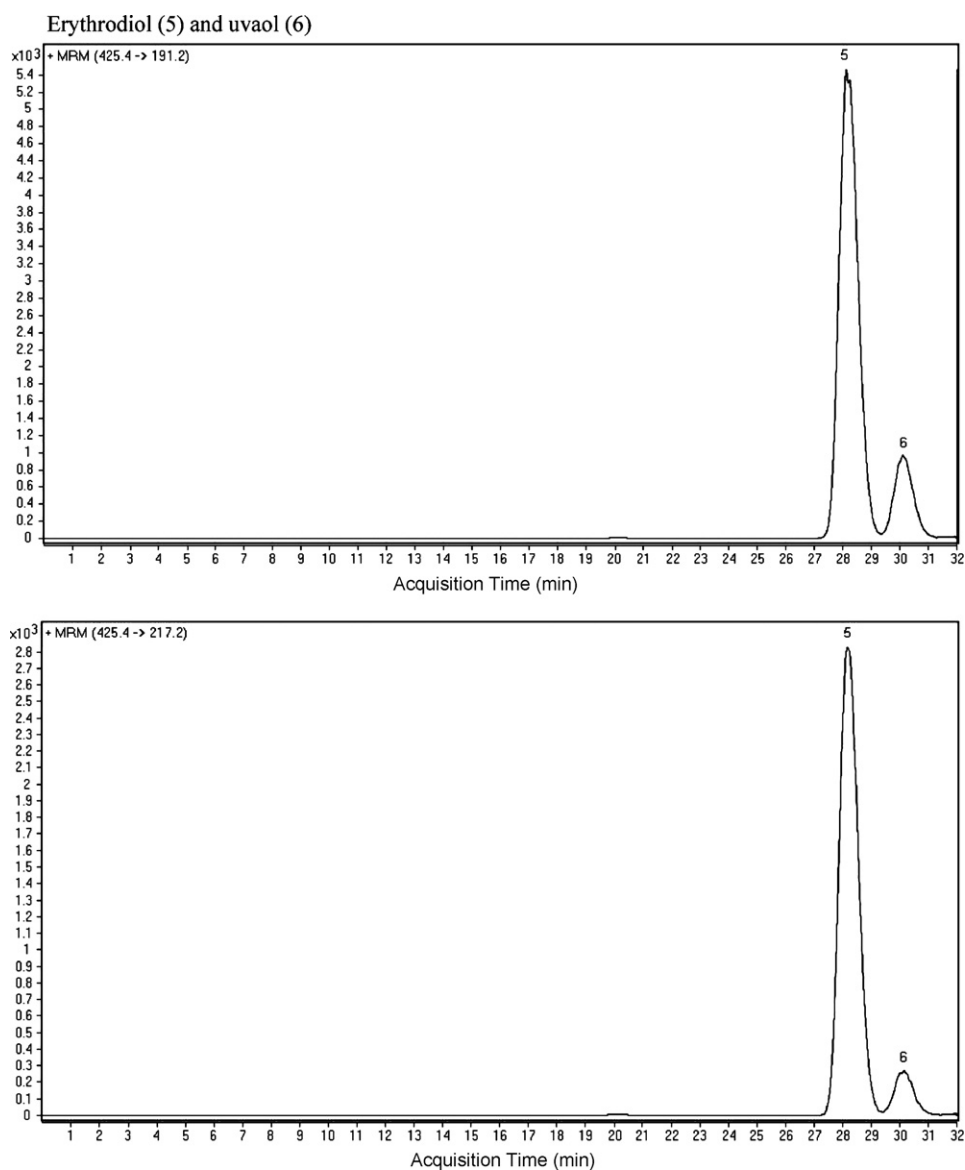


Fig. 2. (Continued)

fingerprinting approach [27] or with a dual system by connection of a photoarray and a mass detector [28], coupled in all instances to LC equipment.

A method for determination of triterpenic compounds in olive leaves is here proposed. The coupling LC–MS–MS with a triple quadrupole (qQq) mass detector has been used for identification, confirmation (by comparison with standards) and quantitation of triterpenic compounds in extracts from olive leaves. The MS–MS step has been optimized by multiple reaction monitoring (MRM) to achieve the demanded levels of sensitivity and selectivity for analysis of this fraction. A microwave-assisted leaching step has been optimized for isolation of the target analytes prior to chromatographic analysis.

2. Experimental

2.1. Samples

Olive leaves from hojiblanca and acebuche varieties were collected in Córdoba, dried at 35 °C for 24 h in an electrical furnace, milled and stored at 4 °C until analysis.

2.2. Reagents

The most representative and commercially available triterpenic compounds found in olive leaves [19] were the target analytes of this research. Thus, erythrodiol and uvaol were purchased from Extrasynthese (Genay, France), oleanolic and ursolic acids were from Sigma–Aldrich (Madrid, Spain). Maslinic acid (>97% purity) isolated by a previously reported protocol [29] was a gift from A. García-Granados (University of Granada, Spain). Betulinic acid, also from Sigma, was used as internal standard. Methanolic stock standard solutions of 1000 $\mu\text{g mL}^{-1}$ were prepared for each analyte and stored at –20 °C. Standard dilutions in methanol were prepared daily. Analytical-grade ethanol from Panreac (Barcelona, Spain) was used in the leaching step.

Deionized water (18 M Ω cm) from a Millipore Milli-Q (Bedford, MA, USA) water purification system and acetonitrile and methanol of LC–MS grade from Scharlab (Barcelona, Spain) were used for preparation of chromatographic mobile phases. Ammonium formate from Agilent (Waldbronn, Germany) and ammonium hydroxide from Scharlab were used as additives in the mobile phases to enhance ionization required for MS detection.

2.3. Apparatus and instruments

A Microdigest 301 microwave-assisted digester of 200 W maximum power (Prolabo, Paris, France) furnished with a micro-processor programmer (Prolabo) was used for the leaching step.

Analyses were performed by reversed-phase LC followed by ESI in the positive mode and MS–MS detection. Liquid chromatography was performed with an Agilent (Palo Alto, CA, USA) 1200 Series LC system. This consists of a binary pump, vacuum degasser, autosampler and a thermostated column compartment. Detection was carried out with an Agilent 6410 Triple Quadrupole LC/MS. The data were processed using a MassHunter Workstation Software from Agilent for qualitative and quantitative analysis. An Inertsil ODS-2 C₁₈ analytical column (4.0 mm i.d. × 250 mm; 5 μm particle size, GL Sciences Inc., Tokyo, Japan) was used for chromatographic separation.

2.4. Proposed leaching procedure

Two grams of milled leaves and 16 mL of extractant mixture (80/20, ethanol–water) were placed into the quartz extraction vessel. The mixture was spiked with internal standard (50 μL of 100 μg mL⁻¹). This was positioned for 5 min in the microwave-

irradiation zone at 180 W irradiation power. After extraction, the suspension was centrifuged at 2000 × g and the extract 1/10 diluted in water prior to injection into the liquid chromatograph.

2.5. LC–MS–MS separation-detection

The separation was carried out under isocratic conditions during the whole chromatographic process. The mobile phase was 90% acetonitrile, 7.9% water and 2% methanol with 0.05% ammonia and 0.05% ammonium formate (pH 9.1). The chromatographic analysis took 32 min at a flow-rate of 1 mL min⁻¹. The temperature of the analytical column was 5 °C and the injection volume 10 μL.

The entire eluate was electrosprayed, ionized in positive mode and monitored by MS–MS detection in MRM mode, which was carried out by optimization of the product ions obtained by fragmentation of the isolated precursor ion for each analyte. This was achieved by setting the optimum voltage of the first quadrupole, which operates as a mass filter, and that of the collision cell for fragmentation of precursor ions. The flow-rate and temperature of the drying gas (N₂) were 13 L min⁻¹ and 350 °C, respectively. The nebulizer pressure was 35 psi and the capillary voltage 4000 V. The dwell time was set at 250 μs.

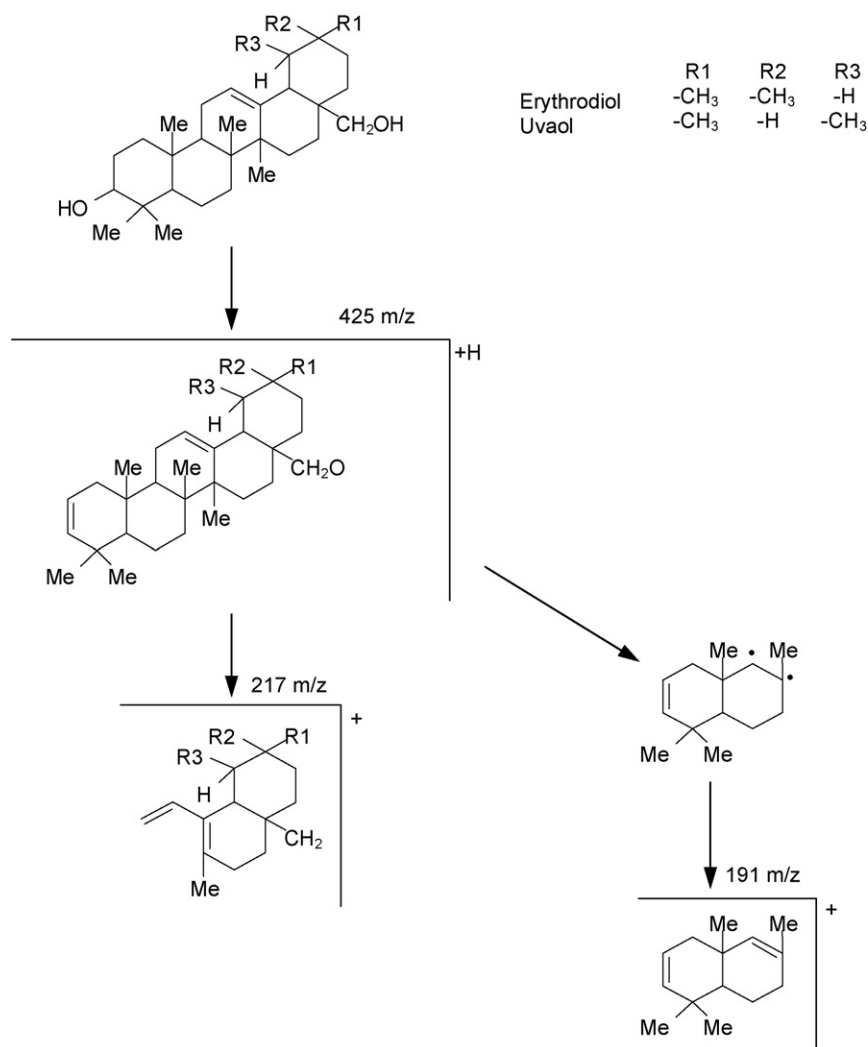


Fig. 3. Tentative fragmentation pathways for triterpenic compounds by MS–MS determination.

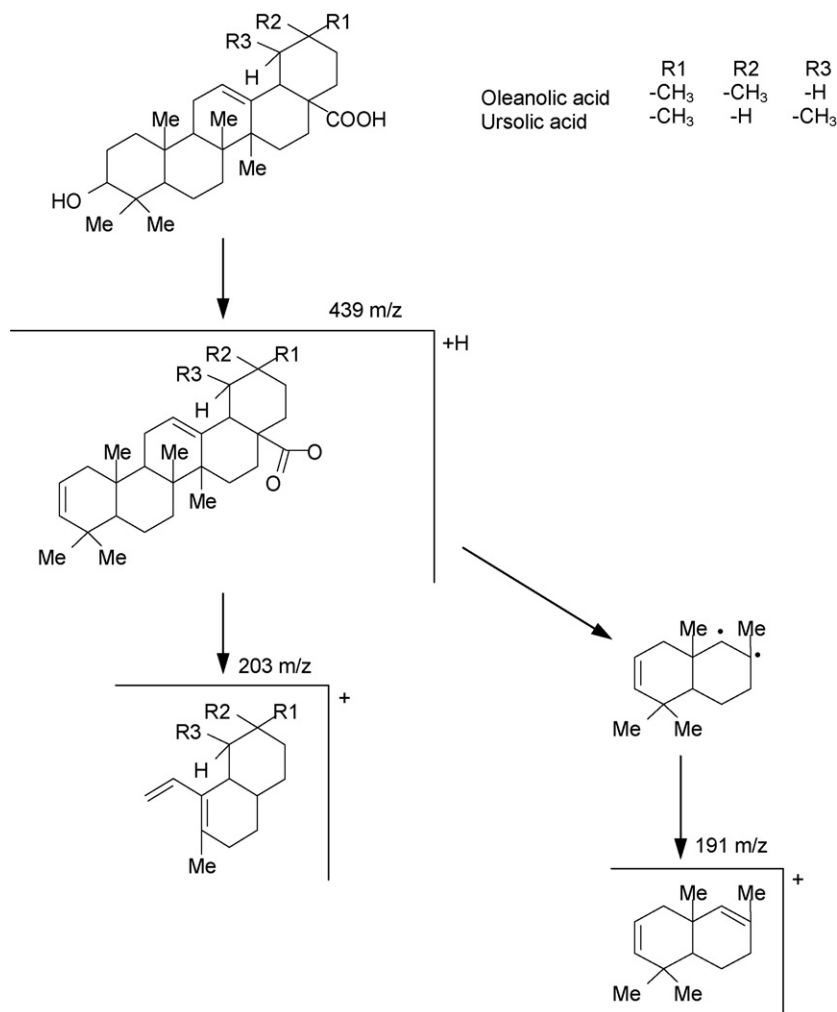


Fig. 3. (Continued)

3. Results and discussion

3.1. Optimization of the liquid chromatographic method

Chromatographic separation is a key step for determination of these compounds taking into account that ursolic and oleanolic acids on the one side and, erythrodiol and uvaol, on the other side, are isomers. The main variables with influence on the chromatographic separation were optimized by a univariate approach in order to obtain the best separation of the analytes in the shortest time. This study was carried out with standard solutions; then, the optimum conditions were tested with extracts. The variables optimized were composition of the mobile phase, flow-rate and temperature of the analytical column compartment. Table 1 shows these variables, the ranges studied and their optimum values as well as the solvents used in the optimization of the mobile phase composition. The most critical variables were the temperature and the pH of the mobile phase. Low temperatures within the range studied (5–35 °C) favoured the separation of the target analytes being 5 °C the optimum value. Concerning the pH of the mobile phase, acid pHs favoured the separation of the triterpenic acids while basic pHs improved that of triterpenic dialcohols. A compromise solution was to set the pH at 9.1 as shows the chromatogram of Fig. 1 obtained with a standard solution under the optimum chromatographic conditions. The study was carried out in scan mode, in

which only the second mass filter is operating to detect ions within a limited mass range (between 50 and 600 m/z) with a scan time of 500 ms. Betulinic acid was used as internal standard due to its physical and chemical behaviour similar that of the target analytes and its absence in olive leaves. The other peaks present in the chromatogram were identified as the solvent front and interferences from incomplete purification of maslinic acid, which was isolated in the laboratory.

In addition, this analysis enables the selection of the precursor ion for all analytes, which are listed in Table 2. The precursor ion for all triterpenes was $[M-H_2O]^+$ by loss of a water molecule, except for maslinic acid, which was $[M-H_2O-COO]^+$ by additional cleavage of the carboxylic group.

3.2. Optimization of the detection method by MS–MS

The strategy followed in the optimization of the MS–MS method was based on multiple reaction monitoring. Similarly to the chromatographic performance, this study was carried out both with standards and extracts. The optimum values for each parameter and triterpenic compound are shown in Table 2. Two different transitions were monitored for each analyte to achieve an extra level of selectivity, which is of particular interest for confirmatory analysis of complex-matrix samples by comparison with standards. Fig. 2 shows the selected transition used for quantitation of each

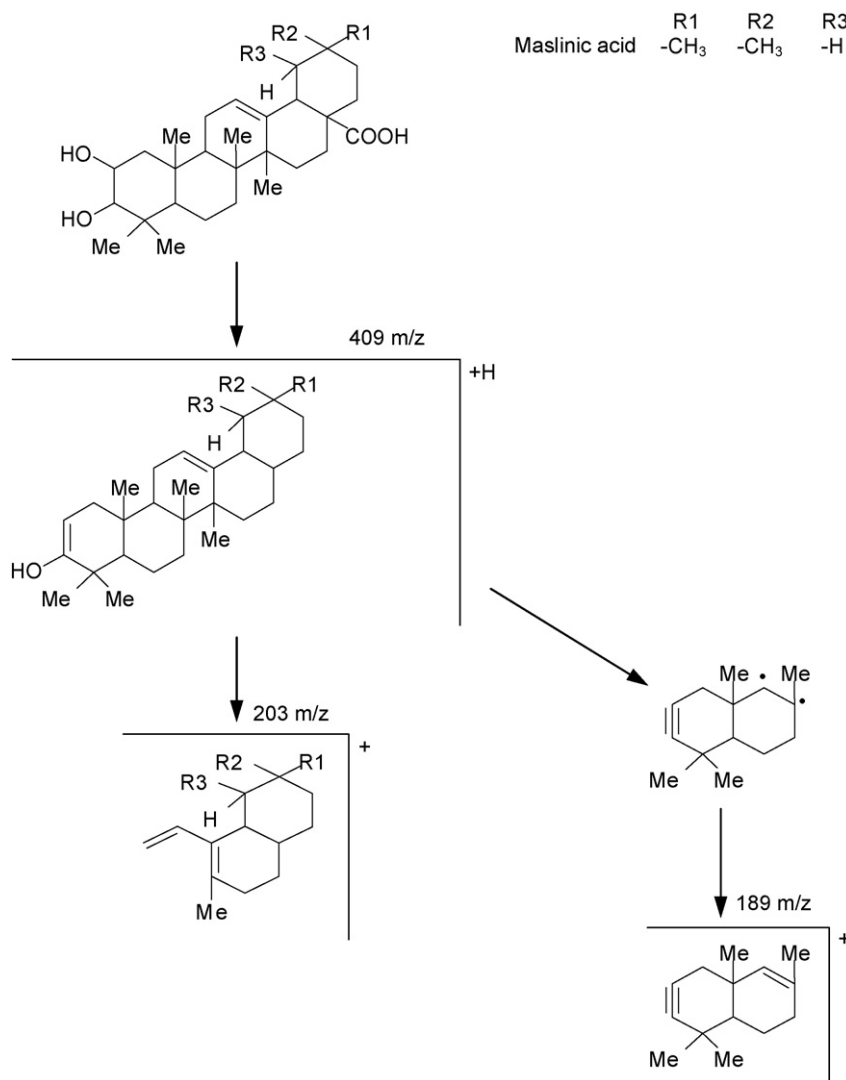


Fig. 3. (Continued)

triterpene. As can be seen, most of the analytes were quantified by two transitions as fragmentation of their precursor ions led to two product ions with a similar intensity. These product ions are 203 and 191 m/z for oleanolic and ursolic acid and 217 and 191 m/z for erythrodiol and uvaol. In the case of maslinic acid, additional quantification with the product ion corresponding to 189 m/z did not improve significantly in terms of sensitivity due to its low intensity. The demand for a powerful tool for confirmatory analysis and quantitation of terpenic compounds justifies the use of LC-MS-MS in MRM mode. Additionally, although the qQq is not a mass analyser suited for qualitative analysis, fragmentation pathways can be tentatively elucidated to set fingerprints characteristic of each analyte. Fig. 3 shows the tentative fragmentation scheme for each analyte from precursor to product ions. A common pattern for all analytes is that their precursor ions are generated in the electrospray source by dehydration resulting in peaks of 425 m/z for erythrodiol and uvaol and 439 m/z for oleanolic and ursolic acids. In the case of maslinic acid, the carboxylic group is additionally cleaved resulting in a peak of 409 m/z . The schemes for generation of product ions are characterized for the target triterpene compounds by fragmentation through the oleanane structure. As a consequence, the double bond changes its position and fingerprinting product ions are obtained for triterpene dialcohols and acids. For triterpene

dialcohols, two product ions are generated from fragmentation of the oleanane structure: 191 m/z , which is characteristic in general of pentacyclic triterpene compounds in olive leaves and, 217 m/z characteristic of triterpene dialcohols that keeps the methylene group after cleavage of the hydroxyl group. As stated above, the transitions from precursor ion to these product ions were used for quantitation because of its similar intensity. For triterpene acids, the fingerprinting product ion corresponds to 203 m/z being common for oleanolic, ursolic and maslinic acids. Oleanolic and ursolic acids also provide the product ion characteristic of triterpene compounds (191 m/z) found in olive leaves, which had an intensity similar to that of the former. For this reason, both transitions were used with quantitation purposes. The other major product ion is different for maslinic acid because of its substitution in two positions

Table 3

Optimization of the microwave-assisted leaching of triterpene compounds from olive leaves.

Variable	Tested range	Optimum value
Power (W)	100–180	180
Ethanol (%)	60–100	80
Irradiation time (min)	1–15	5

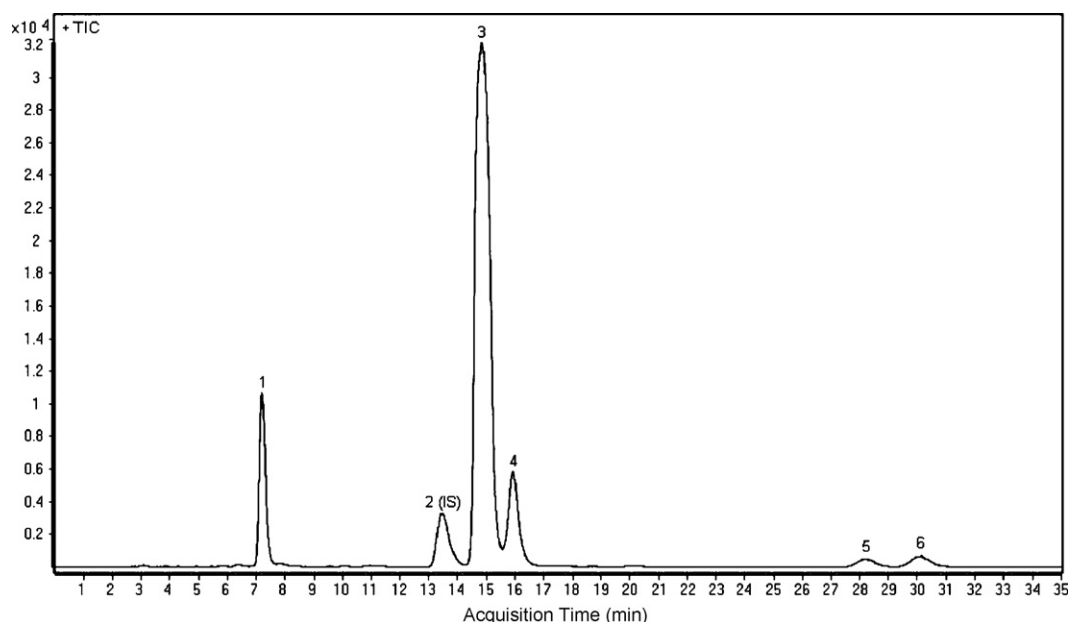


Fig. 4. Total ion chromatogram provided by analysis of the hojiblanca variety. (1) Maslinic acid, (2) betulinic acid (IS), (3) oleanolic acid, (4) ursolic acid, (5) erythrodiol and (6) uvaol.

with an alcohol group. Thus, an additional dehydration process led to the formation of a triple bond resulting in a product peak of 189 *m/z*.

Once the number of transitions was established, the influence of the dwell time on the sensitivity was checked, resulting the best value 250 ms. Longer dwell times did not provide significant improvement.

3.3. Optimization of the microwave-assisted leaching of triterpenic compounds

The role of the main variables involved on the leaching step was optimized. These potential variables were the irradiation power, irradiation time and extractant composition. The response variable used in this study was the extraction efficiency expressed as the ratio between the peak area of each analyte and that of the internal standard. The optimization of the extractant composition was carried out testing different ethanol–water ratios to obtain quantitative isolation of the target compounds [25].

A full two-level factorial design allowing four degrees of freedom and involving 11 randomized runs including three centre points was built for a screening study of the behaviour of the three variables previously cited. The upper and lower values given to each variable were selected from the available data and experience gathered in preliminary experiments. The best results were obtained with 80% ethanol and 180 W irradiation power. A 20% of water was required to solubilise more polar compounds. The tested and the

optimum values obtained for each variable, which were used in further experiments, are shown in Table 3.

A kinetics study was performed to determine the time required for total removal of triterpenic compounds from the olive leaves, which was obtained after irradiation for 5 min. The extracts obtained with longer times provided similar results with non-detected degradation. Fig. 4 shows the chromatogram in TIC mode provided by analysis of the hojiblanca olive variety under optimal conditions.

3.4. Characterization of the method for triterpenes quantification

Calibration plots were run by using the ratios between the peak area of each compound vs. that of the IS as a function of the concentration of each compound. Seven concentration levels were used to build the calibration curves.

The limits of detection (LODs) and quantification (LOQs) were calculated with the MRM chromatograms from extracts using the quantitation transitions. The peak area-to-averaged background noise ratio was calculated, for which the background noise was estimated by the peak-to-peak baseline near the analyte peak. LODs and LOQs were then calculated on the basis of a minimal accepted value of the signal-to-noise (S/N) ratio of 3 and 10, respectively. The values of LODs obtained ranged from 0.26 to 0.91 ng; meanwhile for LOQs the values ranged from 0.87 to 3 ng, for 10 μL injection volume in all instances. The regression coefficients ranged between 0.979 and 0.998 for the linear dynamic range tested for each analyte, which was from the LOQs to 150 $\mu\text{g mL}^{-1}$.

In order to evaluate the precision of the proposed method, inter-day and intra-day variability were evaluated in a single experimental set-up with duplicates [30]. Two extract analyses per day were performed on 7 days. The intra-day assay variability, expressed as relative standard deviation, was from 2.92 to 5.23% for the target analytes, while inter-day assay variability ranged from 4.29 to 7.76%. These results demonstrate the suitability of the proposed method for determination of the target analytes in olive leaf extracts in terms of sensitivity and precision.

Table 4

Concentrations of each triterpene found with the proposed method in two olive leaf varieties expressed in $\mu\text{g/g}$ ($n = 5$).

Triterpene/variety	Hojiblanca	Acebuches
Erythrodiol	2653 \pm 107	3411 \pm 98
Uvaol	2398 \pm 76	2801 \pm 60
Oleanolic acid	13028 \pm 356	8497 \pm 202
Ursolic acid	4861 \pm 182	3792 \pm 151
Maslinic acid	2997 \pm 137	3353 \pm 122

3.5. Comparison of the efficiency of the microwave-assisted leaching method with the conventional method

The isolation of triterpenic compounds, usually carried out by maceration with vigorous agitation, requires at least 5 h to achieve quantitative removal. The use of auxiliary energies to assist the extraction of the target compounds from olive leaves has been reported in a previous publication [25]. Ultrasonic energy enabled acceleration of the leaching process, which was complete in 20 min. In the method proposed here, microwaves have provided a shorter leaching time as only 5 min is needed to isolate the target compounds. The efficiency of this alternative has been checked by comparison with a reference method as conventional maceration. Quantitation was performed by the LC–MS–MS method here reported. The results show that the microwave-assisted method provides leaching efficiencies similar to those of the conventional method as they range from 93 to 112%. This study also enables the validation of the overall method proposed in this research for determination of triterpenic compounds in olive leaves, which were of hojiblanca variety in this study.

3.6. Applicability of the proposed method

The presence of triterpenic compounds in olive leaves is well known [19] and their healthy properties are plenty probed, as commented under “Introduction”. LC–MS–MS was employed to quantify those present in the extracts. The developed method was applied to hojiblanca and acebuche variety in order to prove its feasibility. The concentration of each triterpene was calculated as the arithmetic mean of five experiments under the optimum working conditions. The results obtained show that the composition of triterpenes in the target varieties is characterized by the high concentration of oleanolic acid in comparison to the other compounds. As Table 4 shows, hojiblanca has the highest amount of triterpenic acids while dialcohols are more abundant in acebuche, in agreement with previous studies [25].

4. Conclusions

A method based on LC–MS–MS has been developed for confirmatory analysis and determination of triterpenic compounds in olive leaves. The MS–MS step has been carried out by the MRM mode, which enables identification of the target analytes by comparison with standards with high selectivity even at very low concentrations. The high selectivity and sensitivity obtained demonstrate the suitability of the proposed method for determination of these compounds in extracts from olive leaves. Liquid chromatography provides advantages over GC as avoidance of derivatization and separation accomplished in less than 20 min.

Quantitative isolation of the target analytes is achieved by microwave-assisted extraction in only 5 min. This means that the analytical process is drastically shortened, particularly as compared

with conventional protocols based on long sample preparation steps. Thus, the proposed method can be an interesting tool in the pharmaceutical industry to take profit from this abundant raw material in Spain for extraction of terpenic valuable compounds or from other plants.

Acknowledgement

Spain's Ministry of Science and Innovation is gratefully acknowledged for financial support (Project no. CTQ2006-01614).

References

- [1] R.P. Borris, *J. Ethnopharmacol.* 51 (1996) 29.
- [2] J.D. McChesney, S.K. Venkatamaran, J.T. Henri, *Phytochemistry* 68 (2007) 2015.
- [3] M.D. Luque de Castro, J.L. Luque-García, *Acceleration and Automation of Solid Sample Treatment*, Elsevier, Amsterdam, 2002.
- [4] M.D. Luque de Castro, F. Priego-Capote, *Analytical Applications of Ultrasound*, Elsevier, Amsterdam, 2006.
- [5] M.C. Henry, C.R. Yonker, *Anal. Chem.* 78 (2006) 3909.
- [6] J. Zhao, X.Q. Zhang, S.P. Li, F.Q. Yang, Y.T. Wang, W.C. Ye, *J. Sep. Sci.* 29 (2006) 2609.
- [7] M.A. Strege, *J. Chromatogr. B* 725 (1999) 67.
- [8] D.Z.L. Bastos, I.C. Pimentel, D.A. de Jesús, B.H. de Oliveira, *Phytochemistry* 68 (2007) 834.
- [9] J.M. Siqueira, R.R. Peters, A.C. Gazola, P.B. Krepsky, M.R. Farias, A. Giles, A.J. de Brum-Fernandes, R.M. Ribeiro do Valle, *Life Sci.* 80 (2007) 1382.
- [10] K.L. Mankani, V. Krishna, B.K. Manjunatha, S.M. Vidya, S.D. Singh, Y.N. Manohara, I.J. Kuppast, *J. Nat. Remedies* 6 (2006) 147.
- [11] T. Akihisa, Y. Nakamura, M. Tagata, H. Tokuda, K. Yasukawa, E. Uchiyama, T. Suzuki, Y. Kimura, *Chem. Biodivers.* 4 (2007) 224.
- [12] Z.J. Wu, M.A. Ouyang, C.Z. Wang, Z.K. Zhang, J.G. Shen, *J. Agr. Food Chem.* 55 (2007) 1712.
- [13] D. Yu, Y. Sakurai, C.H. Chen, F.R. Chang, L. Huang, Y. Kashiwada, K.H. Lee, *J. Med. Chem.* 49 (2006) 5462.
- [14] J.E. Angeh, X. Huang, I. Sattler, G.E. Swan, H. Dahse, A. Haertl, J.N. Eloff, *J. Ethnopharmacol.* 110 (2007) 56.
- [15] A.D. Rocha, A.B. de Oliveira, J.D. de Souza Filho, J.A. Lombardi, F.C. Braga, *Phytother. Res.* 18 (2004) 463.
- [16] I.M. Villasenor, A.P. Canlas, K.M. Faustino, K.G. Plana, *J. Ethnopharmacol.* 92 (2004) 53.
- [17] M. Sánchez, C. Theoduloz, G. Schmeda-Hirschmann, I. Razmilic, T. Yanez, J.A. Rodríguez, *Life Sci.* 79 (2006) 1349.
- [18] M. Yoshikawa, T. Morikawa, K. Yamamoto, Y. Kato, A. Nagatomo, H. Matsuda, *J. Nat. Prod. Res.* 68 (2005) 1360.
- [19] T. Albi, Á. Guinda, A. Lanzón, *Grasas Aceites* 52 (2001) 275.
- [20] G. Janicsak, K. Veres, A.Z. Kakasy, I. Mathe, *Biochem. Syst. Ecol.* 34 (2006) 392.
- [21] G. Janicsak, K. Veres, M. Kallai, I. Mathe, *Chromatographia* 58 (2003) 295.
- [22] G. Boskou, F.N. Salta, S. Chrysostomou, A. Mylona, A. Chiou, N.K. Andrikopoulos, *Food Chem.* 94 (2006) 558.
- [23] F. Modugno, E. Ribechini, M.P. Colombini, *J. Chromatogr. A* 1134 (2006) 298.
- [24] A. Otto, M.J. Simpson, *Biogeochemistry* 74 (2005) 377.
- [25] N. Sánchez-Ávila, F. Priego-Capote, M.D. Luque de Castro, *J. Chromatogr. A* 1165 (2007) 158.
- [26] A. Frank, M. Unger, *J. Chromatogr. A* 1112 (2006) 255.
- [27] K. He, G.F. Pauli, B. Zheng, H. Wang, N. Bai, T. Peng, M. Soller, Q. Zheng, *J. Chromatogr. A* 1112 (2006) 241.
- [28] B. Jiang, F. Kronenberg, P. Nuntanakorn, M.H. Qiu, E.J. Kennelly, *J. Agr. Food Chem.* 54 (2006) 3242.
- [29] A. García-Granados, A. Martínez, J.N. Moliz, A. Parra, F. Rivas, *Molecules* 3 (1998) M88.
- [30] D.L. Massart, B.G.M. Vandeginste, L.M.C. Buydens, S. De Jong, P.J. Lewi, J. Smeyers-Verbeke, *Handbook of Chemometrics and Qualimetrics, Part A*, Elsevier, Amsterdam, 1997.



Long-wavelength homogeneous enzyme immunoassay for the determination of amikacin in water samples

M.L. Sánchez-Martínez, M.P. Aguilar-Caballos, A. Gómez-Hens*

Department of Analytical Chemistry, University of Córdoba, Campus of Rabanales, Marie-Curie Annex building, 14071 Córdoba, Spain

ARTICLE INFO

Article history:

Received 20 June 2008

Received in revised form 31 October 2008

Accepted 14 November 2008

Available online 21 November 2008

Keywords:

Homogeneous enzyme immunoassay

Amikacin

Cresyl Violet

Long-wavelength fluorimetry

Stopped-flow mixing technique

Water samples

ABSTRACT

A simple and rapid homogeneous enzyme immunoassay involving the use of the malic dehydrogenase enzyme and a long-wavelength fluorophor, the oxazine Cresyl Violet, is proposed for the determination of the antibiotic amikacin in water samples. An enzymatic tracer has been synthesized by covalent binding of amikacin to malic dehydrogenase via a carbodiimide derivative. Free tracer catalyses the reaction between Cresyl Violet and malic acid giving rise to a decrease in the fluorescence of the fluorophor. Kinetic curves for this reaction have been monitored at λ_{ex} 585 and λ_{em} 624 nm using the stopped-flow mixing technique, being the initial rate measured in only 2–3 s. The dynamic range of the method is 1–15 ng mL⁻¹ and the detection limit is 0.3 ng mL⁻¹, using aqueous standard solutions or water samples. The precision, obtained at 1 and 5 ng mL⁻¹ and expressed as relative standard deviation, was 6.0 and 9.6%, respectively. The method has been applied to the analysis of drinking, river and wastewater samples. The sample pre-treatment involved a solid-phase extraction step for the clean-up of the samples. A recovery study was carried out to validate the method, being the values obtained in the range 80–114%, with a mean value of 96.7%.

© 2008 Elsevier B.V. All rights reserved.

1. Introduction

The extensive use of antibiotics in human and veterinary medicine may result in residues that can be present in aquatic environment. Most of these compounds are water-soluble and can be excreted in urine to a large extent, so that hospital effluents and municipal wastewater are important sources of antibiotic residues [1]. More than thirty antibiotics have been found in sewage influent and effluent samples, in surface waters and even ground and drinking water [2]. The control of these residues is of great interest as they induce resistance of pathogens through continuous exposure. However, concentration limits of antibiotics in the aquatic environment have not been still regulated. With the aim of contributing to the availability of simple and rapid analytical methods for the control of antibiotics in water samples, a fluorimetric homogeneous enzyme immunoassay (EIA) is here described for amikacin determination.

Amikacin is an aminoglycoside antibiotic used for treating infections caused by Gram-negative bacteria resistant to other aminoglycosides. This compound is excreted almost entirely no metabolised in urine, therefore it is expected to be present in wastewater. Methods described for amikacin determination in biological samples mainly involve the use of liquid chromatography [3–7] and immunoassay [3,8–10]. Several detection systems, such

as photometry [4], mass spectrometry [5] and chemiluminescent detection [6] have been used for the development of the chromatographic methods. The best detection limit (LOD) (50 ng mL⁻¹ in urine) was obtained by using the inhibitory effect of amikacin on the chemiluminescent signal provided by the luminol-hydrogen peroxide system catalysed by copper(II) [6]. This approach has been also used for the determination of several aminoglycoside antibiotics in water samples, obtaining a LOD for amikacin of 0.7 ng mL⁻¹ [11]. Other detection systems described for amikacin determination in pharmaceuticals have been evaporative light scattering [12] and pulsed electrochemical detection [13], which reach LODs of 2.2 µg mL⁻¹ and 0.2 µg mL⁻¹, respectively.

The conventional homogeneous enzyme immunoassay method for amikacin determination is based on the use of glucose-6-phosphate dehydrogenase (G6PDH) as label to obtain the tracer with amikacin [8]. Enzyme activity of free tracer is measured spectrophotometrically at 340 nm by the conversion of the oxidized form of nicotinamide adenine dinucleotide (NAD⁺) to its reduced form (NADH). An LOD of 2.5 µg mL⁻¹ is reached for amikacin in serum samples. The method described here involves the use of long-wavelength fluorimetric measurements, which improve the detection limit obtained in the homogeneous EIA with photometric detection. The enzyme L-malic dehydrogenase has been used to obtain the tracer, which is about five-times cheaper than G6PDH, and the oxazine Cresyl Violet (λ_{ex} 585, λ_{em} 624 nm) has been chosen for the measurement of the free tracer activity. Cresyl Violet reacts with malic acid in the presence of the free tracer, obtaining

* Corresponding author.

E-mail address: qa1gohea@uco.es (A. Gómez-Hens).

a decrease in the fluorescence of the oxazine. The initial rate of this reaction, which has been measured automatically using stopped-flow mixing technique, is proportional to the enzyme activity of the free tracer and, bearing the competitive format of this EIA in mind, to the amikacin concentration.

The use of long-wavelength organic dyes are gaining acceptance in fluorimetric analysis due to some desirable properties: (1) good photostability, owing to the low energy required to excite them, (2) low probability of quenching deactivation processes, because of their short lifetimes, and (3) relatively good spectral selectivity, due to their long excitation and emission wavelengths [14], in contrast to that exhibited by conventional fluorophores. A long-wavelength fluorophore, Nile Blue, has been recently described as label for the determination of amikacin using fluorescence polarization immunoassay (FPIA) [15]. The LOD obtained in serum samples was $0.1 \mu\text{g mL}^{-1}$, which is slightly better than that reported using conventional FPIA ($0.8 \mu\text{g mL}^{-1}$) [16], in which fluorescein is used as the label. Thus, in addition to extend the use of homogeneous EIA to environmental analysis, another objective of this study has been to show the usefulness of long-wavelength fluorescence measurements to develop a simple, sensitive and rapid EIA.

2. Experimental

2.1. Instrumental

An SLM Aminco Bowman (Urbana, IL; USA) Model 8100 photon-counting spectrofluorimeter, equipped with a 450 W xenon arc source and a R928 photomultiplier tube, was used. The instrument was furnished with a stopped-flow module [17], which was fitted with an observation cell of 1 cm path-length and controlled by the associated electronics. The solutions in the cell compartment were kept at a constant temperature of 34°C by circulating water from a thermostated tank. A 24-port Visi-Prep vacuum device from Supelco (Bellefonte, PA, USA) and commercial cartridges (500 mg/6 mL) (Análisis Vínicos, Tomelloso, Spain), of a strong cation-exchange sorbent incorporating sulfonylpropyl-groups (PRS), were used to perform a SPE step.

2.2. Reagents

All reagents used were of analytical grade. Cresyl Violet acetate, 1-ethyl-3-(3-dimethylamino-propyl) carbodiimide (EDAC), malic dehydrogenase from porcine heart (catalogue number M-2634, EC number 1.1.1.37, MW 70,000), L(-)-malic acid disodium salt and amikacin were purchased from Sigma (Sigma-Aldrich, St. Louis MO, USA). Anti-amikacin antibodies were supplied by Abbott (Amikacin reagent pack for TD_X/TD_XFL_X, Abbott Laboratories, IL, USA). A stock solution of amikacin (3.5 mM) was prepared in phosphate buffer (pH 7.5, 0.05 M), and working dilutions of amikacin, tracer and antibodies were prepared using the same buffer solution. A Cresyl Violet acetate stock solution (2 mM) was prepared in distilled water by using an ultrasonic bath to achieve the complete dissolution of the oxazine dye in water.

2.3. Procedures

2.3.1. Synthesis of the tracer

The procedure of tracer synthesis involved the mixture of 10 mg of EDAC with $400 \mu\text{L}$ of enzyme, which corresponds to a ratio EDAC:enzyme (2850:1). Immediately after, 5 mg amikacin and $600 \mu\text{L}$ phosphate buffer solution (pH 7.5) were added. The reaction mixture was stirred for 3 h in the dark at room temperature. Then, the tracer was purified by size exclusion chromatography using a HiTrapTM desalting column, which was previously equilibrated with 25 mL of phosphate buffer at 4 mL min^{-1} . After the

application of 1 mL of tracer solution, the elution was carried out using 10 mL of phosphate buffer at 2 mL min^{-1} and $350 \mu\text{L}$ fractions were collected. The tracer was found in the fractions 6 and 7. One blank without enzyme was used to find the appropriate fraction of the tracer.

2.3.2. Determination of amikacin

An aqueous solution containing tracer (0.1 nM), antibody (1.1 nM), amikacin standard or sample at final concentrations in the range $1\text{--}15 \text{ ng mL}^{-1}$ and phosphate buffer solution (0.05 M , pH 7.5), was used to fill one of the 5 mL reservoir syringes of the stopped-flow module. This solution was previously incubated for 15 min. The other syringe was filled with a premixed aqueous solution containing malic acid ($39 \mu\text{M}$), Cresyl Violet ($10 \mu\text{M}$) and phosphate buffer (0.05 M , pH 7.5). In each run, 0.25 mL of the solution of each syringe was mixed in the mixing chamber and the variation of fluorescence intensity with time throughout the reaction was monitored at $\lambda_{\text{ex}} 585 \text{ nm}$ and $\lambda_{\text{em}} 624 \text{ nm}$ for 20 s. Data were processed by the computer furnished with a linear regression program for application of the initial rate method. The analytical parameter used was $B_0 - B$, in which B_0 and B are the initial rates obtained in the absence and in the presence, respectively, of amikacin. The initial rate was measured in ca. 2–3 s, being the integration time used 0.5 s . All measurements were carried out at $34.0 \pm 0.1^\circ\text{C}$. Each standard or sample was assayed in triplicate.

2.3.3. Analysis of water samples

Each acidified water sample (pH 2) was microfiltered through $0.45 \mu\text{m}$ Nylon disks under vacuum. Then, 100 mL water aliquots were subjected onto a solid-phase extraction step using commercial cartridges of PRS, previously conditioned with 10 mL of methanol and 10 mL of acid acetic of pH 2. After sample application, a cleaning step with 5 mL of acetic acid (pH 2) was done. Finally, cartridges were eluted with 5 mL of phosphate buffer (0.05 M , pH 7.5) and $250 \mu\text{L}$ of this solution were treated as described above for amikacin determination.

3. Results and discussion

3.1. Study of the chemical system

With the aim of developing a fluorimetric EIA for amikacin determination in water samples using long-wavelength measurements, the fluorescent behaviour of several fluorophores in the presence of malic acid and malic dehydrogenase has been studied. Cresyl Violet, Nile Blue and Azure A were assayed for this purpose, using stopped-flow mixing technique for the monitoring of the kinetic behaviour of these systems. The fluorescence of these compounds was not modified in the absence of the enzyme, but a decrease in the fluorescence intensity was obtained in its presence, being the initial rate of the system directly related to the enzyme activity. The best initial rate values were obtained with Cresyl Violet, choosing this fluorophore to develop the immunoassay system.

The synthesis of the amikacin-enzyme tracer was carried out using a carbodiimide method, which involves the use of the water-soluble carbodiimide (1-ethyl-3-(3-dimethylamino-propyl) carbodiimide (EDAC). A (2850:1) molar ratio EDAC:enzyme was enough to ensure the maximum efficiency in the coupling of the activated enzyme to the amino groups of amikacin. Then, the tracer was purified by size-exclusion chromatography to remove the excess of small molecules, being the tracer found between fractions 6 and 7. The activity of the enzyme was determined by the reaction of the tracer with NAD^+ and malic acid and the fluorescent signal due of the enzymatically formed NADH was measured at $\lambda_{\text{ex}} 340$ and $\lambda_{\text{em}} 450 \text{ nm}$. This signal was interpolated in the

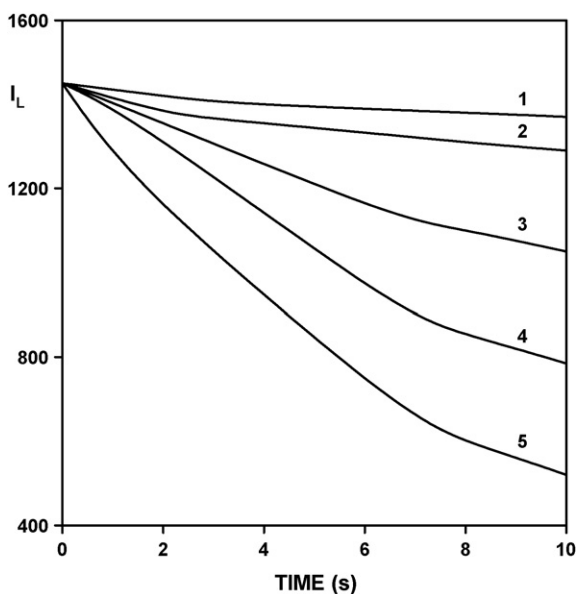


Fig. 1. Kinetic curves obtained at different amikacin concentrations (1) 0, (2) 1, (3) 2.5, (4) 5, and (5) 12.5 ng mL⁻¹. [antibody] = 1.1 nM, [tracer] = 0.1 nM, [phosphate] = 0.05 M, pH = 7.5, pre-incubation time = 15 min. [Cresyl Violet] = 10 μM, [malic acid] = 39 μM.

curve obtained after the reaction of known amounts of enzyme to calculate the effective enzyme activity found in the tracer fraction.

The stopped-flow mixing technique has been used to obtain the initial rate of the enzymatic reaction. The study of the distribution of the reagents in the two drive syringes of the stopped-flow module showed that it plays an important role on the kinetic behaviour of the system. Different configurations were assayed to obtain the highest differences in the initial rates obtained in the presence and in the absence of the analyte. The best results were obtained when the immunoreagents were placed in one syringe and malic acid and Cresyl Violet were placed in the other one. The kinetic curves obtained at different amikacin concentrations are depicted in Fig. 1 in which can be seen that the initial rate can be correlated with the analyte concentration.

3.2. Influence of variables

The variables affecting the system were optimised by the univariate method. All reported concentrations are initial concentrations in the syringes (twice the actual concentrations in the reaction mixture at time zero after mixing). Each kinetic result was

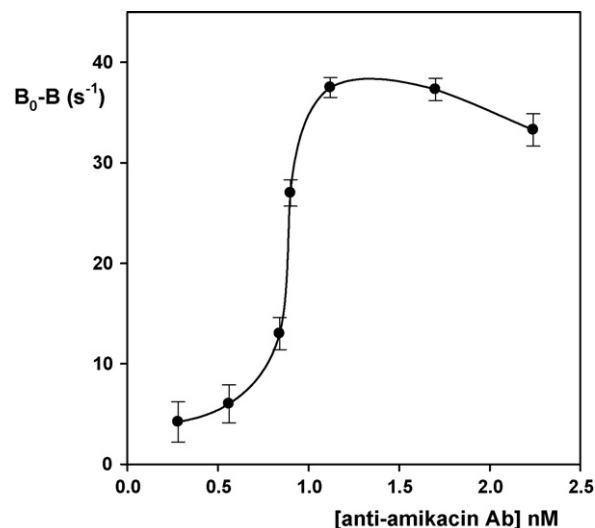


Fig. 2. Optimisation of concentration of anti-amikacin antibodies. [tracer] = 0.1 nM, [amikacin] = 5 ng mL⁻¹ [phosphate] = 0.05 M, pH = 7.5, temperature = 34 °C, [Cresyl Violet] = 12 μM, [malic acid] = 35 μM, pre-incubation time = 15 min.

the average of three measurements. The analytical parameter used was $B_0 - B$, in which B_0 and B are the initial rates obtained in the absence and in the presence of the analyte. Those values yielding the minimum possible standard deviation for the initial rate, under conditions in which the reaction order with respect to the species concerned was zero or near zero, were taken as optimal.

It was checked that the incubation of the immunoreagents is required before placing the mixture in the corresponding drive syringe of the module, in order to reach the equilibrium of the immunochemical reaction. The incubation time was evaluated in the range 5–25 min. A time of 15 min was enough to obtain adequate results. The influence of tracer concentration on the system was studied in the range 0.07–0.4 nM, using 5 ng mL⁻¹ amikacin concentration, finding that 0.1 nM gave the best results. Fig. 2 shows the optimisation study of the antibody concentration, choosing 1.1 nM as the optimum value. The pH of the system was studied in the range 7–9.5, as Fig. 3a shows. The best results were obtained at pH 7.4–7.7, so that a 0.05 M phosphate buffer solution of pH 7.5 was used to adjust this variable. The study of the influence of malic acid concentration on the system (Fig. 3b) showed that the best results were obtained at 39 μM. The concentration of Cresyl Violet was studied in the range 6.0–20.0 μM, being selected 10 μM as optimum. Finally, the influence of the temperature on kinetics was studied in the range 25–40 °C and a value of 34 °C was chosen.

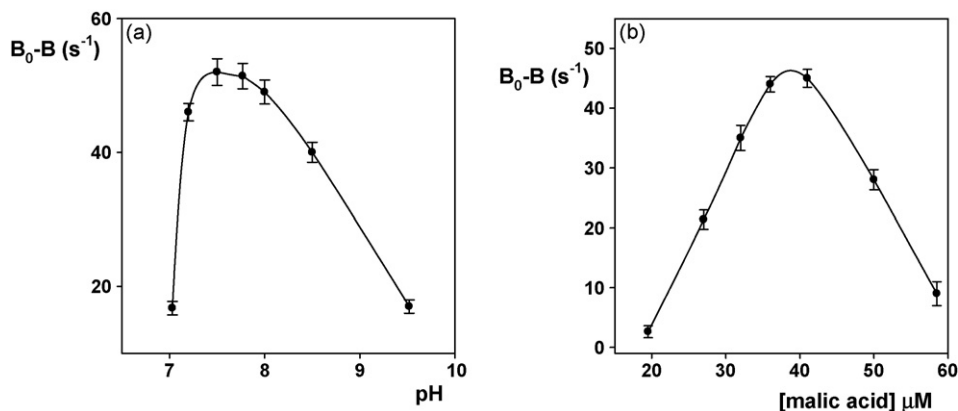


Fig. 3. Influence of pH (a) and malic acid concentration (b) on the system. [amikacin] = 5 ng mL⁻¹, [antibody] = 1.1 nM, [tracer] = 0.1 nM, [phosphate] = 0.05 M, pre-incubation time = 15 min. In (a) [Cresyl Violet] = 12 μM, [malic acid] = 35 μM. In (b) [Cresyl Violet] = 10 μM, pH = 7.5.

3.3. Analytical features of the proposed method

Kinetic data were obtained from the fluorescence intensity–time curves monitored at λ_{ex} 585 and λ_{em} 624 nm under the optimum conditions. The initial rate was measured in only ca. 2–3 s and, as indicated above, the analytical parameter was the difference in the values obtained in the absence (B_0) and in the presence (B) of the analyte. Fig. 4 shows the calibration curve obtained, from which it can be seen that the method presents a dynamic range of 1–15 ng mL⁻¹. The calibration curve was processed by non linear regression using the Sigma Plot 2001 software and fitted to a 3-parameter sigmoidal curve, given by the mathematical expression (1):

$$y = \left\{ \frac{a}{[1 + e^{-(x-x_0)/b}]} \right\} \quad (1)$$

where y is $B_0 - B$ and x is the amikacin concentration expressed in ng mL⁻¹. The values of a , b and x_0 were 153 ± 3 , 3.1 ± 0.1 and 7.3 ± 0.2 , respectively. The correlation coefficient was 0.9999, which suggests a good fit of the experimental data to the regression curve. The LOD calculated following IUPAC recommendations [18] was 0.3 ng mL⁻¹, which is lower than that reported using the conventional homogeneous EIA [8]. The precision was determined by calculating the relative standard deviation at two analyte concentrations, 1 and 5 ng mL⁻¹, obtaining 6% and 9.6% values, respectively.

The selectivity of the method mainly depends on anti-amikacin antibodies. Anti-amikacin antibodies were quite selective for amikacin, although the assay presented cross-reactivity towards its precursor kanamycin. Other aminoglycoside antibiotics, such as dibekacin, tobramycin, netilmicin, gentamicin and vancomycin, did not interfere amikacin determination when assayed at their upper therapeutic limit, which agrees with the brochure provided by the manufacturer.

3.4. Applications

The method was applied to the analysis of four different water samples: drinking, river, influent and effluent wastewater. These samples were subjected to a previous sample pre-treatment using PRS cartridges, which allowed sample clean-up. Although weak cation exchange materials are normally used for the extraction

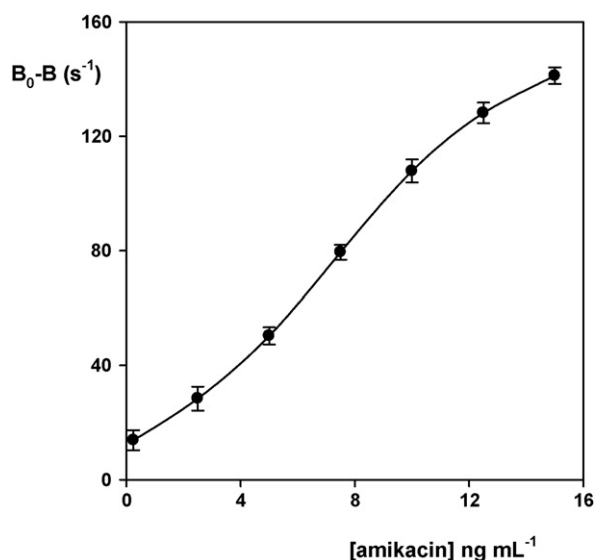


Fig. 4. Calibration curve for amikacin. [antibody] = 1.1 nM, [tracer] = 0.1 nM, [phosphate] = 0.05 M, pH = 7.5, pre-incubation time = 15 min. [Cresyl Violet] = 10 μ M, [malic acid] = 39 μ M.

Table 1

Recoveries for amikacin added to water samples.

Water sample	Amikacin concentration (ng mL ⁻¹)		
	Added	Found ^a	Recovery (%)
Drinking water	2.5	2.8 \pm 0.2	112
	5.0	5.0 \pm 0.1	100
	10.0	8.4 \pm 0.4	84
Wastewater (influent)	2.5	2.5 \pm 0.2	100
	5.0	4.2 \pm 0.1	84
	10.0	9.0 \pm 0.1	90
Wastewater (effluent)	2.5	2.4 \pm 0.2	96
	5.0	5.0 \pm 0.3	100
	10.0	9.5 \pm 0.9	95
River water	2.5	2.7 \pm 0.2	108
	5.0	5.7 \pm 0.4	114
	10.0	8.0 \pm 0.5	80

^a Mean \pm SD ($n = 3$).

of aminoglycoside antibiotics in water samples [19], it has been also reported the separation of these compounds by means of a strong cation exchange column at mild conditions [11]. This allows the elimination of potential interferences from sample matrix that would interfere the immunochemical or the enzymatic reaction. Afterwards, 250- μ L aliquots of these sample extracts were analysed following the procedure above described for the determination of amikacin. The analyte was not found in any sample. A recovery study was performed by adding three different amounts of amikacin to different aliquots of each sample and the results were calculated by interpolating in the calibration graph. The recovery values obtained ranged from 80 to 114% with a mean value of 96.7% (see Table 1).

4. Conclusions

The method presented here reports a simple and rapid homogeneous enzyme immunoassay for the determination of amikacin in water samples. The performance of fluorescence measurements at long-wavelength provides to the method with an adequate spectral selectivity and a low LOD. The use of the stopped-flow mixing technique enables the automation of kinetic measurements, which are obtained in only 2–3 s shortly after mixing. The application of the method to water samples is possible by the use of a previous SPE step.

Acknowledgement

Authors gratefully acknowledge financial support from the Spanish DGI (Dirección General de Investigación) Grant no. (CTQ2006-03263/BQU).

References

- [1] K. Kummerer, Chemosphere 45 (2001) 957.
- [2] N. Kemper, Ecolog. Indicat. 8 (2008) 1.
- [3] D.A. Stead, J. Chromatogr. B 747 (2000) 69.
- [4] S. Nicoli, P. Santi, J. Pharm. Biomed. Anal. 41 (2006) 994.
- [5] C.Y. Lu, C.H. Feng, J. Chromatogr. A 1156 (2007) 249.
- [6] J.M. Serrano, M. Silva, J. Chromatogr. B 843 (2006) 20.
- [7] G. Brajanoski, J. Hoogmartens, K. Allegaert, E. Adams, J. Chromatogr. B 867 (2008) 149.
- [8] J. Centofanti, in: D. Wild (Ed.), The Immunoassay Handbook, Stockton Press, New York, 1994, p. 216.
- [9] D.R. Mendu, P.P. Chou, S.J. Soldin, Ther. Drug Monit. 29 (2007) 632.
- [10] F. Vételé, M. Manchon, A. Mialon, C. Berny, P. Baltassat, Annales Biol. Clin. 60 (2002) 723.
- [11] J.M. Serrano, M. Silva, J. Chromatogr. A 1117 (2006) 176.
- [12] E.G. Galanakis, N.C. Megoulas, P. Solich, M.A. Koupparis, J. Pharm. Biomed. Anal. 40 (2006) 1114.

- [13] N.H. Zawilla, B. Li, J. Hoogmartens, E. Adams, J. Pharm. Biomed. Anal. 43 (2007) 168.
- [14] A. Gómez-Hens, M.P. Aguilar-Caballo, Trends Anal. Chem. 23 (2004) 127.
- [15] M.L. Sánchez-Martínez, M.P. Aguilar-Caballo, A. Gómez-Hens, Anal. Chem. 79 (2007) 7424.
- [16] TDx/TDxFLx Amikacin, Ref. 9508-60/-85, Abbott Laboratories, IL, USA, <http://www.abbottdiagnostics.com/>.
- [17] A. Loriguillo, M. Silva, D. Pérez-Bendito, Anal. Chim. Acta 199 (1987) 29.
- [18] G.L. Long, J.D. Winefordner, Anal. Chem. 55 (1983) 712A.
- [19] M.S. Díaz-Cruz, D. Barceló, Anal. Bioanal. Chem. 386 (2006) 973.



Amperometric determination of choline with enzyme immobilized in a hybrid mesoporous membrane

Takeshi Shimomura^{a,*}, Tetsuji Itoh^b, Touru Sumiya^a, Fujio Mizukami^b, Masatoshi Ono^a

^a Funai Electric Advanced Applied Technology Research Institute Inc. (FEAT), TCI 37A, 2-1-6 Sengen, Tsukuba-shi, Ibaraki 305-0047, Japan

^b National Institute of Advanced Industrial Science and Technology (AIST), 4-2-1 Nigatake, Miyagino-ku, Sendai-shi, Miyagi 983-8551, Japan

ARTICLE INFO

Article history:

Received 14 September 2008

Received in revised form 4 November 2008

Accepted 4 November 2008

Available online 18 November 2008

Keywords:

Biosensor

Enzyme immobilization

Choline oxidase

Hybrid mesoporous membrane

ABSTRACT

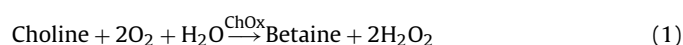
Choline sensor is successfully prepared by using immobilized enzyme, i.e., choline oxidase (ChOx) within a hybrid mesoporous membrane with 12 nm pore diameter (F127M). The measurement was based on the detection of hydrogen peroxide, which is the co-product of the enzymatic choline oxidation. The determination range and the response time are 5.0–800 μM and approximately 2 min, respectively. The sensor is very stable compared to the native enzyme sensor and 85% of the initial response was maintained even after storage for 80 days. These results indicate that ChOx is successfully immobilized and well stabilized, and at the same time, enzyme reaction proceeds efficiently. Such ability of hybrid mesoporous membrane F127M suggests great promise for effective immobilization of enzyme useful for electrochemical biosensors.

© 2008 Elsevier B.V. All rights reserved.

1. Introduction

A number of sensors have been developed for the determination of choline, the determination of which is important in biological sciences of human bile, serum, amniotic fluid, brain extracts and pharmaceutical products [1–3]. For example, the choline sensor can be used for the determination of choline-containing phospholipids or choline esterase activity in blood. Among them, enzyme choline oxidase (ChOx) based amperometric biosensor is promising method for the detection of choline in clinical, industrial and environmental areas, as it offers a simple, inexpensive, rapid operation [4–8].

Amperometric biosensors for choline were previously described being based on a variety of different immobilization techniques [4–10]. They are based on the enzyme reaction where ChOx oxidizes choline to betaine and hydrogen peroxide as products [Eq. (1)]. This is the most commonly followed by direct electrochemical oxidation of hydrogen peroxide at a conventional electrode [Eq. (2)]. The electrochemical current, which depends on the substrate concentration and the enzyme activity, is recorded as a sensor response.



However, the enzyme immobilized by conventional methods such as cross-linking and entrapping in polymeric gels cannot always exhibit satisfactorily high response due to the loss of enzyme activity. No method has been proposed that is generally applicable for all enzymes. For this reason, enzyme immobilization process is one of the most important factors for enzyme based biosensors.

On the other hand, enzyme encapsulation within mesoporous silica materials has been considered as a suitable host because it can render enzymes more mechanically robust and stable with time [11–13]. In addition, they have inherent characteristics of high surface area and pore volume, tunable pore size accommodating dimensions of enzymes, and mechanical stability [14,15]. This entrapment method also has the distinct advantage that since the immobilization requires no covalent bond, the native properties of the enzymes are maintained. Thus, they are considered as a suitable host for enzyme immobilization useful for the electrochemical biosensors.

In this article, ChOx is immobilized within hybrid mesoporous membranes having 3-D concentric spherically layered structure with 12 nm pore diameter (F127M) [16] and the resulting ChOx-immobilized membrane (ChOx-F127M) is applied for amperometric biosensing for choline determination. Sensitivity, response time, and stability of this sensor are reported in the following sections.

* Corresponding author. Tel.: +81 29 886 6500; fax: +81 29 886 6511.
E-mail address: shimomura.t@funai-atrri.co.jp (T. Shimomura).

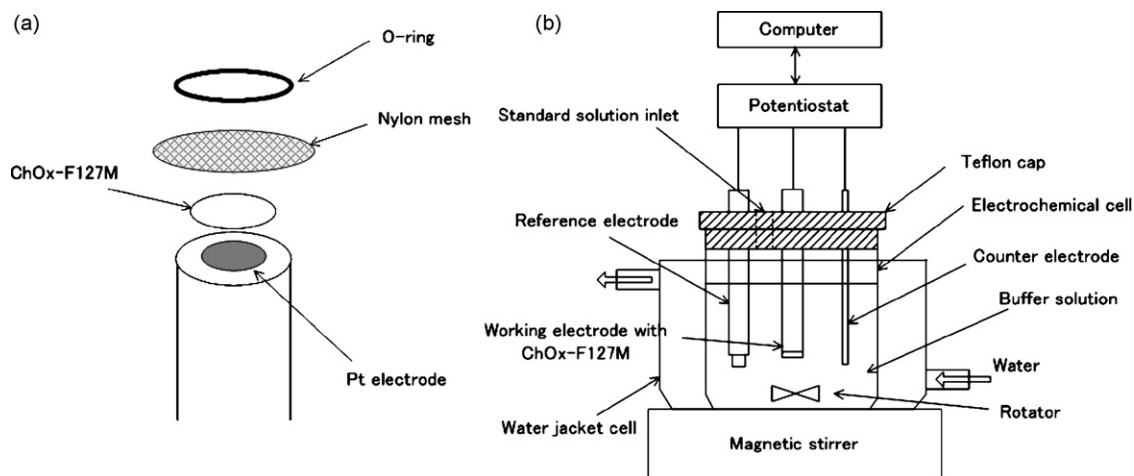


Fig. 1. Schematic diagram of the electrochemical cell setup. (a) Fabrication of ChOx-immobilized working electrode with ChOx-F127M conjugate. (b) The entire measurement system for the detection of choline solutions.

2. Experimental

2.1. Chemicals

Choline oxidase (ChOx, E.C. 1.1.3.17, from *Alcaligenes* sp., 10 units/mg) was obtained from Toyobo Co., Ltd. Tetraethyl orthosilicate (TEOS), ethanol, and HCl solution were obtained from Wako Pure Chemical Industries, Ltd. Pluronic F127 and porous alumina membrane with pore size of 0.2 μm (Anodisk 47) were obtained from BASF Corporation and Whatman plc, respectively. All other reagents were of analytical grade and were obtained from commercial sources. Choline standard solutions were prepared from choline chloride by dilution with distilled water.

2.2. Preparation of enzyme immobilized membranes (ChOx-F127M)

The hybrid mesoporous membrane, F127M with a channel diameter of 12 nm, was prepared by using Pluronic F127 as structure-directing agent [16]: pluronic F127 (0.92 g) was dissolved in a mixture of ethanol (17.66 g), HCl (0.2 g of 1 M aqueous solution), and water (1.38 g). This mixture was stirred at 60 °C for 1 h under a reflux condenser. Then, TEOS (2.0 g) was added to the mixture, and the final mixture was stirred at 60 °C for 6 h to give the precursor solution. A porous alumina membrane (membrane diameter = 47 mm, pore diameter = ca. 0.2 μm , thickness = ca. 60 μm) was set in an ordinary membrane filtration apparatus and 4 ml of the precursor solution was dropped onto the alumina membrane. Moderate aspiration was applied so that the precursor solution

penetrated the columnar alumina pores, then the membrane was dried in air at room temperature. The sample was calcined at 600 °C for 10 h in air and thus we obtained the mesoporous membrane, F127M.

By making use of this, enzyme immobilized membrane, i.e., ChOx-F127M conjugate, was prepared as follows: F127M was immersed in 2.5 ml of 10 mg/ml ChOx solution (phosphate buffer, pH 8.0) for 48 h at 4 °C to establish an adsorption equilibrium. The amounts of ChOx adsorbed into the silica-nanochannels of the F127M were estimated by carrying out the thermal gravimetric and differential thermal analysis (TG/DTA) for this ChOx-F127M conjugate and the estimated value was ca. 5 mg per 1 g of the ChOx-F127M.

2.3. Preparation of the sensor

The system consisted of three electrodes: an Ag/AgCl reference electrode, a platinum (Pt) auxiliary electrode, and a platinum (Pt) working electrode (i.d.: 3 mm) covered with enzyme immobilized hybrid mesoporous membrane.

The working electrode was constructed from the ChOx-F127M conjugate, by placing the prepared ChOx-F127M conjugate membrane (previously cut into circular disks of diameter 4 mm and washed in distilled water three times before use) on the nylon mesh. This enzymatic membrane was placed directly on the working electrodes via rubber O-rings and construct a choline sensor. The ChOx-F127M conjugate was stored phosphate buffer (pH 8.0) at 4 °C when not in use and the working electrode was first polished with 1 μm diamond particles, and then 0.05 μm alumina parti-

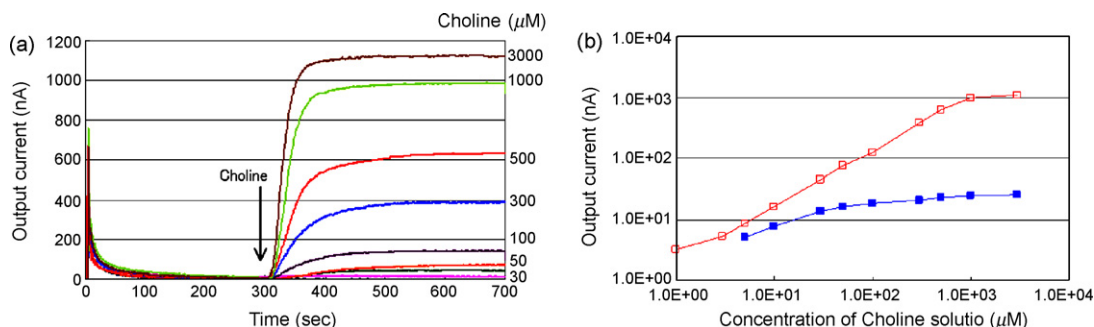


Fig. 2. Typical responses (a) and calibration curve (b) of ChOx-F127M biosensor to injections of aqueous choline solutions. Open symbols for ChOx-F127M sensor (5.6 μg ChOx) and closed symbols for the corresponding native ChOx sensor (5.7 μg ChOx). The electrode potential: +0.6V vs. Ag/AgCl.

cles prior to the fabrication. The electrochemical detection system was based on amperometric measurement: a constant potential of 0.60 V vs. Ag/AgCl was applied with a computer-controlled HSV-100 potentiostat (Hokuto Denko Corporation, Japan) and the resulting current from the generation of hydrogen peroxide was measured.

2.4. Procedure

The sensor is immersed in a 10 ml cell of 0.1 M phosphate buffer (pH 8.0) and maintained at $35 \pm 1^\circ\text{C}$ with thermostated water circulation. After the transient current had settled ($t = 300$ s), 10 μl aliquots of known concentrations of choline standard solutions in phosphate buffer (pH 8.0) were injected into the cell by micropipette. A schematic diagram is shown in Fig. 1.

3. Results and discussion

The choline sensor was placed into the measuring cell and operated under constant voltage of 0.60 V (vs. Ag/AgCl). Fig. 2a and b shows typical amperometric responses and corresponding calibration curve for the sensor to injections of different concentrations of the choline solution (10 μl aliquots), ranging from 1.0 μM to 3000 μM , into the cell (the concentrations of choline in all experiments denote final concentration of choline in the measurement cell). For comparison, the results for native ChOx sensor (i.e., equivalent amount of enzyme (5.7 μg ChOx) as immobilized enzyme (5.6 μg ChOx) in ChOx–F127M sensor was dissolved in the measurement solution) are also shown in the following figures. The ChOx–F127M sensor gave a linear relation ($y = 1.25x + 7.83$) for the range 5.0–800 μM with a correlation coefficient of 0.99, and the current became saturated above 800 μM . The lower detection limit was 5.0 μM , based on three times measurements with the standard deviation of the blank. This calibration range is better than the practical range reported in the literatures [4–10]. A Lineweaver–Burk plots resulted in a straight line, the apparent Michaelis–Menten constant of ChOx–F127M sensor calculated from the plot was found to be 228 μM , whereas that of native ChOx sensor was found to be 16 μM . This difference may be attributed to the effective enzyme concentration for these sensors; the concentration of enzyme around the working electrode for ChOx–F127M sensor is much higher than that for native ChOx sensor.

The average time to reach 90% of the current at steady state for each concentration was approximately 2 min for ChOx–F127M sensor and there was few fluctuation of the response while being the steady state. This is satisfactory rapid and is comparable with the results reported so far [8–10], which means that the diffusion of choline to the ChOx–F127M is sufficiently rapid at practical level. (We discuss the merit of ChOx–F127M based on its structure later in this section.) Reproducibility was tested by repeated 10 μl injections of 100 μM choline solutions; the coefficient of variation for ten injections was 4.8% and the coefficient of variation for five individual sensors was 7.4%. Thus, the response of the sensor was considered to be satisfactory repeatable.

Then, the effect of the pH on the choline sensor was studied for native ChOx sensor or ChOx–F127M sensor in different buffers at $35 \pm 1^\circ\text{C}$. The results are shown in Fig. 3, where the output current of the sensors are expressed as the percentage of the maximum response attained at appropriate optimal pH. We can observe that, at pH 8.0, the current responses have a huge difference by using different buffers (0.1 M phosphate buffer and 0.1 M borate buffer). This difference could be attributed to the different composition of these buffers. It is well known that many factors included in buffer solutions can cause conformational changes in protein, and these can affect enzymatic activity. In our case, it is possible that some

components including sodium tetraborate ($\text{Na}_2\text{B}_4\text{O}_7$) and its ions in 0.1 M borate buffer may affect the reduction of enzymatic activity for ChOx. In fact, in the native ChOx sensor, the use of borate buffer resulted in a significant reduction of response (55%) compared with the use of phosphate buffer. On the other hand, it should be noted that only a slight reduction of response (10%) was seen for the ChOx–F127M sensor; although the size of components in borate buffer is considered to be small enough to enter the pores of F127M, they seem to be trapped on the surface of F127M before going into the F127M pores where it could affect the enzyme, by interacting with SiOH groups, SiO^- ions, defects in the materials, etc.

Moreover, as is seen from Fig. 3, the response of native ChOx sensor decreases more quickly at pH lower than 8.0, whereas the ChOx–F127M sensor kept its good response over this pH range. A broadening of sensor output, i.e., enzyme activity, for ChOx–F127M sensor may be due to the stabilization effect by the encapsulation of ChOx in the pore of hybrid mesoporous membrane, of which the pore size is close to that of ChOx ($\sim 8.8 \text{ nm} \times 7.0 \text{ nm} \times 4.6 \text{ nm}$ [17]) can retard or prevent the denaturation against the change of pH. Although the highest pH value for the response of ChOx–F127M sensor was not determined from Fig. 3 due to the influence of different buffers, it would appear that favorable pH ranges for both sensors are at pH 8.0–8.6.

Fig. 4 shows the storage stability of the choline sensor, which was investigated by measuring the responses of biosensor prepared from the conjugates stored at 4°C in phosphate buffer of pH 8.0. In practice, current responses to 100 μM choline were measured and each response was normalized to the initial value. Native ChOx sensor stored at 4°C over a period of 80 days resulted in loss of enzyme activity and 60% decrease in response was observed, whereas the decrease in response was only about 15% after the 80 days for ChOx–F127M sensor. Thus, the enzyme immobilization with hybrid mesoporous membranes increases the stability of the biosensor. It indicates that encapsulation of ChOx with hybrid mesoporous membrane can retard or prevent the denaturation and/or aggregation processes [18–20].

Finally, we discuss the interface where the reaction takes place in ChOx–F127M sensor. The experimental result about pH dependence shows that the ChOx–F127M sensor is insensitive to the influence of pH and buffer solutions than the native ChOx sensor. This indicates that effective enzymes used in the reaction for ChOx–F127M sensor are encapsulated ones in pores of F127M. The result about storage stability of the sensors also supports this speculation. On the other hand, encapsulation of ChOx in

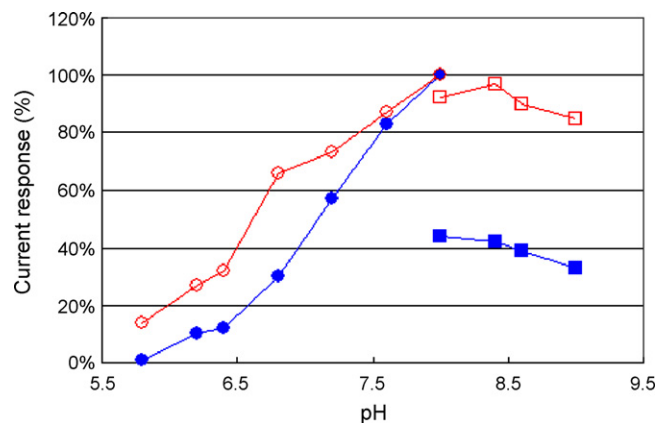


Fig. 3. Response of the ChOx–F127M sensor and native ChOx sensor in different buffer solutions at several pH values to addition of choline solutions giving final concentration of 100 μM . (○, ●) 0.1 M phosphate buffer; (□, ■) 0.1 M borate buffer. Open symbols for ChOx–F127M sensor and closed symbols for the corresponding native ChOx sensor.

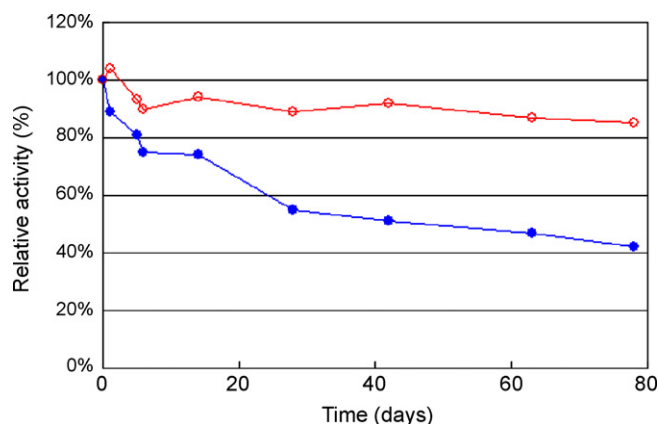


Fig. 4. Storage stability of native (●) and immobilized, i.e., ChOx–F127M, (○) choline sensors in 0.1 M phosphate buffer (pH 8.0). In this experiment, 100 μ M choline solution was used.

pores of F127M might cause a disadvantage for ChOx–F127M sensor in the reaction process compared to native ChOx sensor due to its spatial restriction. In fact, the response starting time of ChOx–F127M sensor after injection of the substrate is not so rapid for the lower concentrations of choline solutions although it is sufficiently rapid at practical level. However, since hybrid mesoporous membrane, F127M, has columnar mesoporous silica structure composed of close-packed silica-nanochannels within a porous alumina membrane and each channel allows transport of molecules across the membrane, the enzymes, ChOxs, could be immobilized appropriately-dispersed with high density in this structured material so as to prevent them from aggregation and to maximize their enzymatic activity. This structure of ChOx–F127M may compensate for the disadvantage of reaction efficiency due to the spatial restriction and then ChOx–F127M sensor shows good response with high current value even if enzymes are encapsulated in pores of F127M.

4. Conclusion

We have illustrated that immobilized enzyme, i.e., choline oxidase (ChOx) within hybrid mesoporous membrane with 12 nm

pore diameter (F127M) successfully offers a suitable amperometric detection of choline. The biosensor consists of Pt electrode and enzyme immobilized membrane (ChOx–F127M) which are attached on the sensing region of the electrode. The measurement was based on the detection of hydrogen peroxide as a co-product in enzyme reaction. In our study, the sensor showed the determination range of 5.0–800 μ M and the response time of approximately 2 min, broad pH-response property and long storage stability (sensor output was maintained about 85% after the 80 days), showing that enzyme choline oxidase (ChOx) is successfully immobilized, well stabilized and enzyme reactions efficiently proceed at practical level. Thus, our study suggests that the hybrid mesoporous membrane F127M could be used as an excellent enzyme immobilization process for enzyme based biosensors.

References

- [1] L. Campanella, M. Mascini, G. Palleschi, M. Tomassetti, *Clin. Chim. Acta* 151 (1985) 71–83.
- [2] L. Campanella, M. Tomassetti, G. De Angelis, M.P. Sammartino, M. Cordatore, *Clin. Chim. Acta* 169 (1987) 175–182.
- [3] L. Campanella, M. Tomassetti, M.P. Sammartino, *Analyst* 113 (1988) 77–88.
- [4] H.G. Xue, Z.Q. Shen, *Chin. J. Chem.* 20 (2002) 784–788.
- [5] H. Gülce, Y.S. Aktas, A. Gülce, A. Yildiz, *Enzyme Microb. Technol.* 32 (2003) 895–899.
- [6] M.A. Rahman, D. Park, Y. Shim, *Biosens. Bioelectron.* 19 (2004) 1565–1571.
- [7] S.S. Razola, S. Pochet, K. Grosfils, J.M. Kauffmann, *Biosens. Bioelectron.* 18 (2003) 185–191.
- [8] S. Yabuki, F. Mizutani, T. Katsura, *Sens. Actu. B* 20 (1994) 159–162.
- [9] L. Svobodova, M. Snejdarkova, K. Tothb, R.E. Gyurcsanyib, T. Hianik, *Bioelectrochemistry* 63 (2004) 285–289.
- [10] H. Kudo, T. Goto, T. Saito, H. Saito, K. Otsuka, K. Mitsubayashi, *Microchim. Acta* 160 (2007) 421–426.
- [11] C.L.Y. Shin, J. Liu, E.J. Ackerman, *J. Am. Chem. Soc.* 124 (2002) 11242–11243.
- [12] U.T. Bornscheuer, *Angew. Chem. Int. Ed.* 42 (2003) 3336–3337.
- [13] Y. Han, S.S. Lee, J.Y. Ying, *Chem. Mater.* 18 (2006) 643–649.
- [14] J. Fan, C. Yu, F. Gao, J. Lei, B. Tian, L. Wang, Q. Luo, B. Tu, W. Zhou, D. Zhao, *Angew. Chem. Int. Ed.* 42 (2003) 3146–3150.
- [15] J.L. Blin, C. Gerardin, C. Carteret, L. Rondehuser, C. Selve, M.J. Stebe, *Chem. Mater.* 17 (2005) 1479–1486.
- [16] A. Yamaguchi, H. Kaneda, W. Fu, N. Teramae, *Adv. Mater.* 20 (2008) 1034–1037.
- [17] O. Quaye, G.T. Lountos, F. Fan, A.M. Orville, G. Gadda, *Biochemistry* 47 (2008) 243–256.
- [18] T. Itoh, K. Yano, Y. Inada, Y. Fukushima, *J. Mater. Chem.* 12 (2002) 3275–3277.
- [19] T. Itoh, R. Ishii, T. Ebina, T. Hanaoka, Y. Fukushima, F. Mizukami, *Bioconjug. Chem.* 17 (2006) 236–240.
- [20] Y. Urabe, T. Shiomi, T. Itoh, A. Kawai, T. Tsunoda, F. Mizukami, K. Sakaguchi, *Chem. Bio. Chem.* 8 (2007) 668–674.



A direct RP-HPLC method for the determination of furanic aldehydes and acids in honey

Nadia Spano^a, Marco Ciulu^a, Ignazio Floris^b, Angelo Panzanelli^a, Maria I. Pilo^a, Paola C. Piu^a, Severyn Salis^a, Gavino Sanna^{a,*}

^a Università degli Studi di Sassari, Dipartimento di Chimica, Via Vienna 2, 07100 Sassari, Italy

^b Università degli Studi di Sassari, Dipartimento di Protezione delle Piante, Via E. De Nicola 1, 07100 Sassari, Italy

ARTICLE INFO

Article history:

Received 16 July 2008

Received in revised form 29 October 2008

Accepted 14 November 2008

Available online 24 November 2008

Keywords:

Honey

5-Hydroxymethyl-2-furaldehyde (HMF)

Furfural

2-Furaldehyde

3-Furaldehyde

2-Furoic acid

3-Furoic acid

ABSTRACT

In this study 5-hydroxymethyl-2-furaldehyde (HMF), 2-furaldehyde, 3-furaldehyde, 2-furoic acid and 3-furoic acid are contemporarily determined in honey using a swift and direct RP-HPLC approach. The validation protocol was performed in terms of detection and quantification limits, precision (by repeatability and reproducibility), linearity and accuracy (by recovery tests); the acceptability of the precision and accuracy results was positively verified using Horwitz's model and AOAC guidelines, respectively. The method was tested on 18 honey samples of different ages, and botanical and geographical origin. HMF and 2-furaldehyde correlated highly with the age of the samples, whereas no correlation was observed with regards to 2-furaldehyde and 2-furoic acid. Hypotheses relating to the formation of minority furanic compounds are also proposed.

© 2008 Elsevier B.V. All rights reserved.

1. Introduction

Of all the saccharidic foodstuffs, honey offers some of the most favourable conditions for the formation of furanic aldehydes: high concentrations of saccharides, low pH values and water activity, as well as the presence of organic acids. The most important of these is 5-hydroxymethyl-2-furaldehyde (HMF), the spontaneous formation of which may take two main routes: the Maillard reaction (nonenzymatic browning) [1] and the acid-catalyzed dehydration of hexoses [2]. For this reason, HMF is a well-known parameter relating to the freshness and quality of honey [3,4]. Indeed, besides aging, HMF concentrations in honey increase as a function of several factors: free acidity, water quantities, botanical origin and stress during storage. Hence, high concentrations of HMF are also indicative of, not only botanical origin [5] and method of isolation [6,7], but also undesirable phenomena such as quality deterioration [8], adulteration [9], overheating [10] and stress during storage. On the other hand, the presence of potentially toxic compounds (such as reactive aldehydes) in foods has been attracting increasing attention ever since consumer protection and quality control gained importance [11]. In particular, according to some studies HMF ranks among the substances posing the risk of

cytotoxic [12], genotoxic [13] and mutagenic activity [14,15]. On the other hand, contrasting studies suggest that HMF probably does not pose a serious risk to human health [16]. In conclusion, differing views persist and the subject is still a matter for debate.

The International Honey Commission (IHC) collaboratively tested three methods for the determination of HMF: two are spectrophotometrical methods (Winkler's [17] and White's methods [18]), whereas the third was a RP-HPLC [19] method. Comparison of their performance was reported by Zappalà et al. [20]. Spectrophotometric methods are fast but low on specificity and sensitivity, on the other hand, the RP-HPLC method is more accurate and sensitive than the spectrophotometric ones, but is quite slow. In addition, the application of this method to HMF evaluation in strawberry tree honey samples has recently evidenced a specific and heavy bias [21].

Other furanic aldehydes and acids can be present in honey, albeit in minor amounts and not always at concentrations high enough to be quantified. While 2-furaldehyde (2-F) and 2-furoic acid (2-FA) originate in variable amounts from reactions such as hydrolysis [22] and oxidative degradation of ascorbic acid [23], respectively, the origin of 3-furaldehyde (3-F) and 3-furoic acid (3-FA), that have sometimes been quantified in honey samples [24], has yet to be ascertained.

While the scientific literature reports an array of analytical methods for the determination of HMF in honey [17–19,21,25–29],

* Corresponding author. Tel.: +39 079 229500; fax: +39 079 229959.

E-mail address: sanna@uniss.it (G. Sanna).

very few contributions also address the evaluation the most common furanic acids and aldehydes [19,24,30]. In this context, it is important to remember the important contributions made by Nozal et al. [24] that reported a RP-HPLC method capable of determining HMF, 2-F, 3-F, 2-FA, 3-FA and methyl anthranilate in honey and honeydew samples in the same chromatographic run. However, the method does not allow direct analysis of the sample, as a clean-up step is needed in order to remove interference and increase sensitivity.

Pursuing our interest in assessing chromatographic and electroanalytical methods for the determination of trace compounds and elements in honey [21,31–33] and honey-based [10] products, we decided to carry out experimental work aimed at proposing and fully validating a direct RP-HPLC method capable of determining the most important furanic aldehydes and acids (i.e. HMF, 2-F, 3-F, 2-FA and 3-FA) in the same analytical run without any pre-treatment of the sample.

2. Experimental

2.1. Samples

Eighteen honey samples were collected from different geographical areas in Italy (Sardinia, Piedmont and Tuscany) and France (Corsica). Twelve of these were of the strawberry tree (*Arbutus unedo* L.) type, two were of thistle cardoon (*Cynara cardunculus*) and the remainder were of eucalyptus (*Eucalyptus* spp.), cistus (*Cistus* L.), chestnut (*Castanea sativa*) and multifloral honey. The attribution of the botanical origin for strawberry tree honey samples was checked by using literature chemical methods [32], whereas a well-recognized melissopalynological approach [34] was used for the samples of different botanical origin. All samples were stored at 4 °C before analysis. Prior to each analytical determination the samples were homogenized for 15 min with an Ultra-turrax mixer mod. T18 (IKA, Staufen, Germany).

2.2. Equipment

2.2.1. Sample preparation

The sample solutions were prepared by dissolving 1 g of homogenized honey with ultra pure water (Merck, Milan, Italy) and then filling to the mark in a 10 ml volumetric flask. Sample solutions were injected through a PVDF (13 mm and 0.45 µm) model 6722 filter from Alltech, Sedriano, Italy.

2.2.2. Chemicals

The chromatographic solvents used were a 0.1 mol L⁻¹ H₂SO₄ solution in ultra pure water (resistance higher than 18 MΩ) and methanol (HPLC grade, Riedel de Haen, Milan, Italy). All solvents used were filtered beforehand through a 0.45 µm membrane, from Millipore, Bedford, MA, to remove any impurities. The chromatographic standards (2-furaldehyde, 3-furaldehyde, 2-furoic acid, 3-furoic acid and 5-hydroxymethyl-2-furaldehyde) were purchased from Lancaster, Milan, Italy.

2.2.3. RP-HPLC analysis

The HPLC equipment was comprised of a Series 200 binary pump, a sampling valve, a 20 µl sample loop and a Series 200 UV-vis variable wavelength detector, all from PerkinElmer, Milan, Italy. Separation was performed on an Alltima C18 column 250 mm × 4.6 mm, 5 µm particle size (Alltech, Sedriano, Italy) fitted with a guard cartridge packed with the same stationary phase. Data were elaborated using Turbochrom Workstation Software (PerkinElmer, Milan, Italy). Each sample was prepared and injected in triplicate.

Table 1

Chromatographic conditions for furanic aldehydes and acids determination in honey.

Elution program		
Time (min)	Solution A = 0.1 mol L ⁻¹ of H ₂ SO ₄ in water (%)	Solution B = methanol (%)
0–2	90	10
9	70	30
9–11	70	30
16	40	60
16–21	40	60
22	90	10
22–23	90	10

Operative wavelengths: 280 nm until 11.5 min, then 240 nm; flow rate: 1.2 mL min⁻¹.

3. Results and discussion

3.1. Assessment of the RP-HPLC method

The method proposed is a development of another proposed by the authors in the past [21], that is capable of evaluating HMF quantities in honey with excellent precision and accuracy, even in the presence of considerable and still unknown sources of interference such as that of homogentisic acid (i.e. the chemical marker of botanical origin of strawberry tree honey [32,35]). The application of this method to the analysis of a standard solution of the five analytes (C = 2 mg L⁻¹ each) provided evidence of high retention times and marked tailoring for the 2-FA and 3-FA peaks. As a consequence of this, the H₂SO₄ solution concentration (solvent A) was raised to 0.1 mol L⁻¹; this represents an optimal compromise between resolution and length of the chromatographic run. On the other hand, pure methanol was chosen as solvent B. The elution program is reported in Table 1.

As the spectra of each compound revealed maxima at different wavelengths: HMF (284 nm), 2-F (277 nm), 3-F (224 nm), 2-FA (253 nm) and 3-FA (239 nm), two different wavelengths (280 and 240 nm) were chosen in order to provide optimum sensitivity for each analyte. In this way, a rapid and sensitive RP-HPLC method that highlights separation at the baseline level of all species was assessed. Within 17 min all the target compounds were completely eluted, and the whole chromatographic run was accomplished in 23 min. Fig. 1 shows the chromatogram obtained by analyzing a mixture of standards.

3.2. Furanic compounds in honey samples

Fig. 2 displays three typical chromatograms of the furanic compounds present in different samples while Table 2

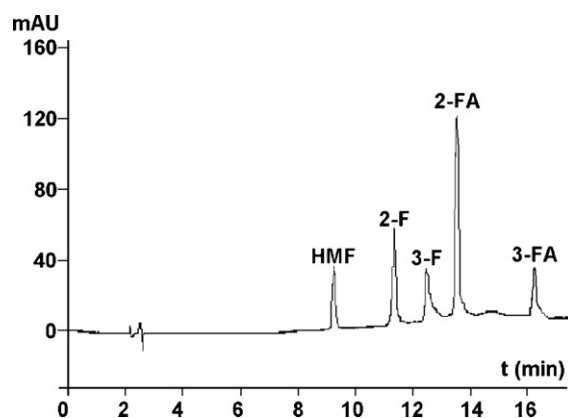


Fig. 1. Chromatogram of a standard mixture of HMF, 2-F, 3-F, 2-FA and 3-FA. C = 2 mg L⁻¹ each. See experimental section for further details.

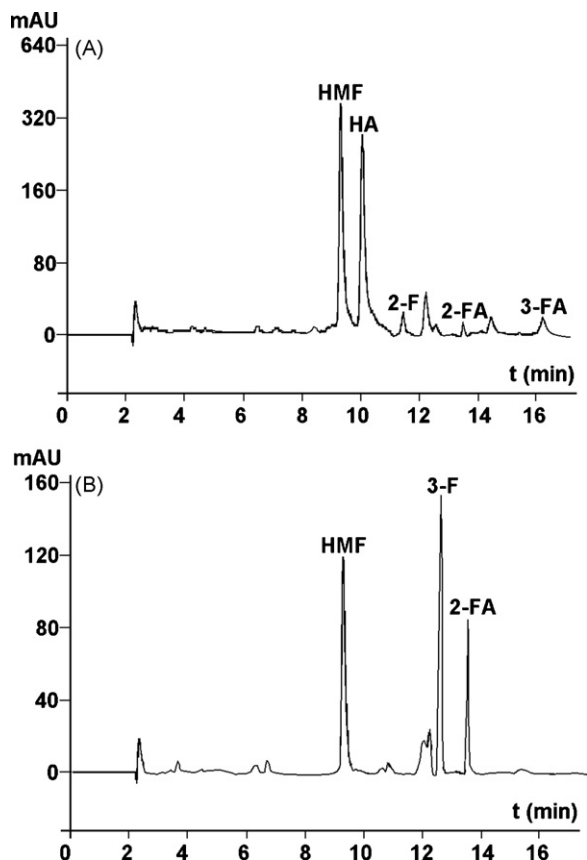


Fig. 2. Chromatograms of: (A) a strawberry tree honey (sample SS3); (B) a thistle honey (sample T1). Peak HA is 2,5-dihydroxyphenylacetic acid (homogentisic acid), *i.e.* the marker of botanical origin of strawberry tree honey.

reports the average concentrations measured in all honeys considered.

As expected, HMF was found in all samples at concentrations of between $0.97 \pm 0.20 \text{ mg kg}^{-1}$ (sample Ch, produced in 2006) and $150.9 \pm 1.6 \text{ mg kg}^{-1}$ (sample SS5, produced in 1998). Fig. 3 shows a very good linear correlation between the age of the samples of strawberry tree honey and the relevant HMF amounts measured.

2-F was found to be over its quantification limit in nine samples, all collected between 1998 and 2002. In these honeys, that are all

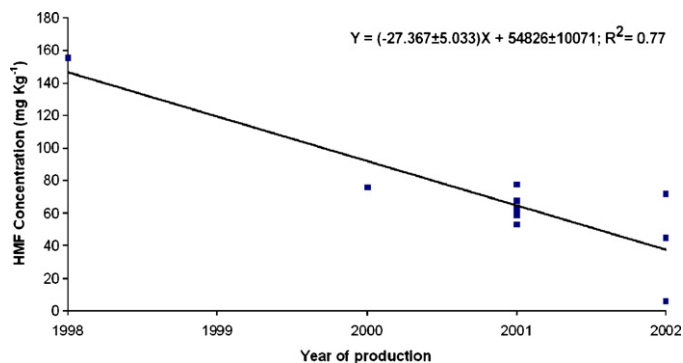


Fig. 3. Correlation between data obtained from the HMF concentration in strawberry tree honey samples (*y*-axis) and the relevant year of production (*x*-axis).

of the strawberry tree variety, the 2-F concentration ranged from $0.94 \pm 0.16 \text{ mg kg}^{-1}$ (SS5) to $2.85 \pm 0.09 \text{ mg kg}^{-1}$ (SP1). These values are generally much higher than those observed by Nozal et al. [24], although it must be borne in mind that in the latter study only fresh samples were analyzed. The age effect probably prevails over that of botanical origin, because some of the freshest strawberry tree samples (SS4, SC1 and SC2), displayed 2-F amounts below the quantification limit. This finding was corroborated by the very high correlation (R^2 value of 0.88) between the 2-F concentration and the year of production of the honey. Furthermore, all honeys collected in the period 2003–2006 displayed total absence of the analyte. On the other hand, the concentrations of 2-F and HMF appear to correlate only weakly (R^2 value of 0.37), and this finding suggests the existence of different degradation pathways affecting the formation of these aldehydes. In particular, the Maillard reaction can account for the formation of HMF, whereas the oxidative degradation of ascorbic acid can give rise to 2-F.

2-FA was quantified in ten samples, at concentrations ranging from $0.35 \pm 0.01 \text{ mg kg}^{-1}$ (SS3) to $3.81 \pm 0.14 \text{ mg kg}^{-1}$ (SU1), not too far from values reported by Nozal et al. [24]. Unlike 2-F, only a slight negative correlation (R^2 value of 0.24) was observed between 2-FA concentrations measured in the strawberry tree honey and the age of the samples (*i.e.* the highest 2-FA concentration was observed in the freshest samples). Furthermore, both HMF and 2-FA concentrations were seen to be affected by a slight negative correlation (R^2 value of 0.43), whereas no correlation was observed between 2-F and 2-FA. 2-FA may be an intermediate species in a more com-

Table 2

Average concentrations of furanic aldehydes and acids in the samples of honey analyzed ($n = 3$).

Sample	Geographical origin	Botanical origin	Year of production	HMF ($\text{mg kg}^{-1} \pm \text{S.D.}^a$)	2-F ($\text{mg kg}^{-1} \pm \text{S.D.}$)	3-F ($\text{mg kg}^{-1} \pm \text{S.D.}$)	2-FA ($\text{mg kg}^{-1} \pm \text{S.D.}$)	3-FA ($\text{mg kg}^{-1} \pm \text{S.D.}$)
SS1	Sardinia	Strawberry tree	2000	75.8 ± 1.0	1.44 ± 0.01	<0.30 ^b	0.79 ± 0.02	<0.09 ^b
SS2	Sardinia	Strawberry tree	2001	53.3 ± 2.1	0.97 ± 0.02	<0.30 ^b	<0.04 ^b	<0.09 ^b
SS3	Sardinia	Strawberry tree	2001	67.83 ± 0.80	0.96 ± 0.04	<0.30 ^b	0.35 ± 0.01	0.84 ± 0.03
SS4	Sardinia	Strawberry tree	2002	5.90 ± 0.20	<0.04 ^b	<0.30 ^b	<0.04 ^b	<0.09 ^b
SS5	Sardinia	Strawberry tree	Unknown	150.7 ± 1.6	0.94 ± 0.16	<0.30 ^b	0.51 ± 0.01	<0.09 ^b
ST1	Tuscany	Strawberry tree	2001	62.5 ± 1.2	1.18 ± 0.02	<0.30 ^b	1.28 ± 0.05	<0.09 ^b
ST2	Tuscany	Strawberry tree	2001	78.0 ± 1.2	1.24 ± 0.03	<0.30 ^b	1.04 ± 0.02	<0.09 ^b
ST3	Tuscany	Strawberry tree	2002	71.9 ± 1.4	1.04 ± 0.02	1.66 ± 0.04	2.90 ± 0.07	<0.09 ^b
SP1	Piedmont	Strawberry tree	1998	155.8 ± 1.8	2.85 ± 0.09	<0.30 ^b	0.63 ± 0.01	<0.09 ^b
SC1	Corsica	Strawberry tree	2001	59.0 ± 1.9	<0.04 ^b	<0.30 ^b	<0.04 ^b	<0.09 ^b
SC2	Corsica	Strawberry tree	2002	44.97 ± 0.07	<0.04 ^b	<0.30 ^b	<0.04 ^b	<0.09 ^b
SU1	Umbria	Strawberry tree	2001	63.7 ± 1.7	1.00 ± 0.03	<0.30 ^b	3.81 ± 0.14	<0.09 ^b
T1	Sardinia	Thistle	2005	11.62 ± 0.37	<0.04 ^b	2.58 ± 0.09	2.15 ± 0.08	<0.09 ^b
T2	Sardinia	Thistle	2006	3.57 ± 0.75	<0.04 ^b	<0.30 ^b	<0.04 ^b	<0.09 ^b
E	Sardinia	Eucalyptus	2004	10.36 ± 0.13	<0.04 ^b	3.94 ± 0.15	3.49 ± 0.17	<0.09 ^b
MF	Sardinia	Multifloral	2003	13.34 ± 0.16	<0.04 ^b	<0.30 ^b	3.24 ± 0.02	<0.09 ^b
Cs	Sardinia	Cistus	2006	1.43 ± 0.31	<0.04 ^b	<0.30 ^b	<0.04 ^b	<0.09 ^b
Ch	Sardinia	Chestnut	2006	0.97 ± 0.20	<0.04 ^b	<0.30 ^b	<0.04 ^b	<0.09 ^b

^a Standard deviation.

^b Under the quantification limit, LoQ.

Table 3
Validation parameters data for the furanic compounds quantified in honey ($n=5$).

Analytes	Sensitivity		Linearity	R^2	Repeatability		Reproducibility		Bias
	LoD (mg L ⁻¹)	LoQ (mg L ⁻¹)	Concentration range (mg L ⁻¹)		CV% _{exp,r} ^a	HorRat _r ^b	CV% _{exp,R} ^c	HorRat _R ^d	Recovery (% ± S.D. ^e)
HMF	0.003	0.010	0.01–100	0.9994	0.99	0.20	1.47	0.19	97 ± 14
2-F	0.001	0.004	0.01–200	0.9992	0.35	0.04	0.97	0.07	83.34 ± 0.62
3-F	0.010	0.030	0.05–200	0.9939	1.63	0.15	2.97	0.19	99.8 ± 7.4
2-FA	0.001	0.004	0.05–100	0.9996	0.44	0.05	1.80	0.13	81.0 ± 2.8
3-FA	0.009	0.027	0.05–100	0.9991	0.03	0.004	3.54	0.27	82.90 ± 0.90

^a CV%_{exp,r} is the experimental coefficient of variation of repeatability.

^b HorRat_r is the ratio between CV%_{exp,r} and the theoretical repeatability data (CV%_{H,r}) according to Horwitz's theory.

^c CV%_{exp,R} is the experimental coefficient of variation of reproducibility.

^d HorRat_R is the ratio between CV%_{exp,R} and the theoretical reproducibility data (CV%_{H,R}) according to Horwitz's theory.

^e Standard deviation.

plex degradation pathway: this acid can be quickly formed from specific precursors that are not always present in the honey (e.g. ascorbic acid [23]), and then slowly consumed in further reaction steps, responsible for the low 2-FA concentrations measured in older samples.

Finally, the determination of 3-F provided values up the relevant quantification limit only for three honey samples and that of 3-FA for only one. While the 3-F concentrations ranged from 1.66 ± 0.04 mg kg⁻¹ (sample ST2) to 3.94 ± 0.15 mg kg⁻¹ (sample E), the amount of 3-FA measured in the SS3 sample is equal to 0.84 ± 0.03 mg kg⁻¹. Only a few tentative conclusions can be drawn from these data. The analytical values are in the same concentration range as that reported by Nozal et al. [24] and, as in the work cited, these analytes can be quantified only in less aged samples. These findings lead us to suppose that 3-F and 3-FA can be either minority constituents of honey or decomposition products obtained by way of a fast reaction pathway from species which are not always present in this matrix.

3.3. Validation

3.3.1. LoD and LoQ

LoD and LoQ were calculated according to the Upper Limit Approach (ULA1) method [36]. For each analyte, four different aqueous solutions at concentrations close to expected LoD were prepared and analyzed. Each measure was performed in triplicate. LoD and LoQ values are reported in Table 3.

Although the current meaning associated with the expression "detection limit" in the past led to numerical values that spanned three orders of magnitude [37], it is well known that the application of the ULA1 approach provides LoD values that are always higher than those obtained using alternative methods (e.g. that of "three times the maximum height of the noise"). Nevertheless, data hereby reported resemble very closely those published elsewhere [24].

3.3.2. Precision

Precision was evaluated by means of repeatability and reproducibility measures.

Repeatability was evaluated by way of five consecutive replicates of the analysis on the same honey sample, and expressed in terms of percent coefficient of the experimental variation (CV%_{exp,r}).

Reproducibility was also expressed in a similar way (CV%_{exp,R}) as the result of five analyses of the same honey sample performed over different analytical sessions within 1 month. All the precision data are reported in Table 3.

Average repeatability ranged from 0.03% (3-FA) to 1.63% (3-F), whereas average reproducibility values ranged from 0.97% (2-F) to 3.54% (3-FA). On the whole, the precision data obtained are comparable with the best values reported in the literature [24]. In addition, Horwitz's theory [38] was used to establish the acceptability level

of the precision data. Hence, a theoretical CV% was calculated on the basis of the concentration level expected for repeatability and reproducibility measures. If the HorRat ratio (*i.e.* the ratio between experimental and theoretical CV%) is less than 1.5, the experimental data can be deemed acceptable. Data reported in Table 3 show that HorRat values for repeatability and reproducibility are always considerably lower than 1.5, *i.e.* within the relevant intervals of acceptable variation.

3.3.3. Linearity

Linearity was determined for each analyte in a concentration range covering at least three decades and spanning from values close to each LoQ to hundreds of mg L⁻¹. As shown in Table 3, satisfactory to very good correlation coefficients (R^2) were observed for the different analytes, ranging from 0.9939 for 3-F to 0.9996 for 2-FA. Moreover, graphical analysis performed on the residuals of the regression line for each compound allowed us to exclude any "hidden" deviations from linearity in all cases.

3.3.4. Accuracy

Accuracy was estimated by recovery tests performed on each analyte, as Certified Reference Materials were not available.

After homogenisation, 80 g of sample Ch was divided into four 20 g aliquots. While the aliquots from 2 to 4 were treated with a suitable volume (1.0, 2.0 or 3.0 mL, respectively) of a freshly prepared bulk solution containing 100 mg L⁻¹ of HMF and 20 mg L⁻¹ of 2-F, 3-F, 2-FA and 3-FA, respectively, no addition was made to aliquot 1 of the sample. Subsequently, varying volumes of ultrapure water were also added to aliquots from 1 to 3 (3.0, 2.0 or 1.0 mL, respectively). After these additions, each aliquot underwent all the analytical procedures previously described. Each analysis was performed in triplicate. Average recoveries, ranging from 81.0% for 2-FA to 99.8% for 3-F, are summarized in Table 3.

The acceptability of these data was verified according to the guidelines described in the AOAC manual for peer-verified methods [39]. Since the concentration range of all five analytes is in the realm of between tens of mg kg⁻¹ (HMF) and units of mg kg⁻¹ (2-F, 3-F, 2-FA and 3-FA), respectively, for these mass ratios the AOAC guidelines consider recovery levels between 80% and 110% to be "acceptable". Since our recovery data are in all cases well within this range, we may conclude that these values are acceptable.

4. Conclusions

A swift and direct RP-HPLC method allowing the contemporary quantification of HMF, 2-F, 3-F, 2-FA and 3-FA in honey samples has been assessed and completely validated. The method has been tested on 18 honey samples of different ages, and geographical and botanical origin. Results show the different presence and concentration levels of the analytes. With the exception of HMF, no compound was quantified in all samples. 2-F and 2-FA, that are

the most frequent analytes, are both present in half of the samples in a concentration range in the realm of the mg kg^{-1} , whereas 3-F was observed in three honey samples and 3-FA in only one. The presence of possible correlation between HMF, 2-F and 3-F concentrations, as well as age and geographical/botanical origin of the samples was verified, and hypotheses relating to the formation of minority furanic compounds have been proposed. Finally, validation parameters demonstrate that the method has low LoD and LoQ values, a wide linearity interval and very good precision. Accuracy was also found to be acceptable according to AOAC guidelines.

References

- [1] A.J. Tomlinson, J.P. Landers, L.A.S. Lewis, S. Naylor, J. Chromatogr. A 652 (1993) 171.
- [2] H.D. Belitz, W. Grosch, Food Chemistry, Springer-Verlag, Berlin, 1999.
- [3] Joint FAO/WHO food standard programme. Alinorm 01/25. Codex Committee On Sugars, 7th session. London, United Kingdom, February 9–11, 2000, and Codex Alimentarius Commission, 24th session, Geneva, Switzerland, July 2–7, 2001. Also available in the web at the address: www.codexalimentarius.net/download/report/277/AI01_25e.pdf.
- [4] EU Directive/110/2001 of 02/12/2001 (L 10/47). Also available in the web at the address: <http://europa.eu.int/eur-lex/lex/LexUriServ/LexUriServ.do?uri=CELEX:32001L0110:EN:HTML>.
- [5] B. Fallico, M. Zappalà, E. Arena, A. Verzera, Food Chem. 85 (2004) 305.
- [6] E. Alissandrakis, P.A. Tarantilis, P.C. Harizanis, M. Polissiou, J. Sci. Food Agric. 85 (2005) 91.
- [7] I. Jerkovic, J. Mastelic, Z. Marijanovic, Ž. Klein, M. Jelic, Ultrason. Sonochem. 14 (2007) 750.
- [8] M.H.J. Kim, J. Richardson, J. Chromatogr. 593 (1992) 153.
- [9] M. Ozcan, D. Arslan, D.A. Ceylan, Food Chem. 99 (2006) 24.
- [10] N. Spano, M. Ciulu, I. Floris, A. Panzanelli, M.I. Pilo, P.C. Piu, R. Scanu, G. Sanna, Food Chem. 108 (2008) 81.
- [11] J. Scultheiss, D. Jensen, R. Galensa, J. Chromatogr. A 880 (2000) 233.
- [12] L. Nassberger, Hum. Exp. Toxicol. 9 (1990) 211.
- [13] W.R. Bruce, M.C. Archer, D.E. Corpet, A. Medline, S. Minkin, D. Stamp, Y. Yin, X.M. Zhang, Mutat. Res. 290 (1993) 111.
- [14] Y.J. Surh, A. Liem, J.A. Miller, S.R. Tannenbaum, Carcinogenesis 15 (1994) 2375.
- [15] X.M. Zhang, C.C. Chan, D. Stamp, S. Minkin, M.C. Archer, W.R. Bruce, Carcinogenesis 14 (1993) 773.
- [16] C. Janzowski, V. Glaab, E. Samimi, J. Schlatter, G. Eisenbrand, Food Chem. Toxicol. 38 (2000) 801.
- [17] O. Winkler, Z. Lebensm. Unters. Forsch. 102 (1955) 160.
- [18] J.W. White, J. Assoc. Off. Anal. Chem. 62 (1979) 509.
- [19] H.J. Jeuring, F.J.E.M. Kuppers, J. Assoc. Off. Agric. Chem. 63 (1980) 1215.
- [20] M. Zappalà, B. Fallico, E. Arena, A. Verzera, Food Control 16 (2005) 273.
- [21] N. Spano, L. Casula, A. Panzanelli, M.I. Pilo, P.C. Piu, R. Scanu, A. Tapparo, G. Sanna, Talanta 68 (2006) 1390.
- [22] G. Bonn, O. Bobleter, J. Radioanal. Chem. 79 (1983) 171.
- [23] M. Sawamura, K. Takemoto, Y. Matsuzaki, H. Ukeda, H. Kusunose, J. Agric. Food Chem. 42 (1994) 1200.
- [24] M.J. Nozal, J.L. Bernal, L. Toribio, J.J. Jiménez, M.T. Martín, J. Chromatogr. A 917 (2001) 95.
- [25] C. Corradini, D. Corradini, J. Microcolumn Sep. 6 (1994) 19.
- [26] C.H. Risner, M.J. Kiser, M.E. Dube, J. Food Sci. 71 (2006) C179.
- [27] E. Teixido, F.J. Santos, L. Puignou, M.T. Galceran, J. Chromatogr. A 1135 (2006) 85.
- [28] A.E. Edris, M. Murkovic, B. Siegmund, Food Chem. 104 (2007) 1310.
- [29] E. Teixido, E. Moyano, F.J. Santos, M.T. Galceran, J. Chromatogr. A 1185 (2008) 102.
- [30] F. Lo Coco, C. Valentini, V. Novelli, L. Ceccon, J. Chromatogr. A 749 (1996) 95.
- [31] G. Sanna, M.I. Pilo, P.C. Piu, A. Tapparo, R. Seeber, Anal. Chim. Acta 15 (2000) 165.
- [32] R. Scanu, N. Spano, A. Panzanelli, M.I. Pilo, P.C. Piu, G. Sanna, A. Tapparo, J. Chromatogr. A 1090 (2005) 76.
- [33] N. Spano, I. Piras, M. Ciulu, I. Floris, A. Panzanelli, M.I. Pilo, P.C. Piu, G. Sanna, RP-HPLC chromatographic profile of the free amino acids in the strawberry tree (*Arbutus unedo* L.) honey, J. Assoc. Off. Agric. Chem., accepted for publication.
- [34] J. Louveaux, A. Maurizio, G. Vorwohl, Bee World 59 (1978) 139.
- [35] P. Cabras, A. Angioni, C. Tuberoso, I. Floris, F. Reniero, C. Guillou, S. Ghelli, J. Agric. Food Chem. 47 (1999) 4064.
- [36] J. Mocak, A.M. Bond, S. Mitchell, G. Schollary, Pure Appl. Chem. 69 (1997) 297, IUPAC recommendation, document 550/35/87.
- [37] L.A. Currie, Chemom. Intell. Lab. Syst. 37 (1997) 151.
- [38] W. Horwitz, Anal. Chem. 54 (1982) 67A.
- [39] AOAC Peer Verified Methods Program, Manual on policies and procedures, AOAC International, Arlington, VA, 1993.



Short communication

Direct determination of arsine in gases by inductively coupled plasma–dynamic reaction cell–mass spectrometry

Jung Ki Suh, Namgoo Kang*, Jin Bok Lee

Division of Quality of Life, Korea Research Institute of Standards and Science, 1 Doryong-Dong, Yuseong-Gu, Daejeon 305-340, Republic of Korea

ARTICLE INFO

Article history:

Received 26 August 2008

Received in revised form 22 October 2008

Accepted 22 October 2008

Available online 5 November 2008

Keywords:

Arsine

Dynamic reaction cell

ICP–DRC–MS

Metal hydride

Measurement uncertainty

ABSTRACT

Reliable determination of arsine (AsH_3) in gases is of great importance due to stringent regulations associated with health, safety and environmental issues. It is, however, challenging for an analyst to determine trace airborne arsine concentrations without specifically designed collection procedures using adsorption, desorption, dissolution or impinging techniques. To circumvent such technical barrier, we have newly developed a direct analytical method, characterized by introduction of an arsine gas sample into stable plasma stream, followed by gas-phase oxidation of arsine with molecular oxygen in a dynamic reaction cell (DRC) equipped within the inductively coupled plasma–mass spectrometry (ICP/MS) system, followed by subsequent detection of AsO^+ ion. This preliminary work used trace arsine concentrations ($161 \mu\text{g m}^{-3}$, $322 \mu\text{g m}^{-3}$, and $645 \mu\text{g m}^{-3}$) gravimetrically prepared in N_2 balance. The proposed method was optimized for the important experimental parameters such as the flow rates of the reaction gas, the arsine sample, and the carrier gas. This method was then validated by demonstrating good figure-of-merits including the low limit of detection ($0.10 \mu\text{g m}^{-3}$), good linearity ($r^2 > 0.9915$), low measurement uncertainty (0.66%), and high speed of analysis (< 6 min). The proposed method is expected to be potentially applicable to the determination of arsine in real workplace air after appropriate modifications are made.

© 2008 Elsevier B.V. All rights reserved.

1. Introduction

Arsine (AsH_3) is a metal hydride and the most reducing form (–III) of arsenic species, existing as a gas at ambient temperature and pressure. Arsine is being frequently used as a dopant as in the processing of semiconductors in the microelectronics industry, and inorganic synthesis. This chemical may be evolved during numerous industrial production processes that can lead to the accidental formation and liberation of arsine fumes: smelting and refining of metals (zinc), plating, galvanizing, soldering, electrolytic processing of hydrogen.

Since arsine is highly toxic depending on its concentration, human exposure to arsine in workplace poses a potential health hazard that may result in severe toxic effects such as arsenic intoxication. Most cases of arsine poisoning do not result from its use but from accidental on-site generation as by-product of a chemical reaction involving a metal containing an arsenic impurity and an acid or a strong alkali [1]. The permissible exposure limits of arsine established by National Institute for Occupational Safety and Health (NIOSH), Occupational Safety and Health Associ-

ation (OSHA), are 0.002 mg m^{-3} during 15 min [2] and 0.2 mg m^{-3} (0.05 ppmv) [3], respectively. The American Committee of Government in Health (ACGIH) suggested strict exposure limit of 0.016 mg m^{-3} (0.005 ppmv) as the notice of international change as of 2004. There is a high potential for the generation of arsine gas when inorganic arsenic is exposed to nascent (freshly formed) hydrogen. Such codes indicate that appropriate work practices be implemented to reduce the risk of worker poisoned by gaseous arsine.

Since early 1980s many have developed sampling and analytical techniques of arsine in gases including ambient air. It is first reported that airborne arsine gas can be trapped on filtering media such as a silver nitrate impregnated filter paper [4] or can be adsorbed onto synthetic resin activated carbon [5]. Afterwards, “indirect” determination methods have been conventionally used in practice, requiring specific sampling techniques. The NIOSH method 6001 requires collection of arsine by adsorption using solid sorbent tube with activated coconut shell charcoal, followed by desorption/dissolution using dilute nitric acid, followed by analysis using graphite furnace–atomic absorption spectroscopy (GF–AAS). The NIOSH method indicates its collection efficiency of $< 89\%$ [6]. The overall accuracy is $\pm 23.2\%$ and the working range is $0.3\text{--}60 \text{ ppbv}$ as As ($0.001\text{--}0.2 \text{ mg m}^{-3}$) for a 10-L air sample [2]. The OSHA method 1D-105 requires collection of arsine by

* Corresponding author. Tel.: +82 42 868 5221; fax: +82 42 868 5042.
E-mail address: nkang@kriss.re.kr (N. Kang).

adsorption using mixed cellulose ester filters, chemically treated cellulose backup pads, and an arsine sampling tube (containing glass and activated coconut shell charcoal), followed by desorption/dissolution using dilute nitric acid/nickel solution, followed by analysis using heated graphite atomizer–atomic absorption spectroscopy (HGA–AAS). Due to the uncertainty associated with collection of samples, this method has a significant drawback of large overall accuracy of $\pm 20\%$ [3].

A wide range of sampling techniques are reported such as filtration, dissolution of the particles on filters, impactors, electrostatic precipitators, and impingers, are available especially for arsenic species [7]. To date, many have made efforts for the best collection of arsine in gases only to fail to resolve the issue of enhancing sampling efficiency. It is thus evident that a good analytical approach depends largely upon the efficiency of the collection techniques. Indirect methods are by nature limited in accurate analysis of arsine due to the low accuracies originated from sampling efficiency and require cumbersome, time-consuming procedures.

Although more accurate, precise and rapid determination of arsine from sample gases without sampling is in high demand, information on quantitative determination of arsine in a gas sample is very rare. An ultrasonic time-of-flight method was developed for application to continuous concentration monitoring of in situ electrochemically generated arsine with a limited applicability to very high concentrations of arsine (2–90%) [8]. A direct method based on gas chromatography–mass spectrometry was recently proposed for analysis of volatile arsenic species including arsine [9]. The determination of arsenic (As) in HCl by inductively coupled plasma–mass spectrometry (ICP–MS) was reported nearly two decades ago [10].

To the best of our knowledge, however, inductively coupled plasma–dynamic reaction cell–mass spectrometry (ICP–DRC–MS) has never been reported for the direct determination of trace arsine in gas samples. We therefore explored the first-ever attempt and present the preliminary results for the direct determination of arsine samples prepared in N_2 by ICP–DRC–MS. We herein demonstrate the validity of the proposed method by investigating optimization of operating conditions, and evaluating linearity, limit of detection, and measurement uncertainties using arsine reference gases. We present results from the determination of arsine in real samples collected from workplace ambient air. The results from this preliminary work are expected to open the new horizon for the practical application to the direct determination of arsine in real workplace air.

2. Experimental

2.1. Working principle

Although an ICP–DRC–MS analytical system can be used to determine total arsenic including arsine, arsine oxides, etc., it is not possible to differentiate arsine only from other arsenic species within the system. As long as an ICP–DRC–MS is used for the determination of As^+ ($m/z=74.9215$), there can be a significant molecular interference from other chemical species such as $ArCl^+$ ($m/z=74.9286$) and $CaCl^+$ ($m/z=74.9314$) which can occur as a result of gas-phase argon plasma reactions with Cl-containing constituents in a gas sample. Since the m/z value of $ArCl^+$ or $CaCl^+$ is similar to that of As^+ , $ArCl^+$, once formed, can result in severe interference with detection of As^+ [11]. The proposed method therefore used direct injection of an arsine gas sample into optimized plasma stream in which molecular oxygen reacts with arsine in an ICP–DRC–MS analytical system, followed by detection of AsO^+ ($m/z=90.9165$).

2.2. Instrumentation

The instrumental system used in this study consists of an ICP–DRC–MS analytical system (PerkinElmer Sciex Elan 6100 DRC Plus; Concord, Ontario, Canada) equipped with a dynamic reaction cell (DRC) within the system, the inlet line of the sample gas, the inlet line of the nebulizer gas (argon), a mass flow controller (MFC), and the reference gas cylinder of arsine in N_2 . A schematic diagram as illustrated in Fig. 1 briefly shows each system compartment. Instead of a nebulizer and spray chamber system used for the injection of a liquid sample, we used a gas injection system designed for a gas sample to be directly transported into the plasma stream within the ICP–MS.

2.3. Selection of operating conditions

The instrumental characteristics and operating parameters for the ICP–DRC–MS analytical system are listed in Table 1. The numerical values were obtained by reflecting the best results from experimental runs. The radio-frequency (RF) power and the nebulizer gas flow rate were set to obtain maximum sensitivity, while curbing the formation of double charged and oxide ions. The voltage of the cylinder lens, the rod offset voltages of both the quadrupole and the dynamic reaction cell, and the Mathieu stability parameters a and q of the cell quadrupole were set for the maximum ion transmission. The RF amplitude of the DRC, the cell path voltage including the cell entrance and exit lenses and the AC-only pre-filter rod offset were set. The reaction gas to generate (AsO^+) at $m/z=90.9165$ is gaseous O_2 and its flow were optimized at 0.35 mL min^{-1} . The reaction gas flow rate was adjusted by the MFC of the instrument. The signal detection parameters were set to

Table 1

The operating conditions of the ICP–DRC–MS for detection of AsO^+ used in this work.

Operating parameter	Operating condition
<i>Sample introduction system</i>	
Flow rate of arsine sample	1.0–5.0 mL min ⁻¹
Flow rate of carrier gas	Ar, 0.9 L min ⁻¹
Injector	Quartz (2.0 mm i.d.)
RF generator	Free-running design (40 MHz)
ICP RF power	1300 W
Flow rate of plasma gas	Ar, 17 L min ⁻¹
Flow rate of auxiliary gas	Ar, 1.30 L min ⁻¹
<i>DRC system</i>	
Cone material of sampler	1.1 mm diameter Pt
Cone material of skimmer	0.9 mm diameter Pt
Ion optics	Grounded metal stop disk plus single cylinder lens, voltage ramped with mass (Autolens®)
Lens voltage at $m/z=90.9165$	6.7 V
Cell type	Dynamic reaction cell
Cell path voltage	-17 V
Cell rod offset	-11 V
Flow rate of reaction gas	O_2 , 0.35 mL min ⁻¹
Parameter a	0
Parameter q	0.45 (O_2)
Mass analyzer	Quadrupole
Quadrupole rod offset	0
Detector	Dual analog/digital discrete dynode
Analog stage voltage	-1906 V
Pulse stage voltage	900 V
<i>Signal detection</i>	
Acquisition mode	Peak-hopping
Dwell time	100 ms
Sweeps/reading	50
Reading/replicates	1
Replicates	50

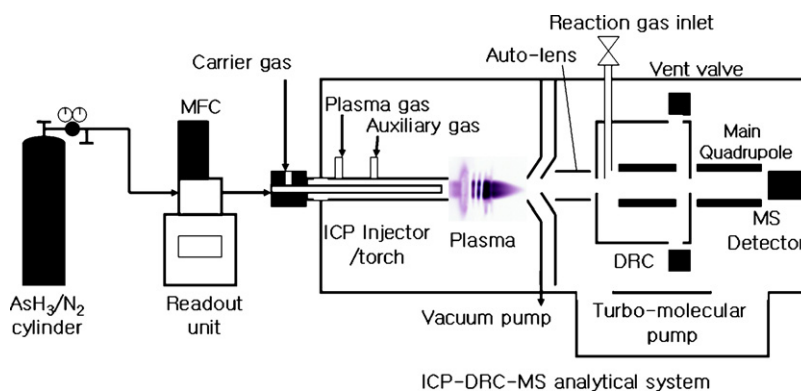


Fig. 1. A schematic representation of the ICP-DRC-MS analytical system used for the arsine determination.

achieve the best analytical performances within a reasonable measurement time period.

2.4. Reagents and preparation of arsine samples

Oxygen (99.999%) was used as the reaction gas. A mother reference gas cylinder for arsine (2.63%) in the balance gas of N_2 was purchased from a specialty gas company (Daehan GasFill Corporation; Yong-In, South Korea). A total of 3 daughter cylinders were gravimetrically prepared by filling a determined amount of arsine from the mother cylinder and by adding high purity N_2 gas, based on the international guide [12]. The gravimetrically prepared concentrations of the three different cylinders were $161 \mu\text{g m}^{-3}$ (49.8 ppbv), $322 \mu\text{g m}^{-3}$ (99.7 ppbv), and $645 \mu\text{g m}^{-3}$ (199.9 ppbv), respectively.

3. Results and discussion

3.1. Optimization of major experimental parameters

Experimental variables such as flow rates of various gases including carrier gas (Ar), reaction gas (O_2) and sample gas (arsine) are important factors for controlling the signal intensities from the ICP-DRC-MS system. These flow rates need to be optimized in order to search for the best operating conditions.

Prior to establishing the best operating conditions, ICP-MS signal responses as a function of reaction gas flow rates were investigated. A total of 10 different flow rates with an increased interval of 0.1 mL min^{-1} from 0 mL min^{-1} to 1.0 mL min^{-1} were tested. The results shown in Fig. 2 suggest that the maximal signal response would be located between 0.3 mL min^{-1} and 0.4 mL min^{-1} . Based on these results, 0.35 mL min^{-1} was chosen as the optimized con-

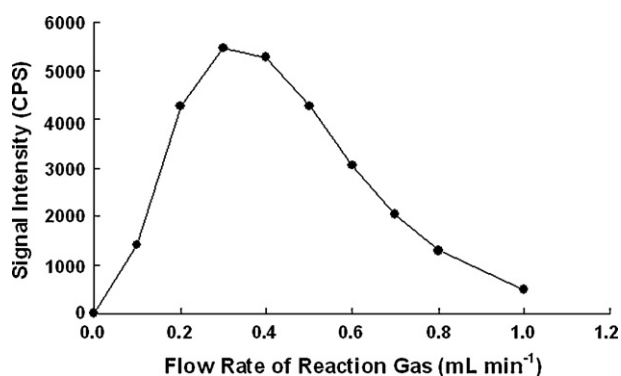


Fig. 2. Signal intensity optimized as to reaction gas (O_2) flow rates.

dition for every subsequent runs through this study. These results demonstrate that the formation of AsO^+ readily occurs upon the reaction with O_2 . With increase in the reaction gas flow rate increases the rate of AsO^+ generation builds up, consequently enhancing the instrumental sensitivity. On the contrary, the reaction gas supply is in excess, the collision of the reaction gas with arsenic atom occurs. As a consequence, the number of arsenic atoms that can reach the detector decreases, which lowers the sensitivity.

ICP-MS signal responses need to be optimized also as to varying flow rates of the carrier gas. For the carrier gas, a total of 8 different flow rates ranging from 0.5 L min^{-1} to 1.2 L min^{-1} were tested. The results as shown in Fig. 3 indicate that the maximal signal intensity value could be obtained around 0.9 L min^{-1} . This value was consistently employed for the all subsequent ICP-MS runs.

Arsine sample introduction flow rates that can affect ICP-MS signal responses were investigated. A total of 5 different flow rates ranging from 1 mL min^{-1} to 5 mL min^{-1} with an interval of 1 mL min^{-1} were tested at the two different arsine concentrations ($161 \mu\text{g m}^{-3}$ and $645 \mu\text{g m}^{-3}$). The results from Fig. 4 shows R^2 values of 0.9915 and 0.9955 for the respective two concentrations, suggesting relatively good linear relationship between the arsine concentrations and the ICP-MS signal intensities within the tested range.

3.2. Linearity, repeatability and limit of detection

Validation processes for the proposed method were conducted as recommended by an international guide [13]. In order to investigate the linearity and repeatabilities for the proposed method, ICP-MS signal intensities were examined as a function of arsine concentrations ranging from $161 \mu\text{g m}^{-3}$ to $645 \mu\text{g m}^{-3}$ at the

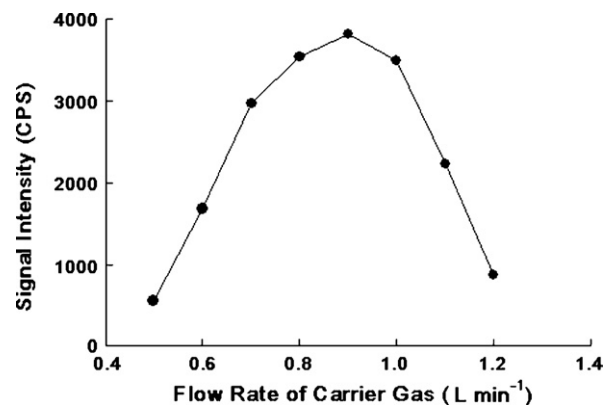


Fig. 3. Signal intensity optimized as to carrier gas (Ar) flow rates.

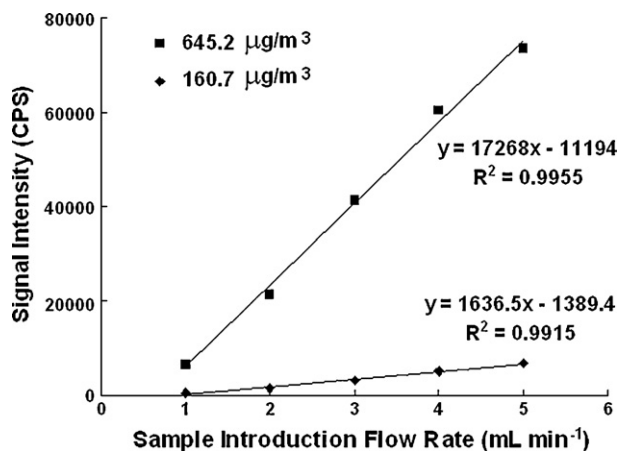


Fig. 4. Signal intensity affected by arsine sample introduction flow rates.

low and high flow rates of sample introduction (2 mL min^{-1} and 5 mL min^{-1}). As shown in Fig. 5, the results indicate R^2 of 0.9999 and 0.9991 under the two different conditions, suggesting very good linear relationships occurred between the ICP–MS signal intensities and the tested arsine concentration within the tested ranges.

The repeatability was investigated by the results from 5 replicate injections ($n=4$) for each arsine sample including a blank sample. The background signal intensities were very low (average value of 148.9 CPS) with a relative standard deviation (RSD) of 3.9%. The preparation of the arsine standards in terms of RSD values for all data points from the samples shown in Fig. 5 were within 0.7%, indicating that this proposed method is very reliable in the aspect of repeatability.

The limit of detection (LOD) for arsine concentrations using the proposed method was determined based on the following criterion [14]:

$$C_{DL} = \frac{t_{(1-a, n-1)} \cdot S_b}{m} \quad (1)$$

where C_{DL} = LOD expressed in concentration ($\mu\text{g m}^{-3}$), $t_{(1-a, n-1)}$ = Student's t statistic at a specified confidence level and degree of freedom (dimensionless), S_b = the standard deviation of the background computed from at least 10 replicate measurements (counts per second; CPS), m = the slope of the analytical calibration curve ($\text{CPS } \mu\text{g}^{-1} \text{ m}^{-3}$).

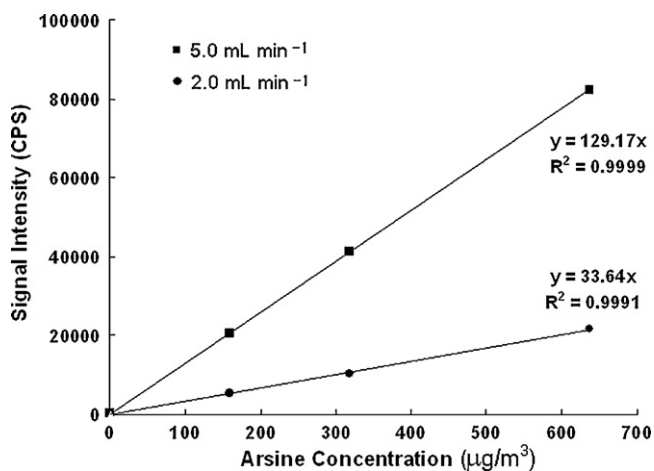


Fig. 5. Relationship between sample concentrations and signal intensities.

The assigned value of the t statistics, $t_{(1-a, n-1)}$, for 10 replicates ($n=9$) tested in this study is 2.262 at 95% confidence level. Based on 10 independent measurements for the background ion current, the obtained value for the standard deviation of background, S_b , was 5.8 CPS. For the sample injection flow rates of 5 mL min^{-1} , the slope of the calibration curves was $128.86 \text{ CPS } \mu\text{g}^{-1} \text{ m}^{-3}$. With these values, the minimum detectable concentration, C_D , of approximately $0.10 \mu\text{g m}^{-3}$ (0.03 ppbv) was obtained.

3.3. Estimation of measurement uncertainty

To investigate the reliability of the measured concentrations of the arsine samples, uncertainty budget was evaluated based on the ISO/EURACHEM guides [15,16]. A two-point calibration process using the low and high arsine concentrations ($161 \mu\text{g m}^{-3}$ and $645 \mu\text{g m}^{-3}$) was applied to the estimation of a measurement uncertainty for the mid concentration ($322 \mu\text{g m}^{-3}$) between the two reference concentrations. The results indicate that the effective degree of freedom (ν) is 9, the coverage factor (k) at $\nu=9$ is 2.26, and the combined, standard uncertainty (u_c) is $1.06 \mu\text{g m}^{-3}$. Using these values, the expanded uncertainty ($U = k u_c$) is $2.40 \mu\text{g m}^{-3}$ (0.66% as the relative expanded uncertainty). The detailed calculation process for these estimates is presented in Supporting Information. In addition, the initial attempts are being made for the determination of arsine concentrations from the real process samples. Although only some preliminary information is included in Supporting Information, further studies on this topic have to be tackled sufficiently in near future.

4. Conclusions

The biggest advantage of this method compared to previous approaches is that no ‘trapping’ of arsine was required in sampling procedure because gaseous samples can be directly injected into the ICP–MS. In this method no pretreatments of samples were needed which minimized the risks for species conversion during sample capturing and pretreatments. Owing to such merit, an analyst can perform rapid (<6 min), and reliable determination of arsine in a direct manner. Application and validation of the proposed method for the determination of arsine in real workplace air samples will be a high priority task in near future. To be potentially applicable to the determination of arsine in workplace air, appropriate modifications would be necessary for the optimized analytical conditions and validation process because the synthetic air as the balance gas contains gaseous molecular oxygen.

Acknowledgement

This research was financially supported by KRISS Basic Research Fund on the Environmental and Food Metrology and Standards.

Appendix A. Supplementary data

Supplementary data associated with this article can be found, in the online version, at doi:10.1016/j.talanta.2008.10.042.

References

- [1] L.J. Cralley, L.V. Cralley, J.S. Bus, Patty's Industrial Hygiene and Toxicology: Theory and Rationale of Industrial Hygiene Practice, 3rd ed., John Wiley & Sons, New York, 1995.
- [2] NIOSH, National Institute for Occupational Safety and Health Manual of Analytical Methods, Method 5001: Arsine, 1994.
- [3] OSHA, Inorganic Arsenic in Workplace Atmospheres, Method Number ID-105, T-ID105-FV-01-9105-M, Division of Physical Measurements and Inorganic Analyses, OSHA Technical Center, Salt Lake City, Utah, 2007.
- [4] D.L. Keech, N.G. West, Ann. Occup. Hyg. 23 (1980) 273.

- [5] Y. Matsumura, *Ind. Health* 26 (1988) 135.
- [6] L. Helsén, *Environ. Pollut.* 137 (2005) 305.
- [7] U. Telgheder, V.A. Khvostikov, *J. Anal. At. Spectrom.* 12 (1997) 1.
- [8] J.L. Valdes, G. Cadet, *Anal. Chem.* 63 (1991) 366.
- [9] M. Pansar-Kallio, A. Korpela, *Anal. Chim. Acta* 410 (2000) 65.
- [10] R.C. Hutton, M. Bridenne, E. Coffre, Y. Marot, F. Simonet, *J. Anal. At. Spectrom.* 5 (1990) 463.
- [11] M. Grotti, R. Frache, *J. Anal. At. Spectrom.* 22 (2007) 1481.
- [12] ISO 6142: Gas analysis – Preparation of Calibration Gas Mixtures – Gravimetric Method, International Organization for Standardization, Geneva, Switzerland, 2001.
- [13] EURACHEM Guide: The Fitness for Purpose of Analytical Methods. A Laboratory Guide to Method Validation and Related Topics, 1st ed., Eurachem, December 1998.
- [14] H.E. Taylor (Ed.), *Inductively Coupled Plasma–Mass Spectrometry: Practice and Techniques*, Academic Press, New York, 2001, pp. 151–155.
- [15] ISO, *Guide to the Expression of Uncertainty in Measurement*, International Organization for Standardization, Geneva, Switzerland, 1993.
- [16] EURACHEM, *Quantifying Uncertainty in Analytical Measurement*, 1995.



Determination of polybrominated diphenyl ethers in human hair by gas chromatography–mass spectrometry

José L. Tadeo*, Consuelo Sánchez-Brunete, Ester Miguel

Departamento de Medio Ambiente, INIA, Ctra de la Coruña, 7, 28040 Madrid, Spain

ARTICLE INFO

Article history:

Received 16 June 2008

Received in revised form 22 October 2008

Accepted 31 October 2008

Available online 11 November 2008

Keywords:

PBDEs

Hair

GC–MS–SIM

Lipids

ABSTRACT

A rapid analytical method has been developed for the determination of polybrominated diphenyl ethers (PBDEs) in human hair. PBDEs were determined by gas chromatography with electron ionization mass spectrometric detection in the selected ion monitoring mode (GC–MS–SIM). A 200 mg amount of hair samples was overnight digested in 3N HCl and then PBDEs extracted with n-hexane. After clean up of extracts in a Florisil column, PBDEs were analyzed by GC–MS. The method has been validated by spiking human hair at five concentration levels, in the range from 5 to 25 ng/g for most compounds, and PBDEs were quantified using labelled compounds as internal standards. Recoveries of PBDEs were higher than 90%, repeatability was equal or lower than 12.5%, and reproducibility lower than 14%, expressed as relative standard deviation (RSD). Limits of detection (LOD) were in the range 0.08–0.9 ng/g and limits of quantification (LOQ) were between 0.27 and 3.0 ng/g. This method was applied to the determination of PBDEs in hair samples from 16 individuals and 5 PBDE congeners were detected in most of the samples. BDE-209 was the dominant compound found, followed by BDE-47, BDE-99, BDE-100, and BDE-190. BDE-209 was found in 12 out of 16 hair samples, and the total levels of PBDEs ranged from 1.4 to 19.9 ng/g.

© 2008 Elsevier B.V. All rights reserved.

1. Introduction

Polybrominated diphenyl ethers (PBDEs) have been used worldwide as flame retardants in textiles, plastics and electronic circuits. As a consequence of this widespread use along with the persistence of these compounds, PBDEs have been found in environmental matrices as well as in human blood [1], milk [2] and adipose tissues [3,4].

Hair has been used as a bioindicator of human exposure to drugs of abuse or metals and its usefulness in the study of human exposure to some persistent organic environmental contaminants, such as organochlorine pesticides [5,6], PCBs and dioxins [7,8], has been pointed out lately.

Hair is a complex keratinous matrix with a high percentage of proteins (around 88%) and with a lipid content in the range 3–4% [5]. This chemical composition together with the easiness of sampling makes it a suitable matrix for the analysis of organic pollutants and hair has been postulated as a promising bioindicator of the human exposure to persistent contaminants [5,7].

Analytical methods for the determination of organic pollutants in hair are very scarce in the scientific literature [5–8]. Regarding the analysis of PBDEs in hair, only one paper published very recently has been found [9]. In this paper, the extraction of hair samples has been

carried out with n-hexane–acetone (3:1, v/v) by a classical Soxhlet method, which has the disadvantages of using a high volume of organic solvents and a great amount of glassware. In the analysis of other organic contaminants in hair, a miniaturized method using low volumes of extracting solvent, after an acidic or basic digestion, has been employed with good results [6,10–12].

PBDEs have been mainly determined by gas chromatography (GC) with electron capture detection (ECD) or mass spectrometry (MS), being MS preferred because it allows the simultaneous confirmation of residues by their mass spectra. Analyses of the decabromo congener, PBDE 209, the only PBDE allowed in Europe at present, requires the use of a short chromatographic column, usually 10 or 15 m length, due to the high molecular weight and low volatility of this compound [13–15].

The aim of the present work is to develop a rapid and simple method for the determination of PBDEs in human hair samples by GC–MS, based on the digestion of a low amount of hair and using low volumes of extracting solvents. This method will be applied to the determination of hair levels of PBDEs in individuals of different age and gender.

2. Experimental

2.1. Chemicals and reagents

The 14 PBDEs analyzed in this study were 2,2',4 tri-BDE (BDE-17), 2,4,4' tri-BDE (BDE-28), 2,2',4,4' tetra-BDE (BDE-47), 2,3',4,4'

* Corresponding author. Tel.: +34 91 347 6821; fax: +34 91 357 2293.
E-mail address: tadeo@inia.es (J.L. Tadeo).

tetra-BDE (BDE-66), 2,3',4,6' tetra-BDE (BDE-71), 2,2',3,4,4' penta-BDE (BDE-85), 2,2',4,4',5 penta-BDE (BDE-99), 2,2',4,4',6 penta-BDE (BDE-100), 2,2',3,4,4',5 hexa-BDE (BDE-138), 2,2',4,4',5,5' hexa-BDE (BDE-153), 2,2',4,4',5,6' hexa-BDE (BDE-154), 2,2',3,4,4',5',6 hepta-BDE (BDE-183), 2,3,3',4,4',5,6 hepta-BDE (BDE-190) and 2,2',3,3',4,4',5, 5',6, 6' deca-BDE (BDE-209). The standard solution of the PBDEs (5 µg/mL each in isoctane, except for BDE-209 25 µg/mL), purity 99%, was supplied by AccuStandard (New Haven, USA) (Code BDE-COC). The six ¹³C₁₂-labelled internal standards (5 µg/mL in nonane, purity higher than 98%) 2,4,4' tri-¹³C₁₂-BDE (BDE-28L), 2,2',4,4',5,6' hexa-¹³C₁₂-BDE (BDE-154L), 2,2',3,4,4',5',6 hepta-¹³C₁₂-BDE (BDE-183L), were supplied by Wellington Laboratories (Guelph, Ontario, Canada) (Code MBDE-MXB). The internal standard solution used to spike all the samples prior to extraction was prepared at 0.4 µg/mL level in isoctane for each component. Calibration solutions were prepared by diluting the standard solution with isoctane. These solutions were stored at 4 °C in an amber glass container in order to avoid UV degradation.

Standard solutions were made at eight levels in a concentration range 1–100 ng/g for all PBDEs, except BDE-209 which was in the concentration range 5–500 ng/g.

Ethyl acetate, isoctane, methylene chloride and n-hexane, residue analysis grade, were purchased from Scharlab (Barcelona, Spain). Florisil, a magnesium silicate adsorbent, 150–250 µm (60–100 mesh) research grade and anhydrous sodium sulphate were obtained from Merck (Darmstadt, Germany). Silica gel (230–400 mesh) was obtained from Merck (Darmstadt, Germany). Sodium hydroxide and hydrochloric acid 37%, analytical grade reagents, were purchased from Panreac (Barcelona, Spain). The Florisil adsorbent was heated overnight at 140 °C before use. A Milli-Q water purification system from Millipore (Bedford, MA, USA) was used to provide Ultrapure water in this study.

2.2. Collection of hair samples

Hair samples were obtained from 16 individuals (7 females, 2 males and 7 children), all of them living in Madrid (Spain). Adults were in the range of 24–44 years old and children ages ranged from 1 to 11 years old. Hair samples were washed with warm deionized water and shampoo. After drying with paper towel, hair was cut in small pieces, <1 cm, mixed well and stored at 4 °C until analysis.

2.3. Sample preparation and purification

A 3 mL volume of 3N hydrochloric acid was added to 200 mg of hair in a glass tube and incubated overnight at 40 °C. The acidic solution was extracted with n-hexane (4 × 2 mL) with agitation in a Vortex mixer. When a basic digestion was assayed, 3 mL of 2.5 M sodium hydroxide was added to 200 mg of hair, incubated overnight at 40 °C and the solution extracted with n-hexane (4 × 2 mL) as in the acidic digestion. The combined organic phase was concentrated with a gentle stream of air at ambient temperature in a fumehood to ~1 mL. The concentrated extract was purified in a 5 mL glass chromatographic column (5 cm × 10 mm i.d.), with a Teflon frit (1 cm diameter and 20 µm pore, Supelco, Madrid, Spain) at the end, packed with 2 g Florisil and 1 g of anhydrous sodium sulphate on top. The sample extract (1 mL) was transferred to the column and the graduated tube was washed with 2 mL of n-hexane:ethyl acetate (80:20, v/v) that were also transferred to the column. The column was placed in a multiport vacuum manifold, Supelco Visiprep (Madrid, Spain), and PBDEs eluted with n-hexane:ethyl acetate (80:20, v/v) (12 mL). The eluate was collected in a graduated tube, concentrated to dryness with a gentle stream of air at ambient temperature in a fumehood, reconstituted with 100 µL of n-hexane

and 100 µL of a solution of labelled internal standards, BDE-28L, BDE-154L and BDE-183L (1 µg/mL), transferred to a minivial and then analyzed by GC–MS–SIM.

2.4. Lipid content

Hair samples (2 g) were extracted in a Soxhlet extractor using a mixture of methanol–methylene chloride (1:1, v/v) for 24 h. After extraction, the solvent was removed on a rotary evaporator under vacuum and the percentage of lipids in hair was determined gravimetrically. The lipid content of the hair samples was in the range of 2.55–4.20%.

2.5. Apparatus

GC–MS analysis was performed with an Agilent 6890 (Waldbronn, Germany) gas chromatograph equipped with an automatic injector, Model HP 7683, and a mass spectrometric detector (MSD), Model HP 5973N, equipped with an inert ion source. The analysis of tri through deca PBDEs was carried out on a fused silica capillary column ZB-5MS, 5% phenyl polysiloxane as nonpolar stationary phase (15 m × 0.25 mm i.d. and 0.1 µm film thickness), from Phenomenex (Torrance, CA). Operating conditions were as follows: injector port temperature 300 °C; helium (purity 99.995%) as carrier gas at a flow-rate of 1.2 mL/min; pulsed splitless injection mode (pulsed pressure 45 psi = 310 kPa for 1.5 min) and a double-taper glass liner with a nominal volume of 800 µL. The column temperature was maintained at 100 °C for 1 min, then programmed at 10 °C/min to 300 °C; held for 1 min, increased to 320 °C at a rate of 8 °C/min, and held for 5 min. The total analysis time was 29.5 min and the equilibration time 2 min. A 2 µL volume was injected splitless, with the split valve closed for 1.5 min.

The mass spectrometric detector was operated in electron ionization mode with an ionizing energy of 70 eV, scanning from *m/z* 150 to 800 at 3.62 s per scan, an ion source temperature of 300 °C and a quadrupole temperature of 150 °C. The electron multiplier voltage (EM voltage) was maintained 100 V above autotune with a solvent delay of 5 min.

Table 1 lists the PBDEs and the labelled internal standards along with their retention times, selected ions and limits of detection (LOD) and quantification. The SIM program used to determine and confirm PBDEs in human hair is indicated in Table 2. The target and qualifier abundances were determined by injection of standards under the same chromatographic conditions using full-scan with the mass/charge ratio ranging from 150 to 800 *m/z*. PBDEs were confirmed by their retention times, the identification of target and qualifier ions and the determination of qualifier-to-target ratios. Retention times must be within ±0.3 min of the expected time and qualifier-to-target ratios within a 20% range for positive confirmation.

2.6. Quantification

The quantification of PBDEs was accomplished by calibration with internal labelled standards. A calibration solution was prepared with the PBDE standard solution and the labelled internal standard solution. Concentrations of PBDEs were measured by using their relative response factors to the internal standards (B-28L, B-154L and B-183L) spiked to the extracts. The linear range was established by an eight point calibration curve (1, 5, 10, 20, 25, 30, 40 and 50 µg/L) and each calibration level was spiked with 50 µg/L of B-28L, B-154L and B-183L as internal standards. For deca-PBDE, the linear range was established in the range 5–250 µg/L.

Table 1
Retention times, limits of detection and quantification (LOD, LOQ ng/g), and selected ions of the studied PBDEs.

PBDE	Name	IUPAC	t _R	LOD	LOQ	m/z ^a
1	2,2',4 tri-BDE	BDE-17	10.155	0.10	0.33	<u>246</u> , 406, 408
2	2,4,4' tri- ¹³ C ₁₂ -BDE	BDE-28L	10.517	–	–	258, <u>260</u> , 418
3	2,4,4' tri-BDE	BDE-28	10.520	0.12	0.40	<u>246</u> , 406, 408
4	2,3',4,6' tetra-BDE	BDE-71	12.286	0.09	0.30	<u>326</u> , 484, 486, 488
5	2,2',4,4' tetra-BDE	BDE-47	12.537	0.09	0.30	<u>236</u> , 484, 486, 488
6	2,3',4,4' tetra-BDE	BDE-66	12.857	0.12	0.40	<u>236</u> , 484, 486, 488
7	2,2',4,4',6 penta-BDE	BDE-100	13.971	0.08	0.27	<u>404</u> , 564, 566
8	2,2',4,4',5 penta-BDE	BDE-99	14.450	0.10	0.30	<u>404</u> , 564, 566
9	2,2',3,4,4' penta-BDE	BDE-85	15.169	0.09	0.30	<u>404</u> , 564, 566
10	2,2',4,4',5,6' hexa- ¹³ C ₁₂ -BDE	BDE-154L	15.559	–	–	<u>496</u> , 494, 656
11	2,2',4,4',5,6' hexa-BDE	BDE-154	15.560	0.12	0.40	<u>484</u> , 641, 643
12	2,2',4,4',5,5' hexa-BDE	BDE-153	16.187	0.13	0.43	<u>484</u> , 641, 643
13	2,2',3,4,4',5 hexa-BDE	BDE-138	16.910	0.16	0.53	<u>484</u> , 641, 643
14	2,2',3,4,4',5',6 hepta- ¹³ C ₁₂ -BDE	BDE-183L	17.749	–	–	<u>574</u> , 576, 733
15	2,2',3,4,4',5',6 hepta-BDE	BDE-183	17.752	0.18	0.60	<u>564</u> , 721, 723
16	2,3,3',4,4',5,6 hepta-BDE	BDE-190	18.725	0.12	0.40	<u>564</u> , 721, 723
17	2,2',3,3',4,4',5,5',6,6' deca-BDE	BDE-209	23.628	0.9	3.0	<u>400</u> , 799

^a Target ions are underlined.

Table 2
SIM program used to analyze PBDEs in hair.

Group	Time	PBDEs	m/z	Dwell time (ms)	Scan rate (cycles/s)
1	5.00	BDE-17, BDE-28, ¹³ C ₁₂ -BDE-28	246, 260, 406, 408, 418	100	1.91
2	11.30	BDE-71, BDE-47, BDE-66	326, 484, 486, 488	100	2.36
3	13.40	BDE-100, BDE-99, BDE-85	404, 564, 566	100	3.10
4	15.40	¹³ C ₁₂ -BDE-154, BDE-154, BDE-153, BDE-138	484, 494, 496, 641, 643	100	1.91
5	17.40	¹³ C ₁₂ -BDE-183, BDE-183, BDE-190	562, 564, 574, 576, 721, 723	100	1.60
6	21.50	BDE-209	400, 799	100	4.46

3. Results and discussion

3.1. Extraction of PBDEs from human hair

PBDEs may be transported to human hair via two routes, endogenous (dietary exposure) and exogenous (air transport). In order to remove external contamination due to dust or solid particles, hair was washed with shampoo and water before analyses.

The extraction of pollutants from hair has normally been done by using alkaline or acidic digestion [6,12,16]. These two procedures, acidic and basic digestion, were applied to spiked hair samples and similar recoveries >90% were obtained (Table 3). PBDE levels of blank samples were subtracted from their corresponding values obtained in the spiked samples to calculate recoveries. Assays with acidic digestion provided cleaner hair extracts with less interfering compounds than those obtained with alkaline digestion. More-

Table 3
Comparison of recoveries^a of PBDEs with acidic and basic digestion.

PBDEs	Acidic digestion	Basic digestion
BDE-17	99 ± 6	102 ± 7
BDE-28	101 ± 6	105 ± 4
BDE-71	97 ± 6	99 ± 9
BDE-47	96 ± 4	105 ± 8
BDE-66	91 ± 6	109 ± 9
BDE-100	96 ± 3	99 ± 5
BDE-99	98 ± 4	106 ± 5
BDE-85	101 ± 5	95 ± 7
BDE-154	98 ± 6	96 ± 5
BDE-153	96 ± 3	104 ± 6
BDE-138	94 ± 7	92 ± 8
BDE-183	91 ± 4	89 ± 5
BDE-190	102 ± 4	106 ± 9
BDE-209	91 ± 8	91 ± 10

^a Results are the mean of four replicates ± standard deviation at 50 ng/g fortification level (250 ng/g BDE-209).

over, it has been reported that alkaline digestion can cause the degradation of some halogenated compounds such as organochlorine pesticides [17], although this effect was not observed in the PBDEs studied. Dichloromethane and n-hexane, which have been used with good results in previous works on analyses of pollutants in hair [5–7,12,17], were evaluated as extracting solvents. Extraction with dichloromethane resulted in somewhat low recoveries of some PBDEs (<80%) due to the formation of emulsions. Extraction with n-hexane produced good recoveries (>90%), higher than those obtained with dichloromethane. Therefore, acidic digestion followed by extraction with n-hexane was used for the extraction of PBDEs from hair.

Hair samples contain lipids that may cause interferences in the GC analysis and it is convenient to remove them. For this reason, a purification of extracts using a column containing appropriate sorbents has been used by several authors as clean up method [6,7]. Florisil, alumina, and silica gel have been evaluated for the clean up of extracts with various solvents of different polarity. In general, hexane, dichloromethane and their binary mixtures in different proportions have been found to provide the best recoveries for PCBs and organochlorine pesticides [5,17,18]. Good recoveries (>85%) and clean extracts were obtained by other authors using Florisil or silica gel as adsorbents. In our work, the use of Florisil as adsorbent and n-hexane:ethyl acetate (80:20, v/v) as eluting solvent produced clean extracts and good recovery results (Table 3).

3.2. Gas chromatographic determination

PBDEs were determined by gas chromatography–mass spectrometry with selected ion monitoring (GC–MS–SIM). Table 1 lists the PBDEs along with their retention times, and their target and qualifier ions. The SIM program used in the PBDEs analyses is indicated in Table 2. Fig. 1A shows a representative GC–MS–SIM chromatogram of a standard mixture solution containing 10 µg/L of PBDEs (50 µg/L of BDE-209).

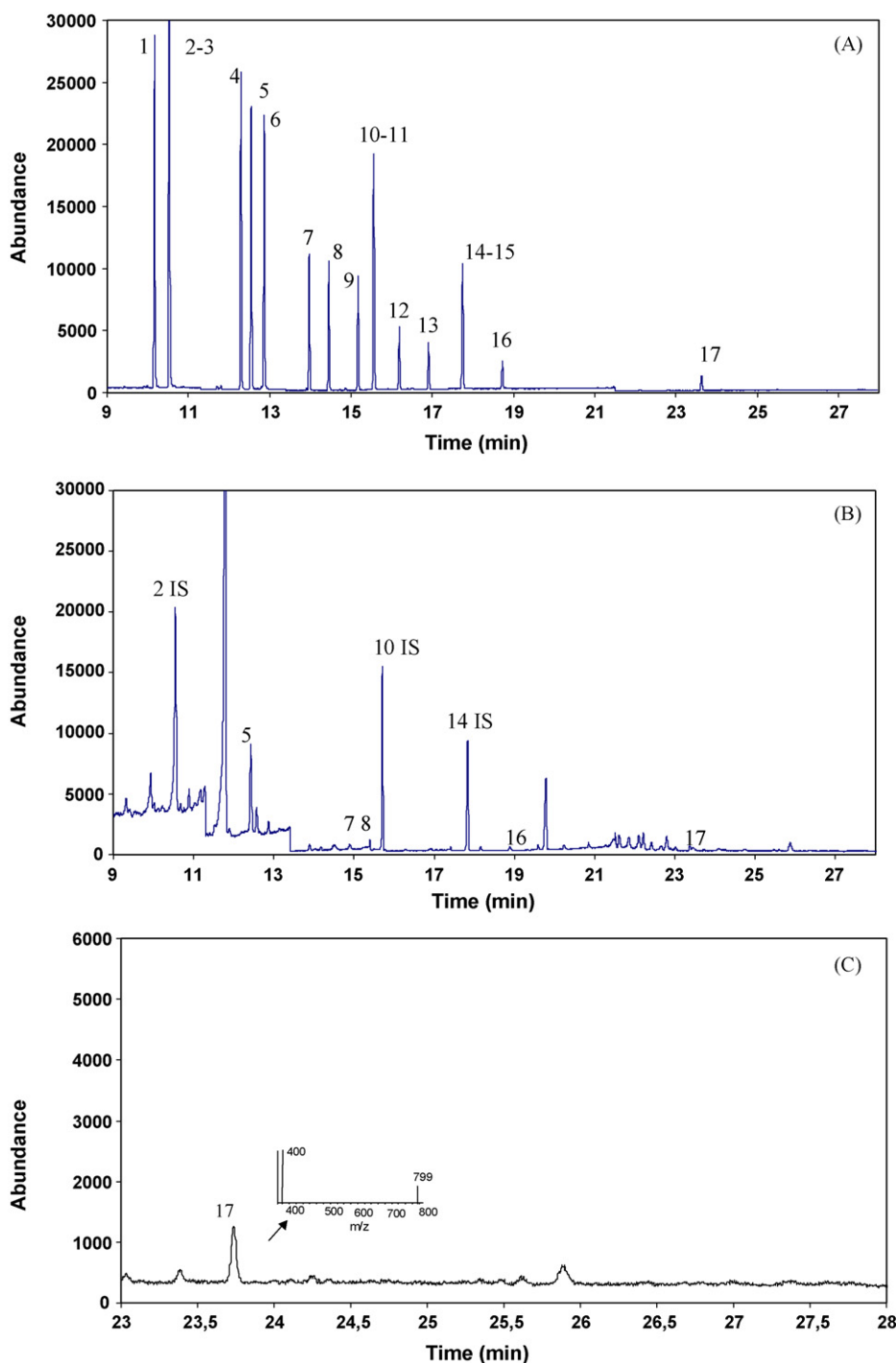


Fig. 1. (A) GC-MS-SIM chromatogram of a PBDEs standard solution containing 10 $\mu\text{g/L}$ (50 $\mu\text{g/L}$ BDE-209). (B) GC-MS-SIM chromatogram of a human hair extract. (C) GC-MS-SIM chromatogram of BDE-209 (4.20 $\mu\text{g/g}$) with the main ions of the mass spectrum obtained from a human hair extract. See Table 1 for peak identification.

3.3. Validation of the method

A multipoint calibration with eight standard solutions at different concentration levels, appropriate to the levels found in hair samples, was used. The internal standard was added to the sample prior to analysis and the concentration of the labelled standard mixture was 50 $\mu\text{g/L}$ for all points. A good linearity of the calibrations curve was obtained in the range 1–50 $\mu\text{g/L}$ for the analysis of tri through hepta PBDEs or 5–250 $\mu\text{g/L}$ for deca PBDE. The correlation coefficient was equal or higher than 0.997 for the

PBDEs analyzed. The analytical data, linearity, correlation coefficient and regression equations of the calibration curve are listed in Table 4.

The repeatability of the chromatographic determination was determined by performing the analysis of a standard solution at 50 $\mu\text{g/L}$. The sample was injected 10 times with an automatic injector and the relative standard deviation (RSD) values obtained for the retention times ranged from 0.006 to 0.014%, whereas for peak areas the values ranged from 5.2 to 12.5% (Table 4). Within-laboratory reproducibility of the chromatographic determination, expressed

Table 4
Calibration data and repeatability^a of the studied PBDEs.

PBDEs	Calibration data		Repeatability (RSD, %) ^b	
	Equation	r	Peak area	t _R
BDE-17	$y = 2.10x + 1.45 \times 10^{-2}$	0.999	7.4	0.014
BDE-28	$y = 1.61x + 1.67 \times 10^{-2}$	0.999	6.8	0.014
BDE-71	$y = 2.38x + 4.21 \times 10^{-2}$	0.998	5.2	0.010
BDE-47	$y = 1.50x + 2.01 \times 10^{-2}$	0.999	8.2	0.011
BDE-66	$y = 1.79x + 2.76 \times 10^{-2}$	0.999	6.4	0.010
BDE-100	$y = 9.17 \times 10^{-1}x + 1.09 \times 10^{-2}$	0.999	7.8	0.008
BDE-99	$y = 1.05x + 3.82 \times 10^{-3}$	0.999	7.6	0.009
BDE-85	$y = 9.73 \times 10^{-1}x + 4.24 \times 10^{-3}$	0.999	6.2	0.009
BDE-154	$y = 1.55x + 4.49 \times 10^{-2}$	0.999	7.2	0.011
BDE-153	$y = 1.49x + 6.47 \times 10^{-3}$	0.998	8.5	0.007
BDE-138	$y = 1.13x + 4.67 \times 10^{-3}$	0.997	7.7	0.008
BDE-183	$y = 1.01x + 6.26 \times 10^{-2}$	0.997	8.8	0.008
BDE-190	$y = 6.59 \times 10^{-1}x + 2.29 \times 10^{-2}$	0.999	7.3	0.008
BDE-209	$y = 4.05 \times 10^{-1}x + 2.73 \times 10^{-2}$	0.997	12.5	0.006

^a Repeatability of the chromatographic method.^b RSD of retention times and peak areas ($n = 10$).**Table 5**
Recoveries^a of the studied PBDEs from human hair.

PBDEs	Fortification levels (ng/g)		
	25	10	5
BDE-17	99 ± 5	94 ± 6	104 ± 2
BDE-28	91 ± 9	102 ± 5	103 ± 4
BDE-71	92 ± 5	98 ± 4	101 ± 1
BDE-47	96 ± 7	105 ± 6	104 ± 1
BDE-66	95 ± 6	104 ± 7	98 ± 5
BDE-100	91 ± 3	99 ± 5	91 ± 4
BDE-99	92 ± 4	104 ± 2	92 ± 5
BDE-85	104 ± 4	95 ± 7	101 ± 5
BDE-154	91 ± 6	99 ± 5	94 ± 6
BDE-153	95 ± 5	104 ± 6	96 ± 5
BDE-138	90 ± 7	96 ± 6	98 ± 4
BDE-183	91 ± 6	100 ± 4	102 ± 2
BDE-190	94 ± 7	101 ± 9	101 ± 3
BDE-209 ^b	92 ± 9	91 ± 9	86 ± 7

^a Results are the mean of four replicates ± standard deviation.^b DE-209 levels were in the range 25–125 ng/g.

as relative standard deviation, was evaluated for 2 weeks and it was lower than 14% for all of the compounds.

The efficacy of the extraction procedure was tested for human hair samples to determine the precision of the analytical procedure for the PBDEs studied. Known amounts of tri through hepta PBDEs (5, 10 and 25 ng/g) and (25, 50 and 125 ng/g) for deca-PBDE were added to four sample replicates. These enriched samples were extracted and analyzed with the method described above. Unspiked "blank" samples were previously analyzed to determine the possible presence of PBDEs and the contribution of each PBDE in the "blank" sample was subtracted from the corresponding value obtained in spiked samples to calculate the recovery values. The recoveries obtained for the spiked samples ranged between 86 and 105% (Table 5), thus fulfilling the requirements of the IUPAC [19].

Low limits of detection and quantification (LOQs), defined as the concentration that would result in a signal-to-noise ratio (S/N) of 3:1 and 10:1, respectively, were obtained due to the selectivity of the analytical procedure and the high sensitivity of GC–MS–SIM, allowing the determination of PBDEs at the levels found in hair samples. The LODs and LOQs corresponding to the different PBDEs are shown in Table 1. The range of LODs obtained was similar to those obtained for the determination of other compounds like PCBs and organochlorine pesticides in human hair [6,17].

3.4. Analysis of PBDEs in human hair

The developed method was applied to the determination of PBDEs in human hair samples obtained from nine adults (seven woman, with ages ranging from 24 to 44 years old, and two men of 23 and 32 years old) and seven children from 1 to 11 years old. In Tables 6 and 7, the individual hair levels of the 9 adults and the 7 children are presented. Five PBDEs were quantified in most of the

samples and the concentration reported for each compound was the average of four replicates. The total content of PBDEs found in hair was in the range from 3.2 to 11.1 ng/g for women, from 7.8 to 19.9 ng/g for men and from 1.4 to 8.3 ng/g hair for children. These values were compared with those reported very recently in the only one paper found in the scientific literature [9]. In this paper, a study was conducted to determine the hair levels of PBDEs and other poly-halogenated aromatic hydrocarbons in Chinese residents in several electronic waste disassembly sites. For the sites where PBDE 209 levels were available the mean reported values ranged from 10.15 to 18.23 ng/g, which are similar, although in the higher range, to those found for adults in our work. They also found a very high frequency of PBDE 209 in hair samples from two sites, where it was the predominant PBDE congener. In our work, PBDE content, expressed in ng/g fat, varied from 34 to 629 ng/g, in a similar range, although somewhat higher, than the levels found in breast adipose samples, which varied from 17 to 462 ng/g [3,18]. A representative chromatogram of a hair sample and the corresponding ion chromatogram of BDE-209 (4.20 μg/g) with the main ions of its mass spectrum are depicted in Fig. 1B and C.

The PBDEs congeners found in most samples were BDE-47, BDE-99, BDE-100, BDE-190 and BDE-209. The deca-BDE was the prominent compound detected in almost all hair samples from adults, with a concentration in the range of 3.4–12.9 ng/g hair. The distribution of the total PBDE content among the different congeners found in hair from adults and children samples is depicted in Fig. 2. Although the PBDE profile was similar in all the studied samples, two additional compounds (BDE-138 and BDE-183) were detected in some hair samples from children (Table 7). The composition of PBDE congeners was dominated by BDE-209, and this may be due to the banning of the penta-BDE and octa-BDE mixtures, being the BDE-209 the only PBDE allowed in the EU at

Table 6
Concentrations of PBDEs in human hair collected from 9 adults^a.

PBDEs	1 F	2 F	3 F	4 F	5 F	6 F	7 F	1 M	2 M
BDE-47	0.55 ± 0.01	3.9 ± 0.7	0.51 ± 0.01	0.31 ± 0.03	0.81 ± 0.06	0.31 ± 0.06	0.6 ± 0.1	1.6 ± 0.3	2.1 ± 0.1
BDE-100	0.38 ± 0.08	0.8 ± 0.2	0.5 ± 0.1	0.37 ± 0.04	0.32 ± 0.07	0.68 ± 0.07	1.34 ± 0.01	0.30 ± 0.02	1.63 ± 0.05
BDE-99	0.85 ± 0.01	1.8 ± 0.4	0.57 ± 0.04	0.30 ± 0.03	0.60 ± 0.03	0.34 ± 0.07	0.96 ± 0.04	1.3 ± 0.2	2.1 ± 0.1
BDE-190	0.42 ± 0.06	0.6 ± 0.2	0.4 ± 0.2	0.49 ± 0.02	1.1 ± 0.1	0.6 ± 0.2	0.6 ± 0.3	0.50 ± 0.08	1.21 ± 0.06
BDE-209	8.5 ± 0.5	3.6 ± 0.4	3.4 ± 0.2	4.5 ± 0.4	4.6 ± 0.5	1.3 ± 0.2	7.5 ± 0.6	4.2 ± 0.6	12.9 ± 0.8
ΣPBDEs ng/g hair	10.7 ± 0.6	10.7 ± 0.7	5.4 ± 0.3	6.1 ± 0.5	7.4 ± 0.8	3.2 ± 0.6	11.1 ± 0.9	7.8 ± 0.9	19.9 ± 1.2
ΣPBDEs ng/g fat	419 ± 24	330 ± 20	189 ± 12	182 ± 14	193 ± 22	75 ± 13	372 ± 29	293 ± 34	629 ± 36

F: female, M: male. Total content of PBDEs is expressed in ng/g hair and ng/g fat.

^a Results are the mean of four replicates. Adults were in the range of 24–44 years old.

Table 7
Concentrations of PBDEs in human hair collected from seven children^a.

PBDEs	1	2	3	4	5	6	7
BDE-47	0.52 ± 0.08	0.53 ± 0.05	0.38 ± 0.05	0.51 ± 0.05	0.37 ± 0.04	0.31 ± 0.02	0.65 ± 0.04
BDE-100	0.41 ± 0.08	0.37 ± 0.07	0.33 ± 0.03	0.32 ± 0.02	0.58 ± 0.07	0.30 ± 0.04	0.31 ± 0.06
BDE-99	0.9 ± 0.2	0.88 ± 0.06	0.33 ± 0.06	0.8 ± 0.1	0.52 ± 0.03	0.38 ± 0.05	1.22 ± 0.08
BDE-138	0.44 ± 0.06	0.8 ± 0.2	n.d.	n.d.	n.d.	n.d.	0.6 ± 0.1
BDE-183	0.24 ± 0.05	n.d.	0.28 ± 0.06	n.d.	n.d.	n.d.	n.d.
BDE-190	0.7 ± 0.1	0.5 ± 0.1	0.34 ± 0.07	0.6 ± 0.1	0.51 ± 0.07	0.42 ± 0.05	0.48 ± 0.08
BDE-209	5.1 ± 0.4	4.5 ± 0.4	3.6 ± 0.2	3.9 ± 0.3	n.d.	n.d.	n.d.
ΣPBDEs ng/g hair	8.3 ± 0.6	7.5 ± 0.7	5.3 ± 0.3	6.1 ± 0.5	2.0 ± 0.2	1.4 ± 0.2	3.2 ± 0.2
ΣPBDEs ng/g fat	324 ± 22	235 ± 21	137 ± 7	204 ± 16	61 ± 7	34 ± 4	97 ± 6

Total content of PBDEs is expressed in ng/g hair and ng/g fat. n.d.: <method detection limit.

^a Results are the mean of four replicates. Children were in the range of 1–11 years old.

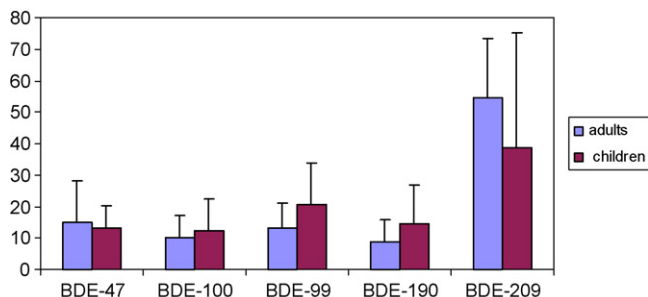


Fig. 2. Percentage of PBDE congeners in adults and children hair.

present [20]. In general, BDE-209 has been determined in a few other studies in human samples [1,21], probably because of its difficult determination due to its low volatility and high molecular weight. BDE-99 is the following congener in importance found in hair, which is agreement with the results reported on PBDE levels in hair of the European hedgehog [22]. This fact may be explained, in accordance to that paper, by the direct transport of unaltered BDE-99 to external tissues. Moreover, a significant relationship was reported in the cited paper between PBDE concentration in hair and endogenous tissues, which indicates that hair may be used in biomonitoring as an indicator of endogenous concentrations. BDE-190 was detected in all samples and, although this congener has not been previously reported in human hair, it has been found in sludge and aquatic organisms [23,24]. The main prominent congener found in other human samples is BDE-47 [3], as a consequence of the metabolism of higher molecular congeners.

4. Conclusions

A rapid and sensitive gas chromatography–mass spectrometric method using a short silica capillary column has been developed to determine 14 PBDEs in human hair. The use of mass spectrometry in the mode of selected ion monitoring allows the quantification and confirmation of residues down to 0.27–3 ng/g, according to the different PBDEs studied, which makes the GC–MS–SIM method suitable for the analysis of PBDEs at the low levels found in hair. Validation of the method was carried out by spiking human hair in the range of expected values and PBDEs were quantified using labelled compounds as internal standards. The developed method

was applied to the analysis of human hair obtained from individuals with different age and genre. In the examined hair samples, BDE-290 was the prominent congener detected in most cases, followed by BDE-99, BDE-47, BDE-190 and BDE-100. The total content of PBDEs found was in the range of 1.4–19.9 ng/g hair.

Acknowledgements

This study was financed by the Ministry of Education and Science–National Institute for Agricultural and Food Research and Technology, INIA, Project number RTA 2005-00090. We thank Mr. Felipe Fernandez for his help with the preparation of samples. Also, we would like to thank donors for providing hair samples.

References

- [1] R.A. Hites, Environ. Sci. Technol. 38 (2004) 945.
- [2] M. Schuhmacher, H. Kivirata, T. Vartiainen, J.L. Domingo, Chemosphere 67 (2007) S295.
- [3] J. She, M. Petreas, J. Winkler, P. Visita, M. McKinney, D. Kopec, Chemosphere 46 (2002) 697.
- [4] B. Gomara, L. Herrero, L.R. Bordajandi, M.J. González, Rapid Commun. Mass Spectrom. 20 (2006) 69.
- [5] A. Covaci, P. Schepens, Chromatographia 53 (2001) 366.
- [6] A. Covaci, M. Tutudaki, A.M. Tsatsakis, P. Schepens, Chemosphere 46 (2002) 413.
- [7] T. Nakao, O. Aozasa, S. Ohta, H. Miyata, Arch. Environ. Contam. Toxicol. 49 (2005) 124.
- [8] K.-W. Schramm, T. Kuettnner, S. Weber, K.L. Westfalischer, Chemosphere 24 (1992) 351.
- [9] G. Zhao, Z. Wang, M.H. Dong, K. Rao, J. Luo, D. Wang, J. Zha, S. Huang, Y. Xu, M. Ma, Sci. Total Environ. 397 (2008) 46.
- [10] T. Nakao, O. Aozasa, S. Ohta, H. Miyata, Chemosphere 48 (2002) 885.
- [11] K. Neuber, G. Merkel, F.E. Randow, Toxicol. Lett. 107 (1999) 189.
- [12] A. Toriba, Y. Kuramae, T. Chetianukornkul, R. Kizu, T. Makino, H. Nakazawa, K. Hayakawa, Biomed. Chromatogr. 17 (2003) 126.
- [13] M. Song, S. Chu, R.J. Letcher, R. Seth, Environ. Sci. Technol. 40 (2006) 6241.
- [14] U. Sellstrom, C.A. De Wit, N. Lundgren, M. Tysklind, Environ. Sci. Technol. 39 (2005) 9064.
- [15] A. Binelli, C. Roscioli, L. Guzzella, J. Chromatogr. A 1136 (2006) 243.
- [16] Y. Nakahara, J. Chromatogr. B 733 (1999) 161.
- [17] L. Altshul, A. Covaci, R. Hauser, Environ. Health Perspect. 112 (2004) 1193.
- [18] L. Zupancic-Kralj, J. Jan, J. Marsel, Chemosphere 22 (1992) 1861.
- [19] M. Thompson, S. Ellison, A. Fajgely, P. Willets, R. Wood, Pure Appl. Chem. 74 (2002) 835.
- [20] Directive 2003/11/EC European Parliament Report Official Journal L 042 15/02/2003.
- [21] C. Thonmsen, V. Horpestad, G. Becher, J. Chromatogr. B 846 (2007) 252.
- [22] H.D. Havé, A. Covaci, J. Scheirs, P. Schepens, R. Verhagen, W. De Coen, Environ. Sci. Technol. 39 (2005) 6016.
- [23] R.C. Hale, M. Alaea, J.B. Manchester-Neesvig, H.M. Stapleton, M.G. Ikonoumou, Environ. Int. 29 (2003) 771.
- [24] K.D. North, Environ. Sci. Technol. 38 (2004) 4484.



Arsenic speciation in natural water samples by coprecipitation-hydride generation atomic absorption spectrometry combination

Mustafa Tuzen^a, Demirhan Çıtak^a, Durali Mendil^a, Mustafa Soylak^{b,*}

^a Gaziosmanpaşa University, Faculty of Science and Arts, Chemistry Department, 60250 Tokat, Turkey

^b Erciyes University, Faculty of Art and Science, Department of Chemistry, 38039 Kayseri, Turkey

ARTICLE INFO

Article history:

Received 21 July 2008

Received in revised form 19 October 2008

Accepted 24 October 2008

Available online 31 October 2008

Keywords:

Arsenic

Speciation

Preconcentration

Coprecipitation

Hydride generation atomic absorption spectrometry

ABSTRACT

A speciation procedure for As(III) and As(V) ions in environmental samples has been presented. As(V) was quantitatively recovered on aluminum hydroxide precipitate. After oxidation of As(III) by using dilute KMnO_4 , the developed coprecipitation was applied to determination of total arsenic. Arsenic(III) was calculated as the difference between the total arsenic content and As(V) content. The determination of arsenic levels was performed by hydride generation atomic absorption spectrometry (HG-AAS). The analytical conditions for the quantitative recoveries of As(V) including pH, amount of aluminum as carrier element and sample volume, etc. on the presented coprecipitation system were investigated. The effects of some alkaline, earth alkaline, metal ions and also some anions were also examined. Preconcentration factor was calculated as 25. The detection limits (LOD) based on three times sigma of the blank ($N: 21$) for As(V) was $0.012 \mu\text{g L}^{-1}$. The satisfactory results for the analysis of arsenic in NIST SRM 2711 Montana soil and LGC 6010 Hard drinking water certified reference materials for the validation of the method was obtained. The presented procedure was successfully applied to real samples including natural waters for arsenic speciation.

© 2008 Elsevier B.V. All rights reserved.

1. Introduction

Elements at trace levels have negative and positive functions at various systems in human body [1–3]. Arsenic is known to cause negative effects in the human body even at a low intake level [4,5]. Arsenic is widely distributed in the environment [6]. Arsenic is mainly used for production of pesticides, plant desiccants, and wood preservatives [6]. The toxicity of arsenic depends on its binding form. Inorganic forms of arsenic are more toxic than organic species, with arsenic(III) being more toxic than arsenic(V) [7,8]. As(V) can replace phosphate in several biochemical reactions, whereas As(III) may react with critical thiols in proteins and inhibit their activity [9]. Acute and chronic poisoning involves the respiratory, gastro-intestinal, conjunctivitis, hyperkeratosis, hyperpigmentation, cardiovascular diseases, disturbance in the peripheral vascular and nervous systems [8,10]. Arsenic is carcinogenic and may cause lung cancer, bladder cancer, liver cancer, renal cancer, and skin cancer [8]. Because of its toxicity and possible carcinogenicity, it is important to speciation of arsenic(V) and

arsenic(III) in environmental samples including natural waters and biological fluids.

The direct determination of arsenic species by instrumental analytical techniques like atomic absorption spectrometry, inductively coupled plasma optical emission spectrometry, etc. is not possible [11–16]. The determination of arsenic species by these instrumental techniques is possible by applying sample treatment procedures including solvent extraction, solid phase extraction, coprecipitation and cloud point extraction, etc. prior to determination step [17–25]. These procedures are generally two steps. In the first step, one species of arsenic quantitatively recovered, other species is not. In the second step, the species not quantitatively recovered is reduced or oxidized to quantitatively recovered species. Then the first step is applied to this sample. At second step, total element concentration is determined. The difference of second step to first step gives the levels of the species that is not quantitatively recovered. Our procedure is based on coprecipitation of arsenic(V) on the precipitate of aluminum(III) hydroxide while arsenic(III) is not coprecipitation at the our working conditions.

In the presented work, a method for the determination of arsenic(III), arsenic(V) and total arsenic in environmental samples by HG-AAS has been established. The analytical parameters for the quantitative recoveries of arsenic species were investigated.

* Corresponding author. Tel.: +90 352 4374933; fax: +90 352 4374933.

E-mail addresses: soylak@erciyes.edu.tr, msoylak@gmail.com (M. Soylak).

2. Experimental

2.1. Instrument

A PerkinElmer AAnalyst 700 atomic absorption spectrometer equipped with MHS-15 Mercury/Hydride System was used in this study. All measurements were carried out using high purity argon. A hollow cathode lamp operating at 18 mA was used and a spectral bandwidth of 0.7 nm was selected to isolate the 193.7 nm arsenic line. Peak height was used for quantitation [26].

A pH meter, Sartorius pp-15 Model glass-electrode was employed for measuring pH values in the aqueous phase. Nuve model NF 800 centrifuge was used to centrifuge of solutions. Milestone Ethos D closed vessel microwave system (maximum pressure 1450 psi, maximum temperature 300 °C) was used. Digestion conditions for microwave system for the samples were applied as 2 min for 250 W, 2 min for 0 W, 6 min for 250 W, 5 min for 400 W, 8 min for 550 W, ventilation: 8 min [27–29].

2.2. Reagents and solutions

All chemicals used in this work, were of analytical reagent grade and were used without further purification. Deionized water (Milli-Q Millipore 18.2 M Ω cm⁻¹, resistivity) was used for all dilutions. Laboratory glassware was kept overnight in a 10% (v/v) HNO₃ solution and then rinsed with deionized double distilled water.

A 1000 mg L⁻¹ stock solution of As(III) was prepared by As₂O₃ (Merck). Similarly, a 1000 mg L⁻¹ stock solution of As(V) was prepared by dissolving KH₂AsO₄ (Sigma). Accurately diluted solutions of As(III) and As(V) were prepared daily using standard stock solutions. The calibration curve was established using the standard solutions prepared in 1 mol L⁻¹ HNO₃ by dilution from stock solutions. The calibration curve solutions were prepared daily. The calibration standards were not submitted to the preconcentration procedure. Stock solutions of diverse elements were prepared from high purity compounds.

NaBH₄ (0.3%) (w/v) in NaOH (0.1%) (w/v) was prepared. 0.75 g KI and 1.25 g (+) ascorbic acid in 100 mL water was dissolved. 0.01 M KMnO₄ was prepared in water. These solutions were prepared fresh daily.

Phosphate buffer solution (H₂PO₄⁻/H₃PO₄) were prepared by mixing of appropriate volumes of 1 mol L⁻¹ sodium dihydrogen phosphate and phosphoric acid solutions for pH 2. Acetate buffer solutions (CH₃COO⁻/CH₃COOH) were prepared by mixing of appropriate volumes of 1 mol L⁻¹ acetic acid and 1 mol L⁻¹ sodium acetate solutions for pH 4. Phosphate buffer solutions (H₂PO₄⁻/HPO₄²⁻) were prepared by mixing of appropriate volumes of 1 mol L⁻¹ sodium dihydrogen phosphate and 1 mol L⁻¹ sodium hydrogen phosphate for pH 5 and 6. Ammonium buffer solutions were prepared by mixing of appropriate amounts of 1 mol L⁻¹ ammonia and 1 mol L⁻¹ ammonium chloride solutions for pH 8–10.

2.3. Analytical procedure for As(V)

The Al(OH)₃ coprecipitation method for arsenic speciation was tested firstly with model solutions. One ml of 1% (w/v) Al³⁺ from Al(NO₃)₃ solution was added to 20 mL of solution containing 0.25 μ g of As(V). Then the pH of the solution was adjusted related pH by the addition of related buffer solution. After 10 min for the formation of aluminum hydroxide precipitate, the solution was centrifuged at 2750 rpm for 10 min. The supernatant was removed. The precipitate remained adhering to the tube was dissolved with 0.5 mL of concentrated HCl. The last volume was completed to 10.0 mL with distilled water. The number of replicates for the test

workings was three. Arsenic contents of the solutions were determined by hydride generation atomic absorption spectrometry. For this, samples were pre-reduced from As(V) to As(III) by adding 0.75% KI and 1.25% ascorbic acid [24,25]. Then for arsenic quantification, 1 mL sample was pipetted into a 50 mL volumetric flask where 10 mL of 1.5% HCl was added as diluent. NaBH₄ (0.3%) (w/v) in NaOH (0.1%) (w/v) was used as reducing agent. The analytical measurement was based on peak height. Reading time and argon flow rate was selected as 20 s and 70 mL min⁻¹.

2.4. Oxidation of As(III) to As(V) and determination of total arsenic

To oxidation of As(III) to As(V), the procedure given in literature [24,26] was applied to model solutions and natural water samples. 0.2 mL of 10⁻² M KMnO₄ solution was added to model solution containing 0.25 μ g of As(III) and 0.25 μ g of As(V). After oxidation of As(III) to As(V), the method given in Section 2.3 was applied to the determination of the total arsenic. The levels of arsenic were determined by hydride generation atomic absorption spectrometry. The level of As(III) is calculated by difference of total arsenic and As(V) concentrations.

2.5. Applications

Natural water samples and LGC 6010 Hard drinking water were filtered through Millipore cellulose membrane filter (0.45 μ m pore size). The pH of the samples was adjusted to 9.0 with buffer solution. Then the procedures given in Sections 2.3 and 2.4 were applied to the final solutions. Blank samples were also analyzed. The levels of analyte ions in the samples were determined by hydride generation atomic absorption spectrometry.

NIST SRM 2711 Montana soil (250 mg), sediment from Green river in Tokat city and soil from Tokat city (1.0 g) were digested with 6 mL of concentrated HCl, 2 mL of concentrated HNO₃ and 0.5 mL of concentrated HF in microwave digestion system and diluted to 50 mL with deionized water. The blanks were prepared in the same way as the sample, but omitting the sample. The preconcentration procedure given above was applied to the samples.

To digestion edible mushroom (*Calvatia utriformis*), rice and sausage samples, 1.0 g of sample was digested with 6.0 mL of concentrated HNO₃ and 2.0 mL of H₂O₂ in microwave system. After digestion the samples, the volume of the digested sample was made up to 25.0 mL with distilled water. The blanks were prepared in the same way as the sample, but omitting the sample. The procedures given above were applied to the samples.

3. Results and discussion

The influences of aluminum(III) on the signal of arsenic(III) on hydride generation atomic absorption spectrometric determinations of arsenic species without any pre-treatment. Due to the signals of arsenic in the HGAAS determinations were stable till 25 g L⁻¹ aluminum(III), the concentration of aluminum(III) ions in the final solution for the combination of coprecipitation method with HGAAS must to be exceeded 25 g L⁻¹.

3.1. Effects of pH

The influences of pH of the sample solution on the recoveries of arsenic(III) and arsenic(VI) ions were separately investigated in the pH range of 2.0–10.0 by adjusting pH of the model solutions with buffers given in Section 2. The results for this study were depicted in Fig. 1. Arsenic(V) was quantitatively coprecipitated in the pH range of 8.0–10.0, while arsenic(III) was recovered lower than 10%

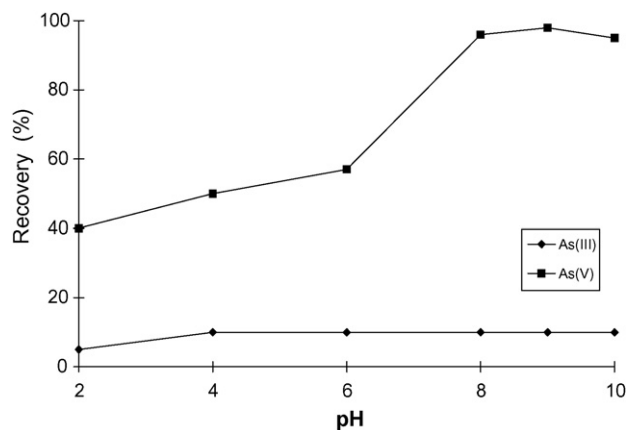


Fig. 1. Relation between pH and arsenic species ($N=3$).

at the all pHs worked. This situation shows that the speciation of arsenic(V) and arsenic(III) is possible at the pH range of 8.0–10.0 by the presented work. For all subsequent coprecipitation works for arsenic(V), pH 9.0 was used.

3.2. Effects of amount of aluminum(III) as carrier element on the recoveries of As(V) on the precipitation

The influences of amounts of aluminum(III) as carrier element on the recoveries of arsenic(V) were also investigated. The results are depicted in Fig. 2. Without aluminum, the recovery for arsenic(V) was below 5% on the presented coprecipitation system. Quantitative recovery values (>95%) for the arsenic(V) ions were obtained for all analyte ions in 1.0–4.0 mg of aluminum(III) as carrier element. All further works were performed with 1 mg (1 mL of 1000 mg L⁻¹) of aluminum(III) ions.

3.3. Effects of sample volume

Due to obtain high preconcentration factor, volume of the sample solution is an important parameter, the effects of the sample volume on the coprecipitation efficiencies of arsenic(V) were examined. Arsenic(V) was quantitatively recovered in the sample volume range of 10–50 mL under optimal working conditions. The precipitate including analytes was successfully dissolved 1.0 mL of concentrated HCl. The final volume was completed to 2.0, 5.0 or

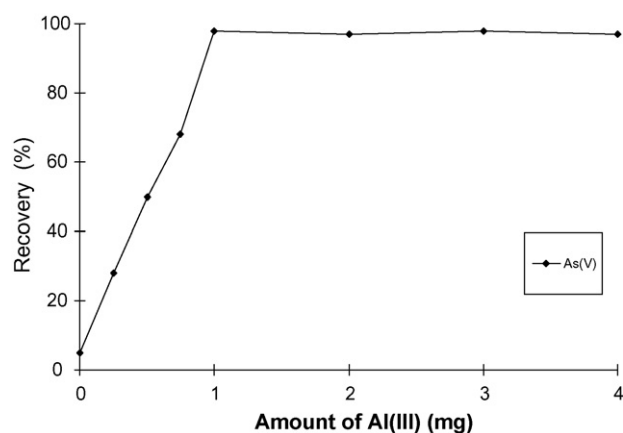


Fig. 2. Influences of amounts of aluminum(III) as carrier element on the quantitative coprecipitation of As(V) (pH: 9, $N=3$).

Table 1
Influences of some foreign ions on the recoveries of As(V), ($N=3$).

Ion	Added as	Concentration (mg L ⁻¹)	Recovery %
Na ⁺	NaCl	20,000	95 ± 3
K ⁺	KCl	5,000	98 ± 2
Ca ²⁺	CaCl ₂	5,000	99 ± 3
Mg ²⁺	MgCl ₂	5,000	100 ± 2
Cl ⁻	NaCl	50,000	98 ± 3
F ⁻	NaF	1,000	95 ± 2
NO ₃ ⁻	KNO ₃	3,000	95 ± 3
SO ₄ ²⁻	Na ₂ SO ₄	5,000	98 ± 2
PO ₄ ³⁻	Na ₃ PO ₄	3,000	95 ± 3
Mn ²⁺	MnSO ₄	50	100 ± 2
Fe ³⁺	FeCl ₃	50	99 ± 2
Cu ²⁺	CuSO ₄	50	95 ± 3
Pb ²⁺	Pb(NO ₃) ₂	50	99 ± 2
Zn ²⁺	ZnSO ₄	50	98 ± 4
Cd ²⁺	Cd(NO ₃) ₂	50	100 ± 2
Ni ²⁺	NiSO ₄	50	98 ± 3
Cr ³⁺	Cr(NO ₃) ₃	50	95 ± 2
As ³⁺	As ₂ O ₃	250	95 ± 2

10.0 mL by deionized double distilled water. The analytes were quantitatively recovered in these studies. The preconcentration factor is calculated by the ratio of the highest sample volume (50 mL) for each analytes and the lowest final volume (2 mL). The preconcentration factor for analytes was 25.

3.4. Interference studies

In order to assess the possible analytical applications of presented coprecipitation procedure for arsenic speciation, the effect of some foreign ions in various real samples was examined with the optimized conditions at above. The recoveries of analyte ions were generally higher than 95%. Tolerable limit was defined as the highest amount of foreign ions that produced an error not exceeding 5% in the determination of analytes by the combination of the coprecipitation method presented and the hydride generation atomic absorption spectrometric determination methods. The results are summarized in Table 1. The tolerable levels of the some heavy metal ions given in Table 1 are suitable for the separation and preconcentration of arsenic(V) in the real samples. It can be seen that the major matrix ions in the food and natural waters show no obvious interference with the preconcentration of arsenic(V) ions.

3.5. Determination of total arsenic

Test solutions that contain different amounts of arsenic(V) and arsenic(III) were prepared to determination of total arsenic. Then oxidation procedure given experimental for arsenic(III) ions to arsenic(V) was applied. Then the presented coprecipitation procedure was applied to these solutions. The results are summarized in Table 2. The quantitative recovery values for total arsenic were obtained. The results show that the proposed coprecipitation method could be applied for the determination of total arsenic in aqueous solutions.

3.6. Analytical performance

The detection limit (LOD) of As(V) was calculated under optimal experimental conditions. The limit of detection for As(V) based on three times the standard deviations of the blank ($k=3$, $N=21$) was 0.012 µg L⁻¹. The precision of the determination of As(V) was evaluated under the optimum conditions mentioned in Section 2.3. For this purpose, the procedure was repeated ten times for As(V) with model solutions containing 0.25 µg of As(V). The recoveries of ana-

Table 2

Total arsenic determinations in spiked test solutions (volume: 50 mL, N = 4).

Added ($\mu\text{g L}^{-1}$)		Found ($\mu\text{g L}^{-1}$)			Recovery (%)			Relative error (%)		R.S.D. (%)	
As(III)	As(V)	As(III)	As(V)	Total As	As(III)	As(V)	Total As	As(III)	As(V)	As(III)	As(V)
0	25	–	24.7 ± 0.9 ^a	24.7 ± 0.9	–	99 ± 2	99 ± 2	–	–1.2	–	3.6
10	15	9.8 ± 0.3	14.6 ± 0.8	24.4 ± 0.7	98 ± 2	97 ± 2	98 ± 2	–2.0	–2.7	3.1	5.5
15	10	14.5 ± 0.5	9.7 ± 0.3	24.2 ± 0.6	97 ± 3	97 ± 3	97 ± 3	–3.4	–3.1	3.4	2.5
25	0	24.1 ± 0.8	–	24.1 ± 0.8	96 ± 2	–	96 ± 2	–3.7	–	3.3	–

^a Mean ± standard deviation.**Table 3**

Speciation of As(III) and As(V) and total arsenic in some natural water samples (sample volume: 50 mL, final volume: 2 mL, N = 4).

Samples	Added ($\mu\text{g L}^{-1}$)		Found ($\mu\text{g L}^{-1}$)			Recovery (%)			Relative error (%)		R.S.D. (%)	
	As(III)	As(V)	As(III)	As(V)	Total As	As(III)	As(V)	Total As	As(III)	As(V)	As(III)	As(V)
Tap water	–	–	0.11 ± 0.01 ^a	0.54 ± 0.03	0.65 ± 0.03	–	–	–	–	–	9.1	5.6
	1.0	1.0	1.10 ± 0.07	1.50 ± 0.10	2.60 ± 0.15	99 ± 2	97 ± 2	98 ± 2	–0.9	–2.7	6.4	6.7
	5.0	5.0	5.01 ± 0.17	5.42 ± 0.20	10.4 ± 0.8	98 ± 2	98 ± 2	98 ± 2	–1.9	–2.2	3.4	3.7
River water	–	–	0.32 ± 0.01	0.65 ± 0.02	0.97 ± 0.04	–	–	–	–	–	3.1	3.1
	1.0	1.0	1.28 ± 0.05	1.59 ± 0.08	2.87 ± 0.12	97 ± 1	96 ± 2	97 ± 1	–3.1	–3.8	3.9	5.0
	5.0	5.0	5.25 ± 0.18	5.53 ± 0.20	10.8 ± 0.9	99 ± 3	98 ± 3	98 ± 3	–1.3	–2.2	3.4	3.6
Sea water	–	–	0.41 ± 0.02	0.78 ± 0.04	1.19 ± 0.07	–	–	–	–	–	4.9	5.1
	1.0	1.0	1.36 ± 0.08	1.72 ± 0.12	3.08 ± 0.17	96 ± 2	97 ± 2	97 ± 2	–3.7	–3.5	5.9	7.0
	5.0	5.0	5.32 ± 0.21	5.81 ± 0.19	11.1 ± 0.7	98 ± 2	101 ± 1	99 ± 2	–1.7	+0.5	3.9	3.3

^a Mean ± standard deviation.

lyte ions were higher than 96%. The relative standard deviation for this work was below 8%.

3.7. Application to real samples

In order to estimate the accuracy of the presented coprecipitation procedure, different amounts of arsenic species were spiked in three different water samples given in Table 3. The resulting solutions were submitted to the presented procedure given in Experimental. The results were given in Table 3. The recovery values for analyte ions were generally higher than 95%. A good agreement

was obtained between the added and measured analyte amounts. These results confirm the validity of the proposed method. The presented method could be applied successfully for the separation, preconcentration and speciation of trace amounts of arsenic species in both spiked and water samples.

The coprecipitation procedure presented was applied to two standard reference materials given in Table 4. The results are in good agreement with the certified values for arsenic. The method has been combined with the microwave assisted digested samples. The results are also given in Table 4. The results have been calculated on the assumption of 100% recovery of analyte ions.

Table 4

The level of total arsenic in certified reference materials and environmental samples after application of the presented procedure (N = 4).

Reference material	Certified value	Our value	Relative error (%)
NIST SRM 2711 Montana soil ($\mu\text{g g}^{-1}$)	105	101 ± 5 ^a	–3.9
LCG 6010 Hard drinking water ($\mu\text{g L}^{-1}$)	52	50 ± 2	–4.0
Sediment from Green river in Tokat city ($\mu\text{g g}^{-1}$)	–	0.29 ± 0.02	–
Soil from Tokat city ($\mu\text{g g}^{-1}$)	–	0.16 ± 0.01	–
Edible mushroom (<i>Calvatia utriformis</i>) ($\mu\text{g g}^{-1}$)	–	0.12 ± 0.01	–
Rice ($\mu\text{g g}^{-1}$)	–	0.20 ± 0.01	–
Sausage ($\mu\text{g g}^{-1}$)	–	0.050 ± 0.002	–

^a Mean expressed as 95% tolerance limit.**Table 5**

Comparative data from some recent studies on speciation of arsenic.

Analytes	Media	Detection system	PF	DL ($\mu\text{g L}^{-1}$)	R.S.D. (%)	Ref.
As(III), As(V)	Molybdate-Triton X-114	ETAAS	52.5	0.01	5	[10]
As(III), As(V)	Ni-pyrrolidine dithiocarbamate	Solid sampling AAS	–	0.02	–	[18]
As(III), As(V), organoarsenic species	Iron(III)-1-pyrrolidinedithioic acid, ammonium salt (APDC)	Energy dispersive X-ray fluorescence spectrometry	–	0.02 mg L ⁻¹	3	[19]
As(III, V) Se(IV, VI), Sb(III, V)	Pb-pyrrolidine dithiocarbamate	Neutron activation analysis	–	1 ng L ⁻¹	–	[20]
Total As	La(III)-ethyl vinyl acetate turning-packed mini column	HG-ICP-OES	28–45	0.007–0.013	0.9–1.3	[21]
As(III)	Amberlite IRA-410	HGAAS	–	30 ng L ⁻¹	4.8	[22]
As(III), As(V)	Hydroxide form anion exchange microcolumn	HGAAS	–	0.07–0.5	–	[23]
As(III), As(V)	Aluminum hydroxide	HGAAS	25	0.012	<8	This study

PF: preconcentration factor, DL: detection limit.

4. Conclusion

The presented coprecipitation procedure was simple and rapid for speciation of arsenic(V) and arsenic(III) in environmental samples. The time required for the coprecipitation and determination was about 30 min. The arsenic ions can be sensitively determined by hydride generation-atomic absorption spectrometry without any influence of aluminum hydroxide. The effect of matrix can be overcome by the method, and the results are satisfying. The method proposed is rapid and has good reproducibility. The preconcentration factor was 25 for 50 mL of sample volume and 2 mL of final volume. The contamination risk for analytes from the carrier element is very low. The usefulness of the method is shown by the control analyses of standard reference materials. The detection limits of analytes are superior to those of preconcentration techniques for analyses. The good features of the proposed method showed that its a convenient and low cost one. Also the method is relatively rapid as compared with previously reported procedures given in Table 5 for the enrichment of analytes [18–23,30,31].

Acknowledgments

The authors are grateful for the financial support of the Unit of the Scientific Research Project of Erciyes University and the Unit of the Scientific Research Projects of Gaziosmanpasa University.

References

- [1] Z.-C. Liang, C.-H. Liang, J.-C. Wang, W.-J. Ho, C.-Y. Wu, *Int. J. Med. Mushrooms* 10 (2008) 181–188.
- [2] A. Kolesarova, J. Slamecka, R. Jurcik, F. Tataruch, N. Lukac, J. Kovacik, M. Capcarova, M. Valent, P. Massanyi, *J. Environ. Sci. Health* 43A (2008) 646–650.
- [3] M.B. Arain, T.G. Kazi, M.K. Jamali, N. Jalbani, H.I. Afridi, J.A. Baig, *J. Hazard. Mater.* 154 (2008) 998–1006.
- [4] Q. Zhang, H. Minami, S. Inoue, I. Atsuya, *Fresen. J. Anal. Chem.* 370 (2001) 860–864.
- [5] A.Q. Shah, T.G. Kazi, M.K. Jamali, M.B. Arain, H.I. Afridi, N. Jalbani, G.A. Kandhro, J.A. Baig, R.A. Sarfraz, R. Ansari, *Food Chem.* 113 (2009) 1351–1355.
- [6] M. Koreňovská, *J. Food Nutr. Res.* 45 (2006) 84–88.
- [7] H.M. Crews, *Spectrochim. Acta* 53 B (1998) 213–219.
- [8] M. Bissen, F.H. Frimmel, *Acta Hydrochim. Hydrobiol.* 31 (2003) 9–18.
- [9] I.A. Katsoyiannis, A.A. Katsoyiannis, *Environ. Monit. Assess.* 123 (2006) 393–406.
- [10] F. Shemirani, M. Baghdadi, M. Ramezani, *Talanta* 65 (2005) 882–887.
- [11] Y. Jiang, Y. Wu, J. Liu, X. Xia, D. Wang, *Microchim. Acta* 161 (2008) 137–142.
- [12] S. Palchaudhuri, A. Sen, *J. Ind. Chem. Soc.* 84 (2007) 1148–1152.
- [13] M.L. Kile, E.A. Houseman, C.V. Breton, T. Smith, O. Quamruzzaman, M. Rahman, G. Mahiuddin, D.C. Christiani, *Environ. Health Perspect.* 115 (2007) 889–893.
- [14] M.G.M. Alam, G. Allinson, F. Stagnitti, A. Tanaka, M. Westbrooke, *Int. J. Environ. Health Res.* 12 (2002) 235–253.
- [15] L. Elci, U. Divrikli, M. Soylak, *Int. J. Environ. Anal. Chem.* 88 (2008) 711–723.
- [16] Y.M. Zhou, A.J. Tong, Y. Akama, *Cellulose Chem. Technol.* 40 (2007) 513–518.
- [17] Y.B. Mao, J. Ling, S.H. Qian, A.Q. Lin, W.J. Zheng, W.Y. Xu, Y.X. Luo, M. Zhang, *Water Environ. Res.* 79 (2007) 1015–1022.
- [18] Q. Zhang, H. Minami, S. Inoue, I. Atsuya, *Anal. Chim. Acta* 508 (2004) 99–105.
- [19] S. Latva, S. Peraniemi, M. Ahlgren, *Analyst* 124 (1999) 1105–1108.
- [20] Y.C. Sun, J.Y. Yang, *Anal. Chim. Acta* 395 (1999) 293–300.
- [21] R.A. Gil, N. Ferrua, J.A. Salonia, R.A. Olsina, L.D. Martinez, *J. Hazard. Mater.* 143 (2007) 431–436.
- [22] L.O. Leal, N.V. Semenova, R. Forteza, V. Cerda, *Talanta* 64 (2004) 1335–1342.
- [23] C.I.S. Narcise, L.C. Co, F.R. del Mundo, *Talanta* 68 (2005) 298–304.
- [24] I. Cano-Aguilera, T.N. Haque, G.M. Morrison, A.F. Aguilera-Alvarado, M. Gutierrez, J.L. Gardea-Torresdey, G. de la Rosa, *Microchem. J.* 81 (2005) 57–60.
- [25] K. Jitmanee, M. Oshima, S. Motomizu, *Talanta* 66 (2005) 529–533.
- [26] Mercury Hydride System User's Guide, Technical Documentation, Perkin Elmer Instruments, Germany, 2000.
- [27] O.D. Uluozlu, K. Kinalioglu, M. Tuzen, M. Soylak, *Biomed. Environ. Sci.* 20 (2007) 203–207.
- [28] M. Tuzen, K.O. Saygi, M. Soylak, *Talanta* 71 (2007) 424–429.
- [29] M. Soylak, M. Tuzen, *J. Hazard. Mater.* 152 (2008) 656–661.
- [30] D. Chen, C. Huang, M. He, B. Hu, *J. Hazard. Mater.* (2008), doi:10.1016/j.jhazmat.2008.09.022.
- [31] C. Xiong, M. He, B. Hu, *Talanta* 76 (2008) 772–779.



Highly-sensitive cholesterol biosensor based on well-crystallized flower-shaped ZnO nanostructures

Ahmad Umar^{a,b,*}, M.M. Rahman^b, A. Al-Hajry^c, Y.-B. Hahn^{b,*}

^a Department of Chemistry, Faculty of Science, Najran University, P.O. Box 1988, Najran 11001, Kingdom of Saudi Arabia

^b School of Semiconductor and Chemical Engineering, BK21 Centre for Future Energy Materials and Devices, Nanomaterials Research Processing Centre, Chonbuk National University, 664-14, 6 Duckjin Dong, 1 Ga Jeonju, Choella-Bukto, Jeonju 561-756, South Korea

^c Department of Physics, Faculty of Science, Najran University, P.O. Box 1988, Najran 11001, Kingdom of Saudi Arabia

ARTICLE INFO

Article history:

Received 10 October 2008

Received in revised form 7 November 2008

Accepted 10 November 2008

Available online 25 November 2008

PACS:

62.23.Hj

82.45.Yz

87.85.Rs

81.05.Dz

81.07.-b

81.10.Bk

Keywords:

ZnO nanostructures

Flower-shaped nanostructures

Cholesterol oxidase

Cholesterol biosensor

ABSTRACT

This paper reports the fabrication of highly-sensitive cholesterol biosensor based on cholesterol oxidase (ChOx) immobilization on well-crystallized flower-shaped ZnO structures composed of perfectly hexagonal-shaped ZnO nanorods grown by low-temperature simple solution process. The fabricated cholesterol biosensors reported a very high and reproducible sensitivity of $61.7 \mu\text{A} \mu\text{M}^{-1} \text{cm}^{-2}$ with a response time less than 5 s and detection limit (based on S/N ratio) of $0.012 \mu\text{M}$. The biosensor exhibited a linear dynamic range from 1.0 – $15.0 \mu\text{M}$ and correlation coefficient of $R = 0.9979$. A lower value of apparent Michaelis–Menten constant (K_m^{app}), of 2.57 mM , exhibited a high affinity between the cholesterol and ChOx immobilized on flower-shaped ZnO structures. Moreover, the effect of pH on ChOx activity on the ZnO modified electrode has also been studied in the range of 5.0 – 9.0 which exhibited a best enzymatic activity at the pH range of 6.8 – 7.6 . To the best of our knowledge, this is the first report in which such a very high-sensitivity and low detection limit has been achieved for the cholesterol biosensor by using ZnO nanostructures modified electrodes.

© 2008 Elsevier B.V. All rights reserved.

1. Introduction

The determination of cholesterol is of vital importance since high serum cholesterol level is related to various clinical disorders, such as heart disease, coronary artery disease, arteriosclerosis, hypertension, cerebral thrombosis, and etc. [1]. In addition to this, the cholesterol and its fatty acids are also important constituents of nerve and brain cells. Hence, the development of reliable and high sensitive method for the active and fast determination of cholesterol is an active research now days. Among various determination methods, the biosensors are receiving a considerable attention due to their selectivity, fast response, reproducibility, and stability. Among various kinds of biosensors, the electrochemical biosensors which are based on the proper immobilization of enzyme on suitable matrixes offers a portable, cheap, and rapid method for the determination of various biological molecules [2–4]. Recently sci-

entists are inclined to use biocompatible nanomaterials as suitable matrixes for the enzyme immobilizations for the effective detection of various biomolecules [2–10]. Among various nanomaterials, the nanomaterials of ZnO are one of the most promising matrixes which can be use for the immobilization of various enzymes due to its numerous exotic properties such as high specific surface area, optical transparency, bio-compatibility, non-toxicity, chemical and photochemical stability, ease of fabrication, electrochemical activities, and so on [11–13]. Moreover, due to the bio-mimetic and high-electron communication features, the nanostructures of ZnO exhibiting a great potential for the fabrication of efficient chemical and biosensors [14–24]. It is observed that the high isoelectric point (IEP) of ZnO is suitable for the low IEP proteins or enzymes. Therefore, ZnO with a high IEP (~ 9.5) should be suitable for the adsorption of the low IEP enzyme (for instance ChOx IEP = ~ 4.9). Furthermore, the ZnO-modified electrode retained the enzyme bioactivity and could enhance the electron transfer between the enzyme and the electrode. Even though having various properties but there are only two reports in the literature in which ZnO nanomaterials are used as supporting matrixes to immobilize the ChOx enzymes for the effective detection of cholesterol [8,9]. Khan et al. developed a cholesterol biosensor based on ZnO nanoparticles-chitosan

* Corresponding authors. Fax: +82 63 270 2306.

E-mail addresses: ahmadumaresn@gmail.com (A. Umar), ybhahn@chonbuk.ac.kr (Y.-B. Hahn).

composite films and got the linear range of 5–300 mg dl⁻¹, detection limit of 5 mg dl⁻¹, and sensitivity of 1.41×10^{-4} A mg dl⁻¹ [8]. Singh et al. also fabricated the cholesterol biosensor based on rf-sputtered ZnO nanoporous thin films and got the linear range of 25–400 mg dl⁻¹ and response time 15 s [9]. The lower sensitivity and higher detection limit of previously fabricated ZnO nanostructures based cholesterol biosensor has been demonstrated in the literature, hence more works are needed to obtain the higher-sensitivity and lower-detection limit of the ZnO nanostructures based cholesterol biosensors.

In this paper, we are reporting an ultra-sensitive cholesterol biosensor based on flower-shaped ZnO structures composed of hexagonal-shaped ZnO nanorods. The fabricated sensor showed a very-high and reproducible sensitivity of $61.7 \mu\text{A mM}^{-1} \text{cm}^{-2}$ with the detection limit of 0.012 μM . Moreover, to the best of our knowledge, this is the first time such a very high-sensitivity and low-detection limit has been achieved for cholesterol biosensors by using ZnO nanostructured modified electrodes.

2. Experimental details

The entire chemicals were used as received without further purification. In a typical reaction process, 0.1 M zinc nitrate solution, made in 50.0 ml deionized water was mixed with the 0.1 M aqueous solution of hexamethylenetetramine (HMTA) (50.0 ml) under stirring at room-temperature. The resultant mixture was stirred continuously for 20 min at room temperature to mix well. Few drops of 1.0 M NaOH solution was added to adjust the pH 10.0 of the solution. The obtained solution was then heated and refluxed with continuous stirring at 100.0 °C for 9 h in necked round bottom flask. During refluxing, temperature of the solution was controlled by inserting manually adjustable thermocouple in the refluxing pot through one of its neck. White precipitates were obtained after completing the reaction which were filtered off, washed thoroughly with deionized water and ethanol, and dried at room temperature.

To fabricate the cholesterol biosensors, the as-synthesized flower-shaped ZnO structures composed of hexagonal-shaped ZnO nanorods were coated onto the surface of a gold (Au) electrode with the area of 3.0 mm². Prior to the modification, the gold electrode was polished with the 0.05 μm alumina slurry and then sonicated in de-ionized water. The surfaces of flower-shaped ZnO structures were immobilized in a solution of ChOx (1.0 mg/mL), prepared in phosphate buffer (PBS, pH ~7.4) 150.0 mM (0.9% NaCl) for 24 h. ChOx was immobilized onto the flower-shaped ZnO structures by physical adsorption technique. The modified electrode was kept overnight for ChOx immobilization and subsequently washed with buffer solution, and dried in nitrogen environment. After drying the modified ChOx/ZnO/Au electrode, a 10 μl Nafion solution was dropped onto the electrode and dried for 24 h at 4.0 °C to form a net-like film on the modified electrode. This step is important for the tight attachment of ZnO flowers and ChOx on the surfaces of the modified electrodes. When, not in use, the ZnO modified gold electrodes (i.e., Nafion/ChOx/ZnO/Au electrodes) were stored in PBS at 4.0 °C. The electrochemical experiments were carried out at room-temperature using an electrochemical analyzer with a conventional three-electrode configuration: a working electrode (ZnO-modified Au electrode), a Pt wire as a counter electrode and Ag/AgCl (sat. KCl) as a reference electrode.

3. Results and discussion

The general morphologies of the as-grown ZnO structures were characterized by FESEM and shown in Fig. 1 (a)–(c). From the low-magnification FESEM, it is confirmed that the grown structures are flower-shaped composed of perfectly hexagonal shaped ZnO nanorods and synthesized in a high-density with uniform

morphologies (figures (a) and (b)). It was observed from the high-resolution FESEM images that the typical lengths and diameters of the perfectly hexagonal nanorods are 300 ± 50 nm and 3 ± 1 μm , respectively. Moreover, it is seen that all the nanorods are joined together through their bases in such a special manner that they made a beautiful-flower-shaped morphologies. The full array of one flower-shaped structure is in the range of 3–4 μm . Inset of Fig. 1 (c) exhibits the exact morphology of the as-synthesized hexagonal-shaped ZnO nanorod grown in the flower-shaped structures. From the image, it is clear that the nanorods are formed with the six crystallographic planes where all the planes are connected each other with the internal angles of $\sim 60^\circ$. Moreover, the as-grown nanorods containing the (0001) top facets enclosed with six equivalents of $\{01\bar{1}0\}$ crystal planes. The exact hexagonal surfaces with facets confirmed the epitaxial growth and therefore the single crystalline nature of the as-grown nanorods. The crystallinity and crystal phases of the deposited ZnO nanorods were observed by the X-ray diffraction (XRD) patterns and shows in Fig. 1 (d). All of the indexed peaks in the obtained pattern are well-matched with that of bulk ZnO which confirms that the synthesized products are single crystalline and possesses a wurtzite hexagonal structures. No other peak related to impurities was detected in the pattern within the detection limit of the X-ray diffraction further confirms that the obtained products are pure ZnO. Further structural characterization of the as-grown hexagonal-shaped ZnO nanorods grown in flower-shaped structures was done by the transmission electron microscopy (TEM) and shown in Fig. 2 (a) and (b). The low-magnification TEM observation shows the exact morphology of the hexagonal-shaped ZnO nanorods assembled in flower-like structures as was seen in FESEM and reveals the full consistency in terms of shape and dimension (Fig. 2 (a)). The typical diameter of the observed nanorod is about 250 nm which possessing a very clean and smooth surfaces with the uniform diameter passim to their lengths. Fig. 2 (b) shows the high-resolution TEM (HRTEM) image which confirm that the as-grown structure is single crystalline with the lattice spacing of 0.52 nm corresponds to the *d*-spacing of [0001] crystal planes of the wurtzite hexagonal ZnO. The corresponding SAED pattern, projected along the $[2\bar{1}\bar{1}0]$ zone axis, is also consistent with the HRTEM observation and confirms that the nanorods are single crystalline with the wurtzite hexagonal phase, and preferentially grown along [0001] direction (inset 2 (b)). The composition and quality of the synthesized nanostructures was examined by FTIR in the range of 400–4000 cm^{-1} and shown in Fig. 2 (c). A strong absorption band at 440 cm^{-1} was observed which was related with the ZnO [25]. Two bands at ~ 3415 and ~ 1632 cm^{-1} are correspond to the O–H stretching and bending modes of vibrations, respectively. Moreover, two very small peaks at ~ 1380 and 879 cm^{-1} are probably due to nitrate (NO_3^-) group as it seems that nitrate is not completely removed during the washing process [26]. Fig. 2 (d) exhibits the UV–vis. absorption spectrum, measured at room-temperature of the as-synthesized flower-shaped ZnO structures. A broad band was observed in the spectrum at 375 cm^{-1} which is a characteristic band for the wurtzite hexagonal pure ZnO [26]. No other peak was observed in the spectrum confirms that the synthesized products are ZnO only.

A schematic of the modification of gold electrode with flower-shaped ZnO structures composed of hexagonal-shaped nanorods, ChOx and Nafion for efficient detection of cholesterol is shown in Fig. 3 (a). Fig. 3 (b) exhibits the cyclic voltammetric (CV) sweep curve for the ZnO-modified gold electrode (Nafion/ChOx/ZnO/Au) without and with 1.0 mM cholesterol in 0.1 M PBS buffer at pH 7.4 in the range of +0.3 to +0.75 V at scan rate of 100 mV/s. No redox peak was observed from the modified electrode in the absence of cholesterol however reversibly a pair of well-defined redox peaks, at +0.3 V (ox.) and +0.1 V (red.), appear from the modified electrode in presence of 1 mM cholesterol which clearly

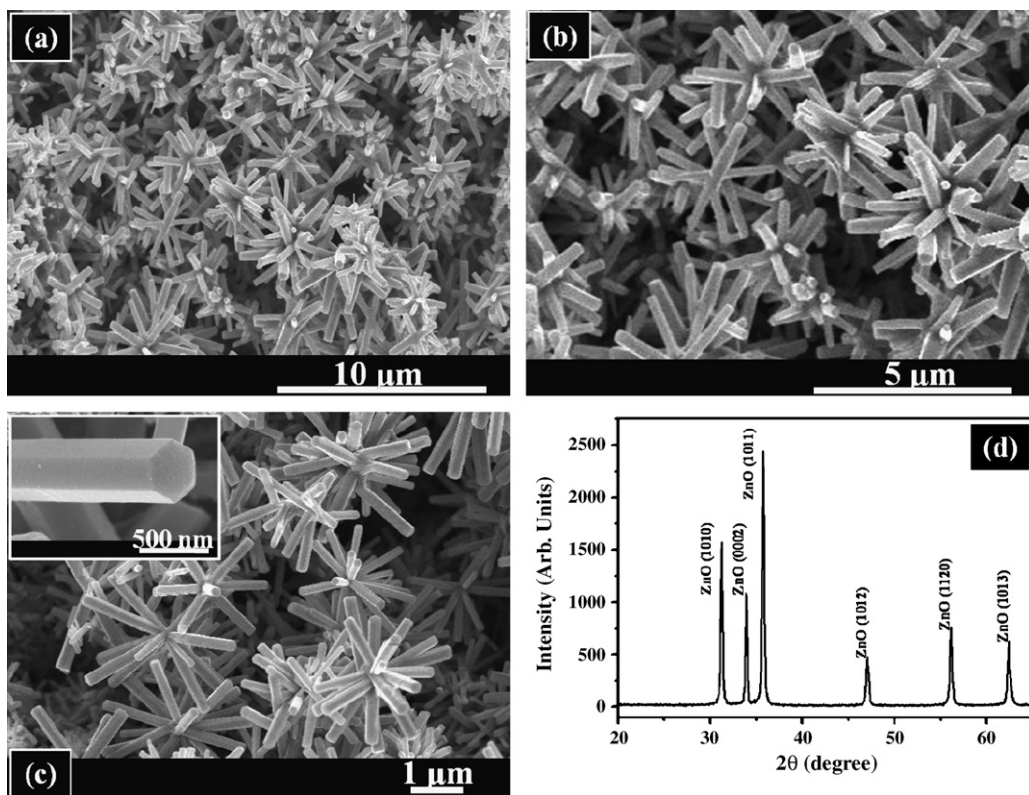


Fig. 1. (a–c) Typical FESEM images and (d) X-ray diffraction pattern of the as-grown flower-shaped ZnO structures composed of perfectly hexagonal-shaped ZnO nanorods.

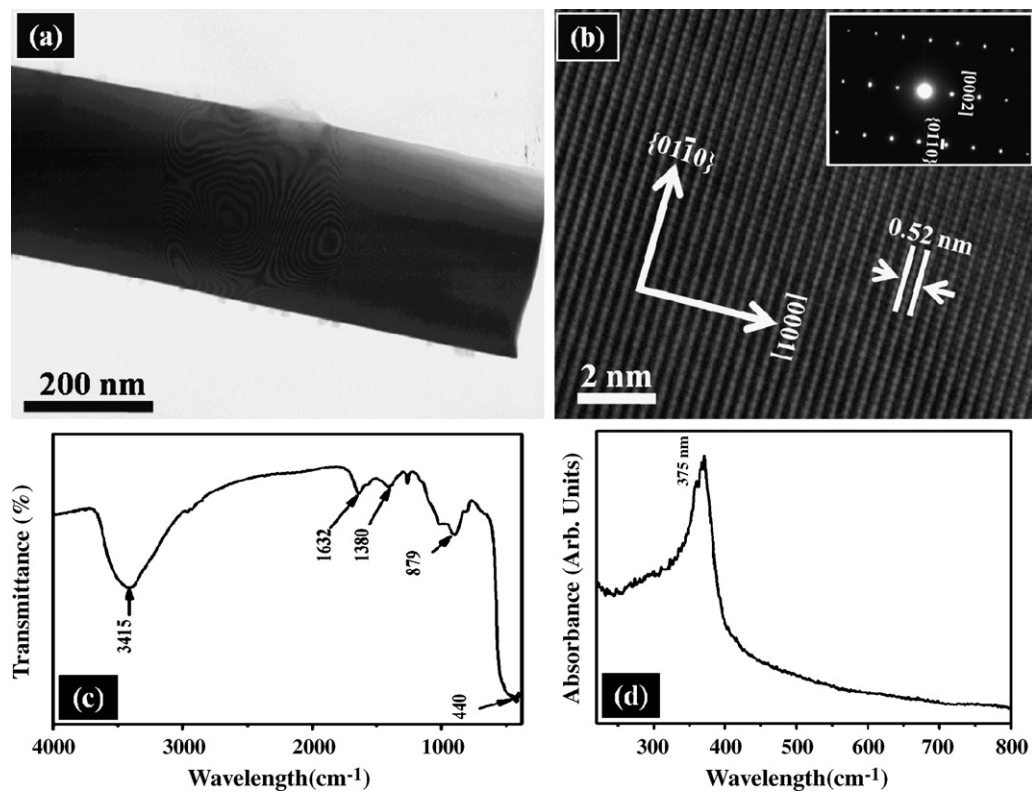


Fig. 2. Typical (a) low-magnification and (b) high-resolution and corresponding SAED pattern (inset); (c) FTIR spectrum and (d) UV-vis spectrum of the as-synthesized flower-shaped ZnO structures composed of perfectly hexagonal-shaped ZnO nanorods.

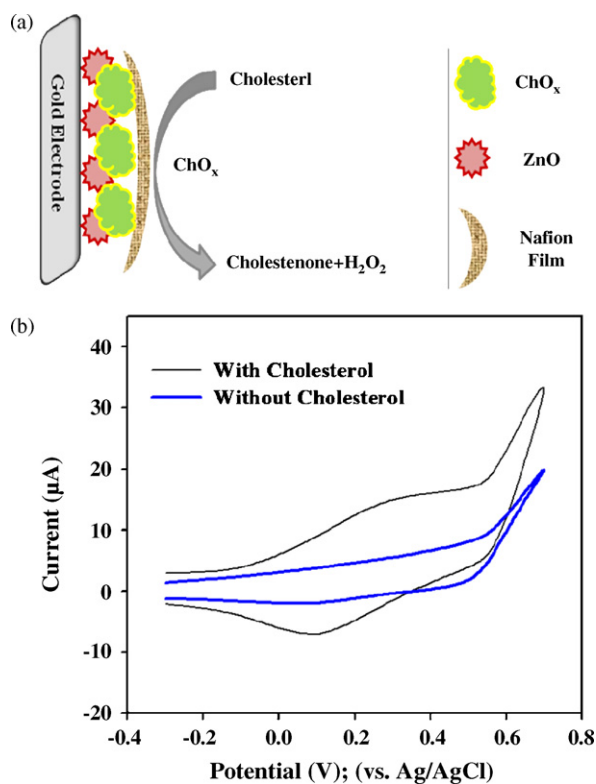


Fig. 3. (a) Schematic of the modification of gold electrode with flower-shaped ZnO structures composed of hexagonal-shaped ZnO nanorods, ChOx and Nafion for efficient detection of cholesterol; (b) cyclic voltammetric sweep curve for the Nafion/ChOx/ZnO/Au electrode without cholesterol and with 1.0 mM cholesterol in 0.1 M PBS buffer (pH 7.4) in the range of -0.3 to $+0.75$ V at scan rate of 100 mV/s.

confirms an electrochemical response from the ZnO-modified electrode in presence of cholesterol. An increase in current from -0.15 to $+0.72$ V has also been observed from the CV curve of Nafion/ChOx/ZnO/Au electrode with cholesterol in PBS compared to without cholesterol in PBS. The origination of a well-defined redox peaks from the CV curve of Nafion/ChOx/ZnO/Au electrode in PBS with 1.0 mM cholesterol are due to the H₂O₂ generation during the oxidation of cholesterol by ChOx. In addition to this, because of high surface area of flower-shaped ZnO structures composed of hexagonal-shaped nanorods, the ChOx attached to the surfaces of ZnO structures facilitates the fast and direct electron transfer

between the active sites of immobilized ChOx and electrode surface which leads to a sharper and well-defined peak. Therefore, cholesterol is efficiently detected with the Nafion/ChOx/ZnO/Au electrodes. The fast and direct electron transfer also improves the sensitivity of the fabricated biosensors. According to the previous report [9], the electrochemical reaction for the detection of cholesterol in presence of cholesterol oxidase is proposed to be as: $\text{Cholesterol} + \text{O}_2 \xrightarrow{\text{ChOx}} \text{cholestenone} + \text{H}_2\text{O}_2$ (Fig. 3 (a)).

Detailed electrochemical response experiments have been carried out on the modified Nafion/ChOx/ZnO/Au electrodes with the addition of different concentrations of cholesterol ranging from 0.1 to 25 μM in 0.1 M PBS buffer (pH 7.4) at scan rate of 100 mV/s. Fig. 4 (a) exhibits the typical CV responses of the ZnO modified electrode at different concentrations of cholesterols. It is clearly seen from the CV curves that as the concentrations of the cholesterol increases, the oxidation current also increases. The magnitude of the oxidation peak appeared at about +0.3 V (due to the oxidation of H₂O₂) increases due to the rising the concentration of H₂O₂ during the enzymatic reactions. Fig. 4 (b) shows the relation between the response current and cholesterol concentration for the fabricated biosensor. It is clearly seen from the graph that the response current increases as the concentration of cholesterol increases and saturated at high concentration of cholesterol which suggests the saturation of active sites of the enzymes at those cholesterol levels. The response time for the fabricated electrode was very fast, i.e. less than 5 s, which exhibit a high electron communication feature of the used ZnO. Under optimized conditions, the steady-state current showed a linear dynamic range of 1.0–15.0 μM (Fig. 4(b)). The correlation coefficient (R) was estimated to be $R = 0.99798$ and the sensitivity was found to be $61.7 \mu\text{A} \mu\text{M}^{-1} \text{cm}^{-2}$ from the fabricated biosensor. To the best of our knowledge, this is the first time such a very high-sensitivity has been achieved for cholesterol biosensors by using ZnO nanostructures modified electrodes. The sensitivity is remarkably higher than other previously reported cholesterol biosensors based on tetraethylorthosilicate [5], polypyrrole films [6], nanoporous CeO₂ films [7], ZnO nanoparticles +chitosan composite [8], and ZnO nanoporous thin films [9], etc. Based on the signal-to-noise ratio ($S/N=3$), the detection limit of the fabricated cholesterol biosensor was estimated to be 0.012 μM which is much lower than previously reported cholesterol biosensor [5–9]. The obtained such a high-sensitivity and detection limit for the fabricated cholesterol biosensor was due to the special morphologies of the used flower-shaped ZnO structures. The used flower-shaped ZnO structures, containing hexagonal-shaped

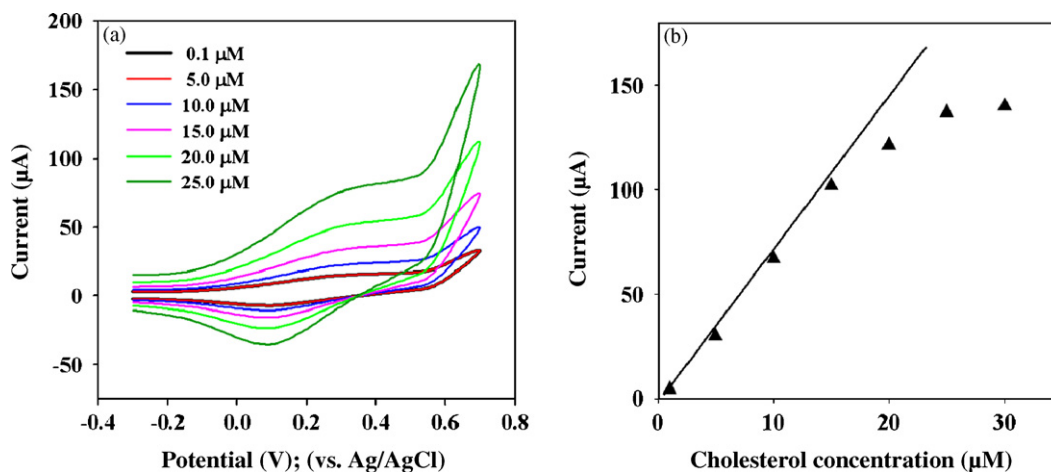


Fig. 4. (a) Electrochemical response of the Nafion/ChOx/ZnO/Au electrode at different concentrations of cholesterol i.e. 0.1, 5.0, 10.0, 15.0, 20.0, and 25.0 μM, into 0.1 M PBS buffer solution (pH 7.4); (b) calibration curve for cholesterol using modified Nafion/ChOx/ZnO/Au electrode.

Table 1
Comparison of the responses of some cholesterol biosensors constructed based on different modified electrode materials.

Electrode materials	Sensitivity ($\mu\text{A } \mu\text{M}^{-1} \text{cm}^{-2}$)	Detection limit (μM)	Apparent Michaelis–Menten constant (K_m^{app}) (mM)	Linear range (μM)	Response time (s)	Reference
Tetraethylorthosilicate	–	0.500	21.2	$2.0\text{--}10.0 \times 10^3$	50	[5]
Polypyrrole films	15.0	–	9.8	$1.0\text{--}8.0 \times 10^3$	–	[6]
Nanoporous CeO_2 film	5.98	–	2.06	$1.3\text{--}10.35 \times 10^6$	15	[7]
ZnO nanoparticles +chitosan composite	14.1	0.125×10^3	0.223	$0.125\text{--}7.76 \times 10^6$	15	[8]
ZnO nanoporous thin films	–	–	2.1	$0.65\text{--}10.35 \times 10^6$	15	[9]
Flower-shaped ZnO structures composed of hexagonal-shaped nanorods	61.7	0.012	2.57	1.0–15.0	5	Current work

nanorods which were attached in three dimensions, exhibited large active surface area. Moreover, it is believed that the active surface area is directly proportional to the sensitivity and detection limit of the fabricated sensors. Hence, due to the large surface area of flower-shaped ZnO structure, large numbers of enzyme biomolecules were immobilized on the surfaces of the used ZnO structure; therefore, the ChOx attached to the surfaces of ZnO structures facilitates the fast and direct electron transfer between the active sites of immobilized ChOx and electrode surface resulting the increase in sensitivity and lowering the detection limit of the fabricated biosensor.

The apparent Michaelis–Menten constant (K_m^{app}) which gives an indication of the enzyme–substrate kinetics for the biosensor can be calculated from the electrochemical version of the Lineweaver–Burk equation $1/i = (K_m^{\text{app}}/i_{\text{max}})(1/C) + (1/i_{\text{max}})$, where i is the current, i_{max} is the maximum current measured under saturated substrate conditions, and C is the cholesterol concentration. The K_m^{app} value of the cholesterol sensor was determined by the analysis of the slope and intercept for the plot of the reciprocals of steady-state current versus cholesterol concentrations, i.e. the Lineweaver–Burk plot of $1/i$ vs. $1/C$ (Fig. 5). According to the Lineweaver–Burk plot, the K_m^{app} is calculated to be 2.57 mM. The lower K_m^{app} value means that the immobilized ChOx passes higher affinity to cholesterol. The observed K_m^{app} value for the fabricated ZnO based cholesterol biosensor is smaller than other previously reported cholesterol biosensors [5,6,10].

To check the effect of pH on the fabricated biosensor was investigated in the pH range of 5.0–9.0 at a fixed cholesterol concentration of 1.0 mM and applied potential in the range of -0.3 to $+0.75$ V at scan rate of 100 mV/s and shown in Fig. 6. It was observed that the

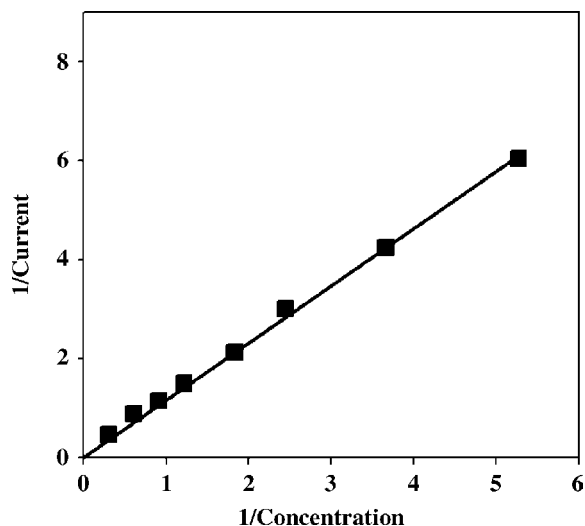


Fig. 5. The plot of $1/\text{current}$ vs. $1/\text{concentration}$ (Michaelis–Menton plot) exhibiting a linear relationship with the steady state current and cholesterol concentration.

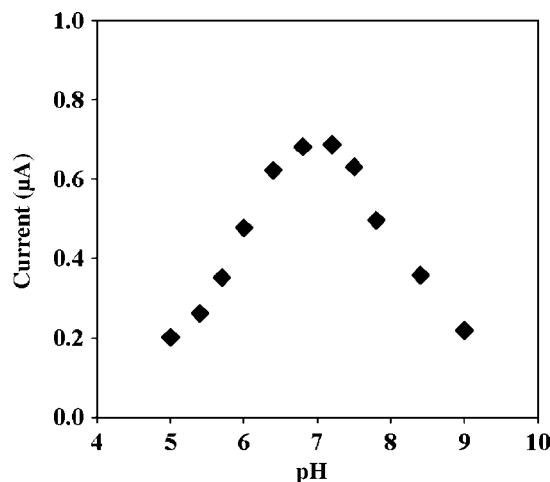


Fig. 6. The effects of pH (5.0–9.0) on the current response of the fabricated cholesterol biosensor based on the modified Nafion/ChOx/ZnO/Au electrode in 0.1 M PBS buffer (pH 7.4) in the range of -0.3 to $+0.75$ V at scan rate of 100 mV/s.

optimum pH range for the ZnO modified electrode is in the range 6.8–7.6. The rise and fall in the pH responses from the modified electrode is due to an effect of pH on the affinity of enzymes for substrate and higher stability of the enzyme in immobilized state. It is assumed that the increasing the hydrogen ion concentration ($\text{pH} < 7$) increases the successful competition of hydrogen ions for any cationic binding sites on the enzyme which results lowering the enzyme activity. Similarly, decreasing the hydrogen ions concentrations ($\text{pH} > 7.0$) means increasing the hydroxyl ions which may leads the conversion of hydroxides and can hinder the enzyme activity causes the reduction in the sensitivity of the biosensor. In this paper, the optimized pH value throughout the experiments was kept at 7.4, due to its compatibility with the human physiological condition.

For comparing, the characteristics and performances of the fabricated biosensor is compared with the previously reported cholesterol biosensors based on the utilization of various materials as the working electrode (Table 1) and it was confirmed that the presented cholesterol biosensor exhibited an excellent performance.

The fabricated biosensors exhibited very good stability and reproducibility. To check the stability of the fabricated biosensor, the experiments were conducted over a long storage period to investigate the storage stability. By repeated experiments (every 2 days) from the stored modified electrodes, it was found that the fabricated biosensors did not show any significant decrease in the sensitivity for more than 32 days, while storing in an appropriate form when not in use (at 4.0°C). It was observed that the sensitivity retained $\sim 83.7\%$ of initial sensitivity up to 32 days which gradually decreases might be due to the loss of the catalytic activity. The above results clearly suggested that the fabricated biosensor can be used for more than 1 month without any significant loss in sensitivity.

4. Conclusions

In summary, a highly-sensitive cholesterol biosensor based on ChOx immobilization on well-crystallized flower-shaped ZnO structures composed of perfectly hexagonal-shaped ZnO nanorods have been fabricated which exhibited a very high and reproducible sensitivity of $61.7 \mu\text{A} \mu\text{M}^{-1} \text{cm}^{-2}$ with a response time less than 5 s and detection limit (based on S/N ratio) of $0.012 \mu\text{M}$. The fabricated biosensor exhibited a lower value of apparent Michaelis–Menten constant (K_m^{app}), of 2.57 mM which presents a high affinity between the cholesterol and ChOx immobilized on flower-shaped ZnO structures. Importantly, to the best of our knowledge, this is the first report in which such a very high-sensitivity and low-detection limit has been achieved for the cholesterol biosensor by using ZnO nanostructures modified electrodes.

Acknowledgements

This work was partially supported by the Korea Research Foundation grant (KRF-2005-005-J07502) and by the Korea Science and Engineering Foundation grant (R01-2006-000-11306-0) funded by the Korean Government (MEST).

References

- [1] M. Nauck, W. Marz, H. Wieland, *Clin. Chem.* 46 (2000) 436.
- [2] A. Umar, M.M. Rahman, S.H. Kim, Y.B. Hahn, *Chem. Commun.* (2008) 166.
- [3] A. Umar, M.M. Rahman, S.H. Kim, Y.B. Hahn, *J. Nanosci. Nanotech.* 8 (2008) 3216.
- [4] A. Umar, M.M. Rahman, Y.B. Hahn, *Talanta* 77 (2009) 1376.
- [5] A. Kumar, R. Malhotra, B.D. Malhotra, S.K. Grover, *Anal. Chim. Acta* 414 (2000) 43.
- [6] S. Singh, A. Chaubey, B.D. Malhotra, *Anal. Chim. Acta* 502 (2004) 229.
- [7] A. Ansari, A. Kaushik, P. Solanki, B. Malhotra, *Electrochem. Commun.* 10 (2008) 1246.
- [8] R. Khan, A. Kaushik, P. Solanki, A. Ansari, M. Pandey, B. Malhotra, *Anal. Chim. Acta* 616 (2008) 207.
- [9] S. Singh, S. Arya, P. Pandey, B. Malhotra, S. Saha, K. Sreenivas, V. Gupta, *App. Phys. Lett.* 91 (2007) 63901.
- [10] C. Bongiovanni, T. Ferri, A. Poscia, M. Viralli, R. Santucci, A. Desideri, *Bioelectrochemistry* 54 (2001) 17.
- [11] A. Umar, Y.B. Hahn, *Appl. Phys. Lett.* 88 (2006) 173120.
- [12] A. Umar, B. Karunakaran, S.H. Kim, E.K. Suh, Y.B. Hahn, *Inorg. Chem.* 47 (2008) 4088.
- [13] A. Umar, Y.B. Hahn, *Cryst. Growth Des.* 8 (2008) 2741.
- [14] Z.R.R. Tian, J.A. Voigt, J. Liu, B. McKenzie, M. McDermott, *J. Am. Chem. Soc.* 124 (2002) 12954.
- [15] G. Sberveglieri, S. Groppelli, P. Nelli, A. Tintinelli, G. Giunta, *Sens. Actuators B* 25 (1995) 588.
- [16] J.A. Rodriguez, T. Jirsak, J. Dvorak, S. Sambasivan, D. Fischer, *J. Phys. Chem. B* 104 (2000) 319.
- [17] F. Zhang, X. Wang, S. Ai, Z. Sun, Q. Wan, Z. Zhu, Y. Xian, L. Jin, K. Yamamoto, *Anal. Chim. Acta* 519 (2004) 155.
- [18] Y. Liu, Y. Yang, H. Yang, Z. Liu, G. Shen, R. Yu, *J. Inorg. Biochem.* 99 (2005) 2046.
- [19] Y. Li, Z. Liu, Y. Liu, Y. Yang, G. Shen, R. Yu, *Analyt. Biochem.* 349 (2006) 33.
- [20] Z.W. Zhao, X.J. Chen, B.K. Tay, J.S. Chen, Z.J. Han, K.A. Khor, *Biosens. Bioelect.* 23 (2007) 135.
- [21] C.D. Corso, A. Dickherber, W.D. Hunt, *Biosens. Bioelect.* 24 (2008) 811.
- [22] Z. Deng, Y. Tian, X. Yin, Q. Rui, H. Liu, Y. Luo, *Electrochem. Commun.* 10 (2008) 818.
- [23] L. Chen, B. Gu, G. Zhu, Y. Wu, S. Liu, C. Xu, *J. Electroanal. Chem.* 617 (2008) 7.
- [24] X. Lu, H. Zhang, Y. Ni, Q. Zhang, J. Chen, *Biosens. Bioelect.* 24 (2008) 93.
- [25] L. Wu, Y. Wu, Lu Wei, *Physica* 28 (2005) 76.
- [26] Y.H. Ni, X.W. Wei, J.M. Hong, Y. Ye, *Mater. Sci. Eng. B* 121 (2005) 42.



Chemometric-assisted MIP-optosensing system for the simultaneous determination of monoamine naphthalenes in drinking waters

Angel Valero-Navarro^a, Patricia C. Damiani^{b,*}, Jorge F. Fernández-Sánchez^a, Antonio Segura-Carretero^a, Alberto Fernández-Gutiérrez^{a,*}

^a Department of Analytical Chemistry, University of Granada, c/Fuentenueva s/n, 18071 Granada, Spain¹

^b Department of Analytical Chemistry, Faculty of Biochemical and Pharmaceutical Sciences, National University of Rosario and Chemical Institute of Rosario (IQUIR), National Centre of Scientific and Technical Research (CONICET), Suipacha Street 570, 2000 Rosario, Santa Fe, Argentina

ARTICLE INFO

Article history:

Received 1 August 2008

Received in revised form 22 October 2008

Accepted 23 October 2008

Available online 6 November 2008

Keywords:

Molecularly imprinted polymers (MIPs)

Optosensors

Chemometric multivariate calibration

Monoamine naphthalene compounds

ABSTRACT

In the present work a chemometric-assisted molecularly imprinted polymer (MIP)-fluorescence optosensing system has been developed for determining monoamines naphthalene compounds in drinking waters. The use of chemometrics for processing flow injection analysis with MIP fluorescence optosensor data allowed the simultaneous determination of the principal monoamine naphthalene compounds 1-naphthylamine (1-NA) and 2-naphthylamine (2-NA) even in presence of potential interferent 1-naphthalenemethylamine (1-NMA). Classical chemometrics tools such as partial least-squares (PLS-1), as well as second-order algorithms like multiway PLS (N-PLS) and unfolded PLS (U-PLS), were successfully applied, assisting fluorescence emission spectra at a fixed excitation wavelength or excitation-emission fluorescence matrices (EEM), respectively, when interferents are considered in the calibration set. The combinations of both N-PLS and U-PLS with residual bilinearization (RBL), achieving the second-order advantage, were satisfactory applied for the simultaneous determination of the main monoamine naphthalene compounds in drinking water, in the presence of a potential interferent without sample pretreatment, even when the later is not modeled in calibration set. Predictive ability, accuracy, figures of merit, as well as advantages and disadvantages of the different strategies were discussed.

© 2008 Elsevier B.V. All rights reserved.

1. Introduction

The contamination of surface and groundwater with aromatic compounds is one of the most important environmental problems of present days [1,2]. Monoamine naphthalene compounds (MANCs) such as 1-naphthylamine (1-NA) and 2-naphthylamine (2-NA) are considered priority contaminants, owing to their acute toxicity and poor biodegradation, as well as substructures of potentially carcinogenic pollutants discharged from pharmaceutical, dyestuff, photographic, agrochemical industries and cigarette smokes. On the other hand, they can also be transformed into toxic *N*-nitroso compounds through a series of reactions in the environment [3–5]. The agencies that regulate 1-naphthylamine are the Environmental Protection Agency (EPA) and the Occupational Safety and Health Administration (OSHA). OSHA regulates 1-naphthylamine as 1 of 13

carcinogens under the General Industry Standard. There is no action level for 1-naphthylamine. The regulation calls for no exposure at any level that can be detected without establishing permissible exposure limits (PELs). Epidemiological studies have shown that occupational exposure to 2-naphthylamine, either alone or present as an impurity in other compounds, causes bladder cancer. It is also considered 1 of 13 OSHA-regulated carcinogens without establishing PELs. These organizations have only established naphthalene (NAPH) allowed levels, because it is considered as a representative of this kind of contaminants and also of other few naphthalene derivatives. EPA recommends that children should not drink water containing more than 0.5 parts of naphthalene per million parts of water (ppm) for more than 10 days, or 0.4 ppm for longer than 7 years. Adults should not drink water with more than 1 ppm for more than 7 years. For water consumed over a lifetime, EPA suggests it should contain no more than 0.02 ppm of naphthalene. In conclusion, these low levels allowed for naphthalene in drinking waters can be considered as referent for levels of its derivatives. It can be noticed that these levels could be so lower (in order of parts per billion parts ppb) so only a few analytical methods can be applied for their determination, mainly based on high-performance liq-

* Corresponding authors.

E-mail addresses: patodamiani@hotmail.com, pdamiani@fbioyf.unr.edu.ar (P.C. Damiani), albertof@ugr.es (A. Fernández-Gutiérrez).

¹ <http://www.ugr.es/local/fqm297>.

uid chromatography (HPLC) with diode-array detection (DAD) and electrochemical detection (ED) and gas chromatography combined with mass spectrometric detection (GC–MS) [6,7]. These methods are expensive for routine environmental control laboratories, and often involve extensive analytical procedures and sample pretreatment.

Molecular imprinting polymer (MIP) technology is now well established for the preparation of tailor-made polymers with cavities that are able to selectivity recognize a target molecule or a group of related compounds [8–10]. Advantages in chemical recognition offered by molecular imprinting technology include the ability to induce receptor sites with outstanding analyze specificity, robustness and stability [11].

In a previous work, the development of a synthetic receptor for monoamine naphthalene compounds using a non-covalent imprinting technique and naphthalene as template has been described [12]. This MIP optosensor was used as an optical flow-through sensor for quantifying these molecules by recording their room-temperature fluorescence emission. The combination of flow injection techniques with detection on an optically active surface packed in a flow-through cell (optosensor) has important advantages such as sensitivity, selectivity, simplicity and low cost for routine environmental control in comparison to commonly reported analytical methods (HPLC, GC–MS) [13].

In this previous work [12], the main monoamine naphthalene compounds (1-NA and 2-NA) were simultaneously determined applying univariate calibration to the fluorescence intensity at an isoemissive point. For this purpose, the signals of 1-NA and 2-NA are required to be absolutely additive, in order to apply a calibration function related to the total NA concentration. It may be noticed that the total content of both analytes was calculated in this case, instead of the individual content. Moreover, under these conditions 1-naphthalenemethylamine (1-NMA) was established as the main interference compound making more difficult the determination of monoamine naphthalene compounds when it is presented in the sample at concentration level equal or higher than 300 ng mL^{-1} .

In the present report, the same MIP optosensor in combination with a flow injection technique was applied to simultaneously determine 1-NA and 2-NA. Two different methodologies were employed in the absence of unexpected sample components: (1) fluorescence emission spectra at a fixed excitation wavelength were processed with the first-order multivariate calibration partial least-squares (PLS) algorithm [14], and (2) excitation-emission fluorescence matrices (EEM) were processed with second-order algorithms such as multiway PLS (N-PLS) and unfolded PLS (U-PLS) [15]. These strategies allowed the simultaneous determination of 1-NA and 2-NA in two different situations: (1) both calibration and test samples contain the analytes, and (2) both calibration and test samples contain the analytes and the interferent 1-NMA.

On the other hand, the combination of both N-PLS and U-PLS with residual bilinearization (RBL) has been applied to excitation-emission fluorescence matrices, achieving the “second-order advantage”, i.e., allowing to quantitate the analytes 1-NA and 2-NA in test samples also containing the interferent 1-NMA, using a calibration set with only binary mixtures of 1-NA and 2-NA [16,17]. It should be noticed that the classical second-order PARAFAC (parallel factor analysis) model did not produce acceptable results in the present samples because of extensive spectral overlapping among the various sample components.

The novelty of this work is the use of chemometrics for assisting a flow injection analysis with MIP fluorescence optosensor data, allowing the simultaneous determination of the principal monoamine naphthalene compound 1-NA and 2-NA, even in presence of unsuspected components which may be present in drinking water samples.

2. Experimental

2.1. Chemicals

Naphthalene, 1-naphthylamine, 2-naphthylamine and 1-naphthalenemethylamine (1-NMA) were obtained from Sigma Chemical Co. bisphenol A (2,2-bis(4-hydroxyphenyl)propane) was purchased from Aldrich (Milwaukee, WI, USA). Phloroglucinol was obtained from Fluka Chemie (Steinheim, Germany). Acetonitrile and diphenylmethan-4,4'-diisocyanate (MDI) were purchased from Merck (Darmstadt, Germany). Tetrahydrofuran (THF) was obtained from Panreac (Madrid, Spain). All reagents were used as received, without further purification.

Freshly prepared ultrapure deionized water (Milli-Q3 RO/MilliQ2 system, Millipore, UK) was used in all experiments.

2.2. MIPs synthesis

MIPs were prepared from bisphenol A (191 mg) and MDI (236.8 mg) as functional monomers, phloroglucinol (50 mg) as an additional cross-linker, naphthalene (30 mg) as template and THF (5 mL) as solvent [12].

The mixture was placed into a glass vial, stirred and stored uncapped in the absence of light for 4 days until complete evaporation of the organic solvent. The resulting polymer monolith was ground in an agate mortar, washed with acetonitrile, and dried at $30\text{--}35^\circ\text{C}$. The ground polymer was dry sieved. Particle sizes of diameters between 80 and $120 \mu\text{m}$ were selected. The template was eliminated easily washed by packing the MIP in a flow cell and passing acetone continuously (5 min of continuous flow).

Non-imprinted polymer (NIP) for control was also prepared and treated exactly in the same way, except that no template molecule was used during the polymerization stage.

2.3. Sample and solution preparation

Stock solutions ($50 \mu\text{g mL}^{-1}$) of the individual MA-NCs and 1-naphthalenemethylamine were prepared by dissolving the appropriate amount of the solid in demineralized water and stored at 4°C in the dark (for a period of up to 1 month). Intermediate stock solutions of 1-NA, 2-NA and 1-NMA were daily prepared by dilution in water of the $50 \mu\text{g mL}^{-1}$ solution.

For the interference studies, solutions of the analytes were prepared by adding the appropriate amount of the interferent to the stock solution and diluting with Milli-Q water.

2.4. Flow-through system and instrumentation

Fig. 1 shows the optosensing manifold used for the luminescence measurements. The polymer particles were packed in a conventional luminescence flow-through quartz cell (Hellma, model 176.052-QS) of 1.5 mm of light path. At the bottom of the cell, a small piece of nylon net was placed to prevent particle displacements by the flow stream. This sensing flow-cell was placed inside the sample holder of the spectrometer and a peristaltic pump (model Minipuls 2, Scharlab, Barcelona, Spain) was used to establish the flow rate. MA-NCs solutions (2 mL), or acetone ($250 \mu\text{L}$) as MIP regenerator, were injected into the carrier flow by means of two conventional six-way injection valves.

Fluorescence spectral measurements were done on a fast Varian Cary-Eclipse fluorescence spectrofluorimeter (Varian Iberica, Madrid, Spain) equipped with a Xenon discharge lamp (peak power equivalent to 75 kW) and two Czerny Turner monochromators, connected to a PC (Cary Eclipse software for Windows 95/98/NT system). Excitation-emission matrices (EEM) for using second-

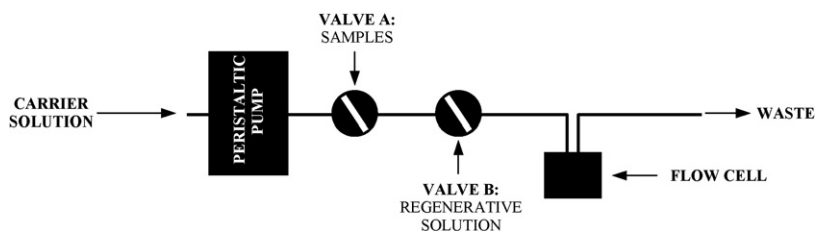


Fig. 1. Optosensing manifold for continuous MA-NCs RTF monitoring.

order data methods (N-PLS, U-PLS, PLS/RBL) were recorded in the excitation range from 300 to 350 nm each 4 nm and in the emission range from 390 to 450 nm each 2 nm, hence the size of each data matrix was $14 \times 31 = 434$ data points per sample matrix. Once EEM matrices have been obtained for each sample, vector data belonging to the first-order data type, such as emission spectra can be extracted in order to apply first-order multivariate calibration method (PLS). The selected excitation and emission wavelength ranges contain the wavelengths corresponding to the excitation and emission maxima for 1-NA and 2-NA when they are immobilized into MIP, i.e., 333/421 and 347/411 nm, respectively, and avoid the scattering signal from the polymeric matrix (Fig. 2).

The pH measurements were performed using a MicropH 2002 meter (Crison, Barcelona, Spain).

2.5. Calibration, validation and spiked drinking waters

For the simultaneous determination of 1-NA and 2-NA in the presence of 1-NMA two strategies were used. First, a calibration set of 19 samples was prepared containing 1-NA and 2-NA according to a central composite design with the central point replicated three times. The resulting concentrations, after applying the above mentioned experimental design using the program Unscrambler[®] 5.0, were in the range of 0–710 ng mL⁻¹ for both analytes (Table 1). Another calibration set of 31 samples containing 1-NA, 2-NA and 1-NMA was constructed with the same software, using a central composite design with three replicates of the central point. The resulting concentrations were in the range of 0–781 ng mL⁻¹ for all analytes (Table 2). The concentration levels were selected considering the linear fluorescence concentration ranges in both cases. Slight differences in concentration ranges for binary and ternary mixtures are the result of using designs with the same concentration values for the two-level full factorial sub-design contained in the central composite design.

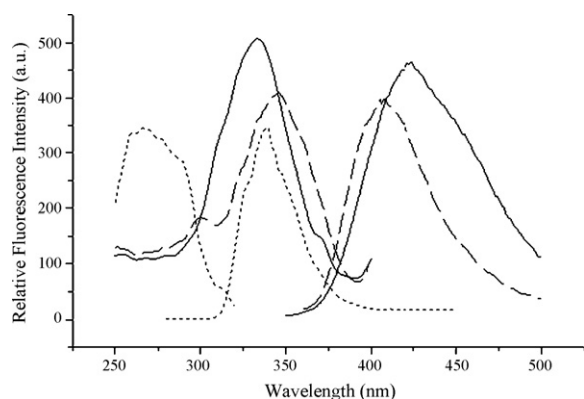


Fig. 2. Room temperature fluorescence excitation and emission spectra of 1-NA (solid line), 2-NA (dash line), and 1-NMA (dot grey line) immobilized into MIP; concentration of MA-NCs = 50 $\mu\text{g mL}^{-1}$, slits_{exc/em} 5/5 nm and detector voltage 750 V.

Table 1

Central composite design for the binary calibration set.

Sample code	1-NA (ng mL ⁻¹)	2-NA (ng mL ⁻¹)
1	0	335
2	0	335
3	710	335
4	710	335
5	335	0
6	335	0
7	335	710
8	335	710
9	70	70
10	70	70
11	600	70
12	600	70
13	70	600
14	70	600
15	600	600
16	600	600
17	335	335
18	335	335
19	335	335

Table 2

Central composite design for the ternary calibration set.

Sample code	1-NA (ng mL ⁻¹)	2-NA (ng mL ⁻¹)	1-NMA (ng mL ⁻¹)
1*	0	335	335
2*	0	335	335
3*	781	335	335
4*	781	335	335
5*	335	0	335
6*	335	0	335
7*	335	781	335
8*	335	781	335
9*	335	335	0
10*	335	335	0
11*	335	335	781
12*	335	335	781
13*	70	70	70
14*	70	70	70
15*	600	70	70
16*	600	70	70
17*	70	600	70
18*	70	600	70
19*	600	600	70
20*	600	600	70
21*	70	70	600
22*	70	70	600
23*	600	70	600
24*	600	70	600
25*	70	600	600
26*	70	600	600
27*	600	600	600
28*	600	600	600
29*	335	335	335
30*	335	335	335
31*	335	335	335

Table 3
Prediction sample set of spiked tap and mineral waters.

Sample code	1-NA (ng mL ⁻¹)	2-NA (ng mL ⁻¹)	1-NMA (ng mL ⁻¹)
Tap water			
W1	100	300	360
W2	100	300	360
W3	360	300	360
W4	500	300	360
Mineral water			
W5	360	100	360
W6	360	100	360
W7	360	500	360

Two validation sets, one with binary mixtures of 1-NA and 2-NA, and an additional one with ternary mixtures of 1-NA, 2-NA and 1-NMA were designed and prepared considering the calibration ranges. A set of tap water samples from the city of Granada, and a set of mineral waters (commonly available in Spain) were spiked with 1-NA, 2-NA and 1-NMA at different levels, considering the linear fluorescence calibration range (Table 3). These samples underwent no previous treatment.

All fluorescence measurements were performed in random order as described below and analyzed using the chemometric algorithms.

2.6. Measurement procedure

The fluorescence measurements were carried out by using the flow-through system described above. The samples were injected in the flow injection system, monitoring the response at the 1-NA and 2-NA fluorescent excitation and emission wavelengths in a kinetic mode. When the system response reached maximum fluorescence intensity, the flow was stopped, and excitation-emission fluorescence matrix for the mixture was collected. The matrix data were then transferred to a microcomputer and processed by applying chemometric analysis.

3. Theory

3.1. Data orders

The various types of instrumental data have been classified on the basis on tensor algebra [18–20]. Within this scheme, when a given instrument produces a single instrumental response for a chemical sample, this datum is a scalar or zeroth-order tensor. Vector data for each sample belong to the first-order type: for example, absorption or emission spectra [UV–visible spectrophotometry, spectrofluorimetry, infrared, near-infrared (NIR), etc.], electrochemical scans (voltammograms, chrono-amperograms), nuclear magnetic resonance spectra, etc. When two first-order instruments are coupled in tandem (e.g., GC–MS, MS–MS, etc.), the order increases from first- to second-order. The latter can also be produced using a single instrument: examples are a spectrofluorometer registering excitation-emission matrices or a diode-array spectrophotometer where a chemical reaction takes place. The data order can be further increased to three if, for example, EEMs are registered as a function of time.

3.2. First-order data

First-order data are processed by suitable first-order multivariate calibration procedures, such as PLS. This involves a calibration step in which the relation between spectra and component concentrations is estimated from a set of reference samples, and a prediction step in which the results of the calibration are used

to estimate the component concentration in an unknown sample spectrum [21]. The PLS-1 version is optimized for the determination of a single analyte of interest, setting the optimum number of loading vectors A in order to avoid overfitting. This is done by applying the leave-one-out cross-validation method described by Haaland and Thomas [22] a set of I calibration spectra is obtained, the model is built with the $(I - 1)$ remaining calibration spectra, and the concentration of the sample left out during the calibration is predicted. This process is repeated a total of I times, until each sample has been left out once. The concentration predicted for each sample is compared with the known concentration of this reference sample. The sum of squared prediction errors for all calibration samples or PRESS is calculated each time a new factor is added to the model. The optimum number is then obtained by computing the ratio $F = \text{PRESS}(A < A^*) / \text{PRESS}(A)$, where A^* leads to the minimum PRESS, and selecting the number of factors corresponding to a probability of less than 75% for $F > 1$.

3.3. Second-order data

3.3.1. U-PLS

U-PLS operates in a similar way to PLS-1, except that second-order data are first vectorized or unfolded along one of the data dimensions, and then a conventional PLS model is built using these unfolded data and the nominal analyte concentrations [16]. Cross-validation can also be employed to estimate the number of calibration latent variables.

3.3.2. N-PLS

Multivariate regression methods such as N-PLS extend the traditional PLS algorithm to higher orders, using the multidimensional structure of the data for model building and prediction [15]. In the case of three-way data, the model is given by the following equation:

$$x_{ijk} = \sum_{f=1}^N t_{if} w_{jf}^j w_{kf}^k + e_{ijk} \quad (1)$$

where x_{ijk} is the fluorescence intensity for sample i at excitation wavelength j and emission wavelength k , N is the number of components, t_{if} is an element of the score matrix \mathbf{T} , w_{jf}^j and w_{kf}^k are elements of two \mathbf{W} loading matrices, and e_{ijk} is a residue not fitted by the model. The model finds the scores yielding maximum covariance with analyte concentrations as the dependent variable. The advantage of using N-PLS over bidimensional regression is a stabilization of the decomposition involved in Eq. (1), which potentially gives increased interpretability and better predictions.

3.3.3. N-PLS/RBL and U-PLS/RBL

If unexpected constituents occur in a test sample, neither the U-PLS nor N-PLS scores for the latter sample can be used for analyte prediction using the trained model. In this case, it is necessary to resort to a technique which is able to: (1) detect the new sample as an outlier, indicating that further actions are necessary before prediction, and (2) isolate the contribution of the unexpected component from that of the calibrated analytes, in order to recalculate appropriate scores for the test sample. U-PLS and N-PLS will consider a sample as an outlier if the residuals of the test data reconstruction are abnormally large in comparison with the typical instrumental noise. In such a case, residual bilinearization can be employed to model the presence of unexpected sample components using principal component analysis (PCA), which allows one to estimate profiles for the unexpected components in the three data dimensions [16,17]. The RBL procedure consists in keeping con-

stant the matrix of calibration loadings, and varying the test sample scores in order to model the test data as a sum of contributions: (1) one modeled by the calibration loadings and (2) one due to the potential interferences. The number of unexpected components in the PCA phase can be assessed by comparing the final residuals of the RBL model with the instrumental noise level. Once the RBL step is finished, and the correct test sample scores have been found, they are employed to provide the analyte concentration as is regularly done in all PLS models.

3.3.4. Figures of merit

Figures of merit such as sensitivity can be estimated for all PLS models, including those coupled to RBL [23]. The analytical sensitivity (γ) and its inverse are also useful [24–26], because they do not depend on the type of measured signal. Finally, the limit of detection (LOD) can be estimated and reported.

3.3.5. Software

All PLS models were applied using suitable MATLAB routines [27], implemented in a graphical user interface available at <http://www.chemometry.com/Index/Links%20and%20downloads/Programs.html>. The N-PLS code is available on the internet at <http://www.models.life.ku.dk/source/>.

4. Results and discussion

4.1. Spectral behavior of the analytes

In solution, naphthalene emits fluorescence at 332 nm exciting at 286 nm, while 1-NA and 2-NA show emission at 445 and 410 nm, when excited at 309 and 333 nm, respectively [12]. When they are immobilized into MIP, 1-NA emits at 421 nm exciting at 333 nm, while 2-NA emits fluorescence at 411 nm when excited at 347 nm (see Fig. 2). The wavelengths corresponding to excitation and emis-

sion maxima in the solid phase are very similar to those obtained in solution, thus it can be concluded that there is no chemical interaction between MA-NCs and MIP.

A significant spectral overlap is apparent between both emission and excitation spectra of analytes (Fig. 2). In a previous work, an iso-emissive point was selected (342/415 nm for excitation/emission wavelengths) for the total determination of both analytes, after it was demonstrated that the signals are additive [12]. The total amount of 1-NA and 2-NA was determined in this latter case. On the other hand, considering the spectral characteristics of the present sample components, the combination of spectral derivatives and zero-crossing could not be successfully applied. Moreover, an additional compound (1-NMA) is a potential interferent because: (1) it emits fluorescence in the working spectral range, and (2) it interacts with MIP, showing the “lowest minimum interferent concentration” (300 ng mL⁻¹), which is the concentration of interferent producing a signal equal or higher than 10% of the fluorescence response produced by the solutions of 1-NA and 2-NA [12]. This implies that chemometrics could be useful for treating fluorescence data in order to simultaneously determine 1-NA and 2-NA in drinking waters, even in the presence of interferences such as 1-NMA or complex background matrices. In this work, first- and second-order multivariate calibration methods were applied for simultaneous determination of 1-NA and 2-NA in drinking water and in the presence of 1-NMA.

4.2. Multivariate calibration results

4.2.1. Results using a binary calibration set

One of the calibration sets described in Section 2 includes two monoamine naphthalene compounds (1-NA and 2-NA), while all other sample components are unsuspected compounds which are not modeled by the calibration set (see Table 1).

Table 4

Second-order multivariate calibration methods. Prediction for test samples (T) and spiked drinking water samples (W) using the binary calibration set.

Samples	Nominal concentrations (ng mL ⁻¹)		Predicted concentrations (ng mL ⁻¹) ^a				
	1-NA	2-NA	N-PLS/RBL ^b		U-PLS/RBL ^b		
			1-NA	2-NA	1-NA	2-NA	
T1	0	335	2 (4)	353 (8)	1 (4)	305 (4)	
T2	710	335	613 (2)	325 (6)	691 (8)	342 (4)	
T3	335	0	350 (3)	22 (1)	313 (5)	20 (5)	
T4	70	600	71 (1)	555 (3)	79 (3)	614 (8)	
T5	600	600	670 (3)	615 (4)	594 (4)	570 (6)	
RMSEP ^c (ng mL ⁻¹)			28	17	11	20	
REP ^d			8	7	3	5	
Samples	Nominal concentrations (ng mL ⁻¹)			Predicted concentrations (ng mL ⁻¹)			
	1-NA	2-NA	1-NMA	N-PLS/RBL ^e		U-PLS/RBL ^e	
				1-NA	2-NA	1-NA	2-NA
W1	100	300	360	90 (7)	270 (9)	92 (9)	328 (9)
W2	100	300	360	93 (8)	284 (8)	95 (9)	270 (8)
W3	360	300	360	313 (8)	309 (7)	326 (9)	286 (8)
W4	500	300	360	401 (9)	262 (9)	411 (9)	275 (6)
W5	360	100	360	347 (1)	96 (1)	395 (4)	109 (8)
W6	360	100	360	371 (8)	93 (2)	328 (8)	103 (9)
W7	360	500	360	359 (9)	511 (8)	343 (9)	483 (1)
RMSEP ^c (ng mL ⁻¹)				31	24	30	18
REP ^d				9	7	9	7

^a Average of three replicates, standard deviations in parentheses.

^b Number of latent variables for 1-NA, 2; for 2-NA, 4; $N_{\text{uns}} = 0$.

^c Root mean square error of prediction.

^d Relative error of prediction.

^e Number of latent variables for 1-NA, 2; for 2-NA, 4; $N_{\text{uns}} = 1$.

Table 5
Second-order multivariate calibration methods. Prediction for test samples (T) and spiked drinking water samples (W) using ternary calibration set.

Samples	Nominal concentrations (ng mL ⁻¹)			Predicted concentrations (ng mL ⁻¹) ^a			
	1-NA	2-NA	1-NMA	N-PLS/RBL ^b		U-PLS/RBL ^b	
				1-NA	2-NA	1-NA	2-NA
T1	0	335	335	3 (4)	366 (6)	15 (5)	345 (3)
T2	710	335	335	692 (3)	330 (6)	721 (6)	312 (3)
T3	335	335	335	321 (3)	293 (7)	374 (5)	326 (5)
T4	70	70	335	77 (2)	71 (3)	71 (3)	72 (8)
T5	70	600	600	69 (4)	636 (4)	70 (4)	618 (7)
RMSEP ^c (ng mL ⁻¹)				8	16	11	10
REP ^d %				3	6	3	3
Samples	Nominal concentrations (ng mL ⁻¹)			Predicted concentrations (ng mL ⁻¹)			
	1-NA	2-NA	1-NMA	N-PLS/RBL ^e		U-PLS/RBL ^e	
				1-NA	2-NA	1-NA	2-NA
W1	100	300	360	91 (7)	265 (9)	87 (5)	302 (1)
W2	100	300	360	90 (9)	279 (8)	93 (9)	290 (7)
W3	360	300	360	345 (9)	267 (7)	348 (4)	267 (9)
W4	500	300	360	433 (9)	274 (5)	442 (8)	268 (5)
W5	360	100	360	328 (8)	80 (6)	372 (8)	102 (8)
W6	360	100	360	386 (8)	103 (9)	375 (9)	108 (9)
W7	360	500	360	397 (8)	510 (7)	331 (9)	487 (3)
RMSEP ^c (ng mL ⁻¹)				24	17	13	11
REP ^d %				8	5	4	4

^a Average of three replicates, standard deviations in parentheses.

^b Number of latent variables for 1-NA, 3; for 2-NA, 3.

^c Root mean square error of prediction.

^d Relative error of prediction.

^e Number of latent variables for 1-NA, 3; for 2-NA, 3.

A set of validation samples (T) was prepared considering the calibration concentration ranges of both analytes 1-NA and 2-NA. Then, second-order data (excitation-emission fluorescence matrices) were obtained, and the samples were predicted applying second-order algorithms. The number of latent variables A was determined by leave-one-out cross-validation using the calibration samples, and were $A=2$ for 1-NA and $A=4$ for 2-NA. Considering that two fluorescent compounds are included in both calibration sets it is logical to think that two factors are needed for each analyte. However, four factors are required for 2-NA, which may be due to the presence of background effects. The results are shown in Table 4.

Prediction samples (W) were obtained by adding Granada tap water and mineral waters commonly sold in Spain with naphthalene compounds considering the calibration concentration ranges, and also the potential interferent 1-NMA at a "minimum interferent concentration" of 300 ng mL⁻¹. Second-order data were obtained, and analytes were predicted applying second-order multivariate methods. The recoveries for the second-order multivariate algorithms U-PLS and N-PLS were not satisfactory (Table 4), using as latent variables $A=2$ for 1-NA and $A=4$ for 2-NA. When U-PLS and N-PLS are combined with residual bilinearization (see Section 3) the number of latent variables was identical, while $N_{\text{uns}}=1$, due to the contribution to the signal from the unsuspected interferent (i.e., 1-NMA). Prediction results obtained applying PLS/RBL are shown in Table 4. The good results suggest that the second-order advantage is fully applied using both PLS/RBL combinations [28]. The value of $N_{\text{uns}}=1$ indicates that 1-NMA is really an interferent. Taking into account that this compound is not included in the calibration set, its signal was not modeled by the calibration data, hence the second-order advantage is absolutely necessary. Table 4 also shows RMSEP and REP% values. They are reasonably good in view of the concentration ranges and matrix complexity. An accuracy test based on the elliptical joint confidence region (EJCR) for the slope and intercept

of predicted versus nominal concentration values was also performed [29]. The elliptical region contained the theoretical point of slope = 1 and intercept = 0, as is shown in Fig. 3G–J. This fact indicates that prediction results for spiked drinking water are accurate. Figures of merit were also determined for both analytes in all samples. The analytical sensitivities (SEN) in water samples were 0.15 and 0.09 mL ng⁻¹ for 1-NA and 2-NA, respectively, leading to the inverse values (γ_n^{-1}) of 6.5 and 11.0 ng mL⁻¹, reasonable considering the concentration range. The limit of detection was 20 ng mL⁻¹ for both analytes [26,27].

4.2.2. Results using ternary calibration set

The alternative ternary calibration set described in Section 2 includes the monoamine naphthalene compounds of interest (1-NA and 2-NA) as well as the potential interferent 1-NMA (see Table 2).

A set of ternary test samples was prepared and predicted using this calibration set and second-order multivariate calibration methods N-PLS and U-PLS, in order to evaluate their predictive abilities.

A set of ternary prediction samples of spiked tap and mineral waters was prepared and measured as described above and predicted applying the second-order multivariate algorithms U-PLS and N-PLS. The satisfactory results shown in Table 5 suggest that the second-order advantage is not necessary, since the interferent is considered in the calibration set. Three factors are needed for each fluorescent compounds applying either the U-PLS or the N-PLS algorithm.

Statistical analysis for prediction and test results showed good RMSEP and REP% values both for N-PLS and U-PLS, and the elliptical regions contained the theoretical points of slope = 1 and intercept = 0, as displayed in Fig. 3C–F [29]. Figures of merit were also calculated: for N-PLS, analytical sensitivities 0.14 and 0.13 FU mL ng⁻¹, inverse values of analytical sensitivities 7.4 and 7.1 ng mL⁻¹ and limits of detection 11 and 20 ng mL⁻¹ for 1-NA and 2-NA, respectively. In case of U-PLS, the values were: analytical sen-

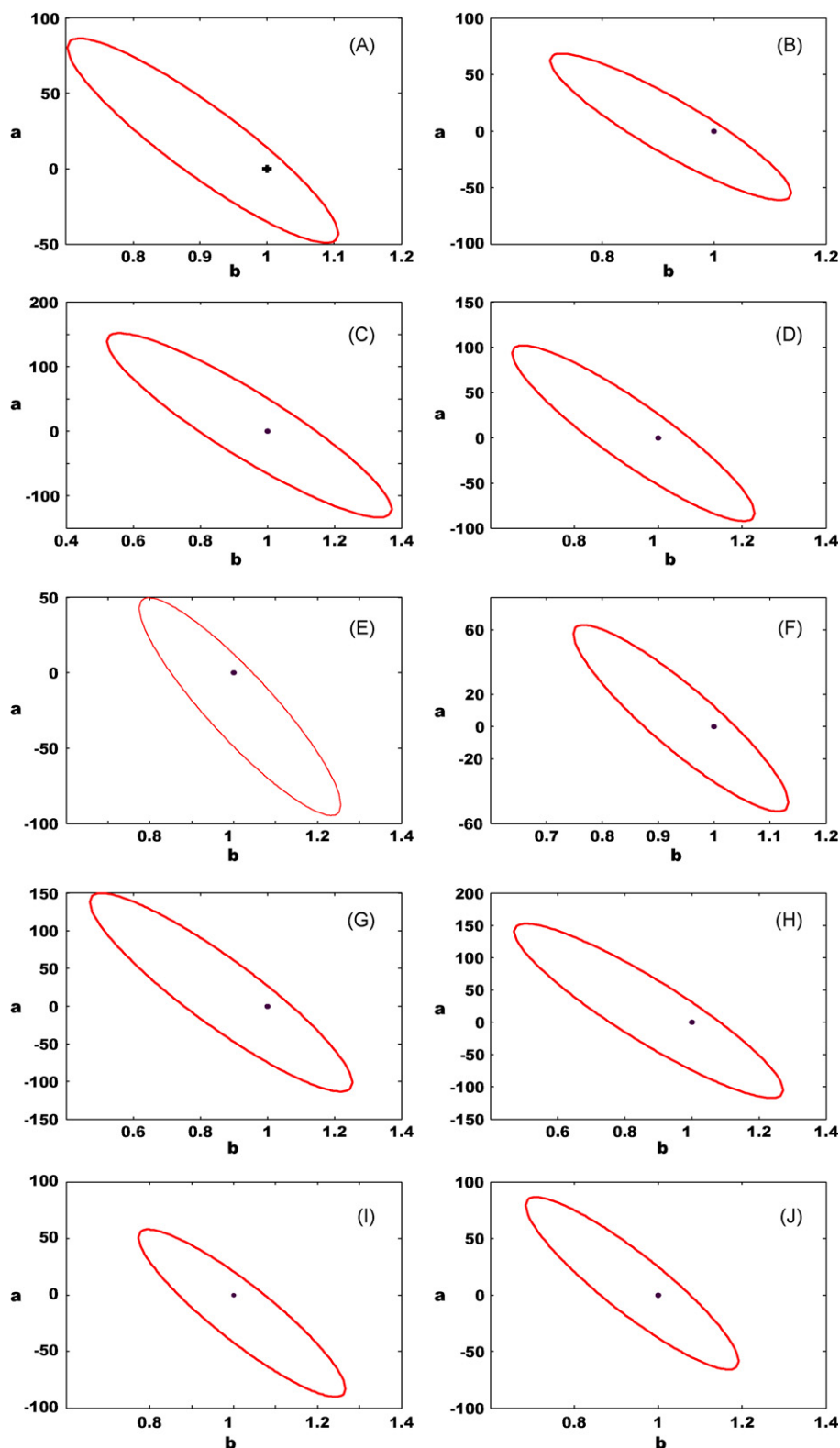


Fig. 3. Test of accuracy based on elliptical joint confidence regions (EJCR). (A) PLS-1 for 1-NA, (B) PLS-1 for 2-NA, (C) N-PLS for 1-NA, (D) U-PLS for 1-NA, (E) N-PLS for 2-NA, (F) U-PLS for 2-NA, (G) N-PLS/RBL for 1-NA, (H) U-PLS/RBL for 1-NA, (I) N-PLS/RBL for 2-NA, and (J) U-PLS/RBL for 2-NA. The red line indicates the elliptical joint confidence region. The point marked in black is the ideal point (0,1) for intercept (a) and slope (b), respectively. (For interpretation of the references to color in this figure legend, the reader is referred to the web version of the article.)

sitivities, 0.23 and 0.15 mL ng⁻¹, inverse of analytical sensitivities, 4.2 and 6.0 ng mL⁻¹ and limits of detection of 12 and 23 ng mL⁻¹ for 1-NA and 2-NA, respectively. These values indicate no serious difference between the employed algorithms.

Another alternative in the case of using ternary calibration samples for predicting ternary samples was to apply first-order multivariate calibration methods such as PLS-1. Once emission-excitation matrices were recorded, emission fluorescence vector

Table 6
Prediction for test samples (T) and spiked drinking waters applying the first-order multivariate calibration method PLS-1 using the ternary calibration set.

Samples	Nominal concentrations (ng mL ⁻¹)			Predicted concentrations (ng mL ⁻¹) ^a	
	1-NA	2-NA	1-NMA	PLS-1	
				1-NA ^d	2-NA ^d
T1	0	335	335	0 (4)	364 (3)
T2	710	335	335	740 (2)	350 (4)
T3	335	335	335	320 (5)	337 (6)
T4	70	70	335	67 (1)	64 (8)
T5	70	70	600	67 (3)	69 (7)
RMSEP ^b (ng mL ⁻¹)				11	11
REP ^c %				5	5
Samples	Nominal concentrations (ng mL ⁻¹)			Predicted concentrations (ng mL ⁻¹) ^a	
	1-NA	2-NA	1-NMA	PLS-1	
				1-NA ^d	2-NA ^d
W1	100	300	360	107 (5)	250 (9)
W2	100	300	360	100 (5)	268 (8)
W3	360	300	360	362 (5)	289 (8)
W4	500	300	360	450 (9)	287 (4)
W5	360	100	360	329 (8)	98 (8)
W6	360	100	360	366 (7)	108 (7)
W7	360	500	360	351 (7)	480 (9)
RMSEP ^b (ng mL ⁻¹)				17	26
REP ^c %				6	9

^a Average of three replicates, standard deviations in parentheses.

^b Root mean square error of prediction.

^c Relative error of prediction.

^d Number of factors: 3 for 1-NA and 2 for 2-NA.

data were extracted for each sample, and these first-order data were processed using first-order multivariate calibration methods.

The sets of ternary test samples and spiked tap and mineral waters were also resolved applying PLS-1, being $A=3$ for 1-NA, meanwhile $A=2$ for 2-NA. It is logical to think that three factors were needed for both analytes considering that at least three fluorescence compounds are present in samples. Really the recoveries as well as the figures of merit were very similar using two or three factors for 2-NA, but the probability (P) was slightly lower using two factors, suggesting that the interference of 1-NMA is negligible in this case may be due to the weak emission signal of the interferent in the score range selected from 390 to 450 nm. Despite this weak signal seems to be important for determining 1-NA and so three factors are needed. The results are shown in Table 6. Figures of merits were: analytical sensitivities, 0.065 FU mL ng⁻¹ for 1-NA and 0.047 mL ng⁻¹ for 2-NA; inverse values, 15 ng mL⁻¹ for 1-NA and 21 ng mL⁻¹ for 2-NA; limits of detection, 15 ng mL⁻¹ for 1-NA and 33 ng mL⁻¹ for 2-NA [23]. Accuracy was also studied, and the elliptical region contained the theoretical point of slope = 1 and intercept = 0, as shown in Fig. 3A and B. It can be noticed that ternary samples could be resolved using ternary calibration, either by applying second-order methods such as N-PLS and U-PLS, or by applying first-order method such as PLS-1. Although the first-order method seems to be simpler and first-order data acquisition faster, second-order methods are more sensitive as can be concluded by comparing the estimated figures of merit, because they resort to multiple measurements at more sensors [30,31]. Besides, emission and excitation matrices can be easily obtained by a fast-scanning spectrofluorometer. Therefore, if second-order data can be recorded, they are preferred over first-order ones.

5. Conclusions

In the present report, a MIP fluorescence optosensor in combination with a flow injection technique was applied to simultaneously

determine 1-NA and 2-NA in drinking waters. Fluorescence data were processed applying different multivariate calibration algorithms allowing the quantization of both principal monoamines naphthalene compounds even in presence of a potential interferent 1-NMA without sample pretreatment. Classical first-order algorithm such as PLS-1 was applied for processing fluorescence emission spectra data at a fixed wavelength and shows satisfactory results for 1-NA and 2-NA when the interferent is considered in the calibration set, it means both calibration and test samples contain the analytes and the interferent 1-NMA. Second-order algorithm like multiway PLS and unfolded PLS were used for assisting excitation-emission fluorescence matrices, allowing the determination of both analytes of interest also when the potential interferent signal is modeled during calibration, both calibration and test samples include the analytes and the interferent. Comparing figures of merit second-order data seems to be more sensitive. Taking into account this fact and also considering that, emission and excitation matrices can be easily obtained by a fast-scanning spectrofluorometer, if second-order data can be obtained, they are preferred over first-order ones. However, these second-order algorithms showed bad results when the interferent is not included in the calibration set used for prediction. Although, when they are combined with residual bilinearization, prediction results are satisfactory, suggesting that the second-order advantage is fully applied using both PLS/RBL combinations. Moreover, if second-order data can be recorded, they are preferred over first-order ones, because the calibration set involves less samples if three sample components are considered in the test samples. Second-order algorithms with the second-order advantage could be performed using a binary calibration set containing 19 samples in order to predict the analytes in the presence of interferents, or using a ternary calibration set of 31 samples including the interferent in the calibration set without the second-order advantage. The binary calibration is preferred because less experimental samples are required. First-order algorithms could only be applied using a ternary calibration

set, i.e., including the interferent in the calibration set, and thus more experimental samples are involved. Moreover, first-order algorithms require the construction of a sufficiently representative calibration set of samples, which should span all the variability expected in unknown samples. For this reason, in this work the interferent 1-NMA must be included in the calibration set involving more experimental samples.

Acknowledgments

The authors thank to the Spanish Ministry of Education (FPU grant reference AP2006-01147 and project CTQ2007-60079), the Regional Government of Andalusia (excellence projects RNM-666 and P07-FQM-02625) and Andalusian Water Agency (agreement 2243) for their financial support. The National University of Rosario, CONICET (Nacional Centre of Scientific and Tecnical Research) and ANPCyT (Nacional Agency of Scientific and Tecnical Promotion) are also acknowledged for financial support. The authors also gratefully thanks Prof. Dr. Alejandro C. Olivieri, international recognized for his experience in chemometric analysis, for his helpful collaboration in the present work.

References

- [1] K.C. Lee, Y. Ku, *Sep. Sci. Technol.* 31 (1996) 2557.
- [2] F.Q. Liu, J.L. Chen, A.M. Li, Z.H. Fei, Z.L. Zhu, Q.X. Zhang, *Chin. J. Polym. Sci.* 21 (2003) 317.
- [3] A.M. Li, Q.X. Zhang, J.L. Chen, Z.G. Fei, L. Chao, W.X. Li, *React. Funct. Polym.* 49 (2001) 225.
- [4] L.Z. Zhu, B.L. Chen, *Environ. Sci. Technol.* 34 (2000) 2997.
- [5] R. Stabbert, K.H. Schäfer, C. Biefel, K. Rustemeier, *Rapid Commun. Mass Spectrom.* 17 (2003) 2125.
- [6] R.M. Black, R.J. Clarke, R.W. Read, M.T.J. Reid, *J. Chromatogr. A* 662 (1994) 301.
- [7] A.L. Jenkins, S.Y. Bae, *Anal. Chim. Acta* 542 (2005) 32.
- [8] K. Haupt, K. Mosbach, *Chem. Rev.* 100 (2000) 2495.
- [9] A. Merkoci, S. Aegret, *TrAC Trends Anal. Chem.* 21 (2002) 717.
- [10] I. Sánchez Barragán, J.M. Costa Fernández, R. Pereiro, A. Sanz Medel, A. Salinas, A. Segura, A. Fernández Gutiérrez, A. Ballesteros, J.M. González, *Anal. Chem.* 77 (2005) 7005.
- [11] E.L. Holthoff, F.V. Bright, *Anal. Chim. Acta* 594 (2007) 147.
- [12] A. Valero-Navarro, J.F. Fernández-Sánchez, A. Salinas-Castillo, R. Mallavia, A. Segura-Carretero, A. Fernández-Gutiérrez, *Biosens. Bioelectr.* (unpublished work).
- [13] S. Casado Terrones, J.F. Fernández Sánchez, B. Cañabate Díaz, A. Segura Carretero, A. Fernández Gutierrez, *J. Pharm. Biomed. Anal.* 38 (2005) 785.
- [14] B.K. Lavine, *Anal. Chem.* 70 (1998) 209R.
- [15] R. Bro, *J. Chemom.* 10 (1996) 47.
- [16] J. Öhman, P. Geladi, S.J. Wold, *J. Chemom.* 17 (2003) 274.
- [17] A.C. Olivieri, *J. Chemom.* 19 (2005) 253.
- [18] E. Sánchez, B.R. Kowalsky, *Anal. Chem.* 58 (1986) 496.
- [19] E. Sánchez, B.R. Kowalsky, *J. Chemom.* 2 (1998) 247.
- [20] E. Sánchez, B.R. Kowalsky, *J. Chemom.* 4 (1990) 29.
- [21] N.M. Faber, J. Ferré, R. Boqué, *Chemom. Intell. Lab. Syst., Lab. Inf. Manage.* 55 (2001) 67.
- [22] D.M. Haaland, E.V. Thomas, *Anal. Chem.* 60 (1988) 1193–1202.
- [23] A.C. Olivieri, N.M. Faber, J. Ferré, R. Boqué, J. Kalivas, H. Mark, *Pure Appl. Chem.* 78 (2006) 633.
- [24] L. Cuadros Rodríguez, A.M. García Campaña, C. Jiménez Linares, M. Román, *Ceba. Anal. Lett.* 26 (1993) 1243.
- [25] A. Lorber, *Anal. Chem.* 58 (1986) 1167.
- [26] G.M. Escandar, P.C. Damiani, H.C. Goicoechea, A.C. Olivieri, *Microchem. J.* 82 (2006) 29.
- [27] MATLAB 7.0, The MathWorks Inc., Natick, MA, USA.
- [28] A.C. Olivieri, *Anal. Chem.* 77 (2005) 4936.
- [29] A.G. González, M.A. Herrador, A.G. Asuero, *Talanta* 48 (1999) 729.
- [30] G.M. Escandar, N.M. Faber, H.C. Goicoechea, A. Muñoz de la Peña, A.C. Olivieri, R.J. Poppi, *Trends Anal. Chem.* 26 (2007) 752–765.
- [31] A.C. Olivieri, *Anal. Chem. (Perspect.)* 80 (2008) 5713–5720.



Pore-functionalized polymer membranes for preconcentration of heavy metal ions

T. Vasudevan^a, Sadananda Das^b, Suparna Sodaye^b, A.K. Pandey^{b,*}, A.V.R. Reddy^b

^a Research Reactor Services Division, Bhabha Atomic Research Centre, Trombay, Mumbai 400 085, India

^b Radiochemistry Division, Bhabha Atomic Research Centre, Trombay, Mumbai 400 085, India

ARTICLE INFO

Article history:

Received 21 July 2008

Received in revised form 30 October 2008

Accepted 30 October 2008

Available online 7 November 2008

Keywords:

Functionalized membrane

Acidic monomer

Ethylene glycol methacrylate phosphate

UV-grafting

Metal ions

Radiotracers

Selectivity

ABSTRACT

Functionalized membranes containing carboxylate, phosphate and sulfonate groups were prepared by UV-initiator induced graft polymerization of the functional monomer (acrylic acid, ethylene glycol methacrylate phosphate (EGMP) and 2-acrylamido-2-methyl-1-propane sulfonic acid) with a crosslinker (methylenebisacrylamide) in the pores of poly(propylene) host membranes. The functionalized membranes thus obtained were characterized by gravimetry, FTIR spectroscopy, radiotracers and scanning electron microscopy for the degree of grafting and water uptake, presence of functional groups, ion-exchange capacity, and physical structure of the membranes, respectively. The uptakes of Cs⁺, Ag⁺, Sr²⁺, Cd²⁺, Hg²⁺, Zn²⁺, Eu³⁺, Am³⁺, Hf⁴⁺ and Pu⁴⁺ ions in the functionalized membranes were studied as a function of acidity of the equilibrating aqueous solution. Among the functionalized membranes prepared in the present work, the EGMP-grafted membrane (with phosphate groups) showed acid concentration dependent selectivity towards multivalent metal ions like Eu³⁺, Am³⁺, Hf⁴⁺ and Pu⁴⁺. The solvent extraction studies of EGMP monomer in methyl isobutyl ketone (MIBK) solvent indicated that divalent and trivalent metal ions form complexes with EGMP in 1:2 proportion, but the distribution coefficients of trivalent metal ions were significantly higher than for the divalent ions. The uptakes of Eu³⁺ ions in monomeric EGMP (dissolved in MIBK) and polymeric EGMP (in the forms of crosslinked gel and membrane) were studied as a function of concentration of H⁺ ions in the equilibrating solution. This study indicated that polymeric EGMP has better binding ability towards Eu³⁺ as compared to monomeric EGMP. The variation of distribution coefficients of Eu³⁺/Am³⁺ in gel and membrane as a function of H⁺ ion concentration in the equilibrating aqueous solution indicated that ionic species held in the membrane and gel were not same. These results indicated that proximity of functional groups (phosphate) plays an important role in metal ion binding with polymeric EGMP.

© 2008 Elsevier B.V. All rights reserved.

1. Introduction

Membranes with functional groups have applications in the chemical sensors, fuel cell, separation science, electrodialysis, and as a host for nanoparticles [1–5]. Most of the commercially available membranes are ion-exchange membranes. Therefore, these membranes cannot be used for the applications that require selective recognition of target ions. The target ion specific membrane is a key issue not only in development of the chemical sensors but also in developing separation schemes for various applications, e.g. the radioactive waste reprocessing. At present, target specific membranes are being developed by physically immobilizing specific ligands in a polymer matrix. These membranes are known as supported liquid membranes and polymer inclusion

membranes. The supported liquid membranes (SLMs) are formed by the physical immobilization of the organic phase containing a mobile carrier (extractant) into the pores of a microporous host membrane. As the organic phase is held in the pores of the host membrane by capillary force, the long-term stability of the SLM is a major concern for its wide scale industrial applications [6]. In order to overcome the stability problems associated with the SLM, a new class of membranes called polymer inclusion membranes (PIMs) have been developed [7]. The PIMs are prepared by physical immobilization of a selective extractant into a plasticized polymer matrix. The PIMs have been reported to have better stability than SLMs. These membranes find extensive applications to prepare the electrochemical and optical chemical sensors [2]. However, the transport of ions across PIM has been found to be slower than SLM and fixed-site carrier membrane. This is due to fact that viscosity of the liquid fraction and hydrophobicity of PIM are considerably higher than those for other two classes of membrane [8].

* Corresponding author. Tel.: +91 22 25590641; fax: +91 22 25505150/25505151.
E-mail address: ashokk@barc.gov.in (A.K. Pandey).

The membranes can be made quite stable by linking functional groups covalently with the polymer chains in the membrane. Such membranes can be synthesized by grafting a monomer on polymer chains and subsequently generating required functional group by chemical modification of the precursor chemical groups on grafted polymer chains. This class of membranes is termed as fixed-site membranes, functionalized membranes, or adsorptive membranes. The membranes used for the metal ions separation have been prepared by anchoring monomers 4-vinyl benzyl chloride (converted to phosphonate ester or triethyl ammonium) [9], 4-vinylpyridine [10–11], acrylonitrile (converted to amidoxime) [12–14], acrylic/methacrylic acid [15] and monomer containing benzo-18-crown-6 crown ether functional groups [16] in the host microporous membrane. Ethylene glycol methacrylate phosphate (EGMP) and 2-acrylamido-2-methyl-1-propane sulfonic acid (AMPS) grafted membranes have not been studied for metal ions separations. However, these monomers have been used for preparing the proton conducting composite materials [17,18].

The objective of the present study is to develop a functionalized flat sheet membrane that can be used as a sorbent for the preconcentration of heavy metal ions. In the present work, the functionalized membranes have been prepared by anchoring carboxylic, phosphate and sulfonate groups in the pores of a microporous host substrate by UV photoinitiator induced *in situ* polymerization of the monomer (acrylic acid (AA)/EGMP/2-acrylamido-2-methyl-1-propane sulfonic acid (AMPS)) along with a crosslinker methylenebisacrylamide. The membranes are characterized in terms of degree of grafting, ion-exchange capacity, water uptake capacity, and physical and chemical structures. Studies on the uptake of Cs⁺, Ag⁺, Sr²⁺, Cd²⁺, Hg²⁺, Zn²⁺, Eu³⁺, Am³⁺, Hf⁴⁺ and Pu⁴⁺ in the membranes were carried out as a function of acidity of the equilibrating solution. The extraction of multivalent ions in organic phase consisting of monomer EGMP dissolved in methylisobutyl ketone solvent (MIBK), EGMP gel, and EGMP membrane have also been studied to understand the mechanism of sorption of ions in the EGMP sorbents.

2. Experimental

2.1. Reagents and apparatus

Analytical reagent grade chemicals and de-ionized water (18 M Ω /cm) purified by model QuantumTM from Millipore (Mumbai, India) were used throughout the present studies. EGMP, AMPS, AA, N-N'-methylenebisacrylamide (MBA), and α,α' -dimethoxy- α -phenyl acetophenone (DMPA) were obtained from Sigma-Aldrich (Steinheim, Switzerland). Tetrahydrofuran (THF), MIBK, and N-N'-dimethylformamide (DMF) were obtained from Merck (Mumbai, India). Radiotracers ²²Na, ^{110m}Ag, ¹³⁷Cs, ^{85,89}Sr, ^{115m}Cd, ²⁰³Hg, ⁶⁵Zn, ¹⁵⁴Eu, ²⁴¹Am, ²³⁹Pu and ¹⁸¹Hf dissolved in aqueous solutions were obtained either from the Board of Radiation and Isotope Technology, Mumbai, India or produced by reactor neutron irradiation of appropriate target samples in our laboratory. The γ -activities of the radiotracers in the membrane and equilibrating solution were monitored by using either a high purity germanium (HPGe) detector or a well-type NaI(Tl) detector based gamma ray spectrometer. All the samples and standard containing radioactivity were counted in identical sample-detector geometry. The thickness of the membrane samples was measured using a digital micrometer (Mitutoyo, Japan) with a precision of ± 0.001 mm.

2.2. Preparation of functionalized membranes and gel

The monomer (AA, EGMP, or AMPS) along with a crosslinker, MBA and an UV initiator (α,α' -dimethoxy- α -phenyl acetophenone)

were dissolved in tetrahydrofuran (THF) and dimethylformamide (DMF) mixture. AMPS was first dissolved in water-methanol (1:1) mixed solvent, and then added to the grafting solution. The amounts of crosslinker and monomer were adjusted in the polymerization solution to get 4–5 mol% of crosslinking. The amount of UV-initiator was taken as 1 wt.% as this was found to be minimum quantity required to initiate the graft-polymerization. For grafting, the microporous host poly(propylene) membrane (6×6 cm² area, 60% porosity, 0.2 μ m pore diameter and 59 μ m thickness) was soaked in the polymerizing solution, and sandwiched the grafting solution filled membrane between two transparent polyester sheets to prevent any possible loss of grafting solution filled in the pores. Care was taken to remove excess grafting solution and air bubbles trapped between the membrane and polyester sheets covering the membrane surface. Finally, the sandwiched membrane was exposed to 365 nm UV light in a multilamp photoreactor (Heber Scientific, model No. HML-SW-MW-LW-888) for a period of 20 min. After irradiation in the photoreactor, the membrane was washed thoroughly with THF, methanol and distilled water to remove the un-grafted components, and then conditioned with a aqueous solution having 0.25 mol L⁻¹ NaCl. The membrane sample was dried for 8–10 h under vacuum and weighed to obtain the weight of grafted membrane. The crosslinked EGMP gels were prepared by using same polymerizing solution in a 15 mL beaker, which was exposed to 365 nm UV light for 20 min in the photoreactor. After gelation, the crosslinked EGMP gels were washed to remove un-polymerized components and conditioned with 0.25 mol L⁻¹ NaCl.

2.3. Characterization of membranes

The degree of grafting in the membrane sample was calculated using weights of membrane sample before and after grafting. The water uptake capacity of the functionalized membranes was also determined by gravimetry using the following equation:

$$\text{water uptake capacity(\%)} = \frac{(W_{\text{wet}} - W_{\text{dry}})}{W_{\text{dry}}} \times 100 \quad (1)$$

where W_{wet} is the weight of the wet membrane sample and W_{dry} is the weight of the same membrane sample dried under vacuum. The membrane samples were powdered in liquid nitrogen and mixed with KBr for FTIR measurements. FTIR spectra of the samples were recorded using the spectrophotometer (8400-model) procured from Shimadzu, Japan. The KBr powder was used as an internal standard in the measurements. The ratio of the KBr to membrane samples was maintained to be 100:1. Diffused reflectance assembly was used for recording the spectra.

The ion exchange capacities of the functionalized membranes were measured by acid-base titration. The weighed membrane sample (2×2 cm²) in H⁺ form was equilibrated with 10 mL of 0.5 mol L⁻¹ NaCl for 5–6 h with a constant stirring at 25–27 °C. After equilibration, the membrane sample was taken out from the solution and droplets adhering on the surface of membrane were washed with de-ionized water. The amount of H⁺ ions (moles) liberated in the solution (final volume of 20 mL) was measured by potentiometric titration with standard NaOH solution. The ion-exchange capacity of the membrane was computed with the experimentally measured moles of H⁺ ions liberated in the equilibrating solution and weight of the dried membrane sample.

2.4. Uptake of metal ions

For uptake studies, 2×2 cm² pieces of membranes were equilibrated with 5 mL solutions containing desirable metal ions in different acidities for 24 h without stirring or 3 h with stirring at room temperature 25 °C. Buffer was not used in the uptake

experiments. The equilibration time was based on the experiments that indicated the minimum equilibration time for quantitative uptake of metal ions in the membrane samples. The radiotracers of ^{22}Na , $^{110\text{m}}\text{Ag}$, ^{137}Cs , $^{85,89}\text{Sr}$, $^{115\text{m}}\text{Cd}$, ^{203}Hg , ^{65}Zn , ^{154}Eu , ^{241}Am , ^{239}Pu and ^{181}Hf were used for the uptake studies. The concentrations of these radiotracers in the equilibrating solution were sub-ppm level depending upon the radioactivity of the radiotracer. The uptake of metal ions (except for ^{239}Pu) in the membrane was monitored by γ -activity of the solutions (5 mL) before and after equilibration of membrane samples, using a NaI(Tl) scintillation detector. The γ -activity of radiotracer used in these experiments was 40,000–50,000 counts/min in 5 mL solution. The uptake of ^{239}Pu in the membrane was obtained by α -scintillation counting of the samples taken before and after equilibration from the feed solution. The α -activity of the equilibrating solution (5 mL) was adjusted to obtain 10,000 counts/min in α -scintillation counting of its 50 μL sample. A 50 μL sample of the equilibrating solution was added to 5 mL of standard organic liquid scintillation cocktail and assayed by scintillation counting. The uptake of radiotracers in the membrane was obtained from Eq. (2).

$$\text{ions uptake(\%)} = \frac{(C_{\text{before}} - C_{\text{after}})}{(C_{\text{before}})} \times 100 \quad (2)$$

where C_{before} and C_{after} are the α -scintillations/ γ -activity (counts/s) of the radiotracer in the samples taken from feed solution before and after equilibrating with the membrane sample, respectively.

2.5. Extraction study

Monomer EGMP was dissolved in solvent isobutylmethyl ketone (MIBK) to prepare organic phase having EGMP concentration in the range of 0.50–3.75 molL⁻¹. The equal volumes (5 mL) of organic phase and aqueous phase containing a radiotracer ($^{65}\text{Zn}/^{154}\text{Eu}/^{241}\text{Am}$) were mixed in an equilibration tube, and shaken for 2 h in a constant temperature bath kept at 25 °C. The acidity and ionic strength of the aqueous phase were adjusted with HNO₃ and NaNO₃, respectively. After equilibration, organic and aqueous phases were separated by ultracentrifugation. Finally, aliquots of 0.5 mL from each phase were taken for the radioactivity counting. The distribution coefficient (K_d) as a function of EGMP monomer concentration in MIBK was obtained from the ratio of measured radioactivity in organic to aqueous phase after equilibration.

The K_d values of EGMP membrane and gel were also measured by equilibrating a known weight of solid sample (0.05 g) in 5 mL of aqueous phase for overnight with constant stirring at room temperature (25–27 °C). The aqueous phase was prepared by adding a known radioactivity of radiotracer ($^{154}\text{Eu}/^{241}\text{Am}$) in aqueous solution whose ionic strength and acidity were adjusted with NaNO₃ and HNO₃, respectively. After equilibration, the 0.5 mL sample was taken from the aqueous phase for monitoring the radioactivity. The K_d values of Eu³⁺ and Am³⁺ ions between gel/membrane and aqueous

phase were calculated from following equation:

$$K_d = \frac{(C_o - C)V}{CW} \quad (3)$$

where C_o , C , V and W denote initial and equilibrium radioactivity of the radiotracer in aqueous phase, volume of the equilibrating aqueous phase, and weight of dried gel/membrane, respectively.

3. Results and discussion

The functionalized membranes were prepared by *in situ* graft polymerization of monomer (acrylic acid/2-acrylamido-2-methyl-1-propane sulfonic acid/ethylene glycol methacrylate phosphate) with a 5 mol% crosslinker into the pores of microporous poly(propylene) host membrane. Un-grafted monomers from the pores of the membrane were removed completely by repeated washing with DMF and methanol. These cycles were continued until weight of the membrane sample remained constant. The grafting of monomer along with crosslinker in poly(propylene) microporous membranes samples was confirmed gravimetrically after removal of the un-grafted materials. It was observed that the amount of grafting in the host poly(propylene) (PP) membrane could be controlled by adjusting the quantity of monomer and relative amounts of other components in the polymerization solution filled in the pores of the host membrane. As given in the Table 1, the functionalized membranes with a varying degree of grafting could be obtained in the present work. The grafting of monomers up to 180 wt.% did not affect thickness of the host poly(propylene) membrane (59 μm) significantly as thickness of the membranes samples after grafting was found to be within $\pm 2 \mu\text{m}$ of the nascent host membrane. Higher degree of grafting was found to increase the thickness of a membrane. For example, the thickness of the membrane was increased from 59 to 70 μm after grafting to the extent of 290 wt.%. This indicated that higher degree of grafting leads to formation of the surface layer on host poly(propylene) membrane. The surface morphology of the membranes was studied by the scanning electron microscope, and images thus obtained are shown in Fig. 1. It can be seen from the comparison of the SEM micrographs of the host and grafted membranes that pores of the membrane are completely filled with the grafted polymer irrespective of their chemical composition. The comparison of FM-3 (290 wt.% grafted EGMP) and FM-6 (120 wt.% grafted AMPS) shows that higher degree of grafting leads to the flat surface without any microstructure. These indicate that higher degree of grafting leads to surface deposition, and the grafted polymer is confined to the pores only when grafting is below 180 wt.%.

3.1. Characterization of membranes

All the functionalized membranes synthesized in the present work were found to take up water readily. These membranes were found to be dimensionally stable, and did not change their

Table 1

Degree of monomer grafting in poly(propylene) microporous membranes and the water uptake capacities of the functionalized membranes. The membranes with higher degree of grafting were obtained by increasing the concentration of monomer in the grafting solutions.

Id.	Composition of grafting solution		Degree of grafting (wt.%)	Water uptake (wt.%)	Ion-exchange capacity (meq/g)
	Monomer	Crosslinker (mol%)			
FM-1	EGMP	4	120 \pm 10	–	–
FM-2	EGMP	5	170 \pm 12	52 \pm 5	1.0 \pm 0.1
FM-3	EGMP	4	290 \pm 10	–	–
FM-4	AA	4	80 \pm 6	–	–
FM-5	AA	5	174 \pm 10	84 \pm 5	0.3 \pm 0.1
FM-6	AMPS	5	120 \pm 10	138 \pm 8	1.8 \pm 0.1

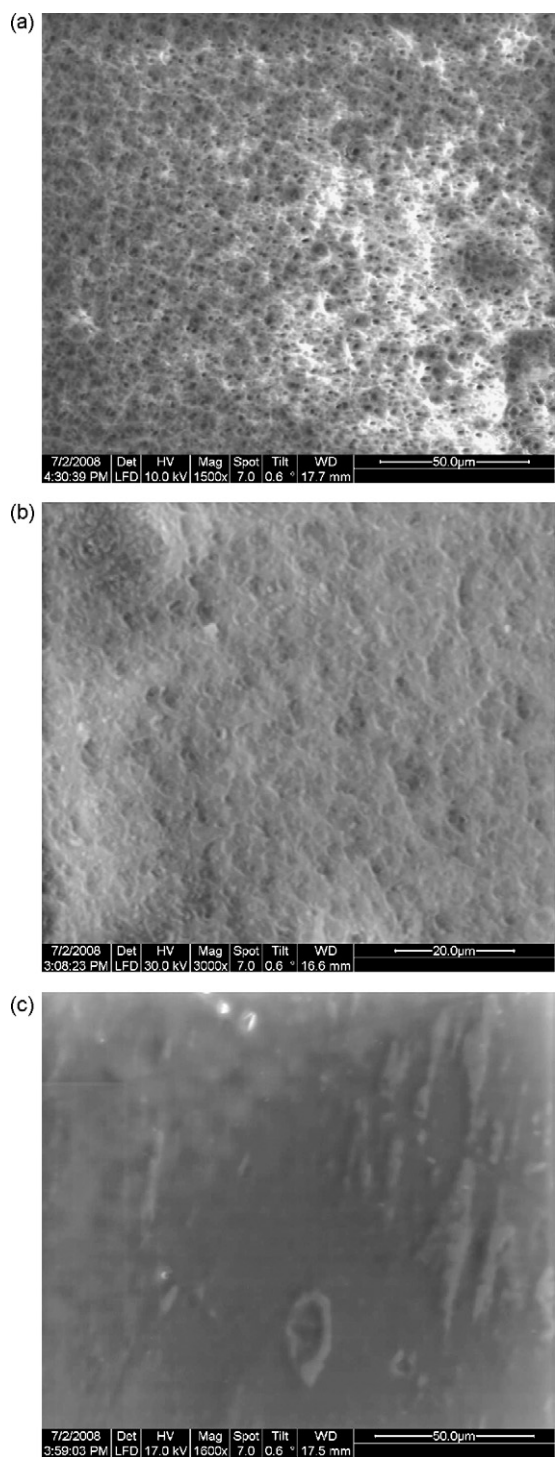


Fig. 1. Scanning electron microscopic images of (a) poly(propylene) host membrane (b) grafted AMPS membrane (FM-6), and (c) grafted EGMP membrane (FM-3).

dimensions when swollen in the water. The two factors responsible for the dimension stability of the functionalized membrane are: (i) poly(propylene) acts as a mechanical containment and (ii) crosslinking of the grafted polymer would prevent the swelling of the polymer chains. The latter is responsible for preventing the swelling of the membranes with higher degree of grafting. As shown in Table 1, the water uptake capacity of the functionalized membrane was dependent on the nature of the functional groups anchored in the membrane. The highest water content was

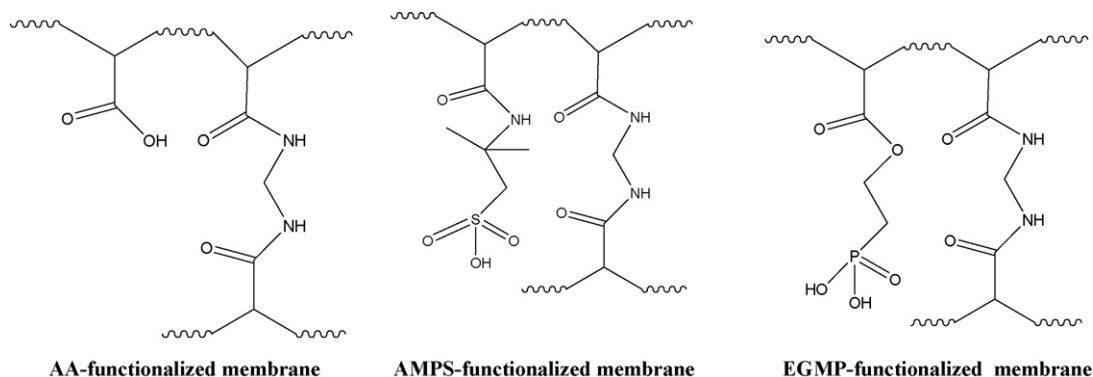
obtained in the membrane having $-\text{SO}_3\text{H}$ group which is stronger than $-\text{COOH}$ and $-\text{PO}(\text{OH})_2$ acid groups.

The chemical structures of functionalized membranes were studied by FTIR spectroscopy. The FTIR spectrum of un-grafted PP membrane shows the absorption bands at 2930, 1450 and 1370 cm^{-1} corresponding to $-\text{CH}_2$ and $-\text{CH}_3$ vibrations, respectively. The FTIR spectrum of AMPS-grafted poly(propylene) membrane showed the additional vibration bands of sulfonyl group at 1035 cm^{-1} (S–O), 1210 and 1370 cm^{-1} (S=O), 1450 cm^{-1} ($-\text{SO}_2-$), and amide carbonyl group at 1645 cm^{-1} (C=O). The FTIR spectra of EGMP monomer and EGMP-grafted membrane showed similar bands corresponding to free P=O (1330 and 1350 cm^{-1}), associated P=O (1171 and 1170 cm^{-1}), C=O (1715 and 1720 cm^{-1}), and P–OH vibrations at ≈ 1000 , 2400 – 2200 cm^{-1} , and a broad band in the region of 3400 – 3000 cm^{-1} . The FTIR spectrum of EGMP-grafted membrane showed a shift in the free P=O and C=O vibration bands to a higher frequency with respect to EGMP monomer. Also, the C=C stretching frequency observed at 1640 cm^{-1} in the FTIR spectrum of EGMP monomer has disappeared after grafting it in the poly(propylene) host membrane. The frequencies discussed were assigned based on the comparison of FTIR spectra with the characteristic frequencies reported in the literature for these groups [19]. The comparison of the host and grafted membranes described above confirmed the presence of the $-\text{SO}_3\text{H}$, $-\text{PO}(\text{OH})_2$, and C=O groups in the functionalized membranes. The possible chemical structures of the functionalized polymer anchored in the pores of membranes are shown in Scheme 1. As can be seen from the chemical structures, there would be considerable extent of the intra and inter-chain hydrogen bonding that are not shown in chemical structures of functionalized polymers given in Scheme 1. The ion-exchange capacities of the AA, EGMP and AMPS membranes were found to be 0.3, 1.0 and 1.8 meq/g, respectively. This trend in the ion-exchange capacity was expected based on the acid groups present in these membranes (see Scheme 1).

3.2. Uptake studies

In order to characterize the functionalized membranes in terms of their selectivity towards different valence metal ions, the membrane samples were equilibrated with the solutions containing a radiotracers of the ions like Cs^+ , Ag^+ , Sr^{2+} , Cd^{2+} , Hg^{2+} , Zn^{2+} , Eu^{3+} , Am^{3+} , Hf^{4+} and Pu^{4+} at different acidities. The comparisons of uptake of the monovalent ions (Cs^+) and divalent ions (Cd^{2+}) in the AA, AMPS and EGMP membranes from aqueous solutions having pH ranging from 1–6 are shown in Figs. 2 and 3, respectively. It can be seen from these figures that the uptake profiles of monovalent and divalent in AMPS and EGMP membranes are similar. The uptake of Cs^+ and Cd^{2+} are quantitative ($>80\%$) below pH 3 and 2, respectively, and thereafter falls steeply on decreasing the pH of the equilibrating solution. The uptakes of Cs^+ and Cd^{2+} in AA membrane were considerably lower than AMPS and EGMP membranes, and quantitative only for Cd^{2+} ions above pH 5. This may be attributed to the fact that AA contains $-\text{COOH}$, which is a weak acid group.

The uptake of trivalent ions ($\text{Eu}^{3+}/\text{Am}^{3+}$) and tetravalent ions (Pu^{4+}) in AMPS and EGMP membranes were studied as these membranes take up monovalent and divalent ions quantitatively at acidic pH range as described above. The uptake of Eu^{3+} and Am^{3+} ions in both these membranes is shown in Fig. 4. The uptake profiles of trivalent ions as a function of feed acidity was found to be similar in both the membranes. These membranes sorb trivalent ions quantitatively ($>90\%$) from solution having acidity up to 0.2 mol L^{-1} , and sharply decrease on increasing the acidity above 0.2 mol L^{-1} . It is also seen from Fig. 4 that the AMPS and EGMP membranes are slightly more selective towards Eu^{3+} ions as compared to Am^{3+} ions. Fig. 5 shows the uptake profiles of Pu^{4+} ions in AMPS and EGMP



Scheme 1. Chemical structures of the functionalized polymer grafted in the pores of poly(propylene) host membranes.

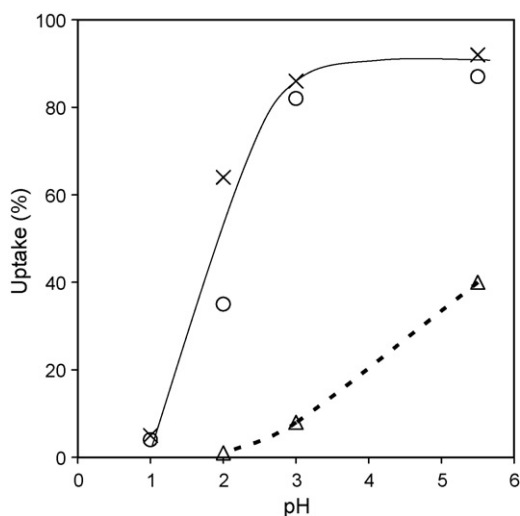


Fig. 2. Cs⁺ uptake in AA (Δ), AMPS (x), and EGMP (○) membranes as a function of pH of equilibrating solution.

membranes. As can be seen from Fig. 5, the trends in the uptake of Pu⁴⁺ ions in EGMP and AMPS membranes as a function of acidity are quite different. Uptake of Pu⁴⁺ in AMPS membrane is negligible from solution having H⁺ ions concentration above 1 mol L⁻¹, whereas EGMP membrane takes up Pu⁴⁺ at acid concentration as high as 4 mol L⁻¹. This indicates that Pu⁴⁺ is held in AMPS mem-

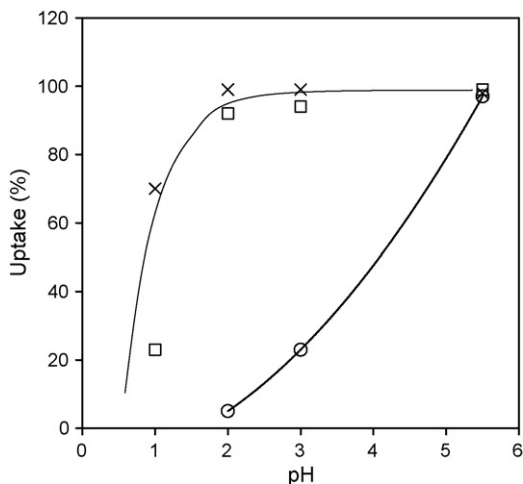


Fig. 3. Cd²⁺ uptake in AA (○), AMPS (x), and EGMP (□) membranes as a function of pH of equilibrating solution.

brane by its electrostatic interactions with sulfonic acid groups. In EGMP-membrane, Pu⁴⁺ must be held by electrostatic as well as covalent interactions with phosphate groups, which gives rise to its quantitative uptake even at very high acidity.

The sulfonic acid functionalized membrane (AMPS-membrane) is nonselective due to a narrow range of reaction free energy values for the exchange with various metal ions. The carboxylic acid membrane (AA-membrane) is less acidic, thus limiting its usefulness in the low pH environments. Of intermediate strength is phosphate functionalized membrane (EGMP-membrane). This is clearly reflected in their ion-exchange capacities (Table 1). The sorption of different valence ions like Ag⁺, Sr²⁺, Zn²⁺, Hg²⁺, Eu³⁺, Am³⁺ and Hf⁴⁺ in EGMP-membrane as a function of log₁₀ of HNO₃ concentration in the equilibrating aqueous feed is shown in Fig. 6. It can be seen from this figure that the uptake profiles are dependent on oxidation states of the ions, and there is no appreciable difference in the uptake behavior of different ions having same valency. This gives rise to a possibility of selectivity uptake of higher valence ions in the EGMP at higher acidity.

All the metal ions could be desorbed quantitatively from AMPS-membranes in 2 mol L⁻¹ HNO₃. In the case of EGMP-membrane, the desorption of Pu(IV) and Hf(IV) was not found to be possible with

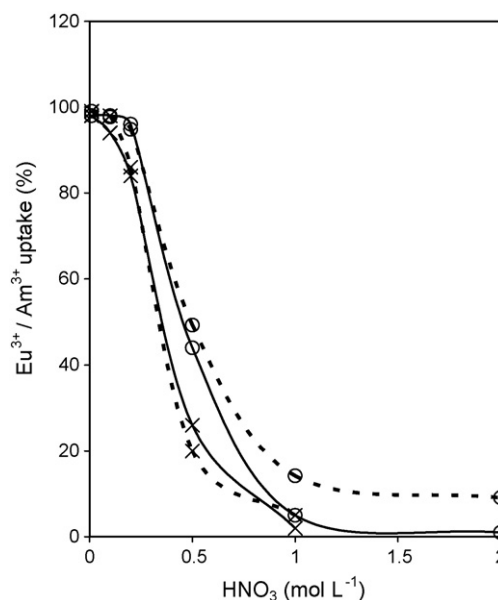


Fig. 4. Sorption of Eu³⁺ (○) and Am³⁺ (x) in AMPS and EGMP membranes as a function of feed acidity. Solid and broken lines represent AMPS and EGMP membranes, respectively.

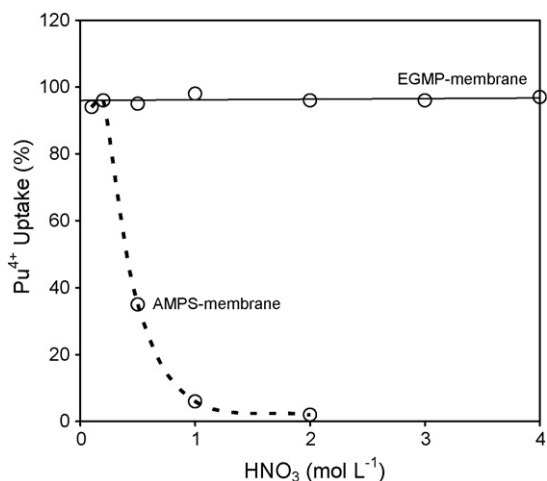


Fig. 5. Comparison of Pu⁴⁺ sorption in EGMP and AMPS membranes as a function of acid concentration in the aqueous feed.

the acid up to 4 mol L⁻¹. It was observed that 30–40% of Pu⁴⁺ could be desorbed by equilibration of EGMP-membrane with aqueous solution of 0.2 mol L⁻¹ disodium salt of EDTA for overnight without stirring.

3.3. Comparison of uptake in monomer and polymeric EGMP

The Eu³⁺ uptake in EGMP monomer (dissolved in MIBK), EGMP-gel and EGMP-membrane were studied as a function of HNO₃ concentration in the equilibrating feed solution, and shown in Fig. 7. It can be seen from this figure that uptake of Eu³⁺ in monomeric EGMP increases with increase in the concentration of EGMP, and get saturated at EGMP concentration of 3.5 mol L⁻¹ in MIBK solvent. However, the Eu³⁺ uptake profiles in polymeric EGMP (gel and membrane) were considerably higher than that in monomeric EGMP solution. This seems to suggest that the binding of Eu³⁺ ions is much stronger in polymeric EGMP than its monomeric form. Similar observations were reported for other functionalized polymers [20,21]. It is also seen in Fig. 7 that the trends of Eu³⁺ uptake profiles of EGMP solution, gel and membrane are significantly different.

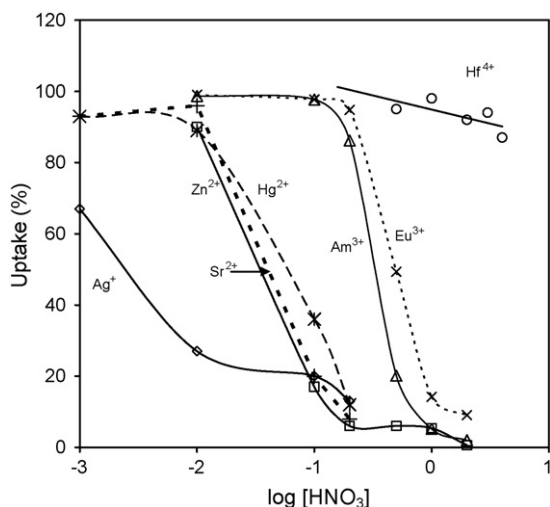


Fig. 6. Sorption of different valence ions in EGMP membrane as a function of log₁₀ of HNO₃ concentration in the equilibrating aqueous feed.

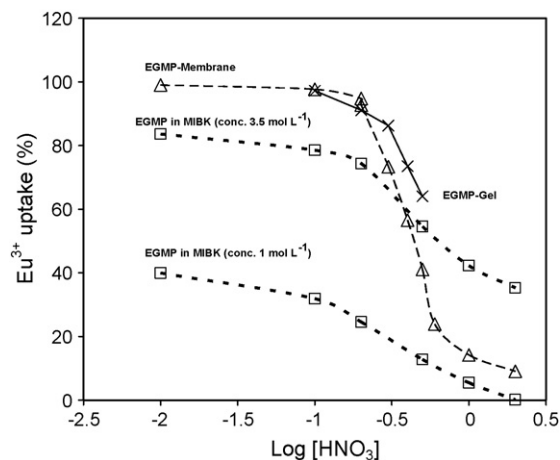


Fig. 7. Eu³⁺-uptakes in solution of monomeric EGMP, EGMP-gel, and EGMP-membrane as a function of log₁₀ of acid concentration in the aqueous feed.

3.4. Extraction studies

In order to understand the formation of metal ion complexes in EGMP-membrane, the solvent extraction studies of Zn²⁺, Eu³⁺ and Am³⁺ ions in organic phase containing EGMP-monomer in MIBK were carried out. The variation of distribution coefficients (K_d) of these ions as a function of EGMP concentration [LH₂] in organic phase is shown in Fig. 8. It is seen from this figure that K_d values increase linearly as a function of EGMP concentration in all the cases. K_d values of Eu³⁺ and Am³⁺ were found to be similar, but significantly higher the K_d values of Zn²⁺ at a given concentration of the ligand. K_d values for Eu³⁺ and Am³⁺ gets saturated at 2.5 mol L⁻¹ concentration of EGMP. This may be due to the formation of hydrogen bonded micelle like species of EGMP monomer at higher concentration, which would inhibit the accessibility of some of the binding sites to the metal ions. Though the K_d values of Zn²⁺ were significantly lower than that for Eu³⁺ and Am³⁺, their constant

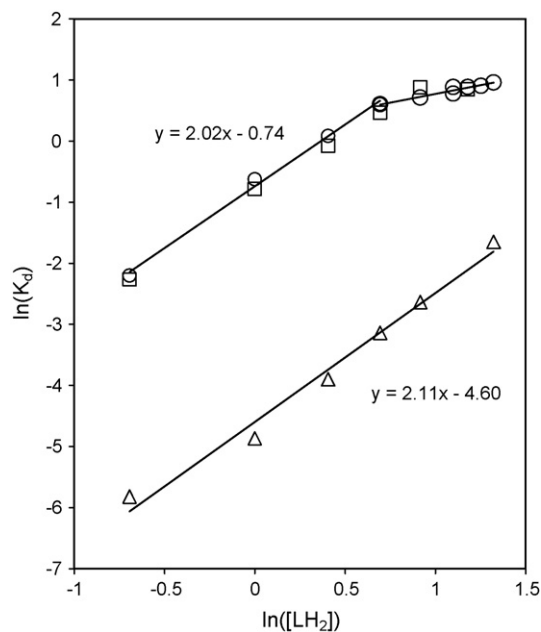


Fig. 8. Variation of logarithm of distribution coefficients of Am³⁺ (□), Eu³⁺ (○), and Zn²⁺ (△) as a function of logarithm of the concentration of EGMP monomer (LH₂) dissolved in the isobutylmethyl ketone.

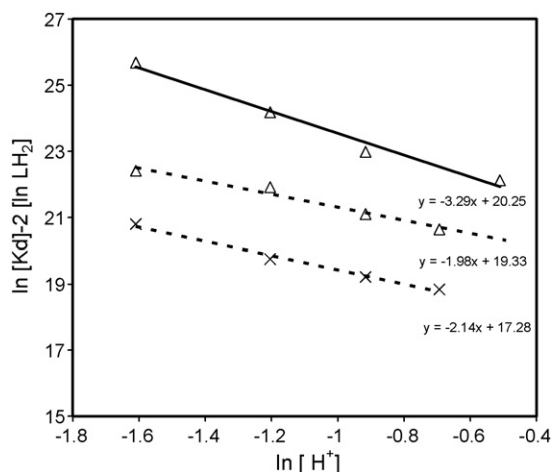
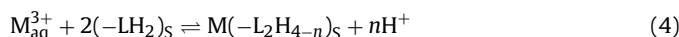


Fig. 9. Slope analysis for the extraction of Am^{3+} (\times) and Eu^{3+} (Δ) ions. Solid and broken lines represent EGMP-membrane and EGMP-gel, respectively.

slope value 2 in the plot of $\ln K_d$ vs. $\ln[\text{LH}_2]$ (Fig. 8) indicates that two EGMP units are involved in binding with Zn^{2+} , Eu^{3+} , and Am^{3+} ions.

The extraction of ions in EGMP-sorbent involves ion-exchange process as the uptake of ions decreases with increase in the concentration of H^+ ions. This means Eu^{3+} and Am^{3+} ions are extracted in EGMP-sorbent by an ion-exchange reaction between these trivalent ions and hydroxyl groups of phosphate moiety in EGMP-sorbent. The stoichiometric equation involved in the uptake of $\text{Eu}^{3+}/\text{Am}^{3+}$ in gel and membrane can be represented based on solvent extraction studies as follow:



where M^{3+} and $-\text{LH}_2$ denote $\text{Eu}^{3+}/\text{Am}^{3+}$ ions and phosphate groups in the EGMP-sorbents, respectively. The subscripts *aq* and *s* denote aqueous and sorbent phases, respectively. Based on this equation, the extraction constant can be expressed as:

$$\ln K_{\text{ex}} = \ln \frac{[\text{M}(\text{L}_2\text{H}_{4-n})_s]}{[\text{M}^{3+}]} - 2 \ln[(\text{LH}_2)] + n \ln[\text{H}^+] \quad (5)$$

$$\ln K_{\text{ex}} = \ln K_d + \ln(1 + \beta_1[\text{NO}_3^-] + \beta_2[\text{NO}_3^-]^2) - 2 \ln[(\text{LH}_2)] + n \ln[\text{H}^+] \quad (6)$$

where $[\text{LH}_2]$ and $[\text{H}^+]$ denote the concentrations of unreacted $-\text{LH}_2$ in the sorbent and hydrogen ion in the aqueous solution, respectively. β_1 and β_2 denote the stability constants for the nitrate complexes $\text{M}(\text{NO}_3)_2^+$ and $\text{M}(\text{NO}_3)^+$, respectively. Since the ionic strength was kept constant, the second term in Eq. (6) can be considered to be almost constant. Therefore, Eq. (6) can be simplified as:

$$\ln K'_{\text{ex}} = \ln K_d - 2 \ln[(\text{LH}_2)] + n \ln[\text{H}^+] \quad (7)$$

The slope analysis was performed using experimentally measured K_d as a function of H^+ ion concentration in the equilibrating solution, keeping constant concentration of radiotracer and weight of EGMP-sorbent. Fig. 9 shows the variation of $(\ln K_d - 2 \ln[(\text{LH}_2)])$ vs. $\ln[\text{H}^+]$ for Eu^{3+} and Am^{3+} uptake in the gel or membrane. It is seen from Fig. 9 that the slope is 2 for Eu^{3+} and Am^{3+} uptake in the gel, and 3 for Eu^{3+} uptake in the membrane. As slope represents *n* in Eq. (7), it appears that $\text{Eu}(\text{NO}_3)_2^+$ and Eu^{3+} are complexed with phosphate moiety of EGMP in the gel and membrane, respectively. The EGMP-gel can swell in water, but EGMP-anchored in the pores of membrane cannot swell as membrane acts as mechani-

cal containment that mitigates the impact of osmotic pressure. The swelling would lead to increase in the effective distance between fixed-sites (phosphate moiety of the EGMP) of the sorbent. This seems to suggest that the proximity of the functional groups plays an important role in binding of the multivalent ions in solid sorbent.

4. Conclusions

The functionalized membranes with three different acidic groups viz. $-\text{SO}_3\text{H}$, $-\text{PO}(\text{OH})_2$, and $-\text{COOH}$ were prepared by UV initiated grafting of functional monomers in the pores of poly(propylene) host membrane. The presence of required functional groups in the membrane was confirmed by FTIR spectroscopy. It was observed that the grafting yield could be controlled by adjusting the concentration of the monomer in grafting solution. The functionalized membranes developed in the present work were found to be hydrophilic. It was observed that the spacing of functional groups in the EGMP-sorbent influence binding of the species of the multivalent ions with functional groups. The uptake of different valence metal ions in the membranes as a function of the feed acidity indicated that the EGMP-grafted membrane (with phosphate groups) can be made selective towards higher valence metal ions by adjusting the feed acidity. The selectivity of the other functionalized membranes towards different valence ions was not as promising as in the case of EGMP-grafted membrane. Thus, EGMP-membrane reported in the present work can be used as the adsorptive membrane for selective preconcentration of the actinides and lanthanides.

Acknowledgments

Authors are thankful to Dr. V.K. Manchanda, Head, Radiochemistry Division, BARC, Mumbai for his keen interest in the present work, and Dr. P.K. Pujari for his valuable suggestions during the course of this work. Authors also thank J. K. Banerjee, Radiometallurgy Division, BARC, for SEM of the membranes.

References

- [1] K.A. Mauritz, R.B. Moore, Chem. Rev. 104 (2004) 4535.
- [2] E. Bakker, P. Bühlmann, E. Pretsch, Chem. Rev. 97 (1997) 3083.
- [3] A. Sachdeva, S. Sodaye, A.K. Pandey, A. Goswami, Anal. Chem. 78 (2006) 7169.
- [4] M. Ulbricht, Polymer 47 (2006) 2217.
- [5] C.R. Martin, M. Nishizawa, K. Jirage, M. Kang, S.B. Lee, Adv. Mater. 13 (2001) 1352.
- [6] A.J.B. Kemperman, D. Bargeman, Th.V.D. Boomgaard, H. Strathmann, Sep. Technol. 31 (1996) 2733.
- [7] L.D. Nghiem, P. Morname, I.D. Potter, J.M. Perera, R.W. Cattrall, S.D. Kolev, J. Membr. Sci. 281 (2006) 7.
- [8] Y.M. Scindia, A.K. Pandey, A.V.R. Reddy, J. Membr. Sci. 249 (2005) 143.
- [9] K.L. Thunhorst, R.D. Noble, C.N. Bowman, J. Membr. Sci. 128 (1997) 183.
- [10] A.M. Mika, R.F. Childs, M. West, J.N.A. Lott, J. Membr. Sci. 136 (1997) 221.
- [11] R.F. Childs, A.M. Mika, A.K. Pandey, C. McCrory, S. Mouton, J.M. Dickson, Sep. Purif. Technol. 22–23 (2001) 507.
- [12] Y. Kobuke, I. Tabushi, T. Aoki, T. Kamaishi, I. Hagiwara, Ind. Eng. Chem. Res. 27 (1988) 1461.
- [13] T. Kawai, K. Saito, K. Sugita, A. Katakai, N. Seko, T. Sugo, J.-I. Kanno, T. Kawakami, Ind. Eng. Chem. Res. 39 (2000) 2910.
- [14] S. Das, A.K. Pandey, A. Athawale, V. Kumar, Y.K. Bhardwaj, S. Sabharwal, V.K. Manchanda, Desalination 232 (2008) 243.
- [15] E.A. Hegazy, B. El-Gammal, F.H. Khalil, T.M. Mabrouk, J. Appl. Polym. Sci. 102 (2006) 320.
- [16] K.L. Thunhorst, R.D. Noble, C.N. Bowman, J. Membr. Sci. 156 (1999) 293.
- [17] G. Zukowska, J. Williams, J.R. Stevens, K.R. Jeffrey, A. Lewera, P.J. Kulesza, Solid State Ionics 167 (2004) 123.
- [18] M. Kufaci, A. Bozkurt, M. Tülü, Solid State Ionics 177 (2006) 1003.
- [19] J. Coates, in: R.A. Meyers (Ed.), Encyclopedia of Analytical Chemistry, John Wiley & Sons Ltd., Chichester, 2000, pp. 10815–10837.
- [20] T. Hirotsu, S. Katoh, K. Sugasaki, M. Seno, T. Itagaki, J. Chem. Soc. Dalton Trans. (1986) 1983.
- [21] H. Nishikawa, E. Tsuchida, J. Phys. Chem. 79 (1975) 2072.



Single-drop micro-extraction and diffuse reflectance Fourier transform infrared spectroscopic determination of chromium in biological fluids

Devsharan Verma, Santosh Kumar Verma, Manas Kanti Deb*

School of Studies in Chemistry, Pt. Ravishankar Shukla University, Raipur, Chhattisgarh 492 010, India

ARTICLE INFO

Article history:

Received 25 July 2008

Received in revised form 8 November 2008

Accepted 10 November 2008

Available online 25 November 2008

Keywords:

Single-drop micro-extraction

DRS-Fourier transform infrared

spectroscopy

Quantitative determination of Cr(VI)

Biological fluids

ABSTRACT

The present paper deals with a new micro-extraction procedure for selective separation of Cr(VI) in the form of a metaloxy anionic species namely dichromate ($\text{Cr}_2\text{O}_7^{2-}$) with *N*¹-hydroxy-*N*¹,*N*²-diphenylbenzamidine (HOA) in to dichloromethane and its subsequent and rapid diffuse reflectance Fourier transform infrared spectroscopic (DRS-FTIR) determination employing potassium bromide matrix. The diffuse reflectance Fourier transform infrared spectroscopy gives both qualitative and quantitative information about the dichromate. The determination of chromium is based on the analytical peak selection, among the various vibrational peaks, at 902 cm^{-1} . The micro-extraction was based on the liquid–liquid solvent extraction (LLSE) principle. The dichromate binds with the nitrogen and oxygen atoms of *N*¹-hydroxy-*N*¹,*N*²-diphenylbenzamidine (HOA) and forms 1:2, Cr(VI):HOA complex in 0.1 mol L^{-1} HCl medium. The formation of above complex, in the acidic medium, is confirmed by the appearance of chocolate-brown color in the micro-extract. The speciation studies of Cr(III) and Cr(VI) is done by conversion of Cr(III) into Cr(VI) utilizing H_2O_2 as an oxidizing agent. The chemistry of pure dichromate and that of its HOA complex is discussed. The limit of detection (LoD) and the limit of quantification (LoQ) of the method are found to be $0.01\text{ }\mu\text{g g}^{-1}$ $\text{Cr}_2\text{O}_7^{2-}$ and $0.05\text{ }\mu\text{g g}^{-1}$ $\text{Cr}_2\text{O}_7^{2-}$, respectively. The standard deviation value and the relative standard value at a level of $10\text{ }\mu\text{g Cr}_2\text{O}_7^{2-}/0.1\text{ g KBr}$ for $n = 10$ is found to be $0.26\text{ }\mu\text{g Cr}_2\text{O}_7^{2-}$ and 2.6%, respectively. The relative standard deviation ($n = 8$ and 6) for the determination of dichromate ($\text{Cr}_2\text{O}_7^{2-}$) in real human biological fluid samples is observed to be in the range 3.1–7.8%.

© 2008 Elsevier B.V. All rights reserved.

1. Introduction

The dubious behavior of chromium has fascinated chemists over the years. On one hand exposure to high-chromium concentration, especially hexavalent chromium leads to toxicity due to its ability to oxidize biomolecules, notably DNA [1,2] and exert its noxious influence on the cell, causing carcinogenic effects; and on the contrary it has been recognized as an essential trace mineral required for normal sugar and fat metabolism. Organic chromium potentiates the action of insulin and is the active component of a substance called GTF (glucose tolerance factor), along with vitamin B₃ and amino acids.

Determination of very low-chromium concentrations in “unexposed” biological material (animal and human tissues, blood, urine, food, as well as water and air) is extremely difficult and many problems still need to be solved [3]. An accurate assessment of human exposure and nutritional chromium requirements depends

on reliable analytical results. Thus, the need for new procedures on determination of chromium with low-detection limit, high-sample throughput, applicability to low-sample size, etc., particularly in biological samples wherein sample size is a real challenge to the chemist, is a perpetual demand for the purpose of clinical diagnosis. Speciation of chromium often involves a separation steps, such as ion exchange [4,5], capillary electrophoresis [6,7], nano-material micro-column separation [8], and solid-phase extraction (SPE) [9]. Various methods have been used for subsequent determination of chromium, for instance, spectrophotometry [10], atomic absorption spectrometry (AAS) [4,9], inductively coupled plasma-atomic emission spectrometry (ICP-AES) [8] and inductively coupled plasma-mass spectrometry (ICP-MS) [7]. However, these methods are only suitable for relatively large sample volumes.

In many common analytical methods, the volume of the sample is very small. In GC, HPLC and graphite furnace atomic adsorption spectrometry (GF-AAS), this volume is usually around 5–20 μL , while in diffuse reflectance Fourier transform infrared spectroscopy (DRS-FTIR) it is around 3–10 μL . The chromatographic techniques often suffer from disadvantages such as incomplete derivatization, being time-consuming and entailing complicated operating procedures. The determination of Cr(VI) using GF-AAS have also some

* Corresponding author. Tel.: +91 771 2593367.

E-mail address: debmanas@yahoo.com (M.K. Deb).

limitations in terms of high cost of instruments used in routine analysis, matrix effects, effect of temperature, reagent ratios, cooling time and required special type furnace tube. Several procedures have been developed for the separation and pre-concentration of contaminants from environmental matrices, such as: liquid–liquid extraction (LLE) [11–13], co-precipitation [14,15]. However, disadvantages such as significant chemical additives, solvent losses, large secondary wastes, unsatisfactory enrichment factors and high-time consumption, limit the application of these techniques. These problems could be addressed by the development of modular and compact processes that provide adequate separation and preconcentration without complex processes. The solvent micro-extraction technique effectively overcomes these difficulties by reducing the amount of organic solvent as well as allowing sample extraction and preconcentration to be done in a single step. The technique is faster and simpler than conventional methods. It is also inexpensive, sensitive and effective for the removal of interfering matrices. Solvent micro-extraction is a form of solvent extraction with phase ratio values higher than 100 [16]. Compared with the conventional solvent extraction, micro-extraction may provide poorer analyte recovery, instead the concentration in the organic phase greatly enhances and thus the detection limit may go down further. In addition, the amount of the used organic solvent is highly reduced and only one step of manipulation is necessary, therefore, problems of contamination and loss of analytes vanishes.

Some of the recently proposed organic reagents for the determination of chromium include 8-hydroxyquinoline [17], 1,5-diphenylcarbohydrazide [18], 2,6-pyridinedicarboxylic acid [19], tributylphosphate [20], etc. However, most of these methods suffer from a number of limitations such as interference by large number of ions, low-metal recovery, and lack of sensitivity, stringent reaction conditions and high-blank values. In the present work an attempt has been made to develop a new method for low-level determination of hexavalent chromium, in terms of dichromate ($\text{Cr}_2\text{O}_7^{2-}$) ion, in biological samples. The determination is based on micro-extraction of $\text{Cr}_2\text{O}_7^{2-}$ with N^1 -hydroxy- N^1,N^2 -diphenylbenzamidine or simply hydroxyamidine (HOA) in to dichloromethane and its subsequent simple and rapid diffuse reflectance Fourier transform infrared spectroscopic (DRS-FTIR) determination at 902 cm^{-1} after spiking the micro-extract over KBr substrate. The optimization procedures for liquid–liquid extraction, micro-extraction, DRS-FTIR determination and the merits of the method are discussed.

2. Materials and methods

2.1. Instrumentation

Fourier transform infrared spectra were recorded with a FTIR 8400S Shimadzu Corporation Analytical and Measuring Instruments Division, Kyoto, Japan. Diffuse Reflectance FTIR (DRS-FTIR) spectrometer equipped with an L-alanine doped deuterated triglycine sulfate (DTGS) detector was used. A single beam Sytronics spectrophotometer 104 was used for characterization of the chromium complex. A Sartorius electronic balance, AG GÖTTINGEN Germany, model CP225D (precision $10\text{ }\mu\text{g}$) was used for measurement of weight. Variable volume ($10\text{--}100\text{ }\mu\text{L}$) micropipette, GlaxoSmithKline Pharmaceuticals Ltd., Finland was used for handling liquid volumes. Calibrated glass apparatus were used for volumetric measurements. Because of the high sensitivity of the method, special care was taken during handling of all glassware to avoid contamination. Glassware were cleaned with Ultrasonic Cleaning Bath, Spectra Lab India, model UCB-40 using mild detergent and after proper washing, rinsed with ultrapure water. Millipore ultra purifier system was used to obtain pure distilled

water. For homogenous stirring of reaction mixture 5 MLH magnetic stirrer, Remi Equipments Pvt. Ltd., India was used.

2.2. Reagents and solutions

A standard solution containing $1.0\text{ mg Cr(VI) mL}^{-1}$ was prepared by dissolving 2.828 g of $\text{K}_2\text{Cr}_2\text{O}_7$ in ultra pure water and diluting to 1 L with water. The solution was standardized spectrophotometrically by 1,5-diphenylcarbazide method [22]. Appropriately diluted solutions of the above standard chromium(VI) solution were used for further work. Merck, AR grade dichloromethane was used for all extraction process. Potassium bromide used in this analysis was of infrared spectrometric grade, Merck KGaA 64271 Darmstadt, Germany. In the present work, 0.5 , 5 and 10 mol L^{-1} HCl were employed for extraction of the metal. N^1 -Hydroxy- N^1,N^2 -diphenylbenzamidine (HOA) or hydroxyamidine was synthesized as according to the literature [23] and its solution in dichloromethane (0.15% , w/v or 0.0173 mol L^{-1}) was used for extraction purposes.

2.3. Procedure for single-drop micro-extraction (SDME) of chromium(VI)

A 8-mL vial (Kimble Glass, Vineland, NJ, USA) with a stirring bar ($8\text{ mm} \times 1.5\text{ mm}$, Fisher) is placed on a magnetic stirrer; 5 mL of water containing 0.25 mL HCl (0.5 mol L^{-1}) and $10\text{ }\mu\text{g}$ of dichromate is placed in the vial. The vial is sealed with a polytetrafluoroethylene (PTFE)-coated silicon septum. The $10\text{-}\mu\text{L}$ gas-tight Hamilton manual injection syringe (Model 1701, Hamilton, Bonaduz, AG Switzerland) filled with $5\text{ }\mu\text{L}$ of dichloromethane containing HOA (0.01 mol L^{-1} chelating agent) is injected into the acidified solution containing dichromate sample. The needle tip is immersed into the solution and fixed about 1 cm below the surface of the sample liquid. Then the $5\text{ }\mu\text{L}$ of the above extractant is squeezed out of the needle and kept suspended at the needle tip. The solution is stirred at 300 rpm for 5 min . After the extraction is complete, the drop is retracted back in the microsyringe, and the needle is removed from the sample vial. The needle is wiped with a tissue paper to remove any possible water contamination. Experiments are performed by taking all the required precautions; absence of air bubble is ensured by washing the syringe several times with organic solvent. Precision of method is improved by positioning the needle in an aqueous sample at a fixed length with stands and clamps.

2.4. Procedure for DRS-FTIR determination of chromium(VI)

The above extracted microdrop of dichloromethane containing Cr(VI)–HOA complex is immediately sucked back carefully into the microsyringe keeping it dipped into the aqueous phase. The microsyringe is then taken out from the vial. Then the microdrop is delivered over 0.1 g pre-weighed and finely ground KBr kept in a 5-mL microbeaker through microsyringe tip. Then KBr-matrix is dried over a water bath at a temperature around 60°C for 2 min . After drying, KBr-matrix is thoroughly mixed using a spatula. The sample holder is filled with this dried KBr-matrix and analyzed by the DRS-FTIR. The optimum conditions set for DRS-FTIR analysis of the samples are shown in Table 1.

3. Results and discussion

3.1. Single-drop micro-extraction (SDME) of chromium(VI)

The conventional LLE [17–19] utilizes large amounts of solvents that are often hazardous, and is time-consuming and laborious to perform. Therefore techniques aimed at overcoming such drawbacks have been developed such as solid-phase micro-extraction

Table 1
Instrumental specifications set for the DRS-FTIR analysis of samples for dichromate.

Particulars	Description
Instrument	Fourier transform infrared spectroscopy, 8400S Shimadzu Corporation, Kyoto, Japan
Technique	Diffuse reflectance infrared Fourier transform spectroscopy
Software	IR solution
Sample volume	About 5 μL
Sample form	Liquid
Apodization function	Happ-Ganzel
Resolution	4 cm^{-1}
No. of scanning	35
Measurement mode	Absorption
Spectral range (peak identification)	1100–400 cm^{-1}
Spectral range (quantitative analysis) ^a	930–890 cm^{-1}
Beam	Internal
Detector	L-Alanine-doped deuterated triglycine sulfate
Mirror speed	2.8 mm s^{-1}

^a Baseline correction range for all analysis.

(SPME) [19–20], liquid-phase micro-extraction (LPME) [20–21], etc. The single-drop micro-extraction, however, offers large enrichment factors (EFs). Because of large ratio between the volume of sample solution and acceptor phase, a high EF, defined as the ratio of analyte concentration in the acceptor phase to that in the sample solution, can be obtained.

The dichromate combines with the nitrogen and oxygen atoms of *N*¹-hydroxy-*N*¹,*N*²-diphenylbenzamidine (HOA) and forms 1:2, Cr(VI):HOA complex in 0.1 mol L^{-1} HCl medium. Further, the formation of above complex is confirmed by the appearance of chocolate-brown color in the micro-extract. In the present method of single-drop micro-extraction, the dichromate is extracted by liquid-liquid extraction procedure from solutions containing the analyte at microgram level. Compared to LLSE, the SDME extraction of chromium shows relatively narrow range of HOA concentration that is suitable for quantitative analysis. However, the upper limit of the concentration range of HOA required for maximum enrichment of chromium complex in dichloromethane droplet remained intact at an optimum microdrop volume and reaction time of 5 μL and 5 min, respectively. The maximum and steady absorbance intensity of the $\text{Cr}_2\text{O}_7^{2-}$ -HOA impregnated KBr substrate is seen when dichromate is extracted with a single drop of 0.007–0.01 mol L^{-1} hydroxyamidine solution prepared in dichloromethane. Fig. 1(a) and (b) shows the experimental setup for the extraction process.

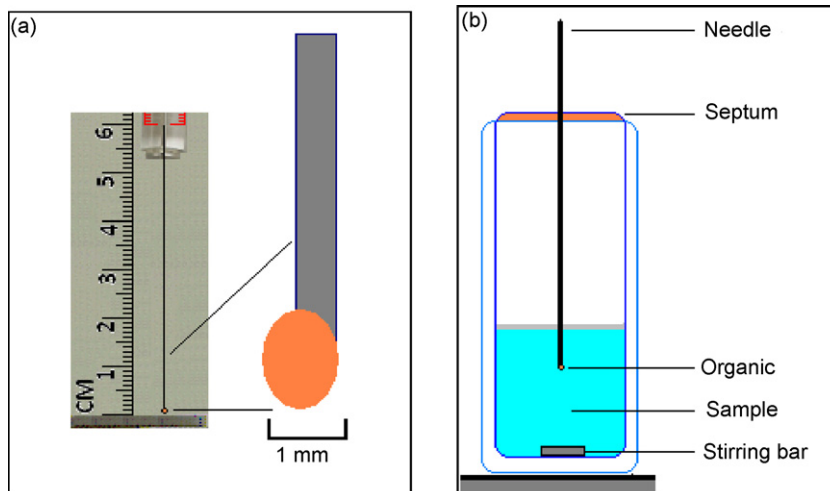


Fig. 1. Experimental setup (a) for the SDME extraction and dropsizes generated during SDME process (b).

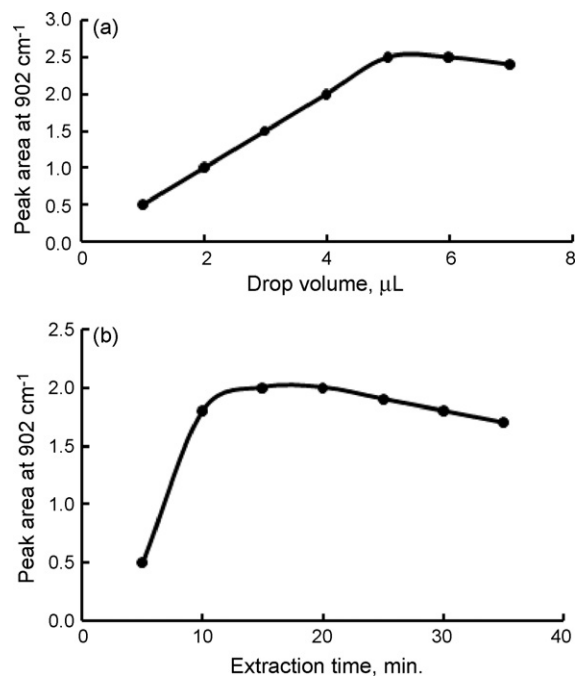


Fig. 2. The effect of extraction efficiency on increasing the microdrop volume in SDME extraction (a) and micro-extraction time on the completeness of formation of chromium complex into microdrop solvent (b).

3.1.1. Optimization of microdrop volume

In SDME the volume of the organic drop does not remain constant during the extraction because no solvent is completely immiscible with water. However, a slight decrease in drop volume is acceptable because it will occur to the same extent for standard and the sample [24]. The effect of microdrop volume on the analytical FTIR signal of 10 μg dichromate per 5 mL of aqueous phase reacted with HOA in dichloromethane was determined. A 5 mL test volume of acidified aqueous phase containing 10 μg dichromate was reacted with 5–7 μL of 0.01 mol L^{-1} solution of HOA in dichloromethane. The results indicated that increasing the microdrop volume enhanced the extraction efficiency, Fig. 2(a). However, larger drop volumes such as 7 μL could be prone to accidental dislodgement. Therefore, drop volume of 5 μL was used in subsequent experiments.

Table 2
Infrared absorption bands and different modes of vibration for some dichromate ions.

Ionic species	Vibrational modes	Absorption peak range reported earlier (cm ⁻¹)	Characteristic absorption peaks found in the present work (cm ⁻¹)
Potassium dichromate	Asymmetric stretching (ν_3)	990–880 (strong)	950, 902 and 885 strong (unresolved)
	Symmetric stretching (ν_1)	840–720 (strong)	775, and very strong (sharp)
	Bending vibrations (ν_4)	380–340 (weak)	Not observed (due to dilution factor)
Ammonium dichromate	Asymmetric stretching (ν_3)	966–924 (very strong)	950 and 901 strong
	Symmetric stretching (ν_1)	910–880 (sharp)	883 strong (sharp)
	Bending vibrations (ν_4)	745–560 (broad)	740 weak broad
Calcium dichromate	Asymmetric stretching (ν_3)	990–35 (strong, broad)	940 very strong
	Symmetric stretching (ν_1)	910–890 (medium, sharp)	905 sharp
	Bending vibrations (ν_4)	750–710 (medium, spited)	748 broad
Sodium dichromate	Asymmetric stretching (ν_3)	950–934 (strong, broad)	940 very strong, broad
	Symmetric stretching (ν_1)	910–890 (medium, sharp)	909 medium
	Bending vibrations (ν_4)	780–740 (medium, spited)	750 strong broad

3.1.2. Optimization of extraction time (reaction time)

Time extraction is very important parameter for discussion it affects the amount of the extracted dichromate. It is obvious that sufficient time must be considered for the optimum extraction process. Once the size of the microdrop volume was selected the time of the reaction was also adjusted for experiment.

Like SPME and LPME, SDME is also a process dependent on equilibrium [25]. The amount of analyte extracted at a given time is dependent on the mass transfer of analyte from aqueous samples to the organic solvent drop. This procedure requires a period of time for equilibrium. The extraction time profile was performed by monitoring the variation of relative peak area DRS-FTIR with exposure time under the experimental condition and stirring at 300 rpm. As can be seen in Fig. 2(b), the relative peak area of dichromate increased with extraction time up to 10 min. After 10 min, the amount of analytes extracted shows a much slower increase. At the 12 min time point, the amount extracted reaches the largest value, then a plateau is observed till as much as 20 min exposure time for the ligand in organic drop to interact with relatively large aqueous volume. However, due to considerable miscibility of the two phases and hence the commencement of loss of samples, a slight decline in the curve was obtained, thereafter. Therefore, in all subsequent optimized experiments, 10 min extraction time was used.

3.2. DRS-FTIR determination of dichromate

3.2.1. Detection of qualitative vibrational (infrared) peaks for dichromate

Dichromate being the multi-atomic metaloxy anion, its dipole moment changes during various types of oscillation and hence information about its presence is well reflected by DRS-FTIR. The descriptions on characteristic IR absorption bands for dichromate as found in the literatures [26,27], were used for the interpretation of the FTIR spectra of dichromate functional group in the present work. All the characteristics IR absorption bands for dichromate are checked by employing standard samples. This paper qualitatively identifies the presence of dichromate species by the study of spectra of its pure salt or compound. The presence of dichromate are commonly reported to be related to strong absorption bands at 948, 902, 885 and 775 cm⁻¹. In the present work, the spectral study of the solutions prepared using K₂Cr₂O₇ salt shows four strong (broad and sharp) absorption bands at 948, 902 and 885 and 775 cm⁻¹. Infrared absorption band found at 948 cm⁻¹ is though very strong but due to its bluntness and multiple splitting in to several sub-peaks it is of no analytical interest. The splitted bands with maxima at 885 and 775 cm⁻¹ are relatively medium and sharp but show undefined baselines. Thus, a comparably strong and sharp

peak with well-defined baseline observed at 902 cm⁻¹ was selected as the analytical peak for quantification of dichromate. Two-point baseline corrections were performed between 1000 and 700 cm⁻¹ in all cases for the observation of all qualitative spectral peaks due to Cr₂O₇²⁻. Table 2 shows the FTIR absorption bands for the different modes of vibration of dichromate (Cr₂O₇²⁻) when taken in different forms.

3.2.2. Comparison on spectral peaks for Cr₂O₇²⁻ ion and Cr₂O₇²⁻-HOA complex

A comparison on the spectral peaks obtained for pure dichromate ion, taken in the form of potassium dichromate, was made with that obtained for Cr₂O₇²⁻-HOA complex in LLSE, in order to see whether both provide the similar spectral characteristics. Fig. 3(a) and (b) shows the spectra scanned of dichromate before and after extraction with HOA, i.e., Cr₂O₇²⁻ in its purest form and in complexed form. It was pleasant to observe that there was absolutely no change in the position of spectral peaks produced due to both the species, apart from the few those produced due to the presence of some functional groups in the HOA. The four corresponding peaks at 948, 902, 885 and 775 cm⁻¹ found for the pure dichromate were also seen exactly at the same position for the Cr₂O₇²⁻-HOA complex. This probably indicates that even after coordinating with the organic ligand, HOA, Cr₂O₇²⁻ does not loose its structure and symmetry identity and it appears as if Cr-O bonds are as free to oscillate in the complexed form as in the pure form. Thus, the similar appearance of spectral peak positions formed the criteria for identification of the Cr₂O₇²⁻ ion in single-drop micro-extract.

3.3. Advantage of complexation of Cr(VI) in single-drop micro-extraction

While the present work has been established by performing IR spectral scans of standard Cr₂O₇²⁻ using K₂Cr₂O₇, the other dichromates such as (NH₄)₂Cr₂O₇, CaCr₂O₇, Na₂Cr₂O₇, etc. may also persist in a complex matrix in solid or liquid states together with K₂Cr₂O₇. Since in solid crystalline form the various vibrational modes of Cr₂O₇²⁻ in all above complexes generate absorption maxima with a substantial drift around 902 ± 05 cm⁻¹, it may possibly be difficult to quantitatively determine the total Cr(VI) in real samples using the spectral peaks of K₂Cr₂O₇ alone as the standard, due to possible overlapping of maxima for different complexes of Cr₂O₇²⁻. However, this drift value for position of absorption maxima in liquids is though relatively less due to decreased atomic interaction but cannot be ignored. Table 2 shows the reported values of spectral peaks obtained for different dichromates. Thus, the pure spectra of Cr₂O₇²⁻ when used in the form K₂Cr₂O₇ alone can

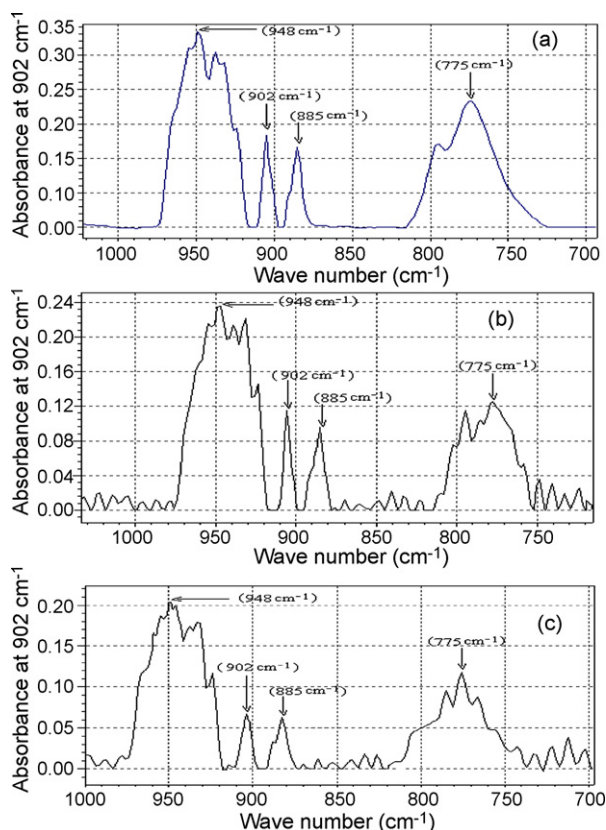


Fig. 3. DRS-FTIR spectra of dichromate; before (a) and after extraction with HOA (b), i.e., $\text{Cr}_2\text{O}_7^{2-}$ in its purest form and in complexed form, and $\text{Cr}_2\text{O}_7^{2-}$ -HOA complex extracted by SDME process from a real human blood serum sample (c).

not be used for quantification of Cr(VI) in real samples. The problem of possible spectral overlapping due to different such dichromate species could be solved by isolating the dichromate ions in solutions through complexing them with organic ligand such as HOA into a separate immiscible phase. Thus, single-drop micro-extraction of Cr(VI) serves two important aspects, first to eliminate any possible interference due to the presence of associated metal ions in real samples and secondly to remove the possible drift and overlapping of spectra at maxima due to the possible presence of different dichromate species in real samples.

3.4. Quantitative and analytical Infrared peak selection for dichromate determination

The peak at 948, 885 and 775 cm^{-1} loses their sharpness and constant baseline in its spectral position upon variation in dichromate concentration for the reasons not identified. Although the IR peak observed at 902 cm^{-1} is relatively less strong at high-

dichromate concentration compared to the peaks at 948 cm^{-1} but due to consistency in spectral position and its quantitative behavior this peak at 902 cm^{-1} for asymmetric stretching vibration (ν_3) was chosen for the quantitative determination of dichromate in the pure compound and in the real samples. The calibration curve method was used for the analysis.

3.5. The Kubelka Munk spectrum and calibration curves

The equation given below executes Kubelka Munk conversion for a spectrum measured by the diffuse reflection method. This conversion is required to enable use of a reflectance spectrum measured by the diffuse reflection method for search or quantitative analysis. $f(R) = (1 - R)^2/2R = k/s$, where k = molecular extinction coefficient; s = scattering coefficient; R = reflectance (power spectrum of sample/power spectrum of dilution material, KBr).

The Kubelka Munk conversion uses the formula above to invert a reflectance spectrum measured by the diffuse reflection method into a quasi-quantitative spectrum that correlates with the concentration of the sample.

Thus, the calibration curves for peak height and peak area were prepared by utilizing the respective Kubelka Munk spectrum obtained for the minimum and maximum dichromate concentration range, in the concentration ratio 1:1000, of the equivalent amount of dichromate in the same ratio. The software IR Solution converts automatically the reflectance spectrum into the Kubelka Munk spectrum for smoothening of the baseline. The data on full range of the concentration were plotted against the respective absorbance values, calibration curve no. (CCn 1). The corresponding absorbance data were obtained at 902 cm^{-1} for large number of standard series with as little as $0.05\text{ }\mu\text{g}$ dichromate/ 0.1 g KBr and as high as $50\text{ }\mu\text{g}$ dichromate/ 0.1 g KBr. The absorbance data obtained for the Kubelka Munk spectrum were processed by the software Table Curve 2D v5.01.01. This absorbance versus concentration plot shows a straight line with excellent correlation coefficient value of 0.984. The slope and the intercept for this straight line were -0.056 and 0.104 , respectively.

The peak area is another important parameter for the quantification of dichromate because dichromate concentration was found directly proportionate to the peak area. In much the same way as discussed above, the full range of concentration (0.05 – $50\text{ }\mu\text{g}$ dichromate/ 0.1 g KBr) were also plotted against the respective peak areas obtained for a series of full concentration range (CCn 2). The peak area data obtained for the Kubelka Munk spectrum showed excellent linearity for this curve also with correlation coefficient, slope and intercept value for the st. line equation $y = mx + c$ as 0.974 , -0.376 and 0.758 , respectively.

Table 3 shows some other important statistical data for the calibration curve no. 1 and calibration curve no. 2 along with the calibration curve equations. The other statistical parameters such as DF Adj r^2 , Fit Std Err and Fstat as obtained for two sets of X–Y data using the software Table Curve 2D have been shown in Table 3. As

Table 3
Statistical data for the calibration curves prepared for dichromate concentrations.

Calibration curve no.	Concentration range ($\mu\text{g Cr}_2\text{O}_7^{2-}/0.1\text{ g KBr}$)	Statistical data ^a for the x–y plot (conc. vs. absorbance and peak area) for the st. line equation, $y = a + bx$								
		Intercept (a)	Slope (b)	St. line equation ^b ($y = a + bx$)	Correlation coefficient (r)	CD r^2	DF Adj r^2	Fit Std Err	Fstat	R.S.D. (n=8) ($\pm\%$)
1 ^c	0.05–50	0.104	–0.056	$125C_{\text{Cr}_2\text{O}_7^{2-}} = 13.0 - 7.0\text{ Abs}$	0.985	0.999	0.963	0.031	297.162	2.4
2 ^d	0.05–50	0.758	–0.376	$125C_{\text{Cr}_2\text{O}_7^{2-}} = 94.0 - 1.0\text{ Abs}$	0.974	0.996	0.961	0.229	183.752	2.2

^a Data processed by the software Table Curve 2D v5.01.01.

^b $C_{\text{Cr}_2\text{O}_7^{2-}}$ = concentration of dichromate— $\mu\text{g}/0.1\text{ g KBr}$; Abs = absorbance at quantitative peak; A_{peak} = area under the peak.

^c Data for full range plot of dichromate concentration vs. absorbance.

^d Data for full range plot of dichromate concentration vs. peak area.

a st. line fit turns out to be more ideal, the r^2 value approaches 1.0 (0 represent a complete lack of fit), the standard error decreases toward zero, and the F -statistic goes toward infinity. Thus, the data shown in Table 3 verifies the ideal rank of the calibration curves.

3.6. Interference studies

In the present work, the study on possible interferences due to presence of various types of ions has been carried out. Such as interferences in micro-extraction process, due to solvents and interferences in the DRS-FTIR determination of dichromate due to solvent effects, and other ionic interferences in the determination.

Chloroform and dichloromethane are equally capable of extracting the chromium–HOA complex with high-% efficiency (>99%) in a single extraction. The strong reason of the selection of dichloromethane, as a solvent in the extraction process, is its relatively less toxicity than the chloroform. The boiling point of dichloromethane is 39.8–40.0 °C so the dichloromethane was completely vaporized when the vaporization process after extraction and before determination was carried out. So there was no chance to interfere of dichloromethane in the determination and in fact we have not found any infrared peaks for the dichloromethane.

Although large number of organic ligands such as 1,5-diphenylcarbohydrazide [18], 2,6-pyridinedicarboxylic acid [19] and tributylphosphate [20] are reported for LLSE of chromium but their selectivity towards other metal ions, particularly Fe(III) which is also an important constituent in biological fluids, is questionable. The HOA was a strong and co-principal component in the micro-extraction process because it was used as selective complexing agent for Cr(VI). Therefore it was very important to study the interferences of the HOA in the determination. We have compared the scanned FTIR spectra of the inorganic dichromate sample and its HOA complex in dichloromethane in KBr substrate and found the dichromate peak unaffected due to the presence of HOA in the HOA-dichromate complex. The IR peak for dichromate could be easily identified in the spectra scanned of dichromate as well as in the spectra of HOA-dichromate complex.

The above-discussed interferences are internal interferences, so the next interference study was based on the effect of foreign species. To study the inter-ionic effect on the change in the position of spectral band and intensity for standard dichromate a large number of inorganic and organic multi-atomic anionic and cationic chemical species were introduced in the analyte solution prior to the SDME process. The inter-ionic effect of foreign species was checked using the quantitative IR peak at 902 cm^{-1} at a level of $10\text{ }\mu\text{g}$ dichromate contained in a single drop of test solution which is equivalent to a volume of $5\text{ }\mu\text{L}$ and sprayed over 0.1 g KBr matrix. In addition to the standard dichromate solution spiked over KBr matrix, varied known amounts of the foreign species was also introduced and the matrix was then analyzed as in the procedure. The band position and spectral intensity of dichromate remained unchanged even in the presence of at least 120-fold molar excess of the following tested multi-atomic cationic and anionic species including BO_3^{3-} , PO_4^{3-} , AsO_4^{3-} , CO_3^{2-} , SeO_3^{2-} , AsO_3^{2-} , MoO_4^{2-} , FeO_4^{2-} , SiO_4^{2-} , CN^- , OH^- , SCN^- , NO_2^- , ClO_2^- , NO_3^- , ClO_3^- , ClO_4^- , BrO_3^- , IO_3^- , IO_4^- , HCO_3^- , MnO_4^- , NH_4^+ , formate, acetate, oxalate, succinate, cinnamate and citrate. Mono-atomic anions and cations like, Cl^- , Br^- , I^- , F^- , Na^+ , K^+ , Ca^{2+} , Mg^{2+} , etc., have absolutely no diverse effect in the quantitative determination of dichromate since they do not possess dipole change, however their effect are seen only below 200 cm^{-1} .

3.7. LoD, LoQ and statistical parameters

The limit of detection (LoD) [28]; defined as the lowest amount of analyte causing a signal distinguishable from noise 99% of the

time that it is analyzed or better and determined by considering more absorbance than three times the standard deviation of seven replicate analysis of the blank absorbance and limit of quantification (LoQ) [28]; defined as the limit at which the difference between two different values may reasonably well be identified and determined by considering five times the product value of standard deviation of analysis of seven standard samples containing the similar analyte concentration through the entire analytical process and one-sided t -distribution ($t=3.14$, for 6 degrees of freedom), standard deviation, relative standard deviation and correlation coefficient (r), of the method were calculated for dichromate calibration graph no. 1. The LoD of the method is calculated to be $0.01\text{ }\mu\text{g g}^{-1}\text{ Cr}_2\text{O}_7^{2-}$. The LoQ value is calculated to be $0.05\text{ }\mu\text{g g}^{-1}\text{ Cr}_2\text{O}_7^{2-}$. The standard deviation value and the relative standard value at a level of $10\text{ }\mu\text{g Cr}_2\text{O}_7^{2-}/0.1\text{ g KBr}$ for $n=10$ is found to be $0.26\text{ }\mu\text{g Cr}_2\text{O}_7^{2-}$ and 2.6%, respectively.

3.8. Application to the real samples

The use of stainless needle was avoided for sample withdrawal process due to possible metallic contamination, if any. Hence, a propene intravenous cannula was used instead for sampling of blood and cerebrospinal fluid [29]. After discarding the first 2 mL of blood due to possible contamination, next 2 mL was withdrawn from a vein in the forearm using a standard plastic Venflon cannula (Viggo AB, Sweden) and sample was transferred to an acid-washed polypropylene centrifuge tube. After clotting and centrifuging, the serum sample was transferred to an acid-washed 2 mL capped sample vial and preserved at $4\text{--}10\text{ }^\circ\text{C}$. A $0.2\text{--}0.5\text{ mL}$ serum was separated and diluted with 1% (v/v) HCl acid in a volume ratio of 1:4. A $0.5\text{--}1.0\text{ mL}$ cerebrospinal fluid from spine was sampled with the help of trained surgical practitioner avoiding traumatic states and the sample was treated similarly with nitric acid. Chromium could then be determined in human serum without ashes and digestion, by using DRS-FTIR in KBr matrix after SDME process with use of no chemical modifiers unlike the other methods [30]. The speed of analysis was increased because there is no requirement of sample digestion.

A 5 mL urine sample was poured into acid washed 25 mL polyethylene container and to this 0.5 mL of AR grade concentrated hydrochloric acid was added. A portion of it was taken directly for SDME extraction and DRS-FTIR determination using KBr matrix as described earlier in the text. Fig. 3(c) shows the DRS-FTIR spectra of $\text{Cr}_2\text{O}_7^{2-}$ –HOA complex extracted by SDME process from a real human blood serum (CSF) sample. Table 4 shows the results of analysis of some blood, cerebrospinal fluid and urine samples for their chromium contents.

In the present method, the Cr content in few randomly sampled patients was found to be in the ranges $1.3\text{--}3.1\text{ }\mu\text{g L}^{-1}$ (R.S.D., $n=8$, 3.1–4.5%), $1.2\text{--}7.4\text{ }\mu\text{g L}^{-1}$ (R.S.D., $n=8$, 4.0–7.8%) and $5.9\text{--}16.5\text{ }\mu\text{g L}^{-1}$ (R.S.D., $n=8$, 3.7–5.7%) in CSF, blood and urine, respectively. These values are almost similar to the values already reported by certain other researchers, e.g., Aguilar et al. [31] found Cr level of $14.6\pm 6.3\text{ }\mu\text{g L}^{-1}$ in a group of 43 volunteers, El-Yazigi et al. [32] reported the control group value of $6.6\text{ }\mu\text{g L}^{-1}$, in CSF. For a non-exposed population, chromium values of 0.22 and $0.23\pm 0.01\text{ }\mu\text{g L}^{-1}$ in blood have been reported [33,34], whereas a range of $0.08\text{--}0.5\text{ }\mu\text{g L}^{-1}$ was reported by Caroli et al. [35]. However, for an exposed population, even values in the order of tens of microgram per liter have been reported [36]. Cr in serum of healthy people from Brazil has been reported in the range $0.20\text{--}0.58\text{ }\mu\text{g L}^{-1}$ by Nunes and his coworkers [37]. Another research has shown Cr in serum value of $6.5\pm 2\text{ }\mu\text{g L}^{-1}$ [38]. Chromium concentration ranges, in the urine samples, were reported to be in the ranges $2.5\text{--}29.5\text{ }\mu\text{g L}^{-1}$ for a group of 60 diabetics and $5.9\text{--}12.3\text{ }\mu\text{g L}^{-1}$ for 21 normal and healthy volunteers [39].

Table 4
Analysis of chromium by DRS-FTIR technique in cerebrospinal fluid, blood and urine samples.

Samples	Amount of chromium found ^a (μg/L)				F-value ^b (sd_1^2/sd_2^2 , $sd_1 > sd_2$)		t-Value ^c ($\pm t = (\bar{x} - \mu) \frac{\sqrt{N}}{s}$)	
	Present method				DRC-ICP-MS method ⁴⁰			
	Cr _{total}	Cr(VI)	Cr(III)	R.S.D. (Cr _{total}) (%) ($n = 8^d, 6^e$)	Cr _{total}	R.S.D. (%) ($n = 4^{d,e}$)		
Cerebrospinal fluid^{f,d}								
1.	1.9	0.7	1.2	3.5	2.2	4.6	2.981	2.213
2.	3.1	1.3	1.8	3.1	3.4	4.2	2.981	1.986
3.	2.8	0.8	2.0	4.5	3.0	4.8	2.644	2.108
4.	2.2	0.6	1.6	3.6	1.9	3.7	1.856	2.116
5.	1.3	–	1.3	4.3	1.0	3.9	2.234	1.840
Blood^{f,d}								
1.	3.4	0.8	2.6	7.8	3.7	6.5	3.476	1.840
2.	1.2	–	1.2	6.7	1.5	6.5	2.954	1.986
3.	6.2	1.7	4.5	7.1	5.9	7.6	3.895	0.908
4.	4.0	1.2	2.8	5.9	3.7	6.2	2.478	2.116
5.	7.4	2.5	4.9	5.8	7.1	7.1	3.887	1.840
6.	2.1	–	2.1	4.0	1.9	7.2	2.743	0.908
Urine^{f,e}								
1.	5.9	1.6	4.3	5.0	5.8	5.6	4.231	2.221
2.	12.1	2.0	10.1	5.1	11.9	5.9	3.982	2.305
3.	8.7	1.9	6.8	4.8	8.3	5.8	2.998	2.198
4.	7.8	2.1	5.7	5.7	7.3	6.2	3.568	2.305
5.	16.5	3.1	13.4	3.7	15.8	4.9	3.893	2.221
6.	13.6	3.2	10.4	4.1	14.1	4.8	4.212	2.198

^a Single-drop micro-extraction DRS-FTIR method.

^b Tabulated *F*-values at 95% confidence level are as follows: for $N_1 = 8, N_2 = 4$ (or $\nu_1 = 7, \nu_2 = 3$), 4.35; for $N_1 = 6, N_2 = 4$ (or $\nu_1 = 5, \nu_2 = 3$), 5.41.

^c Tabulated *t*-values at 95% confidence level are as follows: for $N_1 = 8$ (i.e., for $\nu_1 = N_1 - 1, 7$ degrees of freedom), 2.365; for $N_1 = 6$ (i.e., for $\nu_1 = N_1 - 1, 5$ degrees of freedom), 2.571.

^d 10 μg Cr(VI) spiked in biological cerebrospinal fluid and blood samples.

^e 5 μg Cr(VI) spiked in biological urine samples.

^f Samples obtained from the hospitalized patients having complaints of different kinds of ailments from Pt. Jawaharlal Nehru Memorial Medical College Hospital, Raipur, C.G., India.

To validate the present method, the total chromium content only in the tested real samples was compared by the ICP-MS (PerkinElmer, Elan DRC-e model) technique [40] with flow rate ($L \text{ min}^{-1}$) of 0.9, 1.1 and 15 for nebulizer, auxiliary and plasma gas respectively as standard operating conditions. A high degree of closeness of the analytical data was obtained among the two methods with R.S.D. values ranging between 3.1–7.8% and 3.7–7.6% for

the present method and the earlier reported method [40], respectively.

In the present work, the *F*-test was performed at 95% probability to compare the result of the present method with that of the earlier reported method. Because in all cases the values of $F(sd_1^2/sd_2^2)$ were less than the tabulated *F*-values at 95% confidence level the difference between the results of present method and that of the

Table 5
Comparison of characteristic features of some of the selected techniques used for determination of chromium.

Methods	Linear dynamic range (μg L ⁻¹)	Detection limit (μg L ⁻¹)	Analysis time (min)	Sample volume (μL)	Interferences	References
Inductive coupled plasma mass spectrometry (DRC-ICP-MS) ^a	–	Below 0.05	10	14,000	⁴⁰ Ar ¹² C ⁺ and ⁴⁰ Ar ¹³ C ⁺ and polyatomic ions, in absence of DRC	[40]
Liquid–liquid extraction spectrophotometry (LLSE) ^a	7.5–350	7.5	7–10	12,000	Fe ³⁺ , V ⁵⁺	[42]
Graphite furnace atomic absorption spectrometry (GF-AAS) ^a	0–80	0.047	20	5,000	Na ⁺ , Mg ²⁺ , Ca ²⁺ , Cl ⁻	[43]
Electrothermal atomization–laser induced fluorescence spectrometry (ETA-LIFS) ^a	–	4	5–10	20	Cl, Ar, S, N	[44]
Sequential injection analysis (SIA) ^a	200–1,000	45	30	100	Mo ⁶⁺ , Fe ³⁺ , nitrate, iodate, bromate and peroxy-disulfate	[45]
Flow injection analysis (FIA) ^a	11,000–5,000	0.11	30	10	–	[46]
Single-drop micro-extraction-GC (SDME-GC) ^a	–	0.5	30	2	–	[47]
Single-drop micro-extraction-DRS-FTIR (SDME-DRS-FTIR) ^b	5–500	8 ng/0.1 g on KBr matrix or 0.8 μg mL ⁻¹	3	2	No interference	Present method

^a Large quantities and a number of consumables (chemicals, solvents, gases, etc.) are required.

^b Microamounts and small number of consumables are required.

earlier method are not significant. Similarly, the *t*-test was done at 95% confidence. Again, in all cases, the calculated *t*-values were less than the tabulated values of *t*, indicating no statistical difference between the results obtained by the two methods.

3.9. Chemical speciation of chromium

It is well known that chromium exists in Cr(III) and Cr(VI) oxidation states in environmental [20] and biological samples [41]. In the present work, 1.5 mL of H₂O₂ (30%, v/v) was used as oxidizing agent to convert all Cr(III) to Cr(VI). The HOA is an organic ligand which complexes with Cr(VI) only and not with Cr(III) under the optimized condition. Hence, for speciation analysis, total amount of chromium was found by oxidizing all Cr(III) to Cr(VI), by addition of H₂O₂, prior SDME process. SDME-DRS-FTIR without prior oxidation gave the Cr(VI) only and the difference from total chromium gave Cr(III).

3.10. Analytical recovery of chromium

Since there was no certified reference materials available for cerebrospinal fluid (CSF), the recovery of chromium from pooled CSF samples (*n* = 7) was determined by spiking standard Cr at a level of 10 µg L⁻¹. Similar recovery procedures were also adopted for blood serum and urine samples employing SDME extraction followed by DRS-FTIR analysis. Good recoveries of chromium were found as 96.2 ± 0.3% (*n* = 7), 96.8 ± 0.9% (*n* = 6) and 97.4 ± 0.8% (*n* = 6) for CSF, blood and urine samples, respectively.

4. Conclusions

Analytical requirements for the measurement of Cr in cerebrospinal fluid (CSF), blood and urine are very stringent in order to ensure a reliable sample and hence accurate data. The analysis of microcomponents with the limitations of small available sample size, e.g., in case of cerebrospinal fluid, is a real challenge to the analytical chemist. The newly developed hyphenated technique SDME-DRS-FTIR could be efficiently employed in such cases where available sample size is very small. The present method requires no large amount of consumables and hence is also cost effective. The possibility of chemical speciation of chromium(III) and chromium(VI) in real samples available in small size adds on to the novelty of this technique. The comparison on characteristic features of some of the selected techniques used for determination of chromium shows the suitability of the present method, Table 5.

Acknowledgements

The authors are thankful to the Head, School of Studies in Chemistry, Pt. Ravishankar Shukla University, Raipur, C.G., India for providing laboratory facilities. The authors are thankful to Prof. N.L. Phuljhele, Pt. Jawaharlal Nehru Memorial Medical College, Raipur for providing the biological fluid samples.

References

- [1] G. Darrie, in: L. Ebdon, L. Pitts, R. Cornelis, H. Crews, O.F.X. Donard, P. Quevauviller (Eds.), Trace Element Speciation for Environment, Food and Health, Royal Society of Chemistry (RSC), Cambridge, UK, 2001.
- [2] P. O'Brien, A. Kortenkamp, Environ. Health Perspect. 102 (1994) 3.
- [3] J.M. Ottaway, G.S. Fell, Pure Appl. Chem. 58 (1986) 1707.
- [4] M.T.S. Cordero, E.I.V. Alonso, A.G.D. Torres, J.M.C. Pavón, J. Anal. At. Spectrom. 19 (2004) 398.
- [5] J.W. Ball, R.B. McCleskey, Talanta 61 (2003) 305.
- [6] Y. Nakashima, H. Shen, K. Kusuyama, S. Himeno, Anal. Sci. 15 (1999) 725.
- [7] C.F. Yeh, S.J. Jiang, J. Chromatogr. A 255 (2004) 1029.
- [8] P. Liang, T. Shi, H. Lu, Z. Jiang, B. Hu, Spectrochim. Acta B 58 (2003) 1709.
- [9] D.M. Adriá-Cerezo, M. Llobat-Estellés, A.R. Mauri-Aucejo, Talanta 51 (2000) 531.
- [10] L.V. Mulaudzi, J.F.V. Staden, R.I. Stefan, Anal. Chim. Acta 467 (2002) 51.
- [11] B. Welz, Atomic Absorption Spectroscopy, VCH, Amsterdam, 1985.
- [12] A.N. Anthemidis, G.A. Zachariadis, J.A. Stratis, J. Anal. At. Spectrom. 18 (2003) 1400.
- [13] T. Kakoi, T. Toh, F. Kubota, M. Goto, S. Shinkai, F. Nakashio, Anal. Sci. 14 (1998) 501.
- [14] L. Elci, U. Sahin, S. Oztas, Talanta 44 (1997) 1017.
- [15] C. Guéguen, J. Dominik, D. Perret, Fresen. J. Anal. Chem. 370 (2001) 909.
- [16] E. Carasek, J.W. Tonjes, M. Scharf, Talanta 56 (2002) 185.
- [17] P. Liang, L. Yang, B. Hu, Z. Jiang, Anal. Sci. 19 (2003) 1499.
- [18] I. Bojanowska, Polish J. Environ. Stud. 2 (2002) 117.
- [19] Z. Chen, R. Naidu, A. Subramanian, J. Chromatogr. A 927 (2001) 219.
- [20] A. Ouejhani, M. Dachraoui, G. Lalleve, J.F. Fauvarque, Anal. Sci. 19 (2003) 1499.
- [21] E. Psillakis, N. Kalogerakis, TrAC Trend Anal. Chem. 22 (2003) 565.
- [22] E.B. Sandell, Colorimetric Determination of Traces of Metals, Interscience Publ. Inc., New York, 1959, pp. 392–397.
- [23] K. Satyanarayana, R.K. Mishra, Anal. Chem. 46 (1974) 1609.
- [24] F.F. Canwell, M. Losier, in: J. Pawliszyn, D. Barcelo (Eds.), Wilson & Wilson's Comprehensive Analytical Chemistry, vol. 37, Elsevier, Amsterdam, 2002, pp. 297–340.
- [25] L. Zhao, H.K. Lee, J. Chromatogr. A 919 (2001) 381.
- [26] R.A. Nyquist, R.O. Kagel, Infrared Spectra of Inorganic Compounds, Academic Press, New York, 1971.
- [27] Y.I. Sai, S.C. Kuo, Atmos. Environ. 40 (2006) 1781.
- [28] G.D. Christian, Analytical Chemistry, 5th ed., John Wiley & Sons Inc., New York, 2001.
- [29] G. Schlemmer, B. Welz, Spectrochim. Acta B 41 (1986) 1157.
- [30] Orhan Acar, Anal. Sci. 22 (2006) 731.
- [31] M.V. Aguilar, C.J. Mateos, M.C.M. Para, J. Trace Elem. Med. Biol. 16 (2002) 221.
- [32] A. El-Yazigi, C.R. Martin, E.D. Siqueira, Clin. Chem. 34 (1988) 1084.
- [33] C.P. Case, L. Ellis, J.C. Turner, B. Fairman, Clin. Chem. 47 (2001) 275.
- [34] C. Minoia, E. Sabbioni, P. Apostoli, R. Pietra, L. Pozzoli, M. Gallorini, G. Nicolaou, L. Alessio, E. Capodaglio, Sci. Total Environ. 95 (1990) 89.
- [35] S. Caroli, A. Alimonti, E. Coni, F. Petrucci, O. Senofonte, N. Violante, CRC Crit. Rev. Anal. Chem. 24 (1994) 363.
- [36] R.R. Lauwerys, P. Hoet P, in: R.R. Lauwerys, P. Hoet (Eds.), Industrial Chemical Exposure: Guidelines for Biological Monitoring, 3rd ed., Lewis, Boca Raton, 2001, pp. 77–87.
- [37] B.R. Numes, C.G. Magalhaes, J.B. Borba da Siva, J. Anal. At. Spectrom. 17 (2002) 1335.
- [38] E. Bulska, K. Wrobel, A. Hulanicki, Fresen. J. Anal. Chem. 342 (1992) 740.
- [39] V. Arancibia, M. Valderrama, K. Silva, T. Tapia, J. Chromatogr. B 785 (2003) 30.
- [40] C. Bonnefoy, A. Menudier, C. Moesch, G. Lachatre, J.-M. Mermet, Anal. Bioanal. Chem. 383 (2005) 167.
- [41] B.D. Kerger, B.L. Finley, G.E. Corbett, D.G. Dodge, D.J. Paustenbach, J. Toxicol. Environ. Health 50 (1997) 67.
- [42] W. Chen, G. Zhong, Z. Zhou, P. Wu, X. Hou, Anal. Sci. 21 (2005) 1189.
- [43] A. Xue, S. Qian, G. Huang, L. Chen, J. Anal. At. Spectrom. 15 (2000) 1513.
- [44] M. Ezer, S.A. Elwood, J.B. Simeonsson, J. Anal. At. Spectrom. 16 (2001) 1126.
- [45] P.C.C. Oliveira, J.C. Masini, Analyst 123 (1998) 2085.
- [46] J. Wang, K. Ashley, E.R. Kennedy, C. Neumeister, Analyst 122 (1997) 1307.
- [47] M.Y. Lin, C.W. Whang, J. Chromatogr. A 1160 (2007) 336.



Microwave-assisted extraction for qualitative and quantitative determination of brominated flame retardants in styrenic plastic fractions from waste electrical and electronic equipment (WEEE)

Francisco Vilaplana^{a,b}, Amparo Ribes-Greus^b, Sigbritt Karlsson^{a,*}

^a Department of Fibre and Polymer Technology, School of Chemical Science and Engineering, KTH - Royal Institute of Technology, Teknikringen 56-58, SE-10044 Stockholm, Sweden

^b Instituto de Tecnología de Materiales (ITM), Escuela Técnica Superior de Ingeniería del Diseño (ETSID), Universidad Politécnica de Valencia, Camino de Vera s/n, E-46022 Valencia, Spain

ARTICLE INFO

Article history:

Received 16 May 2008

Received in revised form 17 October 2008

Accepted 24 October 2008

Available online 31 October 2008

Keywords:

Microwave-assisted extraction

Brominated flame retardants

Polymers

HPLC–UV

ABSTRACT

A fast method for the determination of brominated flame retardants (BFRs) in styrenic polymers using microwave-assisted extraction (MAE) and liquid chromatography with UV detection (HPLC–UV) was developed. Different extraction parameters (extraction temperature and time, type of solvent, particle size) were first optimised for standard high-impact polystyrene (HIPS) samples containing known amounts of tetrabromobisphenol A (TBBPA) and decabromodiphenyl ether (Deca-BDE). Complete extraction of TBBPA was achieved using a combination of polar/non-polar solvent system (isopropanol/n-hexane) and high extraction temperatures (130 °C). Lower extraction yields were, however, obtained for Deca-BDE, due to its high molecular weight and its non-polar nature. The developed method was successfully applied to the screening of BFRs in standard plastic samples from waste electrical and electronic equipment (WEEE); TBBPA could be fully recovered, and Deca-BDE could be identified, together with minor order polybrominated diphenyl ether (PBDE) congeners.

© 2008 Elsevier B.V. All rights reserved.

1. Introduction

Brominated flame retardants (BFRs) are organic compounds containing bromine, which are added to polymers and other materials to improve their fire-resistant properties in diverse applications, such as textiles, building materials and insulation, vehicle equipment, and electrical and electronic equipment [1]. In polymeric materials, brominated flame retardants can be either chemically bonded to the polymeric matrix or incorporated as additives at a high concentration (around 10–15%, w/w). BFRs constitute a heterogeneous family of halogenated organic compounds, where tetrabromobisphenol A (TBBPA), polybrominated diphenyl ethers (PBDEs), hexabromocyclododecane (HBCD), and polybrominated biphenyls (PBBs) have been traditionally employed in polymers. It has been shown that BFRs are present in the environment and are bio-assimilable, with increasing concentrations in water, air, soil, and biota; the effects of BFRs on the environment and human health are not well known [2,3]. Concern about these additives has encouraged restrictive legislation that regulates the

employment of BFRs in polymeric components for electronic and electrical equipment and the management of their residues. Waste from electrical and electronic equipment (WEEE) contains approximately 18% plastics, mainly styrenic polymers such as acrylonitrile–butadiene–styrene (ABS), high-impact polystyrene (HIPS) and polystyrene (PS).

Different reviews have been published in recent years that deal with the analysis of BFRs in different matrices. The analytical procedures usually involve different steps, including sample pre-treatment, extraction, clean-up and fractionation, and extract analysis using chromatographic techniques [4–8]. For the determination of additive BFRs in polymeric matrices, an efficient extraction step is mandatory prior to the chromatographic determination. Liquid extraction from polymers is traditionally performed by Soxhlet extraction, which requires lengthy extraction times and consumes high solvent volumes. Different advanced solvent extraction techniques, including supercritical-fluid extraction (SFE), pressurised liquid extraction (PLE), ultrasonic-assisted extraction (UAE), and microwave-assisted extraction (MAE), have been introduced recently and are available in many laboratories as routine extraction procedures with shorter extraction times, lower solvent consumption and automation possibilities [9]. Some studies have been devoted to the determination

* Corresponding author. Tel.: +46 8 790 8581 fax: +46 8 100775.
E-mail address: sigbritt@kth.se (S. Karlsson).

of BFRs in different polymeric samples, using Soxhlet extraction with methanol/isopropanol as solvents [10], SFE [11], PLE with iso-octane [12], and ultrasonication with isopropanol [13] as extraction techniques prior to extract analysis. For detection, liquid chromatography (HPLC) with either ultraviolet (UV) or mass spectrometry (MS) have proven to be robust methods for the quantification of the relatively high concentrations of BFRs in plastic fractions from WEEE [5,12,13]. However, no studies have been reported for the use of microwave-assisted extraction for the determination of BFRs in polymeric matrices.

MAE is based on the application of microwave energy to heat the solvent employed in the liquid–solid extraction. The instrumental equipment consists of several closed extraction vessels to which the sample and the solvent system are introduced, with temperature and pressure control allowing the heating of the solvent system under pressure above its normal boiling point [14–16]. The solvent remains in liquid phase in these high temperature conditions, promoting analyte diffusion and swelling between polymer and solvent. Parameters such as the nature of the extractive solvents, the extraction temperature and the particle size influence the extraction yield [14,15]. The employed solvent system must contain some component with dielectric permittivity, to absorb the microwave energy and therefore be heated; mixtures of polar/non-polar solvents are commonly employed for MAE (acetone/n-hexane, isopropanol/cyclohexane, dichloromethane/xylene) [9]. Microwave-assisted extraction has been successfully employed to extract a wide range of additives (antioxidants, stabilisers, plasticisers) from polymer matrices, especially polyolefins as polyethylene (HDPE and LDPE), polypropylene (PP), and poly(vinyl chloride) (PVC) [17–19] or silicones as polydimethyl siloxane (PDMS) [20], with high effectivity, low solvent consumption, and short extraction times. MAE has also been useful for the analysis of the oligomer content in poly(ethylene terephthalate) (PET) [21] and for the identification of contaminants and low molecular weight compounds in recycled polyolefins from packaging wastes [22].

The aim of this study was to develop and optimise an analytical procedure for the determination of BFRs in styrenic samples from WEEE using MAE and HPLC–UV. Two model flame retardants, TBBPA and Deca-BDE, with HIPS as the polymeric matrix, were chosen for the method development due to two main reasons: (i) TBBPA and Deca-BDE are currently the most employed BFRs in electrical and electronic products and (ii) both BFRs have diverse properties such as volatility, size, and polarity, which allows to obtain interesting conclusions regarding their influence on extraction efficiency. Different extraction parameters (solvent system, extraction temperature and time, particle size) were varied to optimise the recovery rates during extraction. The proposed analytical procedure was further applied and evaluated for the identification and quantification of BFRs in samples from recycled plastic WEEE fractions.

2. Theoretical approach to solvent extraction of additives from polymers

Solvent extraction of additives from polymeric matrixes is a complex mass transfer operation, where different interconnected parameters are involved, related to the own kinetics of the transport process, the interaction between the solvent and the polymer, and the polymeric structural properties. In particular, microwave-assisted extraction from polymers is a batch process whose kinetics involves three interconnected mass transfer steps: (i) diffusion of the analytes in the core of polymer particles; (ii) transfer of the analytes from the polymer surface to the solvent boundary layer;

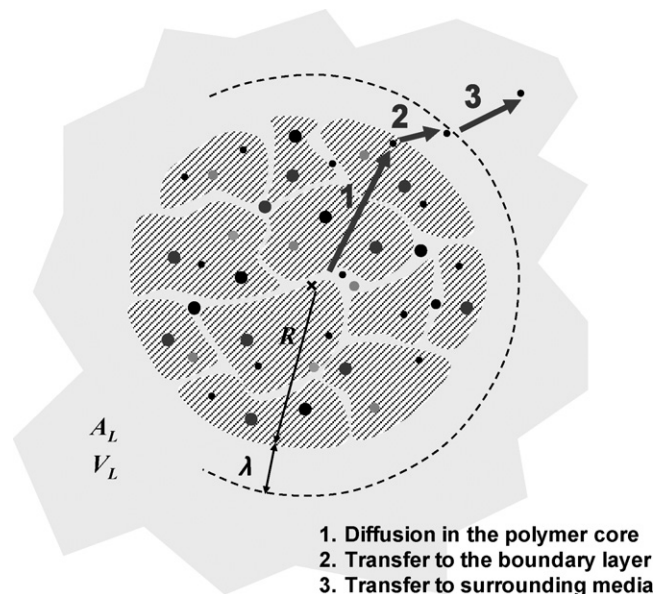


Fig. 1. Kinetic steps in the extraction of low molecular weight compounds from polymers.

(iii) mass transfer of the analytes into the extractive solvent (Fig. 1) [23]. Diffusion of additives from a spherical particle can be mathematically modelled using second Fick's law:

$$\frac{\partial c(t, r)}{\partial t} = \frac{D}{r^2} \left[r^2 \frac{\partial c(t, r)}{\partial r} \right] \quad t > 0 \quad 0 < r < R \quad (1)$$

where $c(t, r)$ represents the concentration of the additive in the polymeric core as a function of time t and the radial coordinate r ; D is the diffusion coefficient of the additives in the polymeric core; R is the radius of the spherical polymeric particles.

Similarly, the differential material balance for the interface polymer/solvent can be modelled as follows:

$$\frac{\partial c(t, r)}{\partial t} = \frac{D_L}{r^2} \left[r^2 \frac{\partial c(t, r)}{\partial r} \right] \quad t > 0 \quad R < r < R + \lambda \quad (2)$$

where D_L is the diffusion coefficient of the additive in the liquid phase; λ is the thickness of the solvent boundary layer.

Finally, the differential material balance for the additive mass transfer into the liquid phase of the batch microwave-assisted extraction vessel can be modelled:

$$V_L \frac{\partial c^L(t)}{\partial t} = -A_L D_L \frac{\partial c(t, R + \lambda)}{\partial r} \quad c^L(0) = 0 \quad (3)$$

where $c^L(t)$ is the concentration of the additive in the liquid phase; A_L is the interfacial area between polymer and solvent; V_L is the solvent volume.

As it can be observed, the mass transport phenomena involved in solvent extraction depend theoretically on geometrical parameters related to particle size and surface area, and on the temperature-dependent diffusion coefficients in the polymeric (D) and the solvent (D_L) phases. In particular, the nature of the diffusion coefficient in polymeric materials has been a matter of constant study in polymer science due to the complex interrelations between solute mobility and polymeric molecular relaxations [24]. Transport properties in polymeric materials depend on their structural properties, e.g. if they are elastomers, amorphous, or semicrystalline polymers. Anomalous diffusion, where phase transformations in the polymer may accompany the sorption of solvent molecules, is expected for glassy polymers such as HIPS exposed to solvent extraction using microwave-assisted extraction. In this case,

Table 1
Solubility parameters for the materials employed in the study.

Materials	Hildebrand	Hansen solubility parameters (HSP)		
	δ (MPa ^{1/2})	δ_D (MPa ^{1/2})	δ_P (MPa ^{1/2})	δ_H (MPa ^{1/2})
n-Hexane	14.9 ^a	14.9 ^{a,b}	0 ^{a,b}	0 ^{a,b}
Isopropanol	23.5 ^a	15.8 ^{a,b}	6.1 ^{a,b}	16.4 ^{a,b}
Methanol	29.7 ^a	15.1 ^{a,b}	12.3 ^{a,b}	22.3 ^{a,b}
Polystyrene	18.6 ^{a,c}	17.5 ^b	2.3 ^b	3.4 ^b
Polybutadiene	17.1 ^{a,c}	21.3 ^b	5.8 ^b	4.3 ^b
TBBPA	26.1 ^d	20.2 ^b	9.1 ^b	13.8 ^b
Deca-BDE	n.a.	n.a.	n.a.	n.a.

n.a.: not available.

^a Value taken from Ref. [27].

^b Value taken from Ref. [26].

^c Value taken from Ref. [28].

^d Value calculated using the HSP from Ref. [26].

solvent/polymer interactions have to be taken into account, to assess the extent of polymeric swelling. Solvent/polymer interactions have been traditionally assessed using Hildebrandt solubility parameters (δ) and Flory–Huggins interaction parameters (χ) [25]. Recently, Hansen solubility parameters (HSD) have been introduced to better understand interactions between solvents and polymers, by identifying three different components in the cohesive energy density: atomic dispersion force parameter (δ_D), molecular permanent dipole–permanent dipole polar cohesive energy parameter (δ_P), and molecular hydrogen bonding electron exchange parameter (δ_H). Affinity between solvents and polymers is based on the principle of “like seeks like”, in which substances with closer solubility parameters will have higher affinity with each other [26]. Table 1 displays the Hildebrand and Hansen solubility parameters for the compounds employed in the current work.

3. Experimental

3.1. Chemicals and polymeric samples

Two commercial brominated flame retardants, tetrabromobisphenol A technical grade (TBBPA) (4-4'-isopropylidene bis(2,6-dibromophenol), 97% purity, M_w 543.9 g/mol, CAS number 79-94-7) and decabromodiphenyl ether, technical grade (Deca-BDE, 95.0% purity, M_w 959.22 g/mol, CAS number 1163-19-5) both provided by Sigma–Aldrich (Sweden), were employed as model compounds for the development of the extraction method from styrenic plastics. The solvents for the extraction and analysis of the BFRs (n-hexane, isopropanol, methanol, tetrahydrofuran, and water) were all chromatographic grades and provided by Acros Organics (Sweden).

Virgin HIPS, Polystyrol 486 M (BASF Española, Spain) was employed as the polymeric matrix for the development of the extraction method for determination of BFRs in styrenic plastics. Standard samples of HIPS containing 50 mg/g TBBPA and 50 mg/g Deca-BDE were prepared by solution in tetrahydrofuran (THF) in a stirred vessel at room temperature. After drying at 25 °C, the polymer was granulated in a Moretto Granulator (Moretto, Italy). To analyse the influence of particle size on extraction efficiency, the polymeric granules (5 mm average diameter) were further grinded into powder (1 μ m average diameter) using a rotary mill with liquid nitrogen.

Standard samples from WEEE were used to verify the applicability of the analytical method for the determination of BFRs in styrenic components from electrical and electronic applications. These standard WEEE samples were provided by Gaiker Centro Tecnológico (Spain) and their approximate composition is shown in Table 2.

3.2. Microwave-assisted extraction (MAE)

MAE was carried out in MES 100 microwave extraction equipment (CEM Corp., North Carolina, USA), with a nominal power of 1000 W. Approximately 0.5 g of the standard HIPS sample with BFRs (in either granule or powder form) was introduced with 10 ml of the extractive solution inside MAE closed vessels. Isopropanol/methanol (IP/MeOH, 1:1, v/v) and isopropanol/n-hexane (IP/hexane, 1:1, v/v) were employed as extractive solutions. Different extraction times (20, 30, 45, and 60 min) and extraction temperatures (90, 110, and 130 °C) were tested to optimise the method. The extracts were evaporated to close to dryness and the residue was re-dissolved with 50 ml THF. The solutions were filtered with a 0.45 mm pore HPLC Teflon filter (Sorbent AB, Sweden) and placed in HPLC vials, which were kept at 4 °C until further analysis. Each extraction was performed three times and the average of the calculated HPLC–UV concentration was assumed as the representative value.

3.3. High-performance liquid chromatography (HPLC–UV)

The analyses of the extracts containing BFRs were performed by high-performance liquid chromatography, employing Hewlett Packard HPLC 1090 equipment (Palo Alto, CA, USA). The chromatograph was equipped with a diode-array detector (DAD) Waters 990 (Milford, MA, USA) and an auto-sampler Waters 712 WISP (Milford, MA, USA). Chromatographic separation was achieved using a reverse phase system consisting on a 5 μ m frit filter, a Supelguard Discovery 18 guard column (20 mm \times 4 mm, 5 μ m), and a C18 Hypersyl ODS column (250 mm \times 4.6 mm, 5 μ m), all supplied by Supelco (Sweden). The measurements were carried out at 35 °C, employing an isocratic methanol/water (95/5%, v/v) mobile phase at a flow of 1 ml/min. After some previous experiments, the DAD detector was fixed at a wavelength of 220 nm.

Quantification of TBBPA and Deca-BDE was performed by external calibration, using 7 seven-point calibration curves obtained by injection of standard solutions containing 1–1000 μ g/ml of the technical flame retardants.

4. Results and discussion

4.1. Development of the detection method by HPLC–UV

The optimisation of the spectrometric detection was achieved by injection of standard solutions of the analytes in THF in the range 1–1000 μ g/ml into the HPLC–UV. The initial chromatographic parameters (column, mobile phase, mobile flow, temperature) were first directly chosen from previous bibliographic results [12], and further adjustments were performed to satisfy the requirements for successful separation and detection. Previous experiments with the DAD detector and the standard BFRs were performed and, as a result, a single wavelength of 220 nm was selected for the sake of simplicity. The retention times, limit of detection (LOD), limit of quantification (LOQ), and the linearity range for TBBPA and Deca-BDE have been calculated for the developed HPLC–UV method and are presented in Table 3.

Table 2
Composition of the standard WEEE samples containing BFRs.

WEEE sample	Matrix	Flame retardant		Additive	
		Type	Conc. (mg/g)	Type	Conc. (mg/g)
ABS-GVL2-07	ABS	Deca-BDE	100	Sb ₂ O ₃	50
ABS-GVL2-11	ABS	TBBPA	100	Sb ₂ O ₃	50
SB-GVL2-07	SB	Deca-BDE	100	Sb ₂ O ₃	50

Table 3
Chromatographic parameters (retention time, limit of detection, limit of quantification, and linearity range) for the proposed analytical method.

Analyte	Retention time, t_R (min)	LOD (S/N = 3) ($\mu\text{g/ml}$)	LOQ (S/N = 10) ($\mu\text{g/ml}$)	Linearity range ($\mu\text{g/ml}$) (regression coefficient)
TBBPA	11.1	0.49	1.63	5–1000 (0.9962)
Deca-BDE	20.6	0.21	0.68	1–1000 (0.9971)

4.2. Evaluation of different extraction conditions for the recovery of BFRs from styrenic polymers using MAE

Different extraction parameters (type of extractive solvent, extraction time, extraction temperature, and particle size) were evaluated to optimise MAE recovery of TBBPA and Deca-BDE from standard HIPS samples with known BFR content. BFR content quantification was performed by analysis of the MAE extracts using HPLC–UV. Fig. 2 shows an example of a chromatogram of the polymeric extract after MAE at 130 °C and 60 min using isopropanol/n-hexane as solvent. Two clear peaks corresponding to TBBPA (at 11.1 min) and Deca-BDE (at 20.6 min) can be observed; different peaks around 14–15 min are also found in the chromatograms, which correspond to styrenic oligomers present in the HIPS matrix, as verified by the extract analysis from virgin HIPS without flame retardants. It is worth mentioning that Deca-BDE is especially sensitive to debromination into lower order PBDEs when exposed to UV and sunlight radiation and/or during long-term solution in alcohols [4]. The extracted samples and the technical standard solutions were therefore analysed shortly after preparation, and no further sign of Deca-BDE debromination induced

by microwaves or during storage could be observed in the chromatograms.

The calculated concentration and the relative standard deviation (R.S.D.) for TBBPA and Deca-BDE in the standard HIPS samples using different extractive conditions is presented in Table 4. It can be observed that TBBPA extraction can be optimised by varying the conditions to reach calculated concentrations similar to the theoretical ones of the standard HIPS samples. In the case of Deca-BDE, however, the extractive conditions with MAE offer a calculated concentration value far below the theoretical value, with maximum extraction recoveries of approximately 30%. This could be due to the different molecular weight and polarity of the two extracted BFRs; the extraction efficiency of additives using MAE is highly conditioned by the molecular weight of the analytes to be extracted [9], so the high molecular weight and low polarity of Deca-BDE (959.17 g/mol) could hinder its complete extraction from the polymeric matrix in comparison with TBBPA (543.87 g/mol).

The selection of the extractive solution plays a critical role in MAE of additives from polymeric matrices. From an operational point of view, the solvent system must possess certain dielectric permittivity to absorb microwave energy and thus be heated. The solvent system should have, in addition, high affinity for both the analytes to be extracted and the polymeric matrix, inducing certain swelling effects in the polymer but without causing the dissolution of any matrix component [23]. Finally, from an occupational health perspective, the employment of hazardous solvents should be avoided. The selection of the extraction solvents was therefore difficult, due to the nature of the matrix (in the case of HIPS, a blend of polystyrene and polybutadiene), and the low quantity of solvent systems that satisfy *a priori* the aforementioned requirements; solvent mixtures with different polar nature such as isopropanol/methanol (1:1, v/v) and isopropanol/n-hexane (1:1, v/v) were thus considered. As the results of Table 4 show, the type of solvent clearly affects the extraction recovery and therefore the calculated concentration of BFRs in the standard HIPS solvent. A mixed polar/non-polar extractant solution such as isopropanol/n-hexane offers higher calculated concentrations of TBBPA and Deca-BDE than a polar mixture such as methanol/isopropanol, due to the higher affinity for both matrix and analytes as assessed using the values of the solubility parameters in Table 1.

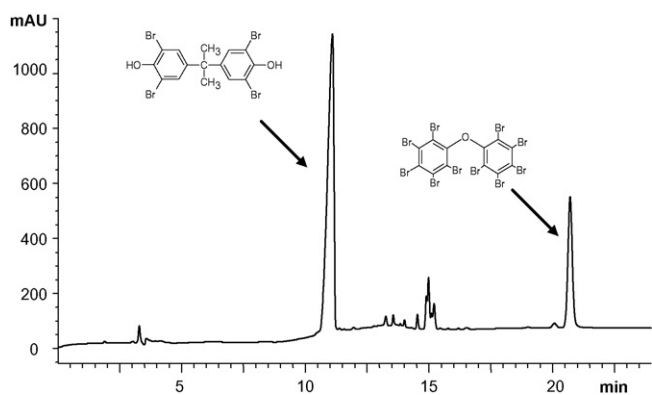


Fig. 2. Chromatogram of the MAE extracts of the standard HIPS sample containing BFRs (solvent: isopropanol/n-hexane, 30 min, 130 °C).

Table 4
Calculated concentration of BFRs in the standard HIPS samples using microwave-assisted extraction under different conditions.

Solvent	Sample size	Extraction temperature (°C)	Extraction time (min)	Calculated concentration, mg/g (R.S.D., %)	
				TBBPA	Deca-BDE
IP/MeOH (1:1, v/v)	Granule	90	30	10.44 (7.46)	2.82 (11.29)
			30	27.16 (1.11)	5.04 (3.10)
	Powder	130	20	33.37 (3.32)	7.77 (3.44)
			30	33.97 (4.87)	7.98 (3.70)
	Granule	130	45	39.69 (4.05)	8.99 (0.42)
			60	41.98 (2.16)	9.27 (5.06)
IP/hexane (1:1, v/v)	Granule	90	30	45.91 (7.1)	11.01 (14.1)
			30	36.62 (2.33)	5.46 (1.49)
	Powder	130	30	38.00 (4.59)	6.92 (3.18)
			20	37.65 (5.69)	9.36 (0.80)
	Granule	130	30	44.93 (0.91)	10.77 (6.55)
			45	46.06 (1.53)	12.04 (7.82)
Powder	130	60	48.55 (1.31)	13.69 (8.75)	
		60	48.19 (3.4)	16.54 (12.7)	

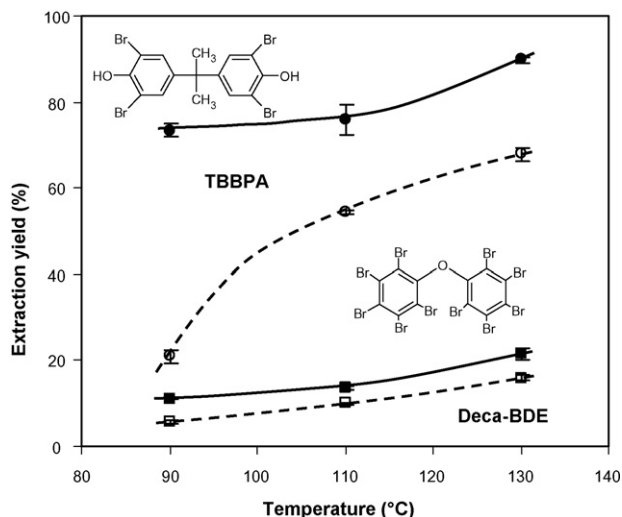


Fig. 3. Influence of the extraction temperature on the recovery of BFRs by MAE at an extraction time of 30 min, employing as solvents (full symbol, —) isopropanol/n-hexane; (hollow symbol, ---) isopropanol/methanol: (●) TBBPA; (■) Deca-BDE.

Particle size also influences the calculated TBBPA and Deca-BDE concentrations after MAE extraction (Table 4). Higher extraction rates were obtained for HIPS powder than for HIPS granules, due to enhanced diffusion of the analytes from the polymer core to the polymer surface as presumed from Eq. (1). However, this increase in extraction rate with decreasing particle size is less significant than expected, especially in the case of Deca-BDE, indicating that the addition of an additional cryogenic reduction size step in the analytical procedure may not be worthwhile in terms of recovery rates. This result suggests that diffusion of BFRs in the polymeric core may not be the limiting step in the solvent extraction process [23], and other external parameters may be adjusted to favour the extraction kinetics and increase the recovery rates.

Extraction temperature substantially influences the extraction efficiency and the calculated BFR concentration from standard HIPS samples. The extraction yield of Deca-BDE and TBBPA especially are greatly improved by using higher extraction temperatures, both with methanol/isopropanol and isopropanol/n-hexane as extractive solutions, as observed in the plot of extraction yield versus extraction temperature in Fig. 3. Temperature acts upon each stage of the solvent extraction process of low molecular weight compounds from polymeric particles, affecting both diffusion coefficients D and D_L (Eqs. (1–3)). Higher temperatures result in higher diffusion rates of the analytes, both in the polymer core and in the boundary layer around the polymer surface. Higher temperatures also increase the solubility of the analytes in the extractive solvents and enhance the mass transfer from the boundary layer to the solvent bulk. The swelling ratio between the polymeric matrix and the solvent is also clearly influenced by extraction temperature. Finally, temperature plays an essential role in the polymeric structure, in terms of the mobility of polymeric chains directly related to their viscoelastic behaviour and the glass transition temperature (T_g). In our study, HIPS is basically constituted by PS with a low content of PB rubber; taking into account that the T_g of PS is around 90 °C, temperatures above this range should favour polymer mobility and therefore a marked increase in extraction rates for additives, which is confirmed by the results in Fig. 3.

The extraction time was optimised for an extraction temperature of 130 °C using both solvent systems (Fig. 4). A near complete recovery of TBBPA can be achieved with an extraction time of 60 min with isopropanol/n-hexane as the extractive solution, whereas only a partial recovery (30%) can be obtained for

Deca-BDE under the same conditions. Employing these conditions (extraction with microwaves at 130 °C with isopropanol/n-hexane during 60 min), the method detection limits combining extraction and HPLC–UV detection and taking into account the calculated recovery rates for both analytes are 50 µg/g polymer for TBBPA and 75 µg/g polymer for Deca-BDE, far below the maximum concentration limits for BFRs in plastic products specified in 0.1% (w/w) by European legislation. In general, the extraction yields for TBBPA and Deca-BDE are similar or even higher than that reported by other authors using SFE with CO₂ and 1-propanol [11]. Other more aggressive extraction conditions and/or procedures may be therefore employed when a complete recovery of Deca-BDE were needed. In fact, almost complete recovery of Deca-BDE was reported in the aforementioned study [11], employing toluene as solvent modifier in the SFE method, which dissolves the HIPS matrix. The proposed analytical method combining MAE and HPLC–UV detection offers, finally, excellent reproducibility ($n=3$) for the calculated BFR concentrations, with low R.S.D. values for the different extractive conditions proposed.

4.3. Extraction of brominated flame retardants from standard WEEE samples

The analytical method developed for the determination of BFRs in standard styrenic polymeric samples was further applied to the identification and quantification of BFRs in standard recycled polymeric samples from waste electrical and electronic equipment (WEEE). The samples described in Table 2 were therefore extracted using MAE and their extracts were analysed using HPLC–UV. Fig. 5 shows the chromatograms of the extracts for the standard WEEE samples. The sample ABS-GVL2-07 exhibits, in addition to the main peak corresponding to Deca-BDE ($t_R = 20.6$ min), other minor peaks that may correspond to other PBDE congeners with lower bromination degree at $t_R = 20.0$ min, $t_R = 19.4$ min, and $t_R = 18.9$ min, either originally contained in the technical grade Deca-BDE used in the manufacture of the plastic component, or due to the debromination of the BFR during service life and further recycling (Fig. 5a). Sample ABS-GVL2-11 shows a single clear peak corresponding to TBBPA at $t_R = 11.1$ min, proving that the flame retardant has been successfully extracted from the polymeric matrix (Fig. 5b). Finally, different peaks can be observed in the chromatogram

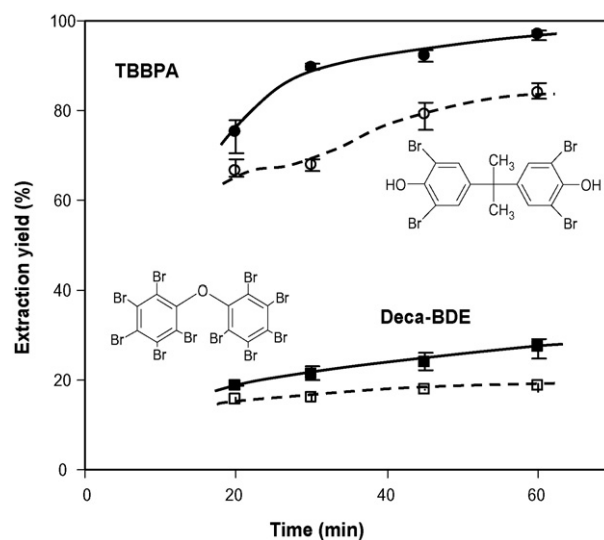


Fig. 4. Influence of the extraction time on the recovery of BFRs by MAE at a temperature of 130 °C, employing as solvents isopropanol/n-hexane (full symbol, —) or isopropanol/methanol (hollow symbol, ---): (●) TBBPA; (■) Deca-BDE.

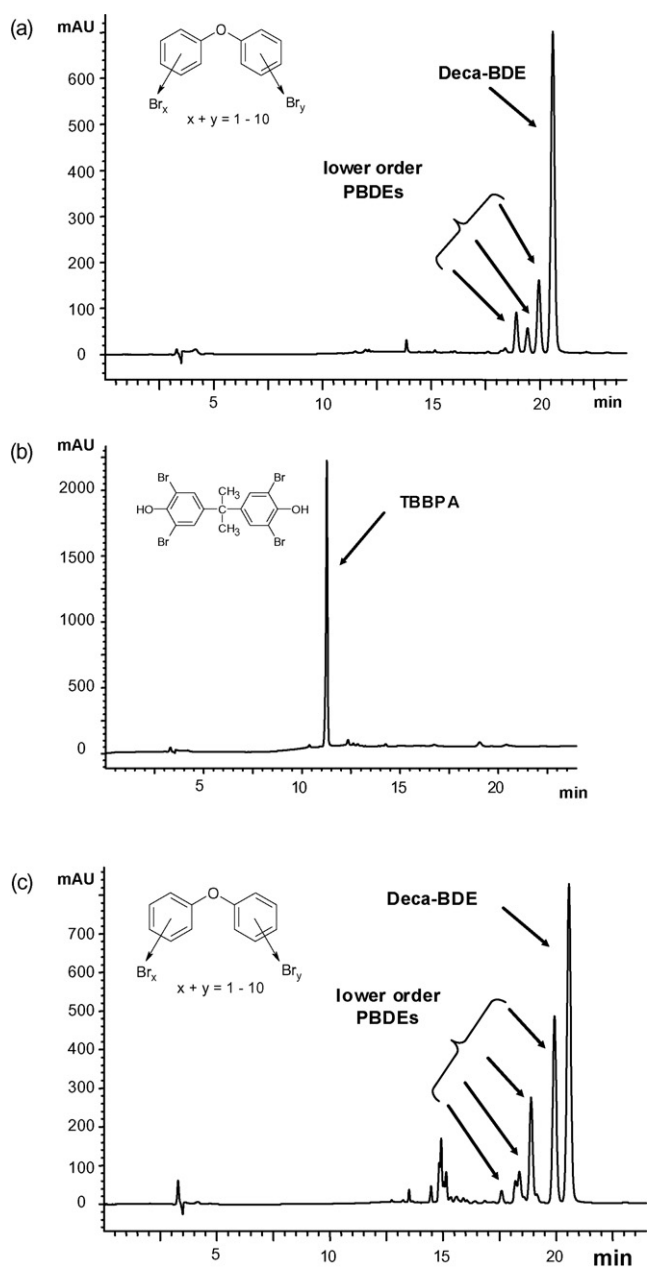


Fig. 5. Chromatograms for the extracted standard WEEE samples using MAE (solvent: isopropanol/n-hexane, 60 min, 130 °C): (a) ABS-GVL2-11; (b) SB-GVL2-07; (c) ABS-GVL2-07.

Table 5

Calculated concentration of BFRs in the standard WEEE samples using microwave-assisted extraction.

Sample	Matrix	BFR	Extraction solvent	Calculated concentration, mg/g (R.S.D., %)
ABS-GVL2-11	ABS	TBBPA	IP/MeOH	124.14 (3.18)
			IP/hexane	109.53 (0.90)
SB-GVL2-07	SB	Deca-BDE	IP/MeOH	10.83 (24.60)
			IP/hexane	26.90 (11.28)
ABS-GVL2-07	ABS	Deca-BDE	IP/MeOH	18.23 (6.12)
			IP/hexane	29.03 (20.04)

corresponding to sample SB-GVL2-07, the main peak assigned to Deca-BDE at $t_R = 20.6$ min and other peaks that may be attributed to other PBDE congeners at $t_R = 19.9$ min, $t_R = 18.9$ min, and $t_R = 18.4$ min (Fig. 5c).

The calculated concentration of TBBPA and Deca-BDE in the standard WEEE samples is provided in Table 5. It is worth mentioning that for the case of samples ABS-GVL2-07 and SB-GVL2-07, the Deca-BDE concentration has been calculated considering only the main peak at $t_R = 20.6$ min and not the other peaks assigned to minor congeners. The calculated concentration for TBBPA is very similar to the approximate theoretical concentration provided by the supplier, proving the complete extraction of this flame retardant, whereas the concentration of Deca-BDE is lower and a complete recovery cannot be achieved.

5. Conclusions

An analytical method based on MAE and HPLC–UV for the determination of BFRs in styrenic polymers was developed for standard HIPS containing TBBPA and Deca-BDE. The extractive conditions (solvent system, extraction temperature and time, and particle size) influence the extraction yields of the BFRs, and their effects have been discussed in terms of mass transfer and polymer structure. Mixed polar/non-polar solvents such as isopropanol/n-hexane offered higher recovery rates due to higher affinity to the analytes and greater swelling effect on the matrix. Temperature had a remarkable effect on the extraction; high temperatures above the glass transition of the polymer should be used to improve diffusion rates and to speed recovery of the analytes. However, decreasing the particle size had only a minor influence on the extraction recovery, which suggests that the diffusion of the additives in the polymer core may not be the limiting stage in the extraction. Complete TBBPA recovery from the polymeric matrix was achieved by adjusting the extraction parameters. The complete extraction of Deca-BDE proved to be a complex analytical process, which may require more extreme extraction conditions (temperature, time) or even other extraction processes with higher pressure and increased affinity for extraction solvents. The method was successfully applied to identify and determine the presence of BFRs in standard WEEE samples, which proves the idoneity of the proposed analytical procedure for the fast screening for the presence of BFRs in recycled WEEE samples.

Acknowledgements

The authors would like to acknowledge the Ministerio de Medio Ambiente (Project 555/2006/3-6.1) for the financial support, co-financed by FEDER European Funds. Francisco Vilaplana thanks the Ministerio de Educación y Ciencia (Spanish Government) for the concession of a pre-doctoral research position (Programa FPU). BASF Española S.A. and Gaiker Centro Tecnológico are acknowledged for providing the materials. Royal Institute of Technology (KTH) and Universidad Politécnica de Valencia (UPV) are thanked for additional economical support.

References

- [1] M. Alae, P. Arias, A. Sjobin, A. Bergman, *Environment International* 29 (2003) 683–689.
- [2] C.A. de Wit, *Chemosphere* 46 (2002) 583–624.
- [3] R.C. Hale, M.J. La Guardia, E. Harvey, M.O. Gaylor, T.M. Mainor, *Chemosphere* 64 (2006) 181–186.
- [4] A. Covaci, S. Voorspoels, J. de Boer, *Environment International* 29 (2003) 735–756.
- [5] A. Covaci, S. Voorspoels, L. Ramos, H. Neels, R. Blust, *Journal of Chromatography A* 1153 (2007) 145–171.
- [6] J. de Boer, R.J. Law, *Journal of Chromatography A* 1000 (2003) 223–251.

- [7] T. Hyotylainen, K. Hartonen, Trends in Analytical Chemistry 21 (2002) 13–30.
- [8] E. Eljarrat, D. Barceló, TrAC Trends in Analytical Chemistry 23 (2004) 727–736.
- [9] H.J. Vandenburg, A.A. Clifford, K.D. Bartle, J. Carroll, I. Newton, L.M. Garden, J.R. Dean, C.T. Costley, Analyst 122 (1997) 101R–116R.
- [10] M. Riess, R. van Eldik, Journal of Chromatography A 827 (1998) 65–71.
- [11] A.M. Altwaiq, M. Wolf, R. van Eldik, Analytica Chimica Acta 491 (2003) 111–123.
- [12] M. Schlummer, F. Brandl, A. Maurer, R. van Eldik, Journal of Chromatography A 1064 (2005) 39–51.
- [13] M. Pohlein, A.S. Llopis, M. Wolf, R.V. Eldik, Journal of Chromatography A 1066 (2005) 111–117.
- [14] M. Letellier, H. Budzinski, Analusis 27 (1999) 259–271.
- [15] V. Lopez-Avila, R. Young, W.F. Beckert, Analytical Chemistry 66 (1994) 1097–1106.
- [16] J.L. Luque-Garcia, M.D. Luque de Castro, Trends in Analytical Chemistry 22 (2003) 90–98.
- [17] J.M. Cano, M.L. Marín, A. Sánchez, V. Hernandis, Journal of Chromatography A 963 (2002) 401–409.
- [18] W. Freitag, O. John, Angewandte Makromolekulare Chemie 175 (1990) 181–185.
- [19] B. Marcato, M. Vianello, Journal of Chromatography A 869 (2000) 285–300.
- [20] K. Fateh-Alavi, S. Karlsson, U.W. Gedde, Journal of Applied Polymer Science 93 (2004) 2185–2192.
- [21] C.T. Costley, J.R. Dean, I. Newton, J. Carroll, Analytical Communications 34 (1997) 89–91.
- [22] W. Camacho, S. Karlsson, Polymer Degradation and Stability 71 (2000) 123–134.
- [23] X. Lou, H.-G. Janssen, C.A. Cramers, Analytical Chemistry 69 (1997) 1598–1603.
- [24] J. Crank, The Mathematics of Diffusion, Clarendon Press, Oxford, 1986.
- [25] H.J. Vandenburg, A.A. Clifford, K.D. Bartle, R.E. Carlson, J. Carroll, I.D. Newton, Analyst 124 (1999) 1707–1710.
- [26] C.M. Hansen, Hansen Solubility Parameters: A User's Handbook, CRC Press–Taylor & Francis Group, Boca Raton, 2007.
- [27] E.A. Grulke, in: J. Brandrup, E.H. Immergutand, E.A. Grulke (Eds.), Polymer Handbook, John Wiley & Sons, Inc., New York, 1999.
- [28] P.A. Small, Journal of Applied Chemistry 3 (1953) 71.



Uncertainty due to volumetric operations is often underestimated

Bruno Wampfler*, Matthias Rösslein

Empa, Swiss Federal Laboratories for Materials Testing and Research, Lerchenfeldstrasse 5, CH-9014 St. Gallen, Switzerland

ARTICLE INFO

Article history:

Received 29 July 2008

Accepted 29 October 2008

Available online 7 November 2008

Keywords:

Measurement uncertainty

Combined standard uncertainty

Titration

Volumetric measurement

Weighing

Collaborative study

Reproducibility standard deviation

ABSTRACT

Fifteen international titration standards were evaluated to determine minimum and maximum combined standard uncertainties. Assuming most thorough performance of the analyses revealed minimum values, whereas maximum values of uncertainty were obtained assuming that the analyses had been done under high time pressure. Minimum and maximum uncertainties were compared with the corresponding reproducibility standard deviations. Since the combined standard uncertainty is expected to lie between the reproducibility standard deviation and the maximum combined standard uncertainty, realistic standard uncertainties of individual influence quantities of volumetric and weighing procedures could be calculated. This top-down approach revealed up to 4 times higher uncertainties for volumetric operations compared to the bottom-up approach according to the current literature. Hence, uncertainty due to volumetric operations is obviously strongly underestimated. The present study additionally contains a ranking of the contributions to the uncertainty of titrimetric results.

© 2008 Elsevier B.V. All rights reserved.

1. Introduction

There are several guidelines which specify how to evaluate the uncertainty of a measurement result (e.g. [1–3]). Although these guidelines are very helpful to chemical analysts, a certain expertise is needed to obtain meaningful uncertainty estimates. When quantifying influence quantities, the analysts often are forced to choose a value within a wide range. When analysts tend to choose either rather low or rather high values, the resulting uncertainty will be under- or overestimated, respectively. This can be examined by comparing the calculated combined standard uncertainties (u_c) with the corresponding reproducibility standard deviations (s_R) from collaborative studies. s_R is a useful quantity for a rough estimation of the combined standard uncertainty [4,5]. As s_R does not include all contributions to uncertainty [4,5], u_c is expected to be higher than s_R . Nevertheless, most uncertainty evaluations lead to $u_c < s_R$ [6–8]. The authors [7] suggest that calibration procedures cause underestimation, whereas weighing and volumetric operations give rise to combined standard uncertainties close to or higher than the corresponding s_R values. If this is true uncertainty calculation in titrimetry would provide meaningful value of u_c with respect to the corresponding value of s_R . Titrimetry is based on volumetric determination of the amount of an analyte which stoichiometrically reacts with the reference substance. Since the concentration of the reference substance is known, the

amount of the analyte can be calculated from the volume of the reference solution which is required to reach the end point. Thus, titrimetry is based solely on gravimetric and volumetric operations. Accurately considered estimates of contributions to the uncertainty nevertheless are often unrealistically small according to our experience in titrimetric procedures, when following the EURACHEM/CITAC guide [2]. Metrologists suggest applying even smaller uncertainties for volumetric operations [9]. This might be applicable in metrological laboratories, where relative combined standard uncertainties of less than 0.04% are reached in titrimetry (e.g. [10]). Collaborative studies of field and application laboratories however seldom yield relative reproducibility standard deviation of less than 1%. The present paper aims at listing realistic standard uncertainties that can be used for the evaluation of the standard uncertainty of weighing and volumetric operations at the level of research and application laboratories. For this purpose, 15 titration procedures approved as international standards (AOAC, ASTM, DIN/EN, ISO, IUPAC) were investigated and their reported s_R values were compared with u_c values evaluated in the present study. u_c was calculated twice for each procedure: in the first calculation we assumed that the analyses were performed most accurately (minimum combined standard uncertainty, $u_{c,min}$), whereas in the second one it was assumed that the analyses were done under high time pressure (maximum combined standard uncertainty, $u_{c,max}$). Since $u_c > s_R$, and $u_{c,min}$ is considered under the most optimistic conditions, one can expect that $u_{c,min} < s_R < u_c < u_{c,max}$. In the present study, appropriate values for the quantification of individual influence quantities were evaluated from a set of international standards fulfilling this

* Corresponding author. Tel.: +41 274 77 86; fax: +41 274 77 88.
E-mail address: bruno.wampfler@empa.ch (B. Wampfler).

condition. These values can be used in future uncertainty evaluations.

2. Procedure

2.1. International standards

Only international standards have been considered whose precision values are known as repeatability standard deviation (s_r) and reproducibility standard deviation (s_R) or as repeatability limit (r) and reproducibility limit (R). Given limits were divided by the expansion factor 2.8 [11] to get the corresponding standard deviations. Different international standards from different fields of activity were consciously chosen, thus covering all important titration methods and involving a broad range of analytes and matrices (see Table 1). When evaluating the combined standard uncertainty, repeatability standard deviation is usually taken from validation data. In the present study, the repeatability standard deviation s_r from the corresponding collaborative study was used instead. In international standards, the quoted equation of the measurand does usually not completely reflect all steps performed during the application of the method. For instance, several constant parameters are often combined into one single constant, and this constant is then presented in the equation of the measurand as a single number without any units. This might facilitate the use of standard methods, but many of the parameters hidden behind such a number have an uncertainty. Therefore, all equations of the measurand were expanded to permit the complete and correct evaluation of influence quantities.

2.2. Evaluation of the measurement uncertainty

The measurement uncertainty was evaluated following the methodology of the Eurachem/CITAC Guide “Quantifying Uncertainty in Analytical Measurement” [2]. This guide describes a pragmatic and practice oriented approach to evaluate the uncertainty of volumes by involving capacity tolerance of volumetric instruments and volume change caused by temperature variation. In the present study, a third influence quantity was included when volumetric flasks and pipettes were used, namely the volume bias due to inexact filling up to the meniscus. Such bias can be caused by non-horizontal focusing on the graduation line. In addition, capacity tolerances are only valid for pure water with its typical concave meniscus. They are probably larger for organic solvents or for aqueous solutions containing surface active agents. Uncertainty due to temperature variation can accurately be calculated via density of the involved solutions [12]. The Eurachem/CITAC guide describes a

more manageable way by neglecting the dependence of the volumetric expansion coefficient on the temperature. We followed Eurachem’s guide as this approach is easier to perform. The calculations were performed using the software UncertaintyManager® [13,14]. The software required the following parameters as input: equation of the measurand, manufacturers and types of instruments used for the measurement, steps of sample preparation, and validation data including conditions under which precision had been determined. The model of the uncertainty influences (cause-and-effect diagram) is built automatically. The software additionally suggested values for the quantification of the individual contributions. These values were taken from the database of the software whose data content is based on specifications of manufacturers of equipment as well as on ISO standards. The suggestions were adapted according to whether the minimum or the maximum uncertainty was calculated. Finally, the calculation was made using the Monte Carlo method [15,16] with 100,000 runs. The approach is described in detail by the following example.

2.3. Calculation of the minimum and maximum combined standard uncertainty explained by using ASTM D 4377-00 (Water in crude oils)

ASTM Standard D 4377-00 (method 15) describes a common Karl Fischer titration. Karl Fischer reagent is standardized by titration of a weighed portion of water:

$$\gamma_{KFR} = \frac{m_R}{V_{TR}} \quad (1)$$

where γ_{KFR} (mg/ml) is the water equivalence of the Karl Fischer reagent, m_R (mg) is the mass of water added, and V_{TR} (ml) is the volume of the reagent required to titrate the added water.

In order to determine the water content of crude oil, methanol with some additives is dried in a titration vessel by adding Karl Fischer reagent until the electrometric end point is reached. An aliquot of the previously homogenized crude oil is added and, after having stirred to homogenize the mixture, titrated to the electrometric endpoint again using Karl Fischer reagent. Water content is calculated according to the following equation:

$$w = \frac{V_{TS} \cdot \gamma_{KFR}}{m_S} \cdot \frac{1}{10} \quad (2)$$

where w (%) is the mass fraction of the analyte, V_{TS} (ml) is the Karl Fischer reagent required to titrate the sample, m_S (g) is the mass of the sample aliquot, and 1/10 is the factor for converting to percent.

Table 1
International standards used in the present study.

No	Analyte/matrix	Standard method	Titration method
1	Iodine value of edible oils	IUPAC 2.205	Redox
2	Peroxide value of edible oils	IUPAC 2.501	Redox
3	Methyltriocetylammmoniumchloride in raw materials and products	DIN/EN 14668	Tenside, two phases
4	Anionic tensides in detergents and cleansers	DIN/EN 14669	Tenside, two phases
5	Saponification value of oils and fats	DIN EN ISO 3657	Acid-base
6	Acid value of refined palm oil	IUPAC 2.201	Acid-base, non-aqueous
7	Nitrogen in milk	ISO/FDIS 8968-3	Acid-base
8	Lead in PbS-concentrates	ISO 11441	Complexometry
9	Total hardness in water	ASTM D 1126-02	Complexometry
10	Calcium hardness in water	ASTM D 1126-02	Complexometry
11	Chloride in cheese	ISO 5943	Precipitation
12	Chloride in aggregates	DIN EN 1744-1	Precipitation
13	Water in pet foods	AOAC 991.02	Karl Fischer
14	Water in spray-dried coffee extract	DIN 10772-2	Karl Fischer
15	Water in crude oils	ASTM D 4377-00	Karl Fischer

Table 2

Input quantities and their values used to calculate minimum and maximum combined standard uncertainty of the water content in crude oils determined according to the standard ASTM D 4377-00 (method 15).

Uncertainty	$m_{R,gr}$ (mg)	$m_{R,ne}$ (mg)	$m_{S,gr}$ (g)	$m_{S,ne}$ (g)	V_{TS} (ml)	V_{TSbl} (ml)	V_{TR} (ml)	V_{TRbl} (ml)	${}^2f_{Rrep}$	f_{Srep}	f_H
Minimum	5020.0	5000.0	20.0000	18.0000	4.01	0.01	4.01	0.01	1.000	1.000	1.000
Maximum	5010.0	5000.0	19.0000	18.0000	2.01	0.01	2.01	0.01	1.000	1.000	1.000

Eq. (3) is obtained by combining Eqs. (1) and (2):

$$w = \frac{m_R}{m_S} \cdot \frac{V_{TS}}{V_{TR}} \cdot \frac{1}{10} \quad (3)$$

This equation does not reflect all experimental operations that must be performed according to the ASTM standard. So m_S is determined by 4 measurements. An aliquot of the sample is withdrawn with a syringe and injected into the titration vessel after the filled syringe has been weighed ($m_{S,gr}$). The empty syringe is back weighed ($m_{S,ne}$) and m_S is calculated by subtracting $m_{S,ne}$ from $m_{S,gr}$. Furthermore, the usual zero setting made before each measurement is also a weighing measurement. Thus, 4 weighing operations are involved to determine m_S :

$$m_S = (m_{S,gr} - m'_0) - (m_{S,ne} - m''_0) \quad (4)$$

where $m_{S,gr}$ is the weight (g) of the syringe filled with the required amount of sample, $m_{S,ne}$ is the net weight (g) of the syringe after injection of the sample into the vessel, m'_0 and m''_0 are the weights (g) of two individual zero settings.

Since m'_0 and m''_0 have the value 0 g, they do not influence w , but they contribute to the uncertainty. In order to keep the formulae concise, zero settings are usually not quoted (see Eq. (5)); however, their contributions to the uncertainty are taken into account. The weight of the reference, m_R , is determined in the same manner as the one of the sample, m_S . The volumes V_{TS} and V_{TR} are each defined by two equivalence points, i.e. by the endpoint of the previous drying of the solvent using Karl Fischer reagent and by the endpoint of the water determination. Thus, V_{TS} and V_{TR} should be replaced by volume deviations (see Eq. (5)). In order to include the repeatability, two auxiliary factors, f_{Rrep} , and f_{Srep} , bearing the dimensionless value of 1 are additionally inserted. The standard uncertainty of f_{Rrep} corresponds to the repeatability due to the standardization of the Karl Fischer reagent, whereas the one of f_{Srep} represents the repeatability of the water determination using the Karl Fischer reagent previously standardized. f_H is the auxiliary value to consider the inhomogeneity of the sample. The expanded equation used to identify the influence quantities is given by:

$$w = \frac{m_{R,gr} - m_{R,ne}}{m_{S,gr} - m_{S,ne}} \cdot \frac{V_{TS} - V_{TSbl}}{V_{TR} - V_{TRbl}} \cdot \frac{1}{10} \cdot f_{Rrep} \cdot f_{Srep} \cdot f_H \quad (5)$$

where $m_{R,gr}$ is the weight (mg) of the syringe filled with the required amount of water, $m_{R,ne}$ is the net weight (mg) of the syringe after the addition of water, V_{TSbl} and V_{TRbl} are auxiliary values

(=0 ml) used to consider the uncertainty of the equivalence point at the end of the solvent drying, f_{Rrep} (=1) is a dimensionless factor used to consider the repeatability of the standardization, f_{Srep} (=1) is a dimensionless factor used to consider the repeatability of the sample titration, f_H (=1) is a dimensionless factor used to consider the inhomogeneity of the sample.

The ASTM standard D 4377-00 provides partially distinct information about the parameters of Eq. (5). The weight of the reference ($m_{R,gr} - m_{R,ne}$) has optionally a value of 10 or 20 mg. The weight of the sample ($m_{S,gr} - m_{S,ne}$) depends on the expected water content: 5 g of the sample is taken if the water content lies between 0 and 0.3%, 2 g is taken if the water content is 0.3–1%, and 1 g is taken if the water content is 1–2%. All weights are measured to the nearest 0.1 mg. Volumes are measured to the nearest 0.01 ml. Repeatability r that has been determined in a collaborative study depends on the water content:

$$r = 0.032 \cdot \sqrt[3]{w} \quad (6)$$

r is usually calculated by multiplying the repeatability standard deviation s_r with a coverage factor of 2.8 [11]. When applying this factor, s_r follows the function

$$s_r = \frac{0.032}{2.8} \cdot \sqrt[3]{w} = 0.0114 \cdot \sqrt[3]{w} \quad (7)$$

The input quantities which have been used to calculate minimum and maximum combined standard uncertainty are listed in Table 2. If the expected value of the measurand amounts to 1 g of water per 100 g of crude oil, as assumed in the present example, the ASTM standard method permits to use either 1 or 2 g of the sample. Since the weighing of 1 g has a higher impact to the uncertainty, it was used to calculate the maximum combined standard uncertainty. Weighing of 2 g was used to calculate the minimum combined standard uncertainty. The same principle was applied when weighing either 10 or 20 mg of water to calibrate the Karl Fischer reagent.

In order to identify and quantify uncertainty sources, different assumptions to evaluate minimum and maximum uncertainty were made (see Table 3). The specifications of the widely used balances Mettler-Toledo AT 201 and AT 200 provided a basis for the weighing operations. Both of them meet the requirements of the ASTM standard. For the evaluation of the sources of volumetric operations, influences by stirring and by the condition of the electrode were determined experimentally (unpublished results).

Table 3

Assumptions for the calculation of minimum and maximum combined standard uncertainty of the water content in crude oils determined according to the standard ASTM D 4377-00 (method 15).

	Minimum uncertainty	Maximum uncertainty
Weighing operations	• Mettler-Toledo AT201	• Mettler-Toledo AT200
Volumetric operations	• Metrohm 701 KF Titrimo • Buret of optimum volume (5 ml) • Stirring speed: predetermined* • Electrode in good condition*	• Metrohm 701 KF Titrimo • Buret of high volume (50 ml) • Stirring speed: ad hoc* • Electrode in medium condition*
f_{Rrep}	$u(f_{Rrep}) = 0.01/\sqrt{3}$	$u(f_{Rrep}) = 0.01\sqrt{3}$
f_{Srep}	$s_r (w = 1\%) = 0.011$	$s_r (w = 1\%) = 0.011$
f_H	No contribution	$0.0125/\sqrt{3} = 0.0072$

* Influences have been quantified experimentally (unpublished results).

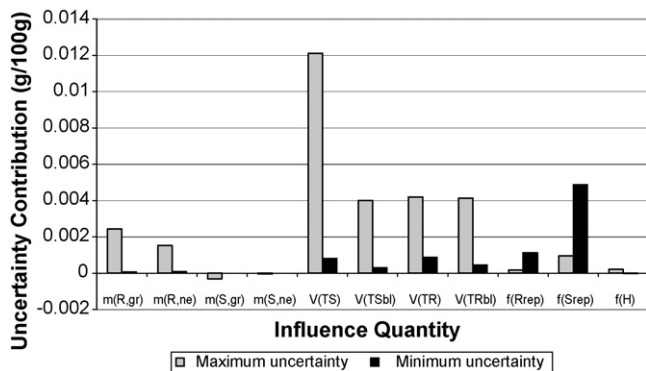


Fig. 1. Contribution of the individual influence quantities to the combined standard uncertainty when assuming accurate processing of the analyses (minimum uncertainty) and processing under high time pressure (maximum uncertainty), respectively. Contribution of the influence quantity x_i means decrease of the combined standard uncertainty if the contribution of x_i would be neglected on the condition that the other contributions are kept constant. Description of the parameters: see Eq. (5).

When performing a collaborative study, repeatability is usually determined without repetition of the standardization procedure, i.e. the within-laboratory variation of the standardization of the Karl Fischer reagent is not included in s_r . Therefore, this contribution was involved using an additional influence quantity ($f_{Rrep} = 1$). Its uncertainty or repeatability, respectively, was obtained from the ASTM standard, upon which duplicate standardization results should agree within 2%. The standard uncertainty of f_{Rrep} thus amounts to $0.01/\sqrt{3}$ when assuming a rectangular distribution. The contribution of a possible sample inhomogeneity (f_H) was neglected in case of minimum uncertainty whereas the maximum inhomogeneity was estimated from the test of the homogenization efficiency of unknown mixers according to annex A1 of the ASTM standard: mixers should only be used, if the relative span width of several determinations under different stirring conditions is not more than 5%. Since stirring conditions are required to be better defined when the actual analyses are performed, half this value was chosen, i.e. $\pm 1.25\%$, assuming a rectangular distribution (factor $\sqrt{3}$).

Uncertainty calculation revealed a combined standard uncertainty ranging from 0.016 g/100 g (minimum uncertainty) to 0.058 g/100 g (maximum uncertainty). These values are valid for a water content of 1 g/100 g in crude oil. Fig. 1 depicts the contributions of the individual input quantities building up the expanded equation of the measurand (Eq. (5)). Regarding maximum uncertainty, highest contributions were caused by titrimetric procedures, followed by weighing procedures of the reference ($m_{R,gr} - m_{R,ne}$). The high influence of weighing measurements might be surprising. However, it must be noticed that a deviation of only 10 mg water is weighed using a suboptimal balance for that purpose (see Tables 2 and 3). The contribution decreases asymptotically against 0 with increasing weight deviations; the weighing operation $m_{S,gr} - m_{S,ne} = 1$ g thus did not contribute significantly to the combined standard uncertainty. The negative value of $m_{S,gr}$ is due to the fact that the Monte Carlo method works on the basis of random variations [15,16]. Precision (f_{Rrep} , f_{Srep}) and inhomogeneity (f_H) of the sample were influence quantities of lower importance. When switching to minimum uncertainty, a decrease of all individual contributions except those of the precision was noted. f_{Rrep} and f_{Srep} increased strongly because their absolute values were kept constant in both cases (see Table 3). Thus, both precision values had a higher relative impact in the case of minimum uncertainty than in the case of maximum uncertainty.

Table 4 Interlaboratory comparison values and uncertainty spans concerning the international standards discussed in the present paper.

Method	1 (g/100 g)	2 (g/100 g)	3 (mmol/100 g)	4 (mmol/100 g)	5 (g C18:1/100 g)	6 (g/100 g)	7 (mg KOH/g)	8 (g/100 g)	9 (g/100 g)	10 (g/100 g)	11 (g/100 g)	12 (g/100 g)	13 (g/100 g)	14 (g/100 g)	15 (g/100 g)
Content	73	3.3	202	50	190	12	0.50	70	0.013	0.0075	2.0	0.021	25	4.4	1.0
s_r	0.57	0.12	0.71	0.35	0.72	0.030	0.0020	0.15	0.00010	0.000076	0.0070	0.00036	0.30	0.084	0.011
s_R	0.82	0.31	1.7	1.1	1.8	0.17	0.0030	0.26	0.00028	0.00025	0.021	0.0012	0.40	0.12	0.040
u_{Cmin}	0.81	0.12	1.2	0.42	1.0	0.057	0.0022	0.23	0.00015	0.00015	0.012	0.00042	0.39	0.10	0.016
u_{Cmax}	1.9	0.15	3.3	1.2	1.8	0.18	0.011	0.65	0.00036	0.00036	0.021	0.0013	0.60	0.14	0.058
s_R/u_{Cmin}	1.01	2.59	1.41	2.62	1.8	2.98	1.36	1.13	1.87	1.67	1.75	2.86	1.03	1.2	2.5

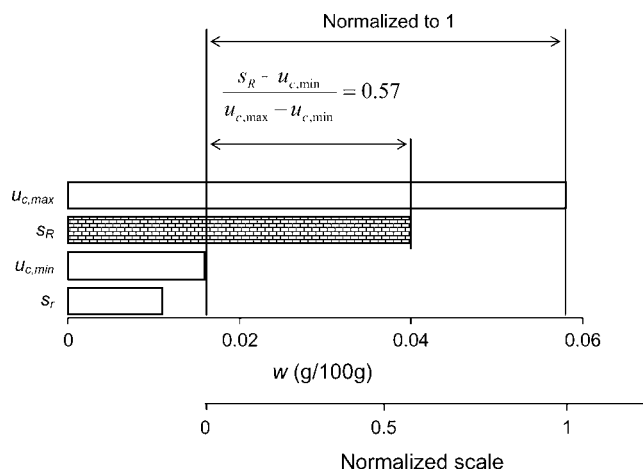


Fig. 2. Normalization of the characteristic reliability values s_R , $u_{c,min}$, and $u_{c,max}$ of the water content in crude oil determined according to the standard ASTM D 4377-00 (method 15).

3. Results and discussion

The fifteen international standards listed in Table 1 were investigated in analogy to the example above. The results are shown in Table 4. In order to generate a straightforward figure, the results were normalized as depicted in Fig. 2, where the determination of water in crude oil (method 15) again is taken as an example. The histogram shows the four values s_r , $u_{c,min}$, s_R , and $u_{c,max}$. If the deviation $u_{c,max} - u_{c,min}$ is normalized to one, $s_R - u_{c,min}$ can be expressed as a fraction expected to be between 0 and 1. Thus, the normalized s_R fraction amounts to 0.57 (hatched bar in Fig. 2). Fig. 3 depicts the normalized results of the investigated international standards. Most normalized s_R fractions lie within the expected interval, i.e. between 0 and 1. Values ≥ 1 were exhibited by method 2 (peroxide value of edible oils), by method 5 (saponification value of oils and fats), and by method 11 (chloride content in cheese). Values ≥ 1 are obtained if $s_R \geq u_{c,max}$. This indicates a vague specification of the measurand leading to an incomplete set of influence quantities. Normalized s_R fractions close to zero were related with

ratios $s_R/s_r < 2$ (methods 1, 7, 8, and 13). Although s_R/s_r typically lies between 1.5 and 2.0 for chemical food and drug analyses [17], 10 of the 15 investigated titration methods show s_R/s_r ratios between 2.4 and 5.7. These high ratios might be caused by usually small relative repeatability of titration results (significantly below 1%), whereas inter-laboratory variations might be in the same range as those of other analytical methods. The international standard to determine the peroxide value (method 2) specifies precision values that are unusually large for titrimetric methods: $s_{r,rel} = 3.6\%$; $s_{R,rel} = 9.4\%$. It is evident that such poor precision is not due to the measurement operations but to the high reactivity of peroxide. Therefore, the maximum combined standard uncertainty is far from exceeding the reproducibility standard deviation, thus leading to an extremely high normalized s_R fraction of 6.3. Such variation can be covered by addition of a dimensionless factor to the equation of the measurand. The value of this factor equals 1. Its standard uncertainty should cover the variation due to the reactivity of hydrogen peroxide and must be estimated. Since it represents the main contribution, such estimation leads to a low reliability of the combined standard uncertainty. The slightly too high normalized s_R fraction of method 5 (saponification value) might be due to influences of carbon dioxide contamination, sample inhomogeneity, or incomplete saponification in some laboratories involved in the collaborative studies, whereas in method 11 (chloride in cheese) inhomogeneity probably was underestimated. Normalized s_R fractions considerably higher than 1 were also obtained for method 15 (determination of water in crude oil), when assuming water contents to be lower than 1 g/100 g (not shown in this paper). As pointed out in this international standard, loss and contamination of water crucially contribute to the uncertainty. In the frame of the present study, it has been tried to expand the equation of the measurand by factors which allow for these additional contributions. The results will be published elsewhere.

One goal of the present study was to generate values that can be recommended to quantify influence quantities of basic operations, such as weighing, dilution, volumetric dosage, or end point recording of titration. It is obvious that recommended values should lead to combined standard uncertainties that are higher than $u_{c,min}$ but lower than $u_{c,max}$, thus revealing values between 0 and 1 with respect to Fig. 3. Since variations due to sample and analyte

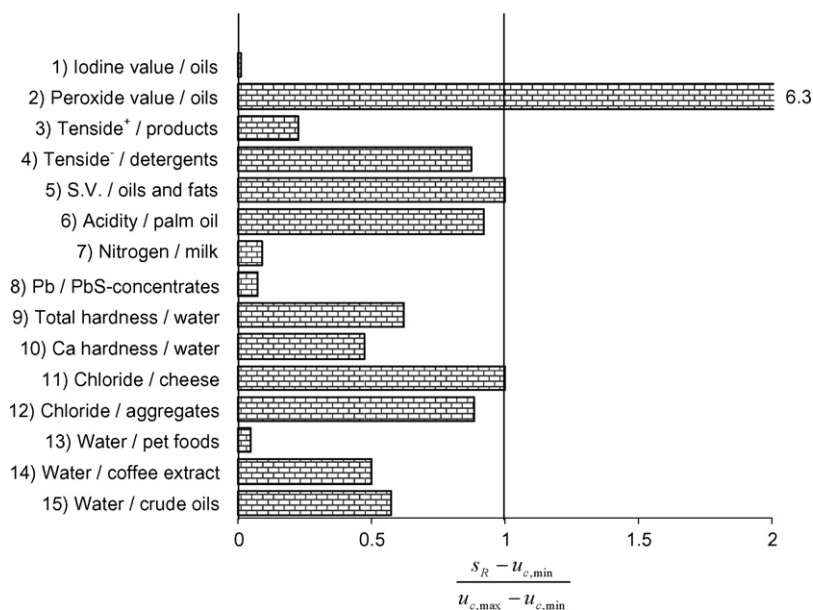


Fig. 3. Reproducibility standard deviations s_R compared with the maximum combined standard uncertainties $u_{c,max}$ (histogram normalized according to Fig. 2).

Table 5
Contributions of individual influence quantities to the combined standard uncertainties of the fifteen investigated international standards.

Method	Repeatability		Mass	Volume			Molecular Mass	Purity RM
	Sample	Reference		Titration	Flask 100 ml–1 l	Volumetric pipette 10–25 ml 50–100 ml		
1) I.V./oils	+++		n	+		+++	n	+
2) P.V./oils	+++		n					
3) Tenside ⁺ /product	++	+	n	++	++	++	n	n
4) Tenside ⁻ /detergent	+++	++	n	++		+	n	+
5) S.V./oils + fats	+++	+	+	++	n		n	++
6) Acidity/palm oil	++	+	n	+		+++	n	+
7) Nitrogen/milk	++	+	n	+	n		n	+++
8) Lead/PbS	+++	n	n	++		+	+	++
9) Total hardness	+++	++	++	+	n		n	n
10) Calcium hardness	+++	++	++	+	n		n	n
11) Chloride/cheese	+++	+	n	++		+	n	++
12) Chloride/aggregates	+++	+	n	+	n	+	n	+
13) Water/pet food	+++	+	n	+		++	n	++
14) Water/coffee	+++	++	n	+				n
15) Water/crude	+++	+	+	++				

properties (e.g. inhomogeneity, contamination, loss or instability) are considerably higher under reproducibility conditions than under repeatability conditions, methods with s_R close to $u_{c,min}$ (low value for $s_R/u_{c,min}$) are assumed to be influenced mainly by basic operations. Six methods revealed $s_R/u_{c,min}$ quotients below 1.5 (methods 1, 3, 7, 8, 13, and 14, see Table 4). Their normalized s_R fractions are equal or smaller than 0.23, except for method 14 (see Fig. 3). This means that all individual contributions to the minimum combined standard uncertainty, $u_{x,min}$, should be augmented by 23% of the deviation ($u_{x,max} - u_{x,min}$) to get combined standard uncertainties that are equal or higher than the corresponding s_R values. Although the reproducibility standard deviation s_R is a good first estimate for the combined standard uncertainty u_c , the latter is usually underestimated by s_R [4,5]. This might also be true in titrimetry although only basic operations were addressed, because participants of a collaborative study may tend toward the means of allowed ranges of experimental conditions. In order to allow for this underestimation we augmented the $u_{x,min}$ values by 30% instead of 23% and calculated the recommended individual contributions $u_{x,rec}$ according to the following equation:

$$u_{x,rec} = u_{x,min} + 0.3(u_{x,max} - u_{x,min}) \quad (8)$$

where $u_{x,rec}$ is the recommended value to quantify the influence quantity x , $u_{x,min}$ is the minimum standard uncertainty of the influence quantity x , $u_{x,max}$ is the maximum standard uncertainty of the influence quantity x .

Table 5 qualitatively depicts the results for all fifteen international standards. Repeatability is the most important influence quantity. As the calculations revealed, the repeatability of the reference determination cannot be neglected. Further important contributions are delivered by the titration (stirring, end point, temperature of organic solvents), volume measurements below 50 ml using a glass pipette (volume, temperature when organic solvents are used), and purity of reference materials. Mass measurements can be neglected in most cases. The contribution is only considerable if masses below 50 mg are measured with a usual micro balance (e.g. working on the electromagnetic force compensation principle) (method 15). However, international standards 5, 9 and 10 also show relevant contributions due to weighing operations although at least 200 mg is measured. The reason lies in the description how accurate the weight should be measured and how the weight should be introduced into the equation of measurand. According to the international standards 9 and 10, 0.2000 g of CaCO₃ reference standard should be weighed. Since

Table 6
Values for the quantification of influence quantities in titrimetry, revealed by the top-down approach.

Repeatability	Most important contribution; to be determined experimentally during validation. Note: reference or calibration measurements, respectively, should also be involved.
Mass:	Not relevant if adequate balances are used. Exception: important contribution by the linearity of the balance when masses below 50 mg are measured; amount of the contribution according to manufacturer's manual.
Volume/titration:	Water, without daily or hourly determination of the titer: important contribution, $u_{rel} = 0.4\%$ ($V = 10$ ml); $u_{rel} = 0.3\%$ (15 ml); $u_{rel} = 0.2\%$ (25–35 ml); $u_{rel} = 0.15\%$ (45 ml). Water, with daily or hourly determination of the titer of the standard solution: contribution in most cases significantly below the values quoted above. Organic solvent, without periodic volume calibration: important contribution, $u_{rel} = 0.5\%$ ($V = 10$ ml); $u_{rel} = 0.45\%$ (15 ml); $u_{rel} = 0.4\%$ (25–50 ml); organic solvent, with daily or hourly volume calibration: important contribution, $u_{rel} = 0.35\%$ (all volumes, due to temperature variation).
Volumetric flask:	Water: no relevant contribution if volume ≥ 100 ml; organic solvents: relevant contribution from all volumes, $u_{rel} = 0.35\%$ ($V \geq 100$ ml). Note: volumes <100 ml were not investigated.
Volumetric pipette:	Water: relevant contribution if volume ≤ 50 ml, $u_{rel} = 0.25\%$ ($V = 10$ –25 ml); $u_{rel} = 0.15\%$ (50 ml); organic solvents: relevant contribution from all volumes, $u_{rel} = 0.45\%$ ($V = 25$ ml); 0.35% (≥ 200 ml)
Molecular mass:	No relevant contribution
Reference material:	Contribution depends on the purity of the reference material (RM); values recommended: certified RM according to the certificate; RM without certificate (e.g. Titrisol, cationic reference solutions): $u_{rel} = 0.3\%$. Note: manufacturers often declare too small uncertainty limits for their uncertified products (e.g. 1000 ± 1 ppm for cationic standard solutions, corresponding to $u_{rel} = 0.06\%$ if rectangle distribution is assumed).
Recovery:	Most important contribution to the uncertainty; to be determined experimentally during validation;
Inhomogeneity:	Can be important depending on the individual sample; uncertainty to be estimated

this target weight is introduced into the equation of the measurand as part of a constant, it must be met exactly. The contribution of the weighing to the uncertainty is therefore not given by the balance but by the capability to achieve this target value. According to our experience, a substance can be dosed on a balance approximately to ± 3.5 mg, corresponding to a standard uncertainty of 1.5 mg (triangle distribution). As can be seen from Table 5, this uncertainty exhibits a relevant contribution to the combined standard uncertainty. International standard 5 explicitly allows a relative weight limit of $\pm 0.25\%$. The resulting relative standard uncertainty of 0.14% slightly contributes to the combined standard uncertainty.

4. Conclusions

The conclusions summarized in Table 6 were drawn on the basis of Table 5 and Eq. (8). Repeatability was found to contribute most importantly to the combined standard uncertainty of titrimetric results. Precision of reference measurement is not negligible; it should be included when repeatability is determined during validation of a method. The uncertainty of weight measurements can be neglected for masses above 50 mg if a suitable balance is used and if convection due to temperature gradients and electrostatic charging of the sample can be avoided. Weight measurements < 50 mg were found to cause relevant contributions unless highly precise balances (e.g. comparators) are used in air-conditioned rooms. Titration volumes have a relevant impact. For aqueous solutions, we recommend to quantify their relative uncertainties with values lying between 0.15 and 0.4%, depending on the measured volume. Alternatively, an absolute standard uncertainty of 0.05 ml for volumes up to 50 ml can be applied. However, the contribution can significantly be reduced by daily or even hourly determination of the titer. When dosing organic standard solutions, the relative standard uncertainty amounts to 0.35–0.5%. Contributions of volumetric flasks ≥ 100 ml and pipettes > 50 ml have found to be negligible. Contributions of volumetric pipettes ≤ 25 ml should be quantified by 0.25% for water and by 0.45% for organic solvents. Organic solvents still have an impact at high volumes because their volumetric expansion coefficients are considerably higher than that of water, thus causing a sensitive dependence on temperature change. Further relevant contributions can occur from purity of the reference material, from recovery value as well as from inhomogeneity of the sample. Recovery and inhomogeneity should be determined during validation, whereas the uncertainty due to the purity of reference material can be learnt from the certificate.

When no certificate is available, it is recommended to assume a relative standard uncertainty of at least 0.3%. This is also valid for non-certified reference solutions whose tolerance is declared to be unrealistically small (e.g. 0.1%).

Compared to the bottom-up approach according to the EURACHEM/CITAC guide [2], the present top-down approach revealed up to 4 times higher uncertainties for volumetric operations. Hence, it is to assume that uncertainty due to volumetric operations is often strongly underestimated. The recommendations listed in Table 6 apply when analytical results should be compared with those from other laboratories, i.e. when comparability is required. In case of production process control, for example, smaller uncertainty values might be justified on the condition that all relevant influence quantities are under an appropriate control.

Acknowledgements

The authors thank Jörg Frank and Dieter Strohm from Metrohm AG, Herisau, Switzerland, as well as Sergio Rezzonico for fruitful discussions about titration. K. Kehl is thanked for his measurements regarding uncertainty contributions due to stirring and due to the condition of electrodes. The work was co-financed by the Swiss Confederation's Innovation Promotion Agency (CTI).

References

- [1] ISO, Guide to the Expression of Uncertainty in Measurement, ISO, Geneva, 1993.
- [2] EURACHEM/CITAC, Quantifying Uncertainty in Analytical Measurement, LGC, Teddington, 2000.
- [3] ISO, ISO/TS 21748:2004 Guidance to the Use of Repeatability, Reproducibility and Trueness Estimates in Measurement Uncertainty Estimation, ISO, Geneva, 2004.
- [4] Analytical Methods Committee, Analyst 120 (1995) 2303.
- [5] S.L.R. Ellison, Accred. Qual. Assur. 3 (1998) 95.
- [6] V.J. Barwick, S.L.R. Ellison, Anal. Commun. 35 (1998) 377.
- [7] M. Thompson, S. Guffog, S. Stangroom, P. Osborne, P. Key, R. Wood, Analyst 127 (2002) 1669.
- [8] S. Populaire, E.C. Giménes, Accred. Qual. Assur. 10 (2006) 485.
- [9] R. Kadis, Talanta 64 (2004) 167.
- [10] H. Felber, S. Rezzonico, M. Märiässy, Metrologia 40 (2003) 249.
- [11] ISO, ISO 5725-6:1994 Accuracy (Trueness and Precision) of Measurement Results—Part 6: Use in Practice of Accuracy Values, ISO, Geneva, 1994.
- [12] B. Wampfler, M. Rösslein, H. Felber, J. Chem. Educ. 83 (2006) 1382.
- [13] B. Wampfler, Trac—Trends Anal. Chem. 25 (7) (2006), vii.
- [14] W.D. Beinert, M. Rösslein, S. Rezzonico, Nachrichten aus der Chemie 56 (2008) 356.
- [15] M.A. Herrador, A.G. González, Talanta 64 (2004) 415.
- [16] ISO, GUM-Supplement 1: Propagation of distribution using a Monte Carlo method, under review.
- [17] R. Albert, W. Horwitz, Anal. Chem. 69 (1997) 789.



Sensitivity enhancement of SPR biosensor with silver mirror reaction on the Ag/Au film

Liyang Wang, Ying Sun, Jian Wang, Xiaonan Zhu, Fei Jia, Yanbo Cao, Xinghua Wang, Hanqi Zhang, Daqian Song*

College of Chemistry, Jilin University, Changchun 130012, PR China

ARTICLE INFO

Article history:

Received 23 July 2008

Received in revised form 8 November 2008

Accepted 10 November 2008

Available online 25 November 2008

Keywords:

Wavelength modulation

Surface plasmon resonance

Silver mirror reaction

Ag/Au film

ABSTRACT

Based on well-known silver mirror reaction the Ag film was formed on Au film modified by self-assembled monolayer (SAM) of 1,6-hexanedithiol (HDT). The sensitivity of the biosensor based on this Ag/Au film is enhanced compared to that based on Au film. When the surface plasmon resonance (SPR) biosensor based on this Ag/Au film was used to determine human IgG, the range of concentrations of human IgG that could be determined is 0.30–40.00 $\mu\text{g mL}^{-1}$. The lowest concentration (0.30 $\mu\text{g mL}^{-1}$) that could be detected was about 8 times lower than that obtained by the biosensor without modification by Ag film (2.50 $\mu\text{g mL}^{-1}$), which demonstrated that the biosensor based on Ag/Au film could make the resonant wavelength move to longer wavelength following with the sensitivity enhancement of the SPR biosensor.

© 2008 Elsevier B.V. All rights reserved.

1. Introduction

In recent years, sensors based on surface plasmon resonance (SPR) have become more and more important in studying molecular interactions [1]. SPR uses light of defined wavelength [2], angle of incidence [3], and polarity [4] on an Au-coated sensor chip to measure changes in refractive index on the opposite side of the Au film. The most important characteristics of SPR sensor are its versatility and capability in real time monitoring the association or dissociation of biomolecules on the surface of the sensor without the need for fluorescence or labeling of the biomolecules [5]. These characteristics made the SPR technique an easy, convenient and reliable one for determining the concentration and molecular weight, monitoring change in structure, measuring kinetic constant and binding specificity of individual biomolecules. SPR sensors are especially suitable for the determination of interactions between biological molecules [6]. The sensor chip surface is usually coated with a thin hydrogel matrix or sulfhydryl compound bearing covalently immobilized receptor molecules such as antibody for specific analyte capture. Complex formation with ligands such as antigen leads to a change in the refractive index, which can be monitored in real time. Great progress has been made in the field of SPR for the determination of antibody, antigen [7–10], enzymes [11], receptors [12], growth factors [13], glycoproteins [14], nucleic acids [15,16] and drugs [17].

With the development of life science, there is a growing requirement for higher sensitive detection technologies in analysis and the detection of biological samples with low concentration and molecular weight has attached more and more importance. So the studies of sensitivity enhancement of SPR biosensor have also been developed and various measurement formats have been adopted for SPR biosensor [5]. Over the years, colloidal Au and sandwich assay are the techniques most commonly applied for enhancing the sensitivity of wavelength modulation SPR biosensor [18–20]. Other methods also have been used to the sensitivity enhancement of SPR biosensor, such as the use of dispersion from a dye [21], long range surface plasmon resonance (LRSPR) [22], inhibition assay [23], surface functionalization for self-referencing [24], and the use of thin films of titanium dioxide [25]. Based on the theoretical analysis, sensitivity of wavelength modulation SPR biosensor is enhanced with the shift of resonant wavelength towards longer wavelength [5]. In our previous work [26], the sensitivity enhancement of SPR biosensor was also performed by changing baseline solution. In addition, SPR sensor based on wavelength modulation may benefit from the use of Ag [5]. Ag film is ideal for surface plasmon generation, since the behavior of the dielectric constant near the Fröhlich frequency gives rise to an intense absorption in the visible region of the spectrum [28]. In the present paper, we focus on the development of approach to enhance the sensitivity of SPR biosensor by using silver mirror reaction method [27,28] to deposit the Ag film on Au film.

SPR refers to the optical excitation of surface plasmons or charge-density waves at the interface between a conductor and a dielectric. The conductor is a metal that has a high free-electron

* Corresponding author. Tel.: +86 431 85168399; fax: +86 431 85112355.
E-mail address: analchem@jlu.edu.cn (D. Song).

density to support the charge-density waves. Au and Ag are the ideal candidates as metal films in the visible light region. Ag film produces a sharper peak than Au and shows better sensitivity, which could be used to enhance the biosensor sensitivity [29]. The Au film was well stability, strong adhesion with the glass and no reaction with the inorganic ions in the reaction system. As a result, Au film can be used as the substrate due to its stability in the SPR biological systems. In the paper, silver mirror reaction was used to deposit the Ag film on Au substrate film. In order to avoid Ag film falling off from the Au substrate film as weak adhesion, 1,6-hexanedithiol (HDT) was used to modify the Au film, and then thin Ag film was formed on this film by silver mirror reaction. Subsequently, 3-mercaptopropionic acid (MPA) was used to connect Ag film with biological components. In this method, Ag film could be existed stably between HDT and MPA, and this could cause a large shift of the resonant wavelength. The sensitivity of SPR sensor could be enhanced with the shift of resonant wavelength towards longer wavelength. Meanwhile, Ag film gains a more distinct SPR spectrum than Au film and generates a high field enhancement.

2. Experimental

2.1. Reagents

Human IgG and rabbit anti-human IgG were purchased from Beijing Biosynthesis Biotechnology Company. 3-Mercaptopropionic acid was purchased from Sigma. 1,6-hexanedithiol was purchased from Jkchemical. 1-Ethyl-3-(3-dimethylaminopropyl)carbodiimide (EDC) and *N*-hydroxysuccinimide (NHS) were purchased from Pierce. Silver nitrate, glucose, ammonia water, sodium hydroxide and all other chemicals were of analytical reagent grade. All solutions were prepared with ultrapure water. Human IgG and rabbit anti-human IgG were stored at -20°C , and all other biological reagents were stored at 4°C . PBS buffer (0.01 mol L^{-1} , pH 7.4) was used as running buffer.

2.2. Equipment

In this paper, the wavelength modulation SPR biosensor installed in our laboratory was used. It is working with Kretschmann configuration to achieve the resonant condition by attenuated total reflection (ATR) in a prism. A K9 glass slide was used whose diameter and thickness were 12 and 0.7 mm, respectively. A 2 nm adhesive layer of Cr followed by a 50 nm layer of Au was deposited on the glass slide, then the glass slide with Au film was put on base of a prism (K9 glass) using a suitable index matching oil (cedar oil). A halogen tungsten lamp is used as the excitation light source in conjunction with a constant voltage transformer. The light from this source passes through a polarizer and two lenses and becomes TM-polarized parallel light. The parallel polychromatic light beam passes through the optical prism and excites surface plasmon at the interface between the Au film and the analyte. The output light is guided into the optical fiber and then enters the full wave spectrophotometer (Ocean Optics, Inc., USA). A 2048 element charge-coupled device (CCD) linear array detector was used as the detector. A $100\ \mu\text{L}$ volume flow cell was used. The interaction between the analyte in the solution and the biomolecular element immobilized on the SPR biosensor produces a change in refractive index (RI) profile that is observed as a shift in the SPR resonant wavelength. The surface plasmon resonance manifests itself on a characteristic dip in the wavelength dependence on the intensity of reflected light and the intensity of reflected light is minimum value at the resonant wavelength. A schematic diagram of a typical multilayer SPR device is shown in Fig. 1. Here, two kinds of sensing membranes were used. The sensing membrane based on Au film consists of Au film, MPA layer and antibody layer, and that based

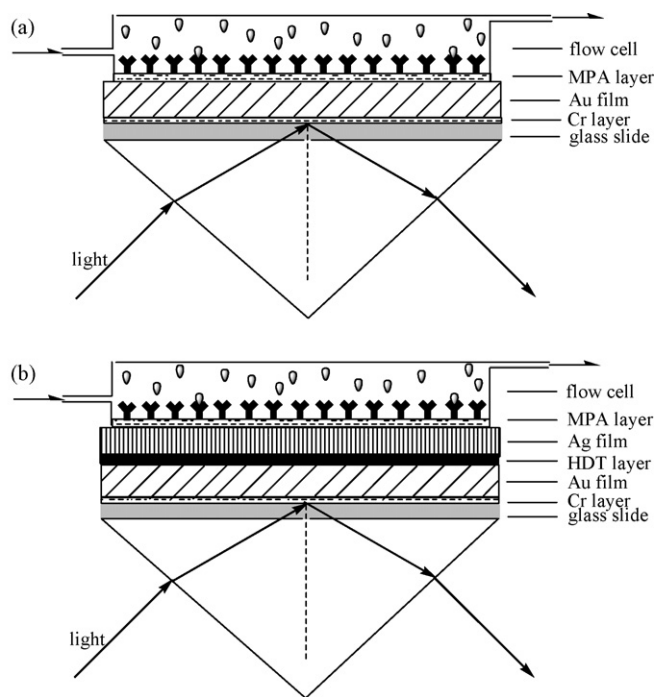


Fig. 1. Schematic diagram of the SPR sensor based on Au film (a) and Ag/Au film (b). (Y) Antibody, (O) antigen.

on Ag/Au film consists of Au film, HDT layer, Ag film, MPA layer and antibody layer.

2.3. Procedures

2.3.1. SPR biosensor based on Au film

The glass slide with Au film was first rinsed with ethanol and deionized water respectively. Then glass slide was fixed under the flow cell (Fig. 1a). Deionized water was injected into the flow cell. After the resonant wavelength kept constant, 10 mmol L^{-1} MPA was injected into the flow cell for 6 h. Then PBS was injected into the flow cell as the baseline solution. After $-\text{COOH}$ group was activated with NHS under the catalysis of EDC for 20 min, rabbit anti-human IgG ($50\ \mu\text{g mL}^{-1}$) was injected into the flow cell for 12 h to organize the processing antibody on the sensing membrane and thus the biosensor membrane was stable. Then, 1 mol L^{-1} ethanolamine hydrochloride (pH 8.5) was used to block the non-specific binding sites on the biosensor surface for 10 min. Finally, at room temperature, different concentrations of human IgG diluted with PBS buffer were separately injected into the flow cell over the immobilized antibody surface prepared and shifts of the resonant wavelength ($\Delta\lambda$) were measured as time prolonged. After 40 min, PBS buffer was injected over the surface to monitor the dissociation of antigen from antibody for 30 min. When the antigen was completely dissociated from the antibody surface, another sample containing human IgG at different concentration was injected into the flow cell.

2.3.2. SPR biosensor based on Ag/Au film

The glass slide with Au film was first cleaned with ethanol and deionized water respectively. Then, the glass slide was immersed into ethanol solution containing the HDT at the concentration of 12.5 mmol L^{-1} for 24 h. Au film was rinsed several times with ethanol and deionized water, and dried with gaseous nitrogen.

After the immobilization of HDT, a thin Ag film was formed on the modified Au film by means of the silver mirror reaction. The concentration of AgNO_3 is an important factor affecting

the thickness of Ag film. The different concentrations of AgNO_3 (0.2%; 0.4%; 0.6%; 0.8%; w/w) were used to prepare Ag film on Au film. 55 μL 5% NaOH solution was added into 3 mL AgNO_3 aqueous solution until a fine brown precipitate of Ag_2O was formed. Then 6% ammonia solution was added into this mixture drop by drop until the precipitate was completely dissolved to form $[\text{Ag}(\text{NH}_3)_2]^+$. Then 6% AgNO_3 solution was added until the solution became pale brown/yellow. After 1 drop of 6% ammonia water was added, the solution became transparent again. This $[\text{Ag}(\text{NH}_3)_2]^+$ solution was mixed with 1 mL 35% glucose solution and 0.5 mL methanol. Then the solution went black. The glass slide with the modified Au film was immersed in this solution and left for approximately 1 h under 35 °C. After that, the glass slide was ultrasonically cleaned with distilled water for 60 s and immersed in PBS buffer for 10 min, then ultrasonically cleaned again for 30 s. Finally, the glass slide was rinsed with distilled water and dried with gaseous nitrogen.

After the glass slide with modified Au film was fixed under the flow cell (Fig. 1b), deionized water was first injected into the flow cell. Then, 10 mmol L^{-1} MPA was injected into the flow cell for 6 h. The next procedures were the same as that mentioned above.

2.3.3. Regeneration

When the immunoassay was finished, the prism was taken away from the flow cell. The glass slide was ultrasonically cleaned with ethanol and distilled water respectively, then dried with gaseous nitrogen. The Au film could be used repeatedly. All measurements using this system were carried out at room temperature under atmospheric pressure.

3. Results and discussion

3.1. Preparation of Ag/Au film

Au and Ag are the most widely used metals for the SPR experiments [5]. At the wavelength of 632.8 nm, the dielectric constant ($\varepsilon = \varepsilon_r + \varepsilon_i$, where ε_r and ε_i are the real and the imaginary part of dielectric constant respectively) of Au is $-10.92 + 1.49i$ and Ag is $-18.22 + 0.48i$. The response curve of SPR is very sensitive to ε_r and ε_i , because they account for reflection and absorption of light in the metal, respectively [29]. The sharpest peak is produced by the metal whose dielectric constant has the highest $|\varepsilon_r/\varepsilon_i|$ ratio ($|\varepsilon_r/\varepsilon_i|$ for Ag is 38.0 and $|\varepsilon_r/\varepsilon_i|$ for Au is 7.33) [30–32]. Compared with Au, Ag has higher $|\varepsilon_r/\varepsilon_i|$ ratio and shows better sensitivity. Ag film could be used to enhance the sensitivity of the biosensor, while Au film can be used as the substrate due to its stability in the SPR biological systems.

The Ag film formed on Au substrate film without the modification by HDT is easy to be destroyed, so HDT layer was constructed on the Au film. The glass slide with Au film was immersed in HDT ethanol solution for 24 h and a monolayer of HDT was formed on the Au surface. As HDT is a disulfide compound, one of sulfhydryl groups is connected with Au and the other can be connected with Ag. After the immobilization of HDT on the Au film, the Ag film could be formed on the modified Au film by means of the silver mirror reaction. The thickness of Ag film produced by the silver mirror reaction is related to the concentration of AgNO_3 in solution. As the increase of concentration of AgNO_3 from 0.2% to 0.8%, the thickness of Ag films was changed from 10 to 15 nm, which were measured by Dektak 150 Surface Profiler. This indicates that the thickness of Ag/Au film is 60–65 nm. From a series of experiments, it was found that the thickness of Ag/Au film in 60–65 nm has the almost same effect on the sensitivity of SPR biosensor. In this paper, 0.4% AgNO_3 was chosen for preparing the Ag film by the silver mirror reaction.

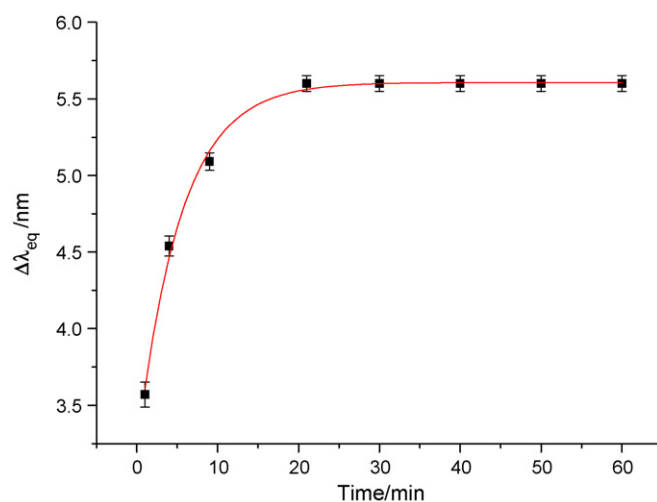


Fig. 2. Kinetic adsorption curve of MPA on the sensor surface based on Au film.

After the silver mirror reaction on the Au film, the glass slide with modified Au film was fixed under the flow cell. When the water was injected into the flow cell, a red-shift of the resonant wavelength for the sensor based on Ag/Au film could be seen. The shift of resonant wavelength was 21.89 nm compared to the sensor based on Au film. This is due to the change of the thickness of the SPR biosensor film and the interparticle interactions in the Ag/Au film. In wavelength modulation SPR biosensor, the shift of resonant wavelength towards long wavelength could increase the sensitivity of the sensor [5].

3.2. Preparation of the MPA self-assembled monolayer

The formation of monolayer is driven by a strong, specific interaction between the thiol and the metal surface. Due to the strong affinity, the traditional method of antibody immobilization was performed by sulfhydryl compounds [33]. In the biosensor based on Au film, the adsorption curve of MPA by self-assembly on the Au film is shown in Fig. 2. It can be seen clearly that the shift of the resonant wavelength reached about 80% of its total shift within 20 min and after 6 h the maximum shift of the resonant wavelength for the formation of this monolayer is 7.13 nm. These results indicate that the MPA monolayer was formed well.

For the biosensor based on Ag/Au film, HDT can effectively connect Au and Ag film and the stable molecular self-assembled layer can be formed. After the modified Au film was fixed under the cell flow, MPA was injected into the flow cell for 6 h. Then the biosensor surface was rinsed with water to remove unbound MPA. The adsorption curve of MPA at the Ag film is shown in Fig. 3. It can be seen clearly that the shift of the resonant wavelength reached about 75% of its total shift within 1 h. After 6 h, the maximum shift of resonant wavelength for the formation of this monolayer is 49.78 nm. This experimental result indicated that a good monolayer membrane of MPA was formed.

For the biosensor based on Ag/Au film, the immobilization of MPA on the Au film was fast while the shift of the resonant wavelength was not significant. Compared with Au film, the rate of immobilization of MPA on Ag film was slower and the shift of the resonant wavelength was more significant. These results are in agreement with the theory that the sensitivity of SPR biosensor based on Ag film is much higher than that based on Au film and the sensitivity of the sensor increases with the shift of resonant wavelength towards longer wavelength in wavelength modulation SPR biosensor [34].

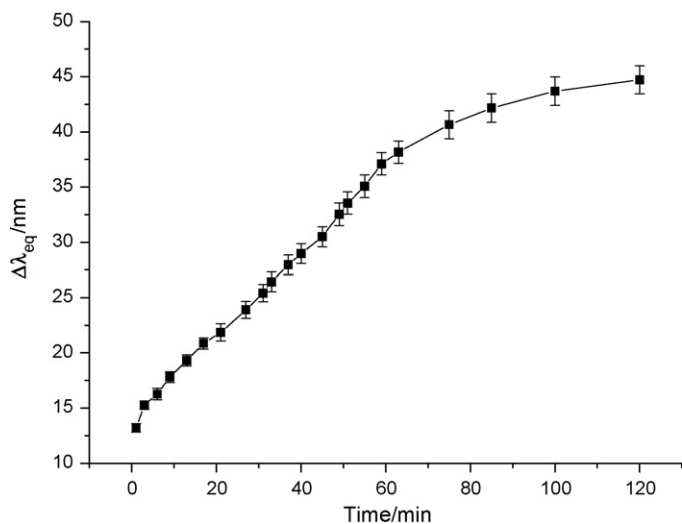


Fig. 3. Kinetic adsorption curve of MPA on the sensor surface based on Ag/Au film.

3.3. Immobilization of rabbit anti-human IgG

After $-\text{COOH}$ group reacted with NHS under the catalysis of EDC for 20 min, the rabbit anti-human IgG diluted with PBS buffer at the concentration of $50 \mu\text{g mL}^{-1}$ was injected into the flow cell to perform its binding on the activated surface. The assembling curve of antibody on surface of sensor based on Au film is shown in Fig. 4. It can be seen that rabbit anti-human IgG sensing membrane formed well within 1 h. The maximum resonant wavelength shift for the immobilization of rabbit anti-human IgG is 11.19 nm. The assembling curve of antibody on surface of sensor based on Ag/Au film is also shown in Fig. 4. It can be seen that the shift of the resonant wavelength is fast at first and then slow and the sensor response seems to increase steadily within 1 h. Rabbit anti-human IgG sensing membrane also formed well on the sensing film within 1 h and the maximum resonant wavelength shift for immobilization of rabbit anti-human IgG is 14.19 nm.

For the immobilization of antibody, the shifts of resonant wavelength are 12.21 and 20.27 nm for the sensor based on Au film and Ag/Au film after 12 h, respectively. When PBS buffer was injected into the flow cell, almost no change was observed. These results indicated that the surface prepared with MPA is a strong response to antibody and antibody was bound steadily on the biosensor sur-

Table 1

The shifts of resonant wavelength for constructing sensing membrane.

Sensing layer	Sensor based on Au film $\Delta\lambda_1$ (nm)	Sensor based on Ag/Au film $\Delta\lambda_2$ (nm)
Ag film	0	21.89 ± 1.02
MPA	7.13 ± 0.25	49.78 ± 1.28
Rabbit anti-human IgG	12.21 ± 0.51	20.27 ± 0.51

face. Then, 1 mol L^{-1} ethanolamine hydrochloride (pH 8.5) was used to block the non-specific binding sites on the biosensor surface. The shifts of resonant wavelength for constructing sensing membrane are shown in Table 1. It can be seen from Table 1 that compared with the sensor based on Au film, the total shift of the resonant wavelength based on Ag/Au film was 72.60 nm after rabbit anti-human IgG was bound on the biosensor surface.

3.4. Determination of human IgG

At room temperature, after the rabbit anti-human IgG was immobilized on the surface of the biosensor, human IgG at different concentrations was separately injected into the flow cell. The shifts of resonant wavelength due to antibody–antigen immunoreaction were measured. The monitoring of SPR response of the adsorption and the dissociation of human IgG can be carried out in real time. The SPR biosensor based on Au film shows a good response to human IgG in the concentration range $2.50\text{--}40.00 \mu\text{g mL}^{-1}$. The minimum shift of resonant wavelength is 0.51 nm at $2.50 \mu\text{g mL}^{-1}$ and the maximum shift of resonant wavelength is 3.80 nm at $40.00 \mu\text{g mL}^{-1}$. The SPR biosensor based on Ag/Au film shows a good response to human IgG in the concentration range $0.30\text{--}40.00 \mu\text{g mL}^{-1}$. The minimum shift of resonant wavelength is 0.51 nm at $0.30 \mu\text{g mL}^{-1}$ and the maximum shift of resonant wavelength is 6.09 nm at $40.00 \mu\text{g mL}^{-1}$. The lowest concentration determined by the sensor based on Ag/Au film is about 8-fold lower than that obtained by the sensor based on Au film. Fig. 5 shows the relationship between the shift in the resonant wavelength and the concentrations of human IgG. When the Ag/Au film was used, the thickness of the sensing membrane increased. This caused the resonant wavelength to move to longer wavelength, which enhances the sensitivity of the biosensor. On the other hand, when a thin film of Ag was deposited on Au substrate film, the Ag film can change the SPR features of the substrate and has its own localized surface plasmon due to the collective oscillations of its conduction electrons. So, the coupling of the localized surface plas-

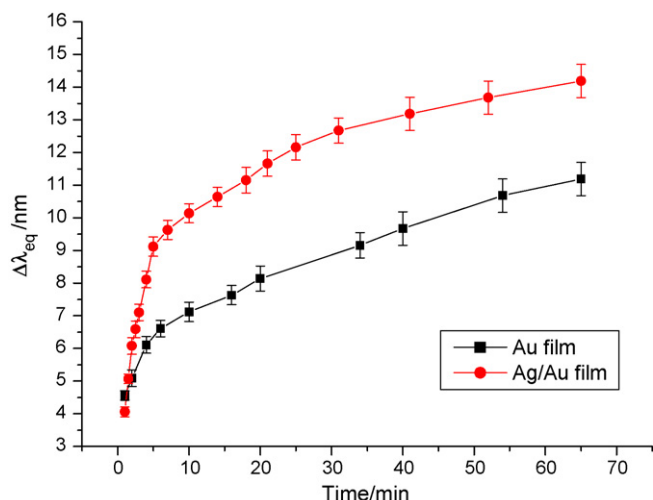


Fig. 4. Kinetic assembling curves of rabbit anti-human IgG on the MPA monolayer.

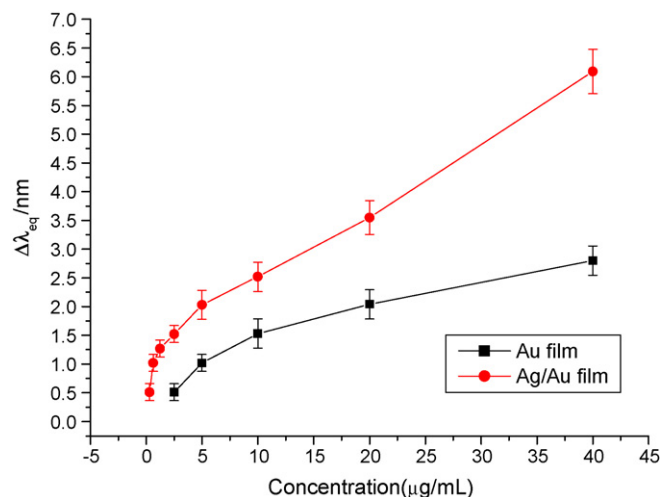


Fig. 5. The relationship between the concentration of human IgG and the shift in the resonant wavelength $\Delta\lambda_{\text{eq}}$.

mon of the Ag film with the propagating plasmon in the Au film could enhance the sensitivity of the SPR biosensor [35]. Due to the two factors, the limit of determination for human IgG obtained by the biosensor based on Ag/Au film was about eight times lower than that obtained by the biosensor based on Au film alone.

4. Conclusion

The sensitivity enhancement of SPR biosensor by Ag/Au film is presented. Self-assembled monolayer (SAM) of HDT was formed on the Au film and a well-known experiment as the silver mirror reaction was used to form thin Ag film. By using Ag/Au film, SPR biosensor gains a more distinct SPR spectrum than that obtained with bare Au film, which makes the resonant wavelength of the SPR spectrum move to the longer wavelength. The biosensor based on Ag/Au film, was therefore found to be more sensitive. The limit of determination with sensor based on Ag/Au film is about eight times lower than that obtained with the sensor based on Au film alone.

Acknowledgements

This work was supported by National Natural Science Foundation of China (No. 20727003) and Science and Technology Developing Foundation of Jilin Province (No. 20070551).

References

- [1] X. Liu, D.Q. Song, Q.L. Zhang, Y. Tian, L. Ding, H.Q. Zhang, Trends Anal. Chem. 24 (2005) 10.
- [2] B. Liedberg, I. Lundström, E. Stenberg, Sens. Actuators B 11 (1993) 63.
- [3] R.C. Jorgenson, S.S. Yee, Sens. Actuators B 12 (1993) 213.
- [4] A.A. Kruchinin, Y.G. Vlasov, Sens. Actuators B 30 (1996) 77.
- [5] J. Homola, S.S. Yee, G. Gauglitz, Sens. Actuators B 54 (1999) 3.
- [6] B. Liedberg, C. Nylander, I. Lundström, Biosens. Bioelectron. 10 (1995) 1.
- [7] W. Lee, B.K. Oh, W.H. Lee, J.W. Choi, Colloids Surf. B 40 (2005) 143.
- [8] X. Liu, Y. Sun, D.Q. Song, Q.L. Zhang, Y. Tian, H.Q. Zhang, Talanta 68 (2006) 1026.
- [9] S. Toyama, A. Shoji, Y. Yoshida, S. Yamauchi, Y. Ikariyama, Sens. Actuators B 52 (1998) 65.
- [10] X. Liu, D.Q. Song, Q.L. Zhang, Y. Tian, H.Q. Zhang, Talanta 62 (2004) 773.
- [11] E. Fujii, T. Koike, K. Nakamura, S. Sasaki, K. Kurihara, D. Citterio, Y. Iwasaki, O. Niwa, K. Suzuki, Anal. Chem. 74 (2002) 6106.
- [12] B. Hock, M. Seifert, K. Kramer, Biosens. Bioelectron. 17 (2002) 239.
- [13] M. Wong, C. Fong, M. Yang, Biochim. Biophys. Acta 1432 (1999) 293.
- [14] C. Bertucci, S. Cimitan, L. Menotti, J. Pharm. Biomed. Anal. 32 (2003) 697.
- [15] M. Minunni, S. Tombelli, M. Mascini, A. Bilia, Talanta 65 (2005) 578.
- [16] J.L. Wang, F. Wang, Z.A. Xu, Y.Z. Wang, S.J. Dong, Talanta 74 (2007) 104.
- [17] R.L. Rich, Y.S.N. Day, T.A. Morton, D.G. Myszka, Anal. Biochem. 296 (2001) 197.
- [18] X. Liu, Y. Sun, D.Q. Song, Q.L. Zhang, Y. Tian, S.Y. Bi, H.Q. Zhang, Anal. Biochem. 333 (2004) 99.
- [19] F. Wang, J.L. Wang, X.Q. Liu, S.J. Dong, Talanta 77 (2008) 628.
- [20] Y. Li, J. Ren, H. Nakajima, B.K. Kim, N. Soh, K. Nakano, T. Imato, Talanta 77 (2008) 473.
- [21] A. Hanning, J. Roeraade, J.J. Delrow, R.C. Jorgenson, Sens. Actuators B 54 (1999) 25.
- [22] G.G. Nenninger, P. Tobiška, J. Homola, S.S. Yee, Sens. Actuators B 74 (2001) 145.
- [23] K.V. Gobi, M. Sasaki, Y. Shoyama, N. Miura, Sens. Actuators B 89 (2003) 137.
- [24] M.G. Manera, G. Leo, M.L. Curri, P.D. Cozzoli, R. Rella, P. Siciliano, A. Agostiano, L. Vasanelli, Sens. Actuators B 100 (2004) 75.
- [25] C. Boozer, Q.M. Yu, S.F. Chen, C.Y. Lee, J. Homola, S.S. Yee, S.Y. Jiang, Sens. Actuators B 90 (2003) 22.
- [26] Y. Sun, X. Liu, D.Q. Song, Y. Tian, S.Y. Bi, H.Q. Zhang, Anal. Chim. Acta 569 (2006) 21.
- [27] Y. Saito, J.J. Wang, D.A. Smith, D.N. Batchelder, Langmuir 18 (2002) 2959.
- [28] Y. Saito, J.J. Wang, D.N. Batchelder, D.A. Smith, Langmuir 19 (2003) 6857.
- [29] M. Mitsushio, K. Miyashita, M. Higo, Sens. Actuators A 125 (2006) 296.
- [30] W.H. Weber, S.L. McCarthy, Phys. Rev. B 12 (1975) 5643.
- [31] R.D. Olney, R.J. Romagnoli, Appl. Opt. 26 (1987) 2279.
- [32] J.W. Sadowski, J. Lekkala, I. Vikholm, Biosens. Bioelectron. 6 (1991) 439.
- [33] T.Y.B. Leung, M.C. Gerstenberg, D.J. Lavrich, G. Scoles, F. Schreiber, G.E. Poirier, Langmuir 16 (2000) 549.
- [34] J. Homola, Sens. Actuators B 41 (1997) 207.
- [35] L.A. Lyon, M.D. Musick, M.J. Natan, Anal. Chem. 70 (1998) 5177.



Wall-jet conductivity detector for microchip capillary electrophoresis

Joseph Wang^{a,*}, Gang Chen^{b,*}, Alexander Muck^{c,*}

^a Department of Nanoengineering, University California San Diego, La Jolla, CA 92093, USA

^b School of Pharmacy, Fudan University, Shanghai 200032, China

^c Mass Spectrometry Group, Max Planck Institute for Chemical Ecology, Hans-Knöll-Str. 8, 07745 Jena, Germany

ARTICLE INFO

Article history:

Received 27 August 2008

Received in revised form 24 October 2008

Accepted 31 October 2008

Available online 11 November 2008

Keywords:

Capillary electrophoresis
Conductivity detection
Hybrid detection electrodes
Microchip
Miniaturization
Wall-jet

ABSTRACT

A new end-column ‘hybrid’ contactless conductivity detector for microchip capillary electrophoresis (CE) was developed. It is based on a “hybrid” arrangement where the receiving electrode is insulated by a thin layer of insulator and placed in the bulk solution of the detection reservoir of the chip, whereas the emitting electrode is in contact with the solution eluted from the channel outlet in a wall-jet arrangement. The favorable features of the new detector including the high sensitivity and low noise, can be attributed to both the direct contact of the ‘emitting’ electrode with the analyte solution as well as to the insulation of the detection electrode from the high DC currents in the electrophoretic circuit. Such arrangement provides a 10-fold sensitivity enhancement compared to currently used on-column contactless conductivity CE microchip detector as well as low values of noise and easy operation. The new design of the wall-jet conductivity detector was tested for separation of explosive-related methylammonium, ammonium, and sodium cations. The new detector design reconsiders the wall-jet arrangement for microchip conductivity detection in scope of improved peak symmetry, simplified study of inter-electrode distance, isolation of the electrodes, position of the wall-jet electrode to the separation channel, baseline stability and low limits of detection.

© 2008 Elsevier B.V. All rights reserved.

1. Introduction

There has been a considerable advance in development of detection techniques for micro total analysis systems (μ -TAS) in the past few years [1]. Among techniques currently employed, laser-induced fluorescence detection (LIF) still dominates [2–4]. However, its sensitivity and selectivity often requires derivatization procedures, complicated focusing of optical microscope detection systems and expensive instrumentation. Accordingly, some advantageous features of these microanalytical systems are compromised. Therefore, there has been a considerable activity towards the development of alternative detection methods [5]. Considerable attention has been given to electrochemical detection modes such as conductivity or amperometry [6–8].

Conductivity detection is a universal detection technique based on measuring the conductivity between two electrodes through which a high frequency alternating current is passed. Conductiv-

ity detection has been widely used for capillary electrophoresis (CE) microchip systems [9,10] allowing the monitoring of ionic species down to the micromolar level. Such detectors in CE electrophoretic separation systems are commonly designed as “on-column” devices and less often in “end-column” modes [11–14]. Considering the connection of the sensing electrodes and the electrophoretic buffer, the “contact” mode, utilizing direct galvanic link to the solution, and capacitively coupled “contactless” mode have been used. In the latter, the electrodes are electrically isolated from solution. It can offer several advantages over the contact mode, including the absence of electrolytic reactions, effective isolation from high separation voltages or a simplified alignment of the detector. Most conventional CE systems are based on two or three electrode on-column contactless conductivity measurements with tubular or semitubular electrodes placed over the separation capillary [15–17]. Contact on-column arrangement was reported by Zare and coworkers [18] and the first contact end-column “wall-jet” setup was published by the same group later [19]. In their work, the platinum wire sensing electrode was mounted directly in the end of electrophoretic capillary. The conductivity was measured between the sensing and ground electrodes, which also acted to complete the electrophoretic circuit. Another example of an end-column conductivity detector employed a conductive epoxy sensing electrode placed by the side of the capillary end with a hydrophilic polymer strip connecting the capillary outlet with the solution in the

Abbreviations: C⁴D, combined contact/contactless conductivity detector; CCD, contactless conductivity detector; CD, contact conductivity detector; CE, capillary electrophoresis; PMMA, poly(methylmethacrylate).

* Corresponding author. Fax: +1 858 534 9553.

E-mail addresses: josephwang@ucsd.edu (J. Wang), gangchen@fudan.edu.cn (G. Chen), amuck@ice.mpg.de (A. Muck).

outlet vessel. Improved baseline and effective shielding from the high-voltage circuitry was reported, yielding submillimolar limits of detection [20].

All previous arrangements have been already employed for the capillary format. For microchip arrangement, only on-column contact (CD) [21–23] or contactless conductivity detection (CCD) [24–26] modes have been reported. While different on-column conductivity electrode geometries have been already compared for integrated planar CE systems [27], the potential of the end-column conductivity detectors has not been investigated.

This article reports for first time on an end-column ‘hybrid’ capacitively coupled C^4D for microchip CE demonstrating the detection of explosive-related ions, which earn a high priority in the view of the current danger of terrorist activities [28,29]. Our new detection system brings new insights into contact/contactless conductivity sensing in a wall-jet format, which has been preferred by many other electrochemical sensing schemes in CE microchip methods. The present design utilizes the inherent advantages of both the contactless conductivity detection, such as low noise and isolation from the high-voltage electrophoretic circuit, with the higher sensitivity and simplified geometry of the contact mode measurements in an alternative system where the receiving electrode is isolated by a thin layer of insulator and placed in the bulk solution of the detection reservoir of the chip while the emitting electrode is in contact with the solution in a wall-jet orientation to the separation channel outlet. Such arrangement assures high signal to noise ratios and an easy operation.

The attractive performance characteristics of the hybrid wall-jet capacitively coupled microchip conductivity detector are reported in the following sections. To the best of our knowledge, no such detector arrangement has been reported for conductivity detection in both capillary and microchip systems.

2. Experimental

2.1. Apparatus

A top view of the CE microchip with the wall-jet CCD is given in Fig. 1. The (70 mm × 24 mm) PMMA microchip (manufactured at the Institut für Mikrotechnik Mainz (IMM, Mainz, Germany)) had a 50 mm long separation channel (between the injection cross and the channel outlet reservoir) and an 18 mm long injection channel (between the sample and unused reservoirs); the channels crossed each other halfway between the sample and the unused reservoirs 9 mm from the run buffer reservoir, and had a 50 μm × 50 μm square cross section [30]. The end of the chip was cut off as shown in Fig. 1. The PMMA chip was fixed in a laboratory-built plexiglas holder with silicone grease providing proper sealing [31]. Short pipet tips were inserted into the fluidic ports of the chip to connect to the injection (Fig. 1B), running buffer (Fig. 1C) and unused (Fig. 1D) reservoirs on the holder to establish solution contact between the channel on the chip and corresponding reservoirs on the chip holder. The homemade high-voltage power supply had an adjustable voltage range between 0 and +4000 V; platinum wires were used to connect the high-voltage electrodes in the solution reservoirs (Fig. 1G) and the electronic circuitry of the conductivity detector (placed on the top of the chip using a laboratory stand).

2.2. Electrode fabrication

The wall-jet ‘emitting’ electrode (Fig. 1E) consisted of a platinum wire (300 μm diameter) inserted axially in the plastic screw of the system using an epoxy resin. The disc end of the electrode was polished with 0.05 μm alumina slurry. The position of the ‘wall-jet’

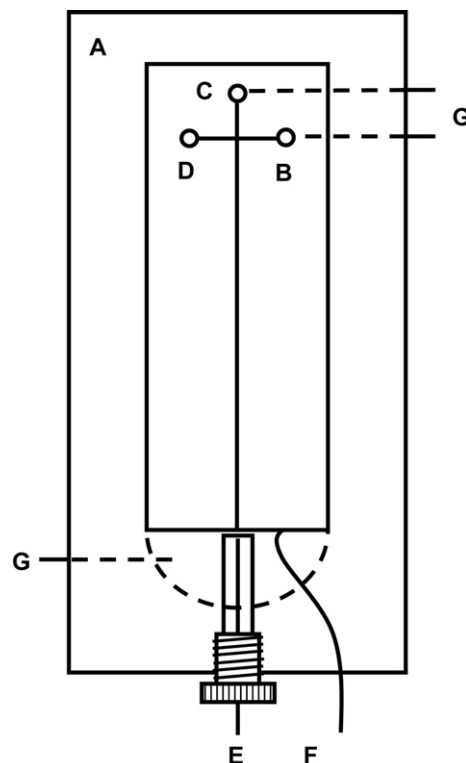


Fig. 1. Schematic diagram of the CE microchip coupled with wall-jet CCD detection. Acrylic holder with PMMA microchip (A), sample reservoir (B), run-buffer (C) and unused (D) reservoirs, plastic screw with the wall-jet emitting electrode (E) in the detection reservoir, receiving electrode (F), and platinum electrodes (G) for the high-voltage circuit.

electrode could be changed by turning the plastic screw by a desired angle. A 9° turn resulted in 30 μm shift between the channel outlet and the electrode along the separation channel. A thin insulated copper wire (0.3 mm × 50 mm) served as the ‘receiving’ electrode (Fig. 1F). To provide proper isolation of the end of the electrode from the DC currents in the detection reservoir, the PVC insulation was pulled over the cut end of the wire and sealed by pressing the excess of plastic in heat. For the full contactless arrangement, the emitting electrode was insulated by casting 2 μL of 5% (w/v) polystyrene in toluene on the disc electrode and dried in air. The detection reservoir was equipped by a poly(vinylchloride) (PVC) L-shaped 125 μm thick rectangular spacer across the whole width of the detection reservoir, to hold the receiving electrode. The position of this electrode could be adjusted by placing its end into 1 mm holes arranged in the shorter arm of the spacer, with a 1.2 mm distance between them. Thus, the distance between the sensing electrodes could easily be controlled. The ‘emitting’ electrode wire was tin-soldered directly to the detector electronics; the wall-jet electrode was connected to the detector using a thin copper wire. The length of the wires was minimized to prevent induction of electric noise.

2.3. Electronic circuit

The electronic circuit of the contactless detector was designed according to a previously reported scheme [32]. The circuit was equipped with a passive RC filter (time constant, 0.01 s) followed by a voltage follower (LF 356) to the circuit output to minimize electrical noise and to allow for convenient data reading. A HP 8116A function generator (Hewlett-Packard, Palo Alto, CA, USA) was used for generating the sinusoidal signal (usually with a frequency of 200 kHz with peak-to-peak amplitude of 10 V). The

electronic circuit was placed in a shielding box to protect the electronics from external electric fields. One side of the box was open; this side was placed as close as possible to the detection reservoir, to act also as a shield for the sensing electrodes. For data collection, a PCI-6035E 200 kS/s, 16 bit A/D board with NI-DAQ driver software for WIN 2000/NT and a program written in LabView 6.0.2 Full Development Version software were used (all National Instruments, Austin, TX, USA). The electronic components were purchased from local suppliers.

2.4. Reagents

Histidine (His), 2-(*N*-morpholino)ethanesulfonic acid (MES), methyl ammonium, ammonium chloride, and sodium chloride were purchased from Sigma. The run buffer (20 mM, pH 6.1) was prepared by dissolving MES and His in deionized water. Stock solutions of the target cations (ammonium, methylammonium, and sodium at 100 mM concentrations) were prepared daily by dissolving the corresponding salts in the run buffer. All chemicals were used without any further purification.

2.5. Electrophoretic procedure

The channels of the plastic chip were treated before use by rinsing with deionized water for 10 min. Reservoirs (C) and (D) on the microchip holder (Fig. 1) were filled with the electrophoretic run buffer solution, while reservoir (B) was filled with the sample mixture (target ions dissolved in the run buffer). After an initial 20 s electrokinetic sample loading in the injection channel, the sample was injected by applying a potential of +1000 V for 1 s between the sample reservoir (B) and the grounded outlet reservoir. This drove the sample “plug” into the separation channel through the intersection. The analytical separation was preceded by switching the high-voltage contacts, the separation potential was subsequently applied to the run buffer reservoir (C) with the outlet reservoir grounded and all other reservoirs floating.

Safety considerations. The high-voltage power supply can cause electrical shock. It should be handled with extreme care. Methyl ammonium is a toxic substance and other used chemicals are irritants. Skin or eye contact and accidental inhalation or ingestion should be avoided.

3. Results and discussion

The new detection system brings new insights into contact/contactless conductivity sensing in a wall-jet format, which has been preferred by many other electrochemical sensing schemes in CE microchip methods. The performance of the new hybrid wall-jet CCD detector was evaluated for electrophoretic separation of ammonium, methylammonium, and sodium ions. Electropherograms obtained with the ‘hybrid’ detector design (Fig. 2C) (in which the emitting electrode was bare while the receiving electrode was insulated to sense only capacitive changes of the AC signal) have been compared to those obtained at the wall-jet ‘full’ contactless (Fig. 2B) and on-column contactless (Fig. 2A) conductivity detection schemes. In such arrangement, the new wall-jet configuration exhibits over 10-fold sensitivity enhancement compared to the wall-jet contact conductivity detector. The direct contact of the ‘emitting’ electrode with solution avoids the additional capacitive effects of the insulator and the double layer capacitance of the solution-capillary wall on the emitted signal, which is present in the on-column contactless arrangement. Such effects observed even at optimum frequencies for the ‘full’ contactless wall-jet arrangement (with the emitting electrode coated

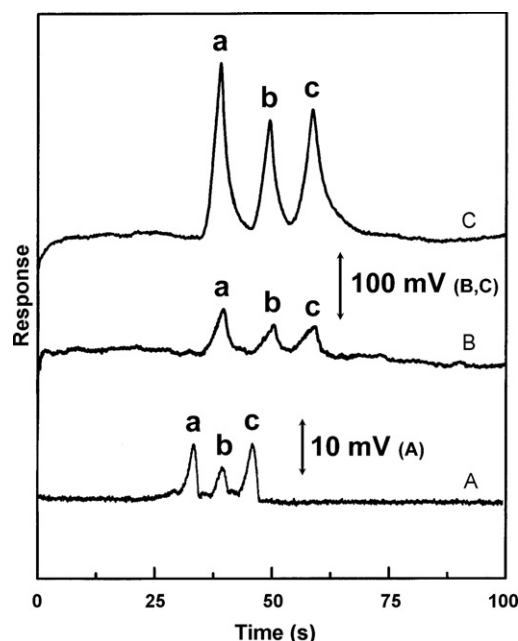


Fig. 2. electropherograms showing the separation of 1 mM ammonium (a), methyl ammonium (b), and sodium (c) using on-column contactless conductivity detector (A) and wall-jet disc electrodes with (B) and without (C) polystyrene membrane coated. Operation conditions: (A) separation voltage, +1000 V; injection voltage, +1000 V; injection time, 1 s; frequency, 200 kHz; peak-to-peak amplitude, 10 V; sinusoidal ac waveform; running buffer, MES/HIS (20 mM, pH 6.1); the distance between the emitting (wall-jet disc) and receiving electrodes, 3.6 mm; the distance between wall-jet disc electrode and the outlet of separation channel, 30 μ m.

with polystyrene membrane) which displays smaller signals and a higher noise (Fig. 2B). The exact reason for the increase sensitivity associated with the bare emitting electrode in the hybrid system is still not fully understood, however, we assume that placing the bare emitting electrode near the high-voltage ground electrode and the channel outlet also levels off potentials generated between the separation channel and the detector. This is expected to improve the detector performance [6]. Although the wall-jet configuration results in some degree of extracolumn band-broadening, such arrangement provided significant peak shape improvements and a baseline resolution compared to the on-column design. The migration times of the analytes in the on-column contactless arrangement are slightly shorter due to the shorter length of the separation channel (45 mm vs. 50 mm in the case of end-column arrangement, respectively).

The arrangement using the wall-jet electrode as the ‘emitting’ one was compared to a reversed scheme with the wall-jet electrode set as ‘receiving’ (Fig. 3). The system in which the bare emitting electrode is combined with an insulated receiving electrode (Fig. 3B) provides approximately 100 times higher signal-to-noise characteristics compared to an arrangement with an insulated emitting and bare wall-jet receiving electrodes (Fig. 3A). Such behavior is attributed to the fact that the high-voltages and DC currents at the channel outlet directly effect the input signal of the detection circuit, resulting in increased noise and inferior signal. The favorable features of the new detector, including the high sensitivity and low noise, can be attributed to both the direct contact of the ‘emitting’ electrode with the analyte solution as well as to the insulation of the detection circuitry by insulating the receiving electrode from the high DC currents in the electrophoretic circuit. Thus, no electrophoretic currents pass through the detector.

Several experimental parameters affecting the response were examined and optimized. The distance between the two sens-

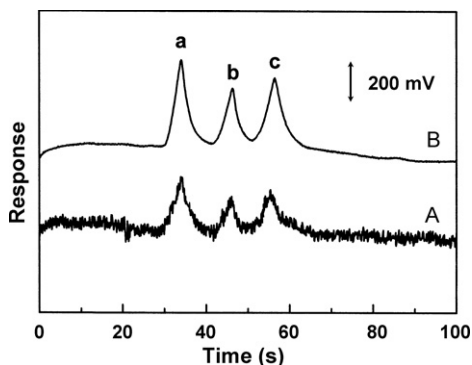


Fig. 3. Electrophoregrams showing the separation of 1 mM ammonium (a), methyl ammonium (b), and sodium (c) using bare wall-jet disc electrode as 'receiving' electrode (A) and 'emitting' electrode (B). Other conditions, as in Fig. 2.

ing electrodes was adjusted using a plastic spacer. The holder enabled to vary the distance of the 'receiving' electrode vs. the fixed-positioned 'emitting' electrode over the 1.2–6 mm range. The dependence of the signal on the electrode distance was found to increase slowly with maximum response obtained for 3.6 mm distance (Fig. 4A). Further increase in electrode distance led to increased electronic noise and more rapid decrease of the signal. The influence of the distance between the emitting electrode and the channel outlet on the peak height was studied over the 15–75 μm range (Fig. 4B). The response was nearly unaffected by changing the distance between 15 and 30 μm , decreased rapidly between 30–60 μm , and then more slowly. Most favorable S/N characteristics were obtained for 30 μm .

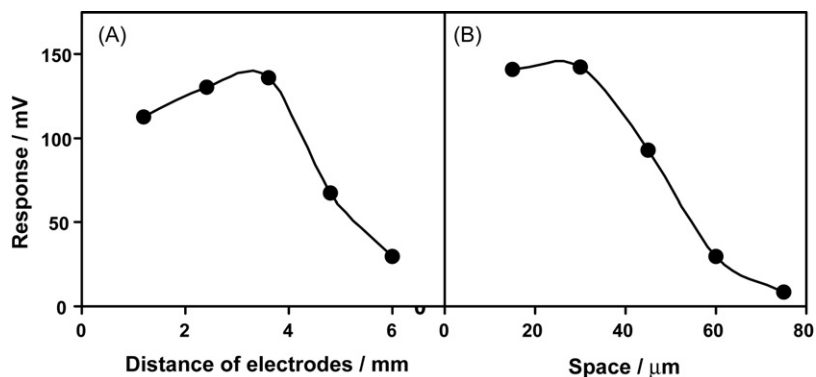


Fig. 4. Effect of (A) the distance between the 'emitting' and 'receiving' electrodes and (B) the space between wall-jet disc electrode and the channel outlet upon the response for 0.5 mM ammonium ion. Other conditions, as in Fig. 2.

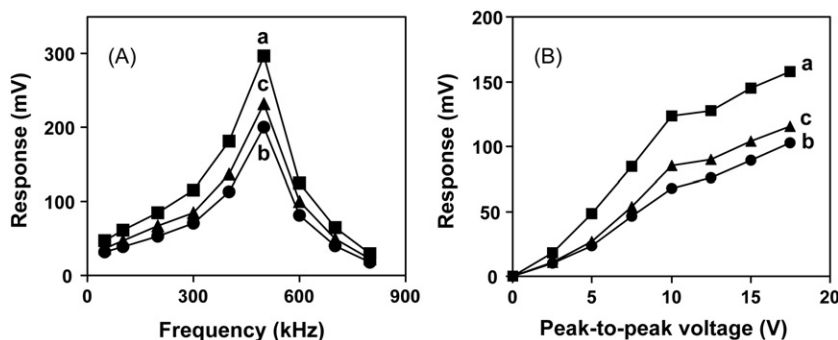


Fig. 5. Influence of (A) the applied ac voltage frequency and (B) the applied ac voltage upon the detector output. (A) Sample containing 1 mM ammonium (a), methyl ammonium (b), and sodium (c); peak-to-peak amplitude, 5 V. (B) Sample containing 0.5 mM ammonium (a), methyl ammonium (b), and sodium (c). Other conditions, as in Fig. 2.

As expected, the response of the wall-jet C⁴D is strongly influenced by the operation frequency and the amplitude of the applied voltage. The influence of the applied frequency is shown in Fig. 5A. For ammonium, methylammonium and sodium, the signal was initially increasing with increase of the frequency. The curves were recorded pointwise over the 50–800 kHz range. The response increases slowly in the region of 50–300 kHz, then more rapidly with a peak at 500 kHz and decreasing in the same manner to 800 kHz. However, unstable and distorted peaks were observed for operation frequencies higher than 300 kHz, probably due to the characteristics of the operational amplifier [13]. The response of all ions increased linearly with the peak-to-peak amplitude of the alternating voltage between 2.5 and 10 V, and then more slowly (Fig. 5B). Optimal response (S/N characteristics) was obtained for peak-to-peak voltage of 10 V. All subsequent work employed a frequency of 200 kHz and amplitude of 10 V_{pp}.

Fig. 6 shows the influence of the separation voltage upon the detector performance. As expected, increasing the separation voltage from +600 to +2500 V significantly decreases the migration times of the test ions from 56 to 26 s, from 80 to 30 s and from 97 to 35 s, for ammonium, methylammonium and sodium, respectively (A–E). The shorter migration times observed at higher electrical fields are coupled to substantially sharper peaks. However, separation voltages over +2000 V caused higher influence of the detection circuit and resulted in lower stability of the baseline. Over the studied voltage range, the separation voltage had a negligible influence on the baseline noise. Also, minimum peak broadening should be noted, which corresponds to other data reported on end-column conductivity detectors.

The end-column wall-jet conductivity microchip detector displays a well-defined concentration dependence. Fig. 7 displays

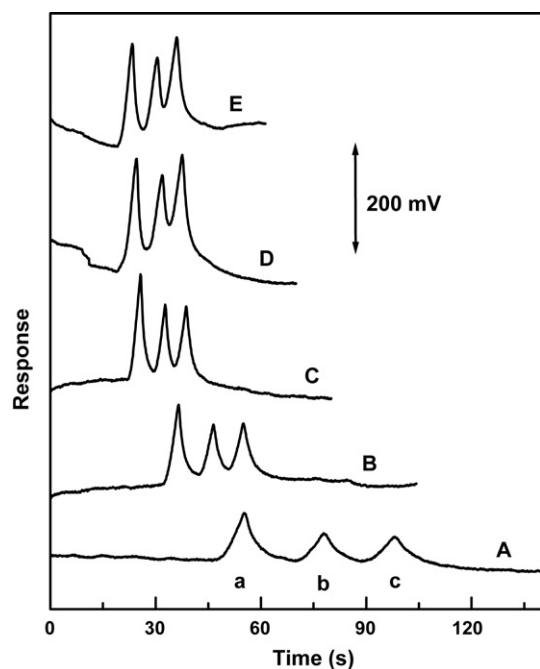


Fig. 6. Influence of the separation voltage upon the response for 0.5 mM ammonium (a), methyl ammonium (b), and sodium (c). Other conditions, as in Fig. 2.

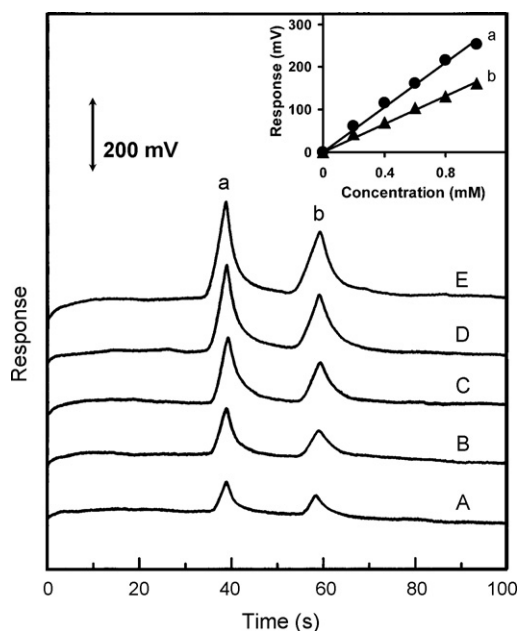


Fig. 7. Electropherograms for mixtures containing increasing levels of ammonium (a) and sodium (b) in increments of 0.2 mM (A–E). Also shown (as insets) are the resulting calibration plots. Other conditions, as in Fig. 2.

electropherograms for sample mixtures containing increasing levels of ammonium (a) and sodium (b) ions in 200 μM steps. A linear range of two orders of magnitude (correlation coefficients higher than 0.996) was obtained for ammonium and sodium. Detection limits of 5 μM ammonium and 3 μM sodium were estimated based on the response characteristics of a mixture containing 10 μM of these cations ($S/N=3$, not shown). The improved sensitivity was coupled to very good reproducibility and stability. No decrease in response sensitivity was observed for series of eight consecutive

measurements which provided relative standard deviation values as low as 4.1% for sodium, 4.7% for methylammonium and 5.2% for ammonium ions.

4. Conclusions

The analytical performance of the CE microchip with a new combined contact/contactless end-column conductivity detector clearly demonstrates the advantages of the new design. A great improvement in signal-to-noise ratio was achieved, with limits of detection as low as 3 and 5 μM (for ammonium and sodium, respectively). The new setup offers improved Gaussian peak shapes in comparison to the contactless modes. The simplified construction of the detector allows for convenient replacement, positioning and alignment of the sensing electrodes as well as spatial integration with amperometric detection in commercial applications. In comparison to previously reported end-column capillary systems, the baseline stability was dramatically improved due to effective isolation of the detector circuit from the high-voltage. Such conductivity CE microsystem can be used in a wide range of analytical applications, providing a versatile alternative to UV and other optical means of detection. Further improvements of the detector sensitivity are expected by application of high-voltage conductivity detection schemes and new detection geometries.

References

- [1] P.S. Dittrich, K. Tachikawa, A. Manz, *Anal. Chem.* 78 (2006) 3887–3907.
- [2] B. Kuswandi, N. Nuriman, J. Huskens, W. Verboom, *Anal. Chim. Acta* 601 (2007) 141–155.
- [3] C.L. Colyer, T. Tang, N. Chiem, D.J. Harrison, *Electrophoresis* 18 (1997) 1733–1741.
- [4] M.L. Chabiny, D.T. Chiu, J.C. McDonald, A.D. Stroock, J.F. Christian, A.M. Karger, G.M. Whitesides, *Anal. Chem.* 73 (2001) 4491–4498.
- [5] J. Tanyanyiwa, S. Leuthardt, P.C. Hauser, *Electrophoresis* 23 (2002) 3659–3666.
- [6] M. Pumera, *Talanta* 74 (2007) 358–364.
- [7] J.G. Alves Brito-Neto, J.A. Fracassi da Silva, L. Blanes, C.L. do Lago, *Electroanalysis* 17 (2005) 1198–1206.
- [8] J. Wang, *Anal. Chim. Acta* 507 (2004) 3–10.
- [9] F. Laugere, G.W. Lübking, A. Berthold, M.J. Bastemeijer, M.J. Vellekoop, *Sens. Actuators A* 92 (2001) 109–114.
- [10] J. Lichtenberg, N.F. de Rooij, E. Verpoorte, *Electrophoresis* 23 (2002) 3769–3780.
- [11] A.J. Zemmann, E. Schnell, D. Volger, G.K. Bonn, *Anal. Chem.* 70 (1998) 563–567.
- [12] F.J.A. da Silva, C.L. do Lago, *Anal. Chem.* 70 (1998) 563–567.
- [13] P. Tüma, F. Opekar, K. Štulík, *Electrophoresis* 23 (2002) 3718–3724.
- [14] S. Polesello Valsecchi, S. M. J. Chromatogr. A 834 (1999) 103–116.
- [15] E. Baltussen, R.M. Guijt, G. van der Steen, F. Laugere, S. Baltussen, G.W.K. van Dedem, *Electrophoresis* 23 (2002) 2888–2893.
- [16] K. Mayrhofer, A.J. Zemmann, E. Schnell, G.K. Bonn, *Anal. Chem.* 71 (1999) 3828–3833.
- [17] B. Gaš, J. Zuska, P. Coufal, T. van de Goor, *Electrophoresis* 23 (2002) 3520–3527.
- [18] X. Huang, T.K.J. Pang, M.J. Gordon, R.N. Zare, *Anal. Chem.* 59 (1987) 2747–2749.
- [19] X. Huang, R.N. Zare, *Anal. Chem.* 63 (1991) 2193–2196.
- [20] P. Tüma, F. Opekar, I. Jelínek, K. Štulík, *Electroanalysis* 11 (1999) 1022–1026.
- [21] J.E. Prest, S.J. Baldock, P.R. Fielden, B.J. Treves Brown, *Analyst* 126 (2001) 433–437.
- [22] M. Galloway, W. Strykowski, A. Henry, S.M. Ford, S. Lopis, R.L. McCarley, S.A. Soper, *Anal. Chem.* 74 (2002) 2407–2415.
- [23] M. Galloway, S.A. Soper, *Electrophoresis* 23 (2002) 3760–3768.
- [24] M. Pumera, J. Wang, F. Opekar, I. Jelínek, J. Feldman, H. Löwe, S. Hardt, *Anal. Chem.* 74 (2002) 1968–1971.
- [25] F. Laugere, R.M. Guijt, J. Bastemeijer, G. van der Steen, A. Berthold, E. Baltussen, P. Sarro, G.W.K. van Dedem, M. Vellekoop, A. Bossche, *Anal. Chem.* 75 (2003) 306–312.
- [26] C.L. do Lago, H.D.T. da Silva, C.A. Neves, J.G.A. Brito-Neto, J.A.F. da Silva, *Anal. Chem.* 75 (2003) 3853–3858.
- [27] B. Grass, D. Siepe, A. Neyer, R. Hergenröder, *Fres. J. Anal. Chem.* 371 (2001) 228–233.
- [28] M. Pumera, *Electrophoresis* 29 (2008) 269–279.
- [29] J. Wang, M. Pumera, G. Collins, F. Opekar, I. Jelínek, *Analyst* 127 (2002) 719–723.
- [30] J. Wang, M. Pumera, M.P. Chatrathi, A. Escarpa, R. Konrad, A. Griebel, W. Dörner, H. Löwe, *Electrophoresis* 23 (2002) 596–601.
- [31] J. Wang, B. Tian, E. Sahlin, *Anal. Chem.* 71 (1999) 5436–5440.
- [32] P. Tüma, F. Opekar, I. Jelínek, *Electroanalysis* 12 (2001) 989–992.



Imaging of nutrient elements in the leaves of *Elsholtzia splendens* by laser ablation inductively coupled plasma mass spectrometry (LA-ICP-MS)

Bei Wu^{a,b}, Miroslav Zoriy^b, Yingxu Chen^a, J. Sabine Becker^{b,*}

^a Department of Environmental Engineering, Zhejiang University, Hangzhou 310029, China

^b Central Division of Analytical Chemistry, Research Center Jülich, D-52425 Jülich, Germany

ARTICLE INFO

Article history:

Received 12 June 2008

Received in revised form 21 October 2008

Accepted 31 October 2008

Available online 13 November 2008

Keywords:

Imaging

Laser ablation ICP-MS

Elsholtzia splendens

Elemental distribution

Plant leaves

ABSTRACT

Laser ablation inductively coupled plasma mass spectrometry (LA-ICP-MS) was used for the quantitative imaging of nutrient elements (such as K, Mg, Mn, Cu, P, S and B) in the leaves of *Elsholtzia splendens*. The plant leaves were scanned directly with a focused Nd:YAG laser in the laser ablation chamber. The ablated material was transported with argon as carrier gas to a quadrupole-based ICP-MS (ICP-QMS), and the ion intensities of $^{39}\text{K}^+$, $^{24}\text{Mg}^+$, $^{55}\text{Mn}^+$, $^{63}\text{Cu}^+$, $^{31}\text{P}^+$, $^{34}\text{S}^+$ and $^{11}\text{B}^+$ were measured by ICP-QMS to study the distribution of the elements of interest. The imaging technique using LA-ICP-MS on plant leaves does not require any sample preparation. Carbon ($^{13}\text{C}^+$) was used as an internal standard element to compensate for the difference in the amount of material ablated. Additional experiments were performed in order to study the influence of the water content of the analyzed leaves on the intensity signal of the analyte. For quantification purposes, standard reference material (NIST SRM 1515 Apple Leaves) was selected and doped with standard solutions of the analytes within the concentration range of 0.1–2000 mg L⁻¹. The synthetic laboratory standards together with the samples were measured by LA-ICP-MS. The shape and structure of the leaves was clearly given by LA-ICP-MS imaging of all the elements measured. The elemental distribution varied according to the element, but with a high content in the veins for all the elements investigated. Specifically, Cu was located uniformly in the mesophyll with a slightly higher concentration in the main vein. High ion intensity was measured for S with a high amount of this element in the veins similar to the images of the metals, whereas most of the B was detected at the tip of the leaf. With synthetic laboratory standard calibration, the concentrations of elements in the leaves measured by LA-ICP-MS were between 20 μg g⁻¹ for Cu and 14,000 μg g⁻¹ for K.

© 2008 Elsevier B.V. All rights reserved.

1. Introduction

As a particular challenging task in the life sciences—the study of the elemental distribution, element species or biomolecules in biological tissue is attracting more and more attention in the emerging field of bioanalytics [1]. Up to now, many techniques have been applied to investigate the distribution and location of elements including both bulk nutrients and trace elements in biological samples. With respect to plants, scanning electron microscopy coupled with electron dispersive X-ray spectroscopy (SEM-EDXS) [2], proton induced X-ray analysis (PIXE) [3] and synchrotron radiation X-ray fluorescence (SRXRF) [4,5] have been used to investigate element locations at the tissue and/or subcellular level.

Mass spectrometric techniques provide multi-element and isotope analysis in the field of plant research. Secondary ion mass

spectrometry (SIMS), such as time-of-flight (TOF) SIMS, is well developed and has been used to image metals and metal-containing species in plant science for many years [6,7]. NanoSIMS has been performed on longitudinal sections of *Alyssum lesbiacum* leaves at the cellular level [8]. Elemental images measured by SIMS also revealed high concentrations of nickel in the peripheral regions of the large unicellular stellate leaf hairs (trichomes) and in the epidermal cell layer [8]. However, a major problem in SIMS analysis is the strong matrix dependence of the ion yields and, as a consequence, it is difficult to quantify the analytical data due to inherent matrix effects [9].

As one of the most important gentle ionization techniques for the imaging of large biomolecules, proteins, peptides and polymers, matrix-assisted laser desorption/ionization mass spectrometry (MALDI-MS) is able to analyze typically thin sections of tissue samples (5–20 μm thickness). Imaging MALDI-MS provides a new and powerful tool to analyze the distribution of metabolites within plant tissues. Ion images of longitudinal and cross sections of a wheat stem (*Triticum aestivum*) after postanthesis treatment were

* Corresponding author. Tel.: +49 2461 612698 fax: +49 2461 612560.
E-mail address: s.becker@fz-juelich.de (J.S. Becker).

obtained by means of MALDI-MS with a TOF analyzer by Robinson et al. [10]. Imaging MALDI-MS was also used to study the cellular distribution of metabolites in mycorrhizal orchid roots [11].

Laser ablation inductively coupled mass spectrometry (LA-ICP-MS) is becoming the method of choice for the trace and isotope analysis of solid samples and is already the most important laser-induced sampling technique in inorganic mass spectrometry due to the advantage of direct solid sampling by focused laser irradiation on the sample surface and its ability to provide direct information on elemental distribution [1]. Besides the analysis of geological, ceramic and metallurgical samples, LA-ICP-MS also can be applied to the imaging of soft tissues such as cryostat-cut slices of brain tissues and plant leaves with relatively high spatial resolution and good sensitivity [1,12–14]. Compared to the other two imaging mass spectrometric techniques, LA-ICP-MS offers in situ analysis of solid samples with respect to metals and non-metals at the trace concentration level mostly without sample preparation and without charging effects during the measurements. This results in a very low risk of foreign contamination and allows small- and large-scale samples to be analyzed. Furthermore, LA-ICP-MS allows easy quantification procedures using different analytical procedures developed at Research Center Jülich [1]. For example, if no suitable standards are available, matrix-matched laboratory standards can be prepared or solution-based calibration can be applied for quantification purposes [15].

An important research topic is studying the accumulation and distribution of metals and non-metals by metal-tolerant/hyperaccumulator plants. *Elsholtzia splendens* is a Cu-tolerant plant usually found in copper mining areas of southern China [16]. The Cu concentration in the leaves can reach 1000 mg kg^{-1} in solution cultivation [17]. The plant is considered to be an appropriate choice for phytoextracting the highly concentrated Cu in metal-contaminated soils. Corresponding research is being undertaken with respect to the mechanisms for Cu tolerance and accumulation. Cross-sections of the stems and leaves of *E. splendens* have been examined by SRXRF and revealed a significant correlation between Cu and Ca, Mn, Fe, Zn, P and S in distribution [5]. However, an element image of the whole tissue is still lacking and each element needs to be quantified. Normally, the leaf samples are cut into thin slices in a cryostat and then used to study the elemental distribution in the tissues. However, with this method it is difficult to present the whole shape and structure of the leaves. And possible contamination may be introduced during the sample preparation. Therefore direct element imaging in plant tissues is more attractive and reliable, because no sample preparation guarantees less foreign contamination during the experimental procedures. In the present study, the unsectioned leaves of *E. splendens* were used for an elemental distribution study by quantitative imaging of the nutrient elements (K, Mg, Mn, Cu, P, S and B) using laser ablation ICP-MS. Synthetic laboratory standards were used to quantify the analytical data.

2. Experimental

2.1. Instrument and LA-ICP-MS measurement procedure

A quadrupole-based ICP mass spectrometer (ICP-QMS, Agilent 7500) coupled to the laser ablation system (New Wave UP 266) was used for imaging essential elements in the grown leaves of *E. splendens*. Laser ablation of the leaves was performed using a Nd:YAG laser (wavelength: 266 nm, repetition frequency: 20 Hz, spot size: $160 \mu\text{m}$). The ablated material was transported into the inductively coupled plasma (ICP) using argon as the carrier gas. The experimental parameters of LA-ICP-MS were optimized with respect to

Table 1
Optimized experimental parameters of LA-ICP-MS.

ICP-MS	ICP-QMS, Agilent 7500ce
RF power (W)	1500
Carrier gas flow rate (L min^{-1})	1.2
Mass resolution $m/\Delta m$	300
Number of passes	1
Analysis time (h)	10
Laser ablation system	New Wave UP 266
Wavelength of Nd:YAG laser (nm)	266
Ablation mode	Scanning-line per line
Laser pulse duration (ns)	20
Repetition frequency (Hz)	20
Energy output	50%
Scan speed ($\mu\text{m s}^{-1}$)	40
Spot diameter (μm)	160
Distance between lines (μm)	300

the maximum ion intensity of $^{103}\text{Rh}^+$ using a Rh standard solution of $2 \mu\text{g L}^{-1}$. Maximum ion intensity was observed at an ICP RF power of 1500 W and a carrier gas flow rate of 1.2 L min^{-1} for the transport of ablated material to the ICP-MS. The plant leaves were investigated by LA-ICP-MS with respect to the nutrient element accumulation and distribution of K, Mg, Mn, Cu, P, S and B, under optimized experimental parameters as summarized in Table 1.

2.2. Standard preparation and quantification procedure

Standard reference material NIST SRM 1515 Apple Leaves was selected for the quantification of analytical data. Another standard reference material NIST SRM 1547 Peach Leaves was used to validate the analytical procedure. One gram of each leaf standard was weighed and pressed under 8 atm. The leaves of *E. splendens* were dried at 75°C until constant weight was reached, ground into fine powder, and then pressed under the same conditions with the standards. The pressed samples were fixed onto double-sided adhesive tape and measured for five lines by laser ablation ICP-MS. After measurement, the samples were used for further microwave digestion and element determination by quadrupole-based ICP-MS (Elan 6100). The digestion procedure has been described elsewhere [18].

Based on the above results, standard reference material NIST SRM 1515 Apple Leaves was applied for synthetic laboratory standard calibration. The standard preparation methods were developed in our lab at Research Centre Jülich. Six dilutions containing a mixture of elements of interest (K, Mg, Mn, Cu, P, S and B) with concentrations from 0.1 to 5 mg L^{-1} for Cu, from 1 to 20 mg L^{-1} for B, from 1 to 50 mg L^{-1} for Mn, from 10 to 500 mg L^{-1} for Mg, from 10 to 1000 mg L^{-1} for P and S, and from 100 to 2000 mg L^{-1} for K were prepared from a mixture of standard stock solution, and then added to the standard reference material. After absorption for 48 h, the materials were dried, ground into fine powder and pressed under 8 atm. These standards were scanned first with five lines each, and then the leaf of *E. splendens* was scanned line by line with a focused laser beam. To compensate for the possible inhomogeneity of the materials due to the preparation procedures, each measured value was corrected by the ion intensity of $^{13}\text{C}^+$.

2.3. Plant cultivation and sample preparation

Seeds of *E. splendens* were collected from copper mining areas in Zhejiang province, China. After soaked in distilled water overnight, the seeds were placed in sand at 25°C for germination. The seedlings were selected and carefully transferred to plastic containers filled with nutrient solution containing macronutrients in μM : $1000 \text{ Ca}(\text{NO}_3)_2$, 500 MgSO_4 , $500 \text{ K}_2\text{HPO}_4$, and micronutrients

Table 2

Validation of analytical procedure of LA-ICP-MS using standard reference material NIST SRM 1547 Peach Leaves.

	Certified concentration in Peach Leaves ($\mu\text{g g}^{-1}$)	Measured concentration in Peach Leaves by LA-ICP-MS using Ni as internal standard ($\mu\text{g g}^{-1}$)
B	29 ± 2	28 ± 3
Mg	4320 ± 80	4155 ± 256
P	1370 ± 70	1309 ± 102
S	2000	1775 ± 231
K	24300 ± 300	23536 ± 1267
Mn	98 ± 3	90 ± 10
Cu	3.7 ± 0.4	3.0 ± 0.4

in μM : 23 H_3BO_3 , 27 Fe(III)-EDTA , 4.5 MnSO_4 , 0.5 NaMoO_4 , 0.8 CuSO_4 , 0.5 ZnSO_4 . The pH of the nutrient solution was adjusted to 5.7. Ten seedlings were planted in one pot. The plants were grown in an environment-controlled room at a temperature of 25 °C, an illumination period of 12 h/day and a relative humidity of 21%. The nutrient solution was refreshed every three days. After 30 days of growth, the grown leaves (the fourth up from the root) were cut off from the stems, washed with Milli-Q water, and fixed to double-sided adhesive tape. The leaves were put into the laser ablation chamber and scanned together with the standards. To avoid individual differences in the elemental distribution in the leaves, at least ten pairs of distichous leaves were collected from ten plants grown in different pots. Three leaves were selected randomly and measured by LA-ICP-MS. For each element measured, the three leaves showed the similar images. The images shown were taken from the leaf which presented the best resolution.

3. Results and discussion

3.1. Quantification of analytical data

In solid-state mass spectrometry, semi-quantitative measurements are helpful for characterizing the material, especially if no suitable certified reference material is available for the quantification procedure [1]. In the present work, standard reference material NIST SRM 1515 Apple Leaves was used for this purpose. Another standard reference material NIST SRM 1547 Peach Leaves was used to validate the analytical procedure. Ni was chosen as the internal standard element. The concentrations of elements in Peach Leaves measured by LA-ICP-MS were in agreement with the certified values (Table 2). Applying relative sensitivity coefficients (RSCs) to the leaves of *E. splendens*, the concentrations measured by LA-ICP-MS were in agreement with those determined by ICP-MS after microwave digestion of the leaves (Table 3). The difference in element concentrations measured by LA-ICP-MS and ICP-MS can be explained by the possible inhomogeneity of the sample. There-

Table 3

Comparison of the nutrient element concentrations in the leaves of *Elsholtzia splendens* measured by LA-ICP-MS (using standard reference material NIST SRM 1515 Apple Leaves for calibration) and measured by ICP-MS after microwave digestion.

	Element concentration determined by ICP-MS after digestion ($\mu\text{g g}^{-1}$)	Measured concentration by LA-ICP-MS using Ni as internal standard ($\mu\text{g g}^{-1}$)
B	73 ± 1	75 ± 3
Mg	2234 ± 174	2303 ± 139
P	5138 ± 91	5328 ± 166
S	3285 ± 350	3313 ± 299
K	13290 ± 552	14078 ± 1170
Mn	155 ± 5	158 ± 3
Cu	6.11 ± 0.08	6.86 ± 0.12

Small differences can be explained by the possible inhomogeneity of the sample.

fore standard reference material NIST SRM 1515 Apple Leaves was suitable for quantifying the images of element in the leaves of *E. splendens* measured by LA-ICP-MS.

Synthetic laboratory standards are usually prepared for the quantification of analytical results in solid-state mass spectrometry when no suitable certified reference material is available [1]. The methods were developed and applied successfully to quantify the images of elements in soft tissues in our lab at Research Centre Jülich [19]. In the present work, the standard reference material NIST SRM 1515 Apple Leaves spiked with a known concentration of the elements was used. To compensate for the possible inhomogeneity of the materials due to the preparation procedures and the water content in the samples, ^{13}C was used as an internal standard [19,20]. Fig. 1 shows the calibration curves representing the ratio of analyte ion intensity to that of $^{13}\text{C}^+$ plotted against the added concentration in the standards. High linear correlation coefficients of the calibration curves ($R^2 > 0.99$) were obtained from the prepared laboratory standards. Furthermore, the concentration values extrapolated by the calibration curves agreed with the certified values in the standard reference material Apple Leaves (Table 4). The distribution profiles of the elements of interest in the leaves of *E. splendens* were quantified using these calibration curves. The observed concentrations of analytes in the sample were in the range of $20 \mu\text{g g}^{-1}$ for Cu and $14,000 \mu\text{g g}^{-1}$ for K.

3.2. The effect of water content in the samples on ion intensities

Since the leaves of *E. splendens* used in the present work were freshly cut off from the plants without any other sample preparation, the water content in the samples should be considered as a factor to the ion intensities of analytes monitored by LA-ICP-MS. To illustrate the water content effect, nine fresh leaves of *E. splendens* were dried to reach different water content in the samples, and then scanned by the laser beam. As shown in Fig. 2, a linear correlation ($R^2 = 0.9874$) between the ion intensity of $^{13}\text{C}^+$ and amount of water in the leaves was observed. The higher water content in the samples, the lower ion intensities of analytes were found. During the long-time measurement, the argon gas flow led to a drying of the leaves, so that the water content of the leaves dropped from $77 \pm 5\%$ to $35 \pm 3\%$. However, similar reproducibilities of ^{13}C and other measured analytes were observed during the measurement. Therefore, the measured ion intensity of $^{13}\text{C}^+$ could be applied to correct the effect of water content on other elements.

3.3. Elemental distribution in the leaves of *E. splendens*

In order to obtain two-dimensional images of elemental distribution in the leaves of *E. splendens*, the leaves were collected without sample preparation and ablated line by line using a focused laser beam. The images of the nutrient elements K, Mg, Mn, Cu,

Table 4

Comparison of analyte concentration in NIST SRM 1515 Apple Leaves measured by LA-ICP-MS (via calibration curves) with certified values.

Analyte measured	Certified concentration in Apple Leaves ($\mu\text{g g}^{-1}$)	Estimated analyte concentration ($\mu\text{g g}^{-1}$)
^{11}B	27 ± 3	27 ± 2
^{24}Mg	2710 ± 80	2601 ± 135
^{31}P	1560 ± 110	1531 ± 90
^{34}S	1800	1960 ± 181
^{39}K	16100 ± 200	15180 ± 989
^{55}Mn	54 ± 3	56 ± 2
^{63}Cu	5.64 ± 0.24	6.23 ± 0.58

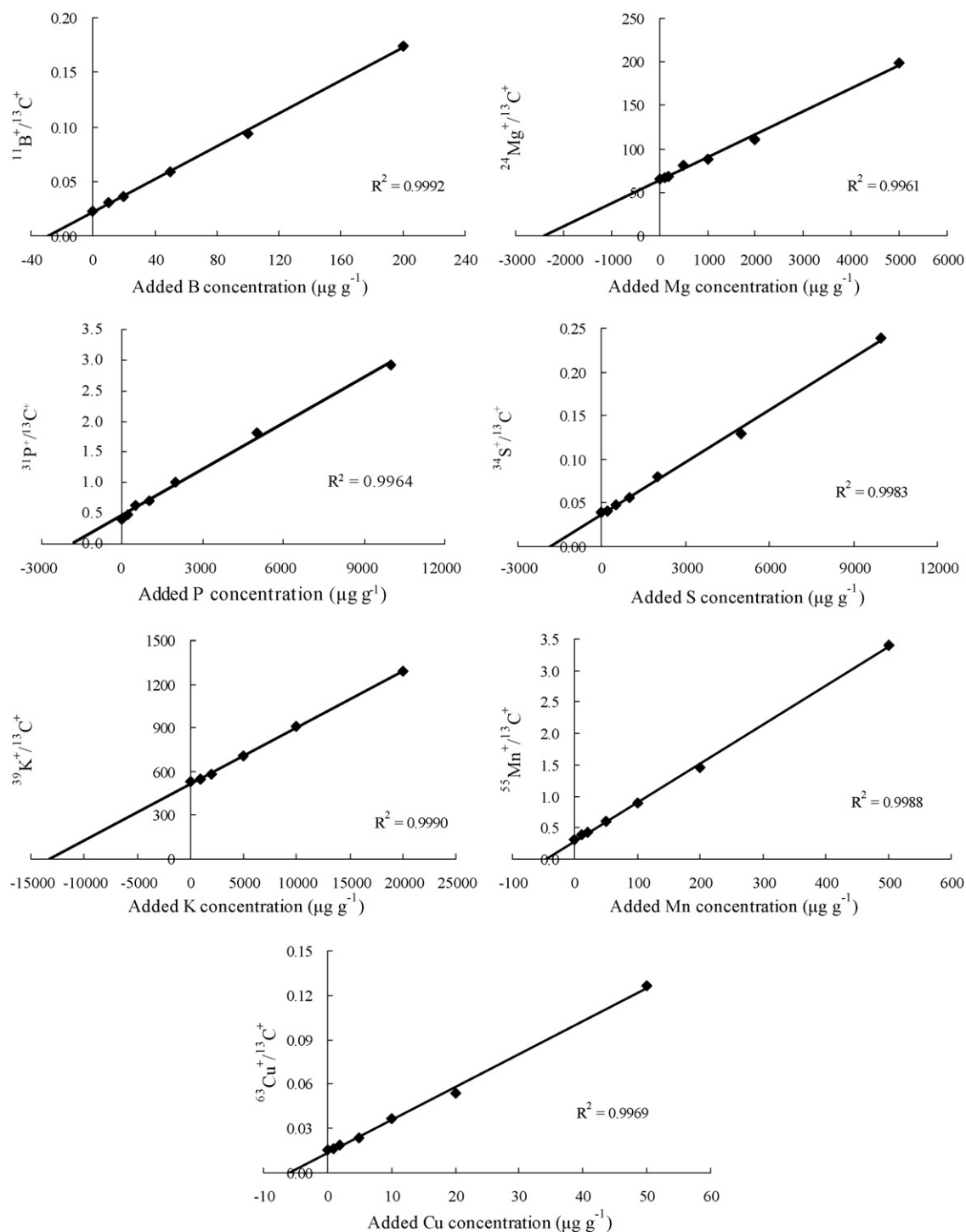


Fig. 1. Calibration curves measured by LA-ICP-MS using prepared laboratory standards NIST SRM 1515 Apple Leaves doped with standard solutions of the analytes of known concentration.

P, S and B measured by LA-ICP-MS in the leaves of *E. splendens* are shown in Fig. 3. All the elements measured could be clearly pictured by LA-ICP-MS. The images for macronutrients, such as K and Mg, were better than those for micronutrients like Cu.

^{13}C was also monitored as well as other analytes during the measurement. As given in Fig. 3, the image of $^{13}\text{C}^+$ showed that C displayed an evenly distributed pattern in the leaves except for the main veins since more material was ablated due to the differ-

ence in the thickness of the main vein and the mesophyll. Because the leaves were scanned line by line from the tip to the bottom of the leaves, an increased ion intensity of $^{13}\text{C}^+$ was observed due to drying of the samples in the course of the measurements. Nevertheless, using the ion intensity of $^{13}\text{C}^+$ for internal standardization to compensate for the different amounts of ablated material including the water content effect is possible.

In the leaves of *E. splendens*, all the measured nutrient elements were clearly observed in the veins of the leaf, indicating the

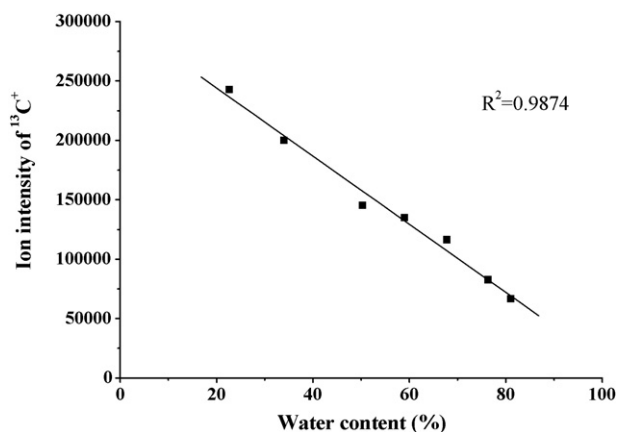


Fig. 2. Dependence of $^{13}\text{C}^+$ ion intensity on water content in the leaves of *E. splendens*.

importance of veins as a pathway for the transport of both macro- and micronutrient elements (Fig. 3). Similarly, in other species of plants, essential elements such as K, Fe, Zn and Ca were also found focused in the veins [4,21,22]. Nevertheless, the distribution differed depending on the element. The highest ion intensity for K of up to 6×10^7 cps was found in the main vein, whereas in the mesophyll the K content was lower. Becker et al. [18] observed that under certain experimental conditions there was no significant interference of $^{38}\text{Ar}^1\text{H}^+$ on $^{39}\text{K}^+$ at low hydrogen flow rates measured by quadrupole-based ICP-MS (ICP-QMS). In the present work, the interference of $^{38}\text{Ar}^1\text{H}^+$ on $^{39}\text{K}^+$ can be neglected due to the agreement of K concentration measured by LA-ICP-MS and the certified value in the standard reference material Peach Leaves. A similar distribution pattern was also found for Mn and P. As an important non-metal element, inhomogeneous distribution of P has been found in various materials such as brain tissues [23] and plant tissues [5]. Furthermore, it is interesting to notice that a co-association between metals and P was observed in the leaves. P serves as a constituent of proteins, nucleic acids, membrane, and adenosine triphosphate (ATP), participating in substance metabolism and energy exchange [24]. With respect to Mg, the mesophyll near the main vein was found to contain the highest amount as well as the main vein itself. In the present work, in order to investigate the interference of possibly formed $^{12}\text{C}^{12}\text{C}^+$ on $^{24}\text{Mg}^+$ when using ICP-

QMS to measure plant tissues, the concentration of Mg in standard reference materials NIST 1547 Peach Leaves measured by LA-ICP-MS was compared with the certified value (Table 2). Also the Mg concentrations in the leaves of *E. splendens* measured by LA-ICP-MS were in agreement with those measured by ICP-MS (Elan 6100) after digestion (Table 3). The results showed that the interference was not significant due to the agreement between the two values. Cu was located uniformly in the mesophyll with a slightly higher concentration in the main vein. Cu was deposited within the leaf tissues of *Sesbania drummondii* in the parenchyma as shown by SEM [25]. As a Cu-tolerant plant, *E. splendens* has the ability to accumulate a high content of Cu in its roots and leaves. The maximum Cu content in the main vein can reach $20 \mu\text{g g}^{-1}$ measured by LA-ICP-MS. In addition, high ion intensity was measured for S with a high amount of this element in the veins similar to the images of the metals. S is an important component of amino acids and proteins including metallothioneins (MTs) and phytochelatins (PCs), which are involved in the chelating and detoxification processes of heavy metals and could be responsible for the plant's metal tolerance [26,27]. Other studies have proved that there is a significant relationship between S distribution and metal location [5]. The present results suggested the possibility of studying sulfur-containing metal ligands together with the metals using LA-ICP-MS. In contrast to other elements, most of the B (up to $90 \mu\text{g g}^{-1}$) was detected at the tip of the leaf, even though a high concentration of B was also found in the veins and at the edge of the leaf (Fig. 3). With increasing interest in boron and boron-tolerant plants [28,29], LA-ICP-MS would provide a promising future method for the imaging of boron in plants.

4. Conclusions

In the present work, it was demonstrated that laser ablation ICP-MS is a powerful analytical technique for directly imaging both macro- and micronutrients in the plant leaves without sample preparation, and the resolution of this technique is sufficient for all the elements measured. The method was able to quantify the analytical data with synthetic laboratory standard calibration. The LA-ICP-MS method will provide an easy and effective tool in the field of the phytosphere with respect to distribution of elements, and will open up a new window onto in vivo ionic imaging of plant tissues.

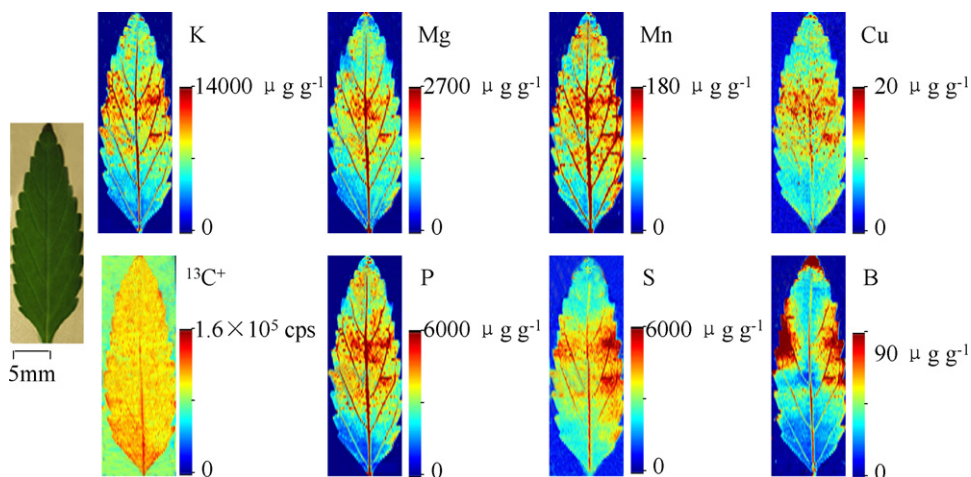


Fig. 3. Two-dimensional distribution of $^{13}\text{C}^+$ and quantitative images of nutrient elements K, Mg, Mn, Cu, P, S and B measured by LA-ICP-MS in the leaves of *E. splendens*.

Acknowledgements

The work was financially supported by the Key Project of the National Natural Science Foundation of China (40432004). The first author is grateful for support for this work by the China Scholarship Council and Helmholtz Association of German Research Centres. The authors would like to thank Dr. A.J. Kuhn (Institute of Chemistry and Dynamics of the Geosphere 3: Phytosphere, Research Centre Jülich) for kindly providing the greenhouse for plant cultivation.

References

- [1] J.S. Becker, *Inorganic Mass Spectrometry: Principles and Applications*, John Wiley and Sons, Chichester, UK, 2007.
- [2] M.P. Isaure, B. Fayard, G. Saffet, S. Pairis, J. Bourguignon, *Spectrochim. Acta Part B* 61 (2006) 1242.
- [3] F.J. Ager, M.D. Ynsa, J.R. Domínguez-Solís, C. Gotor, M.A. Respaldiza, L.C. Romero, *Nucl. Instrum. Methods Phys. Res. B* 189 (2002) 494.
- [4] M.P. Isaure, A. Fraysse, G. Deves, et al., *Biochimie* 88 (2006) 1583.
- [5] J.Y. Shi, Y.X. Chen, Y.Y. Huang, W. He, *Micron* 35 (2004) 557.
- [6] E.F. Verhaeghe, A. Fraysse, J.L. Guerquin-Kern, T.D. Wu, G. Devès, C. Mioskowski, C. Leblanc, R. Ortega, Y. Ambroise, P. Potin, *J. Biol. Inorg. Chem.* 13 (2) (2008) 257–269.
- [7] C. Dérue, D. Gibouin, M. Demarty, M.C. Verdus, F. Lefebvre, M. Thellier, C. Ripoll, *Microsc. Res. Technol.* 69 (2006) 53.
- [8] K.E. Smarta, M.R. Kilburna, C.J. Saltera, J.A.C. Smithb, C.R.M. Grovenor, *Int. J. Mass Spectrom.* 260 (2007) 107.
- [9] D. Touboul, F. Halgand, A. Brunelle, R. Kersting, E. Tallarek, B. Hagenhoff, O. Laprevote, *Anal. Chem.* 76 (2004) 1550.
- [10] S. Robinson, K. Warburton, M. Seymour, M. Clench, J. Thomas-Oates, *New Phytol.* 173 (2007) 438.
- [11] M. Burrell, L. Bendall, C. Earnshaw, M. Clench, D. Read, J. Leake, *Comp. Biochem. Phys. A* 146 (2007) 222.
- [12] J.S. Becker, R.C. Dietrich, A. Matusch, D. Pozebon, V.L. Dressler, *Spectrochim. Acta Part B* 63 (2008) 1248.
- [13] J. Dobrowolska, M. Dehnhardt, A. Matusch, M. Zoriy, N. Palomero-Gallagher, P. Koscielniak, K. Zilles, J.S. Becker, *Talanta* 74 (2008) 717.
- [14] J.S. Becker, M.V. Zoriy, C. Pickhardt, N. Palomero-Gallagher, K. Zilles, *Anal. Chem.* 77 (2005) 3208.
- [15] J.S. Becker, M. Zoriy, C. Pickhardt, J.Su. Becker, *Int. J. Mass Spectrom.* 242 (2005) 135.
- [16] J. Song, F.J. Zhao, Y.M. Luo, S.P. McGrath, H. Zhang, *Environ. Pollut.* 128 (2004) 307.
- [17] M.J. Yang, X.E. Yang, V. Romheld, *Plant Nutr.* 25 (2002) 1359.
- [18] J.S. Becker, K. Füllner, U.D. Seeling, G. Fornalczyk, A.J. Kuhn, *Anal. Bioanal. Chem.* 390 (2008) 571.
- [19] J.S. Becker, A. Matusch, C. Depboylu, J. Dobrowolska, M.V. Zoriy, *Anal. Chem.* 79 (2007) 6074.
- [20] A. Kindness, C.N. Sekaran, J. Feldmann, *Clin. Chem.* 49 (2003) 1916.
- [21] I. Orlic, R. Siegele, D.D. Menon, S.J. Markich, D.D. Cohen, R.A. Jeffree, D.C. McPhail, A. Sarbutt, E. Stelcer, *Nucl. Instrum. Methods B* 190 (2002) 439.
- [22] M.Y. Miah, M. Chino, *Bot. Bull. Acad. Sinica* 40 (1999) 135.
- [23] J.S. Becker, M.V. Zoriy, M. Dehnhardt, C. Pickhardt, K. Zilles, *J. Anal. Atom Spectrom.* 20 (2005) 912.
- [24] H. Marschner, *Mineral Nutrition of Higher Plants*, Academic Press ING (London) Ltd., London, UK, 1986.
- [25] S.V. Sahi, M. Israr, A.K. Srivastava, J.L. Gardea-Torresdey, J.G. Parsons, *Chemosphere* 67 (2007) 2257.
- [26] W.G. Keltjens, M.L. van Beusichem, *Plant Soil* 203 (1998) 119.
- [27] S. Clemens, *Planta* 212 (2001) 457.
- [28] K. Miwa, J. Takano, H. Omori, M. Seki, K. Shinozaki, T. Fujiwara, *Science* 318 (2007) 1417.
- [29] T. Sutton, U. Baumann, J. Hayes, N.C. Collins, B.J. Shi, T. Schnurbusch, A. Hay, G. Mayo, M. Pallotta, M. Tester, P. Langridge, *Science* 318 (2007) 1446.



A novel molecularly imprinted sensor for selectively probing imipramine created on ITO electrodes modified by Au nanoparticles

Xiaoli Xu^a, Guoliang Zhou^a, Huixiang Li^a, Qian Liu^b, Song Zhang^{a,*}, Jilie Kong^{a,*}

^a Department of Chemistry & Institutes of Biomedical Sciences, Fudan University, Shanghai 200433, PR China

^b Department of Surgery, Children's Hospital of Chongqing Medical University, Chongqing 400014, PR China

ARTICLE INFO

Article history:

Received 23 July 2008

Received in revised form 21 October 2008

Accepted 23 October 2008

Available online 5 November 2008

Keywords:

Molecularly imprinted polymers

Au nanoparticles

Imipramine

Electrochemistry

ABSTRACT

A sensitive molecularly imprinted electrochemical sensor was created for selective detection of a tricyclic antidepressant imipramine by combination of Au nanoparticles (Au-NPs) with a thin molecularly imprinted film. The sensor was fabricated onto the indium tin oxide (ITO) electrode via stepwise modification of Au-NPs by self-assembly and a thin film of molecularly imprinted polymers (MIPs) via sol-gel technology. It was observed that the molecularly imprinted film displayed excellent selectivity towards the target molecule imipramine. Meanwhile, the introduced Au-NPs exhibited noticeable catalytic activities towards imipramine oxidation, which remarkably enhanced the sensitivity of the imprinted film. Due to such combination, the as-prepared sensor responded quickly to imipramine, within only 1 min of incubation. The differential voltammetric anodic peak current was linear to the logarithm of imipramine concentration in the range from 5.0×10^{-6} to 1.0×10^{-3} mol L⁻¹, and the detection limits obtained was 1.0×10^{-9} mol L⁻¹. This method proposed was successfully applied to the determination of imipramine in drug tablets, and proven to be reliable compared with conventional UV method. These results reveal that such a sensor fulfills the selectivity, sensitivity, speed and simplicity requirements for imipramine detection, and provides possibilities of clinical application in physiological fluids.

© 2008 Elsevier B.V. All rights reserved.

1. Introduction

Molecularly imprinted polymers (MIPs) have been so far widely applied in the chemical sensing area for various intentions due to the tailor-made affinity and specificity for the model analyte [1–3]. Routine method of MIP preparation includes polymerization and condensation of organic or inorganic functional monomers. Marx and co-workers showed that the inorganic SiO₂-based MIP film offered some advantages over the organic acrylic polymeric film, including easier preparation, higher selectivity to the template, lower nonspecific binding and faster kinetics of adsorption [4,5]. However, as a sensing material, diffusion of the analytes across the inorganic MIP film needs to be accelerated in order to obtain a quick response. Furthermore, in order to effectively convert the binding signals from the molecular recognition to detectable electrical signals, the proper design of the signal transducer still remains challenging to enhance sensitivity of this sensing system [6]. Recently, the expanding availability of a variety of new materials with unique properties at the nanoscale dimension, e.g. Au-NPs, has attracted

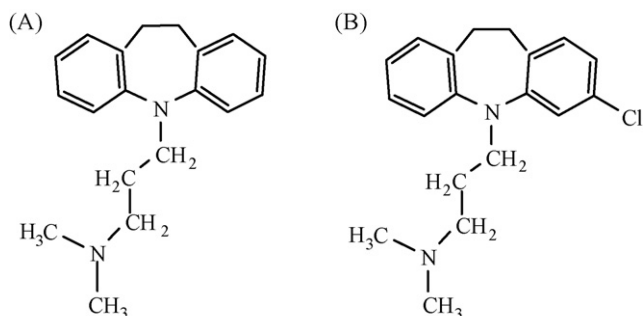
widespread attention in their utilization for the bioassay, especially for the electrochemical detection [7–9]. That urges us to develop a highly sensitive electrochemical sensor through combination of Au-NPs with inorganic MIP techniques to selectively detect trace amount of real samples.

There has appeared studies combining Au-NPs into the design of MIP sensors as sensing elements, due to the unique properties of Au-NPs, including stable physical and chemical character, small dimensional size, and excellent catalytic activities [10–12]. Matsui et al. reported a SPR sensor with Au-NPs embedded in the MIPs which effectively enhanced the signal intensity [13,14]. Compared with the expensive SPR, electrochemical method is more attractive for routine analysis because it combines sensitivity with convenience, speed, and low costs. However, only a few studies reported the combination of electrochemical method and molecular imprinting technology. Gao et al. developed a sensitive dopamine sensor on APTES functionalized ITO electrodes coated with thin silica MIP films [15]. Considering the potential catalytic activities of the Au-NPs and the advantages of electrochemical method, we chose to functionalize the ITO electrode with self-assembled Au-NPs in order to enhance electrochemical performance of MIP sensor in our study.

Imipramine (Scheme 1A), a tricyclic antidepressant, has been widely used for the treatment of many kinds of depression [16].

* Corresponding authors. Tel.: +86 21 6564 2405; fax: +86 21 6564 1740.

E-mail addresses: songzhang@fudan.edu.cn (S. Zhang), jlkong@fudan.edu.cn (J. Kong).



Scheme 1. Molecular structure of imipramine (A) and clomipramine (B).

For therapy, appropriate amount of the drug is required to obtain optimum therapeutic effects, and minimize severe side-effects and toxicity [17]. Therefore selective and sensitive detection of imipramine is preciously important for its clinical applications. Only a few reports are concerning the electrochemical measurements of imipramine, in which it was investigated by graphite polyurethane composite electrodes [16], highly boron-doped diamond electrodes [17], and functionalized carbon paste electrodes [18–20]. Due to the inherent specificity of MIPs, the novel Au-NP functionalized MIP electrodes were fabricated in order to detect imipramine with high sensitivity and selectivity. The function of Au-NPs and the selectivity of the MIP film towards imipramine were investigated by differential pulse voltammetry in detail.

2. Experimental

2.1. Chemicals

Chloroauric acid (HAuCl_4) and sodium borohydride (NaBH_4) were purchased from Shanghai Chemical Reagents Co. (Shanghai, China). 3-Mercaptopropyltrimethoxysilane (MPMSi) was purchased from Fluka Co. (Buchs, Switzerland). Tetraethoxysilane

(TEOS, 99%) and phenyl trimethoxysilane (PTMOS, 85%) were received from Acros Organics. Polyethylene glycol (PEG, MW400) was received from Shanghai Pudong Gaonan Chemical Plant (Shanghai, China). Imipramine hydrochloride ($\text{C}_{19}\text{H}_{23}\text{N}_2\cdot\text{HCl}$) and its drug tablets, and clomipramine hydrochloride ($\text{C}_{19}\text{H}_{23}\text{ClN}_2\cdot\text{HCl}$) were kindly supplied by Sine JiuFu Pharmaceutical Company (Shanghai, China). Prior to determination, the tablets were ground into powder, dissolved in water, filtered and diluted to certain volume. All the other chemicals were of analytical grade and used as received. All water used was demineralized.

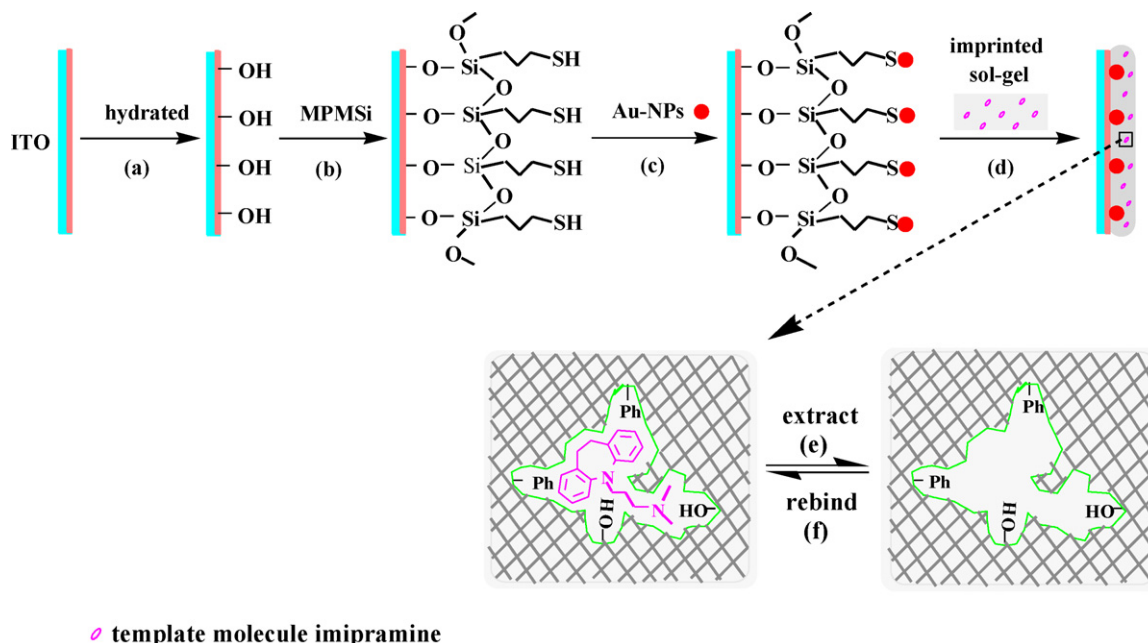
2.2. Apparatus

All electrochemical experiments were carried out on a CHI1030 multichannel voltammetric analyzer (CH Instruments, Cordova, TN, USA). The conventional three-electrode system was employed, i.e., a platinum wire and a saturated calomel reference (SCE) as the counter electrode and the reference electrode, respectively. The ITO glass (Laibao Electrical Co., Shenzhen, China), cut into $1.0\text{ cm} \times 2.0\text{ cm}$, was used as the working electrode (the effective electrode area, 1.0 cm^2).

UV-vis absorption spectra were obtained on a HP8453 ultraviolet-visible spectrophotometer (Agilent Company, USA). The size and morphology of Au-NPs were observed by transmission electron microscopy (TEM) using a JEOL model JEM-2010 (HR, Japan) at 200 kV. Scanning electron microscopy (SEM) was performed on a Philips XL30 Microscope (Japan). The surface morphology of the ITO electrode in each modification step was investigated by a Nanoscope Multimode IV atomic force microscope (AFM; Digital Instruments, Santa Barbara, CA) in the tapping mode.

2.3. Preparation of the Au-NPs

The Au-NPs were prepared according to the literature [21]. In the beginning, HAuCl_4 (0.5 mL, 0.01 M) and sodium citrate (0.5 mL, 0.01 M) were added to 18 mL of purified water and stirred vigorously at room temperature (RT). Then 0.5 mL of fresh ice-cold 0.1 M



Scheme 2. Schematic representation of the fabrication protocol of the MIP/Au-NP/ITO sensor. From left to right: (a) the hydrated process, (b) the mercapto-modifying process by a silanization reaction, (c) the self-assembly of Au-NPs, (d) the modification of the MIP film by a sol-gel technique. The insert diagrams are the interaction principle between the MIP film and imipramine during the extraction (e) and rebinding (f) process.

NaBH_4 was added, and the solution color changed from light yellow to wine red. After the stirring was stopped, the solution was stored at 4°C before use.

2.4. Fabrication of the MIP/Au-NP/ITO electrode

The fabrication protocol of such a sensor was shown in Scheme 2. Firstly, in order to enhance electron transfer on the electrode interface, a functional layer of Au-NPs was modified on the ITO electrode by self-assembly (Scheme 2a–c). In the beginning, the ITO electrodes were hydrated to introduce hydroxyl groups according to a previous report [22]. In Scheme 2b, mercapto groups were coupled onto the ITO plates by immersion in MPMSi (1 wt%, in ethanol) for 0.5 h at RT. After that, the plates were thoroughly washed with absolute ethanol to remove the physically adsorbed MPMSi molecules, and dried under a stream of nitrogen. The MPMSi/ITO electrodes were then prepared. Subsequently, the MPMSi/ITO electrodes were immersed in Au colloid solution for 2 h to introduce Au-NPs by self-assembly (Scheme 2c). After rinsed carefully with water, and dried with nitrogen, the Au-NP functionalized ITO electrodes (Au-NP/ITO) were obtained.

Secondly, a selective and sensitive MIP film towards the targeted antidepressant imipramine was modified on the Au-NP/ITO by sol–gel technology (Scheme 2d). The monomer mixture of the sol consisted of 3.0 mL (13.5 mmol) of TEOS, 0.27 mL (1.1 mmol) of PTMOS, 3.3 mL (9.45 mmol) of PEG, 3.0 mL of ethoxyethanol, 1.0 mL of H_2O , and 0.1 mL of concentrated HCl. The mixture was stirred at RT for some time. Then 1.0 mL of this sol was mixed with 0.1 mL of 0.1 M imipramine hydrochloride in ethanol, and was used for imprinted films. For contrast, the left original sol without imipramine was used for nonimprinted films [5,23]. Finally, the electrodes were immersed in the imprinted or nonimprinted sol for 1 min, then they were taken out, and left to dry overnight in a covered Petri dish at RT, the MIP/Au-NP/ITO and NMIP/Au-NP/ITO electrodes were thus obtained.

The interaction principle between the MIP film and imipramine during the extraction and rebinding process was showed in the insert diagrams (Scheme 2e and f). As noted, reversible interactions, including π – π interaction of phenyl groups, hydrogen bonds with nitrogen heteroatoms, and electrostatic interaction, between the template molecule imipramine and the insoluble polymer network were formed in the modified MIP film. The doped imipramine was extracted from the MIP/Au-NP/ITO electrode by repetitive immersion in absolute ethanol (Scheme 2e). Obviously the left rigid cavities where the template formerly resided contained rebinding groups, therefore imipramine could selectively interact with the MIP/Au-NP/ITO electrode (Scheme 2f). The incubation was carried out in 100 mM phosphate buffer solution (PBS, pH 6.8) containing proper amount of imipramine.

2.5. Electrochemical measurements

Electrochemical measurements were carried out on the three-electrode system which was immersed in a 10 mL cell containing 100 mM PBS (pH 2.3). Differential pulse voltammetry (DPV) were performed from 0.6 to 1.2 V, the pulse amplitude was 50 mV, the pulse width was 50 ms, the pulse period was 0.2 s and the potential increment was 4 mV. All the measurements were performed at RT.

3. Results and discussion

3.1. Characterization of the MIP/Au-NP/ITO electrode

The immobilization of Au-NPs on the ITO electrode was examined by UV–vis spectrometry and AFM images. The freshly prepared

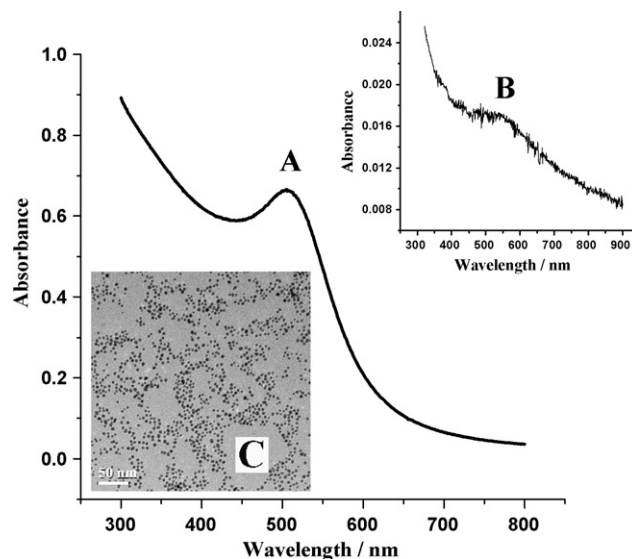


Fig. 1. UV–vis absorption spectra of the Au-NP solution (A) and the Au-NP/ITO (B). The insert (C) is the TEM image of the Au-NPs.

Au colloid exhibited a characteristic absorption at ca. 520 nm (Fig. 1A), as previously reported [24]. At the same wavelength the Au-NP/ITO still exhibited some absorption (Fig. 1B), but no absorption was found on the MPMSi/ITO (not shown). The TEM image (Fig. 1C) showed that the Au-NPs were precisely uniform with an average diameter of ca. 3.5 nm. All these results demonstrate that the Au-NPs were effectively coupled onto the electrode. In addition, AFM images provide the surface morphology information of the MPMSi/ITO (Fig. 2A) and the Au-NP/ITO (Fig. 2B). After the MPMSi/ITO was immersed in the Au-NP solution, the surface roughness increased from 31 Å (Fig. 2A) to 70 Å (Fig. 2B). The rougher surface of the Au-NP/ITO also suggests the successful self-assembly of the Au-NPs on the MPMSi/ITO. Here, the introduction of the Au-NP monolayer might enhance electron transfer on the electrode interface.

The surface morphology and the thickness of the MIP film on the Au-NP/ITO were also investigated by AFM and SEM. It was found that the surface roughness of the MIP/Au-NP/ITO increased from 28 Å (Fig. 2C) to 32 Å (Fig. 2D) when the template molecule imipramine was extracted from the MIP film. The morphology change might also imply the effective extraction of the template. In addition, the MIP film thickness was approximately 400 nm calculated by SEM (Fig. 2E).

3.2. Electrochemical responses of the MIP/Au-NP/ITO electrode

Typical DPV responses of the MIP/Au-NP/ITO are shown in Fig. 3A. Since the template molecule is electroactive, the electrode showed an apparent anodic peak at 0.884 V before extraction (Fig. 3A-a). In order to investigate the rebinding ability of the MIP film, the MIP/Au-NP/ITO was then eluted repeatedly with absolute ethanol until there was no current response observed in the DPV measurements (Fig. 3A-b), which also verifies the effective extraction of the template.

The rebinding ability of the MIP/Au-NP/ITO was tested by DPV experiments. After the incubation in 1.0 mM imipramine for 10 min, the MIP/Au-NP/ITO (Fig. 3B-a) exhibited a much higher current response compared with the ITO electrode just modified with the MIP film (the MIP/ITO, Fig. 3B-b) or the nonimprinted film (the NMIP/ITO, Fig. 3B-c). The excellent sensitivity and selectiv-

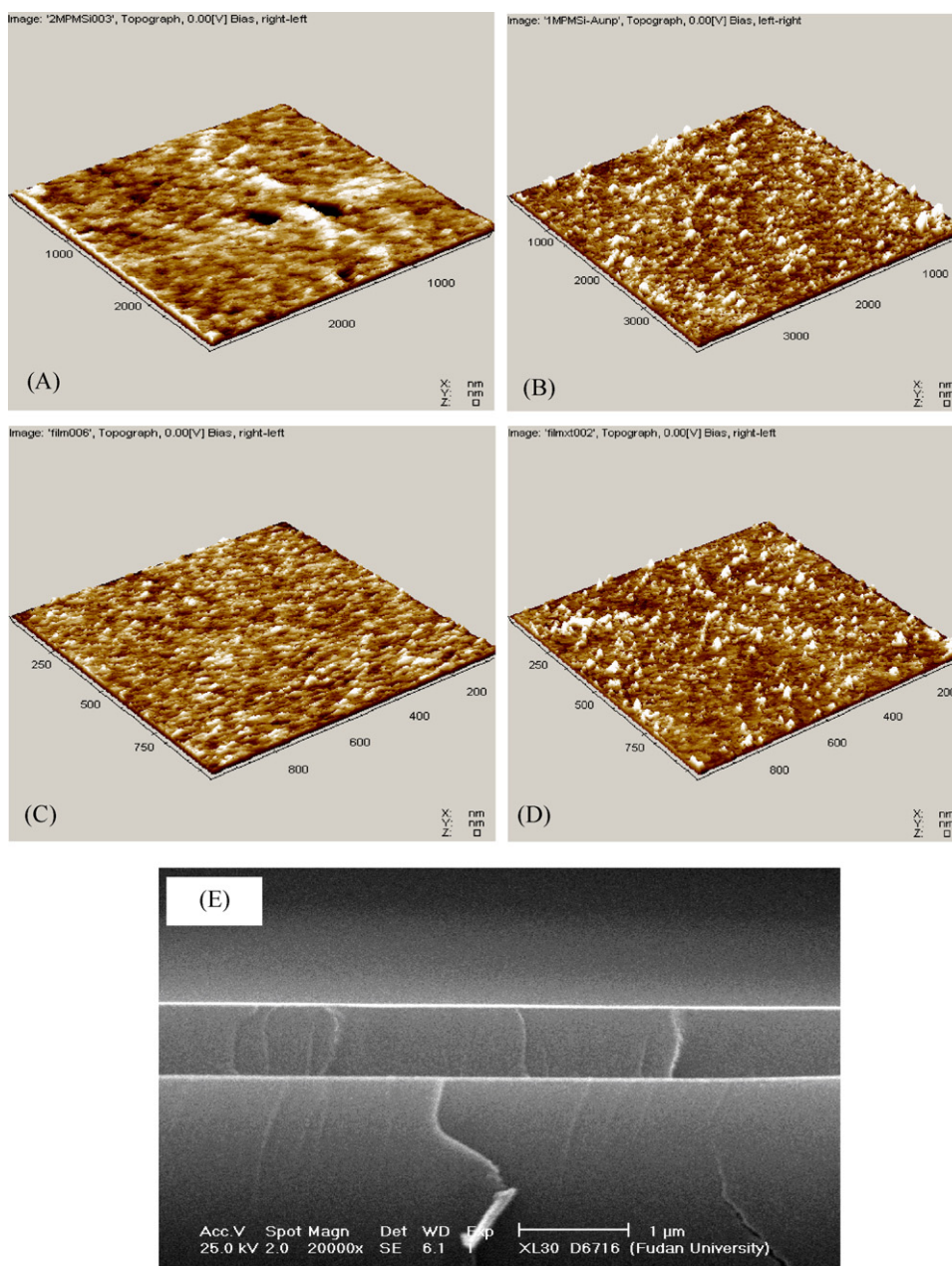


Fig. 2. AFM images of the MPMSi/ITO (A) and the Au-NP/ITO (B), and the MIP/Au-NP/ITO before extraction (C) and after extraction (D). The SEM image of the MIP/Au-NP/ITO (E). The surface roughness of the AFM images was 31 Å (A), 70 Å (B), 28 Å (C) and 32 Å (D), respectively.

ity of the MIP/Au-NP/ITO towards imipramine could be ascribed to the presence of the Au-NP functional monolayer and the selective MIP film. As observed, when the Au-NPs were introduced on the MIP/Au-NP/ITO, the current signal was amplified further than that on the MIP/ITO. It is inferred that the Au-NPs can catalyze the oxidation of imipramine by enhancing electron transfer on the electrode interface. Due to the inherent specificity of the MIP film, imipramine could interact with it selectively in the cavities with rebinding groups. Therefore, both the MIP/Au-NP/ITO and the MIP/ITO showed much better responses than the NMIP/ITO. By the way, the flat response of the NMIP/ITO could be attributed to the shortage of selective sites in the nonimprinted film, it also indicates the low nonspecific interaction between imipramine and the inorganic film prepared by sol-gel technology in our work.

3.3. Effect of scan rate

To examine the predominant type of mass transport, a study was carried out using Linear Sweep Voltammetry. With scan rate increasing, the anodic peak of the MIP/Au-NP/ITO grew (Fig. 4). It was observed that anodic peak current was linear to the square root of scan rate in the range of 10–300 mV s^{-1} , the regression equation was $I_p = 0.181 + 0.260v^{1/2}$ (I_p (μA), v (mV s^{-1}), $r = 0.991$). This indicates the electrode process is diffusion-controlled. In addition, the anodic peak potential and the logarithm of scan rate showed a linear relationship, following the equation: $E_p = 0.934 + 0.00641 \ln v$ (E_p (V), $r = 0.999$). According to the equation [25]: $E_p = E^\Phi + m[0.78 + \ln(D^{1/2}/k_s) - 0.5 \ln m] + 0.5 m \ln v (m = RT/(1 - \alpha)nF)$, the $n(1 - \alpha)$ was calculated to be 1.79. The n was previously estimated to be 2 [16], therefore, α was 0.11 in this case.

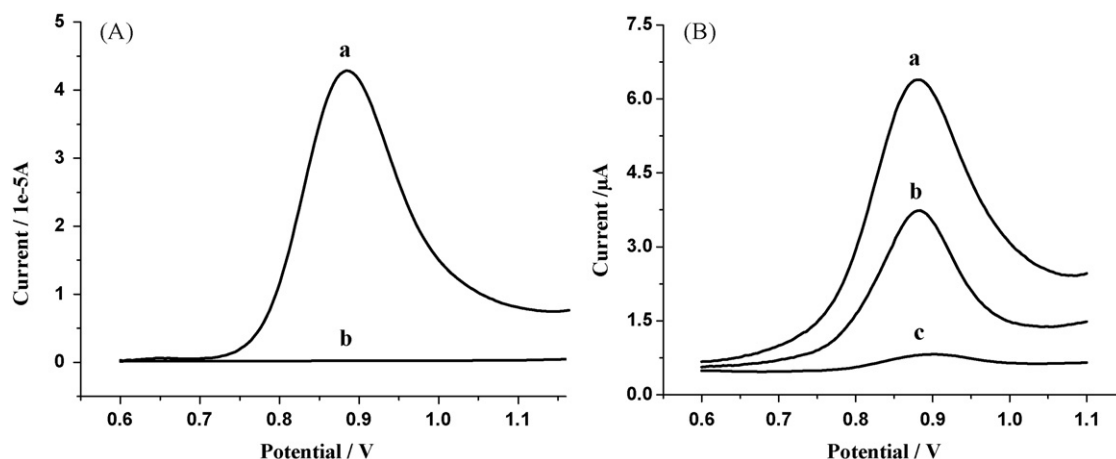


Fig. 3. (A) Typical DPV responses of the MIP/Au-NP/ITO before extraction (a) and after extraction (b). (B) DPV responses of the MIP/Au-NP/ITO (a), the MIP/ITO (b) and the NMIP/ITO (c) after incubation in 1.0 mM imipramine for 10 min. Supporting electrolyte: 100 mM PBS (pH 2.3).

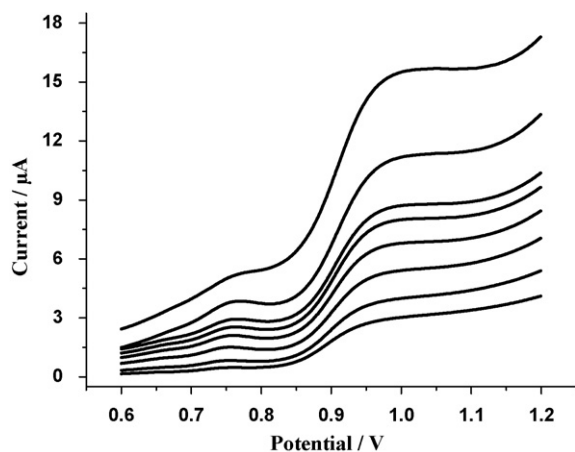


Fig. 4. Influence of scan rate on the response of the MIP/Au-NP/ITO by Linear Sweep Voltammetry. Scan rate: 10, 20, 40, 60, 80, 100, 200, and 300 mV s^{-1} (from bottom to top). Sample interval: 1 mV. Quiet time: 2 s. The electrode was incubated and tested in 1.0 mM imipramine. Other conditions as in Fig. 3.

3.4. Optimization of the analytical conditions

3.4.1. Influence of the amount of PTMOS and PEG on the response of the sensor

The effects of the amount of PTMOS on the DPV responses of the MIP/Au-NP/ITO were examined in Fig. 5A. With the molar

ratio between PTMOS and TEOS (PTMOS/TEOS) increasing from 0.01 to 0.20, a peak current response was found at the ratio 0.08 for the MIP/Au-NP/ITO (Fig. 5A-a), while the low current responses of the NMIP/Au-NP/ITO remained almost unchanged (Fig. 5A-b). Generally, PTMOS acts as a functional monomer in the silica matrix providing π - π interaction with the target molecule imipramine. With its amount growing, more phenyl groups, provided in the MIP film, will strengthen the π - π interaction with imipramine and leads to the increase of the current responses initially. However, when the ratio exceeded 0.08, the current of the MIP/Au-NP/ITO decreased gradually. It is inferred that the structure of the film becomes denser and less porous with too much PTMOS, since the hydrolyzation and condensation rate of TMOS is much quicker than TEOS [5]. Hence the ratio 0.08 was chosen as the best PTMOS/TEOS.

On the other hand, the effect of the amount of PEG on the DPV responses of the MIP/Au-NP/ITO was shown in Fig. 5B. Here, the signals were recorded on the MIP/Au-NP/ITO before the extraction of imipramine. With the molar ratio between PEG and TEOS (PEG/TEOS) increasing from 0.1 to 2.0, the anodic peak current responses were found growing quickly at first, and then increased slowly after the ratio 0.7. The presence of PEG makes the silica structure of the MIP film more porous and flexible, quick diffusion of the analyte imipramine can be easily attained in such a film. Consequently, the current responses increased noticeably in the beginning. However, too much PEG will enhance the fluidity of the matrix and reduce the stability of the film, especially in aqueous

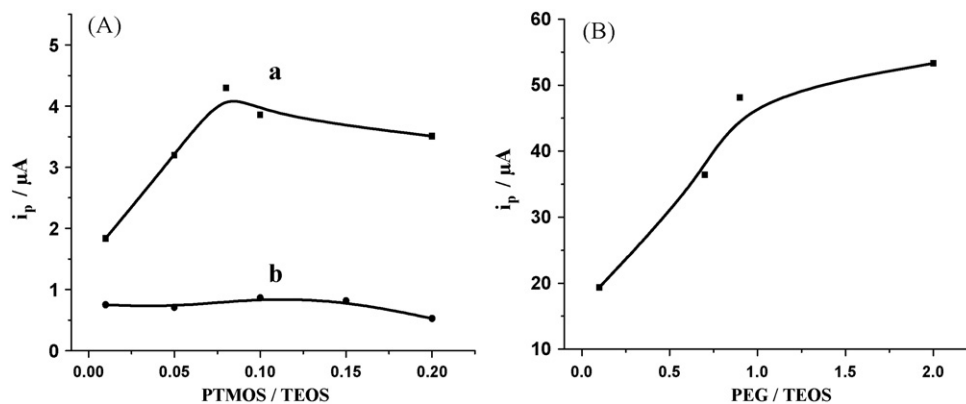


Fig. 5. (A) Influence of the ratio PTMOS/TEOS on the anodic peak current of the MIP/Au-NP/ITO (a) and the NMIP/Au-NP/ITO (b). The electrodes were incubated in 1.0 mM imipramine for 10 min. (B) Influence of the ratio PEG/TEOS on the anodic peak current of the MIP/Au-NP/ITO before extraction. Other conditions as in Fig. 3.

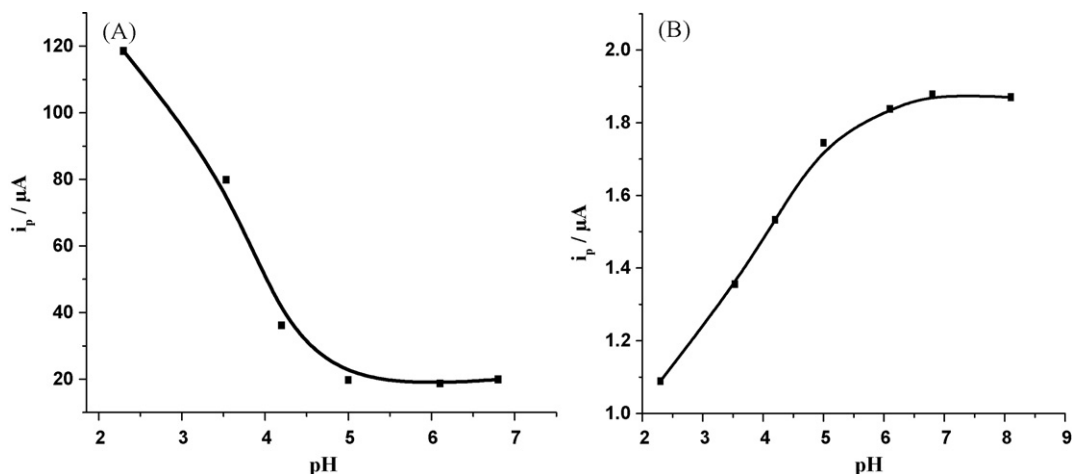


Fig. 6. (A) Influence of pH of the supporting electrolyte (100 mM PBS) for DPV detection on anodic peak current of $5.0 \times 10^{-4} \text{ mol L}^{-1}$ imipramine on a bare ITO electrode. (B) Influence of pH of imipramine solution ($3.0 \times 10^{-5} \text{ mol L}^{-1}$) for incubation of the MIP/Au-NP/ITO on anodic peak current of imipramine. Incubation time: 10 min. Other conditions as in Fig. 3.

solution [23]. It caused the slow growth of the currents from 0.7 to 2.0. Hence the ratio of 0.7 was chosen as the best PEG/TEOS.

3.4.2. Influence of pH

The effect of pH of the supporting electrolyte solution on the DPV response of imipramine was tested in Fig. 6A. The anodic peak current of imipramine (0.5 mM) on the bare ITO electrode decreased gradually, when the pH value of the supporting electrolyte solution (100 mM PBS) increased from 2.3 to 6.8. Since the ITO electrode surface is composed of a sensitive layer of conductive indium tin oxide, pH 2.3 was chosen in order to prevent the ITO electrode from being eroded at lower pH. Meanwhile the anodic peak potential shifted negatively with pH increasing from 4.2 to 6.8, following the linear equation: $E_p = 1.002 - 0.0243 \text{ pH}$ (E_p (V), $r = 0.990$), meaning H^+ is involved in the oxidation of imipramine.

The effect of pH of imipramine solution for incubation of the MIP/Au-NP/ITO on the DPV response of imipramine was also examined in Fig. 6B. For the same incubation time of 10 min in 100 mM PBS containing $3.0 \times 10^{-5} \text{ mol L}^{-1}$ imipramine, the peak current increased with the pH value of the incubation solution growing. At the pH values larger than 6.8, the peak currents attained a plateau, which implied that the target molecule preferably interacted with the selective interface of the MIP/Au-NP/ITO at these pH values.

Hence, a mild condition at pH 6.8 was chosen for the incubation solution.

3.5. Dependence of anodic peak current on incubation time

Different peak current responses of the MIP/Au-NP/ITO, the MIP/ITO and the NMIP/ITO were observed with the incubation time increasing from 1 min to 1 h in 1.0 mM imipramine in Fig. 7. The MIP/Au-NP/ITO kept the highest current responses (a) compared with the MIP/ITO (b) and the NMIP/ITO (c) for the same incubation time, which shows the excellent selectivity and sensitivity of the prepared sensor. The improved sensitivity of the MIP film could be attributed to the introduction of the Au-NPs on the MIP/Au-NP/ITO, for the Au-NPs could help enhance electron transfer on the electrode interface, and promoted the oxidation of imipramine, thus amplified the electrical signal produced by the selective molecular recognition of imipramine. What is more, it was found that the MIP/Au-NP/ITO responded quickly to the target molecule even after 1 min of incubation in Fig. 7a. The speedy response results from the porous MIP film with plentiful selective binding sites, the Au-NP

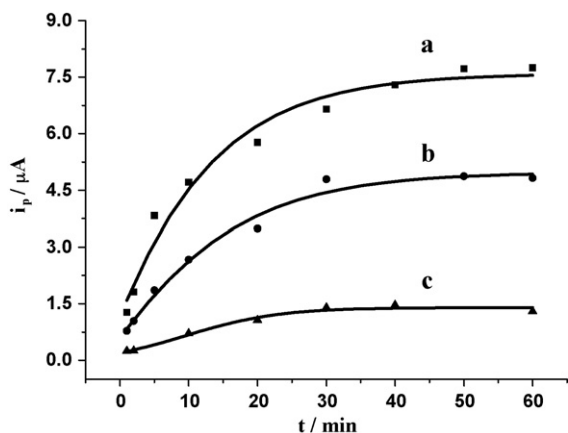


Fig. 7. Dependence of anodic peak current on incubation time for the MIP/Au-NP/ITO (a), the MIP/ITO (b) and the NMIP/ITO (c). The electrodes were incubated in 1.0 mM imipramine. Other conditions as in Fig. 3.

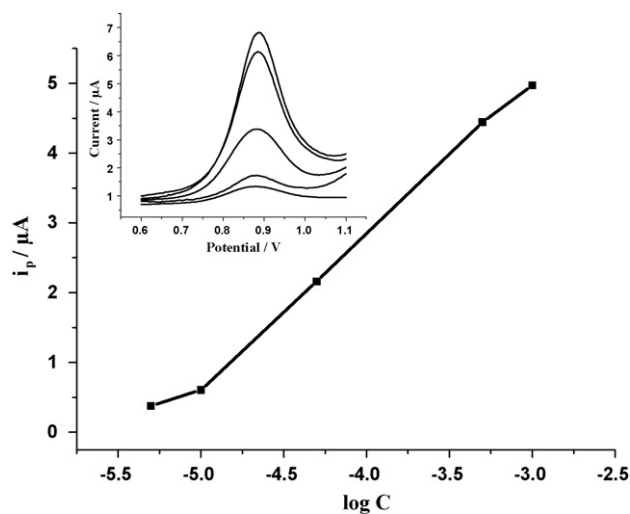


Fig. 8. Dependence of anodic peak current on logarithm of imipramine concentration on the MIP/Au-NP/ITO. The insert showed the DPV responses of 5.0×10^{-6} , 1.0×10^{-5} , 5.0×10^{-5} , 5.0×10^{-4} , and $1.0 \times 10^{-3} \text{ mol L}^{-1}$ imipramine (from bottom to top) after 10 min of incubation. Other conditions as in Fig. 3.

Table 1
Measurement results of imipramine in drug tablets.

Sample (15.0 µg/mL) number	Add (µg/mL)	Expected (µg/mL)	Found (µg/mL)	Recovery (%)
0	0	–	14.9	–
1	15.0	30.0	29.8	99.3
2	30.0	45.0	43.9	97.6
3	45.0	60.0	60.8	101.3
4	60.0	75.0	75.3	100.4

functional monolayer with electrochemical catalytic activities, and the optimization of the analytical conditions.

3.6. Calibration curve and interference

Under the optimal analytical conditions, the determination of imipramine with different concentrations was performed. The anodic peak current was linear to the logarithm of the concentration of imipramine from 5.0×10^{-6} to 1.0×10^{-3} mol L⁻¹ (Fig. 8). The linear regression equation was expressed as $i_p = 11.259 + 2.092 \log C$ (i_p (µA), C (mol L⁻¹), $r = 0.997$). The detection limit was estimated to be 1.0×10^{-9} mol L⁻¹, comparable to that obtained by the carbon paste electrode modified with cyclodextrin [18]. For eight parallel measurements of the MIP/Au-NP/ITO incubated in 100 mM PBS (pH 6.8) containing 1.0 mM imipramine, the R.S.D. of peak current was calculated to be 2.5%. The DPV response of the MIP/Au-NP/ITO was also investigated within a week, during which the peak current did not change noticeably. That indicates the satisfactory stability of the electrode, which could be ascribed to the rigid structure of the MIP film.

The influence of foreign compounds was also tested by the MIP/Au-NP/ITO. Clomipramine (Scheme 1B), another antidepressant drug widely used in clinical treatment of depression [26], is an analogue of imipramine with only one more chlorine atom of its molecular formula. When the electrode was incubated in 0.5 mM clomipramine for 1 h, the peak current was just commensurate with the response produce by 0.1 mM imipramine. It was also found that several kinds of surfactants such as Tween-20, Triton X-100, and sodium dodecyl sulfate did not interfere. Furthermore, 100-fold epinephrine, vitamin C, antipyrine, norfloxacin, allopurinol, thiamine, glucose, phenylalanine, captopril, or hydroxyzine had no obvious effect on the determination. Therefore, satisfactory selectivity of imipramine was obtained by such a kind of sensor.

3.7. Applications

The method was applied to detect imipramine in drug tablets. The pretreatment and determination procedures were the same as described in Section 2. The analytical results were shown in Table 1, and the recovery was 97.6–101.3%. The imipramine content was calculated to be 24.8 mg per tablet (its declared content was 25 mg). In addition, the accuracy of this method was examined by comparison with the result of the Chinese Pharmacopoeia method (the UV absorbance of imipramine at 251 nm in 0.1 M HCl solution was cho-

Table 2
Measurement results of parallel determinations in drug tablets.

Sample (15.0 µg/mL)	Number					
	1	2	3	4	5	6
EC	14.8	15.3	13.9	15.8	14.3	15.4
UV	15.3	14.9	14.4	15.1	14.9	15.6

Statistical analysis results: $F_{ex} = 3.08$, smaller than the F_{crit} value (5.05, at 5% probability level); $t_{exp} = 0.505$, smaller than the corresponding t_{crit} value (2.23, at the 95% confidence level).

sen as the quantitative criterion) [27]. The analytical results were shown in Table 2. By means of F -test and t -test analysis, both the calculated F -value (3.08) and t -value (0.505) are smaller than theoretical values (5.05 and 2.23, respectively, at the 95% confidence level). It means that the method proposed could be reliably used for routine analysis.

4. Conclusion

A sensitive and selective electrochemical sensor was fabricated for detection of the antidepressant imipramine via stepwise modification of Au-NPs and a thin MIP film on ITO electrodes. The excellent performance of the MIP/Au-NP/ITO electrode towards imipramine can be ascribed to the Au-NP functional monolayer with electrochemical catalytic activities and the porous MIP film with plentiful selective binding sites. Moreover, as observed, the sensor responded quickly to imipramine even after 1 min of incubation. Under the selected analytical conditions, the anodic peak current was linear to the logarithm of imipramine concentration from 5.0×10^{-6} to 1.0×10^{-3} mol L⁻¹ with the detection limit of 1.0×10^{-9} mol L⁻¹. The Au-NP functionalized MIP sensor, with high selectivity, sensitivity, and speed meets the requirements of imipramine detection, and it could be potentially applied in clinical analysis of physiological samples.

Acknowledgements

This work was supported by Shanghai Leading Academic Discipline Project (Project Number: B109 and 08XD14009), the NSFC (20675018, 90606014, 20890020 and 20525519), SH908-HD1, Huoyindong Foundation (no. 94009), CSTC 2007BB5260 and Fudan University.

References

- [1] R.J. Umpleby, S.C. Baxter, A.M. Rampey, G.T. Rushton, Y.Z. Chen, K.D. Shimizu, J. Chromatogr. B 804 (2004) 141.
- [2] C. Alexander, H.S. Andersson, L.I. Andersson, R.J. Ansell, N. Kirsch, I.A. Nicholls, J. O'Mahony, M.J. Whitcombe, J. Mol. Recognit. 19 (2006) 106.
- [3] E.L. Holthoff, F.V. Bright, Anal. Chim. Acta 594 (2007) 147.
- [4] S. Marx, Z. Liron, Chem. Mater. 13 (2001) 3624.
- [5] S. Fireman-Shoresh, D. Avnir, S. Marx, Chem. Mater. 15 (2003) 3607.
- [6] A. Walcarius, D. Mandler, J.A. Cox, M. Collinson, O. Lev, J. Mater. Chem. 15 (2005) 3663.
- [7] A.N. Shipway, M. Lahav, I. Willner, Adv. Mater. 12 (2000) 993.
- [8] S. Zhang, F. Huang, B.H. Liu, J.J. Ding, X. Xu, J.L. Kong, Talanta 71 (2007) 874.
- [9] R.N. Goyal, V.K. Gupta, M. Oyama, N. Bachheti, Electrochem. Commun. 8 (2006) 65.
- [10] M.C. Daniel, D. Astruc, Chem. Rev. 104 (2004) 293.
- [11] J.D. Zhang, M. Oyama, Anal. Chim. Acta 540 (2005) 299.
- [12] Z.S. Wu, J.S. Li, M.H. Luo, G.L. Shen, R.Q. Yu, Anal. Chim. Acta 528 (2005) 235.
- [13] J. Matsui, K. Akamatsu, S. Nishiguchi, D. Miyoshi, H. Nawafune, K. Tamaki, N. Sugimoto, Anal. Chem. 76 (2004) 1310.
- [14] J. Matsui, K. Akamatsu, N. Hara, D. Miyoshi, H. Nawafune, K. Tamaki, N. Sugimoto, Anal. Chem. 77 (2005) 4282.
- [15] N. Gao, Z. Xu, F. Wang, S.J. Dong, Electroanalysis 19 (2007) 1655.
- [16] R.A. de Toledo, M.C. Santos, K.M. Honorio, A.B.F. da Silva, E.T.G. Cavalheiro, L.H. Mazo, Anal. Lett. 39 (2006) 507.
- [17] T.A. Ivandini, B.V. Sarada, C. Terashima, T.N. Rao, D.A. Tryk, H. Ishiguro, Y. Kubota, A. Fujishima, J. Electroanal. Chem. 521 (2002) 117.
- [18] A. Ferancova, E. Korgova, R. Miko, J. Labuda, J. Electroanal. Chem. 492 (2000) 74.
- [19] J. Wang, M. Bonakdar, C. Morgan, Anal. Chem. 58 (1986) 1024.
- [20] I. Biryol, B. Uslu, Z. Kucukyavuz, J. Pharm. Biomed. Anal. 15 (1996) 371.
- [21] B.D. Busbee, S.O. Obare, C.J. Murphy, Adv. Mater. 15 (2003) 414.
- [22] C.M. Ruan, L.J. Yang, Y.B. Li, Anal. Chem. 74 (2002) 4814.
- [23] G. Shustak, S. Marx, I. Turyan, D. Mandler, Electroanalysis 15 (2003) 398.
- [24] K.R. Brown, D.G. Walter, M.J. Natan, Chem. Mater. 12 (2000) 306.
- [25] E. Laviron, J. Electroanal. Chem. 101 (1979) 19.
- [26] F. Huang, S. Qu, S. Zhang, B.H. Liu, J. Kong, Microchim. Acta 161 (2008) 149.
- [27] Chinese Pharmacopoeia Committee, Chinese Pharmacopoeia (Part II), 1st ed., Chemical Industry Press, Beijing, 2005, p. 475.